

Lecture Notes in Networks and Systems 536

Olga Arsenyeva
Tatiana Romanova
Maria Sukhonos
Yevgen Tsegelnyk *Editors*

Smart Technologies in Urban Engineering

Proceedings of STUE-2022

 Springer

Lecture Notes in Networks and Systems

Volume 536

Series Editor

Janusz Kacprzyk, Systems Research Institute, Polish Academy of Sciences,
Warsaw, Poland

Advisory Editors

Fernando Gomide, Department of Computer Engineering and Automation—DCA,
School of Electrical and Computer Engineering—FEEC, University of Campinas—
UNICAMP, São Paulo, Brazil

Okyay Kaynak, Department of Electrical and Electronic Engineering,
Bogazici University, Istanbul, Turkey

Derong Liu, Department of Electrical and Computer Engineering, University
of Illinois at Chicago, Chicago, USA

Institute of Automation, Chinese Academy of Sciences, Beijing, China

Witold Pedrycz, Department of Electrical and Computer Engineering, University of
Alberta, Alberta, Canada

Systems Research Institute, Polish Academy of Sciences, Warsaw, Poland

Marios M. Polycarpou, Department of Electrical and Computer Engineering,
KIOS Research Center for Intelligent Systems and Networks, University of Cyprus,
Nicosia, Cyprus

Imre J. Rudas, Óbuda University, Budapest, Hungary

Jun Wang, Department of Computer Science, City University of Hong Kong,
Kowloon, Hong Kong

The series “Lecture Notes in Networks and Systems” publishes the latest developments in Networks and Systems—quickly, informally and with high quality. Original research reported in proceedings and post-proceedings represents the core of LNNS.

Volumes published in LNNS embrace all aspects and subfields of, as well as new challenges in, Networks and Systems.

The series contains proceedings and edited volumes in systems and networks, spanning the areas of Cyber-Physical Systems, Autonomous Systems, Sensor Networks, Control Systems, Energy Systems, Automotive Systems, Biological Systems, Vehicular Networking and Connected Vehicles, Aerospace Systems, Automation, Manufacturing, Smart Grids, Nonlinear Systems, Power Systems, Robotics, Social Systems, Economic Systems and other. Of particular value to both the contributors and the readership are the short publication timeframe and the world-wide distribution and exposure which enable both a wide and rapid dissemination of research output.

The series covers the theory, applications, and perspectives on the state of the art and future developments relevant to systems and networks, decision making, control, complex processes and related areas, as embedded in the fields of interdisciplinary and applied sciences, engineering, computer science, physics, economics, social, and life sciences, as well as the paradigms and methodologies behind them.

Indexed by SCOPUS, INSPEC, WTI Frankfurt eG, zbMATH, SCImago.

All books published in the series are submitted for consideration in Web of Science.

For proposals from Asia please contact Aninda Bose (aninda.bose@springer.com).

More information about this series at <https://link.springer.com/bookseries/15179>

Olga Arsenyeva · Tatiana Romanova ·
Maria Sukhonos · Yevgen Tsegelnyk
Editors


Smart Technologies in Urban Engineering


Proceedings of STUE-2022


 Springer


 **stue**
conference

Editors

Olga Arsenyeva 
O.M. Beketov National University of Urban
Economy in Kharkiv
Kharkiv, Ukraine

Maria Sukhonos 
O.M. Beketov National University of Urban
Economy in Kharkiv
Kharkiv, Ukraine

Tatiana Romanova 
A. Pidhomyi Institute of Mechanical
Engineering Problems of the National
Academy of Sciences of Ukraine
Kharkiv, Ukraine

Yevgen Tsegelnyk 
O.M. Beketov National University of Urban
Economy in Kharkiv
Kharkiv, Ukraine

ISSN 2367-3370

ISSN 2367-3389 (electronic)

Lecture Notes in Networks and Systems

ISBN 978-3-031-20140-0

ISBN 978-3-031-20141-7 (eBook)

<https://doi.org/10.1007/978-3-031-20141-7>

© The Editor(s) (if applicable) and The Author(s), under exclusive license
to Springer Nature Switzerland AG 2023

This work is subject to copyright. All rights are solely and exclusively licensed by the Publisher, whether the whole or part of the material is concerned, specifically the rights of translation, reprinting, reuse of illustrations, recitation, broadcasting, reproduction on microfilms or in any other physical way, and transmission or information storage and retrieval, electronic adaptation, computer software, or by similar or dissimilar methodology now known or hereafter developed.

The use of general descriptive names, registered names, trademarks, service marks, etc. in this publication does not imply, even in the absence of a specific statement, that such names are exempt from the relevant protective laws and regulations and therefore free for general use.

The publisher, the authors, and the editors are safe to assume that the advice and information in this book are believed to be true and accurate at the date of publication. Neither the publisher nor the authors or the editors give a warranty, expressed or implied, with respect to the material contained herein or for any errors or omissions that may have been made. The publisher remains neutral with regard to jurisdictional claims in published maps and institutional affiliations.

This Springer imprint is published by the registered company Springer Nature Switzerland AG
The registered company address is: Gewerbestrasse 11, 6330 Cham, Switzerland

Preface

The International Conference on Smart Technologies in Urban Engineering (STUE) was aimed to bring together leading academic scientists, researchers, and stakeholders within the industry in order to exchange and share their experiences, best practices, and research results concerning all aspects of innovations in the area of Smart Technologies in Urban Engineering.

The Conference STUE-2022 was held on June 9–11, 2022, to commemorate the 100th anniversary of the O.M. Beketov National University of Urban Economy in Kharkiv. To ensure safety and security of every participant, the Conference was held online. During this Conference, technical exchanges between the research communities were carried out in the forms of keynote speeches, panel discussions, as well as special sessions.

This book contains selected papers dealing with relevant topics including Smart City, Transport Technologies and Logistics, Energy, Environment and Sustainable Development, Electrical Engineering, Computational and Information Technologies, and Materials Engineering and Manufacturing. All the contributions offer plenty of valuable information and would be of great benefit to the experience exchange among scientists in urban engineering.

The organizers of STUE-2022 made great efforts to ensure the success of this Conference. We hereby would like to thank all the members of the STUE-2022 Program Committee and Organizing Committee, the reviewers for their effort in reviewing and soliciting the papers, and all authors for their contribution to the formation of a common intellectual environment for solving relevant scientific problems.

We are also grateful to Springer—Janusz Kacprzyk and Thomas Ditzinger—as the editor responsible for the series “Lecture Notes in Networks and Systems” for their great support in publishing these selected papers.

Olga Arsenyeva
Tatiana Romanova
Maria Sukhonos
Yevgen Tsegelnyk

Organization

Steering Committee

Honorary Chair

Volodymyr Babaiev

O.M. Beketov National University of Urban
Economy in Kharkiv, Kharkiv, Ukraine

Executive Chair

Maria Sukhonos

O.M. Beketov National University of Urban
Economy in Kharkiv, Kharkiv, Ukraine

Program Committee Chair

Ihor Biletskyi

O.M. Beketov National University of Urban
Economy in Kharkiv, Kharkiv, Ukraine

Publication Chair

Yevgen Tsegelnyk

O.M. Beketov National University of Urban
Economy in Kharkiv, Kharkiv, Ukraine

International Program Committee

Olga Arsenyeva

O.M. Beketov National University of Urban
Economy in Kharkiv, Kharkiv, Ukraine

Oleksandr Astakhov

Forschungszentrum Jülich FZJ, Jülich, Germany

Zoran Avramović

Pan-European University “APEIRON”, Banja
Luka, Bosnia and Herzegovina

Liliana-Laura Bădiță

National Institute of Research and Development
in Mechatronics and Measurement Technique,
Bucharest, Romania

Paula Bajdor	Częstochowa University of Technology, Czestochowa, Poland
Jan Bauer	Czech Technical University in Prague, Prague, Czech Republic
Grega Bizjak	University of Ljubljana, Ljubljana, Slovenia
Artem Boyarchuk	National Aerospace University “Kharkiv Aviation Institute”, Kharkiv, Ukraine
Daniela-Doina Cioboată	National Institute of Research and Development in Mechatronics and Measurement Technique, Bucharest, Romania
İlhami Çolak	Nişantaşı Üniversitesi, Istanbul, Turkey
Dmytro Diadin	O.M. Beketov National University of Urban Economy in Kharkiv, Kharkiv, Ukraine
Mircea Constantin Duică	Universitatea Valahia din Targoviste, Targoviste, Romania
Ludmiła Filina-Dawidowicz	West Pomeranian University of Technology in Szczecin, Szczecin, Poland
Andrii Galkin	O.M. Beketov National University of Urban Economy in Kharkiv, Kharkiv, Ukraine
Robert Głębocki	Warsaw University of Technology, Warsaw, Poland
Kapil Gupta	University of Johannesburg, Johannesburg, South Africa
István Gábor Gyurika	University of Pannonia, Veszprém, Hungary
Liisa Halonen	Aalto University, Espoo, Finland
Łukasz Kaczmarek	Lodz University of Technology, Lodz, Poland
Dmytro Klets	Reform Support Team at the Ministry of Infrastructure of Ukraine, Kyiv, Ukraine
Olga Kordas	KTH Royal Institute of Technology, Stockholm, Sweden
Dmitriy Kritskiy	National Aerospace University “Kharkiv Aviation Institute”, Kharkiv, Ukraine
Chitresh Kumar	O. P. Jindal Global University, Sonipat, India
Valeriy Kuznetsov	Railway Research Institute IK, Warsaw, Poland
Igor Litvinchev	Member of Mexican Academy of Sciences, Nuevo León State University, Monterrey, Mexico
Oleksii Lobashov	O.M. Beketov National University of Urban Economy in Kharkiv, Kharkiv, Ukraine
Elżbieta Macioszek	Silesian University of Technology, Gliwice, Poland
José Antonio Marmolejo-Saucedo	Universidad Panamericana, Ciudad de Mexico, Mexico
Pavel Neyezhnikov	National Scientific Centre “Institute of Metrology”, Kharkiv, Ukraine

Teresa Pereira	Instituto Politécnico de Viana do Castelo, Viana do Castelo, Portugal
Luca Persia	Sapienza Università di Roma, Rome, Italy
Sergiy Plankovskyy	O.M. Beketov National University of Urban Economy in Kharkiv, Kharkiv, Ukraine
Vladyslav Pliuhin	O.M. Beketov National University of Urban Economy in Kharkiv, Kharkiv, Ukraine
Socorro Rangel	UNESP-Universidade Estadual Paulista, Sao Paulo, Brazil
Tatiana Romanova	A. Pidhorneyi Institute of Mechanical Engineering Problems of the National Academy of Sciences of Ukraine, Kharkiv, Ukraine
Şeref Sağıroğlu	Gazi University, Ankara, Turkey
Tibor Schlosser	Slovak University of Technology in Bratislava, Bratislava, Slovakia
Yochanan Shachmurove	City University of New York, New York, USA
Vladimir Shpachuk	O.M. Beketov National University of Urban Economy in Kharkiv, Kharkiv, Ukraine
Olga Shypul	National Aerospace University “Kharkiv Aviation Institute”, Kharkiv, Ukraine
Natalia Smetankina	A. Pidhorneyi Institute of Mechanical Engineering Problems of the National Academy of Sciences of Ukraine, Kharkiv, Ukraine
Marta Starostka-Patyk	Częstochowa University of Technology, Czestochowa, Poland
Petro Stetsyuk	V.M. Glushkov Institute of Cybernetics of the National Academy of Sciences of Ukraine, Kyiv, Ukraine
Yurii Stoyan	Corresponding Member of the National Academy of Sciences of Ukraine, A. Pidhorneyi Institute of Mechanical Engineering Problems of the National Academy of Sciences of Ukraine, Kharkiv, Ukraine
Tibor Szalay	Budapest University of Technology and Economics, Budapest, Hungary
Joshua Thomas	UOW Malaysia KDU Penang University College, Georgetown, Malaysia
Aurel Mihail Țițu	Lucian Blaga University of Sibiu, Sibiu, Romania
Juri Tolujev	Fraunhofer Institute for Factory Operation and Automation IFF, Magdeburg, Germany
Yevgen Tsegelnyk	O.M. Beketov National University of Urban Economy in Kharkiv, Kharkiv, Ukraine
Dmytro Tugay	O.M. Beketov National University of Urban Economy in Kharkiv, Kharkiv, Ukraine
Jüri Vain	Tallinn University of Technology, Tallinn, Estonia

Petar Sabev Varbanov

Brno University of Technology, Brno, Czech Republic

Georges Zissis

Paul Sabatier University—Toulouse III, Toulouse, France

Organizing Team

Olga Ivanova

O.M. Beketov National University of Urban Economy in Kharkiv, Kharkiv, Ukraine

Maria Osinska

O.M. Beketov National University of Urban Economy in Kharkiv, Kharkiv, Ukraine

Lidiia Piddubna

O.M. Beketov National University of Urban Economy in Kharkiv, Kharkiv, Ukraine

Sergiy Plankovskyy

O.M. Beketov National University of Urban Economy in Kharkiv, Kharkiv, Ukraine

Vladyslav Pliuhin

O.M. Beketov National University of Urban Economy in Kharkiv, Kharkiv, Ukraine

Alona Starostina

O.M. Beketov National University of Urban Economy in Kharkiv, Kharkiv, Ukraine

Alina Trotsai

O.M. Beketov National University of Urban Economy in Kharkiv, Kharkiv, Ukraine

Valeriya Yesina

O.M. Beketov National University of Urban Economy in Kharkiv, Kharkiv, Ukraine

Organizers



Ministry of Education and Science of Ukraine



O.M. Beketov National University of Urban Economy in Kharkiv



Academic and Research Institute of Energy, Information and Transport Infrastructure

Contents

Computational and Information Technologies

Formalization of Converting Processes and it Validation in Spatial Data Infrastructure	3
Oleksandr Zarytskyi, Oleksandr Kostenko, and Maryna Bulaienko	
Using Optimization to Construct Naturally Parametrized Curve with Cubic Curvature	14
Olha Khomiak, Petro Stetsyuk, Volodymyr Zhydkov, and Luis Infante	
Relaxed Containment in Circular Packing Problems	25
Tatiana Romanova, Georgiy Yaskov, Igor Litvinchev, Petro Stetsyuk, Andrii Chuhai, and Sergiy Shekhovtsov	
<i>Phi</i>-Functions for Objects Bounded by the Second-Order Curves and Their Application to Packing Problems	35
Mykola Gil and Volodymyr Patsuk	
Optimization of Design Process Based on 3D-Model	45
Nataliia Vergunova and Sergey Vergunov	
Pulse Wave Propagation Velocity and Assessment of Arterial Vessel Elasticity	57
Volodymyr Kyrychenko, Tetiana Kulbashevska, Viktor Sergieiev, and Lidiia Piddubna	
Mathematical Modeling of Signal Detection in Non-gaussian Correlated Noise	65
Daniil Smirnov, Elena Palahina, and Volodymyr Palahin	
Evaluation of Endothelium Regulation of Vascular Tone	75
Viktor Sergieiev, Volodymyr Kyrychenko, Tetiana Kulbashevska, and Ihor Biletskyi	

Dimensionality Reduction of Diabetes Mellitus Patient Data Using the T-Distributed Stochastic Neighbor Embedding 86
 Ievgen Meniailov, Serhii Krivtsov, and Tetyana Chumachenko

Machine Learning and Web Integrated Chatting Forum Which Detected Mental Health of the User 96
 Mangesh Ghonge, Tejas Kachare, Siddharth Kakade, Snehal Shintre, and Siddharth Nigade

Classification of Cardiovascular Disease Using AdaBoost Method 107
 Kseniia Bazilevych, Mykola Butkevych, and Halyna Padalko

Retaining Wall Surface Optimization 115
 Volodymyr Babaiev, Valeriy Shmukler, and Oleg Kalmykov

Adaptive Blockchain Solution to Fight Against Financial Corruption in an Organization 128
 Premanand Ghadekar, Tejas Kachare, Sagar Sikchi, Talib Hussain, and Pradunya Maladhari

Analytical Solution of Modified Mackey-Glass Equation 140
 Roman Voliansky, Nina Volianska, Oleksiy Sinkevych, Serhii Serhiienko, and Valeriy Kuznetsov

Efficient Policy Representation for Markov Decision Processes 151
 Anahita Khademi and Sepehr Khademian

Modeling of Distributed Mosaic Systems of Mobile Bionic Robots 163
 Oleksandr Prokhorov, Oleg Fedorovich, Valeriy Prokhorov, Oleksii Shatalov, and Yuriy Pakhomov

Electrical Engineering

Investigation of the Electrical Parameters of an Advanced High-Energy Ignition System 177
 Kostyantyn Korytchenko, Mario Janda, Olga Shypul, Serhiy Krivosheev, and Oleksandr Yeresko

Determination of Massive Rotary Electric Machines Parameters in ANSYS RMXprt and ANSYS Maxwell 189
 Vladyslav Pliuhin, Mykola Zablodskiy, Maria Sukhonos, Yevgen Tsegelnyk, and Lidiia Piddubna

Inverse Multi-parameter Identification of Plane Objects Electrophysical Parameters Profiles by Eddy-Current Method 202
 Ruslana Trembovetska, Volodymyr Halchenko, and Constantine Bazilo

The Urgency of Using Adaptive Observers to Identify the Parameters of the DC Electric Drive 213
 Vasyi Stopkin, Anatoliy Nikolenko, Vitaliy Kuznetsov, Mykola Tryputen, and Oleksandr Kuzenkov

Mathematical Modeling of Rod-Type Piezoelectric Transducers for Application in Smart Urban Engineering Technologies 225
 Constantine Bazilo, Maksym Bondarenko, Liudmyla Usyk, Viacheslav Tuz, and Emil Faure

Improvement of a Linear Screw Piezo Motor Design for Use in Accurate Liquid Dosing Assembly 237
 Volodymyr Halchenko, Dmytro Bacherikov, Sergey Filimonov, and Nadiia Filimonova

Design of Event Based State Feedback Controller for Linear Time Invariant Systems 248
 Arepalli Vedavyas, Avadh Pati, Sunil Kumar Mishra, and Bhargav Appasani

Interpretation of Dynamic Models Based on Neural Networks in the Form of Integral-Power Series 258
 Oleksandr Fomin, Sergii Polozhaenko, Valentyn Krykun, Andrii Orlov, and Daria Lys

Miller Decoder for UHF and SHF RFID Application 266
 Sarada Musala, Kesanasetty Leela Sravani, Cristian Ravariu, and Avireni Srinivasulu

Energy, Environment and Sustainable Development

Implementation of Sustainable Development Goals in Business Entities 277
 Paula Bajdor and Marta Starostka-Patyk

Cluster Analysis Usage as Prerequisite for Implementing Strategies of Countries Startup Ecosystems Development 290
 Mykola Kyzym, Olena Dymchenko, Valentyna Smachylo, Olha Rudachenko, and Nataliia Dril

Load Forecasting and Electricity Consumption by Regression Model 302
 Maria Sukhonos, Volodymyr Babaiev, Vladyslav Pliuhin, Vitaliy Teterev, and Illia Khudiakov

Butterfly Valve PID-Controller for Application in Individual Heating Substations 315
 Olga Arsenyeva, Jiří Jaromír Klemesš, Petar Sabev Varbanov, and Petro Kapustenko

Analysis of Gas Transmission Systems Elements from the Perspective of the Sustainable Development Concept	325
Katerina Paleyeva, Ivan Kaptsov, and Nataliya Kaptsova	
A Technique to Identify Technical Measures Designed to Ensure Environmentally Safe Management in Populated Areas in Ukraine	337
Natalia Teliura, Hanna Khabarova, Alona Reshetchenko, Nataliia Tsapko, and Olga Lomakina	
Removal of Heavy Metals from Sewage Sludge by Using Humic Substances	349
Tamara Shevchenko, Olena Galkina, Serghii Martynov, and Stanislav Dushkin	
Methods of Combined Horizontal Settler Research	360
Stepan Epoyan, Tamara Airapetian, Oleksandr Haiduchok, Gennadiy Sukhorukov, and Oleksandr Kravchuk	
Territorial Planning and Sustainable Development of Refugee Areas	368
Olena Uhodnikova, Kostiantyn Viatkin, Sergii Gordiienko, Roman Viatkin, and Natalia Moroz	
Materials Engineering and Manufacturing	
Use of New Smart Materials and Technologies Based on Titanium Alloys in Urban Engineering	381
Valeriy Kostin, Olena Berdnikova, Svitlana Hryhorenko, Olga Kushnarova, and Evgeniy Titkov	
Detonation Nanodiamonds as Part of Smart Composite Paintwork Materials	393
Galina Gurina, Pavlo Kozub, Svetlana Kozub, Natalia Saienko, and Anna Skripinets	
Improving the Quality of Magnesium-Soluble Biological Alloy for Implants	403
Vadim Shalomoev, Viktor Greshta, and Olga Liutova	
Hydrogen Sensor on the Base of Nanocrystalline SiC Films	412
Oleksandr Semenov, Hanna Dulfan, Denis Lubov, Ihor Biletskyi, and Natalia Teliura	
Determination of Research Guidelines and Establishing of a Test Framework for the Development of New CVD Coating Formulations and New Approach Coating Equipment	420
István Gábor Gyurika, Osamah Ihsan Ali, and Miklós Jakab	

An Approach to Calculate Features of Laser Radiation Absorption in Beryllium and Aluminum Alloys for Smart Welding Processes 432
 Volodymyr Korzhyk, Vladislav Khaskin, Sviatoslav Peleshenko, Volodymyr Shcheretskyi, and Yevhenii Illiashenko

Determination of the Composite Products Moulding Process Parameters with Regulated Degree of Curing 444
 Andrii Kondratiev, Oleksii Vambol, Anton Tsaritsynskyi, Maryna Shevtsova, and Tetyana Nabokina

Two-Stage Optimization of Laminated Composite Elements with Minimal Mass 456
 Natalia Smetankina, Oleksandr Semenets, Alyona Merkulova, Dmytro Merkulov, and Serhii Misura

Temperature Effect on Elastic, Thermomechanical and Thermal Properties of Polymer Composite Materials 466
 Oleksii Vambol, Maryna Shevtsova, Anton Tsaritsynskyi, Tetyana Nabokina, and Andrii Kondratiev

Stiffness and Fatigue of Sandwich Plates with Honeycomb Core Manufactured by Fused Deposition Modeling 477
 Borys Uspensky, Konstantin Avramov, Ihor Derevianko, Oleg Polishchuk, and Oleksandr Salenko

Fuzzy-TOPSIS Hybrid Technique for Multi-response Optimization in Nonconventional Machining of Gears 489
 Thobadingoe Craven Phokane and Kapil Gupta

Increasing the Bearing Capacity of the Compressor Bling Blades by Technological Methods 502
 Dmytro Pavlenko, Oleksandr Tarasov, Daria Tkach, and Yuriy Torba

Optimization of T-Joints Laser Robotic Welding Procedure Parameters from AISI 321 Stainless Steel 513
 Maksym Khokhlov, Artemii Bernatskyi, Olena Berdnikova, Olga Kushnarova, and Oleksandr Siora

The Main Defects and Ways to Improve the Quality of Layer-by-Layer Sintered Gas Turbine Parts 525
 Daria Tkach, Dmytro Pavlenko, Yaroslav Dvirnyk, Oleksii Pedash, and Oleksandr Tarasov

3D Concrete Printing Technology: Implementing Tasks in Ukraine 537
 Oleh Kulaienko and Oleksii Kabus

Investigation of Control Algorithms for Machine Tool Coupled Axes 547
 Oleksandr Aksonov, Yevgen Tsegelnyk, Volodymyr Kombarov, Sergiy Plankovsky, and Yevhen Aksonov

Technological Equipment and Automation Control of the Three-Dimensional Structures Laser Welding Process in Different Spatial Positions 558
 Artemii Bernatskyi, Mykola Sokolovskyi, Volodymyr Lukashenko, Oleksandr Siora, and Nataliia Shamsutdinova

Automation of the Pneumatic Impulse Mandreling Technological Process 569
 Vitalii Voronko, Yuri Dyachenko, Iryna Voronko, Oleksandr Zastela, and Vladyslav Voronko

Ensuring Functional Stability of Technological Processes as Cyberphysical Systems Using Neural Networks 581
 Valentyn Sobchuk, Iryna Zamrii, and Serhii Laptiev

S-Shape Feedrate Profile with Smoothly-Limited Jerk for Threading Movements Synchronization in CNC Machining 593
 Volodymyr Kombarov, Volodymyr Sorokin, Yevgen Tsegelnyk, Sergiy Plankovskyy, and Yevhen Aksonov

Smart City

World Experience of Smart City Development 609
 Tetiana Pushkar, Daria Serogina, Krystyna Mykhailova, Hanna Zhovtyak, and Hanna Sobolieva

Perspectives on Socially and Environmentally Just Circular Cities: The Case of Naples (Italy) 621
 Patrizia Ghisellini, Renato Passaro, and Sergio Ulgiati

Regional Waste Management System Improvement Strategy Based on Sustainable Development Principles 632
 Olga Khandogina, Natalia Mushchynska, Olena Dymchenko, and Nataliia Obukhova

Application of an Innovative Monolithic Mechanical Seismometer for Urban Vibroscape Monitoring 644
 Marco Casazza, Rocco Romano, and Fabrizio Barone

The Sustainable and Smart Mobility Strategy: Country Comparative Overview 656
 Olga Kunytska, Luca Persia, Norbert Gruenwald, Diana Datsenko, and Malgorzata Zakrzewska

Definition of the e-Scooter Sharing Stations Number and Location Under a Lack of Data: A Case Study of the City District in Dnipro . . . 669
 Olha Svichynska, Kateryna Serhiienko, Stanislav Svichynskyi, and Vitalii Chyzyh

Transport Technologies and Logistics

Changing Drivers’ Cognitive Characteristics at Twilight in Freight Transportation 683
 Oleksii Prasolenko, Dmytro Burko, and Vitalii Chumachenko

Informational Characteristics of Objects to the Driver’s Perception Field in Urban and Suburban Conditions 695
 Iryna Lynnyk, Svitlana Chepurna, Kateryna Vakulenko, and Nadiia Kulbashna

Real Time Driver Alertness System Based on Eye Aspect Ratio and Head Pose Estimation. 707
 Ronak Mundra, Avireni Srinivasulu, Cristian Ravariu, Appasani Bhargav, and Sarada Musala

Modeling the Impact of Technology and Arranging Commuter Passenger Transportation by Competing Modes of Transport 717
 Tetiana Hrushevskya, Oleh Strelko, Anatoliy Horban, Liubov Soloviova, and Oleksandra Soloviova

Effective Functioning of Intelligent Transport Systems as One of the Main Factors for Supporting Sustainable Urban Development 729
 Viktor Danchuk, Antonio Comi, and Olga Kunytska

Influence of the City Transport Route Network Discrete Model Geometrical Parameters on a Quality of a Passenger Traffic System Operation 740
 Serhii Pustiulha, Volodymyr Samchuk, Viktor Samostian, Valentyn Prydiuk, and Valerij Dembitskij

Improvement of the System of Arranging Commuter Passenger Transportation Based on the Kyiv Transport Hub 752
 Oleh Strelko, Tetiana Hrushevskya, Vasyl Gaba, Yuliia Berdnychenko, and Hanna Kyrychenko

Public Transit Crowding Estimation Indicators: Comparative Analysis, Conditions of Application, Interaction 764
 Denys Ponkratov, Yuriy Davidich, Denys Kopytkov, Ganna Samchuk, and Yevhen Kush

A Formal Method of Trust Computation in VANET: A Spatial, Temporal and Behavioral Approach 775
 Abdullah Alharthi, Qiang Ni, Richard Jiang, and Mohammad Ayoub Khan

Research of the Freight Trains Movement Stability with a Network Effect 785
 Andrii Prokhorchenko, Mikhail Kravchenko, Olena Malakhova, Grygorii Sikonenko, and Halyna Prokhorchenko

Efficiency Assessments of the Parking and Time Restrictions Implementation in Kharkiv by Applying the Logistics Sustainability Index Methodology 795
Mariia Olkhova, Dmytro Roslavytsev, Antonio Comi, and Olga Plyhun

Directions for Improving the Efficiency of Intermodal Transport 808
Ludmiła Filina-Dawidowicz, Alla Selivanova, Daria Możdrzeń, and Sara Stankiewicz

Analysis of Urban Freight Distribution Management Methods on the Principles of “Green Logistics” 820
Olesia Hriekova

Efficiency of “Green” Logistics Technologies in Multimodal Transportation of Dangerous Goods 831
Denis Lomotko, Oleksandr Ohar, Dmytro Kozodoi, Vitalii Barbashyn, and Mykola Lomotko

The Strategic Positioning in the International Maritime Logistics 842
Iuliia Samoilyk and Viktoriia Nykonchuk

Urban Street and Road Network Reconstruction Problems 854
Lina Hasenko, Tetyana Lytvynenko, Viktoriia Ivasenko, and Mohamed Elgandour

Author Index 865

Computational and Information Technologies



Formalization of Converting Processes and its Validation in Spatial Data Infrastructure

Oleksandr Zarytskyi^(✉) , Oleksandr Kostenko , and Maryna Bulaienko 

O. M. Beketov National University of Urban Economy in Kharkiv, 17 Marshala Bazhanova Street, Kharkiv 61002, Ukraine

oleksandr.zarytskohyi@kname.edu.ua

Abstract. For transition to European standards for infrastructure development and spatial data (SD) bank supply following the Directive of the European Parliament and of the Council of Europe (INSPIRE), which is mandatory for all member states and candidates to join the EU, it is necessary to ensure uniform requirements for the content of electronic documents on individual spatial objects. Significant archives of information require automation of the converting process for differentiated databases of SD to updated rules of digitally describing all instances of SD. The main processes of data conversion are considered, based on which the formation technology of acceptable or missed information for spatial data infrastructure is constructed. The paper examines that affine transformation is recommended for cases where geometric distortions of SD are heterogeneous. It has been found that the process of converting spatial and attributive information is more complicated. It is shown that the converting of archival information is realized through a set of functional rules following a set of regulated rules (SRR). It is noted that conversion involves the process of bringing disparate SD in line with the new standards and classifications of SD. The processes of transforming disparate SD between coordinate systems and converting existing data sets relative to old and new classifiers have been formalized. It is established that verification and validation tools allow for detecting disaccord and forming the basis for further data ordering.

Keywords: Spatial data · Coordinate transformation · Converting · Validation

1 Introduction

At present, there is an increase in the complexity of infrastructure and the density of buildings for various purposes. Currently, there is a high need for proper registration of the legal status of spatial data (SD) in part of accounting for parcels and another real estate. Since 2007, the European Union standards for the development of SD infrastructure (INSPIRE) have been elaborated [1, 2].

Changes in the set of regulated rules (SRR) can be caused in particular by a process such as reforming the administrative and territorial structure of the country, which leads to a change in the addressing and subordination of objects and SD as a whole.

At the same time, until now, the interagency homogeneity of SD in existing thematic geoinformation systems (GIS) has not been achieved. There is a significant duplication

and conflict of information [3] in registers and systems both in paper and electronic form. Individual SD is still absent from regional information systems.

In departmental institutions related to regional resources in each of the countries over the past twenty years, a significant amount of SD has been accumulated. The processes of accumulation and presentation of such information took place in some cases without uniform technical regulations and methodological principles. Requirements for the structure, composition, and quality of SD were not coordinated. The data using the sundry classification systems and program-technological means were recorded.

Among decision-makers (DM) sufficiently differentiated information by the format of presentation is collected and updated. Thus, the existing state of regional resources is characterized by the following number of problems:

- mainly departmental principle of regional resources formation;
- significant duplication of project work among DM and users;
- lack of a unified system of national standards for SD products;
- lack of available metadata on the results of SD creation work;
- lack of organizational structure and network of GIS centers responsible for creating and supplying SD databases (DB) at the national, regional, and local levels [4–6].

Among DM in the subject area of SD, there are difficulties in using significant arrays of archival materials affiliated with to change of coordinate systems that are constantly being improved.

The analysis of these tasks indicates the need to improve the processes of formation and use of regional resources and the development of SD infrastructure.

Thus, at present, a basis for a concerted technological policy has been created regarding uniform methodological principles and technical regulations for the creation of SD under the new structure.

In recent years, work has intensified on the standardized digital form of presenting basic SD sets [7]. At present, significant archives of information have been formed, which are quantitatively and qualitatively differentiated. Such conditions today complicate the transition of enterprises and institutions to new standards of work. At the same time, it remains economically viable to use existing archival information. The issues of DB converting remain relevant [8].

Even with an identical visualization of SD database objects, attributive information differs significantly. Without proper reorganization of information, the use of archives in the new SD infrastructure is impossible.

It is necessary to automate the process of converting differentiated DB SD to the updated rules for the digital description of all instances of SD [7, 9]. To switch to European standards for maintaining an SD bank, it is necessary to ensure uniform requirements for the content of electronic documents about individual spatial objects.

2 The Main Conceptual Provisions on the Processes of Converting and Validating Spatial Data

A significant part of the attributive information in GIS requires determination in spatial coordinates. An unambiguous coordinate description of SD in a particular coordinate

system can be provided by transformation. Coordinate transformation is the determination of transition parameters as a result of constructing an interpolation or approximation function by reference (combined) points, the coordinates of which are specified in the input and output coordinate systems.

The algorithm for working with the transformation field and the accuracy of the definition of SD depends on the optimal dimensions of the side of the triangular finite element (as an element of the triangulation surface of space) and its area.

SD converting is the conversion of SD from one format to another while maintaining the basic logical and structural content of information. By converting way the conversion of disparate SD to new SD standards and classifications is provided. There is also a direct connection with the SRR.

In order for information systems to be viable, the data sets used in them need due checking [10]. It is necessary to provide for the converting of disparate archival SD for the possibility of further analysis and processing, that is, SD must meet the requirements of the existing SRR. In the process of converting differentiated SD sets into a single digital description space, some of the data may not be appropriate. Verification and validation tools allow you to mark various kinds of inconsistencies and determine the degree of adequacy of the data obtained after the conversion.

Verification is a checking process when converting SD archives, which is proof that the probable fact or statement is true. Validation is a procedure that gives a high degree of confidence that a particular process, method, or system will consistently lead to results that meet predetermined acceptability criteria. Validation as opposed to verification relies on SRR. The combination of the presented methods can ensure the acceptability of using archived sets of disparate SD to increase the efficiency and adaptability of national spatial data infrastructures (NSDI).

Detected inconsistencies in validation will prompt to look for the right additional methods and recovery solutions for missed data.

Summarizing the above processes of information interaction formation, we will present information technology that provides NSDI with valid SD and marks the missing data (see Fig. 1).

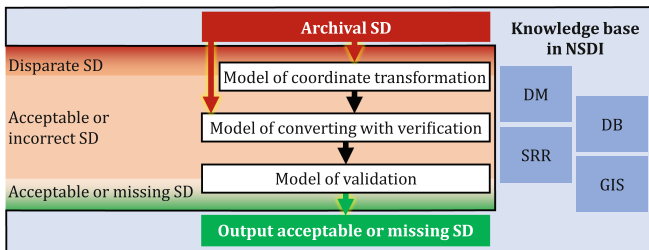


Fig. 1. SD converting and validation technology.

The main processes of data conversion are considered, based on which the formation technology of acceptable or missed information for SD infrastructure has been constructed.

3 Models of Converting Archived Spatial Data

3.1 General Formulation of the Problem

Suppose there is a set of disparate archival SD (I^D) in archived data sets (Ω^1) $I^D \subseteq \Omega^1$, which can represent part of the objects of the coordinate space $I^D = \{SD_i^D\}_{i=1,k}^-$, where k – total number of instances of disparate archive SD. Any object of the archive can be characterized by a tuple of parameters $\forall i, SD_i^D \rightarrow (G^A, \Theta)$, where: G^A – set of coordinates described in the old coordinate system $A = (X^A, Y^A, Z^A)$, which consists of the corresponding domains of coordinate axes X^A, Y^A, Z^A ; Θ – set of attribute parameters according to the old rules of digital data description, in which one or more attribute parameters reproduce a relationship with the geometry of an object.

Defined instances of the set I^D can: refer to a certain coordinate space and have a property g , which indicates membership to outdated coordinate systems; be described according to a specific digital classifier and have a property a , which concerns non-modern rules for the digital description of instances. Conceptually, these properties reflect the different scope and content of information about objects. This considered variability complicates the rapid application of such data.

In order to archive arrays of disparate SD (I^D) was processed along with another SD (I), where $I = \{SD_j\}_{j=1,n}^-$, n – total number of acceptable instances, it is necessary to provide an appropriate, that is, a single-valued digital description of the (Ω^2) $I \subseteq \Omega^2$. Converted SD (I) acquires the following properties: i – matching an instance of convertible and verified SD, q – membership to the modern coordinate system, b – presentation under the new rules for digital description of instances (see Fig. 2).

Note that a properly described object can be characterized by a tuple of parameters $\forall j, SD_j \rightarrow G^B, \Psi$, where: G^B – set of coordinates described in the new coordinate system $B = (X^B, Y^B, Z^B)$, which consists of the corresponding domains of coordinate axes X^B, Y^B, Z^B ; Ψ – set of attribute parameters according to the updated rules of digital data description.

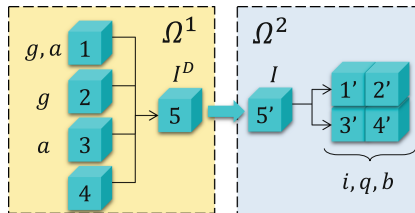


Fig. 2. Graphical representation of the model of converting archival SD to a single-valued coordinate and attributive space. Blocks: 1–4 – different SD variants, 1’-4’ – converting results, 5 and 5’ – generic SD sets according before and after conversion.

3.2 Geometric Component of SD Converting

In the converting model to SD geometry components, it is advisable to apply coordinate transformation based on affine transformation by finite elements [11, 12]. The process of affine transformation occurs over instances of the SD set by transforming from the old coordinate space A , which may include a basic coordinate system and number of derived systems that describe the geometry I^D , to the new coordinate space B , which meets the requirements of modern methods of positioning and the current SRR.

To solve the problems of ambiguous differences between outdated and modern descriptions of the coordinate space, it is necessary to design a transformation field into a limited area (administrative divisions, capacity of object, etc.) [12, 13]. Transformation field (analogue of National Transformation Version 2 (NTv2) [14, 15]) is a model of a limited area with vertices spatially defined in both coordinate systems, which ensures the transformation of coordinates (see Fig. 3).

With the help of set-theoretic approach in a single unified form, the process of affine transformation between coordinate systems is formalized. $A \tau_a B$, as a bijective reflection:

$$\text{transform} : G^A \rightarrow G^B, \quad (1)$$

where $G^A = \left\{ \left(x_g^A, y_g^A, z_g^A \right)_{g=1,p} \mid x_g^A \in R, y_g^A \in R, z_g^A \in R \right\}$ – set of coordinate (geometric) parameters in the coordinate system A , and $G^B = \left\{ \left(x_g^B, y_g^B, z_g^B \right)_{g=1,p} \mid x_g^B \in R, y_g^B \in R, z_g^B \in R \right\}$ – set of coordinate (geometric) parameters in the coordinate system B , where p – number of coordinate compositions, $\left(x_g^A, y_g^A, z_g^A \right) \tau_a \left(x_g^B, y_g^B, z_g^B \right)$ – geometric coordinates of the g -th coordinate compositions, accordingly, in two coordinate spaces.

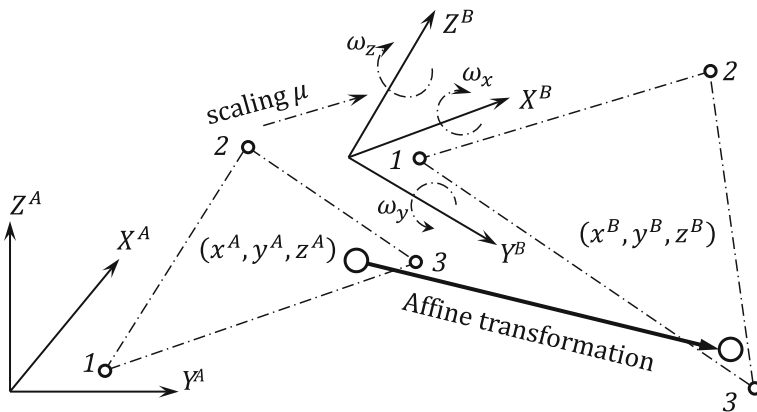


Fig. 3. Illustration of the transformation model: ω_x , ω_y , ω_z – angles of rotation around the corresponding coordinate axes X -abscissa, Y -ordinate and Z - applicate.

Affine transformation is recommended for cases where SD distortions are heterogeneous, that is, they have different character in its different areas. A given set of points is triangulated (is divided into finite triangular elements). The region given by each triangle is transformed by an affine transformation constructed by three reference points corresponding to the vertices of the triangle.

SD outside the triangular grid is transformed in the same way as the nearest triangle. In order for the boundaries to be erected when drawing up a mosaic coverage from individual fragments of SD, common reference points are provided at the boundaries of the fragments.

It is the conversion of the 1st order (affine) that allows you to limit yourself to three reference points, which from an economic and practical point of view is profitable. At the same time, it is worth to remember that affine transformation can compensate only for general distortions like displacement, rotation and stretching. That is, the affine transformation will be able to transform the parallelogram into a rectangle but will not be able to make a rectangle from a trapezoid of general appearance.

The size of the area that can be shown on the plan, without going beyond the specified accuracy on the plane is determined by the formula:

$$r = \sqrt{3 \cdot R^2 \cdot m_t}, \quad (2)$$

where R – radius of the terrestrial globe; m_t – the specified accuracy of the points of the reference network in map; r – radius of the circle within which the specified accuracy is ensured.

Allowable distance, taking into account the conditions of the formula (2), will be equal to the value of the $2r$. In other words, the diameter of such a circle can be considered as the largest value of the side of a finite triangular element. The maximum area at such an allowable distance is reached only in an equilateral triangle and it is founded on the formula:

$$S_{ET} = \frac{l^2 \cdot \sqrt{3}}{4}, \quad (3)$$

where l – side of an equilateral triangle. Replaced with value $2r$ and we get

$$S_{ET} = r^2 \cdot \sqrt{3}. \quad (4)$$

3.3 Converting of Spatial and Attributive Information

Unlike affine transformation, the process of converting spatial and attributive information seems somewhat more complicated. Conceptually, it should take place in such a sequence:

- open a working data set based on the old classifier;
- start the converting process using the developed tool;
- get a working map with a set of data based on a new classifier.

In general, in the converting model, the components of the SD description include the following sets: classes, their instances and attributes of instances. Thus, SD working sets $\Omega^1 = \{Xo, No, Po\}$ and $\Omega^2 = \{Yo, Mo, Qo\}$ formalized as three-dimensional arrays, where regions are represented by classes (Xo, Yo), rows – instances (No, Mo), columns – attributes (Po, Qo).

$$Xo = \{x_i^o\}_{i=1,\overline{c}}, Yo = \{y_j^o\}_{j=1,\overline{e}},$$

where x_i^o та y_j^o – instances of sets Xo and Yo accordingly; c – number of classes in the old classifier, e – number of classes in the new classifier;

$$No = \{n_k^o\}_{k=1,\overline{h}}, Mo = \{m_l^o\}_{l=1,\overline{u}},$$

where n_k^o та m_l^o – instances of sets No and Mo accordingly; h – number of instances (objects) in a working set Ω^1 , u – number of instances (objects) in a working set Ω^2 ;

$$Po = \{p_r^o\}_{r=1,\overline{v}}, Qo = \{q_t^o\}_{t=1,\overline{w}},$$

where p_r^o та q_t^o – instances of sets Po and Qo accordingly; v – number of attributes in the old classifier, w – number of attributes in the new classifier.

A single instance of a three-dimensional array looks as follows:

- element $p_{i,k,r}^o \in \Omega^1$ is an instance attribute $n_{i,k}^o \in No$ of class $x_i^o \in Xo$;
- element $q_{j,l,t}^o \in \Omega^2$ is an instance attribute $m_{j,l}^o \in Mo$ of class $y_j^o \in Yo$;
- if $n_k^o \notin x_i^o$ ($m_l^o \notin y_j^o$), then $n_{i,k}^o \in \emptyset$ ($m_{j,l}^o \in \emptyset$);
- if $p_r^o \notin n_k^o$ ($q_t^o \notin m_l^o$), then $p_{i,k,r}^o \in \emptyset$ ($q_{j,l,t}^o \in \emptyset$).

Conversion of archival information is carried out through a set of functional rules (F) according SRR [7, 16] and formalized as a surjection reflection for classes $e \leq c$, bijective – for instances (objects) $u = h$, injection – for attributes $w \geq v$ (see Fig. 4).

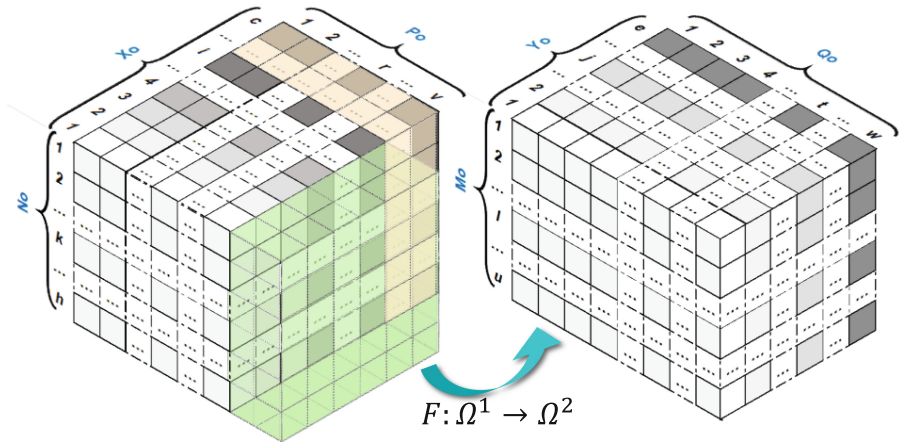


Fig. 4. Model of SD converting.

Each class has its own combination of attributes, but their total number in the classifier is static. Provided that each class consists of all possible attributes of the classifier, the non-essential and unrelated attributes will simply remain empty [7].

If a single instance of the model $n_{i,k}^o$ describe through its attributes $n_{i,k}^o = \{p_r^o\}_{r=\overline{1,v}}$, then all classes of the model can be represented through the entire set of attributes of related instances as follows:

$$X^o = \left\{ \left\{ \left\{ p_r^o \right\}_k \right\}_i \right\}_{i=\overline{1,c}, k=\overline{1,h}, r=\overline{1,v}},$$

similarly for a set of Ω^2 .

$$Y^o = \left\{ \left\{ \left\{ q_t^o \right\}_l \right\}_j \right\}_{j=\overline{1,e}, l=\overline{1,u}, t=\overline{1,w}}.$$

During converting conversion of digital description of vectorial data must pass through a set of functional rules (F) [7, 16] when converting. These rules are functions of dependency of individual attributes of the set Ω^2 from one or more attributes Ω^1 :

$$q_{j,l,t}^o = f_{j,l,t} \{ p_{i,k,1}^o, p_{i,k,2}^o, \dots, p_{i,k,r}^o, \dots, p_{i,k,v}^o \},$$

or, unifying the description of variables to the general form, receive:

$$q_{j,l,t}^o = f_{j,l,t} \{ Xo, No, Po \}. \quad (5)$$

Rules F enable verification of all convertible data sets. Expression through the specified functions of all components of the working set Ω^2 forms the core of the conversion process (see Fig. 4).

To check the model of converting to adequacy in the work, an approach to validation of convertible data is proposed.

3.4 Adequacy of Converting Results and Validation

Converting and validation involve the process of bringing a disparate I^D following the current SRR, that is, new standards and classifications of SD.

According to the semantic context, information about the object should be presented without significant differences. The same cannot be said for the naming, typing and encoding of all data of the same spatial object in two (or more) structures for representing the old classification. Direct transition an array of attribute values without losing or distorting data is not possible [7, 8].

Ordering of SD will allow to fill DB with homogeneous arrays of archival materials, which will give a significant positive result in the implementation of the NSDI.

Checking for the adequacy of any data array converting results is an important step in filling DB. At paper [17] introduces approaches that allow DM and GIS users to mark missed information in large SD arrays. Checking different data sets for correctness forms its criteria according to SRR and displays the result in a text format document.

At work [18] the validation process is used to detect and correct errors in the file system. The application discussed in this study checks and detects errors among system parameters and saves the test results to CSV files.

Checking methods play an important role in identifying possible errors or inconsistencies. Thus, in [19] validation with the appropriate criterion of requirements is considered as a heterogeneous process based on use of various independent methods.

To ensure the validation process, it needs to perform the following tasks:

- to analyze the value I ;
- to form a number of checking rules;
- to realize the validation process and get the result of the checking in the reporting form as marking of the missed SD in DB (I^M).

Since validation is used in different areas, it is used in different ways depending on the data constraints for checking.

Symbol-by-symbol checking. Such verification is performed in the user interface provided and can serve as a lexical analysis of the compiler to detect inadmissible characters, so it is also called “lexical”.

Verification of separate values. This checking is set in a separate field and is performed during data entry and after entering when the field loses focus. Such verifications by analogy with compiler terminology are called “syntactic”.

Set of input values. Checking occurs after the program has received data. During this validation, so-called “semantic” verification is performed, aimed not only at individual values but also at the relationships between them.

System status check after data processing. This method is used when the verification of input data cannot be performed, that is, the data are processed with the ability to return everything to its original state. Such verification is often called “transactional”.

So, validation is proof that the process works as it should. The above method of checking the state of the system after data processing is completely subject to the tasks of this study.

As a result of validation among the entire volume of SD (I) according to the developed verification rules, it can be determined the SD set (I^V), which is valid in relation to the SRR, and the marked set SD (I^M), containing data of varying degrees of inconsistency. Characteristic property for I^V is v , which corresponds to valid instances of SD. Characteristic property for I^M is m , which characterizes inappropriate (missed) SD. These sets have a common property $z \in RSR$, which determines the regulatory compliance of SD instances. Taking into account the results of the converting, the possible results of the validation process are formalized: $I^M \in \Omega^2, I^M = \{1'', 2'', \dots\}$ – marked SD instances that do not match SRR, $I^V \in \Omega^2, I^V = \{3'', 4'', \dots\}$ – valid SD instances, i.e. corresponding to SRR (see Fig. 5).

Verification and validation tools allow to mark inconsistencies and serve as reliable auxiliary tools for further tasks of unsealing such data in the process of information interaction. This prompts the development of additional deployment methods of the NSDI, which should provide for the reproduction of missing data.

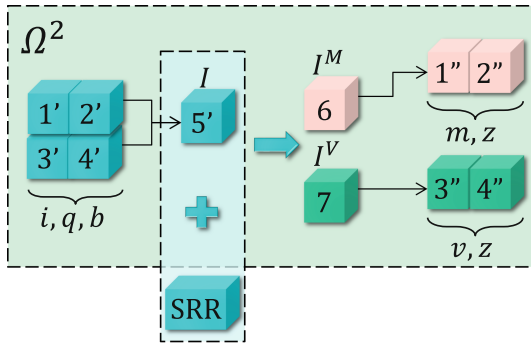


Fig. 5. SD validation process according to SRR requirements. Blocks: 1'–4' – converting results with verification; 5' – sets of SD after conversion; 6 – set of omitted SD; 7 – set of valid SD; 1'', 2'' – instances of SD that do not correspond to SRR; 3'', 4'' – valid instances of SD.

4 Conclusion

Thus, an affine transformation is recommended for cases where geometric distortions of SD are heterogeneous. It is noted that the converting provides the process of putting the disparate SD in order with the new standards and classifications of SD. A new structure of information interaction is proposed due to models of disparate SD transformation between coordinate systems and converting of existing data sets relative to old and new classifiers. It is established that verification and validation tools allow to detect inconsistencies and to form the basis for further ordering of data.





References

1. Baumann, P., Escriu, J.: INSPIRE coverages: an analysis and some suggestions. *Open Geospatial Data, Software and Standards* **4**(1), 1–22 (2019). <https://doi.org/10.1186/s40965-019-0059-x>
2. Feng, M.: Geodata for everyone - model-driven development and an example of INSPIRE WFS service. *Open Geospatial Data, Software and Standards* **1**(1), 1–8 (2016). <https://doi.org/10.1186/s40965-016-0007-y>
3. Ali, A., Emran, N.A., Asmai, S.A.: Missing values compensation in duplicates detection using hot deck method. *Journal of Big Data* **8**(1), 1–19 (2021). <https://doi.org/10.1186/s40537-021-00502-1>
4. Abdolmajidi, E., Harrie, L., Mansourian, A.: The stock-flow model of spatial data infrastructure development refined by fuzzy logic. *Springerplus* **5**(1), 1–20 (2016). <https://doi.org/10.1186/s40064-016-1922-1>
5. Karabegovic, A., Ponjavic, M., Ferhatbegovic, E., Karabegovic, E.: Spatial data and processes integration in local governance of Bosnia and Herzegovina. In: 2018 41st International Convention on Information and Communication Technology, Electronics and Microelectronics (MIPRO), pp. 1298–1303. IEEE, Opatija (2018). <https://doi.org/10.23919/MIPRO.2018.8400235>
6. Idriži, B.: General conditions of spatial data infrastructure. *Int. J. Natu. Eng. Sci.* **12**(1), 57–62 (2018)

7. Zarytskyi, O.V., Kostenko, O.B., Bulaienko, M.V.: Automation of geospatial objects converting into the classifiers according to the European data standards. *Mathematical Modeling and Computing* **7**(2), 228–238 (2020). <https://doi.org/10.23939/mmc2020.02.228>
8. Ouanouki, R., April, A., Abran, A., Gomez, A., Desharnais, J.M.: Toward building RDB to HBase conversion rules. *Journal of Big Data* **4**(1), 1–21 (2017). <https://doi.org/10.1186/s40537-017-0071-x>
9. Zarytskyi, O., Bulaienko, M.: Development of algorithms for the geospatial array visualization module data in xml format. *Municipal Economy of Cities* **6**(166), 8–14 (2021). <https://doi.org/10.33042/2522-1809-2021-6-166-8-14> [in Ukrainian]
10. Rizk, R., McKeever, S., Petrini, J., Zeitler, E.: Diftong: a tool for validating big data workflows. *Journal of Big Data* **6**(1), 1–27 (2019). <https://doi.org/10.1186/s40537-019-0204-5>
11. Klein, F.: Affine transformations. In: *Elementary Mathematics from a Higher Standpoint*, pp. 83–100. Springer, Berlin, Heidelberg (2016). https://doi.org/10.1007/978-3-662-49445-5_7
12. Kucher, O.V., Kurylyak, I.S., Staroverov, V.S., Koshelyuk, N.I.: Study of the method transforming existing geodesic, topographic-cartographic and cadastre materials to the USK-2000 coordinate system. *Engineering Geodesy* **64**, 28–44 (2017). <https://repository.knuba.edu.ua/handle/987654321/2363> [in Ukrainian]
13. Chub, I.A., Novozhylova, M.V.: Determination of descent direction in linearized problem of non-oriented geometric objects arrangement. *Radio Electronics, Computer Science, Control* **2**, 263–270 (2010). <https://doi.org/10.15588/1607-3274-2010-2-17>
14. Markič, Š., Donaubaauer, A., Borrmann, A.: Enabling geodetic coordinate reference systems in building information modeling for infrastructure. In: *Proceeding of the 17th International Conference on Computing in Civil and Building Engineering*, pp. 5–7. Tampere, Finland (2018)
15. Nicolau, R., et al.: Harmonization of categorical maps by alignment processes and thematic consistency analysis. *AIMS Geosciences* **6**(4), 473–490 (2020). <https://doi.org/10.3934/geo-sci.2020026>
16. Baumann, P., Misev, D., Merticariu, V., Huu, B.P.: Array databases: concepts, standards, implementations. *Journal of Big Data* **8**(1), 1–61 (2021). <https://doi.org/10.1186/s40537-020-00399-2>
17. Zarytskyi, O.V., Kostenko, O.B., Bulaienko, M.V., Manakov, V.P.: Marking of incomplete spatially distributed information using validation. *Bionics of Intelligence* **1**(94), 100–106 (2020). [https://doi.org/10.30837/bi.2020.1\(94\).15](https://doi.org/10.30837/bi.2020.1(94).15) [in Ukrainian]
18. Abba, A.H., Hassan, M.: Design and implementation of a CSV validation system. In: *Proceedings of the 3rd International Conference on Applications in Information Technology (ICAIT'2018)*, pp. 111–116. ACM, New York (2018). <https://doi.org/10.1145/3274856.3274879>
19. Maalem, S., Zarour, N.: Challenge of validation in requirements engineering. *Journal of Innovation in Digital Ecosystems* **3**(1), 15–21 (2016). <https://doi.org/10.1016/j.jides.2016.05.001>



Using Optimization to Construct Naturally Parametrized Curve with Cubic Curvature

Olha Khomiak¹ , Petro Stetsyuk¹ , Volodymyr Zhydkov¹ ,
and Luis Infante² 

¹ V.M. Glushkov Institute of Cybernetics of the NAS of Ukraine, 40 Academician Glushkov Avenue, Kyiv 03187, Ukraine

khomiak.olha@gmail.com, stetsyuk@incyb.kiev.ua

² Nuevo Leon State University, 66455 Monterrey, Nuevo Leon, Mexico

Abstract. The article describes a mathematical model and an algorithm to construct a curve passing through two given points and having given tangent angles and curvature values. The conditions imposed on the curve are formulated by four nonlinear integral equations with respect to four unknown variables. Finding a solution of this system of equations is reduced to a non-smooth optimization problem solved by a modification of r -algorithm. Computational results are presented for a corresponding problem in aerodynamics.

Keywords: Natural parameterization · Cubic curvature · r -Algorithm · Nonsmooth optimization

1 Introduction

Naturally parameterized smooth curves are used widely in practice where it is desirable to describe flow, smooth trajectory [1], path or shapes derived from thereof. The derived shapes are, for example, aerodynamic and hydrodynamics cowls, nozzles, wings, propellers and turbine blades.

Usually, there are used simpler curves, like Bezier [2], B-splines [3], because they are much more easily implemented and calculable for the purposes of machine graphics. Also, there often used compound curves, like [4], for piecewise approximation; also, adaptive type curve building used [5, 6], and overall there are many physically based methods to choose correct curve parametrization approach for given case [7–11]. However, most of them have a flaw of being not “fully” smooth (stepwise second or further derivatives etc.). While it generally does not matter for CAM, for manufacturing errors usually much more than errors of curve approximation, it matters for design, calculation and simulation, where insufficient non-smoothness may throw off most methods.

Design works often require quick approximate methods for deriving a nozzle contour with high functioning parameters. This additionally constraints geometric contour properties, which could be provided by applied geometry methods, geometric modelling of 2D curves in particular [12]. These methods utilize natural parametrization algorithm methods [13, 14] and curvature distribution functions for providing contour

geometric properties which in turn must satisfy gasodynamic requirements. Also, naturally parametrized curves like that are useful in other areas, like load calculation [15]. Curves in natural parametrization are actively used in Mykolaiv school works of applied geometry [16, 17]. Using curvature constraints and input is effective while designing turbine blade profiles [17], as well as designing nozzle profiles [18]. Let's note, that for naturally parametrized curves, using linear or quadratic curvature distribution law, you can avoid "waviness" of curvature, which can appear in cases of building 2D curves by widely known Bezier-Bernshtein method [20].

In the paper we suggest building shapes on the basis of a curve with polinomially varied curvature, which is void of deficiencies listed above. Practical application of such curves is hampered by lack of proper math and software tools, which our work is intended to correct. The material is presented in five sections. Section 2 presents the geometric formulation of the problem of constructing a curve in natural parameterization with a cubic curvature and considers the corresponding system of non-linear integral equations (SNIR). Section 3 presents the optimization problem for finding the SNIR solution and the method for its solution using a modification of Shor's r -algorithm [20]. Section 4 describes the application of the developed program for the construction of S-shaped fragments of the outer contour of the nozzle and the method of approximation (smoothing) of the contour of the central body.

2 Problem Formulation

2.1 Geometric Model of the Problem

The problem (see Fig. 1) is as follows. You need to connect the points $A(x_A, y_A)$ and $B(x_B, y_B)$ by two-dimensional curve in natural parameterization using cubic law of curvature distribution (the curve is determined by the length S , where the curvature $k(s) = as^3 + bs^2 + cs + d$ has a cubic dependence on the length of the curve) so that at the points A and B the given values of tangent angles φ_A, φ_B and curvature values k_A, k_B were achieved. The angles φ_A and φ_B are measured in radians.

For the curve $x(s), y(s), s > 0$ in natural parameterization the value of tangent angle $\varphi(s)$ at the point $(x(s), y(s))$ is defined by the formula

$$\varphi(s) = \varphi(0) + \int_0^s k(s)ds = \varphi(0) + \frac{as^4}{4} + \frac{bs^3}{3} + \frac{cs^2}{2} + d \times s, \quad (1)$$

and the coordinates $x(s)$ та $y(s)$ by formulas

$$x(s) = x(0) + \int_0^s \cos \varphi(s)ds, \quad y(s) = y(0) + \int_0^s \sin \varphi(s)ds. \quad (2)$$

Here the curvature $k(s) = as^3 + bs^2 + cs + d$ is given as a cubic function from the curve length s , where a, b, c, d are the given coefficients.

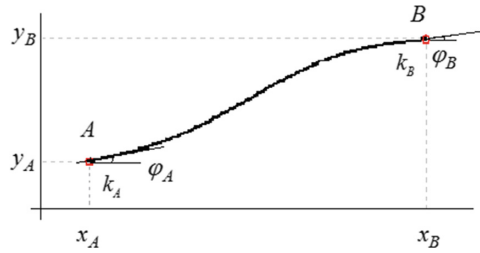


Fig. 1. Initial data for the geometric model of the problem.

2.2 The System of Nonlinear Integral Equations

Let S be the curve length from the point (x_A, y_A) to the point (x_B, y_B) . The system of four nonlinear equations and one linear equation corresponds to finding the parameters of curvature a, b, c, d and length S :

$$x_B = x_A + \int_0^S \cos\left(\varphi_A + \frac{as^4}{4} + \frac{bs^3}{3} + \frac{cs^2}{2} + d \times s\right) ds, \tag{3}$$

$$y_B = y_A + \int_0^S \sin\left(\varphi_A + \frac{as^4}{4} + \frac{bs^3}{3} + \frac{cs^2}{2} + d \times s\right) ds, \tag{4}$$

$$\varphi_B = \varphi_A + \frac{aS^4}{4} + \frac{bS^3}{3} + \frac{cS^2}{2} + d \times S, \tag{5}$$

$$k_A = d, \quad k_B = aS^3 + bS^2 + cS + d. \tag{6}$$

The system (3)–(6) has five unknowns: a, b, c, d – four coefficients of the quadratic function, S – the total length of the curve. The system includes four nonlinear equations, among which Eqs. (3) and (4) are integral and depend on the unknown parameters of the subintegral functions and the unknown upper limit for the definite integral.

Integral Eqs. (3) and (4) connect the coordinates of the points $A(x_A, y_A)$ and $B(x_B, y_B)$ by formulas (2). Nonlinear Eq. (3) is the equation for the angle φ_B at the point B , which according to formula (1) is determined by the given angle φ_A at the point A . Two Eqs. (6), the first of which is linear, define the conditions for curves $k_A = k(0)$ and $k_B = k(S)$ accordingly at the points A and B .

From the linear equation in (6) follows $d^* = k_A$, therefore, system (3)–(6) can be substituted by the system of four nonlinear equations with four unknowns a, b, c, S . To find solutions of this system, let's consider a method based on the modification of the r -algorithm [21, 22] for solving the problem of minimizing the non-smooth function (sum of modules of residual of Eqs. (3)–(6)) subject to constraint for the length S to ensure its positive feasible value.

3 Optimization Problem and Algorithm for Its Solution

3.1 Optimization Problem

Let's consider the conditional problem of minimizing sum of modules of residual functions for Eqs. (3)–(6), which has the form [23], find

$$f^* = f(a^*, b^*, c^*, S^*) = \min_{a,b,c,S} \left\{ f(a, b, c, S) = \sum_{i=1}^4 |f_i(a, b, c, S)| \right\} \quad (7)$$

subject to

$$S_{\min} \leq S \leq S_{\max}, \quad (8)$$

$$-\frac{\pi}{2} \leq \varphi_A + a \frac{i^4 S^4}{4N^4} + b \frac{i^3 S^3}{3N^3} + c \frac{i^2 S^2}{2N^2} + k_A \frac{iS}{N} \leq \frac{\pi}{2}, \quad i = 1, \dots, N, \quad (9)$$

where the residuals for Eqs. (3)–(6) are given by the following functions

$$f_1(a, b, c, S) = x_B - x_A - \int_0^S \cos\left(\varphi_A + \frac{as^4}{4} + \frac{bs^3}{3} + \frac{cs^2}{2} + k_A s\right) ds, \quad (10)$$

$$f_2(a, b, c, S) = y_B - y_A - \int_0^S \sin\left(\varphi_A + \frac{as^4}{4} + \frac{bs^3}{3} + \frac{cs^2}{2} + k_A s\right) ds, \quad (11)$$

$$f_3(a, b, c, S) = \varphi_B - \varphi_A - \frac{aS^4}{4} - \frac{bS^3}{3} - \frac{cS^2}{2} - k_A S, \quad (12)$$

$$f_4(a, b, c, s_p) = k_B - aS^3 - bS^2 - cS - k_A, \quad (13)$$

N is the number of equal subintervals on the interval $[0, S]$ for discretization of the function $\varphi(s) = \varphi_A + \frac{as^4}{4} + \frac{bs^3}{3} + \frac{cs^2}{2} + k_A s$, $s \in [0, S]$.

Here, the objective function (7) is non-smooth and means minimizing the sum of the modules of functions (10)–(13) – residual functions for Eqs. (3)–(6). Constraints (8) guarantee positive values for the length S , which is the upper limit for certain integrals in the residual functions (10) and (11). Here $S_{\min} = \sqrt{(x_B - x_A)^2 + (y_B - y_A)^2}$ – minimum distance between points (x_A, y_A) and (x_B, y_B) , $S_{\max} > S_{\min}$ – parameter to control the upper limit on S – the total length of the curve.

Constraint (9) ensures the existence of the unique global minimum for problem (7)–(9). It uses the complement of problem (7)–(8) by a discrete analogue of the continuous constraint

$$-\frac{\pi}{2} \leq \varphi(s) = \varphi_A + \frac{as^4}{4} + \frac{bs^3}{3} + \frac{cs^2}{2} + k_A s \leq \frac{\pi}{2}, \quad s \in [0, S]. \quad (14)$$

Constraint (14) means that the angles of inclination of the tangents at any point of the curve do not exceed the specified range $\varphi(s) \in [-\pi/2, \pi/2]$, that is, the function $y(x)$ on the interval $[x_A, x_B]$ is uniquely defined. If $S_{\max} \geq S^*$, then the problem (7)–(9) has

a unique point of the global minimum, which coincides with the solution of the system (3)–(6) with the smallest total length of the curve.

If finding the local minimum for problem (7)–(9) results in $f^* = 0$, then the global minimum point is found $(a^*, b^*, c^*, S^*)^T$, components of which together with $d^* = k_A$ are solution of the system (3)–(6). If we obtain $f^* > 0$, then the point $(a^*, b^*, c^*, d^* = k_A, S^*)^T$ is not solution of the system (3)–(6).

3.2 Algorithm for Solving the Optimization Problem

Problem (7)–(9) is a problem of minimization of non-smooth function, which is defined not for all values, but only for those that are positive and allow to calculate definite integrals for functions $f_1(a, b, c, S)$ and $f_2(a, b, c, S)$. To find the point of the global minimum in the problem (7)–(9) a modification of the r -algorithm [21] can be used, which takes into account this feature of the problem. At the point where the generalized gradient of the objective function is undefined, the modification of the r -algorithm uses the generalized gradient to one of the violated constraints (8) and (9).

We give the formulas for calculating the generalized gradient of the objective function (7). Let the vector $g_f = (\partial f / \partial a, \partial f / \partial b, \partial f / \partial c, \partial f / \partial S)^T$ be generalized gradient of the objective function $f(a, b, c, S) = \sum_{i=1}^4 |f_i(a, b, c, S)|$. The components of the generalized gradient are calculated by the formulas:

$$\begin{aligned} \frac{\partial f}{\partial a} &= \sum_{i=1}^4 \text{sign}(f_i) \frac{\partial f_i}{\partial a}, & \frac{\partial f}{\partial b} &= \sum_{i=1}^4 \text{sign}(f_i) \frac{\partial f_i}{\partial b}, \\ \frac{\partial f}{\partial c} &= \sum_{i=1}^4 \text{sign}(f_i) \frac{\partial f_i}{\partial c}, & \frac{\partial f}{\partial S} &= \sum_{i=1}^4 \text{sign}(f_i) \frac{\partial f_i}{\partial S}, \end{aligned} \quad (15)$$

where

$$\frac{\partial f_1}{\partial a} = + \int_0^S \frac{s^4}{4} \sin\left(\varphi_A + \frac{as^4}{4} + \frac{bs^3}{3} + \frac{cs^2}{2} + k_A s\right) ds, \quad \frac{\partial f_3}{\partial a} = -\frac{S^4}{4}, \quad (16)$$

$$\frac{\partial f_2}{\partial a} = - \int_0^S \frac{s^4}{4} \cos\left(\varphi_A + \frac{as^4}{4} + \frac{bs^3}{3} + \frac{cs^2}{2} + k_A s\right) ds, \quad \frac{\partial f_4}{\partial a} = -S^3,$$

$$\frac{\partial f_1}{\partial b} = + \int_0^S \frac{s^3}{3} \sin\left(\varphi_A + \frac{as^4}{4} + \frac{bs^3}{3} + \frac{cs^2}{2} + k_A s\right) ds, \quad \frac{\partial f_3}{\partial b} = -\frac{S^3}{3}, \quad (17)$$

$$\frac{\partial f_2}{\partial b} = - \int_0^S \frac{s^3}{3} \cos\left(\varphi_A + \frac{as^4}{4} + \frac{bs^3}{3} + \frac{cs^2}{2} + k_A s\right) ds, \quad \frac{\partial f_4}{\partial b} = -S^2,$$

$$\frac{\partial f_1}{\partial c} = + \int_0^S \frac{s^2}{2} \sin\left(\varphi_A + \frac{as^4}{4} + \frac{bs^3}{3} + \frac{cs^2}{2} + k_A s\right) ds, \quad \frac{\partial f_3}{\partial c} = -\frac{S^2}{2}, \quad (18)$$

$$\frac{\partial f_2}{\partial c} = - \int_0^S \frac{s^2}{2} \cos\left(\varphi_A + \frac{as^4}{4} + \frac{bs^3}{3} + \frac{cs^2}{2} + k_A s\right) ds, \quad \frac{\partial f_4}{\partial c} = -S,$$

$$\begin{aligned}\frac{\partial f_1}{\partial S} &= -\cos\left(\varphi_A + \frac{aS^4}{4} + \frac{bS^3}{3} + \frac{cS^2}{2} + k_AS\right), \quad \frac{\partial f_3}{\partial S} = -aS^3 - bS^2 - cS - k_A, \\ \frac{\partial f_2}{\partial S} &= -\sin\left(\varphi_A + \frac{aS^4}{4} + \frac{bS^3}{3} + \frac{cS^2}{2} + k_AS\right), \quad \frac{\partial f_4}{\partial a} = -3S^2 - 2S - c.\end{aligned}\tag{19}$$

In the modification of r -algorithm at the point where the generalized gradient of the objective function is undefined, it is substituted by a generalized gradient to one of the violated two-side constraints (8) or (9). Four violated constraints $g_i(\circ) \leq 0$, $i = 1, \dots, 4$ are used for this purpose, which are selected in the order: $g_1(S) = S_{\min} - S$, $g_2(S) = S - S_{\max}$ – for two-side constraints (8),

$$\begin{aligned}g_5(a, b, c, S) &= \max_{i=1}^N \left\{ -\frac{\pi}{2} - \varphi_A - a\frac{i^4 S^4}{4N^4} - b\frac{i^3 S^3}{3N^3} - c\frac{i^2 S^2}{2N^2} - k_A\frac{iS}{N} \right\}, \\ g_4(a, b, c, S) &= \max_{i=1}^N \left\{ \varphi_A + a\frac{i^4 S^4}{4N^4} + b\frac{i^3 S^3}{3N^3} + c\frac{i^2 S^2}{2N^2} + k_A\frac{iS}{N} - \frac{\pi}{2} \right\}\end{aligned}$$

– for two-side constraints (9). If constraints (8), (9) are satisfied, then a generalized gradient of the objective function (7) is used, which is calculated by Eqs. (15)–(19).

The algorithm for solving problem (7)–(9) is implemented in Octave language using the octave function **ralgb5a**. It either finds the global minimum of the objective non-smooth function, or signals that the system of constraints (8)–(9) is incompatible. This may be the case in the absence of a solution in system (3)–(6) under constraints (8), (9), and in the case where the algorithm stops at a "suboptimal" point, given that for large values of the parameter S_{\max} the problem (7)–(8), which does not take into account the constraints (9), is multi-extremal.

The generalized gradients of the objective function (7) are calculated by formulas (15)–(19), and the definite integrals, both in formulas (10), (11) and in formulas (16), (17), (18) for the components of generalized gradients, calculated by the trapezoidal rule. So, for example, in formula (10) the definite integral is calculated by the formula

$$\begin{aligned}\int_0^S \cos(\varphi(s))ds &\approx \left(\frac{\cos \varphi(0) - \cos \varphi(S)}{2} + \sum_{i=1}^N \cos(\varphi(s_i)) \right) h = \\ &= \left(\frac{\cos \varphi(0) + \cos \varphi(S)}{2} + \sum_{i=1}^{N-1} \cos(\varphi(s_i)) \right) h,\end{aligned}$$

where $h = S/N$, N is the number of subintervals on the interval $s \in [0, S]$, for discretization of the function $\cos(\varphi(s)) = \cos(\varphi_A + as^4/4 + bs^3/3 + cs^2/2 + k_A s)$, and the definite integral from (16) is calculated by the formula

$$\begin{aligned}\int_0^S \frac{s^4}{4} \sin(\varphi(s))ds &= \left(-\frac{S^4}{4} \sin(\varphi(S)) + \sum_{i=1}^N \frac{s_i^4}{4} \sin(\varphi(s_i)) \right) h = \\ &= \left(\frac{S^4}{4} \sin(\varphi(S)) + \sum_{i=1}^{N-1} \frac{s_i^4}{4} \sin(\varphi(s_i)) \right) h.\end{aligned}$$

4 Computational Results

Using various boundary conditions at interval ends in problem (7)–(9), it is possible to build various S-like curves (having one inflection point) by given curvature plot. Varying inflection point position within interval it is possible to model various external contours of aerodynamic nozzles (Laval, Frankl, Stanton). The method can be used for profiling compressor turbine blades by defining skeletal profile (principal airfoil cross-sections) line using S-like curve.

Algorithm for (7)–(9) problem solution is tested on several problems of building external contours of Laval nozzle fragments. Figure 2 illustrates overall look of external contour nozzle fragment in supersonic area for various k_1 values, scaled to fit.

Comparison of two solutions for (3)–(6) for $x_1 = y_1 = 0$, $x_2 = 2$, $y_2 = 1$, $\varphi_1 = \varphi_2 = 0$, $k_2 = 0$ and two values $k_1 = 0$ and $k_1 = 2$, that correspond to S-like curves, is represented on Fig. 3. On the figure the curves are in solid and dotted lines (top left), plots for tangent angles (top right), plots for curvature and its derivative (bottom). From the curvature plots it can clearly be seen that both curves are S-like, for they have a single inflection point, matching to zero curvature.

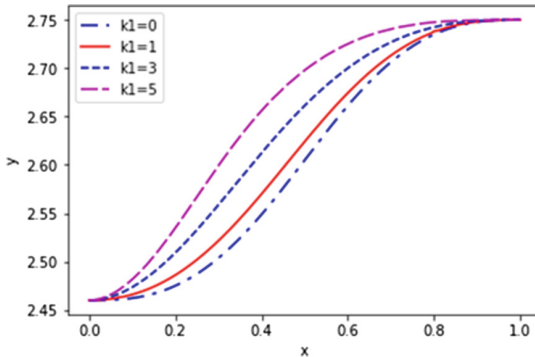


Fig. 2. Fragments of the outer contour of the nozzle for different k_1

Algorithm for (7)–(9) problem solution was used in approximation (smoothing) method for center body contour, which consists in representing two of its intervals using S-like curves, where first curve models subsonic part of central nozzle and second part models supersonic part of the central nozzle. Each of the S-like curves is a flat one with cubic law of curve distribution by natural parametrization. It is obtained either as a result of minimizing sum of squares of distances from curve to the given set of contour points (least square method), or as a result of minimizing sum of distances from curve to the given set of contour points (least modulo method).

Unlike other smoothing methods, including smoothing methods using spline-functions, the presented method guarantees smooth change in contour curvature, provided by natural parametrization with cubic law of curvature distribution. Let's present results of the approximation method, using example of the point-defined contour, setting derivatives at end points as zero (see Table 1).

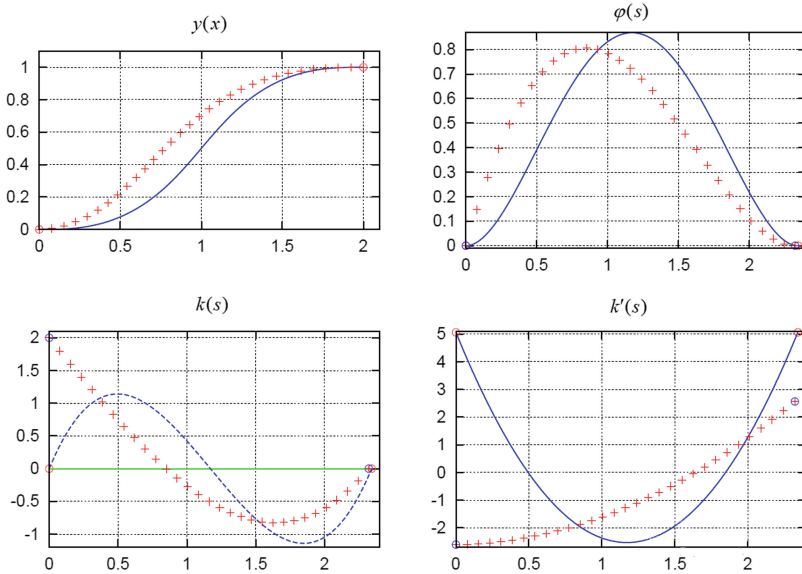


Fig. 3. Two S-curves for the system (3)–(6): $k_1 = 0$ and $k_1 = 2$

Table 1. Point-defined contour, which includes 14 points.

i	x_i	y_i	i	x_i	y_i
1	-216.680000	78.840891	8	-93.151429	150.726455
2	-199.388394	82.662538	9	-81.003369	156.694929
3	-182.333640	92.146215	10	-64.809795	162.158593
4	-170.482179	102.580692	11	-48.383973	166.193093
5	-147.849809	117.679087	12	-31.324910	168.943913
6	-120.476549	134.114910	13	-14.712846	170.439555
7	-93.151429	140.646664	14	0.000000	170.830030

Using the least modulo method optimal values of curvature at border points of contour fragments, which are found accurate to the curvature intervals discretization, there is a curvature $k_1 = 2.42103$ in leftmost point of the fragment, and there is a curvature $k_2 = -0.52632$ in rightmost fragment point. They correspond to approximating flat curve illustrated on Fig. 4. It can be easily seen from Fig. 4 plots that all 14 points are approximated quite well with obtained S-like curve.

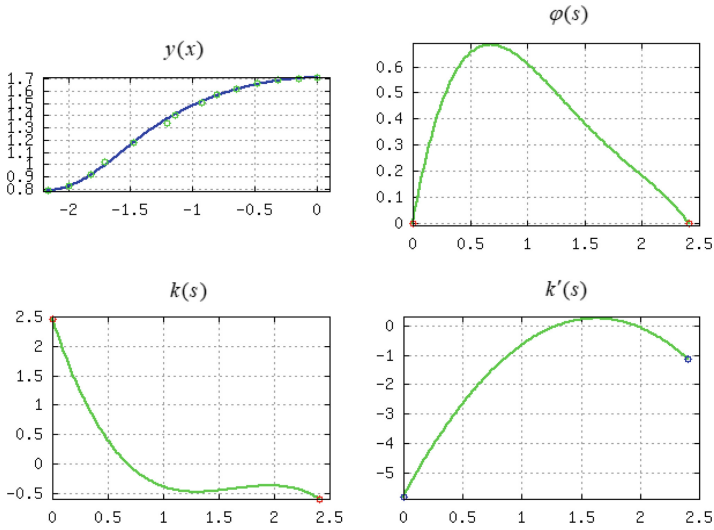


Fig. 4. Approximating curve with cubic curvature distribution law

5 Conclusion

The method developed in the paper, which includes a mathematical model and algorithm, can be used to profile transition channels of variable cross-section with the required geometric properties (along with the Bezier-Bernstein method). This method can be used to profile the compressor blades by specifying the skeletal line of the profile using an S-shaped curve. It can be used to design S-shaped fragments of the outer contour of the nozzle and the contour of the central body. The choice of curve values and allows to control the shape of the curve in such a way that at the base (reference) points the characteristics of the curve correspond to the specified characteristics of the projected profile.

Suggested approach for S-like contour building can be used to develop a geometric model of building external and internal contours of nozzle with central body. Such nozzle design is one of actual problems for increasing parameters of modern aviation engines, namely thrust and energy characteristics for given constraints on dimension and mass of the nozzle [24]. Developed mathematical model, algorithm and, in future, software could be used for profiling fragments of nozzles and bypasses of jet engines [25]. Alongside Bezier-Bernstein, suggested method can be used for building bypass channel profiles of variable cross-section with necessary geometry properties. For example, using the method can model profile fragments that can be presented as convex (concave), monotonously rising and falling. Choice of curvature values can guide curve shape in such a way to set necessary designed profile parameters at reference points.

Further developments shall include advanced constraints, like limits on maximum curvature, limits on monotonicity of curvature distribution; also, less computationally intensive estimation algorithms are desired. Well developed, this can be excellent addition in CAD toolbox, as well as other specialized cases.

Acknowledgement. The authors would like to thank Oleksii Lykhovyd for his help in preparing this paper.

References

1. Kombarov, V., Sorokin, V., Tsegelnyk, Y., Plankovskyy, S., Aksonov, Y., Fojtů, O.: S-Shape Feedrate Scheduling Method with Smoothly-Limited Jerk in Cyber-Physical Systems. In: Cioboată, D.D. (ed.) ICORSE 2021. LNNS, vol. 305, pp. 54–68. Springer, Cham (2022). https://doi.org/10.1007/978-3-030-83368-8_6
2. Shikhar Jaiswal, A.: Shape Parameterization of Airfoil Shapes Using Bezier Curves. In: Bajpai, R.P., Chandrasekhar, U. (eds.) Innovative Design and Development Practices in Aerospace and Automotive Engineering. LNME, pp. 79–85. Springer, Singapore (2017). https://doi.org/10.1007/978-981-10-1771-1_13
3. Han, S., Lee, Y.S., Choi, Y.B.: Hydrodynamic hull form optimization using parametric models. *J. Mar. Sci. Technol.* **17**(1), 1–17 (2012). <https://doi.org/10.1007/s00773-011-0148-8>
4. Segui, M., Castelar, Y., Botez, R.M.: Wing airfoils generation based on a new parametric curve for aerodynamic optimization application. In: Paper presented at the CASI AERO-2019 Conference, Canadian Aeronautics and Space Institute, Montreal, pp. 14–16 (May 2019)
5. Anderson, G.R., Aftosmis, M.J.: Adaptive shape parameterization for aerodynamic design. In: NASA/TM–2015–Seedling Phase 2 Final Report. NASA (2015)
6. Chen, W., Fuge, M.: BézierGAN: automatic generation of smooth curves from interpretable low-dimensional parameters. arXiv preprint, [arXiv:1808.08871](https://arxiv.org/abs/1808.08871) (2018)
7. Samareh, J.A.: Survey of shape parameterization techniques for high-fidelity multidisciplinary shape optimization. *AIAA J.* **39**(5), 877–884 (2001). <https://doi.org/10.2514/2.1391>
8. Melin, T., Gårdhagen, R.: Aerodynamic validation of a parametric airfoil. In: 5th CEAS Air & Space conference Challenges in European Aerospace, p. 133. CEAS, Delft (2015)
9. Winslow, J., Otsuka, H., Govindarajan, B., Chopra, I.: Basic understanding of airfoil characteristics at low Reynolds numbers (10^4 – 10^5). *J. Aircr.* **55**(3), 1050–1061 (2018). <https://doi.org/10.2514/1.C034415>
10. Montero, M., Navarro, G.: Aerodynamic performance simulation of three selected airfoils. *Universidad Ciencia Y Tecnología* **25**(111), 201–211 (2021). <https://doi.org/10.47460/uct.v25i111.532>
11. Xu, J., Han, Z., Song, W., Li, K.: Efficient aerodynamic optimization of propeller using hierarchical kriging models. *J. Phys: Conf. Ser.* **1519**, 012019 (2020). <https://doi.org/10.1088/1742-6596/1519/1/012019>
12. Chen, J., et al.: Improvement of airfoil design using smooth curvature technique. *Renewable Energy* **51**, 426–435 (2013). <https://doi.org/10.1016/j.renene.2012.10.006>
13. Do Carmo, M.P.: *Differential Geometry of Curves and Surfaces: Revised and Updated*, 2nd edn. Dover Publications, Mineola (2016)
14. Fomenko, A.T., Mishchenko, A.S.: *A Short Course in Differential Geometry and Topology*. Cambridge Scientific Publishers, Cottenham (2009)
15. Maksimović, S., Borković, A.: A new class of plane curves with arc length parametrization and its application to linear analysis of curved beams. *Mathematics* **9**(15), 1778 (2021). <https://doi.org/10.3390/math9151778>
16. Borisenko, V.D., Ustenko S.A., Ustenko I.V.: Geometric modeling of S-shaped skeletal lines profile of axial compressor blades. *Herald of Aeroenginebuilding* (1), 45–52 (2018). <https://doi.org/10.15588/1727-0219-2018-1-7> [in Ukrainian]

17. Borisenko, V., Ustenko, S., Ustenko, I., Kuzma, K.: Development of a method for geometrical modeling of the airfoil profile of an axial turbomachine blade. *Eastern-European Journal of Enterprise Technologies* **5**(1), 29–38 (2019). <https://doi.org/10.15587/1729-4061.2019.180915>
18. Stetsyuk, P.I., Tkachenko, O.V., Khomyak, O.M., Gritsay, O.L.: Constructing the external contour of the frankl nozzle using S-shaped curves with quadratic distribution of the curvature. *Cybern. Syst. Anal.* **56**(6), 963–977 (2020). <https://doi.org/10.1007/s10559-020-00317-7>
19. Petkevič, R., et al.: Numerical study of powder flow nozzle for laser-assisted metal deposition. *Mathematics* **9**(22), 2913 (2021). <https://doi.org/10.3390/math9222913>
20. Golovanov, N.: *Geometric Modeling: The Mathematics of Shapes*, CreateSpace Independent Publishing Platform (2014)
21. Stetsyuk, P.I.: Theory and software implementations of shor's r -Algorithms*. *Cybern. Syst. Anal.* **53**(5), 692–703 (2017). <https://doi.org/10.1007/s10559-017-9971-1>
22. Stetsyuk, P.I.: r -Algorithms and ellipsoids. *Cybern. Syst. Anal.* **32**(1), 93–110 (1996). <https://doi.org/10.1007/BF02366587>
23. Stetsyuk, P.I., Tkachenko, O.V., Zhydkov, V.O.: Using Shor's r -algorithm for building naturally parametrized curve having cubic curvature. In: *Proceedings of the 7-th International Conference on Control and Optimization with Industrial Application*, vol. I, pp. 389–391. Baku, Azerbaijan (2020)
24. Heath, C., et al.: Aerodynamic shape optimization of a two-stream supersonic plug nozzle. In: *53rd AIAA Aerospace Sciences Meeting*, p. 2015–1047. AIAA (2015). <https://doi.org/10.2514/6.2015-1047>
25. Kraiko, A., Kraiko, A., P'yankov, K., Tillyaeva, N.: Contouring the nozzles producing a uniform supersonic flow or a thrust maximum in the presence of a curvilinear sonic line. *Fluid Dynamics* **47**(2), 223–238 (2012). <https://doi.org/10.1134/S001546281202010X>



Relaxed Containment in Circular Packing Problems

Tatiana Romanova¹ , Georgiy Yaskov¹ , Igor Litvinchev² , Petro Stetsyuk³ ,
Andrii Chuhai¹ , and Sergiy Shekhovtsov¹ 

¹ A. Pidhorneyi Institute of Mechanical Engineering Problems of the NAS of Ukraine,
2/10 Pozharsky Street, Kharkiv 61046, Ukraine
yaskov@ipmach.kharkov.ua

² Nuevo Leon State University, 66455 Monterrey, Nuevo Leon, Mexico

³ V.M. Glushkov Institute of Cybernetics of the NAS of Ukraine, 40 Academician Glushkov
Avenue, Kyiv 03187, Ukraine

Abstract. One of the most important challenges in modeling structures of materials is development and application of new intelligent technologies. To study mechanical properties, e.g., density, a small cuboidal core of the material is extracted from a large volume for further analyses. Due to the cutting edges, material particles may not belong completely to the core volume. This gives rise to a new class of packing problems where the standard containment conditions (all particles are entirely in the container) are substituted by a relaxed containment (all centers of the particles are in the container). A 2D version of this non-standard problem is presented and formulated as a nonlinear programming problem considering non-overlapping and relaxed containment constraints. A new solution technique is proposed combining a fast algorithm for generating feasible starting points and a local optimization procedure based on nonlinear programming. Computational results are provided and illustrated with several examples.

Keywords: Intelligent technology · Packing problem · Mathematical modeling · Nonlinear optimization · Material structure

1 Introduction

The problem of studying structural properties of various materials, powders, rocks arises in modern scientific research in materials science [1, 2], additive technologies [3–6], petrography [7, 8]. These studies are intended for creating new materials with specified parameters, increasing the efficiency of technological processes [9] and determining the optimal composition of composite materials [1].

There are two ways of conducting this research. The first way leads to expensive laboratory studying the structure of materials using valuable high-precision spectral microscopes. The second way allows creating an intellectual information system [9] for computer modeling the structure of materials instead of expensive natural experiment. The mathematical basis of this information system can be geometric design [10, 11].

Tackling the geometric design problem enables to determine the optimal placement of a given set of geometric objects in a given domain. According to the approach, the particles of the material under study can be presented by a set of geometric objects of a given shape. The space form can be determined as a result of earlier material studies. The essence of the problem is to find a dense placement of material particles in a given domain and study material properties (e.g., material porosity, permeability, filtration parameters, strength parameters).

Laboratory research exploits a spectral microscope a fragment of material having rectangular form is investigated, a rectangular area is taken as a placement area at simulation modeling.

When conducting experimental research using a microscope, a rectangular fragment of the material is tested. For these reasons a rectangular area is taken as a placement domain in simulation modeling. In so doing, the material particles are cut by the frontier of the studied fragment (e.g., a rectangle). In this regard, for adequate computer simulation of the material structure one should take into account that the particles placed may not fully belong to the placement domain.

In this paper a mathematical model for placing particles (circles) in a rectangular area is proposed. Instead of the standard containment conditions (the circles are entirely in the container), the relaxed containment is used (the centers of the circles are in the container). A modification of the jump algorithm [12] considering the relaxation of containment conditions and a concept of adding artificial circles is developed.

The proposed mathematical model and solution algorithm can be used in the intelligent technologies creating for modeling the structure of materials.

2 State-of-the-Art

Nowadays a great number of investigations of circle packing problem (CPP) are known. Authors consider a big variety of different models and methods for solving CPP as precise as heuristic [13–15].

In [16] up-to-date mathematical models of packing problems are reviewed. The authors of the paper emphasize that the *phi*-function technique [11, 17, 18] is a promising tool for analytical description of interactions of geometric objects.

Packing congruent circles with the packing factor $\pi\sqrt{3}/6 \approx 0.91$ is known to be the densest one for circles. Paper [19] considers different optimization methods for solving open dimension problems (ODP) of packing spheres. One of the simplest algorithm is based on optimization by groups of variables. The method yields a feasible solution of the problem which is not in general a local minimum. The approach is known as the block-coordinate descent method [20].

Huang et al. [21] proposed greedy algorithms for packing circles into a rectangle of given sizes. The first heuristic packs the next circle according to the maximum-hole degree rule. The second heuristic is a self-look-ahead search strategy that chooses the next circle to be packed and calculates its position. In [22] the optimized CPP is reduced to a linear integer programming problem of large dimension due to a finite grid of

approximation of the container. In [23] the approach is adopted for so-called circular-like objects that can be presented as circles in a certain metric. In [24] a metaheuristic binary monkey algorithm is used to solve the grid approximation. The paper [25] proposes hybrid algorithms combining beam and binary interval search with an open-strip generation procedure and a multi-start separate-beams strategy for solving the circular ODP.

An idea of increasing the number of variable parameters considering radii of circles as variables is proposed in [12]. Special ways for construction of starting points are developed. A multi-stage jump strategy which allows movement from one local minimum to another decreasing the objective is presented. Constructed is an additional rigid system of constraints which ensures the convergence of variable radii to the origin values.

The best-known solutions for packing equal and non-equal circles into various containers are available at E. Specht's website [26].

3 Problem Formulation

Let a set of circles $S_i(\mathbf{u}_i) = \{(x, y) \in \mathbf{R}^2 : (x-x_i)^2 + (y-y_i)^2 - (\rho_i)^2 \leq 0\}$ be given. Here $\mathbf{u}_i = (x_i, y_i)$ and $\rho_i > 0$ are centers and radii of the circles $S_i(\mathbf{u}_i)$, $i \in I = \{1, 2, \dots, n\}$. The circles should be placed in a rectangle $R(b) = \{(x, y) \in \mathbf{R}^2 : 0 \leq x \leq a, 0 \leq y \leq b\}$ (domain) where a is fixed and b is a variable.

The problem is formulated as follows. Find a vector $\mathbf{u} = (\mathbf{u}_1, \mathbf{u}_2, \dots, \mathbf{u}_n) \in \mathbf{R}^{2n}$ which provides placing centers \mathbf{u}_i of non-overlapping circles $S_i(\mathbf{u}_i)$, $i \in I$, inside the optimized rectangle $R(b)$.

A mathematical model of the packing problem can be presented as a nonlinear programming problem

$$b^* = \min b, \text{ s.t. } \mathbf{V} = (\mathbf{u}, b) \in W \subset \mathbf{R}^{2n+1} \quad (1)$$

where

$$W = \{\mathbf{V} \in \mathbf{R}^{2n+1} : \varphi_{ij}(\mathbf{u}_i, \mathbf{u}_j) \geq 0, i < j \in I, \varphi_i(\mathbf{u}_i, b) \geq 0, i \in I\}, \quad (2)$$

$$\begin{aligned} \varphi_{ij}(\mathbf{u}_i, \mathbf{u}_j) &= (x_i - x_j)^2 + (y_i - y_j)^2 - (\rho_i + \rho_j)^2, \\ \varphi_i(\mathbf{u}_i, b) &= \min\{x_i, b - x_i, y_i, b - y_i\}. \end{aligned}$$

The inequality $\varphi_{ij}(\mathbf{u}_i, \mathbf{u}_j) \geq 0$ ensures non-overlapping of $S_i(\mathbf{u}_i)$ and $S_j(\mathbf{u}_j)$, $i < j \in I$, while $\varphi_i(\mathbf{u}_i, b) \geq 0$, $i \in I$ provides containment of centers of $S_i(\mathbf{u}_i)$, $i \in I$ into the rectangle $R(b)$.

The inequality $\varphi_i(\mathbf{u}_i, b) \geq 0$, $i \in I$ is equivalent to the inequality system

$$\begin{cases} x_i \geq 0, \\ a - x_i \geq 0, \\ y_i \geq 0, \\ b - y_i \geq 0. \end{cases}$$

Unlike typical packing models, in the problem (1)–(2) the circles can be placed beyond the boundary of the rectangular domain. We refer to this condition as “a relaxed containment”. This allows more precise computer simulation of the material fragment.

The objective function is a width b of the rectangle $R(b)$ and so it is linear. The model involves $n(n - 1)/2$ quadratic, inversely convex, and $4n$ linear inequalities.

The problem (1)–(2) is NP-hard. The number of local minima increases dramatically when increasing the number of circles to be packed. Searching for the global minimum is possible for a small number of circles.

4 Solution Algorithm

Our algorithm is aimed to search for a good local minimum the problem (1)–(2). It depends on advantageous choice of starting points and development of powerful technique that makes use of peculiarities of the mathematical model. We use the technique that supposed to introduce auxiliary variable metric characteristics of the circles or the domain [12]. This allows rearrange circles in the domain maximizing the packing density. A smart search of local extrema is used.

A solution strategy of the problem (1)–(2) involves three main stages: 1) generating feasible starting points; 2) searching for local minima; 3) transition from one local minimum to another, solving auxiliary nonlinear programming problems.

4.1 Constructing Starting Feasible Arrangements

A starting point is chosen in a random way making for a wide variety of initial configurations of the circles. A value $b = b^0$ which ensures packing circles S_i with radii ρ_i , $i \in I$, in $R(b^0)$ is firstly evaluated having regard to the best known packing factors and areas occupied by the circles. Radii ρ_i of the circles S_i , $i \in I$, are supposed to become variable and are designated as r_i . Then $\mathbf{r} = (r_1, r_2, \dots, r_n) \in \mathbf{R}^n$ is a vector of radii and $\mathbf{X} = (\mathbf{u}, \mathbf{r}) \in \mathbf{R}^{3n}$ is a vector of variables. A circle S_i with radius r_i moved by the vector \mathbf{u}_i is denoted as $S_i(\mathbf{u}_i, r_i)$.

After that, a point $\mathbf{X}^0 = (\mathbf{u}^0, \mathbf{0}) = (\mathbf{u}^0, \underbrace{0, \dots, 0}_n)$ where \mathbf{u}^0 is chosen randomly providing $\mathbf{u}_i \in R(b^0)$, $r_i = 0$, $i \in I$ (Fig. 1) is taken. Next, radii r_i are reconstituted to origin values ρ_i . To this end the following auxiliary problem is solved.

Problem

$$\max \sum_{i=1}^n r_i, \text{ s.t. } \mathbf{X} \in G \subset \mathbf{R}^{3n}, \quad (3)$$

where

$$G = \{ \mathbf{X} \in \mathbb{R}^{3n} : \varphi_{ij}^r(\mathbf{u}_i, \mathbf{u}_j, r_i, r_j) \geq 0, i < j \in I, \quad (4)$$

$$\varphi_i(\mathbf{u}_i, b^0) \geq 0, \phi_i(r_i) = \rho_i - r_i \geq 0, r_i \geq 0, i \in I\},$$

$$\varphi_{ij}^r(\mathbf{u}_i, \mathbf{u}_j, r_i, r_j) = (x_i - x_j)^2 + (y_i - y_j)^2 - (r_i + r_j)^2 \geq 0.$$

A local maximum point $\mathbf{X}^{0*} = (\mathbf{u}^{0*}, \rho_1, \rho_2, \dots, \rho_n)$ for the problem (3)–(4) is calculated (Fig. 2). Then a local minimum of the problem (1)–(2) (Fig. 3) is found, starting from the point $\mathbf{V}^0 = (\mathbf{u}^{0*}, b^0)$. As a result, a point $\mathbf{V}^{1*} = (\mathbf{u}^{1*}, b^{1*})$ is obtained.

After that l artificial circles are added. The circles should touch either three another circles, or two circles, or one circle. The center point (x_p, y_p) of an artificial circle can be found by solving systems of the form

$$\begin{cases} (x_i^{1*} - x_p)^2 + (y_i^{1*} - y_p)^2 - (\rho_i + r_p)^2 = 0, & i \in I, \\ (x_j^{1*} - x_p)^2 + (y_j^{1*} - y_p)^2 - (\rho_j + r_p)^2 = 0, & j \in I, j \neq i, \\ (x_k^{1*} - x_p)^2 + (y_k^{1*} - y_p)^2 - (\rho_k + r_p)^2 = 0, & k \in I, k \neq i, k \neq j, \end{cases}$$

$$\begin{cases} (x_i^{1*} - x_p)^2 + (y_i^{1*} - y_p)^2 - (\rho_i + r_p)^2 = 0, & i \in I, \\ (x_j^{1*} - x_p)^2 + (y_j^{1*} - y_p)^2 - (\rho_j + r_p)^2 = 0, & j \in I, j \neq i, \\ f_1 = 0, \end{cases}$$

$$\begin{cases} (x_i^{1*} - x_p)^2 + (y_i^{1*} - y_p)^2 - (\rho_i + r_p)^2 = 0, & i \in I, \\ f_1 = 0, \\ f_2 = 0 \end{cases}$$

where functions f_1 and f_2 are linearly independent and take one of the form: x_p or y_p or $b^{1*} - y_p$ or $a - x_p$. The center points (x_p, y_p) providing the circles non-overlapping combined with the relaxed containment conditions are selected, such that $r_p < \rho^- = \min\{\rho_1, \rho_2, \dots, \rho_n\}$. Two artificial circles are shown in dotted line in Fig. 3.

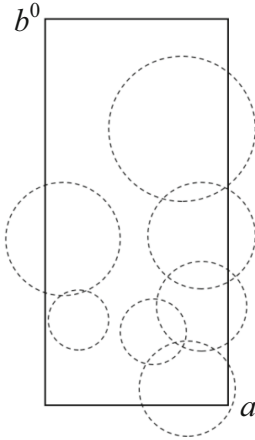


Fig. 1. An example of starting arrangement of circles.

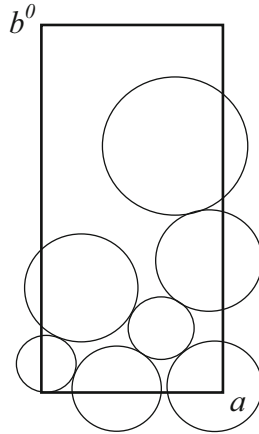


Fig. 2. A local maximum point for the problem (3)–(4).

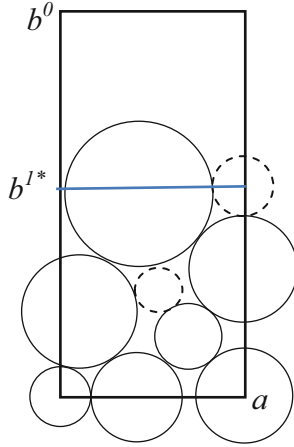


Fig. 3. A local minimum point for the problem (1)–(2) and artificial circles.

We use the notation $\mathbf{V}^{1*} = (\mathbf{u}^{1*}, b^{1*})$ of a local minimum point for the problem (3)–(4).

4.2 Rearranging Circles

Radii of artificial circles are close to radii of original circles. It means that there is an unoccupied area of the domain and therefore circles can be rearranged optimizing the size of the rectangle. The point $\mathbf{X}^{1*} = (\mathbf{u}^{1*}, \rho_1, \rho_2, \dots, \rho_n)$ is taken and the following auxiliary problem is solved:

$$\max \sum_{i=1}^n r_i^2, \text{ s.t. } \mathbf{X} = (\mathbf{u}, \mathbf{r}) \in D \subset \mathbf{R}^{3n}, \tag{5}$$

$$D = \{\mathbf{X} \in \mathbf{R}^{3n}, \varphi_{ij}^r(\mathbf{u}_i, \mathbf{u}_j, r_i, r_j) \geq 0, i < j \in I, \varphi_i(\mathbf{u}_i, b^{1*}) \geq 0, \rho^+ - r_i \geq 0, r_i - \rho^- \geq 0, i \in I\}, \tag{6}$$

where $\rho^+ = \max\{\rho_1, \rho_2, \dots, \rho_n\}$. A total area of the circles is maximized while $\rho^+ - r_i \geq 0$ and $r_i - \rho^- \geq 0$. A local maximum point $\mathbf{X}^{2*} = (\mathbf{u}^{2*}, \mathbf{r}^{2*})$ of the problem (5)–(6) is found.

The circles $S_i(\mathbf{u}_i, r_i)$, $i \in I$, are rearranged according the increasing order of the origin radii $\rho_{j_1} \leq \rho_{j_2} \leq \dots \leq \rho_{j_n}$, $j_1, j_2, \dots, j_n \in I$. Values of r_i in (6) are set to be not greater than ρ_i , $i \in I$. The obtained point is denoted by $\mathbf{X}^3 = (\mathbf{u}^3, \mathbf{r}^3)$.

A new value $b^0 = b^{1*}$ is taken and the problem (3)–(4) is solved starting from the point $\mathbf{X}^3 = (\mathbf{u}^3, \mathbf{r}^3)$ without artificial circles. Let $\mathbf{X}^{3*} = (\mathbf{u}^{3*}, \mathbf{r}^{3*})$ be a local maximum point of the problem (3)–(4). If $r_i^{3*} = \rho_i$, $i \in I$, then a new feasible starting point $\mathbf{V}^0 = (\mathbf{u}^{3*}, b^{1*})$ for the problem (1)–(2) is obtained. If there exists $r_i^{3*} < \rho_i$, $i \in I$, then $\mathbf{V}^0 = (\mathbf{u}^{3*}, b^{1*}) \notin W$. In this case new positions for artificial circles are chosen or a new starting point for the problem (3)–(4) is generated. The process is repeated several times. The best local minimum of the problem (1)–(2) found by our algorithm is taken as the final result.

5 Computational Results

Several benchmark instances from [26] for $n = 20 \dots 50$ circles are tested. The runtime is limited by 5 min for each example. To solve nonlinear optimization problems the IPOPT solver is applied [27].

Example 1. $n = 20$, $a = 8.5$. A starting value $b^0 = 15$ is chosen. An illustration of the local minimum point for the problem (1)–(2) is shown in Fig. 4. The objective function value is $b^* \approx 8.1237$ (local minimum). The corresponding packing of the circles is illustrated in Fig. 5. Radii and center coordinates of the circles are given in Table 1.

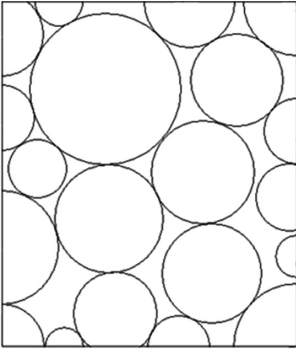


Fig. 4. An illustration of the local minimum point for the problem (1)–(2) for $n = 20$.

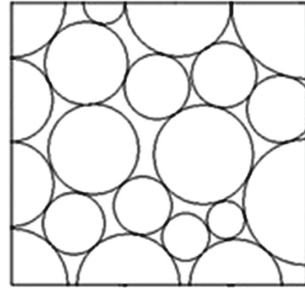


Fig. 5. An illustration of the local minimum point for the problem (1)–(2) for $n = 20$ after the circles rearrangement.

Table 1. Radii and centre points for 20 circles.

i	r_i	x_i	y_i	i	r_i	x_i	y_i
1	0.566	1.8801	2.3274	11	1.229	2.9066	8.5
2	0.612	8.1237	5.833	12	1.309	3.9063	6.1453
3	0.68	1.3913	3.4736	13	1.325	0	2.0298
4	0.85	2.2953	4.708	14	1.43	3.7701	2.9691
5	0.891	1.7787	6.705	15	1.484	0	5.1311
6	0.934	6.0558	2.3654	16	1.525	8.1237	3.696
7	0.947	5.7302	4.3139	17	1.551	8.1176	8.4952
8	0.961	5.0805	0.7406	18	1.636	0	8.5
9	1.189	6.3965	6.3434	19	1.819	2.401	0
10	1.21	5.3457	8.5	20	2.171	8.1237	0

Example 2. $n = 30$, $a = 9.5$. A starting value $b^0 = 17$ is chosen. The objective function value is $b^* \approx 10.4393$ (local minimum). The corresponding packing of the circles is illustrated in Fig. 6.

Example 3. $n = 50$, $a = 9.5$. A starting value $b^0 = 30$ is chosen. The objective function value is $b^* \approx 20.3554$ (local minimum). The corresponding packing of the circles is illustrated in Fig. 7.

Computational results show that concentration of circles along the frontier of the rectangle is increased in contrast to models without relaxation of the containment conditions.

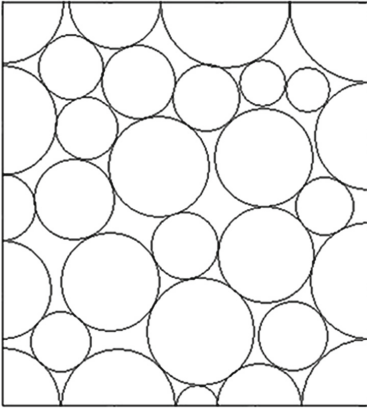


Fig. 6. An illustration of the local minimum point for the problem (1)–(2) for $n = 30$ after the circles rearrangement.

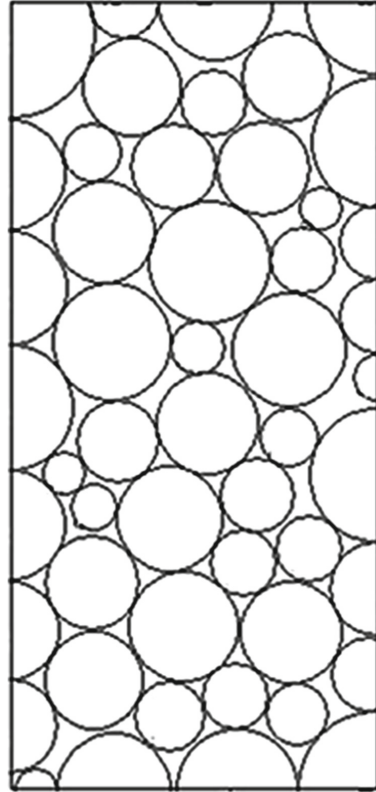


Fig. 7. An illustration of the best local minimum point for the problem (1)–(2) for $n = 50$ the circles after rearrangement.

6 Conclusion

To create an intelligent system for modeling the structure of various materials, an approach to simulation modeling of a rectangular fragment of the material structure is proposed in the paper. For mathematical modeling and computer simulation of the material

fragment, a relaxation of the containment constraints in of the circles packing problem is proposed. The numerical experiments show the efficiency of our algorithm. The proposed approach can be extended to the three-dimensional case.

Acknowledgement. The research is supported by National Research Foundation of Ukraine (grant #2020.02/0128), Volkswagen Foundation (grant #97775, grant #9C086).

References

1. Duriagina, Z.A., et al.: Determination of the best microstructure and titanium alloy powders properties using neural network. *J. Achiev. Mater. Manuf. Eng.* **87**, 25–31 (2018). <https://doi.org/10.5604/01.3001.0012.0736>
2. Ungson, Y., et al.: Filling of irregular channels with round cross-section: modeling aspects to study the properties of porous materials. *Materials* **11**, 1901 (2018). <https://doi.org/10.3390/ma11101901>
3. Duriagina, Z., et al.: Optimized filling of a given cuboid with spherical powders for additive manufacturing. *J. Oper. Res. Soci. China* **9**(4), 853–868 (2020). <https://doi.org/10.1007/s40305-020-00314-9>
4. Araújo, L., Özcan, E., Atkin, J., Baumers, M.: Analysis of irregular three-dimensional packing problems in additive manufacturing: a new taxonomy and dataset. *Int. J. Prod. Res.* **57**, 5920–5934 (2019). <https://doi.org/10.1080/00207543.2018.1534016>
5. Mehrpouya, M., et al.: The potential of additive manufacturing in the Smart Factory Industrial 4.0: A review. *Appl. Sci.* **9**, 3865–3899 (2019). <https://doi.org/10.3390/app9183865>
6. Kritskiy, D., et al.: Powder mixtures analysis for laser cladding using OpenCV library. In: Nechyporuk, M., et al. (eds.) *Integrated Computer Technologies in Mechanical Engineering – 2021*. LNNS, vol. 367, pp. 924–937. Springer, Cham (2022). https://doi.org/10.1007/978-3-030-94259-5_72
7. Kravchenko, O., Suvorova, I., Baranov, I., Goman, V.: Hydrocavitation activation in the technologies of production and combustion of composite fuels. *Eastern-European Journal of Enterprise Technologies* **4**, 33–42 (2017). <https://doi.org/10.15587/1729-4061.2017.108805>
8. Kravchenko, O., Velighotskiy, D., Avramenko, A., Habibullin, R.: An improved technology of a complex influence on productive layers of oil and gas wells. *Eastern-European Journal of Enterprise Technologies* **6**, 4–9 (2014). <https://doi.org/10.15587/1729-4061.2014.29316>
9. Pashchenko, F.F., et al.: Intelligent technologies in decision-making support systems. In: *Proceedings of the 2020 International Conference Engineering and Telecommunication (En&T)*, pp. 1–4 (2020). <https://doi.org/10.1109/EnT50437.2020.9431248>
10. Fasano, G., Pintér, J.D. (eds.): *Modeling and Optimization in Space Engineering*. SOIA, vol. 144. Springer, Cham (2019). <https://doi.org/10.1007/978-3-030-10501-3>
11. Stoyan, Y., et al.: Optimized Packings in Space Engineering Applications: Part I. In: Fasano, G., Pintér, J.D. (eds.) *Modeling and Optimization in Space Engineering*. SOIA, vol. 144, pp. 395–437. Springer, Cham (2019). https://doi.org/10.1007/978-3-030-10501-3_15
12. Stoyan, Y., Yaskov, G.: Packing unequal circles into a strip of minimal length with a jump algorithm. *Optimization Letters* **8**(3), 949–970 (2013). <https://doi.org/10.1007/s11590-013-0646-1>
13. Hifi, M., Yousef, L.: A local search-based method for sphere packing problems. *Eur. J. Oper. Res.* **274**, 482–500 (2019). <https://doi.org/10.1016/j.ejor.2018.10.016>
14. Stetsyuk, P.I.: Shor’s r-Algorithms: Theory and Practice. In: Butenko, S., Pardalos, P.M., Shylo, V. (eds.) *Optimization Methods and Applications*. SOIA, vol. 130, pp. 495–520. Springer, Cham (2017). https://doi.org/10.1007/978-3-319-68640-0_24

15. Blyuss, O., Koriashkina, L., Kiseleva, E., Molchanov, R.: Optimal placement of irradiation sources in the planning of radiotherapy: mathematical models and methods of solving. *Computational and Mathematical Methods in Medicine* 2015, Article ID 142987 (2015). <https://doi.org/10.1155/2015/142987>
16. Leao, A.A.S., Toledo, F.M.B., Oliveira, J.F., et al.: Irregular packing problems: A review of mathematical models. *Eur. J. Oper. Res.* **282**, 803–822 (2020). <https://doi.org/10.1016/j.ejor.2019.04.045>
17. Yaskov, G., Romanova, T., Litvinchev, I., Shekhovtsov, S.: Optimal Packing Problems: From Knapsack Problem to Open Dimension Problem. In: Vasant, P., Zelinka, I., Weber, G.-W. (eds.) *ICO 2019. AISC*, vol. 1072, pp. 671–678. Springer, Cham (2020). https://doi.org/10.1007/978-3-030-33585-4_65
18. Pankratov, A., Romanova, T., Litvinchev, I.: Packing ellipses in an optimized convex polygon. *J. Global Optim.* **75**(2), 495–522 (2019). <https://doi.org/10.1007/s10898-019-00777-y>
19. Stoyan, Y., et al.: Optimized packing multidimensional hyperspheres: a unified approach. *Math. Biosci. Eng.* **17**, 6601–6630 (2020). <https://doi.org/10.3934/mbe.2020344>
20. Wright, S.J.: Coordinate descent algorithms. *Math. Program.* **151**(1), 3–34 (2015). <https://doi.org/10.1007/s10107-015-0892-3>
21. Huang, W.Q., Li, Y., Akeb, H., Li, C.M.: Greedy algorithms for packing unequal circles into a rectangular container. *J. Oper. Res. Soc.* **56**, 539–548 (2005). <https://doi.org/10.1057/palgrave.jors.2601836>
22. Galiev, S.I., Lisafina, M.S.: Linear models for the approximate solution of the problem of packing equal circles into a given domain. *Eur. J. Oper. Res.* **230**, 505–514 (2013). <https://doi.org/10.1016/j.ejor.2013.04.050>
23. Litvinchev, I., Ozuna, L.: Approximate packing circles in a rectangular container: valid inequalities and nesting. *J. Appl. Res. Technol.* **12**, 716–723 (2014). [https://doi.org/10.1016/S1665-6423\(14\)70088-4](https://doi.org/10.1016/S1665-6423(14)70088-4)
24. Torres-Escobar, R., Marmolejo-Saucedo, J.A., Litvinchev, I.: Binary monkey algorithm for approximate packing non-congruent circles in a rectangular container. *Wireless Netw.* **26**(7), 4743–4752 (2018). <https://doi.org/10.1007/s11276-018-1869-y>
25. Lopez, C., Beasley, J.: A formulation space search heuristic for packing unequal circles in a fixed size circular container. *Eur. J. Oper. Res.* **251**, 64–73 (2016). <https://doi.org/10.1016/j.ejor.2015.10.062>
26. Specht, E.: The best known solutions of the circular open dimension problem (CODP), <http://www.packomania.com>. Accessed 25 Feb 2022
27. Wächter, A., Biegler, L.: On the implementation of an interior-point filter line-search algorithm for large-scale nonlinear programming. *Math. Program.* **106**, 25–57 (2006). <https://doi.org/10.1007/s10107-004-055>



Phi-Functions for Objects Bounded by the Second-Order Curves and Their Application to Packing Problems

Mykola Gil  and Volodymyr Patsuk^(✉) 

A. Pidhoryni Institute of Mechanical Engineering Problems of the NAS of Ukraine,
2/10 Pozharsky Street, Kharkiv 61046, Ukraine
patsuk@ipmach.kharkov.ua

Abstract. For non-oriented convex 2D objects whose frontiers are defined by the second order curves an approach of constructing the non-intersection and containment conditions analytically is proposed. For pairs of ellipses or objects bounded by a parabola mutual non-intersection conditions are constructed. For these objects including the case of ellipses being circles the containment conditions are provided as well. The equations of the objects frontiers are used to describe the placement conditions as a system of equalities and inequalities. Solving the systems allows to construct corresponding *phi*-functions for their use in a various packing problems. A problem of packing circles in an ellipse of minimal size saving constant eccentricity is considered as an application.

Keywords: Ellipses · Parabola · Non-intersection · Containment · Nesting

1 Introduction

Constructing conditions for mutual non-intersection of objects in analytical or algorithmic form is of great importance in a wide variety of applied fields: robotics, medicine, cutting of materials [1], packaging, packing, etc. These problems are well investigated, e.g., in [2–5].

In layout optimization problems of circles [6–8] and spheres [9–12], whilst *phi*-functions remain simple, complexities arise at both stages of modelling and solving. It is due to a non-linear disconnected solution domain with multi-connected components, without regarding that the region into which the objects have to be placed may be even convex [13–15].

At the same time, the construction of mutual non-intersection and inclusion conditions for objects with frontiers being not some of the mentioned simple curves is much more difficult, and the results in this area are less numerous. For example, Birgin *et al.* [16] successfully apply a special space transformation to optimization packing problems of ellipses, simplifying the problem. In [17] the quasi-*phi*-functions technique is proposed and used for modelling ellipses layout problems allowing formulating and solving them as MIP problems. In [18–20] quasi-*phi*-functions and *phi*-functions are developed

for objects with piecewise linear frontiers. In [21] quasi-*phi*-functions are applied for describing non-intersection conditions of ellipsoids allowing continuous rotations and *phi*-functions for containment conditions of ellipsoids (using their projections) into a cylinder. In [19, 20] Lagrangian multipliers are used for constructing mathematical model for layout optimization problem for ellipses and ellipsoids respectively.

At the same time, until now little attention has been paid to construction of non-intersection and inclusion conditions for objects bounded by other curves of the second order [22, 23]. Such curves are also the subject of the study below. The proposed approach has the advantage that it allows working with non-convex domains (complements to convex domains), while quasi-*phi*-functions of such regions have not been constructed yet. At the same time, universal properties of smooth objects are used, which makes it possible to extend this approach to other types of objects. The proposed approach extends ideas described in [24].

2 Conditions of Objects Non-intersection

Consider firstly non-intersection and containment conditions for the general case, then for some particular cases of objects bounded by the second-order curves such as ellipses and parabolas.

2.1 A System of Equations Defining Non-intersection Conditions

Let \bar{S}_i , $i = 1, 2$, be a pair of convex objects, whose frontiers are specified by canonical equations $f_1(X, Y) = 0$, $f_2(\bar{X}, \bar{Y}) = 0$, in their own coordinate systems XOY , $\bar{X}O\bar{Y}$, respectively. Let us denote by $f_i(x, y) = 0$, $i = 1, 2$, the equations determining the frontiers of objects $S_i(u_i, \vartheta_i)$ in the main coordinate system xoy . Here $u_i = (x_i, y_i)$ and ϑ_i are placement parameters of the object \bar{S}_i (the position of the origin and the rotation angle of its own coordinate system with respect to xoy). Assume that $(x_i, y_i) \in \text{int}\bar{S}_i$ and the signs of the equations are also chosen so that $f_i(x_i, y_i) < 0$. Let us denote an object homothetic to the object S_2 with a homothetic coefficient γ by S_2^γ . We can assert that objects $S_1\{u_1, \vartheta_1\}$ and $S_2\{u_2, \vartheta_2\}$ do intersect, that is $S_1 \cap S_2 = \emptyset$, if there exists such a point (x^*, y^*) for which the following conditions are met.

1. Points (x_1, y_1) and (x_2, y_2) are situated on the opposite sides of the tangent to S_1 at the point (x^*, y^*) .
2. The point (x^*, y^*) is not an interior point of the object S_2 .
3. The point (x^*, y^*) belongs to the frontiers of objects S_1 and S_2^γ .
4. The slopes of the tangents to the objects S_1 and S_1^γ at (x^*, y^*) are equal.

In an analytical form, conditions 1–4 can be represented as a system of equalities and inequalities:

$$\left\{ \begin{array}{l} -G(x_2, y_2) \cdot G(x_1, y_1) > 0, \\ f_2(x^*, y^*) \geq 0, \\ f_1(x^*, y^*) = 0, \\ \left. \frac{\partial f_1}{\partial y} \right|_{(x^*, y^*)} \cdot \left. \frac{\partial f_2}{\partial x} \right|_{(x^*, y^*)} - \left. \frac{\partial f_1}{\partial x} \right|_{(x^*, y^*)} \cdot \left. \frac{\partial f_2}{\partial y} \right|_{(x^*, y^*)} = 0, \end{array} \right. \quad (1)$$

where $G(x, y) \equiv (y - y^*) \frac{\partial f_1}{\partial y} \Big|_{(x^*, y^*)} + (x - x^*) \frac{\partial f_1}{\partial x} \Big|_{(x^*, y^*)} = 0$ is the equation of the tangent to the object S_1 at the point (x^*, y^*) .

The values x^*, y^* (for given $x_i, y_i, \vartheta_i, i = 1, 2$) can be obtained from the equalities of the system (1) with some computational method. Then the fulfillment of the inequalities for the obtained values guarantees the non-intersection of the objects S_1 and S_2 . If, for these values x^*, y^* , the second inequality of the system turns into an equality, then a tangency of objects have place. As an example, consider the implementation of the proposed approach for an ellipse and a region bounded by a parabola.

2.2 Non-intersection Conditions for an Ellipse and a Region Bounded by a Parabola

Suppose that in some coordinate system xoy we have a parabola $S_1\{u_1, \vartheta_1\}$ and an ellipse $S_2\{u_2, \vartheta_2\}$ with placement parameters $u_1(x_1, y_1), \vartheta_1$ and $u_2 = (x_2, y_2), \vartheta_2$ which in their own coordinate systems XOY and $\bar{X}O\bar{Y}$ are given by the equations $\bar{f}_1(X, Y) \equiv Y - pX^2 = 0$ and $\bar{f}_2(\bar{X}, \bar{Y}) \equiv B^2\bar{X}^2 + A^2\bar{Y}^2 - A^2B^2 = 0$ respectively; A, B are the semi-axes of the ellipse.

Let us choose the coordinate system XOY as the main one, with respect to which we have a parabola $S_1\{\bar{u}_1, \bar{\vartheta}_1\}$ and an ellipse $S_2\{\bar{u}_2, \bar{\vartheta}_2\}$, where $\bar{u}_1 = (0, 0), \bar{\vartheta}_1 = 0, \bar{u}_2 = (X_0, Y_0), \bar{\vartheta}_2 = \vartheta_2 - \vartheta_1$. Here, $Y_0 = (x_2 - x_1) \sin \vartheta_1 + (y_2 - y_1) \cos \vartheta_1$ are obtained using the rotation operator $\begin{pmatrix} \cos \vartheta_1 & -\sin \vartheta_1 \\ \sin \vartheta_1 & \cos \vartheta_1 \end{pmatrix}$. Taking into account the coordinate transformation the frontier equation of $S_2\{X_0, Y_0, \bar{\vartheta}_2\}$ in the system XOY takes the form $f_2(X, Y) = 0$ where $f_2(X, Y) \equiv A^2[-(X - X_0) \sin \bar{\vartheta}_2 + (Y - Y_0) \cos \bar{\vartheta}_2]^2 + B^2[(X - X_0) \cos \bar{\vartheta}_2 - A^2B^2]$.

A region $S_1\{0, 0, 0\}$ bounded by a parabola is characterized by the set of points (\bar{X}, \bar{Y}) for which $\bar{Y} - p\bar{X}^2 \geq 0$. Let (X^*, Y^*) be some point belonging to the parabola $S_1\{0, 0, 0\}$ and the frontier of the ellipse $S_2^Y\{X_0, Y_0, \bar{\vartheta}_2\}$. The slope coefficients $k_i, i = 1, 2$, of the tangents to S_1 and S_2^Y at the point (X^*, Y^*) have the form $k_1 = 2pX^*, k_2 = -\frac{(X^* - X_0)L + (Y^* - Y_0)S}{(X^* - X_0)S + (Y^* - Y_0)R}$ where $L = B^2 \cos^2 \bar{\vartheta}_2 + A^2 \sin^2 \bar{\vartheta}_2, R = B^2 \sin^2 \bar{\vartheta}_2 + A^2 \cos^2 \bar{\vartheta}_2, S = (B^2 - A^2) \sin \bar{\vartheta}_2 \cos \bar{\vartheta}_2$. Then condition 4 from the Sect. 2 (equality of the slope coefficients, which is preserved under orthogonal transformations of space) at a point (X^*, Y^*) in this case is represented in the form

$$\chi(u_1, \vartheta_1, u_2, \vartheta_2, X^*) \equiv (S + 2pRX^*)(pX^{*2} - Y_0) + (L + 2pSX^*)(X^* - X_0) = 0. \tag{2}$$

The equation of the tangent line to the parabola at the point (X^*, Y^*) has the form

$$F(X, Y) \equiv Y - 2pX^*X + pX^{*2} = 0.$$

Then the conditions of being disjoint for the ellipse $S_2\{u_2, \vartheta_2\}$ and the region bounded by the parabola $S_1\{u_1, \vartheta_1\}$, in accordance with (1), can be represented as a system of

inequalities

$$\begin{cases} F(u_1, u_2, X^*) \equiv -Y_0 + 2pX^*X - pX^{*2} \geq 0, \\ f_2(u_1, \vartheta_1, u_2, \vartheta_2, X^*) \equiv B^2[(X^* - X_0) \cos \bar{\vartheta}_2 + (pX^{*2} - Y_0) \sin \bar{\vartheta}_2]^2 + \\ + A^2[-(X^* - X_0) \sin \bar{\vartheta}_2 + (pX^{*2} - Y_0) \cos \bar{\vartheta}_2]^2 - A^2B^2 \geq 0, \end{cases}$$

where X^* is one of the solutions of (2). These conditions can also be represented as the *phi*-function $\Phi(u_1, \vartheta_1, u_2, \vartheta_2) = \max_{X_i^*} \min\{f_2(u_1, \vartheta_1, u_2, \vartheta_2, X^*), F(u_1, u_2, X^*)\}$, where $X_i^*, i = 1, 2, \dots$, are the roots of Eq. (2).

3 Conditions of an Object Containment in a Given Region

Consider now the conditions of containment for some pairs of objects bounded by second-order curves.

3.1 Conditions of a Circle Containment in an Ellipse

Let an ellipse $S_1\{0, 0, 0\}$ and a circle $S_2\{x_0, y_0\}$ be given in the coordinate system xoy and let the frontier equations of them be $g_1(x, y) \equiv b^2x^2 + a^2y^2 - a^2b^2 = 0$ and $g_2(x, y) \equiv (x - x_0)^2 + (y - y_0)^2 - r_0^2 = 0$ respectively, where a, b ($a > b$) are the semi-axes of the ellipse, r_0 is the radius of the circle, $r_0 \leq b$, x_0, y_0 are the placement parameters of the circle.

Let us denote by S_2^γ the circle of radius γ_0 centered at the point (x_0, y_0) . Then the circle $S_2\{x_0, y_0\}$ is an inclusion into the ellipse $S_1\{0, 0, 0\}$, i. e. $S_1 \cup S_2 = S_2$, if there exists a point (x^*, y^*) for which the following conditions are satisfied:

1. The point (x^*, y^*) is not the inner point of the circle $S_2\{x_0, y_0\}$.
2. The center of the circle (x_0, y_0) is inside the ellipse $S_1\{0, 0, 0\}$.
3. The point (x^*, y^*) belongs to the strip bounded by straight lines $x = \bar{x}$ and $x = -\bar{x}$, where \bar{x} is the abscissa of the contact point of the ellipse $S_1\{0, 0, 0\}$ and the circle $S_2\{\bar{x}_0, 0\}$ of radius r_0 with the placement parameters $(\bar{x}_0, 0)$.
4. The point (x^*, y^*) belongs to the frontiers of $S_1\{0, 0, 0\}$ and $S_2^\gamma\{x_0, y_0\}$.
5. The slopes of the tangents to $S_1\{0, 0, 0\}$ and $S_2^\gamma\{x_0, y_0\}$ at (x^*, y^*) are equal. In this case $k_1 = -b^2x^{*2}/a^2y^{*2}$, $k_2 = -(x^* - x_0)/(y^* - y_0)$. The value \bar{x} can be obtained by solving the equation system

$$\begin{cases} (\bar{x} - \bar{x}_0)^2 + \bar{y}^2 - r_0^2 = 0, \\ b^2\bar{x}^2 + a^2\bar{y}^2 - a^2b^2 = 0, \\ b^2\bar{x}\bar{y} - a^2\bar{y}(\bar{x} - x_0) = 0, \end{cases}$$

which implements the conditions of point (\bar{x}, \bar{y}) belonging to the circle $S_2\{\bar{x}_0, 0\}$ and an ellipse $S_1\{0, 0, 0\}$, as well as the equality of the directions of the tangents to the circle and the ellipse at (\bar{x}, \bar{y}) . The solution to this system is $\bar{x} = \pm \frac{a^2}{b} \sqrt{\frac{b^2 - r_0^2}{a^2 - b^2}}$, $\bar{y} = \pm \sqrt{\frac{a^2 r_0^2 - b^4}{a^2 - b^2}}$ provided that $r_0 > \frac{b^2}{a}$ (the radius of curvature of the circle is greater than the radius of

curvature of the ellipse at the point $(a, 0)$) Otherwise $\bar{x} = a, \bar{y} = 0$. Taking into account that $x^* = a \cos t^*, y^* = b \sin t^*$, condition 9 is represented in the form

$$\varphi(x_0, y_0, t^*) \equiv (a^2 - b^2) \sin t^* \cos t^* + by_0 \cos t^* - ax_0 \sin t^* = 0. \tag{3}$$

Thus, the conditions 5–9 (the conditions for the inclusion of a circle into an ellipse) in the analytical representation are reduced to a system of inequalities of the form

$$\begin{cases} g_2(x_0, y_0, t^*) \equiv (a \cos t^* - x_0)^2 + (b \sin t^* - y_0)^2 - r_0^2 \geq 0, \\ g_1(x_0, y_0) \equiv -b^2x_0^2 - a^2y_0^2 + a^2b^2 \geq 0, \\ h_1(t^*) \equiv \bar{x} - a \cos t^* \geq 0, \\ h_2(t^*) \equiv \bar{x} + a \cos t^* \geq 0, \end{cases} \tag{4}$$

where t^* is one of the solutions to Eq. (3), which can be found using one of the computational methods.

It should be noted that the conditions for inclusion $S_2\{x_0, y_0\}$ into $S_1\{0, 0, 0\}$ can be considered as conditions for non-intersection of objects $\mathbb{R}^2 \setminus \text{int}S_1\{0, 0, 0\}$ and $S_2\{x_0, y_0\}$, that is, represented in the form of the *phi*-function

$$\Phi(x_0, y_0, t^*) = \max_{t_i^*} \min\{g_2(x_0, y_0, t^*), g_1(x_0, y_0), h_1(t^*), h_2(t^*)\},$$

where $t_i^*, i = 1, 2, \dots$ are the roots of Eq. (3).

3.2 Conditions of an Ellipse Containment into an Ellipse

Let an ellipse S_1 be given in a coordinate system $\bar{x}\bar{o}\bar{y}$, and an ellipse S_2 be given in a coordinate system $x'oy'$ rotated with respect to $\bar{x}\bar{o}\bar{y}$ by an angle ϑ and with the origin at a point $(\bar{x}_0\bar{y}_0)$; let the equations of their frontiers be $b^2\bar{x}^2 + a^2\bar{y}^2 - a^2b^2 = 0$ ($a > b$) and $B^2x'^2 + A^2y'^2 - A^2B^2 = 0$ ($A > B$) respectively. We will assume that $b \geq B$, since otherwise the inclusion of the ellipse into the ellipse cannot take place. In this case, the conditions for including an ellipse in an ellipse can be reduced to conditions for including a circle into an ellipse as follows. Take the new coordinate system $\bar{X}'O\bar{Y}'$ rotated by an angle ϑ with respect to $\bar{x}\bar{o}\bar{y}$. Assuming $\bar{X}'_0 = \bar{x}_0 \cos \vartheta + \bar{y}_0 \sin \vartheta, \bar{Y}'_0 = -\bar{x}_0 \sin \vartheta + \bar{y}_0 \cos \vartheta$ the ellipse S_1 can be described as $b^2(\bar{X}'/2 \cos \vartheta - \bar{Y}'/2 \sin \vartheta)^2 + a^2(\bar{X}'/2 \sin \vartheta + \bar{Y}'/2 \cos \vartheta)^2 - a^2b^2 = 0$ and the ellipse S_2 is described by $B^2(\bar{X} - \bar{X}'_0)^2 + A^2(\bar{Y} - \bar{Y}'_0)^2 - A^2B^2 = 0$.

Let us apply a compression along the axis $O\bar{X}'$ based on the formulas $\bar{X}' = (A/B)X, \bar{Y}' = Y$. Then, in the new coordinate system XOY , the equation of the frontier of the ellipse S_1 has the form

$$b^2(AX \cos \vartheta - BY \sin \vartheta)^2 + a^2(AX \sin \vartheta + BY \cos \vartheta)^2 - a^2b^2B^2 = 0,$$

and the ellipse turns into a circle whose frontier is described by the equation $(X - X_0)^2 + (Y - Y_0)^2 - B^2 = 0$ where

$$\begin{aligned} X_0 &= (B/A)(\bar{x}_0 \cos \vartheta + \bar{y}_0 \sin \vartheta), \\ Y_0 &= -\bar{x}_0 \sin \vartheta + \bar{y}_0 \cos \vartheta. \end{aligned} \tag{5}$$

We transform the equation of the ellipse S_1 into the form

$$a_{11}X^2 + 2a_{12}XY + a_{22}Y^2 + 2a_{13}X + 2a_{23}Y + a_{33} = 0 \quad (6)$$

where $a_{11} = A^2(a^2 \sin^2 \vartheta + b^2 \cos^2 \vartheta)$, $a_{12} = AB(a^2 - b^2) \sin \vartheta \cos \vartheta$, $a_{22} = B^2(a^2 \cos^2 \vartheta + b^2 \sin^2 \vartheta)$, $a_{33} = -a^2 b^2 B^2$, $a_{13} = a_{23} = 0$.

In the new coordinate system xoy formed by rotating the axes by an angle corresponding to the equation

$$\operatorname{tg} 2\varphi = \frac{2a_{12}}{a_{11} - a_{22}}, \quad (7)$$

the equation of the form (6) is reduced to canonical form $\bar{b}^2 x^2 + \bar{a}^2 y^2 - \bar{a}^2 \bar{b}^2$, where $\bar{a}^2 = -\frac{1}{\lambda_2} \frac{A}{D}$, $\bar{b}^2 = -\frac{1}{\lambda_1} \frac{A}{D}$. Here λ_1, λ_2 are the roots of the characteristic equation $\lambda^2 - J\lambda + D = 0$, where $J = a_{11} + a_{22}$, $D = a_{11}a_{22} - a_{12}^2$, $A = (a_{11}a_{22} - a_{12}^2)a_{33}$.

After simple transformations, we have

$$\bar{a}^2 = \frac{-2a_{33}}{a_{11} + a_{22} - \sqrt{(a_{11} - a_{22})^2 + 4a_{12}^2}}, \quad \bar{b}^2 = \frac{-2a_{33}}{a_{11} + a_{22} + \sqrt{(a_{11} - a_{22})^2 + 4a_{12}^2}}. \quad (8)$$

It should be noted that the transition from the coordinate system XOY to xoy (rotation through the angle 2φ corresponding to Eq. (7) was carried out in accordance with the transition formulas $x = X \cos 2\varphi + Y \sin 2\varphi$, $y = -X \sin 2\varphi + Y \cos 2\varphi$, where $\sin 2\varphi = \frac{2a_{12}}{\sqrt{(a_{11} - a_{22})^2 + 4a_{12}^2}}$, $\cos 2\varphi = \frac{a_{11} - a_{22}}{\sqrt{(a_{11} - a_{22})^2 + 4a_{12}^2}}$.

Accordingly, the coordinates \bar{x}_0, \bar{y}_0 of the center of the circle in the coordinate system xoy are determined as follows

$$\bar{x}_0 = X_0 \cos 2\varphi + Y_0 \sin 2\varphi, \quad \bar{y}_0 = -X_0 \sin 2\varphi + Y_0 \cos 2\varphi, \quad (9)$$

where X_0, Y_0 have the form (5).

Thus, in the coordinate system xoy we have an ellipse $S_1\{0, 0, 0\}$ and a circle $S_2\{\bar{x}_0, \bar{y}_0\}$, the frontiers of which are given by equations $f_1(x, y) \equiv \bar{b}^2 x^2 + \bar{a}^2 y^2 - \bar{a}^2 \bar{b}^2 = 0$, $f_2(x, y) \equiv (x - \bar{x}_0)^2 + (y - \bar{y}_0)^2 - B^2 = 0$ respectively, where \bar{a}^2, \bar{b}^2 are determined from (8) and \bar{x}_0, \bar{y}_0 are determined from (9).

Then the condition of containment of the ellipse S_2 in S_1 , similarly to (4) is

$$\begin{cases} g_2(\bar{x}_0, \bar{y}_0, t^*) \equiv (\bar{a} \cos t^* - \bar{x}_0)^2 + (\bar{b} \sin t^* - \bar{y}_0)^2 - B^2 \geq 0, \\ g_1(\bar{x}_0, \bar{y}_0) \equiv -\bar{b}^2 \bar{x}_0^2 - \bar{a}^2 \bar{y}_0^2 + \bar{a}^2 \bar{b}^2 \geq 0, \\ h_1(t^*) \equiv \hat{x} - \bar{a} \cos t^* \geq 0, \\ h_2(t^*) \equiv \hat{x} + \bar{a} \cos t^* \geq 0, \end{cases}$$

where $\hat{x} = \pm \sqrt{(\bar{b}^2 - B^2)/(\bar{a}^2 - \bar{b}^2)}$, $\hat{y} = \pm \sqrt{(\bar{a}^2 B^2 - \bar{b}^4)/(\bar{a}^2 - \bar{b}^2)}$, t^* is one of the solutions of the equation

$$\bar{\varphi}(\bar{x}_0, \bar{y}_0, t^*) \equiv (\bar{a}^2 - \bar{b}^2) \sin t^* \cos t^* + \bar{b} \bar{y}_0 \cos t^* - \bar{a} \bar{x}_0 \sin t^* = 0 \quad (10)$$

In addition, these conditions can be represented as a *phi*-function $\Phi(\bar{x}_0, \bar{y}_0, t^*) = \max_{t_i^*} \min\{g_2(\bar{x}_0, \bar{y}_0, t^*), g_1(\bar{x}_0, \bar{y}_0), h_1(t^*), h_2(t^*)\}$, where $t_i^*, i = 1, 2, \dots$, are the solutions of (10).

3.3 Conditions for an Ellipse Inclusion into a Region Bounded by a Parabola

Let a region D bounded by a parabola $y = px^2$ and an ellipse $S\{x_0, y_0, \vartheta\}$ with placement parameters x_0, y_0, ϑ be given in the coordinate system xoy . In its own coordinate system $X'OY'$, rotated by angle ϑ with respect to xoy and with the origin at the point x_0, y_0 , the ellipse is defined by the equation $B^2X'^2 + A^2Y'^2 - A^2B^2 = 0$. Let us introduce a new coordinate system $x'oy'$ rotated by angle ϑ with respect to xoy . Taking into account the coordinate system transformation formulas, the equations of the parabola and the ellipse take the form $x' \sin \vartheta + y' \cos \vartheta = p(x' \sin \vartheta - y' \cos \vartheta)^2$ and $B^2(x' - x'_0)^2 + A^2(y' - y'_0)^2 - A^2B^2 = 0$, respectively, where $x'_0 = x_0 \cos \vartheta + y_0 \sin \vartheta, y'_0 = -x_0 \sin \vartheta + y_0 \cos \vartheta$. It is shown in [24] that the conditions for inclusion of $\bar{S}(X_0, Y_0)$ into the region \bar{D} can be represented in the form of the *phi*-function $\Phi(X_0, Y_0, Y^*) = \max_{Y_i^*} \min\{g_2(X_0, Y_0, Y^*), g_1(X_0, Y_0), h(Y^*)\}$ where $Y_i^*, i = 1, 2, \dots$, are the roots of equation $\varphi(X_0, Y_0, Y^*) \equiv p'(Y^* - Y_0) + Y^*((1/2p')Y^{*2} - X_0) = 0, \sqrt{B^2 - p'^2} \leq Y^* < \sqrt{2p'X_0}$, if $Y_0 \geq 0, -\sqrt{2p'X_0} < Y^* < -\sqrt{B^2 - p'^2}$, if $Y_0 < 0$.

4 An Application to Solving a Problem of Packing Circles into an Ellipse

Let us have an ellipse $E_0 = E_0(a, b) = S_0$ with semi-axes a, b and the circles $C_i = S_i, i = 1, 2, \dots, n$ with their own coordinate systems $x_i o_i y_i$ such that $\mathbf{o}_0 = \mathbf{o}_0^{[0]} = (0, 0)[0]$.

Denote $\Delta_{ij}^{\mathbf{o}} = \mathbf{o}_j^{[0]} - \mathbf{o}_i^{[0]} = (\Delta_{ijx}^{\mathbf{o}}, \Delta_{ijy}^{\mathbf{o}})$ (the notation $\mathbf{v}^{[i]}$ means that we consider the coordinate system of an object S_i). We consider a, b as variables with $a/b = \text{const}$. Otherwise, it can be expressed as $(\gamma a, \gamma b)$ where γ is the homothety coefficient. Then the NLP problem for obtaining a packing of C_i into the minimal ellipse $E_0(a, b, \gamma)$ can be stated as

$$\begin{aligned} &\gamma \rightarrow \min, \\ &s.t. \\ &\Phi_{S_i, S_j}(\Delta_{ij}^{\mathbf{o}}) \geq 0, \Phi_{S_i, S_0(\gamma)}^{\subset}(\mathbf{o}_i^{[0]}, \gamma) \geq 0, \end{aligned}$$

where $\Phi_{S_i, S_j}(\Delta_{ij}^{\mathbf{o}})$ is the *phi*-function of $S_i, S_j, \Phi_{S_i, S_0(\gamma)}^{\subset}(\mathbf{o}_i^{[0]}, \gamma)$ is the *phi*-function of C_i and $\mathbb{R}^2 \setminus \text{int}S_0(\gamma)$.

The explicit equations of the contour curves of the objects $S_i, i = 0, 1, 2, \dots, n$ in their own coordinate systems $x^{[i]} \mathbf{o}_i^{[i]} y^{[i]}$ have the forms

$$\mathbf{w}_i^{[i]}(t) = (\xi_i(t), \eta_i(t)), t \in T_0 = [0, 2\pi],$$

and in the coordinate system $x^{[0]} \mathbf{o}_0^{[0]} y^{[0]}$:

$$\mathbf{w}_i^{[0]}(t) = (\xi_i(t), \eta_i(t)) + \mathbf{o}_i^{[0]} = (\xi_i(t) + o_{ix}, \eta_i(t) + o_{iy}), t \in T_0$$

For $S_0(\gamma)$ we have $\mathbf{w}_0^\gamma(t) = (\xi_0^\gamma(t), \eta_0^\gamma(t)) = (\gamma\xi_0(t), \gamma\eta_0(t))$.

For computing $\Phi_{S_i, S_0(\gamma)}^C(\mathbf{o}_i^{[0]}, \gamma)$ the set of pairs of the frontier points can be obtained such that some element of this set provides the exact normalized *phi*-function value. It can be done by solving the following system:

$$\begin{cases} \mathbf{k}_0^\gamma(t) = -\mu\mathbf{k}_i(\tau), \\ (\mathbf{k}_0^\gamma(t), \mathbf{w}_i(\tau) - \mathbf{w}_0^\gamma(t)) = 0, \\ \mu < 0. \end{cases} \tag{11}$$

where $\mathbf{k}_0^\gamma(s) = \frac{d(\gamma\mathbf{w}_0(s))}{ds} = \gamma \frac{d(\mathbf{w}_0(s))}{ds}$ and the first equation is a vector one and splits into two scalar equations.

The non-intersection conditions for circles are known, those for ellipse and a circle when solving (11) leads us to the quartic equation (if we consider a normalized *phi*-function), namely the following one

$$-\zeta^4 4b\Delta_{ijy} + (-2a^2 - 2a\Delta_{ijx} + 2b^2)\zeta^3 + (2a^2 - 2a\Delta_{ijx} - 2b^2)\zeta + b\Delta_{ijy} = 0.$$

It can be solved either numerically or exactly.

Thus an optimization problem is obtained and solved using the Interior point optimizer (IPOpt) [25]. Solution examples are shown in Figs. 1 and 2.

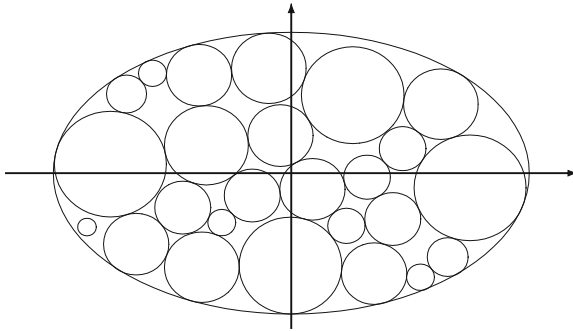


Fig. 1. Packing 25 circles into an ellipse; $a/b = 1.59375$, $a_{\min} = 50.989$; the radii are 2, 3 (3 times), 4, 4.3, 4.4, 5 (2 times), 6 (3 times), 7 (5 times), 8 (3 times), 9, 11 (2 times), 12 (2 times).

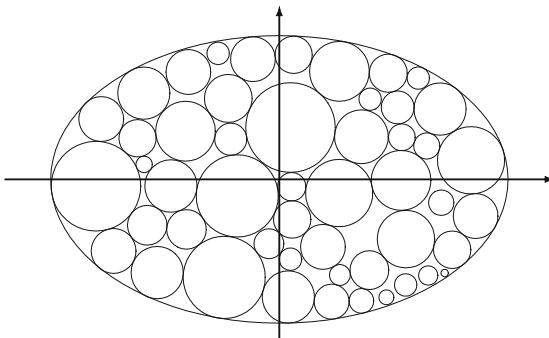


Fig. 2. Packing 50 circles into an ellipse; $a/b = 1.59375$, $a_{\min} = 61.3025$.

5 Conclusion

The proposed approach allows to construct *phi*-functions for a family of objects bounded by the second order curves. In some cases, a direct analytical representation is possible with use of the quartic equation solutions. However, it is quite cumbersome. Therefore, the proposed approach of constructing *phi*-functions is reduced to a numerical solution of an equation with one variable.

This approach for constructing *phi*-functions was applied to a problem of packing circles in an ellipse with minimization of the ellipse size. Numerical results and runtime values show the efficiency of the approach.

References

1. Plankovskyy, S., Tsegelnyk, Y., Shypul, O., Pankratov, A., Romanova, T.: Cutting irregular objects from the rectangular metal sheet. In: Nechyporuk, M., Pavlikov, V., Kritskiy, D. (eds.) Integrated Computer Technologies in Mechanical Engineering. AISC, vol. 1113, pp. 150–157. Springer, Cham (2020). https://doi.org/10.1007/978-3-030-37618-5_14
2. Chernov, N., Stoyan, Y., Romanova, T.: Mathematical model and efficient algorithms for object packing problem. Comput. Geom. **43**(5), 535–553 (2010). <https://doi.org/10.1016/j.comgeo.2009.12.003>
3. Stoyan, Y., Romanova, T.: Mathematical models of placement optimisation: two- and three-dimensional problems and applications. In: Fasano, G., Pintér, J.D. (eds.) Modeling and Optimization in Space Engineering, pp. 363–388. Springer New York, New York, NY (2013). https://doi.org/10.1007/978-1-4614-4469-5_15
4. Kritskiy, D., Pohudina, O., Kovalevskiy, M., Tsegelnyk, Y., Kombarov, V.: Powder mixtures analysis for laser cladding using OpenCV library. In: Nechyporuk, M., Pavlikov, V., Kritskiy, D. (eds.) Integrated Computer Technologies in Mechanical Engineering - 2021: Synergetic Engineering, pp. 924–937. Springer International Publishing, Cham (2022). https://doi.org/10.1007/978-3-030-94259-5_72
5. Stoyan, Y., Pankratov, A., Romanova, T.: Placement problems for irregular objects: mathematical Modeling, optimization and applications. In: Butenko, S., Pardalos, P.M., Shylo, V. (eds.) Optimization Methods and Applications. SOIA, vol. 130, pp. 521–559. Springer, Cham (2017). https://doi.org/10.1007/978-3-319-68640-0_25
6. Litvinchev, I., Ozuna, E.L.: Approximate packing circles in a rectangular container: valid inequalities and nesting. J. Appl. Res. Technol. **12**(4), 716–723 (2014). [https://doi.org/10.1016/S1665-6423\(14\)70088-4](https://doi.org/10.1016/S1665-6423(14)70088-4)
7. Plankovskyy, S., Shypul, O., Tsegelnyk, Y., Pankratov, A., Romanova, T., Litvinchev, I.: Circular layout in thermal Deburring. In: Shkarlet, S., Morozov, A., Palagin, A. (eds.) MODS 2020. AISC, vol. 1265, pp. 111–120. Springer, Cham (2021). https://doi.org/10.1007/978-3-030-58124-4_11
8. Torres-Escobar, R., Marmolejo-Saucedo, J.A., Litvinchev, I.: Binary monkey algorithm for approximate packing non-congruent circles in a rectangular container. Wireless Netw. **26**(7), 4743–4752 (2018). <https://doi.org/10.1007/s11276-018-1869-y>
9. Hifi, M., Yousef, L.: A local search-based method for sphere packing problems. Eur. J. Oper. Res. **274**(2), 482–500 (2019). <https://doi.org/10.1016/j.ejor.2018.10.016>
10. Duriagina, Z., et al.: Optimized filling of a given cuboid with spherical powders for additive manufacturing. J. Oper. Res. Soc. China **9**(4), 853–868 (2020). <https://doi.org/10.1007/s40305-020-00314-9>

11. Pintér, J.D., Kampas, F.J., Castillo, I.: Globally optimized packings of non-uniform size spheres in \mathbb{R}^d : a computational study. *Optim. Lett.* **12**(3), 585–613 (2017). <https://doi.org/10.1007/s11590-017-1194-x>
12. Burtseva, L., Salas, B.V., Romero, R., Werner, F.: Recent advances on modelling of structures of multi-component mixtures using a sphere packing approach. *Int. J. Nanotechnol.* **13**(1–3), 44–59 (2016)
13. Stoyan, Y., Yaskov, G.: Optimized packing unequal spheres into a multiconnected domain: mixed-integer non-linear programming approach. *Int. J. Comput. Math. Comput. Syst. Theory* **6**(1), 94–111 (2021). <https://doi.org/10.1080/23799927.2020.1861105>
14. Stoyan, Y., et al.: Optimized packing multidimensional hyperspheres: a unified approach. *Math. Biosci. Eng.* **17**(6), 6601–6630 (2020). <https://doi.org/10.3934/mbe.2020344>
15. Stetsyuk, P.I., Romanova, T.E., Scheithauer, G.: On the global minimum in a balanced circular packing problem. *Optim. Lett.* **10**(6), 1347–1360 (2015). <https://doi.org/10.1007/s11590-015-0937-9>
16. Birgin, E.G., Bustamante, L.H., Callisaya, H.F., Martínez, J.M.: Packing circles within ellipses. *Int. Trans. Oper. Res.* **20**(3), 365–389 (2013). <https://doi.org/10.1111/itor.12006>
17. Romanova, T., et al.: Optimal layout of ellipses and its application for additive manufacturing. *Int. J. Prod. Res.* **59**(2), 560–575 (2021). <https://doi.org/10.1080/00207543.2019.1697836>
18. Pankratov, A., Romanova, T., Litvinchev, I.: Packing ellipses in an optimized convex polygon. *J. Global Optim.* **75**(2), 495–522 (2019). <https://doi.org/10.1007/s10898-019-00777-y>
19. Pankratov, A., Romanova, T., Litvinchev, I.: Packing ellipses in an optimized rectangular container. *Wireless Netw.* **26**(7), 4869–4879 (2018). <https://doi.org/10.1007/s11276-018-1890-1>
20. Komyak, V., Komyak, V., Danilin, A.: A study of ellipse packing in the high-dimensionality problems. *East.-Eur. J. Enterp. Technol.* **1**(4 (85)), 17–23 (2017). <https://doi.org/10.15587/1729-4061.2017.91902>
21. Romanova, T., Litvinchev, I., Pankratov, A.: Packing ellipsoids in an optimized cylinder. *Eur. J. Oper. Res.* **285**(2), 429–443 (2020). <https://doi.org/10.1016/j.ejor.2020.01.051>
22. Kallrath, J., Rebennack, S.: Cutting ellipses from area-minimizing rectangles. *J. Global Optim.* **59**(2–3), 405–437 (2013). <https://doi.org/10.1007/s10898-013-0125-3>
23. Kallrath, J.: Packing ellipsoids into volume-minimizing rectangular boxes. *J. Global Optim.* **67**(1–2), 151–185 (2015). <https://doi.org/10.1007/s10898-015-0348-6>
24. Gil, M.I., Patsuk, V.M.: Φ -Functions of 2D objects with boundaries being second-order curves. *Cybern. Syst. Anal.* **56**(5), 802–810 (2020). <https://doi.org/10.1007/s10559-020-00301-1>
25. Wächter, A., Biegler, L.T.: On the implementation of an interior-point filter line-search algorithm for large-scale nonlinear programming. *Math. Program.* **106**(1), 25–57 (2006). <https://doi.org/10.1007/s10107-004-0559-y>



Optimization of Design Process Based on 3D-Model

Nataliia Vergunova^(✉)  and Sergey Vergunov 

O. M. Beketov National University of Urban Economy in Kharkiv, 17 Marshala Bazhanova Street, Kharkiv 61002, Ukraine

Natalia.Vergunova@kname.edu.ua

Abstract. This paper aimed to develop the classification with optimized stages of creation the industrial products using parametric 3D modeling. To achieve this goal, powers of research and design should be involved, including CAD software. The scientific novelty of the work lies in a comprehensive study of optimized design process for well-grounded understanding the stages of creation of a new product, for this matter the detailed classification with stages divided by a certain number of levels was presented. The initial stages of design process are characterized by an analysis of requirements, the intermediate stages by a synthesis of planning, and the final stages by an evaluation of proposals. Each stage can be differentiated into multiple levels. Being passed through these levels, industrial designer comprehensively examines the problems of product creation. For this matter, a real example of practical design experience which covers full design process is also considered.

Keywords: Industrial design · CAD Software · SolidWorks

1 Introduction

At the end of the last century, the new principles of the industrial designer's practice were formed. Based on the use of computer technology they were defined by researchers as computer-based tools of industrial design (CAID) [1]. Application of these tools brought clear benefits to the design work and also had a significant impact on the designers themselves. With these tools, modern designers can go through all the stages of design process more efficiently [2, 3].

Parametric modeling is a convenient and intuitive method of creating a conceptual model of a product and eliminates the need to routinely create different types of product with 2D elements – sketches and drawings in the traditional sense [4]. By selecting the desired views and applying the cuts and cross-sections, the drawing lines will be created automatically precise, regardless of the complexity of the geometry. In this way, it is possible to check the internal schematic of the object when needed and avoid mistakes in design process [5].

Obviously, the three-dimensional model is a much more illustrative and visual representation of the item than the two-dimensional sketches and drawings [6]. For CAD

systems there is no problem in obtaining isometric views of different nature, including assemblies. Both designers and customers can use three-dimensional model to accurately estimate the product, check the layout of the components in the assembly structure. The computer tools of industrial design made it possible to bring the concept of “assembly” to a qualitatively new level, giving it the same status in the design practice as it has in the production process [7, 8].

2 The Main Statements of the Paper

The evolution of computer technology has led to a change in the principles of industrial design and the interaction of the specialists involved in this process. Today, the technical preparation of product manufacturing is typically of a high-tech nature, the electronic model rather than a set of design documents is being developed. The electronic model also includes a 3D model created in one of the CAD systems. Therefore, the revision of the methodology of the manufacturing process is now relevant and necessary to accurately determine the place of design and the designer in industrial production. The search for new processes of product creation is relevant as well.

Although most industrial designers follow their own process in developing the aesthetic and ergonomic aspects of the product, there is an objective design algorithm. With it, industrial designers generate a variety of concepts for the subsequent selection of the most successful ones in terms of shaping and functionality, which corresponds to the technological possibilities and user’s needs.

One of such design algorithms represents the defined and science-based stages of creation the industrial products using parametric 3D modeling:

- 1st Stage – preliminary;
- 2nd Stage – conceptual;
- 3rd Stage – variant shaping;
- 4th Stage – system design;
- 5th Stage – prototyping;
- 6th Stage – accompanying;
- 7th Stage – evaluative (de-facto) [9].

This classification was defined in 2010 in the context of industrial design and designer’s practical work. Ten years later, practical experience and the development of project technologies, the emergence of new software modules – all this helps to clarify the semantic significance of this classification:

- 1st Stage – basic information;
- 2nd Stage – conceptual shaping;
- 3rd Stage – system design;
- 4th Stage – accompanying;
- 5th Stage – personal assessment.

Each stage is a set of concrete steps that are subordinate to the main strategic objective of the stage. These steps are equivalent to “immersion” levels of the designer in

design process. The more precise the orientation, quantity and volume of these steps are, the deeper the level of this “immersion”. Therefore, each of the stages can be differentiated into multiple levels. While passing through these levels industrial designer comprehensively examines the problems of product’s creation.

The number of levels, as well as of the stages of the industrial product development may vary depending on its originality on the market, production volume and different regional factors. If it is about product’s upgrade, the first two steps of classification may be excluded. In this case, the appropriate starting-point of design process is the improvement of the old item. Usually the reason for starting this modernization is the low demand for this product. Another major impact on the process of modernization is a possible appearance of a new competitor with similar products on the market. In this case, company’s mission is to satisfy regular customers first. If company is oriented to the development of a leading product as well as to the achievement of market leadership, then all stages of the design process will be involved. Leading products are developed by a successful combination of style and technology. Leading products help create vivid impressions that are highly appreciated by consumers. Leading products create new markets or redistribute the old ones [10].

The initial stages of design process are characterized by an analysis of requirements, the intermediate stages by a synthesis of planning, and the final stages by an evaluation of proposals. Very rarely the developed product is simple enough, so that only a fraction of the stages are sufficient for its development. More often, the developed product passes through all stages of design process and is specified in gradual levels. It might be argued that product/object/item in some sense is developed many times. Thus, the first product sketches can be returned for additional information and then revised again, in the light of the changes and clarifications made. The cycle of analysis, synthesis and evaluation has to be repeated many times: the whole project progresses in a spiral rather than in a straight line. So the design process or, in other words, the creation of a new product or the modernization of an old one by an industrial designer can be named a project spiral. In this case, the control points of the project spiral are the basic levels of the project stages.

Thus, by identifying the main control points – the levels of the project stages – it is possible to define their essence and to determine their number for each stage [11]. These definitions can be illustrated by a practical example of new product development – a shoe dryer “Sugrev” (TermixPro EC 12/220) designed by the authors of the article for the “Kharkiv Shaver Factory” company in 2019–2020.

3 Classification

3.1 1st Stage – Basic Information

This stage may consist of three levels:

- level 1.1 – awareness of marketing and technical requirements; identification and formulation of user needs;
- level 1.2 – research of analogues of designed product;
- level 1.3 – identification of the prototype of designed product.

At this stage it is important to get a marketing task. It begins with a study of the target market segment for which the product will be produced. Marketers determine potential demand and the market segment capacity, in other words, they identify users whose needs are not sufficiently met and bring this information to the designer. The latter should clearly understand market segmentation and the choice of those parts of the market that the future product can serve in the best way possible. After receiving marketing task, the designer becomes aware of the user's problems: this is achieved through the existing methods and ended as documentation of the consumer needs. The next step is to study the analogues, their advantages and disadvantages, and to identify the special points that should be emphasized. The last level of this stage is to define the prototype of the designed product.

Marketers of "Kharkiv Shaver Factory" company provided a task and defined a range of users for the next product (level 1.1). They also prepared a visual set of modern analogues (level 1.2). Designers made an additional, separate search for analogues in the context of a given task, which broadened their knowledge of similar products and helped to define the customer's needs at present stage (level 1.2). All of these indirect analogues were analyzed and systematized, and the dryer "Brownie", produced by the same company and presented in Fig. 1, was chosen as a direct prototype (level 1.3). The first paragraphs that follows a table, figure, equation etc. does not have an indent, either.



Fig. 1. Shoe dryer "Brownie".

3.2 2nd Stage – Conceptual Shaping

This stage may consist of four levels:

- level 2.1 – selection of materials and manufacturing technologies for designed product;
- level 2.2 – conception of designed product;
- level 2.3 – development of 3D-variations of designed product;
- level 2.4 – selection of artistic image and definition of functional qualities designed product.

This stage begins with an awareness of specification with technical and tactical parameters required for the project. This is followed by a selection of materials and

manufacturing technologies. At the same time the information on the technical limitations of selected materials and technologies is collected. Next comes the development of product concept.

The development of 3D-variations of designed item helps to define the final set of the future product functionality. Unlike the traditional “manual” sketching, three-dimensional modeling allows developing more “3D-blanks” variants of designed object in the same time. Three very important points should be considered:

1. CAD-systems provide the opportunity for the designer to work immediately “in the volume”. In “manual” sketching designer has to draw each side of the object separately, hypothetically imagining the shape or performing additional sketches for this purpose. By means of 3D-modeling designer does all the same at once, like on-line mode, in other words, immediately at the same time.
2. The fixed parameters of CAD system provide the possibility to store in memory the history of model development, which allows changing the shape of a surface or a three-dimensional body by changing the numerical values of parameters or replacing elements in its history. In other terms, this design method provides slight adaptation of shaping principles in designed object. It is also possible to make corrections and changes, to work out nuances, to edit the color-texture solution. Sketches made “by hand” are lacking this opportunity.
3. In terms of design, the advantage of three-dimensional modeling is in clear understanding of the outline of designed object. This is peculiar WYSIWYG – What You See Is What You Get [12] – a method of editing when the changes to the object are immediately visible and understood, since the basic structure of the product does not proportionally change (until global changes are made. This is very unlike “manual” sketches, where the representation of the same object can vary considerably.

The essence of the last level of this design stage is in achieving a reasonable balance (compromise) between the outer form (image) and the set of consumer characteristics (function) of the designed object.



Fig. 2. 3D-variations of designed product.

Design engineers and technologists of “Kharkiv Shaver Factory” provided all the necessary information on production equipment and materials operated by this company (level 2.1). In developing the concept of “Sugrev” shoe dryer (level 2.2) one of the factors that influenced its future shape was the avoidance of the child-oriented image of the fabulous bast shoes from folktales. Based on this information, the designers began to develop 3D-variations of designed product (level 2.3) shown in Fig. 2. It should be noted that the dryer was originally designed in 3D, without traditional manual sketching. It was designed in SolidWorks CAD-system with plugin for complex surfaces – Power Surfacing.

Subsequently, the 3D-variations of shoe dryer, shown in Fig. 3 and 4, were refined, taking into account the element base, location and functionality of product. Figure 5 shows final artistic image (level 2.4) that was chosen at last.



Fig. 3. Refined 3D-variation of designed product.

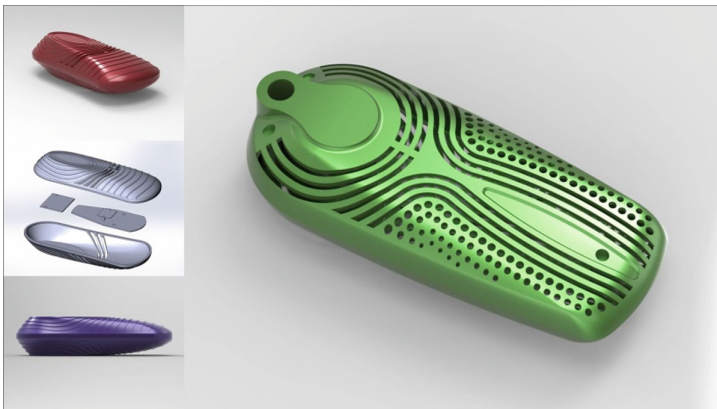


Fig. 4. Refined 3D-variation of designed product.



Fig. 5. Chosen artistic image of shoe dryer.

3.3 3rd Stage – System Design

This stage may consist of four levels: This stage may consist of seven levels:

- level 3.1 – selection of the most appropriate variation of designed product and definition of its structure;
- level 3.2 – definition of the “user – product” interface;
- level 3.3 – color-texture and nuance-figurative solution of designed product;
- level 3.4 – creation of physical or virtual prototype of designed product;
- level 3.5 – technical field tests and adjustment;
- level 3.6 – development of work project;
- level 3.7 – input of parametric 3D model of designed product into manufacturing process.

The result of the “system design” stage is typically a work project consisting of files providing clear and complete understanding of designed product. At this stage, the industrial designer together with the rest of development team – engineers (design engineers and technologists), marketing personnel, sometimes potential users – determines the final version of the future product. Designer also defines the structure of designed product, which is later confirmed by the engineer. The definition of the “user – product” interface is also studied at this stage. To find the solution of particularly complex interfaces, besides consultations with potential users, additional specialists of a narrow profile may be invited. At the same stage, industrial designer refines nuance-figurative and color-texture solution of designed product. Proposed variations for serial production are agreed with the marketing staff.

The main task of prototyping level is to create a prototype of designed product and work out (= prepare) a project for serial production. The key point of this level is a three-dimensional model of the future product made with 3D-printing technologies. In this case, physical prototyping is implied. Prototypes created in this way can be used to evaluate the concept and design of the future product; to analyze its functionality; to

provide the cinematic analysis of its parts; to apply for further technical field tests and to refine the product structure [13, 14].

A virtual prototype of designed product may involve its realistic simulation having material with the relevant physical characteristics for performing the necessary analyses that demonstrate the suitability and efficiency of the product during operation.

In any case, using 3D-modeling and creating a three-dimensional model-prototype eliminates the barriers that separate industrial designers, design engineers, technologists, and production halls. The efficient communication and high level of understanding because of 3D-model and its prototype provides the possibility of making the only sustainable decision while refining and organizing serial production.

After choosing the most appropriate variation of the shoe dryer (level 3.1) represented in Fig. 6, and because of its ease of use, which does not include level 3.2, designers started to work on color-texture and nuance-figurative solution of designed product (level 3.3).



Fig. 6. Final version of shoe dryer.

Design proposals of this level are shown in Fig. 7. The physical prototype of “Sugrev” shoe dryer (Fig. 8) was printed on a 3D printer (level 3.4).

The specialists of “Kharkiv Shaver Factory” provided technical field tests (level 3.5); development of work project (level 3.6); input of parametric 3D model of designed product into manufacturing process (level 3.7). The production model of shoe dryer is shown in Fig. 9.

3.4 4th Stage – Accompanying

This stage may consist of three levels:

- level 4.1 – development of necessary product documentation for designed product;
- level 4.2 – packaging for designed product;
- level 4.3 – advertising and multimedia output for designed product.

The stage is an organic part of the manufacturing process based on three-dimensional model, covering the development of packaging and accompanying documentation, as well as advertising and multimedia output. Complex solutions are in demand on the market today. Designer, the one who created the product, should be able to design



Fig. 7. Color-texture solutions of shoe dryer.



Fig. 8. Physical prototype of shoe dryer.

packaging system for this product; to explain to the user the principles of working with it – functionality, possibilities and management methods.

At first level of the accompanying stage, industrial designer may act as the coordinator for the development of required product documentation for designed product in a group of marketers and engineers. At this level, designer has to “teach” the potential consumer to use the proposed product, understand its functional algorithms. At second level, the leading industrial designer may invite a graphic designer to design the packaging if necessary. At third level, the leading industrial designer may invite a multimedia designer to create advertising and multimedia output (commercials for Television and Internet). In the part of “Sugrev” shoe dryer project, all levels of the fourth stage were developed



Fig. 9. Production model of shoe dryer.

concerning preparation of serial production. It should be noted that the last levels of the third and fourth design stages of proposed classification may occur simultaneously through the three-dimensional modeling.

3.5 Stage – Personal Assessment

This stage may consist of three levels:

- level 5.1 – design evaluation of proposed product;
- level 5.2 – upcycling;
- level 5.3 – recycling.

The stage does not directly concern the process of manufacturing products based on the three-dimensional model. This stage is evaluative and, above all, is more important for self-improvement of designer and for the development of professional skills. In the current market economy the “personal assessment” stage is useful for personal understanding of the level of professionalism and its adequacy in the context of a group of designers involved in product development or colleagues from the design community of one’s city/country. Evaluation of design of the final product is subjective in nature, but it is also possible to determine, at a qualitative level, whether the objectives have been achieved by considering those aspects of the product that are influenced by industrial design [15]. Since the process is subjective and primarily depends on the identity of the designer, different methods are used to make this analysis possible.

One can take an advantage of the product evaluation categories corresponding to the five main design objectives formulated by Dreyfuss in 1967 [16] or focus on the ten principles of good design by Rams (designer of “Braun” company) [17]. Personal criteria of product evaluation can be defined as well. In any case, the self-assessment of the quality of designed product will help to improve personal professionalism.

“Upcycling” and “Recycling” can be considered as two basic approaches of “Sustainable design” aimed at design of spatial environment corresponding to the principles of economic, social and environmental sustainability [18]. In case of “Recycling”, the unused object is recycled into a secondary raw material, which serves as the material for the development of new product. During the “Upcycling” process, the unused object is only purified and disinfected, and subsequently acquires new functional and aesthetic significance due to designer’s work.

The stage of personal assessment was not fully provided towards “Sugrev” shoe dryer. As a separate aspect it is possible to consider the originality of shape of designed product with the extended number of slots and efficient air exchange as a result, for better functioning. The shoe dryer is designed to maximize its useful life, it is serviceable, and the company provides warranty and certified repair services, extending the life of the product. The patent for industrial sample №39751 was obtained for this product on the territory of Ukraine in 2019 [19].

4 Conclusion

The design process of a product based on 3D-model by means of CAD systems has prospects for further development and improvement. Even today, a modern designer is able to create detailed concepts more quickly in large numbers, which can lead to innovative design solutions. Visual realism of computer tools (virtual reality) can increase the efficiency of information exchange among members of the development team and help to eliminate much of the inaccuracy inherent in “manual” sketches traditionally created by designers.

To improve this process, it is necessary to understand the stages of creation of a new product. To achieve this goal, the classification with five stages divided by a certain number of levels was presented. The suitability of these stages was demonstrated by practical design work. First four stages (basic information; conceptual shaping; system design and accompanying) are directly incorporated into manufacturing process. The last – fifth stage (personal assessment) is rather optional and primarily important for self-improvement of designer and for the development of professional skills.

Analytical part of the paper and systematized contemporary design practice can be used in professional training of industrial designers in the higher education system. Writing educational materials and developing specialized training courses also might be considered. The future research is planned to focus on the application and refinement of the identified stages and classification in the development of not a single solution of designed object, but the complex, the ensemble of objects.

References

1. Tovey, M.: Drawing and CAD in industrial design. *Des. Stud.* **10**(1), 24–39 (1989). [https://doi.org/10.1016/0142-694X\(89\)90022-7](https://doi.org/10.1016/0142-694X(89)90022-7)
2. Shyshkin, E., Viatkin, K., Haiko, Y.: Basic methodical design stages of renovation of municipal industrial development. *IOP Conf. Ser.: Mater. Sci. Eng.* **962**(3), 032055 (2020). <https://doi.org/10.1088/1757-899X/962/3/032055>
3. Kondratiev, A., et al.: Self-heating mold for the composite manufacturing. *Polymers* **13**(18), 3074 (2021). <https://doi.org/10.3390/polym13183074>
4. Chahid, Y., et al.: Parametrically designed surface topography on CAD models of additively manufactured lattice structures for improved design validation. *Addit. Manuf.* **37**, 101731 (2021). <https://doi.org/10.1016/j.addma.2020.101731>
5. Nzetchou, S., Durupt, A., Remy, S., Eynard, B.: Semantic enrichment approach for low-level CAD models managed in PLM context: Literature review and research prospect. *Comput. Ind.* **135**, 103575 (2022). <https://doi.org/10.1016/j.compind.2021.103575>
6. Vergunova, N., Vergunov, S.: Optimal model of transportation for people with disabilities: conceptual proposal designed in CAD. *Adv. Comput. Des.* **5**(4), 381–396 (2020). <https://doi.org/10.12989/acd.2020.5.4.381>
7. Favi, C., Mandolini, M., Campi, F., Germani, M.: A CAD-based design for manufacturing method for casted components. *Procedia CIRP* **100**, 235–240 (2021). <https://doi.org/10.1016/j.procir.2021.05.061>
8. Junk, S., Burkart, L.: Comparison of CAD systems for generative design for use with additive manufacturing. *Procedia CIRP* **100**, 577–582 (2021). <https://doi.org/10.1016/j.procir.2021.05.126>
9. Vergunov, S.: 3D-modeling in Ukrainian industrial design at the end of XX and at the beginning of XXI century. Dissertation, Kharkiv State Academy of Design and Arts (2010). [in Ukrainian]
10. Kim, K., Lee, K.P.: Collaborative product design processes of industrial design and engineering design in consumer product companies. *Des. Stud.* **46**, 226–260 (2016). <https://doi.org/10.1016/j.destud.2016.06.003>
11. Vergunov, S.: *Ukrainian Industrial Design: An Inside Look*. Fedorko, Kharkiv (2019). [in Russian]
12. Myers, B.A.: A brief history of human-computer interaction technology. *Interactions* **5**(2), 44–54 (1998). <https://doi.org/10.1145/274430.274436>
13. Skliarov, V., Neyezhnikov, P., Prokopov, A.: Metrological assurance and traceability for Industry 4.0 and additive manufacturing in Ukraine. *Smart Structures and NDE for Industry 4.0* 10602, 114–122 (2018). <https://doi.org/10.1117/12.2292821>
14. Gebhardt, A., Kessler, J., Thurn, L.: *3D Printing: Understanding Additive Manufacturing*. Hanser Publishers, Munich (2019)
15. Ulrich, K.T., Eppinger, S.D., Yang, M.C.: *Product Design and Development*. McGraw-Hill Education, New York (2020)
16. Dreyfuss, H.: *Designing for People*. Skyhorse Publishing Company, New York (2012)
17. Lovell, S.: *As Little Design as Possible*. Phaidon Press, London (2011)
18. Tao, J., Li, L., Yu, S.: An innovative eco-design approach based on integration of LCA, CAD\CAE and optimization tools, and its implementation perspectives. *J. Clean. Prod.* **187**, 839–851 (2018). <https://doi.org/10.1016/j.jclepro.2018.03.213>
19. Voronyi, A.S., Vergunov, S.V., Vergunova, N.S.: Shoe dryer. UA Patent 39751, 25 Jul 2019



Pulse Wave Propagation Velocity and Assessment of Arterial Vessel Elasticity

Volodymyr Kyrychenko^{1,2} , Tetiana Kulbashevskya³ , Viktor Sergeiev^{2,3}  ,
and Lidiia Piddubna³ 

¹ National Aerospace University “Kharkiv Aviation Institute”, 17 Chkalova Street,
Kharkiv 61070, Ukraine

² XAI-Medica Ltd., 4 Zoriana Street, Kharkiv 61070, Ukraine
sergeev@xai-medica.com

³ O. M. Beketov National University of Urban Economy in Kharkiv, 17 Marshala Bazhanova
Street, Kharkiv 61002, Ukraine

Abstract. Evaluation of arterial elasticity is still an urgent task, and the most commonly used and recommended method for this is based on the assessment of pulse wave propagations velocity (PWPV) in the arterial vessels. Unfortunately, this strategy does not fully meet modern requirements due to insufficient accuracy and instability of the results obtained. The analysis of the main sources of errors in the assessment of PWPV of arterial vessels was carried out and ways of their neutralization were proposed. The accuracy of the PWPV estimate can be improved by using the high frequency component of the pulse wave to estimate the time delay. Experimental data, obtained using the “ReoCom” rheographic complex, confirm the correctness of the proposed strategy.

Keywords: Cardiovascular diseases · Rheogram · Velocity of pulse wave propagation · Elasticity of arterial vessels · Peripheral resistance

1 Introduction

Today it is well-known that one of the main early risk factors for cardiovascular diseases and their complications is a decrease in the elastic properties of the walls of arterial vessels [1–4].

Under pulsing of blood flow in the arteries, energy loss of cardiac myocardium for blood transportation becomes substantially smaller just for elastic vessels [5, 6]. This is most noticeable in the presence of the necessary consistency of the elasticity of the arteries with the mass of blood spreading through the vessels, the heart rate and the value of the peripheral resistance [7].

For the purpose of early detection of atherosclerosis and a number of other vascular diseases, various methods of assessing elastic properties of the vascular wall were developed, and one of the most widely used today was the method of the pulse wave propagations velocity (PWPV) measuring [8, 9] in the vascular bed section of interest, most often from the aorta to the vascular area under study.

2 Suggested Methodology for PWPV Assessing

The most commonly used methods for recording pulse waves and measuring PWPV are ultrasound, sphygmography, rheography, or photoplethysmography [10–12]. Synchronous registration of pulsations in different parts of the body allows one to assess PWPV along the course of an arterial vessel located under selected points of the body. For this reason, the time delay Δt between the equivalent points of pulse waves recorded and the distance between points on body.

Unfortunately, regardless of the used method of pulse waves registration in distant points of the body, we will face the same problem – **finding equivalent pulse waves points registered in different points of the body, under conditions of pulse waveform changes during its propagation along the arterial vessel.**

It is evident that arterial system can be considered as some low pass filter (LPF) filter model provoking different attenuations and phase shifts for different spectral components contained in the pulse wave at each specific part of arterial channel, and, therefore provoking the changes of pulse wave under its propagation in the vessel [7, 13]. The found equivalent points of pulse waves can only be apparent equivalents! It was shown in [13] that the position of the minimum of the recorded pulse wave can differ significantly from the real beginning of the pulse wave, therefore, the traditional method for assessing the state of the arterial wall by PWPV will give significant errors due to the impossibility of accurately determining the time delay PW in the vessel under study.

For each vascular region, the error will be strictly individual, depending on the elasticity of the particular artery, the mass of blood moving in it, the value of peripheral resistance of the region, etc. The magnitude of the error will vary from 0, in the smallest arteries, to 70...90 ms in the aorta. Hence, the measurement error in the time interval of pulse wave propagation can be commensurable with per se of propagation time [13].

Unfortunately, this method has existed virtually unchanged for many decades, although the obtained results are far from satisfactory.

Undoubtedly, PWPV could be a very informative indicator of arterial wall condition [14–16], however, it is necessary to find a way to minimize the errors that arise when determining the equivalent points of pulse waves.

This paper is devoted to a new approach to estimating the delay time of a pulse wave, based on the decomposition of a rheosignal into low-frequency and high-frequency components. This makes it possible to reduce the error in determining the delay time of the pulse wave and improve the quality of arterial elasticity assessment.

3 Discussion of the Experimental Results

Experimental records obtained using the “ReoCom” diagnostic complex”, designed by XAI-Medica Ltd., Ukraine [17, 18], are shown below in Fig. 1–3. First, let us consider typical aorta rheogram represented in Fig. 1 (upper curve). The graph of this rheogram first derivative is demonstrated below in Fig. 1.

At what point in time does the aortic valve open, the ejection period begins, and a pulse wave occurs in the aorta? It seems absolutely evident, that everything occurs at the time moment marked by the symbol **a** in the Figures. That is when the aortic cross section

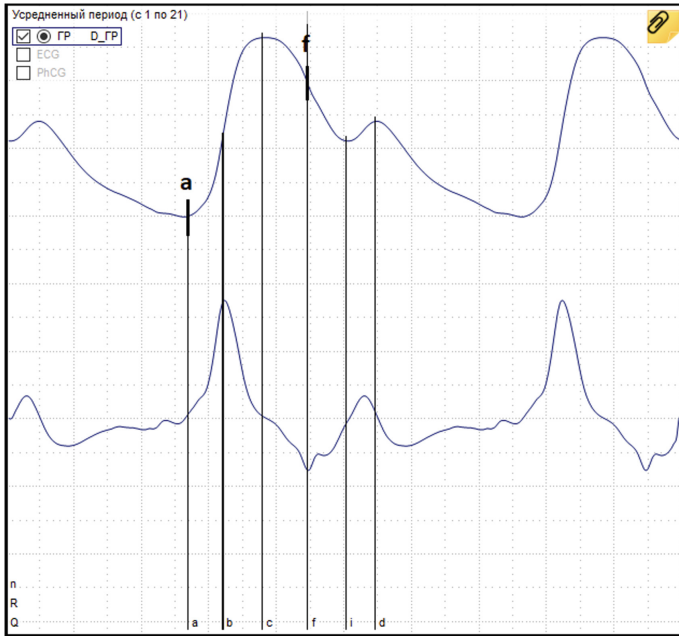


Fig. 1. Aorta rheogram and its first derivative.

begins to increase. What other reason can provoke increasing of aorta cross-section if not unlocking the aortic valve?

We note a few more characteristic points of the considered rheogram. Marker **b**, coinciding with the maximum of the first derivative of the rheogram, marks the moment of the highest rate of aortic blood filling. Marker **c** denotes the moment of greatest stretching of the aortic wall, when the amount of blood coming from the left ventricle into the aorta becomes equal to the amount of blood leaving the aorta through numerous main arteries.

So, suppose that at the moment **a** (the minimum of the rheogram), the aortic valve opens and the aorta cross section begins to increase under the influence of the blood flow coming from the ventricle. During the time interval **a–c**, the amount of blood entering the aorta is greater than the amount of blood going to the periphery, as a result of which the aorta expands and an anacrotia is formed. Further, the amount of blood leaving the aorta becomes greater than that coming from the left ventricle, and the aorta begins to shrink.

At the moment, marked by symbol **f** in the graphs, aortic valve locks up. Appearance of dicrotic tooth can be clearly seen in the below graph of the first derivative shown in Fig. 1. Arrival of blood in the aorta from ventricle lapses and aorta continues to shrink ejecting blood in the main vessels. It continues till to the moment marked by the symbol **i** when cross-section of aorta again begins to increase.

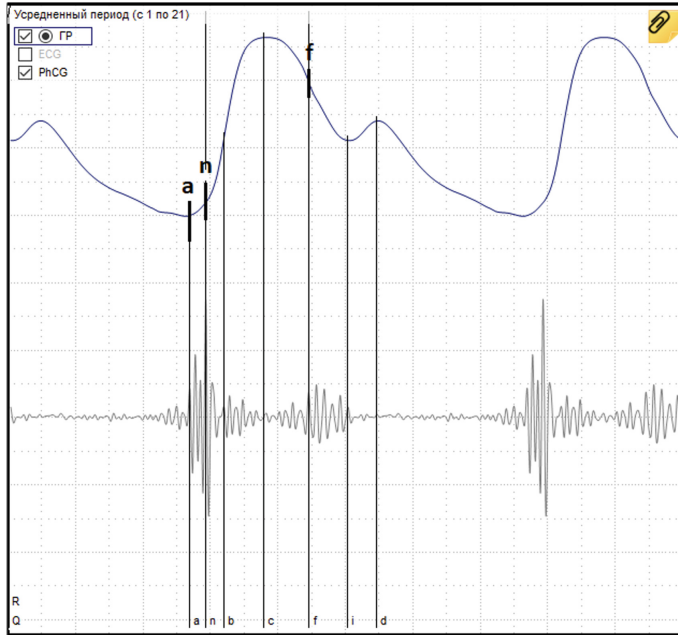


Fig. 2. Aorta rheogram and phonocardiogram.

The following question is arising: where does the blood come from that fills the aorta when the aortic valve is already locked? There can only be one explanation. Through the main arteries into the aorta comes a wave of reflection from the peripheral resistance.

The main arteries return blood to the aorta! It turns out that blood can move through the arteries in both directions! Although, this is not surprising. After all, it has long been known about the mechanism of redistribution of blood flow in the arterial system when the peripheral resistance of the region under load falls. Redistribution is carried out due to the discharge of a certain amount of blood from unloaded regions into the aorta (due to an increase in the tone of the corresponding arterial vessels), and the direction of the generated reflection wave in the area with reduced peripheral resistance.

Now back to the question about beginning of the pulse wave in aorta. Below curve demonstrated in Fig. 2 represents the phonocardiogram recorded synchronously with rheogram. First tone of the phonocardiogram is located within the time interval of anacrotia contained in the rheogram (see Fig. 2). It is well-known [7], that the most high-magnitude oscillations of the first tone correspond to the lock moment of the mitral valve. This time moment is marked by symbol **n** in Fig. 2. The pressure value represent on the graph after marker **n** continues to increase. Approximately during 20...30 ms after the marker **n**, the pressure reaches the diastolic value in aorta. Just in this moment, i.e. in 20...30 ms after the marker **n** in Fig. 2, aortic valve begins to open. This time moment is denoted by the marker **a1** in Fig. 3. It is clear that it is at this point that the ejection period begins and the formation of the pulse wave in the aorta begins.

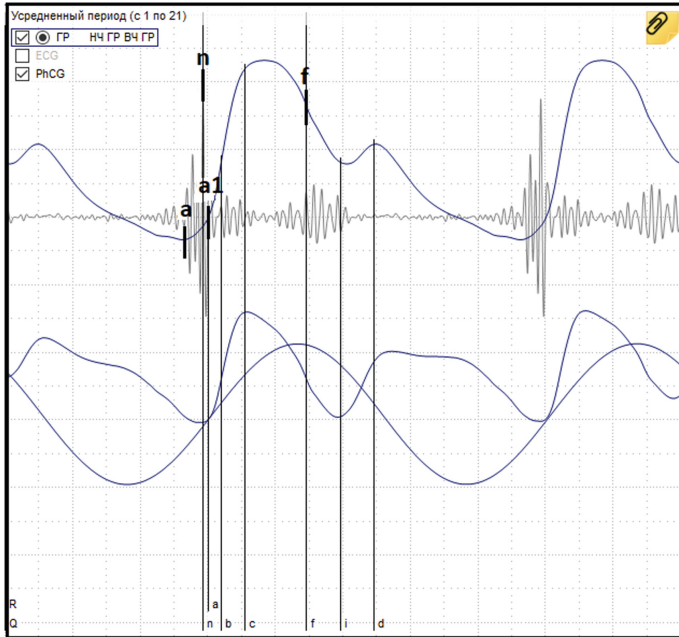


Fig. 3. Aortal rheogram ant its decomposition on low and high frequency components.

It can be clearly seen from Fig. 3 that real beginning of pulse wave (see the location of marker **a1**) has nothing common with rheogram minimum (see the marker **a** in Figs. 1, 2 and 3). Point **a1** in Fig. 3 turned out to be an unremarkable point located in the rising length in the aorta rheogram and significantly displaced relative to the rheogram minimum (point **a**). In the case of the absence of phonocardiogram, considerable errors appear for determination of ejection period and beginning of pulse wave in aorta. These parameters are of very importance for determination of the stroke volume. Noted errors can provoke an error for determination of the pulse wave time delay (approximately of 60 ms), and considerable error for determination of velocity of pulse wave and elasticity of studied main vessels.

So, the minimum of the rheogram can in no way be considered as the beginning of a pulse wave.

Thanks to the phonocardiogram, true beginning of pulse wave in aorta was nevertheless found. However, the following question is arising: what to do for determination of pulse wave beginning in arteries belonging to some other vascular area where phonocardiogram will not be able to help?

Conclusion: the classical method of determining the state of the arterial wall of the main artery by the speed of propagation of the pulse wave in the vessel will give significant errors due to the impossibility of accurately fixing the moments of the beginning of the pulse wave, and, therefore, the impossibility of accurately determining the delay time of the wave when it propagates in the vessel under study.

And one more question: at the cost of what the point of visual beginning of pulse wave was formed (see point **a** in Figs. 1, 2 and 3) and on what depends the value of the shift related to the true beginning of pulse wave from the apparent point?

As C. Caro [7] states when considering the process of pulse wave propagation in the arterial system, – “The wave is more and more delayed relative to the pressure wave directly at the ventricular exit, but, in addition, its amplitude increases significantly and its shape changes”.

It means that arterial system cannot be considered as broadband structure within the frequency range belonging to the pulse wave. Amplitude-frequency characteristic of arterial system has a considerable rise in the low-frequency range. One can say that preferable conditions exist in arterial system for the most low-frequency oscillations contained in the pulse wave spectrum or in rheosignal in the considered case. This means that these fluctuations are slower to decay, and therefore last longer in the arterial system. They interfere with oscillations that are the echoes of oscillation processes related to the previous period. They sum up with reflected oscillations arising by reflection from peripheral resistance. Their magnitudes and phases are varied not only due to the propagation in arterial system with some decay but also under influence of oscillations that are interfered with and that can be formed in sufficiently remote vascular zones.

On the other hand, high-frequency components contained in the pulse wave represent short-time living components. They decay quickly for propagation of the pulse wave. They correspond to the result of the arrival of only last disturbance, i.e. pulse wave last coming. Due to the noted reasons, the amplitude and phase changes in the high-frequency and low-frequency components of the rheosignal will be different when they propagate in the same area of vascular system. Phase of high-frequency contribution will be determined by only phase shift cause by wave propagation. At the same time, the phase of the low-frequency contribution will be determined both by the phase shift caused by the propagation of the pulse wave, and by the phase shift that occurs when the pulse wave is reflected from the periphery, and by the phase shift due to the summation of oscillations of all previous periods. It is clear that the moment of true pulse wave onset will be related exactly to the beginning of growth of the high-frequency component of the pulse wave. Time location of this beginning point will be related only with pulse wave propagation time in the artery channel. It will not depend on the reflection wave from the periphery and the echoes of the oscillatory processes of previous periods.

Taking into account the peculiarities expressed above, it is easy to explain the aorta rheogram minimum shift observed in Figs. 1, 2 and 3 relatively time marker **a1** situated in Fig. 3. The shift is due to the fact, that the beginning of the pulse wave coincides precisely with the beginning of the high-frequency contribution contained in the pulse wave. The **a1** point defines true moment of unlocking of aortal valve and beginning of pulse wave forming in aorta.

Signal growing observed after the point **a** in Figs. 1, 2 and 3 is defined by low-frequency contribution contained in the rheosignal. The latter contribution is formed by summation of low-frequency contribution contained in rheosignal and caused by last heartbeat and low-frequency contribution contained in the rheosignal and caused by reflection from peripheral resistance, as well as low-frequency contribution caused by the echoes of all early existing heartbeat periods. It is clear that the shift of point **a1** in Fig. 3

relative to the rheogram minimum can vary significantly with changes in the peripheral resistance of the studied area. This peculiarity will appear more evidently in the vessels with high elasticity of the sides and large mass of moving blood. As mentioned above, the displacement can reach 60...70 ms, and constitute a significant part of the whole time of pulse wave propagation from the aortic arch to the studied area. It means that the errors related to the estimation of the elasticity of arterial wall can be of large values. The errors will be rather evident in the large vessels with high elasticity and big mass of moving blood.

4 Conclusion

Unfortunately, the most used nowadays method for diagnostics of arterial side condition by evaluation of the velocity of pulse wave propagation in the studied vessel provokes considerable errors. They caused by impossibility of accurate fixation of the pulse wave beginning moments in the studied points. As a result, it is impossible to accurately determine the lag time of the wave during its propagation in the investigated vessel.

This means that the classical method for determining the stiffness of the arterial wall of the main artery by the velocity of the pulse wave in the vessel cannot be used for a high-precision assessment of the state of the arterial vessel wall.

The errors arising in the estimation of PWPV can be significantly reduced by the proposed decomposition strategy for extracting both low-frequency and high-frequency contributions from the pulse wave, and by determining the time delay not between points related to the minimums of rheograms, but between equivalent points corresponding to the beginning high-frequency components of rheograms recorded at points of interest in the arterial system.

References

1. Bai, Y., et al.: Comparison of risk of target organ damage in different phenotypes of arterial stiffness and central aortic blood pressure. *Frontiers in Cardiovascular Medicine* **9**, 839875 (2022). <https://doi.org/10.3389/fcvm.2022.839875>
2. Yu, S., McEniery, C.M.: Central versus peripheral artery stiffening and cardiovascular risk. *Arterioscler. Thromb. Vasc. Biol.* **40**(5), 1028–1033 (2020). <https://doi.org/10.1161/ATVBAHA.120.313128>
3. Kusche, R., Klimach, P., Ryschka, M.: A multichannel real-time bioimpedance measurement device for pulse wave analysis. *IEEE Trans. Biomed. Circuits Syst.* **12**(3), 614–622 (2018). <https://doi.org/10.1109/TBCAS.2018.2812222>
4. Koivistoinen, T., et al.: Pulse wave velocity predicts the progression of blood pressure and development of hypertension in young adults. *Hypertension* **71**(3), 451–456 (2018). <https://doi.org/10.1161/HYPERTENSIONAHA.117.10368>
5. Starodumov, I.O., et al.: Modelling of hemodynamics in bifurcation lesions of coronary arteries before and after myocardial revascularization. *Phil. Trans. R. Soc. A* **380**(2217), 20200303 (2022). <https://doi.org/10.1098/rsta.2020.0303>
6. Gamilov, T., et al.: Computational analysis of coronary blood flow: the role of asynchronous pacing and arrhythmias. *Mathematics* **8**(8), 1205 (2020). <https://doi.org/10.3390/math8081205>

7. Caro, C.G., Pedley, T.J., Schroter, R.C., Seed, W.A.: *The Mechanics of the Circulation*. Cambridge University Press, Cambridge (2012)
8. Shokawa, T., et al.: Pulse wave velocity predicts cardiovascular mortality findings from the Hawaii-Los Angeles-Hiroshima study. *Circ. J.* **69**(3), 259–264 (2005). <https://doi.org/10.1253/circj.69.259>
9. Naka, K.K., et al.: Flow-mediated changes in pulse wave velocity: a new clinical measure of endothelial function. *Eur. Heart J.* **27**(3), 302–309 (2006). <https://doi.org/10.1093/eurheartj/ehi619>
10. Antonchuk, O.N., Nasedkin, K.V., Sharonov, V.B., Shulgin, V.I.: Arterial blood pressure evaluation based on joint processing of the vital signs parameters. *Telecommunications and Radio Engineering* **75**(18), 1679–1693 (2016). <https://doi.org/10.1615/TelecomRadEng.v75.i18.70>
11. Viunytyskiy, O., Shulgin, V., Sharonov, V., Totsky, A.: Non-invasive cuff-less measurement of blood pressure based on machine learning. In: 2020 IEEE 15th International Conference on Advanced Trends in Radioelectronics, Telecommunications and Computer Engineering (TCSET), pp. 203–206. IEEE, Lviv-Slavske (2020). <https://doi.org/10.1109/TCSET49122.2020.235423>
12. Nabeel, P.M., et al.: Local pulse wave velocity: theory, methods, advancements, and clinical applications. *IEEE Rev. Biomed. Eng.* **13**, 74–112 (2019). <https://doi.org/10.1109/RBME.2019.2931587>
13. Sergieiev, V.G., Kiselgov, E.N.: Assessment of the vascular system state on the results of rheographic measurements. *Herald of Epileptology* **1**, 49–62 (2007). [In Russian]
14. Karageorgos, G.M., et al.: Arterial wall mechanical inhomogeneity detection and atherosclerotic plaque characterization using high frame rate pulse wave imaging in carotid artery disease patients in vivo. *Phys. Med. Biol.* **65**(2), 025010 (2020). <https://doi.org/10.1088/1361-6560/ab58fa>
15. Lee, J.G., Joo, S.J.: Arterial stiffness and cardiovascular risk. *The Korean Journal of Internal Medicine* **34**(3), 504–506 (2019). <https://doi.org/10.3904/kjim.2019.110>
16. Hasegawa, H.: Analysis of arterial wall motion for measurement of regional pulse wave velocity. *Japanese Journal of Applied Physics* **57**(7S1), 07LF01 (2018). <https://doi.org/10.7567/JJAP.57.07LF01>
17. Pechenin, A., Kyrychenko, V., Kulbashevskyi, V., Kiselgov, E.: Development of telemedicine system telecom for remote monitoring of patients. *Telecommunications and Radio Engineering* **76**(1), 87–94 (2017). <https://doi.org/10.1615/TelecomRadEng.v76.i1.70>
18. Yukhymenko, L., et al.: Link between brain circulation and nervous mobility of athletes and non-athletes during the orthostatic test. *Journal of Physical Education and Sport* **20**(6), 3660–3670 (2020). <https://doi.org/10.7752/jpes.2020.06493>



Mathematical Modeling of Signal Detection in Non-gaussian Correlated Noise

Daniil Smirnov , Elena Palahina , and Volodymyr Palahin ^(✉) 

Cherkasy State Technological University, 460 Shevchenka Boulevard, Cherkasy 18006, Ukraine
v.palahin@chdtu.edu.ua

Abstract. The development of signal detection systems requires complete information about the type of random processes distributions in communication channels with noise. One of the advanced approaches that allows describe random processes is the use of moment and cumulant description of random variables. This approach makes it possible to significantly simplify the synthesis of signal detection systems in noise with a different type of distribution function. The authors of paper proposed the synthesis of the new cumulant models and methods for signal detection in additive correlated non-Gaussian noise. A stochastic polynomial of finite degree was used to synthesize a decision function, the optimal coefficients of which are found according to the adapted new moment quality criterion decision making. The nonlinear processing of signals in noise and taking into account the parameters of correlated non-Gaussian noise in the form of one-dimensional (1D) and two-dimensional (2D) moments can increase the signal processing efficiency compared to traditional Gaussian random process models.

Keywords: Signal detection · Moment and cumulant description · Correlated non-Gaussian noise

1 Introduction

The development of advanced signal detection systems is of great importance for design and synthesis of communication systems, navigation and radar systems, control systems, etc. [1–3]. For development of new signal detection systems it is necessary to take into account the random distribution of signal which are random under the influence of various types of noise. Classical methods of the statistical hypothesis testing theory are used. According to this theory to solve the problem any kind of distribution density of random processes can be used [4]. The use of normal distribution of random variables has become widespread in practice in the implementation of signal detection systems. However in many cases it becomes impossible to display the real processes with the required accuracy. The action of various destabilizing factors on signals, a complex of noise during multipath propagation of signals, their passage through inhomogeneous media, fluctuation the communication parameters of channels generate a complex signal-noise situation, which is described by non-Gaussian random processes [5]. The use of

the traditional approach to the research and development of systems for processing random non-Gaussian processes is characterized by significant limitations associated with the complexity of their algorithmic implementation. Complications with the classical approach are also due to the fact that random processes can be correlated non-Gaussian random processes [5]. In practice, problems with a limited range of observations often arise, where statistical relationships of random values of a random variable cannot be ignore.

One of the methods of solving the problem is the method of using the probability density function, which is used to describe the random processes. A method based on a threshold system designed to detect a deterministic signal with independent non-Gaussian noise is proposed, the probability density functions are unknown but they are symmetric and unimodal [6]. This method is confirmed by taking a large number of samples in the presence of white noise and low signal. For a specific probability density function as a special correlation detector with strict restrictions different options for signal processing are presented [7]. Based on the suprathreshold stochastic resonance [8], the nonlinear correlative detector is composed of a matched filter. In [9] the structure of a suboptimal detector with a parallel array of two-stage quantizers in non-Gaussian noise is given. A signal detection process based on the probability density function in correlated non-Gaussian noise is presented [10]. Probability density functions are due to limitations and difficulties in calculations, although they have a detailed description of stochastic processes.

The properties of decision functions can be characterized using indicators such as the variance of decision rules and the mean. For example, the deflection criterion in the class of linear-quadratic ($L-Q$) systems has been developed [11–13].

A detailed description of this criterion is given in [14]. But the classical criterion is rather weakly connected with the criterion of deviation and its modifications and does not reveal all the properties of decision-making rules.

The paper proposes another approach, which is based on the moment-cumulant description of random processes. This greatly simplifies their description and takes into account the non-Gaussian distribution density. The aim of the paper is to increase the efficiency of signal detection systems in correlated non-Gaussian noise based on the use of joint moment-cumulant models for representing random variables with the formation of a moment quality criterion for statistical hypotheses testing and polynomial rules for the synthesis of effective methods and computer tools.

2 Moment and Cumulant Models of Correlated Non-gaussian Processes

A multidimensional (denote as MD) probability density function (PDF) is a general mathematical representation of a statistically dependent stochastic process $\xi(t)$. But the PDF is not always known and there may be some difficulty with the estimation of parameters $(\vartheta_1, \vartheta_2, \dots, \vartheta_n)$ function. The method based on cumulant characteristics can be used to describe the properties of such process [15–18]. One-dimensional (denote

as 1D) moments m_i of a random variable ξ are defined via the use of PDF $p(\xi)$

$$E(\xi^i) = \int_{-\infty}^{\infty} \xi^i p(\xi) dx. \quad (1)$$

The MD PDF can represent of statistically dependent random variables [19]. Very often two-dimensional (2D) PDF is taken to describe the statistical characteristics of the relationship of random variables:

$$E(\xi_1^i \xi_2^j) = \int_{-\infty}^{\infty} \int_{-\infty}^{\infty} \xi_1^i \xi_2^j p_2(\xi_1, \xi_2) dx. \quad (2)$$

We can imagine that there are sample values of a stationary random process, and there it is possible to consider individual random variables as sample values. On practice, a widely used example of the statistically dependent values is the relationship for two random variables. The 2D PDF can be use in this case. Take the case of two independent random variables ξ and η with p_ξ and p_η PDF respectively. Then the initial moments of order i look like:

$$m_i^{(\xi)} = E\xi^i = \int_{-\infty}^{+\infty} x^i p_\xi(x) dx, \quad m_i^{(\eta)} = E\eta^i = \int_{-\infty}^{+\infty} y^i p_\eta(y) dy. \quad (3)$$

The random variable ξ and η have the joint moments (i, j) of dimension because they depend on each other. For non-Gaussian statistically independent random variables (let zero mean and variance χ_2) the relationship between the initial moments m_i and cumulants χ_i to fourth order look like

$$m_1 = 0, m_2 = \chi_2, m_3 = \chi_3, m_4 = \chi_4 + 3\chi_2^2. \quad (4)$$

For Gaussian process the cumulants of third, fourth and higher order (χ_3, χ_4, \dots) are equal to zero. For the relationship between samples will be used the joint moments $m_{i,j}$ and cumulants $\chi_{i,j}$ to fourth order:

$$m_{1,1} = \chi_{1,1}, m_{1,2} = \chi_{1,2}, m_{1,3} = \chi_{1,3} + 3\chi_2\chi_{1,1}, m_{2,2} = \chi_{2,2} + \chi_2^2 + 2\chi_{1,1}^2 \quad (5)$$

Note that for the signal detection problem the moment and cumulant description models requires additional research and development. It is possible to make a certain classification, to decompose into certain classes cumulants of ordinary characteristic function with common properties. Let us present some classification of random non-Gaussian variables, which is called as punched random variables. In classes of uncorrelated non-Gaussian random processes based on the punched random variables were proposed and approved [18]. The moment and cumulant models are represented by only a part of the cumulants of all possible sets that correspond to the actual process.

According to the accepted classification there are asymmetrical, excess and asymmetrical-excess random variables of various kinds [18–21].

This paper proposes the development of new models of moments and cumulants of non-Gaussian statistically dependent random variables. On the basis of this models, it

is possible to create signal detection methods using the adapted new moment quality criterion for statistical hypothesis testing [21, 22]. Such methods differ from the classical ones and use cumulant functions of higher orders for taken into account properties of non-Gaussian correlation random processes. Such methods will be used to create a decision rule (DR) of signal detection in correlated non-Gaussian noise.

3 The Moment Quality Criterion Decision Making

Let the random signals $\xi(t)$ be in the time interval $(0, T)$. It is necessary to develop the signal processing algorithms of the stochastic process $\xi(t)$ based on the decision making: a "Yes" the signal $s(t)$ (hypothesis H_1) or a "No" signal (hypothesis H_0) in the input stochastic process $\xi(t)$, where $\xi(t) = s(t) + \eta(t)$, $\eta(t)$ is a stationary correlated non-Gaussian random process that describes the set of cumulants and moments.

We will assume that such the set of moments for hypothesis H_1 will have the form $(m_i^{(v)}, m_{i,j}^{(\tau)})$, and for hypothesis H_0 $(u_i^{(v)}, u_{i,j}^{(\tau)})$, where $\{u_i^{(v)}, m_i^{(v)}\}$ - 1D moments at the time t_v of order i and $\{u_{i,j}^{(\tau)}, m_{i,j}^{(\tau)}\}$ - 2D joint moments of the (i, j) dimension for hypothesis H_0 and H_1 respectively.

The sampling signal $\xi(t)$ of the discrete values $\mathbf{X} = \{x_1, x_2, \dots, x_n\}$ at time t_v for hypothesis H_0 and H_1 look like:

$$\begin{aligned} H_1 : \xi_v &= s_v(\alpha_k) + \eta_v(\gamma_k, \chi_{i,j}^{(\tau)}), \\ H_0 : \xi_v &= \eta_v(\gamma_k, \chi_{i,j}^{(\tau)}), \quad v = \overline{1, n}. \end{aligned} \quad (6)$$

where $s_v(\alpha_k)$ is the useful signal with parameters α_k , $\eta_v(\gamma_k, \chi_{i,j}^{(\tau)})$ is the non-Gaussian random variable with parameters in form of cumulants $\chi_{i,j}^{(\tau)}$, $k = \overline{1, \mu}$.

The Bayesian signal detection algorithm is determined as minimum average risk [1–3]. Then the likelihood ratio look like in the form

$$\Lambda(\mathbf{X}) = P(\mathbf{X}|H_1)/P(\mathbf{X}|H_0). \quad (7)$$

Usually, for most practical cases is mainly done in the assumption that PDF is Gaussian of random process. In these cases it is difficult to describe and to find the parameters of PDF. Therefore, we can apply another approach to obtain the likelihood ratio, which is based on the use of a polynomial decision function [21].

Assume that the probability ratio is a continuous function and it will be represented as a stochastic power polynomial of degree s for sample values x_v

$$\Lambda(\mathbf{X}) = \sum_{v=1}^n \sum_{i=1}^s k_{iv} x_v^i + k_0, \quad (8)$$

where the optimal coefficients k_{iv} and k_0 are found from the minimum of the quality criterion for statistical hypotheses testing [21]:

$$Ku(E, G) = \frac{G_0[\gamma] + G_1[\gamma]}{(E_1[\gamma] - E_0[\gamma])^2}. \quad (9)$$

Criterion $Ku(E, G)$ (9) determines the quality of decision-making using DR (8). This criterion will be called as “The moment quality criterion of upper bounds of error probability” or “Criterion Ku”. From this comes the mean and the variance of the DR (8) with the hypothesis and the alternative will be calculated as:

$$E_{0(s_n)} = \sum_{i=1}^s \sum_{v=1}^n k_{iv} u_i^{(v)}, E_{1(s_n)} = \sum_{i=1}^s \sum_{v=1}^n k_{iv} m_i^{(v)}. \tag{10}$$

$$G_{0(s_n)} = \sum_{i=1}^s \sum_{j=1}^s \sum_{v=1}^n \sum_{k=1}^n k_{iv} k_{jv} F_{(i,j)}^{(\tau)}(H_r) r = 0, 1, \tag{11}$$

where $F_{(i,j)}^{(\tau)}(H_0) = u_{(i,j)}^{(\tau)} - u_i^{(v)} u_j^{(k)}$, $F_{(i,j)}^{(\tau)}(H_1) = m_{(i,j)}^{(\tau)} - m_i^{(v)} m_j^{(k)}$.

The coefficients k_{iv} of the polynomial power stochastic DR (8) have to minimize the probabilities of errors of the first and second kind and are determined from the minimum the criterion $Ku(E, G)$ and look like

$$\sum_{j=1}^s k_{iv} \left(F_{i,j}^{(\tau)}(H_0) + F_{i,j}^{(\tau)}(H_1) \right) = m_i^{(v)} - u_i^{(v)}, v = \overline{1, n}, i = \overline{1, s}. \tag{12}$$

To solve the system of Eqs. (12), numerical methods and Schur complement of a matrix block are used. The 2D joint moments $u_{(i,j)}^{(\tau)}$ and $m_{(i,j)}^{(\tau)}$ were used to determine the correlation function $\rho^{(\tau)}$ which is defined as

$$\rho^{(\tau)} = \begin{pmatrix} 1 & \rho^{(\tau_{1,2})} & \dots & \rho^{(\tau_{1,n})} \\ \rho^{(\tau_{2,1})} & 1 & \dots & \rho^{(\tau_{2,n})} \\ \dots & \dots & \dots & \dots \\ \rho^{(\tau_{n,1})} & \rho^{(\tau_{n,2})} & \dots & 1 \end{pmatrix}. \tag{13}$$

For research, an exponential correlation function was used in the form

$$\rho^{(\tau_{v,k})} = e^{-A|t_v - t_k|},$$

where $\tau_{v,k}$ is the correlation time, A is the scaling factor.

The value of the quality criterion $Ku(E, G, \rho)$ can be used to evaluate the effectiveness of the polynomial DR (1). In addition, it is shown that the inverse value of the quality criterion is the extracted information from input data about discrimination hypotheses H_0, H_1 and look like.

$$Ku(E, G, \rho) = I_{Kus}^{-1}, \text{ or}$$

$$I_{Kus} = G_{1(s_n)} + G_{0(s_n)} = E_{1(s_n)} - E_{0(s_n)}. \tag{14}$$

This value will be used to evaluate the effectiveness of the obtained results.

4 Synthesis of the Signal Detection Algorithms in Correlated Non-gaussian Noise

Let the input signal $\xi(t)$ consist of useful signal a and noise $\eta(t)$ and observed in the time interval $[0, T]$

$$\xi(t) = a + \eta(t), \quad (15)$$

where $\eta(t)$ is the correlated stationary non-Gaussian noise with zero mean and variance χ_2 and is described by a sequence of 1D and 2D moments and cumulants.

Let us present the sampling signal $\xi(t)$, and discrete values $X = \{x_1, x_2, \dots, x_n\}$ at that time t_v for hypothesis H_i ($i = 0, 1$) will take the form:

$$H_1 : x_v = a + \eta_v(\gamma_k, \chi_{i,j}^{(\tau)}),$$

$$H_0 : x_v = \eta_v(\gamma_k, \chi_{i,j}^{(\tau)}), v = \overline{1, n}. \quad (16)$$

Consider a polynomial decision rule for degree $s = 1$.

The algorithm of signal detection in correlated non-Gaussian noise using DR (8) at the first degree of the polynomial $s = 1$ look like

$$\sum_{v=1}^n A_v \left(x_v - \frac{a}{2} \right) \begin{matrix} > 0, \\ < 0, \end{matrix} \begin{matrix} H_1 \\ H_0 \end{matrix} \quad (17)$$

where A_v is the determinant which is obtained from Δ_1 , when v -th column is replaced by units and Δ_1 is determined from the expression

$$\Delta_1 = \det \|F_{(1,1)}^{(\tau)}\| = \det \|\rho^{(\tau_{v,k})}\|, v, k = \overline{1, n}, \quad (18)$$

where $F_{(i,j)}^{(\tau)} = F_{(i,j)}^{(\tau)}(H_0) + F_{(i,j)}^{(\tau)}(H_1)$.

Shown, that the information removed from the samples about discrimination hypotheses H_0, H_1 according to (14) look like

$$I_1 = \frac{q}{\Delta_1} \sum_{v=1}^n A_v \quad (19)$$

and is the inverse of the value of the quality criterion $Ku(E, G)(9)$, where $q = a^2/\chi_2$ - signal-to-noise ratio.

It is shown that if a stationary statistically independent random process is observed, the criterion value $Ku(E, G, \rho)$ is transformed to the following form

$$Ku_1(E, G) = 2/nq \quad (20)$$

and DR (17) is transformed to the classical well-known form

$$\frac{1}{n} \sum_{v=1}^n x_v - \frac{a}{2} \begin{matrix} > \\ < \end{matrix} 0. \quad \begin{matrix} H_1 \\ H_0 \end{matrix} \quad (21)$$

The obtained results of the linear DR (17) do not take into account the non-Gaussian distribution of the random process, since only the first two moments were used to describe it. Increase the degree of the polynomial DR to $s = 2$. Then, the DR will be non-linear and in the general case look like

$$\sum_{v=1}^n k_{1v} x_v + \sum_{v=1}^n k_{2v} x_v^2 + k_0 \begin{matrix} > \\ < \end{matrix} 0, \quad \begin{matrix} H_1 \\ H_0 \end{matrix} \quad (22)$$

where optimal coefficients k_{iv} are defined from equation systems (12) and have the following form

$$k_{1v} = \frac{B_v}{\Delta_2}, \quad v = \overline{1, n}, \quad k_{2v} = \frac{C_v}{\Delta_2}, \quad v = \overline{n+1, 2n}, \quad (23)$$

where B_v is the determinant which obtained from Δ_2 when v -th column ($v = \overline{1, n}$) is replaced by another with $(q^{0.5}, q^{0.5}, \dots, q^{0.5}, q, q, \dots, q)$ elements, C_v is defined in a similar way for $v = \overline{n+1, 2n}$ and Δ_2 looks like

$$\Delta_2 = \det \begin{vmatrix} \|F_{1,1}^{(\tau_{v,k})}\| & \|F_{1,2}^{(\tau_{v,k})}\| \\ \|F_{2,1}^{(\tau_{v,k})}\| & \|F_{2,2}^{(\tau_{v,k})}\| \end{vmatrix}, \quad v, k = \overline{1, n}, \quad (24)$$

In general, the threshold k_0 of the DR (22) with coefficients k_{1v} and k_{2v} is calculated as follows

$$k_0 = -\frac{1}{2\Delta_2} \sum_{v=1}^n (q^{0.5} B_v + C_v (q+1)). \quad (25)$$

Shown, that the DR (22) takes into account the correlated non-Gaussian noise distribution in the form of asymmetry coefficients γ_3 , joint cumulants $\chi_{ij}^{(\tau)}$ and kurtosis coefficients γ_4 , $i, j = \overline{1, 2}$.

The value of the extracted information from input data about discrimination hypotheses H_0, H_1 using DR (22) is defined

$$I_2 = \frac{1}{\Delta_2} \sum_{v=1}^n (q^{0.5} B_v + q C_v). \quad (26)$$

It is possible to synthesize non-linear polynomial DR of a higher degree s , where moments and cumulants of higher orders will be taken into account.

5 Results and Discussion

Adequate new mathematical models of correlated non-Gaussian random processes and polynomial methods of signal detection allows to improve the efficiency of signal processing. The probability of signal detection errors were obtained by using two DR – for linear DR (17) and non-linear DR (22).

The extracted information ratio $I1/I2$ from input data about discrimination hypotheses H_0 and H_1 for polynomial power DR of order $s = 1, 2$ from the SNR and skewness coefficient γ_3 are shown in Fig. 1. In experiment the exponential correlation function was used for simulation. As is shown in Fig. 1, the ratio $I1/I2$ is less than one, and then the value I_2 (26) for non-linear DR is more than the value I_1 (19) for linear DR. The value of the criterion $Ku_2(E, G)$ is less than value of the criterion $Ku_1(E, G)$ and efficiency of non-linear DR (22) is better than linear DR (17). Note that smaller values of the criterion correspond to an increase of signal detection efficiency.

For Gaussian noise the values of the criterion $Ku_1(E, G)$ for $s = 1$ and $Ku_2(E, G)$ for $s = 2$ are the same ($I1/I2 = 1$) when the skewness and kurtosis coefficients are equal to zero ($\gamma_3 = \gamma_4 = 0$). Taking into account the skewness and kurtosis coefficients the values of the criterion $Ku_2(E, G)$ for non linear DR ($s = 2$) are smaller as compared with the criterion $Ku_1(E, G)$ and it correspond to decrease the probability of the first and second kind errors. For example, for $\gamma_3 = 1.3$ the sum probability of errors for the nonlinear DR was decreased in 2 times ($q = 1$ or SNR = 0 dB, kurtosis coefficient $\gamma_4 = 0$ and $n = 100$) and in 1.4 times for $\gamma_4 = 2$ (Fig. 1). The efficiency of signal detection improve with increasing of the polynomial power DR degree.

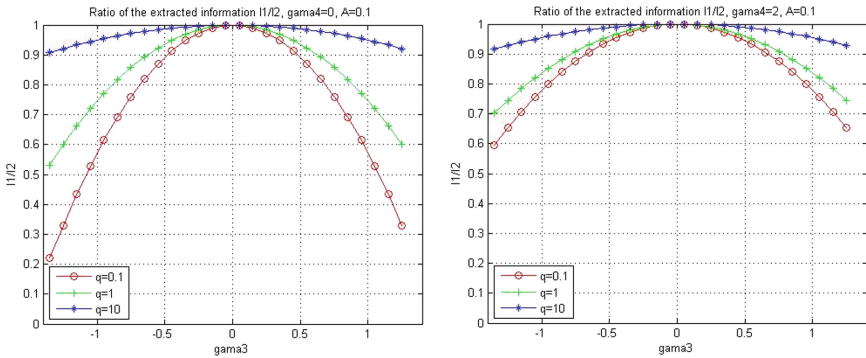


Fig. 1. Comparison of the ratio of the $I1/I2$ from input data about discrimination hypotheses H_0 and H_1 from the γ_3 - skewness coefficient γ_3 for polynomial power DR of order $s = 1, 2$, where $A = 0.1$, coefficients of kurtosis $\gamma_4 = 0$ and $\gamma_4 = 2$.

6 Conclusion

To solve the problems of signal detection in correlated non-Gaussian noise requires a new approach that made it possible to describe the complexity of signal processing. This

approach is based on the use of new mathematical models to describe random processes in the form of higher-order moments and cumulants, including joint moments to describe correlation dependencies. This approach is simpler than the traditional approach using of distribution densities of random processes. The use of stochastic power polynomials for the synthesis of decision rules is proposed. The coefficients of such polynomials power decision rules were determined from the adapted moment quality criterion for statistical hypotheses testing. It is shown that non-linear processing of input data and taking into account the non-Gaussian distribution of sample values can increase the efficiency of signal detection in comparison with the use of traditional and widely used Gaussian models of random processes.

References

1. Van Trees, H., Bell, K., Tiany, Z.: *Detection Estimation and Modulation Theory*. Wiley, New Jersey (2013)
2. Kay, S.M.: *Fundamentals of Statistical Signal Processing*. Prentice Hall PTR, NJ (2008)
3. Lin, C., Chang, Q., Li, X.: A deep learning approach for MIMO-NOMA downlink signal detection. *Sensors* **19**, 2526 (2019). <https://doi.org/10.3390/s19112526>
4. Herzog, M.H., Francis, G., Clarke, A.: *Understanding Statistics and Experimental Design*. LMB. Springer, Cham (2019). <https://doi.org/10.1007/978-3-030-03499-3>
5. Kassam, S.A.: *Signal Detection in Non-Gaussian Noise*. STELE. Springer, New York (1988). <https://doi.org/10.1007/978-1-4612-3834-8>
6. Guo, G., Mandal, M., Jing, Y.: A robust detector of known signal in non-Gaussian noise using threshold systems. *Signal Process.* **92**(11), 2676–2688 (2012). <https://doi.org/10.1016/j.sigpro.2012.04.014>
7. Duana, F., Chapeau-Blondeau, F., Abbott, D.: Non-Gaussian noise benefits for coherent detection of narrow band weak signal. *Phys. Lett. A* **378**, 1820–1824 (2014). <https://doi.org/10.1016/j.physleta.2014.04.061>
8. Hari, V.N., Anand, G.V., Premkumar, A.B., Madhukumar, A.S.: Design and performance analysis of a signal detector based on suprathreshold stochastic resonance. *Signal Process.* **92**(6), 1745–1757 (2012). <https://doi.org/10.1016/j.sigpro.2012.01.013>
9. Rousseau, D., Anand, G.V., Chapeau-Blondeau, F.: Noise enhanced nonlinear detector to improve signal detection in non-Gaussian noise. *Signal Process.* **86**(11), 3456–3465 (2006). <https://doi.org/10.1016/j.sigpro.2006.03.008>
10. Izzo, L., Tanda, M.: Asymptotically optimum diversity detection in correlated non-Gaussian noise. *IEEE Transactions on Communication* **44**(3), 542–545 (1996). <http://ieeexplore.ieee.org/xpl/tocresult.jsp?isnumber=10665> <https://doi.org/10.1109/26.494296>
11. Picinbono, B.: On deflection as a performance criterion in detection. *IEEE Trans. Aerosp. Electron. Syst.* **31**(3), 1072–1081 (1995). <https://doi.org/10.1109/7.395235>
12. Vachkov, G.: Online detection of deviation in performance of multichannel dynamical processes **5**, 1681–1686 (2016). <https://doi.org/10.1109/ICMA.2013.6618168>
13. Solc, T., Mohorcic, M., Fortuna, C.: A methodology for experimental evaluation of signal detection methods in spectrum sensing. *PLoS ONE* **13**(6), 1–31 (2018). <https://doi.org/10.1371/journal.pone.0199550>
14. Biglieri, E., Lops, M.: Linear-quadratic detectors for spectrum sensing. *J. Commu. Netw.* **16**(5), 485–492 (2014). <https://doi.org/10.1109/JCN.2014.000087>
15. Peppas, K., et al.: High-order statistics for the channel capacity of egc receivers over generalized fading channels. *IEEE Commun. Lett.* **22**(8), 1740–1743 (2018). <https://doi.org/10.1109/LCOMM.2018.2846229>

16. Watts, J.P., Smith, P.: Stochastic Processes. An Introduction, Chapman and Hall/CRC (2018)
17. Jammalamadaka, S., Taufer, E., Terdik, G.: Cumulants of multivariate symmetric and skew symmetric distributions. *Symmetry* **13**, 1383 (2021). <https://doi.org/10.3390/sym13081383>
18. Kunchenko, Y.: Polynomial Parameter Estimations of Close to Gaussian Random Variables. Shaker Verlag, Aachen (2002)
19. Vokorokos, L., et al.: Parameters estimation of correlated non-Gaussian processes by the method of polynomial maximization. *IET Signal Proc.* **11**(3), 313–319 (2017). <https://doi.org/10.1049/iet-spr.2016.0142>
20. Palahin, V., et al.: Computer simulation of signal detection in non-Gaussian noise with the Neyman-Pearson moment quality criterion. In: 2018 IEEE 9th International Conference on Dependable Systems, Services and Technologies (DESSERT), pp. 603–608. IEEE, Kyiv (2018). <https://doi.org/10.1109/DESSERT.2018.8409203>
21. Palahina, E., Gamcová, M., Gladišová, I., Gamec, J., Palahin, V.: Signal detection in correlated non-gaussian noise using higher-order statistics. *Circuits Systems Signal Process.* **37**(4), 1704–1723 (2017). <https://doi.org/10.1007/s00034-017-0623-5>
22. Palahin, V., et al.: Computer modeling of noise signals processing system in non-gaussian noise. In: 2018 IEEE 38th International Conference on Electronics and Nanotechnology (ELNANO), pp. 658–662. IEEE, Kyiv (2018). <https://doi.org/10.1109/ELNANO.2018.8477442>



Evaluation of Endothelium Regulation of Vascular Tone

Viktor Sergeiev^{1,2}(✉) , Volodymyr Kyrychenko^{2,3} , Tetiana Kulbashevska¹ ,
and Ihor Biletskyi¹ 

¹ O. M. Beketov National University of Urban Economy in Kharkiv, 17 Marshala Bazhanova Street, Kharkiv 61002, Ukraine

² XAI-Medica Ltd., 4 Zoriana Street, Kharkiv 61070, Ukraine
sergeev@xai-medica.com

³ National Aerospace University “Kharkiv Aviation Institute”, 17 Chkalova Street, Kharkiv 61070, Ukraine

Abstract. The problem of the endothelial function (EF) evaluating is currently very relevant, however, the most widely used and recommended for this method of D. Celermajer today does not satisfy specialists, due to the complexity of the technique, low accuracy and instability of the results obtained. An analysis of the endothelial function assessment by the D. Celermajer method was carried out. The main sources of EF estimation error are determined and the ways of their neutralization are proposed. Improving the accuracy of the endothelium function assessing by the D. Celermajer method is impossible, while maintaining the ultrasonic method for assessing changes in the diameter of an arterial vessel. To simplify the research methodology and improve the accuracy of EF assessment, one should switch to the use of rheographic data. The rheographic method makes it possible to neutralize the identified sources of error in evaluating EF and improve the quality of the assessment.

Keywords: Atherosclerosis · Endothelium dysfunction · Rheography signal · Pulse wave · Vascular tone · Reactive hyperemia

1 Introduction

Nowadays, it is well-known that one of the basic realized risks factors related to the progress of cardiovascular diseases and their complications is decreasing of elasticity of the vascular wall. Most frequently, it caused by atherosclerosis [1–3]. At the middle age, the frequency of detection of arterial involvement approaches to 100% for people without any clinical atherosclerosis developments [2, 3]. It has been also established, that the aging processes affect the arterial vessels on their own account [3, 4]. The main processes occur in the medial and inner layers of the arteries wall. Medial layer becomes very thin, fragmentation and exhaustion of the elasticity fibers take place. The endothelium of arterial vessels is damaged.

First, non-invasive technique for estimation of endothelium condition using flow-dependent vasodilatation (FDV) or endothelium-dependent vasodilatation (EDV) was

suggested by D. Celermajer et. al. [5] in 1992. Nowadays, this technique is considered as the best strategy for estimation of endothelium function [6–9]. This technique is based on the measurement of the brachial artery (BA) diameter by ultra sound (US) system of high resolution before and after arterial occlusion.

It is conventionally accepted to consider dilatation by 9% or more of the resting diameter as a normal BA reaction [10]. Absence of dilatation or spasm should be considered as endothelium dysfunction (ED). In order to identify the causes of the development of changes, it was suggested to perform the test of flow-independent dilatation of the BA after the test of flow-dependent vasodilatation. Reaction for insertion of vasodilatation is computed as difference of BA diameters at 2nd–5th minutes after nitroglycerine intake and initial value related to the artery diameter value at rest in percentage. Degree of increment for BA diameter under endothelium-independent vasodilatation (EIDV) for healthy people under opinion of majority of the authors assembles in average to 14–17% [10].

The close temporal synchronization of the development of endothelial dysfunction in all vessels of the body has now been proved [11–13]. Malfunction of flow-dependent dilatation can be considered as evident predictor for cardiovascular diseases [5–7, 13].

Unfortunately, today, it is necessary allowing that the results obtained by D. Celermajer US technique designed for evaluation of the variation of artery diameter are very often comparable with the measurement instrumental inaccuracy. In addition, other error sources exist.

Let us assume that dependence of artery diameter D_A from the pressure P_A is linear inside it, i.e. $D_A = K \cdot P_A$, where K is the coefficient of artery extensibility. Assume that K value is equal to K_R at rest but after cross-clamping of artery and restoration of blood flow due to influence of NO it will be of K_{NO} value.

In this study, the ratio of artery diameter change ΔD_A is evaluated in the post occlusion period relatively its diameter at rest to the artery diameter at rest D_{AR} , i.e. the following parameter is estimated

$$P_{US} = \frac{\Delta D_A}{D_{AR}} = \frac{P_A(K_{NO} - K_R)}{P_A K_R}. \quad (1)$$

If the measurements of artery diameter variation ΔD_A at rest and after occlusion are performed for the same transmural pressure in artery, P_A value in (1) is cancelled and parameter P_{US} , indeed, will define relative change of extensibility in the studied artery as follows

$$P_{US} = \frac{K_{NO} - K_R}{K_R}. \quad (2)$$

The error of the considered method for assessing the function of the endothelium in this case, will be due not only to the possible instrumental error in assessing the relative change in the diameter of the brachial artery in the sample with reactive hyperemia. In addition, it is necessary to take into account the factor of uncontrolled changes in transmural pressure falls on the post-occlusion period relative to the resting stage. Consequently, the assessment of the relative change in the diameter of the artery will already characterize not only the stiffness of the arterial wall.

To date, the generally accepted method for assessing the elastic properties of arteries is the measurement of pulse wave propagation velocity (PWPV) in the vessel [14–18]. The most commonly used methods for measuring PWPV are ultrasound, sphygmography, rheography, or photoplethysmography [19, 20]. Synchronous registration of pulsations in different parts of the body allows one to assess PWPV along the course of an arterial vessel located under selected points of the body.

For this reason, the time delay Δt between the equivalent points of pulse waves recorded and the distance between points on body.

Unfortunately, regardless of the used method of pulse waves registration in distant points of the body, we will face the same problem – **finding equivalent pulse waves points registered in different points of the body, under conditions of pulse waveform changes during its propagation along the arterial vessel.**

It is evident that arterial system can be considered as some LPF filter model provoking different attenuations and phase shifts for different spectral components contained in the pulse wave at each specific part of arterial channel, and, therefore provoking the changes of pulse wave under its propagation in the vessel [15, 18]. Moreover, the found equivalent points of pulse waves can only be apparent equivalents! It was shown in [18] that the position of the minimum of the recorded pulse wave can differ significantly from the real beginning of the pulse wave, therefore, the traditional method for assessing the state of the arterial wall by PWPV will give significant errors due to the impossibility of accurately determining the time delay pulse wave in the vessel under study.

For each vascular region, the error will be strictly individual, depending on the elasticity of the particular artery, the mass of blood moving in it, the value of peripheral resistance of the region, etc. The magnitude of the error will vary from 0, in the smallest arteries, to 70–90 ms in the aorta. Hence, the measurement error in the time interval of pulse wave propagation can be commensurable with per se of propagation time [18].

Somewhat better results can be obtained when estimating the pulse wave velocity when applying the method outlined in the paper [18].

The latter approach allows identifying more precisely the equivalent points contained in the pulse curves obtained by rheography technique.

But, in our opinion, the best technique for estimation of endothelium state could be fixation of variations of the rheosignals parameters registered for forearm in the test contribution with cross-clamping of shoulder artery part (before and after cross-clamping), and under test with nitroglycerine.

2 Suggested Technique for Estimation of Endothelium Function

It is well-known, that the law of rheosignal variations is defined as [21]:

$$\Delta R(t)_{AR} = \frac{\rho_{Bo}^2 L_A \tilde{S}(t)_{AR}}{\rho_{Bl} S_{Bo}^2}, \quad (3)$$

where ρ_{Bl} is the specific blood resistance; ρ_{Bo} is the specific resistance of the studied body part; S_{Bo} is the body cross-sectional area at the place of the potential rheograph electrodes location; L_A is the length of body part between the potential electrodes;

$S(t)_{AR}$ is the law of change of variable component of cross-sectional area at the place of potential electrodes location under influence of pulse wave (at rest (R) state, till to the cross-clamping of BA).

Due to the variations of the wall elasticity of the forearm arteries, after occlusion of BA and blood flow restoration, the law of changes of variable component of cross-sectional area will be of the value of $S(t)_{ANO}$, that will provoke the following changes of the rheosignal:

$$\Delta R(t)_{ANO} = \frac{\rho_{Bo}^2 L_A \tilde{S}(t)_{ANO}}{\rho_{Bl} S_{Bo}^2}.$$

Parameter $P_{RHEO}(t)$ can be written as:

$$\begin{aligned} P_{RHEO}(t) &= \frac{\Delta R(t)_{ANO} - \Delta R(t)_{AR}}{\Delta R(t)_{AR}} = \frac{\tilde{S}(t)_{ANO} - \tilde{S}(t)_{AR}}{\tilde{S}(t)_{AR}} = \\ &= \frac{(K_{NO}^2 - K_R^2)(P(t)^2 - P(t)_D^2)}{K_R^2(P(t)^2 - P(t)_D^2)} = \frac{K_{NO}^2 - K_R^2}{K_R^2} = P_{RHEO}, \end{aligned} \quad (4)$$

where $\tilde{S}(t)_A = \frac{\pi}{4}(D_A^2(t) - D(t)_{AD}^2) = K^2 \frac{\pi}{4}(P_A^2(t) - P_{AD}^2(t))$ is the difference between of current cross-sectional artery area and the value of cross-sectional area at diastolic pressure; $D_A(t)$ is the law of variation of current diameter of main artery at the place of location of potential rheograph electrodes; $D_{AD}(t)$ is the law of slow variation of current diameter of main artery at the place of location of potential rheograph electrodes under the influence of slowly changing diastolic pressure. Therefore,

$$P_{RHEO} = \frac{K_{NO}^2 - K_R^2}{K_R^2}. \quad (5)$$

As a result of occlusion, due to the developed tissue ischemia and *NO* exposure, the shape of the averaged rheosignal period curve after occlusion will necessarily change in comparison with the averaged rest period. So there won't be a complete identity of the averaged periods after all?

The question is: **how to find the time moments of the equality of the pulse pressure current values in the arterial vessels in the time intervals before and after occlusion?** Besides, current magnitude of the averaged rheosignal amplitude is also the function of pulse pressure in the artery and its rigidity. **How to extract only influence of rigidity variations?**

3 Discussion of the Experimental Results

Let us present the results of a study of endothelial function in an arbitrary patient. Male, 26 years old, no clinical manifestations of atherosclerosis. A forearm rheogram was recorded in two probes.

First probe was performed with reactive hyperemia. The probe duration was of 10 min: the rest stage of 1.5 min + 5 min of occlusion + postocclusion time interval of 3.5 min.

Standard cuff was put in the patient shoulder for measurement of arterial pressure. The cuff did not practically compress the shoulder and it did not create the troubles for the venous outflow. The pressure in the cuff was increased till to the level of systolic pressure + 50 mmHg.

Coherent accumulation of the rheosignal periods was performed in time intervals of 40–60 s (rest period) and 420–440 s (postocclusion period). Obtained experimental results are demonstrated in Fig. 1 (rest period) and Fig. 2 (postocclusion period).

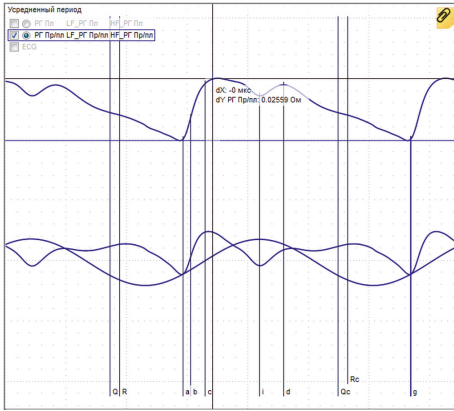


Fig. 1. Rheogram of forearm, rest period.

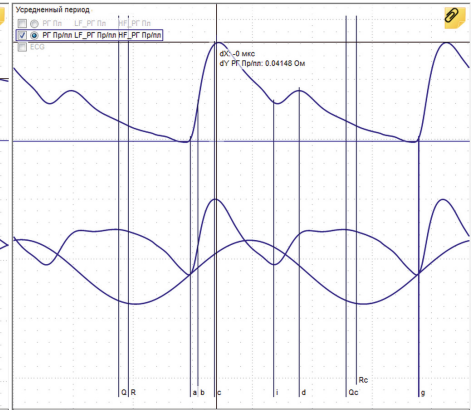


Fig. 2. Rheogram of forearm, postocclusion period.

Second probe was carried out with vasodilator contained 0.5 pill of nitroglycerine by sublingual absorption. Intake of the nitroglycerine was accomplished at the 90th second of the probe. This probe was performed in 15 min after the first probe. Coherent

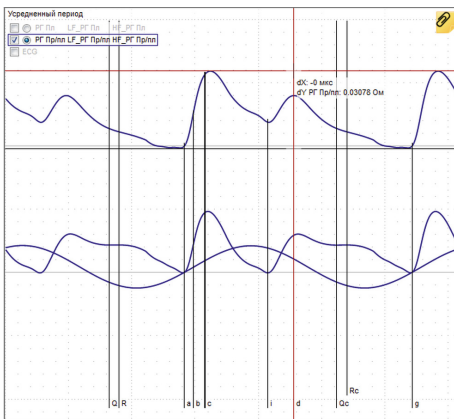


Fig. 3. Rheogram of forearm, rest period.

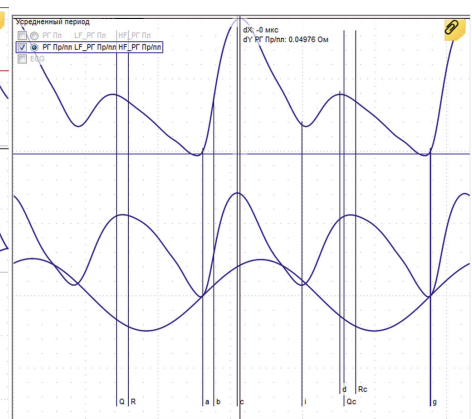


Fig. 4. Rheogram of forearm, registered under nitroglycerine impact.

accumulation of the rheosignal periods was performed for the second probe during 40–60 s (rest period) and 400–420 s (vasodilatation period). Obtained results are represented in Fig. 3 (rest period) and Fig. 4 (vasodilatation period).

Upper curves demonstrated in all of the graphs show averaged rheogram periods and lower curves illustrate the result of rheogram expansion onto low-frequency (LF) and high-frequency (HF) components. This technique was considered in detail in our work [17], carried out with the use of the rheographic complex “ReoCom”, designed by XAI-Medica Ltd., Ukraine [22, 23].

What should be compared in the presented averaged periods of rheograms (before and after exposure) to assess changes in the diameter of the forearm main artery under the influence of *NO* and nitroglycerin? How to exclude the influence of possible variations in transmural pressure existing in the forearm artery at the time intervals of interest? What time intervals have to be selected for the measurements before and after exposure? Let us suppose that we decided to determine the degree of variation in the maximum amplitudes of the averaged rheogram periods before and after exposure (Fig. 1 and Fig. 2, Fig. 3 and Fig. 4).

It is seen from Fig. 2 that the rheogram considerably changed after occlusion and blood restoration in BA. First of all, the amplitude increased by 62% relatively the rest stage. However, the question is: could one affirm that artery diameter increasing is the result of under influence of *NO*? Could we affirm that the rheogram amplitude increasing is of under increasing in artery diameter under influence of pulse waves just due to the artery vasodilatation but not due to increasing of the pulse pressure in the artery? So, the averaged periods obtained in our study before and after occlusion are not identical (Fig. 1 and Fig. 2). Therefore, we cannot confirm that in some selected time intervals relatively, for instance, the locations of the **R** tooth in the electrocardiogram, current pulse pressures in the artery will be of the same value before and after occlusion.

It is known [15], that that pulse pressure along the artery can vary due to the certain hemodynamic processes. It means that in our study the variation of maximum rheowave amplitude can be provoked by not of rigidity variations in the studied artery part but by variations of pulse pressure in the artery. Therefore, estimation of the vessel diameter variations without measurement of pulse variations cannot give true information about the changes in the vessel rigidity.

As we can see, the amplitude of the LF component in Fig. 2 is much greater than the amplitude of the LF component in Fig. 1. Maximum rheogram amplitude could increase also due to the variations of phase relationships between LF and HF rheogram components [18]. The latter peculiarity, in turn, also can be provoked by decreasing of periphery resistance under influence of postocclusion ischemia in the tissues and *NO*.

We suppose that the single feature for variation of wall rigid of the main forearm arteries can be only amplitude of the HF rheogram component (see ascending part, denoted by **a–c**).

The amplitude of the HF component of the rheogram depends solely on the HF component of the source and the stiffness of the arterial wall of the main vessel. If in the post occlusion period or period of influence of nitroglycerin, the amplitude of HF component has been increased, the only reason for this can be as follows – decreasing

of rigidity of artery side in the main arterial vessel under assumption of invariability of the central hemodynamic parameters during experiment.

We believe that in the particular case under study, we have every reason to state that vasodilatation of the forearm main arterial vessels took place at the studied vascular region in the test with reactive hyperemia, and that the observed increasing in the amplitude of the rheogram HF component (by 70.2%) occurred due to this.

It is clear, that increasing of rheogram amplitude by 62% was happened under influence of two reasons – by vasodilatation of the main artery forearm vessels and change of pulse pressure in the artery. Weighting components of these two contributions is difficult to estimate.

Now let's turn to Fig. 3 and Fig. 4, demonstrating the data of the second probe of the study. Comparison of the rheograms in Fig. 3 and Fig. 1 permits to note the following. Bigger maximum amplitude and smaller peripheral resistance, as well as larger amplitude of HF component are observed in Fig. 3. After taking of 0.5 pill of nitroglycerin ($0.5 \text{ mg}/2 = 0.25 \text{ mg}$) sublingually at 90th second of the second probe, the rheogram parameters also has been measured.

Averaged period of rheogram builed for second half probe is represented in Fig. 4. Its maximum amplitude increased by 62.9% with respect to the resting time interval. The amplitude of the HF component of the rheogram increased by 58.1%. Thus, as in the previous probe, however, under nitroglycerin influence, vasodilatation is observed in the artery forearm vessels. However, it is smaller pronounced as compared with the first probe.

Now, we consider the results obtained for a man of 68 years old without any clinical atherosclerosis demonstration. Results of coherent accumulation performed at the rest and post occlusive period, are represented in Fig. 5 and Fig. 6. Analysis of the data in Fig. 5 and Fig. 6 for second patient shows that maximum amplitude of the averaged rheogram in postocclusive period has been increased much smaller (by 10.6%). Amplitude of HF rheogram component also has been increased much smaller (by 16.2%). It allows saying that changing rigidity in the main arteries due to occlusion taken place by much smaller.

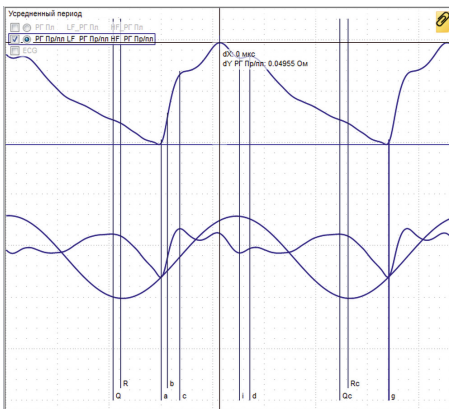


Fig. 5. Rheogram of forearm, rest period.

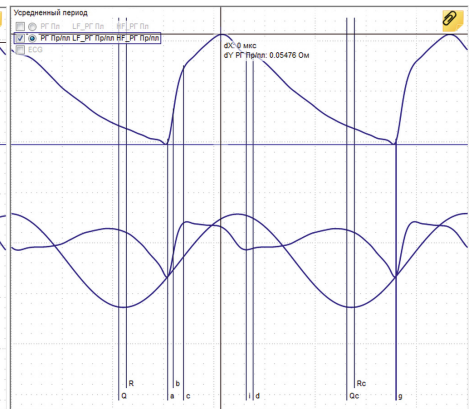


Fig. 6. Rheogram of forearm, postocclusion period.

Now, let us pay attention to the probe for the same patient, performed with nitroglycerin and represented in Fig. 7 and Fig. 8. Note that under influence of endothelium-independent vasodilatation, maximum rheogram amplitude increased by 19%. The magnitude of HF rheogram component increased by 62.6%. In this way, used vasodilator operates and the vessels of the studied region are managed. Moderate increasing of the HF component in the first probe (16.2%) as compared with 62% in the second probe was caused by decreasing of endothelium function.

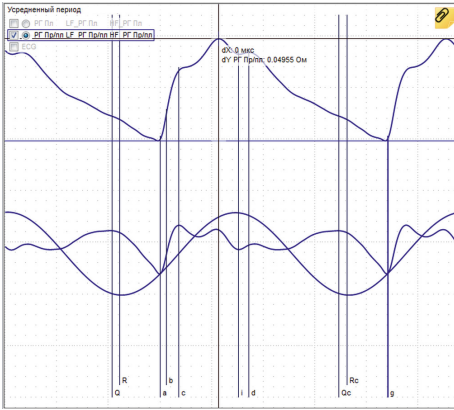


Fig. 7. Rheogram of forearm, rest period.

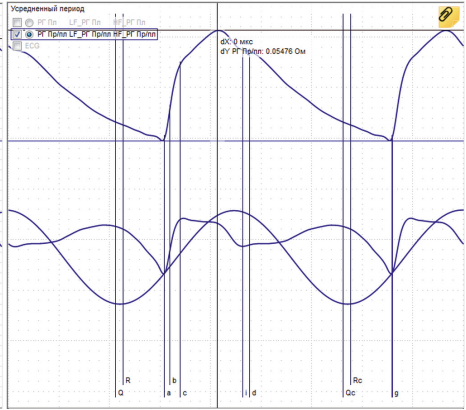


Fig. 8. Rheogram of forearm under influence of nitroglycerin.

Results of coherent accumulation of the probe time intervals with nitroglycerin, i.e. 0.5 pill of nitroglycerin (0.5 mg/2 = 0.25 mg) sublingually are demonstrated in Fig. 7 and Fig. 8. Nitroglycerin has been taken at the 90th second. As above, this probe was performed in 15 min after the first probe.

Let us come back to the expressions (2) and (5) that determine the sensitivity of the endothelium evaluation technique in modification with US and using rheograph:

$$P_{RHEO_{hf}} = \frac{\Delta R_{ANO_{hf}} - \Delta R_{AR_{hf}}}{\Delta R_{AR_{hf}}} = \frac{K_{NO}^2 - K_R^2}{K_R^2}, \tag{6}$$

and let us find $P_{RHEO_{hf}}/P_{US}$ $P_{RHEO_{HF}}/P_{US}$ as:

$$\frac{P_{RHEO_{hf}}}{P_{US}} = \frac{K_{NO} + K_R}{K_R} \approx 2. \tag{7}$$

Expression (7) shows that the sensitivity of method, with using rheographic data is about twice as high as US technique. It can be explained by the same variations of K_{NO} relatively K_R cause twice larger values of P_{RHEO} as compared with P_{US} .

Results of study show that analysis of HF component gives considerably more reliable information about changing the large artery rigidity in forearm area as compared with rheogram amplitude analysis. Since over 30 years of using D. Celermajer methodology, the normative base was created for P_{US} value, one can pass to the conventional

D. Celermajer parameter P_{US} , , however, evaluated by rheographical data. Taking into account (2) and (6) we can write the following:

$$P_{US} = \frac{K_{NO}}{K_R} - 1 = \sqrt{1 + P_{RHEO_{hf}}} - 1.$$

4 Conclusion

The benefits of suggested technique and future ways on its enhancement are represented below as follows:

- suggested technique provides performing of the investigations by using less expensive equipment;
- proposed methodology is more simple as compared with exploiting high resolution US system. It allows disposing the problem of fine orientation US sensor and its long fixation during study, reduce the requirements to experience of operator and obtain more stable data;
- application of coherent accumulation when constructing averaged periods of rheograms makes it possible to significantly reduce the random component of measurement error;
- the proposed technique essentially eliminates error by selecting the moment of measurement of a dynamically changing parameter during the heartbeat period;
- suggested methodology provides disposing the errors arising by possible variations of transmural pressure in the artery due to influence of occlusion or nitroglycerin on the periphery resistance and vessels tone.

It is quite clear that D. Celermajer's method is able to give a correct idea of the endothelium condition only if diastolic pressure in the arterial vessel at time intervals of measuring its diameter in the reactive hyperemia test remains unchanged. In addition, if other reasons related to the variations of the elasticity of artery side are absent except endothelium influence. Unfortunately, neither first nor second condition required according to D. Celermajer methodology does not execute in real life [15, 18].

References

1. Ren, M., Li, X., Xue, M.: Aortic elasticity evaluated by pulsed tissue Doppler imaging of the ascending aorta in different diseases: a systematic review. *Angiology* **72**(5), 403–410 (2021). <https://doi.org/10.1177/0003319721992584>
2. Ziemann, S.J., Melenovsky, V., Kass, D.A.: Mechanisms, pathophysiology, and therapy of arterial stiffness. *Arterioscler. Thromb. Vasc. Biol.* **25**(5), 932–943 (2005). <https://doi.org/10.1161/01.ATV.0000160548.78317.29>
3. McEnery, C.M., Wilkinson, I.B., Avolio, A.P.: Age, hypertension and arterial function. *Clin. Exp. Pharmacol. Physiol.* **34**(7), 665–671 (2007). <https://doi.org/10.1111/j.1440-1681.2007.04657.x>
4. Beckett, N.S., et al.: Treatment of hypertension in patients 80 years of age or older. *N. Engl. J. Med.* **358**(18), 1887–1898 (2008). <https://doi.org/10.1056/NEJMoa0801369>

5. Celermajer, D.S., et al.: Non-invasive detection of endothelial dysfunction in children and adults at risk of atherosclerosis. *Lancet* **340**(8828), 1111–1115 (1992). [https://doi.org/10.1016/0140-6736\(92\)93147-F](https://doi.org/10.1016/0140-6736(92)93147-F)
6. Vanhoutte, P.M., Shimokawa, H., Feletou, M., Tang, E.H.: Endothelial dysfunction and vascular disease – a 30th anniversary update. *Acta Physiol.* **219**(1), 22–96 (2017). <https://doi.org/10.1111/apha.12646>
7. Bonjorno, J.C., et al.: Noninvasive measurements of hemodynamic, autonomic and endothelial function as predictors of mortality in sepsis: a prospective cohort study. *PLoS ONE* **14**(3), e0213239 (2019). <https://doi.org/10.1371/journal.pone.0213239>
8. Chia, P.Y., Teo, A., Yeo, T.W.: Overview of the assessment of endothelial function in humans. *Front. Med.* **7**, 542567 (2020). <https://doi.org/10.3389/fmed.2020.542567>
9. Storch, A.S., et al.: Methods of endothelial function assessment: description and applications. *Int. J. Cardiovasc. Sci.* **30**, 262–273 (2017). <https://doi.org/10.5935/2359-4802.20170034>
10. Corretti, M.C., et al.: Guidelines for the ultrasound assessment of endothelial-dependent flow-mediated vasodilation of the brachial artery: a report of the International Brachial Artery Reactivity Task Force. *J. Am. Coll. Cardiol.* **39**(2), 257–265 (2002). [https://doi.org/10.1016/S0735-1097\(01\)01746-6](https://doi.org/10.1016/S0735-1097(01)01746-6)
11. Accin, J.L., et al.: Colombian study to assess the use of noninvasive determination of endothelium-mediated vasodilatation (CANDEV). Normal values and factors associated. *Endothelium* **8**(2), 157–166 (2001). <https://doi.org/10.3109/10623320109165324>
12. Anderson, T.J., et al.: Close relation of endothelial function in the human coronary and peripheral circulations. *J. Am. Coll. Cardiol.* **26**(5), 1235–1241 (1995). [https://doi.org/10.1016/0735-1097\(95\)00327-4](https://doi.org/10.1016/0735-1097(95)00327-4)
13. Celermajer, D.S., et al.: Endothelium-dependent dilation in the systemic arteries of asymptomatic subjects relates to coronary risk factors and their interaction. *J. Am. Coll. Cardiol.* **24**(6), 1468–1474 (1994). [https://doi.org/10.1016/0735-1097\(94\)90141-4](https://doi.org/10.1016/0735-1097(94)90141-4)
14. Asmar, R., et al.: Assessment of arterial distensibility by automatic pulse wave velocity measurement: validation and clinical application studies. *Hypertension* **26**(3), 485–490 (1995). <https://doi.org/10.1161/01.HYP.26.3.485>
15. Caro, C.G., Pedley, T.J., Schroter, R.C., Seed, W.A.: *The Mechanics of the Circulation*. Cambridge University Press, Cambridge (2012)
16. Shokawa, T., et al.: Pulse wave velocity predicts cardiovascular mortality findings from the Hawaii-Los Angeles-Hiroshima study. *Circ. J.* **69**(3), 259–264 (2005). <https://doi.org/10.1253/circj.69.259>
17. Naka, K.K., et al.: Flow-mediated changes in pulse wave velocity: a new clinical measure of endothelial function. *Eur. Heart J.* **27**(3), 302–309 (2006). <https://doi.org/10.1093/eurheartj/ehi619>
18. Sergieiev, V.G., Kiselgov, E.N.: Assessment of the vascular system state on the results of rheographic measurements. *Herald of Epileptology* **1**, 49–62 (2007). [In Russian]
19. Antonchuk, O.N., Nasedkin, K.V., Sharonov, V.B., Shulgin, V.I.: Arterial blood pressure evaluation based on joint processing of the vital signs parameters. *Telecommun. Radio Eng.* **75**(18), 1679–1693 (2016). <https://doi.org/10.1615/TelecomRadEng.v75.i18.70>
20. Viunytyskiy, O., Shulgin, V., Sharonov, V., Totsky, A.: Non-invasive cuff-less measurement of blood pressure based on machine learning. In: 2020 IEEE 15th International Conference on Advanced Trends in Radioelectronics, Telecommunications and Computer Engineering (TCSET), pp. 203–206. IEEE, Lviv-Slavske (2020). <https://doi.org/10.1109/TCSET49122.2020.235423>
21. Jenkner, F.L.: *Clinical Rheoencephalography: A Non-invasive Method for Automatic Evaluation of Cerebral Hemodynamics*. Ertlbruck, Vienna (1986)

22. Pechenin, A., Kyrychenko, V., Kulbashevskiy, V., Kiselgov, E.: Development of telemedicine system telecom for remote monitoring of patients. *Telecommun. Radio Eng.* **76**(1), 87–94 (2017). <https://doi.org/10.1615/TelecomRadEng.v76.i1.70>
23. Yukhymenko, L., et al.: Link between brain circulation and nervous mobility of athletes and non-athletes during the orthostatic test. *J. Phys. Educ. Sport* **20**(6), 3660–3670 (2020). <https://doi.org/10.7752/jpes.2020.06493>



Dimensionality Reduction of Diabetes Mellitus Patient Data Using the T-Distributed Stochastic Neighbor Embedding

Ievgen Meniailov¹ , Serhii Krivtsov¹ , and Tetyana Chumachenko²  

¹ National Aerospace University “Kharkiv Aviation Institute”, 17 Chkalova Street, Kharkiv 61070, Ukraine

² Kharkiv National Medical University, 4 Nauky Avenue, Kharkiv 61022, Ukraine
t.o.chumachenko@knmu.edu.ua

Abstract. Diabetes Mellitus is a global problem for all countries in the world. Today, about 422 million people worldwide have diabetes, which is more than 6% of the population of the planet Earth. In Ukraine, the mortality rate from diseases associated with high blood sugar has increased by 2.5 times over the past ten years. This study aims to develop a dimensionality reduction model for type 2 diabetic patients using the T-Distributed Stochastic Neighbor Embedding method. The model was developed in Python programming language. As a result of the model operation, the data dimension is reduced to 2 principal components. The transformed dataset makes it possible to increase the efficiency of applying models to diagnose type 2 diabetes mellitus.

Keywords: Dimensionality reduction · Diabetes mellitus · Medical data mining · T-distributed stochastic neighbor embedding

1 Introduction

Diabetes Mellitus is a global problem for all countries in the world. Today, about 422 million people worldwide have diabetes, which is more than 6% of the population of the planet Earth [1]. At the same time, diabetes mellitus is growing every year. If the current growth trends continue, by 2025, the number of patients with diabetes will increase by two times, and by 2030 diabetes will rise to seventh place among the causes of death in the world [2].

One of the main threats posed by diabetes mellitus is an early disability and high mortality from vascular consequences [3]. Among the main consequences of the disease are the following [4]:

- diabetes is the leading cause of blindness;
- the risk of developing a heart attack in diabetes increases by 300%;
- the risk of heart disease increases four times;
- the risk of stroke in diabetes increases four times;

- the likelihood of developing kidney failure is increased by four times;
- diabetes mellitus is the leading atraumatic cause of lower limb amputations.

The most common is type 2 diabetes mellitus [5]. Risk factors for type 2 diabetes:

- overweight, obesity;
- age over 40 years;
- unbalanced nutrition;
- hereditary predisposition to the disease;
- sedentary lifestyle;
- impaired glucose tolerance;
- chronic gastritis or cholecystitis;
- psycho-emotional overload;
- ischemic heart disease, arterial hypertension.

The main symptoms of type 2 diabetes are general weakness, thirst, itching of the skin, weight loss with increased appetite, and prolonged wound healing. The absence of severe clinical symptoms at the onset of the disease leads to late diagnosis, often with the development of complications.

To combat diabetes worldwide, from 2.5% to 15% of the annual health care budget in various countries is allocated, and the associated costs exceed these figures by five times [6].

The problem of diabetes is also relevant to Ukraine. In Ukraine, the mortality rate from diseases associated with high blood sugar has increased by 2.5 times over the past ten years [7]. Today, 2.3 million people live with diabetes in Ukraine, and almost 1 million do not know about their diagnosis. Of all diagnosed patients with type 2 diabetes in Ukraine, 11.3% take insulin preparations, 25% less than in Poland [8]. This is due to difficult access to medicines, which worsened significantly after the Russian invasion of Ukraine in February 2022 [9].

To improve the quality of life of patients with diabetes mellitus and reduce the economic costs of the state for assisting, it is necessary to actively implement measures for the prevention, early detection, and treatment of diabetes and its complications. An effective tool for this is data-driven medicine. At the same time, one of the tasks of using information technologies in medicine is processing data on medical patients to build adequate and accurate models, in particular, reducing the dimension of such data.

With the onset of the global COVID-19 pandemic, the digitalization of all spheres of human activity has significantly increased. Digitalization has also affected medicine. Information technologies are being developed to model epidemic processes [10], not only among the population but also in information systems [11], diagnostics [12], logistics [13], distribution of human resources [14], and other areas directly or directly related to healthcare.

This study **aims** to develop a dimensionality reduction model for type 2 diabetic patients using the T-Distributed Stochastic Neighbor Embedding method.

Research is part of a complex, intelligent information system for epidemiological diagnostics, the concept of which is discussed in [15].

2 Dimensionality Reduction

An excessive amount of data used for a model does not indicate its effectiveness. Moreover, an excessive amount of information characterizing the model's features can lead to a decrease in the efficiency of data analysis. The curse of dimensionality characterizes the problems of working with high-dimensional data [16].

Non-informative features are a source of additional noise and affect the accuracy of model parameter estimation. Also, datasets with many features may contain groups of correlated variables. The presence of these groups of features means duplication of information, which can distort the model's specification and affect the quality of the estimation of its parameters. The higher the dimension of the data, the higher the number of calculations during their processing.

In reducing the dimension of the feature space, two approaches can be distinguished [17]:

- formation of new features by transforming the original data;
- selection of features from the existing initial set.

The search for the most informative features that characterize the used dataset is an approach to dimensionality reduction that does not require the transformation of the original variables. This approach makes it possible to make the model compact and avoid losses associated with the action of uninformative features. At the same time, the selection of informative features consists in finding the best subset of the set of initial variables. The criteria for achieving the result can be the highest modeling quality for a given dimension or the smallest data dimension. The required quality of the model is achieved.

Informativeness of signs is relative. Their selection should provide a high information content of the set of features and not the total information content of the set variables. For example, a correlation between features reduces their overall information content due to duplication of information common to them. Therefore, adding a new feature to the selected ones increases information content to the extent that it contains valuable information not available in the previously selected variables. At the same time, the simplest is the situation in which mutually orthogonal features are selected, and the selection algorithm is implemented by ranking the variables according to information content.

The limitation of feature selection methods to reduce the dimension of space is associated with the assumption of the presence of the necessary features in the initial data, which usually turns out to be incorrect. Another approach to dimensionality reduction is to transform the features into a reduced set of new variables. In contrast to the selection of initial features, the formation of a new feature space involves the creation of new variables, which are usually functions of the original features. These variables, not directly observable, are often called latent or latent [18]. These variables can be endowed with various valuable properties during the creation process, such as orthogonality. In practice, the initial features are usually interconnected, so the transformation of their space into an orthogonal one generates new feature coordinates that do not have the effect of duplicating information about the objects under study.

3 T-Distributed Stochastic Neighbor Embedding Model

The T-distributed stochastic neighbor embedding method is a machine learning technique for data dimensionality reduction. The technique is a modification of the stochastic neighbor embedding method. The procedure is implemented to visualize high-dimensional data by representing each data point in two or three dimensions.

Let it be necessary to embed a set of points in a high-dimensional space $\{x_i | x_i \in X\}$ in a low-dimensional space. Denote the set of points in the low-dimensional space that are obtained after embedding by $\{y_i | y_i \in Y\}$. Then, stochastic neighbor embedding [19] converts distances in high-dimensional Euclidean space between points into conditional probabilities $p_{j|i}$. Where $p_{j|i}$ is the probability that point x_i will choose point x_j as its neighbor among other data points. We assume that point x_i 's probability of finding a neighbor decreases with increasing distance from point x_i following the Gaussian distribution with zero mean and standard deviation σ_i . Accordingly, $p_{j|i}$ can be expressed as

$$p_{j|i} = \frac{\exp\left(-\frac{\|x_i - x_j\|^2}{2\sigma_i^2}\right)}{\sum_{k \neq i} \exp\left(-\frac{\|x_i - x_k\|^2}{2\sigma_i^2}\right)}. \quad (1)$$

Let us define similar probabilities q_{ij} for a low-dimensional space where points of a high-dimensional space are embedded

$$q_{ji} = \frac{\exp\left(-\|y_i - y_j\|^2\right)}{\sum_{k \neq i} \exp\left(-\|y_i - y_k\|^2\right)}. \quad (2)$$

These probabilities are derived from the same propositions for high-dimensional space, except that all Gaussian distributions have a standard deviation for all points. p_{ij} , and q_{ij} will be similar if the spaces nest well. Therefore, the method tries to reduce the difference in the probability distribution. The standard measure for measuring the difference in probabilities is the Kullback-Leibler divergence [20]:

$$KL(P||Q) = \sum_j p_j \log_2 \frac{p_j}{q_j}. \quad (3)$$

We get $|X|$ distributions. Then the objective function to be optimized will look like this:

$$C = \sum_i KL(p_i||q_i) = \sum_i \sum_j p_{j|i} \log_2 \frac{p_{j|i}}{q_{ji}}. \quad (4)$$

The Kullback-Leibner divergence is not a symmetric measure. Therefore, embedding close points into distant ones gives a much larger error value than embedding far points into close ones. The objective function aims to preserve the local structure around the points.

Each parameter value generates its probability distribution P_i , which has entropy

$$H(P_i) = \sum_j p_{j|i} \log_2 p_{j|i}. \quad (5)$$

The entropy increases with the growth of σ_i . In this case, σ_i is calculated using a real binary search for a given value. The points y_i are sampled in a low-dimensional space according to a Gaussian distribution with a small standard deviation expectation of zero. The next step is to optimize the objective function. It is carried out using the gradient descent method. The gradient is

$$\frac{\partial C}{\partial y_i} = 2 \sum_j (p_{j|i} - q_{j|i} + p_{i|j} - q_{i|j})(y_i - y_j). \quad (6)$$

A problem arises when using stochastic neighbor embedding, which follows from the different probability distributions in high and low dimensional spaces. Let there be some high-dimensional space. Let the points x_i be uniformly distributed around the point x_0 in some ball with radius R . The greater the dimension of the space, the more points will fall near the boundary of the ball, so the number of points is close to x_0 will decrease with increasing dimension. It is necessary to embed this space in a plane. Let the points x_i go to the points y_i on the plane. If we put the points x_i into a circle of radius R centered at the point y_0 , many small distances between the points y_i are formed. This is because a sphere's volume in an arrogant space is incomparable with the area of a circle on a plane. Therefore, to simulate small distances on the plane, it is necessary to place the points x_i farther from x_0 than in the original space.

To avoid the problem of crowding, it is necessary to use the Student's t-distribution with one degree of freedom instead of the Gaussian distribution in the low-dimensional space [21]. The Student's t-distribution has a large probability mass in areas separated from zero. Thus, q_{ij} takes the following form:

$$q_{ij} = \frac{(1 + y_i - y_j^2)^{-1}}{\sum_{k \neq i} (1 + y_k - y_j^2)^{-1}}. \quad (7)$$

The numerator value describes the inverse square law for far points in low-dimensional space in this distribution. This allows us to represent not individual points but clusters that interact with each other as separate points.

After replacing the distribution, the gradient of the objective function has also changed, which has the following form:

$$\frac{\partial C}{\partial y_i} = 4 \sum_j (p_{ij} - q_{ij})(y_i - y_j) (1 + y_i - y_j^2)^{-1}. \quad (8)$$

4 Results

For implementation the model we have used open dataset of Diabetes patients: PIMA Indians Diabetes Database. Each instance represents individual patients and their various medical attributes along with diabetes mellitus. Visualization of the dataset is shown in Fig. 1.

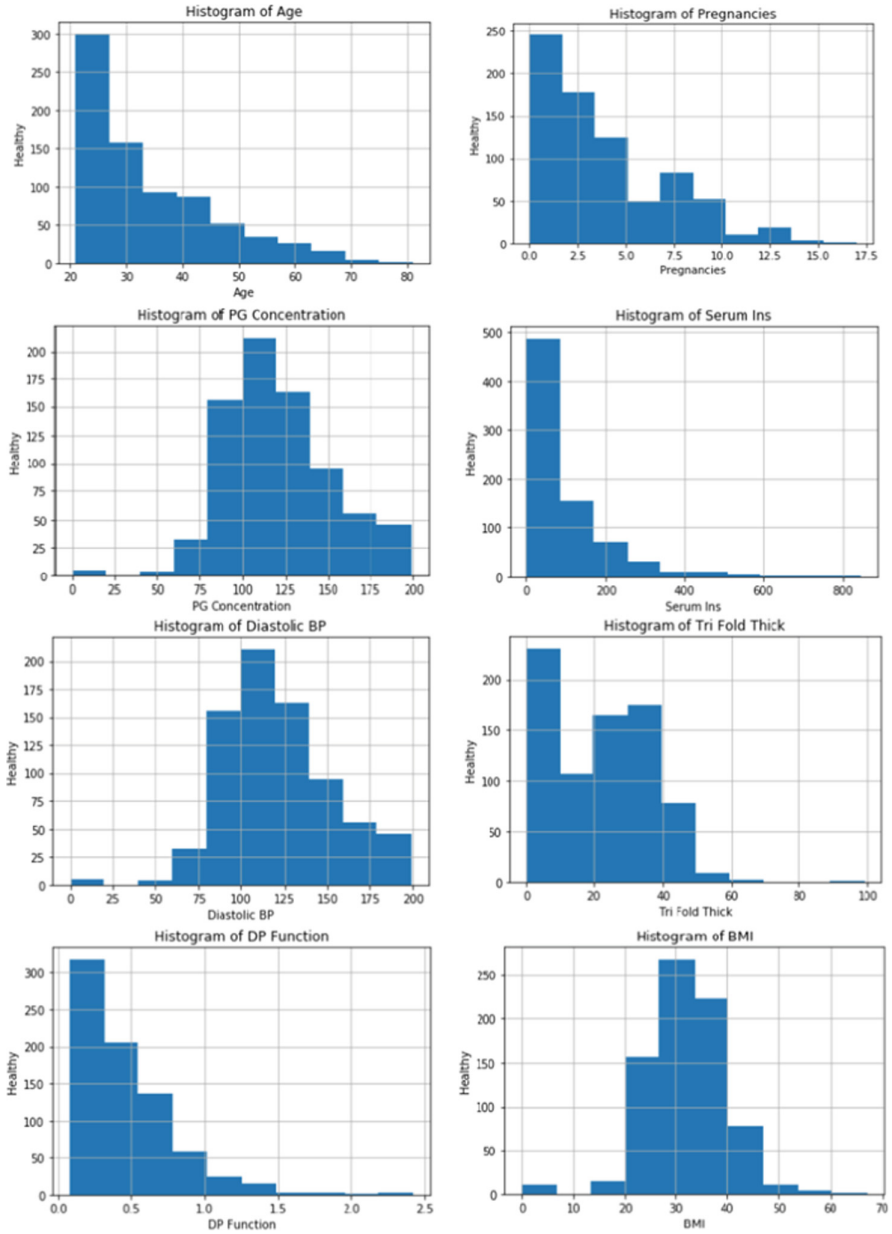


Fig. 1. Distribution of parameters of dataset.

Database has 768 instances and 9 attributes (Table 1).

Table 1. Initial data analysis.

Attribute	Scale type	Range
Pregnancies	Metric	0–17
PGConcentration	Metric	0–199
DiastolicBP	Metric	0–122
TriFoldThick	Metric	0–99
SerumIns	Metric	0–846
BMI	Metric	0–67,1
DPFunction	Metric	0,08–2,42
Age	Metric	21–81
Diabetes	Nominal	Sick/Healthy

The Python programming language was chosen for program realization. In Spyder programming, a T-SNE.py file was created for writing code. Initially, the data set was divided into objects and the objective function, and data processing was performed. The model was then defined using the TSNE class found in the Scikit-learn library, the data dimension was reduced while maintaining the two principal components, and the results were displayed graphically.

In Fig. 2 shown the results of the dimensionality reduction visualization.

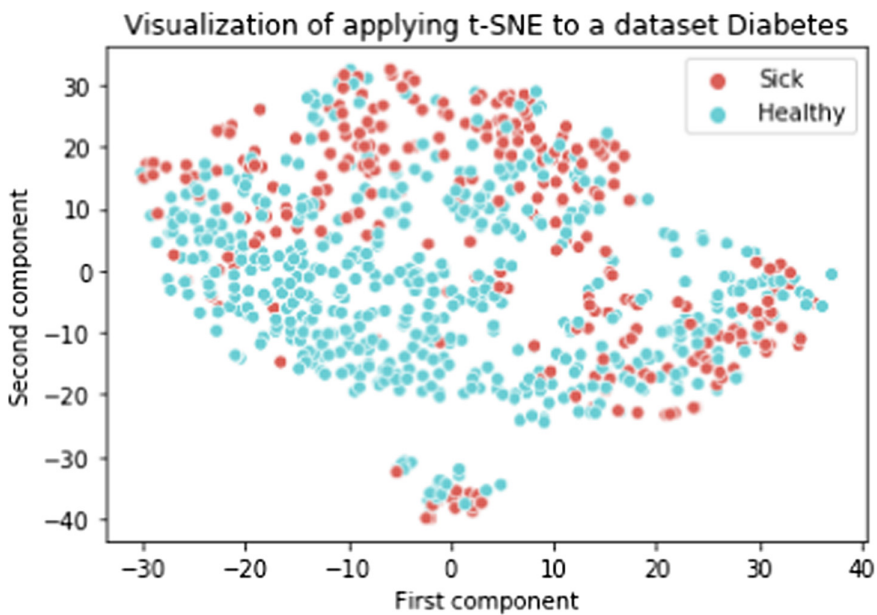


Fig. 2. Visualization of obtained results.

The results of the model made it possible to reduce the sample dimension to 2 principal components. The simulation results are shown in Table 2.

Table 2. Results of model performance.

Indicator	Value
Number of nearest neighbors	91
Mean sigma	0.832929
KL divergence after 250 iterations with early exaggeration	67.918045
KL divergence after 1000 iterations	1.012368
Source array shape	(768, 8)
Array shape after using transform	(768, 2)

5 Conclusion

Dimension reduction is necessary to improve the accuracy and adequacy of modeling, on the one hand, and to reduce the computational complexity of the model, on the other. As part of the study, the T-Distributed Stochastic Neighbor Embedding model was implemented to minimize data dimensionality in patients with type 2 diabetes. As a result of the model operation, the data dimension is reduced to 2 principal components. The transformed dataset makes it possible to increase the efficiency of applying models to diagnose type 2 diabetes mellitus. Future research is planned to develop a web-based information system to provide the classification of Diabetes Mellitus in real time.

Acknowledgements. The study was funded by the National Research Foundation of Ukraine in the frame-work of the research project 2020.02/0404 on the topic “Development of intelligent technologies for assessing the epidemic situation to support decision-making within the population biosafety management”.

References






1. Singer-Englar, T., Barlow, G., Mathur, R.: Obesity, diabetes, and the gut microbiome: an updated review. *Expert Rev. Gastroenterol. Hepatol.* **13**(1), 3–15 (2019). <https://doi.org/10.1080/17474124.2019.1543023>
2. Cloete, L.: Diabetes mellitus: an overview of the types, symptoms, complications and management. *Nurs. Stand.* **37**(1), 61–66 (2022). <https://doi.org/10.7748/ns.2021.e11709>
3. Gillani, S.W., Sulaiman, S.A.S., Abdul, M.I.M., Saad, S.Y.: Physical disability and diabetes mellitus; qualitative exploration of patients’ perception and behavior. *Curr. Diabetes Rev.* **14**(5), 472–480 (2018). <https://doi.org/10.2174/1573399813666170710183736>
4. Bailes, B.K.: Diabetes mellitus and its chronic complications. *AORN J.* **76**(2), 266–282 (2002). [https://doi.org/10.1016/s0001-2092\(06\)61065-x](https://doi.org/10.1016/s0001-2092(06)61065-x)

5. Wu, Y., Ding, Y., Tanaka, Y., Zhang, W.: Risk factors contributing to type 2 diabetes and recent advances in the treatment and prevention. *Int. J. Med. Sci.* **11**(11), 1185–1200 (2014). <https://doi.org/10.7150/ijms.10001>
6. Bommer, C., et. al.: The global economic burden of diabetes in adults aged 20–79 years: a cost-of illness study. *Lancet Diabetes Endocrinol.* **5**(6), 423–430 (2017). [https://doi.org/10.1016/S2213-8587\(17\)30097-9](https://doi.org/10.1016/S2213-8587(17)30097-9)
7. Stuart, R.M., et al.: Diabetes care cascade in Ukraine: an analysis of breakpoints and opportunities for improved diabetes outcomes. *BMC Health Serv. Res.* **20**(1), 409 (2020). <https://doi.org/10.1186/s12913-020-05261-y>
8. Topor-Madry, R., et al.: Prevalence of diabetes in Poland: a combined analysis of national databases. *Diabet. Med.* **36**(10), 1209–1216 (2019). <https://doi.org/10.1111/dme.13949>
9. Editorial: Ukraine: diabetes on the front line. *Lancet Diabetes Endocrinol.* **10**(4), 231 (2022). [https://doi.org/10.1016/S2213-8587\(22\)00084-5](https://doi.org/10.1016/S2213-8587(22)00084-5)
10. Chumachenko, D., et al.: Development of an intelligent agent-based model of the epidemic process of syphilis. In: 2019 IEEE 14th International Conference on Computer Sciences and Information Technologies (CSIT), vol. 1, pp. 42–45. IEEE, Lviv (2019). <https://doi.org/10.1109/STC-CSIT.2019.8929749>
11. Chumachenko, D., Chumachenko, K., Yakovlev, S.: Intelligent simulation of network worm propagation using the Code Red as an example. *Telecommun. Radio Eng.* **78**(5), 443–464 (2019). <https://doi.org/10.1615/TELECOMRADENG.V78.I5.60>
12. Gargin, V., et al.: Application of the computer vision system for evaluation of pathomorphological images. In: 2020 IEEE 40th International Conference on Electronics and Nanotechnology (ELNANO), pp. 469–473. IEEE, Kyiv (2020). <https://doi.org/10.1109/ELNANO50318.2020.9088898>
13. Davidich, N., et al.: Advanced traveller information systems to optimizing freight driver route selection. In: 2020 13th International Conference on Developments in eSystems Engineering (DeSE), pp. 111–115. IEEE, Liverpool (2020). <https://doi.org/10.1109/DeSE51703.2020.9450763>
14. Dotsenko, N., Chumachenko, D., Chumachenko, I.: Modeling of the process of critical competencies management in the multi-project environment. In: 2019 IEEE 14th International Conference on Computer Sciences and Information Technologies (CSIT), vol. 3, pp. 89–93. IEEE, Lviv (2019). <https://doi.org/10.1109/STC-CSIT.2019.8929765>
15. Yakovlev, S., et. al.: The concept of developing a decision support system epidemic morbidity control. In: CEUR Workshop Proceedings 2753, pp. 265–274 (2020)
16. Wang, X., Sloan, I.H.: Brownian bridge and principal component analysis: towards removing the curse of dimensionality. *IMA J. Numer. Anal.* **27**(4), 631–654 (2007). <https://doi.org/10.1093/imanum/drl044>
17. Vikram, M., Pavan, R., Dineshbhai, N.D., Mohan, B.: Performance evaluation of dimensionality reduction techniques on high dimensional data. In: 2019 3rd International Conference on Trends in Electronics and Informatics (ICOEI), pp. 1169–1174. IEEE, Tirunelveli (2019). <https://doi.org/10.1109/ICOEI.2019.8862526>
18. Gao, J., Zhang, J., Tien, D.: Relevance units latent variable model and nonlinear dimensionality reduction. *IEEE Trans. Neural Netw.* **21**(1), 123–135 (2010). <https://doi.org/10.1109/TNN.2009.2034964>
19. Li, H., et al.: Stochastic neighbor embedding with trust region method combining with filter. In: 2020 39th Chinese control conference (CCC), pp. 3194–3199. IEEE, Shenyang (2020). <https://doi.org/10.23919/CCC50068.2020.9188807>

20. Cui, S., Datcu, M.: Comparison of Kullback-Leibler divergence approximation methods between Gaussian mixture models for satellite image retrieval. In: 2015 IEEE International Geoscience and Remote Sensing Symposium (IGARSS), pp. 3719–3722. IEEE, Milan (2015). <https://doi.org/10.1109/IGARSS.2015.7326631>
21. Qiu, M., et al.: T-distributed stochastic neighbor embedding based on cockroach swarm optimization with student distribution parameters. In: 2021 IEEE 12th International Conference on Software Engineering and Service Science (ICSESS), pp. 291–294). IEEE, Beijing (2021). <https://doi.org/10.1109/ICSESS52187.2021.9522161>



Machine Learning and Web Integrated Chatting Forum Which Detected Mental Health of the User

Mangesh Ghonge¹ , Tejas Kachare² , Siddharth Kakade² , Snehal Shintre³ ,
and Siddharth Nigade³ 

¹ Sandip Institute of Technology and Research Centre, Nashik 422213, India

² Vishwakarma Institute of Technology, Pune 411037, India
tejas.kachare18@vit.edu

³ Pune Institute of Computer Technology, Pune 411043, India

Abstract. Nowadays in this 21st century, youth is mainly leaning on chatting forums instead of real-life conversations trying to convey their emotions to their close friends with the help of texts, emojis, etc. On the contrary, the receiver may find it difficult to understand the emotions due to mistyped texts, misunderstandings, or any other issues. Henceforth, this bafflement may lead to more depression, and anxiety and may lead to serious threats to life like suicides. Among all the reasons, almost one-half of the people attempt suicide due to depression, anxiety is the main reason as other people cannot understand them. To overcome this problem of the understanding mood of the people and motivating them, the proposed model can be one of the best applications which can help the depressed user to overcome his/her stress, anxiety, etc. with the help of motivational quotes. The proposed model is a chat-based forum that is designed to monitor the mental health of the user the model consists of two parts: (i) Web Development; (ii) Machine Learning. This application is built with a Machine Learning algorithm and integrated with web development. Web scraping and creation of datasets have been done with the help of 'Tweet' and 'Pandas'. ML model is trained using 'ScikitLearn'. Further, the Machine Learning model is integrated with the chat-based Forum web application with the help of 'Flask'.

Keywords: Data analysis · Web scrapping · Decision tree · Depression detection · Machine learning algorithm · Artificial Intelligence

1 Introduction

In this modern era, people tend to rely on social media and try to avoid public interactions. Henceforth, the count of introverts is increasing day by day. Depression mainly attacks these lonely-natured people. Depression isn't easy to detect as it involves several different aspects. It is one of the major mental disorders which stakes life. Ordinarily, the younger generation falls prey to depression as they are involved more in online domains rather than face-to-face interactions. In this fast-growing world, people don't get enough time

to manage their stress due to hectic schedules. Stress and anxiety have become part of people's daily routines. People avoid the effects of stress and anxiety on their lives without seeking any stress reliever which are the main symptoms of depression. Corporate world employees mainly belong to this category. Symptoms of this acute mental disorder are: constant feeling of being sad; overthinking; suicidal thoughts; lack of sleep; loss of enthusiasm; arduous in concentrating. Likewise, there are many reasons which might cause depression and anxiety which will force people to take on their own lives. This technological world has made people cut contact with the world as people mainly use social media to interact with other people which is one of the major drawbacks of this technical world. People mainly believe in the online form of communication rather than meeting each other. They express their emotions, and opinions through different social media platforms like Facebook, Instagram, Twitter, etc. in the form of texts, audio, videos, and images. We can find people of each generation on this platform and hence this can be an identical dataset. This far-reaching presence of social media has made it quite straightforward for the user data available for analytical surveys.

Textual data is a widespread mode of interaction that is identical and the best way out for performing analysis. Main advantages of using textual data:

- less consumption of memory compared to other forms of data;
- manageable;
- easily available;
- processing is effortless.

Hence, for this purpose, tweets from the Twitter API come in handy and thoroughly satisfy all the above conditions and the extraction of the data is quite effortless to apply the machine learning algorithms to detect depression and anxiety. Detection of the mood with the help of textual data is complicated as compared to image processing. The proposed model is 'A chat-based forum' for detecting the mental health of the user. The main objective of this venture is to detect the depression and anxiety of the users with the help of a machine learning algorithm mainly a Decision tree and reply to them personally with motivational quotes along with the health care helpline numbers. It is a web-based application integrated with machine learning provided with tweets to train the algorithm. Machine learning algorithms can be handy to detect anxiety and forecast depression probability. After the extraction of the dataset variety of processing is done as discussed in the methodology to make it suitable to apply the supervised learning algorithms.

2 Motivation

Mental health plays an important role in day-to-day schedules. People mostly ignore the effects and importance of mental health. Mental health is importantly like Physical health. As people focus on their physical health and do regular exercise, fitness and the smooth functioning of the brain are also important. Interactions of the people has been reduced these days due to online meetings, chatting forums, etc. and hence people prefer to stay lonely which arises the problem of overthinking and anxiety as they don't

share things going on with them. Reduction of physical interaction and overthinking often lead to depression and if isn't detected soon might result in severe and harmful effects like suicidal attempts and even death. Technology is growing faster and Artificial Intelligence along with supervised machine learning algorithms is a vast field and many innovations are being done swiftly. One such innovation is detecting the mental health of people using Artificial Intelligence and machine learning algorithms. A lot of data is available on social media platforms which can be beneficial for applying supervised learning algorithms and creating a chat-based forum to detect the mental state. This approach may solve the problem of depression and anxiety to a certain extent as the user might be able to take necessary precautions and medication or might even consult a doctor which can help to reduce the risk.

3 Problem Definition and Scope

3.1 Problem Definition

“To scent the anxiety and depression on the social media platform using the supervised machine learning algorithms”.

3.2 Scope

Increasing the efficiency and performance of the algorithm can be done by including additional features to derive better results. This project has certain limitations as it can't handle slang and short words. Users generally use slang while chatting and processing this might get us away ahead of precise results. Moreover, an additional feature might be included which can test and differentiate between actual text and sarcasm or jokes. With the help of AI, we can just detect depression, and anxiety and let the user know about that. It depends upon the user how seriously it looks after the matter and takes certain precautions and improve his/her mental health.

4 Literature Review

In [1] dataset used is the tweets extracted from the Twitter API. The data set comprised 10,000 tweets which were further divided into an 80:20 ratio adopted mainly for training and testing respectively. The training word list consists of curated depressed words and tweets were collected at random including negative as well as normal tweets. Supervised learning classification has certain limitations. Sentimental detection mainly depends on the accuracy of the algorithm used. Though support vector machines tend to preprocess the large datasets the accuracy is reduced and due to high complications, human-level accuracy through the prediction of depression isn't granted.

Research work in [2] proposes a new online chatting system, named EmoChat, which automatically identifies the emotions of the users and attaches the identification result to the messages sent by the user, allowing users to know the emotions of each other during the online chatting. EmoChat is a new online chatting mobile application enhanced with emotional information. EmoChat makes users know about each other's emotional

states, thus they will feel more intimate with their conversation partners. Improving the accuracy of the algorithm and reducing the time consumption in future work.

Multiple methods are correlated to determine the levels of depression and enhance accuracy. The study [3] demonstrates a variety of features and a big dataset has enough strength to determine the mental status of the users. Dataset: An online community sourced from live Journal which is a collective blog site where different users can read and write their responses. Privacy rights are being violated. Moreover, Blogs can contain slang and abusive content which might decrease the accuracy of the model if they aren't taken into consideration.

The paper [4] advances toward categorizing the health tweets from the mixed tweets to determine the mental status using K-means clustering and Support Vector Machine. The system's accuracy isn't much effective to predict accurate results and it is restricted to only one language. Moreover, there are only two labels, Positive and Negative which can be extended up to five levels.

The difficulty of detecting depression on social media, as well as several machine learning methods that may be utilized to identify depression, are explored in this study [5]. The use of Ensemble Learning to solve this problem has been proven to be effective. To answer this challenge, we want to discover and apply the best appropriate technique and algorithm. Depression levels can be sent to another or family members or friends. Facebook posts and the Twitter dataset are used. The accuracy of the model is just 74%. Moreover, Facebook posts aren't relatable as people tend to post on the trending posts, and mostly the feed is just the happy side. Also, privacy is another consent. This paper [6] proposes to incorporate weighted and simplified entropy into the decision tree algorithm to improve the ID3 algorithm for the research of data mining algorithms based on a decision tree. On overall performance, the revised method outperforms the commonly used ID3 algorithm, according to the findings of the experiments. A new thorough assessment of machine learning methodologies in predicting mental health disorders is presented in [7]. Furthermore, in doing this systematic review, we use the PRISMA technique. Following the screening and identification processes, they included a total of 30 research publications in their review. The gathered research papers were then organized into categories based on mental health issues such as schizophrenia, bipolar disorder, anxiety and depression, posttraumatic stress disorder, and mental health issues in children. They discussed the findings and the obstacles and constraints that academics working on machine learning in mental health concerns confront. Additionally, they have made specific recommendations for future study and development in the field of mental health using machine learning. This work [8] seeks to give a bibliometric analysis and discussion of ML for mental health research trends on social media.

The purpose of this study [9] is to examine existing literature on the use of DL algorithms in mental health outcome studies. They begin by providing a quick review of current DL approaches. They next go over the literature on the use of DL in mental health outcomes. They divide these relevant articles into four categories based on the application scenarios: clinical data diagnosis and prognosis, genetics and genomics data analysis for understanding mental health conditions, vocal and visual expression data analysis for disease detection, and estimation of mental illness risk using social media data. Finally, they examine the difficulties of employing deep learning algorithms to

increase our understanding of mental illnesses, as well as potential promising prospects for its use in improving mental health diagnosis and treatment. Based on data sources, machine learning techniques, and feature extraction methods, this research offers a critical assessment analysis of mental health detection in Online Social Networks (OSNs) [10]. By defining its data analysis technique, comparison, problems, and limits, the suitability of mental health detection was also evaluated. The purpose of this article [11] is to investigate factors that contribute to mental health problems in chosen higher education students. Using machine learning algorithms, this study tries to categorize students into several categories of mental health disorders, such as stress, depression, and anxiety. The information was gathered from students at a Kuala Terengganu higher education college. Decision Tree, Neural Network, Support Vector Machine, Naive Bayes, and logistic regression are among the techniques used. Decision Tree, Support Vector Machine, and Neural Network are the most accurate models for stress, depression, and anxiety, respectively. The accuracy of five machine learning algorithms in diagnosing mental health concerns was examined using numerous accuracy criteria in this study [12].

Logistic Regression, K-NN Classifier, Decision Tree Classifier, Random Forest, and Stacking are the five machine learning approaches. We examined and executed different strategies, and the most accurate one was the Stacking strategy, which had an accuracy of prediction of 81.75%. The goal of this research [13] is to use machine learning to predict the mental health of medical personnel based on 32 parameters. Through a questionnaire survey, we gathered 32 elements from 5,108 Chinese medical personnel, and the findings of the Self-reporting Inventory were used to assess mental health. They offer a unique prediction model based on an optimization algorithm and a neural network in this study, which can pick and rank the most relevant elements affecting medical personnel's mental health. In addition, to forecast the mental health of medical personnel, they employed stepwise logistic regression, binary bat algorithm, hybrid enhanced dragonfly algorithm, and the suggested prediction model. The findings demonstrate that the suggested model has a prediction accuracy of 92.55 percent, which is higher than current techniques. This approach can be used to forecast worldwide medical workers' mental health. Furthermore, the strategy suggested in this research can aid in the development of a suitable work schedule for medical personnel. This survey [13] study attempts to provide a complete summary of the most recent advancements in this topic. This review investigates and quickly presents several newly proposed algorithm upgrades as well as numerous SA applications. The study [14] begins with an introduction to deep learning before moving on to a thorough examination of its present uses in sentiment analysis. This study [15] looks at methodologies and approaches that have the potential to directly allow opinion-based information-seeking systems. They are particularly interested in approaches that solve the unique issues posed by sentiment-aware applications, as opposed to those that are already present in the more traditional fact-based analysis. They've included content on evaluative text summarizing as well as larger concerns like privacy, manipulation, and economic effect that the proliferation of opinion-oriented information-access services has spawned. The proposed work in [16] integrated two trending technologies i.e., web technology with machine learning.

5 Methodology

5.1 Data Collection

As we tend to create a chat-based application forum similar to social media, social media data can be best suited for this venture. On analyzing different social media platforms, Twitter API tends to be one of the best and is available easily. Twitter feed mainly consists of audio, video, and textual format. Out of these, textual data in the form of comments, and tweets suits best as it is in the shorter format and consists of neutral data. In Fig. 1, the textual data set is easy to analyze as compared to the audio, and video files. A list of words is created which can determine the low mental health which becomes prone to depression. Before converting the dataset into.csv format, the data is filtered to get rid of the unwanted characters which can lower the accuracy of the algorithm or predict false results. At this point, about one-third of the data is filtered out and the rest of the data is then blended with the specific list keywords with the help of JSON objects. After segregating the data from the Twitter servers, the data set is further divided into two parts which generally comprise of training and testing dataset.

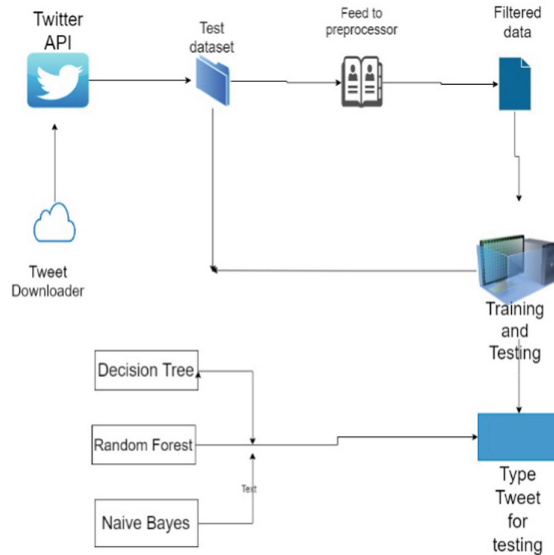


Fig. 1. Methodology.

5.2 Data Preprocessing

The information or the data in the dataset contains a lot of redundant and unstructured information which isn't necessary and if that surplus data isn't processed then it might result in a false outcome. Data preprocessing is obligatory before passing the data to the

training process. Certain Natural language Tools are brought into play while preprocessing the dataset. Dataset consists of filtering the data following certain important steps starting with the Tokenization.

5.3 Tokenization

Tokenization is a process of dividing the dataset or Tweets in the form of Tokens. The dataset extracted from the Twitter API contains slang words, URLs, emojis, mistyped words, punctuation marks, etc. In this process, slang, URLs, emojis, and punctuation marks are filtered out to get the desired results as these might result in misconceptions. Tokenization is followed by stemming.

5.4 Stemming

Stemming is a process of retrenching the texts back to the root type. After scaling back the words of similar types are clustered together. It is followed by removing the stop words which might result in unpredicted results.

5.5 Part of Speech Tagger

Parts of Speech Tagger is a software that is used to enhance the quality of the dataset by categorizing the dataset into a noun, verbs, adjectives, etc. It assigns the parts of speech to each token in the dataset. For example, I'm very depressed. In this given statement, very is an adjective, and depressed is a verb.

5.6 Bag of Word

After segregating the dataset and removing all the redundant stuff, the leftover dataset is preprocessed which is in the lower text format. As the name suggests, similar kind of words is bagged together depending upon how timely they are used, occurrences, mainly into positive affirmation and negative affirmation.

5.7 Training and Testing

Training is one of the key steps to training the algorithm. Once the tweets are segregated into positive and negative tweets. These are fed into an algorithm to make it learn. Based on this information, models are trained. In the testing process, the evaluation of the best algorithm can be done based on confusion metrics.

5.8 Flow Chart

In Fig. 2 shown the flow diagram of the proposed model. In the proposed model data is divided into two parts i.e., the training part and the testing part. So, firstly the data from the dataset is preprocessed. Then after cleaning the data, it gets split into two parts training which is 70% of the dataset, and testing which is 30% of the dataset. After cleaning and splitting the dataset NLP and decision algorithm starts working according to set parameters which at last gives us the derived/expected output.

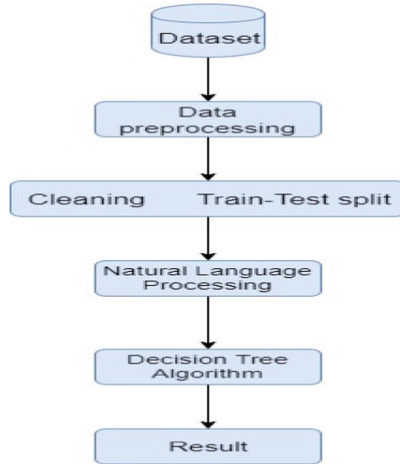


Fig. 2. Flow chart of system.

5.9 Confusion Matrix Diagram

The above confusion matrix shown in Fig. 3 is used to evaluate the result of the proposed model. The predicted values of the machine learning model are compared with the actual target values. Type I and Type II errors can be analyzed easily using the confusion matrix. The four values: true positive, false positive, true negative, and false negative are given in the matrix.

- True positive: These are the values where the predicted and actual values are the same, and both are positive.
- True negative: These are the values where the predicted and actual values are the same, and both are negative.
- False-positive (type I error): The predicted values are predicted falsely. The actual value is negative, but the model predicts a positive value.
- False-negative (type II error): The predicted values are predicted falsely. The actual value is positive, but the model predicts a negative value.

Using these four values precisions, recall, error rate, etc. are calculated.

5.10 Entropy

Consider Fig. 4, the entropy of the algorithm gives an idea of the extent of disordered data item the given set contains. The main objective of the algorithm is to classify the input into two categories orderly. Let us say that we have got “N” sets of the item, and these items fall into two categories, and now in order to group the data based on labels, we introduce the ratio: $P = (n/N)$ and $Q = (m/N) = 1 - p$. The entropy of our set is given by the following equation: $E = -p \log(p) - q \log(q)$.

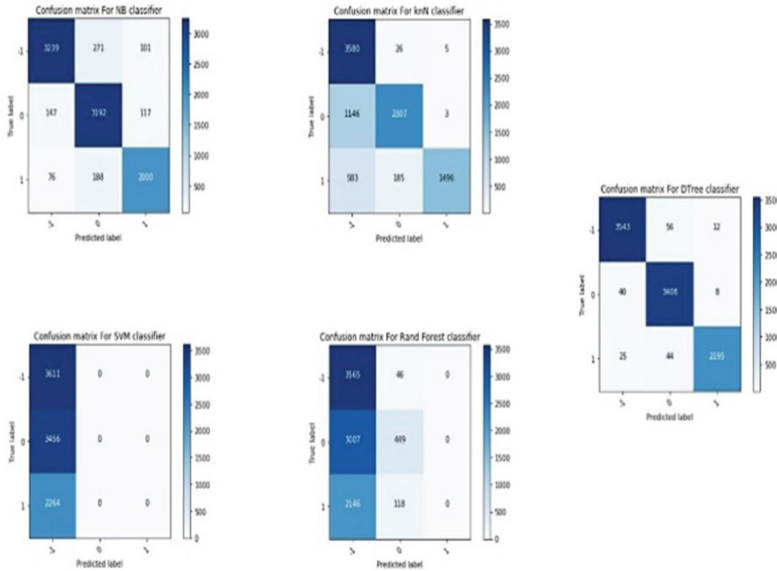


Fig. 3. Confusion matrix diagram.

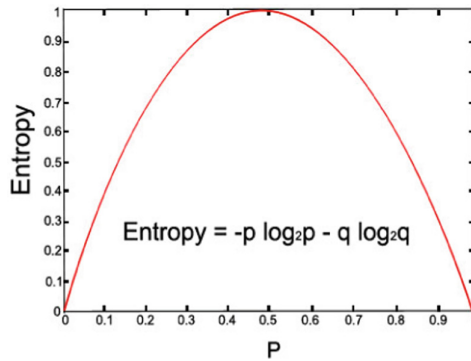


Fig. 4. Entropy.

6 Results

Plumping the efficient and precise algorithm can be predicted with the help of the FI score. Precision and recall are the two main values on which FI score can be found. The calculation formula for the FI score is $2 \times (\text{Recall} \times \text{Precision}) / (\text{Precision} + \text{Recall})$. The following Table 1 shows the accuracy by comparing techniques proposed in this paper. The completion time is also a key in determining the best algorithm of all. Hence, the Decision tree has more completion time as compared to the naïve Bayes classifier and Random Forest algorithm, but the accuracy is the best among all three. Hence, a Decision tree is chosen to be the best-suited algorithm.

Table 1. Accuracy of different machine learning algorithms.

No	Name	F1 score	Accuracy	Time of completion
1	Naive Bayes classifier	0.93794066482645	93.79	2.59778 s
2	Random forest algorithm	0.4910381377488	49.10	2.60996 s
3	Decision tree algorithm	0.985566874804587	98.56	3.40457 s

7 Conclusion

Detecting the depression using supervised machine learning algorithms and integrating it with the web development using Flask has been implemented using Twitter as the dataset successfully to predict the accurate results. The outcomes of the proposed model are precise and accurate as compared to the other supervised machine learning algorithms. Machine learning algorithm has been integrated successfully with web development to create a working application. Existing methods used Naïve Bayes classification and support vector machine. But the results achieved through the decision tree algorithm are more precise and accurate as compared to the rest of the algorithms. The outcomes predicted through Artificial Intelligence won't be perfectly accurate like humans. Misconceptions can be generated due to defects in the dataset errors generated during data preprocessing. This concept of the proposed model can be implemented on all the social media platforms which might help to detect depression reduce the risk at an early stage and might even save lives. In the future, there is a scope of increasing even more accuracy by using different algorithms and even using a more efficient dataset that contains less noise.

In the future we can include an additional feature that can test and differentiate between actual text and jokes, moreover, we can target more precise words by increasing the efficiency of the model.


References

1. Deshpande, M., Rao, V.: Depression detection using emotion artificial intelligence. In: 2017 International Conference on Intelligent Sustainable Systems (ICISS), pp. 858–862. IEEE, Palladam (2017). <https://doi.org/10.1109/ISS1.2017.8389299>
2. Chong, L., Jin, M., He, Y.: EmoChat: bringing multimodal emotion detection to mobile conversation. In: 2019 5th International Conference on Big Data Computing and Communications (BIGCOM), pp. 213–221. IEEE, QingDao (2019). <https://doi.org/10.1109/BIGCOM.2019.00037>
3. Saha, B., Nguyen, T., Phung, D., Venkatesh, S.: A framework for classifying online mental health-related communities with an interest in depression. *IEEE J. Biomed. Health Inform.* **20**(4), 1008–1015 (2016). <https://doi.org/10.1109/JBHI.2016.2543741>
4. Arora, P., Arora, P.: Mining twitter data for depression detection. In: 2019 International Conference on Signal Processing and Communication (ICSC), pp. 186–189. IEEE, Noida (2019). <https://doi.org/10.1109/ICSC45622.2019.8938353>
5. Dabhane, S., Chawan, P.M.: Depression detection on social media using machine learning techniques: a survey. *Int. Res. J. Eng. Technol.* **7**(11), 97–100 (2020)

6. Li, L., Zhang, X.: Study of data mining algorithm based on decision tree. In: 2010 International Conference on Computer Design and Applications, vol. 1, pp. V1–155. IEEE, Qinhuangdao (2010). <https://doi.org/10.1109/ICDDA.2010.5541172>
7. Chung, J., Teo, J.: Mental health prediction using machine learning: taxonomy, applications, and challenges. *Appl. Comput. Intell. Soft Comput.* **2022**, 9970363 (2022). <https://doi.org/10.1155/2022/9970363>
8. Kim, J., Lee, D., Park, E.: Machine learning for mental health in social media: bibliometric study. *J. Med. Internet Res.* **23**(3), e24870 (2021). <https://doi.org/10.2196/24870>
9. Su, C., Xu, Z., Pathak, J., Wang, F.: Deep learning in mental health outcome research: a scoping review. *Transl. Psychiatry* **10**(1), 116 (2020). <https://doi.org/10.1038/s41398-020-0780-3>
10. Abd Rahman, R., et al.: Application of machine learning methods in mental health detection: a systematic review. *IEEE Access* **8**, 183952–183964 (2020). <https://doi.org/10.1109/ACCESS.2020.3029154>
11. Mutalib, S.: Mental health prediction models using machine learning in higher education institution. *Turk. J. Comput. Math. Educ.* **12**(5), 1782–1792 (2021). <https://doi.org/10.17762/turcomat.v12i5.2181>
12. Vaishnavi, K., Kamath, U.N., Rao, B.A., Reddy, N.S.: Predicting mental health illness using machine learning algorithms. *J. Phys: Conf. Ser.* **2161**, 012021 (2022). <https://doi.org/10.1088/1742-6596/2161/1/012021>
13. Medhat, W., Hassan, A., Korashy, H.: Sentiment analysis algorithms and applications: a survey. *Ain Shams Eng. J.* **5**(4), 1093–1113 (2014). <https://doi.org/10.1016/j.asej.2014.04.011>
14. Zhao, S., et al.: Computational emotion analysis from images: recent advances and future directions. In: Ionescu, B., et al. (eds.) *Human Perception of Visual Information*, pp. 85–113. Springer, Cham (2022). https://doi.org/10.1007/978-3-030-81465-6_4
15. Pang, B., Lee, L.: Opinion mining and sentiment analysis. *Found. Trends Inf. Retr.* **2**(1–2), 1–135 (2008). <https://doi.org/10.1561/1500000011>
16. Pralhad, G.P., Abhishek, S., Kachare, T., Deshpande, O., Chounde, R., Tapadiya, P.: Web-based real-time gesture recognition with voice. In: Bhattacharya, M., Kharb, L., Chahal, D. (eds.) *ICICCT 2021. CCIS*, vol. 1417, pp. 119–131. Springer, Cham (2021). https://doi.org/10.1007/978-3-030-88378-2_10



Classification of Cardiovascular Disease Using AdaBoost Method

Kseniia Bazilevych , Mykola Butkevych , and Halyna Padalko  

National Aerospace University “Kharkiv Aviation Institute”, 17 Chkalova Street,
Kharkiv 61070, Ukraine
galinapadalko95@gmail.com

Abstract. The paper is devoted to diagnosing patients with cardiovascular disease. To determine the disease in medical diagnostics, statistical methods are most often used Data Mining, which with large amounts of information and complex relationships can give more accurate estimates, especially with a large number of similar characteristics. The machine learning model for cardiovascular disease classification based on AdaBoost method have been developed using Python programming language. We used dataset of 68783 patients with suspicious of cardiovascular disease. The results of the simulation show enough accuracy for using it in Public Health practice. Implementation of information system can increase diagnosing the cardiovascular disease by medical workers.

Keywords: Machine learning · Classification · Heart disease · Cardiovascular disease · AdaBoost

1 Introduction

Cardiovascular disease is the leading cause of death worldwide. They kill 17.9 million people every year [1]. Cardiovascular diseases are a group of diseases of the heart and blood vessels, which include coronary heart disease, cerebrovascular disease, rheumatic heart disease, and other pathologies. More than 80% of deaths from cardiovascular diseases occur as a result of heart attack and stroke and are premature [2].

The generally accepted classification of cardiovascular diseases includes [3]:

- arterial hypertension;
- coronary artery disease;
- acute coronary syndrome;
- non-coronary diseases;
- heart disease;
- heart failure;
- arrhythmia;
- atherosclerosis;
- phlebeurysm.

The most significant behavioral risk factors for heart disease and stroke are [4]:

- unhealthy food;
- tobacco use;
- alcohol abuse;
- low physical activity.

The consequences of these risk factors are manifested in the form of high blood pressure, overweight, and obesity, high glucose levels, and high blood lipids. These factors can be detected early in primary health care and indicate an increased risk of stroke, heart attack, and other complications associated with cardiovascular disease.

In Ukraine, cardiovascular diseases are the cause of death for 67% of the population [5]. At the same time, Ukraine is the country No. 1 in Europe and No. 2 in the world in the ranking of mortality from cardiovascular diseases. This is due to low awareness of the prevention of cardiovascular diseases and the need for medical supervision for the early detection of diseases. The most popular disease in Ukraine is arterial hypertension, which affects about 31% of people in the world [6].

One of the main conditions for preventing premature death from cardiovascular disease is to identify those at the highest risk of cardiovascular disease and provide them with appropriate treatment.

In recent years, the digitalization of all spheres of human activity has been widely developed. This is due to the global COVID-19 pandemic and the direction of the efforts of scientists around the world to combat it [7]. This area has not bypassed the digitalization of healthcare [8]. Thus, information technologies are used for modeling epidemic processes [9], diagnostics [10], modeling the spread of viruses [11], resource assessment [12], and disease research [13]. For early diagnosis of cardiovascular diseases, it is also effective to use classification methods, the highest results of which are shown by machine learning methods.

The study **aims** to develop a machine learning model for classifying patients with suspected cardiovascular diseases using the AdaBoost method.

Research is part of a complex, intelligent information system for epidemiological diagnostics, the concept of which is discussed in [14].

2 Materials and Methods

Boosting is an ensemble approach to machine learning [15]. Based on the reduction of bias and variance in supervised learning. A weak learning method is defined as a classifier that is weakly correlated with the correct classification. A strong algorithm is a classifier that correlates well with the correct classification.

Boosting benefits:

- Various loss functions can be considered. This makes it possible to solve both regression and classification problems. The ability to choose an arbitrary loss function allows you to focus on the features of the data in the problem.
- It is possible to consider any family of basic algorithms. This allows you to take into account the features of the required task and the data used.

- The method is easy to implement. Therefore, in each variation, it is possible to carry out mathematical and algorithmic optimizations that will speed up the operation of the method.

Boosting Disadvantages:

- The method has high computational complexity. It often requires the construction of hundreds of basic algorithms for composition.
- The method without additional modifications tends to adapt to the data, including stuffing and errors.
- The boosting method is poorly applicable to building a composition from fairly complex algorithms.
- The results of boosting are difficult to interpret.

Boosting is also applicable to the classification problem. In the case of binary classification, this means that $Y = \{-1, 1\}$. It is assumed that each algorithm $h \in H$ returns a real degree of membership of an object to some class, and the resulting answer F is obtained by applying the threshold rule to the composition.

In the case of classification, the loss function of one argument is usually used:

$$L(y, F) = L(yF). \quad (1)$$

that is, the indentation is replaced by the product of the real class and the predicted value.

In this case, there is an approach different from gradient boosting. The gradient of the error functional is understood as the vector of weights of training objects, element-wise multiplied by the correct values of the classes:

$$\nabla Q = \left(\frac{\delta L(y_i F_{m-1})}{\delta F_{m-1}} x_i \right)_{i=1}^N = \left(y_i \frac{\delta L(y_i F_{m-1})}{\delta (y_i F_{m-1})} x_i \right)_{i=1}^N = (y_i w_i)_{i=1}^N. \quad (2)$$

where $w_i = \frac{\partial L(y_i F_{m-1})}{\partial (y_i F_{m-1})} x_i$.

Then the learning algorithm following the principle of maximizing margins has the following form:

$$h(x, a_m) = \operatorname{argmin}_{a_m \in A} \sum_{i=1}^N L(y_i w_i h(x_i, a_m)). \quad (3)$$

W_i can be viewed in terms of the weights that are given to objects and taken into account when training each basic algorithm.

The AdaBoost method [16] implies that an exponential loss function is used:

$$L(y, F) = \exp(-yF). \quad (4)$$

AdaBoost is a classic version of boosting. For it, the main boosting theorem was proved for the first time with analytically calculated optimal bm at each step. Initially, AdaBoost considered the composition of $h \in H$ algorithms that return only values from Y

$= \{-1, 1\}$ ⁶. Subsequently, the method was generalized for $h \in H$ returning the probability of belonging to the class $\{1\}$ ⁷.

Consider a binary classification problem, where x_1, \dots, x_n with comparisons t_1, \dots, t_n , $t_i \in \{-1, 1\}$. Let each test case have a weight w_i whose initial value is $w_i = 1/N$. Let there be a procedure that trains some classifier that produces $y(x) \in \{-1, 1\}$ on weighted data. Then we initialize

$$w_n^{(1)} := \frac{1}{N}. \quad (5)$$

For $m = 1 \dots M$, we train the $y_m(x)$ classifier, which minimizes the error function

$$J_m = \sum_{n=1}^N w_n^{(m)} (y_m(x_n) \neq t_n). \quad (6)$$

Let's calculate the following function

$$\epsilon_m = \frac{\sum_{n=1}^N w_n^{(m)} (y_m(x_n) \neq t_n)}{\sum_{n=1}^N w_n^{(m)}}. \quad (7)$$

$$\alpha_m = \ln\left(\frac{1 - \epsilon_m}{\epsilon_m}\right). \quad (8)$$

Calculate new weights

$$w_n^{(m+1)} = w_n^{(m)} e^{\alpha_m (y_m(x_n) \neq t_n)}. \quad (9)$$

After training, we get:

$$Y_M(x) = \text{sign}\left(\sum_{m=1}^M \alpha_m y_m(x)\right). \quad (10)$$

3 Results

For implementation of the model, we have used open dataset of 68783 patients with suspicions of cardiovascular disease [17]. The parameters of the dataset is presented in Table 1.

Distribution by age is shown on Fig. 1. It is observed that quantity of people with cardiovascular disease is increasing with age. And after 55 years old, the quantity of people with cardiovascular disease is more than people without.

Distribution by weight and height is presented in Fig. 2.

The data set was divided into objects and objective function. This dataset was then split for training and testing. Prediction of the assessment of the accuracy of the condition of a patient with suspected cardiovascular disease was performed using the AdaBoostClassifier class, located in the Scikit-learn library.

Table 1. Initial data analysis.

Attribute	Scale type	Range
Age	Metric	30–65
Gender	Metric	1, 2
Height	Metric	55–250
Weight	Metric	11–200
Systolic pressure	Metric	60–240
Diastolic pressure	Metric	40–190
Cholesterol levels	Metric	1–3
Glucose level	Metric	1–3
Smoke	Metric	0.1
Alcohol	Metric	0.1
Physical activity	Metric	0.1
Cardio disease	Metric	0.1

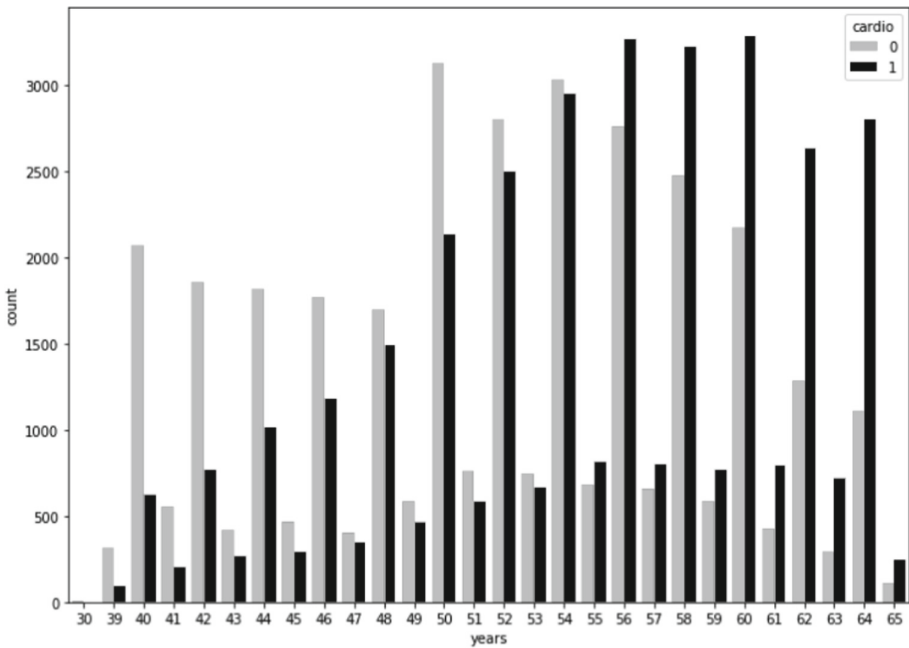


Fig. 1. Distribution patients by age.

The results for distribution of 40% for training and 60% for testing is presented in Table 2.

Table 2. Simulation results (40% – training, 60% – testing).

	Precision	Recall	f1-score	Support
0	0.71	0.79	0.74	13937
1	0.75	0.66	0.70	13577
Micro avg	0.73	0.73	0.73	27514
Macro avg	0.73	0.72	0.72	27514
Weighted avg	0.73	0.73	0.72	27514

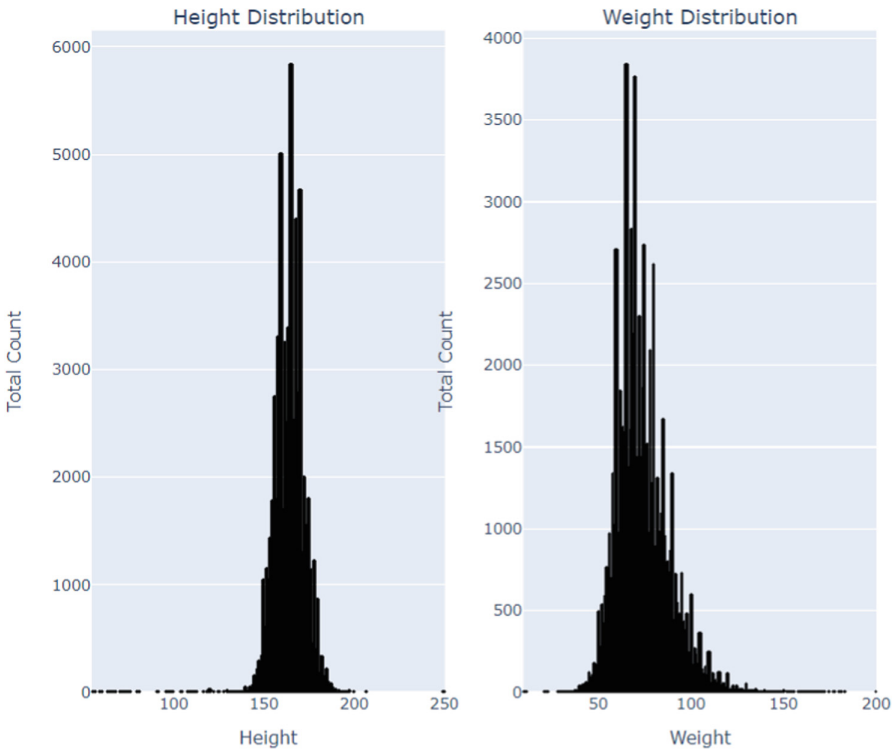


Fig. 2. Distribution of patients by height and weight.

Table 3. Confusion matrix (40% – training, 60% – testing)

10960	2977
4573	9004

Accuracy for 40% for training and 60% for testing is 0.725.

Confusion matrix for distribution of 40% for training and 60% for testing is presented in Table 3.

The results for distribution of 70% for training and 30% for testing is presented in Table 4.

Table 4. Simulation results (70% – training, 30% – testing)

	Precision	Recall	f1-score	Support
0	0,70	0,79	0,75	24304
1	0,76	0,66	0,71	23845
Micro avg	0,73	0,73	0,73	48149
Macro avg	0,73	0,73	0,73	48149
Weighted avg	0,73	0,73	0,73	48149

Accuracy for 70% for training and 30% for testing is 0.727.

Confusion matrix for distribution of 70% for training and 30% for testing is presented in Table 5.

Table 5. Confusion matrix (70% – training, 30% – testing)

19289	5015
8112	15733

4 Conclusion

The problem of classification in medical research is relevant, because. Allows detecting diseases at early stages. The task is especially relevant for patients with suspected cardiovascular diseases. When it should be noted that when classifying, the identification of True Positive and True Negative values is the most significant. In this case, the False Negative value is much more important than False Positive, because does not allow timely assistance to those in need. Thus, we can conclude that the classification accuracy obtained in the study using the AdaBoost model is sufficient for use in practical healthcare.



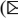

Acknowledgement. The study was funded by the National Research Foundation of Ukraine in the frame-work of the research project 2020.02/0404 on the topic “Development of intelligent technologies for assessing the epidemic situation to support decision-making within the population biosafety management”.

References

1. Van Camp, G.L.: Cardiovascular disease prevention. *Acta Clin. Belg.* **69**(6), 407–411 (2014). <https://doi.org/10.1179/2295333714Y.0000000069>
2. Oksak, G.A., Golovanova, I.A.: Contribution of mortality from cardiovascular disease to overall mortality. *Wiadomosci Lwkarские* **70**(3), 449–455 (2017)
3. Williams, J.W., Giannarelli, C., Rahman, A., et al.: Macrophage biology, classification, and phenotype in cardiovascular disease: JACC macrophage in CVD series (Part 1). *J. Am. Coll. Cardiol.* **72**(18), 2166–2180 (2018). <https://doi.org/10.1016/j.jacc.2018.08.2148>
4. Xia, J.Y., Lloyd-Jones, D.M., Khan, S.S.: Association of body mass index with mortality in cardiovascular disease: new insights into the obesity paradox from multiple perspectives. *Trends Cardiovasc. Med.* **29**(4), 220–225 (2019). <https://doi.org/10.1016/j.tcm.2018.08.006>
5. Terenda, N., Petrashyk, Y., Slobodian, N., Lishtaba, L.: Morbidity and prevalence of cardiovascular diseases in Ukraine: trends and forecasts until 2025. *Georgian Med. News* **282**, 79–82 (2018)
6. Oliveras, A., de la Sierra, A.: New developments in the diagnosis and management of resistant hypertension. *Curr. Med. Chem.* **19**(8), 1210–1218 (2012). <https://doi.org/10.2174/092986712799320592>
7. Abd-Alrazaq, A., Alajlani, M., Alhuwail, D., et al.: Artificial intelligence in the fight against COVID-19: scoping review. *J. Med. Internet Res.* **22**(12), e20756 (2020). <https://doi.org/10.2196/20756>
8. Jandoo, T.: WHO guidance for digital health: what it means for researchers. *Digital Health* **6**, 2055207619898984 (2020). <https://doi.org/10.1177/2055207619898984>
9. Chumachenko, D., et al.: Development of an intelligent agent-based model of the epidemic process of syphilis. In: 2019 IEEE 14th International Conference on Computer Sciences and Information Technologies (CSIT), vol. 1, pp. 42–45. IEEE, Lviv (2019). <https://doi.org/10.1109/STC-CSIT.2019.8929749>
10. Golinelli, D., Boetto, E., Carullo, G., et al.: Adoption of digital technologies in health care during the COVID-19 pandemic: systematic review of early scientific literature. *J. Med. Internet Res.* **22**(11), e22280 (2020). <https://doi.org/10.2196/22280>
11. Chumachenko, D., Chumachenko, K., Yakovlev, S.: Intelligent simulation of network worm propagation using the Code Red as an example. *Telecommun. Radio Eng.* **78**(5), 443–464 (2019). <https://doi.org/10.1615/TELECOMRADENG.V78.I5.60>
12. Dotsenko, N., Chumachenko, D., Chumachenko, I.: Modeling of the process of critical competencies management in the multi-project environment. In: 2019 IEEE 14th International Conference on Computer Sciences and Information Technologies (CSIT), vol. 3, pp. 89–93. IEEE, Lviv (2019). <https://doi.org/10.1109/STC-CSIT.2019.8929765>
13. Arefiev, V., et al.: Complete genome sequence of *Salmonella enterica* subsp. *enterica* serovar Kottbus strain Kharkiv, isolated from a commercial pork production facility in Ukraine. *Microbiol. Resour. Announc.* **9**(49), e01171-20 (2020). <https://doi.org/10.1128/MRA.01171-20>
14. Yakovlev, S., et al.: The concept of developing a decision support system epidemic morbidity control. *CEUR Workshop Proc.* **2753**, 265–274 (2020)
15. Dutta, J., Kim, Y.W., Dominic, D.: Comparison of gradient boosting and extreme boosting ensemble methods for webpage classification. In: 2020 Fifth International Conference on Research in Computational Intelligence and Communication Networks (ICRCICN), pp. 77–82. IEEE, Bangalore (2020). <https://doi.org/10.1109/ICRCICN50933.2020.9296176>
16. Wu, S., Nagahashi, H.: Parameterized AdaBoost: introducing a parameter to speed up the training of real AdaBoost. *IEEE Sig. Proc. Lett.* **21**(6), 687–691 (2014). <https://doi.org/10.1109/LSP.2014.2313570>
17. Ulianova, S.: Cardiovascular disease dataset. <https://www.kaggle.com/datasets/sulianova/cardiovascular-disease-dataset/metadata>. Accessed 8 May 2022



Retaining Wall Surface Optimization

Volodymyr Babaiev , Valeriy Shmukler , and Oleg Kalmykov  

O. M. Beketov National University of Urban Economy in Kharkiv, 17 Marshala
Bazhanova Street, Kharkiv 61002, Ukraine
oleg.kalmykov@kname.edu.ua

Abstract. The paper presents the formulation and implementation of the problem of finding a rational external geometry of a retaining wall. The purpose of the research is to formulate and test the mathematical model of the specified problem. In this connection, the working hypothesis is the assumption of accepting the criteria for rationalizing the system in the form of requirements for minimizing the potential strain energy of system (PSE) on the set of allowable values of variable parameters and equalizing the potential strain energy density (PSED) within the designated model. These criteria are an integral structural part of the bioenergetic optimization method, however, this paper considers the problem of improving external (geometric) parameters based on the exploitation of only the 1st criterion. In the framework of the exploitation of the Coulomb theory, the procedure of formation of the geometry of the structure is defined when the pressure of the ground on it is applied. The simplest example is the algorithm for solving the problem of finding rational geometry of the rear face of a subsurface wall with its given horizontal projection. The essence of the proposed approach is the approximation of the curvilinear forming the rear face of the subsurface wall by a broken line. For each section of the divided structure key dependencies are built for the components of the stress-deformed state of the structure. It is shown that for given soil characteristics, the value of the potential energy of deformation of the system can be described through a combination of the slope angles of each of the sections. The problem is reduced to finding a combination of these angles in which the entered criterion takes the minimum (exact lower bound) value. The conclusion about the representativeness of the obtained solution is made on the basis of the compiled alternative information model. The implementation of the approach is illustrated by a numerical example. The results obtained can be applied in the search for a rational geometry of a retaining wall in the process of building design.

Keywords: Potential strain energy · Surface shape · Lateral pressure · Bioenergy optimization

1 Introduction

Structural elements of buildings and structures that perceive lateral load from a loose material are those in which the magnitude and nature of the load are directly related to the configuration of the component that perceives the load. The generally accepted

theory of non-connected bulk pressure on the side surface, in particular the soil on the retaining walls, is the Coulomb theory [1]. According to this theory, the bulk pressure on the lateral surface is directly related to the coefficient of lateral pressure λ , which in turn depends on the geometrical parameters of the system (the internal friction angle of the bulk, the angle of inclination of the wall to the vertical, the seismic angle, the inclination of the filling, etc.) [2, 3].

A lot of modern scientific research is devoted to the issues of optimizing the parameters of cantilever retaining walls. As a rule, the authors describe the design of a retaining wall by a set of geometric or physical parameters, followed by a search for their rational combination. So, the authors of [4] Mergos and Mantoglou applied the Flower pollination algorithm (FPA) to find the minimum cost of a retaining wall structure by varying the 6 geometric parameters of the system. Bekdas and Temur [5] described the design of the cantilever retaining wall with 5 geometric and 6 physical parameters, and using the Teaching Learning-Based Optimization (TLBO) method, determined the minimum weight of the structure. Papers [6, 7] used the Harmony search algorithm (HAS) to find the minimum cost of a cantilever retaining wall, while the structure was described by 6 geometric parameters. Kaveh *et al.* considered the formulation of the problem of finding the minimum cost of a retaining wall using the Dolphin Echolocation Optimization (DEO) algorithm, describing the design by 7 geometric parameters [8, 9]. The paper [10] compares the Evolutionary strategy (ES), Differential evolution (DE) and Biogeography based optimization algorithm (BBO) algorithms as applied to the problem of finding the optimal parameters of a cantilever retaining wall, which is described by 8 geometric and 12 physical parameters. The above list is a small part of modern research devoted to optimizing the parameters of retaining walls [11]. It is noted that in all the works mentioned above, the design of the cantilever retaining wall was described by a finite number of parameters, and the minimum weight or cost of the structure was taken as the objective function.

The approach proposed in this paper differs in a key way from the known formulations. As a result of setting and solving the problem in the proposed interpretation, we determine the image of a rational construction. In this case, the number of variable parameters is changed within 100. In general, their exact value is set in accordance with the algorithm during the calculation, depending on the rate of convergence of the method.

It is known that the relationship between the lateral static pressure of a loose surface and the curvature of a wall that perceives this pressure can be written as a 4th degree polynomial [12]. According to the developed procedure, the lateral pressure e_{piur} of free-flowing is determined and by solving the equation the inclination angles of the tangent to the curve providing the specified pressure e_{pourse} are determined [13]. Thus, the magnitude and nature of the pressure depend on the curvature of the surface, and vice versa (bielement “retaining wall – soil”). At the same time, each formed retaining wall configuration has a unique lateral pressure distribution inherent only to it, and, consequently, an exclusive distribution of internal forces. If to the bielement “retaining wall – soil” add a restriction, for example, in the form of a constant value of horizontal projection of a wall or to limit maximum movements, it is possible to find a shape of it that will predetermine the minimum accepted criterion. The above provides a basis

for setting and solving the problem of controlling the geometric and/or physical and mechanical parameters of the system. In this paper, an attempt is made to introduce a single criterion that reflects the minimization of the potential energy of deformation of a bielement under given conditions of its support. This approach, among other things, involves the evaluation of a number of traditional attributes that often act as optimization criteria for particular problems (material volume, cost, stiffness, vibration frequencies, etc.) [14, 15].

2 Mathematical Model

In view of the above, an approximate method for searching for a rational surface of a retaining wall is proposed. The essence of the method is as follows. Considered the problem of direct design of a retaining wall. The external geometry of the structure is to be determined. Given that, as a rule, retaining walls are long constructions, their stress-strain state corresponds to a flat deformed state (flat deformation) and the model is considered in the form of a conventional flat curved rod (hereinafter – the rod). The size of the bar in a direction perpendicular to the plane of the drawing shall be taken to be equal to one. The solution is sought by Bionico-Energy (BEO) method [16]. Deformation is considered elastic. Visualization of the problem model is presented in Fig. 1. The initial data here are the vertical (L_y) and horizontal (L_x) generatrix projections of the axes of the flat Cartesian coordinate system and soil parameters providing maximum lateral pressure $q(y)$ (in the form of the weight γ and the angle of internal friction of the soil φ).

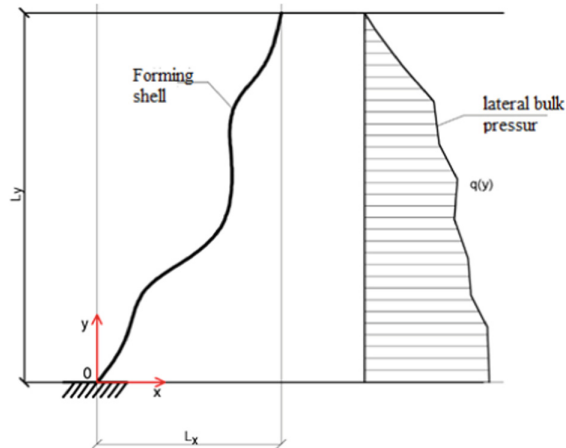


Fig. 1. Towards a problem model.

In the case of constancy of the rigidity of the rod according to its generatrix (arcs), the BEO method in use shall take as a criterion the minimization of the potential strain energy (PSE) of the system. In this case we have:

$$U = \int_0^l \frac{M^2(s)}{2EI} ds + \int_0^l \frac{N^2(s)}{2EA} ds + \int_0^l \frac{\alpha Q^2(s)}{2GA} ds \rightarrow \inf, \quad (1)$$

where E , G are deformation modules of the 1st and 2nd rod material, respectively; A , I is the area and moment of inertia of the rod; $M(s)$, $N(s)$, $Q(s)$ are the bending moment, longitudinal and transverse forces; α is a coefficient depending on the shape of the cross-section; ds is the arc differential.

In the event of a permanent stiffness:

$$U = \frac{1}{2EI} \int_0^l M^2(s) ds + \frac{1}{2EA} \int_0^l N^2(s) ds + \frac{\alpha}{2GA} \int_0^l Q^2(s) ds \rightarrow \inf. \quad (2)$$

Thus, hypotheses and assumptions are accepted in the following form:

- there are no cohesive forces between the particles in the soil;
- the configuration of the retaining wall is considered within the given vertical and horizontal projections of the system ($L_x = B$; $L_y = H$ – initial data);
- the angle of inclination of the retaining wall to the backfill cannot be less than the angle of internal friction of the soil ($\alpha \geq \varphi$);
- the problem is considered as a plane deformation.

Problem (1)–(2) in combination with the specified constraints ($L_x = \text{const}$; $L_y = \text{const}$) is a classical problem of variational calculus. At the same time, it is considered expedient to abandon the formation of the Euler-Lagrange equation by implementing a numerical solution of the problem.

3 Analytical Expression of the System PSE

For the determination of the PSE of a system (2), as noted above, a bi-aggregate is considered, consisting of a retaining wall and the soil acting on it. Accordingly, the following sequence of action is established:

1. The retaining wall is taken as a curvilinear cantilever rod which is rigidly fixed in the base. The wall is divided into n equal in height linear sections. The projection of the height of each of them on the vertical axis is h (Fig. 2).
2. The numbering of sections i starts at the base: bottom section $i = 1$, top section $i = n$.
3. Each section has its unique inclination α_i , which is in the range $\alpha_i [\varphi 90^\circ]$. Then the horizontal projection of each area b_i is:

$$b_i = h/\text{tg}(\alpha_i). \quad (3)$$

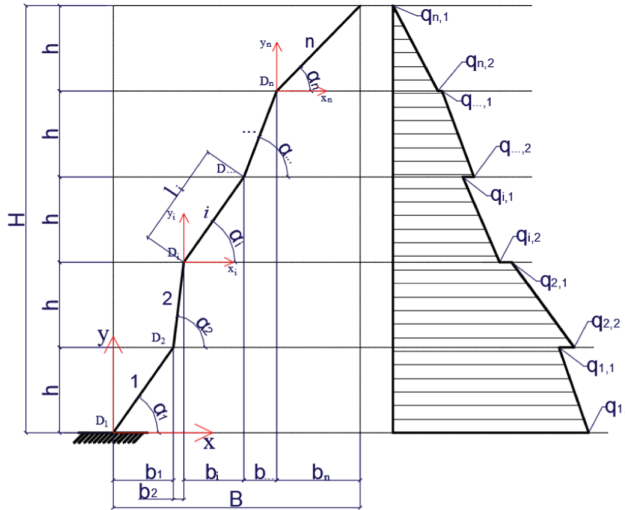


Fig. 2. Approximation of the configuration of the rod and the epius of loading by the linear function.

4. Length of each section l_i :

$$l_i = h / \sin(\alpha_i). \quad (4)$$

5. The distributed pressure at the base and vertices of each of the areas $q_{i,1}$ and $q_{i,2}$ respectively are defined by:

$$q_{i,1} = (H - h \times i) \times \gamma \times K, \quad (5)$$

$$q_{i,2} = [H - h(i - 1)] \times \gamma \times K, \quad (6)$$

$$K = [\operatorname{tg}(45^\circ - (\frac{\varphi + \varphi_i + 270^\circ}{2})) + \operatorname{tg}(\alpha_i + 270^\circ)]^2 \cos(\alpha_i + 270^\circ). \quad (7)$$

6. The distributed soil pressure in the zone of each j -th section is replaced by the resultant force (Fig. 3). The resultant forces are applied at the center of gravity of the j -th trapezoid, and are determined by the expression:

$$Q_j = \frac{q_{i,1} + q_{i,2}}{2} \times h, \quad (8)$$

where the meaning of local coordinate systems and the values of $q_{i,1}$ and $q_{i,2}$ follow from Fig. 2.

7. The coordinates of the point of application of the concentrated force O_i relative to the local coordinate system are defined by:

$$h_{0,i} = h \times m, \tag{9}$$

$$b_{0,i} = h_{0,i} / \text{tg}(\alpha_i), \tag{10}$$

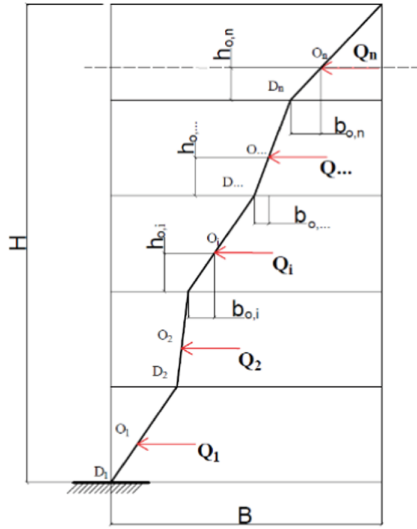


Fig. 3. Alignment of distributed load to concentrated forces.

$$m = \frac{2q_{i,1} + q_{i,2}}{3(q_{i,1} + q_{i,2})}. \tag{11}$$

Length of each section:

$$l_{0,i} = h / \sin(\alpha_i). \tag{12}$$

8. The bending moment epirus from the action of the j -th force will have the view represented in the Fig. 4. The bending moment $M_{i,j}$ at the base of the i -th section (point D_i) of the j -th force is defined as:

$$M_{i,j} = Q_j \times h_{i,j}, \tag{13}$$

where $h_{i,j}$ is the height from the base of the i -th section (D_i) to the j -th force vector (Fig. 3), defined by the expression:

$$h_{i,j} = h \times (j - i) + h_{0,j}. \tag{14}$$

9. Taking into account the pronounced nature of the stress-strain state, the expression for the estimated energy U (2) can be simplified and presented as:

$$U = \frac{1}{2} \int_0^l \frac{M^2}{EI} dx. \quad (15)$$

This position is justified by the small contribution of partial PSE values to (2) the longitudinal and transverse forces compared to the moment.

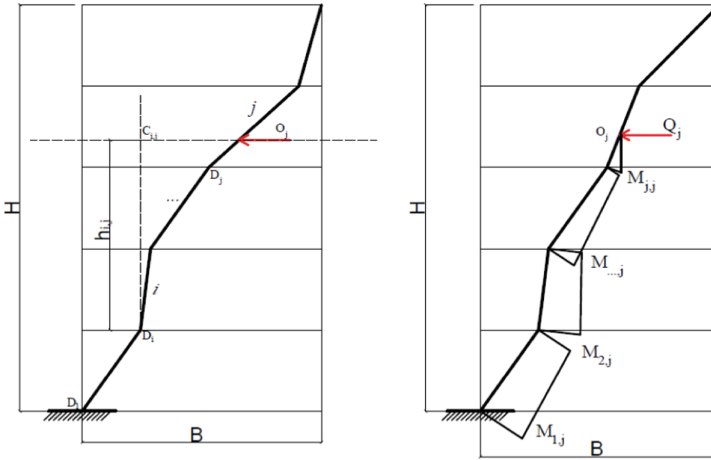


Fig. 4. Construction of the curve moments of the system.

10. Further, it is assumed that the PSE of the system U is equal to the sum of the private PSE $U_{j,tot}$ from the action of each of the forces in areas from 1 to n :

$$U = \frac{1}{EI} \sum_1^n U_{j,tot}. \quad (16)$$

11. The integral (15) is computed numerically by the formula of trapezoids:

$$U_{j,tot} = U_j + \sum_1^{j-1} U_i, \quad (17)$$

where

$$U_i = \frac{(M_{i,j}^2 + M_{i+1,j}^2 + \sqrt{M_{(i,j)}^2 \times M_{(i+1,j)}^2}) \times l_i}{3}, \quad (18)$$

$$U_j = \frac{M_{jj}^2 \times l_{o,j}}{3}. \quad (19)$$

The final task is formulated as follows. Find a combination of α_i , (external parameters) angles in which the PSE of the system (19) takes the minimum value:

$$U(\alpha_i) \rightarrow \inf. \quad (20)$$

4 Numerical Implementation of the Proposed Method

Within the proposed approach, the add-on “Finding a Solution” is used, an Excel function used for optimizing parameters [17]. The add-on allows to find a minimum target function using a generalized method of a given gradient. The data entered into the program are divided into 4 types:

- constants: source information (attributes of the system: characteristics of a loose medium φ , γ , height of system H , number of partition sections, n);
- variable cells: variable (combinations of slope angles of sections α_i);
- target function: the result for which the optimal values of the cells to be changed are selected (deformation energy, U);
- constraints: conditions to be taken into account when optimizing the target function (horizontal projection limitation B).

The following sequence of actions is used for this approach:

1. Input of the task input: φ , γ , H , n .
2. Set arbitrary inclination angles α_i , with limitations: α_i [φ ; 90°]; $B = \text{const}$.
3. Calculations are made using formulae (3) to (19) that determine the PSE of the system.
4. Pp. 2–3 are repeated for other inclination angles as long as the current U value differs by some small value from the previous one:

$$|U^{(k+1)} - U^{(k)}| \leq \delta. \quad (21)$$

The value of $U^{(k+1)}$ is selected as the minimum value and the corresponding combination of α_i values is written. The default accuracy of the calculation is $\delta = 0.000001$.

5. The retaining wall profile is being built.

The application of the Excel “Finding a Solution” option to the solution of the proposed problem makes it possible to determine the optimum topology of retaining walls at random source data. In Fig. 5 shown the resulting configuration of retaining walls for different partitioning grids.

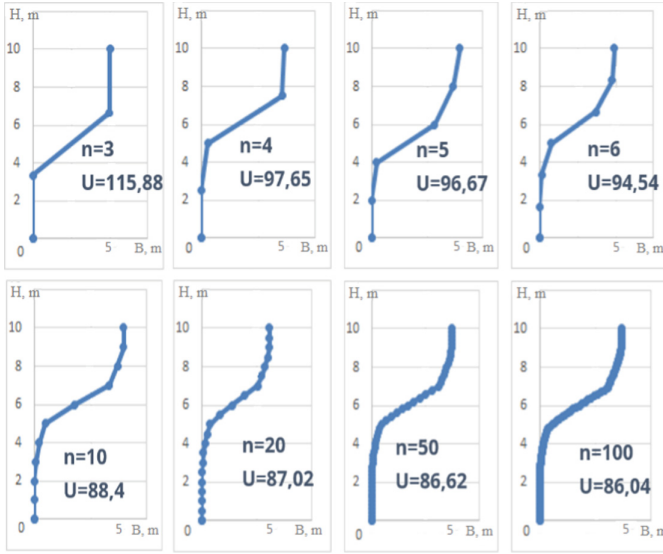


Fig. 5. Configurations of generators according to the number of partition plots.

When a partition mesh is tightened, the growth becomes smoother, the system's PSE indicator is progressively revealed, which, in general, manifests itself in the convergence of achieving a solution to the problem. The variation in the soil weight of the soft γ does not affect the configuration of the subsurface wall that minimizes the PSE of the system. However, the optimal configuration depends directly on the internal friction angle of the loose φ as shown in Fig. 6.

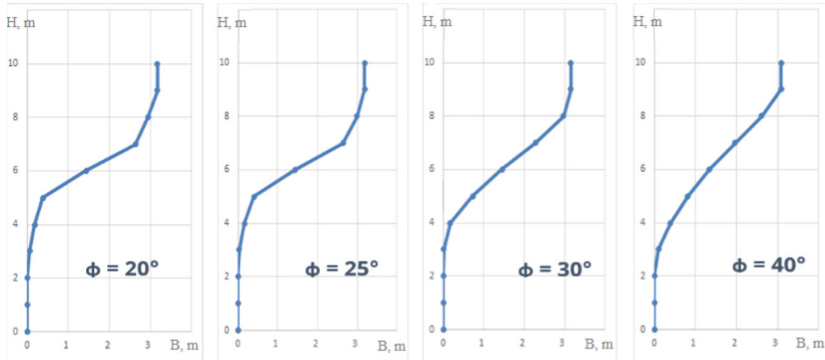


Fig. 6. Configurations of forming according to the accepted angle of internal friction of loose φ .

5 Numerical Verification of the Theoretical Results

In order to evaluate the topology of the retaining wall realized as a result of the proposed public observation, the BEO design block method was used. In this connection, a number of configurations of the generatrix of the retaining wall with a fairly wide range of changes in its geometry are considered. Next, the implementation of the finite element modeling of the compared structures with the determination of the PSE value collected during their deformation.

The “Lyra 10.8” is chosen as a software complex, the distinguishing feature of which compared to analogues is a tab on calculation of the PSE of the system [18]. As part of the analysis, the resulting configuration was compared with 5 similar systems that were built under the same restrictions, but with a difference in the shape of the generatrix (Fig. 7). The specified finite element models are shown in Fig. 8. All systems are a rigid fixed at the base. Initial data – geometrical restrictions ($L_x = \text{const}$; $L_y = \text{const}$) and characteristics of soil for each system are assumed to be the same.

As a result of the calculation, the PSE was determined for each of the above schemes, the displacement of the top of the wall, as well as the main frequency of natural vibrations (Table 1, Fig. 9).

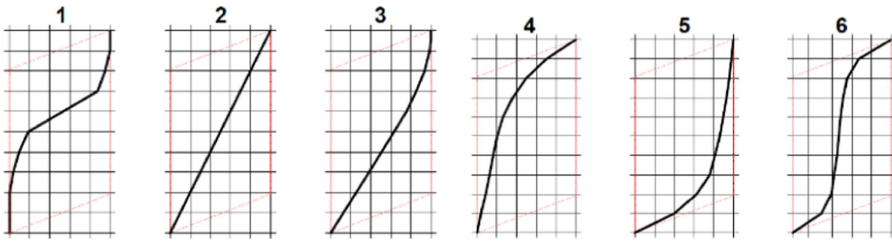


Fig. 7. Surface configurations (profiles) to be investigated.

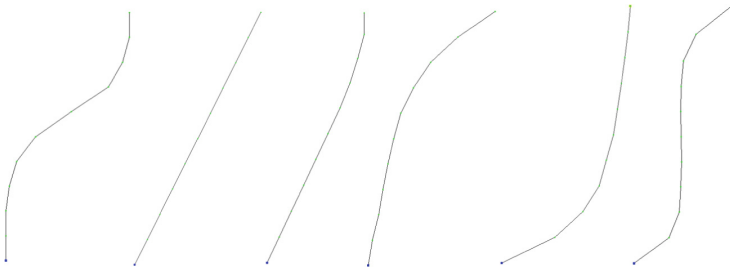


Fig. 8. FE models of the surfaces under consideration.

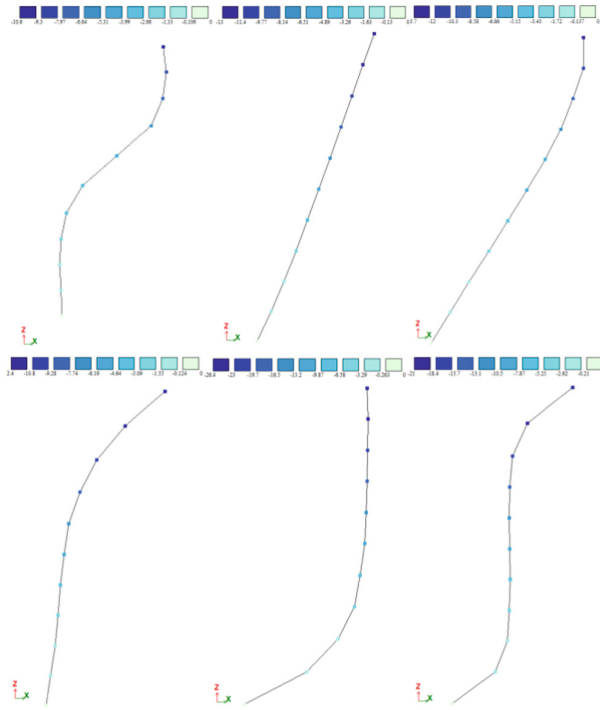


Fig. 9. Movements of the system in the direction of application of the load.

Table 1. Results of calculations.

	Schematic number					
	1	2	3	4	5	6
PSE system, relative units	1.771	2.542	2.721	2.682	7.460	5.923
Maximum movements, mm	10.63	13.03	13.73	12.38	26.33	20.99
Frequency of natural oscillations, Hz	1.771	2.542	2.721	2.682	7.460	5.923

As can be seen from the information in Table 1, scheme 1, the geometry used, obtained by using the proposed use, the minimum PSE of the system. At the same time, this scheme is characterized by the minimum value of the maximum deflection compared to the rest, as well as the minimum frequency of the fundamental tone of natural oscillations. The information provided proves the correctness of the proposed recognition and the representativeness of the criterion for minimizing the PSE system adopted in the work.

6 Conclusion

On the basis of the BEO method, the problem of finding a rational external geometry of the “retaining wall - soil” bielement was formulated and solved. The scientific novelty of the work lies in the formulation and solution of the problem of finding the rational geometry of the logical constructive bielement “retaining wall - soil” based on the introduction of a single generalized control criterion. The practical significance of the work lies in the possibility of using its results in the design of structural elements with predetermined positive properties. The scientific hypothesis of the statement is confirmed by comparing the obtained solution with the results found by alternative, well-tested methods. The numerical implementation of the problem confirms the fact that the formed solution, according to the SEM minimization criterion ($U = 1.771 \text{ r.u.}$), corresponds to an element with a minimum deflection ($f = 10.63 \text{ mm}$) and a minimum frequency of the fundamental tone of natural vibrations ($\omega_o = 0.328 \text{ Hz}$). In conjunction with the possible variation of the stiffness characteristics of the structure, it is permissible to correctly “adjust” the system to specific terrain conditions. In further studies, it is of interest to consider various complicating factors as applied to this problem. We should include other types of structural support, anchoring, multi-layer backfill soil mass, complication of the internal geometry of the structure.


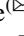



References

1. Khosravi, M.H., Bahaaddini, M., Kargar, A.R., Pipatpongsa, T.: Soil arching behind retaining walls under active translation mode: Review and new insights. *Int J. Min. Geo-Eng.* **52**(2), 131–140 (2018). <https://doi.org/10.22059/ijmge.2018.264011.594754>
2. Jadar, C., Ghosh, S.: Pseudo-dynamic analysis of shallow strip footing considering non-linear rupture surface. *Int. J. Geotech. Eng.* **11**(1), 38–50 (2017)
3. Nimbalkar, S., Choudhury, D.: Design of earth retaining structures and tailing dams under static and seismic conditions. In: 50th Indian Geotechnical Conference (IGC-2015), pp. 1–10. University of Wollongong (2015)
4. Mergos, P.E., Mantoglou, F.: Optimum design of reinforced concrete retaining walls with the flower pollination algorithm. *Struct. Multidiscip. Optim.* **61**(2), 575–585 (2019). <https://doi.org/10.1007/s00158-019-02380-x>
5. Temur, R., Bekdas, G.: Teaching learning-based optimization for design of cantilever retaining walls. *Struct. Eng. Mech.* **57**(4), 763–783 (2016). <https://doi.org/10.12989/sem.2016.57.4.763>
6. Bekdaş, G., Arama, Z.A., Kayabekir, A.E., Geem, Z.W.: Optimal design of cantilever soldier pile retaining walls embedded in frictional soils with harmony search algorithm. *Appl. Sci.* **10**(9), 3232 (2020). <https://doi.org/10.3390/app10093232>
7. Uray, E., Çarbaş, S., Erkan, İ.H., Tan, Ö.: Parametric investigation for discrete optimal design of a cantilever retaining wall. *Challenge J. Struct. Mech.* **5**(3), 108 (2019). <https://doi.org/10.20528/cjsmec.2019.03.004>
8. Kaveh, A., Hamedani, K.B., Bakhshpoori, T.: Optimal design of reinforced concrete cantilever retaining walls utilizing eleven meta-heuristic algorithms: a comparative study. *Periodica Polytech. Civ. Eng.* **64**(1), 156–168 (2020). <https://doi.org/10.3311/PPci.15217>
9. Kaveh, A., Farhoudi, N.: Dolphin echolocation optimization for design of cantilever retaining walls. *Asian J. Civ. Eng. (Build. Hous.)* **17**(2), 193–211 (2016)

10. Gordan, B., Koopialipour, M., Clementking, A., Tootoonchi, H., Tonnizam Mohamad, E.: Estimating and optimizing safety factors of retaining wall through neural network and bee colony techniques. *Eng. Comput.* **35**(3), 945–954 (2018). <https://doi.org/10.1007/s00366-018-0642-2>
11. Gandomi, A.H., Kashani, A.R., Roke, D.A., Mousavi, M.: Optimization of retaining wall design using evolutionary algorithms. *Struct. Multidiscip. Optim.* **55**(3), 809–825 (2016). <https://doi.org/10.1007/s00158-016-1521-3>
12. Babaev, V.N., Shmukler, V.S., Feirushah, S.H., Kalmikov, O.A.: Rational design of retaining walls. *J. Appl. Emerg. Sci.* **3**(1), 94–121 (2012). <https://doi.org/10.36785/jaes.3129>
13. Kalmykov, O., Khalife, R., Grabowski, A.: Search for rational contour of back surface of retaining wall. *AIP Conf. Proc.* **2077**(1), 020024 (2019). <https://doi.org/10.1063/1.5091885>
14. Talatahari, S., Sheikholeslami, R.: Optimum design of gravity and reinforced retaining walls using enhanced charged system search algorithm. *KSCE J. Civ. Eng.* **18**(5), 1464–1469 (2014). <https://doi.org/10.1007/s12205-014-0406-5>
15. Yepes, V., Alcalá, J., Perea, C., González-Vidosa, F.: A parametric study of optimum earth-retaining walls by simulated annealing. *Eng. Struct.* **30**(3), 821–830 (2008). <https://doi.org/10.1016/j.engstruct.2007.05.023>
16. Babaev, V., Ievzerov, I., Evel, S., et al.: *Rational Design of Structural Building Systems*. DOM Publishers, Berlin (2020)
17. Xu, M., Mei, Z., Luo, S., Tan, Y.: Optimization algorithms for construction site layout planning: a systematic literature review. *Eng. Constr. Archit. Manag.* **27**(8), 1913–1938 (2020). <https://doi.org/10.1108/ECAM-08-2019-0457>
18. Geraymovich, Y.D., Yevzerov, I.D., Marchenko, D.V.: The new physically nonlinear finite elements in software package LIRA 10.8. *Int. J. Comput. Civ. Struct. Eng.* **15**(1), 61–66 (2019). <https://doi.org/10.22337/2587-9618-2018-15-1-61-66>



Adaptive Blockchain Solution to Fight Against Financial Corruption in an Organization

Premanand Ghadekar , Tejas Kachare , Sagar Sikchi , Talib Hussain ,
and Pradunya Maladhari 

Vishwakarma Institute of Technology, Pune 411037, India
tejas.kachare18@vit.edu

Abstract. This Blockchain technology is one of the most promising new technologies, having the potential to digitally transform a wide range of systems for better security, autonomy, transparency, auditability, speed, cost savings, and efficiency. These capabilities make blockchain the optimal solution to combat corruption, the issue plaguing society from within. The paper proposes a blockchain model capable of handling finances in any organization by adapting to its financial structure. It has the ability that it can be tailored by the organization on-demand as the organization's structure modifies from the addition of employees or projects under it. Rather than storing entire data on-chain, the blockchain model stores most of the data, that are constantly being updated and created, off-chain and feed them to the blockchain using Chainlink External API. This helps in making the implemented solution scalable and efficient in use for real-life applications.

Keywords: Blockchain · Chainlink · Corruption · Ethereum

1 Introduction

Corruption is defined as the misuse of entrusted power for personal benefit. Corruption stifles economic development, diminishes confidence, and exacerbates inequality, poverty, social division, and environmental calamity. Only by understanding how corruption works and the processes that enable it we can expose it and hold corrupt individuals accountable. Corruption works as an ineffective tax on the company, rising production costs, and decreasing investment profitability. It goes on to say that corruption weakens a country's tax system and revenue collecting capabilities, as well as having an impact on enterprises' growth, productivity, investment patterns, and efficiency [1].

In the fight against government corruption, blockchain has the potential to play a unique role. A blockchain is a distributed database where it gets shared with computer network nodes. The blockchain's unique feature is that it maintains data record integrity and security while also building confidence without the need for a trusted third party [2]. Its technology integrates permanent, tamper-evident record-keeping, real-time transaction transparency and auditability, and automated smart contract capabilities into a single solution. To be sure, blockchain won't be able to prevent all crimes or defeat bad actors on its own. While blockchain can enhance and strengthen existing legal frameworks

and social institutions, the system it is a part of limits its usefulness. Blockchain-based governance may be no more successful at avoiding corruption than present rules and regulations without consistent law enforcement, proper informational inputs, suitable technological know-how, cooperating political elites, and public goodwill [3].

The proposed model is a customizable, adaptive, and robust blockchain solution that allows organizations to define their structure while also assigning authority to entities (e.g., employees). These entities aid in handling transactions among users according to imposed rules and create a scalable solution that can handle large amounts of data generated by each organization in the system. The proposed model, which is based on the blockchain paradigm, may be used by any organization, regardless of its structure.

2 Literature Review

Ray and Abdul Rashid Ibrahim Sanka suggested a paradigm for investigating corruption in developing countries [4], using Nigeria as a case study. They proposed a blockchain architecture to combat public-funds embezzlement, which is the most common form of corruption. They also presented a blockchain architecture and consensus system that would be appropriate for the framework. With the help of this proposed model, all government transactions were simultaneously logged on the blockchain, which is shared by anti-corruption agencies, police, judiciaries, and other associated offices. Edimara Luciano et al. conducted a thorough investigation by first identifying all potential segments where corruption exists [5], and then analyzing which segments can be improved using blockchain technology, thereby mitigating corruption in the segments discovered during the investigation. The purpose of the proposed model was to see how a blockchain might help reduce corruption risks in the Brazilian setting. Hasna El Alaoui El Abdallaou et al. developed a digital architecture for the development of a tool for mapping corrupt activities based on the principles of crowdsourcing, blockchain technology, and smart contracts in [6]. They created an application that gathers, aggregates, displays, and securely saves the reported data on a blockchain-based limited-access ledger. This article focuses on questionable transactions that can be reported to authorities after receiving official confirmation. The suggested model aimed to make data exchange and protection easier, to assure traceability, to achieve complete transparency, to give every person a digital identity, and to map corruption. Using this model reporters would then be able to track and monitor the government's response to actions taken via the application.

The study in paper [7] addresses the uses of blockchain technology as a tool for combating corruption and identifies the obstacles that must be overcome. The paper also mentions that how blockchain technology helps food security, supply-chain management, voting systems, property and real estate management, international trade, and so on. When it comes to security, trust, and integrity, these segments encounter several issues. According to the paper, some of the challenges faced for implementation of technology are Data governance and security, Incumbents' resistance. In [8] Luciano Floridi et al. from Oxford University have introduced the study of how centralized governments are compromised, as well as the approaches and obstacles that blockchain technology will face in resolving the problem. [9] Discusses some of the most common public-sector scams and recommends using smart contracts to automate the bidding process, supplier

qualification, and delivery verification stages of a public-sector procurement method. [11] proposed a model integrating an interactive website with emerging technologies like machine learning.

Matthew Davis et al. proposed a study on how blockchain can tackle the corruptive practices of multinational enterprises in emerging markets [10]. The paper outlines two technologies (public and private blockchain) that may be deployed and utilized to normalize market misconduct using blockchain networks. MNEs might employ either public or private blockchain solutions, depending on the network's requirements and design. However, as previously stated, there are trade-offs for each, best characterized by the so-called Blockchain trilemma. Most public blockchains emphasize security and stability through widespread decentralization and employ incentive mechanisms to encourage people to join. Because so many nodes must agree, the network's performance (transaction throughput) suffers, and scalability suffers as a result (ability to support concurrent users). Private blockchains do not require broad decentralization to safeguard their network since only chosen few have the authority to interact with the ledger. As a result, they tend to offer better speed and scalability, and they do not require their participants to secure the network through reward tokens. The paper concludes that governments' adoption of blockchain technology is contingent on political will (e.g., based on economic forecasts that promise significant economic returns in terms of additional financial resources, a larger tax base, and increased productivity that contributes to society's welfare) and a digital infrastructure. Harmonization of technological standards for blockchain is a key problem that may necessitate not just favorable legislation but also broad participation from powerful firms, professional groups, and other industry organizations. When many industrial players are engaged, blockchain-based governance may not be limited to isolated islands in the sector that can be easily avoided, resulting in a zero-net effect on societal corruption. As a result, blockchain installation necessitates a deliberate effort in which all stakeholders agree to the gradual use of blockchain technology.

In [3] case study by Per Aarvik covers some important things about blockchain technology and how it can be an anti-corruption tool. The study goes over real-world instances of blockchain implementation, such as Georgia's Land Registration Rights, India's Aadhaar Card, Estonia's X-Road, and so on. This study does not go into the future of blockchain, but based on their research and knowledge, they believe that blockchain will be in high demand in the future and will be able to effectively combat corruption. Blockchain features protocols and standards that govern the legal assertions and authority that must be present in the network, ensuring that no illegitimate nodes are added. It is becoming increasingly harder to break through secure networks due to the usage of powerful encryption technologies such as SHA-256 hashing. According to this study, the obstacles that blockchain technology faces include increasing power usage and costs for network transactions. However, because many firms are working on blockchain, answers to these difficulties will ultimately emerge.

The work [12] examines prominent blockchain systems and conducts a comprehensive analysis of the security risks to the blockchain, as well as a survey of the corresponding genuine assaults. Kelsie Nabben explains blockchains as a sociotechnical construct in [13], and she analyses the many types of blockchains as well as the common security

guarantees that blockchains provide. Then, for both public and private blockchains, it takes a sociotechnical security approach, defining blockchain security as people security (Applying Socio-Technical Security to Blockchains Section). The article [14] looks at how blockchain technology is developing and how it might impact a variety of industries, including supply chain management, the Internet of Things (IoT), healthcare, governance, banking, and manufacturing. By reviewing the study through comprehensive literature analysis, also explores and gives insights into the security challenges and dangers linked to blockchain deployments. The paper [15] reviews peer-reviewed literature that tries to leverage blockchain for cyber security aims and provides a comprehensive overview of the most extensively used blockchain security applications.

3 Objectives

Objectives of the work are to monitor each transaction of each node in the system, develop a customizable blockchain solution that gives the organization the ability to define its structure along with assigning authority to entities (e.g., employees) which helps in handling the transactions among the users as per imposed rules and make a scalable solution that is capable of handling large amounts of data generated by each organization in the system.

4 Implementation

For the implementation of the adaptive blockchain solution, a prototype is made using Chainlink API and Ethereum blockchain in the backend.

4.1 Front End

The front end has been created using React.js. Login/Sign-up, addition/deletion of users/nodes in the organizational structure and request for a (blockchain) transaction are the 3 major operations that users can do from the front end. Users will also be allowed to check transaction history.

4.2 Off-Chain Database

An off-chain database takes care of handling most of the user's data, e.g., public key, authority level, organization details, and some personal details. Storing major data off-chain helps us reduce the storage required on blockchain and hence reduce the gas-cost users might have had to pay for basic requests.

4.3 Ethereum Blockchain

The smart contracts deployed on Ethereum handle all the transactions among the users. They take care of the entire authentication and validation, following a set of rules for the transaction.

4.4 Chainlink External API

The chainlink API acts as a mediator between the Off-chain database and the hybrid smart contract on the blockchain.

4.5 Adaptive/Customizable Nature of Mode

The Organization has its structure and follows its hierarchy. The proposed model is customized based on the organization’s hierarchical structure (Fig. 1). This is explained with the help of an example.

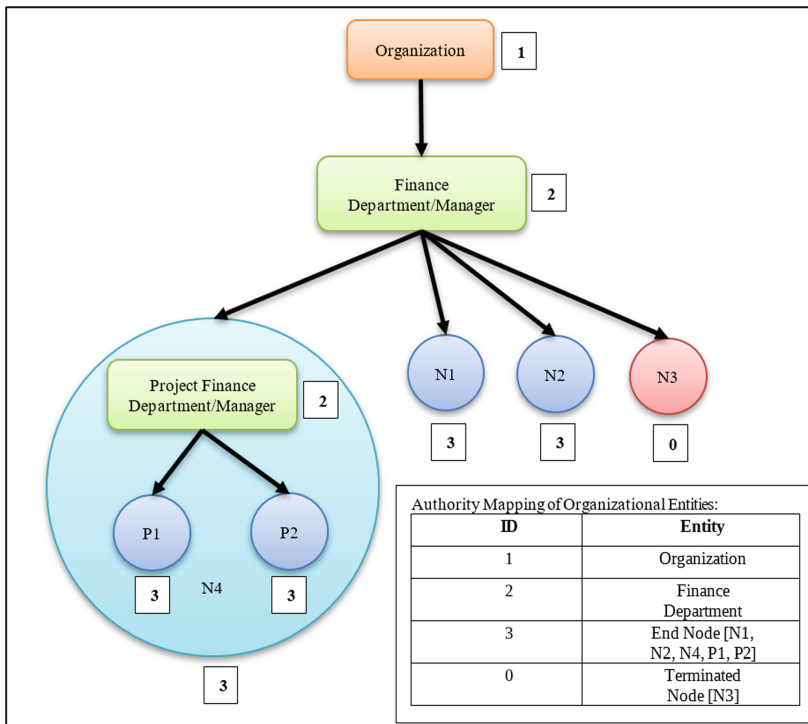


Fig. 1. Hierarchical structure of an organization.

Consider Fig. 1, it defines the hierarchical structure of the Organization and its System. Each Entity in the structure is treated as Node in the diagram (Fig. 2). The end-user/employee of the Organization is the end/leaf node denoted in the circle. The Project Node is the End/Leaf Node when a project is created and after completion of the project, it is considered as the Terminated Node.

Each node has its own number/Authority/ID. The node at the higher depth has a higher ID in magnitude and lesser authority. For example, Organization Node is the root node at Depth 1 and has ID 1, while End Node is the leaf node at Depth 3 (MAX DEPTH) and has ID 3 (MAX ID). The different terminologies mentioned in Fig. 1 are:

- **Organization.** The root node with the highest priority. It has all the rights such as adding new nodes, terminating existing nodes, sending tokens/transactions, updating IDs of other nodes, etc. The ID of this node is always 1. And this node can never be terminated.
- **Finance Manager/Department.** This node is responsible for sending token amounts to all nodes present below its depth. It handles all the transactions inside the organization. The ID of this node will always be greater than or equal to 2.
- **End Node.** This node is the leaf node (can be treated as end-user). This node gets the token amount from nodes present above its depth. The responsibility of this node is to work on the actual tasks. The ID of the end node is the highest in magnitude among all the present nodes in the hierarchy.
- **Terminated Node.** This node is the dead node having Fixed ID 0. Any node can be terminated except the organization itself. The terminated node has no further responsibilities associated with it.
- **Project Node.** The project node is the temporary node. This node is created when a new project is taken by the organization and after completion of the project, it is terminated. This node is treated as an end node in the main hierarchy, but it may have its sub-hierarchy as mentioned in Fig. 1.

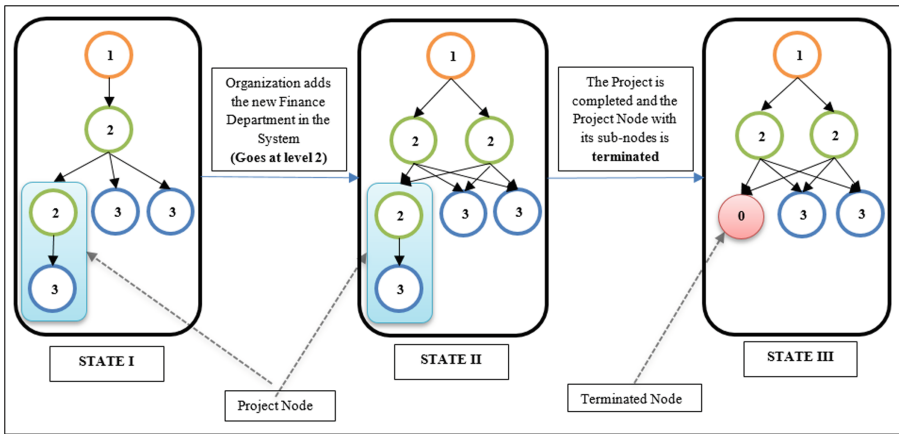


Fig. 2. Different states of organization’s structure.

In Fig. 1. Shown default organizational hierarchy. But different organizations have different structures. The blockchain model proposed is customizable concerning organizational structure. Figure 3 illustrates this point.

The smart contracts written in the back end of the model are adaptive to this behavior of the organizational structure. So, it will not break the network of the different departments/nodes of the hierarchy.

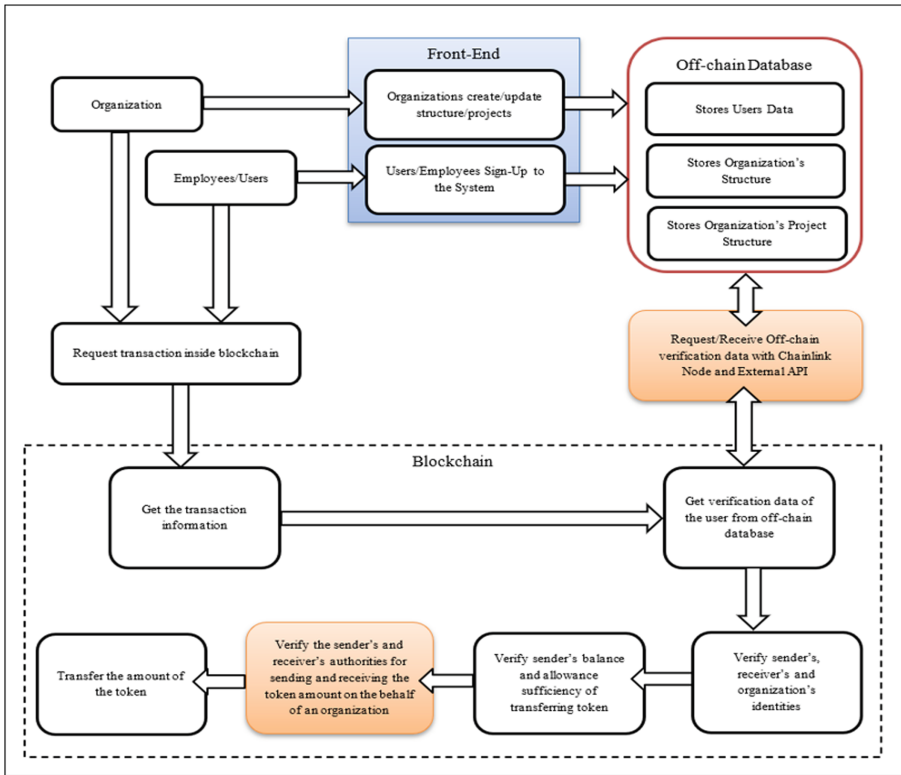


Fig. 3. Proposed adaptive blockchain model/solution.

5 Design and Methodology

5.1 Changing Organization Structure

If a new user needs to be added into the system or the user authority needs to be updated, then it is done as follow.

The employee's public key taken and mapped to the organization. The employee is also assigned an authority level as part of the organization. The employee details are stored in the off-chain database. The structure of the organization transforms based on the employee's authority. A similar process is followed when an organization wants to create a new project or a new contract (e.g., Government contracts to build infrastructure). The updated structure diagram of the organization can be seen in the above diagram. In the following way, the structure of the organization can be changed as per the requirements without affecting the financial management of the organization. A similar process is followed by the organization in case a new project or a new contract (e.g., Govt. Contract to build infrastructure) has been given to the company. The project acts as a new node, part of the organization, with authority level 2. The tokens are sent to the wallet of the project and the manager appointed for the project handles the transactions to be done for

managing the project. In this manner, all the transactions associated with the organization are being managed by the blockchain model.

5.2 Handling User Transaction

The blockchain solution follows the following algorithm for handling transactions between two nodes:

1. Take the amount to be transferred to the receiver as an input. Send request via chainlink external API to off-chain data (userBalance and authorityLevel).
2. Pre-transaction verification:
 - Check if the user is part of the system(organization).
 - The amount to be sent should be greater than 0.
 - Check if the sender's tokenBalance \geq amount to be transferred.
 - Check if the sender's authority is greater than the receiver's authority.
 - Check if the senderAllowance \geq TokenAmount.

Send the tokenAmount from the sender's wallet to the receiver's wallet. Transaction complete.

6 Experimentation

A prototype is required to experiment feasibility of the proposed model and see what the model is going to be capable of doing and further discuss security aspects of it. The model promises an adaptive blockchain solution for keeping transaction records on blockchain and tackling large data processing problems generated by organizations by keeping those data off-chain and feeding them to the blockchain smart contract which keeps a record of the transactions. Data like users' identities, organizations' structure information, and projects information are kept off-chain because they are being created, updated, and removed continuously and requires a flexible storage platform to store, on the other hand, each transaction made by anyone in the system is checked by blockchain for identification of the transaction signer and off-chain data which is feed to the blockchain from off-chain data. As a result, this makes the model adaptive to an organization's structure and can record all transactions happening inside it.

Organizations and individuals can create and storing their identity information in the system which will allow the organizations to create their customized structure and add individuals/employees to the structure and give them a certain level of authority for making transactions on behalf of the organization as it is shown in Fig. 4. That the organization has changed (**user3**) role from terminated to an employee. Additionally, organizations can create projects which have their structure that can be customized by the organization. The functionality of adding people to the organization's structure and updating their status and making the blockchain work with the data provided by off-chain which provides the flexibility makes the model adaptive to the ever-changing data of the organization and at the same time handle it in a robust way.

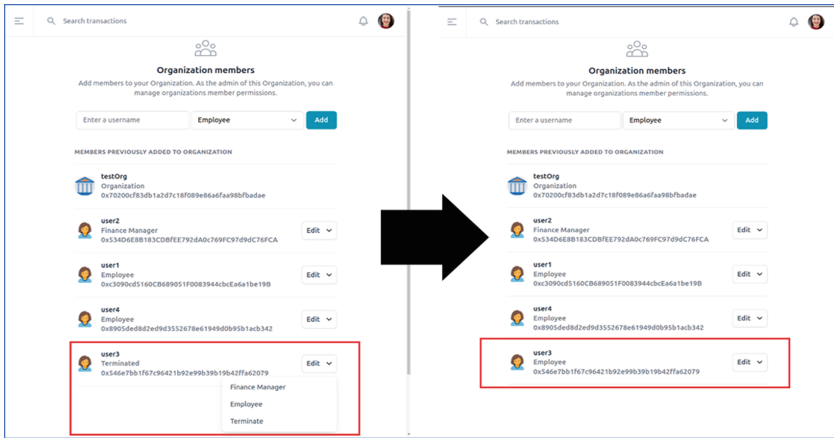


Fig. 4. Organization’s activity – update existing user node in structure.

7 Results

The adaptiveness of the proposed blockchain model/solution has been verified with the help of sample token transactions. Considering the two transactions given in Fig. 5 and Fig. 6., it has been shown that the blockchain solution is giving expected results and successfully following the defined instructions for adaptive nature. The Fig. 6a. Shows that the amount is going to be transferred from Finance Manager (user1) to Employee (user2) present within Organization’s Structure. As per the authority mapping shown in Fig. 1, the Chainlink API/External Adapter gives back the JSON formatted data as output (shown in Fig. 5b. The red box). The data provided from Chainlink API (Fig. 5(b)) states that senderAuthorityID is 2, receiverAuthorityID is 3 (refer Fig. 1), and both the authorities are in the system (allInSystem: 1, 1 stand for TRUE). Since ID 2 is less than ID 3 in magnitude, and both the sender and receiver belong to the organization, the transaction happening is valid. Therefore, the transactionof1PLT token/amount is done along with 0.4PLT token as a Gas Fee (shown in the red-colored box in Fig. 5c).

Now, the Employee (user2) has been terminated by the Organization (shown in Fig. 6a). So, the ID of the Employee has been changed from 3 to 0 (refer Fig. 1.). The transaction does not happen as receiverAuthority is Terminated. Hence, only the Gas Fee has been deducted (Fig. 6c) and the transaction is treated as an invalid transaction. The results show that the blockchain model is robust and can work without any system breaks after changes happen in the organization. The model monitors each financial transaction with the organization and solves the problem of unauthorized transactions happening in the organization.

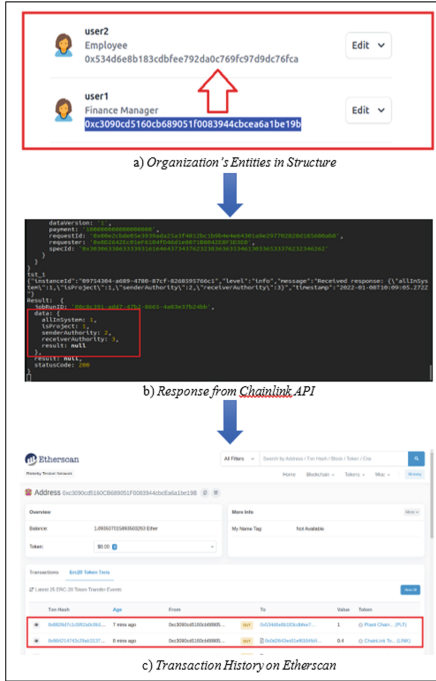


Fig. 5. A valid transaction in the proposed adaptive blockchain model/solution.



Fig. 6. An invalid transaction in the proposed adaptive blockchain model/solution.

8 Limitations

Single Point of Failure. The off-chain database is a vital part of the proposed model to make the blockchain behave adaptively, be permissioned, and provide identity to every participant (e.g., organizations, employees) but all of that doesn't come without a cost. It makes the blockchain rely on a centralized database for any transaction that will be done by the system. In case the connection to the off-chain database is lost, all transactions among the nodes will halt. Validation of authority and authentication of employees, organizations, etc. depends on off-chain data. Hence, the model has the drawback of a single point of failure.

9 Conclusion

The Blockchain model was proposed to aid organizations in their financial needs by monitoring its flow and allowing administrators to control it as per specified rules, hence fighting corruption in the organization. The prepared prototype based on the blockchain model is capable of being applied to every organization irrespective of its structure. The prototype showcases great potential in terms of financial applications and

is scalable as per the organization's demands and proves the worthiness of the proposed blockchain model. The future scope is to develop an adaptive tokenomics standard that every company can use to introduce and issue a new token that can be recognized only by that company (its lifecycle starts and ends within the company). That means that every organization can use its customized tokens. It will help the company use blockchain without worrying about adopting the usual Ethereum token standards that may or may not be suited for their company.



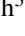


References

1. Dimant, E., Tosato, G.: Causes and effects of corruption: what has past decade's empirical research taught us? a survey: causes and effects of corruption. *J. Econ. Surv.* **32**(2), 335–356 (2018). <https://doi.org/10.1111/joes.12198>
2. Abodei, E., Norta, A., Azogu, I., Udokwu, C., Draheim, D.: Blockchain technology for enabling transparent and traceable government collaboration in public project processes of developing economies. In: Pappas, I.O., Mikalef, P., Dwivedi, Y.K., Jaccheri, L., Krogstie, J., Mäntymäki, M. (eds.) *I3E 2019. LNCS*, vol. 11701, pp. 464–475. Springer, Cham (2019). https://doi.org/10.1007/978-3-030-29374-1_38
3. Aarvik, P.: Blockchain as an Anti-corruption Tool: Case Examples and Introduction (U4 Issue 2020:7). Bergen, U4 Anti-Corruption Resource Centre (2020)
4. Sanka, A.I., Cheung, R.C.: Blockchain: panacea for corrupt practices in developing countries. In: 2019 2nd International Conference of the IEEE Nigeria Computer Chapter (NigeriaComputConf), pp. 1–7. IEEE, Zaria (2019). <https://doi.org/10.1109/NigeriaComputConf45974.2019.8949626>
5. Luciano, E., Magnagnagno, O., Souza, R., Wiedenhöft, G.: Blockchain potential contribution to reducing corruption vulnerabilities in the Brazilian context. In: 2020 Seventh International Conference on eDemocracy & eGovernment (ICEDEG), pp. 135–142. IEEE, Buenos Aires (2020). <https://doi.org/10.1109/ICEDEG48599.2020.9096749>
6. El Alaoui El Abdallaoui, H., El Fazziki, A., Sadgal, M.: Crowdsourcing and blockchain-based e-government applications: corruption mapping. In: Hamlich, M., Bellatreche, L., Mondal, A., Ordenez, C. (eds.) *SADASC 2020. CCIS*, vol. 1207, pp. 86–99. Springer, Cham (2020). https://doi.org/10.1007/978-3-030-45183-7_7
7. Kim, K., Kang, T.: Will blockchain bring an end to corruption? Areas of applications and potential challenges. *Int. J. Inform. Syst. Soc. Change (IJISSC)* **10**(2), 35–44 (2019). <https://doi.org/10.4018/IJISSC.2019040103>
8. Aggarwal, N., Floridi, L.: The opportunities and challenges of blockchain in the fight against government corruption. In: 19th General Activity Report of the Council of Europe Group of States against Corruption (GRECO), pp. 1–4. GRECO (2018)
9. Weingärtner, T., Batista, D., Köchli, S., Voutat, G.: Prototyping a smart contract based public procurement to fight corruption. *Computers* **10**(7), 85 (2021). <https://doi.org/10.3390/computers10070085>
10. Davis, M., Lennerfors, T.T., Tolstoy, D.: Can blockchain-technology fight corruption in MNEs' operations in emerging markets? *Rev. Int. Bus. Strategy* **32**(1), 39–56 (2021). <https://doi.org/10.1108/RIBS-12-2020-0155>
11. Pralhad, G.P., Abhishek, S., Kachare, T., Deshpande, O., Chounde, R., Tapadiya, P.: Web-based real-time gesture recognition with voice. In: Bhattacharya, M., Kharb, L., Chahal, D. (eds.) *ICICCT 2021. CCIS*, vol. 1417, pp. 119–131. Springer, Cham (2021). https://doi.org/10.1007/978-3-030-88378-2_10

12. Li, X., Jiang, P., Chen, T., et al.: A survey on the security of blockchain systems. *Futur. Gener. Comput. Syst.* **107**, 841–853 (2020). <https://doi.org/10.1016/j.future.2017.08.020>
13. Nabben, K.: Blockchain security as “people security”: applying sociotechnical security to blockchain technology. *Front. Comput. Sci.* **2**, 599406 (2021). <https://doi.org/10.3389/fcomp.2020.599406>
14. Idrees, S.M., Nowostawski, M., Jameel, R., Mourya, A.K.: Security aspects of blockchain technology intended for industrial applications. *Electronics* **10**(8), 951 (2021). <https://doi.org/10.3390/electronics10080951>
15. Taylor, P.J., Dargahi, T., Dehghantanha, A., et al.: A systematic literature review of blockchain cyber security. *Digit. Commun. Netw.* **6**(2), 147–156 (2020). <https://doi.org/10.1016/j.dcan.2019.01.005>



Analytical Solution of Modified Mackey-Glass Equation

Roman Voliansky¹ , Nina Volianska² , Oleksiy Sinkevych³ ,
Serhii Serhiienko⁴ , and Valeriy Kuznetsov⁵ 

¹ National Technical University of Ukraine “Igor Sikorsky Kyiv Polytechnic Institute”,
37 Polytechnichna Street, Kyiv 03056, Ukraine
volianskyi.roman@l11.kpi.ua

² Dniprovsk State Technical University, 2 Dniprobudivska Street, Kamyanske 51918, Ukraine

³ National Forestry University of Ukraine, 103 Generala Chuprynka, Lviv 79057, Ukraine

⁴ Kremenchuk Mykhailo Ostrohradskyi National University, 20 Pershotravneva Street,
Kremenchuk 39600, Ukraine

⁵ Railway Research Institute IK, 50 Józefa Chłopickiego Street, 04-275 Warsaw, Poland

Abstract. The paper deals with the design of methodological backgrounds for the study of time-delayed piecewise-linear dynamical systems. These backgrounds allow us to define dynamical system responses to the internal and external disturbances in an analytical way. We define these responses as the piecewise functions of relative system operation time which is used by us to simplify the system model. According to the well-known method of solution of time-delayed differential equations, we split all operation time into equal slices, which are specified by the value of time delay. Due to operating with piecewise-linear right-hand expression in the differential equation, we split each slice into several stages if the output variable in the previous slice reaches the fracture point. Contrary to known methods of analytical solution of time-delayed differential equations the proposed one makes it possible to determine system motions as a function of time delay value and times where piecewise function is fractured. We formalize our approach and propose the algorithm to determine the considered system motions. We use this algorithm to study the Mackey-Glass equation with the constant parameters and piecewise-linear function in the right-hand expression. A comparison of the analytical and numerical solutions of this equation shows that the error does not exceed a step of numerical integration and gives us the possibility to claim the correctness of given formulas. Analysis of our formulas shows that the equation of the modified Mackey-Glass system can be solved analytically in advance and thus its motion can be predicted. This fact requires to use of chaotic systems with piecewise nonlinearity with big caution.

Keywords: Dynamical system · Time-delay system · Piecewise-linear function · Analytical solution

1 Introduction

The piecewise-linear dynamical systems [1, 2], are often used in the modern theory of dynamical systems [3, 4]. One can explain the huge interest in these systems [5], on the

one hand by the simplicity of their technical implementations [6, 7] while systems are being designed and from another hand by the unique features of these systems [8, 9]. For example, a saturation function, which is used in the control systems to prevent plants or processes from damaging, bounds control energy flows [10]. One can find the use of piecewise-linear functions as the membership functions in fuzzy [11, 12] and neuro [13] applications to make intellectual decisions.

In some applications piecewise-linear functions dramatically changes operation modes of dynamical systems. That is why they found their applications in the control [14, 15], energy [16, 17], and communication [18] systems. The various chaotic systems are used to improve the security of the last ones, the Chua [19], and Mackey-Glass [20, 21] systems are among them.

The main requirement for chaotic systems is producing unpredictable motions. Since the systems which are described with piecewise-linear function on some stages of their motions can be specified by linear expressions the problem to study their secured features is the important one.

For the classical nonlinear Mackey-Glass system this problem is solved by using different iterative [22, 23] and intellectual methods [24, 25] we offer to use the exact mathematical methods to study the modified Mackey-Glass system, which is determined by using piece-wise linear functions.

Our paper is organized as follows: at first, we perform modeling of the Mackey-Glass system, then we give the general analytical solution for the time-delayed piecewise-linear differential equation on an example of the Mackey-Glass equation, at third a solution for the specific example is given, at last, we make conclusions.

2 Method

2.1 Mackey-Glass System Modeling

It is a well-known fact that chaotic oscillations occur in the systems which dynamics are described by the time-delayed first-order differential equations. The one of the most studied chaotic systems from the systems of this class is Mackey-Glass system

$$\frac{dy}{dt} = -\gamma y + \beta \frac{y_\tau}{1 + y_\tau^n}, \tag{1}$$

where γ and β are some coefficients, y is an output variable and y_τ means that the output variable is delayed for τ seconds, n is some exponent index.

The continuous nonlinear function in the second summand can be replaced with a piecewise-linear function and motion of dynamical system (1) is described in such a way

$$\frac{dy}{dt} = -\gamma y + \begin{cases} c_{11}y_\tau + c_{10} & \text{if } 0 \leq y_\tau < y_{s1}; \\ c_{21}y_\tau + c_{20} & \text{if } y_{s1} \leq y_\tau < y_{s2}; \\ 0 & \text{otherwise,} \end{cases} \tag{2}$$

here c_{ij} are approximation coefficients.

We call (2) as the modified Mackey-Glass system and we offer to simplify it by transforming into another time domain, where the time is interrelated with the conventional time by following expression [26]

$$T = \gamma t, \quad dT = \gamma dt, \quad \tau_\gamma = \gamma t. \quad (3)$$

We call T as a relative time.

In the new time domain (2) takes the form

$$\frac{dy}{dT} = -y + \begin{cases} d_{11}y_{\tau_\gamma} + d_{10} & \text{if } 0 \leq y_{\tau_\gamma} < y_{s1}; \\ d_{21}y_{\tau_\gamma} + d_{20} & \text{if } y_{s1} \leq y_{\tau_\gamma} < y_{s2}; \\ 0 & \text{otherwise,} \end{cases} \quad (4)$$

where $d_{ij} = \frac{c_{ij}}{\gamma}$ and y_{τ_γ} means signal time delay in a new time domain.

Now we add to the right-hand expression of (4) a control signal u

$$\frac{dy}{dT} = u - y + \begin{cases} d_{11}y_{\tau_\gamma} + d_{10} & \text{if } 0 \leq y_{\tau_\gamma} < y_{s1}; \\ d_{21}y_{\tau_\gamma} + d_{20} & \text{if } y_{s1} \leq y_{\tau_\gamma} < y_{s2}; \\ 0 & \text{otherwise,} \end{cases} \quad (5)$$

We call (5) as the controllable form of modified Mackey-Glass system.

2.2 Solution of Modified Mackey-Glass Equation in an Analytical Way

Let us show the solution of (5). At first, we formulate following initial conditions

$$y(0) = y_0; \quad y(T < 0) = 0. \quad (6)$$

The second assumption in (6) allows us to neglect the third summand in (5) and consider the system motion in the first time slice $0 \leq T < \tau_\gamma$ as defined by the differential equation

$$\frac{dy}{dT} = u - y. \quad (7)$$

The solution of (7) is a trivial one

$$y = u(1 - e^{-T}) + y_0 e^{-T}. \quad (8)$$

Now we back our attention to system (5). This system moves under initial condition y_0 and input signal u for a τ_γ seconds in the first time domain slice. After the right border of this domain is reached the value of system output becomes

$$y(\tau_\gamma) = u(1 - e^{-\tau_\gamma}) + y_0 e^{-\tau_\gamma}. \quad (9)$$

It is clearly understood that the (9) is an initial condition for the system motion in the second time slice. Let us consider the second time slice $[\tau_\gamma, 2\tau_\gamma)$. In this slice the time-delayed piecewise-linear function in the third summand makes its influences in the system motion and one should take it into account. Thus, values of y should be analyzed

and determined in which of three intervals $[0, y_{s1})$, $[y_{s1}, y_{s2})$, or $[y_{s2}, \infty)$ these values are and whether function values reach fracture points. If fracture points are reached by function (8) in the considered time slice, we specify times when these points are reached. One can find these times as solutions of equations

$$y_{s1} = u \left(1 - e^{-T_i} \right) + y_0 e^{-T_i}. \quad (10)$$

for T_i . If all of this times are real numbers or at least one of them is a real number and if these numbers belong to the interval $[0, \tau_\gamma]$, conclusion about reaching of fracture point is made. Several stages of the considered system motion should be studied in this slice.

1. If the initial value of state variable y_0 is greater then y_{s2} , the system dynamic is defined as follows

$$\frac{dy}{dT} = u - y. \quad (11)$$

if the fracture point y_{s2} is reached in the considered time slice, then (11) is considered only in the time interval $[\tau_\gamma, \tau_\gamma + T_{s2})$, where

$$T_{s1} = - \ln \left(\frac{u - y_{s2}}{u - y_0} \right). \quad (12)$$

It is clearly understood, that the system dynamic is described by function (8) and at the second switching point the output coordinate reaches value

$$y(\tau_\gamma + T_{s2}) = u(1 - e^{-\tau_\gamma - T_{s2}}) + y_0 e^{-\tau_\gamma - T_{s2}} = y_{s2}. \quad (13)$$

at the end of the considered time interval.

2. If time T_{s2} is less than τ_γ the system motions continues in the second slice. The motion in this stage continues from the fracture point y_{s2} and described by following differential equation

$$\frac{dy}{dT} - y + u + d_{21}u \left(1 - e^{-T+\tau_\gamma} \right) + d_{21}y_0 e^{-T+\tau_\gamma} + d_{20}. \quad (14)$$

If one analyzes (5), he finds that (14) determine any motions that has initial conditions equals or less y_{s2} and greater than y_{s1} . The main differences between the motion, which starts from value in interval $[y_{s1}, y_{s2})$, and the continued motion are the motion time and initial conditions. If we consider a system motion in the second stage as the continuation of a motion, which is defined by (11), we should take into account that T_{s2} seconds in the second slice already gone. This fact reduce the time, when the value of system trajectory is determined for the next stage or slice. If one solves (14), he gets following function

$$y = (1 + d_{21})u - Td_{21}ue^{-T+\tau_\gamma} + Te^{-T+\tau_\gamma} + d_{21}y_0 + d_{20} + C_1 e^{-T}. \quad (15)$$

here C_1 is an initial condition-dependent factor.

If the system motion start from y_0 less than y_{s2} , one can specify C_1 as follows

$$C_1 = -d_{21}u - d_{21}y_0 - d_{20} - u + y_0, \quad (16)$$

in case of continued motion, the last summand replaced with y_{s2} .

The motion in this stage of the second slice can be finished if the slice border is reached or if output variable reaches a new fractional point. In the first case the state variable value at the stage end can be defined by substituting into (15) motion time T_2 in the second stage

$$y(T_2) = (1 + d_{21})u - T_2 d_{21} u e^{-T_2 + \tau_\gamma} + T_2 e^{-T_2 + \tau_\gamma} + d_{21}y_0 + d_{20} + C_1 e^{-T_2}. \quad (17)$$

The motion time T_2 equals to the second slice length if the system moves from some initial position y_0 and it can be determined as follows

$$T_2 = \tau_\gamma - T_{s2}, \quad (18)$$

if the motion is started in the first stage and it continues in the second stage.

3. If the considered slice is a big enough, the system motion can continue in the third stage. In this case the initial condition for the motion is a fracture point y_{s1} coordinate and system motion is described by the differential equation

$$dy/dT - y + u + d_{11}u(1 - e^{-T + \tau_\gamma}) + d_{11}y_0 e^{-T + \tau_\gamma} + d_{10}. \quad (19)$$

Since it was shown in [27], chaotic oscillations in a modified Mackey-Glass system occurs if a piecewise-linear function, which is used in the system model, has slopes of different signs. For example, if motion in the second stage is accompanied by a decrease in the output variable, then motion in the third stage a accompanied with its increasing and vice versa. A solution of (19) depends on system initial state in the considered stage and can be determined in a similar to (15) way. Thus, if motion starts from some initial condition y_0 , we get

$$y = (1 + d_{11})u - T d_{11} u e^{-T + \tau_\gamma} + T e^{-T + \tau_\gamma} + d_{11}y_0 + d_{10} + (y_0 - d_{11}u - d_{11}y_0 - d_{10} - u)e^{-T}. \quad (20)$$

If motions continues from the previous stage y_0 in the brackets should be replaced with y_{s1} .

Mackey-Glass system continues its motion in the third and second stages until time reaches slice size. The switchings between the third and second stages produce undamped oscillations. The motion in the next slices can be defined by using above-give formulas.

These formulas give us possibility to formulate following **algorithm** for analytical solution for the modified Mackey-Glass equation:

1. System dynamic are rewritten in a relative time domain.
2. Time delay τ_γ and system stop time T_f are specified in relative time. Number of time slices is calculated as follows

$$N_s = \begin{cases} \text{int}\left(\frac{T_f}{\tau_\gamma}\right) + 1 & \text{if } \text{int}\left(\frac{T_f}{\tau_\gamma}\right) \neq \frac{T_f}{\tau_\gamma}; \\ \text{int}\left(\frac{T_f}{\tau_\gamma}\right) & \text{otherwise} \end{cases}, \tag{21}$$

here $\text{int}()$ is a function which calculate integer value of its argument.

3. System motion in the first stage are calculated and initial value of output variable for the second stage is determined.
4. System initial condition is analyzed and operational stage in the second slice is specified.
5. System motion is defined in the considered stage.
6. Changing of the stage and/or slice end is checking.
7. If stage changing found then calculations continue in step 5 with new stage parameters.
8. If slice length is reached then it checked if this slice is the last. Reaching of the last slice end means algorithm stopping.
9. Otherwise new initial value of output variable for the next stage is defined and calculations continue in step 5 with new stage parameters.

The use of this algorithm make it possible to determine Mackey-Glass system motions in the i time slice if the motion in $i - 1$ slice is known. If the motion in this slice is unknown, it can be determined by motion in $i - 2$ slice and so on until initial condition is reached. Thus, solution of modified Mackey-Glass equation can be considered as some recurrent procedure which defines current motion by previous one.

3 Results and Discussion

Let us solve Mackey-Glass system which dynamic is determined by the following differential equation with time-delayed piecewise-linear right-hand expression

$$\frac{dy}{dt} = -y + \begin{cases} 2y_\tau & \text{if } 0 \leq y_\tau < 0.8; \\ -2.9y_\tau + 3.86 & \text{if } 0.8 \leq y_\tau < 1.4; \\ 0 & \text{otherwise,} \end{cases} \tag{22}$$

in the analytical way.

We consider uncontrollable Mackey-Glass system to simplify its study but similar studies can be performed for the controllable one as well.

We assume that time delay $\tau = 4$ and initial condition $y_0 = 1$. System is studied in the time interval $t = [0, 12]$. Above-given time interval and time delay allows us to claim that the system should be studied in three slices. Since the coefficient near y in the first summand of (22) equals to one it is not necessary to transform (22) into relative time.

Let us start from the first one. In this slice system dynamic is defined by the following equation

$$\frac{dy}{dT} = -y. \quad (23)$$

which solution is

$$y_1(t) = e^{-t}. \quad (24)$$

This slice is finished, when time reaches value of 4s and the output variable takes value

$$y_1(4) = e^{-4} = 0.018. \quad (25)$$

Also, during this slice studying, we specify time, when the output variable decreases to value 0.8, which is the first fracture point

$$t_{s1} = -\ln y_1|_{y_1=0.018} = 0.223 \text{ s}. \quad (26)$$

Now we study the second slice. Initial value of delayed state variable equals to one for this slice, that is why we understand that the considered system operates in the second stage and we rewrite (22) by taking into account (25) and applying to (24) time-delay operation

$$\frac{dy}{dt} - y - 2.9y_\tau + 3.86 = -y - 2.9e^{-t+4} + 3.86. \quad (27)$$

and define its solution as follows

$$y_{22}(t) = 3.92 - 158.34te^{-t} + 420.31e^{-t}. \quad (28)$$

At the time 4.223 s the second stage finishes because of value y_1 becomes less then 0.8. After that system motion in the second slice is described by following equation

$$\frac{dy}{dt} - y - 2y_\tau = -y - 2e^{-t+4}. \quad (29)$$

One can solve (29) with begin condition $y(4.223) = 0.28$

$$y_{21}(t) = 109.19te^{-t} - 441.98e^{-t}. \quad (30)$$

Thus, the motion in the second slice can determined with piecewise-linear function

$$y_2(t) = \begin{cases} 3.92 - 158.34te^{-t} + 420.31e^{-t} & \text{if } 4 \leq t < 4.223; \\ 109.19te^{-t} - 441.98e^{-t} & \text{if } 4.223 \leq t < 8. \end{cases} \quad (31)$$

During the second slice values of output variable do not exceed the first fracture point. That is why in the third slice we use the first row of (22) to define system dynamic but we use both branches of (31) and delay them to get y_τ in this slice

$$\frac{dy}{dt} = -y + 2 \begin{cases} 3.92 - 158.34te^{-t+4} + 420.31e^{-t+4} & \text{if } 8 \leq t < 8.223; \\ 109.19(t-4)e^{-t+4} - 441.98e^{-t+4} & \text{if } 8.223 \leq t < 12. \end{cases} \quad (32)$$

Thus, we claim that the third slice has two stages as well. Moreover, generalizing this fact we conclude that number of stages can be increased from slice to slice.

If one takes into account begin conditions for each stage, he can solve (32) as follows

$$y_3(t) = \begin{cases} 7.84 - (8644.5t^2 - 1.15 \cdot 10^5t + 3.79 \cdot 10^5)e^{-t} & \text{if } 8 \leq t < 8.223; \\ (5962.1t^2 - 9595t + 3.86 \cdot 10^5)e^{-t} & \text{if } 8.223 \leq t < 12. \end{cases} \quad (33)$$

In a similar way can be defined and solved equations for other slices.

Thus, we can determine solution of Mackey-Glass system as piecewise-linear function in the considered time range

$$y(t) = \begin{cases} e^{-t} & \text{if } 0 \leq t < 4; \\ 3.92 - 158.34te^{-t} + 420.31e^{-t} & \text{if } 4 \leq t < 4.223; \\ 109.19te^{-t} - 441.98e^{-t} & \text{if } 4.223 \leq t < 8; \\ 7.84 - (8644.5t^2 - 1.15 \cdot 10^5t + 3.79 \cdot 10^5)e^{-t} & \text{if } 8 \leq t < 8.223; \\ (5962.1t^2 - 9595t + 3.86 \cdot 10^5)e^{-t} & \text{if } 8.223 \leq t < 12 \end{cases} \quad (34)$$

In Fig. 1 shown numerical and analytical solution of Mackey-Glass system in the considered time range.

One can see that these results coincide with high accuracy. Error between them does not exceed the calculation step of the numerical method which is used to solve differential equation.

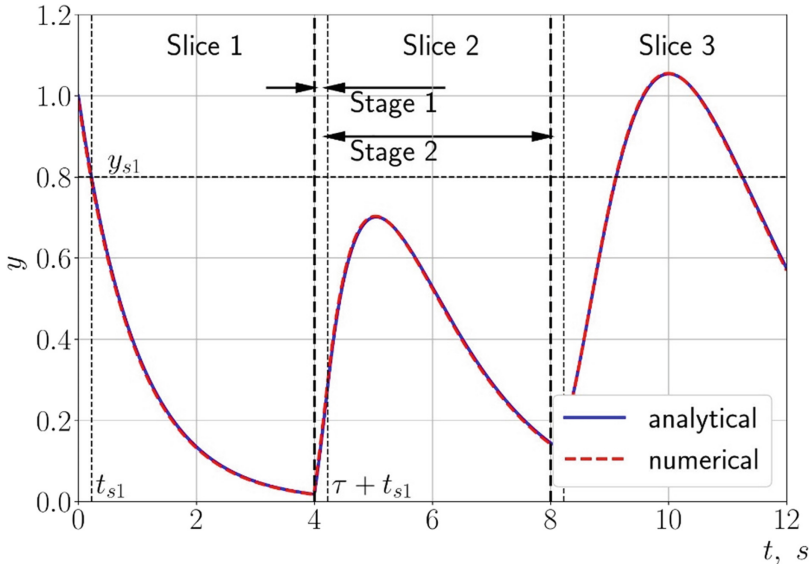


Fig. 1. Results of an analytical and numerical solution of the modified Mackey-Glass equation.

4 Conclusion

The proposed approach makes strong scientific background for the analysis of dynamical systems which is defined by using piecewise-linear functions. It gives the possibility to determine the system's response to internal and external disturbances in an analytical way. Contrary to numerical methods, which are widely used for system analysis and based on numerical solutions of the differential equations, the proposed approach does not depend on the algorithms and parameters of numerical methods and produces the true solution of the differential equations.

On the one hand, it can be recommended to design real-time devices which operate according to the studied models. From another one, our approach proves that chaotic systems with piecewise-linear function should be used with caution because if an unauthorized person has an analytical system motions equation, which can be defined beforehand for the sets of the system parameters, he can study the received chaotic signal and decrypt it. So it can be recommended to improve the security features of dynamical systems by using chaotic systems with nonlinear functions instead of piecewise-linear ones.

We see the development of our work in the design of the detailed decryption algorithms for chaotic systems with piecewise-linear functions to prove our recommendations. Moreover, the possibility to solve differential equations with time-delayed piecewise-linear functions in an analytical way allows us to apply different integral transformations and use methods of system dynamic analysis which is based on these transformations.

References

1. Mu, X., Yu, J., Wang, S.: The extended linear-drift model of memristor and its piecewise linear approximation. *Tsinghua Sci. Technol.* **19**(3), 307–313 (2014). <https://doi.org/10.1109/TST.2014.6838202>
2. Satybaldiev, D.: A new method of piecewise linear approximation of non-stationary time series for similarity measurement. In: 2015 Twelve International Conference on Electronics Computer and Computation (ICECCO), pp. 1–4. IEEE, Almaty (2015). <https://doi.org/10.1109/ICECCO.2015.7416868>
3. Zhai, J., Wu, S., Zhang, L., et al.: A 2-D-canonical piecewise linear function-based behavioral model for concurrent dual-band power amplifiers. *IEEE Microwave Wirel. Compon. Lett.* **28**(11), 1050–1052 (2018). <https://doi.org/10.1109/LMWC.2018.2873191>
4. Hafsi, S., Laabidi, K., Ksouri-Lahmari, M.: Identification of Wiener-Hammerstein model with multisegment piecewise-linear characteristic. In: 2012 16th IEEE Mediterranean Electrotechnical Conference, pp. 5–10. IEEE, Yasmine Hammamet (2012). <https://doi.org/10.1109/MELCON.2012.6196367>
5. Bai, J., Zhai, Q., Zhou, Y.: A compact aggregated unit model for short-term hydro power generation scheduling based on optimal piecewise approximation. In: 2017 36th Chinese Control Conference (CCC), pp. 2882–2886. IEEE, Dalian (2017). <https://doi.org/10.23919/ChiCC.2017.8027803>
6. Volianskyi, R., Sadovoi, O., Volianska, N., Sinkevych, O.: Construction of parallel piecewise-linear interval models for nonlinear dynamical objects. In: 2019 9th International Conference on Advanced Computer Information Technologies (ACIT), pp. 97–100. IEEE, Ceske Budejovice (2019). <https://doi.org/10.1109/ACITT.2019.8779945>

7. Solomentsev, O., Zaliskyi, M., Shcherbyna, O., Kozhokhina, O.: Sequential procedure of changepoint analysis during operational data processing. In: 2020 IEEE Microwave Theory and Techniques in Wireless Communications (MTTW), vol. 1, pp. 168–171. IEEE, Riga (2020). <https://doi.org/10.1109/MTTW51045.2020.9245068>
8. Kuzmin, V.M., Zaliskyi, M.Y., Odarchenko, R.S., Petrova, Y.V.: New approach to switching points optimization for segmented regression during mathematical model building. CEUR Workshop Proc. **3077**, 106–122 (2022)
9. Kuzenkov, O., et al.: Mathematical model of dynamics of homomorphic objects. CEUR Workshop Proc. **2516**, 190–205 (2019)
10. Li, Y., Lin, Z.: Analysis of linear systems with piecewise linear functions in the input. In: 2016 35th Chinese Control Conference (CCC), pp. 5952–5957. IEEE, Chengdu (2016). <https://doi.org/10.1109/ChiCC.2016.7554291>
11. Meng, A., Lam, H.K., Liu, F., Yang, Y.: Filter design for positive T-S fuzzy continuous-time systems with time delay using piecewise-linear membership functions. IEEE Trans. Fuzzy Syst. **29**(9), 2521–2531 (2021). <https://doi.org/10.1109/TFUZZ.2020.3001744>
12. Liu, X., Du, W.: Closed form solutions for the type reduction of general type-2 fuzzy sets with piecewise linear membership functions. In: 2016 IEEE International Conference on Fuzzy Systems (FUZZ-IEEE), pp. 1232–1239. IEEE, Vancouver (2016). <https://doi.org/10.1109/FUZZ-IEEE.2016.7737829>
13. Doleel, P., Rozsival, P., Marika, M.: Piecewise-linear neural network: A tool for modeling of the processes to be controlled. In: 2014 International Conference on Computational Science and Computational Intelligence, vol. 1, pp. 425–430. IEEE, Las Vegas (2014). <https://doi.org/10.1109/CSCI.2014.76>
14. Zagirnyak, M., Serhienko, S., Serhienko, I.: Improvement of the qualitative characteristics of an automatic control system with a fractional-order PID-controller. In: 2017 18th International Conference on Computational Problems of Electrical Engineering (CPEE), pp. 1–4. IEEE, Kutna Hora (2017). <https://doi.org/10.1109/CPEE.2017.8093062>
15. Tryputen, M., et al.: One approach to quasi-optimal control of direct current motor. In: 2019 IEEE 5th International Conference Actual Problems of Unmanned Aerial Vehicles Developments (APUAVD), pp. 190–193. IEEE, Kyiv (2019). <https://doi.org/10.1109/APUAVD47061.2019.8943878>
16. Tryputen, N., Kuznetsov, V., Kuznetsova, Y.: About the possibility of researching the optimal automatic control system on a physical model of a thermal object. In: 2019 IEEE 2nd Ukraine Conference on Electrical and Computer Engineering (UKRCON), pp. 1244–1248. IEEE, Lviv (2019). <https://doi.org/10.1109/UKRCON.2019.8879830>
17. Zagirnyak, M., et al.: Refined calculation of induction motor equivalent circuit nonlinear parameters by an energy method. Eastern-Eur. J. Enterp. Technol. **3**(5–87), 4–10 (2017). <https://doi.org/10.15587/1729-4061.2017.104146>
18. Wang, N., Li, C., Bao, H., Chen, M., Bao, B.: Generating multi-scroll Chua's attractors via simplified piecewise-linear Chua's diode. IEEE Tran. Circ. Syst. I: Regul. Pap. **66**(12), 4767–4779 (2019). <https://doi.org/10.1109/TCSI.2019.2933365>
19. Dhivya, R., Premkumar, R., Nithyaa, A.N.: Real time secured transmission of biosignal using chaotic communication system. In: 2015 IEEE International Conference on Engineering and Technology (ICETECH), pp. 1–4. IEEE, Coimbatore (2015). <https://doi.org/10.1109/ICE TECH.2015.7275045>
20. Amil, P., Cabeza, C., Marti, A.C.: Exact discrete-time implementation of the Mackey-Glass delayed model. IEEE Trans. Circuits Syst. II Expr. Briefs **62**(7), 681–685 (2015). <https://doi.org/10.1109/TCSII.2015.2415651>

21. Hoang, T.M., Son, N.V., Nakagawa, M.: A secure communication system using projective-lag synchronization of multidelay Mackey-Glass systems. In: 2006 First International Conference on Communications and Electronics, pp. 325–330. IEEE, Hanoi (2006). <https://doi.org/10.1109/CCE.2006.350801>
22. Soto, J., Melin, P., Castillo, O.: Optimization of interval type-2 fuzzy integrators in ensembles of ANFIS models for prediction of the Mackey-Glass time series. In: 2014 IEEE Conference on Norbert Wiener in the 21st Century (21CW), pp. 1–8. IEEE, Boston (2014). <https://doi.org/10.1109/NORBERT.2014.6893880>
23. Puthusserypady, S.K., Mahendra, C.: Mackey-Glass based communication scheme: systemf security analysis. In: 2004 Ninth International Conference on Communications Systems, pp. 321–325. IEEE, Singapore (2004). <https://doi.org/10.1109/ICCS.2004.1359391>
24. Farzad, M., Tahersima, H., Khaloozadeh, H.: Predicting the Mackey Glass chaotic time series using genetic algorithm. In: 2006 SICE-ICASE International Joint Conference, pp. 5460–5463. IEEE, Busan (2006). <https://doi.org/10.1109/SICE.2006.315603>
25. Ustundag, B.B., Kulaglic, A.: High-performance time series prediction with predictive error compensated wavelet neural networks. *IEEE Access* **8**, 210532–210541 (2020). <https://doi.org/10.1109/ACCESS.2020.3038724>
26. Voliansky, R., et al.: Chaotic time-variant dynamical system. In: 2020 IEEE 15th International Conference on Advanced Trends in Radioelectronics, Telecommunications and Computer Engineering (TCSET), pp. 606–609. IEEE, Lviv-Slavske (2020). <https://doi.org/10.1109/TCSET49122.2020.235503>
27. Volianskyi, R., Sadovoi, O., Volianska, N., Sinkevych, O.: Root methods for dynamic analysis of the one class chaotic systems. In: 2019 IEEE 14th International Conference on Computer Sciences and Information Technologies (CSIT), vol. 1, pp. 117–121. IEEE, Lviv (2019). <https://doi.org/10.1109/STC-CSIT.2019.8929852>



Efficient Policy Representation for Markov Decision Processes

Anahita Khademi¹  and Sepehr Khademian² 

¹ Vali-e-Asr University of Rafsanjan, Imam Khomeini Square, Rafsanjan, Iran
a.khademi@vru.ac.ir

² Arak University, Ali-Ebne-Abitaleb, Daneshjoo Boulevard, Arak, Iran

Abstract. Storing the optimal policy is an important challenge for autonomous agents and cyber-physical systems where the behavior is modeled by Markov decision processes. In this paper, we propose a symbolic approach to store an optimal policy compactly. We use decision trees for classifying optimal actions that are used to store a compressed representation of an optimal policy. To reduce memory consumption, we propose several approaches that keep the precision of the computed values or provide an approximation of them by considering a threshold for errors in the computed values. The first approach limits the depth of trees to reduce memory consumption. The second one detects and avoids non-important states to have smaller sets of states. The third approach prioritizes states by considering their impact on the precision of results. We use the PRISM case studies to investigate the effectiveness of our approach. Based on our results for the standard case studies, using decision trees and the proposed approaches, the needed memory for storing the optimal policies is reduced by several orders of magnitude, which is promising for embedded systems.

Keywords: Machine learning · Model checking · Markov decision processes · Optimal policy · Decision tree classifier

1 Introduction

Markov Decision Processes (MDPs) are widely used in artificial intelligence [1] and formal verification for modelling the decision making of autonomous systems with uncertain behaviors [2]. In both cases, iterative numerical methods are used to determine the optimal planning policies (as mappings) that compute (or approximate) the optimal (maximal or minimal) probability of reaching a goal state or optimal expected accumulated rewards [3]. There is an interest in recent years in using MDPs to model planning in embedded systems and IoTs [4, 5]. Two general approaches can be applied to use MDPs for planning in such systems. In the dynamic (online) approach, an agent constructs a related MDP and computes the optimal policy at demand. In the static approach (called off-line for the remaining parts), an MDP is constructed once and the optimal policy is computed, to be used as a black box to resolve uncertain decision makings at runtime [4]. The first approach encounters some overheads to the system

which limits its application for embedded systems with limited energy resources. In the second approach, one can compute the optimal policy once and program it to read-only memory (ROM). Exponential blow-up of state space (called state explosion problem) is a well-known obstacle to using explicit representation for MDPs [2, 5]. This problem influences the possibility of using an off-line approach for embedded systems where their memory cost is important.

Several approaches are available to alleviate the state explosion problem. Symbolic model representation is a prominent solution, which is widely used in formal verification and artificial intelligence. In these approaches, symbolic data structures are used to implicitly define the state space of a model [2, 3, 6, 7]. For the case of MDPs, state explosion also introduces the problem of storing optimal policies [8]. To utilize the benefits of an off-line approach for using MDPs in planning and to avoid storing all information of the optimal policies explicitly, we propose an approach to represent it symbolically that results in reducing the memory requirement. Our proposed approach uses decision trees as efficient data structures for representing optimal policies. To do so, we consider a policy as a classifier that maps each state to a class of actions. It provides the opportunity of using classifiers to symbolically represent optimal policies. Using a decision tree classifier as an extension to the binary decision diagrams (BDDs), we have an opportunity in storing the information on optimal policies compactly with low computational overheads.

Notice that the idea of using decision trees for representing optimal policies has been used in previous works [8] and our results show this approach reduces the memory consumption for storing the optimal policies by several orders of magnitude. However, we need more improvements in space consumption for practical autonomous artificial agents that work in a sophisticated environment [9, 10]. Hence, our main focus is to develop new heuristics to have more reduction in space consumption by using decision trees for optimal policies of MDP models.

The space complexity of decision trees depends on variable ordering, the order for which the variables are selected in the structure of a decision tree. Finding the optimal variable ordering for decision trees is an NP-complete problem and several heuristics have been proposed and implemented in decision tree classifiers to find near-optimal variable orderings [8]. To reduce the memory requirement for decision trees our approach is to reduce the number of states that are used for constructing the related decision tree. Based on this idea we follow two classes of approaches. The first class is to detect the set of states of a given model for which the optimal actions do not affect the optimal reachability probability of the initial state of the model. The set of states that cannot reach the goal states, or are not reachable from the initial state under the optimal policy, or those states with only one action should be avoided to computing the related decision tree. The second class of approaches disregards some states or some parts of decision trees while keeping the precision of computations at a given level of accuracy. Considering a threshold for losing the precision of computed value for the optimal reachability probability of the initial state, we proposed a general approach to reduce the memory requirement for the computed decision tree. This approach focuses on more important states and limits the depth of decision trees. Considering these classes of approaches, the main contribution of this paper is as follows:

- we use a decision tree to symbolically represent the optimal policies of MDPs. It can be used for embedded systems with a limited amount of memory that encounter the state explosion problem;
- to reduce memory consumption while keeping the precision of values, we propose a class of approaches that detect those states that do not affect the computed value of the initial state;
- considering a threshold for the precision of computations, we propose a set of approaches for reducing the size of computed decision trees.

BDDs are widely used as a data structure for representing labelled transition systems in a compact way and as an efficient approach for symbolic model checking [2]. Multi-terminal binary decision diagrams (MTBDDs) as an extension to BDDs are used in the case of probabilistic model checking [3, 7]. Our general approach in using decision trees is similar to using MTBDDs for representing optimal policies [12]. However, we develop several new approaches to reduce the set of states and have smaller decision trees.

Several previous works have used classifiers to represent the optimal policies: the deep statistical model checking (DSMC) approach [13] which uses deep learning to represent optimal policies. The main focus of DSMC is on predicting optimal actions for discounted MDPs and no study has been done on its memory consumption. Machine learning is used in [14] for extrapolating the optimal policies by using some small models and domain-level knowledge of the problem, but there is no control on the precision of approximated policies in this work.

Some general approaches have been proposed to reduce the size of decision trees in [8, 13, 15]. However, these approaches do not focus on reducing the size of the training data while keeping the precision of the classifier. Decision trees have been used in [16] to predict the set of states for which the optimal reachability probability is zero or one, a problem that is needed in probabilistic model checking [2, 3].

The rest of this paper is organized as follows. In Sect. 2 we introduce the preliminary definition of MDPs and decision trees. The proposed techniques and related discussions are covered in Sect. 3. Experimental results for evaluating our approaches are available in Sect. 4 and finally, Sect. 5 concludes the paper.

2 Preliminaries

We review some preliminary definitions about MDPs and the decision tree classifier that are needed for the rest of the paper. We use S for a set of states and μ for a set of probability distribution on S where $\sum_{s \in S} \mu(s) = 1$.

Definition 1. A Markov Decision Process (MDP) is a tuple $M = (S, s_0, Act, \delta, R)$ where S is a finite set of states, $s \in S$ is the initial state, $G \subset S$ is a set of goal states, Act is a finite set of actions, $\delta : S \times Act \rightarrow \mu$ is a probabilistic transition function such that determines a probability distribution μ on each state s and enabled action $\alpha \in Act(s)$ and $R : S \times Act \rightarrow R$ is a reward function. For every state $s \in S$, $Act(s)$ denotes the (non-empty) set of enabled actions for s . Actions are used to model non-deterministic choices of a model.

MDPs are transitions systems that model both non-deterministic choices and stochastic aspects of computer systems. Like other variants of transition systems, states are used to capture any possible situations for the system and transitions present its the step-wise progress over the time. Reaching a state $s \in S$ one enabled action $\alpha \in Act(s)$ is selected non-deterministically and the next state s' is stochastically determined with probability $\delta(s, \alpha)(s')$. A discrete-time Markov chain (DTMC) is an MDP for which every state $s \in S$ has exactly one enabled action. A path in an MDP M is a sequence of states and actions and is defined as $\omega = s_0\alpha_0s_1\alpha_1\dots$ where for each $i \geq 0$ we have $\alpha_i \in Act(s_i)$ and $\delta(s_i, \alpha_i)(s_{i+1}) > 0$. A path is finite if it is defined on a finite number of state and actions. To analyse the behaviour of a given MDP M we should define a probability measure on the set of its paths [1]. For DTMCs, a probability measure is defined by constructing a corresponding cylinder set [4]. For MDPs, one should resolve their non-deterministic choices to define a probability measure on its paths. A policy is a decision maker that maps to each state s one enabled action $\alpha \in Act(s)$. In general, for any possible finite path ω , a policy π is defined on its history of states and actions. A memory-less policy is one that only depends on the last state of a path.

2.1 Expected Rewards and Reachability Probabilities

In reinforcement learning, MDPs are used to model the costs or rewards that an agent gains in an environment. In probabilistic model checking a main class of problems reduces to computing reachability probabilities, the probability of finally reaching a goal state when the system starts from an initial state. An important problem in the case of MDPs is to find an optimal policy π^* that optimizes the expected accumulated rewards before reaching a goal state or the probability of reaching a goal state. For any state $s \in S$ and memory-less policy $\pi : S \rightarrow Act$ we use $V^\pi(s)$ as a value function for the expected accumulated rewards where non-deterministic decisions are resolved by π [1]. Such value functions should satisfy the following equation:

$$V^\pi(s) = R(s, \pi(s)) + \sum_{s' \in S} \delta(s, \pi(s)).V^\pi(s'). \quad (1)$$

The optimal policy π^* is a policy that minimizes $V(s)$ for every state $s \in S$. It should satisfy the following system of Bellman equations [3]:

$$V^*(s) = \begin{cases} 0 & \text{if } s \in G \\ \min_{\alpha \in Act(s)} (R(s, \alpha) + \sum_{s' \in S} \delta(s, \alpha) \cdot V^*(s')) & \text{otherwise} \end{cases} \quad (2)$$

In formal verification, MDPs are used to model a stochastic system where the main focus is to study some reachability properties [2]. In this case and for any policy π the value function $V^\pi(s)$ is defined as the probability of finally reaching to one of the goal states and should satisfy:

$$V^\pi(s) = \sum_{s' \in S} \delta(s, \pi(s)).V^\pi(s'). \quad (3)$$

Note that for every goal state $s \in G$ and any possible policy π we have $V^\pi(s) = 1$. A modified version of the *Bellman equation* can be used to compute the minimal (or

maximal) policy π^{min} (or π^{max}). For this case, the model rewards are not important and the value functions are set to one for all goal states. Iterative numerical methods (such as value iteration and policy iteration) are used in practice for computing value functions of (1) or (3). Based on the problem definition we need to compute the optimal policy that minimizes (or maximizes) the probability of reaching a set of bad (or good) states or minimizes the expected accumulated costs. For an intelligent agent in a off-line environment, the optimal policy will be used as a decision maker. In this case, π^* can be computed once and programmed in an intelligent agent or any embedded system. For the remaining parts of this paper, we focus on the optimal reachability probabilities, while similar approaches can be used for optimal expected rewards. Graph-based pre-computation methods can be used before value iteration or policy iteration to compute the set of states that the optimal reachability probability is exactly zero or one. For the case of maximal reachabilities, S_{max}^1 and S_{max}^0 are used for these sets and are defined as:

$$S_{max}^0 = \{ s \in S | V^*(s) = 0 \}, \quad (4)$$

$$S_{max}^1 = \{ s \in S | V^*(s) = 1 \}. \quad (5)$$

Computing these sets can improve the performance of computations and reduce the running times of value or policy iteration depending on the size of these sets. We use them in the next section to reduce the size of decision trees. Although the standard approaches for the value or policy iteration methods are time consuming, the improved methods have been develop that make the computation of optimal policies feasible for most practical problems [3, 6, 12, 17, 18].

2.2 Decision Tree Classifier

Decision trees are one of the well-known supervised machine learning techniques for automatically solving classification problems [15]. In supervised learning, a set of training data are used to generate a hypothesis model for predicting the values of new input data. A decision tree (like other tree-based data structures) includes a set of nodes and branches. Each node is used to make a decision based on a feature value and leaves are labeled by a related class. Decision trees are construed in a top-down manner. Each training data is used to expand or simplify a part of the tree. Although in the worst case the size of a tree grows exponentially in the size of features, it usually leads to a compact model for deciding the membership of objects in their related classes. More details about decision tree classifiers and MTBDDs are available in [12, 15].

2.3 MDP Modeling Methods

Depending on the problem, a modeling approach is used to propose a high-level description of an MDP. In most cases, a set of variables and statements are used to describe the behavior of a system and the way that it works. For example, in the racetrack problem [9], four variables are used to represent the position and speed of a car on a slippery road. The optimal policy should minimize the expected time for reaching a destination from an initial location. Probmela [2] and PRISM [12] are two modeling languages that are

used in probabilistic model checking to providing a high-level description of a model. This description is compiled into a related MDP model. As a result, each state can be considered as a legal valuation of the model variables. As an example, one module of a PRISM program is presented in Fig. 1. This program models the stochastic aspects of the WLAN protocol [6]. This module contains $c1$ and $c2$ as two variables, followed by a set of probabilistic commands. The complete model of this example includes 12 variables.

```

26
27 // FORMULAE FOR THE CHANNEL
28 // channel is busy
29 formula busy = c1>0 | c2>0;
30 // channel is free
31 formula free = c1=0 & c2=0;
32
33 module medium
34
35     // medium status
36     c1 : [0..2];
37     c2 : [0..2];
38     // ci corresponds to messages associated with station i
39     // 0 nothing being sent
40     // 1 being sent correctly
41     // 2 being sent garbled
42
43     // begin sending message and nothing else currently being sent
44     [send1] c1=0 & c2=0 -> (c1'=1);
45     [send2] c2=0 & c1=0 -> (c2'=1);
46
47     // begin sending message and something is already being sent
48     // in this case both messages become garbled
49     [send1] c1=0 & c2>0 -> (c1'=2) & (c2'=2);
50     [send2] c2=0 & c1>0 -> (c1'=2) & (c2'=2);
51
52     // finish sending message
53     [finish1] c1>0 -> (c1'=0);
54     [finish2] c2>0 -> (c2'=0);
55
56 endmodule

```

Fig. 1. A PRISM program.

3 The Proposed Method

The general approach in probabilistic model checking and reinforcement learning is to construct an MDP and apply an iterative method to compute the optimal policy π^* . However, iterative computations are time-consuming and can be used for small models. An off-line approach is an alternative one for large models where the optimal policy is computed once and programmed to a read-only memory [10, 11]. To avoid the challenges of memory limitation in an intelligent agent (or embedded system) we need to have a compact representation of the optimal policy. While a wide range of approaches is available to propose a short description of a given string, we need an approach that can

easily map the optimal action to a given state. For this purpose, we use the decision tree classifier and suppose that the agent works in a fully observable, stochastic but off-line environment, where all needed information is available for planning and does not change during its activities. We first briefly explain how decision trees are constructed and then explain the approaches for reducing the size of trees.

3.1 Decision Tree for Optimal Policies

Consider an optimal policy $\pi : S \rightarrow Act$ that maps the optimal actions to each state of a given MDP M . For each state $s \in S$ its enabled actions are labeled based on their order: the first action is labeled 1, the second action is labeled 2 and so on. Based on this ordering, each policy π can be considered as a mapping that classifies each state s to its related class according to the label of $\pi(s)$. A classifier can be used to represent π . To do so, each variable of the high level description of a model is considered as a feature and each state is represented by its corresponding variable valuations. The states of an MDP model and their selected optimal actions are used for training a classifier. Each state $s \in S$ of an MDP model and its computed optimal action is considered as a training sample to construct a classifier model. To avoid missing any information of an optimal policy π^* we need to use an exact classifier that maps each state to its correct optimal action.

Although a wide range of classification approaches are available in machine learning, we use decision trees that can map each training sample to its exact class. In most implementations of the decision tree classifier, some heuristics are applied to compute a near-optimal feature ordering that minimizes the tree size. Minimizing decision trees provides the opportunity of using them as a compact representation of the optimal policies. In run-time, an agent uses the stored information of decision trees as a black box to make the optimal decisions. It needs not construct the MDP model and instead, it uses the variable valuations as the input to the computed decision tree to determine the corresponding class label.

3.2 Avoiding Useless States to Reduce the Size of Decision Trees

While the proposed approach in the previous section considers all states of a given model to construct the related decision tree for the computed optimal policy, some states may be useless in the computations and can be avoided. We call a state $s \in S$ useless if its optimal action is obvious or its value does not affect $V^*(s_0)$ (the reachability value of the initial state). We consider three classes of useless states and explain how they can be computed. Avoiding these states, we have a smaller set of states for constructing the decision trees. Although there is not a direct relationship between the number of objects for a decision tree and its size, in most cases, their sizes increase when we have a bigger set of objects. These classes of useless states are as follows:

1. The set of states in s_{max}^0 (for maximal reachability) and S_{min}^1 (for minimal reachability) based on (4) and (5). For any possible policy the value of states in these sets are the same and do not depend on the selected actions. For maximal reachability, the probability of reaching to a goal state from any state $s \in S_{max}^0$ is zero. Hence, it is not

- important which action should be selected for this state and we can disregard it in the construction of decision tree. It also holds for the case of minimal reachability.
2. The set of states with only one action. For these states, the agent does not need to make any decision, the available action is also the optimal one and the agent should not refer to the decision tree to select the action.
 3. The set of those states that are not reachable from the initial state under the optimal policy. The standard approach to compile a PRISM program to the corresponding transition system is to consider all states that are reachable from the initial one in S . However, some of these states may not be reachable from s_0 where the actions of the optimal policy are considered. The value of these states does not affect the optimal reachability probability of the initial state and we avoid them for computing the decision trees. Note that these states are needed when we do not have the optimal policy. During this section, we suppose that the optimal policy has been computed previously and is available for this part.

Separating useless states from S , we focus on the remaining states and their optimal actions to build a corresponding decision tree. This decision tree suggests the optimal action for useful states, but may propose any action for useless ones even some ones that are not defined for these states. For example, a useless state may have two actions but the decision tree suggest the third one, which is not defined for it. For the correctness of our approach, the agent can select an action randomly when it encounters to an undefined one.

3.3 Reducing Decision Tree Size by Losing Some Information

Applying the proposed approaches in the previous section may lead to small decision trees that can compute the same reachability probability for the initial state as an optimal policy does. However, one may decide to sacrifice the precision of computations to have a more compact policy representation. Given ϵ as a threshold for tolerating errors in the computed values, we consider several scenarios for having smaller decision trees:

Scenario 1. The standard approach to constructing a decision tree is to consider all features of the problem objects and apply the training step by considering the objects and their corresponding classes. In this case, the decision tree over-fits to the training data and can correctly map each training object to its class. A simple way to improve the generalization of this classifier and also have smaller trees is to avoid one or some features in the structure of trees. This approach decreases tree depth and results in smaller ones. The decision tree classifier applies some heuristics to keep more important features and disregard others when we decide to limit its depth.

Scenario 2. Using Eq. (1) for computing the optimal reachability probabilities (or expected rewards), we need to compute the reachability probability of all states (except S_{max}^1) to have the value for the initial state. However, the impact of state values on the value of the initial state is different among the states. In the previous section we disregard those states that are not reachable from the initial state under the optimal policy. We extend this approach by detecting the set of states for which the probability of reaching from the initial state is negligible. We use the idea of statistical model checking

by considering the optimal policy, i.e., applying a set of simulation runs (traces) and considering those runs that reach a goal state. We consider a counter for each state $s \in \mathcal{S}$ and increment it when a run meets s and finally reaches G . For terminating our approach, we consider an upper bound for the length of traces. Higher values for the counter of each state means, it is more important for computing the value of the initial state. On the other hand, lower values show the impact of the state value is lower for the initial state and we can avoid it for the decision tree. We use a threshold ϵ' for state counters to select them for the training step. If the computation error for the initial state is more than ϵ we can consider a small ϵ' for this scenario and apply it again.

Scenario 3. For any state $s \in \mathcal{S}$, the impact of selecting non-optimal actions on the value of the initial state can be considered as a criterion for selecting or avoiding s for the training step. Consider for example an optimal policy π^* and two states s_1 and s_2 where for all actions of s_1 the computed values are the same and the difference between the minimum and maximum computed values for s_2 is 0.5. It is obvious that selecting a non-optimal action for s_2 can affect the value of the initial state if it reaches to s_2 with high probability. On the other hand the impact of selecting a non-optimal action for s_1 may bring a negligible impact for the value of the initial state. In worst case, non-optimal action for s_1 may be important if the other states select non-optimal actions. We explain it in Fig. 2. Where s_3 is a goal state and s_4 and s_5 are two trap states with one self-loop. Applying the value iteration method, maximal reachability probability is .2 for both s_1 and s_2 . In this case, value iteration computes this value for each of actions (a and b) for these states and a state can give the maximal value if it selects the action b while the other state selects a . However, if both states select b as their actions, their reachability probability will be 0. Hence, we consider this scenario as a heuristic that disregards those states that have the same value under all actions or the difference of values between the best and worst actions is less than a given threshold ϵ'' .

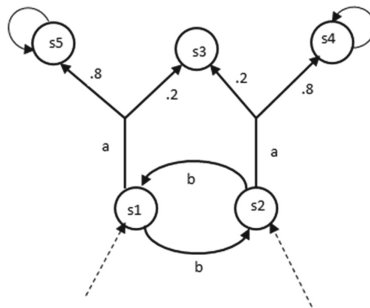


Fig. 2. Some states and transitions of an MDP

Based on these scenarios, we develop a general heuristic that selects some of them by considering an initial threshold values ϵ' or ϵ'' or tree depth d . It constructs a decision tree and applies it as a black box decision maker to approximate the reachability value for the initial state. If the computed error is less than the given threshold ϵ , our heuristic

tries to construct a smaller tree by increasing ϵ' or ϵ'' or decreasing d . Otherwise, the heuristic decreases ϵ' or ϵ'' or increases d .

4 Experimental Results

To compare the impact of our proposed approaches for representing the optimal policies in efficient way, we consider several standard MDP case studies from the PRISM benchmark suite [12]. These models include *Consensus*, *Wlan*, *Firewire* and *Mer* cases that are widely used in the previous works [3, 6]. Each model has one or some parameters where different values for each one result in an instance MDP model. In Table 1 we propose some information of our selected MDP models and our experimental results. For each model, the size of PRISM exported MDP model and stored optimal policy are reported as the original size for the explicit representation of the optimal policies. In the explicit representation, the information of each state and its corresponding optimal action should be stored in the main memory of an embedded system.

For the *Consensus*, *Wlan*, and *Mer* models, we consider the maximal reachability and for the *firewire* models we consider the minimal reachability probabilities. We run PRISM to compute the extremal policy for each case study model. We then use machine learning to construct decision tree models for symbolically represent the optimal policies. All experiments for constructing decision trees have been implemented using the `skit-learn` library in the python programming language running Jupiter notebook. To measure the memory consumption of each decision tree we use the `joblib.dump` command to store its information in a file and report them in Table 1.

Comparing the memory consumption of the explicit method and our proposed implicit method that uses decision tree for the selected case study models, we have at least 99% improvement in all cases, which means the memory consumption is less than 1%. In some cases (*Wlan* for example) decision tree reduces the memory consumption by three orders of magnitude. The results are more promising for larger models where the sizes of decision trees have negligible difference with small models of the same class of MDPs.

The experimental results also show that our state reduction methods (explained in Subsect. 3.2) reduce the memory consumptions in all cases. The improvements are more considerable for the *Consensus* and *Wlan* models where a small part of states are important to construct the optimal policies. Notice that in these cases, our proposed methods keep the precision of computation, i.e. the policies that are represented by the reduced decision trees can be used to compute precise optimal reachability probabilities.

For our last approaches that dismiss some part of information to achieve a smaller decision tree (described in the Subsect. 3.3) we propose both the memory consumption and the precision of computations in the last columns of Table 1. For all cases, except the *Mer* ones memory consumption is less than 10 KB while the precision of computation is at least 85% of exact values.

Table 1. Experimental results for the selected models.

Model (parameters)	Param values	Number of states	Original Size	Standard D.T	Useless state removal D.T	Feature reduction		State prioritizing	
						Space	Precision	Space	Precision
<i>Consensus</i> (N,K)	4.6	63.616	2.8 MB	117 KB	23 KB	7.3 KB	93.1	4.2 KB	92.3
	4.10	104.576	3.8 MB	124 KB	24 KB	8.4 KB	92.5	4.5 KB	89.8
	4.15	155.776	5.3 MB	132 KB	25 KB	9.5 KB	92.2	5 KB	87.5
	4.24	247.936	7 MB	145 KB	27 KB	10 KB	91.8	5.8 KB	85.4
<i>Wlan</i> (TTM)	200	171.542	5.8 MB	87 KB	12 KB	4.7 KB	95.6	1.2 KB	97.5
	800	409.142	14.2 MB	134 KB	15 KB	5.6 KB	94.7	1.4 KB	96.4
	2500	1082.342	35.3 MB	213 KB	19 KB	6.1 KB	95.2	1.5 KB	96.1
<i>Firewire</i> (ddl)	800	289.861	6.2 MB	2.3 KB	1.6 KB	2.2 KB	95	1.1 KB	89
	5000	2856.061	69.3 MB	3.9 KB	3.2 KB	3.7 KB	94.8	1.4 KB	88
<i>Mer</i> (n)	100	592.264	42 MB	1.7 MB	445 KB	243 KB	97.9	179 KB	91.2
	500	2955.064	214 MB	6.4 MB	967 KB	441 KB	96.4	257 KB	93.5

5 Conclusion

In this paper, we use a symbolic approach for storing the information of the optimal policies that can be used for embedded systems and intelligent systems. The proposed approach uses derision trees as classifier to map each MDP state to its optimal action. We propose several approaches to avoid useless states to have smaller decision trees. The results show that using decision tree to represent optimal policies reduces space complexity by two or three orders of magnitude and our heuristics reduce the size of the given trees by one order of magnitude. For the future works, the propose approach can be applied for other classes of models such as probabilistic timed automata or continuous-time Markov models.







References

1. Puterman, M.L.: Markv Decision Processes: Discrete Stochastic Dynamic Programming. John Wiley & Sons, Hoboken (2005). <https://doi.org/10.1002/9780470316887>
2. Baier, C., Katoen, J.P.: Principles of Model Checking. MIT Press, Cambridge (2008)
3. Baier, C., Hermanns, H., Katoen, J.-P.: The 10,000 facets of MDP model checking. In: Steffen, B., Woeginger, G. (eds.) Computing and Software Science. LNCS, vol. 10000, pp. 420–451. Springer, Cham (2019). https://doi.org/10.1007/978-3-319-91908-9_21
4. Tidwell, T.: Utility-aware scheduling of stochastic real-time Systems. Dissertation, Washington University (2011). <https://doi.org/10.7936/K79S1P2H>
5. Zantalis, F., Koulouras, G., Karabetsos, S., Kandris, D.: A review of machine learning and IoT in smart transportation. Future Internet **11**(4), 94 (2019). <https://doi.org/10.3390/fi11040094>
6. Forejt, V., Kwiatkowska, M., Norman, G., Parker, D.: Automated verification techniques for probabilistic systems. In: Bernardo, M., Issarny, V. (eds.) SFM 2011. LNCS, vol. 6659, pp. 53–113. Springer, Heidelberg (2011). https://doi.org/10.1007/978-3-642-21455-4_3

7. de Alfaro, L., Kwiatkowska, M., Norman, G., Parker, D., Segala, R.: Symbolic model checking of probabilistic processes using MTBDDs and the Kronecker representation. In: Graf, S., Schwartzbach, M. (eds.) TACAS 2000. LNCS, vol. 1785, pp. 395–410. Springer, Heidelberg (2000). https://doi.org/10.1007/3-540-46419-0_27
8. Ashok, P., Jackermeier, M., Křetínský, J., Weinhuber, C., Weininger, M., Yadav, M.: dtControl 2.0: Explainable strategy representation via decision tree learning steered by experts. In: Groote, J.F., Larsen, K.G. (eds.) Tools and Algorithms for the Construction and Analysis of Systems. TACAS 2021. LNTCS, vol. 12652, pp. 326–345. Springer, Cham (2021). https://doi.org/10.1007/978-3-030-72013-1_17
9. Gros, T.P., Hermanns, H., Hoffmann, J., Klauck, M., Steinmetz, M.: Deep statistical model checking. In: Gotsman, A., Sokolova, A. (eds.) FORTE 2020. LNCS, vol. 12136, pp. 96–114. Springer, Cham (2020). https://doi.org/10.1007/978-3-030-50086-3_6
10. Kwiatkowska, M., Norman, G., Parker, D.: Probabilistic model checking and autonomy. *Annu. Rev. Control, Robot., Auton. Syst.* **5**, 385–410 (2022). <https://doi.org/10.1146/annurev-control-042820-010947>
11. Pandey, A., Ruchkin, I., Schmerl, B., Garlan, D.: Hybrid planning using learning and model checking for autonomous systems. In: 2020 IEEE International Conference on Autonomic Computing and Self-Organizing Systems (ACSOS), pp. 55–64. IEEE, Washington (2020). <https://doi.org/10.1109/ACSOS49614.2020.00026>
12. Kwiatkowska, M., Norman, G., Parker, D.: PRISM 4.0: verification of probabilistic real-time systems. In: Gopalakrishnan, G., Qadeer, S. (eds.) CAV 2011. LNCS, vol. 6806, pp. 585–591. Springer, Heidelberg (2011). https://doi.org/10.1007/978-3-642-22110-1_47
13. Demirović, E., et al.: MurTree: optimal decision trees via dynamic programming and search. *J. Mach. Learn. Res.* **23**(26), 1–47 (2022)
14. Rataj, A., Woźna-Szcześniak, B.: Extrapolation of an optimal policy using statistical probabilistic model checking. *Fund. Inform.* **157**(4), 443–461 (2018). <https://doi.org/10.3233/FI-2018-1637>
15. Kotsiantis, S.B.: Decision trees: a recent overview. *Artif. Intell. Rev.* **39**(4), 261–283 (2013). <https://doi.org/10.1007/s10462-011-9272-4>
16. Mohagheghi, M., Salehi, K.: Machine learning and disk-based methods for qualitative verification of Markov decision processes. *CEUR Workshop Proc.* **2732**, 74–88 (2020)
17. Mohagheghi, M., Karimpour, J., Isazadeh, A.: Improving modified policy iteration for probabilistic model checking. *Comput. Sci.* **23**(1), 63–80 (2022). <https://doi.org/10.7494/csci.2022.23.1.4139>
18. Mohagheghi, M., Chaboki, B.: Dirac-based reduction techniques for quantitative analysis of discrete-time markov models. In: Barbosa, L.S., Ali Abam, M. (eds.) TTCS 2020. LNCS, vol. 12281, pp. 1–16. Springer, Cham (2020). https://doi.org/10.1007/978-3-030-57852-7_1



Modeling of Distributed Mosaic Systems of Mobile Bionic Robots

Oleksandr Prokhorov¹  , Oleg Fedorovich¹ , Valeriy Prokhorov² ,
Oleksii Shatalov² , and Yuriy Pakhomov³ 

¹ National Aerospace University “Kharkiv Aviation Institute”, 17 Chkalova Street,
Kharkiv 61070, Ukraine

o.prokhorov@khai.edu

² Kharkiv National University of Radio Electronics, 14 Nauky Ave., Kharkiv 61166, Ukraine

³ O. M. Beketov National University of Urban Economy in Kharkiv, 17 Marshala Bazhanova
Street, Kharkiv 61002, Ukraine

Abstract. The paper considers features of using the concept of “mosaic warfare” based on dynamic management of distributed systems of mobile robotics complexes using multi-agent approach. It describes modelling mechanisms for controlling a group of bionic robots for search and rescue operations, reconnaissance and military diversions with the provision of mechanisms for autonomy, adaptation, coordination and collective behavior. The mosaic structure of the distributed system of mobile robotics complexes was suggested. The features of the algorithms of the motion planning, formation of the agents’ trajectory and group control are described. It also describes an agent-based model for the analysis of control processes of a group of unmanned aerial vehicles, unmanned ground vehicles, and ground-based robots.

Keywords: Mosaic warfare · Robotic · Unmanned ground vehicles · Distributed systems · Multiagent systems · Simulation modelling

1 Introduction

The interest of researchers in bionic (technical devices that have a look similar to biological objects) robots and their group control has increased lately.

The development of four-legged (a dog-like) or six-legged (a spider-like) robots is relevant due to the need for mobile robots to investigate unsafe or unstructured terrains. Compared to other mobile robotics platforms, these bionic robots are an excellent movement system in terms of stability, control and low memory. Nowadays, the possibilities of the four-legged robots are studied in various fields, from construction to space exploration and military operations. It should also be noted that the traditional model of development of the defense complex, which is focused on complex and expensive platforms and systems, is not suitable for taking advantage of modern information technology (artificial intelligence, machine learning, unmanned complexes, etc.), which are significantly developing today in the global innovative environment. An alternative

approach is to focus on smaller, purposeful and relatively cheap “units of action” that will have the power of quick and easy scaling and modernization. By creating a dynamic “mosaic” of such units, which act both autonomously and in coordination, it is possible to gain strategic advantage through asymmetric devices, while the supervisor can be made more difficult to solve his military tasks. Such a new concept of “Mosaic Warfare” was proposed by DARPA. Further research requires the development of new methods and models aimed at improving the management of large distributed dynamical systems, including mobile robotics complexes, in unprecedented and critical situations.

This paper considers the peculiarities of modeling of control processes of a group of bionic robots equipped with various sensors and computer vision system, for search and reconnaissance operations, reconnaissance and military sabotage with provision of autonomy, adaptation, coordination, collective behavior, self-renewal and integration mechanisms.

2 Literature Review

The concept of “Mosaic Warfare” of the Defense Projects Agency (DARPA) is considered in [1]. For modeling of distributed mosaic systems the author proposes the developed technology of spacious occupancy, which uses active distributed knowledge networks, solving such problems as real-time collection and integration of widespread resources under unified management and pooling of such resources for collective elimination of undesirable entities. The paper [2] considers the peculiarities of controlling the trajectories of various groups of unmanned air, land and sea transport vehicles on the basis of genetic algorithms. The paper [3] examines the architecture of the unmanned vehicles planning and control system, which includes such modules as sensory data acquisition, voltage detection, delaying, travel planning, control command generation, and control strategy evaluation. The paper [4] considers the features of modelling artificial warfare using the concepts of multi-agent systems. A review of achievements in the field of self-organization in mobile robot systems (or swarming robotic systems) is given in [5]. The paper [6] describes the simulation process on the basis of agents for measuring the overall combat effectiveness in combination with the coefficient of link success based on the ground combat situation. Training in robotics has been a difficult topic for the past several years. The necessity to equip the robot with a tool powerful enough to allow autonomous detection of optimal behavior by means of tests and interference with the environment has been the motive for numerous in-depth research projects. The paper [7] presents the investigation of training algorithms with backing for unmanned ground vehicles for joint study of unknown territory.

The analysis confirmed the relevance and importance of research, which is focused on creating new methods of dynamic control of dispersed systems of mobile robotics complexes through a multi-agent approach within the concept of “Mosaic Warfare”, which will be discussed further.

3 The Concept of “Mosaic Warfare”

The concept of “Mosaic Warfare” is based on a quickly assembled network of sensors, control nodes, as well as joint piloted and unmanned systems with integration of geographically dispersed resources, which must work together as a single system [8]. Thus, one of the ideas behind the “mosaic war” is to take simple systems, combine them into a measure, and ask them to interact and cooperate. One of the key advantages of the asymmetric form of “mosaic warfare” is its ability to add highly effective unmodified elements to the combination of combat operations, which now includes unmanned aerial vehicles (UAVs), unmanned ground vehicles (UGVs) and ground robots.

For example, in the ground forces, instead of relying on large military formations, smaller units could be supplemented with small and medium UGVs and/or UAVs to improve their effectiveness in accomplishing missions. The main idea of such a solution is to be cheap, quick, lethal, bendy and scalable. Instead of creating one excellent combat unit, optimized for a specific purpose, it is proposed to combine small unmanned systems with the existing capabilities in the creative combinations, which are constantly evolving due to modern technologies, such as piecemeal integration and others, to create an advantage on the battlefield and new disadvantages for the opponent. The mosaic concept is well matched with the methods of building distributed systems of agents with a flexible interaction and the possibility of self-adaptation, self-adaptation and stoicism. In multi-agent systems, it is possible to reach its goal when one or several agents collapse or get out of harmony. For example, removal of UAV, which was carrying out the distribution, must not interfere with the actions of other agents, and the whole system must work, if one part is not enough to achieve the global goal. Moreover, such systems can respond to other systems in a non-deterministic/stochastic way and increase the diversity of component variants. For example, agents can arrive and react stochastically in a random way, but structured on other agents in an unspecified environment. However, structured randomness leads to the emergence of systemic behavior, which reveals the desired properties for the purpose of the entire mission. Systems with such properties are easy to assemble and stable. Without well-planned integration, agents can adapt their interaction and reconfigure their own systems. For example, when making decisions on the battlefield, the unmanned ground vehicles must coordinate their actions with a heterogeneous network of unmanned air vehicles and other military units. Thus, in the mosaic approach paradigm the agents can be easily combined to achieve the set goal through non-prescribed steps. These features of a fast ability to self-renew and autonomous composition are the features of the mosaic approach.

4 Bionic Stepping Robots

When carrying out search operations in areas that are not dangerous for people (premises), today they use remotely controlled mobile robots. At this time in the world the most widespread use of ground wheeled, tracked and specialized mobile platforms. The main advantage of their use is the ability to place workers, in this case the operator of a mobile platform, outside the potentially dangerous area, to save the health and life of people. Optimization of work modes of such robots makes it possible to improve their

technical characteristics, and thus increase the efficiency of work, which leads to the possibility of performing fundamentally new operations and reducing the cost of a single operation. This is the general trend in this field of robotics, which Boston Dynamics now demonstrates with its latest developments of craters, Animal and humanoid robots, which are able to perform simple operations of moving objects, as well as to finish the various disadvantages and nerves on the surface of the movement. A special part of robotics occupies the crumbling transfer systems and transport machines based on them. The method of shifting by means of the legs (stepping, running, shearing) is known to be the most widespread in the living nature. The method of stepping is of primary interest for walking on a distance unprepared terrain with obstacles. Traditional wheeled and tracked vehicles leave behind them without a break, expending considerably more energy than shifting by steps, when the interaction with the ground occurs only in the areas of the foot rest. In addition to this, the crotch shifting method is also very easy on the crossed area, even to the point of being able to shimmy, make interruptions, etc. A distinctive feature of this type of work is that the biologic approach is used in the design of the structure. The design and walking algorithm is based on the materials of observations of living skeletons. There is a number of stepping robots:

- two-legged – work with two legs. A classic example is a humanoid robot. These robots work in the same environment as humans and are designed to imitate human behavior. Stability is maintained by calculating each moment and shifting the weight in a strictly defined order. Practical examples include QRIO from Sony, ASIMO from Honda and Atlas from Boston Dynamics;
- three-legged – these machines have three points of contact with the ground and are statically stable, i.e. they are well-balanced and can stand without tipping over. Practical example includes STRIDER by RoMeLa;
- four-legged (Fig. 1), also known as tetrapods, robot-dogs or robot-spiders, have four legs and their walk is similar to that of animals. Being statically stable, they are well balanced in different positions. They can walk by shifting one leg at a time or by shifting a pair of legs;
- hexapod (Fig. 1). These robots have six legs. They have a higher stability in the standing and standing positions. They can swing by shifting each pair of legs one by one or by shifting the legs of each pair alternately.

One of the latest developments in the field of four-legged robots is the Ghost Robotics Vision 60, which in 2021 was tested at Scott Air Force Base in Illinosa (USA) as part of a year-long experimental testing program. Designed to reduce the risks faced by airborne pilots, the Vision 60 is equipped with an armor-mounted screw on the back and equipped with sensors that allow it to operate in a variety of unstable terrain conditions. It is also able to create thermal images, set up infrared imaging and transmit high definition streaming video. Vision 60 can carry up to 13 kg of luggage and move at a speed of up to 1.6 m/s. It is considered to be a fully autonomous rotary-wing operation: although the robot can independently and accurately aim the rotary-wing at the target, it cannot fire without action by a human operator (in line with US military autonomous systems policy, which prohibits automatic target engagement).

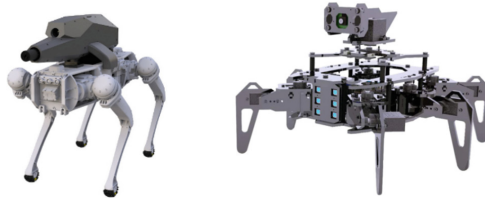


Fig. 1. Bionic robots: four-legged robot-dog Ghost Robotics Vision 60 (left), hexapod for laboratory research Adept RaspClaws (right).

Thus, when carrying out disruptive and sabotage tasks and conducting combat operations in the framework of the “Mosaic Warfare” concept it is advisable to use bionic crushing robots. These robots are able to move by themselves over the terrain and choose the most suitable route to the point of destination, for this purpose the robot uses built-in sensors and navigation systems. The design of these robots today allows without third-party assistance to rise and continue driving. The task of the rover-rovers is to check the danger zones, identify the enemy and the areas to be replaced and indicate the sector of action for combat groups of troops. In general they have a wide range of applications, even to the work in the assault group. In this regard they can operate autonomously. These robots can be equipped with thermal sensors, motion detectors, high-speed thermal and visible light cameras, and the design of the legs gives advantage in maneuverability and lightness, which is one of the advantages in detecting mines.

5 Specifics of Group Robots Management

The Mosaic approach is a transition from acting according to a predetermined scenario, which is aimed at achieving a single goal. Indeed, the classical approach has a defined goal and then uses top-down design techniques to decentralize operations. For example, the operator of the entire battlefield first develops optimal strategies for the agents on a global scale, and then tells each agent how to act based on their local information. However, when one agent leaves the battlefield, which changes the system, the previously developed strategy is no longer globally optimal. The Mosaic approach also differs from the classical deterministic downhill approach, in which the agents are programmed to behave autonomously, which loses adaptability.

In the distributed method, based on the mosaic approach, the task of group work control can be divided into a number of subtasks, among which we can distinguish the following:

- determination of the group structure and formation of its active part, a cluster, as an accumulation of works formed to achieve one or another goal;
- optimal (or close to it) distribution of functions between the groups of workers, as well as reshuffling of these functions when the situation changes;
- implementation of the functions by individual works, which are included in the cluster, to achieve the final goal.

The division of roles in the group is carried out according to the following (Fig. 2):

- sense is a detection agent that performs tasks of inspection of territories or facilities, monitoring, recognition and identification of objects, has data collection sensors, Remote detectors and radars (laser distance meter, for example, is expensive, so it can not be in every member of the group);
- orient – agent-navigator, performs the task of producing a digital picture of the area, route planning, radio traffic, jamming counter-attacks during the implementation of the mission;
- decide – agent commander (leader), may be designated from among unmanned transport vehicles and/or be commanded by a human operator to make decisions (but not necessarily, it can be any command post or a division or combat unit, commanded by a man), performs the task of mission distribution, integration and consolidation of information from the other members of the group, command of the group, re-planning of the mission scenario, liaison with the control center, etc. Examples of commands are attacking a certain enemy object, moving to a certain position, or overloading;
- act – agent-perpetrator, performs actions related to detection, investigation and dissemination, delivery of material and technical equipment to the points of destination, sabotage tasks, attack and destruction of thieves’ objects, etc.

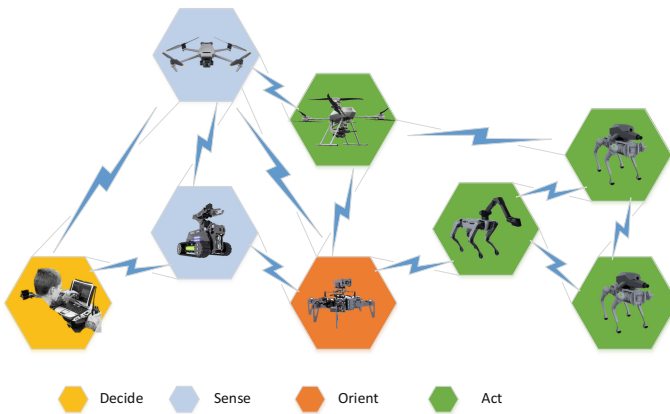


Fig. 2. The roles of unmanned vehicles and their tasks in the group within the mosaic approach.

The number of unmanned vehicles for leaders, detachments and others is calculated according to the area of the territory and the nature of the mission. The payload that is the role of unmanned vehicles can be combined, can be the same in terms of ensuring the required level of assurance of the mission objectives. Of course, in the case of loss of contact with the leading agent, his role can be performed by another agent, or, for example, a roving agent. Mosaic Warfare concept involves dynamic adaptation of all types of resources to perform the mission tasks. Disaggregating units with more than one mission potentially increases the flexibility and adaptability of the force and creates a more difficult situation for the enemy to assess.

Thus, our system is composed of several types of autonomous vehicles, each of which performs one or several roles and is equipped with various monitoring and action capabilities. For example:

- A-UGV: robot-dog for sabotage and attack operations, medium speed, short detection range, 90-degree field of view;
- S-UAV: drone for monitoring, recognition and identification of objects on the territory, high speed, medium range detection, camera, thermal imaging camera;
- S-UGV: area monitoring robot, surveillance, object detection and inspection, low speed, long range detection, 360 degree detection.

So one of the ways in the framework of “Mosaic Warfare” in the ground battle is reasonable to send a unmanned airborne vehicle for ground deployment ahead of the main ground combat forces for disengagement. It can tag enemy troops and equipment. Unmanned system transmits coordinates to the assault group of ground robotic dogs, which are flying in that direction and perform the task to hit the target.

Let us look at how the control of ground robots in a group is carried out. The literature offers a large number of methods of route planning, which use different heuristic techniques, which usually emerge, as a rule, the content sense of the problem solved. This can be methods using a picture of the environment or its description by means of a graph or tree; methods based on the cellular decomposition; methods of potential fields; optimization methods; methods based on integrated technologies and machine learning, etc. Within the framework of our task, path planning algorithms using chaotic dynamics, which are used for obtaining unprecedented trajectories, are particularly popular. Thus, the paper [9] presents a modification of the well-known logistic picture, which is used to create a chaotic generator of pseudo-fluctuations. This sequence is then used to control the robot, which moves along the grid in four or eight different directions. A simple model of pheromones with efficient memory is also suggested to improve the achieved level of coverage [10].

Let’s consider the multi-agent system W of robots-agents A_1, \dots, A_n . In W a global immovable rectangular coordinate system is given xOy . Every agent $A_i, i = 1 \dots n$, presents a model of a mobile robotics complex. For every existing in W agent A_i , at every moment t the location p_i is known inside system xOy .

$$p_i(t) = (x_i, y_i, \theta_i),$$

where x_i, y_i are the coordinates of agent; θ_i is the orientation, given by the corner between the direction of the vector of linear velocity of the agent \bar{v}_i and the axis Ox . Also in the value of the linear v_i and corner ω_i speeds of agents and its constant length l_i . The object movement can be described by the system of differential equations:

$$\begin{cases} x_i = v_i \cos \theta_i, \\ y_i = v_i \sin \theta_i, \\ \theta_i = \omega_i. \end{cases}$$

For all agents of the group the same restrictions are set for the maximum values of their linear v_{\max} and corner ω_{\max} speeds. We have an unpredictable sequence of values

$\rho \in [0, -1]$, which are used to determine the next direction of the vehicle's movement after the probability distribution. Thus, if $\rho < 1/3$, robot turns right ($-\pi/4$); if $1/3 \leq \rho < 2/3$, robot turns left ($\pi/4$); and if $\rho \geq 2/3$, it continues the forward movement. The so-called closeness radius r is set for each transport work. There are, of course, tasks in which the workflow is considered in a structure, for example, the rhombus type. From the practical point of view, in this case, the situation is more appropriate, when the agents move by trajectories that are equidistant from the leader's trajectory. We also consider the approach, which uses the vector of departure taking into account other vehicles in order to identify the next direction of travel. Thus, if there are no other vehicles in the neighbourhood, the algorithm works as a purely chaotic mobility model, where mobility decisions are made in accordance with the probability distribution ρ . Such an algorithm operates in each vehicle using different radius of convergence to optimize the movement taking into account the characteristics of each vehicle in order to improve the distribution of the group members throughout the scenario of the mission, improving hunting and speed of identification of objects, without creating major problems. Initially, we get the current heading for each vehicle in the group relative to the others and check its radius of proximity r over the grid of vehicles of the same type. If some vehicles are closer than r , then the new direction of travel (corner) is calculated according to the corresponding depressing forces. Otherwise, a chaotic approach based on the value of ρ and the guessed distribution of uncertainties is used. For ground robots, the "escape" algorithm is also used, whereby the agent moves away from the target area with the anti-aircraft missile systems and attempts to reach one of the interfaces at a predetermined coordinate. After the "escape" for the agent with the help of an incidental generator is determined the time of the next attempt to continue to the target.

6 Modeling of Combat Mission

We consider the enemy's air defense system (ADS) to be an integrated system consisting of radar stations (radars), surface-to-air complexes (SACs) and devices that ensure their functioning. The most widespread devices of the ADS systems are artillery and missile systems, which ensure the survival of the defended objects in the conditions of a massive attack of the devices of the group of robotic complexes. Artillery and missile systems (as well as radio warfare devices – RWD) are distinguished by the zone of damage (strangulation) – the area of space within which it is ensured that the atmospheric target is destroyed or strangled (in the case of RWD) with a given probability. The zone of influence lies within the range from minimum to maximum range of possible reduction of the targets. Graphically in the projection on the horizontal plane at the all-permissive impact the zone of SACs destruction as well as the zone of targets smothering by RWD are shown in Fig. 3 in the form of circles, where is indicated: AH – radius of impact of artillery SACs; RM and RH – respectively minimum and maximum radius of impact of missile SACs; RM and RH – respectively minimum and maximum radius of impact of RWD units. Missile SACs can engage air targets at long ranges, but cannot engage them at very short ranges. For their part, SACs engage targets at short range, but cannot hit them at greater distances. Thus, the zones of action of missile and artillery SACs are overlapping. The range of targets suffocated by RWD devices is significantly greater

than the range of missile defeat. Thus, the modern ADS is a well-defended, hard-hitting, low-range, high-altitude, low-angle ADS with overlapping zones, capable of effective combat against the enemy's offensive forces. In describing the SACs, we use a right-handed rectangular coordinate system in which we define D as the distance equal to the abnormal range from the radar to the target, and α as the heading (azimuth of the target), moving along the course of the guided missile from the line of sight to the centre to the line of sight to the target. The origin of coordinates in this system can be taken, for example, the center of radar antenna station or the center of the protected object.

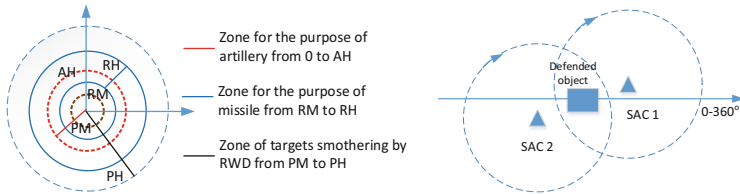


Fig. 3. Zones for the purpose of missile and artillery SACs and RWD and location of the two SACs of ground bases.

Figure 3 graphically shows the model of placement of two ground based air defense systems, where SAC1 and SAC2 are respectively the first and second airborne missile and artillery systems, GS is the defended object. The purpose of the airborne missile system, artillery and missile SAC systems as one of the most important operations is carried out on the basis of information in the form of characteristics of the targets supplied to the combat information and control system from the devices of the visibility systems of the situation. The algorithm of coordinated control of SACs consists of a sequence of actions for the purpose of controlling, ordering and defeating the stations of active interruptions by the RWD system.

7 Multi-agent Modeling

The most accepted way to evaluate the efficiency of complex systems is simulation modeling. To evaluate the developed algorithms and distribution of tasks between unmanned vehicles, we created an agent-based model in AnyLogic system. Each agent was given a predetermined behavior. The overall scenario is the same as the one we discussed earlier. A single drone (or a group) is sent to survey the territory. It surveys the terrain and, having found the objects or obstacles, fills them in on a map of the terrain. The map is shared between all agents, and each agent can take advantage of the combined capabilities of other agents. Combat drones in turn are sent to destroy ground objects, compactly located in a certain surveyed area. In order to destroy targets in the surveyed area, the robots had to form teams based on their individual capabilities and the location of their deployment. When the investigator finds a thief, he signals the closest unmanned vehicles with the necessary capabilities. These vehicles form a team with a robot investigator and head out to complete the mission. Combat drones carry a bomb charge. In

order to successfully complete the mission, the drone must drop the bomb on the military installation.

After completing the mission, the drones return to base using a higher altitude route. Ground operations are represented by spiders and dogs to perform sabotage missions to destroy enemy military objects. Military assets are protected by an ADS system consisting of several radar stations with overlapping target-detection zones and equipped with keyed surface-to-air and ground-to-ground missiles. The radar can simultaneously guide up to two missiles. The missile is launched after the detected robot-agent enters the radar tracking zone, which is a half-sphere with a given radius around the radar. Indeed, the task of detecting unmarked bionic robots is a difficult task, so we have laid a lot of optimism in modeling the capabilities of forces defending themselves by detecting UGV.

In Fig. 4 shown the simulation model for an unmanned ground vehicle, parameters, variations, subs, and functions. The agent’s behavior is defined by means of the state diagrams, which take into account such events as receiving data on the target, successful execution of the task of destroying a hostile object, own hostility to the opposing missile, completion of the mission, and return to the base.

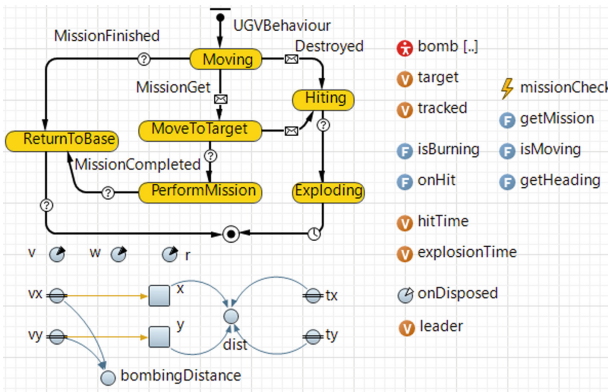


Fig. 4. Imitation model for unmanned ground vehicle.

The model is scalable: it can operate with any number of agents of each type, ADS, opposing objects and the parameters of the number of robotic agents, their speed, the parameters of the operation of the anti-aircraft complex, etc. In Fig. 5 shown the test bench in the process of modeling. To analyze the results in the imitation model, we used as an efficiency criterion a parameter indicating the level of capability to win a battle and the survival rate of the attacking forces, which are calculated as follows. Initially, the activists who remained are calculated at the end of the interaction for both sides. Then they are balanced with the initial assets and calculate their correlation for both parties. In other words, it is simply the coefficient of survival after the end of the battle (Fig. 6).



Fig. 5. The modelling process.

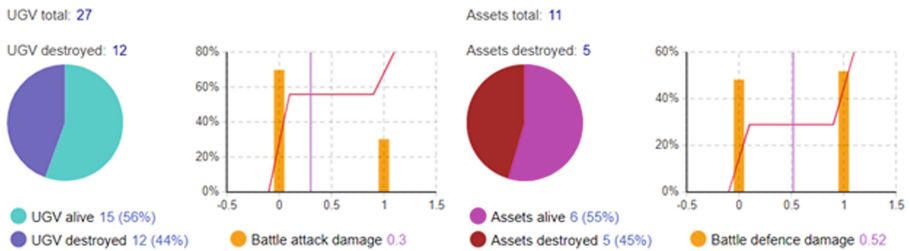


Fig. 6. Resulting data on the survival of the forces attacking and defending.

8 Conclusion

Thus, the paper considers the peculiarities of using the concept of "Mosaic Warfare" based on the dynamic control of distributed systems of mobile robotics complexes using a multi-agent approach. The paper describes modelling of control processes of a group of bionic robots equipped with various sensors and computer vision system for search and reconnaissance operations, reconnaissance and military diversions with the provision of mechanisms of autonomy, adaptation, coordination and collective behavior. During the work implementation the following main tasks were solved: Developed algorithms for formation of groups and clusters of agents; proposed a mosaic structure of a distributed system of mobile robotics complexes; developed algorithms for planning the movement, formation of the agents' trajectory and group control; Developed agent-based optimization model of the control system for a group of unmanned aircraft, unmanned ground vehicles and ground robots; created the system's software interface with 2D and 3D animation. An agent-based approach was used for modeling. All types of agents in this model (robots, radars, missiles, bombs, military units and buildings) are present and interact in a continuous 3D space. The Anylogic modeling environment was used to create the model. Experiments with centralized control with a leader and decentralized control were carried out. The choice of decentralized group control increases the efficiency of operation and the probability of achieving the goal of the mission, as well as

the performance of the task by individual agents. Application of the swarm principle of control is appropriate in conditions of targeted actions aimed at the destruction of enemy forces. This research supports the idea of using several groups of unmanned transport vehicles as a living system for conducting sabotage and combat operations, in which the characteristics of each mobile robotic complex is used to increase the efficiency of the system as a whole. Further investigations will be continued in the complex integration of intellectual algorithms based on the imitation of behavioral reactions and machine learning methods.






References

1. Sapaty, P.S.: Mosaic warfare: from philosophy to model to solutions. *Math. Mach. Syst.* **3**, 17–34 (2019). <https://doi.org/10.34121/1028-9763-2019-3-17-34>
2. Stolfi, D.H., Brust, M.R., Danoy, G., Bouvry, P.: Competitive evolution of a UAV swarm for improving intruder detection rates. In: 2020 IEEE International Parallel and Distributed Processing Symposium Workshops (IPDPSW), pp. 528–535. IEEE, New Orleans (2020). <https://doi.org/10.1109/IPDPSW50202.2020.00094>
3. Khaleghi, A.M., Xu, D., Lobos, A., et al.: Agent-based hardware-in-the-loop simulation for UAV/UGV surveillance and crowd control system. In: 2013 Winter Simulations Conference (WSC), pp. 1455–1466). IEEE, Washington (2013). <https://doi.org/10.1109/WSC.2013.6721530>
4. Ajitha, S., Datta, A., Kumar, T.S.: Multi-agent based artificial war. In: 2017 Ninth International Conference on Advanced Computing (ICoAC), pp. 92–96. IEEE, Chennai (2017). <https://doi.org/10.1109/ICoAC.2017.8441449>
5. Oh, H., Shirazi, A.R., Sun, C., Jin, Y.: Bio-inspired self-organising multi-robot pattern formation: A review. *Robot. Auton. Syst.* **91**, 83–100 (2017). <https://doi.org/10.1016/j.robot.2016.12.006>
6. Lee, J., Shin, S., Park, M., Kim, C.: Agent-based simulation and its application to analyze combat effectiveness in network-centric warfare considering communication failure environments. *Math. Probl. Eng.* **2018**, 2730671 (2018). <https://doi.org/10.1155/2018/2730671>
7. Faryadi, S., Velni, J.M.: A reinforcement learning-based approach for modeling and coverage of an unknown field using a team of autonomous ground vehicles. *Int. J. Intell. Syst.* **36**(2), 1069–1084 (2021). <https://doi.org/10.1002/int.22331>
8. Clark, B., Patt, D., Schramm, H.: Mosaic Warfare: Exploiting Artificial Intelligence and Autonomous Systems to Implement Decision-Centric Operations. CSBA (2020)
9. Petavratzis, E.K., Volos, C.K., Moysis, L., et al.: An inverse pheromone approach in a chaotic mobile robot's path planning based on a modified logistic map. *Technologies* **7**(4), 84 (2019). <https://doi.org/10.3390/technologies7040084>
10. Moysis, L., Petavratzis, E., Volos, C., et al.: A chaotic path planning generator based on logistic map and modulo tactics. *Robot. Auton. Syst.* **124**, 103377 (2020). <https://doi.org/10.1016/j.robot.2019.103377>

Electrical Engineering



Investigation of the Electrical Parameters of an Advanced High-Energy Ignition System

Kostyantyn Korytchenko¹ , Mario Janda^{2,2} , Olga Shypul^{3(✉)} ,
Serhiy Krivosheev¹ , and Oleksandr Yeresko¹ 

¹ National Technical University “Kharkiv Polytechnic Institute”, 2 Kyrpychova Street, Kharkiv 61002, Ukraine

² Comenius University in Bratislava, Mlynska dolina 84248, Bratislava, Slovakia

³ National Aerospace University “Kharkiv Aviation Institute”, 17 Chkalova Street, Kharkiv 61070, Ukraine
o.shipul@khai.edu

Abstract. We studied electrical parameters of the ignition system generating a self-stabilized high-voltage pulsed arc. We observed 2 current pulses generated by the system. The first current pulse appears in the time interval 0 to 3 μ s as a consequence of a high-voltage pulse (about 20 kV) supplied to the spark gap. The discharge current after the first current pulse gradually increases up to 3 ± 1 A, when the second current pulse appears. The delay between two current pulses increases with growing spark gap size from 60 to 125 μ s, corresponding to gap size 0.5 mm and 13 mm, respectively. The energy input in the developed ignition system is given by the discharging of two capacitors. The total energy released in the first current pulse does not exceed 163 mJ. The experimental-computational method was used to measure the energy input for the second pulse. It was found out that the main part of the discharge energy is released in the second current pulse where the deposited energy exceeds 231–541 mJ. Relatively high efficiency of energy deposition in the gas discharge channel up to 58% was observed, increasing with expanding spark gap size to 13 mm.

Keywords: High-energy ignition system · Energy input · Efficiency · Arc resistance · Electrical parameters

1 Introduction

The operation of internal combustion engines with forced ignition under lean mixtures conditions improves their environmental performance. Reliable ignition of lean mixtures requires higher spark ignition energy. High-energy ignition systems are therefore developed for this purpose [1–3]. High energy ignition systems are also used to start gas turbine engines, to ignite fuel oil in boilers and special technological equipment [4, 5], to cold start diesel engines, etc. At the same time, ignition systems are required to ensure reliable ignition of the combustible mixture in a high-speed gas flow [6].

In the presented work, the results of the study of an improved high-energy ignition system are given. The improvement of the considered ignition system is aimed to increase

the reliability of ignition of the combustible mixture under the influence of a high-velocity gas flow on the discharge channel. Previously, we carried out a photographic study of the ignition area [7]. Also studies of the influence of a high-speed gas flow on the development of the discharge process in the considered ignition system were carried out [8]. The presented work is a continuation of previous studies, in which the features of energy release in the developed ignition system are considered in detail.

2 Advanced High-Energy Ignition System Device Operation Principles

A study of an ignition system was made. The system generates a self-stabilized high-voltage pulsed arc obtained according to electrical circuit shown in Fig. 1. This circuit solution is known [9, 10]. However, the circuit was improved by including the switch S_2 in parallel with the capacitor C_2 . In this case, the switch is connected on at a certain time. Adding the switch S_2 makes it possible to provide self-stabilization of the discharge under the influence of a high-speed gas flow on the discharge channel.

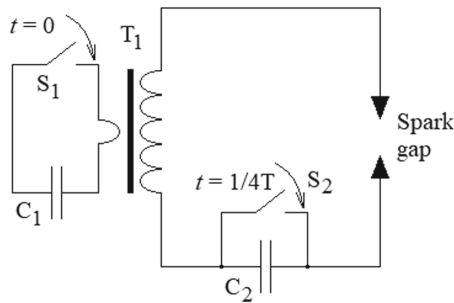


Fig. 1. Schematic diagram of the developed ignition system.

The ignition of a pulsed arc in such a circuit occurs as follows. Initially, capacitors C_1 and C_2 are charged from external voltage sources, which are not shown in the diagram. Next, the switch S_1 is turned on, which leads to the supply of a voltage pulse to the primary winding of the step-up transformer T_1 . This leads to the appearance of a high-voltage pulse on the secondary winding of the transformer, which results in a gas breakdown in the spark gap. After the spark gap is closed, the discharging of the capacitor C_2 through the secondary winding of the transformer T_1 and the spark gap begins. When the current in the discharge circuit reaches its maximum, and the voltage across the capacitor reaches zero, the switch S_2 is turned on. This turn-on time corresponds to the first $1/4$ current cycle. Before turning on the switch S_2 , the energy of the magnetic field is accumulated in the inductance of the transformer winding. Thus, the further flow of the spark discharge is ensured by the release of the energy accumulated in the secondary winding of the transformer.

3 Methodology and Results of the Study of the Electrical Parameters of the Developed Ignition Circuit

The study of the electrical parameters of the developed ignition system was carried out using the following equipment. The spark discharge current during the breakdown was measured by Ion Physics CM-500-L current transformer with a response time of 2 ns where the current signal was registered by Tektronix TBS2104 oscilloscope. Since a high current leads to saturation of the current transformer cores, the measurement of the pulsed arc current was carried out by a CSNM191 Honeywell current sensor with a measurement error of $\pm 0.5\%$ and a response time of less than $1 \mu\text{s}$ where the current signal was registered by Rigol DS1104 oscilloscope. The sensitivity of the CSNM191 sensor after converting the current signal into a voltage signal was $100 \pm 0.51 \text{ A/V}$. Voltage probes TEKTRONIX P6015A and HVP-39pro PINTEK were used to record the voltage. The measurement error of the HVP-39pro probe is 3% of full scale. The voltage across the studied elements of the discharge circuit was determined as a potential difference, where the potentials at the studied points were measured by voltage probes or P6015A or HVP-39pro. Due to the relatively high voltage measurement error of these probes, the capacitor charge voltage was also measured with a UNI-T UT-58C multimeter with a measurement error of $\pm 0.5\%$ in the measurement range under study. Capacitor capacitance was measured using an E7-22 RLC meter with a measurement error of $\pm 0.009 \mu\text{F}$.

The parameters of the elements of the ignition system and the initial voltage on the capacitors C_1 and C_2 were measured. The capacitance of capacitor C_1 was $8.005 \pm 0.009 \mu\text{F}$. The capacitance of capacitor C_2 was $2.708 \pm 0.009 \mu\text{F}$ at a measurement frequency of 1 kHz. The initial charge voltage of capacitors C_1 and C_2 was $828 \pm 6 \text{ V}$, since the charge was carried out from one voltage source. The resistance of the secondary winding of the transformer and connecting wires was determined according to Ohm's law. It is measured that the total resistance of the winding and connecting wires is $R_{\text{wire}} = 0.180 \pm 0.05 \Omega$.

The discharge current flowing through the spark gap and the voltage drop across the spark gap were measured. The results of measuring the discharge current by the CM-500-L current transformer and the voltage by the P6015A voltage probe on the spark gap throughout the entire discharge are shown in Fig. 2.

According to the measurement results, we detect 2 current pulses (Fig. 2, left). The first pulse corresponds to the time interval from 0 to $1-3 \mu\text{s}$. The second pulse takes place in the time interval from $70 \mu\text{s}$ to $90 \mu\text{s}$ (Fig. 2, left). The first pulse is caused by the breakdown of the spark gap, which is confirmed by the presence of a high-voltage voltage pulse (about 20 kV) before the current pulse on the voltage oscillogram (Fig. 2, right). In this case, before the high-voltage pulse, the voltage on the discharge electrodes is equal to the charge voltage of the capacitor C_2 .

The second current pulse is associated with the discharge of capacitor C_2 . Between the pulses, a delay period is marked, which was about $70 \mu\text{s}$ at a spark gap length of 3 mm. During this delay period, a discharge current flows gradually increasing to $3 \pm 1 \text{ A}$. The presence of the delay period is explained by the high inductive resistance of the secondary winding of the transformer. But when saturation of the transformer core is reached, then the inductive resistance decreases. The decrease in inductive resistance

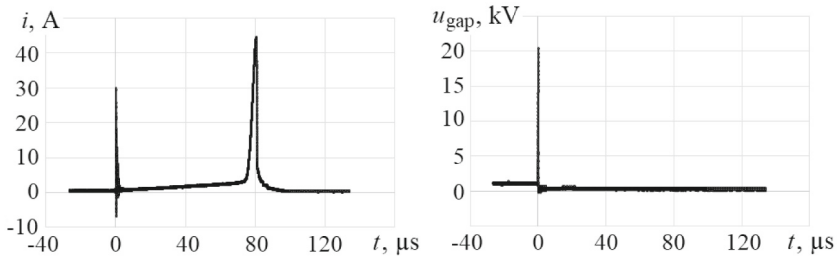


Fig. 2. Oscillograms of current and voltage across the spark gap, recorded by the current transformer CM-500-L and voltage probe P6015A.

leads to a sharp increase in the discharge current caused by the discharge of the capacitor C_2 . In line with the results of measurements of the second current pulse, we observe its increase to 45 A, followed by a sharp decrease after the increase. With the beginning of the first period of pulsations, the voltage across the spark gap decreases to several tens-hundreds of volts (Fig. 2, right).

There was an assumption about the incorrect measurement of the second current pulse by the CM-500-L current transformer due to the presence of a sharp decrease in current after reaching the maximum, since the core saturation may occur in the current transformer. Therefore, the current was additionally measured by the CSNM191 current sensor with a larger current measurement range (± 1000 A) than the CM-500-L current transformer. The results of measuring the discharge current i , flowing through the spark gap, and the voltage u_c on the capacitor C_2 are shown in Fig. 3.

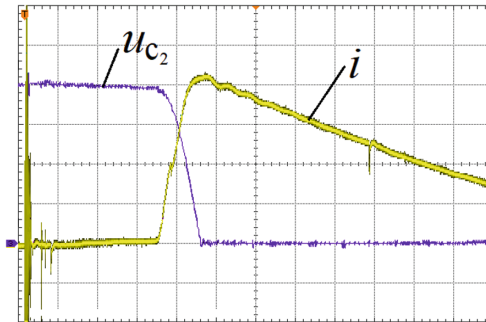


Fig. 3. Oscillogram of the discharge current i flowing through the spark gap and the voltage u_{c2} on the capacitor C_2 . Division scales: current 33.5 A/div, voltage 200 V/div, time 20 μ s/div.

It is detected that the shapes of the measured currents in Fig. 2 (left) and 3 coincide, except for the shape of the current after its rise during the second current pulse. According to the results of measurements with the CSNM191 current sensor, we have the amplitude of the discharge current during the second pulse, reaching more than 135 A. At the maximum current, the voltage across the capacitor C_2 decreases to 0, which corresponds to the theory of electrical engineering. Turning on the switch S_2 excludes the process of

charging the capacitor. Therefore, it is observed the absence of voltage on the capacitor C_2 with further current flow. The further flow of the discharge current is caused by the process of releasing the energy of the magnetic field, accumulated in the inductance of the secondary winding of the transformer, on the resistance of the discharge circuit. As a result, the registered current corresponds to the theory of electrical engineering for the discharge current in the RL circuit.

The first current pulse has been studied in more detail. The results of measuring voltage and current during spark breakdown by a current transformer CM-500-L and by a high-voltage probe are shown in Fig. 4. The length of the spark gap was 3 mm.

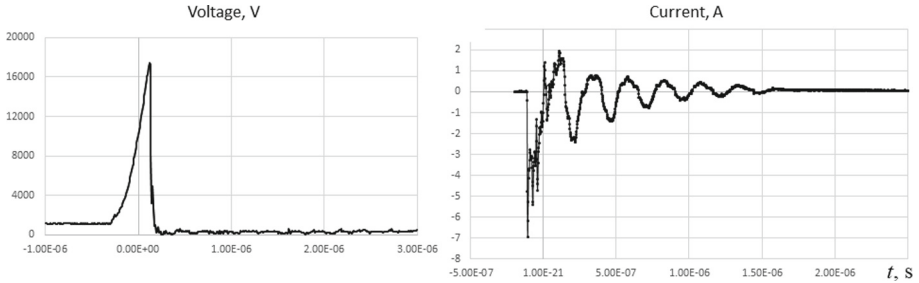


Fig. 4. Spark gap voltage (left) and discharge current (right) recorded by CM-500-L current transformer during the first pulse.

We observe that the increase in the voltage on the secondary winding of the transformer to the breakdown voltage occurs in the case under consideration in less than 0.6–0.7 μs . The breakdown of the spark gap is accompanied by a jump in the discharge current. In this case, the voltage across the spark gap drops sharply with increasing discharge current. An oscillatory-damping process occurs in the discharge circuit with a main oscillation frequency of about 3.3 MHz. Oscillations with such a frequency are possible due to the presence of parasitic capacitance formed between the turns of the secondary winding of the transformer, which leads to a decrease in the inductance of the discharge circuit. The damping of the current oscillations occurs in about 2–3 μs . It should be noted that there are difficulties in measuring the voltage drop across the spark gap after its breakdown.

For the problem of ignition of a combustible mixture, it seems important to estimate the amount of energy deposited into the spark discharge [11]. In the developed ignition system, energy input is carried out as a result of the discharge of capacitors C_1 and C_2 . Let us consider the energy input for the first pulse. The low accuracy of measuring the voltage drop across the spark gap does not allow using these data to calculate the energy deposited into the spark. Therefore, the energy released during the discharge of the capacitor C_1 on the primary winding of the transformer was measured. The switch S_1 in the ignition circuit is switched on for a time $t_1 = 1 \mu\text{s}$. It was measured that the average current in the primary circuit was $i_1 = 200 \text{ A}$. The measurement of the voltage across the capacitor is determined by the expression Δu :

$$\Delta u = \frac{1}{C_1} \int_0^{t_1} i_1 dt. \quad (1)$$

Using the indicated values, we obtain a voltage drop by $\Delta u = 25$ V. With a capacitor charge voltage of 828 V and a subsequent voltage drop to 803 V at $C_1 = 8 \mu\text{F}$, we have that the total energy consumption released at the first pulse does not exceed 163 mJ. It should be noted the low efficiency of conversion of the total energy of the discharge into the energy released in the spark gap, where the efficiency is about 1–50% [12–14].

Consider the energy input for the second pulse because the main energy deposition happens during this time. We use the experimental-computational method for studying the discharge process in a given electrical circuit [15]. We will measure the energy that is deposited into the pulsed arc based on the results of measuring the discharge current under the conditions of the development of the discharge at different lengths of the spark gap. We believe that with an excessively small length of the spark gap, the discharge energy is released on the resistance of the elements of the discharge circuit and is spent on the electrical erosion of the electrodes. With an increase in the length of the discharge gap, these energy losses are supplemented by the release of energy in the gas discharge channel. As a result, with an increase in the length of the discharge gap, an increase in the resistance of the spark channel takes place. According to the results of experimental studies, such an increase in resistance is reflected in a change in the amplitude and duration of the current pulse during the development of a pulsed arc discharge. The discharge current obtained at spark gap lengths of 0.5 mm and 13 mm is shown in Fig. 5.



Fig. 5. Comparison of discharge currents obtained at spark gap lengths of 0.5 mm (left) and 13 mm (right). Division scales: current 35 A/div, time 50 μs /div.

From the obtained current oscillograms, we monitor that an increase in the length of the spark gap leads both to a decrease in the amplitude of the current pulse and the duration of the discharge. It is discovered there is a change in the delay time with a change in the length of the spark gap. The result of the analysis of the delay time between current pulses on the length of the spark gap is presented in Table 1.

Table 1. Dependence of the delay time between current pulses on the length of the spark gap.

Parameter	Volume					
Spark gap length, mm	0.5 ± 0.05	3 ± 0.05	5 ± 0.05	8 ± 0.05	11 ± 0.05	13 ± 0.05
Delay time, μs	60 ± 5	70 ± 5	75 ± 5	90 ± 5	110 ± 5	125 ± 5

An increase in the delay time is associated with a decrease in the discharge current due to an increase in the resistance of the circuit, which increases the saturation time of the transformer core.

Using the results of measurements of the discharge current at different lengths of the discharge gap and the known conditions for the development of the discharge, it seems possible to use these initial data to calculate the change in the resistance of the spark channel with time and to calculate the energy deposited into the gas discharge. Consider the process of discharge current flow in the circuit. Before closing the switch S_2 , the transient process in the electric circuit is described by the equation [16]:

$$L \frac{di}{dt} + i \cdot R_{total} + u_{c_2} = 0, \quad (2)$$

where L is the inductance of the discharge circuit when the transformer core is saturated, u_{c_2} is voltage on the capacitor C_2 .

Let us consider the process of the discharge current flow in the circuit after the switch S_2 , connected in parallel to the capacitor, is closed, while the maximum discharge current is reached. After the switching, the transient process in the electrical circuit is described by the equation

$$L \frac{di}{dt} + i \cdot R_{total} = 0. \quad (3)$$

From Eqs. (2) and (3) it follows that the resistance of the discharge circuit is calculated by the equation

$$R_{total} = \frac{-u_c - L \frac{di}{dt}}{i}. \quad (4)$$

With regard to Eq. (3), in Eq. (4) we have $u_{c_2} = 0$.

For an approximate calculation of the inductance, the results of measuring the amplitude of the current i_{max} , achieved in the first $1/4$ cycle of the second current pulse, and the initial charge voltage of the capacitor $U = u_{c_2}(0)$ can be used. Then the inductance is determined by the expression

$$L = C \frac{U^2}{i_{max}^2}. \quad (5)$$

It is measured that the current amplitude is $i_{max} = 158.8 \pm 1.210.9$ A, the voltage is $U = 828 \pm 6$ V, the capacitance is $C = 2.708 \pm 0.009$ μ F. Hence, we have $L = 73.6 \pm 2.43$ μ H.

After a preliminary assessment of the inductance by expression (5) and a preliminary calculation of the resistance by expression (4), it seems possible to refine the inductance. To do this, we use the expression for calculating the amplitude of the discharge current, counting the resistance of the discharge circuit, in the form

$$i_{max} = U \sqrt{\frac{C}{L}} \cdot e^{-\frac{\pi R_{total}}{4} \sqrt{\frac{C}{L}}}. \quad (6)$$

Thus, the refinement of the inductance L and resistance R_{total} is further carried out by the iteration method, using Eqs. (4) and (6) and the results of measuring the discharge current. In the case of calculating the resistance of the discharge circuit after turning on the switch S_2 , the number of measurement errors that affect the results of the calculation is reduced. This is because only current measurements are used to calculate resistance in an RL circuit, and voltage measurements are not used. Comparison of the results of measuring the resistance in the RLC circuit and the RL circuit in the range of small values is shown in Fig. 6.

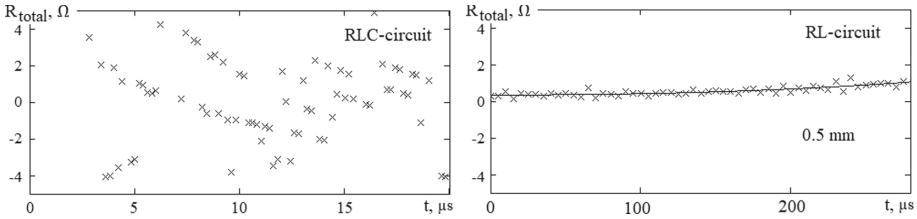


Fig. 6. Comparison of the results of calculating the resistance of the discharge circuit based on the results of measurements in the RLC circuit (left) and RL circuit (right) for a spark gap length of 0.5 mm: × are the calculated values; – is interpolation line.

Since the minimum scatter of the calculated values of the resistance of the discharge circuit takes place in the analysis of the discharge in the RL circuit, these results were used further. According to the results of 5 measurements, it was found that the minimum resistance of the discharge circuit is $R_{total} = 0.362 \pm 0.028_{0,9}$ by a spark gap length of 0.5 mm. It should be noted that the obtained resistance exceeds the measured sum of the resistance of the connecting wires and the resistance of the secondary winding of the transformer by approximately two times. This is due to the fact that the resistance also includes the internal resistance of the capacitor (until it is closed by the switch S_2). In addition, to the resistance should be added the resistance caused by energy losses due to electrical erosion of the discharge electrodes, and energy losses at the resistance of the switch S_2 (after it is turned on). As the discharge current decreases, the resistance of the gas-discharge channel increases. Therefore, there is an increase in resistance discharge circuit in the process of reducing the current in the RL circuit (Fig. 6, right). To confirm this assumption about the effect of the resistance of the gas-discharge channel, we monitor that with an increase in the length of the discharge gap to 13 mm, an increase in the total resistance discharge circuit occurs relatively faster (Fig. 7) than with a length of 0.5 mm (Fig. 6, right).

The reliability of the results of calculating the resistance of the discharge circuit during the second current pulse was verified by checking the presence of an energy balance represented by the equation:

$$\int_0^\infty R_{total} \cdot i^2 dt = \int_0^{t_{1/4}} [R_{total}]_{min} \cdot i^2 dt + \int_{t_{1/4}}^0 R_{total} \cdot i^2 dt = C_2 \frac{U^2}{2}, \quad (7)$$

where $t_{1/4}$ is the duration of the first 1/4 current cycle in the serial RLC circuit.

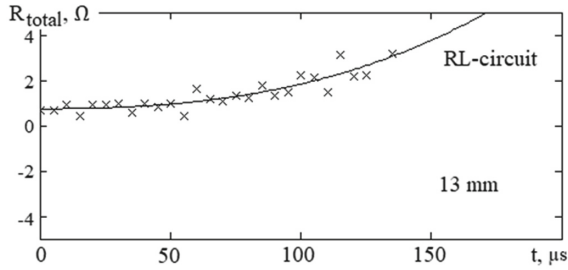


Fig. 7. Total resistance of the discharge circuit according to the results of measurements in the RL circuit for a spark gap length of 13 mm: \times are the calculated values; $-$ is interpolation line.

The calculation assumes that the resistance of the discharge circuit is constant during the first $\frac{1}{4}$ current cycle and equals the minimum resistance $[R_{total}]_{min}$. The results of calculating the energy release in the second current pulse are shown in Fig. 8.

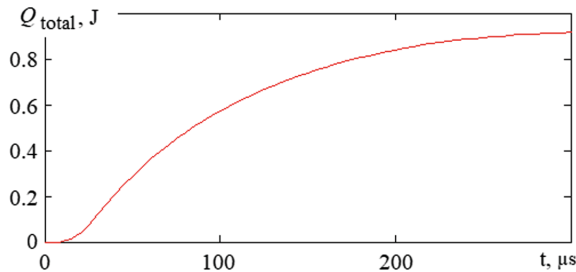


Fig. 8. Dynamics of energy release during the second current pulse by a spark gap length of 0.5 mm.

The experiment was carried out using a copper discharge cathode and an aluminum anode. According to the reference data [17], for the arc discharge current in the range of 20–200 A, the voltage drop across the electrodes is equal to $u_{el} = 18\text{--}22$ V. Hence, it seems possible to calculate the energy release Q_{el} on the discharge electrodes by the expression

$$Q_{el} = \int_0^{\infty} u_{el} i dt. \quad (8)$$

Assuming that $u_{el} = 20$ V and using the measured values of the discharge current over a spark gap length of 0.5 mm, the energy release on the discharge electrodes was calculated using expression (8), which was $Q_{el} = 447$ mJ.

The energy release on the wires is calculated by the expression

$$Q_{wire} = \int_0^{\infty} R_{wire} i^2 dt. \quad (9)$$

At $R_{wire} = 180$ m Ω and using the measured values of the discharge current, it was obtained from expression (9) that $Q_{wire} = 387$ mJ.

To obtain a balance with the total discharge energy Q_{total} , the calculated losses Q_{el} and Q_{wire} should be supplemented with the energy losses due to the internal resistance of the capacitor Q_{cap} . It was obtained by enumeration that if the internal resistance of the capacitor is equal to $R_{cap} = 40 \text{ m}\Omega$, then we will get the presence of an energy balance represented by the expression

$$Q_{total} = Q_{el} + Q_{wire} + Q_{cap}. \tag{10}$$

Using the results of measurements of the current in the RL circuit at different lengths of the spark gap, we obtained the dependence of the minimum resistance of the discharge circuit on the length of the spark gap in the form (Fig. 9).

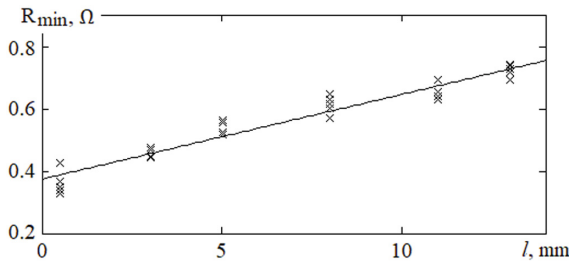


Fig. 9. Dependence of the minimum resistance of the discharge circuit on the length of the spark gap.

With an increase in the length of the spark gap, the difference between the minimum resistance of the discharge circuit at the second current pulse and the average resistance of the discharge circuit during a discharge in the RLC circuit increases. In particular, the calculation of the average resistance of the discharge circuit during a discharge in the RLC circuit was carried out using the measured amplitude values of the discharge current obtained at different lengths of the spark gap using expression (6). The results of such a calculation are presented in Table 2. In the calculation, the average values of the current amplitude based on the results of 5 measurements were used. For comparison, Table 2 also presents the values of the minimum resistance of the discharge circuit at different lengths of the spark gap.

Table 2. Dependence of the average resistance R_{ev} of the discharge circuit during a discharge in the RLC circuit and the minimum resistance R_{min} of the discharge circuit at the second current pulse on the length of the spark gap.

Parameter	Spark gap length, mm					
	0.5	3	5	8	11	13
R_{ev} , m Ω	244	561	679	1163	1289	1415
R_{min} , m Ω	$362 \pm 28_{0,9}$	$457 \pm 14_{0,9}$	$547 \pm 20_{0,9}$	$614 \pm 28_{0,9}$	$650 \pm 25_{0,9}$	$724 \pm 19_{0,9}$

The obtained research results show a tendency for the difference between the average resistance R_{ev} and the minimum resistance R_{min} to increase in the case of an increase in the length of the spark gap. This prevents the minimum R_{min} value from being used as circuit resistance for discharging in an RLC circuit.

The calculation of the discharge energy Q_{ign} released in the gas-discharge channel was carried out according to the expression

$$Q_{ign} = C_2 \frac{U^2}{2} - \int_0^{\infty} R_c i^2 dt - \int_0^{\infty} u_{el} i dt. \quad (11)$$

The results of calculation of the discharge energy Q_{ign} released in the gas discharge channel depending on the length of the spark gap are presented in Table 3. The table also shows the efficiency η_{ign} of energy release in the gas discharge channel.

Table 3. Dependence of the discharge energy Q_{ign} released in the gas-discharge channel on the length of the spark gap.

Parameter	Spark gap length, mm				
	3	5	8	11	13
Q_{ign} , mJ	231	329	445	511	541
η_{ign} , %	24	35	48	55	58

The result obtained on the release of energy in the gas discharge channel shows that the main part of the discharge energy in the developed ignition system is released at the second current pulse. A relatively high efficiency of energy release in the gas discharge channel was also revealed. In this case, a non-linear dependence of the efficiency of energy input into the gas-discharge channel on the length of the spark gap is observed.

4 Conclusion

A study of an ignition system generated a self-stabilized high-voltage pulsed arc was made. The device operation principles of the system are given. The study of the follow electrical parameters of the developed ignition system was carried out. Current, voltage on capacitors, total resistance of discharge circuit was investigated. Generation of two current pulses was observed. Dependence of the delay time between the pulses on the spark gap length was measured. Dependence of the minimum resistance of the discharge circuit on the length of the spark gap was found out. Dependence of the discharge energy released in the gas discharge channel on the length of the spark gap was calculated.

References

1. Dale, J.D., Checkel, M.D., Smy, P.R.: Application of high energy ignition systems to engines. Prog. Energy Combust. Sci. **23**(5–6), 379–398 (1997). [https://doi.org/10.1016/S0360-1285\(97\)00011-7](https://doi.org/10.1016/S0360-1285(97)00011-7)

2. Jose, J.V., Sreenath, V.R.: Review on performance of high energy ignition techniques. *Int. J. Res. Innov. Sci. Technol.* **2**(2), 7–13 (2015)
3. Hayashi, N., Sugiura, A., Abe, Y., Suzuki, K.: Development of ignition technology for dilute combustion engines. *SAE Int. J. Engines* **10**(3), 984–995 (2017). <https://doi.org/10.4271/2017-01-0676>
4. Plankovskyy, S., Popov, V., Shypul, O., et al.: Advanced thermal energy method for finishing precision parts. In: Gupta, K., Pramanik, A. (eds.) *Advanced Machining and Finishing*, pp. 527–575. Elsevier, Amsterdam (2021). <https://doi.org/10.1016/B978-0-12-817452-4.00014-2>
5. Korohodskyy, V., Kryshchyna, S., Migal, V., et al.: Determining the characteristics for the rational adjusting of an fuel-air mixture composition in a two-stroke engine with internal mixture formation. *East.-Eur. J. Ent. Tech.* **2**(5–104), 39–52 (2020). <https://doi.org/10.15587/1729-4061.2020.200766>
6. Watanabe, Y., Houpt, A., Leonov, S.B.: Plasma-assisted control of supersonic flow over a compression ramp. *Aerospace* **6**(3), 35 (2019). <https://doi.org/10.3390/aerospace6030035>
7. Korytchenko, K.V., Kasimov, A.M., Golota, V.I., et al.: Experimental investigation of arc column expansion generated by high-energy spark ignition system. *Prob. Atomic Sci. Technol.* **118**(6), 225–228 (2018)
8. Samoilenko, D., Połaniecki, A., Szost, K., et al.: Influence of high velocity flow on self-stabilized spark discharge of high-energy ignition system. In: *2020 IEEE 4th International Conference on Intelligent Energy and Power Systems (IEPS)*, pp. 313–316. IEEE, Istanbul (2020). <https://doi.org/10.1109/IEPS51250.2020.9263239>
9. Shimojo, H., Inamura, T.: Spark plug igniter comprising a DC-DC converter. US Patent 4,136,301, 7 Jan 1977
10. Porreca, P.J., VanDuyne, E.A.: Dual energy ignition system. US Patent 5,197,448, 23 Aug 1991
11. Essmann, S., Markus, D., Maas, U.: Investigation of the spark channel of electrical discharges near the minimum ignition energy. *Plasma Phys. Technol.* **3**(3), 116–121 (2016). <https://doi.org/10.14311/ppt.2016.3.116>
12. Camilli, L.S., Gonnella, J.E., Jacobs, T.J.: Improvement in spark-ignition engine fuel consumption and cyclic variability with pulsed energy spark plug. *SAE Technical Paper 2012-01-1151* (2012). <https://doi.org/10.4271/2012-01-1151>
13. Lakshmipathi, S.M., Deshpande, S.: Evaluation of spark plug energy and efficiency for two wheeler ignition system. *SAE Technical Paper 2019-26-0330* (2019). <https://doi.org/10.4271/2019-26-0330>
14. Jacobs, T.J., Camilli, L.J., Gonnella, J.E.: Improvement in lean homogenous spark-ignition combustion with pulsed energy spark plug. In: *Internal Combustion Engine Division Fall Technical Conference*, vol. 55096, pp. 439–445. ASME, Vancouver (2012). <https://doi.org/10.1115/ICEF2012-92165>
15. Korytchenko, K.V., Shypul, O.V., Samoilenko, D., et al.: Numerical simulation of gap length influence on energy deposition in spark discharge. *Electr. Eng. Electromech.* **1**, 35–43 (2021). <https://doi.org/10.20998/2074-272X.2021.1.06>
16. Morris, N.M.: Transients in electrical circuits. In: *Mastering Mathematics for Electrical and Electronic Engineering*. MMS, pp. 283–310. Palgrave, London (1994). https://doi.org/10.1007/978-1-349-13193-8_14
17. Raizer, Y.P.: *Gas Discharge Physics*. Springer, Berlin, Heidelberg (1991)



Determination of Massive Rotary Electric Machines Parameters in ANSYS RMxprt and ANSYS Maxwell

Vladyslav Pliuhin¹ , Mykola Zablodskiy² , Maria Sukhonos¹ ,
Yevgen Tsegelnyk¹ , and Lidiia Piddubna¹ 

¹ O.M. Beketov National University of Urban Economy in Kharkiv,
17 Marshala Bazhanova Street, Kharkiv 61002, Ukraine
vladyslav.pliuhin@kname.edu.ua

² National University of Life and Environmental Sciences of Ukraine,
19 Henerala Rodimtseva Street, Kyiv 03041, Ukraine

Abstract. The paper considers simulation results of electromagnetic transient processes of an induction motor with an external solid rotor. Due to the specifics of such type of electric machine, the traditional approach to design and modeling causes difficulties and an ambiguous solution. In this regard, this paper shows the creation of a design object based on the ANSYS RMxprt template specifically for an induction motor with an external solid rotor. Further, the resulting parameterized template was exported to ANSYS Maxwell 2D sheet for further analysis based on the simulation of an electromagnetic field distribution in the dynamic operation mode. The adequacy of the obtained models is guaranteed by the great experience and authority of ANSYS® in generating computational models without user intervention in the key stages of graphic and physical prototypes generation. The formation of equations for obtaining machine parameters based on model graphical objects and components of the electromagnetic field is shown in detail. The simulation results are presented and compared with experimental data. Separately, the extraction of the calculated model parameters at the post-processing stage is shown. The work will be useful to scientific researchers and design organizations in creating digital twins of technical objects.

Keywords: Induction motor · External rotor · Solid rotor · Electromagnetic field · Modeling · Losses · Transients · ANSYS · Maxwell · RMxprt

1 Introduction

The most important achievements of modern science and technology are closely related to the production and use of electrical energy. There is a growing interest in developing efficient ways to convert solar and wind energy into electrical energy [1, 2], in the production of electric vehicles and electric filling stations in all advanced countries of the world. One of the largest consumers of this energy type are electromechanical energy converters and electrical machines (EM) in particular.

In this regard, the problems of improving EM, both in technical terms and in the field of theoretical research, are undoubtedly relevant and will not lose their relevance as long as humanity uses electricity.

The development of a new methodology for designing electromechanical energy converters, the development of software tools to increase their economic competitiveness, the reliability of design synthesis, of course, is an important and urgent task [3, 4]. The calculation of an EM, as a rule, is reduced to solving a system of equations with many unknowns [5–7]. Mathematical modeling includes the description of electromagnetic processes and the solution of a system of equations describing electromagnetic processes, considering the assumptions and variations of the model parameters [8, 9].

The success of the correct, adequate in relation to real prototypes of EM and the correspondence of calculations to experimental results lies in the development of individual mathematical models for a large species diversity of EM [10, 11].

These models have a different nature of the accepted assumptions, considering the features of the design, simplifications, and clarifications. At the same time, a lot of work is devoted to the systematization and classification of both EM and their models, the accumulation of a data bank of models and calculation methods for individual EM [8, 10]. The species diversity of machines has given rise to countless models, and the attempt to classify them has become even more complicated.

A special place in the classification of EM is occupied by a non-standard electric machine, which belongs to the induction type, but has an inverted design with a solid rotor [12]. The design of the screw electric motor (SEM) consists of two stators mounted on a common hollow shaft (Fig. 1).

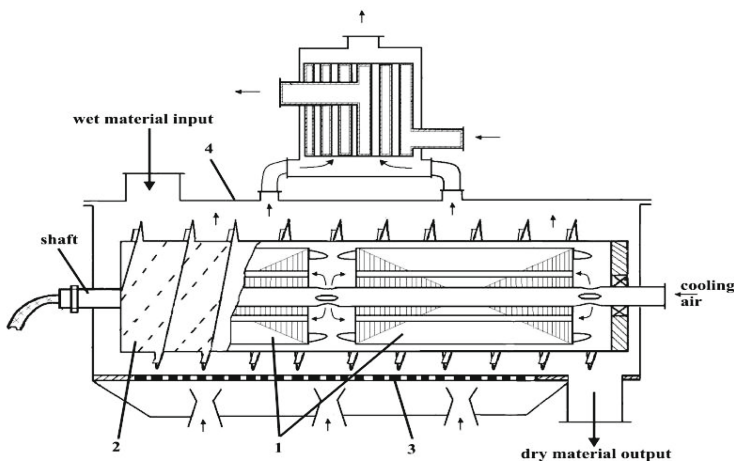


Fig. 1. The design of the screw electric motor: 1 – stators; 2 – solid rotor; 3 – heater; 4 – housing.

Stators (SEM) create oppositely directed electromagnetic torques, providing the necessary speed of rotation of the hollow cylinder of the common solid rotor without the use of a mechanical gearbox. Hollow thin-walled solid rotor with screw loops, in addition to the function of moving the working material, simultaneously provides heating of the latter.

In previous works, an attempt was made to determine the parameters and characteristics of such a machine in various ways, including using ANSYS Maxwell [13, 14]. Despite the positive results obtained, a universal and reliable approach to modeling in the construction and calculation of the model has not been found [12, 15, 16].

Due to the appearance of a new update ANSYS 2022R1, it became possible to improve the calculation method, which is the goal of this work. It will be interesting and useful for readers and scientific researchers to get acquainted with a detailed step-by-step description of the process of creating a computational model in the ANSYS RMXprt and ANSYS Maxwell software packages, the solver configuration, not only for the specific machine under consideration, but also to transfer the obtained research results and methodological approach to other types of EM.

2 Model Settings in ANSYS RMXprt

An eight-pole screw electric motor with an external solid rotor with a power of 45 kW was chosen as a prototype for research.

In the Electrical Machine Type Selection Template Wizard, “Outer-Rotor Induction Machine” is selected under the General category. This category of projects is limited in that it does not allow to directly perform calculations and obtain machine parameters as an output, but it is useful for generating correct exports to Maxwell 2D/3D solutions [17, 18].

At the first stage, after creating the project, it is necessary to choose the configuration of the machine with a solid rotor (Fig. 2). Table 1 shows the parameters that were entered into the forms categories of the project tree.

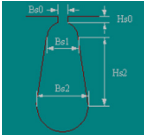
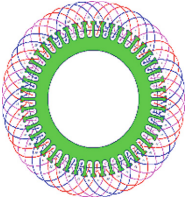
The image shows a screenshot of the 'Properties' dialog box in ANSYS RMXprt. The dialog box has a title bar with a maximize button and a close button. Below the title bar is a table with four columns: 'Name', 'Value', 'Unit', and 'Evaluated V...'. The table contains the following data:

Name	Value	Unit	Evaluated V...
Source Type	AC		
Structure	Outer Rotor		
Stator Type	SLOT_AC		
Rotor Type	SOLID		

Fig. 2. Rotor type selection in the machine category.

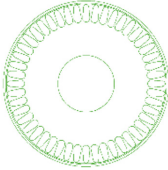
Important in the subsequent calculation of losses in ANSYS Maxwell is the correct setting of steel properties. For stator steel type 2212, a magnetization curve was defined in the material editor (Fig. 3), bulk conductivity 7142857 Sm/m, mass density 7850 kg/m³, composition – lamination.

Table 1. Initial data for the SEM design.

Category	Parameter name	Unit	Value
Stator			
	Number of poles	–	8
	Number of slots	–	48
Stator core			
	Outer diameter	mm	370
	Inner diameter	mm	132
	Length	mm	500
	Stacking factor	–	0.95
	Steel type	–	2212
Stator slot			
	Hs0	mm	1
	Hs2	mm	27
	Bs0	mm	2
	Bs1	mm	13
	Bs2	mm	17
Stator winding			
	Winding layers	–	2
	Parallel branches	–	4
	Conductors per slot	–	24
	Coil pitch	slots	5
	Number of strands	–	3
	Wire wrap	mm	0.28
	Wire size	mm	1.8
Rotor core			
	Outer diameter	mm	384
	Inner diameter	mm	374
	Length	mm	500
	Steel type	–	St3

(continued)

Table 1. (continued)

Category	Parameter name	Unit	Value
Analysis setup			
	Rated output power	kW	45
	Rated voltage	V	220
	Rated speed	rpm	750
	Frequency	Hz	50
	Rated power factor	–	0.8
	Load type	Const. power	

In ANSYS Maxwell the core loss for electrical steel is based on:

$$\rho = K_h B_{max}^2 f + K_c (B_{max} f)^2 + K_e (B_{max} f)^{1.5},$$

where K_h is the hysteresis coefficient; K_c is the classical eddy coefficient; K_e is the excess or anomalous eddy current coefficient due to magnetic domains; B_{max} is the maximum amplitude of the flux density; f is the frequency.

As a result of preliminary calculations for steel type 212, the following characteristic magnetization coefficients were obtained: $K_h = 164.2$, $K_c = 1.3$, $K_e = 1.72$.

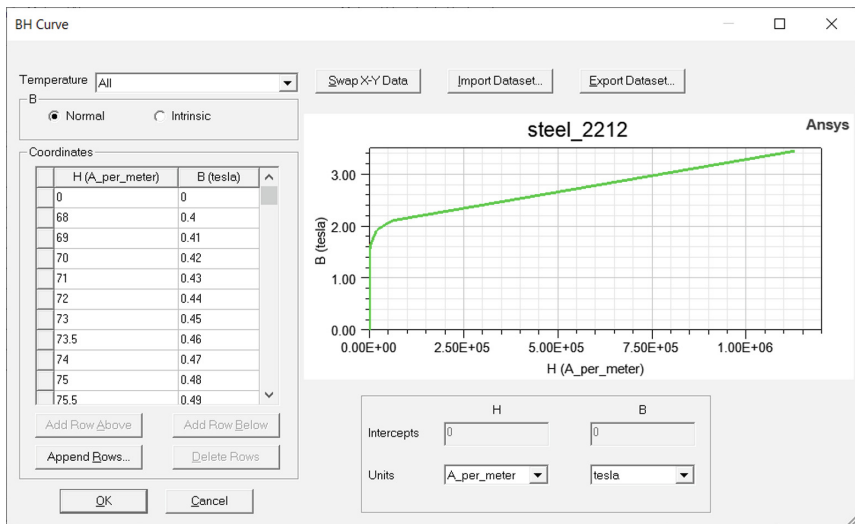


Fig. 3. Type 212 steel magnetization curve.

For steel of a solid rotor of type St3, a magnetization curve was set in the material editor, bulk conductivity 4069000 Sm/m, mass density 7800 kg/m³, composition – solid. Magnetization coefficients ($K_h = 233.89$, $K_c = 1.673$, $K_e = 0$) were determined by

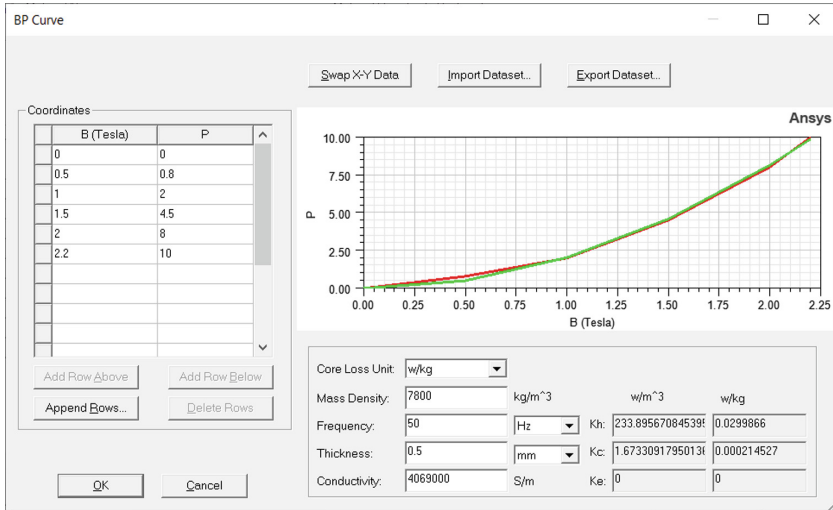


Fig. 4. On the determination of the characteristic magnetization coefficients.

setting a series of specific loss curves at different frequencies in the material properties Core Loss at One Frequency (Fig. 4).

This completes the basic settings of the project, after validating the project, it becomes possible to export it to one of the available formats, in this case – ANSYS Maxwell 2D [19, 20].

3 Model Setup in ANSYS Maxwell

Configuration, excitation settings, winding parameters, material properties and boundary conditions in ANSYS Maxwell are automatically generated during export from ANSYS RMxpvt (Fig. 5).

Since the machine is symmetrical, it is automatically divided into sectors according to the number of poles (in this design – 1/8 part), the full configuration is considered already at the post-processing stage after the field calculation.

To obtain the system of algebraic equations for further solving, the geometry task is divided by Maxwell masher into a small elements. All models' solid entities are split with triangles of the equal size. The set of all triangles is referred to the model finite element mesh, or in other words – the mesh.

In ANSYS Maxwell the field distribution in each element is approximated with a second order quadratic polynomial equation, shown in [21]:

$$A_z(x, y) = a_0 + a_1x + a_2y + a_3x^2 + a_4xy + a_5y^2.$$

Field quantities are calculated for 6 points (3 corners and 3 midpoints) in 2D area. Field quantities inside of each triangle are calculated using a second order quadratic

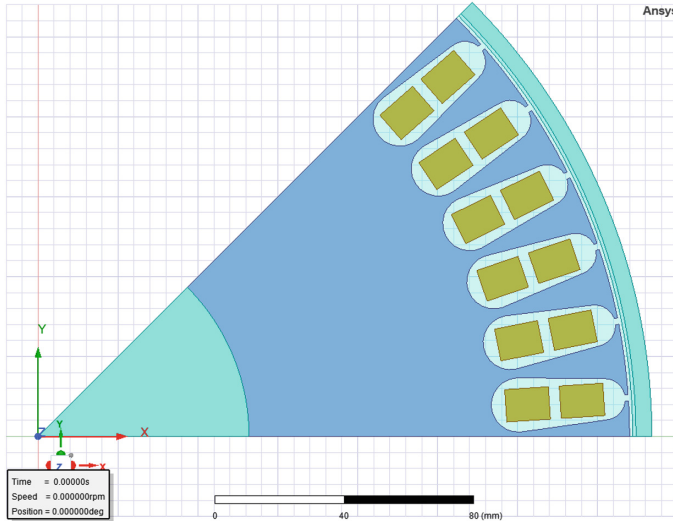


Fig. 5. Model 1/8 of the car in Maxwell 2D.

interpolation approach. In calculation Maxwell uses finite element method variational principle: Poisson's equation $\nabla^2 A = -\mu J$ is replaced with energy functional [20]:

$$F(A) = \frac{1}{2} \int \left(\frac{\nabla A \circ \nabla A}{\mu} + A \circ J \right) dV.$$

Functional $F(A)$ in [20] is minimized with counting the value A at each node in every mesh triangle. After that, over all the triangles, the obtained result in a view of a matrix equation $[S][A] = [J]$ solved using standard matrix solution way:

- Sparse Gaussian Elimination (direct solver);
- Incomplete Choleski Conjugate Gradient Method (ICCG iterative solver).

FEM error evaluation used to approximate solution back into Poisson's equation:

$$\nabla^2 A^{approx} + \mu J = R.$$

Because A is a quadratic function, R has a constant value in each mesh triangle. The local error in every triangle is direct ratio to R .

In addition to the above, Maxwell creates report templates, which, however, are not enough to obtain advanced parameters of the modeled object. The Field Calculator was used to obtain additional calculated parameters. Field calculators has a number of quantities. A feature of this tool is the use of reverse mathematical notation.

Table 2 shows the expressions generated in the field calculator.

Table 2. ANSYS field calculator expressions.

Parameter name	Variable	Expression
Active losses in rotor	P_{rot}	*(Integrate(Volume(Rotor), Ohmic_Loss), 8)
Current in rotor	I_{rot}	Integrate(Surface(Rotor), ScalarZ(<0, 0, Jz>))
Square of current in rotor	I_{rot2}	*(Irot, Irot)
Rotor's resistance	R_2	/(Prot, Irot2)
Module of squared current in rotor	$I_{rot2abs}$	Abs(Irot2)
Ohmic losses in rotor	P_{2_smooth}	Integrate(Volume(Rotor), Ohmic_Loss)
Ohmic losses in 1/8 rotor part	P_{rot1}	/(Prot, 8)
Rotor's resistance in 1/8 rotor part	R_{21}	/(Prot1, Irot2)
Rotor core losses	P_{core}	*(Integrate(Volume(Rotor), Core-Loss), 8)
Core resistance	$R_{2c_coreloss}$	/(+(Prot, Pcore), Irot2)
RMS current in rotor	I_{rot_rms}	/(Irot, sqrt(2))
Square of RMS current in rotor	I_{rot2_rms}	*(Irot_rms, Irot_rms)
RMS resistance in rotor	R_{2_rms}	/(Prot, Irot2_rms)
Solid losses in rotor	$SolidLoss_1$	/(*(Integrate(Volume(Rotor), Pow(ScalarZ(<0, 0, Jz>), 2)), 8), 4069000)
Total RMS resistance in rotor	$R_{2_solid_rms}$	/(SolidLoss1, Irot2_rms)
Total losses in rotor	$TotalLoss_1$	*(Integrate(Volume(Rotor), Total-Loss), 8)

The last modification of the auto-generated project concerned the setup of the model movement system (Fig. 6). In addition to setting the zero-starting speed of the rotor, the moment of inertia of the rotor was set 7.0 kg m² and expressions for mechanical load: if ($time > 0.2$, -120, -10).

Here, up to a time of 0.2 s, the loading torque is 10 Nm, after, according to the set condition, it is 120 Nm. The sign “-” in the expression considers the application of the loading torque, opposite to the direction of rotor rotation.

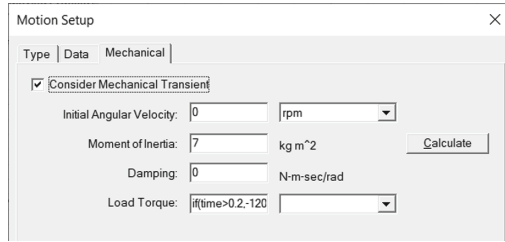


Fig. 6. Model motion system settings.

An additional expression was made to calculate the amount of slip:

$$slip = (n_s - n)/n,$$

where n_s is the field rotation speed in rpm, n is the rotor moving speed, rpm.

In ANSYS RMxprt/Maxwell this equation represented as

$$(750\ rpm - Moving.Speed)/750\ rpm.$$

The *rpm* notation in this expression is required, otherwise the number is incorrectly converted to speed format in *rpm* units.

4 Simulation Results

Modeling in ANSYS Maxwell 2D was performed in a time range of 6 s with a step of 0.0002 s. On a laptop with a mobile processor Intel(R) Core (TM) i5-8250U 1.6 GHz (8 cores / 4 threads) / 16 Gb RAM / SSD, considering the enabled HPC function and saving field patterns every 1000 steps, the calculation of 30000 iterations took 1 h 56 min. Simulation results are shown in Fig. 7, 8, 9, 10 and 11.

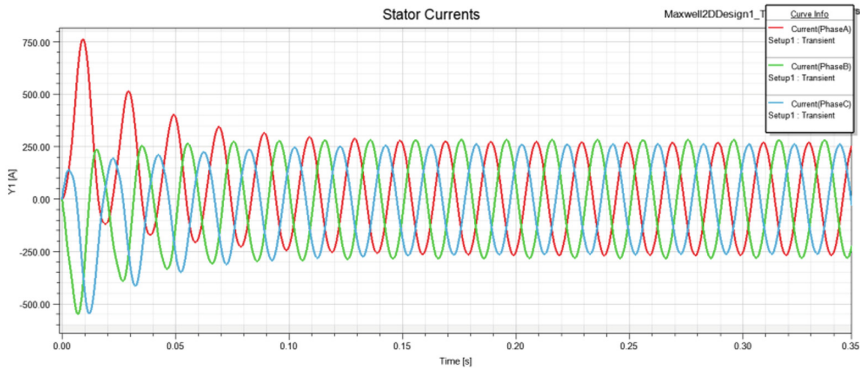


Fig. 7. Currents in the stator winding (starting part shown)

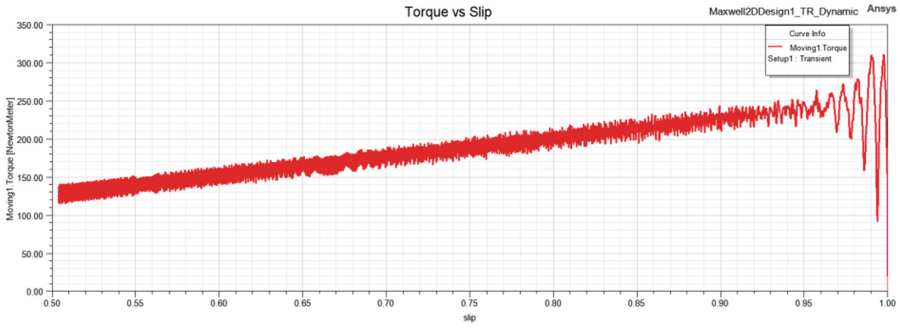


Fig. 8. Moving torque vs slip [equation: $(750 \text{ rpm} - \text{Moving.Speed})/750 \text{ rpm}$].

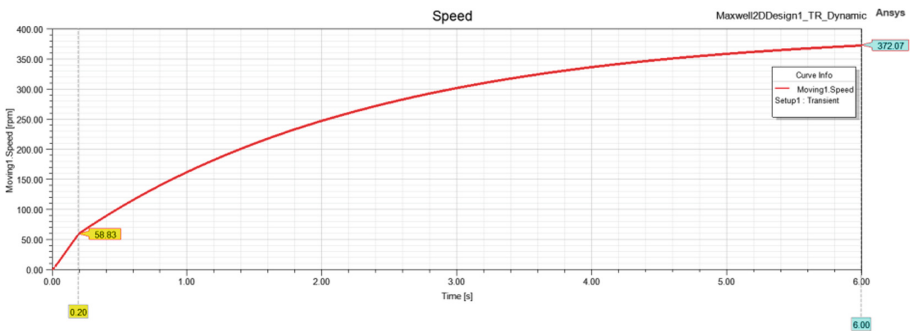


Fig. 9. Moving speed vs time.

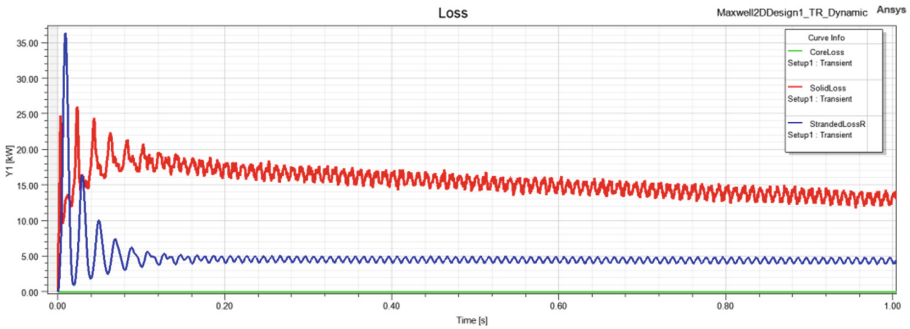


Fig. 10. Losses: solid, stranded in rotor, core.

According to postprocessor analysis, the modulus of force applied to the rotor is 5730 N, the torque is 126 Nm. Comparison chart of experimental and calculated data is shown in Fig. 12 [12, 15, 16, 22].

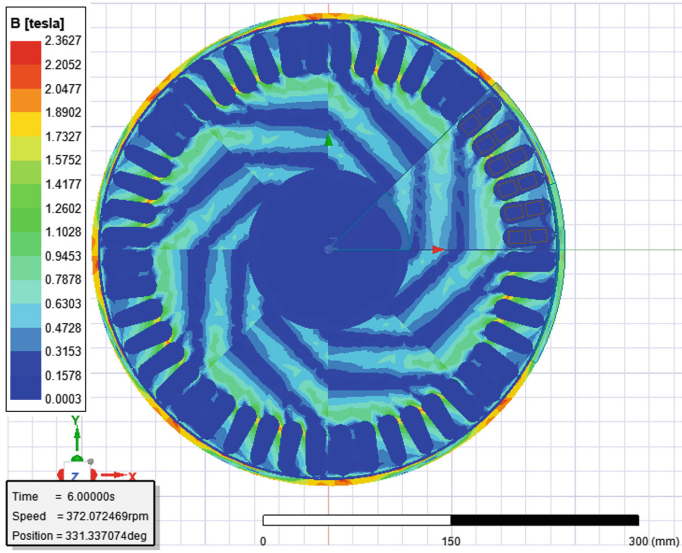


Fig. 11. Flux density distribution.

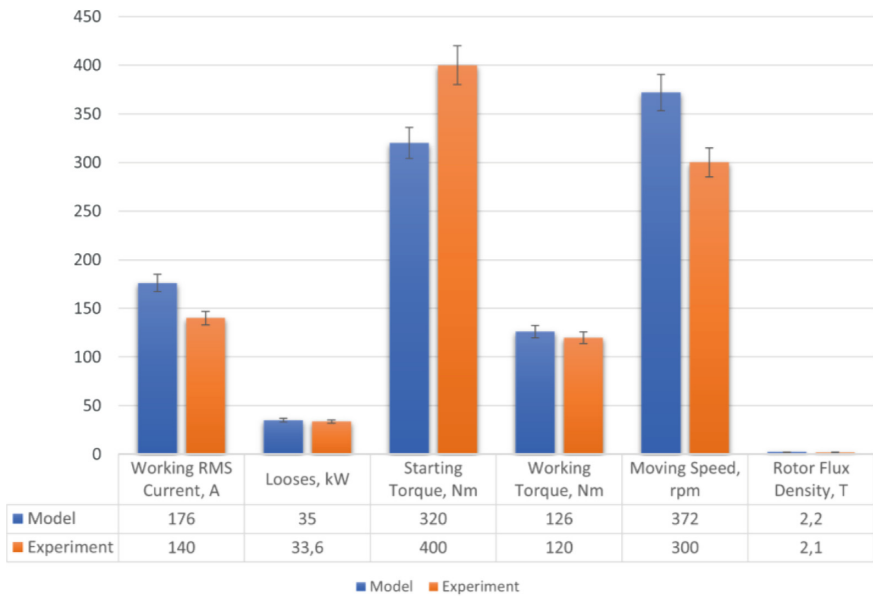


Fig. 12. Comparative diagram of experimental and simulation results.

5 Conclusion

In this paper, the issues of practical modeling of electromagnetic processes in a screw induction electric motor are considered. The specifics of the project configuration consisted in the sequential formation of the model from the ANSYS RMxprt template to the 2D object in ANSYS Maxwell.

The use of a field calculator to generate equations that complement the standard ANSYS Maxwell expressions is shown, which made it possible to obtain values for machine losses, resistances, current and other parameters.

Attention is paid to setting the motion module to consider the moment of inertia of the rotor, the starting speed and the initial angular position, the conditional setting of the machine load torque.

The obtained simulation results allow to get a complete picture of the state of the machine in the start-up mode from zero speed to reaching the working load. Evaluation of the experimental data allows to conclude that the results obtained experimentally are adequate.

Further research of the authors consists in modeling the electromagnetic transient processes of machines with a solid rotor in 3D, as well as creating a motion simulation based on objects imported from ANSYS Maxwell sheet using the ANSYS TwinBuilder (Simplorer) software package.

References

1. Talaat, M., Farahat, M.A., Elkholy, M.H.: Renewable power integration: Experimental and simulation study to investigate the ability of integrating wave, solar and wind energies. *Energy* **170**, 668–682 (2019). <https://doi.org/10.1016/j.energy.2018.12.171>
2. Tugay, D., Kotelevets, S., Korneliuk, S., Zhemerov, G.: Energy efficiency of microgrid implementation with solar photovoltaic power plants. In: 2018 IEEE 3rd International Conference on Intelligent Energy and Power Systems (IEPS), pp. 275–279. IEEE, Kharkiv (2018). <https://doi.org/10.1109/IEPS.2018.8559579>
3. Dineva, A., Mosavi, A., Faizollahzadeh Ardabili, S., et al.: Review of soft computing models in design and control of rotating electrical machines. *Energies* **12**(6), 1049 (2019). <https://doi.org/10.3390/en12061049>
4. Aksonov, Y., Kombarov, V., Tsegelnyk, Y., et al.: Visualization and analysis of technological systems experimental operating results. In: 2021 IEEE 16th International Conference on Computer Sciences and Information Technologies (CSIT), vol. 2, pp. 141–146. IEEE, Lviv (2021). <https://doi.org/10.1109/CSIT52700.2021.9648592>
5. Okhrimenko, V., Zbitnieva, M.: Mathematical model of tubular linear induction motor. *Math. Modell. Eng. Prob.* **8**(1), 103–109 (2021). <https://doi.org/10.18280/mmep.080113>
6. Daukaev, K., Rassölkin, A., Kallaste, A., et al.: A review of electrical machine design processes from the standpoint of software selection. In: 2017 IEEE 58th International Scientific Conference on Power and Electrical Engineering of Riga Technical University (RTUCON), pp. 1–6. IEEE, Riga (2017). <https://doi.org/10.1109/RTUCON.2017.8124818>
7. Lei, G., Zhu, J., Guo, Y., et al.: A review of design optimization methods for electrical machines. *Energies* **10**(12), 1962 (2017). <https://doi.org/10.3390/en10121962>
8. Boldea, I.: *Electric Machines: Steady State, Transients, and Design with MATLAB*. CRC Press, Boca Raton (2009). <https://doi.org/10.1201/9781439882979>

9. Iegorov, O., Iegorova, O., Kundenko, M., Milenin, A.: Single-phase induction motors winding parameters optimization with maximum efficiency. In: 2020 IEEE Problems of Automated Electrodrive. Theory and Practice (PAEP), pp. 1–4. IEEE, Kremenchuk (2020). <https://doi.org/10.1109/PAEP49887.2020.9240878>
10. Pyrhönen, J., Jokinen, T., Hrabovcová, V.: Design of Rotating Electrical Machines. John Wiley & Sons, Chichester (2014). <https://doi.org/10.1002/9780470740095>
11. Hong, C., Huang, W., Hu, Z.: Calculation methods of equivalent circuit parameters for a dual stator solid rotor axial flux induction motor. IET Renew. Power Gener. **12**(16), 1977–1983 (2018). <https://doi.org/10.1049/iet-rpg.2018.5103>
12. Nikolaj, Z., Vladyslav, P., Stanislav, F., Jiri, L.: Dynamic simulation of the double-stator induction electromechanical converter with ferromagnetic rotor. In: 4th International Conference on Power Engineering, Energy and Electrical Drives, pp. 1448–1453. IEEE, Istanbul (2013). <https://doi.org/10.1109/PowerEng.2013.6635828>
13. Schwarz, P., Moeckel, A.: Electric machine design automation with python and ANSYS Maxwell. In: IKMT 2019 – Innovative small Drives and Micro-Motor Systems; 12. ETG/GMM-Symposium, pp. 1–7. VDE, Wuerzburg (2019)
14. Allirani, S., Vidhya, H., Aishwarya, T., et al.: Design and performance analysis of switched reluctance motor using ANSYS Maxwell. In: 2018 2nd International Conference on Trends in Electronics and Informatics (ICOEI), pp. 1427–1432. IEEE, Tirunelveli (2018). <https://doi.org/10.1109/ICOEI.2018.8553912>
15. Zablodskiy, N., Pliugin, V.: 3D magnetic field distribution in a screw double-stator induction motor. In: 2015 16th International Conference on Computational Problems of Electrical Engineering (CPEE), pp. 239–241. IEEE, Lviv (2015). <https://doi.org/10.1109/CPEE.2015.7333386>
16. Zablodskiy, M., Gritsyuk, V., Pliuhin, V., Biletskyi, I.: The surface characteristics features of the electromagnetic field of the rotor of a polyfunctional electromechanical converter. In: 2021 International Conference on Electrical, Computer, Communications and Mechatronics Engineering (ICECCME), pp. 1–5. IEEE, Mauritius (2021). <https://doi.org/10.1109/ICECCME52200.2021.9590872>
17. Giorla, D., Roccella, R., Frano, R.L., Sannazzaro, G.: EM zooming procedure in ANSYS Maxwell 3D. Fusion Eng. Des. **132**, 67–72 (2018). <https://doi.org/10.1016/j.fusengdes.2018.04.096>
18. Tikhonova, O., Malygin, I., Plastun, A.: Electromagnetic calculation for induction motors of various designs by “ANSYS Maxwell”. In: 2017 International Conference on Industrial Engineering, Applications and Manufacturing (ICIEAM), pp. 1–5. IEEE, St. Petersburg (2017). <https://doi.org/10.1109/ICIEAM.2017.8076294>
19. Salkic, H., Softic, A., Muharemovic, A., et al.: Calculation and measurement of electromagnetic fields. In: Bashir, S. (eds.) Electromagnetic Radiation, pp. 195–224. IntechOpen, London (2012). <https://doi.org/10.5772/37631>
20. Duhem, P.M.M.: The Electric Theories of J. Clerk Maxwell. BSPS, vol. 314. Springer, Cham (2015). <https://doi.org/10.1007/978-3-319-18515-6>
21. Ansys: User’s Guide – Maxwell 2D. Ansys Inc (2011)
22. Zablodskiy, M., Pliuhin, V., Chuenko, R.: Simulation of induction machines with common solid rotor. Tech. Electrodrin. **2018**(6), 42–45 (2018). <https://doi.org/10.15407/techned2018.06.042>



Inverse Multi-parameter Identification of Plane Objects Electrophysical Parameters Profiles by Eddy-Current Method

Ruslana Trembovetska^(✉) , Volodymyr Halchenko , and Constantine Bazilo 

Cherkasy State Technological University, 460 Shevchenka Boulevard, Cherkasy 18006, Ukraine
r.trembovetska@chdtu.edu.ua

Abstract. Based on the “accurate” electrodynamic model of Uzal-Cheng-Dodd-Deeds in the interpretation of Theodoulidis, a computer model in the MathCAD software package was created. It allows modeling the measurement process with a surface eddy current probe for objects with continuously changing properties of electrophysical parameters with their piecewise constant approximation. The software product is necessary for the development of a highly productive neural network metamodel which is used to implement the simultaneous inverse identification of the electrical conductivity and magnetic permeability profiles in the process of physical measurements by eddy current probe in real time. The metamodel, which is a model for a model, performs the functions of a carrier of a priori information about the test object obtained at the preliminary preparatory stage as a result of modeling using an “accurate” physical model. This allows us to collect information about the response of the signal of the probe when measuring conditions change, for example, the frequency of excitation of eddy currents in the object, the size of the lift-off between the probe and the conductor surface, varying the profiles of electrophysical parameters, etc. The implementation of the metamodel on neural networks allows us to make it highly productive in the computational sense and use their generalizing properties when constructing it. The computer model was verified by comparing the calculation results for simple measurement cases in the COMSOL Multiphysics software package, which confirmed its sufficiently high accuracy and adequacy. A number of computational experiments with its application have been carried out. They have shown the possibility of distinguishing profiles of electrophysical parameters.

Keywords: Reconstruction · A priori information · Metamodel · Surface probe

1 Introduction

To increase the service life of products in the engineering industry and improve their reliability, technological methods for improving the surface are often used, leading to a change in the structure of the product material in a shallow near-surface region. Structural modifications can also be caused by thermal, mechanical, chemical, including uncontrolled effects that occur at the stages of operation and manufacture of products. Direct

methods of fixing changes in the structure of products are not always acceptable for a number of objective reasons. At the same time, due to the existing rather complex, essentially nonlinear correlation dependence between structural changes and electrophysical parameters of the product material, namely electrical conductivity and magnetic permeability, it is possible not only to track them, but also to quantify them. In this sense, it is of great practical interest to identify the profiles of electrophysical parameters based on the results of measurements by non-destructive methods, in particular eddy current methods, from which it is possible to draw conclusions about the features of the physical processes that led to structural variations [1, 2]. For example, this allows non-destructive methods to test the quality of the technological process of thermal or mechanical hardening of the surface. To increase the reliability of the conclusions, it is very important to reconstruct the profiles of all electrophysical parameters simultaneously within the framework of a single real-time measurement with an eddy current probe.

2 Literature Review

At the moment, a number of approaches and methods are known for solving the problem. Researchers have proposed a variety of solutions to the problem, analyzing which one can note the desire to use multi-frequency measurement methods, improved designs of eddy current probes, which are distinguished by a significant complication of their designs, the use of the phenomena of invariance of definite electrophysical parameters under certain conditions during measurements, or other compensation effects.

In studies [1, 3–5] the authors propose to use the approach with multi-frequency excitation of eddy currents for measurements. This complicates the implementation of the approach due to a number of aspects. In turn, the papers [6–8] demonstrate the possibility of using eddy current probes with rather complex designs for solving the problem, containing a much larger number of constituent elements compared to classical ones. Obviously, their manufacture is associated with a number of technological difficulties. The use of the phenomenon of invariance as in works [9, 10] and compensation techniques [11], as a result, narrows down the possibilities of carrying out measurements only towards one electrophysical parameter. As a rule, the integral values of the parameters of the test objects are mainly determined. Problems of reconstruction of their profiles, i.e. dependences of parameters as a function of one of the coordinates are considered much less frequently.

In the algorithms for solving inverse problems, which include the profile identification problem under consideration, the main attention is drawn to optimization methods. To do this, the model of the direct problem is repeatedly used, the results of the solution of which are considered to be the proposed option for restoring the desired profiles. The optimization algorithm provides for the minimization of root-mean-square or other deviations of the candidate solution from measurements when varying by a set of electrophysical parameters [1, 3, 12–14]. It should be noted that this makes it almost impossible to solve the problem in real time.

All the approaches under consideration are united by one general idea of obtaining additional information about the test objects, which is carried out directly during measurements. This is a limiting factor that also makes it difficult to solve the problem in real time.

The authors proposed in [15, 16] an alternative idea, which consists in a priori accumulation of additional data about objects in previously created neural network meta-models distinguished by high computational productivity, which is especially important for inverse identification. It has been implemented in relation to cylindrical test objects, but can also be applied to plane objects. As a result, the ability to make measurements to identify profiles of electrophysical parameters in real time can be significantly improved.

Thus, as a result of the analysis of recent studies devoted to this issue, the main trends in improving methods for measuring the electrophysical parameters of the material of objects have been established, which should be considered as inverse measurement problems. Their inherent shortcomings are revealed, the elimination of which makes it possible to achieve greater efficiency in solving these problems in real time.

3 Problem Statement

The use of a priori accumulated data on the test objects involves obtaining information about the carrying out measurements as a result of a series of computational experiments using a model of the measurement process with their subsequent saving in the metamodel. As a metamodel, it is considered an approximation highly productive in a computational sense model for an “accurate” physical model of the process of measuring the profiles of electrophysical parameters, i.e., model for model [17]. In the process of information accumulation, possible options and conditions for measurements are simulated, such as, for example, a variation in the conductivity and permeability profiles, followed by recording the amplitude and phase of the output signal of the eddy current probe, changes of the excitation current frequency, simulations of the measurements with different lift-offs between the probe and the surface of the object, etc. The fact of accumulation of such information and its availability before measurements is the main distinguishing feature of this approach, which makes it very effective. The neural network implementation of the metamodel is also important, since it makes full use of the generalizing properties of artificial neural networks.

The purpose of this article is to create a computer model in the form of a software package that implements an “accurate” electrodynamic model of the measurement process using surface eddy current probe as the basis of a method for the simultaneous identification of profiles of electrophysical parameters with a priori accumulation of information necessary to build a metamodel and study the possibility of distinguishing profiles during measurements at different frequencies of excitation of eddy currents.

4 Mathematical Model Formulation

4.1 “Accurate” Electrodynamic Model

Due to high versatility among currently known mathematical models of the process of eddy current measurements with a surface probe the preference was given to the Uzal [18] – Cheng [19] – Dodd – Deeds model [20, 21] in the interpretation of Theodoulidis [22]. It uses a simplified piecewise constant representation of continuously changing electrophysical parameters inside the test object. As a result, the near-surface layer of

the object is considered conditionally multilayered, and the electrophysical parameters are assumed to be constant in each layer. In Fig. 1 shown the geometric model of a surface eddy current probe above a multilayer test object.

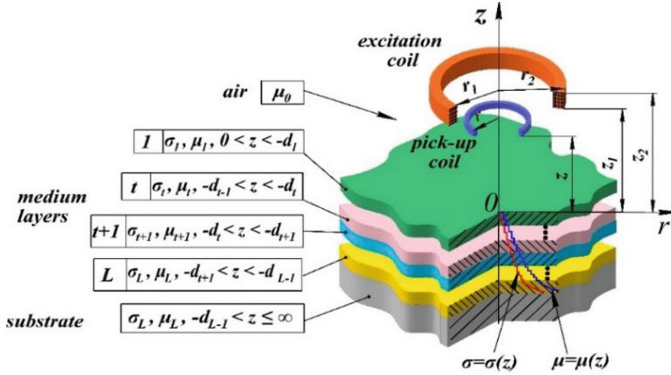


Fig. 1. Geometric model of a surface eddy current probe.

The mathematical model is constructed with following assumptions: media are considered linear, homogeneous and isotropic; excitation current I varies sinusoidally with angular frequency ω . The excitation coil has a rectangular cross section and is characterized by a current density i_0 homogeneous in cross section and a number of turns N . In all areas indicated in (see Fig. 1) the vector potential A , excited by a point source, is described by the Helmholtz partial differential equation written in a cylindrical coordinate system:

$$\frac{\partial^2 A}{\partial r^2} + \frac{1}{r} \cdot \frac{\partial A}{\partial r} - \frac{A}{r^2} + \frac{\partial^2 A}{\partial z^2} = k^2 \cdot A - \mu_0 \cdot I \cdot \delta(r - r_0) \cdot \delta(z - z_0), \quad (1)$$

where $k^2 = j \cdot \omega \cdot \mu_r \cdot \mu_0 \cdot \sigma$; $j = \sqrt{-1}$; δ is the Dirac delta function; r_0, z_0 are the location coordinates of a point source of electromagnetic field; $\mu_0 = 4 \cdot \pi \cdot 10^{-7}$ H/m is the magnetic permeability of free space.

The general solution of Eq. (1) has the following form:

$$A(r, z) = \int_0^\infty [A(\kappa) \cdot J_1(\kappa r) + B(\kappa) \cdot Y_1(\kappa r)] \cdot [C(\kappa) \cdot e^{\lambda z} + D(\kappa) \cdot e^{-\lambda z}] dk, \quad (2)$$

where $\lambda = \sqrt{\kappa^2 + k^2}$; J_1, Y_1 are first order Bessel functions of the first and second kinds.

The unknown coefficients in Eq. (2) are found from the systems of equations written for each media boundary based on the fulfillment of the boundary conditions for the vector potential of the form:

$$\left[\begin{array}{l} A_0 = A_1 \\ \frac{\partial A_0}{\partial z} = \frac{1}{\mu_{r1}} \cdot \frac{\partial A_1}{\partial z} \end{array} \right]_{z=0} \text{ and } \left[\begin{array}{l} A_{t+1} = A_t \\ \frac{1}{\mu_{r+1}} \cdot \frac{\partial A_{t+1}}{\partial z} = \frac{1}{\mu_r} \cdot \frac{\partial A_t}{\partial z} \end{array} \right]_{z=-d_t}. \quad (3)$$

The electromagnetic field in the air in the area below the excitation coil of the eddy current probe is formed by the superposition of its two components: the coil field in free space without a conductor and the field created by eddy currents induced in the test object:

$$A_0 = A^{(s)} + A^{(ec)}. \tag{4}$$

As a result, the mathematical model of the process of eddy current measurements with a surface probe has the form:

$$A_0 = \int_0^\infty J_1(\kappa r) \cdot [C_s \cdot e^{\kappa z} + D_{ec} \cdot e^{-\kappa z}] d\kappa, \tag{5}$$

$$C_s = \frac{\mu_0 \cdot \iota_0}{2} \cdot \frac{\chi(\kappa r_1, \kappa r_2)}{\kappa^3} \cdot (e^{-\kappa z_1} - e^{-\kappa z_2}),$$

$$\iota_0 = N \cdot I(r_2 - r_1)^{-1} \cdot (z_2 - z_1)^{-1},$$

$$\chi(x_1, x_2) = \int_{x_1}^{x_2} x \cdot J_1(x) dx,$$

$$\int_0^z x \cdot J_1(x) dx = -x \cdot J_0(x) + \int_0^z J_0(x) dx,$$

$$\int_0^z J_0(x) dx = 2 \cdot \sum_{k=0}^\infty J_{2k+1}(z),$$

$$D_{ec} = \frac{(\kappa \cdot \mu_{r1} - \lambda_1) \cdot V_{11}(1) + (\kappa \cdot \mu_{r1} +) \cdot V_{21}(1)}{(\kappa \cdot \mu_{r1} + \lambda_1) \cdot V_{11}(1) + (\kappa \cdot \mu_{r1} -) \cdot V_{21}(1)} \cdot C_s,$$

$$V(1) = T(1, 2) \cdot T(2, 3) \cdot \dots \cdot T(L - 2, L - 1) \cdot T(L - 1, L),$$

$$T_{11}(t, t + 1) = \frac{1}{2} \cdot e^{(-\lambda_{t+1} + \lambda_t) \cdot d_t} \left(1 + \frac{\mu_t}{\mu_{t+1}} \cdot \frac{\lambda_{t+1}}{\lambda_t} \right),$$

$$T_{12}(t, t + 1) = \frac{1}{2} \cdot e^{(\lambda_{t+1} + \lambda_t) \cdot d_t} \left(1 - \frac{\mu_t}{\mu_{t+1}} \cdot \frac{\lambda_{t+1}}{\lambda_t} \right),$$

$$T_{21}(t, t + 1) = \frac{1}{2} \cdot e^{(-\lambda_{t+1} - \lambda_t) \cdot d_t} \left(1 - \frac{\mu_t}{\mu_{t+1}} \cdot \frac{\lambda_{t+1}}{\lambda_t} \right),$$

$$T_{22}(t, t + 1) = \frac{1}{2} \cdot e^{(\lambda_{t+1} - \lambda_t) \cdot d_t} \left(1 + \frac{\mu_t}{\mu_{t+1}} \cdot \frac{\lambda_{t+1}}{\lambda_t} \right),$$

$$\lambda_t = \left(\kappa^2 + j \cdot \omega \cdot \mu_0 \cdot \mu_t \cdot \sigma_t \right)^{1/2}, \quad e = -j \cdot \omega \cdot w_u \cdot \oint_{Lc} A_0(P) dl_p,$$

where w_u is the number of turns in the pick-up coil of the probe; e is the electromotive force induced in the pick-up coil of the probe; Lc is the pick-up coil contour of the probe.

4.2 Verification of the Computer Model

Based on this mathematical model a software package was developed in MathCAD 15 package. Its verification was carried out for simple cases of representing the test object, when the number of conditional layers was small. Test calculations were performed by the finite element method implemented in the COMSOL Multiphysics software package (AC/DC Module). The geometric model required for verification is shown in (see Fig. 2). Some selective results of the postprocessor operation are illustrated in (see Fig. 3).

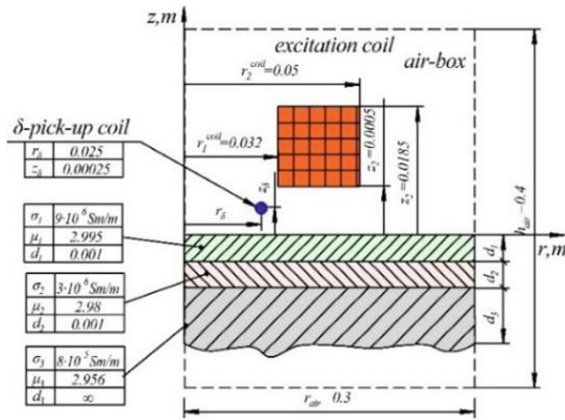


Fig. 2. Geometric model of a surface eddy current probe for test calculations in COMSOL Multiphysics.

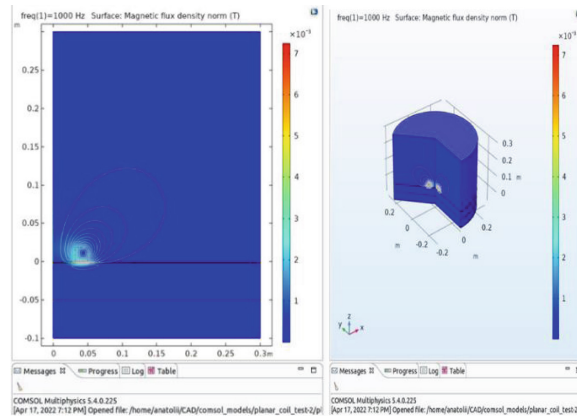


Fig. 3. Some results of calculations in COMSOL Multiphysics.

Comparative results of model calculations are given in Table 1, which contains the calculation data of the component of magnetic induction B_z for a single-layer test object at two control points at a height of $z = 10^{-4}$ m above its surface. The maximum relative error of calculations in amplitude is no more than 2%, and in phase is no more than 1%.

The calculations were carried out with the following initial data: $r_1 = 30 \cdot 10^{-3}$ m; $r_2 = 50 \cdot 10^{-3}$ m; $z_1 = 1 \cdot 10^{-3}$ m; $z_2 = 21 \cdot 10^{-3}$ m; $d_1 = 5 \cdot 10^{-3}$ m; $f = 2 \cdot 10^3$ Hz; $N = 100$; $I = 1$ A; $\mu = 1$; $\sigma = 3.774 \cdot 10^7$ S/m.

Table 1. Verification results for a single-layer test object.

No	Watch point coordinates r , m	Magnetic flux density ($B \times 10^{-5}$), z component (T)		Relative error δ , % amplitude/phase
		Model MathCAD	Model COMSOL	
1	0.04	6.171483–4.718106i	6.239858–4.702572i	0.58/1.06
2	0.055	-9.361975 + 7.764341i	-9.636187 + 7.730765i	1.55/0.66

In Table 2 shown the results of calculating the values of the vector potential at some observation points at a height of $z = 0.25 \cdot 10^{-3}$ m for the case of measuring the parameters of a three-layer test object. Computational experiments were carried out with the following initial data: $r_1 = 32 \cdot 10^{-3}$ m; $r_2 = 50 \cdot 10^{-3}$ m; $z_1 = 5 \cdot 10^{-4}$ m; $z_2 = 18.5 \cdot 10^{-3}$ m; $d_1 = 1 \cdot 10^{-3}$ m; $d_2 = 2 \cdot 10^{-3}$ m; $d_3 = 3 \cdot 10^{-3}$ m; $f = 1 \cdot 10^3$ Hz; $N = 100$; $I = 1$ A; $\mu_1 = 2.995$; $\mu_2 = 2.98$; $\mu_3 = 2.956$; $\sigma_1 = 9 \cdot 10^6$ S/m; $\sigma_2 = 3 \cdot 10^6$ S/m; $\sigma_3 = 8 \cdot 10^5$ S/m. In Fig. 4 illustrates an example of calculating the vector potential at observation point No. 10 using COMSOL Multiphysics.

Table 2. Verification results for a three-layer test object.

No	Watch point coordinates r , m	Magnetic vector potential ($A \times 10^{-6}$), ϕ component (Wb/m)		Relative error δ , % amplitude/phase
		Model MathCAD	Model COMSOL	
1	0	5.75E–5–8.3E–6i	5.752E–5–8.307E–6i	0.045/0.051
2	0.003	0.3658229–0.852211i	0.3597293–0.8519324i	0.286/0.507
3	0.006	0.7469848–0.1725237i	0.7495717–1.725225i	0.054/0.109
4	0.009	1.202462–2.640916i	1.202280–2.640843i	0.0048/0.004
5	0.012	1.754389–3.618694i	1.755918–3.618609i	0.015/0.031
6	0.015	2.45876–4.676426i	2.457401–4.676552i	0.0098/0.022
7	0.018	3.363676–5.827209i	3.364803–5.827082i	0.0067/0.015
8	0.021	4.551144–7.076252i	4.550309–7.076259i	0.142/0.08
9	0.024	6.102589–8.414455i	6.102879–8.414458i	0.0016/0.0023
10	0.025	6.724–8.876i	6.719582–8.875551i	0.027/0.032
11	0.027	8.125535–9.808598i	8.126259–9.808655i	0.0039/0.0046
12	0.003	10.76489–11.18601i	10.72730–11.18507i	0.172/0.212

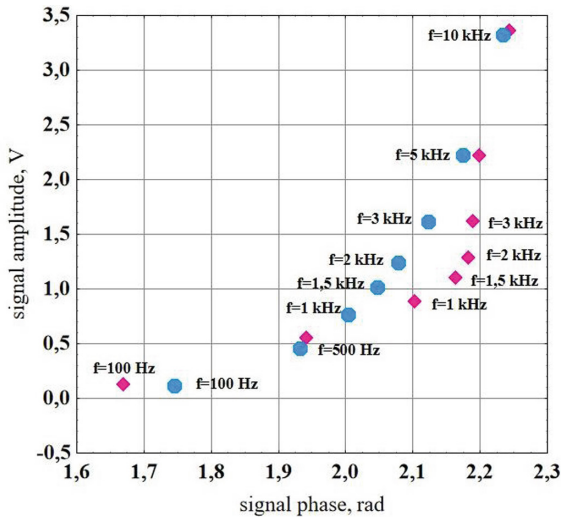


Fig. 5. Simulation results of the measurement process for objects with different profiles of electrophysical parameters.

6 Conclusion

Summarizing, we can note that the studies carried out using the developed software package have shown that there are frequency ranges of excitation of eddy currents, which are more favorable for distinguishing profiles of electrophysical parameters. Of course, these studies require more attention, since they should be carried out separately for magnetic and non-magnetic materials. At the same time, it should be noted that the obtained results do not contradict the known facts, indicating significant difficulties in simultaneously distinguishing between the conductivity and permeability profiles at low frequencies. The created “accurate” electrodynamic model allows, based on the developed effective plan of computer experiments [17], to build a highly productive neural network metamodel, which is a carrier of a priori information about the test object, with its subsequent application at the stage of inverse identification of profiles of electrophysical parameters based on the results of physical measurements by an eddy current probe in real time.

References



1. Sabbagh, H.A., Murphy, R.K., Sabbagh, E.H., et al.: Computational Electromagnetics and Model-Based Inversion. SCIENTCOMP. Springer, New York (2013). <https://doi.org/10.1007/978-1-4419-8429-6>
2. Liu, G.R., Han, X.: Computational Inverse Techniques in Nondestructive Evaluation. CRC Press, Boca Raton (2003). <https://doi.org/10.1201/9780203494486>
3. Yu, Y., Zhang, D., Lai, C., Tian, G.: Quantitative approach for thickness and conductivity measurement of monolayer coating by dual-frequency eddy current technique. IEEE Trans. Instrum. Meas. **66**(7), 1874–1882 (2017). <https://doi.org/10.1109/TIM.2017.2669843>

4. Lee, K., Hao, B., Li, M., Bai, K.: Multiparameter eddy-current sensor design for conductivity estimation and simultaneous distance and thickness measurements. *IEEE Trans. Industr. Inf.* **15**(3), 1647–1657 (2019). <https://doi.org/10.1109/TII.2018.2843319>
5. Pasadas, D.J., Ramos, H.G., Baskaran, P., Ribeiro, A.L.: ECT in composite materials using double excitation coils and resonant excitation/sensing circuits. *Measurement* **161**, 107859 (2020). <https://doi.org/10.1016/j.measurement.2020.107859>
6. Avila, J.R.S., How, K.Y., Lu, M., Yin, W.: A novel dual modality sensor with sensitivities to permittivity, conductivity, and permeability. *IEEE Sens. J.* **18**(1), 356–362 (2017). <https://doi.org/10.1109/JSEN.2017.2767380>
7. Lu, M., Meng, X., Chen, L., et al.: Measurement of ferromagnetic slabs permeability based on a novel planar triple-coil sensor. *IEEE Sens. J.* **20**(6), 2904–2910 (2020). <https://doi.org/10.1109/JSEN.2019.2957212>
8. Lahrech, A.C., Abdelhadi, B., Feliachi, M., et al.: Electrical conductivity identification of a carbon fiber composite material plate using a rotating magnetic field and multi-coil eddy current sensor. *Eur. Phys. J. Appl. Phys.* **83**(2), 20901 (2018). <https://doi.org/10.1051/epjap/2018170411>
9. Yu, Y., Zou, Y., Hosani, M.A., Tian, G.: Conductivity invariance phenomenon of eddy current NDT: Investigation, verification, and application. *IEEE Trans. Magn.* **53**(1), 1–7 (2017). <https://doi.org/10.1109/TMAG.2016.2616328>
10. Wang, C., Fan, M., Cao, B., et al.: Novel noncontact eddy current measurement of electrical conductivity. *IEEE Sens. J.* **18**(22), 9352–9359 (2018). <https://doi.org/10.1109/JSEN.2018.2870676>
11. Lu, M., Huang, R., Yin, W., et al.: Measurement of permeability for ferrous metallic plates using a novel lift-off compensation technique on phase signature. *IEEE Sens. J.* **9**(17), 7440–7446 (2019). <https://doi.org/10.1109/JSEN.2019.2916431>
12. Burkhardt, J.: Determination of the conductivity and thickness of conductive layers on conductive base materials. *Adv. Mech. Eng.* **11**(7), 1–9 (2019). <https://doi.org/10.1177/1687814019854234>
13. Chen, X., Lei, Y.: Electrical conductivity measurement of ferromagnetic metallic materials using pulsed eddy current method. *NDT and E Int.* **75**, 33–38 (2015). <https://doi.org/10.1016/j.ndteint.2015.06.005>
14. Lu, M.: Forward and inverse analysis for non-destructive testing based on electromagnetic computation methods. Dissertation, University of Manchester (2018)
15. Halchenko, V.Y., Tychkov, V.V., Storck, A.V., Trembovetska R.V.: Reconstruction of surface radial profiles of the electrophysical characteristics of cylindrical objects during eddy current measurements with a priori data. The selection formation for the surrogate model construction. *Ukrain. Metrol. J.* **1**, 35–50 (2020). <https://doi.org/10.24027/2306-7039.1.2020.204226> [in Ukrainian]
16. Halchenko V.Y., Storck A.V., Trembovetska R.V., Tychkov V.V.: The creation of a surrogate model for restoring surface profiles of the electrophysical characteristics of cylindrical objects. *Ukrain. Metrol. J.* **3**, 27–35 (2020). <https://doi.org/10.24027/2306-7039.3.2020.216824> [in Ukrainian]
17. Halchenko V.Y., Trembovetska R.V., Tychkov V.V.: Surrogate synthesis of frame eddy current probes with uniform sensitivity in the testing zone. *Metrol. Measure. Syst.* **28**(3), 551–564 (2021). <https://doi.org/10.24425/mms.2021.137128>
18. Uzal, E.: Theory of eddy current inspection of layered metals. Dissertation, Iowa State University (1992)
19. Zhang, J., Yuan, M., Xu, Z., Kim, H.-J., Song, S.-J.: Analytical approaches to eddy current nondestructive evaluation for stratified conductive structures. *J. Mech. Sci. Technol.* **29**(10), 4159–4165 (2015). <https://doi.org/10.1007/s12206-015-0910-7>

20. Bowler, N.: Eddy-Current Nondestructive Evaluation. SSMST. Springer, New York (2019). <https://doi.org/10.1007/978-1-4939-9629-2>
21. Lei, Y.Z.: General series expression of eddy-current impedance for coil placed above multi-layer plate conductor. *Chin. Phys. B* **27**(6), 060308 (2018). <https://doi.org/10.1088/1674-1056/27/6/060308>
22. Theodoulidis, T.P., Kriezis, E.E.: Eddy Current Canonical Problems (With Applications to Nondestructive Evaluation). Tech Science Press, Forsyth (2006)



The Urgency of Using Adaptive Observers to Identify the Parameters of the DC Electric Drive

Vasyl Stopkin¹ (✉) , Anatoliy Nikolenko¹ , Vitaliy Kuznetsov¹ , Mykola Tryputen² , and Oleksandr Kuzenkov³ 

¹ Ukrainian State University of Science and Technologies, 2 Lazaryan Street, Dnipro 49010, Ukraine

vasilstopkin@gmail.com, kaf.et@metal.nmetau.edu.ua

² Dnipro University of Technology, 19 Dmytra Yavornytskoho Avenue, Dnipro 49000, Ukraine

³ Oles Honchar Dnipro National University, 72 Gagarina Avenue, Dnipro 49000, Ukraine

Abstract. The aim of this paper is to analyze the use of surveillance devices in modern digital electric drives with the prospect of modernization of existing DC drives used in the metallurgical industry of the Dnieper region of Ukraine and develop a mathematical model of electric drive with adaptive observer identification of basic coordinates. The urgency of the work is justified, given the large number of outdated control systems for DC electric drives at metallurgical enterprises in the Dnieper region. There are even drives with a generator-DC motor system in the presence of thyristor converters in the excitation windings of motors and generators, such as a generator system – a blooming DC motor 1050 in a rolling shop №1 PJSC “Dnieper Metallurgical Plant”, a generator system – DC motor rolling shop of PJSC “Dnieper Metallurgical Plant”. There are also more modern – for example, digital system thyristor converter – DC motor of the electric drive of a calibration condition in the conditions of rolling shop №7 INTERPIPE NIKO TUBE, Nikopol. The power of the main drives is from 80 kW to 8 MW. Also, the aim of the work is to create a general classical mathematical model of the DC electric drive with observers to identify such parameters as the moment of inertia, the resistance of the armature circuit. The obtained results give an idea of the interdependence of the main parameters of the electric drive, which characterize and influence the dynamic properties of observers – the roots of the characteristic equation, structural coefficients, the frequency of undamped oscillations. The practical value includes recommendations for adjusting the control circuits for regenerative monitoring devices, the coordinates of the electric drive, which are obtained as a result of research on a mathematical model. The recommendations can be used as input, for example in the configuration of control systems, control circuits for digital complete DC electric drives in environments such as the TIA Portal Siemens before the first start-up of electric drives in the plant.

Keywords: DC motor · Thyristor converter · Adaptive observer · Programmable controller · Control circuit · Parameter identification

1 Introduction

At present, the metallurgical enterprises of the Dnieper region have a lot of control systems for DC electric drives, mainly they are used in rolling shops. They are found as obsolete – based on generator-motor systems and relatively new systems thyristor converter – DC motor. Based on this, the urgency of modernization of such electric drives is quite reasonable, given that their structure includes linear regulators, the parameters of which are set during commissioning are not optimal and this reduces the energy efficiency of the unit. For example, in the conditions of PJSC INTERPIPE “NTRP”, the main electric drive of long-term calibration state uses a DC motor with a capacity of 480 kW with a generator-DC motor system, and the main drive of the piercing state has a DC motor with a capacity of 3150 kW – with a converter system direct current. In the conditions of INTERPIPE NIKO TUBE drives of a direct current of a piercing state (3680 kW), the automatic machine of a state (2300 kW), a rolling state (630 kW), a continuous state (1900 kW), a reducing state (1400 kW), a calibrating state (600 kW) are used.

Replacement of analog control systems for such electric drives and obsolete discrete ones with new modern optimal control systems is a promising area of modernization. Such control systems include observers as debugging models for the facility. A necessary condition here, of course, is the presence of an adequate mathematical model of the mechanical part of the electric drive.

In adjustable DC electric drives, the characteristics of motors are determined by electromagnetic parameters (active and inductive windings, time constants, magnetic flux), which may differ from the catalog data due to the instability of the technological process. The actual values of the electromagnetic parameters of DC motors allow us to draw conclusions about their technical condition and, if necessary, adjust the process. In addition, during operation, the current values of the parameters also depend on the load modes and thermal state of DC motors, so it is desirable to monitor the parameters in real time using current information to control, diagnose and protect the electric drive [1–3].

Due to the technical complexity or impossibility of direct measurement of traffic police parameters directly in the process of its operation, it is advisable to use a monitoring device, the operation of which is as follows: measured input and output signals of DC motor, and then, using identification methods, evaluate its parameters [4].

Models of adaptive control systems with observing devices for identifying the moment of inertia, resistance of the motor armature circuit and when combined in the observer system of full order [1] and its adaptation to changes in the resistance of the motor armature circuit are considered. Such a system can be used in the case of a previously unknown change in the resistance of the armature circuit due to the unstable ambient temperature, which leads to a change in the temperature of the armature winding, and hence to a change in resistance.

2 Literature Review

The use of state observers for a two-mass DC electric drive with the possibility of studying the change in the ratio of the moments of inertia of the two masses of the electric drive to reduce speed fluctuations and inconsistencies in the speeds of these masses are considered in [5]. Here is a mathematical model of a full-order observer who uses the measured armature current and supply voltage to change the speed task instead of measuring it directly. Also, the use of an adaptive observer to estimate the speed of the DC drive without a speed sensor is considered in [6].

The issues of robust design of an observer for a DC electric drive with internal load control by a new method based on previously unknown input parameters to assess unmeasured perturbations are considered in [7]. Problems of speed sensor failure and control without it using a state monitor are considered in [8]. The proposed solution allows to provide (restore) engine speed and identification of armature resistance, which is important when operating the engine in variable temperature modes. The stability of the observer is provided by the Lyapunov criterion [9, 10]. In [11], instead of using traditional linear regulators, a fuzzy logic controller in the sensorless control system of a DC motor of independent excitation was proposed, which allowed to improve such technical criteria as overregulation and time of setting the motor speed characteristic.

The issue of designing state monitors to control the DC electric drive without the use of a current sensor is considered in [12]. The proposed observers evaluate the perturbations by reference acceleration, voltage and response to acceleration using the engine model. Back in the 90's there were attempts to design DC drives with control from fuzzy logic systems [13]. The proposed fuzzy control DC system has a speed controller with a load monitor, which is needed to eliminate the steady speed error.

In [14], a method of detecting a fault in order to detect a failure of the belt in the DC drive with the transfer of inertial load through the belt. This method uses a proportional observer of reduced order, developed using the methods of differential algebra. In [15, 16] the control strategy based on linearization of feedback with its use for electric drives of direct current with the matrix observer of identification of electric and mechanical dynamics of the drive is presented. An attempt to use nonlinear adaptive controllers at an unknown load moment in a DC drive to control motor speed is considered in [17]. The unknown parameter is the moment estimated through the law of adaptation, and the stability of the whole system is ensured on the basis of the Lyapunov control function. Another attempt to use fuzzy logic in the control system of the DC drive is given in [18]. It uses a combined adaptive DC system with a step-down power converter controlled by high-frequency pulse-width modulated signals received from the proportional-integral-differential controller.

It is important to consider the modes of operation of the converter in DC control systems. In [19], an adaptive current regulator of a DC motor with independent excitation with a thyristor converter using z-transform was designed. The dynamic characteristics of the adaptive controller are constant for the operation of the converter in the modes of continuous and intermittent currents. This controller can be used for a four-quadrant DC drive with the requirements of accurate and optimal speed control.

Existing control systems for DC electric drive are usually built on the principles of subordinate coordinate control, and the use of observing devices or modified regulators in the control circuits depends on each situation. In [20, 21] the authors considered the position control system of the DC electric drive and proved that the use of proportional-integral-differential algorithm and linear quadratic controller with approach to the state space is sufficient to minimize control errors and inconsistencies.

Paper [22] presents the results of modeling of controlled DC machines powered by thyristor converters in intermittent mode without the use of feedback signals on current and speed. The proposed observer calculates the average value of the intermittent current depending on the generated thyristor opening angle and the change in the current flow angle. Issues of identification of perturbing influences from the mechanical part of the electric drive using an observer are considered in [23, 24]. In [25], a comparative evaluation of the problems of integrating the equations of state observers with the study of sampling methods for the accuracy of integration. Here we compare the methods of Euler, Tustin and vice versa rectangular method in terms of accuracy of integration with the provision of recommendations for their use.

Problems of modeling observers with the use of additional feedback are also considered in [26, 27]. The use of observers is appropriate where the installation of sensors of the coordinates of the electric drive is complicated by the operating conditions of the electric drive, such as the operation of mechanisms in conditions of vibration, significant shock loads, temperatures [28–30]. The general tasks of work concern: maintenance of change of parameters of regulators, at invariable dynamic properties of system; automatic search of optimal operating conditions of the system according to a certain criterion in the absence of initial information about the parameters of the electric drive and external perturbations [31]. The main task of this work is to develop a mathematical model of the DC electric drive that would restore the basic coordinates of the electric drive through the use of appropriate observers. The idea of supplementing the mathematical model [5] with observers to identify the resistance of the armature circle and the moment of inertia will expand the possibilities of applying previously obtained results.

3 Research Methodology

If an unknown change in the moment of inertia occurs in the DC power line system, information from the monitoring device of the moment of inertia identification is used in the control system to stabilize the dynamic characteristics of the drive. We consider the motor current as the influence of control, and the motor speed as the output coordinate. The unknown linear part of the object is characterized by a transfer function:

$$W(p) = \frac{KF}{J1 \cdot p} = \frac{b}{p}. \quad (1)$$

The parameter b belongs to the identification. The block diagram of the observer is indicated by the OS1 block (see Fig. 2).

The algorithm of the observer's identification of the moment of inertia is described by the equation:

$$\begin{cases} \frac{d\hat{\omega}}{dt} = \left(\frac{KF}{J}\right) \cdot I_a + \lambda \cdot K_{s1} \cdot (\omega - \hat{\omega}); \\ \frac{d\frac{KF}{J}}{dt} = \beta \cdot K_{s1} \cdot I_a \cdot (\omega - \hat{\omega}). \end{cases} \quad (2)$$

The \hat{b} score is used to set up the proportional speed controller RS2 (see Fig. 2). The standard adjustment of the current control circuit RC2 (see Fig. 2) according to the modular optimum is performed. With an unknown law of change of the moment of inertia of the electric drive, the adaptive system will have constant dynamic characteristics due to the adjustment of the gear ratio of the speed controller.

An example of calculations in the form of a m-file Matlab electric drive with an adaptive monitoring device to identify the moment of inertia is shown in Fig. 1.

```

1  % Calculation of an electric drive with an adaptive system for
2  % identifying the moment of inertia
3  - nn=750; % rated speed, rpm
4  - Un=950; % rated supply voltage, V
5  - In=436; % rated current, A
6  - Ra=0.0192; % active resistance of the armature circuit, Ohm
7  - J1=5.85; % moment of inertia, kgm^2
8  - p=4; % number of pole pairs
9  - Lamb=2; % motor overload capacity
10 - wn=pi*nn/30; % nominal angular velocity, rad/s
11 - KF=(Un-In*Ra)/wn; % engine design factor
12 - Kk=0.5; % coefficient for compensated machines
13 - La=30*Kk*Un/(pi*p*In*nn); % armature circuit inductance, H
14 - Ta=La/Ra; % electromagnetic time constant, s
15 - Ub=1; % base unit, V
16 - Uzs=10; % task for speed, V
17 - t1=1; % braking start time, s
18 - J2=5; % real moment of inertia of the drive, kgm^2
19 - Ttp=0.005; % uncompensated converter time constant, s
20 - Ktp=Un/Ub; % converter gain
21 - Kc=Ub/(In*Lamb); % current feedback factor
22 - Ks1=Ub/wn; % motor speed feedback factor
23 - Krcp=Ra*Ta/(2*Ttp*Ktp*Kc); % current controller proportional gain
24 - Krci=Ra/(2*Ttp*Ktp*Kc); % gain of the integral part of the current regulator
25 - Krsad=Kc/(4*Ks1*Ttp); % speed controller gain for adaptive system
26 - Krcj1=Kc/J1/(4*Ks1*KF*Ttp); % speed controller gain at j1

```

Fig. 1. Example of calculations in the form of the m-file of the Matlab of the electric drive with the adaptive monitoring device of identification of the moment of inertia

As an example, a DC motor with a capacity of 85 kW, rated current 436 A, supply voltage 220 V, speed 750 rpm. The speed control limit is set at 10 V. Values of unknown observer parameters: $\lambda = 1000$, $\beta = 1$. Braking start time $t_1 = 1$ s. Transition calculation time – 2 s. Step of calculating differential equations – 0.0005 s. Calculation method – Runge-Kutta 4th order.

Mathematical S-model of adaptive to the moment of inertia control system and the classical system of subordinate control of engine speed are shown in Fig. 2.

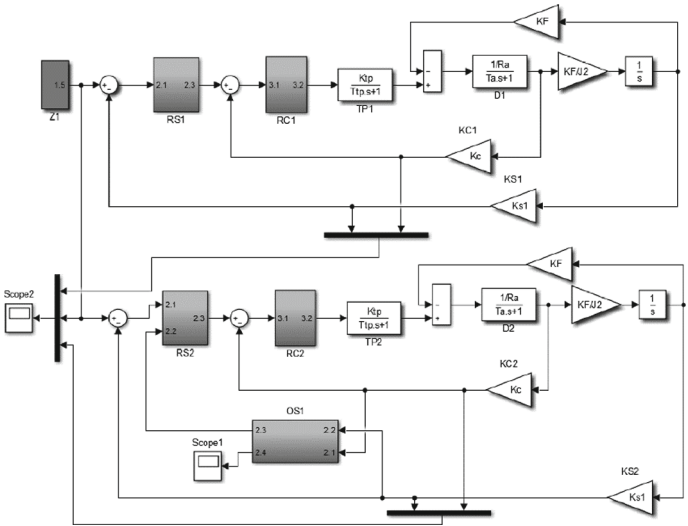


Fig. 2. Mathematical S-model of the control system of adaptive to change of the moment of inertia and classical system of the subordinate control of speed of the DC motor.

Graphs of transients on the speed and current of the adaptive to the moment of inertia of the system are shown in Fig. 3. In Fig. 3 marked: 1 – speed task; 2, 3 – speed when using and without the adaptive OS1 observer; 4, 5 – motor current when using the OS1 adaptive monitor and without it. In Fig. 4 shown the S-model of the speed controller RS2 (see Fig. 2).

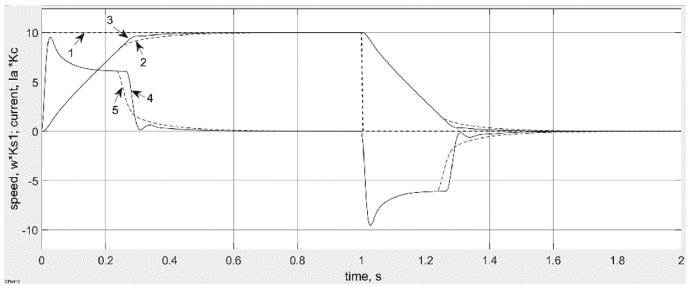


Fig. 3. Graphs of transients in speed and current adaptive to changes in the moment of inertia of the system.

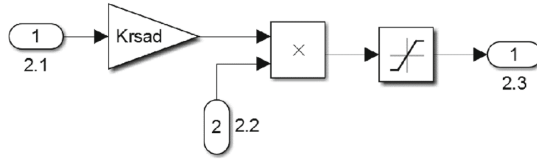


Fig. 4. S-model of the RS2 speed controller

In Fig. 5 shown the S-model of the observer OS1 (see Fig. 2). It is possible to estimate the moment of inertia $J2$ on the signal $KF/J2$.

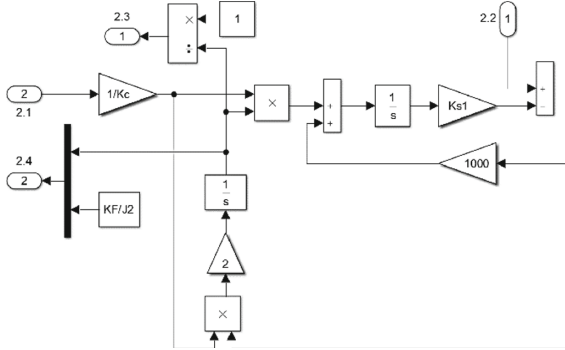


Fig. 5. OS1 observer S-model.

The S-model of the system adaptive to the resistance of the armature circuit of the motor is shown in Fig. 6. The initial data for the S-model are calculations in the form of an m-file (see Fig. 1).

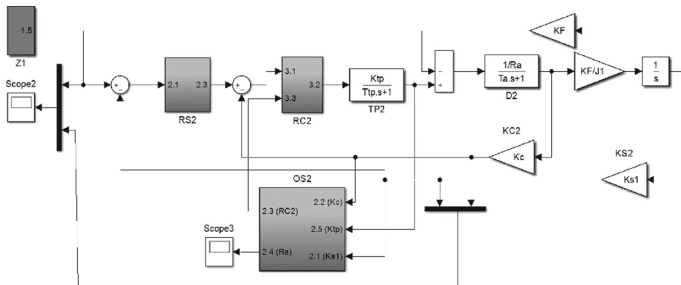


Fig. 6. S-model adaptive to the change in resistance of the armature circuit of the motor system.

In Fig. 7 shown the S-model of the current regulator PC2 (see Fig. 6).

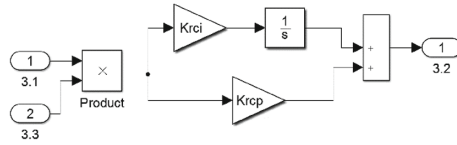


Fig. 7. S-model of current regulator PC2.

The S-model of the electric speed control system adaptive to changes in the moment of inertia and resistance of the motor armature circuit is shown in Fig. 8. Graphs of transients in the electric drive with adaptive to the change of moment of inertia and resistance of the armature circuit control system are shown in Fig. 9.

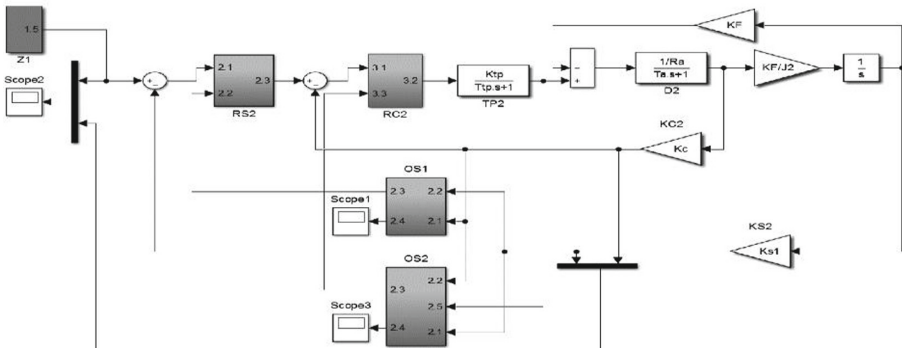


Fig. 8. S-model of the electric speed control system adaptive to changes in the moment of inertia and resistance of the armature circuit of the motor.

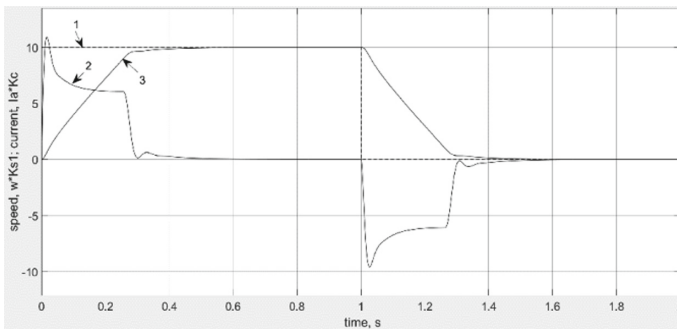


Fig. 9. Graphs of transients in the electric drive with adaptive to the moment of inertia and resistance of the armature circuit: 1 – speed task; 2 – motor current; 3 – speed.

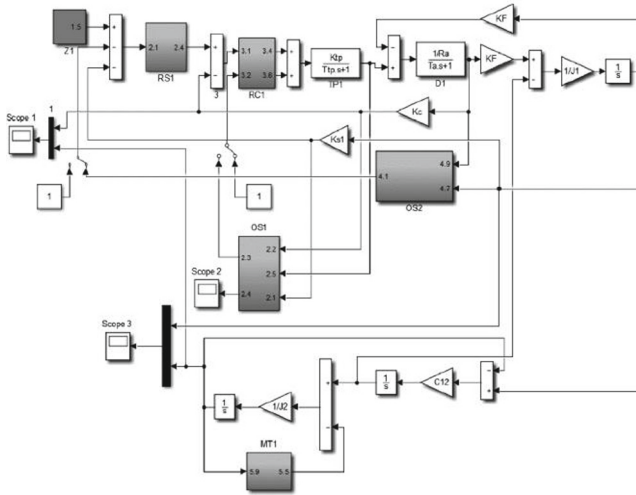


Fig. 10. S-model of the system of adaptive to change of resistance of a circle of an armature of the motor of the electric drive with the observer of full order.

The S-model of the system of adaptive to change the resistance of the armature circuit of the electric motor with a full-order observer is shown in Fig. 10. Graphs of transients in speed and current adaptive to the change in resistance of the armature circuit of the engine speed control system with a state observer when operating under rated load are shown in Fig. 11.

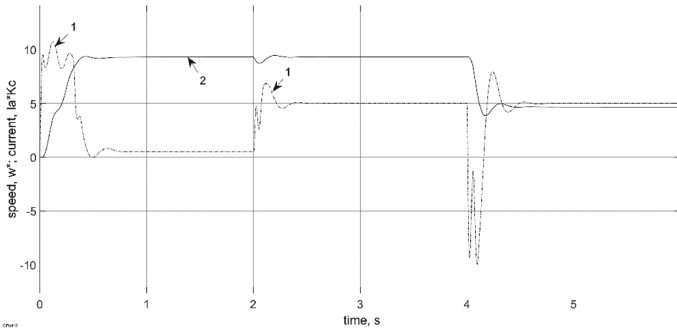


Fig. 11. Graphs of transients on speed and current adaptive to change the resistance of the armature circuit of the DC motor of the speed control system with a condition monitor when operating under rated load.

The load occurs at a time of 2 s. There is no static speed error even if there is a proportional speed control. This is explained by the fact that the system uses two adaptive observing devices that quickly restore the corresponding coordinates of the electric drive. There is a slight fluctuation in current.

4 Results

The developed mathematical model of the electric drive (see Fig. 2) gives the chance at the unknown law of change of the moment of inertia of the electric drive to have constant dynamic characteristics due to change of a transfer factor of the regulator of speed RS2. This is relevant for gearless tracking electric drives, where parametric perturbations of the system may occur due to the variable nature of the motor excitation flow. And the identification of the KF parameter makes it possible to make adjustments to the system. The model of the electric drive (see Fig. 5) gives the chance at the unknown law of change of resistance of an armature of the motor to have constant dynamic characteristics due to change of a transfer factor of a regulator of current RC2.

The developed S-model [5] included a complete OS2 observer. It has been improved (see Fig. 10) by supplementing the adaptive observer to identify the resistance of the OS1 armature circuit. It is now possible to stabilize the dynamic characteristics of the electric drive with an unknown change in the resistance of the armature circuit due to the unstable ambient temperature.

These conclusions were confirmed by the results of research on mathematical models. The moment of inertia of the drive changed – the acceleration time to the nominal speed t_p and the maximum current of the Scope 2 motor, the maximum value of the Scope 1 moment of inertia estimation were compared (see Fig. 8). The resistance of the armature circuit of the motor changed – t_p and the time of the first achievement of the set resistance of the armature circuit Scope 3 were compared (see Fig. 8).

5 Conclusion

A promising area of further research is the development of a mathematical model of the mechanical part of the electric drive according to the technological task of the customer and the use of the already developed mathematical model of the observing electric drive with a specific model of the mechanical part of the drive.

References






1. Tryputen, M., Kuznetsov, V., Serdiuk, T., et al.: One approach to quasi-optimal control of direct current motor. In: 2019 IEEE 5th International Conference Actual Problems of Unmanned Aerial Vehicles Developments (APUAVD), pp. 190–193. IEEE, Kyiv (2019). <https://doi.org/10.1109/APUAVD47061.2019.8943878>
2. Tryputen, N., Kuznetsov, V., Kuznetsova, Y.: About the possibility of researching the optimal automatic control system on a physical model of a thermal object. In: 2019 IEEE 2nd Ukraine Conference on Electrical and Computer Engineering (UKRCON), pp. 1244–1248. IEEE, Lviv (2019). <https://doi.org/10.1109/UKRCON.2019.8879830>
3. Kuzenkov, O., Serdiuk, T., Kuznetsova, A., et al.: Mathematical model of dynamics of homomorphic objects. CEUR Workshop Proc. **2516**, 190–205 (2019)
4. Tryputen, M., Kuznetsov, V., Kuznetsov, V., et al.: Laboratory bench to analyze of automatic control system with a fuzzy controller. Diagnostyka **21**(2), 61–68 (2020). <https://doi.org/10.29354/diag/122357>

5. Stopkin, V., Kuznetsov, V., Kuznetsov, V., et al.: Model of two-mass electric drive of DC electric locomotive with the full order observer. In: 2021 International Conference on Electrical, Communication, and Computer Engineering (ICECCE), pp. 1–6. IEEE, Kuala Lumpur (2021). <https://doi.org/10.1109/ICECCE52056.2021.9514247>
6. Yachiangkam, S., Prapanavarat, C., Yungyuen, U., Po-ngam, S.: Speed-sensorless separately excited DC motor drive with an adaptive observer. In: 2004 IEEE Region 10 Conference TENCN 2004, vol. 500, pp. 163–166. IEEE, Chiang Mai (2004). <https://doi.org/10.1109/TENCN.2004.1414894>
7. Vu, V.P., Do, T.D.: Disturbance observer synthesis for linear systems: Application for DC motor. In 2019 International Conference on System Science and Engineering (ICSSE), pp. 433–436. IEEE, Dong Hoi (2019). <https://doi.org/10.1109/ICSSE.2019.8823127>
8. Hamed, S.B., Hamed, M.B.: Lyapunov function based simultaneous state and parameter estimation in excited DC motor drive. In: 2014 International Conference on Electrical Sciences and Technologies in Maghreb (CISTEM), pp. 1–8. IEEE, Tunis (2014). <https://doi.org/10.1109/CISTEM.2014.7077010>
9. Aftab, M.S., Shafiq, M., Yousef, H.: Lyapunov stability criterion based neural inverse tracking for unknown dynamic plants. In: 2015 IEEE international conference on industrial technology (ICIT), pp. 321–325. IEEE, Seville (2015). <https://doi.org/10.1109/ICIT.2015.7125118>
10. Levin, A.: Decomposition-based Lyapunov stability criterion for multi-component nonlinear systems with common links. In: [1992] Proceedings of the 35th Midwest Symposium on Circuits and Systems, pp. 87–90. IEEE, Washington (1992). <https://doi.org/10.1109/MWSCAS.1992.271327>
11. Thanh, S.N., The, C.N., Xuan, H.H.: Improved performance of a sensorless DC motor control using fuzzy logic. In: 2014 5th International Conference on Intelligent and Advanced Systems (ICIAS), pp. 1–6. IEEE, Kuala Lumpur (2014). <https://doi.org/10.1109/ICIAS.2014.6869506>
12. Kambara, Y., Ohnishi, K.: A design method of observers for bilateral control using DC brushed motor. In: IECON 2015 – 41st Annual Conference of the IEEE Industrial Electronics Society, pp. 000938–000943. IEEE, Yokohama (2015). <https://doi.org/10.1109/IECON.2015.7392220>
13. Feng, X., Chen, B.: Fuzzy-controlled DC drive system with load observer. In: Proceedings of 4th IEEE International Workshop on Advanced Motion Control-AMC'96-MIE, vol. 1, pp. 354–358. IEEE, Mie (1996). <https://doi.org/10.1109/AMC.1996.509432>
14. Martínez-Guerra, R., Garrido, R., Palacios, R., Mendoza-Camargo, J.: Fault detection in a belt-drive system using a proportional reduced order observer. In: Proceedings of the 2004 American Control Conference, vol. 4, pp. 3106–3110. IEEE, Boston (2004). <https://doi.org/10.23919/ACC.2004.1384386>
15. Voliansky, R., Sadovoi, A.: Chua's circuits interval synchronization. In: 2017 4th International Scientific-Practical Conference Problems of Infocommunications. Science and Technology (PIC S&T), pp. 439–443. IEEE, Kharkiv (2017). <https://doi.org/10.1109/INFOCOMMST.2017.8246434>
16. Hozefa, J., Ankit, M., Shadab, S., Bhil, S.K.: Feedback linearization technique for DC series motor with LMI based observer and DREM. In: 2020 International Conference on Smart Grids and Energy Systems (SGES), pp. 407–412. IEEE, Perth (2020). <https://doi.org/10.1109/SGES51519.2020.00078>
17. Roy, T.K., Pervej, M.F., Tumpa, F.K., Paul, L.C.: Nonlinear adaptive controller design for velocity control of a DC motor driven by a DC–DC buck converter using backstepping approach. In: 2016 2nd International Conference on Electrical, Computer & Telecommunication Engineering (ICECTE), pp. 1–4. IEEE, Rajshahi (2016). <https://doi.org/10.1109/ICECTE.2016.7879598>

18. Abhinav, R., Sheel, S.: An adaptive, robust control of DC motor using fuzzy-PID controller. In: 2012 IEEE International Conference on Power Electronics, Drives and Energy Systems (PEDES), pp. 1–5. IEEE, Bengaluru (2012). <https://doi.org/10.1109/PEDES.2012.6484325>
19. Lazim, M.T., BeniYounis, M., Alkhashashna, H.: Analysis and design of adaptive current controller for DC drive using Z-transform. In: 2018 15th International Multi-Conference on Systems, Signals & Devices (SSD), pp. 1305–1310. IEEE, Yasmine Hammamet (2018). <https://doi.org/10.1109/SSD.2018.8570422>
20. Chotai, J., Narwekar, K.: Modelling and position control of brushed DC motor. In: 2017 International Conference on Advances in Computing, Communication and Control (ICAC3), pp. 1–5. IEEE, Mumbai (2017). <https://doi.org/10.1109/ICAC3.2017.8318792>
21. Voliansky, R., Kluev, O., Sadovoi, O., et al.: Anti-swing control system for the one class of underactuated dynamic objects. In: 2020 IEEE Problems of Automated Electrodrive Theory and Practice (PAEP), pp. 1–4. IEEE, Kremenchuk (2020). <https://doi.org/10.1109/PAEP49887.2020.9240849>
22. Adzic, M., Adzic, E., Katic, V.: Modeling of the controlled DC-drives without current and speed feedback. In: 2008 6th International Symposium on Intelligent Systems and Informatics, pp. 1–4. IEEE, Subotica (2008). <https://doi.org/10.1109/SISY.2008.4664921>
23. Voliansky, R., Kuznetsov, V., Pranolo, A., et al.: Sliding Mode Control for DC Generator with Uncertain Load. In: 2020 IEEE 15th International Conference on Advanced Trends in Radioelectronics, Telecommunications and Computer Engineering (TCSET), pp. 313–316. IEEE, Lviv-Slavske (2020). <https://doi.org/10.1109/TCSET49122.2020.235446>
24. Pantonial, R., Kilantang, A., Buenaobra, B.: Performance of a real time disturbance observer in rotational motion electro-mechanical system from stimulated physical actuation. In: TENCON 2012 IEEE Region 10 Conference, pp. 1–6. IEEE, Cebu (2012). <https://doi.org/10.1109/TENCON.2012.6412179>
25. Comanescu, M.: Influence of the discretization method on the integration accuracy of observers with continuous feedback. In: 2011 IEEE International Symposium on Industrial Electronics, pp. 625–630. IEEE, Gdansk (2011). <https://doi.org/10.1109/ISIE.2011.5984230>
26. Szabat, K., Tokarczyk, A., Wróbel, K., Katsura, S.: Application of the multi-layer observer for a two-mass drive system. In: 2020 IEEE 29th International Symposium on Industrial Electronics (ISIE), pp. 265–270. IEEE, Delft (2020). <https://doi.org/10.1109/ISIE45063.2020.9152577>
27. Sieklucki, G.: Optimization of observers in a two-mass system-dual LQ problem. In: 2018 International Symposium on Electrical Machines (SME), pp. 1–6. IEEE, Andrychow (2018). <https://doi.org/10.1109/ISEM.2018.8442808>
28. Kreuawan, S., Gillon, F., Moussouni, F., et al.: Optimal design of traction motor in railway propulsion system. In: 2007 International Aegean Conference on Electrical Machines and Power Electronics, pp. 343–348. IEEE, Bodrum (2007). <https://doi.org/10.1109/ACEMP.2007.4510527>
29. Presură, R.C.N., Enache, S., Nicolae, M.Ş., et al.: The importance of the cross geometry over the optimal design of asynchronous traction motors. In: 2020 International Conference and Exposition on Electrical And Power Engineering (EPE), pp. 72–77. IEEE, Iasi (2020). <https://doi.org/10.1109/EPE50722.2020.9305577>
30. Patrizi, G., Catelani, M., Ciani, L., et al.: Electrical characterization under harsh environment of DC–DC converters used in diagnostic systems. *IEEE Trans. Instrum. Meas.* **71**, 3504811 (2021). <https://doi.org/10.1109/TIM.2021.3129513>
31. Son, Y.I., Kim, I.H., Choi, D.S., Shim, H.: Robust cascade control of electric motor drives using dual reduced-order PI observer. *IEEE Trans. Industr. Electron.* **62**(6), 3672–3682 (2014). <https://doi.org/10.1109/TIE.2014.2374571>



Mathematical Modeling of Rod-Type Piezoelectric Transducers for Application in Smart Urban Engineering Technologies

Constantine Bazilo , Maksym Bondarenko  ^(✉), Liudmyla Usyk ,
Viacheslav Tuz , and Emil Faure 

Cherkasy State Technological University, 460 Shevchenka Boulevard, Cherkasy 18006, Ukraine
m.bondarenko@chdtu.edu.ua

Abstract. This paper presents the process and results of developing a mathematical model of rod-type piezoelectric transducers, which are widely used in various devices and systems that are part of smart technologies for urban engineering and municipal economy (power supply devices for green and intelligent municipal special vehicles, systems for high-precision control of environmental factors affecting the critical infrastructure of the city, etc.). The physical processes taking place in rod-type piezoelectric transducers operating in the mode of longitudinal low-frequency oscillations are considered. The obtained analytical dependences make it possible to determine the main operating parameters (modulus of electrical impedance, frequencies of the first resonance and antiresonance, electromechanical coupling coefficient, etc.) of rod-type piezoelectric transducer depending on its operating frequencies and dimensions. As one of the practical results obtained in the work, there is a proposed generalized algorithm for mathematical modeling of rod-type piezoelectric transducer. Also, in the process of mathematical modeling according to the above algorithm, the dependences of changes in the electrical impedance modulus on the operating frequency of the electromechanical resonance were obtained. The discrepancy between the mathematically calculated and experimentally obtained values of the electrical impedance modulus of an oscillating rod-type piezoelectric transducer in the operating frequency range up to 60 kHz, which have found application in smart technologies of urban engineering, does not exceed 5.2%.

Keywords: Smart technologies · Urban engineering · Mathematical model · Piezoelectric ceramics · Rod-type piezo transducer

1 Introduction

The introduction of new approaches and social technologies to the development of society in the areas of its informatization and virtualization involves the creation of new management strategies in the interaction of the technopolis with the environment [1]. This is fully consistent with the Industry 4.0 initiative, which implies the need to develop and implement new ideas to change the concept of urban infrastructure development [2].

The latter consists in moving away from the traditional hierarchical management functions of the urban economy on the part of the municipality towards their decentralization and subsequent synchronization through the introduction of promising information technologies and innovative technical solutions. To date, the implementation of these ideas is taking place within the framework of modern trends in introducing the Smart City concept into the process of sustainable development of modern cities and megaregions [3]. However, this approach would not work without the involvement in the process of technical implementation of the Smart City concept of device elements and systems based on new functional materials, the most promising of which are piezoelectric ceramics.

Distinctive features of piezoelectric ceramics is that this material has the ability to convert energy in both directions (mechanical energy into electric field energy, and vice versa, electrical energy into mechanical movement energy), has high sensitivity and reliability. This allows the active use of electrical circuit components made of such materials in the design of intelligent systems capable of changing their behavior based on information received from the environment in real time [4–6].

There is a wide range of piezoelectric materials, as well as a variety of circuit solutions for the practical implementation of piezoelectric transducers and devices based on them, especially those that are used in critical city infra-structure systems (power supply devices for green and intelligent municipal special vehicles, high-precision control systems for mechanical loads, flow meters, meteorological, seismic and vibration control, etc.). This, of course, stimulates their further theoretical research, which consists in mathematical modeling of the processes occurring during electromechanical transformations of energy in piezoelectric materials. The ultimate goal of such mathematical modeling of the physical state of vibrating piezoceramic elements is a qualitative and quantitative description of the characteristics and parameters of electrical and elastic mechanical fields arising in them [7], which should significantly reduce the time and cost of calculating the operating parameters used in the development of new piezoelectronic devices.

2 Review of the Problem in Smart City Conditions

Among modern firms and organizations that are investigating the problem of using piezoelectric transducers in Smart City conditions and implementing devices based on such transducers in a modern city, the following ones should be noted: TE Connectivity (USA), PI Ceramic GmbH (Germany), Changzhou Keliking Electronics Co., Ningbo Sanco Electronics Co. (China), Kingstate Electronics Corp. (Taiwan), et al., as well as the work of the following scientists: Jettanasen *et al.* [8], Collins [9], Izadgoshab [10], Valtasaari [11] and others. The main obstacle in the development and distribution of devices for smart technologies of urban engineering, the key element of which are piezoelectric transducers, is the complexity of the mathematical description of the mechanism of operation of such transducers, which would allow taking into account both electrical and mechanical processes occurring in them.

An analysis of recent research in this area has shown insufficient knowledge, and sometimes the absence of an analytical and/or numerical description of mathematical models of piezoelectric transducers of various designs and types, which would take into

account the mechanical processes and phenomena occurring in piezoceramics, and the nature of the relationship between these processes and electrical characteristics of the piezoelectric material. Thus, in [12], the authors propose two methods for calculating transfer functions, namely, the wave equation method and the method based on the A-matrices of the regular line segment. At the same time, the proposed methods are relatively simple for the analysis and calculation of the amplitude-frequency characteristics of piezoelectric radiators. In [13], a combined piezoelectric element is simulated taking into account its electrical and mechanical properties by applying a transfer matrix model of describing the coupled bending vibration. On the basis of such transfer model, an electromechanical coupling model of the proposed transducer is developed, which makes it possible to study its dynamic behavior.

However, despite the prospects of the calculation methods and mathematical models proposed above, as well as a number of other effective methods for modeling piezoelectric transducers (for example, modeling using the finite element method described in [14], which allows a three-dimensional analysis of the effect of various limiting conditions of electromechanical coupling on voltage distribution, electric field strength and electric displacement in the piezoelectric transducer), it should be noted that today there is no algorithm for calculating the components in such mathematical models, which would have a generalized form for all sizes of rod-type piezoelectric transducers. That is why, in order to expand the possibilities of practical application of rod piezoelectric transducers in smart technologies for urban engineering, it is necessary to carry out mathematical modeling and compile its generalized algorithm, according to which the main operating parameters of these transducers can be determined with high accuracy and reliability.

The aim of the paper is to develop a mathematical model of rod-type piezoelectric transducers, the use of which will allow obtaining high-precision and reliable values of the main operating parameters of such transducers, which will expand the possibilities for their further practical application in smart technologies for urban engineering and municipal economy.

3 Piezoelectric Rod-Type Transducers Mathematical Model

Let us consider a rod (Fig. 1) made of PZT-type piezoelectric ceramics [15] polarized along the axis Ox_3 . With the indicated polarization direction, the matrix of piezoelectric modules in the rod material shall be written as:

$$|e_{k\beta}| = \begin{vmatrix} 0 & 0 & 0 & 0 & e_{15} & 0 \\ 0 & 0 & 0 & e_{24} & 0 & 0 \\ e_{31} & e_{32} & e_{33} & 0 & 0 & 0 \end{vmatrix}, \beta \Leftrightarrow i, j, \tag{1}$$

where $e_{15} = e_{24} = (e_{33} - e_{31})/2$ and $e_{31} = e_{32} \neq e_{33}$.

Let us assume that the surfaces of the rod $x_3 = \pm \alpha$ are covered with a thin layer of metal [16] and the electric potential difference $U_0 e^{i\omega t}$ is applied to them (U_0 is amplitude; $i = \sqrt{-1}$; ω is angular frequency of the charge sign reversal; t stands for time), which is induced by an external generator of electrical signals. The amplitude of the external electric field is solely determined by the axial component of the strength vector $E_3^* =$

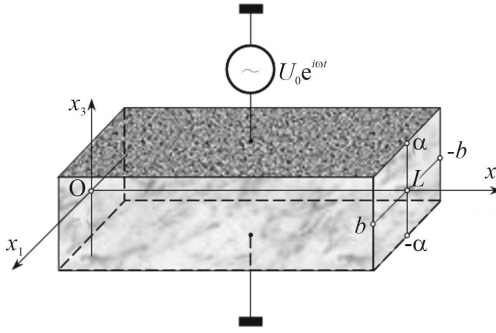


Fig. 1. Calculation scheme for a piezoceramic rod.

$-U_0/2\alpha$ (Fig. 1). Since the piezoelectric properties of the rod material are defined by matrix (1), it can be argued that the Coulomb forces created by the external electric field will cause the rod to perform compression-tension oscillations along the axes of the Cartesian coordinate system (x_1, x_2, x_3) (Fig. 1) [17]. With this type of stress-strain state, there are no shear deformations, and the stress tensor is determined by the diagonal components of the matrix, i.e., by quantities ε_{11} , ε_{22} , and ε_{33} .

The amplitude value of the component of the electric induction vector normal to the metalized surfaces of the rod in the problem under consideration shall be determined as follows

$$D_3 = e_{31}(\varepsilon_{11} + \varepsilon_{22}) + e_{33}\varepsilon_{33} + \chi_{33}^E E_3, \tag{2}$$

where $\varepsilon_{11} = \partial u_1/\partial x_1$; $\varepsilon_{22} = \partial u_2/\partial x_2$; $\varepsilon_{33} = \partial u_3/\partial x_3$ are amplitudes of harmonically time-varying strains; u_k ($k = 1, 2, 3$) stands for amplitudes of the displacement vector components of the material particles of the rod that satisfy the equation of motion (Newton’s second law in differential form), i.e.

$$\partial \sigma_{ij} / \partial x_j + \rho_0 \omega^2 u_i = 0, \quad (i, j = 1, 2, 3), \tag{3}$$

where σ_{ij} are amplitudes of resultant elastic stresses in the rod material; E_3 is amplitude of the axial component of the strength vector of the resulting electric field. When writing relation (2), as in all further entries, material constants of the same magnitude will be denoted by the same symbols (see the first term in formula (2)).

Since $\sigma_{ij} = c_{ijkl}^E \varepsilon_{kl} - e_{kij} E_k$, where c_{ijkl}^E is the matrix of elastic module, then

$$\sigma_{11} = c_{11}^E \varepsilon_{11} + c_{12}^E (\varepsilon_{22} + \varepsilon_{33}) - e_{31} E_3, \tag{4}$$

$$\sigma_{22} = c_{22}^E \varepsilon_{22} + c_{12}^E (\varepsilon_{11} + \varepsilon_{33}) - e_{32} E_3, \tag{5}$$

$$\sigma_{33} = c_{33}^E \varepsilon_{33} + c_{12}^E (\varepsilon_{11} + \varepsilon_{22}) - e_{33} E_3, \tag{6}$$

$$\sigma_{ij} = \sigma_j = 0 \quad \forall i \neq j. \tag{7}$$

The resulting stresses σ_{ij} must satisfy Newton's third law on the side surfaces of the rod. We will assume that the rod is suspended on thin threads in vacuum, which means no forces act on it from the side of the environment. Since the action force is equal to the reaction force, it is necessary to require the fulfillment of the following conditions on the boundary of existing solutions to Eqs. (3), i.e., on the side surfaces of the rod:

$$\sigma_{ij}n_i = 0 \forall x_k \in S, \quad (8)$$

where n_i are components of the unit normal vector to lateral surface S bounding the volume of the rod.

Setting equal to zero the left parts of expressions (4) and (6), we obtain a system of equations for determining strains ε_{11} and ε_{33} through longitudinal strain ε_{22} and axial component E_3 of the strength vector of the resultant electric field.

Having performed the necessary calculations, we obtain the following relations to calculate strains ε_{11} and ε_{33} :

$$\begin{aligned} \varepsilon_{11} &= \left\{ \left[-c_{12}^E c_{33}^E + \left(c_{12}^E \right)^2 \right] \varepsilon_{22} + \left(e_{31} c_{33}^E - e_{33} c_{12}^E \right) E_3 \right\} / \Delta_0, \\ \varepsilon_{33} &= \left\{ \left[-c_{12}^E c_{11}^E + \left(c_{12}^E \right)^2 \right] \varepsilon_{22} + \left(e_{33} c_{11}^E - e_{31} c_{12}^E \right) E_3 \right\} / \Delta_0, \end{aligned} \quad (9)$$

where $\Delta_0 = c_{11}^E c_{33}^E - \left(c_{12}^E \right)^2$.

By substituting expressions (9) into relation (5), we shall obtain Hooke's law for uniaxial compression—tension of a rod with complicated properties as follows

$$\sigma_{22} = Y^E \varepsilon_{22} - e_{32}^* E_3, \quad (10)$$

where Y^E is Young's modulus of a piezoceramic rod, experimentally determined in the mode of a constant (equal to zero) electric field strength; e_{32}^* is piezomodulus for the oscillation mode at constant (equal to zero) normal stresses σ_{11} and σ_{33} . The formulas for calculating values Y^E and e_{32}^* through physical and mechanical parameters of piezoceramics are as follows:

$$Y^E = c_{22}^E + \left(c_{12}^E \right)^2 \left[2c_{12}^E - \left(c_{11}^E + c_{33}^E \right) \right] / \Delta_0, \quad (11)$$

$$e_{32}^* = e_{31} - c_{12}^E \left[e_{31} \left(c_{33}^E - c_{12}^E \right) + e_{33} \left(c_{11}^E - c_{12}^E \right) \right] / \Delta_0. \quad (12)$$

After substituting relation (9) into expression (2), we obtain the law of electric polarization of a dielectric with complicated (piezoelectric) properties for a uniaxial stress state:

$$D_3 = e_{32}^* \varepsilon_2 + \chi_{33}^\sigma E_3, \quad (13)$$

where χ_{33}^σ is the permittivity of the material of the rod for the mode of harmonic oscillations, in which the resulting stresses in the cross-section are equal to zero. The formula to calculate this value is therefore as follows

$$\chi_{33}^\sigma = \varepsilon_{33}^\varepsilon + \left[e_{31}^2 c_{33}^E + e_{33}^2 c_{11}^E - 2e_{31} e_{33} c_{12}^E \right] / \Delta_0. \quad (14)$$

Since shear deformations are absent according to the physical essence of the formulation of the problem being solved, and sources that could create electric fields with components of the strength vector E_1 and E_2 are also absent, it can be argued that the electric induction vector \vec{D} is completely determined by the axial component D_3 . In this case, the condition for the absence of free electricity carriers, namely, $\text{div } \vec{D} = 0$ is written down as follows $\partial D_3/\partial x_3 = 0$, whence it follows that component D_3 does not depend on coordinate x_3 values. This fact can be used to determine value E_3 , which is the vertical component of the strength vector of the resultant electric field within the volume of the strained piezoelectric rod.

Since $\vec{E} = -\text{grad } \Phi$, where Φ is the electric potential of the resulting field, then, obviously, $E_3 = -\partial \Phi/\partial x_3$. In this case, expression (13) can be represented in the following form

$$D_3 = e_{32}^* \partial u_2/\partial x_2 + \chi_{33}^\sigma \partial \Phi/\partial x_3. \tag{15}$$

Integrating the left and right parts of expression (15) along coordinate x_3 and presuming that the longitudinal component of the displacement vector does not change its value within the cross-sectional area of the rod, we obtain the following result considering condition $\partial D_3/\partial x_3 = 0$:

$$2\alpha D_3 = 2\alpha e_{32}^* \partial u_2/\partial x_2 - \chi_{33}^\sigma [\Phi(\alpha) - \Phi(-\alpha)].$$

The square brackets in the last relation contain the amplitude of the difference in electric potentials on the metalized surfaces of the rod, that is, value U_0 . The last relation means that

$$D_3 = e_{32}^* \partial u_2/\partial x_2 - \chi_{33}^\sigma U_0/2\alpha. \tag{16}$$

Comparing expressions (13) and (16) with each other, we arrive to the conclusion that

$$E_3 = -U_0/2\alpha, \tag{17}$$

therefore,

$$\sigma_{22} = Y^E \partial u_2/\partial x_2 + e_{32}^* U_0/2\alpha. \tag{18}$$

whereas all other components of the stress tensor are equal to zero.

Substituting expression (18) into Eq. (3), we obtain

$$\partial^2 u_2/\partial x_2^2 + k^2 u_2 = 0, \tag{19}$$

where $k^2 = \omega^2 \rho_0/Y^E$ is the square wave number of longitudinal low-frequency harmonic oscillations of a piezoceramic rod. The final form of the relationship to calculate component D_3 of the electrical induction vector:

$$D_3 = \frac{U_0(e_{32}^*)^2}{2Y^E\alpha} \left[\text{tg} \left(\frac{kL}{2} \right) \sin kx_2 + \cos kx_2 \right] - \chi_{33}^\sigma \frac{U_0}{2\alpha}. \tag{20}$$

By integrating expression (20) over the area of the electroded surface $x_3 = \alpha$, we can define the amplitude value of the total electric charge Q on this surface

$$Q = U_0 C_0^\sigma F(kL), \quad (21)$$

where $C_0^\sigma = \chi_{33}^\sigma bL/\alpha$ denotes the static electrical capacity of the free piezoceramic rod; $F(kL) = K^2 \operatorname{tg}(kL/2)/(kL/2) - 1$ is the a frequency-dependent function that determines the ratio of the polarization charge Q^{pe} and electric charge Q^* (occurs in a capacitor with capacitance C_0^σ when applying difference of electric potentials U_0 to it; $K^2 = (e_{32}^*)^2/(\chi_{33}^\sigma Y^E)$) denotes the square electromechanical coupling coefficient.

The electrical impedance $Z_{el}(\omega)$ of the rod in the mode of longitudinal vibrations is determined by the following formula

$$Z_{el}(\omega) = -[i\omega C_0^\sigma F(kL)]^{-1}. \quad (22)$$

If $K^2 = 0$, which means the dielectric does not possess piezoelectric properties, then function $F(kL) = 1$, and expression (22) takes the form of a known formula for calculating the reactance of a capacitor with electric capacitance C_0^σ . When $K^2 \neq 0$, which means the dielectric between the electrodes on surfaces $x_3 = \pm x_3$ possesses piezoelectric properties, the function $F(kL)$ vanishes (anti-resonance phenomenon) at a frequency ω_α for which the condition is satisfied

$$K^2 \operatorname{tg}(k_a L/2)/(k_a L/2) - 1 = 0. \quad (23)$$

Thus, the considered type of piezoceramic element vibrations initially creates electromechanical antiresonance, and afterwards—electromechanical resonance.

4 Results and Discussion

In a real situation, when performing measurements $Z_{el}(\omega)$, zeros or infinities of the electrical impedance of an oscillating piezoelectric element can not be observed, which can be explained by energy losses in piezoceramics. In this case, the dynamic Young's modulus Y^E should be determined as follows

$$Y^E = Y_0^E (1 + i/Q_0), \quad (24)$$

where Y_0^E is static Young's modulus, which is determined through the elastic moduli of the piezoceramics according to the formula (11).

In Fig. 2 shown function $1/F(kL)$ modules calculated with the values of the square electromechanical connection $K^2 = 0,05; 0,1; 0,2; 0,4$. Along the abscissa in Fig. 2, the values of the dimensionless wave number $kL/2$ are plotted in fractions of number $\pi/2$, that is, value kL/π . Any change in value K^2 significantly affects the value of the electromechanical antiresonance frequency.

In Fig. 3 shown the modulus of the function values $1/F(kL)$ in the vicinity of the electromechanical resonance frequency when $k_p L/2 = \pi/2$. Thus, Fig. 3 demonstrates that an increase in the quality factor of piezoceramics is accompanied by a decrease in the modulus of the function $1/F(kL)$.

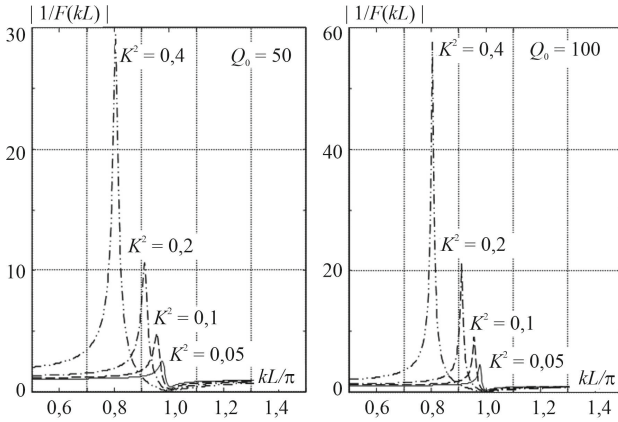


Fig. 2. Frequency dependent change in the modulus of the function $1/F(kL)$ for various values of the square electromechanical coupling coefficient and piezoceramics quality factor.

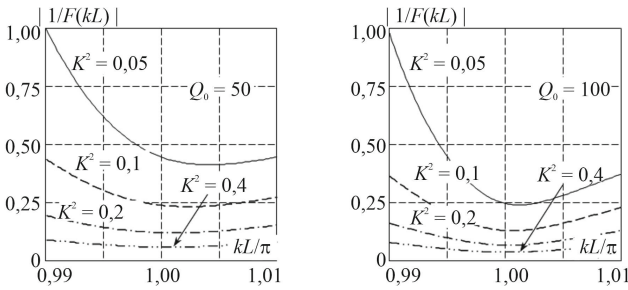


Fig. 3. Variation in the modulus of the function $1/F(kL)$ in the vicinity of the first electromechanical resonance frequency.

In Fig. 4 shown a graph for changes in the electrical impedance modulus of a rod with a square cross-section made of PZT-type piezoceramics. The calculation was carried out according to formula (22). When performing calculations, the following parameter values were accepted: $c_{11}^E = 112 \text{ GPa}$; $c_{12}^E = 62 \text{ GPa}$; $c_{33}^E = 106 \text{ GPa}$; $e_{33} = 18 \text{ Ku/m}^2$; $e_{31} = -7 \text{ Ku/m}^2$; $\rho_0 = 7400 \text{ kg/m}^3$; $\chi_{33}^\epsilon = 8,85 \cdot 10^{-9} \text{ F/m}$; $Q_0 = 80$; $\alpha = \beta = 4 \text{ mm}$; $L = 80 \text{ mm}$. The first resonance—antiresonance stands out vividly against the background of a monotonous decrease in the electrical impedance of the rod with increasing frequency, and therefore can be reliably recorded in the course of an experimental study.

Relations (22) and (23) together with calculation results shown in Figs. 2, 3 and 4 indicate that it is possible to estimate the quantitative values of integral physical and mechanical parameters of piezoceramics basing on the results of studying the dependence of electrical impedance $Z_{el}(\omega)$ of an oscillating piezoceramic rod. These parameters include: Young’s modulus Y^E , piezomodulus e_{32}^* , the permittivity of a free rod χ_{33}^σ , and quality factor of a piezoelectric frame Q_0 .

We shall consider the following quantities to be experimentally determined: rod dimensions α , b , L in meters; rod mass m in kilograms; the frequencies of the first

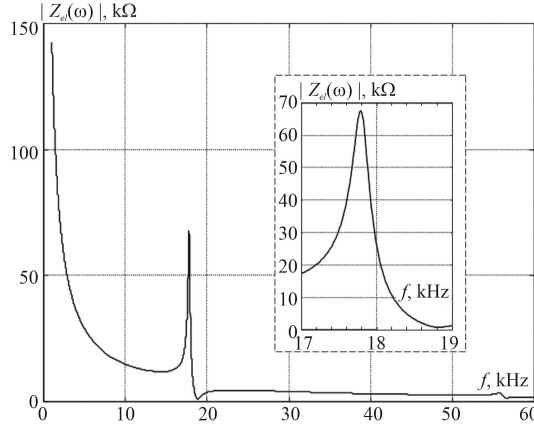


Fig. 4. Electrical impedance modulus of a rod with a square cross-section 8×8 mm and length $L = 80$ mm made of PZT-type piezoceramics.

antiresonance f_α measured to the nearest hertz and frequencies of the first resonance f_r in hertz; modulus of electrical impedance Z_0 at the frequency of the first electromechanical resonance in ohms; electrical impedance modulus $Z_{el}(\omega_l)$, measured in ohms at low frequency f_l , where $f_l \ll f_\alpha$.

The known value $Z_{el}(\omega_l)$ defines the static electric capacitance of the rod $C_0^\sigma = [2\pi f_l \times \times Z_{el}(\omega_l)]^{-1}$. According to the known capacitance, the dielectric constant is found as $\chi_{33}^\sigma = \alpha C_{33}^\sigma / bL$. Since the condition is satisfied at the electromechanical resonance frequency $k_p L / 2 = \pi / 2$, where $k_p = 2\pi f_r / v_{st}$; $v_{st} = (Y^E / \rho_0)^{1/2}$ is the speed with which longitudinal elastic waves propagate in the rod, this condition determines speed as $v_{st} = 2f_r L$. Young's modulus $Y^E = \rho_0 v_{st}^2$ is derived from the known speed v_{st} and density $\rho_0 = m / (4\alpha bL)$. At the frequency of electromechanical antiresonance, the product is $k_\alpha L = (k_p L)(k_\alpha / k_r) = \pi f_\alpha / f_r$. However, the square of the electromechanical coupling coefficient:

$$K^2 = (\pi f_\alpha / 2f_r) / \text{tg}(\pi f_\alpha / 2f_r). \quad (25)$$

If the energy losses in the volume of the piezoceramic rod are determined by formula (24), then the expression for calculating the electrical impedance $Z_{el}(\omega)$ shall be written in the following form:

$$Z_{el}(\omega) = [i / (\omega C_0^\sigma)] \Psi(\omega, \varepsilon), \quad (26)$$

wherein

$$\Psi(\omega, \varepsilon) = \{K^2 \text{tg}[x(1 - i\varepsilon)] / [x(1 - i\varepsilon)]\}^{-1}; \quad (27)$$

$x = k_0 L / 2$; $k_0 = \omega / v_{st}^0$ is wave number determined without considering energy losses in the rod material; $v_{st}^0 = (Y_0^E / \rho_0)^{1/2}$ is speed of longitudinal waves in the rod without considering energy losses; $\varepsilon = (2Q_0)^{-1} \ll 1$ is a small parameter. At the frequency f_r of the first electromechanical resonance, we obtain the following result

$$|Z_{el}(\omega)| = Z_0 = (\varepsilon \pi) / (8f_r C_0^\sigma K^2),$$

whence follows the formula for estimating the quality factor Q_0 at frequency f_r :

$$Q_0 = \pi / (16Z_0 f_r C_0^\sigma K^2) \tag{28}$$

At the same time, it should be noted that the obtained numerical values of the integral parameters Y^E , e_{32}^* and χ_{33}^σ were not able to provide assessment of the numerical values for the actual physical and mechanical parameters of piezoelectric ceramics.

The set of experimental data on the electrical impedance of a piezoceramic rod in various modes of harmonic oscillations provides the necessary database for constructing estimates of the numerical values of the physical and mechanical parameters of piezoelectric ceramics.

The calculation and study of the developed mathematical model was carried out in the MatLab Simulink software [18], which makes it possible to accurately and quickly determine the main parameters of the rod piezoelectric transducer, taking into account its operating frequencies and dimensions, as well as to obtain dependences of changes in the electrical impedance modulus on frequency of the electromechanical resonance.

According to the results of the performed calculations and practical experiments, the experimental (solid line) and calculated (dashed line) curves of the electrical impedance modulus of the piezoceramic rod-type transducer were obtained, (Fig. 5).

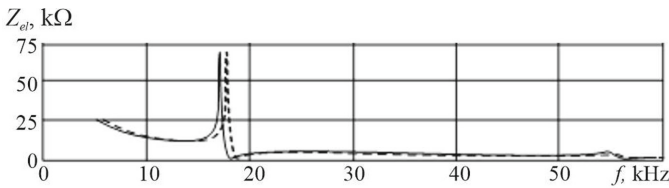


Fig. 5. Experimental (solid line) and calculated (dashed line) dependence curves of the electrical impedance modulus on the operating frequency of the piezoceramic rod-type transducer.

As can be seen from Fig. 5, the calculated results correlate with the experimentally obtained values of the electrical impedance modulus (there is a very strong correspondence between the calculated and experimental data). At the same time, the discrepancy between the results of mathematical modeling and experimental data does not exceed 5.2% for the same values of operating frequencies.

5 Conclusion

Physical processes in rod-type piezoelectric transducers, which have found application in smart technologies of urban engineering and municipal economy, were considered. A description of these processes was obtained by analytical dependences during the operation of such piezoelectric transducers in the mode of longitudinal low-frequency oscillations.

A mathematical model of rod-type piezoelectric transducers was proposed, which can be used to determine the basic operating parameters (modulus of electrical impedance,

first resonance and antiresonance frequencies, electromechanical coupling coefficient, etc.) of such transducers depending on their operating frequency range and dimensions.

A generalized algorithm for calculating the components of the abovementioned mathematical model was given, according to which mathematical modeling of a rod-type piezoelectric transducer was carried out and dependences of changes in the electrical impedance modulus on the operating frequency of the electromechanical resonance were obtained.

It has been established that the discrepancy between the mathematically calculated and experimentally obtained values of the modulus of electrical impedance of oscillating rod-type piezoelectric transducer in the frequency range up to 60 kHz does not exceed 5.2%.

Further research by the authors of the article will be aimed at improving the proposed mathematical model in terms of taking into account the unpredictable effects of the external environment (the action of mechanical static and dynamic loads, the influence of thermal, electromagnetic fields) and internal factors (the formation and development of micro- and macrodefects in piezoceramics, depolarization and phantom repolarization of its domain structures), which will make it possible to carry out a high-precision determination of the terms of its reliable operation under various operating modes in the conditions of the urban economy. It is also planned to develop a test stand for further experimental confirmation of the results of theoretical calculations and mathematical modeling of rod-type piezoelectric transducers.

References

1. Giffinger, R., Kramar, H., Fertner, C., Meijers, E.J.: City-ranking of European medium-sized cities. In: Ostergard, N. (eds.) *Futures of Cities*, pp. 1–12. IFHP (2007)
2. Ng, T.C., Lau, S.Y., Ghobakhloo, M., et al.: The application of Industry 4.0 technological constituents for sustainable manufacturing: A content-centric review. *Sustainability* **14**, 4327 (2022). <https://doi.org/10.3390/su14074327>
3. Razumkov Center: *Smart Infrastructure in Sustainable Urban Development: World Experience and Prospects of Ukraine*. Zapovit, Kyiv (2021) [In Ukrainian]
4. Sharapov, V., Sotula, Z., Kunickaya, L.: *Piezo-Electric Electro-Acoustic Transducers*. MEMS. Springer, Cham (2014). <https://doi.org/10.1007/978-3-319-01198-1>
5. Sherman, C.H., Butler, J.L.: *Transducers and Arrays for Underwater Sound*. Springer, New York (2007). <https://doi.org/10.1007/978-0-387-33139-3>
6. Bazilo, C., Zagorskis, A., Petrishchev, O., et al.: Modelling of piezoelectric transducers for environmental monitoring. In: *Proceedings of the International Conference on Environmental Engineering (ICEE)*, vol. 10, pp. 1–8. Vilnius Gediminas Technical University (2017). <https://doi.org/10.3846/enviro.2017.008>
7. Bazilo, C.V., Bondarenko, M.O., Khlivnyi, V.V., et al.: Mathematical modelling of rod-type piezo-electric transducers for acoustoelectronic devices. *Visnyk NTUU KPI Serii—Radiotekhnika Radioaparatabuduvannia* **86**, 58–67 (2021). <https://doi.org/10.20535/RADAP.2021.86.58-67>
8. Jettanasen, C., Songsukthawan, P., Ngaopitakkul, A.: Development of micro-mobility based on piezoelectric energy harvesting for Smart City applications. *Sustainability* **12**, 2933 (2020). <https://doi.org/10.3390/su12072933>

9. Collins, R.: Piezoelectric Harvesting and Sensing 2019–2039. IDTechEx. <https://www.idtechex.com/en/research-report/piezoelectric-harvesting-and-sensing-2019-2039/646> (2019). Accessed 10 May 2022
10. Izadgoshasb, I.: Piezoelectric energy harvesting towards self-powered Internet of Things (IoT) sensors in smart cities. *Sensors* **21**, 8332 (2021). <https://doi.org/10.3390/s21248332>
11. Valtasaari, S.: Japan—A New Challenger in the Smart City Industry. *Open & Agile Smart Cities*. <https://oascities.org/japan-a-new-challenger-in-the-smart-city-industry/> (2022). Accessed 10 May 2022
12. Naida, S., Zheliaskova, T., Naida, A., et al.: Methods for calculating the transfer functions of broadband plate piezoelectric transducers with transition layers. *J. Nano Electr. Phys.* **13**(6), 06029 (2021). [https://doi.org/10.21272/jnep.13\(6\).06029](https://doi.org/10.21272/jnep.13(6).06029)
13. Wang, L., Wang, J.A., Jin, J.M., et al.: Theoretical modeling, verification, and application study on a novel bending-bending coupled piezoelectric ultrasonic transducer. *Mech. Syst. Signal Process.* **168**, 108644 (2022). <https://doi.org/10.1016/j.ymssp.2021.108644>
14. Zhu, S., Liu, H.: Finite element analysis of the three-dimensional crack and defects in piezoelectric materials under the electro-mechanical coupling field. *J. Intell. Mater. Syst. Struct.* **32**(15), 1662–1677 (2021). <https://doi.org/10.1177/1045389X20983884>
15. Yan, Y., Geng, L.D., Zhu, L.F., et al.: Ultrahigh piezoelectric performance through synergistic compositional and microstructural engineering. *Adv. Sci.* **14**(9), 2105715 (2022). <https://doi.org/10.1002/advs.202105715>
16. Medianykyk, V., Bondarenko, Y., Bazilo, C., Bondarenko, M.: Research of current-conducting electrodes of elements from piezoelectric ceramics modified by the low-energy ribbon-shaped electron stream. *J. Nano Electr. Phys.* **10**(6), 06012 (2018). [https://doi.org/10.21272/jnep.10\(6\).06012](https://doi.org/10.21272/jnep.10(6).06012)
17. Wang, X., Schiavone, P.: Coulomb force on a line charge in an anisotropic piezoelectric bimaterial. *Continuum Mech. Thermodyn.* **34**, 387–394 (2021). <https://doi.org/10.1007/s00161-021-01061-9>
18. Yadav, P., Gaur, P.: Electromechanical modeling and simulation of piezoelectric vibration based energy harvester interfaced with MPPT based electrical circuit using Matlab Simulink. *Int. J. Recent Technol. Eng.* **8**(2S11), 36–40 (2019). <https://doi.org/10.35940/ijrte.B1007.0982S1119>



Improvement of a Linear Screw Piezo Motor Design for Use in Accurate Liquid Dosing Assembly

Volodymyr Halchenko , Dmytro Bacherikov , Sergey Filimonov^(✉) ,
and Nadiia Filimonova 

Cherkasy State Technological University, 460 Shevchenka Boulevard, Cherkasy 18006, Ukraine
s.filimonov@chdtu.edu.ua

Abstract. The purpose of the article is to improve the design of a screw linear piezoelectric motor as a result of the use of bimorph piezoelectric elements, which made it possible to reduce the length of the stiffening ribs of the entire structure. For research, mathematical modelling was used in the environment of the COM-SOL Multiphysics software package, taking into account the relationship between electrostatic and mechanical phenomena. By means of numerical simulation, natural vibration frequencies of the design of a linear ultrasonic motor with bimorph piezoelements are determined. Using the graph of the amplitude-frequency characteristic, the main resonant frequency of the piezoelectric motor is determined. An experimental sample of a screw linear piezoelectric motor was also made, which demonstrated its operability and proved the adequacy of the proposed technical solutions. By conducting experimental studies on the removal of the real amplitude-frequency characteristic of the engine, the validation of the results of numerical experiments was carried out. The data obtained can be used in the design of devices that use piezoceramic actuators, in particular, in the agricultural sector.

Keywords: Agriculture · Dispenser · Piezoelectric motor · Bimorph piezoelectric element

1 Introduction

Today, agriculture is at the forefront of the development of the country's economy and is one of its main sectors. This has been made possible by automating and modernizing farming practices, in particular precision farming.

Agriculture is rapidly using the latest technology to manage and optimize agricultural production. The main implementing technologies are not only GPS navigation, controllers, data communication protocols, farm management software platforms, but also the latest sensors for accurate control, monitoring, analysis and collection of real-time soil data for application them in differentiated sowing and outflow, which are currently relevant [1, 2]. One of the important steps for obtaining a good harvest is spraying and applying rare fertilizers.

With the development of agriculture, the demand for the use of fertilizers and preparations to achieve maximum yields in the fields is increasing. Therefore, the issue of pouring systems and accurate dosage and compliance with specified norms is relevant, which will not lead to overspending of fertilizers and the budget.

To control the dosage of the outflow of liquid fertilizers, special dispensers are used. The main element of the dosing and pouring unit is the control system. It is based on the control of technological operations with the help of dampers, calibrated holes, regulation with the help of electric motors and electromagnetic valves, which are widely used in precision farming systems.

The main disadvantages of existing control systems are inaccurate positioning, excessive consumption of electric current to maintain a constant position of the executive body, which leads to its overheating and miscalibration.

A promising direction in the field of agricultural technologies is the creation and use of engines, the principle of which is based on the inverse piezoelectric effect. The reverse piezoelectric effect consists in changing the linear dimensions of a piezoelectric when an electric field is applied to it.

Due to the simplicity of the design and a number of technical advantages over electromagnetic motors, namely the absence of radiated magnetic fields and the reluctance to their effect, the possibility of miniaturization; a wide range of speeds and torques on the shaft (0.1 ... 1.0 Nm), fire resistance, absence of windings, the possibility of self-locking of the drive shaft without electric current consumption and high positioning accuracy [3, 4] of the order of 0.5 μm , a sufficiently significant pushing (pulling) force up to 10 N, piezoelectric motors are highly efficient in use in all industries, especially modern agricultural machinery and agricultural technologies [5, 6], which is justified by their exceptional unpretentiousness in operating and maintenance conditions.

The object of research is the processes of interaction of transverse bending mechanical vibrations of bimorph piezoelements of a screw linear piezoelectric motor.

The subject of the study is a linear piezoceramic motor with bimorph piezoelements of the design.

The purpose of the paper is to improve the design of a screw linear piezoelectric motor, which makes it possible to increase the amplitude of oscillations of its components, on which, as a result, the improvement of its technical characteristics largely depends.

In the future, we will understand their improvement as an increase in the maximum torque on the shaft, pushing (thrust) force, which is very important for miniature engines, while maintaining the possibility of precise positioning of the shaft position.

Formulation of the problem. To achieve this task, it is necessary to consistently perform a number of tasks: to modernize the design of a screw linear piezoelectric motor by introducing bimorphic piezoelements into its structure, to evaluate the spectrum of natural vibration frequencies of the structure and the corresponding vibration modes, and to determine the resonance frequency of the system of bimorphic piezoelectric elements of engine corresponding to the maximum amplitude of its mechanical oscillations.

2 Literature Review

The disadvantages of the known types of control systems for the dosing and outflow unit, which are widely used in precision farming systems, namely in trailed, mounted and self-propelled sprayers, are: there is no possibility of remote control in the dampers and in the calibration holes, there is a large clogging of the holes and non-compliance with the specified outflow rates, which leads to excessive consumption of fertilizers; regulation by electric motors and solenoid valves is energy-intensive due to significant currents for self-holding.

Also, the disadvantages include the complexity of manufacturing, a significant adjustment step and the complexity of managing these types of systems.

Recently, piezo motors, known as vibration motors, have been actively used, which are a modern alternative to DC motors in terms of providing accurate movement of actuators. The advantages of such motors are high positioning accuracy, speed and sufficiently high power with small overall dimensions, as well as the absence of the need for gear mechanisms to change the drive speed [7, 8]. A significant number of designs of such engines are known [9, 10], including “inch worm” [11], “wedge worm” and others. They differ in complexity and performance indicators derived from the amplitude of oscillations of the resonant system of the engine, where the movement is created by a variable deformation caused at the frequency of the mechanical resonance of the device by an alternating electric field. Comparing designs according to their technical indicators is very difficult: possible advantages in some indicators are not a guarantee of achieving the same results in others. Therefore, the main efforts of researchers are concentrated precisely on the implementation in various designs of engines of the largest amplitude of oscillations of the system, which is the main general trend in design. Therefore, this task of maximum rationalization of the design of the piezoelectric motor chosen by the authors for modernization is solved within the framework of this article.

The most acceptable design of the piezoelectric motor, according to the authors, when using it to control the dispensers of agricultural machinery is a linear screw version of the motor. One of the designs of engines of this type is shown in Fig. 1 [12, 13]. The main structural elements of this piezoelectric motor are: a tetrahedral metal profile (made of non-magnetic material) with an internal thread, a running shaft (worm) and four piezoceramic plates. The piezoceramic plates are attached to the edges of the metal profile, the worm is twisted into the metal profile [14].

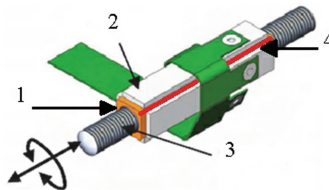


Fig. 1. SQL series piezo motor: 1 – metal profile with thread; 2 – piezoceramics; 3 – running shaft (rod); 4 – four structural stiffeners.

The principle of operation of the engine is as follows. Applying a two-phase voltage to opposite pairs of piezoceramic plates leads to the appearance of mechanical vibrations that are transmitted to the metal profile. As a result, the running shaft rotates and moves linearly relative to the metal profile. By changing the voltage offset in phase by 90°, you can change the direction of movement of the running shaft. These piezo motors operate at frequencies of 30–200 kHz, depending on their overall dimensions. The design parameters of one of the smallest standard sizes of the SQL series piezo motor are illustrated in Fig. 2. Its main technical characteristics are presented in Table 1.

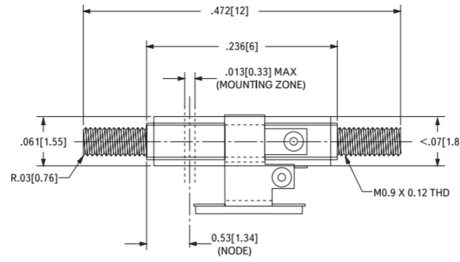


Fig. 2. Structural parameters of SQL series piezo motor SQL.

Table 1. Key Features of SQL Series Piezo Motor.

Parameter	Value
Minimum engine dimensions	1.55 × 1.55 × 6 mm
Power consumption	500 mW (only when moving the rod)
Resolution	0.5 μm
Speed of movement	5 mm/s
Moving effort	More 200 g
Piezo motor resonance frequency	116 kHz
Working resource	300,000 cycles
Piezo motor efficiency	80%

The key disadvantage of this design is the following. When moving from one face to another, long stiffening ribs are formed, which negatively affect the characteristics of the structure. Namely, if the amplitude of vibrations of the faces of the metal profile of the engine decreases, it is necessary to increase the amplitude of the control voltage, etc. That is, it leads to an additional force to counteract the operation of the piezo motor.

Therefore, improving the design of a screw linear piezoelectric motor by reducing the length of the stiffening ribs and obtaining its greater mobility is an important and urgent task, the implementation of which makes it possible to increase the oscillation amplitude of the piezoelectric element system, and, accordingly, significantly improve the technical characteristics of the engine.

3 Materials and Methods

Taking into account the technical features of the design of piezoelectric motors and all the difficulties that arise in their manufacture, the optimal solution is to use numerous modelling methods implemented by special CAD systems [15]. To study the spectrum of natural frequencies of vibrations of the structure and the corresponding modes of vibrations and the choice of its operation mode, as well as to determine the maximum amplitude of oscillations at resonance, a numerical simulation of the operation of a piezoelectric motor was carried out in the COMSOL Multiphysics 3.5 software.

Details of a mathematical model that takes into account multiphysics processes described by a combination of various partial differential equations and some of the main points of calculations using the Piezoelectric Effects module and COMSOL's Solid Mechanics and Electrostatics tools are detailed in [16, 17]. The simulation of the operation of the piezoceramic engine was carried out in the Eigenfrequency Analysis mode to determine the natural vibration frequencies of the structure as a whole and to search for the limiting frequencies necessary for use in the Frequency response mode to determine the main resonant frequency. The computational mesh of finite elements Mesh was chosen as the orthogonal type Normal; it is optimal for carrying out model calculations. The mesh was built by a tetragonal partition, and the studied three-dimensional models were represented by a set of more than a thousand elements for each component of the structure. Direct was used as a solution, in which the SPOOLES numerical method was chosen for solving systems of linear equations with sparse matrices [18, 19].

Modernization of the design of the piezoelectric motor consists in replacing the power part of the structure in the form of a long tetrahedral metal profile with a system of bimorphic piezoelectric elements and a short nut, which simultaneously perform the functions of a power structure, and in this case the design is much smaller rigidity compared to the previous version. Instead of piezoceramic plates, four bimorph piezoelements were introduced into the engine design, shown in Fig. 3. A bimorph piezoelectric element is a thin metal plate to which a piezoelement is glued, the front surfaces of which are covered with electrodes [20, 21]. The use of bimorph piezoelements of a special shape makes it possible to reduce the length of the stiffening ribs and the rigidity of the entire structure as a whole, to give it the necessary mobility. As a material for modelling a piezoelectric motor, a brand of piezoceramics – PZT-5H (TsTS-19) was used [22]. The bimorph piezoelectric elements 2 consist of metal plates made of semi-hard brass L63 with dimensions of $36 \times 12 \times 0.1$ mm, and the piezoelectric elements of piezoceramics with dimensions of $31 \times 6 \times 0.4$ mm.

The thicknesses of piezoelectric elements 2, as well as brass plates 1, remained unchanged during the entire cycle of modelling studies. The bimorph piezoelectric elements are interconnected at the ends of the brass plates by soldering, and the tetrahedral metal nut is fixedly fixed in the center of the piezoelectric motor, where there is a maximum oscillation amplitude. The geometric dimensions of the nut are: side – 12 mm, length – 12 mm and inner diameter – 6 mm. In order to simplify the calculations in the simulation, the influence of the running shaft on the calculation results was neglected.

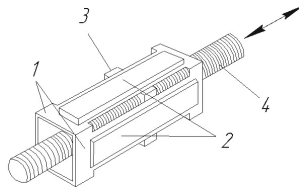


Fig. 3. The design of the piezoelectric motor using bimorph piezoelectric elements and shortened stiffeners: 1 – brass plates; 2 – piezoelectric elements; 3 – square metal nut, 4 – running shaft.

When modelling a piezoelectric motor, the type of boundary conditions Fixed was adopted: piezoelectric element 2 has an electric potential (Electric potential) of 100 V applied to it, and brass plate 1 has a “ground” potential (Ground) applied to the opposite side of the piezoelectric element (see Fig. 3).

The principle of operation of the engine is as follows. When an alternating two-phase electrical voltage is applied, one of which is supplied to a pair of opposite plates of bimorphic piezoelectric elements, and the other with a phase shifted by 90° , to a second pair of opposite similar piezoelements. The common "minus" of the signals is connected to brass plates. This method of excitation leads to the occurrence of mechanical vibrations transmitted to the metal nut. As a result, the running shaft rotates and moves linearly relative to the metal nut. By changing the phase shift of the voltage, you can change the direction of movement of the screw.

4 Numerous Experiments and Results

Even a comparative visual analysis of the designs of a linear piezoelectric motor, presented in Figs. 1 and 3 allows us to assert a relatively significant reduction in the length of the stiffeners in the proposed version, which approximately reaches about 80%. It is obvious that a decrease in the rigidity of the structure as a whole within such limits significantly affects the technical characteristics of a linear screw piezoelectric motor.

Let us prove the increase in the mobility of the proposed design by numerical simulation. An important step in obtaining reliable results of numerical simulation is the construction of a finite element model of the engine design by introducing a mesh Mesh, on which the obtained calculation results significantly depend. On Fig. 4 shows a finite element model of the engine as a result of splitting into finite elements.

It is known that resonance is observed at frequencies close to the frequencies of natural oscillations of the structure. Therefore, the numerical simulation in the COMSOL Multiphysics software package began in the Eigenfrequency Analysis mode, where the natural vibration frequencies of the engine design with bimorph piezoelectric elements were determined. The results of numerical simulation are shown in Fig. 5, where, together with the frequency characteristics, the values of the oscillation amplitude of the mechanical system of the engine are also given in the form of a vertical scale with color gradation and numerical values.

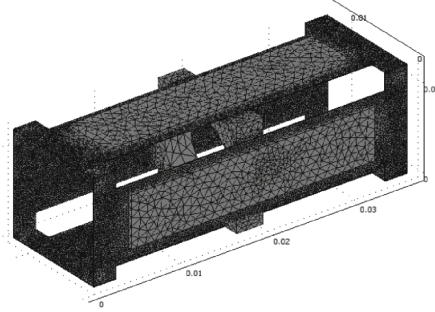


Fig. 4. Model of the piezoelectric motor obtained by the finite element method.

This also made it possible to search for the values of the cutoff frequencies, which are necessary to determine the resonant frequencies in the Frequency response mode. Data analysis of Fig. 5 allows us to establish that the resonant frequencies of the piezoelectric motor design lie approximately in the range of 7000–7300 Hz.

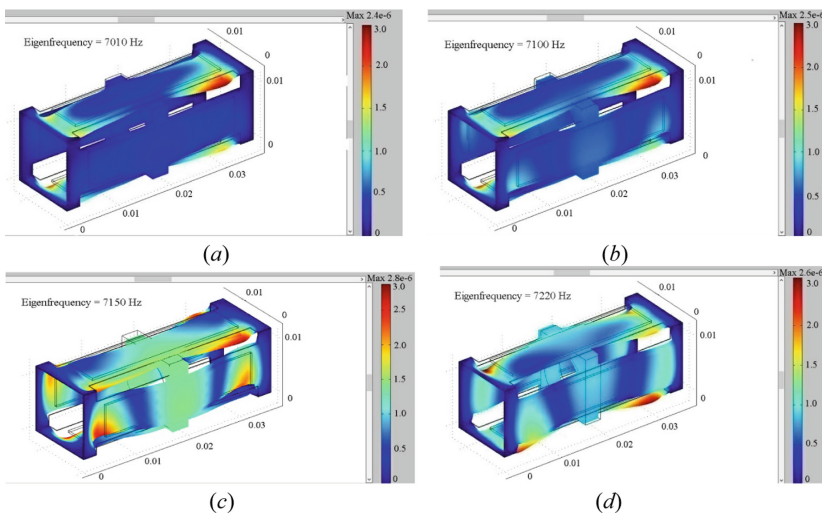


Fig. 5. Results of numerical simulation in the Eigenfrequency Analysis mode with certain natural frequencies of the structure: (a) Eigenfrequency equal to 7010 Hz; (b) Eigenfrequency equal to 7100 Hz; (c) Eigenfrequency equal to 7150 Hz; (d) Eigenfrequency equal to 7220 Hz.

Subsequent calculations were carried out in the Frequency response mode, which made it possible to construct a graph of the amplitude-frequency response (AFR) of the proposed piezoelectric motor, shown in Fig. 6.

In Fig. 6 is shown that the resonant frequencies correspond to 7190 Hz and 7280 Hz. This makes it possible to calculate the maximum oscillation amplitudes of its main elements possible for this engine design.

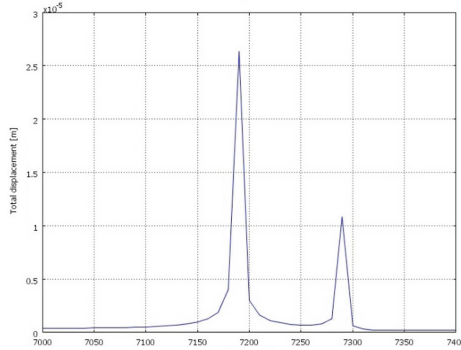


Fig. 6. Frequency response of a piezoelectric motor using bimorph piezoelectric elements.

From Fig. 7 it can be seen that the maximum amplitude of oscillations of the bimorph plates of the piezoelectric motor reaches 2.5×10^{-5} m in their middle part at a resonance frequency of 7190 Hz (see Fig. 7a).

The results of similar numerous experiments for the primary design of a screw piezoelectric motor are presented in Fig. 8. On Fig. 8 is shown that the maximum amplitude of oscillations of the piezoelectric motor plate in the middle part of the structure reaches 2.67×10^{-6} m at a resonant frequency of 20000 Hz.

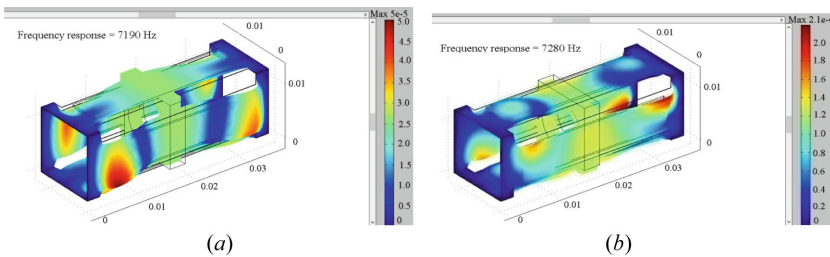


Fig. 7. Results of numerical simulation to determine the resonant amplitude of system oscillations in the Frequency response mode: (a) Frequency response equal to 7190 Hz; (b) Frequency response equal to 7280 Hz.

Based on the simulation results obtained, an experimental sample of a piezoelectric motor based on bimorph piezoelements was developed, shown in Fig. 9.

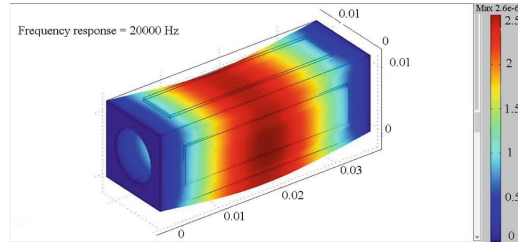


Fig. 8. Results of numerical simulation for determining the resonant amplitude of oscillations of the primary structure system of a screw piezoelectric motor in the frequency response mode.

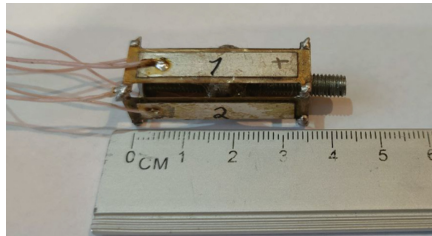


Fig. 9. Experimental sample of the developed linear piezoelectric motor.

In order to prove the adequacy of numerical simulation, experimental studies of the manufactured engine sample were carried out. Due to the significant difficulties in fixing the amplitude of oscillations of the components of the engine structure in the resonant mode of operation, the increase of which was declared for research purposes, a special technique for conducting experiments was created. The main idea of which is to experimentally determine the resonant frequency of a manufactured engine sample and compare it with the theoretically obtained one. It is obvious that it is in this mode that the maximum oscillation amplitude is provided. The experimental procedure is as follows. The experiments were carried out using an intelligent bench complex for the development and research of piezoelectric components [23], created at the Cherkasy State Technological University as part of research work No. 0117U000936. A replaceable electrical voltage in the form of a meander with an amplitude of 12 V was applied to one of the four bimorph plates. Using the direct piezoelectric effect, the electric potential was recorded from the bimorph plate opposite to it using an OWON SDS7102E digital oscilloscope. In Fig. 10 shown the experimental amplitude-frequency characteristic of the engine taken in this way for a potential fixed by the indicated measuring means.

In Fig. 10 convincingly illustrates that the resonant frequencies obtained by mathematical modeling and experimentally practically coincide. There lative comparison errors 0.2%. Therefore, experimental studies confirm the adequacy of the adopted technical solutions.

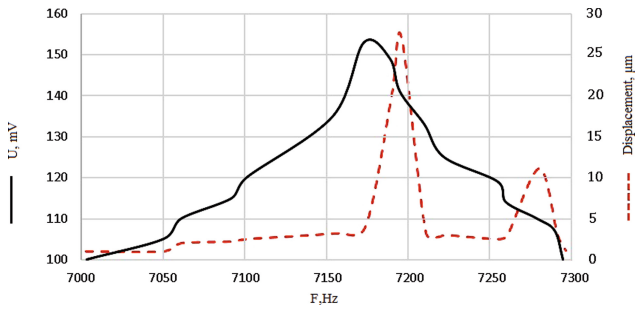


Fig. 10. Experimental and theoretical frequency response of the analyzed sample of the piezoelectric motor.

5 Conclusion

A new original solution for the use of bimorph piezoelements as part of the design of a piezoelectric linear screw engine was proposed and experimentally tested to reduce the effect of stiffeners on its dynamics, which made it possible to increase the amplitude of vibrations of structural elements by approximately 10 times. This is of decisive importance for achieving the maximum torque on the shaft and the pushing (traction) force of the engine. Computer simulation was carried out using the COMSOL Multiphysics 3.5 software package. The frequency at which the maximum amplitudes of oscillations of bimorph piezoelectric plates are provided is determined, which leads to the implementation of the most effective resonant mode of operation of the engine. The data obtained can be used in the design of devices based on linear piezoelectric motors, in particular, in compound dispensers in the agricultural sphere.

In the future, studies are planned aimed at calculating and improving the power characteristics of the developed linear piezoelectric motor of a new design compared to the prototype.

References

1. Donika, M., Balogh, P., Bai, A., et al.: Trends in scientific research on precision farming in agriculture using science mapping method. *Int. Rev. Appl. Sci. Eng.* **11**(3), 232–242 (2020). <https://doi.org/10.1556/1848.2020.00086>
2. Beluhova-Uzunova, R., Dunchev, D.: Precision farming – concepts and perspectives. *Prob. Agri. Econ.* **3**, 142–155 (2019). <https://doi.org/10.30858/zer/112132>
3. Sharapov, V.M., Filimonov, S.A., Sotula, Z.V., et al.: Improvement of piezoceramic scanners. In: 2013 IEEE XXXIII International Scientific Conference Electronics and Nanotechnology (ELNANO), pp. 144–146. IEEE, Kiev (2013). <https://doi.org/10.1109/ELNANO.2013.6552063>
4. Song, S., Shao, S., Xu, M., et al.: Piezoelectric inchworm rotary actuator with high driving torque and self-locking ability. *Sens. Actuators, A* **282**, 174–182 (2018). <https://doi.org/10.1016/j.sna.2018.08.048>
5. Bazilo, C., Filimonov, S., Filimonova, N., Bacherikov, D.: Determination of Geometric Parameters of Piezoceramic Plates of Bimorph Screw Linear Piezo Motor for Liquid Fertilizer Dispenser. In: Hu, Z., Petoukhov, S., Yanovsky, F., He, M. (eds.) *ISEM 2021. LNNS*, vol. 463, pp. 84–94. Springer, Cham (2022). https://doi.org/10.1007/978-3-031-03877-8_8

6. Kiziroglou, M., Temelkuran, B., Yeatman, E., Yang, G.: Micro motion amplification – A review. *IEEE Access* **8**, 64037–64055 (2020). <https://doi.org/10.1109/ACCESS.2020.2984606>
7. Spanner, K., Koc, B.: Piezoelectric motors, an overview. *Actuators* **5**(1), 6 (2016). <https://doi.org/10.3390/act5010006>
8. Hunstig, M.: Piezoelectric inertia motors – A critical review of history, concepts, design, applications, and perspectives. *Actuators* **6**(1), 7 (2017). <https://doi.org/10.3390/act6010007>
9. Brahim, M., Bernard, Y., Bahri, I.: Modelling, design, and real time implementation of robust H-infinity position control of piezoelectric actuator drive. *Int. J. Mechatron. Autom.* **6**(4), 151–159 (2018). <https://doi.org/10.1504/IJMA.2018.095516>
10. Spanner, K., Koc, B.: Piezoelectric motor using in-plane orthogonal resonance modes of an octagonal plate. *Actuators* **7**(1), 2 (2018). <https://doi.org/10.3390/act7010002>
11. Ryndzionek, R., Sienkiewicz, Ł.: A review of recent advances in the single- and multi-degree-of-freedom ultrasonic piezoelectric motors. *Ultrasonics* **116**, 106471 (2021). <https://doi.org/10.1016/j.ultras.2021.106471>
12. Mashimo, T., Izuhara, S.: Review: Recent advances in micromotors. *IEEE Access* **8**, 213489–213501 (2020). <https://doi.org/10.1109/ACCESS.2020.3041457>
13. Chunsheng, Z.: *Ultrasonic Motors: Technologies and Applications*. Springer, Berlin (2011). <https://doi.org/10.1007/978-3-642-15305-1>
14. Shunsuke, I., Tomoaki, M.: Design and characterization of a thin linear ultrasonic motor for miniature focus systems. *Sens. Actuators, A* **329**(4), 112797 (2021). <https://doi.org/10.1016/j.sna.2021.112797>
15. Lu, W., Zhao, L., Jiang, Z., et al.: High accuracy Comsol simulation method of bimorph cantilever for piezoelectric vibration energy harvesting. *AIP Adv.* **9**(9), 095067 (2019). <https://doi.org/10.1063/1.5119328>
16. Halchenko, V., Bondarenko, Y., Filimonov, S., Filimonova, N.: Determination of influence of geometric parameters of piezoceramic plate on amplitude characteristics of linear piezomotor. *Electr. Eng. Electromech.* **2019**(1), 17–22 (2019). <https://doi.org/10.20998/2074-272X.2019.1.03>
17. Halchenko, V., Filimonov, S., Batrachenko, A., Filimonova, N.: Increase the efficiency of the linear piezoelectric motor. *J. Nano Electron. Phys.* **10**(4), 04025 (2018). [https://doi.org/10.21272/jnep.10\(4\).04025](https://doi.org/10.21272/jnep.10(4).04025)
18. Behera, B., Nemade, H.B.: Investigating translational motion of a dual friction-drive surface acoustic wave motor through modeling and finite element simulation. *SIMULATION* **95**(2), 117–125 (2019). <https://doi.org/10.1177/0037549718778770>
19. Sivakumar, N., Kanagasabapathy, H., Srikanth, H.: Analysis of perforated piezoelectric sandwich smart structure cantilever beam using COMSOL. *Mater. Today: Proc.* **5**(5), 12025–12034 (2018). <https://doi.org/10.1016/j.matpr.2018.02.177>
20. Sharapov, V.: *Piezoceramic Sensors*. Springer, Heidelberg (2011). <https://doi.org/10.1007/978-3-642-15311-2>
21. Yu, H., Liu, Y., Tian, X., et al.: A precise rotary positioner driven by piezoelectric bimorphs: Design, analysis and experimental evaluation. *Sens. Actuators, A* **313**(1), 112197 (2020). <https://doi.org/10.1016/j.sna.2020.112197>
22. Bazilo, C.: Modelling of Bimorph piezoelectric elements for biomedical devices. In: Hu, Z., Petoukhov, S., He, M. (eds.) *AIMEE 2019*. AISC, vol. 1126, pp. 151–160. Springer, Cham (2020). https://doi.org/10.1007/978-3-030-39162-1_14
23. Filimonov, S., Bazylo, C., Bondarenko, Y., et al.: Creation of a highly efficient intellectual complex for the development and research of piezoelectric components in instrumentation, medicine and robotics. *Bull. Cherkasy State Technol. Univ.* **3**, 33–43 (2017). [in Russian]



Design of Event Based State Feedback Controller for Linear Time Invariant Systems

Arepalli Vedavyas¹ , Avadh Pati¹ , Sunil Kumar Mishra² ,
and Bhargav Appasani²  

¹ National Institute of Technology, Silchar 788010, India

² Kalinga Institute of Industrial Technology, Bhubaneswar 751024, India
bhargav.appasanifet@kiit.ac.in

Abstract. Control system plays an important role in process automation. This work focuses on designing Event Based State Feedback Control (EBSFC) scheme for controlling Linear Time Invariant (LTI) Systems. The state feedback gain matrix are computed for desired pole placement from pole placement technique. The expressions for triggering and minimum Inter Event Time (IET) are derived for generalized LTI systems. The stability of LTI system with Event Based State Feedback Controller is derived in the sense of Lyapunov stability in the presence of external disturbance. Simulation results are presented for two numerical examples to support the theoretical perspective of the proposed control scheme.

Keywords: State feedback control · Pole placement · Event triggered · Inter event time · Disturbance · Process automation

1 Introduction

The role of control system in process automation for getting desired performance is irreplaceable [1–3]. Discrete periodic implementation of control law is being employed in computer-controlled systems (due to limited processing power). For more resource conservative approach event-based control schemes are addressed in recent years [4–6]. Generally sensing, control signal computation and actuation are the three main steps for implementing and transmitting a control signal. These steps are done at periodic instants due to limited processing power of computers and microprocessors. Although it simplifies the design and analysis, an alternative way of implementing control signal is addressed in recent years [7–9] in which implementation of control is done based on events with benefits like reducing burden on network medium (Wi-Fi, Bluetooth and WLAN etc.). Event Based control (EBC) are aperiodic control schemes that can be used in Network Control Systems (NCS) so that the three steps (form implementing control signal) will be executed whenever there is need. Main difference between time triggered and event triggered/based control is at sensor's mechanism. In the first one sensor measures states or output periodically on the other hand in EBC paradigm sensor will transfer data only when the triggering condition is violated which is generally a function of states or output or a threshold value as shown in [10, 11]. EBC scheme is

inspired from lebesgue sampling technique. Several research are showing interest in EBC schemes due to its responsive nature and its important advantage like reducing network burden (by transmitting data at only triggering instants) and decreasing power consumption so that self-powered remote sensor's battery's lifetime can be increased [12].

State feedback control (SFC) is a control scheme which involves the usage of state vectors to compute the control signal which is used to change the closed loop dynamics of the system. The SFC scheme considered here is pole placement like technique in which control signal is a linear multiplication of matrix K and instantaneous values of states. In continuous time domain, states are available at every instant but in discrete domain availability of states depends on sampling time (in discrete periodic paradigm). In Event based control paradigm (aperiodic discrete) the states are available only when at the triggering instants which depends on violation of triggering condition. The important point to be noted here is states are sampled based on the violation of triggering condition, so the states are fed back aperiodically (but not periodically) through a gain matrix to change the systems to change the system's dynamics.

The organization of this paper is as follows: The notations, assumptions, and basics of and difference between Time-triggered State feedback control (TTSFC) and EBSFC are discussed in Sect. 2. In Sect. 3 theoretical results of the paper are presented regarding triggering condition and minimum IET. Section 4 shows two examples to support the theoretical perspective and discuss how ECSFC behaves and what more can be expected. Finally, in Sect. 5 conclusion, remarks and ideas regarding this work are discussed.

2 Notations and Problem Formulation

Consider a LTI system in state-space representation as shown

$$\dot{x}(t) = Ax(t) + B(u(t) + d(t)), \quad (1)$$

where $A \in R^{n \times n}$ and $B \in R^{n \times 1}$ are constant matrices, $x \in R^{n \times 1}$ is state vector, $u \in R$ is the control signal and $d(t)$ is the bounded matched disturbance with $\|d(t)\| \leq d_0$ (d_0 is the upper bound of disturbance). $\|\cdot\|$ is Euclidean norm.

Assumptions

1. In this work it is assumed that all states are available readily for measurement.
2. A, B pair are controllable.

The control law for state feedback technique is

$$u(t) = -Kx(t). \quad (2)$$

In C.T domain states should be available for every instant so that Control law can be calculated. In event paradigm states are available only at instants at which event condition is violated. So for event paradigm control law at triggering instants given as

$$u(t) = -Kx(t_e) \forall t \in [t_e, t_{e+1}], \quad (3)$$

where t_e is the time at which the event condition is violated in literature is termed as triggering instant as it's the instant at which event is triggered for the calculation of control law. In practical situations a small amount of delay exists between the triggering instant and actuation (delays like transmission delay and time required for processing). In this work delays and data loss are not considered. Between triggering instants zero order hold (ZOH) is used just like in discrete time system at every instant t_e control law is updated. The measurement error ($M_e(t)$) for sampled states are defined for system is

$$M_e(t) = x(t) - x(t_e) \forall t \in [t_e, t_{e+1}]. \tag{4}$$

Above equation plays a very important role in stabilization of the problem and it is not the error caused by noise. It is the difference between previously sent state data and current data of state and its order is same as of state vector.

3 Event Paradigm Based State Feedback Control Technique

The state feedback control technique is updated at only triggering instants which is based on violation of the triggering condition. For deriving event triggering condition, in this work Lyapunov stability criterion is used. Lyapunov function selected is

$$V = \frac{1}{2}x^2(t). \tag{5}$$

On differentiating the above equation, we get:

$$\dot{V} = x^T(t)\dot{x}(t), \tag{6}$$

$$\dot{V} = x^T(t)(Ax(t) + B(u(t) + d(t))). \tag{7}$$

From Eq. (3) and (7) we get

$$\dot{V} = x^T(t)(Ax(t) + B(-Kx(t_e) + d(t))). \tag{8}$$

From Eq. (4) and (8) results

$$\dot{V} = x^T(t)(Ax(t) - BK(x(t) - M_e(t)) + Bd(t)). \tag{9}$$

By solving Eq. (9) we get Eq. (10) which gives two cases for making \dot{V} negative definite so that system will be stable when EB-SFC is used. Furthermore, for making system stable how much measurement error can be allowed can be derived.

$$\dot{V} = x^T(t)(A - BK)x(t) + x^T(t)BKM_e(t) + x^T(t)Bd(t). \tag{10}$$

Choosing K matrix such that $x^T(t)(A - BK)x(t)$ is negative definite.

– Case 1:

if $x^T(t)BKM_e(t) < 0$ and $x^T(t)Bd(t) < 0$ then $\dot{V} < 0$ then system is stable;

- *Case 2:*
when $x^T(t)(A - BK)x(t)$ is negative definite if

$$x^T(t)(A - BK)x(t) > x^T(t)BK M_e(t) + x^T(t)Bd(t), \quad (11)$$

then $\dot{V} < 0$ which results the stability of system. From Eq. (11) by solving for $M_e(t)$ then the inequality obtained Eq. (12) and norm of (12) gives the triggering condition Eq. (13):

$$M_e(t) < (2BK - A)^{-1}((A - BK)x(t_e) - Bd), \quad (12)$$

$$\|M_e(t)\| < \left\| (2BK - A)^{-1}((A - BK)x(t_e) - Bd) \right\|, \quad (13)$$

$$\|M_e(t)\| < \gamma \|(2BK - A)^{-1}((A - BK)x(t_e) - Bd)\|, \gamma \in (0, 1). \quad (14)$$

The Eq. (14) is the triggering condition by which the following remarks are made:

- γ is constant introduced for improve the closeness of performance of Event based control and Continuous control;
- the measurement error's bound should be less as shown in (13) then $\dot{V} < 0$ so that system will be stable;
- selection K must be done such that $[2BK - A]$ is a full rank matrix and $[A - BK]$ is a negative definite matrix;
- new triggering instant is given as

$$t_{e+1} = \inf\{t \in]t_e, \infty[: \|M_e(t)\| < \gamma \left\| (2BK - A)^{-1}((A - BK)x(t_e) - Bd) \right\|\}. \quad (15)$$

The triggering instants relative threshold i.e. the threshold value of the measurement error is not fixed and it depends on the previously sent state data.

From the Eq. (15), the simplified triggering condition is:

$$S1(x(t_e)) = \gamma \|(2BK - A)^{-1}((A - BK)x(t_e) - Bd)\|. \quad (16)$$

To avoid the Zeno phenomenon effect in Event paradigm control there should be minimum amount of inter event time (IET) so that there won't be infinite number of control executions in a finite period of time. The minimum inter event time is derived using [5]

$$\frac{d}{dt}\|M_e(t)\| \leq \left\| \frac{d}{dt}M_e(t) \right\|. \quad (17)$$

Considering (17) to calculate the maximum growth of measurement error as

$$\frac{d}{dt}\|M_e(t)\| \leq \left\| \frac{d}{dt}M_e(t) \right\|,$$

$$\begin{aligned} \left\| \frac{d}{dt} M_e(t) \right\| &= \left\| \frac{d}{dt} (x(t) - x(t_e)) \right\| = \left\| \frac{d}{dt} (x(t)) \right\|, \\ &\leq \|Ax(t) + B(u(t) + d(t))\|, \\ &\leq \|AM_e(t)\| + \|(A - BK)x(t_e)\| + \|B\|d_0. \end{aligned} \tag{18}$$

Let $S2(x(t_e)) = \|(A - BK)x(t_e)\|$ and $S3 = \|B\|d_0$ then (18) can be written as

$$\frac{d}{dt} \|M_e(t)\| \leq \|A\| \|M_e(t)\| + S2(x(t_e)) + S3. \tag{19}$$

Using a comparison lemma [13], the Eq. (19) can be simplified for initial conditions

$$M_e(t_e) = x(t_e) - x(t_e) = 0. \tag{20}$$

By solving (19) we get:

$$\|M_e(t)\| \leq \frac{S2(x(t_e)) + S3}{\|A\|} \left(e^{\|A\|(t-t_e)} - 1 \right). \tag{21}$$

From (16) and (21) we get

$$S1(x(t_e)) = \|M_e(t)\| \leq \frac{S2(x(t_e)) + S3}{\|A\|} \left(e^{\|A\|(t-t_e)} - 1 \right). \tag{22}$$

By solving (22) for $T_i = t - t_e$, Minimum IET will be:

$$T_i \geq \frac{1}{\|A\|} \ln \left[1 + \frac{S1(x(t_e)) \|A\|}{S2(x(t_e)) + S3} \right]. \tag{23}$$

From Eq. (23) it is proven that there will be at least a minimum time will be there so that Zeno phenomenon will be avoided.

4 Simulation Results and Discussions

To validate the proposed scheme, two examples are considered, and theoretical perspective of the proposed work is discussed with simulation results of these two considered systems with and disturbance conditions.

Example 1: Consider a second order LTI system represented in state space as shown:

$$\dot{x}(t) = \begin{bmatrix} 0 & 1 \\ 2 & 3 \end{bmatrix} x(t) + \begin{bmatrix} 0 \\ 1 \end{bmatrix} (u_1(t) + d_1(t)).$$

Here disturbance $d_1(t) = 0.2\text{sint}$ ($d_{01} = 0.2$). The poles of the system are: -0.5616 and 3.5616 , with Initial Conditions: $x_1(0) = 1$ and $x_2(0) = 0.5$. . To make systems stable gain matrix is chosen same as in pole placement. For system the desired pole locations are at $[-1 -2]$. The SFC gain matrices for system 1 is $K_1 = [4 \ 6]$. Control signal for system 1 is:

$$u_1(t) = -4x_1(t_e) - 6x_2(t_e).$$

The simulation results are plotted for example 1 for two cases $\gamma = 0.9$ and 0.5 :

a. Simulation Results with $\gamma = 0.5$

The Fig. 1a and b are plotted for evolution of states of the example 1 with event based domain (EBD) and continuous time domain (CTD). The control Signal and Sampling intervals are given in Fig. 1c and d when $\gamma = 0.5$. The state’s decaying nature ensures that system is stable but not accurately close enough to the pole we want. The reason is the control signal is not available for the system at every instant but available only when the event condition is violated (14).

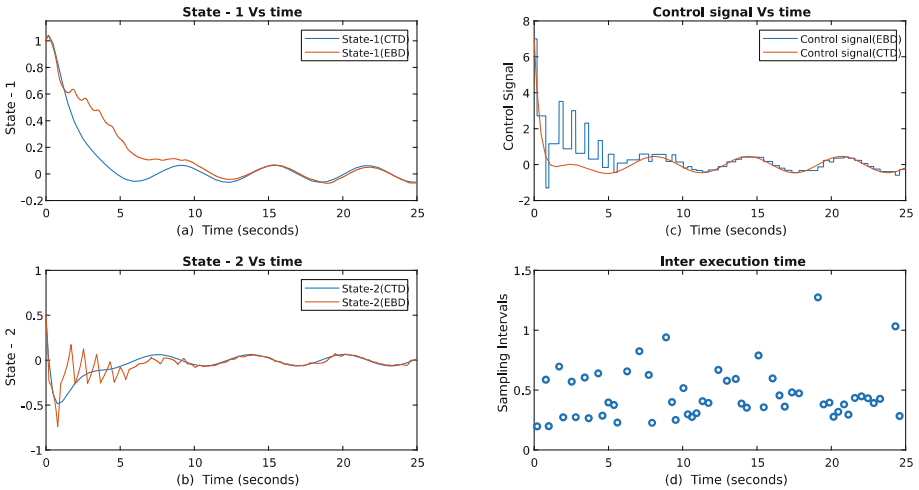


Fig. 1. (a) and (b) Evolution of states of event based domain (EBD) and continuous domain (CTD) with respect to time (sec), (c) Control Signal evolution with respect to time (sec) and (d) Time between two intervals of control signal execution. (In presence of disturbance $d_1(t) = 0.2\text{sint}$ and $\gamma = 0.5$).

b. Simulation Results with $\gamma = 0.9$

The Fig. 2a and b are plotted for evolution of states of the example 1 with event based domain (EBD) and continuous domain (CTD). The control Signal and Sampling intervals are given in Fig. 2c and d (with disturbance $d_1(t) = 0.2\text{sint}$ ($d_{01} = 0.2$)) when $\gamma = 0.9$.

The state’s decaying nature ensures that system is stable with a bound which is due to disturbance. In this case, EBD control signal could not make its states as close as the CTD states this is because the measurement error’s bound (14) is increased without making system unstable. In other words, this can be the least expected performance without making system unstable.

By observing IET plot of system with $\gamma = 0.9$ and $\gamma = 0.5$ it is seen that IET of $\gamma = 0.5$ has lower highest IET value than that of $\gamma = 0.9$ but number of instants is almost same for 25 s and the between successive events IET is more in case of $\gamma = 0.9$.

So it is recommended that if the performance of the system is prioritized γ should be close to 0 than to one but the price we pay to achieve is lesser IETs. On the other hand, if usage of network, communication and computational power shouldn’t be more frequent then γ must be closer to 1 than to 0.

Example 2: Consider a 2-dimensional linearized Moving Cart Inverted Pendulum (IVP) in state space representation [14]:

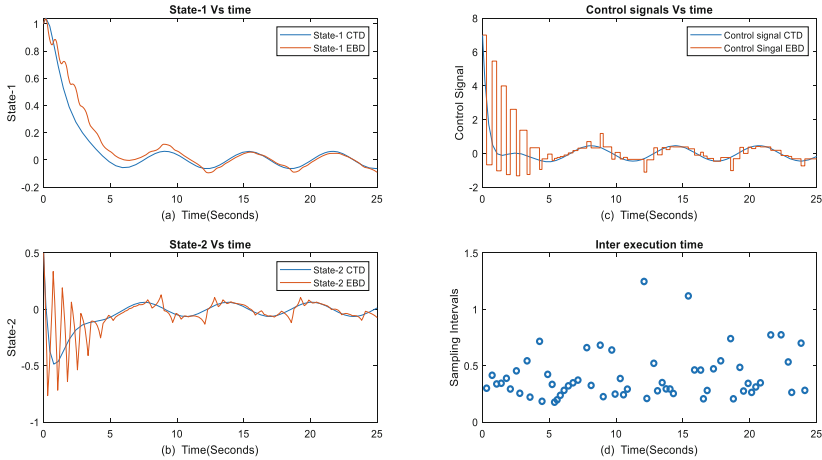


Fig. 2. (a) and (b) Evolution of states of event based domain (EBD) and continuous domain (CTD) with respect to time(sec), (c) Control Signal evolution with respect to time (sec) and (d) Time between two intervals of control signal execution. (In presence of disturbance $d_1(t) = 0.2sint$ and $\gamma = 0.9$).

$$\dot{z}(t) = \begin{bmatrix} 0 & 1 & 0 & 0 \\ 20.601 & 0 & 0 & 0 \\ 0 & 0 & 0 & 1 \\ -0.4905 & 0 & 0 & 0 \end{bmatrix} z(t) + \begin{bmatrix} 0 \\ -1 \\ 0 \\ 0.5 \end{bmatrix} (u_2(t) + d_2(t)).$$

Here disturbance $d_2(t) = 0.5sint$ ($d_{02} = 0.5$). The poles of the system are: 4.5388, -4.5388, 0 and 0, with Initial Conditions: $z_1(0) = 1.5, z_2(0) = 0.1, z_3(0) = 0.5, z_4(0) = 0.1$. . To make systems stable gain matrices are chosen same way as in classical control.

For system the desired pole locations are at $[-1 + i\sqrt{3} -1 -i\sqrt{3} -5 -5]$. The SFC gain matrices for system 1 is $K_2 = [-157.6336 -35.3733 -56.0652 -36.7466]$. Control signal for example 2 is:

$$u_2(t) = 157.6336z_1(t_e) + 35.3733z_2(t_e) + 56.0652z_3(t_e) + 36.7466z_4(t_e).$$

Figure 3a and b shows that both EBD and CTD states are decaying in almost similar way, which shows system is stable. When $\gamma=0.9$ the states of both CTD and EBD are almost similar the reason is the overall amplitude of the state’s behavior at transient time is more compared to the example 1. Note that this is the least expected performance as $\gamma = 0.9$ when compared to $\gamma =0.5$. So γ will depend on system, it may differ for different systems even for same performance. Figure 3c and d shows control signal and IETs for example 2. Here it is shown that for a system like inverted pendulum which is highly nonlinear and unstable system is made stable using EB-SFC but to achieve this the time between successive event is very less when compared to system 1. So while designing the control simulation results are very important for the systems like IVP so that the control engineer could compare periodic and event based control.

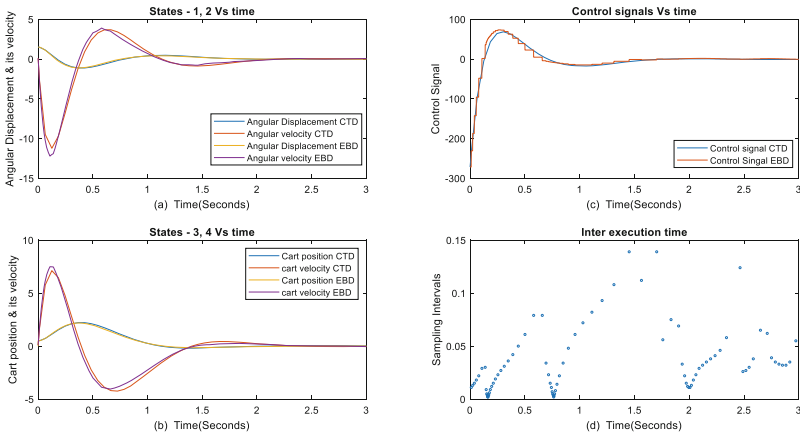


Fig. 3. (a) Angular Displacement and velocity of pendulum evolution with respect to time; (b) Position and velocity of cart evolution with respect to time; (c) Control Signal evolution with respect to time; (d) Time between two intervals of control signal execution. (In presence of disturbance $d_2(t) = 0.5sint$ and $\gamma = 0.9$).

5 Conclusion

In this paper, an Event Based State Feedback Control (EBSFC) scheme is designed for Linear Time Invariant (LTI) System. Mathematical expressions of Event condition and IET of EB-SFC are derived for generalized LTI systems. It is also shown that upon violation of event condition the control law will be applied to the system to make overall performance of the system like CTD in means of γ . . Furthermore, the designed control

scheme is applied on two unstable systems with external disturbances. The simulation results are plotted for event-based domain (EBD) and continuous time domain (CTD) and state that how EB-SFC behaves when the gain matrix of continuous time system is used. The designed controlled scheme gives better result, and it is also tested by two numerical examples but in practical application, the proposed scheme may not be work up-to mark as time delay and data loss are not included in this work as these are very common problem in network control systems. If time delay and data loss are included during the designing of controller, possibly achieve better results for any network control system.

References

1. Heemels, W.P., Johansson, K.H., Tabuada, P.: An introduction to event-triggered and self-triggered control. In: 2012 IEEE 51st IEEE Conference on Decision and Control (CDC), pp. 3270–3285. IEEE, Maui (2012). <https://doi.org/10.1109/CDC.2012.6425820>
2. Su, H., Zhang, H., Jiang, H., Wen, Y.: Decentralized event-triggered adaptive control of discrete-time nonzero-sum games over wireless sensor-actuator networks with input constraints. *IEEE Trans. Neural Networks Learn. Syst.* **31**(10), 4254–4266 (2020). <https://doi.org/10.1109/TNNLS.2019.2953613>
3. Maier, R.: Event-triggered communication on top of time-triggered architecture. In: 21st Digital Avionics Systems Conference, vol. 2, p. 13C5. IEEE, Irvine (2002). <https://doi.org/10.1109/DASC.2002.1053011>
4. Zhuang, W., Liu, Z., Su, H., Zhang, Q.: Event-triggered output feedback control for a class of discrete-time nonlinear systems. In: 2019 Chinese Control Conference (CCC), pp. 739–744. IEEE, Guangzhou (2019). <https://doi.org/10.23919/ChiCC.2019.8866152>
5. Zhu, M., Fan, Y., Chen, J.: Event-triggered and self-triggered control for linear system based on new event condition. In: 2019 Chinese Control Conference (CCC), pp. 4265–4269. IEEE, Guangzhou (2019). <https://doi.org/10.23919/ChiCC.2019.8865910>
6. Abdolmaleki, B., Seifi, A., Arefi, M.M., Shafiee, Q.: Event-triggered voltage control of inverter-based microgrids. In: 2018 9th Annual Power Electronics, Drives Systems and Technologies Conference (PEDSTC), pp. 522–528. IEEE, Tehran (2018). <https://doi.org/10.1109/PEDSTC.2018.8343851>
7. Zhao, Y.B., Liu, G.P., Rees, D.: Packet-based deadband control for internet-based networked control systems. *IEEE Trans. Control Syst. Technol.* **18**(5), 1057–1067 (2009). <https://doi.org/10.1109/TCST.2009.2033118>
8. Kumar, N., Porwal, A., Singh, A.R., et al.: Event triggered control of robot manipulator. In: 2019 6th International Conference on Signal Processing and Integrated Networks (SPIN), pp. 362–366. IEEE, Noida (2019). <https://doi.org/10.1109/SPIN.2019.8711653>
9. Li, H., Fan, Y., Pan, G., Song, C.: Event-triggered remote dynamic control for network control systems. In: 2020 16th International Conference on Control, Automation, Robotics and Vision (ICARCV), pp. 483–488. IEEE, Shenzhen (2020). <https://doi.org/10.1109/ICARCV50220.2020.9305348>
10. Behera, A.K., Bandyopadhyay, B.: Event based robust stabilization of linear systems. In: IECON 2014—40th Annual Conference of the IEEE Industrial Electronics Society, pp. 133–138. IEEE, Dallas (2014). <https://doi.org/10.1109/IECON.2014.7048489>
11. Xing, L., Wen, C., Liu, Z., et al.: An event-triggered design scheme for spacecraft attitude control. In: 2017 12th IEEE Conference on Industrial Electronics and Applications (ICIEA), pp. 1552–1557. IEEE, Siem Reap (2017). <https://doi.org/10.1109/ICIEA.2017.8283085>

12. Feeney, L.M., Nilsson, M.: Investigating the energy consumption of a wireless network interface in an ad hoc networking environment. In: Proceedings IEEE INFOCOM 2001. Conference on Computer Communications. Twentieth Annual Joint Conference of the IEEE Computer and Communications Society (Cat. No. 01CH37213), vol. 3, pp. 1548–1557. IEEE, Anchorage (2001). <https://doi.org/10.1109/INFCOM.2001.916651>
13. van de van de Wouw, N., Lefeber, E., Lopez Arteaga, I. (eds.): Nonlinear systems. LNCIS, vol. 470. Springer, Cham (2017). <https://doi.org/10.1007/978-3-319-30357-4>
14. Katsuhiko, O.: Modern Control Engineering. Pearson (2010)



Interpretation of Dynamic Models Based on Neural Networks in the Form of Integral-Power Series

Oleksandr Fomin^(✉) , Sergii Polozhaenko , Valentyn Krykun , Andrii Orlov ,
and Daria Lys 

Odessa Polytechnic National University, 1 Shevchenko Avenue, Odessa 65044, Ukraine
fomin@op.edu.ua

Abstract. The paper is devoted to the problem of interpretation the dynamic models based on neural network. Proposed approach is conclude in the building of the interpretive model in the form of an analytical integral-power series, saving the dynamic and nonlinear properties of the primary neural network model. The purpose of the paper is development a method for interpreting dynamic models based on neural networks, providing high accuracy of the interpreting models construction. Scientific novelty consists in using of intego-power series in the form of multidimensional weight functions to build analytical models that interpret dynamic neural networks. This method allows to obtain an interpretation of dynamic neural network models while preserving their nonlinear and dynamic properties. Practical usefulness of the developed method consists in providing high accuracy and speed of interpreting models construction, allows to provide modeling of nonlinear dynamic states of objects in both test and functional modes of operation. The proposed method tested on the data of a test nonlinear dynamic object. The results of the experiment demonstrate high accuracy and speed of construction of analytical interpreting models.

Keywords: Explainable neural networks · Nonlinear continuous objects · Time delay neural networks · Multidimensional weight functions

1 Introduction

Modern processes of development, production and operation in most industries are characterized by the increasing role of modeling in the tasks of determining the type of technical state of objects, finding the locations and causes of faults. At the same time, of great interest are applied tasks of modeling complex technical and biological objects belonging to the class of nonlinear dynamic objects with continuous characteristics and unknown structure. Such objects are usually considered as a “black box” [1–3]. Examples of such objects in industry are electric motors [4], cutting tools in metal processing systems [5], in biomedicine – objects of living nature [6], in economics – econometric objects [7] etc.

When modeling black-box-type objects, the neural network approach is widespread, since the process of model building in this case requires only the measurement of input and output data of the object.

Recently, the use of neural networks to describe objects of non-linear dynamic objects with continuous characteristics has expanded significantly. This is due to the fact that complex objects are characterized by some a priori uncertainty: the lack of data on the object, the presence of interference and environmental disturbances. Traditional deterministic methods are not suitable for modeling such objects, while the ability of neural networks to learn under such conditions allows us to obtain good results in most problems.

The purpose of the paper is development a method for interpreting dynamic state models in the form of neural networks, providing high accuracy of the interpreting models construction.

2 Literature Review

Models do not always need interpretation [8–11]. Linear models and low-dimensional decision trees, kNN models [12], when working with features understandable to the researcher are themselves understandable to the researcher and need additional interpretation.

In cases where the use of interpreted models alone does not lead to a satisfactory result, for example when modeling complex objects with nonlinear and dynamic properties, more complex methods, in particular machine learning, are increasingly used [13, 14]. The result is models whose principles are not obvious, and whose features often do not make physical sense.

To interpret such models, one can use interpretable machine learning methods, e.g., LIME or linear regression [15–17], which build surrogate models that locally approximate the original model to a linear one. Another popular approach is based on estimating the importance of features to explain individual model predictions, the SHAP method [18].

The disadvantage of such approaches is that interpolation in these cases reveals the features affecting the model performance, but does not reflect the functional dependence of the result on the revealed features.

Among machine learning models it is important to distinguish neural network models. The relevance of the task of interpreting neural networks is increasing due to the fact that neural networks, which can carry reliable information about the structure and functions of the control object, are increasingly used to model complex objects.

A number of scientific publications are devoted to interpretation of neural network models. Interpretation methods of convolutional neural networks working with visual information images and video [19], sound and speech [20], textual data [21] are widely known. These methods of interpretation are based on visualization of decision-making processes.

Complex objects and processes of the surrounding world (technical and biological objects of control, means of production, control and automation) usually have simpler models based on neural networks [22–24]. Despite this, the methods for interpreting

such models are much less represented in the literature and are usually reduced to linearization [14] or polynomial approximation [25, 26] of neural network models. In this case interpretable models, as a rule, have the form of linear dynamic or nonlinear static dependences, which do not reflect all properties of a real object.

This problem can be solved by using integral-power series based on multidimensional weight functions as interpreting models. The main advantage of these interpretable models is the simultaneous consideration of nonlinear and dynamic properties of the object under study, which provides increasing the accuracy of these models.

As a result of the analytical review of the current state of the problem of interpreting models based on neural networks, the article proposes an approach to building interpreting models based on integral-power series based on multidimensional weight functions. The use of this approach allows to provide simultaneously high accuracy and speed of interpretation of complex research objects.

3 Models of Nonlinear Dynamic Objects with Continuous Characteristics and Unknown Structure

3.1 Models Based on Neural Networks

A simple and effective means for modeling nonlinear dynamic objects with continuous characteristics are time-delay neural networks (TDNN) in the form of three-layer architecture with direct signal propagation [27–29].

The input-output relation for such a model with M inputs and one output is written in the form:

$$y(n) = b_0 + s_0 \sum_{i=0}^K r_i^2 S_i \left(b_i + \sum_{j=0}^M r_{i,j}^1 x(n-j) \right), \tag{1}$$

where b_0, b_i – bias of the output layer neuron and input layer neurons accordingly; S_0, S_i – activation functions of the output layer neuron and input layer neurons accordingly; $r_i^2, r_{i,j}^1$ – weighing coefficients of the output layer neuron and input layer neurons accordingly; K – number of neurons in the input layer.

The output signal is generated by a single neuron, which most often has a linear activation function. The input signal in the form of consecutive sets of input data, shifted one relative to another by one value from the input set, arrives at the neurons of the input layer of the neural network.

If the activation function has the form of a polynomial activation or a hyperbolic tangent function, the “input-output” relation for a three-layer TDNN with M inputs and one output has the form of expressions (2) and (3), respectively [19].

$$y(n) = b_0 + s_0 \sum_{i=0}^K r_i^2 S_i \left(b_i + \sum_{j=0}^M r_{i,j}^1 x(n-j) \right)^n, \tag{2}$$

$$y(n) = b_0 + s_0 \sum_{i=0}^K r_i^2 \text{thn} \left(b_i + \sum_{j=0}^M r_{i,j}^1 x(n-j) \right). \tag{3}$$

This paper does not consider many other classes of neural nets: with several hidden layers, non-significant activation functions, non-deterministic wagons, bell-coupled ones, and so on. They lead to a much more complicated relationship with the discrete Volterra models.

3.2 Models in the Form of Integral-Power Series Based on Multidimensional Weight Functions

For a wide class of nonlinear dynamic objects with continuous characteristics, the dependence between the input $x(t)$ and the output $y(t)$ signals can be written in the form of an integral-power series based on multidimensional weight functions [3, 23, 24, 27]. Thus, for an object with one input and one output in the time domain, the model takes the following form:

$$y(t) = \sum_{n=0}^{\infty} \int_0^t \dots \int_0^t w_n(t, \tau_1, \dots, \tau_n) \prod_{i=1}^n x(\tau_i) d\tau_i, \tag{4}$$

where $x(t)$ and $y(t)$ – input and output signals of the object; $w_n(\tau_1, \dots, \tau_n)$ – multidimensional weight function of the n -th order ($n = 1, 2, 3, \dots$); w_0 – free member of the series; t – current time.

The use of models in the form of integral-degree series is a universal form of representation of the properties of nonlinear dynamic objects with continuous characteristics. To build an interpretive model of a neural network in the form of an integral-power series using multidimensional weighting functions, it is necessary to establish an analytical connection between these models.

3.3 Relationship of Time-Delayed Neural Nets and Integral Models Based on Multidimensional Weight Function

Analyzing the expression (1) and (4) we can conclude that its structure is equivalent. This means that the values of multivariate weight functions can be expressed in terms of the coefficients $r_{i,j}^1$ and r_i^2 , c_h and the bias of the neurons b_j of the network [15, 21, 24]. For an activation function in the form of a second-degree polynomial, this expression can be represented as follows:

$$y(n) = b_0 + s_0 \sum_{i=0}^K c_0 r_i^2 b_i^3 + \sum_{i=0}^K c_1 r_i^2 \sum_{j=0}^M \left(r_{i,j}^1 x(n-j) \right)^3 + \sum_{i=0}^K c_2 r_i^2 b_i^3 \sum_{j=0}^M r_{i,j}^1 x(n-j) + \sum_{i=0}^K c_3 r_i^2 b_i \sum_{j_1=0}^M \sum_{j_2=0}^M r_{i,j_1}^1 r_{i,j_2}^1 x(n-j_1) x(n-j_2). \tag{5}$$

This expression gives estimations of 0–2 orders multivariate weight functions based on TDNN coefficients obtained from network training:

$$w_0 = b_0 + \sum_{i=0}^K c_0 r_i^2 b_i^3, \quad w_1(k) = \sum_{i=0}^K c_1 r_i^2 b_i^2, \quad w_2(k_1, k_2) = \sum_{i=0}^K c_3 r_i^2 b_i \sum_{j_1=0}^M \sum_{j_2=0}^M r_{i,j_1}^1 r_{i,j_2}^1. \tag{6}$$

The method for interpretation of dynamic models based on neural networks in the form of integral-power series is tested on a diagnostic object with nonlinear dynamic characteristics.

4 Results

The accuracy of the proposed method for interpreting models construction is investigated on the example of a nonlinear dynamic diagnostic object of the first order with quadratic nonlinearity in the feedback [26] (Fig. 1).

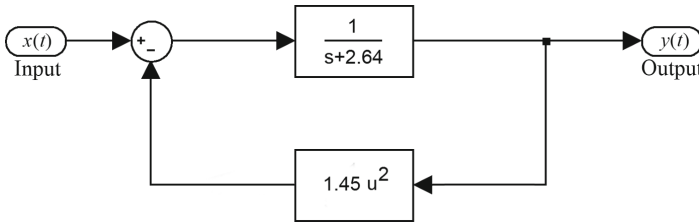


Fig. 1. Structure diagram of the diagnostic object with nonlinear dynamic characteristics.

The analytical expressions for the multivariate weight function of the first order $w_1(t)$ and diagonal section of multidimensional weight function ($\tau_1 = \tau_2 = t$) of the second order $w_2(t, t)$:

$$w_1(\tau_1) = e^{-\alpha\tau_1}, \tag{7}$$

$$w_2(t, t) = \frac{\beta}{\alpha}(e^{-2\alpha t} - e^{-\alpha t}). \tag{8}$$

As a result of the experiment, a TDNN was created and trained. On the basis of the coefficients of the trained neural network $r_{i,j}^1$ and r_i^2 , c_h and b_j the coefficients of the integro-power series using expressions (4) are determined. The resulting model is interpretive for the original TDNN model.

To analyze the accuracy of the interpretive model, the multivariate weight function $w_1(t)$ and the diagonal section of the multivariate weight function $w_2(t, t)$ obtained analytically (7), (8) and obtained by interpreting the trained TDNN (4) are compared. Both resulting models are presented in Fig. 2.

The percentage normalized root-mean-square error was used as a criterion for the accuracy of the interpretive model. The obtained results allow to get nonlinear dynamic model in the form of integral-power series with an expected accuracy of 5–9% as compared to the analytical model. The results of the experiment demonstrated the accuracy of the interpreting model based on integral-power series in the form of multidimensional weight functions (1) within 5–9% with compared to the analytical model.

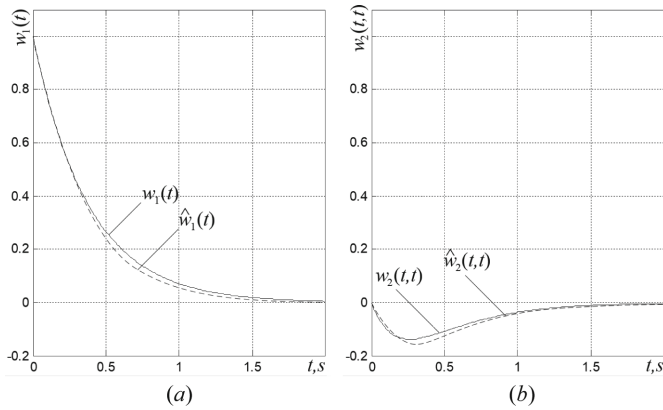


Fig. 2. Comparison of analytical and experimental estimation of the model: (a) first-order multidimensional weight function $w_1(t)$ and its estimation $\hat{w}_1(t)$; (b) the diagonal section of second order multidimensional weight function $w_2(t,t)$ and its estimation $\hat{w}_2(t,t)$.

5 Conclusion

The results of this study are as follows.

- a method for interpreting TDNN neural network models has been developed. The interpreting model is constructed in the form of integral-power series based on multivariate weight functions;
- the interpreted models in the form of integral-power series are able to obtain the acceptable identification accuracy with the preservation of nonlinear and dynamic properties of the object. The method allows to build interpretation models of an object both in test and functional modes;
- the speed of construction of the interpretive model is limited by the training time of the neural network. Therefore, the direction of further research can be methods of increasing the learning speed of TDNN;
- the experimental researches of the offered method of construction of the interpreted model of the diagnostic nonlinear dynamic object show the deviations on 5–9% in comparison with the analytical model of the object.

Thus, the problem of interpretation the dynamic models based on neural network is solved using explainable models in the form of integral-power series based on multivariate weight functions. The method of high accuracy of the interpreting models construction with the preservation of nonlinear and dynamic properties of the object is developed.

References





1. Rudin, C., Radin, J.: Why are we using black box models in AI when we don't need to? A lesson from an explainable AI competition. *Harvard Data Sci. Rev.* **1**(2), 1 (2019). <https://doi.org/10.1162/99608f92.5a8a3a3d>

2. Guidotti, R., Monreale, A., Ruggieri, S., et al.: A survey of methods for explaining black box models. *ACM Comput. Surv.* **51**(5), 93 (2018). <https://doi.org/10.1145/3236009>
3. Favier, G., Kibangou, A.Y., Bouilloc, T.: Nonlinear system modeling and identification using Volterra-PARAFAC models. *Int. J. Adapt. Control Signal Process.* **26**(1), 30–53 (2012). <https://doi.org/10.1002/acs.1272>
4. Fomin, O., Rudkovskiy, O., Ruban, O.: Method for construction the diagnostic features space of switched reluctance motors based on integral dynamic models. *Problemele Energeticii Regionale* **48**(4), 35–44 (2020). <https://doi.org/10.5281/zenodo.4316968>
5. Fomin, O., Derevianchenko, O.: Improvement of the quality of cutting tools states recognition using cloud technologies. In: Ivanov, V., Trojanowska, J., Pavlenko, I., Zajac, J., Peraković, D. (eds.) *DSMIE 2020. LNME*, pp. 243–252. Springer, Cham (2020). https://doi.org/10.1007/978-3-030-50794-7_24
6. Petch, J., Di, S., Nelson, W.: Opening the black box: the promise and limitations of explainable machine learning in cardiology. *Can. J. Cardiol.* **38**(2), 204–213 (2021). <https://doi.org/10.1016/j.cjca.2021.09.004>
7. Mullainathan, S., Spiess, J.: Machine learning: An applied econometric approach. *J. Econ. Persp.* **31**(2), 87–106 (2017). <https://doi.org/10.1257/jep.31.2.87>
8. Marton, S., Lüdtke, S., Bartelt, C.: Explanations for neural networks by neural networks. *Appl. Sci.* **12**(3), 980 (2022). <https://doi.org/10.3390/app12030980>
9. Samek, W., Montavon, G., Lapuschkin, S., et al.: Explaining deep neural networks and beyond: A review of methods and applications. *Proc. IEEE* **109**(3), 247–278 (2021). <https://doi.org/10.1109/JPROC.2021.3060483>
10. Miller, T.: Explanation in artificial intelligence: Insights from the social sciences. *Artif. Intell.* **267**, 1–38 (2019). <https://doi.org/10.1016/j.artint.2018.07.007>
11. Tsoka, T., Ye, X., Chen, Y., et al.: Explainable artificial intelligence for building energy performance certificate labelling classification. *J. Clean. Prod.* **355**, 131626 (2022). <https://doi.org/10.1016/j.jclepro.2022.131626>
12. Sen, J. (ed.): *Machine Learning – Algorithms, Models and Applications*. IntechOpen, London (2021). <https://doi.org/10.5772/intechopen.94615>
13. Schoukens, J., Ljung, L.: Nonlinear system identification: A user-oriented road map. *IEEE Control Syst. Mag.* **39**(6), 28–99 (2019). <https://doi.org/10.1109/MCS.2019.2938121>
14. Meruelo, A.C., Simpson, D.M., Veres, S.M., Newland, P.L.: Improved system identification using artificial neural networks and analysis of individual differences in responses of an identified neuron. *Neural Netw.* **75**, 56–65 (2016). <https://doi.org/10.1016/j.neunet.2015.12.002>
15. Sarkar, G., Saha, J., Md, R.: Development of regression equation for optimizing the materials requirements of lime and sand stabilizing adobe based on consistency and linear shrinkage. *Int. J. Appl. Sci. Eng. Res.* **1**(3), 499–511 (2012). <https://doi.org/10.6088/ijaser.0020101051>
16. Agresti, A.: *Foundations of Linear and Generalized Linear Models*. Wiley, Hoboken (2015)
17. Ribeiro, M.T., Singh, S., Guestrin, C.: “Why should I trust you?”: Explaining the predictions of any classifier. In: *Proceedings of the 22nd ACM SIGKDD International Conference on Knowledge Discovery and Data Mining*, pp. 1135–1144. ACM, New York (2016). <https://doi.org/10.1145/2939672.2939778>
18. Hall, P, Gill, N.: *An Introduction to Machine Learning Interpretability : An Applied Perspective on Fairness, Accountability, Transparency, and Explainable AI*. O’Reilly Media, Sebastopol (2019)
19. Hachchane, I., Badri, A., Sahel, A., Ruichek, Y.: Large-scale image-to-video face retrieval with convolutional neural network features. *IAES Int. J. Artif. Intell.* **9**(1), 40–45 (2020). <https://doi.org/10.11591/ijai.v9.i1.pp40-45>

20. Purwins, H., Li, B., Virtanen, T., et al.: Deep learning for audio signal processing. *IEEE J. Sel. Topics Signal Process.* **13**(2), 206–219 (2019). <https://doi.org/10.1109/JSTSP.2019.2908700>
21. Amanat, A., Rizwan, M., Javed, A.R., et al.: Deep learning for depression detection from textual data. *Electronics* **11**(5), 676 (2022). <https://doi.org/10.3390/electronics11050676>
22. Rao, A.R., Reimherr, M.L.: Non-linear functional modeling using neural networks. arXiv Preprint, <https://arxiv.org/abs/2104.09371> (2021)
23. Govind, G., Ramamoorthy, P.A.: Multi-layered neural networks and Volterra series: The missing link. In: 1990 IEEE International Conference on Systems Engineering, pp. 633–636. IEEE, Pittsburgh (1990). <https://doi.org/10.1109/ICSYSE.1990.203237>
24. Marmarelis, V.Z., Zhao, X.: Volterra models and three-layer perceptrons. *IEEE Trans. Neural Networks* **8**(6), 1421–1433 (1997). <https://doi.org/10.1109/72.641465>
25. Eivazi, H., Veisi, H., Naderi, M.H., Esfahanian, V.: Deep neural networks for nonlinear model order reduction of unsteady flows. *Phys. Fluids* **32**(10), 105104 (2020). <https://doi.org/10.1063/5.0020526>
26. Mitrea, C.A., Lee, C.K.M., Wu, Z.: A comparison between neural networks and traditional forecasting methods: A case study. *Int. J. Eng. Bus. Manage.* **1**(2), 19–24 (2009). <https://doi.org/10.5772/6777>
27. Stegmayer, G., Pirola, M., Orenco, G., Chiotti, O.: Towards a Volterra series representation from a Neural Network model. *WSEAS Trans. Syst.* **3**(2), 432–437 (2004)
28. Sugiyama, M., Sawai, H., Waibel, A.H.: Review of TDNN (time delay neural network) architectures for speech recognition. In: 1991 IEEE International Symposium on Circuits and Systems (ISCAS), pp. 582–585. IEEE, Singapore (1991). <https://doi.org/10.1109/ISCAS.1991.176402>
29. Liu, W., Zhu, L., Feng, F., et al.: A time delay neural network based technique for nonlinear microwave device modeling. *Micromachines* **11**(9), 831 (2020). <https://doi.org/10.3390/mi11090831>



Miller Decoder for UHF and SHF RFID Application

Sarada Musala¹ , Kesanasetty Leela Sravani¹ , Cristian Ravariu² ,
and Avireni Srinivasulu^{3,4} 

- ¹ Vignan's Foundation for Science Technology and Research, Guntur 522213, India
² Politehnica University of Bucharest, 313 Splaiul Independentei, Bucharest, Romania
³ JECRC University, Jaipur 303905, India
avireni@jecrcu.edu.in
⁴ K.R. Mangalam University, Gurugram 103122, India

Abstract. This paper proposes a Miller decoder design for Ultra High Frequency (UHF) and Super High Frequency (SHF), Radio Frequency Identification (RFID) application. In magnetic recording, optical domain, radio frequency identification, and for Visible Light Communication (VLC) the Miller decoder is utilized. Two Miller decoders proposed in this paper. The proposed Miller decoders constructed using digital circuits like D-flipflops and few logic gates. Proposed Miller decoders used D flipflops, logic gates of AND gate, OR gate, XNOR gate and inverters. Whereas the existing Miller decoders used both analog and digital circuits like Phase locked loop, Oscillators, Filters, amplifiers, counters, multiplexers and few logic gates. It means proposed miller decoder circuits are simple in construction and occupies less area when compared to the existing circuits. The proposed designs used less number of blocks because of that power is decreased which is confirmed through simulation and it offers a simpler design with reduced transistor-count. CMOS 180-nm technology on Cadence-platform was used to evaluate the performance of the proposed circuit. A simulation result shows that the power, delay and PDP are better in proposed Miller Decoder-2 when compared to all other designs.

Keywords: Miller decoder · Ultra High Frequency · Super High Frequency · RFID

1 Introduction

The RFID reader is a network-connected device that can be portable or permanently attached. It uses radio waves to transmit signals that activate the tag. Once activated, the tag sends a wave back to the antenna, where it is translated into data.

In Fig. 1 shown the selective I/Q diversity receiver diagram [1]. By using RF Front End the received tag signal is directly transformed and adjusted to digital base band signals in ADC utilizing the RF Front End. Channel filters for dense reader mode (DRM) and DC noise rejecting filters make up the Receiver Filter block. With the help of

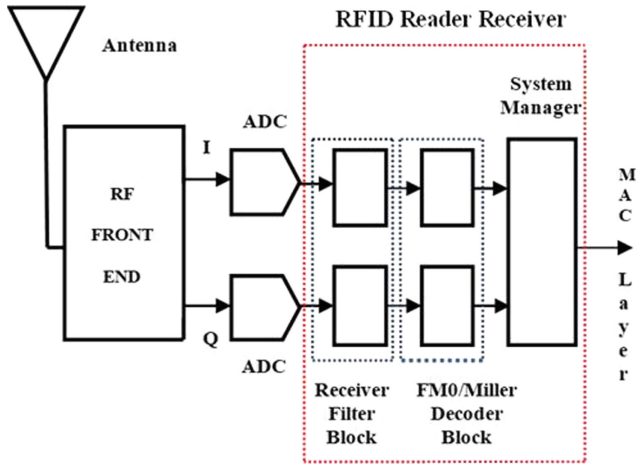


Fig. 1. The selective I/Q diversity receiver [1].

FM0/Miller decoders we can decode the digitalized I and Q channel signals. The system manager can select the relative best signal between I and Q channels.

In recent years the transportation system has begun to integrated with LED-based illumination. Automobile manufacturers have begun to replace halogen lamps with LEDs, while local governments have begun to deploy LED systems to replace traditional street lighting systems and integrate them into traffic lights. As a result, the Miller coding techniques were applied, as well as their suitability for Visible Light Communication (VLC) outside use in an Intelligent Transportation System (ITS) application. According to simulation data, the Manchester code is clearly dominated by the Miller code in terms of bandwidth and channel coexistence [2].

Numerous modulation methods are employed in communication devices, including Non Return-to-Zero (NRZ) and Return-to-Zero (RZ). However, VLC's design incorporates FM0, Manchester, and Miller encodings. In general, the transmitted signal's waveform is anticipated to have a zero mean for robustness reasons; this is also referred to as DC-balance. The transmitted signal is arbitrary binary sequence, which makes dc-balancing problematic. FM0, Manchester, and Miller codes can all supply dc-balance to the broadcast signal. As a result, VLC favours the FM0, Manchester, and Miller encoding methods [3]. In high speed optical communication systems at very high frequencies of the order of GHz the Miller encoding technique is used. Against error delay and noise interference miller code improved its operation [4]. For Dedicated Short Range Communication (DSRC) Applications FM0/ Manchester/Miller Encoding is used [5].

Remaining parts of the paper is thus structured: Second part presents Miller encoding design and coding scheme, third part refers to existing Miller Decoder designs, fourth part presents the designs of Proposed Miller Decoders, fifth part gives simulated results and makes a comparison with the previous works and sixth part concludes the paper.

2 Miller Encoder

In Fig. 2 shown the block diagram of Miller Encoder, which made up of one XNOR gate and one T flip-flop. Inputs to the XNOR gate are Data and Clock. From XNOR gate Manchester data is obtained and it is applied as input to the T flip-flop then Miller encoded output is generated from T flip-flop. For DATA ‘0110010’ the Miller code is ‘00011000111000’ and it is shown in Fig. 3. Table 1 describes the encoding rules of Miller encoder [3].

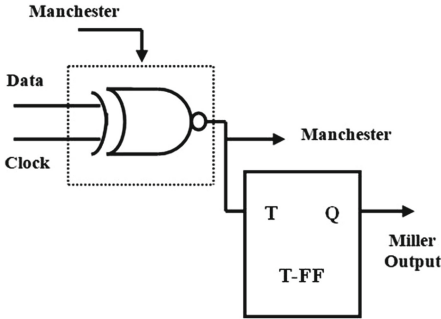


Fig. 2. Block diagram of Miller encoder [6].

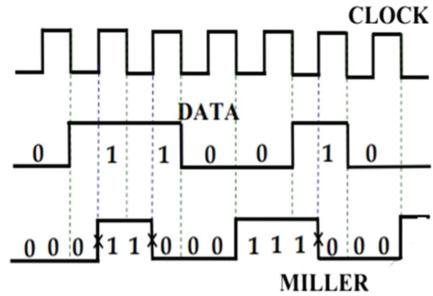


Fig. 3. Waveforms of Miller encoder [7].

Table 1. Table encoding rules of Miller encoder [7].

Previous bit ($i - 1$)	Current bit i	Miller encoding rules
X	1	Bit i 's voltage level remains constant at initially, but the waveform jumps after half a cycle (upward or downward)
0	0	Bit i 's voltage level varies at initially, but does not transit after a half cycle
1	0	Bit i voltage level at initial does not varies nor transit after half cycle

3 Existing Miller Decoders

In this section Digital Miller decoder is explained. This circuit is designed by using one clock oscillator, two inverters, two digital comparators, one OR gate, one AND gate, one counter, three D flip-flops and three Multipliers.

In Fig. 4 shown the block diagram of digital Miller decoder [8]. For an edge detector miller encoded code is applied. It generates pulses based on the rising and falling edges, which are then sent into the counter as reset signals. When compared to Miller code's basic frequency the counter is clocked at a higher frequency. In one time unit interval of the Miller code, an accumulator has a value that is substantially equivalent to the value

to which said counter is advanced. The output from the Counters is used as the input for both the first and second digital comparators. Accumulator output is passed through both the multipliers. For comparison with the counter output the output taken from the first and second multipliers is supplied as second input for both the digital comparators. When the output of the comparator exceeds the output of the first and second multipliers then the output of first and second comparators are produced. To toggle an output of toggle flip-flop the first comparator output is used as an input clock and to reset the flip-flop the second comparator's output is used, to gets its proper state the decoded data is toggled. From this flip-flop miller decoded data is obtained [8–10].

In this section Phase-lock loop based Miller decoder is explained. It is designed by using one Phase detector, one filter and amplifier, two counters, two AND gates, one clock logic, one counter decoder, two D flip-flops and one voltage control oscillator.

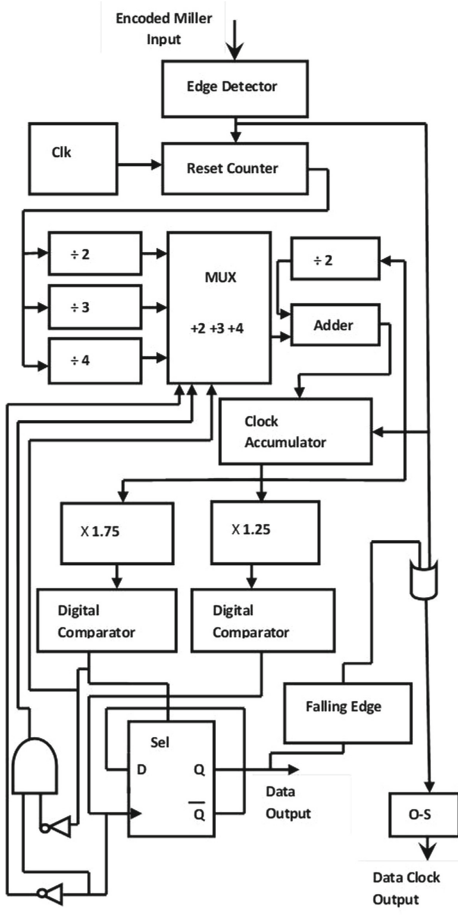


Fig. 4. The digital Miller decoder [8].

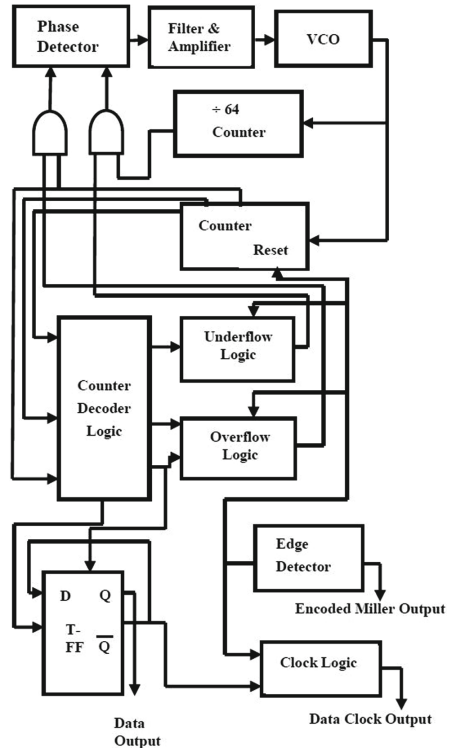


Fig. 5. Phase-lock loop and Miller decoder block diagram [9].

In Fig. 5 shown the block diagram of phase-lock loop based Miller decoder [9]. A phase-lock loop first having a controlled oscillator and at second divisible by N counters to obtain the advantages of this invention. With the help of counters inputs are applied to phase detector produces the phase difference between the counter outputs. To control the oscillator frequency through a low pass filter and an amplifier the output of phase detector is connected to the oscillator. One of the counters receives a reset signal as input. The reset signals occur at integral counter cycles when counters are clocked at lock-on period. For the 1 and 2 time unit widths of the code, the phase-lock loop counters in a Miller decoder are operated at a frequency that provides two, three, and four counter cycles, respectively. The upcoming counter stages from one counter to another counter, does not reset the range of phase lock loop. For the set signal 2 flip-flops time unit output is used, to get reset state in a flip-flop the decrypted data which toggle it to the proper state, for the toggle flip-flop output clock input is given to toggle and used as decoders one-time unit output. The output of the flip-flop is used to generate Miller decoded data [11, 12].

4 Proposed Miller Decoders

The proposed Miller Decoder-1 is shown in Fig. 6. The Miller decoder consists of one negative level D flip-flop, one positive level D flip-flop, one XNOR gate, one AND gate, one OR gate, two Inverters and one positive edge trigger D flip-flop. Miller encoded data stream and clock are applied as inputs for –ve level and +ve level D flip-flops then the output is realized at the –ve and +ve level of code stream. The output of the –ve level D flip-flop and the previous output of Miller Decoded output are given as inputs to the XNOR gate. Output of the –ve Level D flip-flop and inverted output of +ve level D flip-flop are applied as inputs to the AND gate. For OR gates the outputs extracted from the XNOR and AND gates are applied. Output of OR gate and inverted clock are passed through +ve edge trigger D flip-flop to extract the Miller Decoded Output. This proposed circuit occupy lesser area when compared to existing circuits.

In this section proposed Miller decoder-2 using Demux is explained. The proposed Miller decoder-2 block diagram is shown in Fig. 7. It consists of one Demux of 1×2 , one XNOR gate, one AND gate, one OR gate, one Inverter and two positive edge trigger D flip-flop. Miller encoded data stream and clock with one frequency hertz are applied as inputs for 1×2 Demux then the production of pulses are applied as one input to +ve edge trigger D flip-flop and the inversion of pulse is applied as one input to AND gate. Another input applied to +ve edge trigger D flip-flop is Clock with two frequency hertz. The output of +ve edge trigger D flip-flop and the previous output of are given as inputs to the XNOR gate. Inverted output of 1×2 Demux and output of +ve edge trigger D flip-flop are applied as inputs to the AND gate. The outputs extracted from the XNOR and AND gates are applied as inputs to the OR gate. Output of OR gate and clock are passed through +ve edge trigger D flip-flop to extract the Miller Decoded Data. This proposed circuit occupies lesser area when compared to existing circuits.

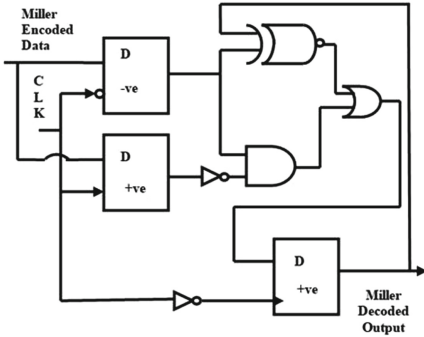


Fig. 6. Proposed Miller decoder-1.

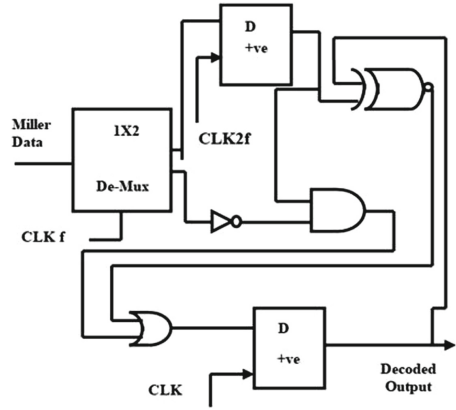


Fig. 7. Proposed Miller decoder-2.

5 Simulation Results

The circuits in Figs. 2, 6 and 7 are simulated by using virtuoso tool in cadence software with CMOS 180-nm technology. The simulations have been carried out with 1.8V supply-rail. By using this software, the transient analysis is performed to check the functionality, and for calculating the power dissipation and propagation delay.

Table 2. Analysis of proposed Miller decoders.

Voltages (V)	Parameters	Proposed Miller decoder-1	Proposed Miller decoder-2
1.7	Power (μ W)	36.14	34.08
	Delay (μ s)	1.8	1.63
	PDP (pJ)	65.05	55.55
1.8	Power (μ W)	48.22	45.78
	Delay (μ s)	2.5	1.97
	PDP (pJ)	120.55	90.18
1.9	Power (μ W)	62.95	59.33
	Delay (μ s)	3.7	3.2
	PDP (pJ)	232.91	189.85
2	Power (μ W)	80.38	78.9
	Delay (μ s)	4.5	4.35
	PDP (pJ)	361.71	343.21

The simulated waveforms of clock, data and miller encoded output of miller encoder is presented in Fig. 8 and the simulated wave forms of clock, miller encoded data and miller decoded output are presented in Figs. 9 and 10 respectively. In Figs. 9 and 10 waveforms the output is with one-bit delay because that bit represents the previous bit which will be applied as one input to the XNOR gate. Table 2 shows the analysis of proposed Miller Decoders and sub modules used in different Miller decoders are shown in Table 3.

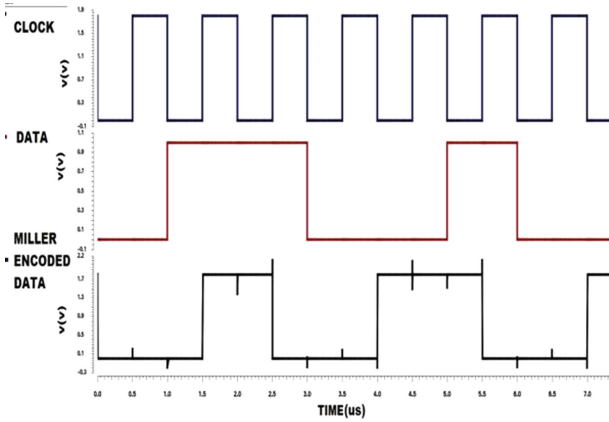


Fig. 8. Transient response of Miller encoder.

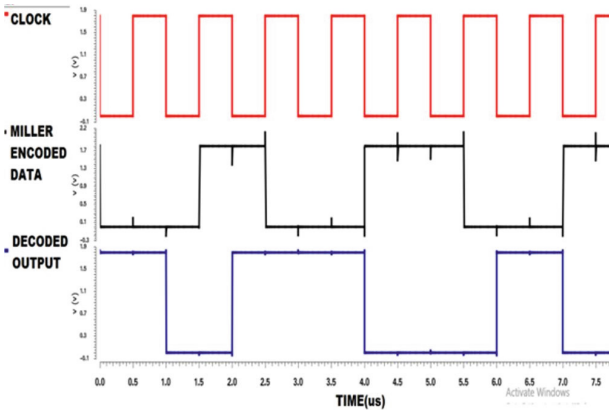


Fig. 9. Transient response of proposed Miller decoder-1.

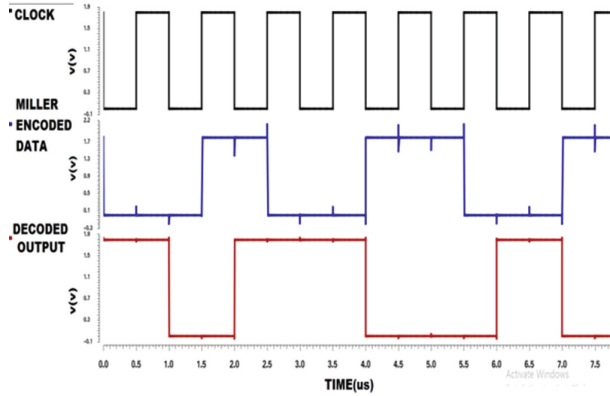


Fig. 10. Transient response of proposed Miller decoder-2.

Table 3. Sub modules used in different Miller decoders.

Circuits	Blocks used for Miller decoder
Digital Miller decoder-1	Clock oscillator-1, inverters-2, ORgate-1, ANDgate-1, Counter-1, Dflip-flop-3, digital Comparators-2, MUX-3
Phase-lock loop Miller decoder-2	Phase Detector-1, Filter & Amplifier-1, Counter-2, AND gate-2, ClockLogic1, Counter Decoder-1, Dflip-flop-2, Voltage Control Oscillator (VCO)-1
Proposed Miller decoder-1	D flip-flop's-3, AND gate-1, XNORgate-1, ORgate-1, Inverters -2
Proposed Miller decoder-2	D flip-flop's-2, 1×2 Demux-1, AND gate-1, XNOR gate-1, ORgate-1, Inverter-1

6 Conclusion

New Miller decoder circuits have been proposed and simulated using 180-nm CMOS technology operating on 1.8V supply-rail. MOSFET inverters, D flip-flops, XNOR gate, AND gate, OR gate, and 1×2 De-mux are used in the proposed Miller decoders. Due to the usage of pure digital circuits, the proposed designs became simple with less area. The simulation results of the proposed Miller Decoders confirmed that it consumes less power because of less number of blocks are used due to the transistors count is reduced. The output of the miller decoder is produced with one-bit delay because it depends on the previous bit, so the future work is design of Miller decoder without delay. The Miller decoder design used for Ultra High Frequency (UHF) and Super High Frequency (SHF), Radio Frequency Identification (RFID) applications like magnetic recording, optical domain, radio frequency identification, and for Visible Light Communication (VLC).

References

1. Kim, S.K., Nam, S.S., Cho, S.H.: A FPGA design of the I/Q signal combining for UHF RFID reader receiver. In: 2010 2nd IEEE International Conference on Network Infrastructure and Digital Content, pp. 556–560. IEEE, Beijing (2010). <https://doi.org/10.1109/ICNIDC.2010.5657831>
2. Cailean, A.M., Cagneau, B., Chassagne, L., et al.: Miller code usage in visible light communications under the PHY I layer of the IEEE 802.15.7 standard. In: 2014 10th International Conference on Communications (COMM), pp. 1–4. IEEE, Bucharest (2014). <https://doi.org/10.1109/ICComm.2014.6866699>
3. Gharat, R., Thorat, S.S. (2017). Miller encoder for outdoor MIMO VLC application. *International J. Sci. Technol. Eng.* **3**(11), 25–28 (2017)
4. Singh, P., Jain, R.: Design of miller encoder using 32 nm UMC CMOS technology at 5 GHz. *Int. J. Innov. Sci. Res. Technol.* **1**(4), 1–5 (2016)
5. Jyothi, Y., Vardhini, P.A.H., Shirisha, M.: SOLS based reused architecture of FM0/Manchester/Miller encoding for DSRC applications. *J. Emerg. Technol. Innov. Res.* **5**(12), 463–465 (2018)
6. Srinivasulu, A., Sravanthi, G., Sarada, M., Pal, D.: FinFET-based Miller encoder for UHF and SHF RFID application. *Int. J. Electron.* **105**(1), 104–115 (2018). <https://doi.org/10.1080/00207217.2017.1354401>
7. Hung, Y.C.: Time-interleaved CMOS chip design of Manchester and Miller encoder for RFID application. *Analog Integr. Circ. Sig. Process* **71**(3), 549–560 (2012). <https://doi.org/10.1007/s10470-012-9850-7>
8. Yarborough Jr., J.M.: Digital Miller Decoder. US Patent 4,454,499, 12 June 1984
9. Yarborough Jr., J.M.: Phase-Lock Loop and Miller Decoder Employing the Same. US Patent 4,456,884, 26 June 1984
10. Patcha, K., Musala, S., Vijayavardhan, K., et al.: Carbon nano tube field effect transistors based ternary Ex-OR and Ex-NOR gates. *Curr. Nanosci.* **12**(4), 520–526 (2016). <https://doi.org/10.2174/1573413712666151216221629>
11. Harinarayan, G.S., Srinivasulu, A.: Three microwave frequency dividers using current source/sink and modified current source inverters. *Act. Passive Electron. Compon.* **2013**, 762706 (2013). <https://doi.org/10.1155/2013/762706>
12. Musala, S., Srinivasulu, A.: Fin-FET based 4-BIT input XOR/XNOR logic circuit. In: IEEE Applied Electronics 2016 International Conference, pp. 219–222. IEEE, Pilsen (2016). <https://doi.org/10.1109/AE.2016.7577277>

Energy, Environment and Sustainable Development



Implementation of Sustainable Development Goals in Business Entities

Paula Bajdor^(✉)  and Marta Starostka-Patyk 

Częstochowa University of Technology, 69 Dabrowskiego Street, 42-201 Częstochowa, Poland
paula.bajdor@pcz.pl

Abstract. Sustainable development is now a commonly implemented concept by various entities, ranging from entire countries to basic economic units. Concerning countries, references to this concept can be found in the constitution; concerning economic entities – it takes the form of collections, reports, or particular documents indicating the company’s involvement in implementing this concept. For many years, the concept of sustainable development has been the subject of extensive research; however, while in theoretical terms, this issue is very widely discussed and presented in practical terms, this topic has still not been fully exhausted. With this in mind, the article presents the practical implementation of the concept of sustainable development in Polish enterprises. Practical implementation took the form of many factors corresponding to the economic, environmental, and social dimensions. The research subject was 410 companies in which the assumptions of the sustainable development concept are implemented. The conducted research and analyses made it possible to determine the degree of implementation of the concept of sustainable development in enterprises and identify significant differences depending on the adopted criteria.

Keywords: Sustainable development · Enterprise · Economic · Ecologic · Social

1 Introduction

The concept of sustainable development is a response to growing concerns that the terrestrial ecosystem may not be able to cope with the effects of human activities, and its purpose is, among others, preventive elimination or reduction of imbalances occurring simultaneously in its three main areas [1]. In the 1970s, the most important role was played by environmental issues, and the undertaken actions or formulated guidelines focused mainly on the methods of its protection [2]. However, with time, the other two pillars of sustainable development were also taken into account - the social and economic aspects, along with the environmental one of course. This, what was at first a call to protect the environment, has been made more specific, including the improvement of living conditions or economic growth [3].

Currently, the goals of sustainable development are implemented by both, organizations at the national level and individual economic entities operating on a given market. The main issue of the sustainable development goals implementation by enterprises has

been, and it is, the subject of constant research. However, for the purposes of this paper, a literature review in the area of sustainable development practical implementation enterprises made it possible to identify a research gap. The research gap takes the form of the lack of detailed research and analyzes concerning the practical implementation of goals in SME enterprises, and in particular the lack of indication of significant differences in the implementation of individual goals depending on the adopted criteria. Identification of the existing research gap made it possible to formulate the research hypothesis “*there are significant differences in the implementation of the sustainable development goals depending on the adopted criteria*”, which will be verified in the course of the conducted research and analyzes.

2 Literature Review

The concept of sustainable development derives in a straight line from the idea of development that has accompanied societies since the dawn of history – a constant striving to discover, learn, improve or make ideas and ideas physically character [4]. The concept of sustainable development was more fully embedded in the 1970s, because from that moment on, this concept became the subject of research, discussion and publication, in which a wide group of scientists participated. Beginning in the 1970s, the concept of sustainable development became the subject of programs, declarations and reports on ecology, society and development issues, which over time became the main pillars, aspects and dimensions of this concept. Currently, it occupies a widely exposed place in discussions concerning the protection of the natural environment [5]. Entering the phrase sustainable development into a search engine results in 438 million views. Currently, this term denotes not only the best known and most cited concept, but also very well documented in various publications. The result of such a broad discourse is most often reports, strategies or declarations containing attitudes, concepts or solutions that fit in with the idea of sustainable development.

It is also possible to distinguish the key stages that break the evolution of sustainable development into three main periods:

1. The first period covers the period from economic theories, in which some theorists recognized the limits of development and environmental requirements, warning against the negative effects of economic development, until 1972, when the First United Nations Conference on the Environment of Man took place, in Stockholm. This conference meant the introduction of the concept of sustainable development and although it did not fully link environmental problems with development, it emphasized the need for changes in the policy of economic development [6]. It can be assumed that this stage is characterized by theoretical considerations that do not translate into practice.
2. The second period covers the years after the Stockholm Conference. The terms development and environment, development without destruction and environmentally compatible development have increasingly been used in publications. In 1980, the International Union for Conservation of Nature (IUCN) put forward the idea of combining economics and the environment through the concept of sustainable

development [7]. In 1983, the United Nations World Commission on Environment and Development (WCED) was established to develop a global change agenda. The aim of this program was to raise awareness and concern about the negative impact of socio-economic development on the environment and natural resources, and to ensure the prospect of long-term and sustainable development compatible with the environment, its protection and conservation [6]. After several years of work, in 1987 a commission of 19 delegates from 18 countries led by Gro Harlem Brundtland (then Prime Minister of Norway) published the *Our Common Future* report, better known as the Brundtland Report, which includes one of the most popular definitions of sustainable development. This report initiated a new global socio-economic policy in which the concept of sustainable development has become a key element in environmental management and other areas of human activity [1]. It can be assumed that this stage is, on the one hand, characterized by theoretical considerations, but containing hints and guidelines for practical application.

3. The third period covers the years after the Brundtland Report and continues today. The concept of sustainable development is currently implemented in many dimensions, on its basis the concepts of sustainable transport, sustainable construction and sustainable fashion were created, and each of them contains tips and guidelines enabling the practical implementation of solutions, resulting in benefits in the economic, ecological and social dimensions [8].

The most popular and well-known definition of sustainable development is the one contained in the report *Our Common Future* [9]: “At the present level of civilization, sustainable development is possible, i.e. development in which the needs of the present generation can be satisfied without reducing the chances of future generations for their satisfaction”. The civilization itself is the level of social development that has been achieved by society in a specific period [10]. Authors of paper [11] sees the concept of sustainable development as “a qualitatively new form of conscious, responsible individual and social life, on the basis of development together with the environment – social and natural, taking into account ecological limitations and social expectations”. According to Jackson [12], the idea of sustainable development appeared as one of the answers to the issues related to economic growth, towards which modern society has been confronted. It is a choice between continuing unsustainable growth, resulting in increasing resource consumption, higher environmental costs, and increasing social inequalities, or moving away from this type of growth. Sustainable development according to [13] assumes the multiplication of goods in line with the efficiency of ecosystems, so that the former do not lose their ability to renew.

Currently, it is also possible to distinguish several common elements of this concept, referred to as paradigms of sustainable development [14–18]:

- man-made socio-economic development for a man who pursues socio-economic-environmental egalitarianism;
- integration of all human activities reduced to three main dimensions: social, environmental and economic;
- identifying this concept with a certain pattern, and even a development program, enabling the implementation of goals and principles in a practical dimension;

- searching for harmony between the main components of this concept – the natural environment, society and economy, as well as striving for their equal treatment and maintaining appropriate proportions between them;
- striving for the desired natural environment constituting the environment of human life and a responsible society implementing the concept of intra- and intergenerational justice.

Nevertheless, the issues resulting from the industrial revolution, i.e. the still unlimited use of human and environmental resources, remain the greatest challenge to sustainable development.

3 Research Methodology

The adopted research procedure included the following stages:

1. Selection of the research area – on the basis of previously conducted research in the field of sustainable development, it was possible to identify a research area that has not yet been thoroughly investigated – the practical implementation of the concept of sustainable development in Polish enterprises.
2. Defining the subject of research – Polish enterprises from the micro, small and medium-sized enterprises sector were selected as the subject of research. The justification for the research conducted among this group of enterprises is the fact that they constitute 99.8% of all enterprises operating in Poland. Table 1 below presents the sample structure in the form of activity characteristics and size.

Table 1. Structure of the research sample.

Main business profile	Micro	Small	Medium	TOTAL
Industry	13	37	60	110 (27%)
Construction	18	17	10	45 (10%)
Trade	33	38	27	98 (24%)
Transport and warehouse management	10	9	8	27 (7%)
Accommodation and gastronomy	4	5	2	11 (3%)
Information and communication	6	4	4	14 (4%)
Real estate market services	4	4	4	12 (3%)
Professional, scientific and technical activity	18	7	6	31 (8%)
Administration and activity	5	4	7	16 (4%)
Education	4	1	1	6 (2%)
Healthcare and social assistance	12	5	3	20 (5%)
Culture, entertainment and recreation	1	1	0	2 (1%)
Other service activities	6	1	1	8 (2%)

In the study, the majority were enterprises employing more than 49 and less than 250 people, operating in the industrial and commercial sectors. The next places were taken by micro-enterprises, also operating in the commercial and construction industries, and conducting scientific, professional and technical activities. At the same time, it should be noted that the presented distribution of enterprises is the result of the earlier layered selection of the research sample. However, in the case of the distribution in terms of the size of enterprises, this distribution is the most proportional, because each group constitutes 1/3 of the entire research sample.

3. Selection and preparation of research tools – a survey questionnaire was selected to conduct research among Polish enterprises, due to the fact that the survey is a simple and quick way to collect large amounts of data on the surveyed enterprises.
4. Development of the questionnaire – on the basis of the conducted literature analysis, a questionnaire was constructed containing 20 questions about sustainable development in Polish enterprises.
5. Conducting a pilot study – a pilot study was carried out on a group of 10 enterprises. Its aim was to eliminate potential inaccuracies so that the respondents had no doubts as to the essence of the questions asked.
6. Introduction of changes to the questionnaire – due diligence in the development of the research tool meant that the conducted pilot study did not indicate the need to make changes to the questionnaire.
7. Implementation of the survey – the main survey was conducted in the period from August to December 2021, among 400 enterprises representing a representative sample of the survey, using CATI and CAWI methods. The respondents of the study were the owners of enterprises, as the assumption was made that they mainly make decisions regarding activities that are part of the sustainable development framework.
8. Verification of the obtained research material – the verification of the obtained primary data did not reveal any errors or omissions.
9. Analysis of the obtained results – the obtained results were the primary data, which were subjected to further analyzes. For this purpose, Statistica software and an Excel spreadsheet were used. The following statistical methods were used: reliability analysis and U Mann-Whitney tests.
10. Verification of hypotheses – the use of above-mentioned statistical methods and carrying out analyzes made it possible to verify the research hypothesis formulated for the purposes of this paper, “there are significant differences in the implementation of the sustainable development goals depending on the adopted criteria”.

Due to the fact that the nature of the answers to individual questions took the form of single or multiple-choice answers and answers on a 6-point Likert scale, before starting the analysis of the obtained test results, an analysis of the reliability of the measuring scale was carried out, using the Alpha Cronbach statistic for this purpose. This statistic is most often used to measure the internal consistency or reliability of a psychometric tool. It is a factor that tests the reliability of the research questionnaires used, and in particular the internal consistency of the tool used. The Cronbach’s alpha statistic is based on the correlation coefficients of all the questions in the questionnaire with the overall score on this scale. Cronbach’s alpha can take values in the range from 0 to 1, with the value

of 0.6 being assumed to be the correct and commonly accepted value, although the aim is for the value of this coefficient to be 0.9. Table 2 below contains the results of the performed descriptive statistics for the issues included in the research questionnaire.

Table 2. Values of descriptive statistics of individual issues included in the questionnaire.

Issue	Mean	Variance	Standard deviation	Cronbach's alpha
Realization of economic goals	62.20	0.40	12.16	0.88
Realization of environmental goals	53.70	0.06	15.66	0.89
Realization of social goals	63.39	0.11	12.11	0.89

4 Research Results

In order to make a comparison between the selected groups, in this case between micro, small and medium enterprises, the non-parametric U'Mann-Whitney test was used. The use of this test made it possible to determine whether there are significant statistical differences between the selected groups of the enterprise in the assessment of economic, environmental and social goals, listed in the Table 3.

Due to the distinguished groups of enterprises from the SME sector, the conducted tests compared:

- micro-enterprises with small ones;
- micro-enterprises with medium-sized ones;
- small and medium-sized enterprises/

The Table 4 presents test values for factors related to the assessment of the significance of differences in the assessment of economic goals implemented by the surveyed enterprises. The results presented in the Table 4 show that:

- micro-enterprises significantly more often indicated the implementation of economic goals in the form of reducing investment risk in strategic areas of the company ($Z = 0.979$; $p = 0.032$); the possibility of using technologically advanced IT resources ($Z = 0.289$; $p = 0.027$) and increasing the number of customers ($Z = 0.069$; $p = 0.045$) than small enterprises. Moreover, they significantly more often indicated better cooperation with clients and partners ($Z = 0.442$; $p = 0.045$) than medium-sized enterprises;
- small enterprises significantly more often indicated the implementation of economic goals in the form of better cooperation with clients and partners and acceleration of enterprise development ($Z = -1.449$; $p = 0.014$) than micro-enterprises and improvement of employee efficiency ($Z = 0.442$; $p = 0.045$) than medium-sized enterprises;

- medium enterprises significantly more often indicated the implementation of economic goals in the form of greater economic efficiency ($Z = -0.389$; $p = 0.045$, $Z = -0.906$; $p = 0.046$) and higher cost predictability and stability ($Z = -0.044$; $p = 0.049$, $Z = -0.252$; $p = 0.048$) than micro and small enterprises. However, in relation to micro enterprises only, medium enterprises significantly more often indicated the implementation of economic goals in the form of improving cooperation between employees ($Z = -0.221$; $p = 0.042$), and the possibility of faster launching innovations compared to small enterprises ($Z = 0.422$; $p = 0.045$).

Table 3. Factors related to the assessment of the significance of differences in the assessment of economic, environmental and social goals.

Goals	Variables
<i>Economical</i>	
Achieving business profits	1.1
Greater economic efficiency (reduced level of investment outlays)	1.2
Reduction of costs related to e.g. the day-to-day operations of the enterprise	1.3
Higher cost predictability and stability	1.4
Reduction of investment risk in strategic areas of the company	1.5
Ability to use technologically advanced IT resources (hardware, software, services)	1.6
Better cooperation with customers and partners	1.7
Improving the company's image	1.8
Increasing the number of customers	1.9
Improving collaboration between employees	1.10
Improving the efficiency of employees	1.11
Better business continuity	1.12
Possibility to standardize and simplify organizational procedures	1.13
Possibility of faster launch of innovations (e.g. new/modified services, processes, products)	1.14
Acceleration of enterprise development (implementation of new business models)	1.15
<i>Environmental</i>	
Use of renewable energy sources	2.1
The use of energy-saving devices	2.2
Reduction of the working time of electronic devices	2.3
The use of efficient heating and emission-reducing systems	2.4
Building insulation (thermal insulation, insulated windows)	2.5

(continued)

Table 3. (continued)

Goals	Variables
Reduction of radiation, noise and noise related to the use of electronic equipment	2.6
Influencing customers towards environmentally friendly behavior	2.7
Resignation from packaging that is difficult to dispose of in favor of those that can be recycled	2.8
Waste segregation by staff	2.9
Automatic shutdown of unnecessary devices and lighting	2.10
Producing and selling environmentally friendly products	2.11
Maximum use of natural daylight	2.12
The use of devices regulating water consumption (aerators, stream pressure regulators, timer stops, photocells)	2.13
Reuse of materials/raw materials	2.14
Recycling of broken, defective or used products	2.15
<i>Social</i>	
Employing based on labor contracts	3.1
Offering work to people from the closest social environment	3.2
Compliance with the provisions resulting from the applicable law	3.3
Conducting activities for the benefit of the local community	3.4
Taking care of safety in the workplace	3.5
Transparency of the career path	3.6
Activities for equality	3.7
Striving to create a friendly atmosphere at work	3.8
Engaging employees in the affairs of the enterprise	3.9
Pay wages on time and pay taxes and fees due	3.10
Development and application of accepted ethical standards related to the conducted activity	3.11
Pro-social activity	3.12
Conducting activities for the development of local culture	3.13
Participation in charity events	3.14

Table 4. U'Mann-Whitney test values for factors related to the assessment of the significance of differences in the assessment of economic goals.

Factor	Micro/small		Micro/medium		Small/medium		Mean		
	Z	p	Z	p	Z	p	Micro	Small	Medium
1.1	-0.415	0.678	-0.378	0.705	0.063	0.950	4.96	4.89	4.92
1.2	1.277	0.202	-0.389	0.045	-0.906	0.046	3.17	3.14	3.9
1.3	1.168	0.243	0.480	0.631	-0.709	0.479	3.96	3.79	3.9
1.4	0.195	0.846	-0.044	0.049	-0.252	0.048	3.07	3.13	3.78
1.5	0.979	0.032	-0.230	0.818	-1.161	0.246	3.94	3.45	3.66
1.6	0.289	0.027	0.449	0.654	0.721	0.471	3.99	3.02	3.11
1.7	-1.449	0.014	0.753	0.045	0.691	0.490	4.06	4.86	3.75
1.8	0.156	0.876	-0.192	0.848	-0.344	0.731	4.81	4.8	4.84
1.9	0.069	0.045	0.038	0.970	-0.028	0.978	4.72	4.11	4.22
1.10	0.535	0.592	-0.221	0.042	-0.305	0.760	4.39	4.32	4.86
1.11	0.610	0.542	0.179	0.858	0.442	0.045	4.14	4.75	4.01
1.12	-1.207	0.227	-0.071	0.943	1.143	0.253	4.29	4.45	4.3
1.13	0.355	0.722	-0.174	0.862	-0.533	0.594	4.2	4.17	4.24
1.14	-0.047	0.963	-0.444	0.657	-0.429	0.046	3.01	3.19	3.99
1.15	-0.076	0.040	-0.122	0.903	-0.064	0.949	3.16	3.96	3.98

Then, it was examined whether there were significant differences in the assessment of environmental goals implemented by the studied groups of enterprises (Table 5).

The results presented in the Table 5 show that:

- micro-enterprises significantly more often indicated the implementation of environmental goals in the form of the use of energy-saving devices ($Z = 0.173$; $p = 0.046$, $Z = 0.141$; $p = 0.048$) and waste segregation by staff ($Z = 0.279$; $p = 0.045$, $Z = 0.204$; $p = 0.038$) than small and medium-sized enterprises. Moreover, they significantly more often indicated the reduction of working time of electronic devices than small enterprises ($Z = 0.215$; $p = 0.030$);
- small enterprises significantly more often indicated the implementation of environmental goals in the form of building insulation ($Z = -0.076$; $p = 0.040$); producing and selling environmentally friendly products ($Z = -1.179$; $p = 0.023$); reuse of materials/raw materials ($Z = -2.550$; $p = 0.011$) and recycling of broken, defective, used products ($Z = -1.451$; $p = 0.014$) than micro enterprises. Moreover, they significantly more often indicated that they gave up packaging that is difficult to recycle in favor of those that can be recycled ($Z = 0.333$; $p = 0.039$) than medium enterprises;
- medium enterprises significantly more often indicated the implementation of environmental goals in the form of the use of renewable energy sources ($Z = -0.353$; $p = 0.024$, $Z = -0.052$; $p = 0.049$) than other groups of enterprises, and automatic

Table 5. U'Mann-Whitney test values for factors related to the assessment of the significance of differences in the assessment of environmental goals.

Factor	Micro/small		Micro/medium		Small/medium		Mean		
	Z	p	Z	p	Z	p	Micro	Small	Medium
2.1	0.312	0.755	-0.353	0.024	-0.051	0.049	2.53	2.41	3.46
2.2	0.173	0.046	0.141	0.048	0.027	0.979	3.98	2.94	2.98
2.3	0.215	0.030	0.101	0.920	0.247	0.805	3.94	3.47	3.44
2.4	0.511	0.610	0.047	0.963	-0.400	0.689	3.47	3.35	3.44
2.5	-0.076	0.040	-0.537	0.591	-0.377	0.706	3.67	4.65	3.76
2.6	0.068	0.946	0.239	0.811	0.160	0.873	3.33	3.32	3.29
2.7	0.871	0.384	-0.019	0.985	-0.859	0.390	3.73	3.54	3.72
2.8	0.153	0.879	-0.227	0.821	0.333	0.039	3.56	4.51	3.59
2.9	0.279	0.045	0.204	0.038	0.118	0.906	5.28	4.24	4.26
2.10	-0.185	0.853	-0.671	0.502	-0.449	0.045	3.97	4.98	4.11
2.11	-1.179	0.023	-0.390	0.697	0.780	0.435	3.36	4.62	3.45
2.12	0.069	0.945	-0.473	0.636	-0.509	0.611	4.25	4.22	4.3
2.13	-1.111	0.267	-1.126	0.260	-0.028	0.977	2.79	2.98	3.01
2.14	-2.550	0.011	-1.589	0.112	0.956	0.339	3.18	3.69	3.49
2.15	-1.451	0.014	-1.199	0.231	0.270	0.787	3.59	4.89	3.84

switch-off of unnecessary appliances and lighting ($Z = -0.449$; $p = 0.045$) than small enterprises.

In the last step, it was examined whether there were significant differences in the assessment of social goals implemented by the studied groups of enterprises (Table 6). The results presented in the Table 6 show that:

- micro enterprises significantly more often indicated the implementation of social goals in the form of engaging employees in the affairs of the enterprise ($Z = 0.580$; $p = 0.046$) than medium enterprises;
- small enterprises significantly more often indicated the implementation of social goals in the form of employing employees based on employment contracts ($Z = -0.551$; $p = 0.045$); conducting activities for the benefit of the local community ($Z = -0.127$; $p = 0.049$); pro-social activity ($Z = -0.279$; $p = 0.048$) and participation in charity actions ($Z = -1.486$; $p = 0.037$) than micro enterprises. Moreover, they more often achieved the goal of engaging employees in the affairs of enterprises ($Z = 0.279$; $p = 0.048$) than medium enterprises;
- medium enterprises significantly more often indicated the implementation of social goals in the form of employing employees based on employment contracts ($Z = -0.465$; $p = 0.042$); conducting activities for the benefit of the local community ($Z =$

Table 6. U'Mann-Whitney test values for factors related to the assessment of the significance of differences in the assessment of social goals.

Factor	Micro/small		Micro/medium		Small/medium		Mean		
	Z	p	Z	p	Z	p	Micro	Small	Medium
3.1	-0.551	0.045	-0.465	0.042	-0.058	0.954	4.09	4.56	4.66
3.2	0.654	0.513	0.572	0.567	-0.090	0.929	4.17	4.06	4.08
3.3	-0.494	0.621	-0.169	0.866	0.341	0.733	5.06	5.13	5.1
3.4	-0.127	0.049	-0.566	0.045	-0.412	0.680	3.59	4.62	4.71
3.5	-0.245	0.807	-0.174	0.862	0.078	0.938	5.12	5.15	5.14
3.6	-0.558	0.577	-0.247	0.040	-0.316	0.042	4.5	4.57	5.55
3.7	-0.427	0.669	-0.959	0.337	-0.517	0.605	4.16	4.26	4.39
3.8	-0.020	0.984	-0.309	0.045	-0.282	0.048	4.19	4.19	5.24
3.9	-0.819	0.413	0.279	0.048	0.580	0.046	4.53	4.64	3.56
3.10	0.498	0.618	-0.485	0.627	-0.986	0.324	5.37	5.25	5.41
3.11	-0.118	0.906	0.306	0.760	0.434	0.664	5.01	5.02	4.95
3.12	-0.279	0.048	-0.449	0.043	-0.753	0.451	3.65	4.63	3.75
3.13	0.723	0.469	-0.171	0.864	-0.882	0.037	3.32	3.22	4.36
3.14	-1.486	0.037	-1.246	0.021	0.352	0.725	2.54	3.83	3.78

-0.566; $p = 0.045$); transparency of the career path ($Z = -0.247$; $p = 0.040$); striving to create a friendly atmosphere at work ($Z = -0.309$; $p = 0.045$); pro-social activity ($Z = -0.449$; $p = 0.043$) and participation in charity actions ($Z = -1.246$; $p = 0.021$) than microenterprises. However, in relation to small enterprises, they significantly more often indicated the implementation of social goals in the form of transparency of the career path ($Z = -0.316$; $p = 0.042$); striving to create a friendly atmosphere at work ($Z = -0.282$; $p = 0.048$) and carrying out activities for the development of local culture ($Z = -0.882$; $p = 0.037$).

5 Conclusion

The conducted research and subsequent analyzes clearly indicated that, depending on the size of the enterprise, there are significant differences in the practical implementation of sustainable development goals in enterprises. Therefore, it can be assumed that the research hypothesis in the form of “*there are significant differences in the implementation of the sustainable development goals depending on the adopted criteria*” has been positively verified. Most differences exist between micro and medium-sized enterprises, they are probably caused by the fact that micro-enterprises employ up to 9 people, and medium-sized enterprises – min. 50, which may already cause the occurrence of many differences, for example in the aspect of achieving social goals.

The conducted research may be of great cognitive value both for business entities and scientists conducting research in the field of sustainable development. With regard to economic organizations, these studies may indicate directions for further proceedings in the process of achieving the goals of sustainable development. For researchers, however, they may constitute an introduction to further, more detailed research in this field.

However, it should not be forgotten that the research and analysis conducted in this article have some limitations – they were primarily focused on Polish enterprises, which may limit the possibility of drawing more general conclusions with regard to all enterprises operating on the market. Therefore, in further research, it is worth focusing on a larger group of enterprises (not limited only to Polish ones), which will allow for a more detailed picture of the practical implementation of the sustainable development goals in economic entities.






References

1. Pieroni, M.P., McAlloone, T.C., Pigosso, D.C.: Business model innovation for circular economy and sustainability: a review of approaches. *J. Clean. Prod.* **215**, 198–216 (2019). <https://doi.org/10.1016/j.jclepro.2019.01.036>
2. Olawumi, T.O., Chan, D.W.: A scientometric review of global research on sustainability and sustainable development. *J. Clean. Prod.* **183**, 231–250 (2018). <https://doi.org/10.1016/j.jclepro.2018.02.162>
3. Aarseth, W., Ahola, T., Aaltonen, K., et al.: Project sustainability strategies: a systematic literature review. *Int. J. Proj. Manag.* **35**(6), 1071–1083 (2017). <https://doi.org/10.1016/j.ijproman.2016.11.006>
4. Geissdoerfer, M., Morioka, S.N., de Carvalho, M.M., Evans, S.: Business models and supply chains for the circular economy. *J. Clean. Prod.* **190**, 712–721 (2018). <https://doi.org/10.1016/j.jclepro.2018.04.159>
5. Pawłowski, A.: Rozwój zrównoważony – największe wyzwanie XXI wieku. In: Sadowski, R.F., Łepko, Z.(eds.) *Theoria i praxis zrównoważonego rozwoju*, pp. 53–64. Towarzystwo Naukowe Franciszka Salezego, Warszawa (2017)
6. Drexhage, J., Murphy, D.: Sustainable development: from Brundtland to Rio 2012. Background paper prepared for consideration by the High Level Panel on Global Sustainability at its first meeting, 19 September 2010
7. IUCN: World Conservation Strategy. IUCN-UNEP-WWF (1980)
8. Čiegis, R., Šimanskienė, L.: The concept sustainable economic development and indicators assessment. *Manag. Theory Stud. Rural Bus. Infrastruct. Dev.* **21**(2), 34–42 (2010)
9. UN: Secretary-General: Report of the World Commission on Environment and Development: Our Common Future. UN, New York (1987)
10. Ghobakhloo, M.: Industry 4.0, digitization, and opportunities for sustainability. *J. Clean. Prod.* **252**, 119869 (2020). <https://doi.org/10.1016/j.jclepro.2019.119869>
11. Kamble, S.S., Gunasekaran, A., Gawankar, S.A.: Achieving sustainable performance in a data-driven agriculture supply chain: a review for research and applications. *Int. J. Prod. Econ.* **219**, 179–194 (2020). <https://doi.org/10.1016/j.ijpe.2019.05.022>
12. Jackson, T.: *Dobrobyt bez wzrostu*. Wydawnictwo Naukowe Uniwersytetu Mikołaja Kopernika, Toruń (2015)
13. Jabbour, C.J.C., de Sousa Jabbour, A.B.L., Sarkis, J., Filho, M.G.: Unlocking the circular economy through new business models based on large-scale data: an integrative framework and research agenda. *Technol. Forecast. Soc. Chang.* **144**, 546–552 (2019). <https://doi.org/10.1016/j.techfore.2017.09.010>

14. Salvia, A.L., Filho, W.L., Brandli, L.L., Griebeler, J.S.: Assessing research trends related to Sustainable Development Goals: local and global issues. *J. Clean. Prod.* **208**, 841–849 (2019). <https://doi.org/10.1016/j.jclepro.2018.09.242>
15. Pezzey, J.C.V., Toman, M.A.: The economics of sustainability: a review of journal articles. *Resources for the Future*, Discussion Paper 02-03 (2002)
16. Kusi-Sarpong, S., Gupta, H., Sarkis, J.: A supply chain sustainability innovation framework and evaluation methodology. *Int. J. Prod. Res.* **57**(7), 1990–2008 (2019). <https://doi.org/10.1080/00207543.2018.1518607>
17. Silvestre, B.S., Țîrcă, D.M.: Innovations for sustainable development: moving toward a sustainable future. *J. Clean. Prod.* **208**, 325–332 (2019). <https://doi.org/10.1016/j.jclepro.2018.09.244>
18. Stanny, M., Czarnecki, A.: *Zrównoważony rozwój obszarów wiejskich zielonych płuc Polski*. Irwir PAN, Warszawa (2011)



Cluster Analysis Usage as Prerequisite for Implementing Strategies of Countries Startup Ecosystems Development

Mykola Kyzym , Olena Dymchenko , Valentyna Smachylo ,
Olha Rudachenko , and Nataliia Dril 

O. M. Beketov National University of Urban Economy in Kharkiv, 17 Marshala Bazhanova
Street, Kharkiv 61002, Ukraine
dymchenkoov@kname.edu.ua

Abstract. In today's world, knowledge, innovations, new ideas and intellectual achievements are becoming the driving forces of the economy. The realities of the modern business environment, which have developed in the context of the intellectualization of the world economy, require a revision of the classical ideas of management regarding the rules of doing business, competition and markets. The issue of socio-economic development of the country as a whole, as well as its individual regions, is solved through the active implementation of innovations. The role of innovative business structures in ensuring sustainable economic development of the world's countries is growing rapidly, this attracts more and more attention from the state, society and the scientific community. Innovative business structures include startup projects that are becoming increasingly popular all over the world, including Ukraine. The process of spreading innovations is inextricably linked to the development of the startup ecosystem. Important components of the startup ecosystem are government institutions, state and local authorities, financial and investment organizations, business, communication and educational support organizations, as well as existing entrepreneurs and their associations. The development of the startup ecosystem can be measured using indexes, among which, such international indexes as StartupBlink and Startup Genome are most fully represented. StartupBlink is of the particular interest, it displays a map of the startup ecosystem and a research center that works to identify the dynamics of startup ecosystems around the world and help accelerate their growth. The paper grouped countries into 5 clusters, which made it possible to identify the features of the development of startup ecosystems, and provide characteristics of each group of countries, and in the future will become the basis for developing recommendations and forming strategies for the development of the startup ecosystem.

Keywords: Startup · Ecosystems · Global Startup Ecosystem Index · Clustering · Cluster analysis

1 Introduction

The issue of socio-economic development of the country as a whole, as well as its individual regions [1, 2], is solved through the active implementation of innovations.

Innovations spreading process is inextricably linked to the development of the startup ecosystem.

Investigation goal: the formation of homogeneous startup ecosystems of the country as a basis for developing strategies for their development.

2 Literature Survey

According to the cenological approach, an ecosystem is understood as “a set of institutions effectively interacting in the economic system” [3]. This interpretation is based only on the material perception of the ecosystem as a set of various organizations and produces a non-material component – an environment that promotes the development of creativity, innovation and entrepreneurial spirit. This assistance is provided by the activities of various people and institutions, among which the main place is given to universities.

In addition, important components of the startup ecosystem are governmental institutions, state and local authorities, financial and investment organizations, business, communication and educational support organizations, as well as existing entrepreneurs and their associations [4].

The development of the startup ecosystem can be measured using indexes, among which, today, such international indexes as StartupBlink [5] and Startup Genome [6] are most fully represented. The formation of these indices and their components is a significant basis for understanding the nature of the components of the startup ecosystem, as well as its development factors.

StartupBlink is of the particular interest, it shows a map of the startup ecosystem and a research center that works to identify the dynamics of startup ecosystems around the world and help accelerate their growth.

The Global Startup Ecosystem Index consists of hundreds of thousands of data points that are processed using an algorithm that takes into account several dozen parameters. The methodology for calculating the StartupBlink ecosystem index includes 3 components: quantitative, qualitative indicators, and an assessment of the business environment.

The quantitative component shows the level of activity of the ecosystem through its stakeholders and other indicators, such as: the number of startups, the number of coworking spaces, the number of accelerators, the number of meetings related to startups, which allows to set the level of activity of the startup ecosystem.

The qualitative component of the rating investigates the parameters that indicate the qualitative results achieved by the ecosystem. These parameters include analyzing the popularity of the best startups in the ecosystem: traffic, domain rating, customer base; availability of branches and research centers; international technology corporations; branches of multinational companies; investment volume; number of startup employees; unicorn companies, exit companies, and pantheons.

The component related to the assessment of the business environment combines business and economic indicators at the national level, with focus on general indicators related to infrastructure, business environment, and the ability of startup founders to work in any country. The main components of the business environment are: ease of doing

business and registering companies; availability of the internet and its speed; investment in R&D; availability of various technological services (payment portals, travel exchange programs, cryptocurrencies); number of patents per capita; level of English proficiency, etc.

Today, the startup topic is very popular in Ukrainian business [7], since it is startups that make up the largest number of innovative and newest products or services, which is a significant prospect for attracting domestic and foreign investment in the economy.

So, a startup ecosystem is such an environment where people and organizations (enterprises) are involved in, and it creates and supports scientific developments and the possibility of their entry into the market.

The modern startup ecosystem in Ukraine is represented by the following components:

- an entrepreneur acting as an expert;
- financial institutions/investors that provide startup capital and contribute to the growth of startups and their entry into the market;
- government/state that has an important role in construction and support of entrepreneurs and implement relevant legislative initiatives;
- corporations/private sector that help in checking ideas, hypotheses, and testing;
- universities that act as the core of the ecosystem and create all the conditions for the development of entrepreneurial education and culture and the fusion of student startups;
- innovative infrastructure that evaluates and, if necessary, helps choose an innovative idea and implement it in a startup.

Within the startup ecosystem, all the participants involved are connected to each other. Entrepreneurs unite to exchange ideas and interact with universities to attract future employees, and investors are learning to understand which types of entrepreneurs, teams, and startups are most likely to succeed and can make an exit - invest money in startups, which makes it possible to raise new capital. However, one should draw attention to the determining role of higher education institutions in the formation of the startup ecosystem.

It is advisable to start forming a local startup ecosystem on the basis of higher education institutions. O.M. Beketov National University of Urban Economy in Kharkiv has practical experience in this area, on the basis of which a holistic ecosystem of support for startup projects has now been formed, this has a positive impact on regional economic and innovative development. The experience of formation can be considered in the structural and time planes.

The main structural elements currently are:

- 1) Beketov startup School junior development school, which is intended for schoolchildren of the Kharkiv region and provides training and development of their own startup project, as well as its presentation at the All-Ukrainian (regional) competition;
- 2) Beketov startup school is designed primarily for applicants, young scientists, teachers, as well as anyone who has their own idea or development for startup projects and provides training according to the developed training program, mentoring and

- expert support, pitching startup projects and business plans and participation in the All-Ukrainian startup festival;
- 3) the goal of the Beketov Business Incubator is to create infrastructural and consulting support for youth entrepreneurship. Currently the business incubator is focused specifically on the successful implementation of startups and business ideas and is a logical part of supporting promising startups that have become graduates of BEKETOV STARTUP SCHOOL;
 - 4) Beketov Science Park is designed for the development of highly scientific developments and further commercialization of scientific and startup projects developed in the previous stages;
 - 5) the “Megapolis” Technology Transfer Center provides university-wide, national and international coordination support for technology transfer for all representatives of the local startup ecosystem of O.M. Beketov National University of Urban Economy in Kharkiv.

The university ecosystem is based on the concept of SMART specializations, is coordinated with the development strategy of the Kharkiv region until 2027 [8] and is focused on the SMART-city direction.

The development of startup ecosystems is due to a variety of support systems that are implemented at different levels: international, national, regional, and local.

Research [9] shows that the presence of a system of support for entrepreneurship by the government at any level already has a positive impact on the intentions of potential entrepreneurs to start a business in any form.

If the support program is effective and newly created business entities are satisfied with it, then this leads to greater efficiency of startups [10]. Accordingly, the formation of the startup ecosystem of a city, region, or state requires a comprehensive combination of the most effective support tools.

The authors of the investigation [9] rely on the conclusions made in [11], where it was established that obtaining management or technological support, supporting the main business functions (marketing, financial management and operational activities), is more effective for low-productive startups, while support in functions such as human resources and capital raising had a great impact on high-performance startups [12]. Therefore, support for entrepreneurship is necessary at all levels, including the regional level.

The use of local support programs, according to [13], has a number of advantages, which should include: a better level of adaptation to the needs of the territory and business; attracting a wider range of subjects, which can provide a wider range of competencies on this issue to the authorities.

Accordingly, in order to optimize local support, one should take into account the factors that will affect the formation of a local startup ecosystem. Thus, in the paper [14], 6 factors that were determined by David J. Storey in 1994 are given: demographics, unemployment, wealth, educational and professional level of the labor force, prevalence of small businesses, level of security with your own housing.

These factors for sure affect the development of the territory, but with different strengths, which will depend on the country, historical, national and cultural background. So, in the context of domestic realities, such a factor as the prevalence of small firms

will not be a determining factor for starting a business, as well as the availability of their own housing, in conditions of distrust of the financial and credit system and existing credit conditions, will not determine it as a start for entrepreneurship.

In addition, the authors can add obstacles caused by the mentality – people are afraid of failure, are not ready to take risks (the three F rule does not work); low business culture, which causes problems of agreement between founders; distrust of traditional investors and businessmen to invest in startups and distrust of government institutions and the credit sector in general.

The guidelines for Local and State Governments to Promote Entrepreneurship [15] indicate that venture funds and incubation centers are often tools for promoting entrepreneurship development by local governments. At the same time, these tools are not always combined effectively. The model being standard is one that combines government, venture funds and business incubators, but, according to [15], it is more expedient to focus it on the entrepreneur and attract existing entrepreneurs. This recommendation is based on a study [16–19] that proves the effectiveness of local connections compared to national or global ones for the success of entrepreneurs. This is due to the fact that both new and existing entrepreneurs move in a single business environment, so successful local businessmen can become sources of useful information, knowledge and motivation for those who start a new business. That is why the local startup ecosystem should create communication between startup makers, scientific institutions, investors who find it difficult to identify local entrepreneurs, and other entrepreneurs who are already operating in this area in this territory.

The role of local self-government bodies is to promote interaction between entrepreneurs and institutions that support entrepreneurship [15]. This allows to create an environment that catalyzes and provides synergy through training, interaction, establishing relationships and discussing problems and receiving feedback from existing entrepreneurs, experts, consultants, trainers [15]. Good examples of promoting the development of the startup movement at the city level are the creation of municipal startup centers in Mariupol and Kharkiv. It is important to provide investments to as many future entrepreneurs as possible during the formation of the ecosystem, which requires competitive selection of the best start-up projects and their initial financial support from the investment fund. According to the authors [15], it is better to provide a smaller amount of investment to a larger number of startups than one large investment, which will create a certain network and group of startups that will be able to support each other and integrate into the local business environment.

3 Methods

Global Startup Ecosystem Index 2021 presents a rating of countries with a total number of 100, where total Score (corresponds to the position in the rating) and Rank Change (from 2020) are marked (shows the change in the rating in 2021 relative to 2020). The research methodology is based on the analysis of the dynamics of countries' ranks of changes in the Global Startup Ecosystem Index rating from StartupBlink, which allows to determine dynamic changes by year (2021–2020), as well as structural changes that led to such changes in the context of index components. For a detailed investigation of

the best practices for developing generalized recommendations for the development of the startup ecosystem, it is proposed to group countries taking into account their rating and the changes that occurred in 2021 compared to 2020. For this purpose, these methods are enhanced by cluster analysis, which forms the homogeneous groups of countries and determines common characteristics. The purpose of cluster analysis is to form relatively homogeneous groups (clusters) in the variable space based on a set of models and methods for aggregating rows in the data matrix. Usage of cluster analysis has a certain sequence of actions and involves the use of several methods [16–19]. Taking into account existing developments, the sequence of cluster analysis will be used in stages: forming a sample for cluster analysis; determining a set of criteria (features) for which clustering is performed; conducting a hierarchical cluster procedure for creating groups of similar objects by various methods in order to form a hypothesis about natural clustering; testing the hypothesis of natural clustering by the k -average method; verification of the reliability of the obtained cluster analysis results.

When defining clusters, one uses the most commonly used integral measure – the square of Euclid’s distance. The Euclidean distance between two points x and y is the shortest distance between them. If the space is two-dimensional or three-dimensional, then this measure is geometrically the length of the straight line connecting these points. In case of n variables, the Euclidean distance is calculated by the formula [16–19]:

$$\text{dist}(x, y) = \sqrt{\sum_{i=1}^n (x_i - y_i)^2}. \quad (1)$$

The square of the Euclidean distance is calculated by the formula:

$$\text{dist}^2(x, y) = \sum_{i=1}^n (x_i - y_i)^2. \quad (2)$$

Compared to Euclidean distance, this measure pays more serious importance to large distances. If the centroid, median, or Ward method is used, it is usually recommended to use this measure [16–19].

It is also necessary to establish the significance and existence of interdependence between certain sample criteria. In order to do this, one conducts additional analysis using statistical methods. Variance analysis is a procedure for comparing the average values for samples, on the basis of which it is possible to draw conclusions about the ratio of the average values of general populations. The overall variability of a variable is divided into two components: intergroup (factor), due to differences in groups (average values), and intragroup (errors), due to random (not taken into account) reasons. The greater the proportion of the distribution between group and intragroup variability (F-ratio), the greater the difference is in the average values of the compared samples, and, accordingly, the higher the statistical significance of this difference [13–16].

Let us define Fischer statistics by the formula:

$$F = \frac{\text{Intergroup variance}}{\text{Intragroup variance}} = \frac{S_1^2}{S_2^2}. \quad (3)$$

Fischer statistics reflects the significant contribution of each metric to cluster differentiation. Positive trend of the significance indicator for $i \rightarrow 0$.

4 Discussion

Since 2013, the StartupBlink website has been updating the Global Startup Ecosystem Index from StartupBlink annually, which is the largest complete ranking of startup ecosystems in 100 countries and 1000 cities in the world.

So, Fig. 1 shows the dynamics of the 20 leaders of countries according to the Global Startup Ecosystem Index from StartupBlink over the past 3 years.

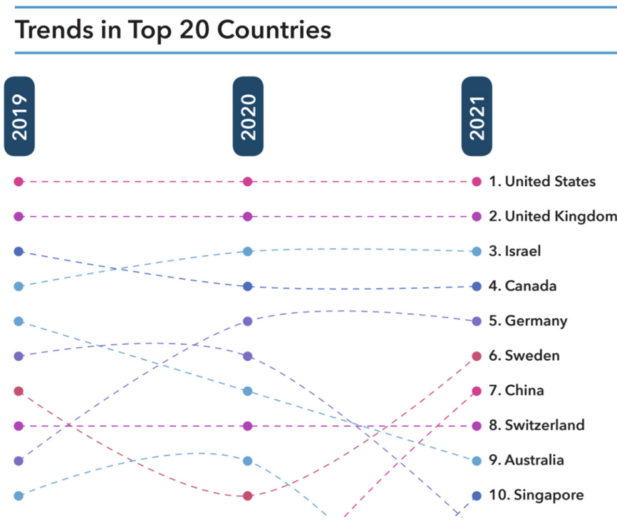


Fig. 1. Leading countries in the Global Startup Ecosystem Index from StartupBlink [5]

Disclosure of the components of the Global Startup Ecosystem Index allows to determine the impact of each of its components on the overall result.

Figure 2 shows the quantitative, qualitative and business components of the leading countries in comparison with Ukraine according to the Global Startup Ecosystem Index from StartupBlink in 2021.

In this list, Ukraine ranked 34th place in 2021 according to the rating, in the previous year the rating of Ukraine was 29th. Among 1000 cities in the world, 6 cities of Ukraine took places in the rating. Kyiv is on the 48th place of the rating, Lviv – 255, Odessa – 394, Kharkiv – 513, Ternopil – 787, and Dnipro – 883.

An ecosystem that decreased in the ranking wasn't necessarily worse than in the previous year. The reduction reflects the faster growth of other higher-ranking ecosystems going up.

At the first stage of cluster analysis, a selection from 100 countries was formed that are represented in the Global Startup Ecosystem Index 2021, 4 of them were included in this rating for the first time in 2021.

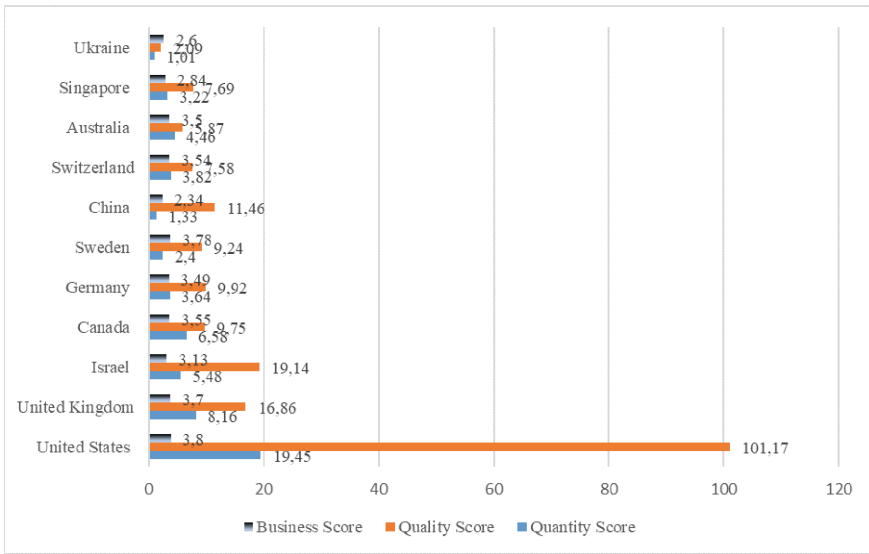


Fig. 2. Leading countries and Ukraine in the International Global Startup Ecosystem Index from StartupBlink, compiled by the authors on the basis of [5].

The second stage allowed to formulate a set of criteria (attributes) according to which clustering is to be held: Total Score and Rank Change (from 2020). Cluster analysis is implemented in the IBM SPSS Statistics trial program. Having made a hierarchical classification by constructing a dendrogram to identify the so-called “natural” clusters, based on the results of clustering by various methods (intra-group connections, far neighbor, Ward method), an assumption was made about the formation of 5 enlarged natural clusters.

Two-step cluster analysis testified a good silhouette measure of connectivity and cluster distribution (Fig. 3).

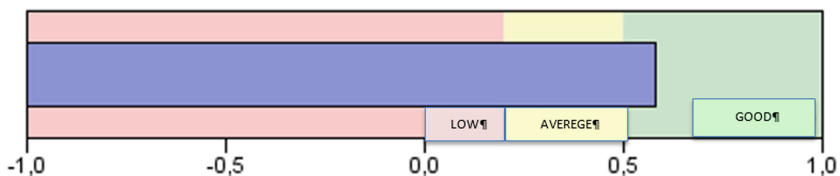


Fig. 3. Two-step cluster analysis using the SPSS Statistics software

Verification of the results of the breakdown of enterprises by clusters, presented in the form of a dendrogram for two factors, was carried out using the k -average method, taking into account the distribution over 5 clusters. The results of cluster analysis are presented in the table using the k -mean method (Table 1).

Table 1. Table of results of clustering countries by Rank Change (from 2020) and Total Score

Cluster	Rank	Country	Rank Change (from 2020)		Total Score		Number of countries
			min	max	min	max	
1	1	United States	0	0	124.42	124.42	1
2	2-18	United Kingdom, Israel, Canada, Germany, Sweden, China, Switzerland, Australia, Singapore, The Netherlands, France, Estonia, Finland, Spain, Lithuania, Russia, Ireland	-6	7	9.633	28.719	17
3	19-24; 26-31; 35-39; 41; 43-44; 47-48; 50; 52; 55; 57-61; 63-64; 68; 74; 79-81; 83-84; 87-88; 93-94; 98	South Korea, India, Japan, Denmark, Belgium, Brazil, Taiwan, Portugal, Austria, Italy, Poland, Norway, Bulgaria, Chile, Croatia, Mexico, Argentina, Romania Luxembourg, Turkey, Colombia, South Africa, Thailand, Philippines, Iceland, Cyprus, North Macedonia, Vietnam, Malta, Kenya, Nigeria, Jordan, Liechtenstein, Lebanon, Jamaica, Georgia, Ghana, Panama, Qatar, Cape Verde, Mongolia, Kuwait, Bangladesh, Somalia, Nepal	-4	5	0.173	8.888	45
4	25; 33; 40; 45; 51; 66; 70; 71; 75-76; 07	United Arab Emirates, New Zealand, Malaysia, Indonesia, Uruguay, Bahrain, Egypt, Saudi Arabia, Pakistan, Kazakhstan, Sri Lanka	7	18	0.245	6.951	11
5	32; 34; 42; 56; 62; 65; 67; 69; 70; 07; 07	Czechia, Ukraine, Latvia, Slovenia, Hungary, Serbia, Greece, Slovakia, Peru, Armenia, Belarus, Rwanda, Moldova, Albania, Tunisia, Bosnia and Herzegovina, Ecuador, Azerbaijan, Paraguay, Morocco, Dominican Republic, Uganda	-19	-4	0.18	6.226	22

The table shows the grouping of countries by cluster, the minimum and maximum boundaries of clusters in the context of two indicators, as well as the number of countries included in each cluster. Further implementation of cluster analysis involves conducting a variance analysis, the results of calculations are presented in the form of a table (Table 2).

Fischer statistics reflects the significant contribution of each indicator to cluster differentiation, with the largest share of the total Score indicator. Validation of variance analysis and Fischer Statistics indicates the validity of such a distribution.

Table 2. Univariate analysis of variance using SPSS Statistics software.

Indicator	Connections	Sum of squares	Degree of freedom	Middle square	<i>F</i>	Value
Rank Change (from 2020)	Between groups	3421.864	4	855.466	75.607	0.00
	In groups	1029.626	91	11.315		
	Total	4451.490	95	–	–	–
Total Score	Between groups	16207.285	4	4051.821	352.460	0.00
	In groups	1046.121	91	11.496	–	–
	Total	17253.406	95	–	–	–

5 Conclusion

The group includes 96 countries (4 countries that were in the rating for the first time were automatically excluded), which formed 5 clusters that differ from each other, but have common characteristics within the selected groups. Each cluster has its own characteristics. So, only one country belongs to cluster 1 – United States – which has been leading with a large gap in this rating for several years and has a maximum Total Score of 124.42.

The second cluster includes countries that are representatives of the top 20 (a total of 17 countries from the 2nd to the 18th place; Total Score: 28,719–9,633) and are characterized by a high level of the index, as well as moderate changes in the range of falling by a maximum of –6 positions (Spain) and growing by a maximum of 7 positions (China). Despite the change in position in the rating, the countries of this cluster are the leaders of the startup movement in the world.

The third cluster is represented by the largest number of countries (45) that are in the range from 19 to 98 positions of the rating and have minor changes in rank in this interval both in the direction of decline (maximum - 4 positions: Brazil, Italy) and in the direction of growth (maximum 5 positions: Turkey, Nigeria, Bangladesh), or do not have any changes in the rating (South Korea, Japan, Denmark, Austria, Thailand, Vietnam, Lebanon, Qatar).

The fourth cluster is represented by countries that achieved rapid growth in the rating in 2021 compared to 2020 (minimum - 7, maximum - 18 positions): a total of 11 countries, among which the highest growth in the rating is demonstrated by United Arab Emirates (+18 positions), Saudi Arabia (+17 positions), Uruguay (+15 positions), New Zealand (+14 positions).

The last, fifth cluster, represented by 22 countries, it also includes Ukraine, which occupies the 34th position in 2021 (Total Score 5,705) and has a drop of -5 points. The countries of this cluster are characterized by a negative rating change in 2021 (from -4 to -19 positions): Azerbaijan (-19 positions), Dominican Republic (-18 positions), Ecuador (-15 positions), Moldova (-13 positions), Hungary, Bosnia and Herzegovina, Morocco (-12 positions), Slovenia, Serbia, Paraguay (-11 positions), Greece (-10 positions). It should also be noted that negative changes have occurred in the startup ecosystems of European countries: Czechia, Latvia, Slovakia, Belarus, Albania.

Thus, the generalization of countries rating in 5 clusters allowed to identify the features of the development of startup ecosystems, to provide characteristics of each group of countries, and in the future to become the basis for developing recommendations and forming strategies for the development of the startup ecosystem.

References

1. Bobrovska, O.Y., Durman, M.O., Kravchenko, T.A., et al.: Management decisions to support and maintain the socio-economic development of the territories. *Estudios de Economía Aplicada* **39**(6) (2021). <https://doi.org/10.25115/eea.v39i6.5266>
2. Kuzmenko, S.H., Filipenko, T.V., Ryabev, A.A., et al.: Current conditions, causes and increase of poverty in Ukraine. *Asia Life Sci.* **22**(2), 43–56 (2020)
3. Gumenna, O.V., Ganushchak-Yefimenko, L.M.: Consumer value formation for knowledge within innovation ecosystem. *Actual Probl. Econ.* **2**, 8–13 (2014). (in Ukrainian)
4. Smachylo, V., Khalina, V., Chayka, D.: Formation of a local start-up ecosystem. *Econ. Soc.* **23**, 1–9 (2021). <https://doi.org/10.32782/2524-0072/2021-23-9>. (in Ukrainian)
5. StartupBlink: The Global Startup Ecosystem Index Report by StartupBlink (2021). <https://www.startupblink.com/blog/global-startup-ecosystem-index/>. Accessed 21 Apr 2022
6. Startup Genome: Key Insights from #GSER2021 (2021). <https://startupgenome.com/report/gser2021>. Accessed 21 Apr 2022
7. Gura, O.: Start-up as a tool for implementation of investment decisions. *Econ. Ecol. Socium* **2**(2), 1–11 (2018). <https://doi.org/10.31520/2616-7107/2018.2.2-1>
8. Kharkiv Regional State Administration: Development Strategy of Kharkiv region for 2021–2027 (2021). <https://kharkivoda.gov.ua/content/documents/1026/102538/files/Стратегія.pdf>. Accessed 21 Apr 2022
9. Lee, W., Kim, B.: Business sustainability of start-ups based on government support: an empirical study of Korean start-ups. *Sustainability* **11**(18), 4851 (2019). <https://doi.org/10.3390/su11184851>
10. Lee, Y.J., Yang, Y.: An impact of startup business performance by entrepreneurs' perceived importance, satisfaction, and level of meeting to expectation over government startup business aid programs. *Asia Pac. J. Bus. Ventur. Entrep.* **13**(1), 31–41 (2018)
11. Solomon, G.T., Bryant, A., May, K., Perry, V.: Survival of the fittest: technical assistance, survival and growth of small businesses and implications for public policy. *Technovation* **33**(8–9), 292–301 (2013). <https://doi.org/10.1016/j.technovation.2013.06.002>

12. Seo, J.H., Perry, V.G., Tomczyk, D., Solomon, G.T.: Who benefits most? The effects of managerial assistance on high-versus low-performing small businesses. *J. Bus. Res.* **67**(1), 2845–2852 (2014). <https://doi.org/10.1016/j.jbusres.2012.07.003>
13. LaunchVic: A startup guide and toolkit for local government: A resource to support startup activities (2017). <https://launchvic.org/files/LV-Startup-Guide.pdf>. Accessed 21 Apr 2022
14. Lesakova, L.: The role of business incubators in supporting the SME start-up. *Acta Polytechnica Hungarica* **9**(3), 85–95 (2012)
15. Motoyama, Y., Wiens, J.: Guidelines for Local and State Governments to Promote Entrepreneurship (2015). <https://doi.org/10.2139/ssrn.2580321>. Accessed 21 Apr 2022
16. Motoyama, Y., Konczal, J., Bell-Masterson, J., Morelix, A.: Think Locally, Act Locally: Building a Robust Entrepreneurial Ecosystem (2014). <https://doi.org/10.2139/ssrn.2425675>. Accessed 21 Apr 2022
17. Guryanova, L.S., Gvozdytskyi, V.S., Dymchenko, O.V., Rudachenko, O.A.: Models of forecasting in the mechanism of early informing and prevention of financial crises in corporate systems. *Finan. Credit Act. Probl. Theory Pract.* **3**(26), 303–312 (2018). <https://doi.org/10.18371/fcaptp.v3i26.144280>
18. Bogiday, I.: Clusterization of agro-industrial enterprises of Ukraine as the basis of effective strategic management. *Agric. Resour. Econ.* **5**(2), 86–98 (2019). <https://doi.org/10.22004/ag.econ.290315>
19. Sotska, Y.I.: Methodological basis of cluster analysis of the competitiveness of Ukrainian banks. *Finan. Credit Act. Probl. Theory Pract.* **2**(19), 177–185 (2015). <https://doi.org/10.18371/fcaptp.v2i19.57261>. (in Ukrainian)



Load Forecasting and Electricity Consumption by Regression Model

Maria Sukhonos , Volodymyr Babaiev , Vladyslav Pliuhin  , Vitaliy Teterev ,
and Illia Khudiakov 

O. M. Beketov National University of Urban Economy in Kharkiv,
17 Marshala Bazhanova Street, Kharkiv 61002, Ukraine
vladyslav.pliuhin@kname.edu.ua

Abstract. A non-standard method of forecasting load and power consumption using a regression model is considered. The training sample is taken as a basis, which is a set of values of the maximum annual load of the power system for the past ten years. The work is devoted to the issues of optimal design of the regression equation in the form of a time polynomial (polynomial) in order to ensure a high value of forecasting for the next five years and to estimate the confidence intervals of the forecast. A feature of this method of forecasting is the ability to find the values of the time series based on its historical values in energy. Which is the basis for planning, managing and optimizing energy production and control. Selection of informative indicators and determination of the type of model are considered separately. The statistical capacity of the model is being tested. However, the absence of autoregressive connections is checked. Calculation of interval estimates of the indicator and forecasting errors. Forecasting by regression model. In contrast to previous research, the authors have shown how to achieve a high rate of forecasting using the Python programming language and NumPy libraries. The results of the work will be useful for machine learning technologies, data science, statistics, energy companies and power systems and others.

Keywords: Energy system · Efficiency · NumPy · Statistics · Machine learning · Data science · Forecasting · Power engineering

1 Introduction

Increasing the security of electricity supply is one of the most important conditions for improving economic efficiency. With the growing use of smart electricity meters and the widespread introduction of various technologies for its production, such as solar panels, etc. [1], there is a lot of data on electricity consumption [2, 3].

Data Science – studies the problems of analysis, processing, and presentation of data in digital form. Combines methods for processing data in large volumes and a high level of parallelism, statistical methods, methods of data mining and the use of artificial intelligence to work with data, as well as methods of designing and developing databases [4, 5]. These data can be presented as multidimensional time series and used not only

to model but also to predict future electricity consumption [6]. Planning and forecasting play an important role in the reliability of electrical networks and enterprises [7, 8]. Forecasting makes it possible to create effective management and optimize the purchase and sale of goods and services to enterprises [9].

By observing the use of electricity, it has become possible to identify and study patterns based on economic and physical indicators in databases, which significantly increases the amount of input information for forecasting.

Given that modern approaches to economic and technical management are increasingly demanding on the accuracy of forecasting, the task of forecasting time series is becoming more difficult along with the development of information technology [10].

The task of forecasting time series is relevant at any time and its solution is an integral part of the daily work of most companies. This problem is solved by creating a forecasting model that adequately describes the research process.

This paper describes the construction of a mathematical model using the principal components method for forecasting electricity volumes. Energy supply is a participant in the wholesale electricity market and an intermediary between the wholesale market and the final consumer [11, 12]. Usually, the amount of electricity that an energy company needs to buy on the wholesale market is equal to the projected amount [13].

It is very important to make a forecast with the least error. Improving the efficiency of electricity generation and supply is an important and urgent task for the energy sector. In case of large errors of deviation from the plan for the energy supply of enterprises, fines are imposed, with possible exclusion from participation in the tender [14]. To reimburse financial costs, the company is forced to raise the price of electricity for consumers [15–17].

Therefore, to solve modern problems in forecasting should use modern methods of solving these problems. Today, significant solutions for forecasting regression models are possible using the Python programming language [18–20]. Namely using the NumPy open-source library. The capability of this library is that it can support multidimensional arrays, including matrices and high-level mathematical functions that are designed to work with multidimensional arrays [21, 22].

NumPy is a library used for mathematical calculations: from basic functions to linear algebra. The full name of the library is Numerical Python extensions, or Numerical Python extensions.

This library is written in C and Fortran. It is a compilation of language, the text of which is converted into machine code – a set of instructions for a particular type of processor. The conversion is done with the help of a special compiler program, thanks to which compilation calculations are much faster and more efficient [16, 21, 22].

The NumPy library [23, 24] provides implementations of computational algorithms in the form of functions and operators optimized for working with multidimensional arrays. As a result, any algorithm that can be expressed as a sequence of operations on arrays and matrices is implemented using NumPy, works as fast as the equivalent code executed in MATLAB.

2 Problem Statement and Initial Data

In the problem to be solved, the training sample is a set of values of the maximum annual load of the power system for the past 10 years. It is needed to choose the regression equation in the form of a time polynomial, perform a load forecast for the next 5 years and estimate the confidence intervals of the forecast.

The set of values observed, and the maximum annual load are given in Table 1.

Table 1. Initial data of electricity consumption.

Year number	1	2	3	4	5	6	7	8	9	10
Consumption, MW	11.37	12.02	13.3	14.41	16.42	17.99	19.02	21.18	22.39	24.78

Python code for creating data sets:

```
x= np.array ([1,2,3,4,5,6,7,8,9,10])
y= np.array
([11.37,12.02,13.3,14.41,16.42,17.99,19.02,21.18,22.39,24.78])
```

Graphic dependence of electricity consumption according to Table 1 shown in Fig. 1.

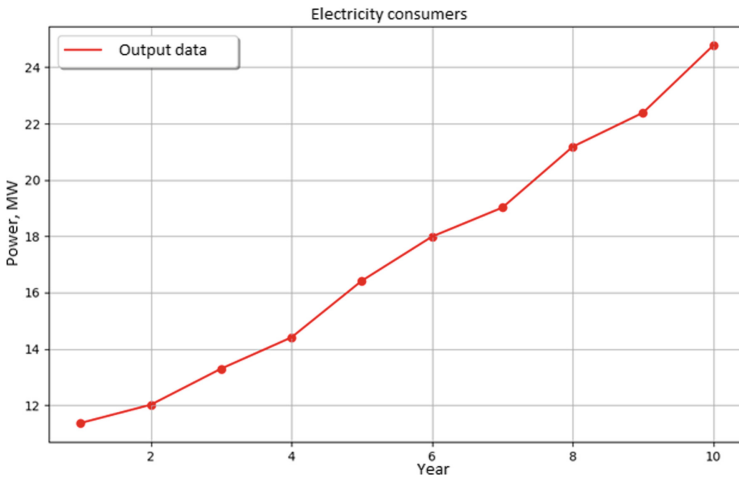


Fig. 1. Graph of electricity consumption according to the original data.

Code in Python for chart:

```
# Adjust the graphics area
plt.figure (figsize= (10,6))
plt.title ('Electricity consumption')
plt.xlabel ('Year')
plt.ylabel ('Power, MW')
plt.grid (True)
# Original data
plt.scatter (x1, y1,color='red')
plt.plot (x1, y1,color='r',label='Output data')
legend= plt.legend (loc='upper
left',shadow=True,fontsize='x-large')
plt.show ()
```

3 Selection of Informative Indicators and Determination of the Model Type

Graphical analysis of the data set (Fig. 1) allows to hypothesize the model as a time polynomial (polynomial):

$$y = a_1x_1 + a_2x_2 + a_3x_3,$$

where $x_1 = 1$; $x_2 = t$; $x_3 = t^2$ (t - time).

Then it is possible to get a vector of sample values of the simulated indicator, and a matrix of sample values X :

$$\overline{Y}_B = \begin{bmatrix} 11.37 \\ 12.02 \\ 13.30 \\ 14.41 \\ 16.42 \\ 17.99 \\ 19.02 \\ 21.18 \\ 22.39 \\ 24.78 \end{bmatrix}; \quad X = \begin{bmatrix} 1 & 1 & 1 \\ 1 & 2 & 4 \\ 1 & 3 & 9 \\ 1 & 4 & 16 \\ 1 & 5 & 25 \\ 1 & 6 & 36 \\ 1 & 7 & 49 \\ 1 & 8 & 64 \\ 1 & 9 & 81 \\ 1 & 10 & 100 \end{bmatrix}.$$

Python code for forming source matrices and calculating *Pearson* correlation coefficients:

```

x= np.array ([1,2,3,4,5,6,7,8,9,10])
y= np.array
([11.37,12.02,13.3,14.41,16.42,17.99,19.02,21.18,22.39,24
.78])
x_size=x.size
X= np.ones ((x_size,3))# matrix 10 x 3, filled with units
for row in range(10):
    for col in range(3):
        if col==1:#column with values of t
            X[row] [col] =x[row]
        if col==2:# column with values of t ^ 2
            X[row] [col] =x[row] **2
# Correlation coefficient
corel= np.corrcoef (x,y)
# Print values
print("Correlation")
print(corel)
print("Y")
print(y)
print("X")
print(X)

```

Point estimates of the coefficients of the model are determined by the ratio:

$$\vec{A} = (X^t X)^{-1} \cdot X^t \vec{Y}_B;$$

$$X^t X = \begin{bmatrix} 10 & 55 & 385 \\ 55 & 385 & 3025 \\ 385 & 3025 & 25333 \end{bmatrix}; X^t \vec{Y}_B = \begin{bmatrix} 172.68 \\ 1074.28 \\ 8045.14 \end{bmatrix}.$$

To obtain the vector of mathematical expectations of point estimates of the coefficients of the model, it is necessary to perform the inversion of the information matrix $M = X_t X$:

$$(X^t X)^{-1} = \begin{bmatrix} 1.3833 & -0.52499 & 0.04166 \\ -0.52499 & 0.241287 & -0.020833 \\ 0.04166 & -0.020833 & 1.89383 \cdot 10^{-3} \end{bmatrix}.$$

Calculating matrices and obtaining model coefficients in Python are as follows:

```

Xt= X.transpose ()# transposed matrix
XtY= np.dot (Xt, y)
XtX= np.dot (Xt, X)
X1= np.linalg.inv (XtX)# inverted matrix
A= np.dot (X1,XtY)

```

The result of the program is shown in Fig. 2.

```

Xt
[[ 1.  1.  1.  1.  1.  1.  1.  1.  1.  1.]
 [ 1.  2.  3.  4.  5.  6.  7.  8.  9. 10.]
 [ 1.  4.  9. 16. 25. 36. 49. 64. 81. 100.]]
XtY
[ 172.88 1074.88 8046.94]
XtX
[[1.0000e+01 5.5000e+01 3.8500e+02]
 [5.5000e+01 3.8500e+02 3.0250e+03]
 [3.8500e+02 3.0250e+03 2.5333e+04]]
XtX-1
[[ 1.38333333 -0.525      0.04166667]
 [-0.525      0.24128788 -0.02083333]
 [ 0.04166667 -0.02083333  0.00189394]]
A
[10.12783333  0.94893182  0.05041667]

```

Fig. 2. The result of the program execution.

4 Calculation of Point Estimates of Indicators and Modeling Errors

Mathematical expectation of Y_m model, or calculated values of the indicator, was found for the model using point estimates of the coefficients of the model by the ratio:

$$Y_m = a_1 x_{1i} + a_1 x_{1i} a_1 x_{1i}; \varepsilon = Y_B - Y_m.$$

The results of calculations on the sample are given in Table 2.

Table 2. Calculation of values and errors of the model.

Indicator	Year of observations									
	1	2	3	4	5	6	7	8	9	10
Y_B	11.37	12.02	13.10	14.41	16.42	17.99	19.02	21.18	22.39	24.78
Y_m	11.089	12.189	13.391	14.696	16.103	17.612	19.224	20.937	22.753	24.671
ε	0.281	-0.169	-0.291	-0.286	0.317	0.378	-0.204	0.243	-0.363	0.109
ε^2	0.0791	0.0285	0.084	0.0818	0.1005	0.1427	0.0415	0.0589	0.1319	0.0118

Python code:

```
Y= np.zeros (10)
e= np.zeros (10)
e2= np.zeros (10)
for row in range(10):
    Y[row] = A [0] * X [row] [0] + A [1] * X [row] [1] + A
    [2] * X [row] [2]
    e[row] = y [row] -Y[row]
    e2[row] =e[row] **2
```

The result of the program is shown in Fig. 3.

```
Y
[11.12718182 12.22736364 13.42837879 14.73022727 16.13290909 17.63642424
19.24077273 20.94595455 22.7519697 24.65881818]
e
[ 0.24281818 -0.20736364 -0.12837879 -0.32022727  0.28709091  0.35357576
-0.22077273  0.23404545 -0.3619697  0.12118182]
e2
[0.05896067 0.04299968 0.01648111 0.10254551 0.08242119 0.12501582
0.0487406 0.05477727 0.13102206 0.01468503]
```

Fig. 3. The result of the program execution.

5 Checking the Statistical Capacity of the Model

The null hypothesis test, which rejects the ability of the regression model, is performed by comparing the variance of the simulated indicator and the variance of the simulation error.

The dispersion ratio is subject to the *Fisher* distribution. To confirm the ability of the model, the value of F_p is calculated and compared with the critical value of the standard F -distribution with high reliability $\beta = 0.99$ (or 0.95) and the number of degrees of freedom of the numerator $(N - 1)$ and denominator $(N - n)$:

$$F_p = \frac{S^2(Y_B)}{S_\epsilon^2}, \quad \text{where } S_\epsilon^2 = \frac{\sum_{i=1}^n \epsilon_i^2}{N - n}.$$

Standard value of the F -distribution with reliability $\beta = 0.99$ and the number of degrees of freedom of the numerator $\lambda_1 = (10 - 1) = 9$ and the denominator $\lambda_2 = (10 - 2) = 8$ is equal to $F_{table} = 5.91$ [15]. Therefore, $F_p = 223 > F_{table}$ and the null hypothesis about the insolvency of the model is rejected, i.e. the adequacy of the type of model and estimates of mathematical expectations of the coefficients is confirmed.

The Python code for determining the F -distribution is given below.

```

N=10 n=2
Sy= (np.sum (y) - y [9]) /N-2)
Sy2=Sy**2
sum_e2= np.sum (e2) - e2 [9]
Se2=sum_e2/ (N-n)
Fp.=Sy/Se2
    
```

6 Forecasting by Regression Model

Forecasting by regression model includes the determination of point and interval estimates of the modeling indicator for a given perspective. Point estimates of the indicator for the year are determined by the model.

$$y_i = a_1x_1 + a_2x_2 + a_3x_3; \text{ or } y = 10.09 + 0.95t + 0.05t^2.$$

Interval estimates for the year are performed based on calculations of forecasting errors in the ratio:

$$S_i = S_\varepsilon \sqrt{1 + \vec{X}_i (X^t X)^{-1} \vec{X}_i^t}.$$

The results of forecasting for a period of 5 years are given in Table 3, and Fig. 4 shows a chart of the calculated forecast.

Table 3. Forecasting the maximum annual load of the power system.

Indicator	Year				
	11	12	13	14	15
$\vec{X}_i (X^t X)^{-1} \vec{X}_i^t$	1.383	2.801	5.145	8.733	13.928
S	0.4762	0.6015	0.7647	0.9625	1.1919
Y	26.69	28.83	31.02	33.34	35.77
ΔY	1.6	2.021	2.569	3.234	4.004

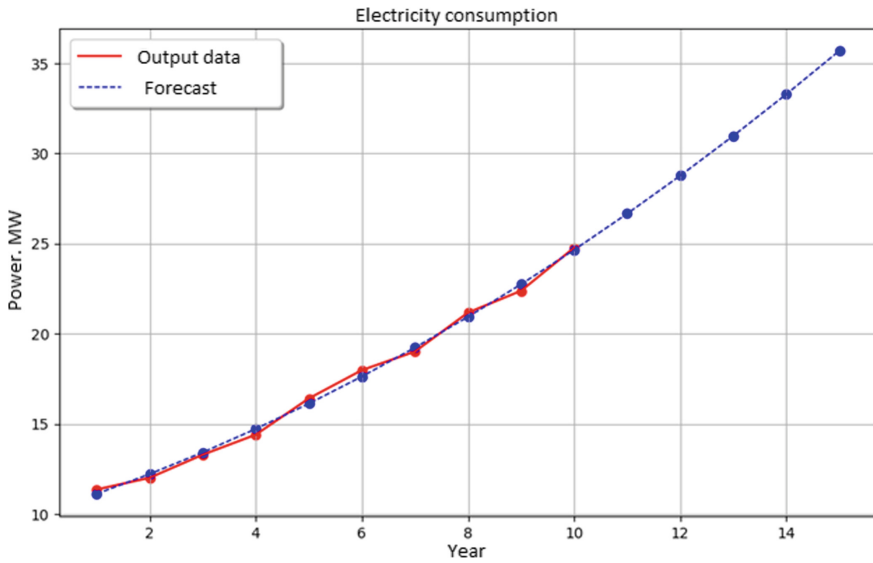


Fig. 4. Graph of electricity consumption forecasting.

Python calculation code:

```

years= np.array
([1,2,3,4,5,6,7,8,9,10,11,12,thirteen,14,15])
num_years=years.size
score= np.zeros (num_years)
yp= np.zeros (num_years)
S11= np.zeros (num_years)
dy11= np.zeros (num_years)
for year in years:
    index=year-1
    yp[index] = A [0] + A [1] *year+ A [2] *year**2
    v1= np.array ([1,year,year**2])
    v2=v1.transpose ()
    score1= np.dot (v1, X1)
    score[index] = np.dot (score1,v2)
    S11[index] = rmse * math.sqrt (1+score[index])
    dy11[index] = tt *S11[index]
# Build graphics
plt.plot (years,yp, '-
', color='blue',linewidth=1,label='Forecast')
plt.scatter (years,yp,color='b')
plt.show ()

```

The result of the program is shown in Fig. 5.

```

Yp
[11.12718182 12.22736364 13.42837879 14.73022727 16.13290909 17.63642424
 19.24077273 20.94595455 22.7519697 24.65881818 26.6665 28.77501515
 30.98436364 33.29454545 35.70556061]
score
[ 0.61818182  0.27878788  0.18333333  0.19545455  0.22424242  0.22424242
  0.19545455  0.18333333  0.27878788  0.61818182  1.38333333  2.80151515
  5.14545455  8.73333333 13.92878788]
S11
[0.33114335 0.29437548 0.28317567 0.28462229 0.28802892 0.28802892
 0.28462229 0.28317567 0.29437548 0.33114335 0.4018785 0.50755223
 0.64532633 0.81214426 1.005807 ]
dy11
[1.11264166 0.98910162 0.95147024 0.95633091 0.96777717 0.96777717
 0.95633091 0.95147024 0.98910162 1.11264166 1.35031177 1.70537551
 2.16829648 2.72880472 3.37951153]

```

Fig. 5. The result of the program execution.

A similar prediction can be made with the NumPy library much more faster:

```

poly_np= np.poly1d (np.polyfit (x, y,2))
yp=poly_np(years)
coeff1=poly_np.coeffs
poly_rmse= np.sqrt (mean_squared_error (y,poly_np((x))))
print("Rmse error =",poly_rmse)
print("Coefficients of the equation")
print(coeff1)
y11=poly_np(11)
print("Forecast for the 11th year =",round(y11, 3))

```

The result of the program is shown in Fig. 6.

```

Rmse error = 0.26031691059052153
Coefficients of the equation
[ 0.05041667  0.94893182 10.12783333]
Forecast for the 11th year = 26.666

```

Fig. 6. The result of the program execution.

Figure 7 shows the forecasting graph obtained by performing specialized Python mathematical statistics libraries.

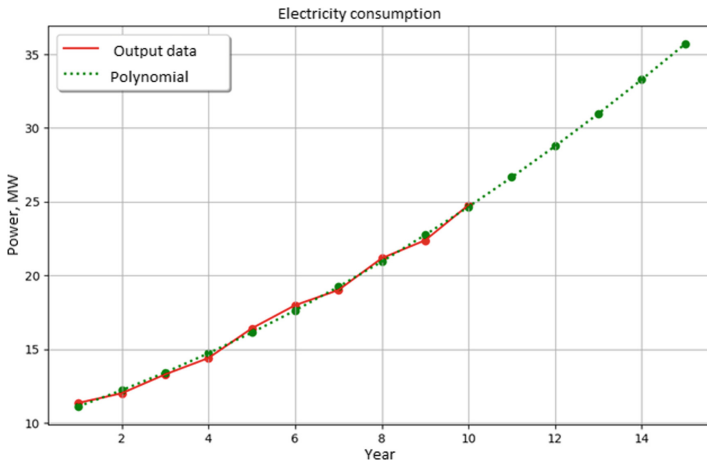


Fig. 7. Graph of electricity consumption forecasting in Python.

7 Conclusion

Forecasting by regression model includes the determination of point and interval estimates of the simulation indicator for a given perspective. The verification of the significance of the model coefficients was performed on the basis of comparing the value of the model coefficient and estimating its error. The ratio of these quantities is subject to the Student distribution.

The theoretical solution of the tasks is proposed to be solved on the basis of modern computational algorithms of machine learning using a programming language, namely NumPy libraries, which not only provides a mathematical model with a large database of statistical materials, but also allows adjusting the current state of the power system.

In energy, Data Science can help solve many problems, such as forecasting electricity consumption, forecasting electricity prices, calculating optimal tariffs, diagnosing energy facilities, optimizing consumption patterns and more.

References





1. Tugay, D., Kotelevets, S., Korneliuk, S., Zhemerov, G.: Energy efficiency of microgrid implementation with solar photovoltaic power plants. In: 2018 IEEE 3rd International Conference on Intelligent Energy and Power Systems (IEPS), Kharkiv, pp. 275–279. IEEE (2018). <https://doi.org/10.1109/IEPS.2018.8559579>
2. Akbar, B., Amber, K.P., Kousar, A., et al.: Data-driven predictive models for daily electricity consumption of academic buildings. *AIMS Energy* **8**(5), 783–801 (2020). <https://doi.org/10.3934/energy.2020.5.783>

3. Bedi, J., Toshniwal, D.: Deep learning framework to forecast electricity demand. *Appl. Energy* **238**, 1312–1326 (2019). <https://doi.org/10.1016/j.apenergy.2019.01.113>
4. Kondratiev, A., Píšťek, V., Purhina, S., et al.: Self-heating mould for composite manufacturing. *Polymers* **13**(18), 3074 (2021). <https://doi.org/10.3390/polym13183074>
5. Aksonov, Y., Kombarov, V., Tsegelnyk, Y., et al.: Visualization and analysis of technological systems experimental operating results. In: 2021 IEEE 16th International Conference on Computer Sciences and Information Technologies (CSIT), Lviv, vol. 2, pp. 141–146. IEEE (2021). <https://doi.org/10.1109/CSIT52700.2021.9648592>
6. Deng, S., Yuan, C., Yang, L., Zhang, L.: Distributed electricity load forecasting model mining based on hybrid gene expression programming and cloud computing. *Pattern Recogn. Lett.* **109**, 72–80 (2018). <https://doi.org/10.1016/j.patrec.2017.10.004>
7. Zahid, M., Ahmed, F., Javaid, N., et al.: Electricity price and load forecasting using enhanced convolutional neural network and enhanced support vector regression in smart grids. *Electronics* **8**(2), 122 (2019). <https://doi.org/10.3390/electronics8020122>
8. Zhou, X., Gao, Y., Yao, W., Yu, N.: A robust segmented mixed effect regression model for baseline electricity consumption forecasting. *J. Mod. Power Syst. Clean Energy* **10**(1), 71–80 (2020). <https://doi.org/10.35833/MPCE.2020.000023>
9. Hong, W.C., Fan, G.F.: Hybrid empirical mode decomposition with support vector regression model for short term load forecasting. *Energies* **12**(6), 1093 (2019). <https://doi.org/10.3390/en12061093>
10. Lee, C.W., Lin, B.Y.: Applications of the chaotic quantum genetic algorithm with support vector regression in load forecasting. *Energies* **10**(11), 1832 (2017). <https://doi.org/10.3390/en10111832>
11. Dovgalyuk, O., Omelianenko, H., Pirotti, A., et al.: Reliability increase of the distribution electric networks operation in the implementation of the energy market in Ukraine. In: 2019 IEEE 6th International Conference on Energy Smart Systems (ESS), Kyiv, pp. 70–75. IEEE (2019). <https://doi.org/10.1109/ESS.2019.8764243>
12. Chen, Q., Balian, A., Kyzym, M., et al.: Electricity markets instability: causes of price dispersion. *Sustainability* **13**(22), 12343 (2021). <https://doi.org/10.3390/su132212343>
13. Mohammed, N.A., Al-Bazi, A.: An adaptive backpropagation algorithm for long-term electricity load forecasting. *Neural Comput. Appl.* **34**(1), 477–491 (2021). <https://doi.org/10.1007/s00521-021-06384-x>
14. Sayenko, Y., Baranenko, T., Kalyuzhnyi, D.: Compensation of reactive power in electrical supply systems of large industrial enterprises. *Przeglad Elektrotechniczny* **91**(11), 77–80 (2015). <https://doi.org/10.15199/48.2015.11.22>
15. Moon, J., Park, J., Hwang, E., Jun, S.: Forecasting power consumption for higher educational institutions based on machine learning. *J. Supercomput.* **74**(8), 3778–3800 (2017). <https://doi.org/10.1007/s11227-017-2022-x>
16. El Sayed, M.A.E.A., Moustafa, H.M.M., Ziedan, I.E.S., Zamel, A.A.: A combined effective time series model based on clustering and whale optimization algorithm for forecasting smart meters electricity consumption. *COMPEL* **41**(1), 209–237 (2021). <https://doi.org/10.1108/COMPEL-04-2021-0150>
17. Saxena, H., Aponte, O., McConky, K.T.: A hybrid machine learning model for forecasting a billing period's peak electric load days. *Int. J. Forecast.* **35**(4), 1288–1303 (2019). <https://doi.org/10.1016/j.ijforecast.2019.03.025>
18. Pluihin, V., Korobka, V., Karyuk, A., et al.: Using Azure Machine Learning Studio with Python scripts for induction motors optimization web-deploy project. In: 2019 IEEE International Scientific-Practical Conference Problems of Infocommunications, Science and Technology (PIC S&T), Kyiv, pp. 631–634. IEEE (2019). <https://doi.org/10.1109/PICST47496.2019.9061447>

19. Pliuhin, V., Pan, M., Yesina, V., Sukhonos, M.: Using Azure Maching Learning cloud technology for electric machines optimization. In: 2018 International Scientific-Practical Conference Problems of Infocommunications. Science and Technology (PIC S&T), Kharkiv, pp. 55–58. IEEE (2018). <https://doi.org/10.1109/INFOCOMMST.2018.8632093>
20. Pliuhin, V., Sukhonos, M., Bileckiy, I.: Object oriented mathematical modeling of electrical machines. In: 2020 IEEE 4th International Conference on Intelligent Energy and Power Systems (IEPS), Istanbul, pp. 267–272. IEEE (2020). <https://doi.org/10.1109/IEPS51250.2020.9263158>
21. Tajeuna, E.G., Bouguessa, M., Wang, S.: A network-based approach to enhance electricity load forecasting. In: 2018 IEEE International Conference on Data Mining Workshops (ICDMW), Singapore, pp. 266–275. IEEE (2018). <https://doi.org/10.1109/ICDMW.2018.00046>
22. Wang, D., Yue, C., ElAmraoui, A.: Multi-step-ahead electricity load forecasting using a novel hybrid architecture with decomposition-based error correction strategy. *Chaos Solitons Fractals* **152**, 111453 (2021). <https://doi.org/10.1016/j.chaos.2021.111453>
23. Roubeyrie, L., Celles, S.: Windrose: a Python Matplotlib, Numpy library to manage wind and pollution data, draw windrose. *J. Open Source Softw.* **3**(29), 268 (2018). <https://doi.org/10.21105/joss.00268>
24. Harris, C.R., Millman, K.J., Van Der Walt, S.J., et al.: Array programming with NumPy. *Nature* **585**(7825), 357–362 (2020). <https://doi.org/10.1038/s41586-020-2649-2>



Butterfly Valve PID-Controller for Application in Individual Heating Substations

Olga Arsenyeva¹ , Jiří Jaromír Klemesš² , Petar Sabev Varbanov² ,
and Petro Kapustenko² 

¹ O. M. Beketov National University of Urban Economy in Kharkiv, 17 Marshala Bazhanova Street, Kharkiv 61002, Ukraine

olga.arsenyeva@kname.edu.ua

² Brno University of Technology, Technická 2896/2, 616 69 Brno, Czech Republic

Abstract. The reduction of the fossil fuels consumption is of great importance nowadays. The heating of residential apartments of domestic houses and hot water supply in the modern metapolicies arises challenges in application of modern technologies. The necessity for reliable regulation of temperatures inside the apartments requires quick-respond and accurate control techniques for the implied equipment. In the present work, the parametric model predictive control technique for water flowrate control of the butterfly type valve used for temperature and flowrate regulation in the individual heat substation of centralized heating system is proposed. The model improves the non-linear characteristics resulting in quality of flow control.

Keywords: Individual heat substation · Model predictive control · Butterfly valve

1 Introduction

To adjust a flowrate when transporting a fluid between two places is crucial for many systems. The main challenge is to produce a constant flow rate, what can be done using efficient and reliable controllers. For the closed-loop operations of flow regulation in industry the proportional integral derivative (PID) controllers are widely used. The PID controllers are widely applied and have the possibility to maintain reasonable efficiency of controlled parameter [1, 2]. When implemented with programmable logic controllers, they can perform poorly in operations with highly nonlinear systems. The parameters of PID control are crucial for reliable operation of the whole system and should be determined causing the minimal error of the system.

The application of Model Predictive Control (MPC) for building energy systems can reduce the energy consumption and increase the reliability [3]. For achieving the high effect of regulation, the MPC requires for the equipment integrated for the regulation. For the central district heating [4], the individual heat substations are commonly used to provide hot water for the radiators in rooms, and to adjust the water temperature, the flow rate control is essential. One of the approaches is to adjust room temperatures according

to the consumer needs [5]. One of the efficient techniques is to use the distributed model predictive control, which can be applied for optimization and control of indoor temperature based on the advancement of circulating water load according to the predicted heat demand as proposed in [6]. The proposed method can increase the control accuracy of the room temperature, the efficiency of water pump by up to 16% and to decrease the energy consumption by 14%. Another approach is the application of artificial neural networks (ANN) for water flow controllers. As flow control is characterized by highly non-linear systems, the heuristic methods and ANN are widely applied. The data presented in [7] show the two times decrease of maximum overshoot and 30% decrease of steady state error, when comparing ANN controller with conventional PID.

The simultaneous optimization of the control system and equipment used in the individual heat substation (IHS) arises new challenges in efficient energy consumption. The approach for rising the efficiency of IHS by simultaneous selection of heat exchanger, circulating water pump and automatic control station is presented in [8]. The outlet temperature adjustment by the flow control for steam heated heat exchanger is observed in [9], where the approach for optimization of plate heat exchanger is suggested. It is emphasized, that the selection of heat exchanger plays crucial role for reliable operation of IHS. The optimization methods for plate heat exchanger selection for different conditions can be found in [10]. The approach for optimal design of modern pillow-plate heat exchangers for the district heating duties is discussed in [11].

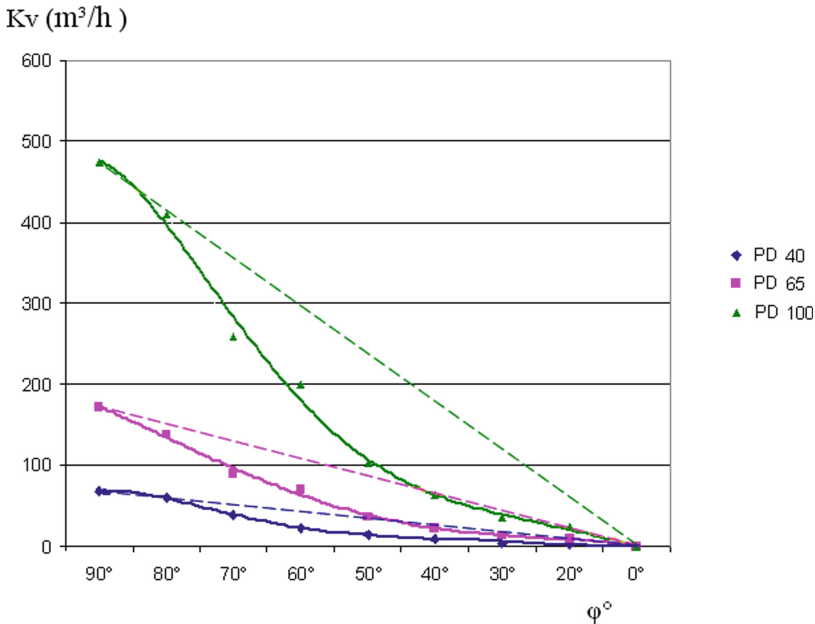


Fig. 1. The flow characteristic curves and coefficient K_v (m^3/h) values versus paddle rotation angle φ for butterfly valves of different diameters (at 20 °C temperature and 1 bar pressure).

The flow rate control can be done by the different types of valves, namely block valves, gated valves, disk-shaped rotary gates, needle valves, ball-valves, saddle valves [12]. In IHS the butterfly type valves are the most commonly used [13]. But such equipment has non-linear dynamic characteristic, that affects the precision of control in case of using it in couple with PID-controllers. Most producers of butterfly valves present the flow characteristic data of their valves in technical manuals. The typical flow characteristic curves and coefficient K_v (m^3/h) values versus paddle rotation angle for butterfly valves of different diameters are presented on Fig. 1 for temperature equal to 20°C and pressure 1 bar. The characteristics of valves with nominal diameters ND 40, ND 65, ND 100 are given. As it can be seen, the valves characteristics are nonlinear and the nonlinearity progresses with the increase of valve passage diameter.

For the regulation techniques the machine learning methods are widely used to improve the accuracy of regulation and to ensure the constant flowrate in the system.

The present work proposes the approach to improve the control quality of butterfly valve for individual heat substations in district heating using the parametric model predictive control. The work uses the microcontroller device and implemented microchip for valve positioning sensor.

2 Linearization of Rotation Angle Characteristics

In order to ensure the reliability of IHS and proper regulation of supply temperature, the scheme represented at Fig. 2 is applied for the flow rate control of the circulating water, going out of the heat exchanger.

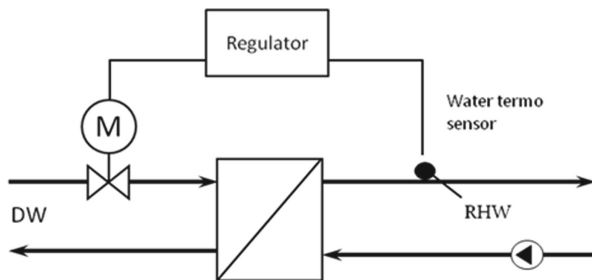


Fig. 2. Scheme of control for heat exchanger used in IHS.

Through the proper configuration of heat exchanger operation, it is possible not only to maintain the temperature at the required value, but also to save the consumption of energy. Therefore, the selection of the regulation valve from the hydraulic point of view is essential for the reliable operation of all IHS.

2.1 The Definition of Valve's Rotation Angle

To create the mathematical model of the valve, which will ensure the proper operation of the valve's rotation angle, it is needed to collect the data of the dynamic characteristic of

the valve K_v . The K_v data and the rotation angle values at each time point were examined. Valve dynamic response data can be presented as a relation of the following form:

$$K_v = b \cdot e^{x/a}, \quad \varphi \leq 75^\circ \tag{1a}$$

$$K_v = c \cdot x - d, \quad \varphi \geq 75^\circ \tag{1b}$$

where the parameters a, b, c, d have different values for each valve size (see Table 1).

Table 1. Values of parameters for Eqs. (1).

Parameter	DN40	DN50	DN65	DN80	DN100
a	19.5	19	21.65	21.3	20.8
b	1	1.5	3.5	5	9
c	0.8	2.2	3.4	5.1	6.4
d	4	86	134	201	102

To reach the set temperature, the controllers generate pulses for the drive, depending on the reaction of the system. When approaching the set value of the controlled parameter, the pulse duration decreases depending on the required accuracy of maintaining the parameter value.

As can be seen from the dynamic characteristics of the valves (Fig. 1), the reaction of the system in different parts of the valve rotation angle at minimum impulses will be different.

To bring the dynamic characteristic to a linear form, a coefficient is found, which is an amendment for the regulating system for each section of the characteristic in the range from 0° to 90° . To do this, the graph of the dynamic response of a given valve is divided into sections ΔF_{ri} , which can be considered linear. Then projections are lowered onto the K_v flow rate scale, forming segments ΔK_{vi} . The projections of the obtained segments fall onto the ideal characteristic, forming the segments ΔF_{ri} , as shown in Fig. 3.

The required correction factor is the ratio of the slope angles of the segments ΔF_{rr} and F_{ri} of the real and ideal dynamic characteristics of the valve.

The equation of the segments for the ideal and real characteristics, respectively:

$$K_{v1} = k_1 \cdot \varphi_i \tag{2a}$$

$$K_{v2} = k_2 \cdot \varphi_r \tag{2b}$$

where the coefficients k_1 and k_2 determine the angle of lines inclination.

For each of the segments, these coefficients can be obtained from Eqs. (2). In this case, the displacement of the segments relative to the φ axis can be neglected.

After the necessary transformations, we get:

$$a = \Delta K_v / \Delta \varphi_i \tag{3a}$$

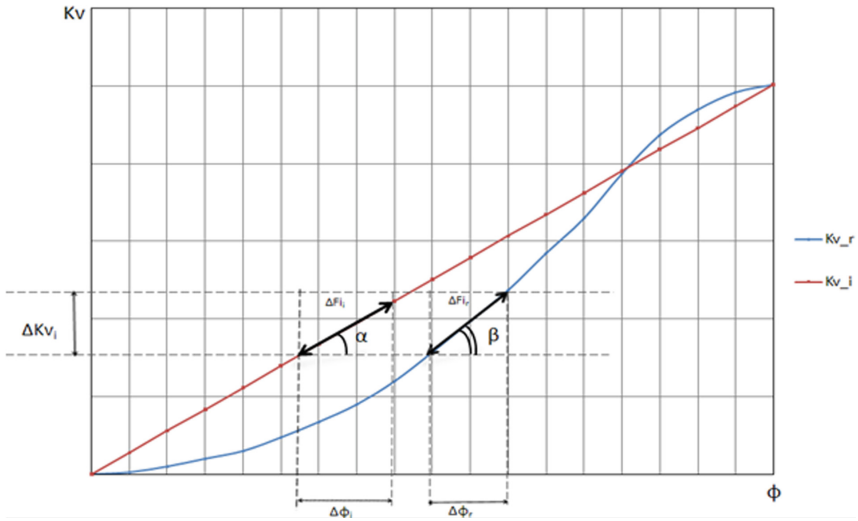


Fig. 3. Linearization of the dynamic coefficients.

$$b = \Delta K_v / \Delta \varphi_r \tag{3b}$$

where $\Delta \varphi_i$ and $\Delta \varphi_r$ are projections of segments corresponding to the ideal and real characteristic on the x-axis.

From Eqs. (3) it is possible to get the ratio of the analyzed characteristics:

$$b/a = \Delta \varphi_r / \Delta \varphi_i \tag{4}$$

Thus, the correction factor is the ratio of the lengths of the projections of the segments of the real and ideal characteristics on the φ -axis.

The resulting correction factors determine the duration of the minimum pulse in each range of the dynamic response of the valve. The duration of the minimum pulse is determined by the accuracy of the regulation calculation. In this case, it is $\pm 0.5^\circ\text{C}$. Thus, the minimum pulse duration is chosen such that when the valve is turned through the n -th angle, the temperature changes by 0.5°C .

2.2 Description of Experimental Set-Up

To study the developed approach, an experimental set-up presented in Fig. 4 was created. The set-up consists of: a direct current source 1 ($I = 4 \dots 20 \text{ mA}$), an electric drive with a positioner, developed by us for the experiment, a phase voltage regulator.

The physical model of the thermal system includes a heater placed in a pipe along which air moves, blown by a fan. A voltage stabilizer is used to select the air flow and stabilize it.

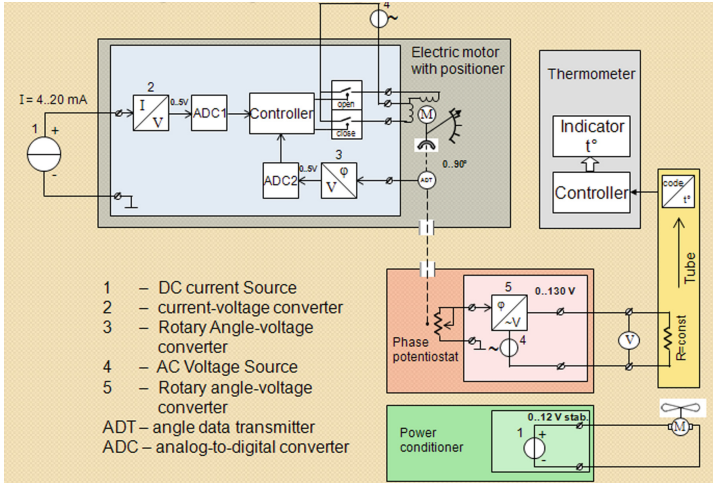


Fig. 4. Principal schema of experimental set-up.

2.3 Hardware Description

DC Current Source. DC current source manufactured by AO Spivdruzhnist-T LLC (Ukraine) was used.

Electric Motor with Positioner. The electric drive with the positioner contains the following units: current-voltage converter 2 converts direct current from 4–20 mA into direct voltage 0-V, has a linear characteristic; ADC1 converts the voltage into a code transmitted to the controller, 2 switches, a motor with a gearbox and an ADT rotation angle sensor, which is installed on the shaft; Angle-voltage converter 3, which has a linear characteristic, ADC2 converts the voltage from converter 3 into a code transmitted to the controller.

The ADC digitizes the signal. The controller also receives a signal from the ADC from the rotation angle sensor. The controller, having received data from two ADCs, processes the error in the position of the electric drive shaft and, if there is an error, issues a command to one of the switches - rotates the shaft in the direction of opening or closing. There is an ADT rotation angle sensor on the shaft, which outputs a signal to the transducer 3, on the same shaft there is a rotation indicator in the form of an arrow with a scale in degrees.

Phase Potentiator. A variable resistor of the phase voltage regulator is rigidly connected to the drive shaft, which is a rotation angle sensor for the phase regulator. The

phase regulator includes a rotation angle converter to voltage 5. Its transfer characteristic is non-linear, which makes the system characteristic close to that of the control object. The voltage at the output of the phases of the regulator is controlled by a voltmeter. Fan with voltage stabilizer: by changing the voltage of the stabilizer, you can change the air flow in the pipe, thus simulating the coolant flow in the system.

3 Results and Discussion

The experimental set-up was designed in such a way that its dynamic response is close to the dynamic response of the valve. In this case, the dependence of the angle of rotation on the input current has a linear form. To linearize this characteristic of the system, the corresponding sections of the characteristic were selected and correction factors were calculated for them. When turning on the rotation angle system implemented on the basis of the test bench model, the results presented in Fig. 5 were obtained. For the rest part of experiment, the experimental set-up was modified as shown in Fig. 6.

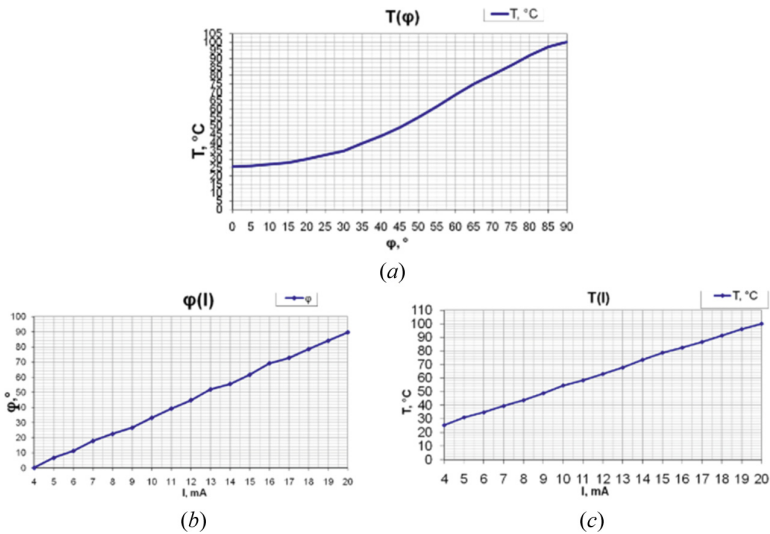


Fig. 5. Results of experiments: (a) temperature change depending on rotation angle; (b) change of rotation angle depending on current; (c) change of temperature depending on current.

The studies were carried out in three modes: at a given air temperature of 33 °C, 45 °C, and 73 °C. The speed of reaching the set temperature was estimated, as well as the fluctuation of the controlled parameter around the set value. The experimental results are presented in Fig. 7.

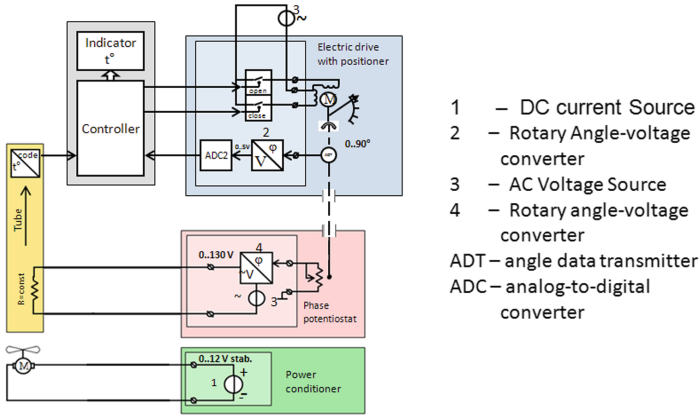


Fig. 6. Principal schema of modified experimental set-up.

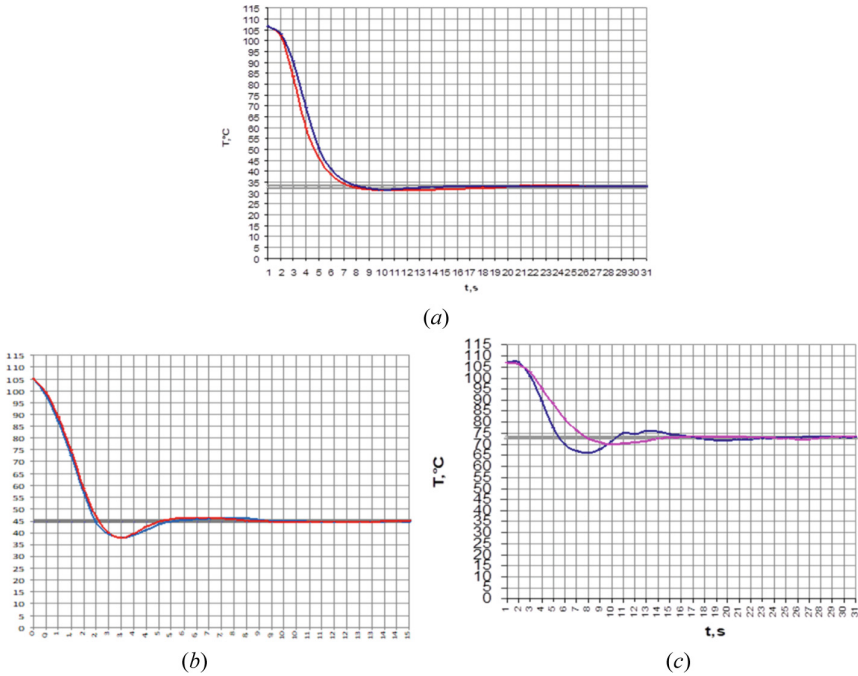


Fig. 7. Experimental results on modified set-up at different temperatures: (a) 33 °C; (b) 45 °C; (c) 73 °C.

From the obtained results, it can be seen that when using the system for taking into account the angle of rotation of the valve, the set temperature is reached faster, while there is a smaller number of oscillations of the controlled parameter around the set value.

4 Conclusion

In this paper the linearization of the rotation angle characteristic was carried out. The realized rotation angle accounting system provides constant regulation quality in every functioning mode of system. It decreases the common oscillation of the system and optimizes system impact on change of value of controlled parameter. The rotation angle accounting system may contain dynamic characteristic data of butterfly valve of any diameter. The further improvement of regulation quality can be achieved by implementing the model of heat exchanger accounting the butterfly valve flow characteristic.

Acknowledgement. This research has been supported by the EU project “Sustainable Process Integration Laboratory – SPIL”, project No. CZ.02.1.01/0.0/0.0/15_003/0000456 funded by EU “CZ Operational Programme Research, Development and Education”, Priority 1: Strengthening capacity for quality research.

References

1. Jagatheesan, K., Anand, B., Samanta, S., et al.: Design of a proportional-integral-derivative controller for an automatic generation control of multi-area power thermal systems using firefly algorithm. *IEEE/CAA J. Automatica Sinica* **6**(2), 503–515 (2017). <https://doi.org/10.1109/JAS.2017.7510436>
2. Garcíadealva, Y., Best, R., Gómez, V.H., et al.: A cascade proportional integral derivative control for a plate-heat-exchanger-based solar absorption cooling system. *Energies* **14**(13), 4058 (2021). <https://doi.org/10.3390/en14134058>
3. Mork, M., Xhonneux, A., Müller, D.: Nonlinear distributed model predictive control for multi-zone building energy systems. *Energy Build.* **264**, 112066 (2022). <https://doi.org/10.1016/j.enbuild.2022.112066>
4. Redko, I., Ujma, A., Redko, A., et al.: Energy efficiency of buildings in the cities of Ukraine under the conditions of sustainable development of centralized heat supply systems. *Energy Build.* **247**, 110947 (2021). <https://doi.org/10.1016/j.enbuild.2021.110947>
5. Lastovets, N., Kosonen, R., Mustakallio, P., et al.: Modelling of room air temperature profile with displacement ventilation. *Int. J. Vent.* **19**(2), 112–126 (2020). <https://doi.org/10.1080/14733315.2019.1579486>
6. Meng, Z., Junqi, Y.U., Anjun, Z.: Distributed model predictive control for central heating of high-rise residential buildings. *J. Asian Archit. Build. Eng.*, 1–13 (2022). <https://doi.org/10.1080/13467581.2021.1987245>
7. Ahmad, B., Prajitno, P.: Design of neural network and PLC-based water flow controller. *J. Phys. Conf. Ser.* **1528**, 012065 (2020). <https://doi.org/10.1088/1742-6596/1528/1/012065>
8. Gao, B., Zhang, L., Tian, Y., Zhou, M.: Analysis on energy saving measures of heat exchange station in central heating system. *Procedia Eng.* **205**, 581–587 (2017). <https://doi.org/10.1016/j.proeng.2017.10.422>
9. Kapustenko, P., Dobromyslova, O., Dobromyslov, O., et al.: Control of plate heat exchanger outlet temperature using butterfly valve and parametric model predictive control technique. *Chem. Eng. Trans.* **18**, 827–832 (2009). <https://doi.org/10.3303/CET0918135>
10. Klemes, J.J., Arsenyeva, O., Kapustenko, P., Tovazhnyanskyy, L.: *Compact Heat Exchangers for Energy Transfer Intensification: Low Grade Heat and Fouling Mitigation*. CRC Press, Boca Raton (2015). <https://doi.org/10.1201/b18862>

11. Arsenyeva, O., Tran, J., Piper, M., Kenig, E.: An approach for pillow plate heat exchangers design for single-phase applications. *Appl. Therm. Eng.* **147**, 579–591 (2019). <https://doi.org/10.1016/j.applthermaleng.2018.08.083>
12. Buffa, S., Fouladfar, M.H., Franchini, G., et al.: Advanced control and fault detection strategies for district heating and cooling systems – a review. *Appl. Sci.* **11**(1), 455 (2021). <https://doi.org/10.3390/app11010455>
13. Zeh, R., Ohlsen, B., Philipp, D., et al.: Large-scale geothermal collector systems for 5th generation district heating and cooling networks. *Sustainability* **13**(11), 6035 (2021). <https://doi.org/10.3390/su13116035>



Analysis of Gas Transmission Systems Elements from the Perspective of the Sustainable Development Concept

Katerina Paleyeva^(✉) , Ivan Kaptsov, and Nataliya Kaptsova 

O. M. Beketov National University of Urban Economy in Kharkiv,
17 Marshala Bazhanova Street, Kharkiv 61002, Ukraine
Kateryna.Palieieva@kname.edu.ua

Abstract. At the beginning of the 21st century, the concept of sustainable development was developed in many countries around the world. It aims to combine environmental, economic and social aspects of modern society. Being an equal member of the world community, Ukraine is constantly taking steps to achieve and maximize the goals of the concept of sustainable urban development. One of the main directions of Ukraine's industry is the fuel and energy complex, one of the components of which is the gas industry. Each direction of the gas industry (extraction; transportation; storage; distribution and sale of natural gas) has a significant impact on the environmental, social and economic components of Ukraine's development. Therefore, considering the gas industry in terms of the concept of sustainable development is an urgent task. One of the directions of the gas industry is the transportation of natural gas which is an important activity of the gas industry. The aim of this paper is to analyze the existing defects of the elements of gas transmission systems and their effects on economic, environmental and social components in terms of the concept of sustainable development. The analysis of the main factors of failures and accidents on Ukrainian and European gas pipelines is carried out. It has been found out that one of the main factors is corrosion. The method of calculating the effect of surfactants on the process of accelerating the accumulation of damage is presented its also presented.

Keywords: Leaks · Corrosion · Environmental safety

1 Introduction

At the beginning of the 21st century, the concept of sustainable development was developed in many countries around the world. It aims to combine environmental, economic and social aspects of modern society. The Sustainable Development Goals were endorsed by the United Nations Summit on Sustainable Development in 2015. They have become a priority for the European and global community in the 21st century. After signing the Association Agreement with the European Union, Ukraine has become an equal member of this community not only mentally but also legally. Therefore, in the framework of this

agreement and on the basis of good will, our state is constantly taking steps to achieve and maximize the goals of the concept of sustainable urban development.

On January 1, 2020, the Law of Ukraine “On the Key Principles (Strategy) of the State Environmental Policy of Ukraine for the Period till 2030” entered into [1]. Among other things, it defines the following principles of state environmental policy:

- meeting the goals of sustainable development;
- promoting balanced (sustainable) development by achieving balanced components of development (economic, environmental, social), focusing on the priorities of balanced (sustainable) development;
- prevention of emergencies of natural and man-made nature, which includes analysis and forecasting of environmental risks based on the results of strategic environmental assessment, environmental impact assessment, as well as comprehensive monitoring of the environment;
- state stimulation of domestic economic entities that reduce greenhouse gas emissions, reduce energy and resource intensity, modernization of production aimed at reducing the negative impact on the environment.

Ukraine is an industrialized country. Therefore, the role of industry in the implementation of the concept of sustainable development in Ukraine is difficult to overestimate. One of the main areas of industry is the fuel and energy complex, which in turn directly or indirectly affects all areas of activity. Ukraine uses a variety of energy sources for its own needs, such as oil, natural gas, coal, nuclear and hydropower, wind and solar energy, etc. Traditionally, today the most popular in Ukraine are fossil resources: natural gas and coal, which together account for more than 60% of the energy balance [2]. Thus, the gas industry is one of the most important components of the fuel and energy complex.

The key to sustainable development is the consideration and harmonious interaction of institutional, social, environmental and economic components [3, 4]. From the point of view of the economic component, the gas industry is strategic. It affects the development of the state as a whole. It also affects the functioning of all sectors of the economy (industry, agriculture, services, utilities, etc.). From the point of view of the social component, the gas industry also has a significant impact. Gas supply to both industry and the public affects the quality of life. On the other hand, gas facilities are often sources of environmental and man-made hazards [5, 6].

The gas industry of Ukraine can be divided into the following areas: natural gas production; transportation of natural gas; natural gas storage; distribution and sale of natural gas to consumers [7].

Each of the areas has an impact on the environmental, social and economic components of Ukraine’s development. Therefore, considering the gas industry in terms of the concept of sustainable development is an urgent task.

The natural gas transportation is a crucial activity performed by the gas industry in which the gas has to be moved from one location to another. Several types of transportation means might be applied to transport the gas, yet it is well known that pipelines represent the most economical means to transport large quantities of natural gas [8].

Gas transportation system is a property production complex, which includes economically, organizationally and technologically interconnected facilities that are designed to transport and supply gas directly to its consumers.

The aim of this paper is to analyze the existing defects of the elements of gas transmission systems and their effects on economic, environmental and social components in terms of the concept of sustainable development.

2 Literature Review

The study of phenomena related to the functioning of gas transmission systems has been and is carried out by specialists and scientists from various fields. Some studies are interdisciplinary because, as noted above, the functioning of gas transmission systems is closely linked to environmental, economic, technological, safety, etc.

Much attention has been paid to the study of the economic component of the functioning of gas transmission systems in the research of Goral [9]. For example, the analysis of the following factors of the macroenvironment of gas enterprises was carried out: construction of bypass gas pipelines, price and tariff policy of the state, ways to diversify gas supply. Also in his works Goral pays attention to the management of gas transmission companies.

Zapukhlyak in research pays [10] attention to the issues of greening of gas transportation companies, and to prove the need for environmental and economic management of gas transportation companies.

Issues of functioning of gas transmission systems are becoming relevant around the world and are the subject of research by scientists from different countries. Thus, in the paper [11] the authors proposed an approach to risk assessment of gas pipeline operation management in an intuitive fuzzy language environment. And the paper [12] discusses increasing the construction of oil and gas pipelines for China's economy and infrastructure.

It should also be noted the paper [13] of a team of foreign authors, which based on bibliometric analysis of the Web of Science (WoS) database conducted a systematic and thorough review to study the safety of oil and gas pipelines. In the course of the work, a total of 598 publications were received and finalized between 1970 and 2019, related to the safety of oil and gas pipelines.

3 Environmental Aspects of Gas Industry Enterprises

The activity of the gas industry at all stages of the life cycle is a significant factor in anthropogenic impact on the environment [14]. As a result of the activities of the gas industry, the air basin, terrestrial and underground water resources, soils, flora and fauna, etc. are affected. Atmospheric air is significantly affected. This is due to the specifics of this industry. Many processes in the gas industry, in particular during gas transportation, are accompanied by emissions of natural gas into the atmosphere.

Emissions of natural gas during the operation of gas transmission system facilities can be divided into [15]: organized – through sources of a certain geometric shape;

unorganized (technical losses) – undirected flows, for example, due to violations of the tightness of equipment; emissions during emergencies.

Organized emissions are caused by certain technological features of the facilities and equipment of the gas transmission system. Unorganized and accidental emissions are caused by disturbances in the operation of facilities and equipment of the gas transmission system. Losses of natural gas entail economic losses, both in the form of lost profits and in the form of fines for emissions. In addition, all emissions, especially unorganized and emergency, pose a risk of fire and explosion. Also, all types of emissions are accompanied by the entry of significant amounts of volatile substances into the atmosphere. Many of these substances are dangerous and harmful. Therefore, there is a negative anthropogenic impact on the environment.

According to statistical reports, in 2019 alone, Naftogaz Group companies released 100 600 tons of pollutants into the atmosphere (excluding carbon dioxide). Figure 1 shows the structure of emissions of pollutants into the atmosphere by the Naftogaz Group for 2016–2020. Based on the results of the analysis, we can conclude that the most significant are methane emissions.

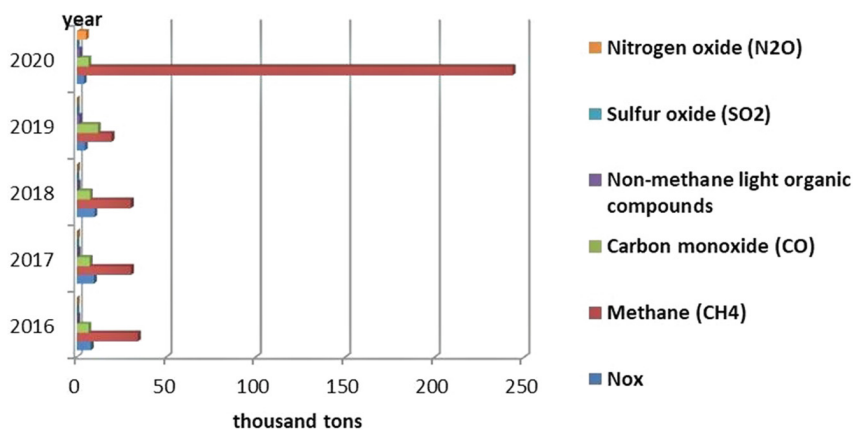


Fig. 1. Structure of pollutant emissions into the atmosphere by the Naftogaz Group.

Volumes of pollutant emissions by individual enterprises of Naftogaz Group for the period 2016–2020 are shown in Fig. 2. For example, in 2019, emissions of pollutants into the atmosphere (excluding carbon dioxide) by individual enterprises of Naftogaz Group were:

- JSC “Ukrtransgaz” – 48 400 tons (2018 – 48 000 tons);
- JSC “Ukrgezvydobuvannya” – 38 500 tons (2018 – 42 900 tons);
- PJSC “Ukrnafta” – 18 100 tons (2018 – 31 000 tons).

In addition, in 2019, 5957 100 tons of dioxide were released into the atmosphere, including:

- JSC “Ukrtransgaz” – 3753 900 tons (2018 – 3707 900 tons),

- JSC “Ukrgezvydobuvannya” – 1676 600 tons (2018 – 1715 200 tons),
- PJSC “Ukrnafta” – 522 500 tons (2018 – 631 100 tons).

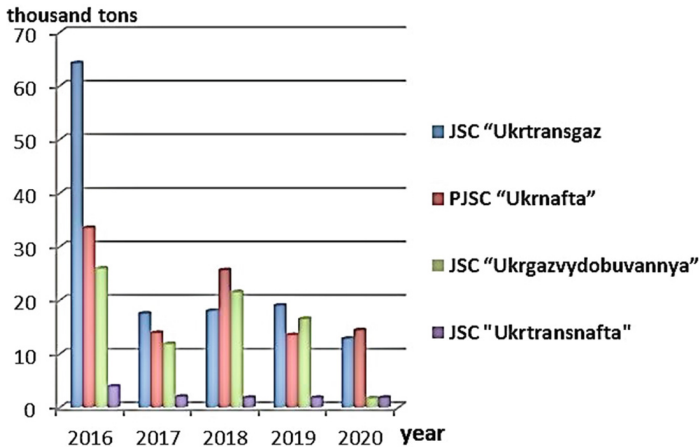


Fig. 2. Volumes of pollutant emissions by individual enterprises of the Naftogaz Group.

The excess of emissions from gas-related enterprises compared to the oil industry is due to the greater number of natural gas reserves in Ukraine and the volume of its transportation through the country compared to oil. These indicators were also influenced by annual changes in the volume of transportation and production of hydrocarbons. However, the presence of the greatest influence of the enterprises of JSC “Ukrtransgaz” was observed during the studied period of four out of five years.

One of the most influential enterprises in the gas industry is GTS Ukraine Operator LLC. This company transports natural gas to Ukrainian consumers and transits gas through Ukraine to Western and Central Europe.

As of 2020, the total length of GTS gas pipelines in Ukraine was approximately 33,190 km, including: main gas pipelines – 20,890,182 km; main gas pipelines-branches – 12197,514 km; distribution gas pipelines – 303,923 km.

In addition, the GTS of Ukraine includes: 57 compressor stations; 86 compressor shops; 1389 gas distribution stations; 63 thousand gas distribution points;- 1.4 million domestic pressure regulators.

According to the Plan for the development of the gas transmission system operator of the Gas Transmission System Operator LLC “Gas Transmission System Operator of Ukraine” for 2020–2029, approved by the Resolution of the NCRECP dated 17.03.2020 № 619 on the balance of the Gas Transmission System Operator as of 2020 were [9]: 5969 km of gas pipelines with a service life of up to 25 years; 12023 km of gas pipelines with a service life of 25 to 40 years; 15198 km of gas pipelines with a service life of over 40 years.

As a result of operation of a significant part of gas pipelines in Ukraine for more than 25 years, the risk of accidents and the possibility of their destruction increases.

It is known that long-term operation of transport pipelines leads to various types of damage. These include damage to the insulating coating of pipes, corrosion damage, cracks in the welds of pipelines and body parts of fittings and more. These damages reduce the reliability and durability of transport pipelines. The presence of these damages reduces the economic and environmental efficiency of the operation of pipeline systems [16].

In particular, it causes the entry of natural gas components into the air, soil and water bodies. Accumulation of these substances in the atmosphere is the cause of gas imbalance, which can intensify global climate change [9]. Also, significant wear and tear of such systems is the reason for the annual increase in the cost of upgrading fixed assets.

According to the data provided in the Energy Strategy of Ukraine for the period up to 2035 “Security, Energy Efficiency, Competitiveness” which was approved by the order of the Cabinet of Ministers of Ukraine dated August 18, 2017 № 605-r. there is a risk of increased accidents and losses of natural gas in distribution networks. This is due to the unsatisfactory condition and suboptimal structure of gas distribution systems [17].

Our state constantly formulates tasks and develops measures to eliminate these shortcomings. Thus, according to the same Energy Strategy of Ukraine for the period up to 2035, “Security, Energy Efficiency, Competitiveness” one of the main tasks of the gas sector is to improve the efficiency of gas distribution networks, GTS mains, underground gas storage infrastructure (UGS) and others [2].

It should be noted that despite the existing shortcomings, the overall reliability of transport pipeline systems is currently approaching European. The failure rate is 0.18–0.2 accidents per 100 km per year.

The following measures should be taken to prevent and eliminate negative economic and environmental unorganized leaks caused by damage to gas pipelines:

- constantly improve the processes of manufacture, installation and repair of elements of gas transmission systems, in particular by automating the technological processes of manufacture;
- try to improve the operating conditions of individual elements and the gas transmission system as a whole;
- to improve the methods and means of monitoring both the elements of gas transmission systems and the state of the atmospheric air at their facilities.

4 Main Factors of Failures and Accidents Analysis

Consider the main factors of failures and accidents that occur in the process of transportation and distribution of gas. Various classifications of the causes of unauthorized leakage of energy in gas transmission systems are used in the literature. In general, the main reasons can be considered [18]:

- leaks in pipelines and fittings;
- ingress of energy (gas, oil, etc.) into the environment due to deformation of structural elements of pipe fittings;

- composition of materials of structural elements of pipe fittings, as well as sealing units of pumps, gas pumping units, etc.;
- unfinished technology of finishing works in technological processes of manufacturing or repair of structural elements of pipeline fittings;
- changes in the structure, shape and size of structural elements of pipe fittings during operation of gas transmission systems (corrosion, abrasive wear, aging of metal under the action of dynamic loads, high pressures and temperatures).

In Europe, the analysis and collection of data on unauthorized gas emissions is carried out by the European Gas Incident Data Group (EGIG) [19]. The EGIG pipeline database contains data collected since 1970. EGIG is currently an association of 17 gas transmission system operators in Europe. Its current members are: Gas Networks Ireland (Ireland), DGC (Denmark), ENAGAS, S.A. (Spain), EUSTREAM (Slovak Republic), Fluxys (Belgium), Gasgrid Finland (Finland), GRTgaz (France), National Grid (UK), NET4GAS (Czech Republic) Gasunie (Netherlands/Germany), Gasconnect GmbH (Austria), Open Grid Europe (Germany), REN Gasodutos S.A. (Portugal), Snam Rete Gas (Italy), Swedegas A.B. (Sweden), SWISSGAS (Switzerland), Terega (France). The total length of the studied gas pipelines in 2019 was more than 140 km. The average age of pipelines is more than 35 years. The total number of incidents for the period from 1970 to 2019 – 1411 incidents.

According to EGIG, the reasons for pipeline failures may be: external obstacles; corrosion; structural defects and material failure; hot false incision; movement on the ground; other, unknown reasons (design error, lightning, etc.).

According to data for the last 10 years, cases of corrosion (26.63%) and external interference (27.17%) occurred with almost the same frequency. However, cases of corrosion are usually smaller.

In terms of the dependence of the frequency of major failures on the size of the leak, it can be noted that the general trend in the distribution of the size of the leak during the study period remained unchanged. Mostly punctures and ruptures are caused by external interference. Corrosion ranks second and remains the main cause of point leaks.

Based on the results of the analysis, the following conclusions can be drawn:

- the frequency of failures decreases with increasing year of construction;
- the failure rate decreases with increasing pipe wall thickness. The occurrence of corrosion does not depend on the wall thickness. But the thinner the wall of the pipeline, the faster it fails. Corrosion on thick pipelines takes longer. Therefore, it is more likely to be detected.

Pipeline owners take various protective measures to prevent leaks due to corrosion. According to statistical data [20], as a result of in-pipe diagnostics of the state of the main gas pipelines of Ukraine, about 5 000–6 000 defects are detected for every 100 km of length. Many of these defects are unacceptable and need to be repaired. Studies of the technical condition of 25% of the main gas pipelines of PJSC “Ukrtransgaz” showed that the loss of more than 60% of the metal is 0.9% of all cases; loss of 41–60% of metal – 5% of cases, and loss of 20–40% of metal – 45.5% of cases.

According to the data on accidents and failures on the main gas pipelines of UMG “Lvivtransgaz” since 1973, most failures and accidents occurred due to lack of welding, mechanical interference and corrosion – about 80% (lack of welding – 36%, mechanical intervention – 31%, lack of corrosion – 26%) [21].

There is also an approach where the classification of defects is in terms of their maintainability and manufacturability of repair [22]. According to this classification, the dangerous defects of pipelines include corrosion, some types of delamination and risks. The percentage of manifestations of these defects to the total number of injuries is: corrosion (metal losses) – 42.8–59.2%; stratification – 24.6–47.1%; stratification with surface yield – 1.5–2.6%; stratification in the peri-suture zone – 6.2–7.7%.

According to the results of the analysis, it can be concluded that one of the main factors of failures during the operation of gas transmission systems is corrosion. It is manifested both in the thinning of the pipe wall, and in corrosion and hydrogen cracking, corrosion-tired crack propagation. These are especially dangerous types of corrosion and mechanical damage, the kinetics of which are difficult to predict [23].

5 Influence of Surfactants on the Accelerating the Accumulation Damage Process

One of the causes of corrosion, changes in the mechanical properties of the metal and decline its durability are adsorption processes. The result of destruction is usually the appearance of cracks. This process has two stages:

- slow destruction (accelerates over time due to the accumulation of damage);
- rapid destruction.

Solving these problems requires different approaches. In the case of slow destruction, it is an increase in the time of growth of cracks (durability) or a decrease in the rate of their development. While maintaining a high level of stress.

In the case of rapid destruction, the task is to limit the destruction that has begun. Let's consider the process of accelerating the accumulation in more detail [24]. Adsorbed by the metal surfactants are typical for this process. These substances penetrate cracks and migrate to their base. During this time, high capillary pressure occurs

$$\Delta p_k = 2\gamma_e \cos\left(\frac{\theta_k}{r}\right), \quad (1)$$

where γ_e is the free surface energy; θ_k is the contact angle; r is the crack radius.

The contact angle is determined by the surface tension at the boundaries of the drop. The better the solids are lubricated, the smaller this angle is. When $\theta_k = 0$ (the material is completely wetted), Eq. (1) will take the form:

$$\Delta p_k = 2\gamma_e \frac{\theta_k}{r}. \quad (2)$$

Capillary pressure significantly accelerates the development of existing cracks. The rate of destruction is equal to

$$v_e = \tau_0 \exp\left(-\frac{v_0 - \gamma_e \sigma}{R_g T}\right) \quad (3)$$

where τ_0 , γ_e are the parameters that characterize the strength properties of materials; v_0 is the initial energy barrier, constant at $\sigma = 0$ (regardless of temperature and material processing); σ is the mechanical stress in the material; R_g is the gas steel; T is the material temperature.

In this expression $v_0 - \gamma_e \sigma$ – a value similar to the activation energy of the destruction process. The parameters τ_0 , v_0 and γ_e characterize the strength properties of the metal under the action of contacting and adsorbing substances (moisture, condensate, methanol, diethylene glycol, oils), which are in the pipeline. Their decrease indicates a decrease in its reliability and durability. Electrolyte ions, especially halogen ions, which reduce the level of surface energy, have significant adsorbing activity against metals. Alcohols, acids and other organic substances are less active.

To determine the strength characteristics of the metal, it is necessary to test the outer and inner surfaces of the sample material of the pipeline, which is in contact with harmful substances. The result of research is the exclusion of the interaction of metal with substances that reduce its surface energy.

The probability of fistulas and destruction of the pipeline also depends on the number of cracks that occur during the manufacture of pipes. These microcracks in the process of operation grow into cracks, fistulas, shells. Therefore, it is important to ensure the necessary metrological control of the presence of microcracks in the manufacturers. Such control will help to find ways to improve the technology of manufacturing pipes. This, in turn, will also help increase the reliability of the main gas pipelines.

Let's consider the section of the pipeline with a surface that has a large number of cracks, fistulas. This contributes to the emergence of stresses of greater intensity when loaded with excess pressure in this area. In addition, the area of fistulas and cracks has less cylindrical stiffness. Therefore, the loss of stability of the considered section will take place at an earlier stage of loading than other sections of the pipeline.

To solve the problem, the area with holes has been supposedly replaced with a solid area. This area has a reduced wall thickness or modulus of elasticity, which takes into account the influence of the field of small holes. Replacement makes it possible to move on to solving the problem of the stability of the shell, composed of circular plates of different stiffness. When the section of the gas pipeline is subjected to internal pressure, axial and circular stresses will occur in its wall. For a solid section of the pipeline, these voltages can be calculated by the formulas

$$\sigma_1 = \frac{q_{in} R_{av}}{2h_{av}}, \quad (4)$$

$$\sigma_2 = \frac{q_{in} R_{av}}{h_{av}}, \quad (5)$$

where σ_1 , σ_2 are respectively axial and circular stress; q_{in} is the internal pressure; R_{av} , h_{av} are respectively, the average radius and thickness of the shell.

The forces in the wall of the area, which has fistulas, cracks, create a tension of the membrane (chain) type. Now to determine the parameters of the weakened section (reduced modulus of elasticity and stress concentration coefficients), you can use a solution for a flat plate. This flat plate must have the same thickness and the same hole system as the weakened section of the pipeline.

6 Conclusion

The gas industry is strategic in terms of economic component. It affects the development of the state as a whole and the functioning of all sectors of the economy (industry, agriculture, services, utilities, etc.). From the point of view of the social component, the gas industry also has a significant impact. Gas supply to both industry and the public affects the quality of life. On the other hand, gas facilities are often sources of environmental and man-made hazards.

As a result of the activity of the gas industry, the air basin, terrestrial and underground water resources, soils, flora and fauna, etc. are subjects to anthropogenic impact. Atmospheric air is significantly affected. This is due to the specifics of this industry. Many processes in the gas industry, in particular during gas transportation, are accompanied by emissions of natural gas into the atmosphere.

The excess of emissions by enterprises related to the gas industry compared to the enterprises of the oil industry can be explained by the greater number of natural gas reserves in Ukraine and the volume of its transportation through the country compared to oil. These indicators were also influenced by annual changes in the volume of transportation and production of hydrocarbons. However, the presence of the greatest influence of the enterprises of JSC “Ukrtransgaz” was observed during the studied period of four out of five years.

A significant part of the gas pipeline of LLC “Operator of the gas transmission system of Ukraine” has a service life of more than 25 years. Due to this, the risk of accidents and the possibility of their destruction increases.

The following measures should be taken to prevent and eliminate the negative economic and environmental consequences of unorganized leaks caused by damage to gas pipelines:

- constantly improve the processes of manufacture, installation and repair of elements of gas transmission systems, in particular by automating the technological processes of manufacture;
- try to improve the operating conditions of individual elements and the gas transmission system as a whole;
- to improve the methods and means of monitoring both the elements of gas transmission systems and the state of the atmospheric air at their facilities.

Corrosion is one of the main factors of failure during operation of gas transmission systems. It is manifested both in the thinning of the pipe wall, and in corrosion and hydrogen cracking, corrosion-tired crack propagation. These are especially dangerous types of corrosion and mechanical damage, the kinetics of which are difficult to predict.

One of the causes of corrosion, changes in the mechanical properties of metal and decline its durability are adsorption processes. To determine the parameters of the weakened section, you can use a solution for a flat plate, which has the same system of holes as the weakened section of the pipeline.






References

1. Verkhovna Rada of Ukraine: On the Key Principles (Strategy) of the State Environmental Policy of Ukraine for the Period till 2030. Law of Ukraine. <https://zakon.rada.gov.ua/laws/show/2697-19#Text>. Accessed 10 May 2022
2. Ministry of Energy of Ukraine: New energy strategy of Ukraine until 2035: Security, energy efficiency, competitiveness. http://mpe.kmu.gov.ua/minugol/control/uk/publish/officialecategory?cat_id=245239555. Accessed 10 May 2022
3. Lelechenko, A.P., Lebedinska, O.Y., Derun, T.M., et al.: Mechanisms of inter-state communications for solving sustainable development problems. *Asia Life Sci.* **22**(2), 1–14 (2020)
4. Gontareva, I., Maryna, B., Babenko, V., et al.: Identification of efficiency factors for control over information and communication provision of sustainable development in higher education institutions. *WSEAS Trans. Environ. Dev.* **15**, 593–604 (2019)
5. Kombarov, V., Kryzhyvets, Y., Biletskyi, I., et al.; Numerical control of fiberglass pipe bends manufacturing. In: 2021 IEEE 2nd KhPI Week on Advanced Technology (KhPIWeek), Kharkiv, pp. 357–362. IEEE (2021). <https://doi.org/10.1109/KhPIWeek53812.2021.9570068>
6. Galkin, A.: Urban environment influence on distribution part of logistics systems. *Arch. Transp.* **42**(2), 7–23 (2017). <https://doi.org/10.5604/01.3001.0010.0522>
7. Miroshnyk, M., Kotukh, V., Kaptsova, N.: Information analysis of energy performance and factors affecting the serviceability of products illustrated by the example in gas industry. In: 2016 13th International Conference on Modern Problems of Radio Engineering, Telecommunications and Computer Science (TCSET), Lviv, pp. 436–438. IEEE (2016). <https://doi.org/10.1109/TCSET.2016.7452081>
8. Ríos-Mercado, R.Z., Borraz-Sánchez, C.: Optimization problems in natural gas transportation systems: a state-of-the-art review. *Appl. Energy* **147**, 536–555 (2015). <https://doi.org/10.1016/j.apenergy.2015.03.017>
9. Goral, L.: Analysis of macro functioning gas transmission companies in the context of the use their potential. *Socio-Econ. Probl. Mod. Period. of Ukr.* **1**(111), 122–126 (2015). (in Ukrainian)
10. Zapukhlyak, I.: Current status and problems of Ukraine’s gas transportation system in the context European integration process. *Econ. Manag. Natl. Econ.* **3**(08), 47–52 (2017). (in Ukrainian)
11. Li, M., Liu, L., Li, Y., Xu, Y.: Evaluating the risk of natural gas pipeline operation management in intuitionistic fuzzy linguistic environments. *Math. Probl. Eng.* **2018**, 3960496 (2018). <https://doi.org/10.1155/2018/3960496>
12. Tan, M.: Current situation and suggestions of pipelines of oil and gas storage and transportation in China. In: International Conference on Education, Management and Computing Technology (ICEMCT 2015), pp. 14–17. Atlantis Press (2015). <https://doi.org/10.2991/ice-mct-15.2015.4>
13. Chen, C., Li, C., Reniers, G., Yang, F.: Safety and security of oil and gas pipeline transportation: a systematic analysis of research trends and future needs using WoS. *J. Clean. Prod.* **279**, 123583 (2021). <https://doi.org/10.1016/j.jclepro.2020.123583>

14. Riva, A., D'Angelosante, S., Trebeschi, C.: Natural gas and the environmental results of life cycle assessment. *Energy* **31**(1), 138–148 (2006). <https://doi.org/10.1016/j.energy.2004.04.057>
15. Kotukh, V., Varlamov, Y., Palieieva, K., Ilinskyi, O.: Solution of the problem of operational reliability and environmental safety of transport pipeline systems. *Mater. Sci. Forum* **1038**, 393–400 (2021). <https://doi.org/10.4028/www.scientific.net/MSF.1038.393>
16. UA TSO of Ukraine: Plan for the development of the gas transmission system operator of the Gas Transmission System Operator LLC “Gas Transmission System Operator of Ukraine” for 2020–2029 (2020). https://tsoua.com/wp-content/uploads/gas-quality/files/TYNDP_2020-2029_18-03-2020.pdf. Accessed 10 May 2022
17. Mandrik, O.: Development of scientific bases of increase of level of ecological safety at transportation of natural gas. Dissertation, Ivano Frankivsk National Technical University of Oil and Gas (2013). (in Ukrainian)
18. Varlamov, Y., Kotukh, V., Ilinskyi, O., Paleyeva, K.: Increasing the level of technogenic and environmental safety of gas transportation systems by implementing the application system for production and repair of their elements. *Technog. Ecol. Saf.* **8**(2), 39–47 (2020). <https://doi.org/10.5281/zenodo.4300758>. (in Ukrainian)
19. Bianchini, A., Guzzini, A., Pellegrini, M., Saccani, C.: Natural gas distribution system: a statistical analysis of accidents data. *Int. J. Press. Vessel. Pip.* **168**, 24–38 (2018). <https://doi.org/10.1016/j.ijpvp.2018.09.003>
20. Mandryk, O.: The analysis of the accidents causes and gas mains damage. *Sci. NLTU Ukr.* **25**(1), 155–162 (2015). (in Ukrainian)
21. Ilnytsky, Y.: Analysis of failures and accidents on the main gas pipelines of UMG “Lviv-transgaz” and measures to prevent their occurrence. *Sci. Bull. IFNTUNG* **2**(32), 210–214 (2012). (in Ukrainian)
22. Yu, W., Song, S., Li, Y., et al.: Gas supply reliability assessment of natural gas transmission pipeline systems. *Energy* **162**, 853–870 (2018). <https://doi.org/10.1016/j.energy.2018.08.039>
23. Halim, S.Z., Janardanan, S., Flechas, T., Mannan, M.S.: In search of causes behind offshore incidents: fire in offshore oil and gas facilities. *J. Loss Prev. Process Ind.* **54**, 254–265 (2018). <https://doi.org/10.1016/j.jlp.2018.04.006>
24. Kaptsova, N.: Improving the efficiency of operation and repair of municipal pipelines. Dissertation, Kharkiv National University of Civil Engineering and Architecture (2018). (in Ukrainian)



A Technique to Identify Technical Measures Designed to Ensure Environmentally Safe Management in Populated Areas in Ukraine

Natalia Teliura¹(✉) , Hanna Khabarova² , Alona Reshetchenko¹ ,
Nataliia Tsapko² , and Olga Lomakina¹ 

¹ O. M. Beketov National University of Urban Economy in Kharkiv, 17 Marshala Bazhanova Street, Kharkiv 61002, Ukraine

natalya.telyura@kname.edu.ua

² Ukrainian Scientific and Research Institute of Ecological Problems, 6 Bakulina Street, Kharkiv 61165, Ukraine

Abstract. The paper describes a technique for identifying appropriate environmental technology options for populated areas. It assesses the relative significance of some factors influencing the implementation of environmental technology options using the analytic hierarchy process as a basis for environmental management and monitoring. It considers key components of the technique, focusing on the objective, comparative assessment process, estimation process and analysis, and characterises the relationships among the adjacent levels and their entities in the hierarchy. The paper demonstrates that the use of systemic analysis helps reduce the likelihood of making bad decisions.

Keywords: Environment and sustainable development · Environmental monitoring technologies · Environmental safety · Agglomeration · Analytic hierarchy process

1 Introduction

The environmentally safe social and economic development is the practice of ensuring that the improvements in the quality of life and living standards occur in parallel with the reduction of adverse impacts on the natural environment [1–3]. The analysis of the existing resource use practices and environmental situation in Ukraine demonstrates the need for ensuring the sustainable management of natural resources and improved quality of the environment [4, 5].

The deterioration of the environment in Ukraine [6, 7] has led to the loss of ecosystem stability and stronger impact of ecological factors on human health as witnessed by the public health data. In this situation, special focus should be concentrated on the development and justification of options for reducing adverse anthropogenic impacts.

Poor resource management practices and accidents often result in the non-compliance with the existing environmental and social guidelines governing natural resource uses [8–10]. The state-of-the art environmentally safe technologies are key to ensuring that the state of the natural environment and resources is improved. Environmentally safe technology solutions that serve to ensure that the environment is protected and natural resources are managed in a sustainable manner are considered the Best Environmental Techniques in EU [11].

The aim of the paper is to reduce the technogenic load on the environment by applying the method of system analysis, based on program-analytical procedures using the method of the hierarchy analysis.

2 Problem Formulation for Analytic Hierarchy Process

This study is underpinned by a hypothesis that can be summarized as follows: a numerical measure should be assigned to each environmentally safe technology option so that to help reduce the likelihood of making a wrong decision. Such complex tasks like this are best resolved using the systemic analysis methods including the analytic hierarchy process (AHP) [12–15] which serves to:

- structure a problem, decompose it and consider the interaction among individual entities;
- formalize the work of experts by breaking down the approval process into a number of stages so that the outcome of each stage is compared with a specific numerical indicator set as a dimensionless variable.

The first stage refers to the 1st level in the hierarchy, which defines the objective of the study as improving the environmental and social safety in populated areas through the implementation of environmental technology measures.

The 2nd level in the hierarchy describes the environmental and social safety sub-criteria (C) for populated areas. The principles underpinning these sub-criteria are enshrined in the Rio Declaration on Environment and Development and Sustainable Development Concept [16]. These principles form an integral part of the objective as the top-level entity of the hierarchy as they explain the sustainable development criteria and serve as indicators to measure progress against these criteria at the same time.

The 2nd level criteria (C) are linked to the 3rd level factors (F), which explain how safety criteria apply to a certain stage in the destructive process and have environmental, social and economic dimensions that influence the choice of a specific environmental technology option:

- a stage in the destructive process;
- conditions affecting human health;
- potential level of funding.

These factors serve to describe the real situation and potential capacity a specific municipality has to deal with it. For example, the potential level of funding available in a municipality is a factor influencing the choice of a specific environmental technology option because funding constraints limit the ability to choose and pay for an expensive option and a less expensive option should be recommended and pursued, and vice versa.

The 4th and 5th levels of the hierarchy represent technical and economic indicators (TEI) of municipalities and level of action (LA), required to improve them.

The 6th level of the hierarchy represents alternative environmental technology options (AETO).

The hierarchy in this study is a linear structure arranged in a manner similar to a water use management system and taking account of relevant environmental factors affecting it [12]. This is a certain type of system which is based on the assumption that the entities thereof can be grouped to form a set. The objective of the analysis is at the top of the system with key criteria standing at the next level. The level below includes hierarchically arranged entities describing the essence of the problem and the list of alternative solutions [12]. Building a hierarchy and identifying entities at each level is a process that shapes the choice of an appropriate alternative environmental technology option.

The hierarchy is structured to have six levels which are described in Table 1 below along with their hierarchical relationships.

Table 1. Relationships between the adjacent levels in the hierarchy.

Top-level entity	Lower-level entities adjoining the top-level entity	Description of relationships
1	2	3
The 1st level of the hierarchy defines the objective of the study as improving the environmental and social safety in populated areas through the implementation of environmental technology measures (ETM)		
The 2nd level of the hierarchy describes the relationships between the objective and the criteria (C) set at this level (i.e. improving an environmental and social safety in populated areas through the implementation of ETM is governed by a number of sub-criteria)		
Improving an environmental and social safety in populated areas through the implementation of ETM	C1: Surface water quality	Reducing anthropogenic pressure serves to improve the ecological status of water bodies, water quality, living (biological) resources, and aquatic species diversity, and abate parasitic diseases
	C2: Community living conditions	An important environmental and social criterion which involves better quality of the environment, improved attractiveness and accessibility of a populated area, reliable public utilities operations and convenient logistics

(continued)

Table 1. (continued)

Top-level entity	Lower-level entities adjoining the top-level entity	Description of relationships
1	2	3
	C3: Economic consequences of changes in the state of the environment in populated areas	Reduced anthropogenic pressure as a result of ETM helps cut costs significantly. Lower levels of bacterial pollution including pathogens help improve the recreational value of an area thus contributing to better economic situation. The economic implications of changes in the state of the environment are an important factor shaping the environmental and social safety in the populated areas
The 3rd level of the hierarchy shows the relationship between the C and F entities (impact on the environmental and social safety level in populated areas (C))		
C1 The state of the environment	F1: A stage in the destructive process	The state and quality of the environment including, inter alia, surface water quality (drinking water sources and recreational waters), which is characterized by the trophic state (oligotrophic, mesotrophic, eutrophic, polytrophic, and hypertrophic)
	F2: Hazard for human health	Whether the state of the environment is hazardous for human health: environmental pollution limits are prescribed in the relevant regulations and guideline documents
	F3: Availability of funding	Mitigation measures designed to tackle the consequences of environmental pollution can be funded from local, regional and national budget. The availability of funding is essential for bringing and maintaining the state of the environment in compliance with the relevant guidelines as it means that resources are available to conduct laboratory measurements, surveys etc.
C2 Living conditions	F1: A stage in the destructive process	Pollution levels in the environment affect living conditions
	F2: Hazard for human health	Pollution levels in the environment limit the ability to use natural resources

(continued)

Table 1. (continued)

Top-level entity	Lower-level entities adjoining the top-level entity	Description of relationships
1	2	3
	F3: Availability of funding	A potential for improving living conditions in populated areas depends on the budget constraints and availability of funding sources including external funding
C3 Economic implications of changes in the state of environment in populated areas	F1: A stage in the destructive process	Increased pollution levels in the environment and mitigation measures needed to tackle the consequences of pollution involve costs and require funding from various sources
	F2: Hazard for human health	Increased pollution levels in the environment and ecosystems and mitigation measures needed to tackle the consequences of pollution involve costs and require funding from various sources, including external funding
	F3: Availability of funding	The poorer the state of the environment the higher the cost of bringing it in compliance with the current standards
The 4th level of the hierarchy shows the relationship between the criteria (C) and technical and economic indicators (TEI) (i.e. how TEI contribute to each specific F)		
F1 A stage in the destructive process	TEI1: The condition of vital infrastructure in a municipality	The poorer the condition of vital infrastructure the higher the level of destructive process
	TEI2: The area occupied by a municipality	The larger the area occupied by a municipality the greater the potential for the destructive process to escalate
	TEI3: The availability of vacant sites for construction and implementation of ETM	The destructive process emerges or escalates if there are no vacant sites for implementing new ETM
	TEI4: Whether the area managed by a municipality is well maintained	The poorer the maintenance the greater the potential for destructive processes
F2 Hazard for human health	TEI1: The condition of vital infrastructure in a municipality	The poorer the condition the higher the risk of an accident
	TEI2: The area occupied by a municipality	The larger the area the higher the potential for health hazard to emerge

(continued)

Table 1. (continued)

Top-level entity	Lower-level entities adjoining the top-level entity	Description of relationships
1	2	3
	TEI3: The availability of vacant sites for construction and implementation of ETM	The lack of vacant sites for implementing new ETM exacerbates the risk of health hazard
	TEI4: Whether the area managed by a municipality is well maintained	The poorer the maintenance of a populated area the higher the potential for health hazard to emerge
F3 Availability of funding	TEI1: The condition of vital infrastructure in a municipality	The better the condition of vital infrastructure the less funding is required
	TEI2: The area occupied by a municipality	The larger the area the more funding is required to ensure compliance with environmental standards
	TEI3: The availability of vacant sites for construction and implementation of ETM	The lack of vacant sites for implementing new ETM could result in higher costs as other, more expensive solutions could be required
	TEI4: Whether the area managed by a municipality is well maintained	The better maintained the area the less funding is required to achieve and maintain compliance with relevant guidelines

The 5th level of the hierarchy shows the relationship between TEI and LA (i.e. how LA contribute to each specific TEI)

TEI1: The condition of vital infrastructure in a municipality	LA1: The need to meet the guidelines governing the collection and management of storm water, snowmelt water and surface runoff in storm sewers	The stable operation of wastewater collection systems greatly depends on maintaining compliance with the guidelines governing the collection and management of storm water, snowmelt and surface runoff in storm sewers
	LA2: The need to introduce the biological treatment of surface runoff and drainage water	The need to introduce the biological treatment of surface runoff and drainage water directly depends on the condition of wastewater collection systems
	LA3: The need to ensure the stable operation of municipal biological treatment systems	The condition of wastewater collection systems comprising the biological treatment process depends on their stable operation

(continued)

Table 1. (continued)

Top-level entity	Lower-level entities adjoining the top-level entity	Description of relationships
1	2	3
TEI2: The area occupied by a municipality	LA1: The need to meet the guidelines governing the collection and management of storm and snowmelt water and surface runoff in storm sewers	The larger the catchment area the greater the need to maintain compliance with the guidelines governing the collection and management of storm and snowmelt water and surface runoff in storm sewers
	LA2: The need to introduce the biological treatment of surface runoff and drainage water	The need for introducing the biological treatment of surface runoff and drainage water is determined by the size of a catchment area
	LA3: The need to ensure the stable operation of municipal biological treatment systems	The need for ensuring the stable operation of municipal biological treatment system only slightly depends on the size of a catchment area
TEI3: The availability of vacant sites for construction and implementation of ETM	LA1: The need to meet the guidelines governing the collection and management of storm water, snowmelt and surface runoff in storm sewers	The actual arrangements for the collection and management of storm water, snowmelt and surface runoff in storm sewers will be directly dependant on the availability of vacant sites for implementing new ETM
	LA2: The need to introduce the biological treatment of surface runoff and drainage water	The availability of vacant sites for implementing new ETM is a key factor to shape the design of biological treatment facilities for surface and drainage runoff
TEI4: Whether the area managed by a municipality is well maintained	LA1: The need to meet the guidelines governing the collection and management of storm water, snowmelt and surface runoff in storm sewers	The level of the populated area maintenance directly reflects how the guidelines governing the collection and management of storm water, snowmelt and surface runoff in storm sewers are met
	LA2: The need to introduce the biological treatment of surface runoff and drainage water	The level of the populated area maintenance is an important factor to be considered when assessing the need for introducing the biological treatment for surface and drainage runoff

(continued)

Table 1. (continued)

Top-level entity	Lower-level entities adjoining the top-level entity	Description of relationships
1	2	3
	LA3: The need to ensure the stable operation of municipal biological treatment systems	The stable operation of the municipal biological treatment facilities only slightly depends on how well the populated area is maintained

The 6th level of the hierarchy describes the alternative environmental technology options (AETO) for each specific populated area

The second stage involves the development of the pairwise comparison matrix for criteria on each level of the hierarchy and calculating weights by comparisons of alternatives for each criterion using a unified pairwise weighting scale specially designed to deal with environmental tasks [12]. The purpose of this exercise is to assess which of the entities on each level of the hierarchy contributes most to the environmental and social safety in the populated areas.

The third stage involves the calculation of local and global priority weights and criteria for the hierarchical model using the results from the second stage. This can be done using the My Priority software that is capable of doing the calculation automatically and efficiently because it includes dialogue tools specifically adjusted to serve this purpose. The global priority weights of alternative options AETO are calculated at the final level of the hierarchy [17].

Finally, the consistency of the model is assessed in order to verify consistency of responses to variation in the values of input parameters which are chosen in each specific case depending on the current situation.

At the 5th stage, the most appropriate AETO is identified based on the largest sum of the global priority weights.

3 Numerical Simulation Results

This computerized technique uses the expert judgments to assess entities in each hierarchical level and then determine the relative importance of these entities within each group. We would like to discuss some specific issues relating to the use of this technique in more detail:

- the pairwise comparison matrix for comparing entities in each level of the hierarchy should be developed by a multidisciplinary team of experts including environmental specialists, urban planners, social experts and economists working with local authorities, industrial and residential developers in each specific municipality where an AETO is planned to be implemented. These experts contribute their expertise to form a square reverse symmetrical matrix of judgments as a basis for Stage 2;

- this matrix is recommended to be developed using a classic situational judgement conversion table where each attribute is assigned a relative importance expressed as a score varying from 1 to 9 [12];
- the calculation of local and global priority weights (weight coefficients) for entities and determination of consistency ratio of matrices should be made with an accuracy of 0.001 as recommended in [12].

As a result, the selected AETO would represent the best choice adjusted to take account of the local environment and populated area where it would be implemented and aligned with the specific requirements applied to this type of technology. This approach also allows us to use various additional information such as direct measurements, forecasts and expert estimates.

Let us consider how this technique can be used to identify the best AETO for a model municipality in Ukraine. The objective is to ensure an improved environmental and social safety in a municipality which has the following characteristics:

- a large city with a population on over 300 thousand people;
- is located in the area experiencing a relatively high anthropogenic pressure;
- has a separate wastewater collection system.

The AHP was applied in this study and all three stages of the AHP process were completed by a team of local experts. The priorities assigned to entities within the hierarchical levels 1–5 were used to identify the priority AETO for the model area.

Figures 1 and 2 illustrate the result the experts came up with at the sixth (final) level of the hierarchy. The data presented in Fig. 1 and 2 (the qualitative and quantitative priorities assigned to entities within the sixth hierarchical level) serve to identify an optimal option based on the prevailing global priority weights.

An option assigned the highest global priority weight is considered as an optimal one. In this example, the analysis of the global priority weights assigned to various options on the 6th level helps identify the best option in terms of ensuring an improved social and environmental safety in the model municipality using the analytic hierarchy process as a tool supporting environmental management, decision making and monitoring.

The paper describes key stages of AHP including setting a goal, comparative assessment, calculation and analysis of relationships between adjoined entities. This systemic analysis approach minimizes the likelihood of misjudgment and ensures that management decisions are justified.

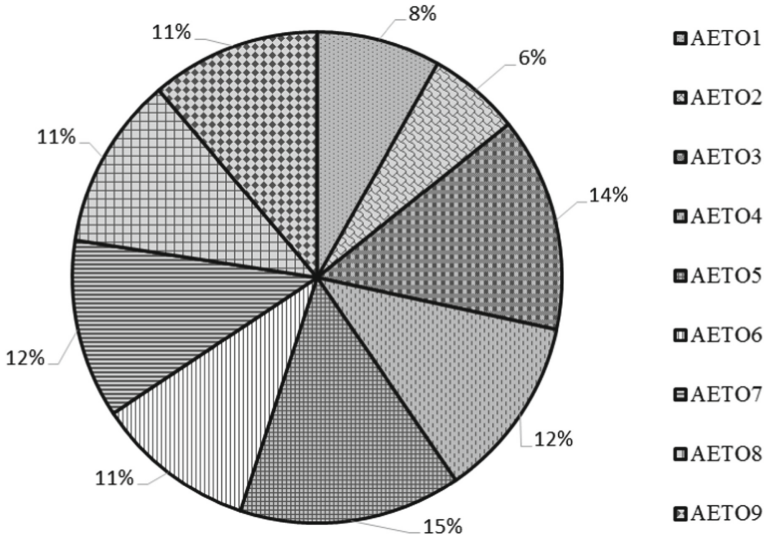


Fig. 1. Global priority weights.

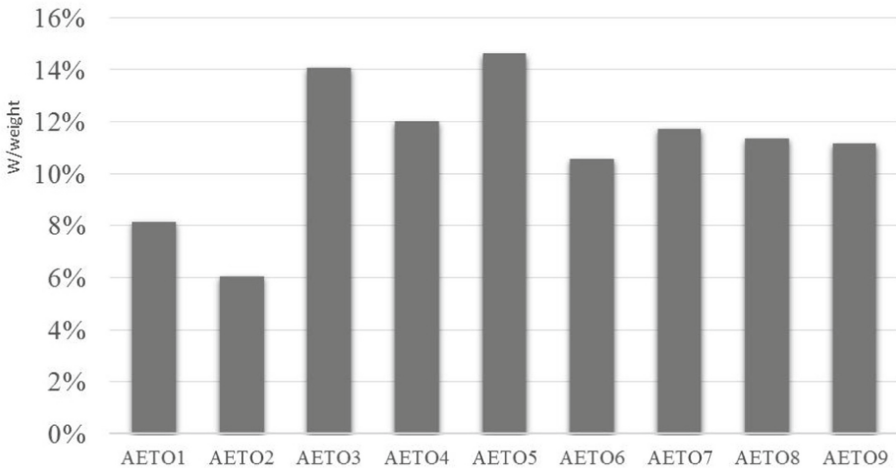


Fig. 2. Global priority weights for the model municipality, %.

4 Conclusion

The technique described herein helps develop a strategy for ensuring the environmental and social safety in populated areas in Ukraine and throughout the world through the formulation of well-grounded recommendations on implementing appropriate AETO.

AHP was applied to assess entities within each group and identify the relationships between entities as described in the table. The hierarchical structuring was used to derive global priority weights. The advantages of the identified AETO were demonstrated for a model municipality.





References

1. Kuzmenko, S.H., Filipenko, T.V., Ryabev, A.A., et al.: Current conditions, causes and increase of poverty in Ukraine. *Asia Life Sci. Supp***22**(2), 43–56 (2020)
2. Diegtiar, O.A., Hornyk, V.H., Kravchenko, S.O., et al.: Improving public water resources policy in Ukraine: municipal and environmental issues. *J. Environ. Manag. Tour.* **11**(3), 669–675 (2020). [https://doi.org/10.14505//jemt.11.3\(43\).20](https://doi.org/10.14505//jemt.11.3(43).20)
3. Kombarov, V., Kryzhyvets, Y., Biletskyi, I., et al.: Numerical control of fiberglass pipe bends manufacturing. In: 2021 IEEE 2nd KhPI Week on Advanced Technology (KhPIWeek), pp. 357–362. IEEE, Kharkiv (2021). <https://doi.org/10.1109/KhPIWeek53812.2021.9570068>
4. Babaev, V., Sukhonos, M., Starostina, A., Beletsky, I.: Improving the processes of cost management in the construction and energy projects. *East.-Eur. J. Enterp. Technol.* **4**(3–82), 10–17 (2016). <https://doi.org/10.15587/1729-4061.2016.75515>
5. Papagiannis, F., Gazzola, P., Burak, O., Pokutsa, I.: An intelligent environmental plan for sustainable regionalisation policies: the case of Ukraine. *Environ. Sci. Policy* **108**, 77–84 (2020). <https://doi.org/10.1016/j.envsci.2020.03.010>
6. Vystavna, Y., Huneau, F., Motelica-Heino, M., et al.: Monitoring and flux determination of trace metals in rivers of the Sevversky Donets basin (Ukraine) using DGT passive samplers. *Environ. Earth Sci.* **65**(6), 1715–1725 (2012). <https://doi.org/10.1007/s12665-011-1151-4>
7. Yakovlev, V., Vystavna, Y., Diadin, D., Vergeles, Y.: Nitrates in springs and rivers of East Ukraine: distribution, contamination and fluxes. *Appl. Geochem.* **53**, 71–78 (2015). <https://doi.org/10.1016/j.apgeochem.2014.12.009>
8. Teliura, N., Tsapko, N., Khabarova, H., et al.: Selection methodology of ecological safety priorities of sustainable development goals of urban agglomerations. In: Nechyporuk, M., et al. (eds.) *Integrated Computer Technologies in Mechanical Engineering – 2021. LNNS*, vol. 367, pp. 941–950. Springer, Cham (2022). https://doi.org/10.1007/978-3-030-94259-5_73
9. Yeboah-Assiamah, E., Muller, K., Domfeh, K.A.: Institutional assessment in natural resource governance: a conceptual overview. *Forest Policy Econ.* **74**, 1–12 (2017). <https://doi.org/10.1016/j.forpol.2016.10.006>
10. Dmitrieva, O., Khorenzhaja, I., Vasylenko, V., et al.: Choosing the phytoremediation technologies for cleaning various types of wastewater. *East.-Eur. J. Enterp. Technol.* **2**(10), 27–37 (2020). <https://doi.org/10.15587/1729-4061.2020.200591>
11. Teliura, N.O.: Development of the methodological approach to the selection of technologies for environmentally safe water drainage in populated areas. *East.-Eur. J. Enterp. Technol.* **6**(10–96), 55–63 (2018). <https://doi.org/10.15587/1729-4061.2018.148689>
12. Saaty, T.L., Ergu, D.: When is a decision-making method trustworthy? Criteria for evaluating multi-criteria decision-making methods. *Int. J. Inf. Technol. Decis. Mak.* **14**(06), 1171–1187 (2015). <https://doi.org/10.1142/S021962201550025X>
13. Ho, W., Ma, X.: The state-of-the-art integrations and applications of the analytic hierarchy process. *Eur. J. Oper. Res.* **267**(2), 399–414 (2018). <https://doi.org/10.1016/j.ejor.2017.09.007>
14. Mukhin, V., Romanenkov, Y., Bilokin, J., et al.: The method of variant synthesis of information and communication network structures on the basis of the graph and set-theoretical models. *Int. J. Intell. Syst. Appl.* **9**(11), 42–51 (2017). <https://doi.org/10.5815/ijisa.2017.11.06>

15. Galkin, A.: Urban environment influence on distribution part of logistics systems. *Arch. Transp.* **42**(2), 7–23 (2017). <https://doi.org/10.5604/01.3001.0010.0522>
16. Mensah, J.: Sustainable development: Meaning, history, principles, pillars, and implications for human action: literature review. *Cogent Soc. Sci.* **5**(1), 1653531 (2019). <https://doi.org/10.1080/23311886.2019.1653531>
17. Ahmed, S., Ahmed, S., Shumon, M.R.H., et al.: A comparative decision-making model for sustainable end-of-life vehicle management alternative selection using AHP and extent analysis method on fuzzy AHP. *Int. J. Sustain. Dev. World Ecol.* **23**(1), 83–97 (2016). <https://doi.org/10.1080/13504509.2015.1062814>



Removal of Heavy Metals from Sewage Sludge by Using Humic Substances

Tamara Shevchenko¹(✉) , Olena Galkina¹ , Serghii Martynov² ,
and Stanislav Dushkin³ 

¹ O. M. Beketov National University of Urban Economy in Kharkiv,
17 Marshala Bazhanova Street, Kharkiv 61002, Ukraine

Tamara.Shevchenko@kname.edu.ua

² National University of Water Management and Environmental Engineering,
11 Soborna Street, Rivne 33028, Ukraine

³ National University of Civil Defense of Ukraine, 94 Chernyshevskya Street,
Kharkiv 61023, Ukraine

Abstract. The paper discusses the issue of extracting heavy metals from domestic wastewater sludge as fertilizers for agricultural purposes. Currently, the bulk of the formed precipitation is not utilized due to the presence of toxic chemicals in their composition, mainly heavy metals. This is due to the fact that industrial wastewater enters the city sewer network after insufficient treatment. Based on the foregoing, the development of progressive technologies and methods for removing heavy metals from urban wastewater sludge is an extremely urgent and timely task, the successful solution of which will significantly reduce the level of negative impact of this sludge on the environment. A technological scheme for the extraction of heavy metals from domestic wastewater sludge has been developed; the optimal modes of the technological process are given. It has been established that it is advisable to use organic flocculants to intensify the processes of thickening and dehydration of urban wastewater sludge. The most effective are cationic flocculants. Their use intensifies the process of sludge dewatering both in sludge beds and in mechanical dewatering devices – filter presses and centrifuges.

Keywords: Sewage sludge · Humic substances · Carbon-alkaline reagents · Peat · Heavy metals · Dehydration

1 Introduction

The work of water supply and sewerage companies makes a significant contribution to the total amount of waste from cities and industrial enterprises [1]. About 60 thousand m³/day of sludge are formed at sewage treatment plants of Ukraine alone, which are stored on sludge sites specially designated for this purpose. These wastes contain more than 90% of organic matter, which can be a valuable fertilizer for agriculture. However, the presence of heavy metals in these sediments prevents their use in agriculture and leads to the need for storage with the alienation of large areas. In total, more than 1.0

million m³ of such sediments have been accumulated in Ukraine today, for the storage of which 1450 ha of land have been allocated. These repositories of sludge are sources of environmental pollution: groundwater, soil, air. The amount of sludge formed in Kharkiv reaches 3500 m³/day; the area occupied by sludge exceeded 120 ha.

The environmental problem that requires immediate solution is the creation of new effective methods of treatment (disposal and dehydration) and subsequent disposal of urban wastewater [2, 3]. This direction is extremely relevant not only for Ukraine but also for many countries around the world. This sludge is colloidal type suspensions and difficult to filtered. Large volumes, bacterial contamination, the presence of organic substances that can rot quickly with the release of odors, as well as the heterogeneity of composition and properties complicate their processing.

Currently, the disposal of the bulk of the sludge of wastewater is not carried out due to the presence in their composition of toxic chemicals, mainly heavy metals [4]. This is due to the fact that industrial wastewater enters the municipal sewerage network after insufficient treatment. As a result, sludge from municipal sewage treatment plants is directed to dewatering on sludge sites and storage, allocating large plots of land for this purpose [5]. Sludge sites are sources of pollution of soil, groundwater and surface water bodies, air [6]. The size of land allocated for these purposes is constantly increasing.

Based on the above, the development of advanced technologies and methods for removing heavy metals from urban wastewater is an extremely urgent and timely task, the successful solution of which will significantly reduce the negative impact of these sediments on the environment. The paper considers the issue of extraction of heavy metals from sewage sludge as fertilizers for agricultural purposes [7, 8].

Raw sludge from primary settling tanks is heterogeneous in composition and is a gelatinous suspension of gray or light brown color. The average humidity of the sludge removed from the primary settling tanks is assumed to be 95–96%. Activated sludge is a suspension containing amorphous flakes, including aerobic bacteria and simple microorganisms with small (mechanical) and adsorbed (dissolved) contaminants of wastewater. Humidity of activated sludge removed from secondary settling tanks after aeration tanks is 99.2–99.5%, and after biofilters – 96–96.5%.

Most sludge sites are arranged on a natural basis. There is a sludge sites lead to intensive pollution of the environment: groundwater, soil, air. This has led to a significant deterioration of the environmental situation in the cities of Ukraine.

The main reason that prevents the disposal of sludge is the presence of toxic chemicals, mainly heavy metals. Best practices in the operation of sewage treatment plants show that improving the toxic properties of sludge cannot be fully addressed by improving the operation of sewage treatment plants. The technological scheme of heavy metals extraction from sewage sludge is developed; the optimal modes of technological process are given. It is established that it is expedient to use organic flocculants to intensify the processes of thickening and dehydration of sludge of wastewater. Cationic flocculants are the most effective. Their use intensifies the process of sludge dehydration both on sludge sites and in mechanical dehydration devices – filter presses and centrifuges [9].

Sewage treatment systems for urban wastewater make a significant contribution to the total amount of waste from cities and industrial enterprises. Sediments are stored on sludge sites. Sediment storage is a source of environmental pollution: soil, groundwater

and surface water bodies, air. Urban sewage sludge contains more than 90% organic matter, which can be a valuable fertilizer for agriculture. However, the presence of heavy metals in urban sewage sludge prevents their use in agriculture.

Different researchers dealt with the issues of physical and chemical properties of sewage sludge and the development of methods for intensification of dehydration and utilization processes. However, the problem of removal of heavy metals and disposal of urban wastewater remains incomplete, and therefore the level of man-made impact of sediment on the environment remains quite high [10].

The analysis of papers [11, 12] and available experience of operation of facilities for domestic (urban) wastewater and sludge treatment showed that currently the tasks of sludge treatment and disposal remain unresolved. This leads to the accumulation of sediment and pollution of the environment (soil, groundwater and surface water bodies, air). It is necessary to develop methods and technologies for the extraction of heavy metals from urban sewage sludge. It was found that the composition of urban sewage sludge generated at urban treatment plants, which have machine-building and metal-lurgical enterprises, contain heavy metals such as iron, copper, nickel, zinc, chromium, manganese, cadmium, arsenic, mercury and a number of others. Heavy metals need to be removed from sewage sludge for disposal as fertilizer in agriculture.

The study of patterns of urban wastewater disposal, which includes raw sludge from primary settling tanks and excess activated sludge from secondary settling tanks, is one of the important technological tasks in solving problems of improving sludge treatment technology.

Based on the generally accepted classification of heterogeneous physicochemical systems, urban wastewater sediments cannot be attributed to any of them [13, 14]. They have the characteristics and properties of both emulsions and suspensions. On the one hand, in the dispersion medium (water) there are particles of organic matter, the surface of which is covered with a layer of sorbs dissolved organic compounds; there is no boundary solid – water. On the other hand, the structural and mechanical properties of this system are largely determined by solid particles. The ratio of the properties of the emulsion and the suspension depends on the dispersion of the solid phase and the associated organic content, which is in the anhydrous part of the precipitate by weight 3–30%, volume 15–70%, and sometimes more. Precipitation humidity is in the range of 95–98%.

The paper [15] considers the main characteristics of sewage sludge during dehydration. The sewage sludge contains mainly organic matter that is difficult to release moisture. There are no exact linear dependences of the filtration time on the rate of the dehydration process. Studies have shown that this process is not linear and depends on many factors. First of all, it is necessary to establish the concentration of organic compounds in the sewage sludge. Other important parameters are the permeability and compressibility of sediments during their dehydration. Comparison of the quantified dewaterability of the fifteen sludges to the relative volatile solids content showed a very strong correlation in the volatile solids range from 40 to 80%. The data indicate that the volatile solids parameter is a strong indicator of the dewatering behavior of sewage sludge.

Sewage sludge contains the nutrients necessary for plants (nitrogen, phosphorus, potassium, microelements) and, in terms of their agrochemical value, is similar to traditional organic fertilizers – manure, and applying them to the soil will improve the composition and structure of the arable soil layer and ensure an increase in plant productivity. Among the organic compounds, the most frequently detected in the municipal sewage sludge include absorbable organic halogens (AOX), linear alkylbenzenesulfonates (LAS), nonylphenols and nonylphenoethoxylates (NP and NPnEOs), di-ethylhexylphthalate (DEHP), polyaromatic hydrocarbons (PAH), polychlorinated biphenyls (PCB), polychlorinated dibenzo-p-dioxins and-furans (PCDD/F) [16]. These compounds have been proven to cause adverse effects, such as reproductive damage, carcinogenicity, and metabolic and obesity diseases. During processing, these organic substances are broken down into simpler ones. However, constant monitoring of their content in urban sewage sludge is necessary. An efficient analytical method for the detection of organic pollutants in sewage sludge has been developed, demonstrating excellent reproducibility and recovery. After removing said organic contaminants from the sewage sludge, it is possible to use the sewage sludge as a fertilizer.

Another problem that limits the use of sewage sludge as a fertilizer is the presence of heavy metals in their composition. This situation is typical for many industrial cities. The paper [17] proposes a three-stage method for the removal of heavy metals from sewage sludge. The results of the study showed that the combination of sonication pre-treatment and alkaline fermentation showed the best results among other cases, resulting in hydrolysis by 33.7%, acidification by 10.5%, metal leaching by 11–33% and a reduction in the bioavailability of potentially toxic substances to 25% heavy metals. Bioleach effluent from the most efficient reactor was subjected to membrane metal recovery. A supported liquid membrane impregnated with a basic carrier successfully recovered soluble metals from bioleach effluents with an efficiency of 39–68%. This study shows that the proposed three-step process, pre-sonication, liquid membrane-supported alkaline fermentation, efficiently produces a stable sludge with reduced heavy metal toxicity and recovers metals from organic waste streams. However, the complexity and relative high cost of this combined treatment should be noted. The complexity of process control and the economic feasibility of this method require the search for new approaches to solving the issue of removing heavy metals from sewage sludge.

Evaluation of the effectiveness of cassava peel extracts for removing heavy metals from sewage sludge was carried out in the article [18]. Mean heavy metal concentrations in the sludge were estimated for copper (2.22 ± 0.2 mg/kg), zinc (52.3 ± 0.1 mg/kg), chromium (1.46 ± 0.1 mg/kg), nickel (5.6 ± 0.01 mg/kg), and lead (1.9 ± 0.1 mg/kg) and were below permissible limits. Optimum heavy metal removal for *Aspergillus niger* fermentation extract at room temperature was achieved on day 12 at pH 3.5 for zinc (74.5%), while optimum heavy metal removal at elevated temperature was achieved on day 9 at pH 3.0 for lead (79.3%). The optimum pH for crude fermentation extracts lies between pH 3.0–4.5 for nickel (76.2%) at room temperature and chromium (76.6%) at elevated temperature. It should be noted that this technology requires a long time to implement the removal of heavy metals from sewage sludge. Such duration of the process can lead to a delay in the processing and disposal of sewage sludge due to the accumulated large volumes of this sludge.

Currently, the disposal of the bulk of sludge generated during urban wastewater treatment is not carried out due to the presence of heavy metals. Sludge sites are a source of pollution of soil, groundwater and surface water bodies, air. The size of land allocated for these purposes is constantly increasing. As a result, it could turn into a real environmental disaster.

The purpose of this study is to investigate the efficiency of detecting metals from exposure to domestic wastewater. This can be exploited by changing the process of domestic wastewater treatment. Continuous change in precipitation with humic reagents, accompanied by the emission of ultrasound. This method makes it possible to reduce the content of metals in sediments with a persistent water content that does not exceed the sanitary standards for the content of metals in food substances for agricultural enterprises. Analysis of experimental data shows that the treatment of sewage sludge allows to effectively removing heavy metals with subsequent disposal of sludge as fertilizer.

2 Flocculating Properties of Humic Substances

Humic substances and, in particular, humic acid are widespread in the environment. For example, humic acid can be obtained from soil, natural waters, peat, low-grade coal (so-called brown coal) and others. It has been established that these substances have properties that allow removing heavy metals from sewage sludge [19–21].

To a large extent, they have an aromatic structure, including phenolic hydroxyl and carboxyl groups capable of attaching metal ions. The molecular weight of humic substances depends on various factors, such as polydispersity, the tendency to combine into large molecules in a particular environment. Molecules of organic or other dissolved compounds can interact with humic substances through ion exchange or interaction with functional groups, as well as a result of hydrophobic interaction. The formation of complex compounds of humic substances with heavy metal ions is established and a high degree of their stability is shown, which increases in the following order: $\text{Fe}^{3+} > \text{Al}^{3+} > \text{Cu}^{2+} > \text{Zn}^{2+} > \text{Ni}^{2+} > \text{Co}^{2+} > \text{Mn}^{2+} > \text{Ca}^{2+} > \text{Mg}^{2+}$. Humic substances in alkaline, neutral or acidic environments form chelated compounds with heavy metals, which are dissolved or adsorbed on suspended particles containing metal compounds. In addition, humic substances, such as humic acid, have the properties of flocculants – polyelectrolytes, which contributes to the intensification of wastewater treatment processes from suspended solids.

The aim of the research is to study the effectiveness of the method of heavy metals extraction from sewage sludge through the use of special sludge treatment technology. This technology consists of the step of continuously mixing the sludge with humic reagents. The second stage involves the simultaneous treatment of sludge with ultrasound. This will reduce the concentration of heavy metals in sewage sludge to concentrations that do not exceed the sanitary norms of heavy metals in fertilizers for agricultural land.

3 Materials and Methods

The paper uses theoretical and experimental research in laboratory-pilot conditions to achieve the aim. The efficiency of the dewatering equipment was evaluated by the amount

of solids removed from the unit of the filtration surface, as well as by the humidity of the dehydrated product.

The precipitates were filtered on a laboratory vacuum filter unit with a filling funnel with a diameter of 100 mm [22, 23], at a constant pressure difference (ΔP) during the filtration cycle. During the operation of the laboratory installation, a layer of sediment is formed on the filter tape. It was found that there is also an intensive clogging of the pores of the filter tape with colloidal or similar particles. This leads to a rapid decrease in the filtration rate in subsequent cycles. Therefore, in the experiments as a filter partition used a tape with a pre-washed on it a layer of disposable lignite reagent [24].

The paper considers the technology of removal of heavy metals from urban wastewater with the help of humic substances. Removal of heavy metals from domestic sewage sludge is carried out with constant stirring of sludge with humic reagents with a linear velocity of 0.2–0.5 m/s with simultaneous sonication at a frequency of 2.5–5.5 kHz for 1–1.5 min. 1–2% solution of humic substances of brown coal and peat with a dose of 10–50 mg/kg of dry matter was used for sludge treatment.

4 Research Results

The efficiency of removal of heavy metals from sewage sludge depending on the dose of reagent is given in Table 1 and in Fig. 1. Changing the linear velocity directly affects the process of extracting heavy metals from sewage sludge. In Fig. 2 shown the graphs of the influence of changes in the linear mixing velocity on the efficiency of removal of heavy metals from domestic sewage sludge.

Table 1. Efficiency of removal of heavy metals from sewage sludge.

Reagent type	Reagent dose	The content of heavy metals in the sludge, mg/kg dry matter		
		Iron (Fe^{3+})	Copper (Cu^{2+})	Aluminium (Al^{3+})
No reagent	0	4148.5	266.3	8517.5
Lignite	10	2443.47	199.46	4803.87
	20	1837.79	167.50	3764.74
	30	1381.45	108.92	3321.83
	40	850.44	92.94	2614.87
	50	273.80	48.99	1865.33
Peat	10	1883.42	178.15	4582.42
	20	1136.69	145.93	3372.93
	30	900.22	104.12	2861.88
	40	613.98	78.82	2359.35
	50	365.07	39.15	1686.47

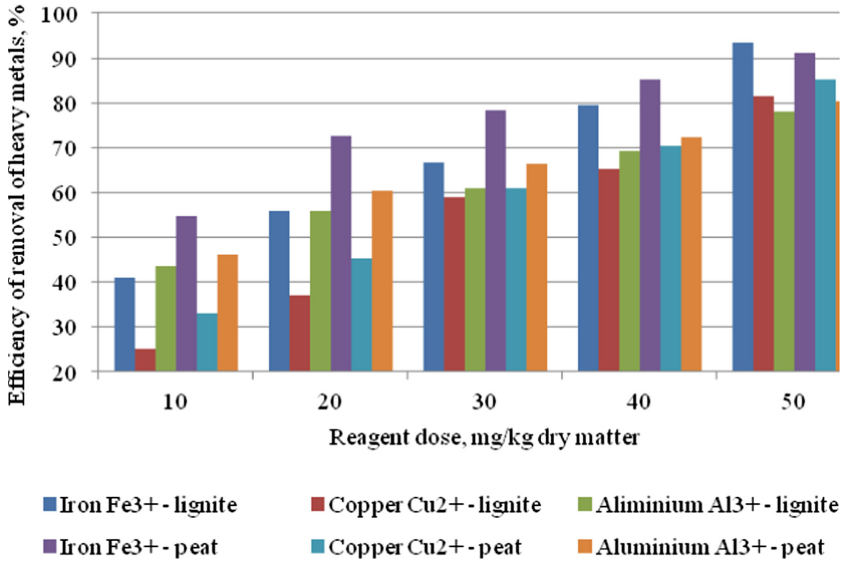


Fig. 1. The effect of the humic substances dose on the efficiency of heavy metals removal from domestic sewage sludge ($V = 0.2$ m/s, $\nu = 2.5$ kHz, $t = 60$ s).

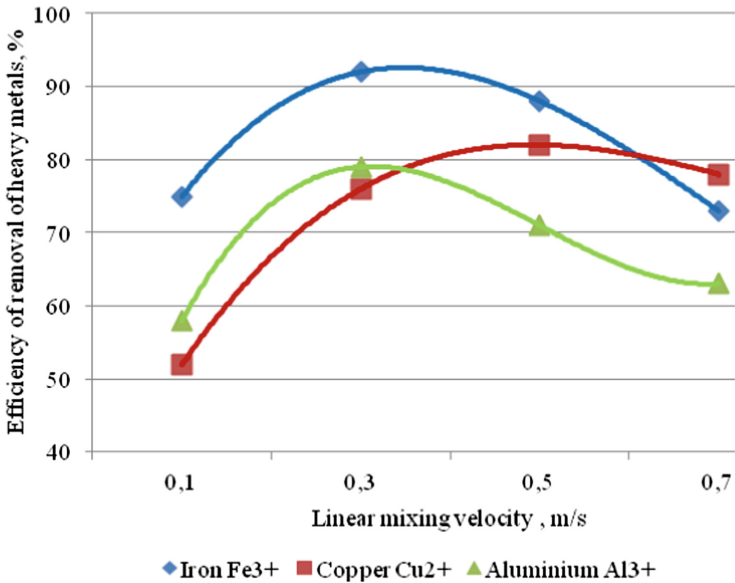


Fig. 2. Influence of linear mixing velocity change on efficiency of removal of heavy metals from sewage sludge.

The effect of changes in the frequency of ultrasound on the efficiency of removal of heavy metals from domestic sewage sludge is shown in Fig. 3. During the experiments, the optimal modes of heavy metals removal from urban wastewater sludge during treatment with humic reagents were established (Table 2).

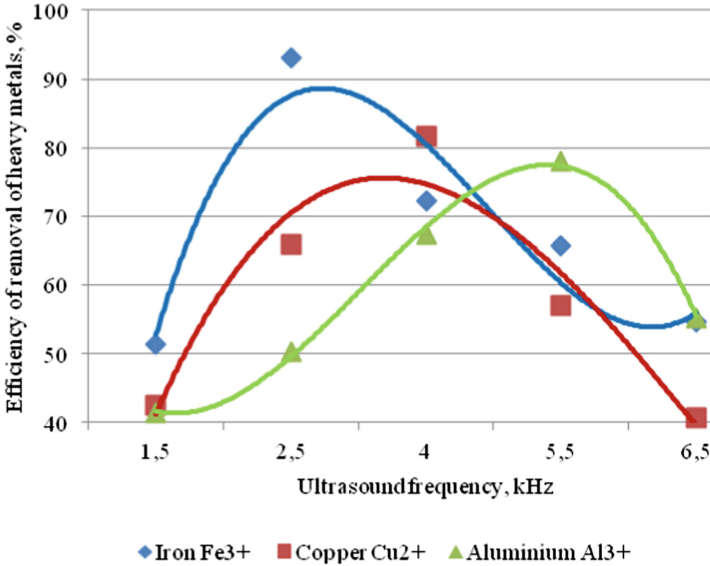


Fig. 3. Influence of ultrasound frequency change on efficiency of removal of heavy metals from sewage sludge.

It was found that the highest efficiency of removal of heavy metals from sewage sludge is observed at the following ultrasound frequencies: iron (Fe³⁺) – 2.5 kHz, copper (Cu²⁺) – 4 kHz, aluminium (Al³⁺) – 5.5 kHz at linear mixing velocity Fe³⁺ and Al³⁺ – 0.3 m/s, Cu²⁺ – 0.5 m/s.

Analysis of experimental data shows that the treatment of sewage sludge with humic reagents effectively removes heavy metals with subsequent disposal of sludge as fertilizer.

Table 2. Optimal modes of heavy metals removal from urban wastewater sludge during treatment with humic reagents.

Reagent type	Reagent dose	The content of heavy metals in the sludge, mg/kg dry matter			Efficiency of removal of heavy metals from sewage sludge
		Name of elements	Before treatment	After treatment	
Lignite	50	Iron (Fe ³⁺)	4148.5	273.9	93.0
		Copper (Cu ²⁺)	266.3	490	81.6
		Aluminium (Al ³⁺)	8517.5	1865.4	78.1
Peat	50	Iron (Fe ³⁺)	4148.5	365.1	91.2
		Copper (Cu ²⁺)	266.3	391	85.3
		Aluminium (Al ³⁺)	8517.5	1686.2	80.2

5 Conclusion

Utilization sludge disposal is an urgent environmental problem. Sludge sites are sources of pollution of soil, ground and surface water bodies, air. The authors proposed a method of extracting heavy metals from wastewater sludge using humic reagents and sonication.

This method involves constant mixing of the sludge with humic reagents at a linear velocity of 0.2–0.5 m/s while simultaneously ultrasound at a frequency of 2.5–5.5 kHz for 1–1.5 min. The developed technological scheme of heavy metals extraction from domestic sewage sludge allows further use of sewage sludge as fertilizer.

References




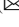


1. Vystavna, Y., Zaichenko, L., Klimenko, N., Rätsep, R.: Trace metals transfer during vine cultivation and winemaking processes. *J. Sci. Food Agric.* **97**(13), 4520–4525 (2017). <https://doi.org/10.1002/jsfa.8318>
2. Vergeles, Y., Butenko, N., Ishchenko, A., et al.: Formation and properties of sediments in constructed wetlands for treatment of domestic wastewater. *Urban Water J.* **13**(3), 293–301 (2016). <https://doi.org/10.1080/1573062X.2014.993178>
3. Marchand, L., Nsanganwimana, F., Cook, B.J., et al.: Trace element transfer from soil to leaves of macrophytes along the Jalle d'Eysines River, France and their potential use as contamination biomonitors. *Ecol. Ind.* **46**, 425–437 (2014). <https://doi.org/10.1016/j.ecolind.2014.07.011>
4. Vystavna, Y., Huneau, F., Motelica-Heino, M., et al.: Monitoring and flux determination of trace metals in rivers of the Seversky Donets basin (Ukraine) using DGT passive samplers. *Environ. Earth Sci.* **65**(6), 1715–1725 (2012). <https://doi.org/10.1007/s12665-011-1151-4>

5. Papagiannis, F., Gazzola, P., Burak, O., Pokutsa, I.: Overhauls in water supply systems in Ukraine: a hydro-economic model of socially responsible planning and cost management. *J. Clean. Prod.* **183**, 358–369 (2018). <https://doi.org/10.1016/j.jclepro.2018.02.156>
6. Vystavna, Y., Yakovlev, V., Diadin, D., Vergeles, Y., Stolberg, F.: Hydrochemical characteristics and water quality assessment of surface and ground waters in the transboundary (Russia/Ukraine) Seversky Donets basin. *Environ. Earth Sci.* **74**(1), 585–596 (2015). <https://doi.org/10.1007/s12665-015-4060-0>
7. Camargo, F.P., Sérgio Tonello, P., dos Santos, A.C.A., Duarte, I.C.S.: Removal of toxic metals from sewage sludge through chemical, physical, and biological treatments—a review. *Water Air Soil Pollut.* **227**(12), 1–11 (2016). <https://doi.org/10.1007/s11270-016-3141-3>
8. Reddy, G.K., Yarrakula, K., Lakshmi, U.V.: Reducing agents enhanced electrokinetic soil remediation (EKSR) for heavy metal contaminated soil. *Iran. J. Chem. Chem. Eng. (Int. Engl. Ed.)* **38**(3), 183–199 (2019)
9. Cieřlik, B.M., Świerczek, L., Konieczka, P.: Analytical and legislative challenges of sewage sludge processing and management. *Monatshefte für Chemie – Chem. Mon.* **149**(9), 1635–1645 (2018). <https://doi.org/10.1007/s00706-018-2255-2>
10. Hudcová, H., Vymazal, J., Rozkořný, M.: Present restrictions of sewage sludge application in agriculture within the European Union. *Soil Water Res.* **14**(2), 104–120 (2019). <https://doi.org/10.17221/36/2018-SWR>
11. Meng, X.Z., Venkatesan, A.K., Ni, Y.L., et al.: Organic contaminants in Chinese sewage sludge: a meta-analysis of the literature of the past 30 years. *Environ. Sci. Technol.* **50**(11), 5454–5466 (2016). <https://doi.org/10.1021/acs.est.5b05583>
12. Dushkin, S.S., Galkina, O.P.: More effective clarification of circulating water at coke plants. *Coke Chem.* **62**(10), 474–480 (2019). <https://doi.org/10.3103/S1068364X19100041>
13. Hamdi, H., Hechmi, S., Khelil, M.N., et al.: Repetitive land application of urban sewage sludge: effect of amendment rates and soil texture on fertility and degradation parameters. *CATENA* **172**, 11–20 (2019). <https://doi.org/10.1016/j.catena.2018.08.015>
14. Dushkin, S., Shevchenko, T.: Applying a modified aluminum sulfate solution in the processes of drinking water preparation. *East.-Eur. J. Enterp. Technol.* **4**(10), 26–36 (2020). <https://doi.org/10.15587/1729-4061.2020.210096>
15. Skinner, S.J., Studer, L.J., Dixon, D.R., et al.: Quantification of wastewater sludge dewatering. *Water Res.* **82**, 2–13 (2015). <https://doi.org/10.1016/j.watres.2015.04.045>
16. Lamastra, L., Suciú, N.A., Trevisan, M.: Sewage sludge for sustainable agriculture: contaminants' contents and potential use as fertilizer. *Chem. Biol. Technol. Agric.* **5**(1), 1–6 (2018). <https://doi.org/10.1186/s40538-018-0122-3>
17. Yesil, H., Molaey, R., Calli, B., Tugtás, A.E.: Removal and recovery of heavy metals from sewage sludge via three-stage integrated process. *Chemosphere* **280**, 130650 (2021). <https://doi.org/10.1016/j.chemosphere.2021.130650>
18. Adeolu, A.T., Adewoye, S.O.: Efficacy of cassava peel extracts for the removal of heavy metals from hospital sewage sludge in Nigeria. *J. Health Pollut.* **9**(23), 190908 (2019). <https://doi.org/10.5696/2156-9614-9.23.190908>
19. Sutradhar, I., et al.: Introducing urine-enriched biochar-based fertilizer for vegetable production: acceptability and results from rural Bangladesh. *Environ. Dev. Sustain.* **23**(9), 12954–12975 (2021). <https://doi.org/10.1007/s10668-020-01194-y>
20. Kobierski, M., Kondratowicz-Maciejewska, K., Banach-Szott, M., Wojewódzki, P., Peñas Castejón, J.M.: Humic substances and aggregate stability in rhizospheric and non-rhizospheric soil. *J. Soils Sediments* **18**(8), 2777–2789 (2018). <https://doi.org/10.1007/s11368-018-1935-1>
21. Śliwińska, A., Drab, M.: Changes in the content of humic substances, reaction and sorption properties occurring in reclaimed land in post-mining areas. *Pol. J. Soil Sci.* **48**(2), 189 (2016). <https://doi.org/10.17951/pjss.2015.48.2.189>

22. Keeley, J., Jarvis, P., Judd, S.J.: Coagulant recovery from water treatment residuals: a review of applicable technologies. *Crit. Rev. Environ. Sci. Technol.* **44**(24), 2675–2719 (2014). <https://doi.org/10.1080/10643389.2013.829766>
23. Dushkin, S.S., Martynov, S., Dushkin, S.S.: Intensification of the work of contact clarifiers during the drinking water preparation. *J. Water Land Dev.* **41**, 55–60 (2019). <https://doi.org/10.2478/jwld-2019-0027>
24. Matsak, A., Tsytlshvili, K., Rybalova, O., et al.: Method of agricultural sewage water purification at troughs and a biosorption bioreactor. *East.-Eur. J. Enterp. Technol.* **5**(10), 15–24 (2018). <https://doi.org/10.15587/1729-4061.2018.144138>



Methods of Combined Horizontal Settler Research

Stepan Epoyan¹ , Tamara Airapetian¹ , Oleksandr Haiduchok²  ,
Gennadiy Sukhorukov² , and Oleksandr Kravchuk³ 

¹ O. M. Beketov National University of Urban Economy in Kharkiv, 17 Marshala Bazhanova Street, Kharkiv 61002, Ukraine

² Kharkiv National University of Civil Engineering and Architecture, 40 Symska Street, Kharkiv 61002, Ukraine
alexandr.haiduchok@kstuca.kharkov.ua

³ Kyiv National University of Construction and Architecture, 31 Povitroflotsky Avenue, Kyiv, Ukraine

Abstract. The main sources for water supply in Ukraine are the rivers Dnieper, Southern Bug, Dniester, Siverskyi Donets, Danube. The quality of these rivers is deteriorating. A two-stage scheme with horizontal settling tanks on the first stage is used for surface water treatment. These facilities are reliable and easy to operate, but require significant space. Source water distribution and clarified water drainage systems are inefficient, so structures are constantly modified, improved systems of distribution of source water and drainage. We propose to use a device of thin-layer settlers in a sedimentation zone for intensification horizontal settler. This work shows the development of methods for studying the model of a combined horizontal settling tank. To increase the efficiency of horizontal settling tanks and the quality of water treatment, a combined horizontal settling tank is proposed. At the beginning of the sedimentation zone, there is a tubular thin-layer settling tank and the clarified water is drained through an end tray with a sinusoidal spout. Studies of settling tanks are usually carried out on models. For this purpose the technique of carrying out experiments on the model of the combined horizontal settler is developed. The design of the combined horizontal settling tank and the method of its research are developed and offered. The proposed technique allows studying the combined horizontal settling tank for water purification in the laboratory.

Keywords: Combined horizontal settling tank · Thin-layer settling tank · Sinusoidal sillway

1 Introduction

Sustainable development of a country is impossible to imagine without the development of a water industry [1]. Natural water, which is found in surface and underground sources, as well as in atmospheric waters, is used for water supply in cities or settlements [2–4]. The main water sources in Ukraine are the rivers Dnieper, Southern Bug,

Dniester, Siverskyi Donets, Danube. Unfortunately, the quality of water in these rivers is deteriorating [5, 6].

In water supply systems of populated cities, treatment plants occupy a significant place because they purify water to the drinking quality. Even in ancient Rome, water purification took place by the method of settling. Water passed through the buildings where the process of precipitation of the suspension took place, and then the sediment was periodically removed. These were the first horizontal settling tanks. Since then, these facilities have changed (new constructions of horizontal settling tanks, new systems of distribution of source water, drainage of clarified water, sludge discharge, calculation of settling tanks have appeared).

2 Literature Review

Nowadays, a two-stage scheme with settling tanks is used for surface water treatment (Fig. 1). If productivity of water treatment plant is near $30000 \text{ m}^3/\text{day}$ or more, the horizontal settlers are used [7]. They are reliable and easy to operate. Unfortunately, their disadvantages are: require large areas for building and systems of distribution of source (primary) water, drainage of clarified water are not effective enough. With increasing water consumption, they do not provide complete drainage of clarified water (part of the clarified water is returned to the settling tank) and from the bottom the drained water with sludge. Thus there is a longitudinal circulation. Solving these problems they are constantly modified and improved systems of distribution of source water, drainage of clarified water, their calculations and designs [8–10].

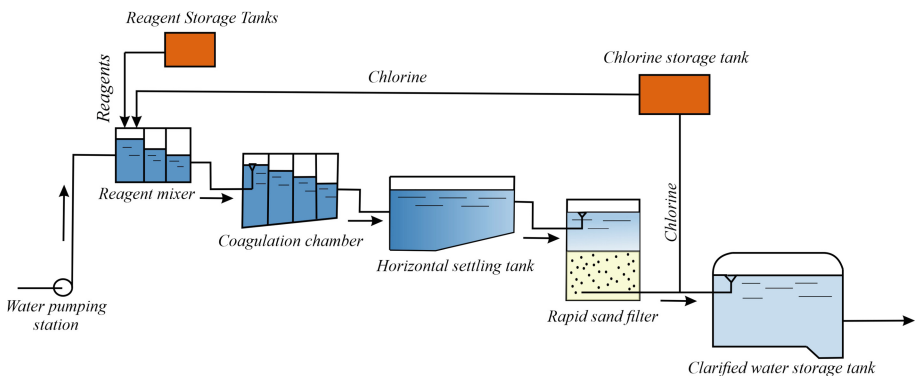


Fig. 1. Two-stage scheme for surface water treatment with horizontal settling tank and rapid sand filter.

In the 1950s, thin-layer settling tanks began to be used, in which the sedimentation of suspended solids occurs by reducing the height [11]. Thin-layer settling tanks (blocks, modules, elements) can be used as independent structures and for intensification or reconstruction traditional settling tanks [12–15]. Thin-layer settling tanks in the direction of sediment movement relative to the movement of treated water are divided into direct-flow, counter-current, combined and transverse [12, 13].

To increase the efficiency of horizontal settling tanks and the quality of water purification, we have proposed a combined horizontal settling tank, in which a tubular thin-layer settling tank is located at the beginning of the sedimentation zone.

The work shows the development of research methods of the model of combined horizontal settling tank to improve the quality of natural water treatment for drinking water supply.

3 Research Methodology

Before starting the study of the combined horizontal settling tank, we take into account the following conditions:

- thin-layer settlers and horizontal settling tank work as one facilities and the water consumption for them is the same, but the main device is a horizontal settling tank;
- turbidity of the water, which is entering in horizontal settling tank, will be less than the source water. This means that the big suspended particles will be deposited in a thin-layer settlers, and the light suspended particles – along the length of the horizontal settling tank;
- the speed of water movement in the thin-layer settlers will be higher than in the horizontal settling tank because the living cross section of water in the thin-layer settlers decreases due to structural elements and their geometric location in horizontal settling tank.

Studies of settling tanks are usually carried out on models [16, 17]. It is necessary to have a geometric similarity between the model and nature facility, to determine the main force of the process. In this case, the main force is the gravity force, due to which the sedimentation of the suspension proceeds. So the hydraulic modeling of the combined horizontal settling tank is carried out according to the Froude criterion [16, 17].

To research the combined horizontal settling tank, it is first necessary to calculate its model in accordance with the full-scale facility. For example, with a scale factor of geometric similarity (L_λ), this is equal to 12:

$$L_\lambda = \frac{L_H}{L_M}, \quad (1)$$

where L_H is the size of the full-scale system; L_M is the size of the model system.

In Fig. 2 shown the model of combined horizontal settling tank for laboratory research. The principle of operation of the combined horizontal settling tank is as follows: source water, which is mixed with the coagulant, gets through hose 1 into the distribution system 2 of the vortex chamber of the flake formation of sludge 3 with vertical walls. Then it flows through the spillway 4 and descends between the spillway wall 4 and the jet-directing wall 5 and rotates under the wall 5 and distributes in the thin-layer settler pipes by reducing the cross-section between the jet-directing wall 5 and the thin-layer settler pipes 6. Next, it passes through a thin-layer settling tank 7, where big suspended particles are deposited, which slides on the tray of pipes 6 and is periodically removed by the hose 8. Partially clarified water from the thin-layer settling

tank 7 falls on the jet-directing combined partition 9, where part of the water passes through the holes 10 and through the visors 11 is evenly distributed in the lower part of the settling tank. Then the entire flow of water enters the end gutter 13 with a spout of wavy shape (sinusoidal shape) 14 and pipelines 15 is diverted. The fine suspended particles stuck in the settling tank are periodically discharged through the pipeline 16.

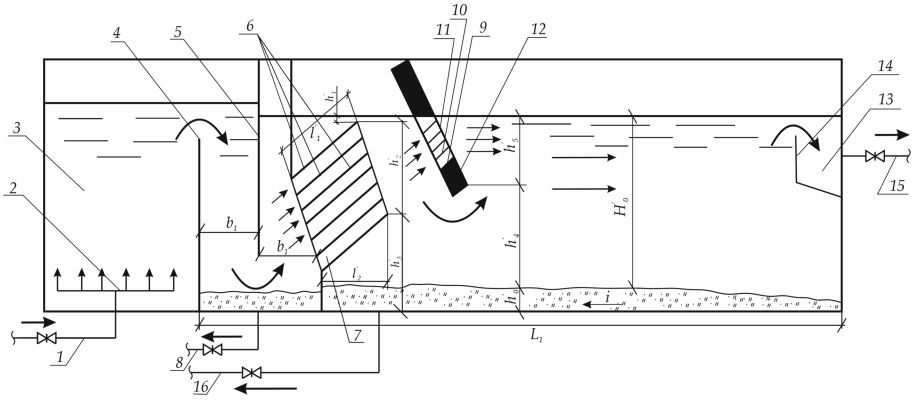


Fig. 2. The model of the combined horizontal settling tank for laboratory research.

In the research of the combined horizontal settling tank on the small model with a coefficient of geometric similarity scale $L_\lambda = 12$, we reduce all the dimensions of the full-scale structure by 12 times. In this case, the geometric dimensions of the model will be next (Fig. 2): the length of the horizontal settling tank (L_1) – 5.8 m; width – 0.25 m; the height of the sedimentation zone – 0.25 m; the height of the block of thin-layer settlers (h_2') – 0.13 m; the length of the block of the thin-layer element (l_1') – 0.09 m; the length of the block of the thin-layer block in horizontal direction – 0.06 m; the number of pipes in the thin-layer block in vertical direction – 16 and horizontally – 30; diameter of pipes – 8 mm; the tilt angle of thin-layer elements – 50° ; the height of the clarified water collection zone (h_1') – 0.03 m; the height of the protection zone (h_3') – 0.08 m; the width of the channel between the chamber for the formation of sludge flakes and thin-layer settlers (b_1) – 0.07 m; the distance of the combined jet-directing partition from the block of thin-layer settlers (l_3') – 0.125 m; the diameter of the holes in the combined jet-directing partition – 8 mm; number of holes in the combined jet-directing partition – 92; the distance between the combined partition from the zone of sediment accumulation (h_4') – 0.17 m; the depth of the combined partition under water level (h_5') – 0.08 m; the height of the accumulation zone (h_0') – 0.04 m; the length of chamber for the formation sludge flakes is 1.5 m; the width and height according to the horizontal settling tank are 0.25 m. The total height of the model will be 0.35 m taking into account the reserve factor.

During modeling by the Froude criterion, the velocity of water in the model of the horizontal settling tank will be [17–21]:

$$V_M = \frac{V_H}{\sqrt{\frac{L_H}{L_M}}} = \frac{V_H}{\sqrt{L_\lambda}}, \quad (2)$$

where V_H is the water velocity in a full-scale facility.

Water consumption, respectively, will be:

$$Q_M = \omega_M \times V_M, \quad (3)$$

where ω_M is the living area of the model.

The water velocity in the elements (pipes) of the thin-layer settling tank is determined by:

$$V_{thin.set.} = \frac{Q_M}{\omega_{thin.set.}}, \quad (4)$$

where $\omega_{thin.set.}$ is the living cross-sectional area of the model of thin-layer settling tank. This parameter is determined by the equation:

$$\omega_{thin.set.} = \omega'_{cross.area} \cdot N, \quad (5)$$

where $\omega'_{cross.area}$ is the living cross-sectional area of the element of the thin-layer settling tank; N is the number of elements of the thin-layer settler. It is determined by the equation:

$$N = \frac{\omega'_e}{\omega_e}. \quad (6)$$

The living cross-sectional area of the element of the thin-layer settling tank is:

$$\omega'_{cross.area} = \frac{\pi \cdot d_{holes}^2}{4}, \quad (7)$$

where d_{holes} is the diameter of the holes in the combined jet-directing partition.

Then the area of one element is equal:

$$\omega_e = \frac{\pi d_1^2}{4}. \quad (8)$$

The area of all elements (Fig. 2) is:

$$\omega'_e = b'_1 \cdot h'_2, \quad (9)$$

where b'_1 is the width of the model; h'_2 is the height of the block of thin-layer settlers.

Studies of the combined horizontal settling tank are carried out at different source water temperatures and different turbidity. To determine the uniformity of the distribution of source water on the elements in the thin-layer settler, a mixture of potassium permanganate is used, which is fed into the source water. The process itself is observed through observation windows. At the same time, the movement of potassium permanganate-stained source water around the jet-directing combined partition is observed through the observation windows (Fig. 2).

The silt of the river Siverskyi Donets is used to darken the source water and aluminum sulfate is used as a coagulant.

4 Results

Before the calculation of the combined horizontal settling tank, the following technological and constructive parameters were adopted:

- the water velocity in a full-scale facility (V_H) is 8 mm/s;
- the living area of the model (ω_M) is 0.0625 m²;
- the outer diameter of the element of the thin-layer settler (d_1) is 12 mm;
- the width of the model (b_1') is 0.25 m;
- the height of the block of thin-layer settlers (h_2') is 0.13 m;
- the diameter of the holes in the combined jet-directing partition (d_{holes}) is 8 mm.

The results of the calculations are shown in Table 1.

Table 1. The results of calculations of the combined horizontal settling tank.

Parameter	Value of calculation
V_M	0.0023 m/s
Q_M	0.0001438 m ³ /s
ω_e	0.000113 m ²
ω'_e	0.0325 m ²
N	288
$\omega'_{cross.area}$	0.00005024 m ²
$\omega_{thin.set.}$	0.01447 m ²
$V_{thin.set.}$	0.00994 m/s or 9.94 mm/s

Water samples are taken in front of the thin-layer settling tank, behind it, behind the jet-directing combined partition and at the outlet of the horizontal settling tank. They are selected at different depths in the amount of at least three. The transparency of the samples is determined by the photoelectrocalorimeter and the weighing method.

The result of water consumption of the model is 0.0001438 m³/s or 0.144 l/s. In this case, the number of elements of the thin-layer settler (N) is 288.

After calculations on the model of the combined horizontal settling tank according to the Froude criterion, the water velocity in the elements (pipes) of the thin-layer settling tank was 9.94 mm/s and the water velocity in the model of the horizontal settling tank was 2.3 mm/s. These parameters indicate the feasibility of hydraulic modeling by Froude criterion.

5 Conclusion

Thus, the combined horizontal settling tank is a facility in which the vortex chamber of flake formation and the horizontal settling tank are combined. A thin-layer settling tank

is arranged in the horizontal settling tank, where suspended solids are deposited. The retained sediment slides on the tray of pipes and is periodically removed. The proposed design allows increasing the efficiency of removal of suspended solids in horizontal settling tanks.

The study of the combined horizontal settling tank is carried out on the small model with the coefficient of geometric similarity scale. This coefficient is equal to 12. This allows finding the technological parameters (the water velocity in the model of the horizontal settling tank, the water velocity in the elements (pipes) of the thin-layer settling tank and the water consumption) using Froude criterion. The numerical values of technological parameters are determined.

The given method of the study of the combined horizontal settling tank is a continuation of our previous studies on this topic. These works are aimed at improving the efficiency of settling tanks, which will reduce operating costs and hydraulic loads on other facilities, increase the uniformity of collection and disposal of clarified water, improve the quality of water treatment and increase the reliability of the facility as a whole.






References

1. Morris, J.: Developing and exploring indicators of water sustainable development. *Heliyon* **5**(5), e01778 (2019). <https://doi.org/10.1016/j.heliyon.2019.e01778>
2. Yakovlev, V., Vystavna, Y., Diadin, D., Vergeles, Y.: Nitrates in springs and rivers of East Ukraine: distribution, contamination and fluxes. *Appl. Geochem.* **53**, 71–78 (2015). <https://doi.org/10.1016/j.apgeochem.2014.12.009>
3. Poff, N.L., Brown, C.M., Grantham, T.E., et al.: Sustainable water management under future uncertainty with eco-engineering decision scaling. *Nat. Clim. Chang.* **6**(1), 25–34 (2016). <https://doi.org/10.1038/nclimate2765>
4. Barannik, V., Borysova, O., Stolberg, F.: The Caspian sea region: environmental change. *Ambio* **33**(1), 45–51 (2004). <https://doi.org/10.1579/0044-7447-33.1.45>
5. Vystavna, Y., Huneau, F., Motelica-Heino, M., et al.: Monitoring and flux determination of trace metals in rivers of the Seversky Donets basin (Ukraine) using DGT passive samplers. *Environ. Earth Sci.* **65**(6), 1715–1725 (2012). <https://doi.org/10.1007/s12665-011-1151-4>
6. Wilkinson, J.L., Boxall, A.B., Kolpin, D.W., et al.: Pharmaceutical pollution of the world's rivers. *Proc. Natl. Acad. Sci.* **119**(8), e2113947119 (2022). <https://doi.org/10.1073/pnas.2113947119>
7. Tretyakov, O., Shevchenko, T., Bezsonnyi, V.: Improving the environmental safety of drinking water supply in Kharkiv region (Ukraine). *East.-Eur. J. Enterp. Technol.* **5**(10), 40–49 (2015). <https://doi.org/10.15587/1729-4061.2015.51398>
8. Epoyan, S., Sukhorukov, G., Volkov, V., Haiduchok, O.: The research of tubular mixer with improved design. *IOP Conf. Ser.: Mater. Sci. Eng.* **907**, 012050 (2020). <https://doi.org/10.1088/1757-899X/907/1/012050>
9. Orlov, V., Martynov, S., Kunitskiy, S.: Energy saving in water treatment technologies with polystyrene foam filters. *J. Water Land Dev.* **31**, 119–122 (2016). <https://doi.org/10.1515/jwld-2016-0042>
10. Polyakov, V., Kravchuk, A., Kochetov, G., Kravchuk, O.: Clarification of aqueous suspensions with a high content of suspended solids in rapid sand filters. *EUREKA: Phys. Eng.* (1), 28–45 (2019). <https://doi.org/10.21303/2461-4262.2019.00827>

11. Martynov, S., Kunytskyi, S., Orlova, A.: A simulation study of surface water purifying through a polystyrene foam filter. *East.-Eur. J. Enterp. Technol.* **5**(10), 19–26 (2017). <https://doi.org/10.15587/1729-4061.2017.109841>
12. Dushkin, S.S., Galkina, O.P.: Thin-layer sedimentation tanks in water clarification at coke plants. *Coke Chem.* **64**(8), 380–385 (2021). <https://doi.org/10.3103/S1068364X21080020>
13. Shamyán, V.L.: Use of various thin-layer settling schemes for industrial wastewater treatment. *J. Arch. Eng. Res.* **1**(1), 43–49 (2021). <https://doi.org/10.54338/27382656-2021.1-8>
14. Bilgin, M., Yurtsever, M., Karadagli, F.: Microplastic removal by aerated grit chambers versus settling tanks of a municipal wastewater treatment plant. *J. Water Process Eng.* **38**, 101604 (2020). <https://doi.org/10.1016/j.jwpe.2020.101604>
15. Muralikrishna, I.V., Manickam, V.: *Environmental Management: Science and Engineering for Industry*. Elsevier, Amsterdam (2017)
16. Hirom, K., Devi, T.T.: Application of computational fluid dynamics in sedimentation tank design and its recent developments: a review. *Water Air Soil Pollut.* **233**(1), 1–26 (2022). <https://doi.org/10.1007/s11270-021-05458-9>
17. Prešeren, T., Steinman, F., Širok, B., Bajcar, T.: The theoretical densimetric Froude number values with favourable effect on the clarifier performance. *Chem. Eng. Process.: Process Intensif.* **74**, 97–105 (2013). <https://doi.org/10.1016/j.cep.2013.09.001>
18. Lopez, P.R., Lavín, A.G., López, M.M., de las Heras, J.L.: Flow models for rectangular sedimentation tanks. *Chem. Eng. Process.: Process Intensif.* **47**(9–10), 1705–1716 (2008). <https://doi.org/10.1016/j.cep.2007.09.020>
19. Bürger, R., Diehl, S., Farås, S., Nopens, I.: On reliable and unreliable numerical methods for the simulation of secondary settling tanks in wastewater treatment. *Comput. Chem. Eng.* **41**, 93–105 (2012). <https://doi.org/10.1016/j.compchemeng.2012.02.016>
20. Gao, H., Stenstrom, M.K.: Development and applications in computational fluid dynamics modeling for secondary settling tanks over the last three decades: a review. *Water Environ. Res.* **92**(6), 796–820 (2020). <https://doi.org/10.1002/wer.1279>
21. Tetzlaff, D., Priddy, G.: Sedimentary process modeling: from academia to industry. In: Merriam, D.F., Davis, J.C. (eds.) *Geologic Modeling and Simulation*. CAES, pp. 45–69. Springer, Boston, MA (2001). https://doi.org/10.1007/978-1-4615-1359-9_4



Territorial Planning and Sustainable Development of Refugee Areas

Olena Uhodnikova^(✉) , Kostiantyn Viatkin , Sergii Gordiienko ,
Roman Viatkin , and Natalia Moroz 

O. M. Beketov National University of Urban Economy in Kharkiv, 17 Marshala Bazhanova
Street, Kharkiv 61002, Ukraine
uhodnikova.olena@kname.edu.ua

Abstract. The paper analyzes the state and prospects of the development of the territories of Ukraine in the conditions of counteraction to military aggression and post-war reconstruction. The basic needs to be addressed to the IDPs have been identified. By analyzing statistical data, household needs are identified among the main needs that have arisen in internally displaced persons. To meet these needs, the problems of increased workload and logistics – building a safe route for the delivery of food and household items. A cartographic projection of the movement of internally displaced persons has been developed based on the results of the analysis of statistical data on population movements from February 24, 2020 to the time of the study. It has been determined that changes during military aggression may lead to further population displacement, so the location of the population in the territories that received the largest number of internally displaced persons is temporary both in terms of population relocation and post-occupation change of territories of active ground combat operations. The international experience of solving the problems of accommodation of internally displaced persons was analyzed, which allowed to identify the negative aspects of the construction of such towns and solve them through research. Possible elements of integrated territorial planning of temporary development of territories for accommodation of internally displaced persons were considered, considering the need to ensure the goals of sustainable development. As a result, proposals have been developed for mechanisms to provide temporary housing for persons whose housing has been damaged because of the war, both in the territories where displaced persons have moved and then in the territories liberated from occupation. Therefore, the requirements for the functional component of modular towns should be linked to the requirements of the Concept of Sustainable Development.

Keywords: Sustainable development · Post-war reconstruction · Territorial development · Territorial planning

1 Introduction

The military aggression against Ukraine on February 24, 2022 was the cause of the socio-economic crisis that arose due to the forced movement of the population from the

territories of active hostilities. Almost 5.6 million people have been granted refugee status by countries of the European Union. 7.7 million people in Ukraine have been forcibly displaced. These humanitarian and social challenges became the biggest challenges for Europe after the Second World War. Many people were left homeless in areas of active hostilities due to constant bombing, artillery, and tank shelling. Thus, while the first challenge for Europe has been the issue of temporary accommodation and a number of humanitarian issues, the new challenge will be the creation of temporary housing in safe areas and socio-economic assistance to those who have been forced to leave their homes and damaged their homes. Therefore, it is expedient to analyze the ways of solving the problem of accommodation of the population that was forced to leave their homes both at the level of temporary arrangement and to solve the problems of post-war reconstruction of the country.

2 Literature Review

The issue of transformations of sustainable development processes in the context of military conflicts, their prevention, and the use of elements of sustainable development in the postwar reconstruction system is an important public topic, so the work of many scholars is devoted to its solution [1, 2]. In particular, the issue of sustainable development in the post-war reconstruction was considered in the study of Strasser *et al.* [3], analyzed advanced technologies in the development of the transformational potential of territories in the face of new challenges. Fazey *et al.* [4] systematized the study of energy and social areas of development, considering the goals of sustainable development. Pel *et al.* [5] conducted a study of social challenges in the new realities of society. Törnberg [6] in his research defined the typology of social change in the face of new challenges, based on the study of transformational processes. Aguilar *et al.* [7] studied the processes of renovation and restoration of post-conflict societies. Wittmayer *et al.* [8] investigated transformational processes through the application of social innovations to construct social systems. Augustinus and Barry [9] identified public initiatives that can be implemented to ensure sustainable development. Fisher [10] identified some aspects of territorial management in the context of political challenges, considering the prospects of their sustainable development. The conditions of military aggression in Ukraine have created unique challenges for the sustainable development of modern society, so it is advisable to search for new mechanisms for managing the sustainable development of territories in modern socio-economic conditions.

3 Research Methodology

According to UN statistics, as of May 2, 2022, the number of refugees was 5,597,483 people [11]. Among the countries that received refugees, 3.07 million were sheltered by Poland, 836.1 thousand people were sheltered by Romania, 534.8 thousand people – Hungary, more than 448 thousand people – Moldova, 382 thousand people – Slovakia [12]. Statistics on internally displaced persons show that the number of persons who have officially received the status of internally displaced persons is 3.4 million [13].

According to the results of a survey conducted by the Ministry of Digital Transformation of Ukraine, the basic needs that needed to be addressed by internally displaced persons were identified. The results of the survey are presented in Fig. 1.

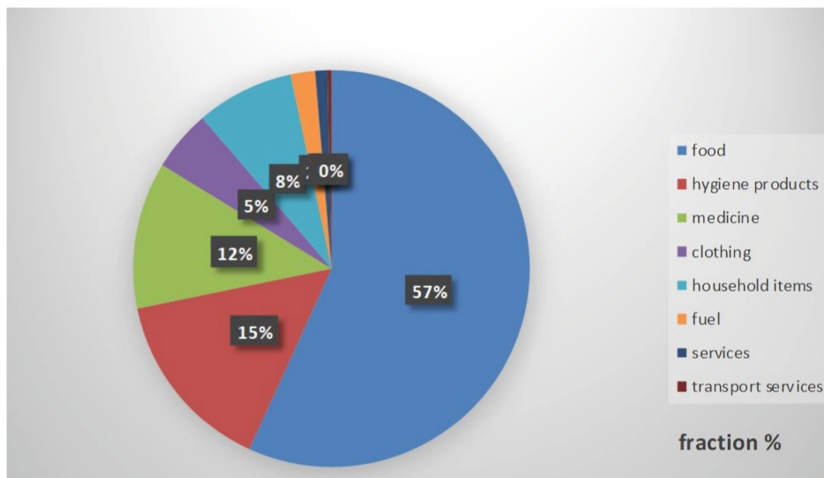


Fig. 1. The structure of the needs of internally displaced persons [14].

Thus, among the main needs of IDPs are household needs: food, hygiene products, medicines and more. Speaking about the social burden in the EU, it is appropriate to determine that the growing number of refugees increases the burden on the social system, and determines the need to increase the amount of food, medicine, and household items supplied in the territory. As for the territories of Ukraine where there are no active ground battles, the population has moved there from areas of active hostilities. It also increases the load on the territory of Ukraine, mainly in the West and in the Central regions. Part of the population has moved from uncontrolled and evacuated areas and areas under temporary occupation, so to meet the needs of these areas there is not only the problem of increased workload but also the problem of logistics - building a safe route for food and household items.

The authors have developed a cartographic projection of displaced persons under the results of the analysis of statistical data on population movements from February 24, 2020 to the time of the study (Fig. 2).

Thus, because of mapping the flows of displaced persons to Ukraine, we see that the largest number of people moved from Donetsk and Luhansk regions (as a percentage of the permanent population in this area, the number of displaced persons is over 80%). We are talking about the processes of decentralization – moving from cities to rural and urban areas and moving outside the regions. Significant population movements are observed in Kyiv, Chernihiv, Sumy and Kharkiv oblasts. The largest number of internally displaced persons was in the Lviv region (approximately 400,000). The greatest load is observed in the western regions of Ukraine (Lviv, Zakarpattia, Ivano-Frankivsk regions). The large flow of IDPs in these areas is associated not only with their remoteness from



Fig. 2. Cartographic projection of displaced persons, compiled by the authors on the basis of [15].

the area of active ground combat operations, but also with their approach to the state border of Ukraine. Thus, further changes in the course of the war may lead to further population displacement, so the relocation of the population to the territories hosting the largest number of internally displaced persons is temporary both in terms of relocation to the liberated territories in terms of population movement due to the change of territories of active ground combat operations.

4 Results

Analyzing the processes of relocation of internally displaced persons, it was concluded that temporary modular housing should be in the western regions of Ukraine, taking into account the possibility of its further relocation to the liberated territories in order to return to a peaceful life. Together with the UN, the construction of modular houses for internally displaced persons began in Lviv. The modular town will consist of 88 residential buildings, which can accommodate 350 people. Electricity and heating will be supplied to the modular campus. Similar modular towns have been built in areas of other military conflicts. Examples are the modular town in Kharkiv region for IDPs from Donetsk and Luhansk oblasts with the beginning of the military conflict in eastern Ukraine in 2014, the modular town for IDPs in Georgia on the outskirts of Tbilisi, the modular town in Bosnia and Herzegovina and others [16].

It should be noted that the operation of these houses, despite the temporary nature of such towns, in the above areas, these houses are without any changes since the start of hostilities, for example, in Kharkiv region, the temporary town has been operating for 8 years. It should be noted that because such houses are not designed for long-term use, there are problems with utilities, the need for repairs and modernization [16].

In Fig. 3 shown the aftermath of a fire in a model refugee town in Bosnia and Herzegovina. The fire was caused by the mismatch of electrical wiring to the required load in the town due to the use of heating devices because the heating in the town is insufficient to ensure the normal functioning of people [17].



Fig. 3. Results of a fire due to overload of the electrical network in the modular town, Bosnia and Herzegovina [17].

Therefore, among the requirements for the functional component of modular towns, it is advisable to identify the following requirements, which can be related to the requirements of the Concept of Sustainable Development (Table 1).

Thus, analyzing the goals of sustainable development and their role in creating modular towns for migrants, the main requirements for the following facilities are identified:

- the possibility of fast assembly and disassembly, possibility of movement – transport mobility,
- the ability to accommodate the maximum number of people in the shortest possible time,
- ensuring operational safety,
- providing the residents of the town with quality utilities,
- to create conditions for ensuring the goals of sustainable development by rationalizing the space of modular towns.

Table 1. The requirements for the functional component of modular towns are related to the requirements of the concept of sustainable development [3–6, 9, 10, 18–21]

Sustainable development goals	Settlement requirements	Ways to solve the problem
1. Overcoming poverty	Creating additional jobs	Possibility of temporary employment of displaced persons in the field of housing and communal services directly from the modular town, Possibility of employment of internally displaced persons in the system of social infrastructure created in the modular town, Creation of coworking with the involvement of forcibly displaced persons to work remotely with the provision of technical capabilities (organizational equipment, high-speed Internet), Involvement of residents in agriculture through the creation of greenhouses in the town
2. Overcoming hunger	Food shortages due to occupation of agricultural lands and complicated logistics	Creation of greenhouses with vertical landscaping near modular towns, which are able to provide food and work for the townspeople
3. Good health	Ensuring access to medicines and medical services, prevention of epidemics and diseases	Formation of mobile outpatient clinics to meet the needs of modular camps and conduct current medical examinations
4. Quality education	Formation of access to education and new skills	Creating opportunities for coworking space for remote retraining of specialists, obtaining additional skills and providing leisure for children

(continued)

Table 1. (continued)

Sustainable development goals	Settlement requirements	Ways to solve the problem
5. Gender equality	Issues of gender equality are complicated in military conflicts	Ensuring the processes of gender equality by finding ways to ensure the realization of the potential of men and women on equal terms
6. Clean drinking water	There is a reduction in the amount of clean drinking water with increasing population	Creation of modular settlements in places with access to groundwater sources, which will simplify the possibility of access to water
7. Renewable energy	Increasing the load on the network due to the increase in the number of electrical devices	Consideration of the possibility of creating modular towns next to farms with alternative energy sources to use this energy for their power supply
8. Economic growth	Decreased economic growth	Financing of startups developed by residents of modular towns aimed at reviving economic development through the crowdfunding exchange
9. Innovation and infrastructure	Infrastructure overload	Establishment of mobile social security institutions in towns with many inhabitants with the possibility of their further transportation to the territories liberated from hostilities
10. Reducing inequality	Issues of equality are complicated by military conflicts	Ensuring the processes of equality of all categories of the population
11. Sustainable development of cities and communities	Overpopulation in the absence of potential resources to provide for the population	Connecting modular cities with the infrastructure of the territories where they are located
12. Responsible consumption	In conditions of imperfect processes of providing the population with products and services, irrational consumption may increase	Rationalization of the process of providing the population by analyzing the requests and finding the minimum cost of providing them

(continued)

Table 1. (continued)

Sustainable development goals	Settlement requirements	Ways to solve the problem
13. Combating climate change	Man-made impacts on the territory cause climate change	Creating conditions for vertical landscaping will help address issues of man-made impact, the proximity of the location to the existing infrastructure will reduce the number of movements and emissions of carbon dioxide
14, 15. Conservation of land and sea ecosystems	Man-made human impact on nature threatens the sustainability of ecosystem development	Development of vertical landscaping, alternative energy sources, locality of means of providing household needs of the population will contribute to the preservation of ecosystems
16. Peace and justice	Rising domestic problems due to war and forced displacement	Development of volunteering on the territories of modular towns
17. Partnership for sustainable development	There are no effective global problem-solving and security systems	Providing an integrated approach to the placement and equipment of modular houses will promote sustainable development

5 Conclusion

Thus, because of the study, trends in the development of territories in the context of military conflict and postwar reconstruction were identified. Statistical data were analyzed and a cartographic projection of the movements of internally displaced persons on the territory of Ukraine was developed. Based on the analysis of population movements, areas that could potentially be attractive for the accommodation of modular settlements for migrants were identified. Due to changes in the military situation at the front and changes in the flow of migrants, it is necessary to create modular houses that can be moved, including to the liberated territories. The proposals of the authors of the article are related to the developed mechanisms for ensuring the goals of sustainable development for the sustainable development of the territories where the modular towns are located.

References






1. Lelechenko, A.P., Lebedinska, O.Y., Derun, T.M., et al.: Mechanisms of inter-state communications for solving sustainable development problems. *Asia Life Sci.* **22**(2), 1–14 (2020)
2. Gontareva, I., Maryna, B., Babenko, V., et al.: Identification of efficiency factors for control over information and communication provision of sustainable development in higher education institutions. *WSEAS Trans. Environ. Dev.* **15**, 593–604 (2019)
3. Strasser, T., de Kraker, J., Kemp, R.: Network leadership for transformative capacity development: roles, practices and challenges. *Glob. Sustain.* **5**, e11 (2022). <https://doi.org/10.1017/sus.2022.6>
4. Fazey, I., Schöpke, N., Caniglia, G., et al.: Transforming knowledge systems for life on earth: visions of future systems and how to get there. *Energy Res. Soc. Sci.* **70**, 101724 (2020). <https://doi.org/10.1016/j.erss.2020.101724>
5. Pel, B., Haxeltine, A., Avelino, F., et al.: Towards a theory of transformative social innovation: a relational framework and 12 propositions. *Res. Policy* **49**(8), 104080 (2020). <https://doi.org/10.1016/j.respol.2020.104080>
6. Törnberg, A.: Prefigurative politics and social change: a typology drawing on transition studies. *Distinktion: J. Soc. Theory* **22**(1), 83–107 (2021). <https://doi.org/10.1080/1600910X.2020.1856161>
7. Aguilar, M., Sierra, J., Ramirez, W., et al.: Toward a post-conflict Colombia: restoring to the future. *Restor. Ecol.* **23**(1), 4–6 (2015). <https://doi.org/10.1111/rec.12172>
8. Wittmayer, J.M., Backhaus, J., Avelino, F., et al.: Narratives of change: how social innovation initiatives construct societal transformation. *Futures* **112**, 102433 (2019). <https://doi.org/10.1016/j.futures.2019.06.005>
9. Augustinus, C., Barry, M.B.: Land management strategy formulation in post-conflict societies. *Surv. Rev.* **38**(302), 668–681 (2006). <https://doi.org/10.1179/sre.2006.38.302.668>
10. Fisher, D.: Freeze-framing territory: time and its significance in land governance. *Space Polity* **20**(2), 212–225 (2016). <https://doi.org/10.1080/13562576.2016.1174557>
11. Official site of the National Institute for Strategic Studies. <https://niss.gov.ua/en/general-information>. Accessed 05 May 2022
12. Official site of Office of the United Nations High Commissioner for Refugees. <https://www.unhcr.org/ua/>. Accessed 05 May 2022
13. Trofimtseva, O.: Ukraine ranks 20th in the world and 11th in Europe in the area of agricultural land under organic production (2019). <https://www.kmu.gov.ua/news/ukrayina-zajmaje-20-te-misce-u-sviti-ta-11-te-misce-v-yevropi-za-ploshcheyu-silskogospodarskih-ugid-zajnya-tih-pid-organichnim-virobnictvom-olga-trofimceva>. Accessed 05 May 2022
14. Official site of the Ministry and the Committee for Digital Transformation of Ukraine. <https://thedigital.gov.ua/>. Accessed 05 May 2022
15. Official site of Information and Analytical Portal of the AIC of Ukraine. <https://agro.me.gov.ua/ua>. Accessed 05 May 2022
16. Fulford, L.: For Ukrainians displaced by war, five years in a grey container block. *The New Humanitarian* (2019). <https://www.thenewhumanitarian.org/news/2019/09/10/Ukraine-internally-displaced-idps-conflict-Kharkiv>. Accessed 05 May 2022
17. Arsenijević, D.: Unbriable Bosnia and Herzegovina: The Fight for the Commons. *Nomos Verlagsgesellschaft*, Baden-Baden (2014)
18. Giles-Corti, B., Moudon, A.V., Lowe, M., et al.: Creating healthy and sustainable cities: what gets measured, gets done. *Lancet Glob. Health* **10**(6), e782–e785 (2022). [https://doi.org/10.1016/S2214-109X\(22\)00070-5](https://doi.org/10.1016/S2214-109X(22)00070-5)

19. de Sa, T.H., Mwaura, A., Vert, C., et al.: Urban design is key to healthy environments for all. *Lancet Glob. Health* **10**(6), e786–e787 (2022). [https://doi.org/10.1016/S2214-109X\(22\)00202-9](https://doi.org/10.1016/S2214-109X(22)00202-9)
20. Lowe, M., Adlakha, D., Sallis, J.F., et al.: City planning policies to support health and sustainability: an international comparison of policy indicators for 25 cities. *Lancet Glob. Health* **10**(6), e882–e894 (2022). [https://doi.org/10.1016/S2214-109X\(22\)00069-9](https://doi.org/10.1016/S2214-109X(22)00069-9)
21. Cerin, E., Sallis, J.F., Salvo, D., et al.: Determining thresholds for spatial urban design and transport features that support walking to create healthy and sustainable cities: findings from the IPEN Adult study. *Lancet Glob. Health* **10**(6), e895–e906 (2022). [https://doi.org/10.1016/S2214-109X\(22\)00068-7](https://doi.org/10.1016/S2214-109X(22)00068-7)

Materials Engineering and Manufacturing



Use of New Smart Materials and Technologies Based on Titanium Alloys in Urban Engineering

Valeriy Kostin^(✉) , Olena Berdnikova , Svitlana Hryhorenko ,
Olga Kushnarova , and Evgeniy Titkov 

E. O. Paton Electric Welding Institute of the National Academy of Science of Ukraine,
11 Kazymyra Malevycha Street, Kyiv 03150, Ukraine
kostin@paton.kiev.ua

Abstract. One of the promising areas of development of modern titanium alloy metallurgy is the development and manufacture of low-alloy titanium alloys for the aerospace industry, chemical and energy engineering, military industry, medicine. The experimental low cost alloys of titanium Ti-2.8Al-5.1Mo-4.9Fe (pseudo- β -alloy) and Ti-1.5Fe-0.4O (pseudo- α -alloy) were received by electron beam melting (EBM) with intermediate capacity. Metallographic, structural, X-ray structural analysis, electron microscopic studies of the lumen were performed, CCT diagrams of transformation titanium alloys were obtained and critical cooling rates were determined, physical and computer modeling of phase transformations in experimental titanium alloys was performed. It was found that the low cost titanium alloy Ti-2.8Al-5.1Mo-4.9Fe is a two-phase pseudo- β alloy, while the alloy Ti-1.5Fe-O is a two-phase pseudo- α titanium alloy. It was found that in the alloy Ti-2.8Al-5.1Mo-4.9Fe hardening occurs due to the formation of dispersed particles of titanium intermetallic Mo_9Ti_4 and Fe_2Ti , while in the alloy Ti-1.5Fe-O – disperse-strengthening particles of titanium oxides Ti_3O_5 , $\text{Ti}_4\text{Fe}_2\text{O}$ and FeTiO . The low cost titanium alloy Ti-2.8Al-5.1Mo-4.9 Fe has higher strength values compared to the strength of the alloy Ti-1.5Fe-O, but lower plasticity and toughness. The critical cooling rate for the experimental titanium alloy Ti-2.8Al-5.1Mo-4.9Fe is 20 °C/s.

Keywords: Low cost titanium alloys · Electron beam melting · Microstructure · Titanium alloys · Dispersive particles · Structural transformations · Gleeble 3800 · Structure modeling

1 Introduction

The successful development of modern urban economy requires, on the one hand, the introduction of new computer smart control systems, and, on the other hand, the creation of an appropriate infrastructure for our cities. To successfully solve this complex problem, it is necessary to develop and implement new smart technologies for the design and production of modern building structures. Currently, most building structures are made of steels of various compositions and strength classes – low-alloy, stainless, high-strength, weather-resistant, etc. In some cases, titanium and its alloys could become a

worthy replacement for steels. Titanium alloys have high specific strength, corrosion resistance, wear resistance and other outstanding properties. However, the main deterrent to the widespread use of titanium alloys in urban infrastructure is its relatively high cost. Therefore, one of the urgent problems of modern materials science is to reduce the cost of their production and the production of structures from them for various purposes.

Titanium and its alloys as structural materials have an excellent set of mechanical and operational properties that allow them to be used in various industries. Titanium-based alloys are widely used in aerospace, chemical and energy engineering, military industry, medicine [1–6].

One of the factors hindering the widespread use of titanium alloys in other industries is the high cost of titanium alloys, due to their alloying system, high cost of raw materials used and technology of their production. Reducing the cost of products involves the development of alloys using cheap raw materials, alloys with high technological characteristics, as well as technological processes that provide higher energy and materials efficiency.

The main directions of development of new compositions of low alloys of wide application are: reduction of the content in the alloy of expensive and deficient alloying elements (Mo, Ta, Zr, Nb, W); doping with cheap eutectoid-forming elements (Fe, Cr) and the use of interstitial elements (O, N).

The most promising in terms of reducing the price of raw materials is the use of scrap titanium alloys of different composition with a preliminary calculation of the required degree of their “doping” and the direct use of titanium sponge [7, 8].

In terms of ensuring higher efficiency of consumer energy use and application of energy-saving technologies, the use of electron-beam melting (EBM) technology with intermediate capacity is considered promising. EBM technology can serve as an effective smart technology for the production and connection of titanium alloys.

Changing the alloying system of low-alloy titanium alloys leads to changes in the kinetics of phase transformations, and as a consequence to changes in their structural-phase composition.

A common method of classification of titanium alloys is the classification of alloys by phase composition. The coefficient of β -stabilization of titanium alloys is often used for this purpose. For α -alloys $K_\beta = 0$, for pseudo- α -alloys $K_\beta < 0.25$, for two-phase ($\alpha + \beta$)-alloys $K_\beta = 0.3 \dots 0.9$, for alloys of transition class $K_\beta = 1.0 \dots 1.4$ [9]. Pseudo- β -alloys have $K_\beta = 1.4 \dots 2.4$, and the polymorphic transformation proceeds according to the scheme $\beta \rightarrow (\beta + \alpha)$. In the stable state, they have $(\beta + \alpha)$ structure with a predominance of β -phase.

The development of low-alloy titanium alloys went mainly in two directions. The first group of low-alloy titanium alloys consisted of alloys with a reduced amount of vanadium (up to 2...3 wt% V), which increases both strength properties and plasticity characteristics due to dispersion strengthening [10], increasing the ability of α -phase to plastic deformation (Ti-3Al-2.5V, etc.) [11]. Alloys of the second group were created as cheaper analogues of the alloy Ti-6Al-4V (Ti 6-4), not inferior to it in mechanical and technological properties, the so-called RMI Low cost (Ti-5.5Al-1Fe, etc.) [12].

In order to reduce the cost of high-strength high-alloy titanium alloys, TIMETAL (USA) has developed an alloy of Ti-1.5Al-6.8Mo-4.5Fe (Low Cost Beta – LCB) which

is characterized by a strength of at least 1000 MPa in the annealed state, and a strength of at least 1400 MPa after standard heat treatment. TIMETAL LCB alloy is used for the manufacture of high-strength products, including springs for some car models [13, 14].

However, the main disadvantages of low-alloy titanium alloys are the insufficient level and instability of properties due to the heterogeneity of the structural-phase composition, chemical micro homogeneity and the release of intermetallic phases along the grain boundaries.

Therefore, the aim of the study was to investigate the influence of the alloying system of low-alloy titanium alloys on the features of phase and structure formation and mechanical properties in ingots obtained by the method of electron beam melting with intermediate capacity.

2 Material and Methods

Ingots of two low-alloy titanium alloys Ti-2.8Al-5.1Mo-4.9Fe (pseudo- β -alloy, alloy #1) and Ti-1.5Fe-0.4O (pseudo- α -alloy, alloy #2) were smelted by the method of electron-beam melting (EBM) with intermediate capacity [15, 16]. They found application in research practice and industry for alloys with low content of gases, impurities and non-metallic inclusions. The use of EBM allowed to improve the quality of ingots of low-alloy titanium alloys and reduce the cost of semi-finished products through the use of up to 100% of scrap and waste of titanium production during smelting. After machining, the ingots were subjected to hot deformation treatment on a reversible rolling mill Skoda 355/500 [15]. The chemical composition of the experimental alloys is given in Table 1.

Table 1. Chemical composition of experimental low-alloy titanium alloys (% wt.).

Alloy	Chemical composition, % wt							
	Al	Fe	Mo	Nb	Ni	Si	O	Ti
#1	2.778	4.87	5.125	–	–	–	0.15	rem
#2	0.006	1.53	0.004	0.003	0.023	0.032	0.40	rem

Low-alloy titanium alloy Ti-1.5Fe-0.4O contains 1.53% Fe and 0.4% O (Table 1). The solubility of iron in α -titanium is quite small and is only 0.2%, so a significant content of oxygen can cause iron oxides, and a significant content of iron – intermetallic TiFe in the metal structure. The coefficient of β -stabilization of the alloy Ti-1.5Fe-0.4O is equal to $K_{\beta} = 0.34$, which corresponds to low-alloy ($\alpha + \beta$)-alloys. However, the significant content of oxygen, which is a stabilizer of the α -phase, allows it to be attributed to pseudo- α -alloys. The structure of the alloy is dominated by α -phase, but pseudo- α -alloys contain a small amount of β -phase at the level of 5...15%.

Low-alloy titanium alloy Ti-2.8Al-5.1Mo-4.9Fe contains 2.7% Al, 4.87% Fe and a significant proportion of molybdenum 5.125% Mo. The amount of oxygen does not exceed 0.15% O. The coefficient of β -stabilization of the alloy Ti-2.8Al-5.1Mo-4.9Fe is $K_{\beta} = 1.55$ (Table 2), which allows us to refer it to the class of pseudo- β -alloys of titanium.

The coefficient of β -stabilization of this alloy is slightly less than that of the traditional low alloy TIMET LCB $K_{\beta} = 1.64$ and is equal to the coefficient of β -stabilization of the alloy VT19.

Table 2. Parameters of chemical composition of low-alloy titanium alloys.

Name	Alloy system	K_{β}	[Mo] eq %	[Al] eq %	Type of structure
Alloy #1	Ti-2.8Al-5.1Mo-4.9Fe	1.55	17.1	4.2	Pseudo- β
Alloy #2	Ti-1.5Fe-0.4O	0.34	3.75	5.0	Pseudo- α
TIMETAL LCB	Ti-1,5Al-6,8Mo-4,5Fe	1.64	18.1	3.0	Pseudo- β
BT 19	Ti-5,5Mo-5,5Cr-3,5Fe-3Al-Zr	1.56	17.2	4.1	Pseudo- β
WT 23	Ti-5Al-4,5V-2Mo-1Cr- 0.6Fe	–	8.1	6.0	$\alpha + \beta$

Chemical digestion of the samples had two stages: first in 4% nitric acid solution (HNO_3) and subsequent electrolytic etching in chromic anhydride reagent.

Studies of the microstructure were performed on a light microscope “NEOPHOT 32” at a magnification of $\times 100 \dots 1000$, which was equipped with an OLYMPUS digital camera with image recording and archiving system. The surface of the fracture was examined on a scanning electron microscope JSM-840 from JEOL Japan and a surface analysis system JAMP 9500F from JEOL Japan. Microhardness was measured on a hardness tester M-400 from “LECO” USA at a load of 10 g.

Research of dislocation structure, microdiffraction patterns and phase composition was carried out by the method of transmission electron microscopy (TEM) on a transmission electron microscope JEM-200CX from “JEOL” Japan ($U = 200 \text{ kV}$, $I = 50 \text{ mA}$).

3 Results and Discussion

Microstructure of the titanium alloy #1 (Ti-2.8Al-5.1Mo-4.9Fe) is presented in Fig. 1. Analysis of the structure of the source metal of the studied alloy #1 showed that it consists of equilibrium polyhedral β -grains both in the near-surface layers and in depth. The size of β -grains is $150 \dots 500 \mu\text{m}$ with a uniform distribution of dispersed particles of α -phase on the body of the grain. The size of α -particles is $1 \dots 2 \mu\text{m}$. Along the boundaries of some grains there is a fringe with α -phase with a thickness of $5 \dots 10 \mu\text{m}$ in which a decrease in the amount of molybdenum and iron is observed (Fig. 2).

Studies of the structure allow us to conclude that in the microstructure of the original titanium alloy #1 dispersed particles of α -phase of different shapes and sizes are distinguished. The dimensions of the phases vary from $15 \mu\text{m}$ to $1 \mu\text{m}$. In addition, dispersed particles of intermetallics of various shapes with a size of much less than $1 \mu\text{m}$ were detected in α -phase plates, which makes it necessary to conduct transmission electron

microscopic studies. It should be noted that in the alloy #1 (Ti-2.8Al-5.1Mo-4.9Fe) there is a significantly higher content of dispersed particles of intermetallics in comparison with the metal of the alloy #2 (Ti-1.5Fe-0.4O). The hardness of the base metal is ~3500...3760 MPa, the amount of β -phase ~71% [17].

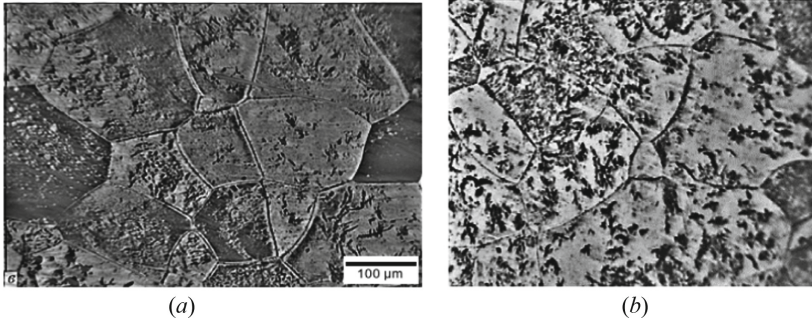


Fig. 1. Microstructure of the source metal of the investigated alloy #1 (Ti-2.8Al-5.1Mo-4.9Fe): (a) – light microscopy ($\times 200$); (b) – electron microscopy ($\times 1000$).

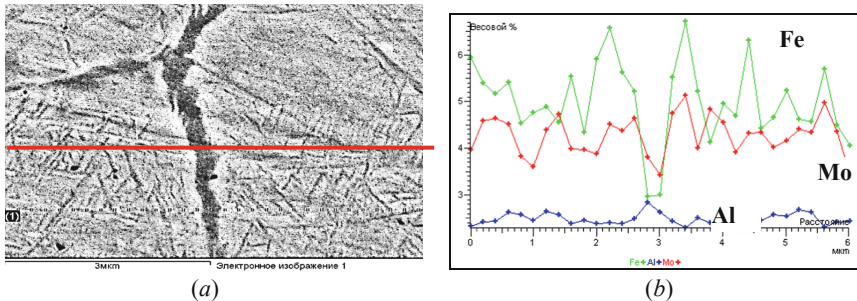


Fig. 2. Edge of α -titanium phase along grain boundaries in titanium alloy #1 (Ti-2.8Al-5.1Mo-4.9Fe): (a) – microstructure ($\times 3000$); (b) – distribution of elements along the line.

The microstructure of the source metal of low-alloy titanium alloy #2 (Ti-1.5Fe-0.4O) is presented in Fig. 3. The structure of the pseudo- α -alloy #2 is dominated by α -phase with a small amount of β -phase (5...15%). The structure consists of large polyhedral grains of the primary α -phase, within which there is a batch structure.

Studies have shown that the structure inside the grain consists of a lamellar α -phase collected in the colony, in the intervals between the plates of which is the β -phase. The α -phase plates have a thickness of 3...7 μm , the β -phase layers between the plates are about 1 μm . In addition to these phase components, and against the background of α plates and between them are likely to be dispersed particles less than 1 μm .

In order to determine the composition of dispersed particles of intermetallics, energy dispersion analysis was performed on the JAMP 9500F system and found that increased iron content was detected in the β -phase of titanium and in dispersed intermetallic particles observed in α -phase. The hardness of the base metal is ~2600...2850 MPa.

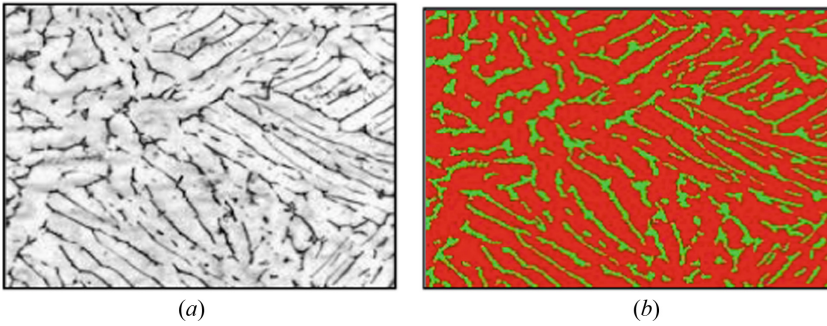


Fig. 3. Microstructure of the source metal of the studied alloy #2 (Ti-1.5Fe-O): (a) – light microscopy ($\times 500$); (b) – the corresponding binary image to determine the proportion of phases.

Translucent method TEM electron microscopy studied the fine structure and phase separations in the studied titanium alloys. In the titanium alloy #1 (Ti-2.8Al-5.1Mo-4.9Fe) dispersed phase emissions of different shape and size were detected (Fig. 4a). Namely: Mo_9Ti_4 particles with a size $(0.02\dots 0.12) \times (0.04\dots 0.17) \mu\text{m}$; dispersed globular particles of Fe_2Ti with a size of $0.01\dots 0.04 \mu\text{m}$; intermetallics Ti_3Al in the form of dark bands in α -phase plates of size $(0.01\dots 0.04) \times (0.03\dots 0.11) \mu\text{m}$. Mo_9Ti_4 layers are also observed between the α -phase plates of size $(0.04\dots 0.13) \times (0.13\dots 0.5) \mu\text{m}$. The volume fraction of phase emissions is 5...11 vol% Ti_3Al , 27...38 vol% Fe_2Ti , 5...24 vol% Mo_9Ti_4 , 10...18 vol% layers of Mo_9Ti_4 . This is the composition of particles in titanium alloys was established in the works [18, 19].

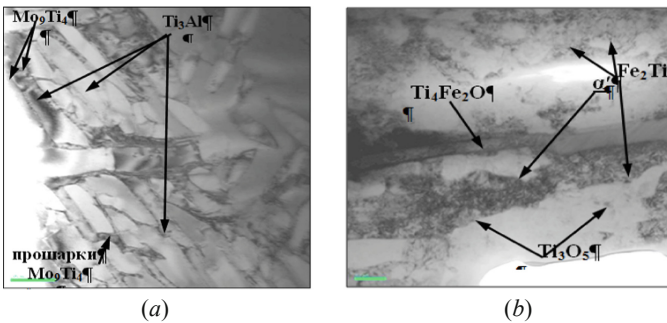


Fig. 4. Structure of the studied titanium alloys and phase distribution in them: (a) – alloy #1 (Ti-2.8Al-5.1Mo-4.9Fe); (b) – alloy #2 (Ti-1.5Fe-0.4O) $\times 52000$.

Studies of the fine structure of titanium alloy #2 (Ti-1.5Fe-O) revealed (Fig. 4b) that the structure has phase separations of different shapes and sizes. In α' -phase plates dispersed globular particles of Fe_2Ti with a size of $0.01\dots 0.04 \mu\text{m}$; bar oxides Ti_3O_5 size $(0.01\dots 0.03) \times (0.05\dots 0.08) \mu\text{m}$ and a small number of complex compounds FeTiO_5 $(0.07\dots 0.09) \times (0.14\dots 0.21) \mu\text{m}$. In the β -phase stripes were detected globular particles of FeTiO_5 of size $(0.07\dots 0.09) \times (0.14\dots 0.21) \mu\text{m}$. The volume fraction of phase

emissions is 4...23 vol% Ti_3O_5 , 8...10 vol% $FeTiO_5$, 6...12 vol% Ti_4Fe_2O and 12...35 vol% Fe_2Ti .

Thus, in the alloy #1 (Ti-2.8Al-5.1Mo-4.9Fe) hardening occurs due to the formation of dispersed particles of titanium intermetallics Mo_9Ti_4 and Fe_2Ti , while in the alloy #2 (Ti-1.5Fe-O) due to the increased level of oxygen (0.4% O) dispersed particles are mainly complex oxides of titanium Ti_3O_5 , Ti_4Fe_2O and $FeTiO_5$ with a small number of particles of intermetallic Fe_2Ti .

Mechanical tests obtained in [20] of the studied low-alloy titanium alloys #1 (Ti-2.8Al-5.1Mo-4.9Fe) and #2 (Ti-1.5Fe-O) are given in Table 3. Analysis of the results of mechanical tests showed that the low-alloy titanium alloy #1 (Ti-2.8Al-5.1Mo-4.9Fe) has higher strength values: temporary tensile strength – 1015 MPa, yield strength – 939 MPa compared to the strength of the alloy #2 – 731 MPa and 713 MPa, respectively. But the alloy #2 has excellent ductility: elongation 13.7% and impact strength 39 J/cm².

Table 3. Mechanical properties of the studied low-alloy titanium alloys.

Alloy name	Tensile strength σ_t , MPa	Yield strength σ_y , MPa	Relative elongation δ , %	Impact strength, KCV, J/cm ²
#1	1015	939	1.9	3.6
#2	731	712	13.7	39

It is proposed that in order to further increase the plasticity of the pseudo- β titanium alloy #1 it is necessary to carry out appropriate heat treatment. In order to determine the optimal modes of heat treatment, physical modeling was performed on the example of titanium alloy VT23 (Table 2) and computer modeling of phase transformations on the studied titanium alloy #1 (Ti-2.8Al-5.1Mo-4.9Fe) and thermokinetic diagrams (CCT) of phase transformations were constructed. The choice of titanium alloy VT23 for physical modeling was due to the fact that this is the only titanium alloy with a publicly available experimental CCT to compare the results of the experiment with. The research was carried out with the involvement of a Gleeble 3800 automated dynamic system for modeling (simulation) of the thermo deformation state of metals. The method of differential dilatometric analysis was used to determine the critical temperatures of phase transformations. When using this technique, the critical temperatures are determined not as is traditionally accepted, tangential to the dilatogram, but by the results of the first derivative of the dilatometer temperature data. This method allows to more accurately identify minor changes in the size of the titanium alloy sample that occur during dilatometric testing.

As a result of dilatometric tests and analysis of the obtained data, the critical temperatures of structural-phase transformation for titanium alloy VT23 were established.

It is shown that for samples cooled at cooling rates of 0.5 and 6 °C/s during the conversion there is a peak increase in the values of the first derivative of dilatometric data, while for samples 20 and 34 °C/s there is a peak decrease. This indicates the different

nature of the formation of structural-phase components during the transformation for the titanium alloy VT23.

Comparison of the experimental CCT diagram with the CCT obtained in [21] showed quite close values of the temperatures of formation of the structural-phase components of the α - and β -phases (Fig. 5).

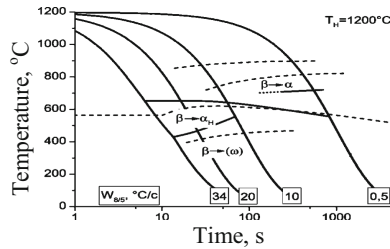


Fig. 5. Comparison of the experimental CCT diagram for titanium alloy VT23 (—) with the diagram obtained in [21] (-----).

Some differences in these results can be explained by different conditions of thermal exposure during dilatometric tests. It should also be noted that the slight dilatometric effect obtained on samples of titanium alloy VT23 was significantly lower than that obtained in titanium alloy VT6. A slight dilatometric effect indicates that only a small part of the metal was involved in the structural-phase transformation.

Compared to the VT6 alloy, the maximum heating temperature was only 1200 °C against 1350 °C when constructing the CCT of the titanium alloy VT23 and there was no exposure at the maximum temperature. That is, to obtain a “contrasting” dilatometric effect in the construction of titanium alloys CCT, it is necessary to ensure sufficient exposure of the metal at high temperatures to convert a larger volume of titanium alloy metal in the β -phase. Thus, the results obtained in the physical modeling of phase transformations in titanium alloys on the Gleeble 3800 device will allow to build with sufficient accuracy the CCT of low-alloy titanium alloys and determine the transformation temperatures and the proportion of phases formed. In addition to physical modeling (simulation) of phase transformations, mathematical (computer) modeling of phase transformations in low-alloy titanium alloys was performed.

One of the main approaches for calculating equilibrium state diagrams is the CALPHAD method (CALCulation of PHase Diagrams) [22], which is based on a comparative analysis of calculated data with experimental information about the phase equilibria in the system and the thermodynamic properties of the phases and its components. The thermodynamic properties of each phase are described by a mathematical model, the parameters of which are calculated. After that, it is possible to recalculate the phase diagram and thermodynamic properties of the components of the phase system.

Gibbs energy is used as the main parameter of the model because most of the data are obtained at certain values of temperature and pressure. In addition, any thermodynamic quantity can be obtained from Gibbs energy. The values of the parameters included in the formula for calculating the Gibbs energy G_φ , enthalpy H_φ and entropy S_φ of any phase within the CALPHAD approach are given in the SGTE database (Scientific Group

Thermodata Europe) [23] for all elements in different phase states. After the parameters of the G_φ , H_φ , S_φ individual phases are determined, the properties of the final alloy are calculated using well-proven models of the mixture, which allow to calculate the contribution of each phase to the total Gibbs energy of the whole system (Fig. 6).

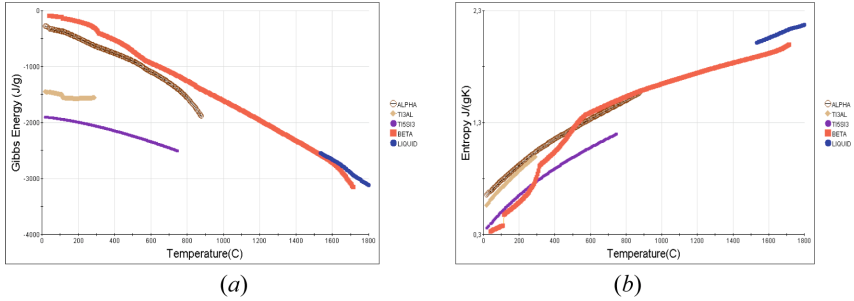


Fig. 6. Influence of temperature on the calculated Gibbs energy (a) and entropy (b) of titanium alloy Ti-2.8Al-5.1Mo-4.9Fe separately by phases.

CALPHAD software package allowed to calculate the thermophysical properties of titanium alloy Ti-2.8Al-5.1Mo-4.9Fe depending on the test temperature.

Currently, a number of mathematical models of phase transformations have been developed, which, based on combining thermodynamics and kinetics of structural transformations of multicomponent systems of different materials, including titanium alloys, allow to build an equilibrium state diagram of such systems and isothermal transformations (TTT) [24].

For example, according to Johnson–Mehl–Avrami–Kolmogorov (JMAK) theory, for a titanium alloy the change in the volume fraction of α -phase x during the decay of β -phase at constant temperature T under the assumption that the emitted particles of α -phase have a spherical shape, can be described by the following Eq. (1) [25]:

$$x = \frac{V}{V_{eq}} = 1 - \exp\left(-\frac{\pi}{3}N_rG_r^3t^4\right), \quad (1)$$

where V is the volume fraction of α -phase isolated during time t , V_{eq} is the equilibrium fraction of α -phase in the metal at temperature T , N_r is the rate of α -phase evolution, $m^{-3}s^{-1}$; G_r is the growth rate of α -phase particles, m/s.

For practical calculations, Eq. (1) is usually used in generalized form (2) [26]:

$$x = 1 - \exp(-kt^n), \quad (2)$$

where k and n are constants and are usually determined empirically and depend on the temperature, particle shape of the α -phase and other parameters of transformation.

The isothermal transformation diagram (TTT) constructed in this way, using the known rules of additivity [27], can be converted into a continuous cooling diagram.

According to the CALPHAD method for low-alloy titanium alloy Ti-2.8Al-5.1Mo-4.9Fe, a calculated diagram of phase transformations was obtained (Fig. 7a), which

allows estimating the temperature of the beginning of $\beta \rightarrow \alpha$ transformation, the required cooling rate to obtain a certain ratio β/α phases (Fig. 7b), the time of transformation, the critical rate of transformation at which the martensite-like α'' -phase begins to form. The diagram shows the temperature of the beginning of the transformation $\beta \rightarrow \alpha$ (850...875 °C), for cooling rates 0.01...10 °C/s and end temperature $\beta \rightarrow \alpha$ conversion (600...660 °C) for the same speeds.

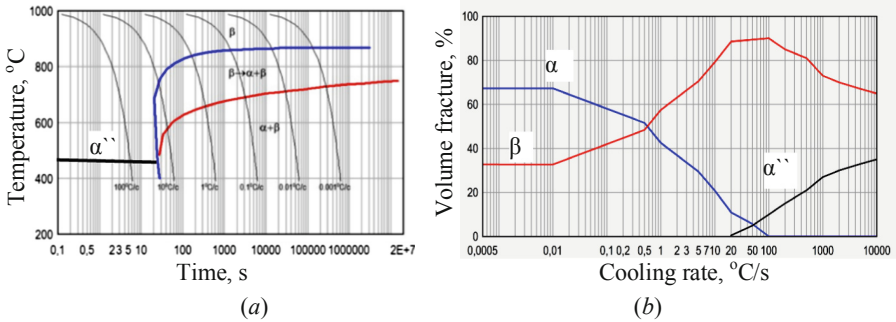


Fig. 7. Calculation diagrams: (a) – CCT diagram; (b) – the effect of cooling rate on the proportion of phases in the low-alloy titanium alloy Ti-2.8Al-5.1Mo-4.9Fe.

Critical cooling rate, above which the martensite-like α'' -phase begins to form for the studied titanium alloy Ti-2.8Al-5.1Mo-4.9Fe is 20 °C/s (Fig. 7b). The analysis of the obtained results showed that with the increase of cooling rate the amount of α -phase continuously decreases, the amount of β -phase first increases, and after the start of α'' -phase formation, decreases (Fig. 7b). The maximum amount of β -phase is formed in the range of cooling rates 50...100 °C/s, but the amount of α'' -phase begins to increase, which limits the plastic properties of the alloy.

Thus, the use of computational methods for modeling structural-phase transformations in low-alloy titanium alloys allows to optimize their structural-phase composition and improve mechanical properties.

4 Conclusion

It has been established that economically alloyed titanium alloys are promising materials for the construction and creation of elements of urban infrastructure, which have high strength, ductility, good resistance to atmospheric corrosion, good welding and processing.

The use of low-cost titanium alloys makes it possible to create a wide range of two-phase titanium alloys, which makes it possible to largely control their structure and, as a result, mechanical and physical-technological properties.

It was found that the low-alloy titanium alloy #1 (Ti-2.8Al-5.1Mo-4.9Fe) is a two-phase pseudo- β alloy in which the share of titanium beta-phase is 89.02% and titanium alpha-phase is 10.98%. Titanium alloy #2 (Ti-1.5Fe-O) is a two-phase pseudo- α alloy of titanium in which the share of alpha phase is 90.42% and beta phase – 9.58%.

It is established that in the alloy #1 (Ti-2.8Al-5.1Mo-4.9Fe) hardening occurs due to the formation of dispersed particles of titanium intermetallics Mo_9Ti_4 and Fe_2Ti , while in the alloy #2 (Ti-1.5Fe-O) – dispersion-strengthening particles of titanium oxides Ti_3O_5 , $\text{Ti}_4\text{Fe}_2\text{O}$ and FeTiO_5 (due to elevated oxygen levels of 0.4% O) with a small amount of intermetallics Fe_2Ti .

Analysis of the results of mechanical tests showed that the low-alloy titanium alloy #1 (Ti-2.8Al-5.1Mo-4.9Fe) has higher strength values: temporary tensile strength – 1015 MPa, yield strength – 939 MPa compared to the strength of the alloy #2 – 731 MPa and 713 MPa, respectively. But the alloy #2 has excellent plasticity: elongation of 13.7% and impact strength KCV_{+20} – 39 J/cm².

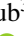
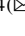
References

1. Pushp, P., Dasharath, S.M., Arati, C.: Classification and applications of titanium and its alloys. *Mater. Today: Proc.* **54**(2), 537–542 (2022). <https://doi.org/10.1016/j.matpr.2022.01.008>
2. Tshephe, T.S., Akinwamide, S.O., Olevsky, E., Olubambi, P.A.: Additive manufacturing of titanium-based alloys – a review of methods, properties, challenges, and prospects. *Heliyon* **8**(3), e09041 (2022). <https://doi.org/10.1016/j.heliyon.2022.e09041>
3. Hiramatsu, N.: Aviation and space (Materials). *J. Japan Weld. Soc.* **83**(2), 117–123 (2014). <https://doi.org/10.2207/jjws.83.117>
4. Froes, F.H., Whittaker, M.: Titanium and its alloys. In: Caballero, F.G. (eds.) *Encyclopedia of Materials: Metals and Alloys*, vol. 1, pp. 287–293. Elsevier, Oxford (2022). <https://doi.org/10.1016/B978-0-12-819726-4.00066-1>
5. Kumar, A., Misra, R.D.K.: 3D-printed titanium alloys for orthopedic applications, In: Froes, F.H., Qian, M. (eds.) *Titanium in Medical and Dental Applications*, pp. 251–275. Woodhead Publishing, Cambridge (2018). <https://doi.org/10.1016/B978-0-12-812456-7.00012-3>
6. Loboda, P., Zvorykin, C., Zvorykin, V., et al.: Production and properties of electron-beam-welded joints on Ti-TiB titanium alloys. *Metals* **10**(4), 522 (2020). <https://doi.org/10.3390/met10040522>
7. Yanko, T., Brener, V., Ovchinnikov, O.: Production of spherical titanium alloy powders used in additive manufacturing from titanium scrap. In: *MATEC Web of Conferences*, vol. 321, p. 07008 (2020). <https://doi.org/10.1051/mateconf/202032107008>
8. Smythe, S.A., Thomas, B.M., Jackson, M.: Recycling of titanium alloy powders and swarf through continuous extrusion (ConformTM) into affordable wire for additive manufacturing. *Metals* **10**(6), 843 (2020). <https://doi.org/10.3390/met10060843>
9. Ahmed, M., Pereloma, E.V.: Observation of simultaneous operation of deformation twins in both α and β phases in metastable β titanium alloy. *J. Alloy. Compd.* **910**, 164794 (2022). <https://doi.org/10.1016/j.jallcom.2022.164794>
10. Hryhorenko, G., Akhonin, S., Berdnikova, O., et al.: Fine structure of heat-resistant titanium alloys welded joints. In: 2019 IEEE 9th International Conference Nanomaterials: Applications & Properties (NAP), pp. 01MIT02-1. IEEE, Odessa (2019). <https://doi.org/10.1109/NAP47236.2019.219071>
11. Ding, C., Liu, C., Zhang, L., et al.: Design of low-cost and high-strength titanium alloys using pseudo-spinodal mechanism through diffusion couple technology and CALPHAD. *Materials* **14**(11), 2910 (2021). <https://doi.org/10.3390/ma14112910>
12. Singh, P., Pungotra, H., Kalsi, N.S.: On the characteristics of titanium alloys for the aircraft applications. *Mater. Today: Proc.* **4**(8), 8971–8982 (2017). <https://doi.org/10.1016/j.matpr.2017.07.249>

13. Hong, S.H., Hwang, Y.J., Park, S.W., et al.: Low-cost beta titanium cast alloys with good tensile properties developed with addition of commercial material. *J. Alloy. Compd.* **793**, 271–276 (2019). <https://doi.org/10.1016/j.jallcom.2019.04.200>
14. Chirico, C., Romero, A.V., Gordo, E., Tsipas, S.A.: Improvement of wear resistance of low-cost powder metallurgy β -titanium alloys for biomedical applications. *Surf. Coat. Technol.* **434**, 128207 (2022). <https://doi.org/10.1016/j.surfcoat.2022.128207>
15. Kostin, V., Taranova, T., Zvorykin, V.: Fracture of electron beam welding joints of titan alloys. *Solid State Phenom.* **316**, 333–339 (2021). <https://doi.org/10.4028/www.scientific.net/SSP.316.333>
16. Akhonin, S., Markovsky, P., Berezos, V., et al.: Producing of high-strength titanium alloy Ti-1.5Al-6.8Mo-4.5Fe by EBM method. *Electrometall. Today* (1), 9–16 (2018). <https://doi.org/10.15407/sem2018.01.02>
17. Akhonin, S.V., Belous, V.Y., Selin, R.V., Kostin, V.A.: Influence of TIG welding thermal cycle on temperature distribution and phase transformation in low-cost titanium alloy. *IOP Conf. Ser.: Earth Environ. Sci.* **688**, 012012 (2021). <https://doi.org/10.1088/1755-1315/688/1/012012>
18. Chang, H.C., Lee, C.S., Chen, S.H., et al.: Study of Ti/W/Cu, Ti/Co/Cu, and Ti/Mo/Cu multilayer structures as Schottky metals for GaAs diodes. *J. Electron. Mater.* **33**(7), L15–L17 (2004). <https://doi.org/10.1007/s11664-004-0251-2>
19. Oufella, L.S., Benchettara, A.: Influence of fluoride on the electrochemical behavior of a new synthesized Ti-10Ta-2Mo alloy for biomedical applications. *J. Fundam. Appl. Sci.* **8**(3), 731–752 (2016). <https://doi.org/10.4314/jfas.v8i3.5>
20. Ivasishin, O.M., Akhonin, S.V., Savvakina, D.G., et al.: Effect of microstructure, deformation mode and rate on mechanical behavior of electron-beam melted Ti-6Al-4V and Ti-1.5Al-6.8Mo-4.5Fe alloys. *Prog. Phys. Metals* **19**(3), 309–336 (2018). <https://doi.org/10.15407/ufm.19.03.309>
21. McQuillan, M.K.: Phase transformations in titanium and its alloys. *Metall. Rev.* **8**(1), 41–104 (1963). <https://doi.org/10.1179/mtlr.1963.8.1.41>
22. Agren, J.: CALPHAD – an approach to predict microstructural stability. In: Caballero, F.G. (eds.) *Encyclopedia of Materials: Metals and Alloys*, vol. 4, pp. 497–509. Elsevier, Oxford (2022). <https://doi.org/10.1016/B978-0-12-819726-4.00042-9>
23. van de Walle, A.: Reconciling SGTE and ab initio enthalpies of the elements. *Calphad* **60**, 1–6 (2018). <https://doi.org/10.1016/j.calphad.2017.10.008>
24. Fukuda, T., Kawamura, T., Kakeshita, T.: Time-temperature-transformation diagram for the martensitic transformation in a titanium-nickel shape memory alloy. *J. Alloy. Compd.* **683**, 481–484 (2016). <https://doi.org/10.1016/j.jallcom.2016.05.120>
25. Liu, G., Zhang, D., Yao, C.: A modified constitutive model coupled with microstructure evolution incremental model for machining of titanium alloy Ti-6Al-4V. *J. Mater. Process. Technol.* **297**, 117262 (2021). <https://doi.org/10.1016/j.jmatprotec.2021.117262>
26. Xu, J., Zeng, W., Zhang, X., Zhou, D.: Analysis of globularization modeling and mechanisms of alpha/beta titanium alloy. *J. Alloy. Compd.* **788**, 110–117 (2019). <https://doi.org/10.1016/j.jallcom.2019.02.205>
27. Kumara, C., Segerstark, A., Hanning, F., et al.: Microstructure modelling of laser metal powder directed energy deposition of alloy 718. *Addit. Manuf.* **25**, 357–364 (2019). <https://doi.org/10.1016/j.addma.2018.11.024>



Detonation Nanodiamonds as Part of Smart Composite Paintwork Materials

Galina Gurina¹ , Pavlo Kozub² , Svetlana Kozub³ , Natalia Saienko⁴  ,
and Anna Skripinets⁴ 

¹ O. M. Beketov National University of Urban Economy in Kharkiv, 17 Marshala Bazhanova Street, Kharkiv 61002, Ukraine

² Kharkiv National University of Radio Electronics, 14 Nauky Avenue, Kharkiv 61166, Ukraine

³ Kharkiv National Medical University, 4 Nauky Avenue, Kharkiv 61022, Ukraine

⁴ Kharkiv National University of Civil Engineering and Architecture, 40 Sumska Street, Kharkiv 61002, Ukraine

saienko.nataliia@kstuca.kharkov.ua

Abstract. The development of materials using fillers of polymer matrices with micron and submicron levels of dispersion has largely exhausted itself in achieving a new level of performance. New breakthrough solutions can be reached using the principles of nanotechnology, using the nano dispersed state of reinforcing components, the synthesis of which is very promising both theoretically and practically from the point of view of creating smart composite paints and varnishes. Such nano dispersed particles are nanodiamonds – promising representatives of carbon nanostructures, which have a crystal lattice characteristic of ordinary diamond: planaxial class of cubic syngony, two face-centered Brave lattices, shifted relative to each other by 1/4 of the main diagonal from each diagonal, but 10 nm. The aim of the work was to study the effect of nanodiamond particle additives on the physical-mechanical and optical properties of nanocomposite paints and prediction of their further use in various industries. It is established that the introduction of nanodiamonds leads to the increased wear resistance of paints and varnishes and leads to a decrease in ultraviolet radiation under the coating. According to research, detonation nanodiamonds are recommended for the production of water-based nanocomposite acrylic polymers in various industries to create coatings to absorb ultraviolet radiation and improve their physical and mechanical properties.

Keywords: Nanodiamonds · Paint coatings · Wear resistance · Ultraviolet radiation

1 Introduction

A promising way to solve the problems of chemistry and chemical technologies development in Ukraine is the creation of innovative materials based on polymer nanocomposites with low content of environmentally harmful components and high physical and mechanical characteristics and improved functional properties [1–3]. The development

of materials using fillers of polymer matrices of micron and submicron level of dispersion to achieve a new level of performance has largely exhausted itself [4, 5]. New breakthrough solutions can be reached using the principles of nanotechnology, namely the transition to the nano disperse state of reinforcing components, the synthesis of which is very promising both theoretically and practically from the point of view of creating smart composite paints and varnishes [6–8]. Such nano disperse particles are nanodiamonds – promising representatives of carbon nanostructures [9, 10].

Nanodiamonds or ultrafine diamonds are a group of carbon nanostructures that have a crystal lattice characteristic of ordinary diamond: a planaxial class of cubic syngony, two face-centered Bravais lattices, shifted relative to each other by 1/4 of the main diagonal, but the size of each to 10 nm. In dry form, nanodiamonds are light gray polydisperse powder [11–13].

It should be noted that the structure of nanodiamonds depends on the conditions of their synthesis, purification, and further processing. Thus, in the case of wet synthesis, the shape is close to spherical, while in dry synthesis, diamond nanocrystals close to the ideal structure are formed. Nanodiamonds, which are obtained during the explosion in a closed volume of condensed explosives with a negative oxygen balance, are a special type of diamond material. These are typical nanomaterials with an average grain size of 4 nm, which have a predominantly spherical shape, so they were used in this work.

Nanodiamonds have a three-layer structure which includes: a diamond core with a size of 4 to 6 nm, which contains 70 to 90% of carbon atoms in the sp³-hybridization state; a transition shell (intermediate layer) around the nucleus with a thickness of 0.4 to 1 nm, consisting of X-ray amorphous carbon structures and containing from 10 to 30% of sp²-hybridized carbon atoms; surface layer, in which, in addition to carbon atoms, there are other heteroatoms (N, O, H), which form a number of functional groups. Nitrogen atoms are fairly evenly distributed across all layers of nanodiamond.

The structure of the intermediate layer of the nanodiamond particle is inhomogeneous. The shell, which is directly on the border with the diamond core, consists of continuous layers of carbon in the form of onions, formed by groups of six atoms, the so-called hexagons. The transition shell also contains graphite-like monolayers concentrated in its peripheral parts and amorphous carbon.

A characteristic feature of nanostructures is that the carbon atoms in them have a coordination number inherent in ordinary diamond, equal to 4. Each carbon atom is surrounded by four other similar atoms. The extreme atoms on the surface have nothing to be surrounded by, and this leads to the creation of various uncompensated valences. Therefore, the properties of the surface layer of diamond differ from the properties of its inner layers. In the surface layer, carbon atoms can bind not only to each other but also to other heteroatoms: Nitrogen, Hydrogen and Oxygen, forming different functional groups. Functional groups in the surface layer were identified as hydroxyl, which is part of sorbed water and tertiary alcohols; amino groups in the composition of amides; carboxyl groups; carbonyl groups consisting of ketones, acid anhydrides, esters, and lactones. Bonds between Carbon and Hydrogen in the form of CH-, CH₂-, and CH₃-groups, as well as C-O-C bonds, have been identified.

A small particle has a larger surface area to volume ratio than a large particle. Accordingly, the role of surface atoms and groups in nanodiamonds increases significantly compared to ordinary diamonds. Thus, nanodiamond particles have the properties of diamond – strength, and stability, but acquire a number of unique properties: they are very small, they have a very large specific surface area and high surface energy, and due to the presence of functional groups, they can be modified, such as to “sew” various molecules, for examples like medicine and drugs. Today, among a large number of areas of the practical application of nanodiamonds, three main areas prevail: 70% of nanodiamonds are used for finishing polishing; 25% of nanodiamonds are used in electroplating; 5% – in oil compositions [14].

In the near future, extremely wide areas of application of nanodiamonds may be the production of polymer-diamond compositions, charge-transfer catalysts, and modified bio-resistant concrete [15].

Numerous studies have also shown the effectiveness of nanodiamonds in polymer composites and films based on polyfluorinated elastomers, perfluorinated hydrocarbons, polysiloxanes, polyisoprenes, butadiene-styrene rubbers, polyurethanes, and other substances. The introduction of nanodiamonds in general increases the elastic strength characteristics and provides in some cases the unique tribotechnical properties of polymers [15, 16].

Particles of detonation nanodiamonds, obtained in non-stationary, extremely harsh conditions of an explosion, have not the usual smooth surface, but on the contrary – “bacterium” of functional groups. Hence the whole set of unpredictable properties and non-standard areas of their use. Nanodiamonds are being used in practice as selective adsorbents and catalyst carriers, and in the future nanodiamonds are planned to be used in the medical field, for example, for the targeted movement of drugs in the body and tissue regeneration.

The lack of information in the scientific and technical literature on systematic studies of the influence of nanodiamonds as modifiers in paint coatings determines the relevance of the work.

The aim of this paper was to study the effect of nanodiamond particle additives on the physical-mechanical and optical properties of nanocomposite paints and coatings for further prediction of their use in various industries.

2 Materials and Methods

Primal CM-219 EF water-dispersion acrylic dispersion (Rohm and Haas) was used to determine the effect of detonation nanocomposites on the physico-mechanical and optical properties of paint coatings. The compositions were prepared using a bead mill by dispersing water pastes with nanodiamonds (VPNA) and without nanodiamonds (VPD). Orotan 731 AER dispersant, cellulose and associative polyurethane thickeners, and Foamaster NXZ defoamer were used. As a coalescent – Texanol NX-795. Acrylic dispersion was added to the obtained water pastes at a speed of 280 rpm [17, 18].

To study the effect of nanodiamonds on physical and mechanical properties of coating based on aqueous acrylic dispersions acrylic aqueous dispersions with nanodiamonds and without nanodiamonds were coated with steel plates to measure the resistance of

coatings to impact, tin plates to determine the elasticity of coatings and glass plates and to determine the conditional hardness of coatings. The concentration of nanodiamonds varied from 0.2 to 0.5% as the most interesting in terms of their application technology and coating price.

After preparing samples physico-mechanical properties of paint coating were determined by standard methods.

The relative hardness is determined by the pendulum instrument (according to ISO 1522) by comparing the damping time of the pendulum oscillations on the sample with the “glass number”.

Impact resistance of the coatings was determined (according to ISO 6272) using a device measuring the maximum height from which a load of 1 kg does not cause visible mechanical damage to the surface of the test plate with paint coating under a free fall of load.

Elasticity and bending strength of coatings (according to ISO 1519) were measured around a set of cylindrical rods with diameters from 1 mm to 32 mm. The method consists in determining the minimum diameter of a metal cylindrical rod the bending of which of the painted metal plate does not cause mechanical destruction or peeling of the paint film at a certain thickness.

The adhesion of paint coating was determined by the method of lattice cuts (according to ISO 2409).

The thickness of the coatings (according to ISO 2808) was 30 μm for all samples and was determined using a thickness gauge NOVOTEST TP-1 (L) for metals and dielectric products.

The wear resistance of the coatings was determined according to ISO 5470 by abrasion of the coating due to the mechanical action of a jet of quartz sand.

Conditional viscosity was measured using a viscometer type VZ-246 (ISO 2431).

The absorption efficiency of UV radiation was studied by changing the intensity of radiation of fluorescent pigments sensitive to different spectral ranges of UV radiation. The concentration of nanodiamonds in the suspension was 7% to obtain a more accurate value of the degree of absorption.

For this color and color coordinates of secondary radiation were determined using a portable spectrophotometer NS810. The task of experimental quantitative determination of pigment color is the calculation of color coordinates, chromaticity coordinates, color tone, color purity, and brightness in the standard colorimetric system XYZ. The obtained values allow us to graphically represent the color in Cartesian coordinates x and y on a color graph.

In addition to a certain color by color coordinates X, Y, Z , color coordinates x, y and z in combination with the color coordinate Y , it is possible to determine the color by color tone λ , pure color P , and brightness \underline{Y} . The color tone is characterized by the dominant wavelength λ , ie the co-wavelength corresponding to the maximum on the reflection spectrum of the sample. It can be determined on a color chart by given or calculated chromaticity coordinates x , in this sample. The purity of color P is determined by the ratio of photometric brightness of monochromatic radiation and total brightness of radiation. On the color graph, the value of color purity P is determined by the ratio of the distance from the white point to the point with the coordinates of the chromaticity

of the sample (x, y) and the length of the segment drawn to the line of spectral colors. Brightness (L) characterizes the amount of light reflected by the sample.

As a result, the research methodology made it possible to study the most important technological parameters of both the suspension and the finished coating in the most important range of filler concentrations.

3 Results and Discussion

The results of the influence of detonation of nanocomposites on the physical and mechanical properties of water-dispersion paint coatings for the optimal composition (0.3% nanodiamonds) which are given in Table 1 show a significant increase in the conditional hardness of the coating (almost 60%) and wear resistance (almost 140%).

Wherein the viscosity of the aqueous acrylic dispersion was slightly lower than the viscosity of the aqueous acrylic dispersion with nanodiamonds and was 44 s and 48 s, respectively (at 20 ± 0.5 °C).

Table 1. Physico-mechanical properties of pure acrylic dispersion (VP) coatings and coatings based on compositions of aqueous acrylic dispersion with nanodiamonds (VPND).

Property	VP	VPND
Conditional hardness of coatings, un	0.38	0.61
Impact resistance of coatings, cm	50	50
Resistance of coatings to bending, mm	2	2
Adhesion of coatings, points	0	0
Wear resistance kg/kg	3.80×10^{-7}	1.58×10^{-7}

A more detailed study of the temperature dependence of the conditional hardness of samples based on an aqueous acrylic dispersion and an aqueous acrylic dispersion with the addition of nanodiamonds in the range from 0.2% to 0.5% (Fig. 1) revealed an extreme nature of the dependence on the concentration of nanodiamonds.

For all samples there is a single type of dependence of hardness on temperature, which is characterized by a minimum at temperatures of 50–90 °C. More clearly the differences in the change in hardness from temperature are found in the logarithmic coordinates for hardness, which are shown in Fig. 2.

The results showed that the introduction of nanodiamonds in the amount of 0.5% leads to a decrease in conditional hardness at medium temperatures (30–70 °C), the introduction of nanodiamonds of 0.3% increases the hardness for the entire temperature range and in the temperature range of 60–80 °C any amount of nanodiamonds increases the hardness of the coating.

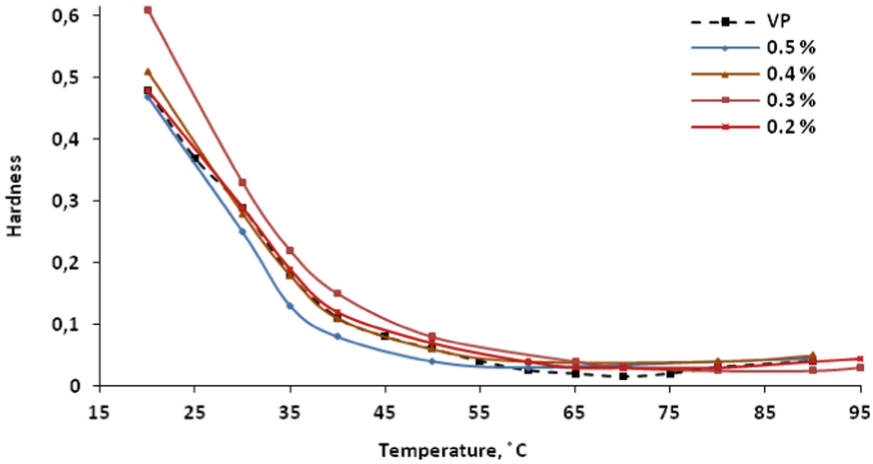


Fig. 1. Temperature dependences of the conditional hardness of coatings depending on the content of nanoparticles.

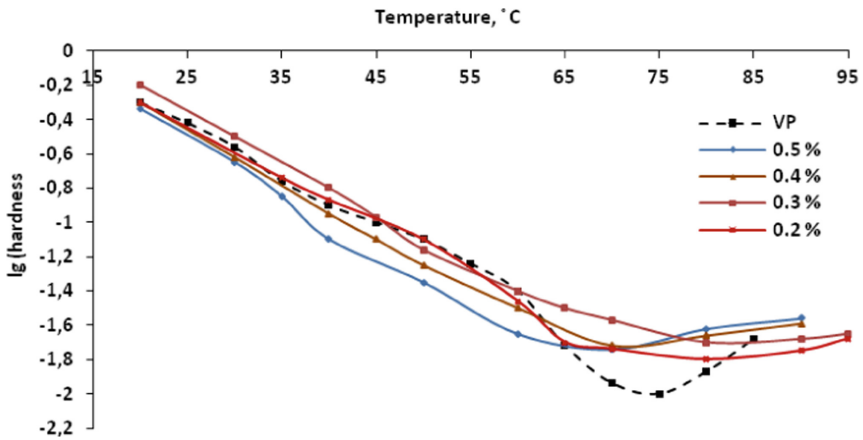


Fig. 2. Logarithmic dependence of the hardness of coatings on the content of nanodiamonds.

This dependence of hardness on from the concentration of nanodiamonds and temperature becomes even more obvious when displayed in relative units (relative to the sample without nanodiamonds) (Fig. 3).

The additive has the greatest effect in the amount of 0.3%, and when it is made, it is possible to increase the hardness not only at temperatures of 70–80 °C, but also when the temperature drops below 20 °C. The dependence of the maximum deviations for the three temperature ranges on the amount of additive shows that for concentrations less than 0.4% increase the hardness reaches 230% relative to the pure material, and even at average temperatures the decrease in strength does not exceed 10%. Nano disperse diamond has the greatest effect on hardness at a temperature of 70–80 °C.

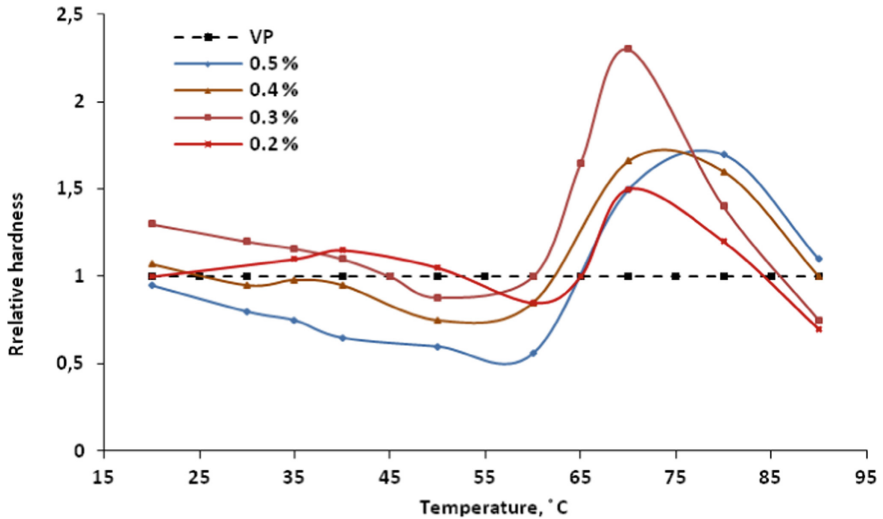


Fig. 3. Temperature dependence of hardness in relative units (in relation to the sample without nanodiamonds).

The experimental results obtained made it possible to create a fairly simple mathematical model that makes it possible to predict the hardness of coating using these two parameters:

$$H = \left(0.962 \frac{T + 273.15}{273.15}\right)^{-20.75} + \left((0.0573 - 0.117|C - 0.3|) \frac{T + 273.15}{273.15}\right)^{14.9}, \quad (1)$$

where H is the hardness, units; T is the temperature, °C; C is the concentration of nanodiamond in suspension, % mass.

As mentioned above, the analysis of the literature indicates the feasibility of studying the absorption of electromagnetic radiation in the ultraviolet region of the spectrum by nanodiamonds. To do this, fluorescent pigments were placed under the film of an acrylic dispersion with nanodiamonds with a D65 light source located above it.

Three samples of luminescent pigments of yellow, green, and red color were taken, for which color coordinates, chromaticity for XYZ, CIELAB colorimetric system and dominant wavelength, saturation and color brightness were determined. The measurement data for pigment samples without a film and pigments with a film with nanodiamonds are given in Table 2. The brightness of fluorescent pigments of red, yellow, and green colors exposed to UV radiation compared to the brightness of pigments under an acrylic-coated filter with nanodiamond nanoparticles for a D65 light source in the CIELAB colorimetric system increased from 22.85 to 27.91, from 57.14 to 60, 48 and from 44.04. The calculated differences in color ΔE in the CIELAB system for pigment samples and samples with nanodiamond filters indicate a significant effect of nanodiamonds included in the coating composition on pigment colors due to a decrease in the effect of ultraviolet radiation on the fluorescence of pigment samples.

Table 2. Color parameters of the studied pigments under UV radiation.

Type of sample	XYZ	CIELAB	λ , P , Y
Red with ND	$X = 4.1058$ $Y = 4.9670$ $Z = 5.9987$	$L = 22.85$ $A = -2.4$ $B = 5.14$	$\lambda = 525$ $P = 5\%$ $Y = 4.6771$
Red	$X = 5.1421$ $Y = 5.7497$ $Z = 6.7823$	$L = 27.91$ $A = -0.17$ $B = -2.14$ $\Delta E = 9.15$	$\lambda = 525$ $P = 10\%$ $Y = 5.7497$
Yellow with ND	$X = 26.2291$ $Y = 25.0617$ $Z = 38.1268$	$L = 57.14$ $A = 7.77$ $B = -11.87$	$\lambda = 565$ $P = 22.22\%$ $Y = 25.0617$
Yellow	$X = 29.1335$ $Y = 28.5971$ $Z = 40.1755$	$L = 60.42$ $A = 5.1$ $B = -8.63$ $\Delta E = 5.5$	$\lambda = 565$ $P = 40\%$ $Y = 28.5971$
Green with ND	$X = 11.6266$ $Y = 13.8998$ $Z = 23.3076$	$L = 44.04$ $A = -12.72$ $B = -13.49$	$\lambda = 568$ $P = 5\%$ $Y = 13.8998$
Green	$X = 16.5657$ $Y = 18.3176$ $Z = 26.0161$	$L = 49.88$ $A = -6.83$ $B = -7.88$ $\Delta E = 10.01$	$\lambda = 568$ $P = 30\%$ $Y = 18.3176$

4 Conclusion

As a result of studying the effect of detonation nanodiamonds on the physical-mechanical and optical properties of water-dispersion paints, it was found that the introduction of nanodiamonds leads to significant increase in the conditional hardness of the coating (almost 60%) and wear resistance (almost 140%) and almost does not change the viscosity of the suspension.

It was determined that the optimal amount of nanodiamonds is 0.3%, providing a 2.4-fold increase in the hardness of the coating, and the most effective effect of nanodiamond additives on the hardness of coatings for temperatures of 60–80 °C.

Based on the results of the experiments, a simple mathematical model was proposed for the dependence of the coating hardness on the concentration of nanodiamonds in suspension and temperature.

As a result of the research, the possibility of creating an effective UV radiation filter based on paint coatings with the inclusion of nanodiamonds has been proved.

Therefore, the results of the study make it possible to recommend the use of detonation nanodiamonds in various industries both to improve the performance properties of paint coatings and to create new optical materials in the field of UV radiation.

References

1. Riaz, U., Nwaoha, C., Ashraf, S.M., Laboratory, M.R.: Recent advances in corrosion protective composite coatings based on conducting polymers and natural resource derived polymers. *Prog. Org. Coat.* **77**(4), 743–756 (2014). <https://doi.org/10.1016/j.porgcoat.2014.01.004>
2. Licea-Jiménez, L., Méndez-Romero, U.A., Méndez-Reséndiz, A., et al.: Polymer coatings based on nanocomposites. In: Rangappa, S.M., et al. (eds.): *Polymer Coatings*, pp. 31–51. CRC Press, Boca Raton (2020). <https://doi.org/10.1201/9780429199226-3>
3. Pourhashem, S., Saba, F., Duan, J., et al.: Polymer/Inorganic nanocomposite coatings with superior corrosion protection performance: a review. *J. Ind. Eng. Chem.* **88**, 29–57 (2020). <https://doi.org/10.1016/j.jiec.2020.04.029>
4. Samui, A.B., Pawar, S.S.: Smart paints. In: Samui, A.B. (eds.): *Smart Polymers*, pp. 41–65. CRC Press, Boca Raton (2022). <https://doi.org/10.1201/9781003037880-3>
5. Ahn, J.H., Choi, D.S., Lee, C.Y.: Resistances of carbon black and polymers in smart paints for temperature sensors. *J. Nanosci. Nanotechnol.* **21**(7), 3716–3720 (2021). <https://doi.org/10.1166/jnn.2021.19209>
6. Nihalani, S., Joshi, U., Meeruty, A.: Smart materials for sustainable and smart infrastructure. *Mater. Sci. Forum* **969**, 278–283 (2019). <https://doi.org/10.4028/www.scientific.net/MSF.969.278>
7. Kingchok, S., Nontasorn, P., Laohhasurayotin, K., et al.: Reversible thermochromic polydiacetylene/zinc-aluminium layered double hydroxides nanocomposites for smart paints and colorimetric sensors: the crucial role of zinc ions. *Colloids Surf., A* **610**, 125733 (2021). <https://doi.org/10.1016/j.colsurfa.2020.125733>
8. Sazou, D., Deshpande, P.P.: Conducting polyaniline nanocomposite-based paints for corrosion protection of steel. *Chem. Pap.* **71**(2), 459–487 (2016). <https://doi.org/10.1007/s11696-016-0044-0>
9. Popov, V.: Several aspects of application of nanodiamonds as reinforcements for metal matrix composites. *Appl. Sci.* **11**(10), 4695 (2021). <https://doi.org/10.3390/app11104695>
10. Kasahara, Y., et al.: Nanodispersion in transparent polymer matrix with high melting temperature contributing to the hybridization of heat-resistant organo-modified nanodiamond. *Polym. Bull.* **75**(9), 4145–4163 (2017). <https://doi.org/10.1007/s00289-017-2259-9>
11. Wang, H., Cui, Y.: Nanodiamonds for energy. *carbon. Energy* **1**(1), 13–18 (2019). <https://doi.org/10.1002/cey2.9>
12. Kirschbaum, T., Petit, T., Dzubiella, J., Bande, A.: Effects of oxidative adsorbates and cluster formation on the electronic structure of nanodiamonds. *J. Comput. Chem.* **43**(13), 923–929 (2022). <https://doi.org/10.1002/jcc.26849>
13. Stelmakh, S., Skrobas, K., Gierlotka, S., Palosz, B.: Atomic structure of nanodiamond and its evolution upon annealing up to 1200°C: real space neutron diffraction analysis supported by MD simulations. *Diam. Relat. Mater.* **93**, 139–149 (2019). <https://doi.org/10.1016/j.diamond.2019.02.004>
14. Alkhtani, M.H., Alghannam, F., Jiang, L., et al.: Fluorescent nanodiamonds: past, present, and future. *Nanophotonics* **7**(8), 1423–1453 (2018). <https://doi.org/10.1515/nanoph-2018-0025>
15. Huang, H., Liu, M., Jiang, R., et al.: Facile modification of nanodiamonds with hyperbranched polymers based on supramolecular chemistry and their potential for drug delivery. *J. Colloid Interface Sci.* **513**, 198–204 (2018). <https://doi.org/10.1016/j.jcis.2017.11.009>
16. Hajiali, F., Shojaei, A.: Network structure and mechanical properties of polydimethylsiloxane filled with nanodiamond—effect of degree of silanization of nanodiamond. *Compos. Sci. Technol.* **142**, 227–234 (2017). <https://doi.org/10.1016/j.compscitech.2017.02.005>

17. Saienko, N.V., Demidov, D.V., Bikov, R.A., Younis, B.N.: Effect of mineral fillers on the wetting of water-based polymer dispersions. IOP Conference Series: Materials Science Eng. **708**, 012103 (2019). <https://doi.org/10.1088/1757-899X/708/1/012103>
18. Saienko, N.V., Bikov, R., Skripinets, A., Demidov, D.V.: Research of the influence of silicate fillers on water absorption and microstructure of styrene-acrylic dispersion coatings. Mater. Sci. Forum **1038**, 61–67 (2021). <https://doi.org/10.4028/www.scientific.net/MSF.1038.61>



Improving the Quality of Magnesium-Soluble Biological Alloy for Implants

Vadim Shalomeev , Viktor Greshta , and Olga Liutova  

Zaporizhzhia Polytechnic National University, 64 Zhukovskoho Street, Zaporizhzhia 69063, Ukraine

liutova@zp.edu.ua

Abstract. Currently, biosoluble materials are widely used for the manufacture of implants, among which the most promising are magnesium alloys. To investigate and test various carbonaceous materials for refining and modifying magnesium melt. The technology of modification of cast magnesium alloys of Mg-Zr-Nd system by dispersed graphite powder is proposed. It is shown that the optimal carbon additive in the amount of 0.05...0.1% improves the mechanical properties due to grain grinding and additional strengthening of structural components. A complex filter containing equal amounts of magnesite, graphite and calcite is proposed, which provides an increased level of refining of the melt to obtain high quality casting. It is shown that the use of a complex carbon-containing filter provides not only efficient refining of the melt, but also its additional modification. In the structure of the alloy there is an increased amount of intermetallic γ -phase, which increases the microhardness of the structural components of the alloy and improves its physical and mechanical characteristics. The structure and properties of the cast magnesium alloy of the Mg-Zr-Nd system during modification with dispersed graphite powder and its filtration through carbon-containing materials have been studied. The developed complex technology for processing the liquid melt of magnesium alloys of the Mg-Zr-Nd system allows to increase the yield of suitable casting and improve its quality.

Keywords: Magnesium alloy · Carbonaceous materials · Filtration

1 Introduction

Currently, biosoluble materials are widely used for the manufacture of implants, among which the most promising are magnesium alloys. Their main advantage is the positive effect of magnesium on the human body [1]. Magnesium is a natural element of the body – it is contained in bone and muscle tissue, is involved in various metabolic processes [2]. In addition, magnesium and its biocorrosion products have excellent biocompatibility.

The technology of obtaining magnesium alloys includes smelting of the alloy in induction, gas furnaces, treatment of liquid melt with flux, casting molds and heat treatment. Improving the quality [3] of implants made of magnesium alloys and improving their mechanical properties [4] can be achieved by improving the methods of modification [5] and refining [6] of the melt.

The main requirements for modifiers of magnesium alloys for medical purposes are the ability to form insoluble centers of crystallization, stable modification effect, low cost, non-deficiency and non-toxicity. The most suitable for these conditions is carbon [7], the main advantage of which is its ability to contaminate the metal with oxide inclusions and reaction products in contact with the melt [8]. Given that carbon is insoluble in magnesium [9] and its particles or carbides can be additional centers of crystallization, the use of carbonaceous materials, in particular graphite, to modify magnesium alloys is a promising direction to improve their quality.

Various fluxes are widely used to protect and refine the liquid magnesium alloy, however, in this case there is a risk of contamination of the metal with flux and its refining products [10], which leads to flux corrosion and reduces the quality of implants. To improve their quality, the melt is filtered before it is poured into the mold [11] using materials capable of adsorbing flux, non-metallic inclusions [12] and providing high quality metal and improved mechanical properties [13].

The following requirements are set for filtration materials [14]: the possibility of easy crushing and sieving, sufficient mechanical strength, inertness of the filter to the chemical composition of the alloy, stable refining effect, low cost and no shortage.

Such requirements are met by calcite, magnesite and graphite, which are widely used in metallurgy. When these materials interact with the magnesium alloy, simultaneously with the refining of the melt, the process of its modification with carbon, which is part of the filter materials, is possible. It is obvious that different carbon-containing materials will have different refining and modifying ability due to their chemical composition and physicochemical properties [15]. Therefore, the correct choice of filter material, which provides increased refining capacity, maximum grinding of metal grains and, as a consequence, increased complex properties of the metal, is an urgent task.

2 Materials and Methods

Magnesium alloy system Mg-Zr-Nd (% wt.: 0.1...0.7 Zn; 0.4...1.0 Zr; 2.2...2.8 Nd; Mg residue) melted in an induction furnace crucible type IPM-500. The refining of the alloy was carried out in a dispensing furnace with batch melt selection and increasing additives of dispersed graphite powder (% wt.: 99.1 C; 0.9 ash) fraction of 0,071 mm were introduced, mixed thoroughly and poured into standard samples for mechanical tests. The samples were heat treated in Bellevue and PAP-4M furnaces according to T6 mode: heating to 540 ± 5 °C, holding for 15 h, cooling in air and aging at 200 ± 5 °C, holding for 8 h, cooling to air.

The efficiency of purification of the melt by filtration materials was compared by the method of determining the characteristics of the surface interaction in different systems. To do this, used the method of “lying drop”. Samples of Mg-Zr-Nd system alloy ($\varnothing 7.5 \times 7.5$ mm) were placed in a graphite heater, which was placed in a quartz glass furnace in the middle of the inductor on substrates of magnesite, calcite and graphite. Surface tension ($\sigma_{s.l.}$), work of cohesion (A_c), adhesion (A_a) and edge wetting angle (K_r), as well as the efficiency of removal of inclusions from the melt during its filtration ($W_{fl.}$) were determined. After melting the metal drop and subsequent crystallization (Fig. 1), the hardened metal samples were cut in half and sections were made. The microstructure of

the metal on the surface of the metal-substrate contact was studied by optical microscopy after etching in 7% alcoholic nitric acid solution. The microhardness of the metal was determined on a microhardness tester from Buehler at an indenter load of 10 g.

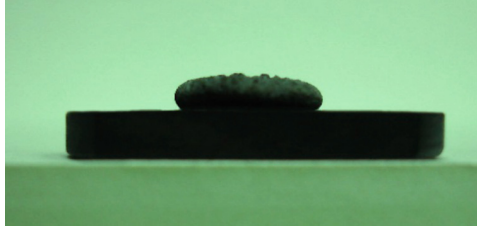


Fig. 1. Drop from a magnesium-based alloy after crystallization on a graphite substrate.

The filtration efficiency through different materials was investigated on a magnesium alloy, after refining with VI-2 flux (% wt.: 38...46 MgCl; 32...43 KCl; 8...10 CaCl₂; 5...9 BaCl₂; 3...5 CaF₂). Pre-heated to a temperature of 500 °C filter materials with a granularity of 10... 50 mm alternately poured on the grid of a removable gutter bowl 100 mm high, mounted above the mold riser, and poured cast samples with a working diameter of 12 mm to determine mechanical properties and metallographic control.

Temporary resistance to rupture (σ_B) and relative elongation (δ) samples with a working diameter of 12 mm were determined on a bursting machine P5 at room temperature. The microstructure of the castings was studied by light microscopy (“Neophot 32”) on heat-treated samples after etching with a reagent consisting of 1% nitric acid, 20% acetic acid, 19% distilled water, 60% ethylene glycol.

The chemical composition of castings from magnesium alloys was monitored using optical emission spectrometers “SPECTROMAXx” and “SPECTROMAXxF”, photoelectric spectrometers MFS-8 and TFS-36.

3 Results and Discussion

The effect of growing additives of fine graphite powder was investigated (0.05%, 0.1%, 0.3%, wt.) on the structure and mechanical properties of the magnesium alloy. The microstructure of the alloy system Mg-Zr-Nd, cast by standard technology, was a δ -solid solution with the presence of eutectoid ($\delta + \gamma$ phase) spherical shape and individual γ -phase intermetallics (Fig. 2a).

The introduction and increase in the concentration of the graphite modifier in the alloy helped to reduce the size and amount of eutectoid secretions (Fig. 2b-d). The value of the micrograin decreased by 1.5 times, and the size of the structural components by 2 times (Table 1). It was found that the microhardness of eutectoid alloys of the cast alloy was significantly higher than the matrix δ -solid solution. In the heat-treated alloy there was an increase in the microhardness of the matrix and a decrease in the hardness of the eutectoid, which indicates an increase in the homogeneity of the heat-treated alloy. The addition of carbon from 0.05% to 0.3% helped to increase the microhardness of the

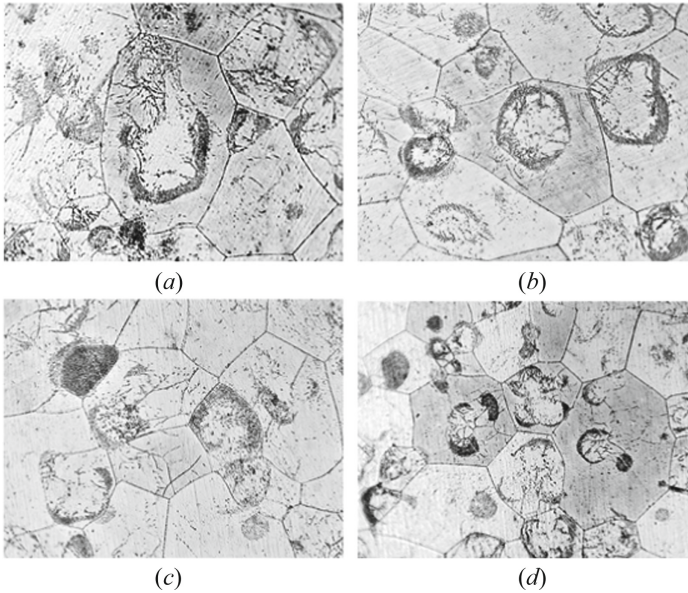


Fig. 2. The microstructure of the magnesium alloy after heat treatment ($\times 350$): (a) – the source metal; (b) – additive 0.05% C; (c) – additive 0.1% C; (d) – additive 0.3% C.

Table 1. Dimensions of structural components and their microhardness in magnesium alloy samples.

Additive modifier (C), % wt	Dimensions of structural components, microns		Microhardness, HV, MPa	
	Eutectoid	Micrograin	Matrix	Eutectoid
Without modif.	60...330	160...280	771.9...899.2	1011.7...1119.5
0.05	60...240	100...210	984.5...1045.0	1292.8...1387.4
0.1	60...200	80...200	1014.5...1054.3	1296.4...1621.7
0.3	50...180	60...180	1065.3...1268.9	1357.5...1787.7

structural components (Table 1) and, as a consequence, increase the strength of the alloy (Table 2).

Modification of the magnesium alloy with fine graphite powder (0.05...0.1%) led to an increase in its plasticity due to the formation of additional centers of crystallization and grinding of metal grains. A further increase in the amount of modifier introduced led to some decrease in the physical and mechanical properties of the material (Table 2).

Based on the above, it can be noted that the modification of the magnesium alloy with carbon up to 0.1% contributed to the increase of its mechanical properties due to the additional strengthening of the structural components of the alloy and grain grinding. Heat treatment increased the homogeneity of the alloy due to the redistribution of

Table 2. Mechanical properties of samples of magnesium alloy with the addition of graphite powder.

Modifier additive (C), % wt	Mechanical properties			
	Without heat treatment		After heat treatment	
	σ_B , MPa	δ , %	σ_B , MPa	δ , %
Without modifier	153	1.9	223	2.9
0.05	163	2.5	231	4.9
0.1	178	3.1	240	4.8
0.3	173	3.0	236	3.5

elements between the axes and axial spaces of the dendrites, which led to the alignment of properties along the cross section of the metal. Addition to the melt of more than 0,1% of carbon led to contamination of the metal with films, increasing the porosity of the material and, consequently, reducing its mechanical properties.

The efficiency of melt cleaning with calcite, magnesite and graphite was compared by determining the characteristics of surface interaction in the systems: «alloy – filter», «flux – filter», «alloy – inclusion», «flux – inclusion».

Analysis of research results (Table 3) showed that the surface tension ($\sigma_{s.t.}$) at the «alloy – gas» boundary in the systems «alloy – carbonate substrate» and «alloy – oxide» was at the level of 71...80 MJ/m².

Table 3. Characteristics of surface interaction between alloy, flux and substrate material (average values).

Material substrates	$\sigma_{s.t.}$, MJ/m ²	θ , °	A_a , MJ/m ²	A_c , MJ/m ²	K_r , MJ/m ²
	alloy / flux	alloy / flux	alloy / flux	alloy / flux	alloy / flux
CaCO3	80/79	128/49	32/131	158/155	-126/-25
MgCO3	71/78	141/53	17/127	141/156	-125/-31
graphite	73/76	155/50	9/124	143/152	-138/-26
SiO2	72/103	131/132	24/35	139/204	-116/-170
Al2O3	75/100	138/144	21/20	149/200	-129/-183
MgO	71/102	149/138	12/29	141/203	-130/-174

The flux spread on carbonate materials and practically did not wet the oxide, which caused different values of surface tension ($\sigma_{s.t.}$) on substrates of oxides and carbonates. Adhesion (A_a) at the interface «flux – substrate of CaCO₃, MgCO₃ and graphite» was 131 MJ/m², 127 MJ/m² and 124 MJ/m², respectively, which is 2...3 times more than the adhesion at the boundary «flux – a substrate of oxides». In the systems «alloy – carbonate

substrate” and “alloy – oxide” lower wetting angle and correspondingly high adhesion work were obtained for the material with CaCO_3 .

The refining property of the flux ($W_{fl.}$) is characterized by the work of adhesion to the metal. Interfacial tension (adhesion) at the boundary “alloy – flux” is: $\sigma_{s.t.} = 79 \text{ MJ/m}^2$; $\theta = 49$. The adhesion of inclusions to the metal among the flux was for SiO_2 , Al_2O_3 and MgO in accordance 140 MJ/m^2 , 143 MJ/m^2 and 132 MJ/m^2 . Given that the refining property of the flux ($W_{fl.}$) increases with decreasing adhesion, we can conclude that the flux adsorbs these inclusions, but more effectively – magnesium oxides (Fig. 3a).

The refining efficiency is characterized by the total binding energy “sorber – inclusion” ($W_{ef.}$) in the system: solid filter (sorber) – metal melt – inclusion (flux). The completeness of the removal of inclusions in the melt was reduced by filtration from calcite to magnesite and graphite – 279 MJ/m^2 , 259 MJ/m^2 and 250 MJ/m^2 respectively (Fig. 3b).

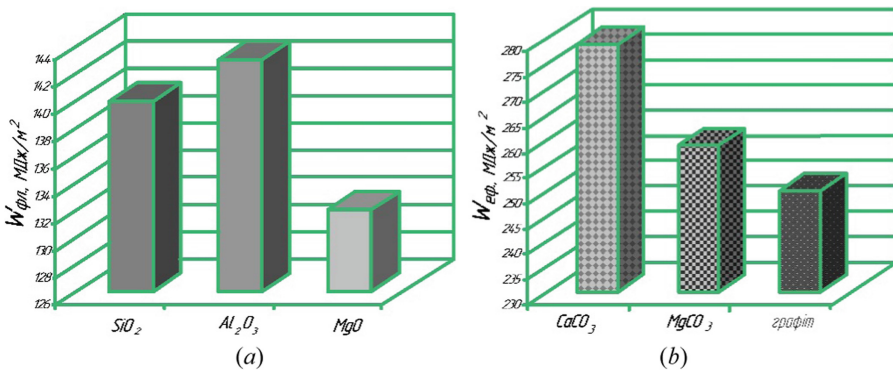


Fig. 3. Refining capacity of the flux to the inclusions (a) and the efficiency of refining the melt with filter materials (b).

The depth of the interaction between the alloy and the filter material was assessed by metallographic analysis. It was found that the magnesium melt penetrated into the filter material with CaCO_3 to a depth of $180 \mu\text{m}$, which significantly exceeded the action of graphite (10 mm) and magnesite (12 mm)(Fig. 4).

An increased (compared to the rest of the droplet volume) number of intermetallics was observed in the surface zone of contact of the investigated drops with the substrate material. It was found that more intermetallics were in the surface zone of the drop in contact with the magnesite substrate. The size of intermetallics reached 25 microns, which is 3...4 times more than in drops in contact with calcite and graphite. The size of micrograin in the material of all investigated drops was at the same level (Table 4).

The microhardness of the δ -solid solution in the surface zones of the drops of all variants was slightly higher than in the center (Table 5). Increased microhardness of the matrix, eutectic and intermetallics was observed in the droplet metal obtained on a magnesite substrate, which is most likely due to the diffusion processes of the substrate elements into the metal melt.

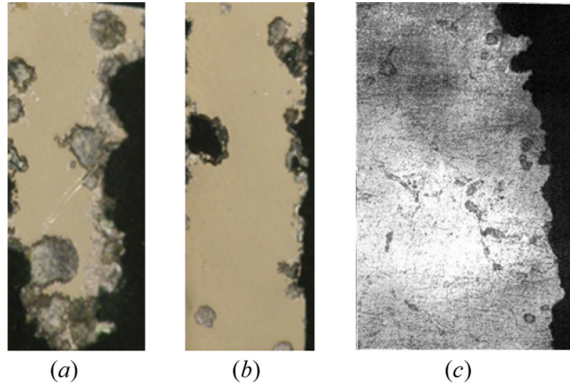


Fig. 4. Microstructure of the limit of interaction of metal with the filter ($\times 500$): (a) – of calcite; (b) – from graphite; (c) – from magnesite.

Table 4. Structural components of melt droplets in contact with various substrates.

Material substrates	Depth of interaction, μm	Micrograin size, μm	Size γ - phases, μm
Calcite	up to 180	80...155	2.0...5.0
Graphite	up to 12	80...185	3.0...7.0
Magnesite	up to 10	75...150	3.0...20.0

Table 5. Microhardness of melt droplets in contact with various substrates.

Material substrates	Microhardness, HV, MPa			
	Matrix		$(\delta + \gamma)$ - phase	γ -phase
	Edge	Center		
Calcite	860.0...978.5	735.4...934.5	1190.4...1372.9	2827.8
Graphite	796.0...899.1	764.8...795.0	1228.8...1894.6	2830.8
Magnesite	897.1...1174.8	827...1032.3	1229.8...2295.9	2825.8...5145.0

Quantitative analysis of the structural components in the studied samples of the studied alloy showed that the interaction of the metal with the substrate materials formed both single intermetallics and their clusters. Their index and average size increased from magnesite to graphite and calcite (Table 6). After the contact of the metal with the substrate materials, the topography and morphology of the inclusions changed.

Filtration of the alloy through magnesite, calcite and graphite contributed to the noticeable sub-grinding of the micrograin metal, especially when using a complex filter containing equal parts of magnesite, graphite and calcite.

Table 6. Quantitative assessment of inclusions in magnesium alloy test samples.

Material substrates	Single inclusions		Accumulation of inclusions	
	Index, I	Medium sized, microns	Index, I	Medium sized, microns
Magnesite	0.00708	3.899	0.00143	9.988
Graphite	0.00910	4.495	0.00125	8.912
Calcite	0.01180	5.673	0.00274	17.15

Mechanical tests have shown that melt filtration increased the strength (σ_B) and plastic (δ) characteristics of the metal. Higher values of mechanical properties and density were obtained on samples made using a complex filter (33% magnesite + 33% graphite + 33% calcite) (Table 7).

Thus, the best properties of the magnesium alloy are achieved by filtration through a complex filter containing calcite, magnesite and graphite. The use of a complex filter [13] in the production of castings from magnesium alloys allows to improve their quality, physical and mechanical properties and increase the yield of suitable castings.

Table 7. Physico-mechanical properties of heat-treated samples of magnesium alloy after different filtration options (average values).

Version filtration	Physical and mechanical properties		
	σ_B , MPa	δ , %	Physical density, g/cm ³
Without filtering	249.0	3.4	1.6951
Magnesite	256.0	4.7	1.6984
Graphite	255.0	4.9	1.6855
Calcite	282.0	5.7	1.6978
Complex	291.0	6.6	1.7298

4 Conclusion

Additives to the magnesium alloy of dispersed graphite powder up to 0.1% improve the mechanical properties of the metal due to the additional strengthening of both solid solution and eutectoid. This changes the parameters of the eutectic transformation and reduces the eutectoid $\delta + \gamma$. Heat treatment increases the homogeneity of the metal between the axes and axial spaces of the dendrites.

It is established that in the process of filtration of magnesium melt through carbon-containing materials (magnesite, calcite and graphite) its effective refining was provided. The use of a filter containing equal amounts of magnesite, graphite and calcite when pouring magnesium alloy provided a reduction in the size of the structural components of the metal by 1.5 times, increased its strength by 20% and ductility almost twice.

It is established that when the filter materials interact with the magnesium melt, it is effectively modified. In the structure of the alloy there is an increased amount of intermetallic γ -phase, which increases the microhardness of the structural components of the alloy and improves its physical and mechanical characteristics.

The use of carbon-containing materials for the modification and refining of magnesium-based alloys is quite effective for improving the quality of medical casting and improving its physical and mechanical properties.

References

1. Suzuki, H., Hirota, M., Amemiya, T., et al.: Cortical bone response of MDF titanium implant. *J. Oral Tissue Eng.* **13**(3), 117–124 (2016). <https://doi.org/10.11223/jarde.13.117>
2. Sinha, R., Sharma, A., Ray, B.R., et al.: Effect of addition of magnesium to local anesthetics for peribulbar block: a prospective randomized double-blind study. *Saudi J. Anaesthesia* **10**(1), 64–67. <https://doi.org/10.4103/2F1658-354X.169478>
3. Cizek, L., Tański, T., Rusz, S., et al.: Microstructure and properties of selected magnesium-aluminum alloys prepared for SPD processing technology. *Arch. Metall. Mater.* **62**(4), 2365–2370 (2017). <https://doi.org/10.1515/amm-2017-0348>
4. Chen, F., Zhang, Y., Zhang, Y.: Effect of graphene on micro-structure and properties of MAO coating prepared on Mg-Li alloy. *Int. J. Electrochemical Science* **12**(7), 6081–6091 (2017). <https://doi.org/10.20964/2017.07.59>
5. Mahmoud, M.G., Samuel, A.M., Doty, H.W., et al.: Effect of rare earth metals, Sr, and Ti addition on the microstructural characterization of A413.1 alloy. *Advances in Materials Science and Eng.* 4712946 (2017). <https://doi.org/10.1155/2017/4712946>
6. Li, Y., Wei, Y., Hou, L., et al.: Effect of erbium on microstructures and properties of Mg-Al intermetallic. *J. Rare Earths* **32**(11), 1064–1072 (2014). [https://doi.org/10.1016/S1002-0721\(14\)60184-8](https://doi.org/10.1016/S1002-0721(14)60184-8)
7. Dieringa, H.: Properties of magnesium alloys reinforced with nanoparticles and carbon nanotubes: a review. *J. Mater. Sci.* **46**(2), 289–306 (2011). <https://doi.org/10.1007/s10853-010-5010-6>
8. Pekguleryuz, M.O., Kainer, K., Kaya, A. (eds.): *Fundamentals of Magnesium Alloy Metallurgy*. Woodhead Publishing, Cambridge (2013). <https://doi.org/10.1533/9780857097293>
9. Chen, H.L., Li, N., Klostermeier, A., Schmid-Fetzer, R.: Measurement of carbon solubility in magnesium alloys using GD-OES. *J. Anal. At. Spectrom.* **26**(11), 2189–2196 (2011). <https://doi.org/10.1039/C1JA10128E>
10. StJohn, D.H., Qian, M.A., Easton, M.A., et al.: Grain refinement of magnesium alloys. *Metall. and Mater. Trans. A.* **36**(7), 1669–1679 (2005). <https://doi.org/10.1007/s11661-005-0030-6>
11. Shalomeev, V., Tsvirco, E., Vnukov, Y., et al.: Development of new casting magnesium-based alloys with increased mechanical properties. *Eastern-European J. Enterprise Technologies* **4**(1), 4–10 (2016). <https://doi.org/10.15587/1729-4061.2016.73384>
12. Belov, V.D., Koltygin, A.V., Belov, N.A., Plisetskaya, I.V.: Innovations in cast magnesium alloys. *Metallurgist* **54**(5), 317–321 (2010). <https://doi.org/10.1007/s11015-010-9313-2>
13. Shalomeev, V., Aikin, N., Chorniy, V., Naumik, V.: Design and examination of the new biosoluble casting alloy of the system Mg–Zr–Nd for osteosynthesis. *Eastern-European J. Enterprise Technologies* **1**(12), 40–48 (2019). <https://doi.org/10.15587/1729-4061.2019.157495>
14. Belikov, S., Shalomeev, V., Tsvirko, E., et al.: Microalloyed magnesium alloys with high complex of properties. In: *Materials Science and Technology Conference and Exhibition 2017 (MS&T17)*, pp. 84–91. MS&T17, Pittsburgh (2017) https://doi.org/10.7449/2017/mst_2017_84_91
15. Zakaria, M.R., Akil, H.M., Kudus, M.H.A., et al.: Hybrid carbon fiber-carbon nanotubes reinforced polymer composites: a review. *Compos. B Eng.* **176**, 107313 (2019). <https://doi.org/10.1016/j.compositesb.2019.107313>



Hydrogen Sensor on the Base of Nanocrystalline SiC Films

Oleksandr Semenov¹(✉) , Hanna Dulfan¹, Denis Lubov² , Ihor Biletskyi¹ ,
and Natalia Teliura¹

¹ O. M. Beketov National University of Urban Economy in Kharkiv, 17 Marshala Bazhanova Street, Kharkiv 61002, Ukraine

oleksandr.semenov@kname.edu.ua

² National Technical University “Kharkiv Polytechnic Institute”, 2 Kyrpychova Street, Kharkiv 61002, Ukraine

Abstract. The chemical resistive sensitivity of nanocrystalline SiC films to molecular hydrogen mixed with air has been studied. Three series of films with different structures were prepared by direct ion deposition. The effect of hydrogen on the resistance of the films was studied in the range of easily flammable hydrogen concentrations H_c (0.5–10%) in a mixture with air. At the operating temperature of the films of 230 °C, it was found that the maximum sensitivity to hydrogen ($S \sim 95\%$, at $H_c = 4\%$) is exhibited by films with a predominantly rhombohedral polytype, an average nanocrystal size of 10–25 nm, and a content of nanocrystals in the volume of 83%.

Keywords: SiC nanocrystals · Thin films · Hydrogen resistive sensitivity · Sensor · Structure · Nanocrystal size

1 Introduction

At present, the topic of hydrogen attracts special attention of scientists and specialists in the development of renewable energy technologies [1–3]. Hydrogen is an environmentally friendly energy carrier with excellent thermophysical properties: high calorific value (142 kJ/g), low minimum ignition threshold (0.017 mJ), wide flammability range (4–75%), as well as a high burning rate. The product of hydrogen combustion is pure water, which again can be a source of hydrogen [4]. On the other hand, this gas is a source of serious danger to people. Hydrogen gas is tasteless, colorless, and odorless, so humans cannot detect it. The low ignition energy and wide flammability range make it highly flammable and explosive. Therefore, it is necessary to quickly and accurately detect hydrogen leaks during the production, storage and use of hydrogen, as well as to control the hydrogen concentration in energy and industrial production [5–8].

There are many types of commercially available hydrogen sensors developed on various physical and chemical principles, including electrochemical, semiconductor, thermoelectric, pellistor, optical and acoustic, et al. [9–11] The most widely used for mass autonomous monitoring of hydrogen impurities in air are semiconductor sensors

that have high sensitivity, fast response, long-term stability and potential for integration into hydrogen detection systems [12–14].

However, this type of hydrogen sensor still suffers from high operating temperatures resulting in high power consumption and potential safety hazards [15]. In addition, cross-selectivity towards other combustible or reducing gases is another important issue that must be addressed in order to improve measurement accuracy [16].

Modern performance criteria for a hydrogen sensor are as follows: detection in the concentration range of 0.01–10% for safety and 1–100% for fuel cells, selectivity to other reducing gases such as NO, CO, H₂S, etc., high sensitivity, high accuracy, short response and recovery, suitable operating temperature (preferably at room temperature), stability to environmental factors (such as temperature and humidity), repeatability, long-term stability and low cost [17–19].

One of the promising materials, the properties of which meet modern requirements for sensitive elements of semiconductor hydrogen sensors, which have chemical inertness, resistance to radiation exposure, and temporal stability of properties, are functional materials based on SiC [20], in particular, films of semiconductor nanocrystalline SiC (nc-SiC) obtained by direct deposition of carbon and silicon ions [21]. Previously, it was found that nc-SiC films containing one predominant cubic polytype exhibit a thermally activated conductivity mechanism, while films containing the main rhombohedral polytype demonstrate a two-channel conductivity mechanism, one of which is based on electron tunneling through a barrier between nanocrystals of different polytypes [22]. The radiation resistance of such films was shown earlier in [23].

In this paper, we investigated the gas sensitivity to hydrogen of thin films of nanocrystalline silicon carbide (nc-SiC), which have a higher reliability and resistance to external influences compared to metal oxides. In this work, studies of the gas sensitivity of nc-SiC films to oxidizing and reducing gases, the results of which were published earlier [24–26], are continued.

2 Experimental Research

The preparation of gas-sensitive nc-SiC layers on single-crystal Al₂O₃ substrates was performed by an original method of direct ion deposition [21, 27]. Three series of nc-SiC films of close thickness (~100 nm) were deposited, differing in structure and phase composition according to the conditions of their preparation. Synthesis of series 3C – C, 3C + 21R – D, and 21R + 3C – F nc-SiC films was performed at different process temperatures, which ensured the variation of structural parameters [27]. The 3C – C series contained a predominantly cubic polytype with an average crystallite size of 5–10 nm, the 3C + 21R – D series had a predominantly cubic 3C polytype with the addition of the 21R rhombohedral polytype and an average nanocrystal size of 8–15 nm, and a batch of films 21R + 3C – F contained predominantly rhombohedral polytype 21R with an admixture of cubic 3C, and the average size of nanocrystals was 10–25 nm. The volume content of crystallites in the films of the given series also varied: from 73% in the first series, 77% in the second, and 83% in the third series. Electron microscopic images of the films and their structural parameters, measured by us earlier, are shown in Fig. 1 and in Table 1.

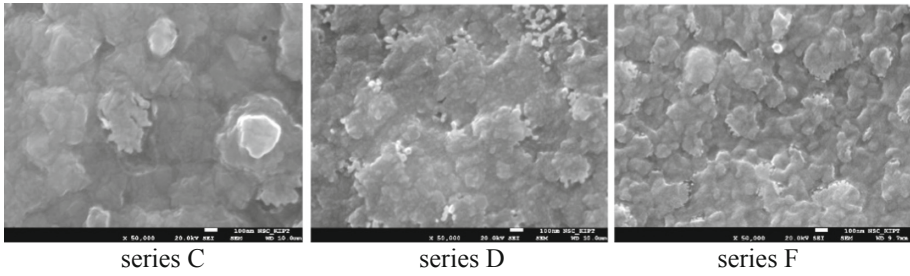


Fig. 1. Scanning Electron Microscopic images of the surfaces of nc-SiC films of various series.

Table 1. Structural characteristics of nc-SiC films

Polytype	Integral ratio Si/C in the film of boundary regions	Crystalline phase content, %	Average size of nanocrystals, nm	Elemental composition of boundary regions
3C – C	1.33	~ 73	~ 5–10	Si, SiO _x
3C + 21R – D	1.41	~ 77	~ 8–15	Si, SiO _x
21R + 3C – F	1.75	~ 82	~ 10–25	Si, SiO _x

The excess of silicon in the films, shown in the table, was contained both in the boundary region and in the nanocrystals. This was evidenced by the electronic conductivity of the films, which indicates self-doping of SiC nanocrystals with silicon [27]. For resistive measurements, rectangular areas of Au/Ni $7 \times 7 \text{ mm}^2$ were plotted at a distance of 2 mm between the boundaries. Before measuring the gas sensitivity, the films were annealed in air at a temperature of 500 °C. The effect of hydrogen in a mixture with atmospheric air was determined by comparing the electrical conductivity of the films under the action of a gas mixture with different concentrations of hydrogen and pure air at different temperatures of the film sample. A number of pure air mixtures were prepared with volume concentrations of hydrogen near its ignition threshold of 4% in the range of 0.5%, 1%, 2%, 4%, 6%, 10%. During measurements, gas mixtures were passed through the volume of the measuring chamber at a rate of $\sim 1 \text{ L/min}$. The gas sensitivity coefficient was estimated using the formula $S(\%) = (Rg - Ra) / Ra \times 100\%$, where Rg and Ra are the film resistance in the presence and absence of hydrogen in air, respectively. The initial resistance of the film samples was about 100 M Ω . Previous studies have shown that the optimal operating temperature of nc-SiC films for recording various gases differed: for O₂, CO, CH₄ [24] it was near 500 °C, for O₃ it was optimal near 280 °C and 330 °C [25]. At the same time, one of the important conditions for the applicability of hydrogen sensors concerns the temperature of the sensor: it should be as low as possible to prevent gas ignition. Previously, we found that the maximum rate of desorption of molecular hydrogen in nc-SiC films occurs near 230 °C [28]. Therefore, this temperature was previously chosen as the working one.

3 Results and Discussion

At the first stage of research, we refined the optimal temperature of the film sensitivity to hydrogen. Figure 2 shows the dependences of the sensitivity of nc-SiC films of three series to molecular hydrogen with a volume concentration of 4% at different temperatures in the range of 50–400 °C. It can be seen from the curves that the maximum sensitivity of all series of films is near 230 °C, which is in good agreement with ours. Data on the temperature dependence of the maximum rate of molecular hydrogen desorption from the surface (and subsurface) of nc-SiC films [29]. Therefore, we carried out further measurements at a working temperature of the films of 230 °C. In addition, it is clear that the sensitivity of the films depends on their structure and differs over the entire temperature range. A higher sensitivity for a hydrogen concentration of 4% was observed in films of the 21R + 3C – F series, which contains the highest concentration of the SiC nanocrystalline phase. The concentration dependences of S for films of all series are shown in Fig. 3. It can be seen from the dependences that the sensitivity of films with a hydrogen concentration increases nonmonotonically. In the range of 0.5–4%, a rapid change in resistance is observed, which then reaches a flat area, and for films of the 21R + 3C – F series, the sensitivity S reaches a maximum value of 0.95–0.98. On films of the first 3C – C and the second series 3C + 21R – D, the maximum sensitivity value reaches approximately 0.7.

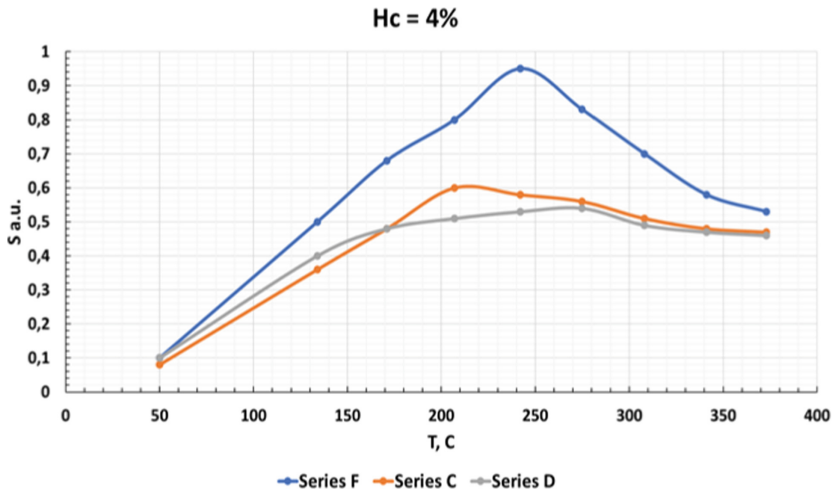


Fig. 2. The hydrogen sensing properties of nc-SiC thin films different structure in dependence working temperature at concentration of the $H_c = 4\%$.

Figure 4 shows variation in the resistance of films of the 21R + 3C – F series to turning on and off the action of hydrogen in real time at a film temperature of 230 °C.

The measurements were carried out at a hydrogen concentration in air of 4% and an optimum temperature of 230 °C film measurement chamber, within approximately 3 – 4 s, the film resistance decreases by two orders of magnitude, and after the gas

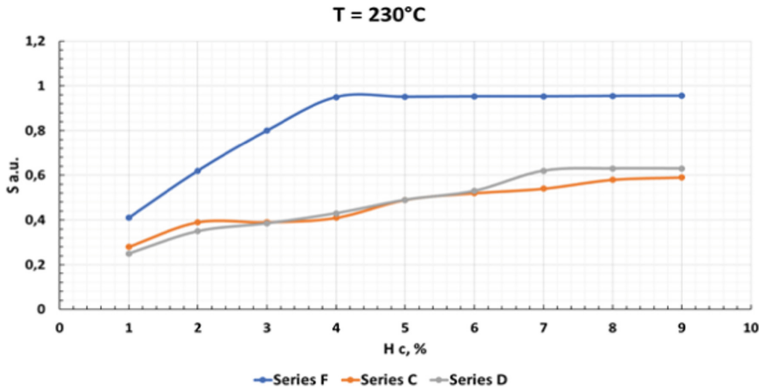


Fig. 3. The concentration dependences of S for nc-SiC films of series F, C and D at the film temperature of 230 °C.

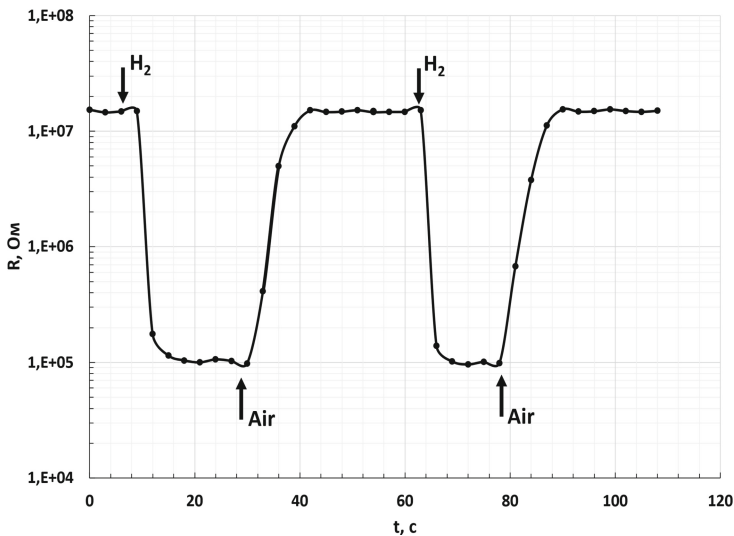


Fig. 4. Changes in the resistance of films of the 21R + 3C – F series to turning on and off the action of hydrogen in real time at a film temperature of 230 °C.

inlet is turned off, it is restored in approximately 10–12 s. The drop in the resistance of the nc-SiC film upon interaction with hydrogen is explained by the reducing effect of hydrogen on the film surface oxidized by atmospheric oxygen. The surface of the nc-SiC film, according to microanalysis and Raman spectroscopy, mainly contains silicon oxides SiO_x. The mechanism of change in the charge state of the surface of a film with oxidized silicon can be seen in Fig. 5, proposed in [30] to explain the effect of hydrogen on the surface of metal oxide semiconductors. The generally accepted mechanism is based on a variation in the area of surface electron depletion due to the reaction between hydrogen and chemisorbed oxygen at the surface.

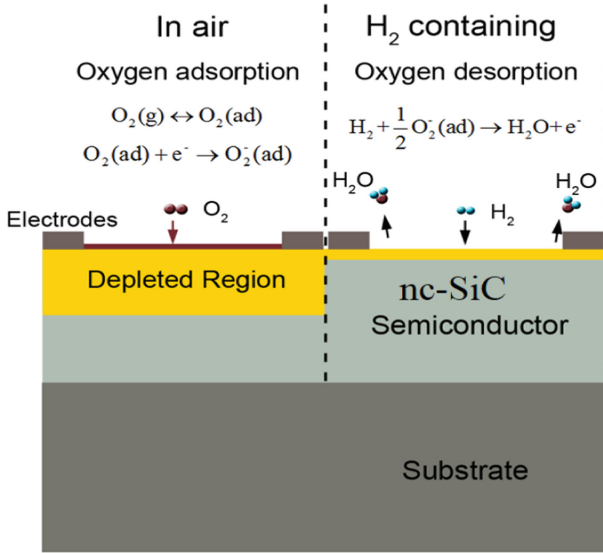


Fig. 5. The hydrogen sensing mechanism of resistance based nc-SiC sensors.

As shown in Fig. 5, in an air atmosphere, oxygen molecules can be adsorbed on the surface of a semiconductor and extract electrons from the conduction band to form oxygen ions. This can lead to the formation of an electron depletion region near the surface, which can significantly increase the resistance due to a decrease in the net carrier density. When the sensor is exposed to a hydrogen atmosphere, the hydrogen molecules react with the adsorbed oxygen species. The redox reaction is exothermic and leads to rapid desorption of H_2O molecules formed from the surface. The released electrons will reduce the thickness of the depletion region and reduce the resistance of the semiconductors. When the sensor is again exposed to the ambient air, the depleted area will be restored by adsorbed oxygen species. The resistance will return to its original level before the hydrogen reaction. Due to the fact that the films are thin and have a developed surface, the response time to the action of hydrogen is extremely short, about 3 s, which is significantly less than the response time of existing semiconductor hydrogen sensors [1]. Accordingly, the recovery time of the sensor sample, relative to existing hydrogen sensors [1], is also extremely short, about 10 s.

4 Conclusion

The chemical resistive sensitivity of nanocrystalline SiC films to molecular hydrogen mixed with air was studied. Three series of films with different structures were prepared by direct ion deposition. The 3C – C series contained a predominantly cubic polytype with an average crystallite size of 5–10 nm, the 3C + 21R – D series had a predominantly cubic 3C polytype with the addition of the 21R rhombohedral polytype and an average nanocrystal size of 8–15 nm, and a batch of films 21R + 3C – F contained

predominantly rhomboeric polytype 21R with an admixture of cubic 3C, and the average size of nanocrystals was 10–25 nm. The effect of hydrogen on the resistance of the films was studied in the range of easily flammable hydrogen concentrations H_c (1–8)% in a mixture with air. The optimal temperature of the maximum sensitivity of films to hydrogen was determined in the region of 230 °C. At an operating temperature of films of 230 °C, it was found that the maximum sensitivity to hydrogen ($S_{95\%}$, at $H_c = 4\%$) is exhibited by films with a predominantly rhombohedral polytype, the average size of nanocrystals 10–25 nm, the content of nanocrystals in the volume of 83%.




References

1. Constantinoiu, I., Viespe, C.: Synthesis methods of obtaining materials for hydrogen sensors. *Sensors* **21**(17), 5758 (2021). <https://doi.org/10.3390/s21175758>
2. Hirscher, M., Yartys, V.A., Baricco, M., et al.: Materials for hydrogen-based energy storage – past, recent progress and future outlook. *J. Alloy. Compd.* **827**, 153548 (2020). <https://doi.org/10.1016/j.jallcom.2019.153548>
3. Kritskiy, D., Pohudina, O., Kovalevskiy, M., et al.: Powder mixtures analysis for laser cladding using OpenCV library. In: Nechyporuk, M., et al. (eds.): *Integrated Computer Technologies in Mechanical Engineering – 2021. LNNS*, vol. 367, pp. 924–937. Springer, Cham (2022). https://doi.org/10.1007/978-3-030-94259-5_72
4. Agrawal, T., Ajitkumar, R., Prakash, R., Nandan, G.: Sodium silicide as a hydrogen source for portable energy devices: a review. *Materials Today: Proceedings* **5**(2), 3563–3570 (2018). <https://doi.org/10.1016/j.matpr.2017.11.605>
5. Buttner, W.J., Post, M.B., Burgess, R., Rivkin, C.: An overview of hydrogen safety sensors and requirements. *Int. J. Hydrogen Energy* **36**(3), 2462–2470 (2011). <https://doi.org/10.1016/j.ijhydene.2010.04.176>
6. Plankovskyy, S., Breus, V., Voronko, V., Karatanov, O., Chubukina, O.: Review of methods for obtaining hardening coatings. In: Nechyporuk, M., Pavlikov, V., Kritskiy, D. (eds.) *ICTM 2020. LNNS*, vol. 188, pp. 332–343. Springer, Cham (2021). https://doi.org/10.1007/978-3-030-66717-7_28
7. Aroutiounian, V.M.: Hydrogen detectors. *Int. Scientific J. Alternative Energy Ecology* **3**(23), 21–31 (2005)
8. Kovač, A., Paranos, M., Marciuš, D.: Hydrogen in energy transition: a review. *Int. J. Hydrogen Energy* **46**(16), 10016–10035 (2021). <https://doi.org/10.1016/j.ijhydene.2020.11.256>
9. Sharma, A., Ahmed, A., Singh, A., et al.: Recent advances in tin oxide nanomaterials as electrochemical/chemiresistive sensors. *J. Electrochem. Soc.* **168**(2), 027505 (2021). <https://doi.org/10.1149/1945-7111/abdee8>
10. Luo, Y., Zhang, C., Zheng, B., et al.: Hydrogen sensors based on noble metal doped metal-oxide semiconductor: a review. *Int. J. Hydrogen Energy* **42**(31), 20386–20397 (2017). <https://doi.org/10.1016/j.ijhydene.2017.06.066>
11. Sun, X., Wang, C., Su, D., et al.: Application of photocatalytic materials in sensors. *Advanced Materials Technol.* **5**(5), 1900993 (2020). <https://doi.org/10.1002/admt.201900993>
12. Wright, J.S., Lim, W., Norton, D.P., et al.: Nitride and oxide semiconductor nanostructured hydrogen gas sensors. *Semicond. Sci. Technol.* **25**(2), 024002 (2010). <https://doi.org/10.1088/0268-1242/25/2/024002>
13. Wang, C., Yin, L., Zhang, L., et al.: Metal oxide gas sensors: sensitivity and influencing factors. *Sensors* **10**(3), 2088–2106 (2010). <https://doi.org/10.3390/s100302088>
14. Potje-Kamloth, K.: Semiconductor junction gas sensors. *Chem. Rev.* **108**(2), 367–399 (2008). <https://doi.org/10.1021/cr0681086>

15. Nikolic, M.V., Milovanovic, V., Vasiljevic, Z.Z., Stamenkovic, Z.: Semiconductor gas sensors: Materials, technology, design, and application. *Sensors* **20**(22), 6694 (2020). <https://doi.org/10.3390/s20226694>
16. Plankovskyy, S., Shypul, O., Tsegelynyk, Y., Pankratov, A., Romanova, T.: Amplification of heat transfer by shock waves for thermal energy method. In: Nechyporuk, M., Pavlikov, V., Kritskiy, D. (eds.) ICTM 2020. LNNS, vol. 188, pp. 577–587. Springer, Cham (2021). https://doi.org/10.1007/978-3-030-66717-7_49
17. Chen, K., Yuan, D., Zhao, Y.: Review of optical hydrogen sensors based on metal hydrides: recent developments and challenges. *Opt. Laser Technol.* **137**, 106808 (2021). <https://doi.org/10.1016/j.optlastec.2020.106808>
18. Hübert, T., Boon-Brett, L., Black, G., Banach, U.: Hydrogen sensors – a review. *Sens. Actuators, B Chem.* **157**(2), 329–352 (2011). <https://doi.org/10.1016/j.snb.2011.04.070>
19. Chauhan, P.S., Bhattacharya, S.: Hydrogen gas sensing methods, materials, and approach to achieve parts per billion level detection: a review. *Int. J. Hydrogen Energy* **44**(47), 26076–26099 (2019). <https://doi.org/10.1016/j.ijhydene.2019.08.052>
20. Zorman, C.A., Parro, R.J.: Micro- and nanomechanical structures for silicon carbide MEMS and NEMS. *physica status solidi (b)* **245**(7), 1404–1424 (2008). <https://doi.org/10.1002/pssb.200844135>
21. Semenov, A.V., Puzikov, V.M., Dobrotvorskaya, M.V., et al.: Nanocrystalline SiC films prepared by direct deposition of carbon and silicon ions. *Thin Solid Films* **516**(10), 2899–2903 (2008). <https://doi.org/10.1016/j.tsf.2007.05.059>
22. Kozlovskiy, A., Semenov, A., Skorik, S.: Electron transport in nanocrystalline SiC films obtained by direct ion deposition. *Superlattices Microstruct.* **100**, 596–604 (2016). <https://doi.org/10.1016/j.spmi.2016.10.013>
23. Semenov, A.V., Lopin, A.V., Puzikov, V.M., Boriskin, V.N.: Effect of irradiation on the properties of nanocrystalline silicon carbide films. *Semiconductors* **43**(10), 1322–1327 (2009). <https://doi.org/10.1134/S106378260910011X>
24. Semenov, A., Kozlovskiy, A., Skorik, S., Lubov, D.: Gas sensing properties of nanocrystalline silicon carbide films. *Micro and Nano Systems Letters* **7**(1), 1–5 (2019). <https://doi.org/10.1186/s40486-019-0084-7>
25. Semenov, A.V., Lubov, D.V., Makhonin, M.V.: Ozone sensitive properties of thin films of nanocrystalline silicon carbide. *J. Nano- and Electronic Physics* **12**(5), 05016 (2020). [https://doi.org/10.21272/jnep.12\(5\).05016](https://doi.org/10.21272/jnep.12(5).05016)
26. Semenov, A.V., Lubov, D.V., Kozlovskiy, A.A.: The chemresistive properties of SiC nanocrystalline films with different conductivity type. *Journal of Sensors* **2020**, 7587314 (2020). <https://doi.org/10.1155/2020/7587314>
27. Semenov, A.V., Puzikov, V.M., Golubova, E.P., et al.: Low-temperature production of silicon carbide films of different polytypes. *Semiconductors* **43**(5), 685–689 (2009). <https://doi.org/10.1134/S1063782609050273>
28. Taki, Y., Kitiwan, M., Katsui, H., Goto, T.: Electrical and thermal properties of off-stoichiometric SiC prepared by spark plasma sintering. *J. Asian Ceramic Societies* **6**(1), 95–101 (2018). <https://doi.org/10.1080/21870764.2018.1446490>
29. Guglya, A., Kalchenko, A., Lyubchenko, E., et al.: Layers of nanocrystalline SiC as a new type of solid-state hydrogen storage. *J. Nanotechnology* **2018**, 3787390 (2018). <https://doi.org/10.1155/2018/3787390>
30. Gu, H., Wang, Z., Hu, Y.: Hydrogen gas sensors based on semiconductor oxide nanostructures. *Sensors* **12**(5), 5517–5550 (2012). <https://doi.org/10.3390/s120505517>



Determination of Research Guidelines and Establishing of a Test Framework for the Development of New CVD Coating Formulations and New Approach Coating Equipment

István Gábor Gyurika^(✉) , Osamah Ihsan Ali , and Miklós Jakab 

University of Pannonia, 10 Egyetem Street, Veszprem 8200, Hungary
gyurika@almos.uni-pannon.hu

Abstract. Within the science of mechanical engineering, different coatings in cutting technology and thermoforming improve the different mechanical properties of tools. Several coating technologies are available to improve tool hardness, abrasion resistance, thermal stability, toughness, chemical stability, but coatings can increase tool life, i.e., the time spent in cutting or the number of products that can be produced with a plastic forming tool. One of the common coating technologies used today is chemical vapor deposition (CVD technology). The authors writing the article are at the beginning of a three-year research process. The research aims to develop new CVD coating compositions and a new approach to CVD coating equipment. Research on new coating formulations aims to achieve higher service life and better mechanical properties. In the development of the coating equipment, a high level of universality and increasing productivity are the basic goals. During the construction and manufacturing planning process of the plant, the effective coating temperature ranges achievable with the new formulations, the optimal coating time, and the best possible use of space for the components that can be placed in the reactor will have to be examined. To start the research of the new compositions, a detailed literature review process was carried out, where the application possibilities and limitations of CVD coatings and the scientific results achieved in recent years were examined. For the future research described in the article, the authors describe the possible directions of development, the already established research background, and the requirements related to the new CVD equipment, which can be compared to the fourth industrial revolution. The detailed literature research process in this article, the definition of development directions, and the research framework together provide the basis for the implementation of an effective research process over three years.

Keywords: Chemical vapor deposition · CVD · Coatings · The substrate · Multi-layers films

1 Introduction

Chemical vapour deposition (CVD) may be define as the deposition of solid in heated surfaces from a chemical reaction on vapour phase. It belong to classes of vapours transfers processes which atomistic in nature, depositions species are atoms or molecules or a combinations [1]. So, CVDs is a techniques that relies on the formation of gaseous species containing the coating element within coating retort/chamber. Otherwise, the gaseous species may be generated external to the coating retort and introduce by delivery system. These gaseous species then allows to come into contact with surface that require coating. The retorts held high temperatures may be up to 2000 °C. Using the CVD method a wide variety of coating may be formed, ranging from soft, ductile coating to those with hard, like ceramics properties. Coatings with hardness's in the range 150–3000 HV (0.1 kg). Coating-formed by the CVD method currently, beings used to combats the severe attritions of component used industrials situation where corrosions, oxidations or wears is experienced [2].

Thin flake films are layers of finely made material from less than one nanometer (many atoms layer) to some hundreds of micro-meters (the references; the man's hair, its around 75 μm thickness) [3]. The significance of the subtle layers in the association of the moment is enormous and subtle layers can be present everywhere. Most of the metal objects around us have their own processing by cutting tool and plastic forming tool which coated with very hard and wear resistant thin layers. Spare parts for the humans body, as the hip joints, often coated with thin layers to create it further bio-compatible. Technologically important thin films can be mono-crystalline, poly-crystalline, or unformed epitaxial, and material characterizations can frequently be fine-tuned to perfection to suit different applications [4].

The substrates with the thin films, it's frequently preferred to starts from atomic or molecule in the vapour phases and place object to coating in vapour, lettings atom and/ or molecule from the vapour build up the thin film on the surfaces of the object. These vapour base thin-film conflation techniques are classified as either physical vapour deposits (PVD) or chemical vapours deposits (CVD), depending whether the films deposits process is driven by physical impact or by chemical reactions respectively. CVDs, target element deliver in form of volatiles molecules, denoted as precursors, and the film is building ups by the series of chemical reactions between precursors, precursor fraction and the substrate. In the general cases, such as these reactions can takes places both in the gas-phase and on the substrate surfaces. However, a configurations of CVD styled atomic layers deposition (ALD) uses only surfaces chemical reaction to building up thin film with great perfection. The precursor molecule are frequently adulterated in a carriers gas make up the main parts of the gas-volumes in the processes, related to the detergent in liquid phase chemical reaction. The carrier gases in CVD most frequently hydrogen, nitrogen or argon, or mixes of these. Correspondingly CVD and ALD process used the plasmas to activation the chemist by open up newer reaction paths electron impact collision and via creation of radicals and ions, the process referee to as Plasma Enhance CVD (PECVD) or alternately Plasmas Assist CVD (PACVD). Likewise the gas phase chemistry can be actuated by photons from the laser, appertained to as Laser Enhance CVD (LECVD). CVD may even be regard as a chemical operation that span numerous classical discipline chemical physic of gas and plasma, surfaces knowledge,

solid states chemistry of inorganic material and organometallic or organic chemistry for precursor conflation [5, 6].

2 Literatures Review and a Brief Historical Perspective

A CVD isn't a very new processes, its original practical usage was develop in the 1880s in the product of incandescence lights to enhance the strengths of filament by coats them with the carbon or metals [1]. CVD develop slow in the coming fifty times and was held down substantially to extract and pyro-metallurgy for the product of very high pure refractory metals such-as tantalum, titanium, and zirconium. Several traditional CVD reaction develop at that moment includes the carbon cycle (the Mond operation), the iodides decomposition (Des Boer Van Arkel operation) and magnesium reduce reaction (Krolls operation) [7, 8].

As previously as 1909, CVD of silicon was related in from SiCl_4 in hydrogen. This procedure stills utilized to productions purified silicon for assiduity, although kindly refine to allows to higher controls in the procedure. It's the original illustration of the CVD used to deposit a layer of a semiconductor substance and, going_s back in time, this is clear that diligence in microelectronics and CVD procedures go hand in hand. The use of organic precursor metals and alloys such as trimethylgallium ($\text{Ga}(\text{CH}_3)_3$, also understood under the name TMG) has therefore been a crucial parameter in the development of form nitride technology. From another point of view, in developing the coating of tools to supply the wear resistant coating in the field of metal and alloy cutting, Wilhelm Rupert of Metalgesellschaft [10] was probably the first experimenter to do so. Coating on tool steel substrate commercially used in the 1950 and it's called the "father" of tools coating. The first TiC coating applied to tungsten carbide substrates a film thickness of 4 μm in 1968. 5B, composite multilayers of TiN and TiCN on TiC composite double layers of aluminum oxide on TiC, TiC on WC and oxycarbone titanium. Consequently: in the period 1968–1985 CVD coating of carbide substrates were quickly accepted and developed rapidly [11]. Nowadays, technology is evolving faster. Below, survey of some literatures review of CVD coatings.

In 2017, Gao *et al.*, Pyrolytic Boron Nitride (PBN), it's high performance material made by hot wall CVD using spent graphite substrates and a deposit temperature range of 1300 °C to 1600 °C total_s pressures of 200 Pa. Result showed that the deposit face of product had pebble suchlike structure and fracture face had apparent laminar structure having preferred exposure (002) parallel to face of substrate at temperature above 1400 °C. Unformed quantum of boron nitride also increased with the increase in the deposit temperature of the proses [12]. In 2018, Ciprian *et al.*, using rotating chemical vapor deposit (RCVD), nanoparticles from molybdenum oxide (MoO_3) with a size of 1.5 to 60 nm were produced. Zinc acetate ($\text{Zn}(\text{OAc})_2 \cdot 2\text{H}_2\text{O}$) was used as the substrate. It was concluded that a direct influence of the deposit time on the essence oxide lading was observed in a time window between 0.9 and 2.7 ks, the essence oxide lading can increase from 1 to 3 by weight [13]. In 2020, Kainz *et al.* delved a gas admixture of TiCl_4 , H_2 , N_2 and Ar for the conflation of TiN. BCl_3 was added to the deposits of the B-containing coatings and N_2 was neglected to gain pure TiB_2 . Tungsten carbide cutting insert with 92 by weight of WC, 6 by weight of Co and 2 by weight of mixed carbide

were used as the substrate from 4.0 to 7.1 μm and the growth rate was between 0.76 and 1.64 $\mu\text{m/h}$. High-energy X-ray diffraction trials in an inert terrain showed that TiN, TiB₂ and ternary TiB_xN_y layers with varied B contents are thermally stable up to 1000 °C. TiN and TiB_xN_y layers drop with the duration of the heating, while TiB₂ shows an enhancement in compressive stresses as well as the deposit temperature. Nano-crystalline TiB₂ shows a farther increase in this grain during the annealing period compared to coarse-granulated columnar. Results indicate that the measure of thermal growth decreases with adding B_s content. Same trend detected for thermal conductivity, which correlate with grain size of coating [14]. In 2020, Sharma *et al.* the studies focused on the design and fabrication of a triangular spirals microstructure on cutting tool coated with CVD insert using femtosecond laser machine on tungsten carbide insert with CVD in TiCN (titanium carbon nitride) and alpha aluminum oxide up to 20 μm . Triangular spiral texture cover 1.12 mm from area with grooved edge in vertical position to the path of the groove width of 10 μm , the wall thickness of 20 μm and the intensity of 10 μm grooves. Triangular spiral structure act as reservoir_s for lubricant and provide additional location for the heat dissipation rate. The laser groove of coating moved away from cutting insert of cutting tools [15]. In 2021, Song *et al.* prepared and evaluated group of Si₃N₄ diamond thick film welded cutting tool using microwave plasma chemical vapor deposition technique. Layers deposited on the Si₃N₄ substrate using microwave CVD plasma (MPCVD) using optimized deposition parameters: microwave_s power 3.5 kW, reagent pressure 20 kPa and concentration in methane 10% confirms that it is desired to improve the smoothness of the surfaces of the layers and to suppress formation of void in intermediate layer of the substrate by using techniques of sandblasting and pretreatment with nanodiamond. The overall performance of the DB cutting tools was tested in an AlSi hypereutectic dry-turning alloy using PCD and fine diamond. WCCo Coats (c.DC devices) in comparison Cuttings effects indicate that, the DB tool outpaced PCD and DC tools in period of service life also outperformed DC tool in position of machining worth [16].

3 Advantage and Limitation of CVD-Processes

CVD processes have numerous vital benefits making it the favored technique at lots of cases. These can brief as following [1, 17]:

1. It can be implemented to a huge kind of base substances which includes ceramic, metals and metallic alloy.
2. It can resist publicity to low and excessive temperature and high difference of temperature.
3. Remain bonded in excessive pressure environment and while surfaces activate because of excessive the adhesion characteristics.
4. Precursor fueloline may be optimized for put on resistance, excessive lubricity, corrosion resistance, fouling resistance, excessive purity, or chemical inertness.
5. Process is flexible for designing, and new technology can be developed.
6. CVD can production grade and/multi layers coating and provides coating for a range of metals alloys and compounds not available by the others mean.

Other benefits of CVD encompass increase of excessive purity and the capacity to manufacture abrupt junctions. Despite all the above benefits, there are a few obstacles as a first-rate one being that it's miles maximum flexible at the temperature of 600 °C and overhead many materials of substrates aren't thermally solid at those temperature. But, the improvement of plasma CVD and metalloorganics CVD in part offsets this problem. Additional obstacles are conditions of getting chemical precursor (the material of start) via excessive vapour pressures which it can be frequently risky and at instances extraordinarily toxics. The by-product of the CVD-reaction likewise are toxics and corrosives also it needs to counteracted, which it can steeply-priced operations. Also, many precursors for CVD, especially the metal-organics, are relatively expensive [17, 18].

4 Process Principle and Deposition Mechanism

Typically the CVD_s technique includes the subsequent stages [19, 20]:

1. Generation the activation gaseous reactant species.
2. Transference of the gaseous species to the reaction chamber.
3. Vaporous-reactants go through gases segment reaction forming intermediate species:
 - At high temperatures overhead decomposition temperature of intermediate species within side reactor, homogeneous-gases reaction can arise wherein the intermediate species go through next decomposition or chemical reactions, creating powders and unstable via-product within side the gases segment. The powder may accrue at the substrate-surfaces and can acts as crystallization centers, and via-product transference far from the deposition chamber.
 - At temperature under the separation of the intermediate segment, diffusion convection of intermediary types throughout border film (very thin film nearby substrate surfaces) arise. These intermediate species ultimately go through stages (4)-(7).
4. Absorptions of gaseous reactant on heat-substrate and heterogeneous reactions happens on the gases stable interface (heat substrates) which production the deposits and derivative species.
5. The deposit will be diffusing alongside the heat substrate surfaces forms the crystallization center and increase of the layers.
6. Gaseous via product eliminated from boundaries layer thru diffusion or convection.
7. The unreacts gaseous precursor and via product may transference far from the depositions chamber. Figure 1 indicates diagram instance of the important thing CVD stages for the duration of deposition.

The famous-precursors using within side the CVD technique are metals/alloys hydride, halide, and halo hydride, and metal-organic compound. Generally, metallic halide and halo hydride are greater stabling than the correspond hydride. The metalorganic-precursor provide the benefit of decrease reactions and deposition temperature than halide and hydride and are much less toxics and pyrophoric. However,

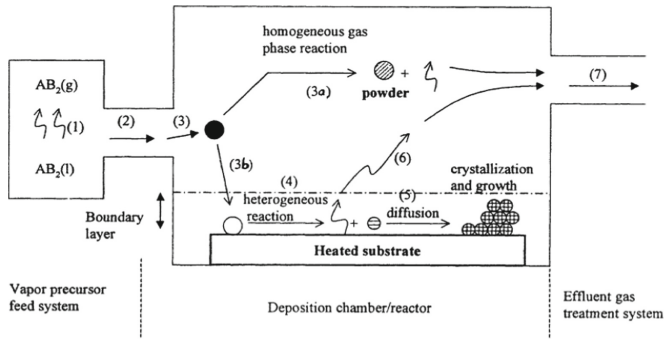


Fig. 1. A chart instance of important thing CVD steps for duration of deposition [19].

maximum metalorganic unstable liquid and requires unique managing of the deposition-pressure. The choice standards of appropriate chemical-precursors for coatings program of the precursors: (a) It stay-stable at room temperatures. (b) It has low vaporization temperatures and high saturation of vapor pressures. (c) It could generate vapor high stability at low temperatures (for example; earlier than decompose or reacts at the high-temperatures). (d) It has appropriate deposition-rate. Low deposition rate to very thin layers application (for example; semiconductor industry) and high deposition rate for thick coating application. (e) undertakes decomposition or chemical reactions at temperatures under the melt temperatures and phases transformation of the substrates relying at the engineering applications. For example, the depositions of high temperatures shielding coating (the oxide) and difficult coating can using halide which generally tends to reacting at high temperatures and provide higher depositions rate. The deposition of the thins-film (Si, Ga-As and SiO₂) can utilize hydride in addition to halide for low-temperatures deposition and lower increase rate for semiconductors application. (f) It has low toxicities, explosive and very-inflammable for protection of managing chemical compounds and eliminating the underacted precursors. This is mainly suitable for huge scales commercial application. For example, metal-organic precursor that commonly few toxic, pyrophorics and dangerous than hydride. (g) Its costs effective for the thin layers/coatings deposition. (h) It's with no trouble to be had at high-purity electronics grade commercially [21, 22].

5 Establishment of the Test Framework

CVD coating process and processing parameters affect the nucleation and growth which in turn influence the microstructure and the properties of the coatings. The kinetics of the nucleation and crystal growth are influenced by the deposition temperature and the concentration of the reactive species. The deposition processes can be divided into two main groups. The homogeneous nucleation occur at high temperature and reactant concentration. This results in the formation of stable solid reaction product in the form of fine powder. The ultra fine powder that nucleated in gas phase will deposit on the surface and may inhibit the nucleation and crystal growth, which will lead poor coating adhesion. Heterogeneous reactions, result in the adsorption of monomers, which diffuse

to the preferred sites to form stable nuclei. Growth will occur by the addition of adsorbed monomers to form crystallites. Heterogeneous reactions can lead to various structures depending on surface quality, and processing parameters. If the substrate surface is not perfectly pure, polycrystalline growth can be observed. This type of nucleation occurs at different substrate surface sites leading to the growth of islands which coalesce to form a polycrystalline layer. The inappropriate configuration of the deposition process can lead to amorphous layer formation. This structure tends to form at low substrate temperatures where the mobility of the absorbed species is relatively low.

In order to identify the quality of the coatings and support the production by the test results, complex material testing methods are required. These investigations should reveal the microstructure, morphology and micro-hardness of the coating and life expectancy for different stresses. A critical phase in the characterization of coatings, produced by different methods is the proper sample preparation. Cross-sectional grinding is essential for microstructure analysis, where a perfectly polished surface required. This polished surface is already suitable for scanning electron microscopic (SEM) analysis. Using backscattered electron imaging, we can determine the thickness of the layers, the heterogeneous nature of the reaction, and the relationship between substrate and deposited coating. With high-resolution secondary electron imaging, we can observe the morphology of the coating formed on the surface, including the crystals that make up the layer. If an energy-dispersive X-ray analyzer (EDS) is also available attached to the SEM, then the elemental composition of the substrate and the layers on the polished surface can be determined. If we measure the elemental composition in each pixel and plot it in the image, we can also create an elemental map, as shown in Fig. 2.

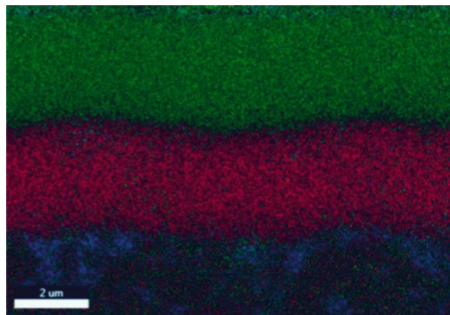


Fig. 2. Element map collected on a polished surface, where blue indicates the WC substrate, TiC and Al₂O₃ layers marked with red and green, respectively.

The purpose of measuring hardness on the polished surface is to determine the degree of hardening and the hardness gradient between the substrate and the coating. If the hardness of the coating is relatively high compared to the substrate, it will lead to surface deformation during stress. Therefore, it is advisable to use materials in the same hardness range for coating. The value of hardness depends to a large extent on the geometry of the measuring head used, to a lesser extent on its material. The Vickers-method is the most common in materials science studies. The measuring head used in Vickers hardness measurement is a tetragonal diamond pyramid that leaves characteristic

square imprints in the material. From the diameter of the imprint, the hardness of the coating can be determined, and from the length of the cracks around the impression, the so-called stress intensity factor (KIC) can be also determined see Fig. 3.

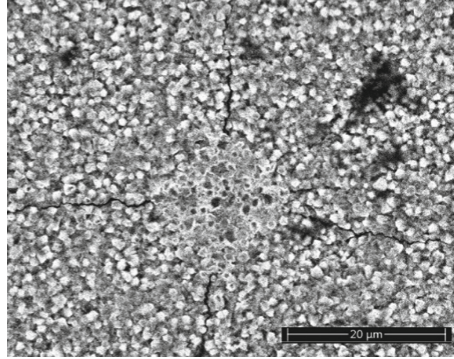


Fig. 3. Impression after hardness measurement, and the evolved cracks at the corners of the pyramid on the surface of a TiN coating.

In order to determine the life expectancy of coatings tribological model tests are required. The purpose of these tests is to design a structure that is optimal for longevity and operation, and to determine the data needed to define maintenance periods, and to control the quality of materials. The most commonly used tribological model testing equipment is the well-known pin-on-disc tribometer. During the model test, the applied load force, temperature, material quality and diameter of the pin and the disc, and the type of friction (dry friction or any lubricant or abrasive suspension applied) should be defined. After the pin-on-disc model test we can determine the fluctuation of the value of the coefficient of friction, the mass of the material worn from the specimen, the magnitude of the stress between the contact surfaces, and analyze the wear cross section to describe the nature of the wear mechanism that occurs during the test. It is technologically important that the disc should be the coated piece in the model test. If the pin is harder than the counterpart, it wears a ditch in the surface of the disc, which affects the wear and friction conditions. By measuring the surface roughness of the wear mark formed on the surface of the disc, we can obtain tribologically important information as follows. When studying the different friction and wear mechanisms, great attention should be paid to the correct interpretation of the surface roughness parameters. The technical content of the average surface roughness R_a is not essential for the interpretation of a given profile and provides only general information from a practical point of view. The most commonly used parameter to characterize different surfaces, along with the roughness height R_z . Regarding the average roughness, it should be mentioned that it can remain almost constant at different measurement locations, it does not provide information on the magnitude of the protruding roughness peaks forming the surface. The maximum peak height (R_p) of the profile gives the average value of the measured profile peaks, but its information content can be questioned, as a local profile deviation can affect the measurement result. If the R_p value is smaller, it indicates a surface divided

by strong and only narrow valleys, while at higher R_p values it is characterized by a much higher intensity abrasion profile with wide valleys and pointed peaks. The quality of the roughness profile is indicated by the R_p / R_z ratio. If the value of the quotient is greater than 0.5, the sliding zone forming the surface profile is needle-like, however, if a rounded roughness profile of less than 0.5 is more favorable from the point of view of friction. From a tribological point of view, the “critical” value of R_p / R_z is defined as 0.3, below which the surface is considered tribologically advantageous, even above these values it is considered tribologically unfavorable.

6 Research Directions in the Developing CVD Coatings Topic

The basic aim of the research, which started at the end of 2020, is to improve the properties of cutting tools and stamping dies by developing new CVD coating recipes and a new approach of coating technologies. The research process for the next 4 years will therefore focus on improving the mechanical properties of these two tools.

6.1 Improvable Mechanical Properties

In the case of tools used in pre-production and component production processes, increasing abrasion resistance can be considered a basic aim. The abrasion resistance extent of tools is in parallel with their lifespan. It is important to note that in the case of cutting tools, the expression ‘tool life’ is used instead of ‘lifetime’. Tool life is the time range passed with effective cutting between two sharpening of the tool. Nowadays, in the time of the monopoly of CNC technology, this definition has changed and it stands for the time range passed with effective cutting between two edge changes of the tool. In the case of tools developed for CNC machine tools, it is a shocking fact that by applying the technological parameters issued in the tool manufacturer’s catalogue, only a tool life of 10–15 min can be reached. In this amount of time, such an extent of crater wear and flank wear is developed, that the tool loses its cutting ability. With the help of new CVD coating recipes, that ensure higher abrasion resistance, the tool life of cutting tools can be increased. If the tool life of the tool can be increased, the CNC machine tools won’t have to be stopped as often in order to change tools. The time of tool change counts as time out of production, therefore, the aim is to minimize this period of time. It is likely however, that in case the result of our research is used by tool manufacturing companies interested in international trade, they will not focus on increasing the tool life, but will offer a higher set of technological parameters to customers, keeping the 10–15-min reference value. The reason for this is that in most cases, only a small fraction of the total cost of production is the cost of the tool, therefore, tool manufacturers recommend higher feed rate, spindle speed and depth of cut values.

In case of stamping dies, we actually mean lifetime. Lifetime is based on the number of finished products that the tool can produce. Thus, while the effective cutting time was the basis for determining the lifetime of cutting tools, the number of pieces produced is taken into account for stamping dies. When designing stamping dies, it is an interesting task to determine the structural material that makes up the tool. Depending on whether we want to carry out individual production, series production or mass production with the

tool, we have to use different structural materials. However, usually the more abrasion-resistant a material is, the more expensive it is. For this reason, the use of new types of CVD coating recipes would have complex advantages, as the coatings would allow us to control the life expectancy even if a cheaper structural material is used. The life cycle of a stamping die ends when the product geometry to be formed by it is somewhere outside the tolerance field. The primary reason for this is tool wear. It is visible therefore, that by using new CVD recipes and technologies, we could change the lifetime of stamping dies in a much wider spectrum than at present. By using a cheaper structural material and a CVD recipe matched to the serial number, we can optimize our tool life cost. This is also important because, unlike cutting tools, stamping dies are extremely expensive, therefore, tool cost is a significant factor in this case.

6.2 Improvement Possibilities of Coating Technologies

The other goal of our research process is to develop a new concept of CVD coating equipment. In this research phase, we need to focus on the combined improvement of several factors in order for our equipment to have a complex advantage system compared to the solutions currently available on international markets.

One such focus point is to expand the capacity of the equipment. A key advantage of CVD coating processes is that the process taking place in the reactor is essentially unaffected by multiple components placed in the correct position. For this reason, as a development direction, one of our goals in the field is to develop a reactor geometry and a holder console that achieves optimal space utilization. The more tools we can coat at the same time, the lower the total coating cost will be. As a result, the cost of tool production can be reduced. The design of the holder console that holds the components is also an important development direction. The basic goal of this direction is to create as much universality as possible. Our research goal is to develop a holder console product family that can handle mounting problems due to different component sizes and geometries as flexibly as possible. For the product family, a construction and production planning process based on group technology must be implemented in order for us to be able to store the typical construction and production parameters of all family members in a complex database.

Coating thickness is also an important development direction. Currently, normally 6–10 μm thick coatings are made with CVD technology. If it is possible to reduce the coating thickness by 1–2 μm without deteriorating the coating properties while maintaining the stability of the coating, we can achieve significant cost savings in the case of mass-produced cutting tools. However, in order to reduce the coating thickness, it is necessary to improve the cohesion properties, since the forces and heat effects generated in the immediate vicinity of the machining tear a thinner coating off the base surface of the tool faster. This development direction therefore imposes a double requirement on us; we must improve the cohesion properties in parallel with developing the technology with which we can produce thinner coatings.

7 Conclusion

The authors of the paper are in the first phase of a research process, the basic goal of which is to produce and test new CVD formulations in order to improve mechanical properties in cutting tools and stamping dies, furthermore, to develop a new concept of CVD coating equipment, for which equipment a holder console family will be developed through construction and production planning operations based on group technology. The article provides a detailed analysis of recent research findings related to CVD technology, while it also presents the currently visible development trends, and summarizes the test system used in the research processes. The article provides an excellent basis for the application of international research results and for the optimization of the developed test system in the next phases of research. Another goal is to create an industry 4.0 compliant data collection system. The system will predict changes in the mechanical properties of the coating based on proposals for changes in the coating compositions.

Acknowledgment. This work was supported by the TKP2020-NKA-10 project financed under the 2020–4.1.1-TKP2020 Thematic Excellence Program by the National Research, Development and Innovation Fund of Hungary.

References

1. Plankovskyy, S., Breus, V., Voronko, V., Karatanov, O., Chubukina, O.: Review of methods for obtaining hardening coatings. In: Nechyporuk, M., Pavlikov, V., Kritskiy, D. (eds.) ICTM 2020. LNNS, vol. 188, pp. 332–343. Springer, Cham (2021). https://doi.org/10.1007/978-3-030-66717-7_28
2. Tarazona, A., Domínguez, T., Oo, Z., et al.: Hot wire chemical vapor deposition for silicon photonics: An emerging industrial application opportunity. *J. Thin Solid Films* **676**(1), 26–30 (2019). <https://doi.org/10.1016/j.tsf.2019.02.048>
3. Ohring, M.: *Materials Science of Thin Films*. Elsevier, Singapore (2006)
4. Martin, P.M.: *Handbook of Deposition Technologies for Films and Coatings*. Elsevier, Amsterdam (2010)
5. Lee, S., Baek, G., Lee, J.H., et al.: Molecular layer deposition of indicone and organic-inorganic hybrid thin films as flexible transparent conductor. *Appl. Surf. Sci.* **525**, 146383 (2020). <https://doi.org/10.1016/j.apsusc.2020.146383>
6. Kai, X., Hao, L., Yan, C., et al.: Preparation of T-carbon by plasma enhanced chemical vapor deposition. *Journal of Carbon* **157**, 270–276 (2020). <https://doi.org/10.1016/j.carbon.2019.10.032>
7. Apera, T., Yama, F., Beh, K.: Influence of temperature and nickel catalyst on the structural and optical properties of indium oxide nanostructured films synthesized by chemical vapor deposition technique. *Mater. Sci. Semicond. Process.* **132**, 105925 (2021). <https://doi.org/10.1016/j.mssp.2021.105925>
8. Bhaskar, B.: Synthesis of Cu catalyzed chemical vapor deposition grown Cu-CNFs on less porous graphite powder. *Mater. Lett.* **305**, 130828 (2021). <https://doi.org/10.1016/j.matlet.2021.130828>
9. Jones, M., Hitchman, L.: *Chemical Vapour Deposition: Precursors, Processes and Applications*. Royal Society of Chemistry, Cambridge (2009)

10. Zhang, Y., Wang, Q., Ramachandran, C.S.: Synthesis of carbon nanotube reinforced aluminum composite powder (CNT-Al) by polymer pyrolysis chemical vapor deposition (PP-CVD) coupled high energy ball milling (HEBM) process. *Diam. Relat. Mater.* **104**, 107748 (2020). <https://doi.org/10.1016/j.diamond.2020.107748>
11. Saketi, S., Olsson, M.: Influence of CVD and PVD coating micro topography on the initial material transfer of 316L stainless steel in sliding contacts – a laboratory study. *Journal of Wear* **388–389**, 29–38 (2017). <https://doi.org/10.1016/j.wear.2016.12.003>
12. Gao, S., Li, S., Zhang, S., et al.: Chemical vapor deposition of pyrolytic boron nitride ceramics from single source precursor. *Ceramics International* **43**(13), 10020–10025, 384 (2017). <https://doi.org/10.1016/j.ceramint.2017.05.016>
13. Ciprian, M., Xu, P., Chaemchuen, S., et al.: MoO₃ nanoparticle formation on zeolitic imidazolate framework-8 by rotary chemical vapor deposition. *Int. J. Microporous Mesoporous Materials* **267**, 185–191 (2018). <https://doi.org/10.1016/j.micromeso.2018.03.028>
14. Kainz, C., Schalk, N., Tkadletz, M., et al.: Thermo-physical properties of coatings in the Ti (B, N) system grown by chemical vapor deposition. *Surf. Coat. Technol.* **384**, 125318 (2020). <https://doi.org/10.1016/j.surfcoat.2019.125318>
15. Sharma, R., Pradhan, S., Bathe, R.: Design and fabrication of spiral triangular micro texture on chemical vapor deposition coated cutting insert using femtosecond laser machine. *Materials Today: Proceedings* **28**(3), 1439–1444 (2020). <https://doi.org/10.1016/j.matpr.2020.04.817>
16. Song, X., Wang, H., Wang, X., Sun, F.: Fabrication and evaluation of diamond thick film-Si₃N₄ brazed cutting tool by microwave plasma chemical vapor deposition method. *J. Mater. Process. Technol.* **291**, 117034 (2021). <https://doi.org/10.1016/j.jmatprotec.2020.117034>
17. Eckart, U., Danny, S.: Process behaviour of micro-textured CVD diamond thick film cutting tools during turning of Ti-6Al-4V. *Procedia CIRP* **87**, 25–30 (2020). <https://doi.org/10.1016/j.procir.2020.02.014>
18. Cherifia, A., Aouinea, M., Decams, M., et al.: Chemical vapor deposition (DLI-CVD) and characterization of multiphasic molybdate-based catalysts for propene oxidation. *Catal. Sci. Technol.* **12**(10), 3261–3271 (2022). <https://doi.org/10.1039/d1cy02021h>
19. Nalwa, H.S. (ed.): *Handbook of Nanostructured Materials and Nanotechnology*, vol. 1. Academic Press, San Diego (2000)
20. John, U., Michael, U.: Optical and electrical characterization of microwave power system chemical vapour deposited (MPS-CVD) graphene on Ni electroplated Cu foil at varying temperatures. *J. Vacuum* **182**, 109767 (2020). <https://doi.org/10.1016/j.vacuum.2020.109767>
21. Kern, K., Schuergraf, K.: *Handbook of Thin Film Deposition Processes and Techniques*. Noyes, Park Ridge (1988)
22. Xu, S., Zhang, L., Wang, B., Ruoff, R.S.: Chemical vapor deposition of graphene on thin-metal films. *Cell Reports Physical Science* **2**(3), 100372 (2021). <https://doi.org/10.1016/j.xcrp.2021.100372>



An Approach to Calculate Features of Laser Radiation Absorption in Beryllium and Aluminum Alloys for Smart Welding Processes

Volodymyr Korzhyk^{1,2} , Vladislav Khaskin^{1,2} , Sviatoslav Peleshenko^{1,2} ,
Volodymyr Shcheretskyi¹  , and Yevhenii Illiashenko¹ 

¹ E.O. Paton Electric Welding Institute of the National Academy of Science of Ukraine, 11 Kazymyra Malevycha Street, Kyiv 03150, Ukraine
shcheretskyi@nas.gov.ua

² Guangdong Welding Institute (Chinese-Ukrainian Paton Institute), 363 Changxing Road, Tian He, Guangzhou 510650, China

Abstract. The paper proposes an approach to determine the absorption of laser radiation in laser and laser-plasma welding, which can be applied as a basis to create a smart control system for these processes. The work shows that during the melting of light alloys, the fraction of absorbed laser radiation increases abruptly from ~ 20% for beryllium and up to two and more times for aluminum. The change of the radiation with a wavelength of $\lambda = 10.6 \mu\text{m}$ (CO₂ laser) to radiation with $\lambda = 1.06 \mu\text{m}$ (fiber or Nd:YAG laser) within welding of light alloys, its absorption increases in about 2,5 times. The usage of plasma melting in hybrid laser-plasma welding makes it possible to increase the penetration depth by 40–75% compared to laser welding, including by improving radiation absorption. To improve the absorption of radiation during the laser-plasma welding, the distance between the center of the anode region of the compressed arc of the non-consumable electrode and the axis of laser radiation should not exceed 1.0 mm. To establish a full-fledged hybrid laser-plasma process, this distance should not exceed 0.5 mm. Experimental verification of the calculated results for aluminum alloys 5083 (1561) and 7075 reveals calculation error is in the range of 15–20% makes it possible to apply the developed method to predict laser and laser-plasma welding of light alloys, including beryllium alloys.

Keywords: Laser radiation · Absorption · Welding · Hybrid · Laser-plasma · Light alloys

1 Introduction

One of the urgent problems of modern science and technology is the creation of smart industries and technologies. In particular, an urgent task is the development of smart welding technologies based on heat sources with a controlled concentration of thermal energy introduced into the metal [1, 2]. To implement such technologies, it is necessary

to use a smart automated system to monitor and process the information. This approach makes it possible to provide the required welding performance, the quality of the resulting welded joint [3], process stability joint [5], and reproducibility of the results [5]. In recent years, the laser [6] or hybrid laser-plasma source [7, 8] has increased usage as a controlled heat source for the welding of metallic materials [9, 10], the same approach was used for laser-arc process [11]. In laser-plasma welding, a focused laser beam with a compressed electric arc has the combined thermal effect on the metal being welded within the common heating zone [12].

At the same time, the regularities of the mutual effect of the laser-plasma heat source components and their joint effect on various metallic materials have not yet been studied enough [13, 14]. The study of the physics of the processes within the components' interaction of the laser-arc source of thermal energy and their combined effect on the welded metal, the development of appropriate mathematical models, and computer simulation of these processes are very urgent scientific and technical problems [15, 16]. These problems include the physical features study of hybrid laser-plasma welding of light alloys based on aluminum and beryllium [17]. This aims to enhance the process productivity by increasing the effective efficiency, i.e., increasing the ratio of the power of the heat source acting in the metal during welding to the total power of the compressed electric arc and laser radiation. One of the ways to increase the effective efficiency of welding is to reduce laser energy losses associated with the reflection of radiation from the welded surface [18].

In the paper the following tasks were solved:

- determination of the absorbing capacity of surfaces of aluminum and beryllium alloys depending on their heating temperature;
- determination of the distance effect between the anode region of the non-consumable electrode compressed arc and the axis of laser radiation on the efficiency of its absorption by the metal being welded;
- experimental verification of the distance effect between the anode region of the non-consumable electrode arc and the laser radiation axis on the penetration depth.

All of these made it possible to achieve the aim of the paper – to study the effect of concomitant heating provided by a compressed direct action electric arc on the conditions of the laser radiation absorption change by aluminum and beryllium alloys during their laser-plasma welding, and also the effect of the distance between the center of the anode region of the compressed arc of a non-consumable electrode and the axis of laser radiation on the reduction of laser energy losses.

2 Research Methodology

2.1 Physical Model

Laser-plasma welding, the same as laser welding, is characterized by the formation of a vapor-gas penetration channel in a welded metal. In the paper [19], the behavior of this channel during welding is described in detail. In particular, it was noted that on

its front wall there is a layer of molten metal, which suffers constant “perturbations” – the formation of curvature in the shape of a step, which periodically moves along the height of the channel. In this case, the removal of material from the front wall is carried out by layers via the step movement from upside to down. The probable explanation is an increase in the amount of molten metal layer on the front wall, formed by the radiation energy transition released by the wall into thermal energy, in combination with hydrodynamic processes in the weld pool.

It is known that part of the radiation energy is absorbed by the welded metal, and its part is reflected. The fraction of absorbed radiation is greater with higher the temperature of the metal. The melt formed on the front wall efficiently absorbs the radiation, however, due to the displacement in the welding process, the front part of the laser beam always hits the low heated metal, which leads to a decrease in the absorption coefficient (Fig. 1a). It is obvious to assume that local heating to certain temperatures of a rather small area of the welded metal, located directly in front of the steam-gas channel on the welding course, will significantly increase the absorption coefficient of laser radiation. For the laser-plasma welding performed according to the scheme shown in Fig. 1b, such local heating is provided by an electric arc of a non-consumable electrode. The goal is to achieve achieving minimum temperatures sufficient for the maximum possible increase in the radiation absorption coefficient, depending on the welding speed and geometry of the welded item.

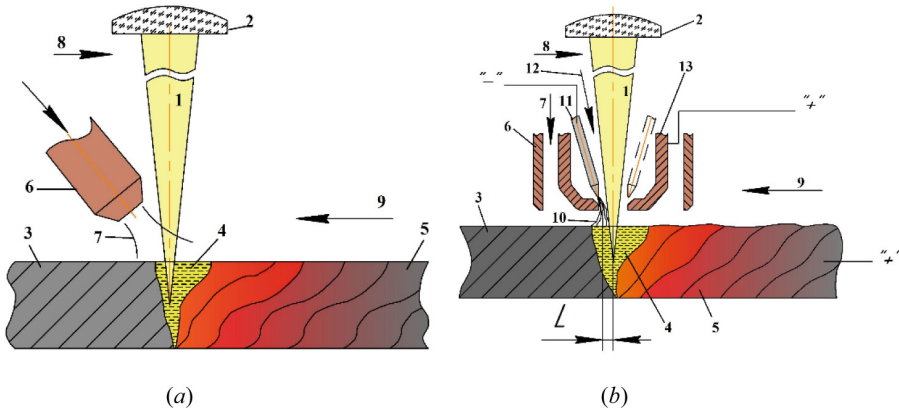


Fig. 1. Scheme of laser (a) and hybrid laser-plasma (b) welding: 1 – laser radiation; 2 – lens; 3 – base metal; 4 – welding pool; 5 – weld metal; 6 – protective nozzle; 7 – protective gas; 8 – gas protection of the lens; 9 – direction of welding; 10 – welding arc; 11 – non-consumable electrode; 12 – plasma gas; 13 – plasma nozzle; L – distance between the conditional point of the anode spot center and the laser radiation axis.

2.2 Mathematical Model

To determine the temperature dependence of the laser radiation absorption coefficient of metallic materials $A(T_s)$, consider the metal (aluminum) in the framework of the nearly

free electron model. In this case, according to the Drude–Zener formulas [20], for the real ϵ_1 and imaginary ϵ_2 parts of the complex permittivity of the metal at the laser radiation frequency $\omega = 2\pi c/\lambda$, where c is the speed of light, λ is the radiation wavelength, it is:

$$\epsilon_1 = 1 - \frac{\omega_p^2}{\omega^2 + \omega_c^2}, \tag{1}$$

$$\epsilon_2 \omega = 4\pi\sigma = \frac{\omega_c \omega_p^2}{\omega^2 + \omega_c^2}, \tag{2}$$

Here ω_p is the frequency of free electrons’ plasma oscillations of the metal; ω_c is the frequency numerically equal to the reciprocal relaxation time of conduction electrons. The value of the plasma frequency is determined by the formula:

$$\omega_p^2 = \frac{4\pi neN_e}{m_e^*}, \tag{3}$$

where e and m_e^* are the charge and effective mass of an electron in a metal [21].

The conduction electron concentration $N_e = V/\Omega$ is determined by the valency V and the atomic volume Ω . The valence value for aluminum was taken as three. The atomic volume was obtained on the basis of experimental data on the aluminum density given in [22]. In the limiting case of a constant field, when $\omega = 0$, the high-frequency optical conductivity σ turns into the static conductivity of the metal:

$$\sigma(0) = \frac{N_e e^2}{m_e^* \omega_c}. \tag{4}$$

The temperature dependence of the relaxation frequency ω_c for the considered metals in the solid-state is taken into account using the following formula [23]:

$$\omega_c = K' T^5 \int_0^{\frac{\theta}{T}} \frac{z^4 dz}{\exp(z) - 1}. \tag{5}$$

where θ is the Debye temperature; K' is a constant that includes the total scattering cross-section of an isolated atom, ion masses, ion density, Debye wavenumber, Debye temperature, and other universal constants [23].

The values ω_c and K' at room temperature for aluminum was taken in accordance with the data from [24], and for beryllium – [25]. For aluminum and beryllium in the liquid state, we took the experimental values from [26]. The calculated data is in Fig. 2.

3 Results and Discussion

3.1 Calculation Results

The temperature dependences in Fig. 2 have the characteristic gap at the melting temperature of the metal T_m . According to formulas (1) and (2), with usage (3)–(5), we are able to plot the real and imaginary parts of the complex permittivity for aluminum and beryllium at certain laser radiation frequency ($\lambda = 1,06 \mu\text{m}$) Fig. 3.

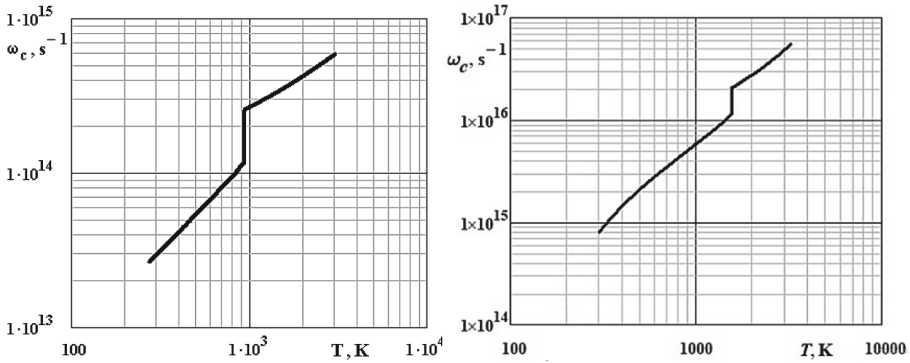


Fig. 2. Dependence of the relaxation frequency $\omega_c(T)$ [s^{-1}] on the temperature T [K] for aluminum (a) and beryllium (b).

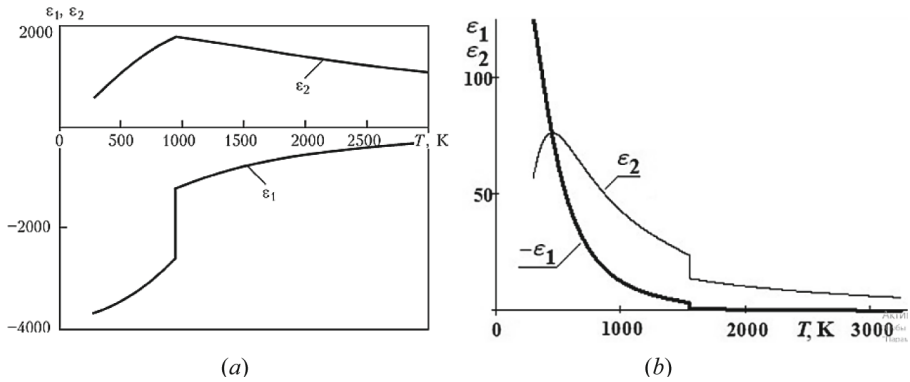


Fig. 3. Dependence of the real ϵ_1 and imaginary ϵ_2 parts of the complex permittivity of aluminum (a) and beryllium (b) on the temperature T [K].

For further calculations, it is convenient to take the real n and imaginary k parts of the complex refractive index of the metal at the laser frequency

$$\sqrt{\epsilon} = \sqrt{\epsilon_1 + i\epsilon_2} = n + ik, \tag{6}$$

by using the following formulas:

$$n = \sqrt{\frac{\sqrt{\epsilon_1^2 + \epsilon_2^2} + \epsilon_1}{2}}, \tag{7}$$

$$k = \sqrt{\frac{\sqrt{\epsilon_1^2 + \epsilon_2^2} - \epsilon_1}{2}}. \tag{8}$$

There are temperature dependences of the real and imaginary parts of the complex refractive index for aluminum and beryllium in Fig. 4.

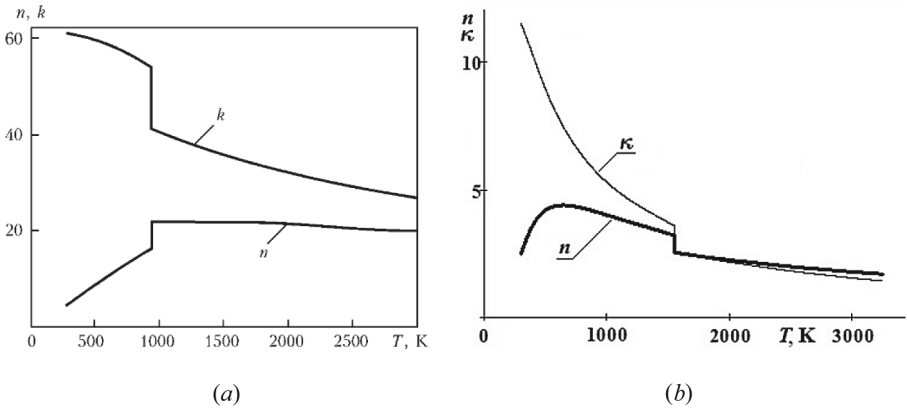


Fig. 4. Dependences of the real n and imaginary k parts of the complex refractive index of aluminum (a) and beryllium (b) on the temperature T [K].

Using the obtained values of n and k , we determine the absorption coefficient of laser radiation normally directed on a flat metal surface (absorption capacity) by the usage of well-known formula:

$$A = \frac{4n}{(1 + n)^2 + k^2} \tag{9}$$

in some cases, a more important parameter is the reflection coefficient (reflectivity), which can be determined by the formula

$$R = 1 - A = \frac{(1 - n)^2 + k^2}{(1 + n)^2 + k^2} \tag{10}$$

In Fig. 5a shown the calculations results of the temperature dependences for the CO₂ laser absorption coefficient for aluminum in the temperature range from room temperature to the metal boiling point T_b and above. Similar calculations were done to determine the absorptive capacity of the aluminum surface in the case of incident Nd:YAG laser radiation ($\lambda = 1,06 \mu\text{m}$) on it. They show the identical behavior of both dependences with a difference that the absolute values of the Nd:YAG laser radiation absorption coefficient are higher than those for CO₂ laser radiation (Fig. 5b). Similar results were obtained for beryllium also (Fig. 6).

Calculated absorption dependences for both types of radiation are in satisfactory agreement with the available experimental data [23, 24]. According to the dependencies shown in Fig. 5 and Fig. 6, to achieve the maximum values of the absorption coefficient, the welded metal surface in the operating area of laser radiation of both wavelengths (10.6 and 1.06 μm) should be heated to the boiling temperature T_b , however, heating up to the melting temperature T_m is enough for a sharp stepwise increase in the absorption capacity.

The comparative analysis (Fig. 5 and Fig. 6) shows that laser welding of beryllium has high energy efficiency at any wavelength of laser radiation.

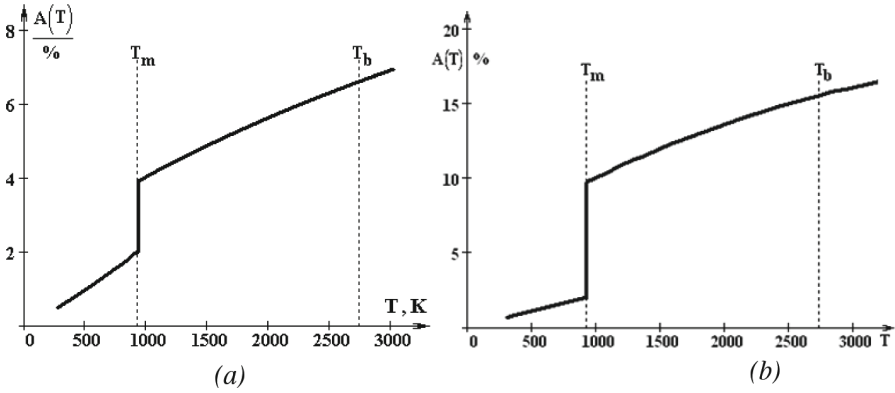


Fig. 5. Absorption capacity A [%] of aluminum on the temperature T [K]: (a) – wavelength $\lambda = 10.6 \mu\text{m}$; (b) – $\lambda = 1.06 \mu\text{m}$.

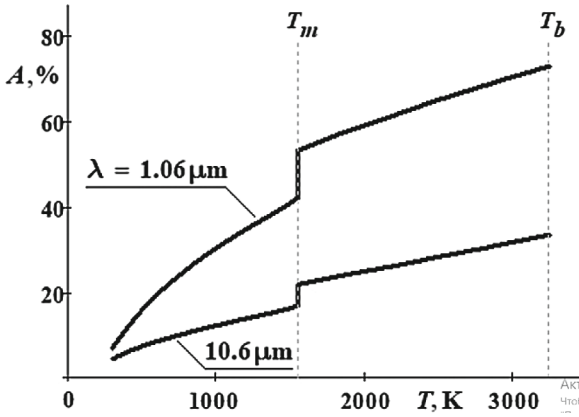


Fig. 6. Absorption capacity A [%] of beryllium on the temperature T [K] for wavelength $\lambda = 10.6 \mu\text{m}$ and $\lambda = 1.06 \mu\text{m}$.

To determine such mode parameters for the laser-plasma welding as the power Q_a of the plasma component and the distance L between the anode region of the non-consumable electrode arc and the laser radiation axis (Fig. 1), it is necessary to solve the corresponding heat equation. To simplify the problem, we consider the stationary case of an aluminum plate is being heating with δ thickness by an arc source, in this case, the heat flux determined as

$$Q_a = \eta I U, \tag{11}$$

where η is the efficiency of a non-consumable electrode arc (usually $\eta = 0.6$ is taken [27]); I is the welding current, A; U is the arc voltage, V.

To simplify the solution of determining the influence of the distance between the anode region of the non-consumable electrode arc and the laser radiation axis on the increase in the effective efficiency of welding, we used an assumption. We assumed

that the spatial distribution of the heat flux introduced into the sample is symmetrical to the axis perpendicular to its surface (i.e., symmetrical to the axis of a laser beam). In this case, the formulation for the mathematical model of sample's heating in the axisymmetric formulation coincides with the known model [28]. In this paper, there are given the initial and boundary conditions, as well as the solution by this model for heating of aluminum plate with a thickness of $\delta = 2$ mm.

Farther we used the model proposed in [28] to calculate the temperature propagation over a plate surface for the laser (heat source with power P_L) and laser-plasma (heat source with power $Q_a = P_L + P_{PL}$) welding. In this case, the welding speed v_w is taken into account within determining the time of heat source exposure, calculated by dependence $\tau = d/v_w$, where d is the size of the laser (d_L) and plasma (d_{PL}) heat source on the surface of the welded plate (we took $d_L = 1.5$ mm, $d_{PL} = 2.2$ mm).

The calculations result for the cases of laser-microplasma (1) and laser (2) welding of aluminum and beryllium plates (for the values of the radiation power $P_L = 400$ W, the welding current $I = 50$ A, the arc voltage $U = 26$ V) are in Fig. 7. The speed of laser-microplasma welding is $v_w = 240$ m/h, for the laser one is $v_w = 180$ m/h. The calculation results show that in the case of a steady-state hybrid welding process, the distance L between the center of the anode region of the compressed arc of the non-consumable electrode and the laser radiation axis should not exceed 0.9 mm. In this case, the compressed arc melts the surface of the welded plate and improves conditions of the laser radiation absorption (Fig. 5, 6).

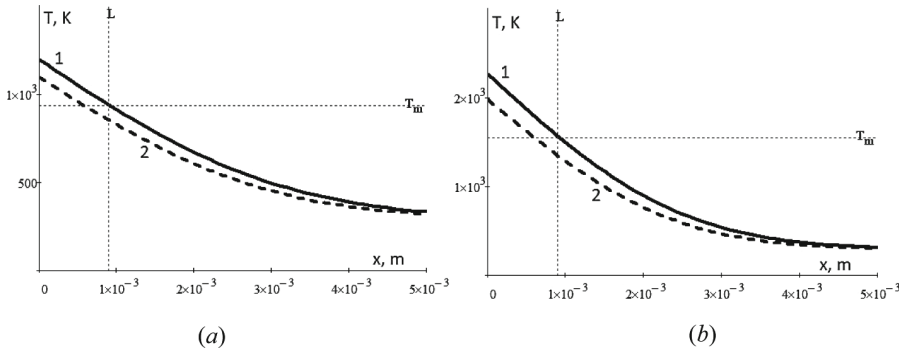


Fig. 7. Temperature distribution T [K] on the surface of aluminum (a) and beryllium (b) plates from the center of the weld in the opposite direction to the welding x [m]: 1 - laser-plasma welding: $P_L = 400$ W, $I = 50$ A, $v_w = 240$ m/h; 2 - laser welding: $P_L = 400$ W, $v_w = 180$ m/h.

3.2 Experimental Study

The experiments verified the results of the proposed optimization method of the hybrid welding efficiency by correcting the distance L between the conditional point of the anode spot center and the laser radiation axis for 5083 (1561) and 7075 aluminum alloys samples with a thickness of $\delta = 2$ mm (performed with the integrated plasma torch of the

original design). In case of laser and hybrid welding, a fiber laser ($\lambda \approx 1.06 \mu\text{m}$) with a power of up to 2.0 kW was used with a power source (welding current up to 100 A) and the original plasma module. Hybrid laser-plasma test welding was performed with argon as plasma-forming and protective gas and gas speed flow of 4 m/min (240 m/h). The welding testing regime was: current $I = 50 \text{ A}$ and arc voltage $U = 26 \text{ V}$. Laser welding was performed at a speed of 3 m/min (180 m/h). The distance between the conditional point of the anode spot center and the laser radiation axis was varied within $L = 0\text{--}2 \text{ mm}$ due to the deflection of the compressed arc away from the laser beam by the plasma gas flow. The experiments' procedure included variations in the laser radiation power P_L with the weld depth h fixation (Fig. 8, 9).

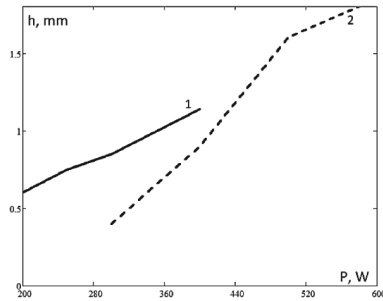


Fig. 8. Penetration depth h [mm] of 5083 alloy samples ($\delta = 2 \text{ mm}$) on the radiation power P_L [W] of the fiber laser welding: 1 – laser-arc ($v_w = 4 \text{ m/min}$, $I = 50 \text{ A}$, $U = 26 \text{ V}$); 2 – laser ($v_w = 3 \text{ m/min}$).

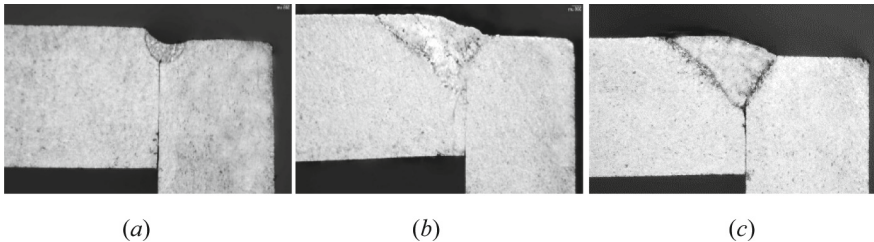


Fig. 9. Cross sections of welds made by laser (a) and laser-plasma (b), (c) welding of 7075 alloy with mode parameters: (a) $P_L = 300 \text{ W}$, $v_w = 3 \text{ m/min}$; (b) $P_L = 300 \text{ W}$, $I = 50 \text{ A}$; $U = 26 \text{ V}$, $v_w = 4 \text{ m/min}$, $L = 0.6 \text{ mm}$; (c) $P_L = 300 \text{ W}$, $I = 50 \text{ A}$, $U = 26 \text{ V}$, $v_w = 4 \text{ m/min}$, $L = 0.4 \text{ mm}$.

4 Conclusion

Analysis of the experimental test shows the following results. There observed the separate action of laser radiation and plasma at $L > 0.9\text{--}1.0 \text{ mm}$. Their joint action is observed at $L < 0.9 \text{ mm}$. A full-fledged hybrid laser-plasma process took place at $L < 0.5 \text{ mm}$. An example of the parameter L effect on the depth of weld and its formation is in Fig. 9. In

case of laser welding of 7075 alloy at $P_L = 300$ W, $v_w = 3$ m/min, the penetration depth is $h \approx 0,4$ mm (Fig. 9a). In the case of laser-plasma welding in the mode $P_L = 300$ W, $I = 50$ A, $U = 26$ V, $v_w = 4$ m/min and L parameter value – 0.6 mm, the penetration depth is $h \approx 0,8$ mm (Fig. 9b). One can see in Fig. 9b that the laser radiation is focused to the right, while the plasma arc is slightly shifted to the left. In the case of laser-plasma welding in the same mode at $L = 0.4$ mm (the displacement of the plasma arc to the left side decreases), the penetration depth increases up to $h \approx 1.0$ mm (Fig. 9c), the formation of the upper bead is also improved. The effect of the plasma component of the hybrid process led to an increase in the penetration depth by 30–60% without taking into account the variation in welding speed (Fig. 9). At the same welding speeds, it is possible to predict an increase in the penetration depth of the hybrid by 40–75% compared to the laser process. The heat distribution along the depth of the welded plate is considerably close to the heat distribution over a surface. According to Fig. 7, at $PL = 400$ W in the laser and laser-plasma processes, the change in penetration depth (at the melting temperature T_m) should be $\sim 35\%$. According to Fig. 9, the experimentally obtained value is $\sim 30\%$. The calculation error is assumed to be close to 15–20% this is acceptable for technological calculations. The results of the study are suitable for predicting laser and laser-plasma welding of aluminum and beryllium alloys. The assessment of the laser radiation absorption during its interaction with the surface of light metals (aluminum, beryllium) became the base of the prediction method of the penetration depth for laser and laser-plasma welding, as well as to visualize the L parameter effect on the components' position of the laser and plasma in the hybrid process. The technique is the basis for a smart automated system to monitor and process information during laser and hybrid welding. As a result of computational experiments, it is stated that at the melting temperature of light alloys, the fraction of absorbed laser radiation increases rapidly to $\sim 20\%$ for beryllium and up to above 2 times for aluminum. The change in radiation wavelength from $\lambda = 10.6 \mu\text{m}$ (CO_2 laser) to $\lambda = 1.06 \mu\text{m}$ (fiber, disk or Nd:YAG laser) for light alloys welding, the laser radiation absorption increases about 2.5 times. The usage of plasma melting in the hybrid laser-plasma welding increases the penetration depth by 40–75% compared to laser one, including through improved radiation absorption. To improve the radiation absorption, the distance between the anode region center of the non-consumable electrode compressed arc and the axis of laser radiation should not exceed 1.0 mm. To provide the full-fledged hybrid laser-plasma process, this distance should not exceed 0.5 mm. Hybrid laser-plasma welding improves the formation of the upper weld bead compared to laser welding. It is stated that reduction of the distance between the anode spot center and the axis of laser radiation improves the quality of weld formation and increases the penetration depth. The calculation method error (15–20%) is considered acceptable to develop smart laser and laser-plasma welding system.

Acknowledgment. The authors express their deep gratitude to Volodymyr Sydorets, his ideas became the theoretical basis of this research.






References

1. Kusano, K., Watanabe, H.: Recent trends in development of high-efficiency TIG welding; high-deposition TIG welding and ultranarrow-gap TIG welding. *Weld. Int.* **16**(12), 986–991 (2002). <https://doi.org/10.1080/09507110209549651>
2. Moglia, F., Raspa, A.: New trends in laser beam welding: how automotive applications are driving the future of laser technologies. *Photonics Views* **17**(5), 26–29 (2020). <https://doi.org/10.1002/phvs.202070508>
3. Reisgen, U., Krivtsun, I., Gerhards, B., Zabirov, A.: Experimental research of hybrid welding processes in combination of gas tungsten arc with CO₂-or Yb:YAG-laser beam. *J. Laser Appl.* **28**, 022402 (2016). <https://doi.org/10.2351/1.4944096>
4. Akhonin, S.V., Belous, V.Y., Selin, R.V.: Electron beam welding, heat treatment and hardening of beta-titanium. *IOP Conference Series: Materials Science Eng.* **582**(1), 012050 (2019). <https://doi.org/10.1088/1757-899X/582/1/012050>
5. Kritskiy, D., Pohudina, O., Kovalevskiy, M., et al.: Powder mixtures analysis for laser cladding using OpenCV library. In: Nechyporuk, M., et al. (eds.): *Integrated Computer Technologies in Mechanical Engineering – 2021. LNNS*, **367**, pp. 924–937. Springer, Cham (2022). https://doi.org/10.1007/978-3-030-94259-5_72
6. Reisgen, U., Zabirov, A., Krivtsun, I., Demchenko, V., Krikent, I.: Interaction of CO₂-laser beam with argon plasma of gas tungsten arc. *Welding in the World* **59**(5), 611–622 (2015). <https://doi.org/10.1007/s40194-015-0236-1>
7. Shelyagin, V., Krivtsun, I., Borisov, Y., et al.: Laser-arc and laser-plasma welding and coating technologies. *The Paton Welding J.* **8**, 44–49 (2005)
8. Berdnikova, O., Poznyakov, V., Bushma, O.: Laser and hybrid laser-arc welding of high strength steel N-A-XTRA-70. *Mater. Sci. Forum* **870**, 630–635 (2016). <https://doi.org/10.4028/www.scientific.net/MSF.870.630>
9. Krivtsun, I.V.: Modelling hybrid plasma-laser processes and integrated plasmatrons. *Weld. Int.* **18**(4), 268–276 (2004). <https://doi.org/10.1533/wint.2004.3253>
10. Khaskin, V.Y., Korzhyk, V.M., Bernatskii, A.V., et al.: Features of synergistic effect manifestation in laser-plasma welding of SUS304 steel, using disc laser radiation. *Paton Welding Journal* **04**, pp. 25–29 (2020). <https://doi.org/10.37434/tpwj2020.04.04>
11. Seyffarth, P., Krivtsun, I.V.: *Laser-arc Processes and their Applications in Welding and Material Treatment*. CRC Press, New York (2002)
12. Krivtsun, I.V., Khaskin, V.Y., Korzhik, V.N., Luo, Z.: Industrial application of hybrid laser-arc welding (Review). *The Paton Welding J.* **7**, 41–46 (2015). <https://doi.org/10.15407/tpwj2015.07.07>
13. Bushma, O.: State-of-the-art of hybrid laser-plasma welding (Review). *The Paton Welding J.* **8**, 18–25 (2015). <https://doi.org/10.15407/tpwj2015.08.04>
14. Hu, L., Huang, J., Liu, C., et al.: Effects of coupling between the laser plasma and two arcs on metal transfer in CO₂ laser double-wire MIG hybrid welding. *Opt. Laser Technol.* **105**, 152–161 (2018). <https://doi.org/10.1016/j.optlastec.2018.02.044>
15. Xu, X., Song, G., Zhao, S., Liu, L.: Effect of distance between the heat sources on energy transfer behavior in keyhole during laser-GTA welding titanium alloy. *J. Manuf. Process.* **55**, 317–325 (2020). <https://doi.org/10.1016/j.jmapro.2020.04.041>
16. Zhu, Y., Cai, Y., Wang, M.: Effects of He content in shielding gases on high-efficient hybrid laser arc welding with C-276 filler metal. *J. Mater. Process. Technol.* **299**, 117367 (2022). <https://doi.org/10.1016/j.jmatprotec.2021.117367>
17. Bunaziv, I., Akselsen, O.M., Ren, X., et al.: Laser beam and laser-arc hybrid welding of Aluminium alloys. *Metals* **11**(8), 1150 (2021). <https://doi.org/10.3390/met11081150>

18. Sokolov, M., Salminen, A.: Improving laser beam welding efficiency. *Phys. Procedia* **6**(09), 559–571 (2014). <https://doi.org/10.4236/eng.2014.69057>
19. Fetzer, F.: Fundamental investigations on the spiking mechanism by means of laser beam welding of ice. *J. Laser Applications* **1**(30), 012009–1–012009–9 (2018). <https://doi.org/10.2351/1.4986641>
20. Noskov, M.M.: Optical and magneto-optical properties of metals. UNTs AN SSSR, Sverdlovsk (1983) [in Russian]
21. Kiselev, A.I., Akashev, L.A., Kononenko, V.I.: Effective mass of electrons in the alloys of aluminum, cesium and binary system Al-3 at. % Ce. *Zhurnal Tekhnich. Fiziki* **74**(3), 20–23 (2004)
22. Zinoviev, V.E.: Thermal Properties of Metals at High Temperatures. Metallurgiya, Moscow (1989). [in Russian]
23. Ujihara, K.: Reflectivity of metals at high temperatures. *J. Appl. Physics* **43**(5), 2376–2383 (1972). <https://doi.org/10.1063/1.1661506>
24. Ordal, M.A., Long, L.L., Bell, R.J., et al.: Optical properties of the metals Al, Co, Cu, Au, Fe, Pb, Ni, Pd, Pt, Ag, Ti and W in the infrared and far infrared. *Appl. Optics* **22**(7), 1099–1119 (1983)
25. Chi, T.C.: Electrical resistivity of alkaline earth elements. *J. Phys. Chem. Ref. Data* **2**(8), 439–497 (1979). <https://doi.org/10.1063/1.555599>
26. Korkmaz, S.D., Korkmaz, S., Resuloglu, F.: A comparative study of electrical resistivity of liquid alkaline earth metals. *AIP Conference Proceedings* **899**, 649–649 (2007). <https://doi.org/10.1063/1.2733390>
27. Dupont, J.N., Marder, A.R.: Thermal efficiency of arc welding processes. *Weld. J.* **74**, 406s–416s (1995)
28. Khaskin, V.Y., Korzhik, V.N., Sydorets, V.N., et al.: Improving the efficiency of hybrid welding of aluminum alloys. *The Paton Welding J.* **12**, 14–18 (2015). <https://doi.org/10.15407/tpwj2015.12.03>



Determination of the Composite Products Moulding Process Parameters with Regulated Degree of Curing

Andrii Kondratiev¹ (✉) , Oleksii Vambol^{1,2} , Anton Tsaritsynskyi² ,
Maryna Shevtsova² , and Tetyana Nabokina² 

¹ O.M. Beketov National University of Urban Economy in Kharkiv, 17 Marshala Bazhanova Street, Kharkiv 61002, Ukraine
andrii.kondratiev@kname.edu.ua

² National Aerospace University “Kharkiv Aviation Institute”, 17 Chkalova Street, Kharkiv 61070, Ukraine

Abstract. Reduction of the time of manufacturing of the composite products of various applications and decrease in energy and labor costs is now a topical issue. The paper presents the results of studies of the main physical-chemical processes occurring in the polymeric composite material during moulding at the heating stage. A model is proposed which allows us to determine the degree of curing of the material at any time at the given temperature and to choose the heating rate of the composite package from the condition of achieving the given degree of curing with the minimum expenditure of time. Occurrence of stresses in the composite package at the heating stage has been studied. It is shown that stress condition at the stage of heating of the composite package is associated with shrinkage in the material. At the initial stage of the heating process, stresses have negative values. When the degree of curing reaches 60...70%, stresses take a positive value. It is shown that the values of stresses at the first stage depend on the heating rate. Thus, the heating rate should be maximum until the degree of curing reaches 60...70%, since shrinkage stresses decrease with the heating rate rising. At the final stage, because of occurrence of the temperature stress condition, the heating rate should be reduced. It is shown that values of stresses related to shrinkage of the material depend on the heating rate; with its increase from 0.5 °C/min to 3 °C/min the values of shrinkage become 3–4 times lower, which is associated with the transition from viscous-flow to solid state within a short period of time. Consequently, the method for determining the temperature and time of moulding for the binder on condition of reaching of the regulated degree of curing with the minimum expenditure of time has been developed.

Keywords: Heating rate · Shrinkage of polymeric material · Temperature stresses · Minimum expenditure of time

1 Introduction

The modern polymeric composite materials (PCM) and structures made of them are increasingly used in the construction sector [1, 2]. Usage of these materials allows to

reduce the weight of building structures, increase corrosion stability and resistance to the impact of adverse climatic factors, extend the overhaul periods, perform repairs and strengthen the structures with the minimum expenditure of resources and time [3, 4]. Products for the construction sector represent about 30% of the global PCM output (about 4 mln tons) [5]. Even now certification of the buildings and structures in accordance with the normative parameters of ISO and Eurocode is possible only with the use of high-quality PCM and modern construction technologies which guarantee maximum safety of an object, its energy efficiency and environmental compatibility [6, 7]. The main areas of PCM application (except traditionally prevailing aerospace industry [8, 9]) are mechanical engineering, power generation sector, manufacturing of sports and leisure goods and healthcare products [10–12]. Currently, increase in the efficiency of the technology of production of structural elements of PCM is associated with high energy costs [13, 14]. In view of this, high importance is given to implementation of the methods to optimize the technology of PCM manufacturing [15]. Optimized mode of heat treatment of PCM and control over all stages of process of their moulding will allow reducing heat treatment cycle and electricity costs due to optimization and control of processes of impregnation and heat treatment combined with gas release kinetics.

Taking the above into account, objective of the work is to develop a method for determining the temperature-time dependence of the moulding process to obtain composite products with the regulated degree of curing for the minimum period of time.

2 Literature Review

During the stage of heating of the PCM package and at the stage of isothermal holding, physico-chemical processes forming the product structure and properties occur in the moulded material. At this stage, viscosity of the binder, upon reaching of the gelation point, begins to increase continuously, with the transition from viscous-flow to solid aggregate state. The change in the binder viscosity is closely related to the increase in the degree of curing (conversion) and molecular weight of the polymer. The degree of curing and dynamics of its change play an exceptional role at the stage of material heating, since from a certain point in time the viscosity reaches the value at which the binder acquires mechanical characteristics allowing it to perceive and transmit the load [16]. Therefore, there is a problem of determining the degree of curing at any time. The value of viscosity and the rate of its change define the PCM properties. The problems of chemical transformations in the binder and release of volatile products are solved in [17, 18]. Nevertheless, the effect of temperature on the PCM characteristics in the process of curing was not taken into account. The results of [19–21] allowed simulating, controlling and regulating the curing process. However, occurrence of the thermal stress-strain behavior was not considered. The phenomena of relaxation and creep occurred in the composite at the stage of temperature holding and cooling were discussed in [22, 23], but distribution of the thermal field in the process of curing was not studied in these papers. Temperature phenomena participate in the occurrence of stresses and deformations at the stage of heating along with shrinkage according to [24]. It is shown that temperature stresses become comparable with shrinkage stresses upon reaching the material viscosity corresponding to 60...70% conversion in the binder. The papers [25, 26] describing the occurrence of stress-strain behavior at the stage of PCM heating to the polymerization

temperature based on experimental studies are of some interest. A particular case of the composite curing by the autoclave method is considered in [27]. In the process of work with prepregs, the issues of optimal technological modes ensuring their regulated quality are solved [28, 29], and the modes of processes are ambiguously harmonized with each other. To determine the degree of curing, there is a number of methods, which describe the process. The Carothers equation, the Arrhenius equation and equations obtained by the approximation of experimental data [16, 30] are used quite often. Unfortunately, each of these methods takes into account the individual factors. The Carothers equation takes into account the molecular structure only, neglecting the kinetics and physics of the process. The results obtained on its basis cannot directly reflect the change in the degree of curing depending on parameters of the moulding process (temperature and time), so they are of little use in production conditions. The Arrhenius equation, which takes into account the process kinetics and gives a complete picture of the change in the degree of curing depending on temperature, is often used for the determination of the degree of material curing. Nevertheless, using the Arrhenius equation, the result can be obtained with a certain degree of accuracy, because of approximate values of the activation energy. In addition, the dependencies for determining the degree of polymerization obtained from these equations are quite difficult to implement in the production process. First of all, this is due to sufficiently large range of resins, hardeners, modifiers and other components of the binder. That in turn leads to a large number of experiments to determine the required design parameters. In most cases, empirical dependences are used to determine the degree of polymerization and describe the kinetics of the curing process [16, 30]; they often include the main parameters of the curing process. However, the dependencies obtained by approximating the experimental data do not fully reflect the mechanism of curing.

3 Research Methodology

To determine the degree of the PCM polymerization, we use the relation derived from the Arrhenius equation [16, 30]:

$$\eta = \frac{1 - e^{-\tau}}{1 + c_1 \cdot e^{-\tau}}. \quad (1)$$

Here, τ is defined as follows:

$$\tau \approx c_2 \frac{t - t_g}{t_p - t} \text{Exp} \left[c_3 \frac{T_p - T(r, t)}{T_g - T(r, t)} \right], \quad (2)$$

where t_g, t_p, T_g, T_p are the time and temperature of gelation and polymerization, respectively; t is the time, min; $T(r, t)$ is the temperature, K; c_1, c_2, c_{13} are the experimentally derived coefficients.

The degree of curing of phenol (LBS-4), epoxy-phenol (5-211B), epoxy (ENFB) binders obtained experimentally was compared with the results derived from the Eq. (1). For this equation, the coefficients c_1, c_2, c_3 , approximating the experimental values were found (Fig. 1). According to the results, it can be said that analytical Eq. (1) describes the curing process with the sufficient degree of accuracy (Table 1).

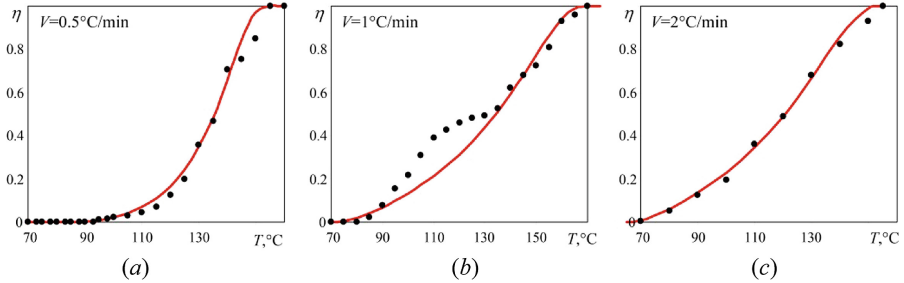


Fig. 1. Dependence of the degree of curing for LBS-4 (a), ENFB (b), 5-211B (c) binders on the temperature (coefficients: $c_1 = 1; c_2 = 0,6; c_3 = 1$): • – experimental; — Eq. (1)

Difference in the results for LBS-4 and 5-211B binders did not exceed 10...20%. For the ENFB binder, the error between the experimental and theoretical values at the initial stage of the curing process was equal to 45...65%. Large error is most likely due to additional exothermal self-heating of the material. The presented dependence (Fig. 1) shows that as from the degree of curing of 10% overshoot of values of the degree of curing occurs, therefore, the temperature in the material itself most likely is significantly higher than that measured by the thermocouple. The error in the final phase of the heating stage for the binders in question did not exceed 5...10%, but it is important to note a slight inhibition of the curing process. In particular, it is observed for the LBS-4 binder (Fig. 1). This is due to transition from the mode of kinetic control to the diffusion one. Increase in the temperature does not cause a significant rise in the reaction rate.

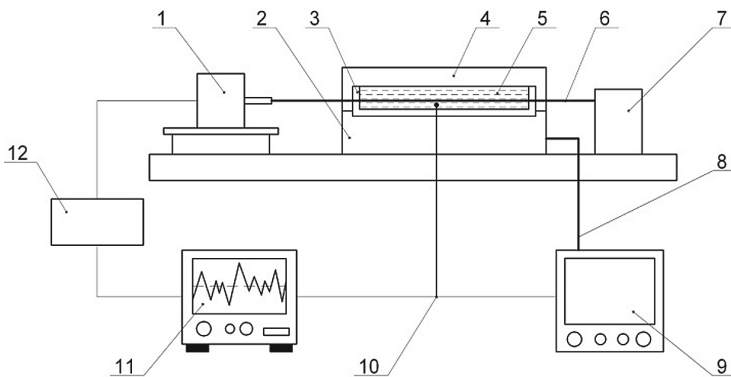
However, Eq. (1) despite its shortcomings gives quite satisfactory result in the determination of the value of the degree of curing, in particular, at the final stage of the moulding process. This dependence allows to reliably determine the moment when the binder begins to perceive and transmit the external mechanical and temperature forces. Therefore, using the Eq. (1) the degree of PCM curing can be determined at any time and temperature. Moreover, this dependence gives an opportunity to theoretically describe the change in the degree of curing with the use of parameters of the process and to construct the rational mode of curing of the binder, which provides the regulated degree of curing in the minimum period of time.

Viscosity of the material, as shown above, is in functional dependency on the temperature and time. With the increase in these parameters, the value of viscosity is also growing. It results in the occurrence of shrinkage stresses in the moulded composite material-product, relating to transformations in the binder and degassing process. At a certain value of viscosity, temperature stresses begin to appear in the moulded PCM package as well.

Table 1. Values of the degree of curing depending on temperature and time of curing for LBS-4, 5-211B, ENFB binders

Binder	T, °C	t, min	η, %		Relative error Δ, %
			theory	experiment	
Phenol (LBS-4)	100	150	1,8	2	10
	120	190	15	12	19
	140	230	62	71	14
	150	250	95	85	11
	160	270	100	100	~0
Epoxy-phenol (5-211B)	80	25	6	5	13
	100	35	23	19	15
	120	45	49	49	~0
	140	55	86	82	4
	155	65	100	100	~0
Epoxy (ENFB)	95	65	10	15	56
	115	85	26	31	63
	135	105	51	53	3
	155	125	86	81	6
	165	135	99	96	3
	175	145	100	100	~0

Experimental determination of stresses in the curing binder was implemented according to the diagram below (Fig. 2).

**Fig. 2.** Layout of the bench for determination of stresses: 1 – loading device; 2 – heater; 3 – bath with a binder; 4 – heat insulation; 5 – binder; 6 – carbon fiber; 7 – rigid body; 8 – supply; 9 – thermo-regulator; 10 – thermocouple; 11 – data recorder; 12 – amplifier

The nature of stresses and their values are determined as follows. A bath with the binder is placed in the heater through which the carbon fiber passes. One end is fixed in the rigid body, and the other one is connected to the loading device and preloaded. To measure the exact temperature value, thermocouples are connected to the bath. Signals from the thermocouples and loading device are transmitted through the amplifier to the data recorder; thus, the value of loading will correspond to each temperature value. Change in the loading value will correspond to stress in the carbon fiber in the binder. All obtained values of forces being higher than the value of preloaded fiber indicate the occurrence of compressive stresses in the binder. On the other side, decrease in forces in the fiber will mean tensile stresses of the binder.

4 Results

As can be seen from the results (Fig. 3), during the heating stage there are compressive stresses in the binder in the initial phase of the process. It indicates the occurrence of stress-strain behavior in the binder, associated with shrinkage phenomena only.

Up to the certain point in time, compressive stresses increase, and then the reverse process occurs, when compressive stresses begin to decrease to zero. After reaching of zero value, the stresses pass from the compressive zone to tensile zone with subsequent growth. The moment of decrease in compressive stresses indicates that the material reaches the value of viscosity, when the stresses associated with the temperature factor can be perceived and transmitted by the material.

It can be seen from the experimental data that stress-strain behavior in the moulded composite material-product before reaching the degree of polymerization of 65...75% occurs because of shrinkage of the material. It should also be noted that formation of shrinkage stresses begins at the stage of gelation and depends on the rate of temperature rise (Table 2).

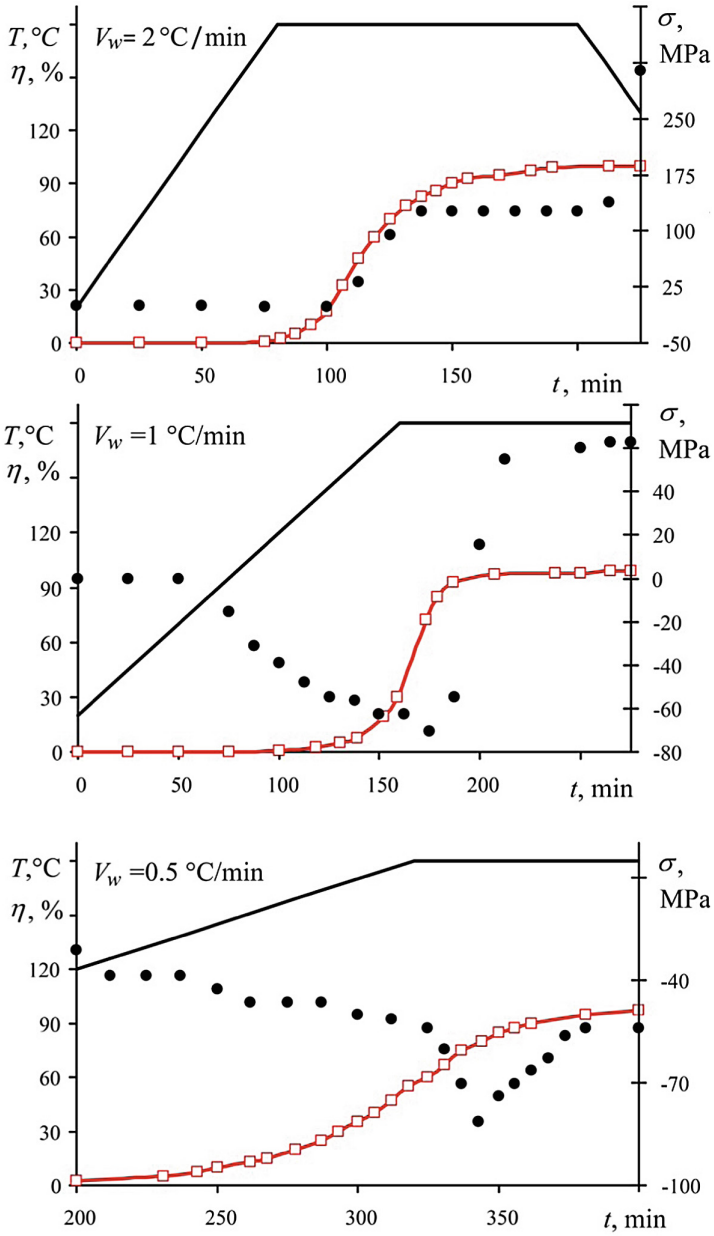
Based on the results derived from the experiments and [16, 30], it can be said that the value of shrinkage stresses depends on the material heating rate: when this rate increases from 0.5 °C/min to 2 °C/min, the shrinkage value becomes 3–4 times lower. First of all, this is due to achievement of high viscosity in the material, as well as removal of volatile fractions in a shorter period of time. In addition, during slow heating of the material (at heating rate of max. 0.75 °C/min) stresses at the heating stage as a whole take the negative values.

Consequently, the rate of heating of the material to the polymerization temperature should be as high as possible because of shrinkage occurring at this stage. However, stress-strain behavior during the process of curing at the selected rate should not lead to any violation of solidity of the material. Besides, process parameters at the stage of heating of the material (temperature and time) should be determined taking into account the influence of the reinforcing material, since after reaching of the degree of curing of 65...75% the binder begins to perceive and transmit stresses. As a result, stresses and deformations occur both in the binder and in the material-product as a whole.

Analysis of experimental and theoretical studies allows us to develop a method for determining the moulding process parameters (temperature and time) which would satisfy the condition of minimum expenditure of time to obtain a product with the maximum degree of curing.

Table 2. Dependence of shrinkage on the rate of temperature rise for various binders

Parameters	Heating rate, °C/min																					
	1					2					3											
	BFOS	LBS-4	ENFB	BFOS	ENFB	BFOS	LBS-4	ENFB	BFOS	LBS-4	ENFB	BFOS	LBS-4	ENFB	BFOS	LBS-4	ENFB					
Shrinkage value, %	8.6	5.8	5.8	6.4	4.2	4.2	4.2	4.2	3.8	2.9	2.9	2.9	2.9	2.5	2.5	2.5	2.8	2.1	2.1	2.2	1.6	1.6
Shrinkage start temperature, °C	90	85	85	90	90	90	90	90	100	95	95	95	95	95	95	95	100	97	97	105	100	100
Curing temperature, °C	190	160	160	190	160	160	160	160	190	160	160	160	160	160	160	160	190	160	160	190	160	160
Temperature of completion of shrinkage recording, °C	150	125	125	172	150	150	150	150	175	155	155	180	160	160	160	160	190	160	160	190	160	160
Duration of shrinkage, min	120	80	80	82	60	60	60	60	50	40	40	40	40	35	35	35	36	25	25	28	20	20



(c)

Fig. 3. Dependence of the degree of curing and shrinkage stresses on the moulding mode for various heating rates: (a) – $V_w = 2 \text{ }^\circ\text{C/min}$; (b) – $V_w = 1 \text{ }^\circ\text{C/min}$; (c) – $V_w = 0.5 \text{ }^\circ\text{C/min}$; \square — degree of curing; \bullet — stresses; — —temperature

Input parameters for determination of the material heating time will be the temperature and time of gelation and temperature of polymerization. Shrinkage values for the various heating rates. The limitations are as follows: maximum possible duration of the heating process, temperature and time of destruction, as well as limitations associated with the equipment used (maximum heating rate, heating rate error, time of response of the heater used).

1. Minimum possible time of the PCM package heating is determined based on the technical capabilities of the equipment used:

$$\tau_{min} = \frac{T_p - T_g}{V_{max}}, \quad (3)$$

where V_{max} – maximum possible heat carrier heating rate.

2. Using the dependence (1), the conversion field is determined in the given time and temperature range ($T_g - T_p$).
3. From the resulting conversion field, the temperature and time of the point $T_\eta(0.6)$, is determined, from which the binder perceives and transmits the forces.
4. Rate of heating of the material is determined, and its value is to satisfy the following conditions:

$$V_w(\sigma, \Delta V_w, T) \rightarrow \left\{ \begin{array}{l} \sigma_\xi \leq [\sigma_\xi] \\ \Delta V_w \rightarrow \min \\ T_v < T_d \rightarrow \min \end{array} \right\}, \quad (4)$$

where σ_ξ are the stresses in the moulded PCM package; ΔV_w is the deviation from the heating rate; T_v is the temperature overshoot; T_d is the destruction temperature.

5. If condition (4) is met, the chosen heating rate is the rational one for the given PCM.
6. The degree of curing of the binder at the end of heating stage at the rate (4) is found from the conversion field.

5 Conclusion

The choice of the analytical dependence for determination of the degree of PCM curing at any time within the given temperature range has been substantiated. Results of comparison of the experimentally derived data and the analytical Eq. (1) allow using it to describe the curing process. The error at the final stage of the process, when the binder begins to perceive and transmit the load, does not exceed 10% for the considered binders. With the use of the experimental results, the relationship between the heating rate and stresses caused by the shrinkage and thermal effect in the moulded material has been established. The value of the degree of curing, from which the binder perceives and transmits stresses, is determined. Based on the analytical Eq. (1), the method for determining process parameters of the moulding mode (temperature and time) for the binder has been developed. Rational parameters of the moulding mode at the heating stage are the minimum time for heating of the material to the polymerization temperature, while the condition for reaching of the regulated degree of the binder curing is to be observed.

Our results provide an opportunity to determine the residual thermal stress–strain behavior of the moulded structure with the required degree of accuracy without a series of experiments. It allows us to solve and indicate range of practical problems:

- to create the rational mode of curing of PCM with the minimum expenditure of energy and time;
- significantly simplify the practical implementation of the developed method and avoid any additional production costs.

References

1. Elfaki, I., Abdalgadir, S.: Composite sandwich structures in advanced civil engineering applications – a review. *Comput. Res. Prog. Appl. Sci. Eng.* **6**, 259–262 (2020)
2. Birman, V., Kardomateas, G.A.: Review of current trends in research and applications of sandwich structures. *Compos. B Eng.* **142**, 221–240 (2018). <https://doi.org/10.1016/j.compositesb.2018.01.027>
3. Gaidachuk, V.E., Kondratiev, A.V., Chesnokov, A.V.: Changes in the thermal and dimensional stability of the structure of a polymer composite after carbonization. *Mech. Compos. Mater.* **52**(6), 799–806 (2017). <https://doi.org/10.1007/s11029-017-9631-6>
4. Otrosh, Y., Kovalov, A., Semkiv, O., et al.: Methodology remaining lifetime determination of the building structures. *MATEC Web Conf.* **230**, 02023 (2018). <https://doi.org/10.1051/mateconf/201823002023>
5. Hsissou, R., Seghiri, R., Benzekri, Z., et al.: Polymer composite materials: a comprehensive review. *Compos. Struct.* **262**, 113640 (2021). <https://doi.org/10.1016/j.compstruct.2021.113640>
6. Yanes-Armas, S., de Castro, J., Keller, T.: Long-term design of FRP-PUR web-core sandwich structures in building construction. *Compos. Struct.* **181**, 214–228 (2017). <https://doi.org/10.1016/j.compstruct.2017.08.089>
7. Manalo, A., Aravinthan, T., Fam, A., Benmokrane, B.: State-of-the-art review on FRP sandwich systems for lightweight civil infrastructure. *J. Compos. Constr.* **21**(1), 1–16 (2017). [https://doi.org/10.1061/\(asce\)cc.1943-5614.0000729](https://doi.org/10.1061/(asce)cc.1943-5614.0000729)
8. Ugrimov, S., Smetankina, N., Kravchenko, O., Yareshchenko, V.: Analysis of laminated composites subjected to impact. In: Nechyporuk, M., Pavlikov, V., Kritskiy, D. (eds.) *ICTM 2020*. LNNS, vol. 188, pp. 234–246. Springer, Cham (2021). https://doi.org/10.1007/978-3-030-66717-7_19
9. Tkachenko, D., Tsegelnyk, Y., Myntiuk, S., Myntiuk, V.: Spectral methods application in problems of the thin-walled structures deformation. *J. Appl. Comput. Mech.* **8**(2), 641–654 (2022). <https://doi.org/10.22055/jacm.2021.38346.3207>
10. Fomin, O., Lovskaya, A., Plakhtiy, A., Nerubatsky, V.: The influence of implementation of circular pipes in load-bearing structures of bodies of freight cars on their physico-mechanical properties. *Sci. Bull. Natl. Min. Univ.* **6**(162), 89–96 (2017)
11. Kombarov, V., Kryzhyvets, Y., Biletskyi, I., et al.: Numerical control of fiberglass pipe bends manufacturing. In: *2021 IEEE 2nd KhPI Week on Advanced Technology (KhPIWeek)*, Kharkiv, pp. 357–362. IEEE (2021). <https://doi.org/10.1109/KhPIWeek53812.2021.9570068>
12. Dveirin, O.Z., Andreev, O.V., Kondrat'ev, A.V., Haidachuk, V.Y.: Stressed state in the vicinity of a hole in mechanical joint of composite parts. *Int. Appl. Mech.* **57**(2), 234–247 (2021). <https://doi.org/10.1007/s10778-021-01076-4>

13. Boitsov, B.V., Gavva, L.M., Pugachev, Y.N.: The stress-strain state of structurally anisotropic panels from composite materials under force and process temperature exposure. *Polym. Sci., Ser. D* **12**, 85–90 (2019). <https://doi.org/10.1134/S1995421219010039>
14. Karpus, V., Ivanov, V., Dehtiarov, I., Zajac, J., Kurochkina, V.: Technological assurance of complex parts manufacturing. In: Ivanov, V., et al. (eds.) *DSMIE 2018. LNME*, pp. 51–61. Springer, Cham (2019). https://doi.org/10.1007/978-3-319-93587-4_6
15. Rodionov, V.V.: Optimization of molding the polymeric composite material with improved characteristics. *Plasticheskie massy* **3–4**, 55–58 (2019). <https://doi.org/10.35164/0554-2901-2019-3-4-55-58>
16. Fedulov, B.N.: Modeling of manufacturing of thermoplastic composites and residual stress prediction. *Aerosp. Syst.* **1**(2), 81–86 (2018). <https://doi.org/10.1007/s42401-018-0018-8>
17. Li, D., Li, X., Dai, J., Xi, S.: A comparison of curing process-induced residual stresses and cure shrinkage in micro-scale composite structures with different constitutive laws. *Appl. Compos. Mater.* **25**(1), 67–84 (2017). <https://doi.org/10.1007/s10443-017-9608-6>
18. Yuan, Z.Y., Wang, Y.J., Yang, G.G., et al.: Evolution of curing residual stresses in composite using multi-scale method. *Compos. B Eng.* **155**, 49–61 (2018). <https://doi.org/10.1016/j.compositesb.2018.08.012>
19. Carlone, P., Rubino, F., Paradiso, V., Tucci, F.: Multi-scale modeling and online monitoring of resin flow through dual-scale textiles in liquid composite molding processes. *Int. J. Adv. Manuf. Technol.* **96**(5–8), 2215–2230 (2018). <https://doi.org/10.1007/s00170-018-1703-9>
20. Lionetto, F., Moscatello, A., Totaro, G., et al.: Experimental and numerical study of vacuum resin infusion of stiffened carbon fiber reinforced panels. *Materials* **13**(21) (2020). <https://doi.org/10.3390/ma13214800>
21. Rocha, H., Semprinoschnig, C., Nunes, J.P.: Sensors for process and structural health monitoring of aerospace composites: a review. *Eng. Struct.* **237**, 112231 (2021). <https://doi.org/10.1016/j.engstruct.2021.112231>
22. Brauner, C., Frerich, T., Herrmann, A.S.: Cure-dependent thermomechanical modelling of the stress relaxation behaviour of composite materials during manufacturing. *J. Compos. Mater.* **51**, 877–898 (2017). <https://doi.org/10.1177/0021998316656924>
23. Cameron, C.J., Saseendran, S., Stig, F., Rouhi, M.: A rapid method for simulating residual stress to enable optimization against cure induced distortion. *J. Compos. Mater.* **55**(26), 3799–3812 (2021). <https://doi.org/10.1177/00219983211024341>
24. Muliana, A.H.: Spatial and temporal changes in physical properties of epoxy during curing and their effects on the residual stresses and properties of cured epoxy and composites. *Appl. Eng. Sci.* **7**, 100061 (2021). <https://doi.org/10.1016/j.apples.2021.100061>
25. Kondratiev, A., Píšťek, V., Purhina, S., et al.: Self-heating mould for composite manufacturing. *Polymers* **13**(18), 3074 (2021). <https://doi.org/10.3390/polym13183074>
26. Kondratiev, A., Píšťek, V., Smovziuk, L., et al.: Stress-strain behaviour of reparable composite panel with step-variable thickness. *Polymers* **13**(21), 3830 (2021). <https://doi.org/10.3390/polym13213830>
27. Fernlund, G., Rahman, N., Courdji, R., et al.: Experimental and numerical study of the effect of cure cycle, tool surface, geometry, and lay-up on the dimensional fidelity of autoclave-processed composite parts. *Compos. A Appl. Sci. Manuf.* **33**, 341–351 (2002). [https://doi.org/10.1016/S1359-835X\(01\)00123-3](https://doi.org/10.1016/S1359-835X(01)00123-3)
28. Deng, B., Shi, Y.Y., Yu, T., Zhao, P.: Influence mechanism and optimization analysis of technological parameters for the composite prepreg tape winding process. *Polymers* **12**(8), 1843 (2020). <https://doi.org/10.3390/polym12081843>

29. Budelmann, D., Schmidt, C., Meiners, D.: Prepreg tack: a review of mechanisms, measurement, and manufacturing implication. *Polym. Compos.* **41**(9), 3440–3458 (2020). <https://doi.org/10.1002/pc.25642>
30. Baran, I., Cinar, K., Ersoy, N., Akkerman, R., Hattel, J.H.: A review on the mechanical modeling of composite manufacturing processes. *Arch. Comput. Methods Eng.* **24**(2), 365–395 (2016). <https://doi.org/10.1007/s11831-016-9167-2>



Two-Stage Optimization of Laminated Composite Elements with Minimal Mass

Natalia Smetankina¹ (✉) , Oleksandr Semenets² , Alyona Merkulova¹ ,
Dmytro Merkulov¹ , and Serhii Misura¹

¹ A. Pidhorneyi Institute of Mechanical Engineering Problems of the National Academy of Sciences of Ukraine, 2/10 Pozharskogo Street, Kharkiv 61046, Ukraine
nsmet@ipmach.kharkov.ua

² Antonov Company, 1 Akademika Tupolieva Street, Kyiv 03062, Ukraine

Abstract. The design of laminated composite structures used in mechanical engineering presents a major challenge in terms of computational cost. The most important aspect in designing laminated structures is the composition selection. An iterative procedure for minimization of the mass of laminated composite elements under an impulse load is offered. Both thicknesses and fiber orientation angles of layers are selected as design variables. The hybrid search method of optimization with adaptive control of the computing process is applied to solving the problem of optimal plate design. Deformation of plates is considered in a linear statement. Calculation of parameters of the stress-strain state of elements is carried out with the finite element method. Mass and deflection optimization of a composite plate subjected to the Tsai-Wu criteria-based design constraint have been carried out. The two-stage approach allows getting a design with the greatest bending stiffness without a significant structure mass increase. The approach makes it possible to develop new composite elements with improved characteristics.

Keywords: Composite plate · Impulse load · Optimal design

1 Introduction

The wide application of modern composite materials in different engineering areas is linked directly to the development of methods for optimal design of laminated composite structures [1, 2]. In practice, composite structures are usually assembled with other components, such as honeycomb or metal panels [3, 4], and are also reinforced by various fibers, particles and films [5, 6]. Design with account for the anisotropy of the mechanical properties of layers, apart from the conventional choice of geometric parameters, provides for determining the optimal structure of the material, i.e. the number and sequence of layers, fiber orientation angles and other parameters [7, 8]. In addition, designing composites requires taking into account a variety of technological defects and imperfections that may occur during their manufacture [9, 10].

Regardless of extensive theoretical developments in optimal design of composite elements of structures, the focus is on problems in optimization of statically loaded structures [11, 12]. A fair number of studies deal with finding structure parameters under conditions of free vibrations whose natural frequency reaches a maximum [13, 14]. The number of papers dealing with optimal design of composite elements under action of unsteady loading is far less [15], making research in this area a topical issue.

2 Literature Review

As a rule, problems in optimal design of laminated composite structures are multicriteria ones [16, 17]. They are usually reduced to minimizing the average-weighted functional where the choice of weight multipliers requires the knowledge of information that can be not known a priori [18].

The paper [19] suggests a procedure for designing laminated truncated conical shells subjected to external hydrostatic compression orientations by using the golden section method. The critical buckling loads of the shells with given materials are maximized with respect to fiber orientations by changing thicknesses, fiber orientations and buckling modes. In the paper [20], the authors suggested a hybrid genetic algorithm that combines a genetic algorithm and a descent local search technique for the optimization of a sandwich composite inter-stage skirt located in the upper bound of the launcher. Total number of plies forming the sandwich composite skin and fiber orientations were considered as design variables. A fully blended design is represented by a stacking sequence of t composites. The paper [21] presents simultaneous maximization of the fundamental frequency and frequency separation between the first two modes by optimizing the fiber angles. A high-fidelity design optimization methodology is developed by combining the high-accuracy of finite element method with iterative improvement capability of metaheuristic algorithms, and genetic optimization algorithms.

However, there is another approach to solving multicriteria problems, viz. using multilevel iteration optimization procedures. The study [22] presents a multi-level optimization method for elastic constant identification of composite materials. The optimization problem is solved by using a stochastic search minimization algorithm at the first level, and the particle swarm algorithm at the second-level algorithm for obtaining the statistics of the new quasi-optimal elastic constants. The paper [23] demonstrates a two-stage method for performing global layup optimization of composite laminates with buckling and manufacturing constraints. In the first stage, the buckling optimization problem is solved changing the lamination parameters and laminate thickness. During the second stage, a global technique is employed to search the optimal stacking sequences to match the optimized lamination parameters obtained in the first stage. The optimization algorithm moreover gives insight on the influence of different lamination parameters and the dominance of certain manufacturing constraints in various locations of the design space.

The aim of this study is the development of a two-stage procedure for minimizing the mass of laminated composite plates under impulse action. The optimization problem is formulated in terms of nonlinear programming.

3 Research Methodology

Let us consider the laminated composite element as a rectangular laminated plate (see Fig. 1) with a constant overall thickness H , assembled of an arbitrary number of anisotropic layers N with constant thickness h_i ($i = \overline{1, N}$). The plate is subjected to a transverse impulse load $p(x, y, t)$. The axes of the material of each layer are oriented arbitrarily with respect the median plane of the plate.

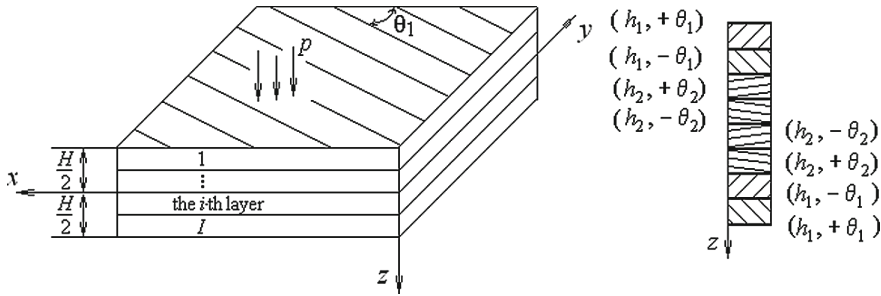


Fig. 1. Laminated plate.

The displacements of the plate points according to the Timoshenko-type theory [24, 25] are presented as follows

$$u_1(x, y, z, t) = u_0(x, y, t) + z\psi_x(x, y, t),$$

$$u_2(x, y, z, t) = v_0(x, y, t) + z\psi_y(x, y, t),$$

$$u_3(x, y, z, t) = w_0(x, y, t) + z\psi_z(x, y, t).$$

Here $u_0(x, y, t)$, $v_0(x, y, t)$, $w_0(x, y, t)$ are displacements of the median plane points in the direction of the coordinate axes; $\psi_x(x, y, t)$, $\psi_y(x, y, t)$ are rotation angles of the normal element, $\psi_z(x, y, t)$ is normal element reduction; t is time.

Assuming a linear elastic strain of the plate, for internal forces and moments we have the following relationships:

$$\mathbf{T} = \mathbf{CE},$$

where

$$\mathbf{T} = [N_x, N_y, N_z, Q_y, Q_x, N_{xy}, M_x, M_y, M_{yz}, M_{xz}, M_{xy}]^T;$$

$$\mathbf{E} = [u_{0,x}, v_{0,y}, \psi_z, w_{0,y} + \psi_y, w_{0,x} + \psi_x, u_{0,y} + v_{0,x},$$

$$\psi_{x,x}, \psi_{y,y}, \psi_{z,y}, \psi_{z,x}, \psi_{x,y} + \psi_{y,x}]^T;$$

$$C = \begin{bmatrix} A_{11} & A_{12} & A_{13} & 0 & 0 & A_{16} & B_{11} & B_{12} & 0 & 0 & B_{16} \\ A_{12} & A_{22} & A_{23} & 0 & 0 & A_{26} & B_{12} & B_{22} & 0 & 0 & B_{26} \\ A_{13} & A_{23} & A_{33} & 0 & 0 & A_{36} & B_{13} & B_{23} & 0 & 0 & B_{36} \\ 0 & 0 & 0 & A_{44} & A_{45} & 0 & 0 & 0 & B_{44} & B_{45} & 0 \\ 0 & 0 & 0 & A_{45} & A_{55} & 0 & 0 & 0 & B_{45} & B_{55} & 0 \\ A_{16} & A_{26} & A_{36} & 0 & 0 & A_{66} & B_{16} & B_{26} & 0 & 0 & B_{66} \\ B_{11} & B_{12} & B_{13} & 0 & 0 & B_{16} & D_{11} & D_{12} & 0 & 0 & D_{16} \\ B_{12} & B_{22} & B_{23} & 0 & 0 & B_{26} & D_{12} & D_{22} & 0 & 0 & D_{26} \\ 0 & 0 & 0 & B_{44} & B_{45} & 0 & 0 & 0 & D_{44} & D_{45} & 0 \\ 0 & 0 & 0 & B_{45} & B_{55} & 0 & 0 & 0 & D_{45} & D_{55} & 0 \\ B_{16} & B_{26} & B_{36} & 0 & 0 & B_{66} & D_{16} & D_{26} & 0 & 0 & D_{66} \end{bmatrix}$$

$$(A_{kl}, B_{kl}, D_{kl}) = \sum_{i=1}^N \int_{z_i}^{z_{i+1}} Q_{kl}^i(1, z, z^2) dz, k, l = \overline{1, 6}.$$

The index after the comma means partial differentiation with respect to the coordinate. Stiffness factor Q_{kl}^i depends on material properties and the orientation of fiber angles θ_i in the i -th layer (see Fig. 1). Expressions for Q_{kl}^i in the general case, when the axes of symmetry of the material layer do not coincide with the directions of coordinate axes, are given in [26].

The finite element method is applied for computing the dynamic behavior of the plate. Apart from transverse shear strain and thickness reduction, the inertia of rotation of the normal was accounted for.

In the general case, the nonlinear programming problem, irrespective of its content, consists in finding the extremum point

$$X^* = \underset{X \in G}{\operatorname{argextr}} F(X)$$

of objective function $F(X)$ with constraints in the form of equalities

$$G_i(X) = 0, i = \overline{1, m_1},$$

and (or) inequalities

$$G_j(\overline{X}) \geq 0, j = \overline{1, m_2},$$

where $X = \{X_i\}$, $i = \overline{1, N}$ is vector of the design variables space; G is admissible domain of change of design variables.

Functions $F(X)$, $G_i(X)$, $G_j(\overline{X})$ are real, continuous and bounded; $F(X)$ is defined on set $G = G(X)$, and $G_i(X)$ and $G_j(\overline{X})$, on its extension $\overline{G} \supset G$.

The optimization problem at each stage is a multiextremum one because the constraints are both non-convex and sliding ones, changing from step to step. With a relatively small problem dimension, the algorithmic implementation of constraints also

increases the time of search for the extremum. Hence, the solution method used is the effective hybrid search optimization one with adaptive control of the computational process [27, 28].

At the first stage of the proposed procedure, the thicknesses of the layers are varied and the plate mass is minimized. At the second stage, the thicknesses of the layers obtained by mass minimization are fixed and the maximum deflection of the plate is minimized by changing the fiber angles in layers. The optimal design is the result of an iterative process that continues until preset accuracy criteria have been achieved.

In the first stage, the design variables of the problem for minimizing the mass of a laminated plate are the thicknesses of layers $X = \{h_k\}$, $k = \overline{1, N}$. It is necessary to find the values of independent parameters $X^* = \{h_k^*\}$, at which the laminated plate mass $F_M(X)$ is minimal, i.e.

$$F_M^* = \min F_M(X), F_M = S \sum_{k=1}^N \rho_k h_k, \tag{1}$$

where S is area of the plate median plane; ρ_k is density of the layer material.

Constraints are imposed on the minimal and maximal thicknesses of each layer

$$h_{min} \leq h_k \leq h_{max}, k = \overline{1, N}. \tag{2}$$

The strength of layers is evaluated using the Tsai-Wu criterion

$$\max_{[0, T] \times x, y \in \Omega} \max (F_i \sigma_i^k + F_{ij} \sigma_i^k \sigma_j^k) \leq 1, \tag{3}$$

where $F_1 = 1/X_T - 1/X_C$, $F_2 = 1/Y_T - 1/Y_C$, $F_3^i = 1/Z_T - 1/Z_C$, $F_{11} = 1/(X_T X_C)$, $F_{22} = 1/(Y_T Y_C)$, $F_{33} = 1/(Z_T Z_C)$, $F_{44} = 1/R^2$, $F_{55} = F_{66} = 1/S^2$, $F_{12} = -0.5/\sqrt{X_T X_C Y_T Y_C}$, $F_{13} = -0.5/\sqrt{X_T X_C Z_T Z_C}$, $F_{23} = -0.5/\sqrt{Y_T Y_C Z_T Z_C}$, X_T, Y_T, Z_T are material ultimate tensile strengths; X_C, Y_C, Z_C are material ultimate compression strengths; R, S are material ultimate shear strengths; σ_i^k are stress components on the material principal axes; Ω is the domain occupied by the plate median plane.

The stresses included in strength criterion (3) are evaluated over a definite time interval $[0, T]$. The length of the interval is taken to be such that all the principal factors characterising the unsteady strain process across the entire domain of change of design variables would appear.

In the second stage, the design variables in the problem of minimizing maximum plate deflection are the fiber angles in layers $X = \{\theta_k\}$, $k = \overline{1, N}$. Constraints are imposed on the minimal and maximal fiber angles in each layer. The plate strength is evaluated using the Tsai-Wu criterion (3).

Hence, it is necessary to find the values of independent variables $X^* = \{\theta_k^*\}$, at which maximum plate deflection $F_w(X)$ is minimal, i.e.

$$F_w^* = \min F_w(X), F_w = \max_{[0, T] \times x, y \in \Omega} \max_{z \in [-\frac{H}{2}, \frac{H}{2}]} [u_3(x, y, z, t)], \tag{4}$$

$$Q_{min} \leq Q_k \leq Q_{max}, k = \overline{1, N}. \tag{5}$$

The objective function does not exceed a certain preset value, i.e.

$$\left| \frac{F_M^n - F_M^{n-1}}{F_M^{n-1}} \right| \leq \varepsilon_M, \quad \left| \frac{F_w^n - F_w^{n-1}}{F_w^{n-1}} \right| \leq \varepsilon_w,$$

where n is iteration number, ε_M , ε_w are positive constants defining the extremum search accuracy. A similar criterion is used for evaluating solution convergence at each iteration of the procedure that combines both stages. Stopping the running of the program, which implements this algorithm, by the number of computations of the objective function is also provided for.

4 Results

The feasibility and effectiveness of the developed mass minimization procedure is illustrated by the example of a simply supported eight-ply symmetrically-structured plate $[\pm\theta^1/\pm\theta^2]_s$. The symmetrical structure of a laminated composite is most often used in real-life applications.

Impulse load $p = P_0H(t)$, where $H(t)$ is Heaviside's function, is uniformly distributed across the entire plate surface. Plate layers are made of a carbon-fiber epoxy composite with the following characteristics and material ultimate strength (3): $E_1 = 132.5$ GPa, $E_2 = E_3 = 10.8$ GPa, $G_{12} = G_{13} = 5.7$ GPa, $G_{23} = 3.4$ GPa, $\nu_1 = 0.24$, $\rho = 1,500$ kg/m³; $X_T = 1,515$ MPa, $Y_T = Z_T = 43.8$ MPa, $X_C = 1,697$ MPa, $Y_C = Z_C = 43.8$ MPa, $R = 67.6$ MPa, $S = 86.9$ MPa. The design variables were restricted by admissible values: $h_{min} = 3$ mm, $h_{max} = 10$ mm, $Q_{min} = 0^\circ$, $Q_{max} = 90^\circ$. The constants defining the extremum search accuracy were as follows: $\varepsilon_M = \varepsilon_w = 10^{-4}$. The length of the characteristic time interval was 0.2 s, and the solution discretization time step was 0.01 s. To search for a rational form of the structure mesh discretization, multivariate numerical studies were performed. The number of finite elements should provide the possibility of a detailed description of the entire change in the studied displacements, strains and stresses. In all the cases considered, a grid of rectangular eight-node finite elements ensured high solution accuracy. The start values were thicknesses and fiber angles belonging to the domain of admissible values determined by inequalities (2), (3) and (5), as well as the values on the boundary and outside the domain of admissible values. In all the cases considered, the number of iterations was within ten.

Table 1 summarizes the results of solving the problem of minimization of plate mass with a different side lengths ratio B/A at $P_0 = 0.1$ MPa; $A = 0.5$ m, $H = \sum_{k=1}^N h_k$ is plate thickness, $H = F_M/(\rho AB)$ (see (1)), u_3 is maximum deflection of the plate at the found optimal design variables. With increasing side lengths ratios, the fiber angles of external layers θ^1 increase in the interval from 45° to 90° . The angles of internal layers θ^2 are close to those within $0^\circ - 5^\circ$. The thicknesses of the layers in optimal plates are virtually equal to their minimum admissible values. Plate mass minimization with the same parameters and loading, when only the first stage is used, yields optimal plate designs with a mass close to that obtained with the two-stage scheme. However, the plate deflection exceeds the values obtained with the two-stage scheme by 10–15%.

In Fig. 2 shown variation the plate thickness H for different iterations of the two-stage procedure for $B/A = 1.5$.

Table 1. Influence of side lengths ratio B/A on the optimal design.

B/A	h^1/h^2 , mm	H , mm	$\pm\theta^1/\pm\theta^2$	u_3 , mm
1.0	3.0988/3.0988	24.790	$\pm 46.8^\circ/\pm 5.70^\circ$	0.6932
1.5	3.0950/3.0913	24.745	$\pm 58.0^\circ/\pm 3.92^\circ$	1.5180
2.0	3.0986/3.0949	24.774	$\pm 78.9^\circ/\pm 7.30^\circ$	2.0809

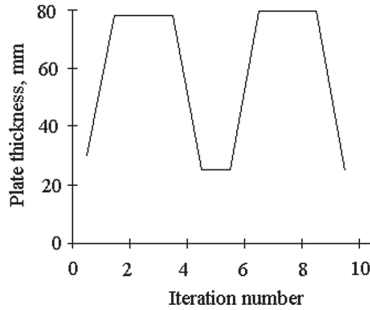


Fig. 2. Changing the plate thickness under the iterative process.

In Fig. 3 shown the deflection u_3 and tensile stress vs. time in the middle point of the plate at $z = -H/2$ for optimal variables obtained for $B/A = 1.5$ (see Table 1).

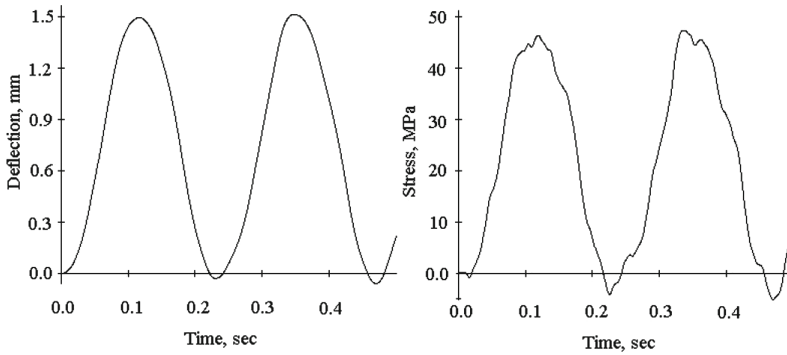


Fig. 3. Changing deflection u_3 and tensile stress vs. time.

If the criterion for evaluating an optimal design is the minimal maximum plate deflection F_w (4), the solution results will change as follows (see Table 2). With such an optimality criterion, the plate mass increased by 0.1–0.38%, and the deflections decreased by 2.3–14.5%. For a plate with a unit side ratio, the optimal angles are 45° , and for other ratios they are close to zero. Numerical analysis showed that optimal designs obtained with minimization of minimum strain energy and minimization of maximum plate deflection are equivalent. Hence, the optimal designs in Table 2 correspond to

maximum stiffness plates, and the mass of the plates did not essentially increase as compared to plates with a minimal mass.

Table 2. Influence of side lengths ratio B/A on the optimal deflection value

B/A	h^1/h^2 , mm	H , mm	$\pm\theta^1/\pm\theta^2$	u_3 , mm
1.0	3.1108/3.1107	24.886	$\pm 45.2^\circ/\pm 45.1^\circ$	0.6772
1.5	3.0984/3.0986	24.788	$\pm 7.30^\circ/\pm 8.50^\circ$	1.3626
2.0	3.0979/3.0982	24.784	$\pm 7.30^\circ/\pm 8.60^\circ$	1.7782

5 Conclusion

A two-stage iteration scheme was developed for minimizing the mass of laminated composite plates under non-stationary loading. The approach suggested produced plate designs with minimal mass and minimal possible maximum deflections. The obtained optimal fiber angles are in good agreement with reinforcement schemes developed experimentally and used in real-life applications. The advantage of the two-stage approach, as compared to the one-stage procedure is that a plate design with the greatest bend stiffness can be obtained without a significant plate mass increase. The effectiveness of the numerical implementation of the suggested procedure (reducing the number of solution search steps) was achieved by applying the hybrid optimization method and using an effective scheme of data exchange between the stages.

The use of a multicriteria objective functional requires careful selection of weight coefficients that are not known in advance. The selection of coefficients is a separate problem that requires an additional numerical study. An incorrect choice of coefficients can lead to an incorrect solution of the optimization problem, and the design variables will not reach their best values. At each stage, the hybrid search method of optimization employs adaptive control for automatically introducing one or several hybrid elements from the accepted set. Hence, the proposed method is more effective for solving a wider class of problems than any one method taken separately.

The practical application of research is seen in designing laminated composite structures of minimum weight under static and dynamic loads in aircraft [29, 30] and civil engineering [31]. The two-level procedure offered allows to obtain an optimal layout of composite laminates, taking into account production and operational constraints. The number of layers as an additional optimization parameter will be taken into account in further studies. The results obtained enable evaluating how close the actual structure is to an optimal one.

References







1. Strelnikova, E., Litvinchev, I., Pankratov, A., et al.: Optimized packings in analysis of 3D nanocomposites with inclusion systems. In: 2020 IEEE KhPI Week on Advanced Technology

- (KhPIWeek), Kharkiv, pp. 377–381. IEEE (2020). <https://doi.org/10.1109/KhPIWeek51551.2020.9250142>
2. Kombarov, V., Kryzhyvets, Y., Biletskyi, I., et al.: Numerical control of fiberglass pipe bends manufacturing. In: 2021 IEEE 2nd KhPI Week on Advanced Technology (KhPIWeek), Kharkiv, pp. 357–362. IEEE (2021). <https://doi.org/10.1109/KhPIWeek53812.2021.9570068>
 3. Rayhan, S.B.: Finite element analysis of oblique bird strike on leading edge of aircraft wing. AIP Conf. Proc. **1980**, 030009 (2018). <https://doi.org/10.1063/1.5044288>
 4. Tkachenko, D., Tsegelnyk, Y., Myntiuk, S., Myntiuk, V.: Spectral methods application in problems of the thin-walled structures deformation. J. Appl. Comput. Mech. **8**(2), 641–654 (2022). <https://doi.org/10.22055/jacm.2021.38346.3207>
 5. Koohbor, B., Rohanifar, M., Kidane, A.: Characterizing fracture response of cracked transversely graded materials. Compos. Struct. **229**, 111439 (2019). <https://doi.org/10.1016/j.compstruct.2019.111439>
 6. Ugrimov, S., Smetankina, N., Kravchenko, O., Yareschenko, V.: Analysis of laminated composites subjected to impact. In: Nechyporuk, M., Pavlikov, V., Kritskiy, D. (eds.) ICTM 2020. LNNS, vol. 188, pp. 234–246. Springer, Cham (2021). https://doi.org/10.1007/978-3-030-66717-7_19
 7. Nikbakt, S., Kamarian, S., Shakeri, M.: A review on optimization of composite structures. Part I: laminated composites. Compos. Struct. **195**, 158–185 (2018). <https://doi.org/10.1016/j.compstruct.2018.03.063>
 8. Haripriya, M., Naga, G., Rao, M., Prasad, B.D.: Review on optimization of metal matrix composite connecting rod. Int. Res. J. Adv. Sci. Hub **2**(7), 94–99 (2020). <https://doi.org/10.47392/irjash.2020.71>
 9. Kondratiev, A., Gaidachuk, V., Nabokina, T., Kovalenko, V.: Determination of the influence of deflections in the thickness of a composite material on its physical and mechanical properties with a local damage to its wholeness. East. Eur. J. Enterp. Technol. **4**(1), 6–13 (2019). <https://doi.org/10.15587/1729-4061.2019.174025>
 10. Dveirin, O.Z., Andreev, O.V., Kondrat'ev, A.V., Haidachuk, V.Y.: Stressed state in the vicinity of a hole in mechanical joint of composite parts. Int. Appl. Mech. **57**(2), 234–247 (2021). <https://doi.org/10.1007/s10778-021-01076-4>
 11. Zhou, X.-Y., Ruan, X., Gosling, P.D.: Thermal buckling optimization of variable angle tow fibre composite plates with gap/overlap free design. Compos. Struct. **223**, 110932 (2019). <https://doi.org/10.1016/j.compstruct.2019.110932>
 12. Uddin, K.Z., Koohbor, B.: Gradient optimization of transversely graded Ti-TiB structures for enhanced fracture resistance. Int. J. Mech. Sci. **187**, 105917 (2020). <https://doi.org/10.1016/j.ijmecsci.2020.105917>
 13. Roque, C.M.C., Martins, P.A.L.S.: Maximization of fundamental frequency of layered composites using differential evolution optimization. Compos. Struct. **183**, 77–83 (2017). <https://doi.org/10.1016/j.compstruct.2017.01.037>
 14. Vosoughi, A.R., Malekzadeh, P., Topal, U., Dede, T.: A hybrid DQ-TLBO technique for maximizing first frequency of laminated composite skew plates. Steel Compos. Struct. **28**(4), 509–516 (2018). <https://doi.org/10.12989/scs.2018.28.4.509>
 15. Zhang, H.M., Xing, Y.F.: Optimization of a class of composite method for structural dynamics. Comput. Struct. **202**, 60–73 (2018). <https://doi.org/10.1016/j.compstruc.2018.03.006>
 16. Nikbakt, S., Kamarian, S., Shakeri, M.: A review on optimization of composite structures – Part II: functionally graded materials. Compos. Struct. **214**, 83–102 (2019). <https://doi.org/10.1016/j.compstruct.2019.01.105>
 17. Li, X., Wang, H., Li, G.: Reanalysis assisted metaheuristic optimization for free vibration problems of composite laminates. Compos. Struct. **206**, 380–391 (2018). <https://doi.org/10.1016/j.compstruct.2018.08.028>

18. Jain, M., Singh, V., Rani, A.: A novel nature-inspired algorithm for optimization: squirrel search algorithm. *Swarm Evol. Comput.* **44**, 148–175 (2019). <https://doi.org/10.1016/j.swevo.2018.02.013>
19. Hu, H.-T., Chen, H.-C.: Buckling optimization of laminated truncated conical shells subjected to external hydrostatic compression. *Compos. B Eng.* **135**, 95–109 (2018). <https://doi.org/10.1016/j.compositesb.2017.09.065>
20. Gharsalli, L., Guerin, Y.: Composite structures optimization using hybrid genetic algorithm for space applications. *AIP Conf. Proc.* **2186**, 170022 (2019). <https://doi.org/10.1063/1.5138101>
21. Kalita, K., Ragavendran, U., Ramachandran, M., Bhoi, A.K.: Weighted sum multiobjective optimization of skew composite laminates. *Struc. Eng. Mech.* **69**(1), 21–31 (2019). <https://doi.org/10.12989/sem.2019.69.1.021>
22. Huang, C.Y., Kam, T.Y.: A multi-level optimization method for elastic constants identification of composite laminates. *Appl. Sci.* **9**(20), 4267 (2019). <https://doi.org/10.3390/app9204267>
23. Liu, X., Featherston, C.A., Kennedy, D.: Two-level layup optimization of composite laminate using lamination parameters. *Compos. Struct.* **211**, 337–350 (2019). <https://doi.org/10.1016/j.compstruct.2018.12.054>
24. Smetankina, N., Kravchenko, I., Merculov, V., Ivchenko, D., Malykhina, A.: Modelling of bird strike on an aircraft glazing. In: Nechyporuk, M., Pavlikov, V., Kritskiy, D. (eds.) *Integrated Computer Technologies in Mechanical Engineering*. AISC, vol. 1113, pp. 289–297. Springer, Cham (2020). https://doi.org/10.1007/978-3-030-37618-5_25
25. Smetankina, N., Merkulova, A., Merkulov, D., Postnyi, O.: Dynamic response of laminate composite shells with complex shape under low-velocity impact. In: Nechyporuk, M., Pavlikov, V., Kritskiy, D. (eds.) *ICTM 2020*. LNNS, vol. 188, pp. 267–276. Springer, Cham (2021). https://doi.org/10.1007/978-3-030-66717-7_22
26. Reddy, J.N.: *Mechanics of Laminated Composite Plates and Shells: Theory and Analysis*. CRC Press, Boca Raton (2004). <https://doi.org/10.1201/b12409>
27. Smetankina, N.V., Postnyi, O.V., Misura, S.Y., et al.: Optimal design of layered cylindrical shells with minimum weight under impulse loading. In: *2021 IEEE 2nd KhPI Week on Advanced Technology (KhPIWeek)*, Kharkiv, pp. 506–509. IEEE (2021). <https://doi.org/10.1109/KhPIWeek53812.2021.9569982>
28. Misura, S., Smetankina, N., Misiura, I.: Optimal design of the cyclically symmetrical structure under static load. In: Nechyporuk, M., Pavlikov, V., Kritskiy, D. (eds.) *ICTM 2020*. LNNS, vol. 188, pp. 256–266. Springer, Cham (2021). https://doi.org/10.1007/978-3-030-66717-7_21
29. Kondratiev, A., Píštěk, V., Purhina, S., et al.: Self-heating mold for the composite manufacturing. *Polymers* **13**(18), 3074 (2021). <https://doi.org/10.3390/polym13183074>
30. Kustron, K., Horak, V., Doubrava, R., Goraj, Z.J.: New hail impact simulation models on composite laminated wing leading edge. *Aircr. Eng. Aerosp. Technol.* **91**(3), 457–465 (2019). <https://doi.org/10.1108/AEAT-02-2018-0089>
31. Davidson, P., Waas, A.M.: Probabilistic defect analysis of fiber reinforced composites using kriging and support vector machine based surrogates. *Compos. Struct.* **195**, 21–31 (2018). <https://doi.org/10.1016/j.compstruct.2018.03.007>



Temperature Effect on Elastic, Thermomechanical and Thermal Properties of Polymer Composite Materials

Oleksii Vambol^{1,2} , Maryna Shevtsova¹ , Anton Tsaritsynskyi¹ ,
Tetyana Nabokina¹ , and Andrii Kondratiev²  

¹ National Aerospace University “Kharkiv Aviation Institute”, 17 Chkalov Street, Kharkiv 61070, Ukraine

² O.M. Beketov National University of Urban Economy in Kharkiv, 17 Marshal Bazhanov Street, Kharkiv 61002, Ukraine
andrii.kondratiev@kname.edu.ua

Abstract. Polymer composite materials are being increasingly used in various industries. The active application of composites calls for increasing their operating temperature range. The aim of the work is to study and analyze the effect of operating temperatures on the physical and mechanical properties of polymer composite materials and to establish dependences of these properties on temperature. It is found that elastic properties decrease as temperature grows. With an increase in temperature to 473 K, the values of the elastic modulus of the binder, the shear modulus, the elastic modulus of unidirectional fiberglass in the direction transverse to the fibers, and the Poisson’s ratio decrease by almost 5 times. The shear modulus also decreases by more than 4.5 times, while the value of the modulus of elasticity along the fiber length direction remains practically unchanged in the studied temperature range. With an increase in temperature, the coefficient of linear thermal expansion of the binder and unidirectional fiberglass in the transverse direction increases almost 1.3 times, while its value along the fiber length direction decreases by no more than 10%. The values of thermal conductivity and heat capacity of the binder increase as temperature grows. The decrease in the stress level of the monolayer in the temperature range is especially noticeable in the transverse direction – it fell by 4.2 times, in the longitudinal direction it decreased by 30%. The results obtained make it possible to carry out a refined calculation of the stress-strain state of a composite structure within the operating temperature range.

Keywords: Temperature dependence · Approximation · Binder · Monolayer

1 Introduction

The introduction of new technologies in the chemical, oil production, oil refining, energy, construction, transport, engineering and other industries have repeatedly increased the relevance of the ever-widening use of polymer composite materials (PCMs) with

improved performance properties [1, 2]. In developing, testing and introducing PCMs, the possibility of a reliable, prompt and relatively inexpensive study of their properties is of great importance [3, 4]. At the same time, of the greatest value are methods and equipment that allow, on the one hand, measuring the most important indicators of PCM properties with a good accuracy, and on the other hand, serve as a tool for studying structural transformations and physicochemical processes that can develop under conditions of PCM operation [5, 6]. Using such methods and equipment facilitates solving a wide range of problems on optimizing the composition, production technology and prediction of properties of the developed PCMs and structures based on them [7, 8]. In case of composites intended for structural purposes, the main attention of researchers is focused on physical and mechanical properties (PMPs) [9, 10]. No less important is information about the dependence of PMPs of composites on temperature, especially considering that PCMs are characterized by a pronounced temperature anisotropy of properties [11, 12].

2 Literature Review

The widespread use of advanced analysis methods makes it possible to carry out complex studies of PCM PMPs [13], and modern equipment greatly facilitates the collection and processing of data obtained as a result of experiments [14]. The paper [15] studies the effect of temperature on PMPs of epoxy adhesives. The results show that the elastic moduli of the binders are stable in the temperature range from 0 to 30 °C, while in the range from 30 °C to 100 °C they decrease linearly and drop sharply when the glass transition temperature is reached. The tensile strength decreases almost linearly with an increase in temperature, the degree of decrease differing depending on the binder type. Similar dependences of PMPs of nanomodified composites on temperature are obtained in the work [16]. The research [17] proposes a method for accelerated testing of PCM PMP depending on temperature. The disadvantage of the proposed method is the possibility of predicting a decrease in PMP values only below the glass transition temperature of the composite. The paper [18] investigates PMPs of glass/epoxy and neat epoxy binders in the temperature range from 0 to 50 °C. The results of the prediction at room temperature show that an increase in stress levels results in acceleration of elastic strain values. In addition, a decrease in elastic properties is achieved by reducing the degree of compliance at a higher stress level at the glass transition temperature. However, regardless of the type of fiber orientation, with an increase in temperature a decrease in the elastic modulus and tensile strength is observed. In the work [19], using molecular dynamics simulation, thermophysical properties of various binders are determined and an original method for calculating the thermal expansion coefficient based on density variation with temperature is proposed. The paper [20] presents the results of experimental studies to establish the dependence of the impact behavior of PCMs on temperature. The results show that an increase in temperature can lead to a clear decrease in the stiffness behavior of PCMs. The work [21] presents results of experimental studies of PMPs of woven composites in the temperature range of 218–448 K. It is shown that the elastic modulus and strength of woven composites decrease with an increase in temperature. The paper [22] experimentally studies the effect of temperature in the range from –100 °C

to 100 °C on the PMPs of carbon fiber reinforced polymers at three-point bending. The results demonstrate that the composites provide enhanced flexural strength at lower temperatures (−60 °C, −100 °C), while relatively poor performance is observed at a higher temperature (100 °C). The work [23] presents the prediction of PMPs of reinforced PCMs using the finite element method. In the research [24], a numerical simulation of the thermomechanical behavior of PCMs with continuous carbon fiber reinforcement exposed to elevated temperatures is performed. The influence of global thermal loads on the PCM is modelled by changing its mechanical properties at the microscale (level of fiber-matrix interaction). The glass transition temperature of the composite, determined as a result of the study, is 42 °C. At this temperature, a significant decrease in the elastic modulus is observed. In the works [25, 26] the PMPs of three-dimensional braided and hybrid composites are studied with the use of a modified multiscale finite element method. The simulation results are in good agreement with the experimental data. Such methods, despite their versatility, have a number of significant drawbacks: cumbersomeness, time-consuming programming, the need for large RAM capacity and a lot of computing time; difficulties in preparing input data and visualizing calculation results, poor stability of the obtained solutions, etc. The paper [27] studies thermomechanical properties of composites. Due to the combination of an equivalent model and mechanical experiments, the simulation of composites has allowed to obtain a minimum spread of parameters. In this regard, the aim of the work is to study and analyze the effect of operating temperatures on PCM PMPs and to establish the temperature dependences of these properties for composites used in critical structures.

3 Research Methodology

The effect of temperature on PCM PMPs depends on the components included in the composition [28, 29]. For example, the values of the longitudinal elastic modulus E_1 , ultimate tensile strength F_{1t} and ultimate compressive strength F_{1c} , Poisson's ratio μ_{12} of the PCM layer insignificantly depend on temperature, since they are determined by the properties of the reinforcing material that do not change much in the specified temperature range, and their elastic properties can be considered constants. At the same time, the transverse elastic modulus E_2 and the shear modulus G_{12} depend on temperature significantly, since they are determined by properties of the matrix [30].

The data on the dependence of PMPs of the binder are taken from the previous experimental studies [31]. The data are approximated by a polynomial of the third degree for the elastic modulus of the binder for the temperature range of 273...473 K, with the reliability of 96%. The obtained equation has the following form:

$$E_b(T) = a_1 - a_2T + a_3T^2 - a_4T^3, \quad (1)$$

where $a_1 = 5635$ MPa, $a_2 = 16.67$ MPa · K^{−1}, $a_3 = 0.064$ MPa · K^{−2}, $a_4 = 1.15 \cdot 10^{-4}$ MPa · K^{−1} are the constants for the binder; T is the temperature, K.

The elastic properties of a unidirectional PCM in the longitudinal direction, with consideration for (1), take the following form [32]:

$$E_1(T) = E_b(T)(1 - \theta) + E_f\theta = \left(a_1 - a_2T + a_3T^2 - a_4T^3 \right) (1 - \theta) + E_f\theta, \quad (2)$$

$$\mu_{12}(T) = \mu_b(1 - \theta) + \mu_f\theta, \quad (3)$$

where θ is the fiber volume fraction, E_f is the elastic modulus of the fiber, μ_f is the Poisson's ratio of the reinforcing material, μ_b is the Poisson's ratio of the binder (almost independent of temperature).

Since the transverse modulus and shear modulus of a unidirectional material are mainly determined by the binder, therefore, their dependence on temperature will be more significant than that of the modulus of elasticity in longitudinal direction [29]. To consider the influence of temperature in the expressions for calculating the modulus of elasticity in the transverse direction and the shear modulus, we will use the following equations [32]:

$$E_2(T) = \left[\frac{1 - \mu_b^2}{E_b(T)} \left(\frac{2 + (k_f - 1) \frac{G_b(T)}{G_f}}{1 + \psi + \theta k_b + \psi (k_f - 1) \frac{G_b(T)}{G_f}} - \frac{2\theta \left(1 - \frac{G_b(T)}{G_f}\right)}{\theta + k_b + \psi \frac{G_b(T)}{G_f}} \right) \right]^{-1}, \quad (4)$$

where $k_b = 3 - 4\mu_b$; $k_f = 3 - 4\mu_f$; $\psi = 1 - \theta$;

$$G_{12}(T) = \frac{E_b(T)}{2(1 + \mu_b)} \frac{1 + \chi\theta}{1 - \chi\theta}, \quad (5)$$

where $\chi = \frac{2G_f(T)(1 + \mu_b) - E_b(T)}{2G_f(T)(1 + \mu_b) + E_b(T)}$.

Based on the above Eqs. (1)–(5) the dependences of the elastic properties on temperature in the temperature range from 273 to 473 K were built for the epoxy binder and fiberglass (Figs. 1, 2, 3 and 4)

As can be seen from the presented dependences (Figs. 1, 2 and 3), the elastic properties decrease as the temperature rises for both the binder and the unidirectional fiberglass. With an increase in the temperature to 473 K, the values of the elastic modulus of the binder, the shear modulus, the modulus of elasticity of unidirectional fiberglass $E_2(T)$ and the Poisson's ratio $\mu_{21}(T)$ decrease by almost 5 times. The shear modulus $G_{12}(T)$ also decreases by more than 4.5 times, while the value of $E_1(T)$ in the studied range remains practically unchanged (Fig. 4).

To study the dependence of the coefficient of linear thermal expansion (CLTE) in a given temperature range at the stage of curing, the results of experiments for the epoxy binder [31] are taken as initial data.

The data are approximated by a polynomial of the third degree for the temperature range of 273...473 K, with the reliability of 96%. The obtained equation is as follows:

$$\alpha_b(T) = b_1 + b_2T + b_3T^2 + b_4T^3, \quad (6)$$

where $b_1 = -3.7 \cdot 10^{-6} \cdot \text{K}^{-1}$, $b_2 = 2.1 \cdot 10^{-7} \cdot \text{K}^{-2}$, $b_3 = 3.75 \cdot 10^{-10} \cdot \text{K}^{-3}$, $b_4 = -9.3 \cdot 10^{-13} \cdot \text{K}^{-4}$ are the constants for the binder.

In the longitudinal direction, the CLTE, with consideration for (6), takes the following form [32]:

$$\alpha_1(T) = \frac{E_f\alpha_f\theta + E_b(T)\alpha_b(T)(1 - \theta)}{E_f\theta + E_b(T)(1 - \theta)}, \quad (7)$$

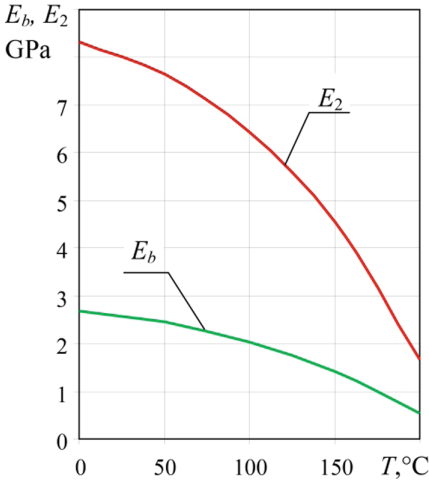


Fig. 1. Dependence of E_c and E_2 on temperature for the fiberglass.

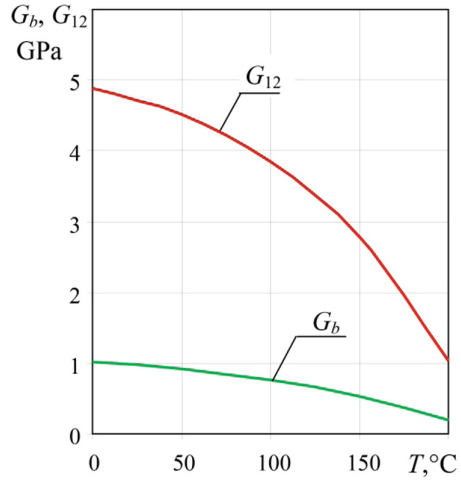


Fig. 2. Dependence of G_c and G_{12} on temperature for the fiberglass.

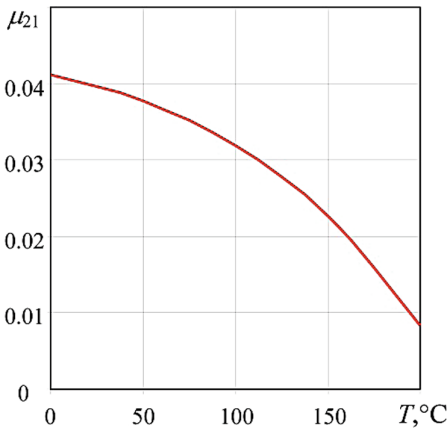


Fig. 3. Dependence of μ_{21} on temperature for the fiberglass.

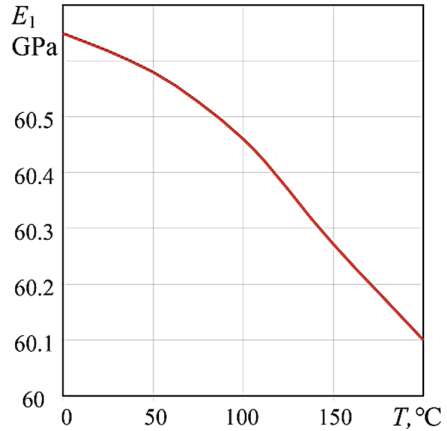


Fig. 4. Dependence of E_1 on temperature for the fiberglass.

where α_f is the CLTE of the reinforcing material (in the specified temperature range for the glass fiber and carbon fiber practically does not change [29]).

In the transverse direction, the equation for the CLTE depending on the temperature is written as follows [32]:

$$\alpha_2(T) = \frac{[\alpha_f \theta + \alpha_b(T)(1 - \theta)][E_f \theta + E_b(T)(1 - \theta)]}{E_f \theta + E_b(T)(1 - \theta)} + \frac{\theta(1 - \theta)(\alpha_b(T) - \alpha_f)(E_f \mu_b - E_b(T)\mu_f)}{E_f \theta + E_b(T)(1 - \theta)}. \quad (8)$$

According to the presented Eqs. (7) and (8), the dependence of the material's CLTE on temperature in a given temperature range is built (Fig. 5). As can be seen from the above dependences, $\alpha_b(T)$ and $\alpha_2(T)$ increase with a growth in temperature, while $\alpha_1(T)$ decreases in this case. This is due to the fact that $E_b(T)$ is a decreasing function in this interval.

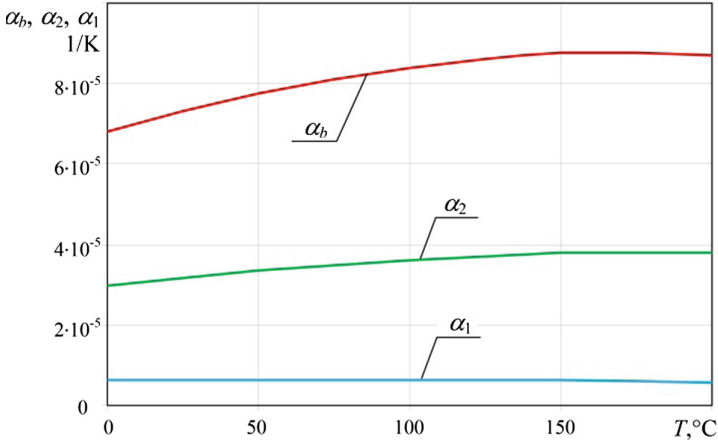


Fig. 5. Dependence of α_b , α_1 , α_2 on temperature for the fiberglass.

With a growth in temperature, the values $\alpha_b(T)$ and $\alpha_2(T)$ increase by almost 1.3 times, while the value $\alpha_1(T)$ decreases by no more than 10%.

In addition to the dependences of the elastic properties and CLTE on temperature, it is necessary to know the values of the thermal parameters of the material in a given temperature range [33]. The temperature difference in the molded product is mainly determined by the thermal conductivity and heat capacity of the material. Based on the experimental studies [31], dependences of thermal conductivity and specific heat capacity of the epoxy binder for the temperature range of 273...473 K are obtained and then approximated by a polynomial of the third degree (Fig. 6).

The dependence of the thermal conductivity is presented in the following form:

$$\lambda_b(T) = c_1 + c_2T + c_3T^2 + c_4T^3, \quad (9)$$

where $c_1 = -0.119 \cdot \text{W}/(\text{m} \cdot \text{K})$, $c_2 = 3.66 \cdot 10^{-3} \cdot \text{W}/(\text{m} \cdot \text{K}^2)$, $c_3 = -1.24 \cdot 10^{-5} \cdot \text{W}/(\text{m} \cdot \text{K}^3)$, $c_4 = 1.4 \cdot 10^{-8} \cdot \text{W}/(\text{m} \cdot \text{K}^4)$ are the constants for the binder.

The dependence of the heat capacity for the specified temperature range is as follows:

$$C_b(T) = c_1 + c_2T + c_3T^2 + c_4T^3, \quad (10)$$

where $c_1 = -8561.1 \text{ kJ}/(\text{kg} \cdot \text{K})$, $c_2 = 68.04 \text{ kJ}/(\text{kg} \cdot \text{K}^2)$, $c_3 = -0.15 \text{ kJ}/(\text{kg} \cdot \text{K}^3)$, $c_4 = 1.11 \cdot 10^{-4} \text{ kJ}/(\text{kg} \cdot \text{K}^4)$ are the constants for the binder.

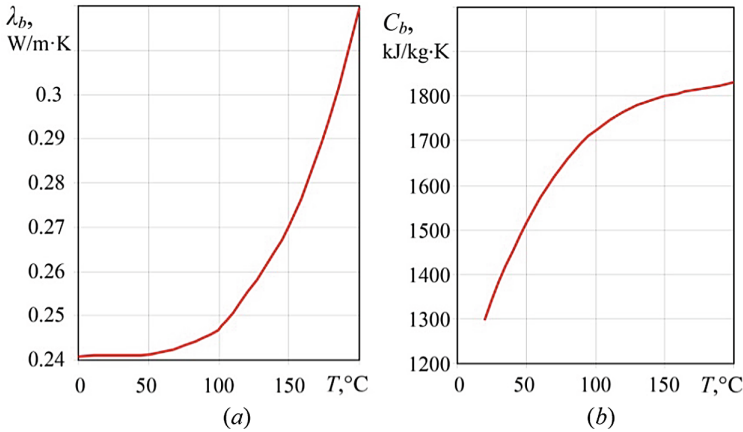


Fig. 6. Dependence of the thermal conductivity (a) and the specific heat capacity (b) of an epoxy-resin binder on temperature.

From the presented dependences (Fig. 6), it can be seen that the values of thermal conductivity and heat capacity of the binder increase as the temperature rises. However, when designing a PCM, it is necessary to consider the parameters of not only the binder but also of the reinforcing material as well as its volume fraction. Since the thermal conductivity of the material depends on the direction, the equations for the thermal conductivity values in the longitudinal and transverse directions can be written in the following form [32] (Fig. 7):

$$\lambda_1(T) = \lambda_f(T)\theta + \lambda_b(T)(1 - \theta), \tag{11}$$

$$\lambda_2(T) = \lambda_b(T) \left(1 + \frac{\theta}{\left(\frac{\lambda_b(T)}{\lambda_b(T) + \lambda_f(T)} + \frac{1-\theta}{2} \right)} \right), \tag{12}$$

where $\lambda_1(T)$, $\lambda_2(T)$ are the thermal conductivity coefficients in the longitudinal and transverse directions, respectively; $\lambda_f(T)$, $\lambda_b(T)$ are the thermal conductivity coefficients of the reinforcing material and the binder, respectively.

The heat capacity of PCMs does not depend on the direction of reinforcement, because it is a volumetric characteristic, therefore, the expression for heat capacity has the following form [32]:

$$C(T) = C_f(T)\theta + C_b(T)(1 - \theta), \tag{13}$$

where $C(T)$ is the coefficient of heat capacity of the PCM; $C_f(T)$, $C_b(T)$ are the heat capacity coefficients of the reinforcing material and the binder, respectively.

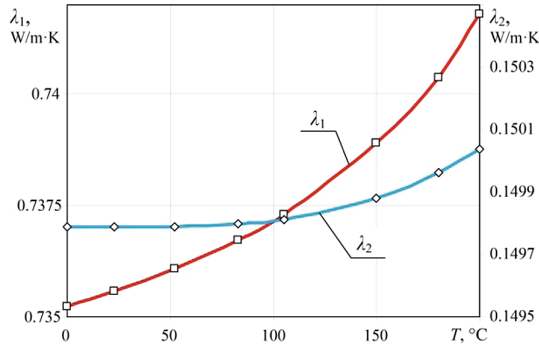


Fig. 7. Dependence of λ_1 , λ_2 on temperature for the fiberglass.

4 Results

Thus, in the course of studying the effect of temperature on the elastic and thermal properties of the PCMs, it can be said that the effect of temperature on the mentioned properties in the transverse direction is quite significant. The change in the PMP values in the longitudinal direction with an increase in temperature is insignificant. Taking into consideration the dependence of the elastic properties of the material on temperature makes it possible to more accurately determine the stress-strain state of the structure. As can be seen from Fig. 8, the decrease in the stress level of the monolayer in the temperature range is especially noticeable in the transverse direction (σ_2 decreased by 4.2 times, τ_{12} by 3.5 times, while σ_1 decreased by 30%). Such behavior is explained by the fact that the properties in the transverse direction are determined by the matrix of the material-product. Moreover, from the above dependences, it can be seen that the properties of the PCM depend on the ratio of its constituent components, therefore, the consideration for the change in stresses in the structure depending on temperature will also depend on this ratio. It can be assumed that the larger the volume of the reinforcing material

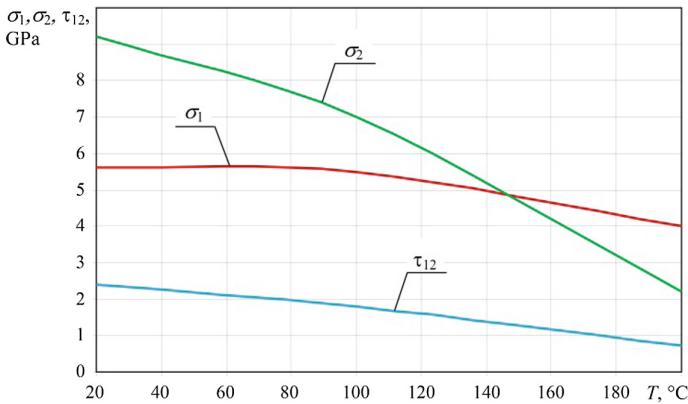


Fig. 8. Dependence of stresses in the monolayer on temperature.

demonstrating stable properties throughout the entire molding process, the smaller the difference between the stress-strain state of the structure, calculated with consideration for temperature, and the stress-strain state, calculated at constant elastic properties.

5 Conclusions

The analytical dependences of the influence of temperature on the elastic, thermomechanical and thermal properties of the PCM are presented. The influence of temperature on the properties of the material has been assessed: thus, in the considered temperature range, the stress level in the monolayer decreased for σ_1 by 30%, for σ_2 by 4.2 times and for τ_{12} by 3.5 times. The presented dependences make it possible to carry out a refined calculation of the stress-strain state of a composite structure in the operating temperature range. Using such dependences facilitates solving a wide range of practical problems on optimizing the composition, production technology and prediction of properties of the developed PCMs and structures based on them.

References






1. Elfaki, I., Abdalgadir, S.: Composite sandwich structures in advanced civil engineering applications – a review. *Comput. Res. Prog. Appl. Sci. Eng.* **6**, 259–262 (2020)
2. Smetankina, N., Merkulova, A., Merkulov, D., Postnyi, O.: Dynamic response of laminate composite shells with complex shape under low-velocity impact. In: Nechyporuk, M., Pavlikov, V., Kritskiy, D. (eds.) *ICTM 2020. LNNS*, vol. 188, pp. 267–276. Springer, Cham (2021). https://doi.org/10.1007/978-3-030-66717-7_22
3. Otrosh, Y., Kovalov, A., Semkiv, O., et al.: Methodology remaining lifetime determination of the building structures. *MATEC Web Conf.* **230**, 02023 (2018). <https://doi.org/10.1051/mateconf/201823002023>
4. Fomin, O., Lovskaya, A., Plakhtiy, A., Nerubatsky, V.: The influence of implementation of circular pipes in load-bearing structures of bodies of freight cars on their physico-mechanical properties. *Sci. Bull. Natl. Min. Univ.* **6**(162), 89–96 (2017)
5. Kombarov, V., Kryzhyvets, Y., Biletskyi, I., et al.: Numerical control of fiberglass pipe bends manufacturing. In: 2021 IEEE 2nd KhPI Week on Advanced Technology (KhPIWeek), Kharkiv, pp. 357–362. IEEE (2021). <https://doi.org/10.1109/KhPIWeek53812.2021.9570068>
6. Otrosh, Y., Rybka, Y., Danilin, O., Zhuravskiy, M.: Assessment of the technical state and the possibility of its control for the further safe operation of building structures of mining facilities. *E3S Web Conf.* **123**, 01012 (2019). <https://doi.org/10.1051/e3sconf/201912301012>
7. Slyvyns'kyi, V., Gajdachuk, V., Kirichenko, V., Kondratiev, A.: Basic parameters' optimization concept for composite nose fairings of launchers. In: 62nd International Astronautical Congress, IAC 2011, Red Hook, NY, vol. 9, pp. 5701–5710 (2012)
8. Deng, B., Shi, Y.Y., Yu, T., Zhao, P.: Influence mechanism and optimization analysis of technological parameters for the composite prepreg tape winding process. *Polymers* **12**(8), 1843 (2020). <https://doi.org/10.3390/polym12081843>
9. Hsissou, R., Seghiri, R., Benzekri, Z., et al.: Polymer composite materials: a comprehensive review. *Compos. Struct.* **262**, 113640 (2021). <https://doi.org/10.1016/j.compstruct.2021.113640>
10. Kondratiev, A., Píšťek, V., Smovziuk, L., et al.: Stress-strain behaviour of repairable composite panel with step-variable thickness. *Polymers* **13**(21), 3830 (2021). <https://doi.org/10.3390/polym13213830>

11. Dveirin, O.Z., Andreev, O.V., Kondrat'ev, A.V., Haidachuk, V.Y.: Stressed state in the vicinity of a hole in mechanical joint of composite parts. *Int. Appl. Mech.* **57**(2), 234–247 (2021). <https://doi.org/10.1007/s10778-021-01076-4>
12. Tkachenko, D., Tsegelnyk, Y., Myntiuk, S., Myntiuk, V.: Spectral methods application in problems of the thin-walled structures deformation. *J. Appl. Comput. Mech.* **8**(2), 641–654 (2022). <https://doi.org/10.22055/jacm.2021.38346.3207>
13. Baran, I., Cinar, K., Ersoy, N., Akkerman, R., Hattel, J.H.: A review on the mechanical modeling of composite manufacturing processes. *Arch. Comput. Methods Eng.* **24**(2), 365–395 (2016). <https://doi.org/10.1007/s11831-016-9167-2>
14. Kumar, A., Sharma, K., Dixit, A.R.: Carbon nanotube- and graphene-reinforced multiphase polymeric composites: review on their properties and applications. *J. Mater. Sci.* **55**(7), 2682–2724 (2019). <https://doi.org/10.1007/s10853-019-04196-y>
15. Ke, L., Li, C.X., He, J., et al.: Effects of elevated temperatures on mechanical behavior of epoxy adhesives and CFRP-steel hybrid joints. *Compos. Struct.* **235**, 111789 (2020). <https://doi.org/10.1016/j.compstruct.2019.111789>
16. Salom, C., Prolongo, M.G., Toribio, A., et al.: Mechanical properties and adhesive behavior of epoxy-graphene nanocomposites. *Int. J. Adhes. Adhes.* **84**, 119–125 (2018). <https://doi.org/10.1016/j.ijadhadh.2017.12.004>
17. Krauklis, A.E., Akulichev, A.G., Gagani, A.I., Echtermeyer, A.T.: Time-temperature-plasticization superposition principle: predicting creep of a plasticized epoxy. *Polymers* **11**, 1848 (2019). <https://doi.org/10.3390/polym11111848>
18. Nosrati, N., Zabett, A., Sahebian, S.: Stress dependency of creep response for glass/epoxy composite at nonlinear and linear viscoelastic behavior. *Int. J. Polym. Sci.* **2022**, 9733138 (2022). <https://doi.org/10.1155/2022/9733138>
19. Hadipeykani, M., Aghadavoudi, F., Toghraie, D.: A molecular dynamics simulation of the glass transition temperature and volumetric thermal expansion coefficient of thermoset polymer based epoxy nanocomposite reinforced by CNT: a statistical study. *Phys. A* **546**, 123995 (2020). <https://doi.org/10.1016/j.physa.2019.123995>
20. Liu, M.J., Xu, J.Z., Fu, T.Y., et al.: Investigations on the internal curing process and mechanical properties of winding composite considering the structure of plant fiber. *J. Appl. Polym. Sci.* **137**(37) (2020). <https://doi.org/10.1002/app.49114>
21. Wang, J., Wen, L., Xiao, J., et al.: The mechanical properties and constitutive model of two woven composites including the influences of temperature, strain rate and damage growth. *Compos. B Eng.* **161**, 502–513 (2019). <https://doi.org/10.1016/j.compositesb.2018.12.137>
22. Jia, Z.A., Li, T.T., Chiang, F.P., Wang, L.F.: An experimental investigation of the temperature effect on the mechanics of carbon fiber reinforced polymer composites. *Compos. Sci. Technol.* **154**, 53–63 (2018). <https://doi.org/10.1016/j.compscitech.2017.11.015>
23. Guo, F.L., Huang, P., Li, Y.Q., et al.: Multiscale modeling of mechanical behaviors of carbon fiber reinforced epoxy composites subjected to hygrothermal aging. *Compos. Struct.* **256**, 113098 (2021). <https://doi.org/10.1016/j.compstruct.2020.113098>
24. Muna, I.I., Mieloszyk, M.: Temperature influence on additive manufactured carbon fiber reinforced polymer composites. *Materials* **14**, 6413 (2021). <https://doi.org/10.3390/ma14216413>
25. Hong, Y., Yan, Y., Tian, Z.Y., et al.: Mechanical behavior analysis of 3D braided composite joint via experiment and multiscale finite element method. *Compos. Struct.* **208**, 200–212 (2019). <https://doi.org/10.1016/j.compstruct.2018.10.017>
26. Massarwa, E., Tabrizi, I.E., Yildiz, M.: Mechanical behavior and failure of glass/carbon fiber hybrid composites: multiscale computational predictions validated by experiments. *Compos. Struct.* **260**, 113499 (2021). <https://doi.org/10.1016/j.compstruct.2020.113499>

27. Wang, Y., Zhang, J., Fang, G., et al.: Influence of temperature on the impact behavior of woven-ply carbon fiber reinforced thermoplastic composites. *Compos. Struct.* **185**, 435–445 (2018). <https://doi.org/10.1016/j.compstruct.2017.11.056>
28. Fedulov, B.N.: Modeling of manufacturing of thermoplastic composites and residual stress prediction. *Aerosp. Syst.* **1**(2), 81–86 (2018). <https://doi.org/10.1007/s42401-018-0018-8>
29. Saba, N., Jawaid, M.: A review on thermomechanical properties of polymers and fibers reinforced polymer composites. *J. Ind. Eng. Chem.* **67**, 1–11 (2018). <https://doi.org/10.1016/j.jiec.2018.06.018>
30. Muliana, A.H.: Spatial and temporal changes in physical properties of epoxy during curing and their effects on the residual stresses and properties of cured epoxy and composites. *Appl. Eng. Sci.* **7**, 100061 (2021). <https://doi.org/10.1016/j.apples.2021.100061>
31. Vambol, O.O., Purhina, S.M., Stavychenko, V.G., Shevtsova, M.A.: Modeling the process of forming composite structures. National Aerospace University “Kharkiv Aviation Institute”, Kharkiv (2016). (in Russian)
32. Vasiliev, V.V., Morozov, E.V.: *Advanced Mechanics of Composite Materials and Structures*. Elsevier, Amsterdam (2018). <https://doi.org/10.1016/C2016-0-04497-2>
33. Kondratiev, A., Přítěk, V., Purhina, S., et al.: Self-heating mould for composite manufacturing. *Polymers* **13**(18), 3074 (2021). <https://doi.org/10.3390/polym13183074>



Stiffness and Fatigue of Sandwich Plates with Honeycomb Core Manufactured by Fused Deposition Modeling

Borys Uspensky¹ (✉) , Konstantin Avramov^{1,2,5} , Ihor Derevianko³ ,
Oleg Polishchuk¹ , and Oleksandr Salenko⁴ 

¹ A. Pidhornyi Institute of Mechanical Engineering Problems of the National Academy of Sciences of Ukraine, 2/10 Pozharskogo Street, Kharkiv 61046, Ukraine
Uspenskiy@nas.gov.ua

² Kharkiv National University of Radio Electronics, 14 Nauky Avenue, Kharkiv 61166, Ukraine

³ Yuzhnoye State Design Office, 1 Kryvoriz'ka Street, Dnipro 49008, Ukraine

⁴ National Technical University of Ukraine "Igor Sikorsky Kyiv Polytechnic Institute", 37 Prosp. Peremohy, Kyiv 03056, Ukraine

⁵ National Aerospace University "Kharkiv Aviation Institute", 17 Chkalova Street, Kharkiv 61070, Ukraine

Abstract. Shear and tension properties of the honeycombs FDM-manufactured from PLA and ULTEM 9085 are analyzed experimentally. Experimental data show that geometrically nonlinear deformations of the honeycomb walls occur during tension. Deformation of the honeycomb cells is accounted in the finite elements simulation of the specimen tension which is performed using the ANSYS commercial software. The simulation takes into account deformations of the equipment and honeycomb cells as well as the geometrical nonlinearity of the honeycomb strain-state. Method of fatigue testing of the sandwich plates with FDM-manufactured honeycomb core is treated. A combination of fatigue tests and numerical simulations of the thin-walled structure in the software ANSYS is used. Fatigue properties of the specimens from the PLA material are obtained to analyze the fatigue of the honeycomb, which is produced by the FDM additive manufacturing. The combination of the experimental and the numerical analysis is used to analyze the fatigue of the sandwich plate. S-N diagrams of the sandwich plate are obtained as a result of such analysis.

Keywords: Honeycomb core · Fused deposition modeling · Shear · Force-strain response

1 Introduction

Additive technologies are used in design and productions of satellites, launch vehicles and aircrafts [1]. The honeycomb core, which is used in the sandwich structures, can be produced by the additive manufacturing [2]. Using the homogenization theory, a honeycomb core can be replaced by an orthotropic solid medium in order to simplify

the calculations [3]. Analytical and numerical methods are developed to calculate the mechanical characteristics of this orthotropic media [4]. Mechanical behavior of honeycomb structures was investigated through in-plane static compression tests in [5]. The shear moduli and shear strength of extruded polystyrene foam were obtained by in-plane shear and asymmetric four-point bending tests in [6]. As follows from the experimental analysis [7], the materials of the parts produced by additive manufacturing are anisotropic. Raster angles, air gaps and printing velocities are affected on the mechanical characteristics of printing parts [8]. As follows from [9], ULTEM 9085 material has great potential for application in aerospace engineering. Fatigue of the samples obtained by the FDM additive technology is treated in several papers. Static and fatigue behavior of an auxetic honeycomb structure manufactured using FDM 3D printing technique was analyzed experimentally in [10]. The papers [11–13] aim is analysis the fatigue behavior of polymeric materials, which is produced by FDM.

The static response and fatigue of the FDM-manufactured honeycombs is analyzed in the present paper. In order to use such structures in aerospace engineering the knowledge of their static and fatigue behavior is required.

2 Honeycomb Core Production

The honeycomb core is manufactured using 3D system Fortus 900 mc. The specimens are fabricated from PLA or ULTEM 9085 materials in order to study the material properties the honeycomb core. The building-up of layers is performed along the honeycomb height. The amount of the layers is equal to 45. The honeycomb height is equal to 10 mm. The printing is performed by PLA filament with diameter 0.2 mm and 0.22 mm ULTEM 9085 filament. All walls of the honeycomb have thickness in two layers. Every wall layer is formed by one passage of the extruder.

The honeycomb cell outline is shown at Fig. 1. The length of the wall l is measured along the inner side of the wall. The dimensions of the ULTEM honeycomb cell are the following: $h = 0.5$ mm; $l = 6.05$ mm, where h is thickness of the cell walls; l is length of the internal side of the cell. The dimensions of the PLA honeycomb cell are: $h = 0.4$ mm; $l = 6.11$ mm. Cartesian coordinate system $x_1x_2x_3$ is used to simulate the honeycomb (Fig. 1b).

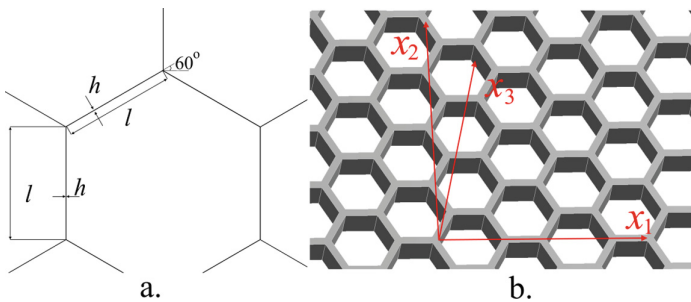


Fig. 1. Honeycomb core: (a) – cell parameters; (b) – honeycomb outline

3 Experimental Analysis

3.1 Shear Characteristics

The tensile machine TiraTest 2300 is used for mechanical testing. Figure 2a shows the outline of the specimen for the honeycomb shear characteristics determination. The specimen consists of two honeycombs 1, which are glued with three loads applications plates 2. The dimensions of the specimen are shown on Fig. 2a in millimeters. The specimens prepared for experimental testing are shown on Fig. 2b. The dimensions of the honeycomb are $120 \times 60 \times 10$ mm. The specimen is mounted in the gripping device (Fig. 3). The direction of the force F coincides with the longitudinal axis of the specimen (the x_1 direction of the honeycomb).

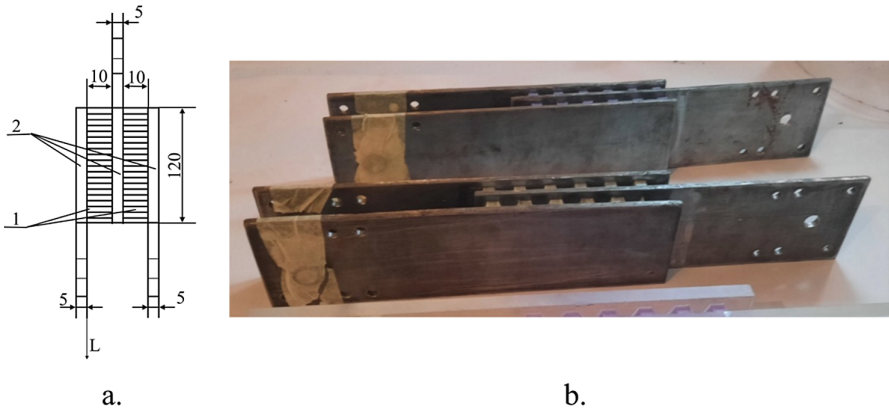


Fig. 2. Specimens: (a) – Outline of honeycomb specimen; (b) – Photo of specimens for shear testing of honeycomb from PLA (top) and from ULTEM 9085 (bottom)

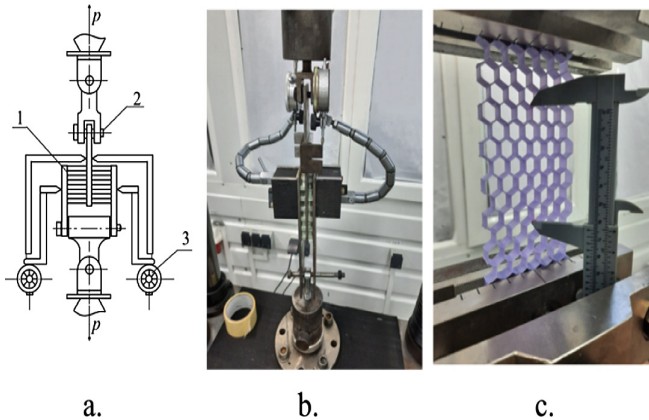


Fig. 3. Layout and photo of experimental test rig: (a) – schematic diagram; (b) – photo; (c) – tension test.

The testing is performed by gradual increase of the force up to the fracture of the samples. The constant velocity of the gripping device is equal to 2 mm/min. The dependences of the forces on the displacements are recorded during the testing. The force

is recorded using the electronic sensor in the range up to 100 kN. The displacements are recorded by using two dial indicators for every honeycomb separately to measure displacements without deformations of the hinges.

3.2 Tension Testing

The tension tests of the honeycombs are carried out on the tensile machine TiraTest 2300. The x_1 direction of the honeycomb (Fig. 1b) is arranged along the line of the tensile force. The specimen attachment is performed using the clamp of the tensile machine TiraTest 2300 (Fig. 3c). The dimensions of the honeycomb between the clamps are $146.2 \times 66.3 \times 10$ mm. Four honeycomb samples are tested.

The testing is performed by increasing the loads up to honeycomb fracturing. The uniform velocity of the clamp motions is equal to 5 mm/min.

3.3 Fatigue Testing

The fatigue tests of the sandwich plates are carried out using electrodynamic shaker. The shaker reproduces the harmonic vertical vibrations in the wide ranges of the frequencies and the amplitudes of the excitation. The shaker harmonic motions excite the flexural harmonic vibrations of the sandwich specimen. The weight is attached at free end of the sandwich plate to reach the required values of the stresses in the honeycomb.

In Fig. 4 shown the attachment of the sandwich plate to the shaker platform 3. Sandwich plate is denoted by 1. The weight with vibrations transducer is installed at the end of the sandwich plate. This vibration transducer records the vibration acceleration. The mass of the weight with transducer is chosen to obtain the necessary values of stresses in the honeycomb for the fatigue tests.

The specimens' tests are performed up to their fracture. The numbers of cycles to the specimen fracture are recorded. The variations of the vibrational eigenfrequencies due to decrease of the sandwich plate stiffness are observed during the fatigue tests. These variations are determined by creations of fatigue damages [9].

The stress-strain states of the sandwich plates are determined numerically by finite element method. S-N diagrams are obtained as a result of the fatigue tests and numeric simulations.

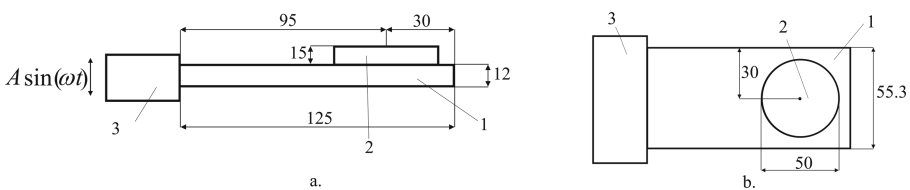


Fig. 4. Outline of sandwich plate attachment: (a) – side view; (b) – top view.

Fatigue testing is performed on 12 sandwich plate specimens with PLA-printed core and carbon composite faces. A carbon composite combined of four cross-ply layers of the prepreg SIGRAPREG C U200-0 is used for the faces.

4 Approach for Numerical Simulations

4.1 Static Response Simulations

Shear Testing. The finite element simulations of the mechanical experiments for determination of the shear characteristics and experiments for the honeycomb tension are carried out in two formulations. Full formulation allows taking into account the influences of every cell deformations. Homogenized formulation is much simpler to handle and is based on the honeycombs homogenization. As a result of the homogenization [14, 15], the honeycomb is replaced by the equivalent orthotropic solid plate of the same dimensions. Homogenization by finite element simulations is deeply discussed in [3]. The simulations of the specimen allow accounting three loads application plates (Fig. 2). The elasticity of the glue joints is not considered.

Tension Testing. The gripping device of the tensile machine TiraTest 2300 provides rigid contact with the sample. The x_1 direction of the honeycomb (Fig. 1b) is positioned vertically. The direct finite element simulation of the honeycomb with account of the cell deformations is performed.

The loading of the sample is performed by preset the displacements of one side Δ_X in order to obtain the uniform sample deformation observed in the experimental analysis. The second end of the spacemen is clamped (Fig. 5).

The weighed values of the stresses σ_X are calculated to obtain the forces, which results in the displacement Δ_X .

4.2 Sandwich Plates Fatigue Calculations

The finite element model is obtained for the stress-strain state calculations of the sandwich plate with the honeycomb. The homogenized model of the honeycomb with the effective mechanical characteristics [3] is obtained to analyze the fatigue properties of the structure.

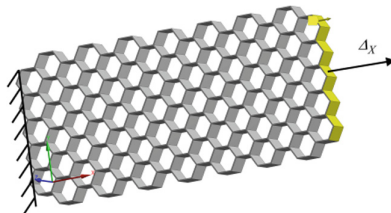


Fig. 5. Boundary conditions on the honeycomb.

4.3 Sandwich Plates Fatigue Calculations

The finite element model is obtained for the stress-strain state calculations of the sandwich plate with the honeycomb. The homogenized model of the honeycomb with the

effective mechanical characteristics [3] is obtained to analyze the fatigue properties of the structure.

In Fig. 6 shown the computational model of the sandwich plate with the weight. Figure 6a shows the computational model, which accounts the detailed honeycomb structure (without homogenization). In this case, the homogenization model of the honeycomb is not applied. The computational model with the homogenized honeycomb core is used for calculation too (Fig. 6b).

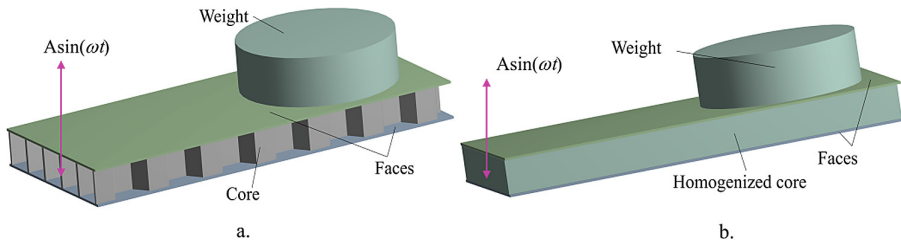


Fig. 6. Sketch of sandwich plate with weight and with different models of honeycomb; (a) - detailed model of honeycomb core (without homogenization); (b) - homogenized model of core.

The ANSYS Workbench is used for the finite element simulations of the sandwich plate. The harmonic response of the sandwich plate under the action of the kinematic excitation $A\sin(\omega t)$ (Fig. 6) is calculated. The frequency of the kinematic excitation ω is equal to the structure eigenfrequency 124.59 Hz. The amplitude of excitation A is equal to the vibrational amplitude of the shaker. Material damping in the form of Rayleigh β -damping [16] is accounted in the structure finite element model. The values of the material damping are identified from the equality of the amplitudes of the weight, which are obtained experimentally and numerically. The vibrational amplitudes of the von Mises stresses are determined from the forced vibrations analysis.

The S-N fatigue diagram is obtained using the numbers of cycles to failure and the amplitude values of the von Mises stresses, which are calculated using the homogenized model of the honeycomb.

5 Results of Experimental Analysis and Numerical Simulations

5.1 Shear Analysis

The numerical simulations and the experimental analysis of honeycomb shear are considered. The values of the concentrated forces F belong to the range $F \in [750; 9829.9]$ N.

In Fig. 7 shown the experimental data and the calculations results of the shear testing of honeycomb from PLA and ULTEM 9085 materials. The values of forces F versus the shear strain γ_{x1x3} are shown on these Figures. The experimental data averaged across the specimens are shown on Fig. 7 by solid lines. The results of the finite element calculations based on the honeycomb direct simulations accounting deformations of the cells and the

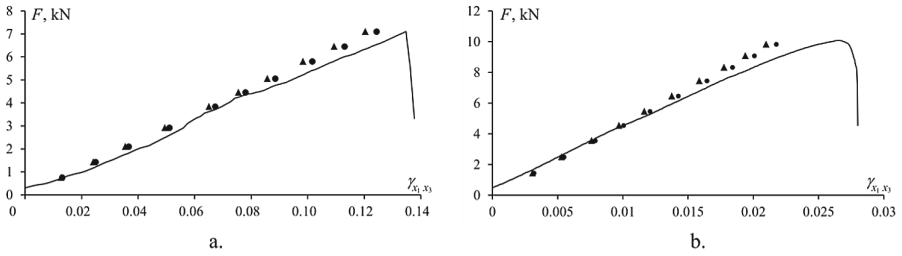


Fig. 7. Forces-shear strains responses of the honeycomb: (a) – PLA; (b) – ULTEM.

equipment are shown by triangular markers. The results of the finite element simulations using the homogenized honeycomb model are shown by round markers.

As follows from the honeycomb experimental analysis, the brittle fracture of the honeycomb is observed. The specimen fractures occur in the honeycomb during the shear testing. The glue joints between steel and honeycomb are not fractured. Figure 8 shows the fractured honeycombs.

Only elastic behavior of the structure is simulated by finite elements method. The data obtained from finite element analysis models are close to the experimental data.

The analysis results (Fig. 7) allow estimating the honeycomb shear modulus G_{x1x3} . Such values obtained from experimental and finite element analysis results are presented in Table 1. Experimental and numerical results are close.

Table 1. Shear modulus G_{x1x3} estimation (MPa) of the honeycomb.

Filament type	Experiment	Direct simulation	Relative difference	Homogenized model	Relative difference
PLA	36.790	40.390	0.097	40.050	0.089
ULTEM	34.383	36.772	0.069	35.423	0.038

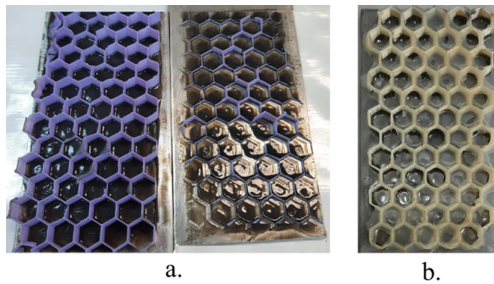


Fig. 8. Fractured PLA honeycomb during shear testing: (a) – PLA specimen; (b) – ULTEM specimen.

5.2 Tension Analysis

As follows from the experimental analysis, before the honeycomb fracturing, the displacements of the honeycomb free edge (Fig. 9) are commensurable with the honeycomb thickness. Therefore, large displacements of the honeycomb must be accounted. Then the nonlinear problem [17–20] is calculated using the commercial software ANSYS.

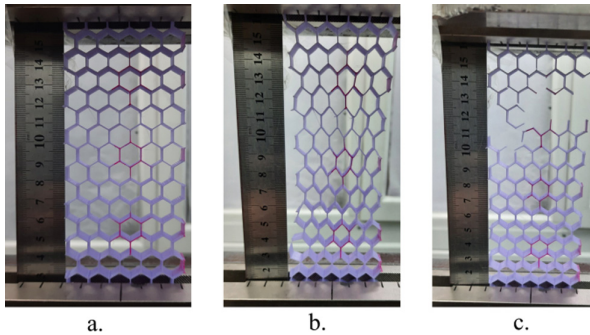


Fig. 9. Tension tests of honeycomb: (a) – sample before tension test; (b) – tensioned sample before fracture; (c) – fractured honeycombs

The honeycomb sample undergoes significant displacements during testing. The longitudinal displacements of the sample edge are equal to $12 \div 17$ mm. In Fig. 9a shown the photo of the honeycomb before loading. In Fig. 9b shown the tensioned specimen before fracture. The photo of the fractured honeycomb is shown in Fig. 9c. The averaged experimental force-displacement response is shown by the solid line on Fig. 10. The results of the finite element simulations of the samples deformations are shown by points on this figure. The majority points are close to the experimental response curve.

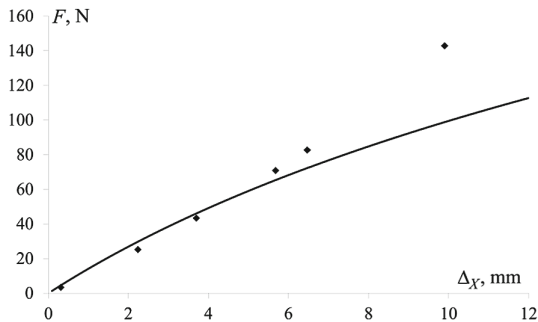


Fig. 10. The experimental results on the honeycomb tension and the data of finite element simulations.

5.3 Fatigue Analysis

The resonance vibrations of the sandwich plates are analyzed. During the experiment an eigenfrequency decrease due to the material wearing is accounted. Analysis of the spectral density of the cantilevered sandwich plate end shows that the vibrations of the sandwich plate end are simple harmonic.

The numbers of cycles to the fracture N_f and the numbers of cycles to the first eigenfrequency change N_C are measured during the fatigue tests. The fractures of the sandwich plates take place in the honeycombs. In Fig. 11 shown the example of the honeycomb fracture.



Fig. 11. Fractured sandwich plate. The crack is observed at honeycomb

The stresses in the honeycomb are estimated using finite element analysis. The data of the experimental fatigue analysis of the specimens and the calculations results of the von Mises stresses in the honeycomb are shown at Fig. 12. The von Mises stresses in the honeycomb σ_{\max} versus the numbers of cycles are shown on Fig. 12. The von Mises stresses in the honeycomb σ'_{\max} , which are obtained by the homogenized model of the honeycomb, are shown on Fig. 12b.

The S-N diagram (Fig. 12a) shows the numbers of cycles up to the variation of the eigenfrequencies N_c on the x-axis. This diagram is obtained both numerically by using the S-N diagram of the PLA material (solid line) and experimentally (dots). The numerical and experimental results are close.

The numbers of cycles to the fracture of the specimens is shown on the x-axis of the S-N diagram (Fig. 12b). The amplitudes of the von Mises stresses are obtained using the homogenized finite element model of the honeycomb. The dots (Fig. 12b) represent experimental data. The solid line shows the result of approximation using least squares technique.

As follows from the experimental data (Fig. 12), the sandwich plate resists well to fatigue loads.

Analysis of sandwich plates' defects is carried out after the structure fracture. Main approach of the analysis is the X-ray photography. The results of the specimens' defects analysis include multiple kinds of fatigue failures such as cracks in the honeycomb, buckling of the honeycomb walls, debonding of faces. Mostly the cracks in the honeycomb are observed. The buckling of the honeycomb walls are observed in two samples. Both cracks and the delamination between the layers are observed in one specimen.

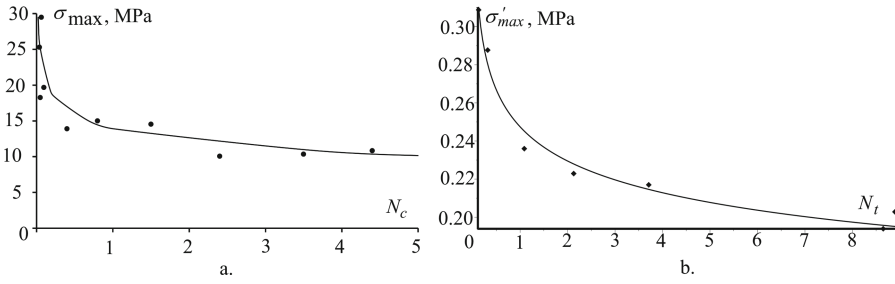


Fig. 12. S-N diagram of the sandwich plate with honeycomb: (a) – the numbers of cycles up to the variations of the eigenfrequencies N_c is shown on the x-axis; (b) – the numbers of cycles to the fracture of specimens are shown on the x-axis

6 Conclusion

An approach for experimental determination of mechanical characteristics of the honeycomb produced by FDM technology is suggested. Shear characteristics of the honeycomb are obtained by tension of the specimen. The honeycombs from PLA and ULTEM materials are analyzed experimentally. The forces-shear strains response and shear moduli are obtained as a result of this experiment. The specimen fractures occur in the honeycomb during the shear testing. The brittle fracture of the honeycomb is observed. The glue joints between the rig and the honeycomb are not fractured.

Tension response of the honeycomb is analyzed experimentally. Before the honeycomb fracturing, the displacements of the honeycomb free edge are commensurable with the honeycomb thickness. Therefore, geometrically nonlinear deformations of the honeycomb are taken place. If values of the tension forces are significant, the honeycomb walls undergo geometrically nonlinear deformations.

The shear and tension experiments are simulated using the finite element analysis. The direct finite element simulations of all cells of two honeycombs with account of the loads applications plates are carried out as well as the simulation using the homogenized honeycomb model. Elasticity of the glue joints is not accounted. The finite element calculations results are close to the experimental data.

The fatigue of the composite sandwich plate with the FDM-manufactured PLA honeycomb is analyzed. The approach for the experimental analysis of the sandwich plate fatigue is suggested. It is based on the resonance vibrational testing of the sandwich plate. The stress-strain state of the samples is calculated using the finite element simulations. Decrease of the structure eigenfrequencies due to the defects formation in the plate is observed during the fatigue tests. After the first measurable variation of the eigenfrequency, the structure undergoes significant numbers of cycles to the fracture.

Two types of S-N diagram of the sandwich plate are considered. The S-N diagram allows prediction of the number of cycles until the first damage of the honeycomb. This diagram is predicted well by the finite element simulations based on the S-N diagram of the PLA material. The S-N diagram to the specimen failure is developed using the homogenized honeycomb model. It allows predicting the number of cycles until the plate's failure.

Acknowledgement. This study was funded by National Research Foundation of Ukraine (grant number 128/02.2020).


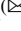

References

1. Matthews, N.: Additive metal technologies for aerospace sustainment. In: Aircraft Sustainment and Repair, pp. 845–862. Butterworth-Heinemann (2018). <https://doi.org/10.1016/B978-0-08-100540-8.00015-7>
2. Xu, M., Liu, D., Wang, P., et al.: In-plane compression behavior of hybrid honeycomb metastructures: theoretical and experimental studies. *Aerosp. Sci. Technol.* **106**, 106081 (2020). <https://doi.org/10.1016/j.ast.2020.106081>
3. Catapano, A., Montemurro, M.: A multi-scale approach for the optimum design of sandwich plates with honeycomb core. Part I: homogenisation of core properties. *Compos. Struct.* **118**, 664–676 (2014). <https://doi.org/10.1016/j.compstruct.2014.07.057>
4. Malek, S., Gibson, L.: Effective elastic properties of periodic hexagonal honeycombs. *Mech. Mater.* **91**, 226–240 (2015). <https://doi.org/10.1016/j.mechmat.2015.07.008>
5. Zhang, P., Arceneaux, D.J., Khattab, A.: Mechanical properties of 3D printed polycaprolactone honeycomb structure. *J. Appl. Polym. Sci.* **135**, 46018 (2017). <https://doi.org/10.1002/app.46018>
6. Yoshihara, H., Maruta, M.: Measurement of the shear properties of extruded polystyrene foam by in-plane shear and asymmetric four-point bending tests. *Polymers* **12**, 47 (2020). <https://doi.org/10.3390/polym12010047>
7. Casavola, C., Cazzato, A., Moramarco, V., Pappalettere, C.: Orthotropic mechanical properties of fused deposition modelling parts described by classical laminate theory. *Mater. Des.* **90**, 453–458 (2016). <https://doi.org/10.1016/j.matdes.2015.11.009>
8. Gerisa, A.W., Lenu, H.G.: Influence of 3D printing process parameters on tensile properties of ULTEM 9085. *Procedia Manuf.* **30**, 331–338 (2019). <https://doi.org/10.1016/j.promfg.2019.02.047>
9. Motaparti, K.P., Taylor, G., Leu, M.C. et al.: Effects of build parameters on compression properties for ULTEM 9085 parts by fused deposition modeling. In: Solid Freeform Fabrication 2016: Proceedings of the 26th Annual International Solid Freeform Fabrication Symposium – An Additive Manufacturing Conference, Austin, TX, pp. 946–977 (2016)
10. Khare, E., Temple, S., Tomov, I., et al.: Low fatigue dynamic auxetic lattices with 3D printable, multistable, and tuneable unit cells. *Front. Mater.* **5**, 45 (2018). <https://doi.org/10.3389/fmats.2018.00045>
11. Shanmugam, V., Das, O., Babu, K., et al.: Fatigue behaviour of FDM-3D printed polymers, polymeric composites and architected cellular materials. *Int. J. Fatigue* **143**, 106007 (2021). <https://doi.org/10.1016/j.ijfatigue.2020.106007>
12. Ezeh, O.H., Susmel, L.: Fatigue strength of additively manufactured polylactide (PLA): effect of raster angle and non-zero mean stresses. *Int. J. Fatigue* **126**, 319–329 (2019). <https://doi.org/10.1016/j.ijfatigue.2019.05.014>
13. Moore, J.P., Williams, C.B.: Fatigue properties of parts printed by PolyJet material jetting. *Rapid Prototyp. J.* **21**(6), 675–685 (2015). <https://doi.org/10.1108/RPJ-03-2014-0031>
14. Bhandaria, S., Lopez-Anido, R.: Finite element analysis of thermoplastic polymer extrusion 3D printed material for mechanical property prediction. *Addit. Manuf.* **22**, 187–196 (2018). <https://doi.org/10.1016/j.addma.2018.05.009>
15. Naveed A., Naeem Z., Hadiya Z.J.: Homogenization of honeycomb cores in sandwich structures: a review. In: Proceedings of 2019 16th International Bhurban Conference on Applied Sciences and Technology, pp. 159–173. IEEE (2019). <https://doi.org/10.1109/IBCAST.2019.8667144>

16. Pan, D.G., Chen, G.D., Gao, L.L.: A constrained optimal Rayleigh damping coefficients for structures with closely spaced natural frequencies in seismic analysis. *Adv. Struct. Eng.* **20**(1), 81–95 (2016). <https://doi.org/10.1177/1369433216646007>
17. Avramov, K.V.: Nonlinear forced vibrations of a cylindrical shell with two internal resonances. *Int. Appl. Mech.* **42**, 169–175 (2006). <https://doi.org/10.1007/s10778-006-0072-5>
18. Qiu, K., Wang, Z., Zhang, W.: The effective elastic properties of flexible hexagonal honeycomb with consideration for geometric nonlinearity. *Aerosp. Sci. Technol.* **58**, 258–266 (2016). <https://doi.org/10.1016/j.ast.2016.08.026>
19. Avramov, K.V., Borisuk, A.: Nonlinear dynamics of one disk asymmetrical rotor supported by two journal bearings. *Nonlinear Dyn.* **67**, 1201–1219 (2012). <https://doi.org/10.1007/s11071-011-0063-x>
20. Avramov, K.V., Strel'nikova, E.A.: Chaotic oscillations of plates interacting on both sides with a fluid flow. *Int. Appl. Mech.* **50**(3), 303–309 (2014). <https://doi.org/10.1007/s10778-014-0633-y>



Fuzzy-TOPSIS Hybrid Technique for Multi-response Optimization in Nonconventional Machining of Gears

Thobadingoe Craven Phokane  and Kapil Gupta  

Department of Mechanical and Industrial Engineering Technology, University of Johannesburg,
John Orr Building (DFC), Johannesburg 2028, South Africa
kgupta@uj.ac.za

Abstract. An optimum combination of process parameters is essential to attain the desired product quality and process productivity in manufacturing. Advanced or nonconventional machining of gears is in trend these days. This paper reports the optimization of wire-EDM parameters by Fuzzy-TOPSIS (Technique for Order of Preference by Similarity to Ideal Solution) integrated hybrid multi-criteria decision making technique. Gear manufacturing by wire-EDM involves conflicting interests such as gear quality and process productivity. For a better gear quality, lower values of surface roughness and micro-geometry errors are desirable, whereas for higher productivity, higher values of gear cutting rate is desirable. This multi-criteria problem has been solved in this work. After cutting gears from wire-EDM via a set of twenty-nine experiments, Fuzzy-TOPSIS has been used to optimize its process parameters. An optimum combination of Voltage – 10 V, Pulse-on Time – 0.8 μ s, Pulse-off Time – 170 μ s and Wire Feed Rate – 15 m/min has been obtained for simultaneous improvement of gear quality and wire-EDM productivity has been achieved. The outcome of this work provides a set of wire-EDM parameters for ready industrial use to manufacture quality gears with good productivity. Further, it is hoped that the scholars and researchers will utilize the Fuzzy-TOPSIS to solve MCDM problems for other manufacturing processes.

Keywords: Fuzzy · Gear · Productivity · Quality · TOPSIS · Wire-EDM

1 Introduction

In past few years, there have been significant attempts on nonconventional machining of gears. Electric discharge machining (EDM), wire-EDM, laser beam cutting, and abrasive water jet machining are mainly the techniques used for gear machining [1–3]. A gear is a machine element and used for motion and power transfer applications in a wide range of instrument, equipment, devices, and machines. To address the specific application requirements, appropriate selection of gear materials and optimum combination of process parameters for gear machining are two essential factors. It is known that materials like brass and aluminium are the best fit for motion transmission requirements and stainless steel is used for making gears which are to be used for torque transfer applications [4]. Machining is a subtractive type manufacturing process for making gears from

a wide range of materials. Due to many limitations of conventional machining [1], the advanced machining is being explored widely. The success of gear machining is based on two factors, namely, gear quality and process productivity. To obtain the same, gear machining should be done on an optimum combination of process parameters. In other words, optimization is one of the main strategies to attain the best quality and productivity in gear machining. An optimization can be done using various statistical and soft computing techniques or by their hybridization.

For multi-criteria decision making problems where conflicting type interests lie, relevant techniques are required to be implemented. Hybrid techniques such as Fuzzy-MOORA, Fuzzy-TOPSIS, Fuzzy-Grey and many other techniques have been used by researchers in the past. Some of the important past work is discussed here as under.

Sahu and Andhare [5] used a combination of Teaching learning-based optimization (TLBO) and genetic algorithm (GA) to minimize surface roughness and machining force while cutting Titanium grade 5 material. Gok [6] employed fuzzy TOPSIS and multi-objective grey design and succeeded for machinability enhancement of ductile iron. MOORA-Fuzzy hybrid technique for surface quality enhancement during wire-EDM of NiTi alloy was used by Majumder and Maity [7]. Tripathy and Tripathy [8] used TOPSIS and grey relational analysis for multi-performance optimization during powder mixed electro-discharge machining of die steel. They obtained increment in material removal rate from 2.564 to 9.87 mm³/min, reduction in tool wear rate from 0.0172 to 0.0034 mm³/min, and surface roughness decreased from 3.8 microns to 1.57 microns. While end milling of Mg hybrid metal matrix composites, an integrated technique of Taguchi-TOPSIS-GRA was used by Gopal and Prakash [9] and minimized the values of machining force and temperature, and surface roughness of the workpiece.

Another successful attempt on advanced machining optimization was done by Dewangan et al. [10] who used grey-fuzzy logic technique and optimized surface integrity related parameters in EDM. Bhaumik and Maity [11] used response methodology together with the fuzzy based desirability function approach for optimization of multi quality characteristics in powder-mixed electric discharge machining of AISI 304SS. Material removal rate was improved from 2.3708 to 2.4591 mm³/min, tool wear rate was decreased from 0.03198 to 0.01066 mm³/min, surface roughness was decreased from 6.33 to 5.124 microns. RSM-Fuzzy-TOPSIS integrated MCDM technique was employed by Tiwary et al. [12] to optimize process parameters of micro-EDM for Ti-6Al-4V. They obtained material removal rate – 0.076780 mg/min, tool wear rate – 0.021691 mg/min, taper – 0.00243, over cut per mm – 0.01023 on optimum setting of pulse-on time – 8 μs, current – 1.5 A, voltage – 30 V, and dielectric pressure – 0.15 kg/cm².

The review of past work indicates that the hybrid optimization techniques are indeed effective and have been effectively used for successful optimization of machining process parameters. Fuzzy-TOPSIS is one of them. When talk about the optimization of gear machining processes then very limited work is found and mainly based on the implementation of statistical technique desirability analysis. There is a scarcity of work on using MCDM based techniques to solve optimization problems in gear machining.

The work reported in this paper fills that gap where Fuzzy-TOPSIS based hybrid technique has been implemented to wire-EDM of gears for multi-performance optimization. The next sections will discuss about the various aspects of this work.

2 Experimental Details and Methodology

Wire-EDM machining of gears is done on a CNC WEDM machine tool with the details as given in [1, 13]. Figure 1 illustrates the sequence of tasks conducted in Wire-EDM gear machining and optimization.

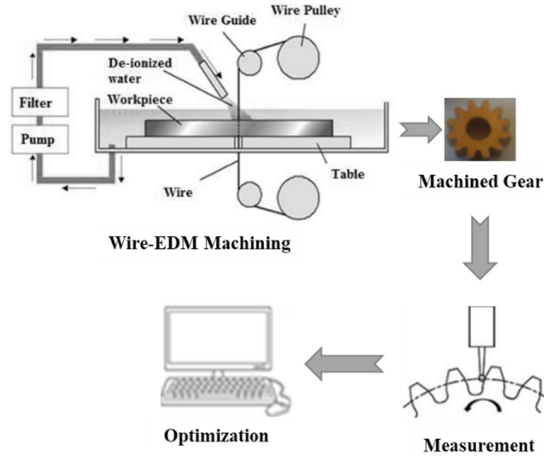


Fig. 1. Sequence of tasks in wire-EDM gear manufacturing.

Wire-EDM parameters considered and to be optimized are detailed in Sect. 3. The optimization is targeted to secure the single set of wire-EDM parameters for the best gear quality and process productivity. The selected gear quality indicators are average and maximum surface roughness Ra and Rmax, and profile error Fa and pitch error Fp. Whereas process productivity indicator is gear cutting rate GCR.

Fuzzy-TOPSIS hybridization uses a set of linguistic data to show opinions of the decision maker, furthermore, the generation of fuzzy decision matrix and normalized fuzzy decision matrix are from the further exploitation of these linguistic data sets [14–16]. The following steps illustrate the computation of fuzzy ideal negative solution and fuzzy ideal positive solution through the adoption of best weightage for each output criteria. Lastly, the calculation and preferred order of the alternatives were determined by the distances of each alternative from the ideal fuzzy negative and ideal fuzzy positive solutions.

Step 1: Fuzzy decision matrix development, where each column denotes one attribute and each row denotes one alternative [14]

$$\tilde{D} = \begin{matrix} A_1 \\ A_2 \\ \vdots \\ A_i \\ \vdots \\ A_m \end{matrix} \begin{bmatrix} \tilde{x}_{11} & \tilde{x}_{12} & \cdot & \tilde{x}_{1j} & \tilde{x}_{1n} \\ \tilde{x}_{21} & \tilde{x}_{22} & \cdot & \tilde{x}_{2j} & \tilde{x}_{2n} \\ \vdots & \vdots & \cdot & \vdots & \vdots \\ \tilde{x}_{i1} & \tilde{x}_{i2} & \cdot & \tilde{x}_{ij} & \vdots \\ \vdots & \vdots & \cdot & \vdots & \vdots \\ \tilde{x}_{m1} & \tilde{x}_{m2} & \cdot & \tilde{x}_{mj} & \tilde{x}_{mn} \end{bmatrix}, \tag{1}$$

where column denotes the attributes ($j = 1, 2, \dots, n$) and each row represents the possible alternatives ($i = 1, 2, \dots, m$). Moreover, \tilde{x}_{ij} represents the performance of attribute X_j and alternative A_i .

Step 2: Fuzzy decision matrix normalization for matrix \tilde{R}

$$\tilde{R} = [\tilde{r}_{ij}]_{m \times r}, \quad i = 1, 2, \dots, m \text{ and } j = 1, 2, \dots, r, \tag{2}$$

\tilde{r}_{ij} value can be computed as follows for the beneficial criteria

$$\tilde{r}_{ij} = \left(\frac{l_{ij}}{n_j^+}, \frac{m_{ij}}{n_j^+}, \frac{n_{ij}}{n_j^+} \right), \tag{3}$$

non-beneficial criteria is computed as follows for the normalized value \tilde{r}_{ij}

$$\tilde{r}_{ij} = \left(\frac{l_j^-}{n_{ij}}, \frac{l_j^-}{m_{ij}}, \frac{l_j^-}{l_{ij}} \right), \tag{4}$$

where $l_j^- = \min l_{ij}$ and $n_j^+ = \max n_{ij}$.

Step 3: Weighted normalized fuzzy decision matrix \tilde{V} computation through finding the product of the user-defined weight for each criterion and the corresponding normalized fuzzy value.

$$\tilde{V} = [v_{ij}]_{m \times r}, \quad i = 1, 2, \dots, m \text{ and } j = 1, 2, \dots, r, \tag{5}$$

$$\tilde{v}_{ij} = \tilde{r}_{ij} \times \tilde{\omega}_j, \tag{6}$$

Step 4: Compute the fuzzy positive ideal and anti-ideal (negative) solutions as follows

$$A^B = \{(\max \tilde{n}_{ij} \mid j \in J); (\min \tilde{n}_{ij} \mid j \in J)\}, \text{ or} \tag{7}$$

$$A^B = \{\tilde{v}_1^+, \tilde{v}_2^+, \dots, \dots, \dots, \tilde{v}_n^+\},$$

$$A^W = \{(\min \tilde{n}_{ij} \mid j \in J); (\max \tilde{n}_{ij} \mid j \in J)\}, \text{ or} \tag{8}$$

$$A^W = \{\tilde{v}_1^-, \tilde{v}_2^-, \dots, \dots, \dots, \tilde{v}_n^-\},$$

where $\tilde{v}_1^+ = (1, 1, 1)$, $\tilde{v}_1^- = (0, 0, 0)$, $j = 1, 2, \dots, n$ the set of positive attributes are represented by J and I is the set of negative attributes.

Step 5: S_i^B and S_i^W computation representing ideal positive and ideal negative solutions of distance as follows:

$$S_i^B = \sum_{j=1}^n d(\tilde{v}_{ij} - \tilde{v}_j^+), \quad i = 1, 2, \dots, m \text{ and } j = 1, 2, \dots, n, \tag{9}$$

$$S_i^W = \sum_{j=1}^n d(\tilde{v}_{ij} - \tilde{v}_j^-), \quad i = 1, 2, \dots, m \text{ and } j = 1, 2, \dots, n, \tag{10}$$

where S_i^B and S_i^W are the distances that respectively denote each alternative form of best and worst fuzzy solution.

Step 6: Determine ranking score/relative closeness C_i^+ of each alternative

$$C_i^+ = \frac{S_i^W}{(S_i^B + S_i^W)}, \quad i = 1, 2, \dots, m, \quad 0 \leq C_i^+ \leq 1. \tag{11}$$

Step 7: Organize a set of alternatives via showing the performance order based on the value of ranking score in descending order and the most preferred alternative will be the one with a maximum value of C_i^+ and vice versa.

Next section presents the implementation of Fuzzy-TOPSIS hybrid method on result data sets of wire-EDM manufacturing of gears.

3 Results and Discussion

Table 1 shows the representation of four controllable factors, namely, Voltage (V), Pulse-on Time (Ton), Pulse-off Time (Toff) and Wire Feed Rate (WF) together with their high, medium and low levels as reported by [13]. Table 3 presents the experimental layout together with the values of gear quality indicators i.e. average surface roughness, maximum surface roughness, profile error, pitch error; and process productivity indicator i.e. gear cutting rate. Fuzzy-TOPSIS has been applied on these data sets. In this study, each alternative was basically identified in terms of specific linguistic variables namely: very low, low, medium low, medium, medium high, high and very high, these were assigned triangular fuzzy numbers (0, 0, 0.1), (0, 0.1, 0.3), (0.1, 0.3, 0.5), (0.3, 0.5, 0.7), (0.5, 0.7, 0.9), (0.7, 0.9, 1.0) and (0.9, 1.0, 1.0) respectively. The main reason for this was to compute the relative weights of the chosen output criteria that is Fa, Fp, Rt, Ra and GCR.

Table 1. Variable parameters and their levels [13].

Variable Parameter	Symbol	Unit	Level and Corresponding Value		
			-1	0	1
Voltage	V	V	5	10	15
Pulse-on time	Ton	μs	0.6	0.8	1.0
Pulse-off time	Toff	μs	90	130	170
Wire feed rate	WF	m/min	9	12	15

Table 2. Linguistic variable used for each alternative.

Linguistic variable	Triangular fuzzy number (TFNs)
Very Poor (VP)	(0, 0, 1)
Poor (P)	(0, 1, 3)
Medium Poor (MP)	(1, 3, 5)
Fair (F)	(3, 5, 7)
Medium Good (MG)	(5, 7, 9)
Good (G)	(7, 9, 10)
Very Good (VG)	(9, 10, 10)

The current study focuses on both quality and productivity of gear manufacturing and for this reason all criteria were given equal importance. The relative weight of each criterion by the decision maker was “very high” where the triangular fuzzy number for this classification is (0.9, 1.0, 1.0). Table 2 gives the linguistic variable based valuation of all the available alternatives. Additionally, the valuation applied 7 different fuzzy linguistic variables.

Table 3. Experimental combination and results for WEDM gear manufacturing [1].

Variable input parameters					Experimental results				
Run	V (V)	Ton (μ s)	Toff (μ s)	WF (m/min)	Total Profile Error “Fa” values (μ m)	Accumulated Pitch Error “Fp” values (μ m)	Average Surface Roughness “Ra” values (μ m)	Maximum Surface Roughness “Rt” values (μ m)	Gear Cutting Rate “GCR” values (mm^3/min)
1	15	0.8	130	15	14.20	30.20	1.70	7.40	38.00
2	10	0.8	90	9	14.50	41.00	2.00	9.20	42.50
3	5	1.0	130	12	14.00	29.40	1.80	8.72	25.68
4	10	0.8	130	12	13.10	12.40	1.40	7.23	28.00
5	15	0.6	130	12	14.00	24.20	1.44	7.14	25.46
6	5	0.8	130	9	14.40	32.10	1.70	8.00	31.40
7	5	0.8	170	12	13.00	19.20	1.35	6.87	17.80
8	10	1.0	130	9	14.60	44.50	1.82	8.85	35.58
9	15	0.8	130	9	14.80	38.60	1.76	8.55	38.00
10	10	0.8	170	15	13.10	18.10	1.28	7.01	27.60

(continued)

Table 3. (continued)

Variable input parameters					Experimental results				
Run	V (V)	Ton (μ s)	Toff (μ s)	WF (m/min)	Total Profile Error "Fa" values (μ m)	Accumulated Pitch Error "Fp" values (μ m)	Average Surface Roughness "Ra" values (μ m)	Maximum Surface Roughness "Rt" values (μ m)	Gear Cutting Rate "GCR" values (mm ³ /min)
11	15	0.8	170	12	14.40	35.00	1.71	7.30	28.20
12	15	1.0	130	12	15.20	40.80	1.92	8.90	42.42
13	10	0.8	130	12	12.80	16.25	1.65	7.00	30.50
14	10	0.8	130	12	12.50	11.80	1.70	6.78	34.50
15	10	0.8	130	12	13.10	15.00	1.60	6.90	27.80
16	15	0.8	90	12	14.80	35.70	1.87	8.70	36.45
17	10	0.8	170	9	13.80	32.40	1.68	7.80	25.54
18	10	1.0	90	12	13.90	38.00	1.97	9.80	40.73
19	5	0.8	90	12	14.30	34.00	1.61	8.20	28.00
20	10	0.8	130	12	13.00	18.20	1.76	7.11	32.00
21	10	0.6	90	12	14.20	28.35	1.63	7.30	28.16
22	10	0.6	170	12	11.70	9.40	1.40	7.00	24.00
23	10	0.8	90	15	13.50	25.10	1.55	8.23	32.45
24	10	1.0	130	15	14.00	27.00	1.74	8.70	37.17
25	5	0.6	130	12	13.30	20.65	1.14	6.72	16.08
26	10	0.6	130	9	13.50	25.00	1.49	7.45	30.64
27	10	1.0	170	12	14.60	32.80	1.65	7.90	28.80
28	5	0.8	130	15	13.00	22.40	1.25	6.75	22.10
29	10	0.6	130	15	12.00	16.00	1.18	6.90	20.26

The assessment process results are given in Table 4. The conversion of the data sets into suitable triangular fuzzy numbers, formulated the fuzzy decision matrix. Table 5 illustrates the results from the conversion process. The assignment of fuzzy linguistic variables is done by calculating the difference between maximum and minimum value determined for each criterion then divided by 7 (representing the 7 linguistic variables) to find an adding/subtracting factor. Since criteria Fa, Fp, Ra and Rt are smaller-is-better, the range is set from the minimum value of each, then the adding factor is added repeatedly to form 7 ranges of data sets which are assigned the linguistic variables where the minimum value is classified as "VG" and the maximum value as "VP". Conversely for GCR where higher-is-better, the process begins with the maximum value and the subtracting factor is subtracted repeatedly to form 7 ranges of data sets which are assigned the linguistic

Table 4. Results of the assessment.

Output responses					Fuzzy linguistic variables				
Fa (μm)	Fp (μm)	Ra (μm)	Rt (μm)	GCR (mm^3/min)	Fa (μm)	Fp (μm)	Ra (μm)	Rt (μm)	GCR (mm^3/min)
14.20	30.20	1.70	7.40	38.00	P	MP	MP	G	G
14.50	41.00	2.00	9.20	42.50	P	VP	VP	P	VG
14.00	29.40	1.80	8.72	25.68	MP	F	P	MP	MP
13.10	12.40	1.40	7.23	28.00	MG	VG	MG	G	F
14.00	24.20	1.44	7.14	25.46	MP	MG	MG	VG	MP
14.40	32.10	1.70	8.00	31.40	P	MP	MP	MG	MG
13.00	19.20	1.35	6.87	17.80	MG	G	G	VG	VP
14.60	44.50	1.82	8.85	35.58	P	VP	P	MP	G
14.80	38.60	1.76	8.55	38.00	VP	P	P	MP	G
13.10	18.10	1.28	7.01	27.60	MG	G	G	VG	F
14.40	35.00	1.71	7.30	28.20	P	P	MP	G	F
15.20	40.80	1.92	8.90	42.42	VP	VP	VP	MP	VG
12.80	16.25	1.65	7.00	30.50	MG	G	MP	VG	F
12.50	11.80	1.70	6.78	34.50	G	VG	MP	VG	MG
13.10	15.00	1.60	6.90	27.80	MG	G	F	VG	F
14.80	35.70	1.87	8.70	36.45	VP	P	P	MP	MG
13.80	32.40	1.68	7.80	25.54	MP	MP	MP	MG	MP
13.90	38.00	1.97	9.80	40.73	MP	P	VP	VP	VG
14.30	34.00	1.61	8.20	28.00	P	MP	F	F	F
13.00	18.20	1.76	7.11	32.00	MG	G	P	VG	MG
14.20	28.35	1.63	7.30	28.16	P	F	F	G	F
11.70	9.40	1.40	7.00	24.00	VG	VG	MG	VG	MP
13.50	25.10	1.55	8.23	32.45	F	F	F	F	MG
14.00	27.00	1.74	8.70	37.17	MP	F	MP	MP	MG
13.30	20.65	1.14	6.72	16.08	F	MG	VG	VG	VP
13.50	25.00	1.49	7.45	30.64	F	F	MG	G	F
14.60	32.80	1.65	7.90	28.80	P	P	MP	MG	F
13.00	22.40	1.25	6.75	22.10	MG	MG	VG	VG	P
12.00	16.00	1.18	6.90	20.26	VG	G	VG	VG	P

variables where the maximum is classified as “VG” and the minimum value will be “VP”.

Table 5. Fuzzy decision matrix.

Run	Fa (μm)	Fp (μm)	Ra (μm)	Rt (μm)	GCR (mm^3/min)
1	(0, 1, 3)	(1, 3, 5)	(1, 3, 5)	(7, 9, 10)	(7, 9, 10)
2	(0, 1, 3)	(0, 0, 1)	(0, 0, 1)	(0, 1, 3)	(9, 10, 10)
3	(1, 3, 5)	(3, 5, 7)	(0, 1, 3)	(1, 3, 5)	(1, 3, 5)
4	(5, 7, 9)	(9, 10, 10)	(5, 7, 9)	(7, 9, 10)	(3, 5, 7)
5	(1, 3, 5)	(5, 7, 9)	(5, 7, 9)	(9, 10, 10)	(1, 3, 5)
6	(0, 1, 3)	(1, 3, 5)	(1, 3, 5)	(5, 7, 9)	(5, 7, 9)
7	(5, 7, 9)	(7, 9, 10)	(7, 9, 10)	(9, 10, 10)	(0, 0, 1)
8	(0, 1, 3)	(0, 0, 1)	(0, 1, 3)	(1, 3, 5)	(7, 9, 10)
9	(0, 0, 1)	(0, 1, 3)	(0, 1, 3)	(1, 3, 5)	(7, 9, 10)
10	(5, 7, 9)	(7, 9, 10)	(7, 9, 10)	(9, 10, 10)	(3, 5, 7)
11	(0, 1, 3)	(0, 1, 3)	(1, 3, 5)	(7, 9, 10)	(3, 5, 7)
12	(0, 0, 1)	(0, 0, 1)	(0, 0, 1)	(1, 3, 5)	(9, 10, 10)
13	(5, 7, 9)	(7, 9, 10)	(1, 3, 5)	(9, 10, 10)	(3, 5, 7)
14	(7, 9, 10)	(9, 10, 10)	(1, 3, 5)	(9, 10, 10)	(5, 7, 9)
15	(5, 7, 9)	(7, 9, 10)	(3, 5, 7)	(9, 10, 10)	(3, 5, 7)
16	(0, 0, 1)	(0, 1, 3)	(0, 1, 3)	(1, 3, 5)	(5, 7, 9)
17	(1, 3, 5)	(1, 3, 5)	(1, 3, 5)	(5, 7, 9)	(1, 3, 5)
18	(1, 3, 5)	(0, 1, 3)	(0, 0, 1)	(0, 0, 1)	(9, 10, 10)
19	(0, 1, 3)	(1, 3, 5)	(3, 5, 7)	(3, 5, 7)	(3, 5, 7)
20	(5, 7, 9)	(7, 9, 10)	(0, 1, 3)	(9, 10, 10)	(5, 7, 9)
21	(0, 1, 3)	(3, 5, 7)	(3, 5, 7)	(7, 9, 10)	(3, 5, 7)
22	(9, 10, 10)	(9, 10, 10)	(5, 7, 9)	(9, 10, 10)	(1, 3, 5)
23	(3, 5, 7)	(3, 5, 7)	(3, 5, 7)	(3, 5, 7)	(5, 7, 9)
24	(1, 3, 5)	(3, 5, 7)	(1, 3, 5)	(1, 3, 5)	(5, 7, 9)
25	(3, 5, 7)	(5, 7, 9)	(9, 10, 10)	(9, 10, 10)	(0, 0, 1)
26	(3, 5, 7)	(3, 5, 7)	(5, 7, 9)	(7, 9, 10)	(3, 5, 7)
27	(0, 1, 3)	(0, 1, 3)	(1, 3, 5)	(5, 7, 9)	(3, 5, 7)
28	(5, 7, 9)	(5, 7, 9)	(9, 10, 10)	(9, 10, 10)	(0, 1, 3)
29	(9, 10, 10)	(7, 9, 10)	(9, 10, 10)	(9, 10, 10)	(0, 1, 3)

Table 5 details the data sets of the fuzzy decision matrix to be normalized using Eq. (3). The normalized fuzzy decision matrix was then multiplied with the respective relative weights of each machining criterion and their corresponding values, the resultant matrix values were then converted into crisp values and presented in Table 6.

Table 6. Crisp values for weighted normalized fuzzy decision matrix.

Crisp values					
Run	Fa (μm)	Fp (μm)	Ra (μm)	Rt (μm)	GCR (mm^3/min)
1	0.133	0.297	0.297	0.843	0.843
2	0.133	0.033	0.033	0.133	0.937
3	0.297	0.490	0.133	0.297	0.297
4	0.683	0.937	0.683	0.843	0.490
5	0.297	0.683	0.683	0.937	0.297
6	0.133	0.297	0.297	0.683	0.683
7	0.683	0.843	0.843	0.937	0.033
8	0.133	0.033	0.133	0.297	0.843
9	0.033	0.133	0.133	0.297	0.843
10	0.683	0.843	0.843	0.937	0.490
11	0.133	0.133	0.297	0.843	0.490
12	0.033	0.033	0.033	0.297	0.937
13	0.683	0.843	0.297	0.937	0.490
14	0.843	0.937	0.297	0.937	0.683
15	0.683	0.843	0.490	0.937	0.490
16	0.033	0.133	0.133	0.297	0.683
17	0.297	0.297	0.297	0.683	0.297
18	0.297	0.133	0.033	0.033	0.937
19	0.133	0.297	0.490	0.490	0.490
20	0.683	0.843	0.133	0.937	0.683
21	0.133	0.490	0.490	0.843	0.490
22	0.937	0.937	0.683	0.937	0.297
23	0.490	0.490	0.490	0.490	0.683
24	0.297	0.490	0.297	0.297	0.683
25	0.490	0.683	0.937	0.937	0.033
26	0.490	0.490	0.683	0.843	0.490
27	0.133	0.133	0.297	0.683	0.490
28	0.683	0.683	0.937	0.937	0.133
29	0.937	0.843	0.937	0.937	0.133

Table 7. Fuzzy-TOPSIS results.

Run	Euclidean distance ideal best S_i^B	Euclidean distance ideal worst S_i^W	$S_i^B + S_i^W$	Performance score C_i	Rank
1	1.217	1.209	2.426	0.498	16
2	1.710	0.914	2.624	0.348	27
3	1.440	0.653	2.093	0.312	28
4	0.580	1.589	2.169	0.733	2
5	0.973	1.342	2.315	0.580	13
6	1.262	0.997	2.259	0.441	17
7	0.947	1.597	2.545	0.628	10
8	1.589	0.863	2.452	0.352	25
9	1.589	0.863	2.452	0.352	25
10	0.530	1.661	2.191	0.758	1
11	1.381	0.977	2.358	0.414	19
12	1.690	0.941	2.631	0.358	24
13	0.826	1.474	2.300	0.641	8
14	0.695	1.667	2.362	0.706	4
15	0.687	1.520	2.207	0.689	5
16	1.606	0.715	2.322	0.308	29
17	1.305	0.837	2.141	0.391	21
18	1.639	0.946	2.585	0.366	23
19	1.286	0.840	2.126	0.395	20
20	0.885	1.525	2.410	0.633	9
21	1.119	1.137	2.256	0.504	15
22	0.688	1.715	2.403	0.714	3
23	0.929	1.121	2.050	0.547	14
24	1.222	0.916	2.138	0.429	18
25	1.039	1.504	2.543	0.591	12
26	0.819	1.305	2.125	0.614	11
27	1.401	0.849	2.250	0.377	22
28	0.880	1.577	2.457	0.642	7
29	0.809	1.765	2.573	0.686	6

Table 7 presents results of Fuzzy-TOPSIS with the ranks where the Euclidean distance ideal best and the Euclidean distance ideal worst are determined by Eq. (9) and 10 respectively, then finding the sum of the two distances and the performance score (C_i) is found by Eq. (11).

Fuzzy-TOPSIS hybrid technique has resulted in the optimum combination of wire-EDM parameters corresponding to experiment 10 with a rank of 1. It can be said that for simultaneous improvement of gear surface quality and productivity of the wire-EDM process, the machining should be on Voltage – 10 V, Pulse-on Time – 0.8 μ s, Pulse-off Time – 170 μ s and Wire Feed Rate – 15 m/min.

4 Conclusion

In the present work, procedure of implementing hybrid MCDM technique Fuzzy-TOPSIS for simultaneous optimization of gear quality and process productivity during Wire-EDM has been reported. The results of this multi-performance optimization are Voltage – 10 V, Pulse-on Time – 0.8 μ s, Pulse-off Time – 170 μ s and Wire Feed Rate – 15 m/min for the best values of gear quality in terms of profile error – 13.10 μ m, pitch error – 18.10 μ m, average roughness – 1.28 μ m, maximum roughness – 7.01 μ m, and process productivity with gear cutting rate 27.60 mm³/min. Further, by making amendments in weights etc., for the desired response, machining parameters can be optimized. The optimized parameters of Wire-EDM are for ready industrial reference and can be utilized to obtain the quality gears at the high productivity by Wire-EDM. The outcomes of the present work further encourage researchers and scholars to utilize the Fuzzy-TOPSIS like hybrid optimization techniques to solve multi-criteria decision making problems in other manufacturing processes.

Acknowledgment. The optimization work is supported by the Royal Academy of Engineering UK Grant TSP1332.

References

1. Gupta, K., Jain, N.K.: Near-Net Shape Manufacturing of Miniature Spur Gears by Wire Spark Erosion Machining. MFMT, Springer, Singapore (2017). <https://doi.org/10.1007/978-981-10-1563-2>
2. Anghel, C., Gupta, K., Jen, T.C.: Analysis and optimization of surface quality of stainless steel miniature gears manufactured by CO₂ laser cutting. *Optik* **203**, 164049 (2020). <https://doi.org/10.1016/j.ijleo.2019.164049>
3. Phokane, T., Gupta, K., Gupta, M.K.: Investigations on surface roughness and tribology of miniature brass gears manufactured by abrasive water jet machining. *Proc. Inst. Mech. Eng. C J. Mech. Eng. Sci.* **232**(22), 4193–4202 (2018). <https://doi.org/10.1177/0954406217747913>
4. Davis, J.R. (ed.): *Gear Materials, Properties, and Manufacture*. ASM International (2005)
5. Sahu, N.K., Andhare, A.B.: Multiobjective optimization for improving machinability of Ti-6Al-4V using RSM and advanced algorithms. *J. Comput. Des. Eng.* **6**(1), 1–12 (2019). <https://doi.org/10.1016/j.jcde.2018.04.004>
6. Gok, A.: A new approach to minimization of the surface roughness and cutting force via fuzzy TOPSIS, multi-objective grey design and RSA. *Measurement* **70**, 100–109 (2015). <https://doi.org/10.1016/j.measurement.2015.03.037>
7. Majumder, H., Maity, K.: Prediction and optimization of surface roughness and micro-hardness using GRNN and MOORA-fuzzy-a MCDM approach for nitinol in WEDM. *Measurement* **118**, 1–13 (2018). <https://doi.org/10.1016/j.measurement.2018.01.003>

8. Tripathy, S., Tripathy, D.K.: Multi-attribute optimization of machining process parameters in powder mixed electro-discharge machining using TOPSIS and grey relational analysis. *Eng. Sci. Technol. Int. J.* **19**(1), 62–70 (2016). <https://doi.org/10.1016/j.jestch.2015.07.010>
9. Gopal, P.M., Prakash, K.S.: Minimization of cutting force, temperature and surface roughness through GRA, TOPSIS and Taguchi techniques in end milling of Mg hybrid MMC. *Measurement* **116**, 178–192 (2018). <https://doi.org/10.1016/j.measurement.2017.11.011>
10. Dewangan, S., Gangopadhyay, S., Biswas, C.K.: Multi-response optimization of surface integrity characteristics of EDM process using grey-fuzzy logic-based hybrid approach. *Eng. Sci. Technol. Int. J.* **18**(3), 361–368 (2015). <https://doi.org/10.1016/j.jestch.2015.01.009>
11. Bhaumik, M., Maity, K.: Multi-objective optimization of PMEDM using response surface methodology coupled with fuzzy based desirability function approach. *Decis. Sci. Lett.* **6**(4), 387–394 (2017). <https://doi.org/10.5267/j.dsl.2017.1.004>
12. Tiwary, A.P., Pradhan, B.B., Bhattacharyya, B.: Application of multi-criteria decision making methods for selection of micro-EDM process parameters. *Adv. Manufact.* **2**(3), 251–258 (2014). <https://doi.org/10.1007/s40436-013-0050-1>
13. Gupta, K., Jain, N.K.: Analysis and optimization of micro-geometry of miniature spur gears manufactured by wire electric discharge machining. *Precis. Eng.* **38**(4), 728–737 (2014). <https://doi.org/10.1016/j.precisioneng.2014.03.009>
14. Nădăban, S., Dzitac, S., Dzitac, I.: Fuzzy TOPSIS: a general view. *Procedia Comput. Sci.* **91**, 823–831 (2016). <https://doi.org/10.1016/j.procs.2016.07.088>
15. Palczewski, K., Salabun, W.: The fuzzy TOPSIS applications in the last decade. *Procedia Comput. Sci.* **159**, 2294–2303 (2019). <https://doi.org/10.1016/j.procs.2019.09.404>
16. Pathak, S. (ed.): *Intelligent Manufacturing. MFMT*, Springer, Cham (2021). <https://doi.org/10.1007/978-3-030-50312-3>



Increasing the Bearing Capacity of the Compressor Bling Blades by Technological Methods

Dmytro Pavlenko¹ (✉) , Oleksandr Tarasov² , Daria Tkach¹ , and Yuriy Torba³ 

¹ Zaporizhzhia Polytechnic National University, 64 Zhukovskoho Street, Zaporizhzhia 69063, Ukraine

dvp@zntu.edu.ua

² Donbas State Engineering Academy, 72 Akademichna Street, Kramatorsk 84313, Ukraine

³ Ivchenko-Progress SE, 2 Ivanova Street, Zaporizhzhia 69068, Ukraine

Abstract. The paper applies to settling the actual, scientific and technical problem of increasing the load-carrying capacity of compressor impeller blades made of heat-resistant nickel alloy EhK79 by technological methods. By using the system approach to the investigation of surface layer characteristics of blade aerodynamic surfaces together with process operations, the application of high-speed milling and strain hardening is substantiated for increasing the strength margin of blades concerning multi-cycle fatigue resistance. Established are the reasons for blades breakage in the course of the operation and basic principles of forming surface layer characteristics of aerodynamic surfaces during shape formation by high-speed line-by-line milling and strain hardening at ultrasonic installation. Determined are the rational process conditions and ranges of process operation factors as well as the range of rational levels of surface cold working of blade aerodynamic surfaces, in which the maximum strength margin is ensured. The issues of forming the surface layer characteristics of centrifugal wheel vanes made of Ni-based EhK79, heat-resistant alloy during high-speed line-by-line milling have been considered. The effects of strain hardening with balls on endurance limits within the range of operating temperatures have been investigated. Technological recommendations are advised on machining and hardening processing of vanes, which provide for the increase of their load-bearing capacity.

Keywords: Compressor impeller · Surface layer characteristics · Residual stresses · Surface cold working · Flexible parameters · Endurance limit · High-speed milling · Strain hardening

1 Introduction

The rotor blades are the critical parts of the rotor of a gas turbine engine, limiting the resource of its operation. To increase the margin of their strength and reduce the mass of the rotor, various advanced materials are used [1]. Due to increased requirements for strength characteristics of the materials that are used for the manufacture of the

high-pressure turbine and compressor disks (Fig. 1), new nickel-based high-temperature alloys such as EpH742, EhK79, EhK151, EpH975, and other alloys are widely used actually in all up-to-date gas turbine engines [2, 3]. These alloys feature high ultimate strength of 1300 to 1500 MPa and an operating temperature of 850 to 975 °C.

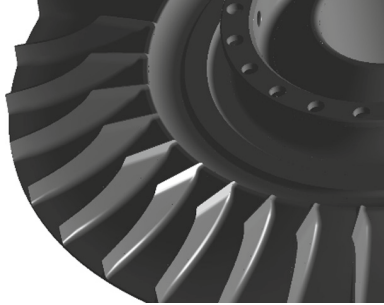


Fig. 1. Fragment of centrifugal compressor bling with blades.

Possessing high strength, these alloys are characterized by extremely poor machinability. For example, the machining factor for the EpH742 alloy is 0.75 of that for the EI698 alloy and as low as 0.5 for the EhK79 alloy. In this case, recommended cutting speed is 3 to 3.5 times lower than that for the EI698 alloy. Poor machinability is the main cause of heavy wear of the tool cutting edges during machining, which causes the generation of residual tensile stresses in the surface layer of the workpieces. From the point of view of bearing capacity, the residual tensile stresses are unfavorable ones. In addition, excessive hardening of the surface layer takes place. Considering the important and ambiguous role of the strain hardening of the surface layer for parts operating at elevated temperatures, a rational degree of hardening must be determined. This will make it possible to control the quality of the surface at all stages of the technological cycle of manufacturing blades to achieve their maximum bearing capacity.

2 Literature Review

It is known that technological heredity in the surface layer of parts is formed at all stages of their processing [4, 5]. In this case, cutting usually contributes to the formation of unfavorable tensile residual stresses [6]. Heat treatment promotes partial or complete relaxation of stresses. Hardening treatment leads to the formation of favorable compressive residual stresses [7].

The reasons for the ambiguity of the role of hardening are both a direct decrease in the strength of the deformed material and the relaxation of residual stresses at high temperatures. Thus, the residual stresses arising during finishing are particularly important [8]. It is known that tensile stresses deteriorate the dynamic strength and chemical resistance of materials. Compressive stresses in the surface layer lead to an increase in the endurance limit. Rough surfaces and machining artifacts are also areas where compressive residual stresses are extremely effective. The influence of various stress

concentrators, including material defects and inclusions, which also reduce the strength of parts [9], can be effectively eliminated due to technological compressive stresses. They also play a significant role in increasing the endurance of parts with structural stress concentrators [10, 11] and in retardation of crack propagation rate [12]. Different methods for the stress concentrators eliminate like deburring of engineered parts [13] and sticking minimization [14]. Are investigated. The exclusive role of surface strain hardening of parts operating under variable loads is known and beyond doubt [15]. The effectiveness of surface hardening has been confirmed for titanium [16], steel [17], aluminum [18], and other alloys. However, the question of the role of hardening parts made of iron-nickel alloys and operating at elevated temperatures remains debatable. Obviously, a rational degree of deformation of the surface layer exists.

The main criterion for the performance of materials under conditions of variable loading is fatigue resistance at operating temperature [19, 20]. To increase the fatigue resistance of gas turbine engine parts, methods of surface-plastic hardening with free shot are widely used. At the same time, to calculate the margin of safety and service life, as well as to optimize the modes of surface hardening, it is necessary to have information about the influence of the characteristics of the surface layer on fatigue resistance. Taking into account the anomalous temperature dependence of the endurance limit inherent in some nickel and other alloys having a face-centered cubic lattice [2], the issue of the effect of surface hardening on fatigue resistance at operating temperatures is relevant.

The purposes of the present publication are the determination of the mechanism of generation of characteristics in the surface layer on compressor impeller vanes for the up-to-date aircraft engine, that is made of the EhK79 [16Co-12Cr-5Mo-3Nb—3.3Al-3W-3Ti—0.8V-Ni(base)] nickel-base superalloy during machining and hardening, investigation of the effect of strain hardening on the durability of vanes within operating temperatures range as well as the development of recommendations aimed at technological ensuring bearing capacity.

3 Materials and Methods

Advanced machining technology that is based on high-speed cutting was used to generate blade geometry. The airfoil portions of the blades were finished with the aid of the Starrag ZS-500 high-speed machining center by using milling cutters that were made of Swiss hard alloy that is similar to the VK10HOM alloy by machining. Row milling was used for finishing. During machining, the cutting area was sufficiently flushed with coolant. After machining, the quality of the surface layer was checked by surface roughness, value, sign, and nature of the distribution of residual stresses and rate of surface hardening. The rate of surface hardening means the relation between microhardness of specimen surface and microhardness of its core expressed in per cents.

The main criterion for the quality of the surface layer was the endurance limit of flat laboratory samples at operating temperature. Cantilever-supported flat specimens were tested in lateral bending on a piezoelectric shaker with a vibration acceleration control sensor under resonance conditions under a symmetric loading cycle. The 1% decrease in frequency relative to the initial frequency was taken as a failure criterion of the specimen. The endurance limit was determined by the “ladder” method. The average

value of the endurance limit was calculated for failed specimens and full-scale blades via the following formula:

$$\bar{\sigma} = \sigma_0 + \Delta\sigma \left(\frac{A}{N} - \frac{1}{2} \right) \quad (1)$$

where σ_0 is the lowest stress value in tests, $A = \sum_{i=1}^n i \cdot r_i$; $I = 0, 1, 2 \dots n$; n is the serial number of load level, r_i is the number of equal events (failures or non-failures) at the i -th load level, and $N = \sum_{i=0}^n r_i$ is the total number of equal events.

According to the results of testing the samples by the least-squares method, the parameters of the equation of the left branch of the endurance curve were determined in semilogarithmic coordinates:

$$\sigma(N) = b - k \lg(N). \quad (2)$$

The degree of surface hardening was assessed by the change in the microhardness of the surface layer before and after treatment:

$$S = \frac{H_{\mu}^{surf} - H_{\mu}^{int}}{H_{\mu}^{int}} \cdot 100\%, \quad (3)$$

where H_{μ}^{surf} is the surface microhardness after hardening, MPa; H_{μ}^{int} is the initial microhardness of the surface, MPa.

The endurance limit was determined for samples with different degrees of work hardening of the surface layer. The deformation hardening of the surface layer of the aerodynamic surfaces of the blades was carried out due to the kinetic energy of steel balls in an ultrasonic field. Hardening was carried out according to the regime: the diameter of the balls is 1.6 mm; hardening time 10–15 min; processing intensity 4.1–4.2 mV; the total mass of the balls is 400 g.

The effect of surface hardening was evaluated by the amount of work hardening and residual stresses in the surface layer. The study of residual stresses in the surface layer of the blade airfoil was performed by drilling small holes, by the standard of the American Society for Testing and Materials ASTM E837 [21]. The measurements were carried out on a SINT RESTAN MTS 3000 plant (Italy).

Hardening of the surface layer was investigated by measuring the microhardness at various distances from the surface on “oblique sections”. The measurement was performed on a Vickers microhardness tester model HVA-1 with an indenter load of 50 g.

4 Result and Discussion

Development of the up-to-date machining technology and ensuring the favorable combination of characteristics of the surface layer of the parts that are made of up-to-date

super alloys nowadays is considered to be one of the actual problems in aero-engine manufacture.

To determine the mechanism of generation of stress on the surface layer and surface roughness of vane airfoil depending upon milling conditions, an experiment with two factors that were varied at two levels was run. The following milling conditions were used as factors: machine tool spindle speed, rpm (X_1); minute milling cutter feed, mm/min (X_2). Response functions were described by the following surface equation:

$$Y(X_1, X_2) = a + b_1X_1 + b_2X_2. \tag{4}$$

The intervals of variation of factors were chosen depending on the area where they were determined and the technical feasibility of the experiment (Table 1).

Table 1. Levels of factors during implementation of experiments.

Factor	Interval of variation	Level -1	Level 0	Level +1
N , rpm (X_1)	160	800	960	1120
S , mm/min (X_2)	60	300	360	420

To prevent experimental error, each experiment at the given levels was carried out two times, and results were averaged. Table 2 shows the experimental design matrix and obtained values of response functions. Obtained response functions are as follows:

– for residual stress:

$$\sigma_0 = -210 - 15 \cdot X_1 - 30 \cdot X_2;$$

– for airfoil roughness in a longitudinal direction:

$$Ra = 0.31 + 0.04 \cdot X_1 + 0.0017 \cdot X_2;$$

– for airfoil roughness in a transverse direction:

$$Ra = 0.6 - 0.07 \cdot X_1 + 0.16 \cdot X_2$$

where X_1 is the machine tool spindle speed in coded scale; X_2 is the minute milling cutter feed in coded scale.

Since coefficients at independent variables in the received regression equation that describes the dependence of the vane airfoil roughness in a longitudinal direction depending upon milling conditions are statistically insignificant for the given level of significance, it may be considered that in the above range change in milling conditions affects only roughness in the transverse direction, i.e. row height.

Analysis of the effect of the high-speed milling conditions on residual stress in the surface layer shows that compressing residual stresses are generated in the surface layer of the blades irrespective of the machining conditions. The peculiarity of the residual

Table 2. Experiment design matrix and obtained values of response functions.

Condition No.	Coded scale		Natural scale of factors		Hardening rate, %	Max. compressing residual stresses, MPa		Roughness in the longitudinal direction, μm		Roughness in the transverse direction, μm	
	X1	X2	X ₁ rpm	X ₂ mm/min		S	σ_0	S ²	Ra	S ² 10 ⁻⁵	Ra
1	+1	+1	1120	420	25	250	24.5	0.700	19.8	0.384	16.2
2	-1	+1	800	420	28	230	21.4	0.813	15.3	0.255	15.9
3	+1	-1	1120	300	30	200	16.8	0.358	16.2	0.329	15.4
4	-1	-1	800	300	30	160	26.0	0.526	14.6	0.303	16.7
Estimated coefficients variance						-	22.18	-	16.5	-	16.1

stress after milling was that neither value nor nature of the distribution of the residual stresses was independent of the place of specimen cutting in the vane airfoil, which testifies to identical machining of the airfoil portion and stability of the cutting procedure. Diagrams of residual stresses had under layer maximum at a depth of 15 to 25 microns from the surface, which is typical for the residual stresses, generated under the action of power factor (Fig. 2).

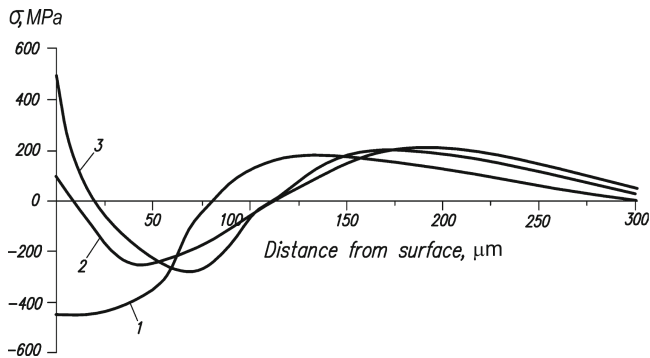


Fig. 2. Diagram of average values distribution in the surface layer after high-speed row milling using different conditions: 1 – condition No. 1; 2 – condition No. 2; 3 – condition No. 3.

The main cause of propagation of compressing residual stresses in the surface layer of the vane after high-speed row milling is as follows: at high-speed machining, the main amount of heat is concentrated in chips and it has no sufficient amount of time to be transferred into surface layer while normal component of cutting force does not depend upon cutting speed and may reach considerable value. As a result, the action of strengthening the power factor exceeds that of heating and weakening one thereby causing the generation of favorable compressing stresses in the surface layer.

The established empirical dependencies between milling conditions and characteristics of the surface layer show that the value of the residual stresses is dependent both on milling cutter feed and machine tool spindle rpm, i.e. cutting speed. As they are increased, residual compressing stresses of high levels are generated in the surface layer. The surface roughness of the airfoil portion similar to the value of the residual stresses is dependent on machining conditions. An increase in the minute feed of the milling cutter causes an increase in the value of the microasperity while the increase in cutting speed results in a decrease in microasperity. The rate of hardening of the surface layer of the vanes practically was independent of milling conditions and its value was within 25 to 30% (Table 1). Irrespective of the machining conditions, high-speed row milling ensured the accuracy of shape, dimensions, and the positional relationship between airfoil portions of the vanes.

Taking into consideration the fact that the condition of the surface layer of parts that work under conditions of alternating loading largely affects their bearing capacity is necessary during the development of the production process for the manufacture of the compressor impeller vanes to provide for hardening operations. They are aimed at the generation of a favorable combination of characteristics of the surface layer of the vane airfoil portions thereby ensuring their maximum endurance.

In order to investigate the effect of hardening of vane surface layer on endurance, 7 lots of plane specimens (14 to 16 pcs) were subjected to ultrasonic hardening with the use of steel beads having dia. of 1.6 mm and the time of hardening was varying (Table 3). The specimens were tested within a range of operating temperature, i.e. 20 °C, 500 °C, and 700 °C.

Table 3. Microhardness of the surface layer of specimens after ultrasonic hardening

No.	Average microhardness $H\mu$, MPa	Rate of hardening S , %	Standard deviation $S_{H\mu}$, MPa	Coefficient of variation, ν
1	2717	Initial	95	0.035
2	3070	13	141	0.046
3	3342	23	110	0.033
4	3451	27	120	0.035
5	3695	36	121	0.033
6	4103	51	117	0.028
7	4619	70	118	0.026

Fatigue testing was carried out based on $2 \cdot 10^7$ cycles at the cantilever bending of specimens loaded by the forces of inertia of their weight. Fatigue curves testing temperatures irrespective of the surface layer condition (Fig. 3 and 4) consisted of the oblique and horizontal branches.

Fatigue test results of the investigated batches of specimens at normal and high temperatures showed (Fig. 5) that the fatigue value of initial specimens increases as

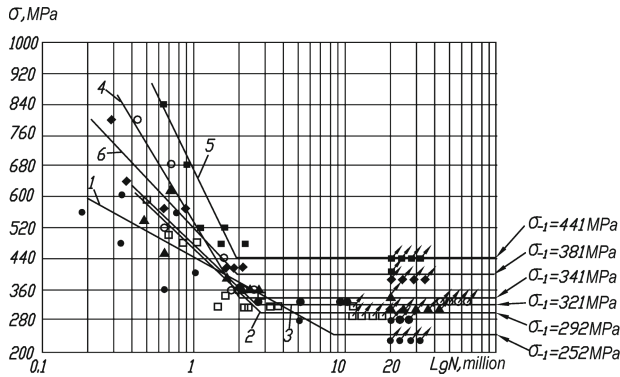


Fig. 3. Fatigue curves of the specimens at $t = 20\text{ }^{\circ}\text{C}$: 1(●) – initial specimens; 2(□) – $S = 23\%$; 3(▲) – $S = 27\%$; 4(○) – $S = 36\%$; 5(■) – $S = 51\%$; 6(◇).

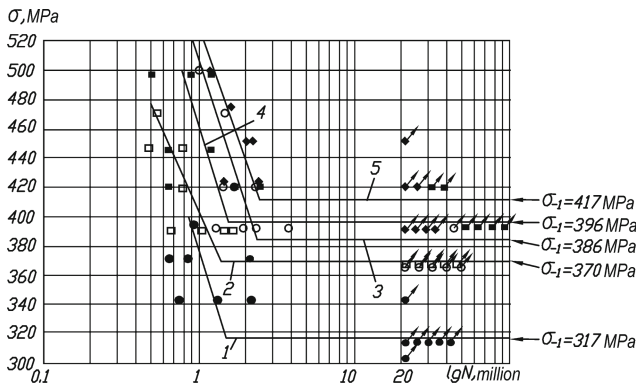


Fig. 4. Fatigue curves of the specimens at $t = 500\text{ }^{\circ}\text{C}$: 1(●) – initial specimens; 2(□) – $S = 23\%$; 3(○) – $S = 36\%$; 4(■) – $S = 51\%$; 5(◆) – $S = 70\%$.

the temperature increases. Thus, at the temperatures of $500\text{ }^{\circ}\text{C}$ and $700\text{ }^{\circ}\text{C}$, the fatigue value of the specimens is higher than at $20\text{ }^{\circ}\text{C}$ by 25.8% and 65.5% accordingly. Surface cold-work hardening both at normal and high temperatures brings about the increase of the fatigue value and reduction of endurance dissipation till failure. But with the increase of the testing temperature to $500\text{ }^{\circ}\text{C}$ the intensity of the fatigue value increase is getting reduced as the cold-work hardening increases.

The rational range of cold-work hardening level of the vanes airfoil surface layer can be assumed as 45 to 55%, within which we observe the peak of endurance value at temperature $20\text{ }^{\circ}\text{C}$ and asymptotic approximation to maximum endurance value at temperature $500\text{ }^{\circ}\text{C}$.

To make provision for a rational level of the airfoil surfaces of the vanes of the compressor full-scale centrifugal impeller we investigated the matter what was the effect of hardening time on the cold work hardening level (Fig. 6).

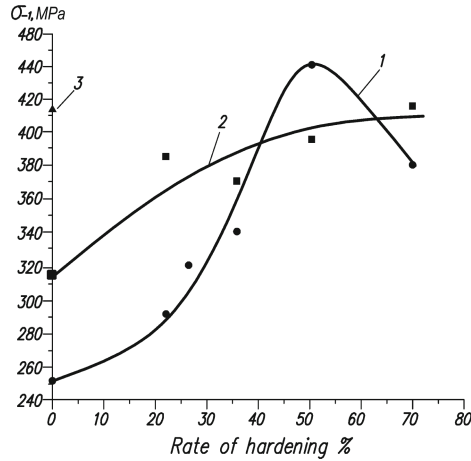


Fig. 5. Dependence of specimens' fatigue value on testing temperature and cold-work hardening level: 1(●) – $t = 20\text{ }^{\circ}\text{C}$; 2(■) – $t = 500^{\circ}$; 3(▲) – $t = 700\text{ }^{\circ}\text{C}$.

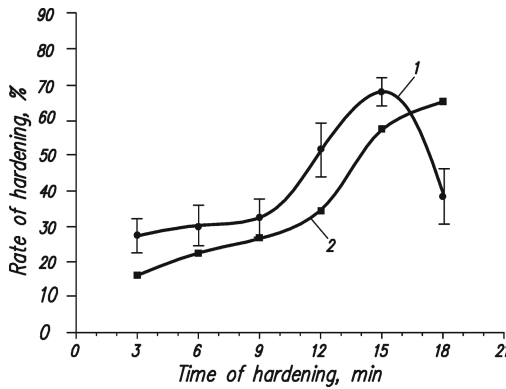


Fig. 6. Dependence of cold-work hardening level of the airfoil (1) and an end portion (2) of compressor centrifugal impeller vanes on hardening time 1 – hardening time, min; 2 – cold-work hardening level, %.

The results of the investigation showed that the required cold-work hardening level of the surface layer of the vane airfoil and end portion can be provided for 12 to 14 min. When hardening with balls having a diameter of 1.6 mm in the wave concentrator of the cup type.

Complex investigations of the rules of drawing up characteristics of the surface layer of the parts made of EhK79 alloy during machining and hardening processing and their effects on endurance within the range of operating temperatures made it possible to develop technological recommendations and organization and technological measures to increase operating reliability of compressor centrifugal impeller vanes.

5 Conclusion

It is the most expedient to perform form-building geometry of compressor centrifugal impeller vanes using high-speed row milling. The rational high-speed row milling is as follows: minute milling feed – 300 mm/min; spindle rotational speed with milling cutter dia. 12 mm – 1150 rpm (the actual cutting speed 42–43 m/min). When using such machining conditions, the considerable compression residual stresses are getting formed in the surface layer of the vanes and the surface roughness does not exceed the value specified in the compressor centrifugal impeller vanes' working drawing.

Strain hardening of the vanes' surface layer with steel balls at ultrasonic hardening installation is an effective technological method for their bearing capacity to increase under conditions of normal and high temperatures. The rational range of the vanes' surface layer cold - work hardening level is from 45 to 55%, in which maximum fatigue value is observed.

Ultrasonic hardening of compressor centrifugal impeller vanes made of EhK79 alloy shall be implemented in the wave concentrator of the cup type with steel grade balls having a diameter of 1.6 mm. The rational condition of compressor centrifugal impeller vanes' ultrasonic hardening is as follows: hardening intensity - from 50 to 55 mA, hardening time - from 12 to 14 min. Under such conditions and hardening conditions in the surface layer in the vane airfoil and end portion the most rational combination of characteristics, from the fatigue viewpoint, is formed.






References

1. Pavlenko, D., Dvirnyk, Y., Przysowa, R.: Advanced materials and technologies for compressor blades of small turbofan engines. *Aerospace* **8**(1), 1 (2021). <https://doi.org/10.3390/aerospace8010001>
2. Sims, C.T., Stoloff, N.S., Hagel, W.C.: *Superalloys II*. Wiley, New York (1987)
3. Kabanov, I.V., Lomberg, B.S., Sidorina, T.N.: Development of superalloy production at the electrostal metallurgical plant. *Metallurgist* **61**(7–8), 565–568 (2017). <https://doi.org/10.1007/s11015-017-0533-6>
4. Plankovskyy, S., Popov, V., Shypul, O., et al.: Advanced thermal energy method for finishing precision parts. In: Gupta, K., Pramanik, A. (eds.) *Advanced Machining and Finishing*, pp. 527–575. Elsevier, Amsterdam (2021). <https://doi.org/10.1016/B978-0-12-817452-4.00014-2>
5. Baurova, N.I., Zorin, V.A., Prikhodko, V.M.: Technological heredity and identification of technological processes. *Polym. Sci. Ser. D* **8**(3), 219–222 (2015). <https://doi.org/10.1134/s199542121503003x>
6. Shen, X., Zhang, L., Ren, C.: Influence of milling conditions on the surface quality in high-speed milling of titanium alloy. In: Lin, S., Huang, X. (eds.) *CSEE 2011. CCIS*, vol. 214, pp. 423–429. Springer, Heidelberg (2011). https://doi.org/10.1007/978-3-642-23321-0_66
7. Vyshnepolskyi, Y., Pavlenko, D., Tkach, D., Dvirnyk, Y.: Parts diamond burnishing process regimes optimization made of INCONEL 718 Alloy via selective laser sintering method. In: 2020 IEEE 10th International Conference Nanomaterials: Applications and Properties (NAP), Sumy, p. 02SAMA01-1. IEEE (2020). <https://doi.org/10.1109/NAP51477.2020.9309661>
8. Liang, H., Kan, Y., Chen, H., et al.: Effect of cutting process on the residual stress and fatigue life of the welded joint treated by ultrasonic impact treatment. *Int. J. Fatigue* **143**, 105998 (2021). <https://doi.org/10.1016/j.ijfatigue.2020.105998>

9. Shapoval, A., Savchenko, I., Markov, O.: Determination coefficient of stress concentration using a conformed display on a circle of a single radius. *Solid State Phenom.* **316**, 928–935 (2021). <https://doi.org/10.4028/www.scientific.net/SSP.316.928>
10. Mcevilly, A.J., Kasivitanuay, J.: *Metal Failures: Mechanisms, Analysis, Prevention*. Wiley, Hoboken (2013)
11. Plankovskyy, S., Shypul, O., Tsegelnyk, Y., Pankratov, A., Romanova, T.: Amplification of heat transfer by shock waves for thermal energy method. In: Nechyporuk, M., Pavlikov, V., Kritskiy, D. (eds.) *ICTM 2020. LNNS*, vol. 188, pp. 577–587. Springer, Cham (2021). https://doi.org/10.1007/978-3-030-66717-7_49
12. Praveenkumar, K., Mylavarapu, P., Sarkar, A., et al.: Residual stress distribution and elevated temperature fatigue behaviour of laser peened Ti-6Al-4V with a curved surface. *Int. J. Fatigue* **156**, 106641 (2022). <https://doi.org/10.1016/j.ijfatigue.2021.106641>
13. Gillespie, L.K.: *Deburring and Edge Finishing Handbook*. Society of Manufacturing Engineers, Dearborn (1999)
14. Kombarov, V., Sorokin, V., Tsegelnyk, Y., et al.: Numerical control of machining parts from aluminum alloys with sticking minimization. *Int. J. Mechatron. Appl. Mech.* **1**(9), 209–216 (2021). <https://doi.org/10.17683/ijomam/issue9.30>
15. Schneider, M.J., Chatterjee, M.S.: Introduction to surface hardening of steels. In: Dossett, J.L., Totten, G.E. (eds.) *Steel Heat Treating Fundamentals and Processes*. ASM Handbook, vol. 4A, p 389–398. ASM International (2013). <https://doi.org/10.31399/asm.hb.v04a.a0005771>
16. Wen, Y., et al.: Evaluation of mechanical behavior and surface morphology of shot-peened Ti-6Al-4V alloy. *J. Mater. Eng. Perform.* **29**(1), 182–190 (2020). <https://doi.org/10.1007/s11665-020-04565-8>
17. Čiuplys, V., Čiuplys, A., Vilys, J., Kvedaras, V.: Increasing of carbon steel durability by surface hardening. *Medziagotyra* **16**(1), 24–28 (2010)
18. Kim, S.H., Kim, Y.J., Ahn, J.-H.: Surface hardening of Al alloys through controlled ball-milling and sintering. *J. Nanosci. Nanotechnol.* **12**(7), 5514–5518 (2012). <https://doi.org/10.1166/jnn.2012.6320>
19. Suresh, S.: *Fatigue of Materials*. Cambridge University Press, Cambridge (1998). <https://doi.org/10.1017/CBO9780511806575>
20. Ramesh Babu, H., Böcker, M., Raddatz, M., et al.: Experimental and numerical investigation of high-temperature multi-axial fatigue. *J. Eng. Gas Turbines Power* **144**(4), 041003 (2022). <https://doi.org/10.1115/1.4053153>
21. ASTM E837-08: Standard test method for determining residual stresses by the hole-drilling strain-gage method. ASMT International, West Conshohocken (2008). <https://doi.org/10.1520/E0837-08E02>



Optimization of T-Joints Laser Robotic Welding Procedure Parameters from AISI 321 Stainless Steel

Maksym Khokhlov^(✉) , Artemii Bernatskyi , Olena Berdnikova ,
Olga Kushnarova , and Oleksandr Siora 

E.O. Paton Electric Welding Institute of the National Academy of Science of Ukraine, 11
Kazymyra Malevycha Street, Kyiv 03150, Ukraine
maksymkhokhlov@gmail.com, bernatskyi@paton.kiev.ua

Abstract. Enterprises that produce finished products from sheet material are usually focused on fulfilling orders of a wide range. The wide range and small volumes of batches of products force such enterprises to often readjust their technological equipment. Due to the fact that the readjustment affects the entire technological chain of sheet material processing, flexible technological solutions are of high value. Introduction of the robotic welding complexes allows to pass quickly from one to another operation of laser welding of various details. Reducing the weight of products by reducing the thickness of welded parts is a common trend for the above industries. It aims to reduce the cost of products to increase their competitiveness. At the same time, reducing the thickness of parts encourages manufacturers to find ways to increase the structural strength of products. The task for technologists is to optimize the parameters of technological processes of welding to obtain high-quality welded joints with not only the required design, but also with a given geometry, the necessary parameters of the structure and the level of physical and mechanical properties. The aim of this work is to optimize the parameters of laser welding procedure of AISI 321 stainless steel T-joints according to three different technological procedures for their further use in the library of robotic welding complex. The optimal modes for three welding procedures are established, which ensure the production of defect-free structures, the formation of a given geometry and the highest level of mechanical properties.

Keywords: Robotics · Laser welding · Parameters · Optimization · Technological procedure · Stainless Steel

1 Introduction

Competition in the market in various industries encourages manufacturers to find effective and flexible ways to improve technological processes, equipment and product quality while reducing production costs [1–3]. The main directions of development of modern technological systems in production include the following: Smart Manufacturing and Industry 4.0 Strategy [4]; extensive use of computational methods in engineering [5–7];

application of machine learning [8]; use of artificial neural networks and fuzzy logic systems [9]; use of modern CAD systems for design [10]; mathematical modeling and forecasting the properties of various structures [11–13]; introduction of intelligent production systems [14]; production automation [15]; improvement and increasing involvement of robotics in production processes [16]; use of optimization methods in engineering [17–19], etc. At the same time, competition in the market also stimulates the development of research aimed at creating and improving modern technological processes of materials processing, which include beam technologies [20–22]. The technological processes that use laser beam include 3D prototyping [23–25], welding [26–28], surface treatment, coating and cladding [29–31], etc. Laser welding technologies have found their use in the manufacture of various products in many industries [32–34]: rocketry; aircraft construction; production of railway cars; automotive industry; chemical industry, etc. Reducing the weight of products by reducing the thickness of welded parts is a common trend for the above industries. It is aimed at reducing the cost of products to increase their competitiveness [35–37]. At the same time, reducing the thickness of parts encourages manufacturers to find ways to increase the structural strength of products. The task for technologists is to optimize the parameters of welding processes to obtain high-quality welded joints not only of the required design, but also with a given geometry, with the necessary parameters of the structure and the level of physical and mechanical properties.

The aim of this work is to optimize the parameters of laser welding procedure of AISI 321 stainless steel T-joints according to three different technological procedures for their further use in the library of robotic welding complex.

Enterprises that produce finished products from sheet material are usually focused on fulfilling orders of a wide range. The wide range and small volumes of batches of products force such enterprises to often readjust their technological equipment. Due to the fact that the readjustment affects the entire technological chain of sheet material processing, flexible technological solutions are of great value. The introduction of robotic welding systems allows to quickly switch between laser welding operations of various parts. The ability to perform readjustment and reprogramming of the station in a short time during the performance of welding technological tasks, is provided by technological equipment for fixation of parts and programming in offline mode. An integrated approach to the technological chain in the processing of sheet material provides a noticeable economic effect to the owner of the station. Therefore, the task of creating “libraries” of pre-worked welding procedures becomes relevant.

The introduction of laser welding can reduce the percentage of defective products and the complexity of their manufacture, and also increase productivity compared to other types of welding. It is expected that when using variations in temperature and time parameters of the laser welding process of thin-sheet stainless steels, a fine-grained weld structure will be obtained, which will provide similar strength and ductility characteristics to the base metal.

However, known laser welding methods also have drawbacks. Laser exposure is characterized by a rigid thermal cycle that causes changes in the structure of the material, the occurrence of stresses and deformations, that lead to microdefects, significantly impairing the mechanical properties, and, consequently, reducing the reliability and durability of products. To eliminate these shortcomings, it is necessary to study the

structural features that are associated with the emergence of internal stresses and can lead to the formation of microcracks. In this regard, it was necessary to conduct detailed research at different structural levels using complex methods that will investigate the structural-phase state of welded joints formed by laser welding.

2 Materials and Research Methods

T-joints made of stainless steel are widely used in the manufacture of thin-walled housings of various parts and products. Depending on the purpose and operating conditions of individual parts and products in general, on the geometry and properties of these joints, designers may have different technical requirements. To meet these requirements, it is necessary to test the welding procedure in accordance with the requirements of EN ISO 15614-11:2016 “Specification and qualification of welding procedures for metallic materials. Welding procedure test. Electron and laser beam welding”. The resulting welding procedures can be used in the manufacture of welded T-joints with a given geometry, structure and properties by means laser welding.

In this study, the authors were tasked with testing the parameters of laser welding of AISI 321 stainless steel T-joints by three different technological procedures for their further use in the library of robotic welding.

T-joints were welded using industrial robot manipulator “FANUC M710” and laser “ROFIN-SINAR” “DY044” from AISI 321 stainless steel: 1.2 mm thick sheets were used for ribs, and 0.8 mm thick sheets - for shelf.

Metallographic studies of the structure of welded joints for all procedures were performed using a light microscope Versamet-2 (Japan) at magnifications $\times 50 \dots 500$. The images were recorded with the OLYMPUS digital camera that the microscope is equipped with. Microhardness (HV) was measured under a load of 100 g on an M-400 hardness tester (USA, Leco). Base metal, weld metal, fusion line were studied in detail in welded joints. Studied structural parameters are: grain sizes (D); width (h) and length (l) of crystallites; crystallite form factor ($\alpha = l/h$); the width of the transition zones (δ).

3 Results and Discussion

The technological procedures of laser welding differed as follows. According to the first task, it was necessary to obtain a welded T-joint with a slot weld on the side of the shelf in one pass (Fig. 1). The optimization criterion was to obtain the highest possible value of strength for uniaxial static tensile testing, geometry of the joint was not considered.

The optimization of laser welding parameters in one pass in the pulsed mode of laser beam generation was performed according to the first procedure of T-joints welding. Ranges of parameters changes of modes are: power of laser radiation in a pulse $P_{max} = 3.0\text{--}4.4$ kW; pulse frequency 100–250 Hz; the focus deepening of the laser beam radiation 2.0–4.0 mm relative to the surface of the samples; welding speed 50–100 mm/s. The maximum value of strength in the uniaxial static tensile testing was obtained using the following parameters (hereinafter – mode I): power of laser radiation in the pulse $P_{max} = 4.4$ kW; pulse frequency 250 Hz; the focus deepening of laser radiation by 4 mm; welding speed 75 mm/s.

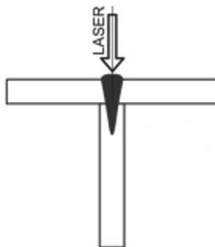


Fig. 1. Scheme of laser welding of T-joints with slot weld.

According to the second task, in addition to obtaining the highest possible value of strength for uniaxial static tensile testing, a necessary condition was to obtain a given geometry with guaranteed formation of fillets on both sides of the rib. To perform this task, according to the second procedure, laser welding was performed in two passes one after the other, with a step of a given distance from the plane of symmetry of the welded T-joint rib. The value of this parameter varied in the range 0.2–0.5 mm. Welding was performed in a continuous mode of laser radiation generation with a power P from 3.0 to 4.4 kW with a defocus value ΔF from -4 to $+4$ mm at a welding speed $V = 50$ – 300 mm/s. Optimal results regarding the formation of a given geometry and obtaining the welded joint with the highest strength were obtained using laser radiation with a power of 4.4 kW without defocusing at a speed of 100 mm/s with a 0.3 mm step from the plane of symmetry of the rib for each of the passages (hereinafter – mode II).

An additional optimization criterion, according to the third task, was the guaranteed formation of the upper reinforcement bead. Also maintained the conditions for obtaining the highest possible value of strength for uniaxial static tensile testing and the necessary condition to obtain a given geometry with guaranteed formation of fillets on both sides of the rib. Therefore, the search for optimal parameters of laser welding by the third technological procedure was performed in three passes. The first two of which corresponded in their parameters to the modes of the second technological procedure described in the previous paragraph. An additional third pass was performed for the proper formation of the upper reinforcement bead in the continuous mode of laser radiation generation while varying the parameters of technological modes in the following ranges: $P = 1.0$ – 3.0 kW; ΔF from $+10$ to $+30$ mm; $V = 1$ – 50 mm/s. The optimal mode for the third pass during welding (hereinafter – mode III): the continuous mode of laser radiation generation with power $P = 1.5$ kW; with defocusing value $\Delta F + 20$ mm; welding speed 25 mm/s.

The structure of the base metal of AISI 321 steel is austenitic with a grain size of $D = 10$... 20 μm and microhardness $HV = 2280$... 2360 MPa (Fig. 2a).

The characteristic zones investigated in the welded joint obtained by laser welding in mode I (Fig. 2b) are: 1 – the center of the weld (Fig. 3a); 2 – weld in the lower area (Fig. 3b); 3 – lateral section of the weld (Fig. 3c); 4 – fusion line in the upper plate (Fig. 3d); 5 – fusion line in the area of connection of two plates (Fig. 3e); 6 – fusion line in the lower plate (Fig. 3f).

Data on the distribution of microhardness (HV) and sizes of grain structure are given in Table 1. As a result of metallographic studies of the structure of the welded joint of

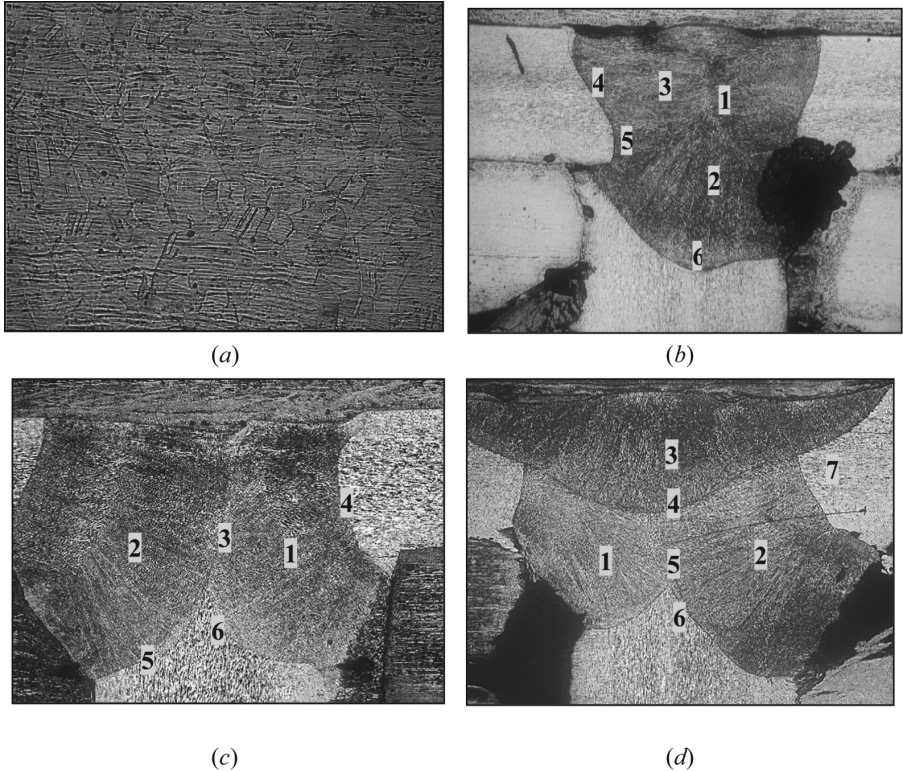


Fig. 2. Microstructure of the base metal ((a) $\times 500$) and general view of welded joints with designation of characteristic zones of research: (b) mode I; (c) mode II; (d) mode III ($\times 50$).

mode I shows the following. Weld metal in zones 1–3 (Fig. 2b, Fig. 3a–c) is characterized by the formation of a dendritic austenitic structure with a crystallite size $h \times l = 5 \dots 12 \times 30 \dots 100 \mu\text{m}$ with a coefficient of their shape $\alpha \sim 2 \dots 8$ at $HV = 2530 \dots 2540 \text{ MPa}$. Characteristically, in the zone 1 α decreases to $3 \dots 4$.

During the transition from the weld metal in zones 4–5 to the base metal of the upper plate, a narrow transition zone (width $\delta = 20 \mu\text{m}$) with a dispersed structure at $h \times l = 2 \dots 5 \times 5 \dots 10 \mu\text{m}$ and $HV = 2620 \dots 2700 \text{ MPa}$ (Fig. 3d, e) is observed on the weld side. On the steel side along the fusion line, the size of the austenitic grain is $D = 10 \dots 20 \mu\text{m}$ at a microhardness $HV = 2510 \dots 2540 \text{ MPa}$. On the opposite side of the weld (left section) in the fusion line of weld metal and steel microhardness HV and the size of the grain structure have similar values. Thus, the structure in these areas is homogeneous.

During the transition from the weld to the base metal (zone 6, Fig. 2b) on the weld side in the transition zone ($\delta = 30 \mu\text{m}$) $h \times l = 4 \dots 10 \times 30 \dots 50 \mu\text{m}$, $HV = 2510 \dots 2640 \text{ MPa}$ (Fig. 3f). On the steel side near the fusion line in the transition zone ($\delta = 20 \mu\text{m}$) $h \times l = 5 \dots 10 \times 10 \dots 15 \mu\text{m}$ and $HV = 2700 \dots 2740 \text{ MPa}$. In zone 6 in comparison with zones 4–5 along the fusion line there is a slight increase of α to $4 \dots 5$ in the weld metal.

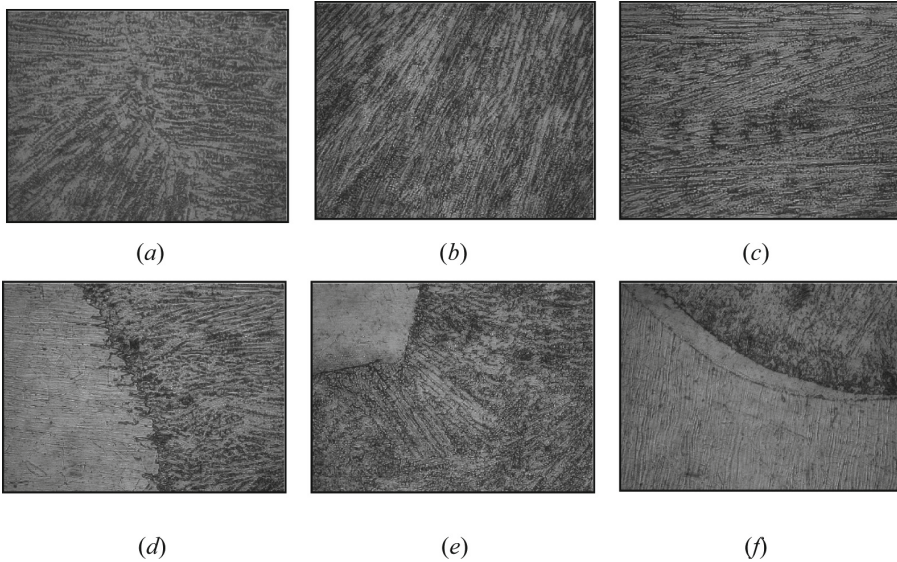


Fig. 3. The microstructure of the welded joint obtained in mode I in the studied zones: (a) – 1; (b) – 2; (c) – 3; (d) – 4; (e) – 5; (f) – 6 ($\times 500$).

Thus, studies of the structure of the weld metal obtained in mode I found that the dendritic structure has a homogeneous and uniform nature, both in size and microhardness. A slight increase in microhardness is observed in the transition zone along the fusion line on the weld side. Thus, this mode can be successfully applied in the absence of specific requirements for the geometry of the welded joint. However, the presence of a stress concentrator in the form of unmelted sections of the T-joint, potentially reduces the crack resistance of the joint welded in mode I.

As a result of metallographic studies of the structure of the welded joint obtained by laser welding in mode II, the following is shown. Characteristic zones were investigated in the welded joint (Fig. 2c): 1, 2 – the center of the welds (Fig. 4a, b); 3 – welds in the area of their joint (Fig. 4c); 4 – side section of the weld along the fusion line (Fig. 4d); 5, 6 – fusion line in the lower plate (Fig. 4e, f). Micro-hardness (HV) and structural parameters are given in Table 1.

The weld metal (zones 1–2, Fig. 2c) is characterized by the formation of a homogeneous dendritic structure. The size of the crystallites in the first weld is $h \times l = 4 \dots 10 \times 30 \dots 110 \mu\text{m}$ with the coefficient of their shape $\alpha \sim 9$ at $\text{HV} = 2540 \dots 2740 \text{ MPa}$ (Fig. 4a). The size of the crystallites in the second weld (zone 2, Fig. 2c) is almost the same with the coefficient of their shape $\alpha \sim 10$ with a slight decrease in HV to $2510 \dots 2640 \text{ MPa}$ (Fig. 4b). In the welds joint zone (zone 3, Fig. 4c) the dendritic component has a structure with microhardness $\text{HV} = 2280 \dots 2380 \text{ MPa}$. The width of this zone $\delta = 50 \mu\text{m}$. In the upper area of the joint zone of the first and second welds there is a slight increase in microhardness to $\text{HV} = 2680 \dots 2700 \text{ MPa}$.

In the upper plate during the transition from the base metal (zone 4, Fig. 2c) to the metal of the first weld in the fusion line on the steel side, the austenitic grain size $D =$

Table 1. Grain structure parameters and microhardness of weld metal.

Welded joint zones of the mode I (Fig. 2b)						
Parameters	1	2	3	4	5	6
$h, \mu\text{m}$	8...12	5...12	5...12	2...3	2...5	4...10
$l, \mu\text{m}$	30...40	30...100	30...100	5...10	5...10	30...50
HV, MPa						
<u>min</u>	2530	2540	2540	2620	2700	2510
<u>max</u>				2700		2640
Welded joint zones of the mode II (Fig. 2c)						
Parameters	1	2	3	4	5	6
$h, \mu\text{m}$	4...10	4...10	10...20 ^a	4...12	8...15 ^a	–
$l, \mu\text{m}$	30...110	50...120		50...120		
HV, MPa						
<u>min</u>	2540	2510	2680 ^b	2360	2600	–
<u>max</u>	2740	2640	2700 ^b 2280 ^c 2380 ^c	2600	2640	
Welded joint zones of the mode III (Fig. 4d)						
Parameters	1	2	3	4	5	6
$h, \mu\text{m}$	3...8	3...8	2...5	2...5	2...5	2...5
$l, \mu\text{m}$	30...120	30...120	10...100	40...120	20...30	20...50
HV, MPa						
<u>min</u>	2240	2430	2360	2450	2270	2300
<u>max</u>	2450	2450	2740	2470	2270	2450

^a grain; ^b upper area; ^c lower area

10...20 μm at microhardness HV = 2360 MPa (Fig. 4d). From the side of the weld in the transition zone ($\delta \sim 50 \mu\text{m}$) $h \times l = 2...3 \times 8...15 \mu\text{m}$ at HV = 2360 MPa. Similar structural parameters are observed from the side of the second weld.

During the transition to the base metal of the lower plate (zones 5–6, Fig. 2c), the dendritic structure is lowered to $h \times l = 3...5 \times 5...70 \mu\text{m}$ at HV = 2540...2680 MPa. In the transition zone ($\delta = 50...60 \mu\text{m}$) from the weld side HV increases to 2640...2850 MPa (Fig. 4e, f). In the fusion line on the steel side, the austenitic grain size is $D = 10...20 \mu\text{m}$ at HV = 2280 MPa.

Thus, studies of the metal structure of the welded joint, obtained in mode II, show that the dendritic structure in the weld metal has a uniform character, both in size and microhardness. Such structural characteristics indicate the uniform strength of the weld obtained in this mode. This mode can be successfully applied if it is necessary to form fillets.

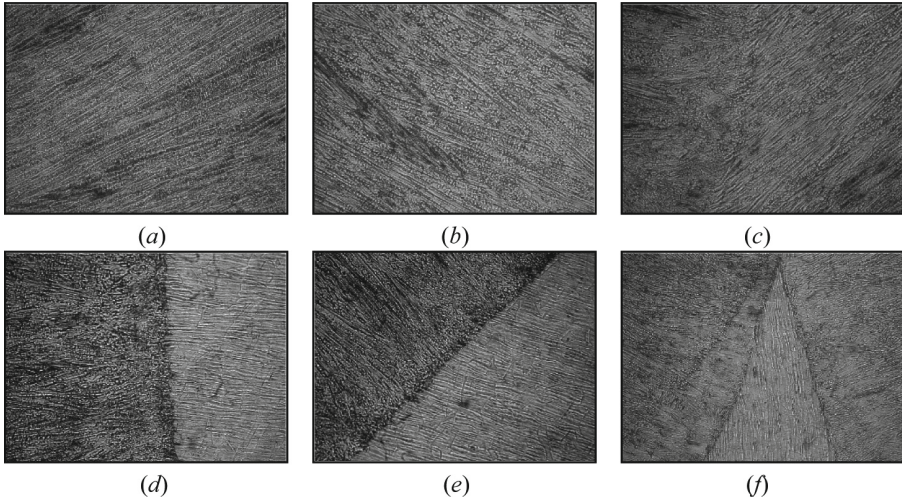


Fig. 4. The microstructure of the welded joint obtained in mode II: (a) – zone 1; (b) – zone 2; (c) – zone 3; (d) – zone 4; (e) – zone 5; (f) – zone 6 ($\times 500$).

As a result of metallographic studies of the structure of the welded joint obtained in mode III, the following is shown. The structural parameters of the metal of the joint being tested are given in Table 1.

Characteristic zones investigated in the welded joint (Fig. 2d) are: 1–3 – center of welds (Fig. 5a–c); 4, 5 – welds in their joint area (Fig. 5d, e); 6 – fusion line in the lower plate (Fig. 5g); 7 – side section of the weld along the fusion line (Fig. 5h).

The weld metal is characterized by the formation of a dendritic structure with the size of crystallites in the first weld (zone 1) $h \times l = 3 \dots 8 \times 30 \dots 120 \mu\text{m}$ with a shape coefficient $\alpha \sim 10 \dots 15$ at $\text{HV} = 2240 \dots 2450 \text{ MPa}$ (Fig. 5a). The size of the crystallites in the second weld (zone 2) doesn't change, the microhardness is almost the same (Fig. 5b).

The weld metal in zone 3 is characterized by the formation of a dendritic structure with a crystallite size $h \times l = 2 \dots 5 \times 10 \dots 100 \mu\text{m}$ with a shape coefficient $\alpha \sim 5 \dots 20$ at microhardness: $\text{HV} = 2640 \dots 2740 \text{ MPa}$ (upper); $\text{HV} = 2450 \dots 2470 \text{ MPa}$ (lower), (Fig. 5c). The slight increase in HV in the upper part of the weld is due to the cooling conditions of the metal. In this case, the weld metal in zone 3 is characterized by the general structure refinement.

In zone 4, the dendritic component has a structure with size $D = 2 \dots 5 \times 10 \dots 20 \mu\text{m}$ and microhardness $\text{HV} = 2270 \dots 2470 \text{ MPa}$ (Fig. 5d). Along the joint line of the welds in zone 5 the width of the transition section is $20 \dots 30 \mu\text{m}$, $D = 2 \dots 5 \times 20 \dots 30 \mu\text{m}$, $\text{HV} = 2270 \text{ MPa}$ (Fig. 5e).

In zone 6 along the transition line from the weld metal to the base metal on the weld side in the transition zone ($\delta \sim 50 \mu\text{m}$) $h \times l = 2 \dots 5 \times 20 \dots 50 \mu\text{m}$ at $\text{HV} = 2300 \dots 2450 \text{ MPa}$ (Fig. 5g). On the steel side in the fusion line, the size of the austenitic grain is $D = 8 \dots 20 \mu\text{m}$ at a microhardness of $\text{HV} = 2280 \text{ MPa}$.

Along the transition line from the base metal to the weld metal in zone 7 on the steel side in the fusion line, the austenitic grain size is $D = 5 \dots 20 \mu\text{m}$ at microhardness HV

= 2210...2280 MPa (Fig. 5h). On the side of weld metal in the transition zone ($\delta \sim 10 \dots 20 \mu\text{m}$) $h \times l = 2 \dots 5 \times 10 \dots 20 \mu\text{m}$ at HV = 2380...2410 MPa.

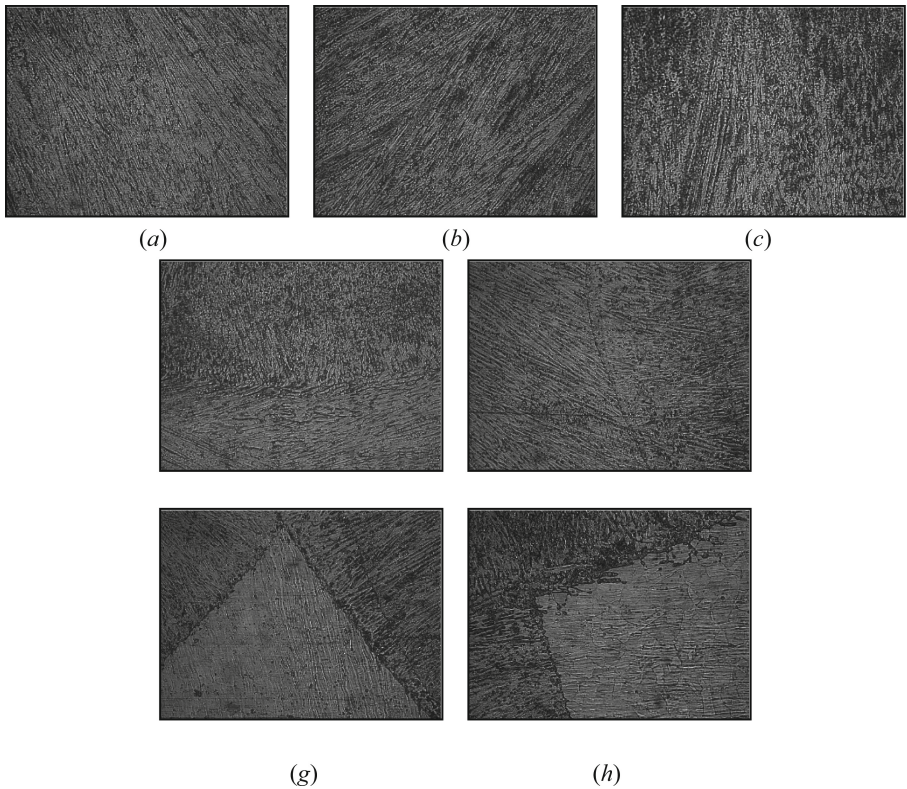


Fig. 5. The microstructure of the welded joint obtained in mode III: (a) – zone 1; (b) – zone 2; (c) – zone 3; (d) – zone 4; (e) – zone 5; (g) – zone 6; (h) – zone 7 ($\times 500$).

Thus, studies of the structure of metal in the welded joint obtained using mode III found that the dendritic structure in the weld metal has a homogeneous character, both in size and microhardness. Welded joints are characterized by a defect-free structure and by the formation of fillets and the upper reinforcement bead. This allows to ensure a high level of mechanical properties, namely the strength and crack resistance of the welded joint metal.

For all three selected optimal modes, the appropriate control programs were compiled for the “FANUC M710” robot. They were tested in the production of various products where T-joints of various configurations were present.

4 Conclusion

The library of technological modes of the robotic welding complex has been expanded by testing the parameters of laser welding of AISI 321 stainless steel T-joints according to three different technological procedures. The optimal modes for three welding procedures are established, which ensure the production of defect-free structures, the formation of a given geometry and the highest level of mechanical properties.

References

1. Magalhães, K.M., Rebello da Fonseca Brasil, R.M., de Macêdo Wahrhaftig, A., et al.: Influence of atmospheric humidity on the critical buckling load of reinforced concrete columns. *Int. J. Struct. Stab. Dyn.* **22**(01), 2250011 (2022). <https://doi.org/10.1142/S0219455422500110>
2. Zavdoveev, A., Poznyakov, V., Baudin, T., et al.: Effect of heat treatment on the mechanical properties and microstructure of HSLA steels processed by various technologies. *Mater. Today Commun.* **28**, 102598 (2021). <https://doi.org/10.1016/j.mtcomm.2021.102598>
3. Bibik, S., Strelko, O., Nesterenko, H., et al.: Formulation of the mathematical model for the planning system in the carriage of dangerous goods by rail. *IOP Conf. Ser. Mater. Sci. Eng.* **985**(1), 012024 (2020). <https://doi.org/10.1088/1757-899X/985/1/012024>
4. Oluyisola, O.E., Bhalla, S., Sgarbossa, F., Strandhagen, J.O.: Designing and developing smart production planning and control systems in the industry 4.0 era: a methodology and case study. *J. Intell. Manuf.* **33**(1), 311–332 (2021). <https://doi.org/10.1007/s10845-021-01808-w>
5. Semenov, I., Krivtsov, I., Demchenko, V., et al.: Modelling of binary alloy (Al–Mg) anode evaporation in arc welding. *Model. Simul. Mater. Sci. Eng.* **20**(5), 055009 (2012). <https://doi.org/10.1088/0965-0393/20/5/055009>
6. Lobanov, L.M., Kostin, V.A., Makhnenko, O.V., et al.: Forecasting of structural transformations in heat affected zone steel of 15KH2NMFA at anti-corrosion cladding. *Probl. Atomic Sci. Technol.* **2**(126), 89–96 (2020)
7. Tiutkin, O., Neduzha, L., Kalivoda, J.: Finite-element analysis of strengthening the subgrade on the basis of boring and mixing technology. *Transp. Probl.* **16**(2), 189–197 (2021). <https://doi.org/10.21307/tp-2021-034>
8. Paturi, U.M., Cheruku, S.: Application and performance of machine learning techniques in manufacturing sector from the past two decades: a review. *Mater. Today Proc.* **38**, 2392–2401 (2021). <https://doi.org/10.1016/j.matpr.2020.07.209>
9. Bakhtiyari, A.N., Wang, Z., Wang, L., Zheng, H.: A review on applications of artificial intelligence in modeling and optimization of laser beam machining. *Opt. Laser Technol.* **135**, 106721 (2021). <https://doi.org/10.1016/j.optlastec.2020.106721>
10. Kolosnichenko, M., Yezhova, O., Pashkevich, K., et al.: The use of modern digital technologies in the design and technology VET in Ukraine. *J. Tech. Educ. Train.* **13**(4), 56–64 (2021). <https://doi.org/10.30880/jtet.2021.13.04.005>
11. Ostash, O.P., Kulyk, V.V., Poznyakov, V.D., et al.: Fatigue crack growth resistance of welded joints simulating the weld-repaired railway wheels metal. *Arch. Mater. Sci. Eng.* **86**(2), 49–55 (2017). <https://doi.org/10.5604/01.3001.0010.4885>
12. Aharkov, O.V., Tverdomed, V.M., Boiko, V.D., et al.: Influence of the structural design of rail fastenings on ensuring the stability of track gauge in operating conditions. *IOP Conf. Ser. Mater. Sci. Eng.* **708**(1), 156807 (2019). <https://doi.org/10.1088/1757-899X/708/1/012001>
13. Akhonin, S.V., Milenin, A.S., Pikulin, A.N.: Modeling of processes of evaporation of alloying elements in EBSM of cylindrical ingots produced from Ti-base alloys. *Problemy Spetsial'noj Electrometallurgii* **1**, 21–25 (2005)

14. May, M.C., Schmidt, S., Kuhnle, A., et al.: Product generation module: automated production planning for optimized workload and increased efficiency in matrix production systems. *Procedia CIRP* **96**, 45–50 (2021). <https://doi.org/10.1016/j.procir.2021.01.050>
15. Zdobyt'skyi, A., Lobur, M., Klymkovych, T., et al.: Use of methods and technologies of additive production for optimization of parameters of designs. *IOP Conf. Ser. Mater. Sci. Eng.* **1016**(1), 012019 (2021). <https://doi.org/10.1088/1757-899X/1016/1/012019>
16. Javaid, M., Haleem, A., Singh, R.P., Suman, R.: Substantial capabilities of robotics in enhancing Industry 4.0 implementation. *Cogn. Robot.* **1**, 58–75 (2021). <https://doi.org/10.1016/j.cogr.2021.06.001>
17. de Sousa, W.T., Jr., Montevechi, J.A., de Carvalho Miranda, R., Campos, A.T.: Discrete simulation-based optimization methods for industrial engineering problems: a systematic literature review. *Comput. Ind. Eng.* **128**, 526–540 (2019). <https://doi.org/10.1016/j.cie.2018.12.073>
18. Plankovskyy, S., Myntiuk, V., Tsegelnyk, Y., Zadorozhnyi, S., Kombarov, V.: Analytical methods for determining the static and dynamic behavior of thin-walled structures during machining. In: Shkarlet, S., Morozov, A., Palagin, A. (eds.) *MODS 2020. AISC*, vol. 1265, pp. 82–91. Springer, Cham (2021). https://doi.org/10.1007/978-3-030-58124-4_8
19. Fomin, O., Lovska, A., Skliarenko, I., Klochkov, Y.: Substantiating the optimization of the load-bearing structure of a hopper car for transporting pellets and hot agglomerate. *East. Eur. J. Enterp. Technol.* **1**(7), 103, 65–74 (2020). <https://doi.org/10.15587/1729-4061.2020.193408>
20. Laukhin, D., Poznyakov, V., Kostin, V., et al.: Features in the formation of the structural state of low-carbon micro-alloyed steels after electron beam welding. *East. Eur. J. Enterp. Technol.* **3**, 25–31 (2021). <https://doi.org/10.15587/1729-4061.2021.234783>
21. Nesterenkov, V.M., Orsa, Y.V., Khripko, K.S.: Renewal of elements and construction units of gas turbine engines by means EBW. *IOP Conf. Ser. Mater. Sci. Eng.* **582**(1), 012049 (2019). <https://doi.org/10.1088/1757-899X/582/1/012049>
22. Akhonin, S.V., Belous, V.Y., Selin, R.V.: Electron beam welding, heat treatment and hardening of beta-titanium. *IOP Conf. Ser. Mater. Sci. Eng.* **582**(1), 012050 (2019). <https://doi.org/10.1088/1757-899X/582/1/012050>
23. Korzhyk, V., Khaskin, V., Voitenko, O., et al.: Welding technology in additive manufacturing processes of 3D objects. *Mater. Sci. Forum* **906**, 121–130 (2017). <https://doi.org/10.4028/www.scientific.net/MSF.906.121>
24. Gadagi, B., Lekurwale, R.: A review on advances in 3D metal printing. *Mater. Today Proc.* **45**, 277–283 (2021). <https://doi.org/10.1016/j.matpr.2020.10.436>
25. Peleshenko, S., Korzhyk, V., Voitenko, O., et al.: Analysis of the current state of additive welding technologies for manufacturing volume metallic products (review). *East. Eur. J. Enterp. Technol.* **3**(1–87), 42–52 (2017). <https://doi.org/10.15587/1729-4061.2017.99666>
26. Shelyagin, V.D., Bernatskyi, A.V., Berdnikova, O.M., et al.: Effect of technological features of laser welding of titanium-aluminium structures on the microstructure formation of welded joints. *Metallofizika i Noveishie Tekhnologii* **42**(3), 363–379 (2020). <https://doi.org/10.15407/mfint.42.03.0363>
27. Poznyakov, V.D., et al.: Cold cracking resistance of butt joints in high-strength steels with different welding techniques. *Strength Mater.* **51**(6), 843–851 (2020). <https://doi.org/10.1007/s11223-020-00132-7>
28. Bernatskyi, A., Sydorets, V., Berdnikova, O., et al.: Research of technology for repair of heat exchangers of nuclear power plants by laser welding. *Solid State Phenom.* **313**, 94–105 (2021). <https://doi.org/10.4028/www.scientific.net/SSP.313.94>
29. Kritskiy, D., Pohudina, O., Kovalevskiy, M., et al.: Powder mixtures analysis for laser cladding using OpenCV Library. In: Nechyporuk, M., Pavlikov, V., Kritskiy, D. (eds.) *ICTM 2021*.

- LNNS, vol. 367, pp. 924–937. Springer, Cham (2022). https://doi.org/10.1007/978-3-030-94259-5_72
30. Berdnikova, O., Kushnarova, O., Bernatskyi, A., et al.: Structure peculiarities of the surface layers of structural steel under laser alloying. In: 2020 IEEE 10th International Conference Nanomaterials: Applications and Properties (NAP), Sumy, pp. 02IT01-1–02IT01-4. IEEE (2020). <https://doi.org/10.1109/NAP51477.2020.9309615>
 31. Berdnikova, O., Kushnarova, O., Bernatskyi, A., et al.: Structure features of surface layers in structural steel after laser-plasma alloying with 48(WC–W₂C)+ 48Cr+ 4Al powder. In: 2021 IEEE 11th International Conference Nanomaterials: Applications and Properties (NAP), Odessa, pp. 1–4. IEEE (2021). <https://doi.org/10.1109/NAP51885.2021.9568516>
 32. Stavridis, J., Papacharalampopoulos, A., Stavropoulos, P.: Quality assessment in laser welding: a critical review. *Int. J. Adv. Manuf. Technol.* **94**(5–8), 1825–1847 (2018). <https://doi.org/10.1007/s00170-017-0461-4>
 33. Sheikhabaee, H., Mirahmadi, S.J., Pakmanesh, M.R., Asghari, S.: Investigating sensitivity to process parameters in pulsed laser micro-welding of stainless steel foils. *Opt. Laser Technol.* **148**, 107737 (2022). <https://doi.org/10.1016/j.optlastec.2021.107737>
 34. Yang, J., Oliveira, J.P., Li, Y., et al.: Laser techniques for dissimilar joining of aluminum alloys to steels: a critical review. *J. Mater. Process. Technol.* **301**, 117443 (2022). <https://doi.org/10.1016/j.jmatprotec.2021.117443>
 35. Lobanov, L.M., Pashchyn, M.O., Mikhodui, O.L., Goncharov, P.V., Sydorenko, Y.M., Ustyomenko, P.R.: Influence of the accompanying heating on the efficiency of electrodynamic treatment of AMg6 aluminum alloy welded joints. *Strength Mater.* **53**(2), 222–226 (2021). <https://doi.org/10.1007/s11223-021-00278-y>
 36. Kombarov, V., Sorokin, V., Tsegelnyk, Y., et al.: Numerical control of machining parts from aluminum alloys with sticking minimization. *Int. J. Mechatron. Appl. Mech.* **1**(9), 209–216 (2021). <https://doi.org/10.17683/ijomam/issue9.30>
 37. Wang, J., et al.: Numerical study on the temperature field of underwater flux-cored wire arc cutting process. *Int. J. Adv. Manuf. Technol.* **91**(5–8), 2777–2786 (2017). <https://doi.org/10.1007/s00170-016-9913-5>



The Main Defects and Ways to Improve the Quality of Layer-by-Layer Sintered Gas Turbine Parts

Daria Tkach¹(✉) , Dmytro Pavlenko¹ , Yaroslav Dvirnyk² , Oleksii Pedash² ,
and Oleksandr Tarasov³ 

¹ Zaporizhzhia Polytechnic National University, 64 Zhukovskoho Street, Zaporizhzhia 69063, Ukraine

dvt@zp.edu.ua

² Motor Sich JSC, 15 Motorobudivnykiv Avenue, Zaporizhzhia 69068, Ukraine

³ Donbas State Engineering Academy, 72 Akademichna Street, Kramatorsk 84313, Ukraine

Abstract. The paper investigates the possibility of improving the quality of engine parts in the process of layer-by-layer synthesis at the stage of prepress. It was found that in the processes of manufacturing parts using 3D printing, the mechanical properties of the final products are influenced by various factors, such as the quality of the powder for printing and the parameters of layer-by-layer synthesis. The most common defects in 3D printing are investigated in this work. It is shown that the quality of the product is significantly affected by the formation of internal stresses, which leads to warping of the product, and the incorrect design of the supports also leads to the need for additional machining. For a preliminary assessment of the influence of printing modes on the properties of products, the stress-strain state was modeled in the ANSYS environment for various modes and strategies of layer-by-layer synthesis of an engine part. Residual stresses and deformation of products were assessed depending on the printing strategy, the position of the part was determined corresponding to the minimum level of warpage of the part during the printing process. The approach proposed in the work allows at the stage of prepress to develop recommendations for choosing the position of the part and modes of layer-by-layer synthesis, depending on the purpose of the engine parts. But the limitation is the significant resource consumption of this process. The main defects arising in the details in the layer-by-layer synthesis process and ways to eliminate them are classified.

Keywords: Additive manufacturing · Finite element method · Stresses · Deformation · Defects · Processing parameters

1 Introduction

An increase in the number of products made of metals and alloys obtained by layer-by-layer synthesis methods is associated with the wide possibilities of manufacturing geometrically complex parts, the possibility of reducing the mass of products, and quickly obtaining a separate product. At the same time, the process of additive manufacturing of

products from metallic materials faces a number of problems: a limited range of materials that can be used to obtain high-quality products; uneven microstructure; porosity; various defects due to the peculiarities of the process and the stress-strain state of the part. However, due to the advantages of this process, the modern industry is interested in the development of additive manufacturing of products from metal powders. Thus, to obtain high-quality products, the structure, and properties of which will be reproduced from product to product, it is necessary to carry out comprehensive studies on the influence of the parameters of the layer-by-layer synthesis process on the physical and mechanical properties.

The solution for a preliminary assessment of possible defects and correction of printing modes is to simulate the process using numerical simulation systems. This will allow a preliminary assessment of possible defects: warpage of the product due to the formation of inhomogeneous internal stresses, separation of the product from the substrate, and other possible defects.

Since the equipment for selective laser sintering allows a fairly wide variety of production parameters, using different sets of parameters can provide different properties of the resulting products. In addition, using finite element modeling methods, it is possible to optimize the location of products in the working space: to ensure the most rational placement of products to ensure not only high mechanical properties of products, but also to reduce the number of rejects, loss of powder and accelerate the production of products.

2 Literature Review

The numbers of goods production for gas turbine via the layer-by-layer synthesis methods increases every year. Major aircraft engine manufacturers pay significant attention to the development of 3D printing technology for metals and alloy parts [1, 2]. The manufacture of aircraft parts is associated with a number of problems: porosity, a decrease in the mechanical properties of products, warpage of the parts, which leads to the impossibility of accomplishing the layer-by-layer synthesis process. Thus, studying the possibility of improving the quality of gas turbine parts for ground installations and aviation is an urgent task. The possibility of using blanks from powders for parts of gas turbine is expanding due to the development of technologies for improving the level of their properties [3]. The methods of compaction by severe plastic deformation [4] and with combined static dynamic loading of powders by pressing and impact forces [5] are being developed. At the same time, the change in the mechanical [6] and physical [7] properties of materials require additional study.

The scientific literature shows a significant amount of research on the features of the additive manufacturing of metal parts. In industry, the most commonly used powders are obtained by gas atomization because they have higher quality [8]. Taking into account the peculiarities of the process of synthesizing parts from powders, the quality of the feedstock has a significant effect on the properties of parts. In work [9] it is shown that the use of titanium powders with a low content of gas impurities makes it possible to ensure their use in the semifinished product at the level of the corresponding regulatory documentation. Obviously, the powders used for synthesis must meet similar conditions.

Quality control for such industries is an important condition for obtaining high-tech products, so the authors of [10] propose the use of computer vision methods, which will improve the quality of products obtained by SLS methods.

The researchers paid special attention to the study of the characteristics of the molten bath. It was found that the smallest number of defects is formed in the conduction mode [11]. When the keyhole mode occurs, the metal evaporates from the pool, porosity and a number of other defects appear [12]. The combination of parameters like the power source power, spot width, and scanning speed actually controls the energy density of the radiation source and, accordingly, by controlling them, you can adjust the quality of the workpiece [13]. The main defects and reasons for its occurrence were investigated in [14]. In this study, the defects in 3D printed Zr-based bulk metallic glasses fabricated by selective laser melting under different energy densities have been investigated via both experimental and simulation approaches. It was shown that different defects, including balling, interlayer pores, open pores, and metallurgical pores, are detected in the 3D-printed. They are depending on the energy inputs. The work provides an in-depth understanding of defect formation in the SLM process and provides methods for eliminating these defects to enhance the mechanical performance of 3D prints. Despite this, it does not give comprehensive knowledge to control the printing process to eliminate the formation of defects. There are no fully classifications of the main problems of obtaining gas turbine parts using the technology of selective laser sintering of powders.

The typical metallurgical defects associated with SLM such as balling effect are significantly affected by line energy density are shown in the article [15]. The authors of [16] noted that the process instabilities intrinsic to the localized laser-powder bed interaction cause the formation of various defects in the laser powder bed fusion additive manufacturing process. The possibility of the elimination of large spatters through controlling laser-powder bed interaction instabilities by using nanoparticles was shown. Two mechanisms work synergistically to eliminate all types of large spatters: nanoparticle-enabled control of molten pool fluctuation eliminates the liquid breakup induced large spatters and nanoparticle-enabled control of the liquid droplet coalescence eliminates liquid droplet colliding induced large spatters are proposed.

The most common defect is the porosity of the finished product, which leads to a significant decrease in its mechanical properties [17]. The work [18] established: samples built horizontally usually have a higher level of porosity than samples built vertically. Incorrectly selected parameters of additive manufacturing can also lead to the formation of balls splashed out of the melt bath, which reduces the quality of adhesion of layers and the quality of the surface of the printed part [19]. Features of the formation of a product by layer-by-layer synthesis (high-temperature gradients and rapid solidification of the melt pool) can lead to the formation of significant residual stresses, warping, and cracking of parts [20].

The possibilities of manufacturing products by layer-by-layer synthesis are also limited by the range of materials that can currently be used in additive manufacturing. Nickel-based and titanium-based powders, a new generation of aluminum alloys, and titanium aluminide are suitable for additive manufacturing, and parts for gas turbine engines [21, 22]. But in each case, different approaches for the technology of synthesis must be used. By controlling the printing parameters, it is possible to form grains of a

given morphology, which directly affects the properties of the product. Further improvement of the mechanical properties of the product is possible using post-processing methods. In work [23] to expand the area of application of parts made of non-compact alloys, it is proposed to use methods of local surface-plastic deformation.

The literature review shows that the regimes and strategy layer-by-layer synthesis determines the quality of a surface layer and the bulk of the metal parts. A decrease in porosity leads to a significant increase in the endurance limit of parts [24]. In this regard, the optimization of printing modes in order to control the morphology of the pore space is an urgent task.

Considering many factors that have an influence on the quality of the details, using numerical modeling to technology preparing, optimization and development is an actual task. The results of works [25, 26] show the high efficiency of using these methods in the development of new processes in mechanical engineering, which, accordingly, can also be used in the design of technological processes of additive manufacturing. In particular, the work [27] shows the possibility of using numerical simulation to optimize the topology of an article obtained by selective laser melting. Thus, they should be applicable to the tasks described above as broadly as possible.

Considering that it is impossible to eliminate all defects in the printing process, the authors of the work [28] noted, that hot working, as an important group of post-processing routes for additive manufacturing technology, has to be used to reduce the solidification/processing defects and anisotropy of properties, grain refinement, improvement of mechanical properties, processing of preformed parts, and increasing the applicability domain. For example, a promising approach to improving the quality of products produced by SLS is the thermal energy method and modifications [29]. This method makes it possible to improve the quality of the surface of products obtained by SLS and, accordingly, to improve their operational properties. The numerical methods for modeling the stress-strain state of the layer-by-layer synthesis parts to assess their strength should be used [3, 30]. Obtaining products with a satisfactory set of physical and mechanical properties by this method requires comprehensive research to ensure the quality of blanks at the stage of 3D printing by controlling the modes and strategy of printing, as well as the spatial orientation of the blank.

Despite a large number of available studies on the physics of the process and the influence of printing parameters and further post-processing on the properties of products, it can be argued that further research is needed in the field of manufacturing aircraft products. Printing parameters are key factors in producing parts with high mechanical properties, and alloys used in gas turbine are often insufficiently studied.

3 Materials and Methods

To improve the operational properties of critical parts of gas turbine obtained by layer-by-layer synthesis, it is necessary to conduct several studies. At the same time, at the first stage of research, to achieve the set task, it is necessary to establish the most common defects in additive manufacturing and establish the reasons for their occurrence. Based on the available data, the model of the part was built and a finite element method to investigate its stress-strain state was used to find the influence of printing parameters on its

stress-strain state and the appearance of possible printing defects. Modeling the process of layer-by-layer synthesis of material in the ANSYS program was done in Workbench Additive environment. In this work, the term layer-by-layer synthesis of material means selective laser sintering/melting (SLS). The essence of the project was to solve the non-stationary thermal problem “Transient Thermal” coupled with the stationary strength calculation module “Static Structural”.

As a result of this calculation, it was possible to analyze the heat-stressed state of the part in the process of layer-by-layer formation at each printing layer, at the end of the printing process. The final model of the part understudy with quantitative parameters of deformations arising under the influence of temperature stresses was obtained. Taking into account the resulting deformations, it is possible to provide the necessary additional stages of post-processing thermal treatment and compensate for the original solid model. The calculations were carried out using a computer with the following characteristics: processor – Intel Xeon E5-2699V3, 18 cores at 3.6 GHz; RAM - DDR4, 128 GB. The time for calculating the SLS process by the numerical method in the Workbench Additive environment directly depends on the number of layers modeled, and, consequently, on the position of the part in space during the printing process. There are two options for the location of the part: horizontal, corresponding to the design coordinate system, and vertical, the most advantageous to minimize residual deformations. The solid model of the part itself, together with the base plate, were designed in the Space Clame CAD system.

The modeling process uses a cubic grid with an element size of 0.5 mm for the part and 3 mm for the base. The cell size for the part is selected from the requirements that it should be 10–20 times larger than the applied layer, which in this case is 30 microns. The above ratio, based on the developer’s information and calculation experience, gives the optimal accuracy to the calculation time ratio. Moreover, there is an interesting phenomenon associated with the fact that with an increase in the accuracy of the model, i.e. by decreasing the cell size, the calculation accuracy remains unchanged, and the required computing power increases significantly.

The following parameters were set as initial data: powder material – Ti-6Al-4V; the thickness of the applied layer – 30 microns; shading distance – 0.14 mm; scanning speed (laser) - 1200 mm/s; downtime between layers – 10 s; base (slab) temperature – 80 °C; convection coefficient of gas and powder – 5...10 W/mm².°C; ambient temperature – 22 °C; overhang angle – 45°.

4 Results and Discussion

In order to establish the priority tasks of modeling the production of products by layer-by-layer synthesis, the most common defects were studied. Detachments of the supporting structures (Fig. 1) are caused by uneven internal stresses and weak design of the supporting structures. Uneven heat dissipation at the edges and in the center leads to warping at the ends. In this case, the formed internal stresses are likely to exceed the value of the strength limit of the resulting material, which leads to separation. This defect is especially characteristic of a workpiece made of titanium alloys, which is probably due to the low limit of the strength of the initial material in comparison with the formed residual

stresses. In order to avoid this defect, it is possible to use such methods as heating the substrate and the printing process optimization.

Some printing defects are associated with defects in the design of the supports. In particular, when printing massive parts, it may be necessary to use massive support structures with a block structure. The use of such supports after printing has led to problems with their removal after printing (Fig. 2).

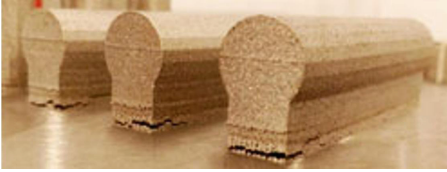


Fig. 1. Detachments caused by significant internal stresses.



Fig. 2. Hard-to-remove massive part supports.

In order to remove the supports shown in the image, it was necessary to use a blade tool on a lathe, since a simple tool (pliers, fortune, cutters) could not remove the support of such a structure.

Another problem associated with the design of the supports is their lack of rigidity during the printing process. In Fig. 3 is shown this defect – two thin plates inside are not connected by a common wall and are grown separately due to which there was some warping and a stop of printing with non-fusion of layers, as can be seen in the image there is no local adhesion of the layers. The subsequent resumption of the printing process led to the absence of filling the indicated place with powder and missing its adhesion. The conical type of support turned out to be ineffective and led to the separation of the main product from the supporting structure, the block structure of the supports is more effective in this case (Fig. 4). An uncalibrated laser of the setup can lead to a defect shown in Fig. 5. The image shows uneven penetration of the product: in a specific area of the build platform, the laser melted the powder too much.

Insufficient filling of the construction zone with powder due to the small number of revolutions of the leveling roller can lead to the separation of the primary layers of the part from the array of supporting structures and, subsequently, to the stop of the print job and local remelting of some details (Fig. 6). Based on the previously constructed model and the specified parameters, the first results of the influence of printing parameters on the stress-strain state of the selected part were obtained.

The process of calculating this problem on the above system took 12 h, while 60 GB of RAM was used. The problem was solved in 504 steps for thermal analysis and 264 steps for strength analysis, while the print time of the part is 12649 s.

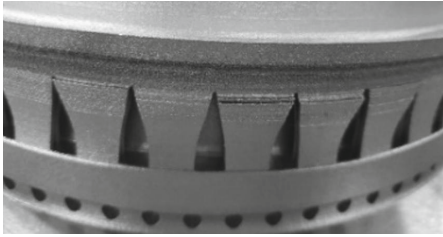


Fig. 3. Unfused layers due to warpage of the product.

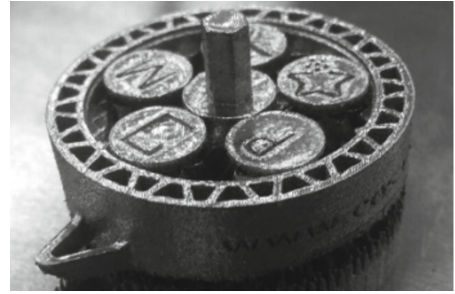


Fig. 4. Separation of the main product from support.



Fig. 5. The uneven penetration of the build area due to an uncalibrated laser.

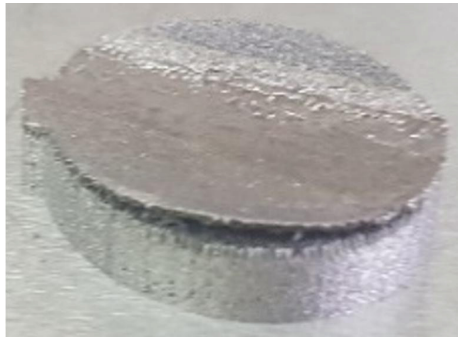


Fig. 6. Detachment of the part from the supporting structures due to the insufficient filling of the area with powder.

At the end of the calculation, the following results were received: temperature distribution fields at each of the 504 construction steps (Fig. 7); stress distribution fields at each of the 264 construction steps (Fig. 8). At the final stage, the results of the deformation (warping) of the part were obtained after the printing process was completed and the supports were removed (Fig. 9). Having available data on the amount of deformation along three axes, it is possible to put the results obtained in the original solid model of the part and, thereby, compensate for the warpage of the resulting product.

Permanent deformation can be minimized by finding the initial optimum position of the part during printing. For this purpose, the Space Clame CAD modeling program was used as an auxiliary tool. This program has a built-in Additive Prep module, which allows you to determine the optimal position of the part, depending on the priorities set. In Fig. 10 shown a triangle of priorities, in accordance with which the optimal position of the part in space is selected. The aforementioned priority triangle has mutually exclusive factors such as support volume, print time, and tendency to warp.

In Fig. 10*b, c, d* shown maps of the corresponding priorities, where green corresponds to the least number of supports, print time, and tendency to warp, and red, on the contrary,

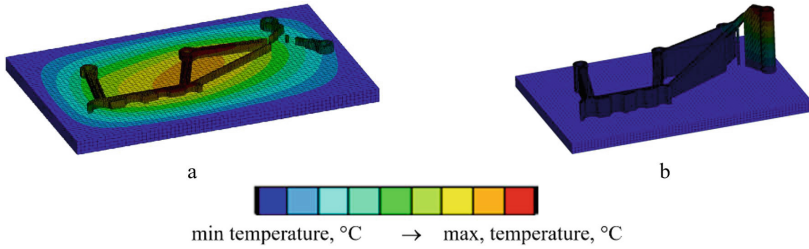


Fig. 7. Temperature field at 40 (a) and 500 (b) construction steps.

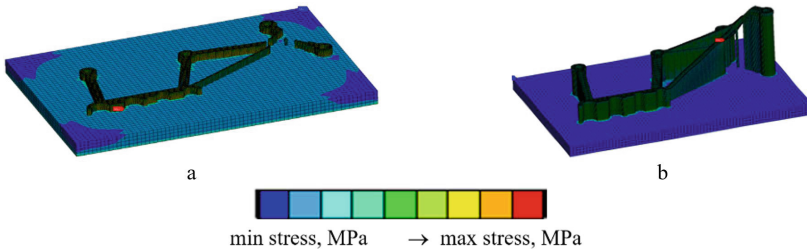


Fig. 8. Field of equivalent stresses at 20 (a) and 250 (b) construction steps.

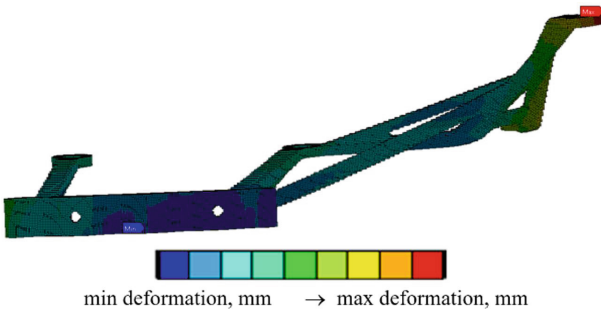


Fig. 9. Field of the part deformation at the end of the printing process and removal of supports.

to the largest corresponding values. The algorithm of this triangle of priorities allows you to obtain preliminary results on the optimal location of the part (for example, based on the minimum warpage) without calculations. However, it must be remembered that these are preliminary results and they cannot be accepted as final without carrying out verified calculations. Taking into account the requirements for the minimum residual distortion of the investigated part, it was previously found its optimal position in terms of minimum residual deformations.

Such an arrangement of the part (vertical) will lead to an increase in both the time of calculation and of the actual process of printing the part. However, in reality, when printing a given part in a vertical position, it becomes possible to arrange a larger number of such parts in a plane and thereby compensate for an increased printing time. At this

position of the part, the calculation with similar parameters to the previous one took 56 h instead of 12 h. In this case, almost 120 GB of RAM was involved.

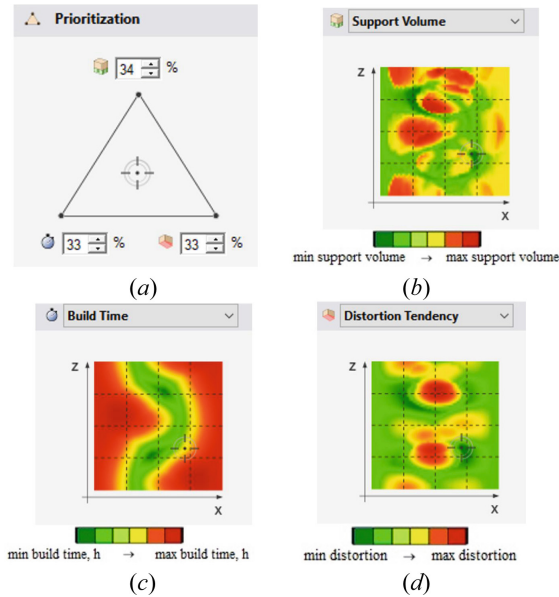


Fig. 10. Triangle of spatial position priorities (a), map of part position c in accordance with the volume of supports (b), construction time (c) and tendency to deformation (d).

The use of finite element analysis to simulate the stress-strain state of a part in the process of layer-by-layer synthesis makes it possible to exclude the appearance of many of the defects. So, modeling has the main influence on the quality of the part at the stage of preparing the model and choosing a printing strategy. Varying the position of the workpiece in space, modes, and strategy of layer-by-layer synthesis makes it possible to eliminate such defects as detachment of the workpiece from the substrate, delamination, etc. Also at this stage, it is effective to optimize both the shape of the part, taking into account the features of the printing technology, and the system of technological supports. In combination with the spatial orientation of the workpiece, which takes into account the influence of the printing direction on the anisotropy of mechanical and physical properties, this makes it possible to reduce material consumption while maintaining the functional properties of the part. Optimization also reduces print times and improves the energy efficiency of the process.

By classifying the main printing defects based on the stage of their manifestation, their causes, types, impact on the production process, and methods for their elimination, it can be seen (Fig. 11) that modeling can influence more than a third of them. Based on the developed classifier, studies aimed at improving the quality of products and reducing their cost can be systematized.

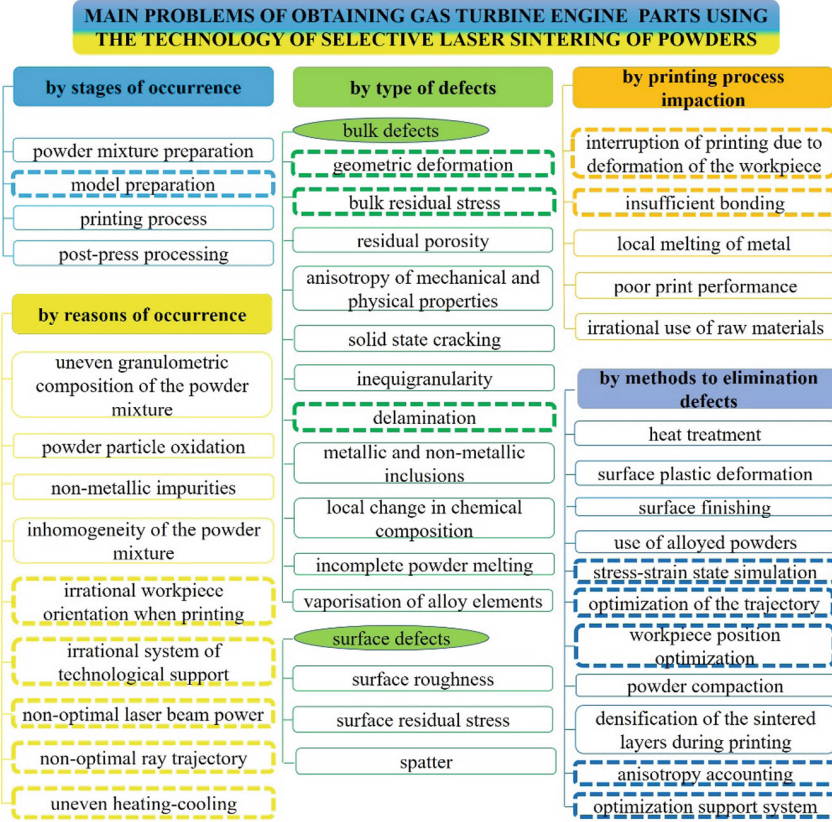


Fig. 11. Classifier of the main defects of the layer-by-layer sintered gas turbine parts. The dotted line marks defects that can be eliminated by modeling.

5 Conclusion

Thus, it has been established that in the process of 3D printing of parts from titanium and heat-resistant nickel alloys, such characteristic defects as detachment of the part from the substrate, unfused layers, the uneven penetration of the build area, warping and detachment of the parts from the supporting structures are possible. The effectiveness of applying numerical modeling to optimize printing has been established. It is shown that the Workbench Additive environment module of the ANSYS software package allows solving a wide range of problems related to the assessment of stresses and deformations of a part in the process of layer-by-layer synthesis. This allows you to optimize the design of supports and the orientation of the part in the working space of the camera and to exclude the appearance of characteristic defects. Using a triangle of spatial position priorities allows you to optimize your print for such parameters as a volume of supports, construction time, and tendency to deformation. To effectively implement the numerical simulation of complex-profile parts of gas turbine, it is necessary to use a computer with at least 18 cores of a processor at 3.6 GHz and 128 GB of RAM. The use of simulation

of the stress-strain state of parts in the process of layer-by-layer laser synthesis makes it possible to exclude the appearance of more than a third of the main defects.

References

1. Badum, L., Leizeronok, B., Cukurel, B.: New insights from conceptual design of an additive manufactured 300 W micro gas turbine toward unmanned aerial vehicle applications. *J. Eng. Gas Turbines Power* **143**(2) (2021). <https://doi.org/10.1115/1.4048695>
2. Wang, M., Du, Y.: Research progress of additive manufacturing of TiAl alloys. *Hangkong Xuebao/Acta Aeronautica et Astronautica Sinica* **42**(7) (2021)
3. Pavlenko, D., Dvirnyk, Y., Przysowa, R.: Advanced materials and technologies for compressor blades of small turbofan engines. *Aerospace* **8**(1), 1 (2021). <https://doi.org/10.3390/aerospace8010001>
4. Pavlenko, D.V., Beygel'zimer, Y.E.: Vortices in noncompact blanks during twist extrusion. *Powder Metall. Met. Ceram.* **54**(9–10), 517–524 (2016). <https://doi.org/10.1007/s1106-016-9744-9>
5. Tarasov, A.F.: The staticodynamic forming of powders preforms on press-hammers. *Kung Cheng Je Wu Li Hsueh Pao/J. Eng. Thermophys.* **19**(6), 5–9 (1998)
6. Karpinos, B.S., Pavlenko, D.V., Kachan, O.Y.: Deformation of a submicrocrystalline VT1-0 titanium alloy under static loading. *Strength Mater.* **44**(1), 100–107 (2012). <https://doi.org/10.1007/s11223-012-9354-9>
7. Pavlenko, D.V., Tkach, D.V., Danilova-Tret'yak, S.M., Evseeva, L.E.: Thermophysical properties and temperature of the start of titanium recrystallization in different structural states. *J. Eng. Phys. Thermophys.* **90**(3), 685–696 (2017). <https://doi.org/10.1007/s10891-017-1616-8>
8. Fayazfar, H., Salarian, M., Rogalsky, A., et al.: A critical review of powder-based additive manufacturing of ferrous alloys: process parameters, microstructure and mechanical properties. *Mater. Des.* **144**, 98–128 (2018). <https://doi.org/10.1016/j.matdes.2018.02.018>
9. Pavlenko, D.V.: Assessment of gas saturation of titanium alloys synthesized from powders using twist extrusion. *Powder Metall. Met. Ceram.* **56**(5–6), 273–282 (2017). <https://doi.org/10.1007/s1106-017-9895-3>
10. Kritskiy, D., Pohudina, O., Kovalevskiy, M., et al.: Powder mixtures analysis for laser cladding using OpenCV library. In: Nechyporuk, M., Pavlikov, V., Kritskiy, D. (eds.) *ICTM 2021. LNNS*, vol. 367, pp. 924–937. Springer, Cham (2022). https://doi.org/10.1007/978-3-030-94259-5_72
11. Dezfoli, A., Hwang, W.S., Huang, W.C., et al.: Determination and controlling of grain structure of metals after laser incidence: theoretical approach. *Sci Rep* **7**, 41527 (2017). <https://doi.org/10.1038/srep41527>
12. Qi, T., Zhu, H., Zhang, H., et al.: Selective laser melting of Al7050 powder: melting mode transition and comparison of the characteristics between the keyhole and conduction mode. *Mater. Des.* **135**, 257–266 (2017). <https://doi.org/10.1016/j.matdes.2017.09.014>
13. Maamoun, A., Xue, Y., Elbestawi, M., Veldhuis, S.: Effect of selective laser melting process parameters on the quality of Al alloy parts: powder characterization, density, surface roughness, and dimensional accuracy. *Materials* **11**, 2343 (2018). <https://doi.org/10.3390/ma11122343>
14. Xing, W., Ouyang, D., Chen, Z., Liu, L.: Effect of energy density on defect evolution in 3D printed Zr-based metallic glasses by selective laser melting. *Sci. China Phys. Mech. Astron.* **63**(2), 1–7 (2019). <https://doi.org/10.1007/s11433-019-1485-8>
15. Xiang, Y., et al.: Forming and defect analysis for single track scanning in selective laser melting of Ti6Al4V. *Appl. Phys. A* **124**(10), 1–12 (2018). <https://doi.org/10.1007/s00339-018-2056-9>

16. Qu, M., Guo, Q., Escano, L.I., et al.: Controlling process instability for defect lean metal additive manufacturing. *Nature Commun.* **13**(1) (2022). <https://doi.org/10.1038/s41467-022-28649-2>
17. Ngo, T.D., Kashani, A., Imbalzano, G., et al.: Additive manufacturing (3D printing): a review of materials, methods, applications and challenges. *Compos. B Eng.* **143**, 172–196 (2018). <https://doi.org/10.1016/j.compositesb.2018.02.012>
18. Qiu, C., Adkins, N., Attallah, M.: Microstructure and tensile properties of selectively laser-melted and of HIPed laser-melted ti-6Al-4V. *Mater. Sci. Eng. A* **578**, 230–239 (2013). <https://doi.org/10.1016/j.msea.2013.04.099>
19. Kruth, J.P., Froyen, L., van Vaerenbergh, J., et al.: Selective laser melting of iron-based powder. *J. Mater. Process. Technol.* **149**(1), 616–622 (2004). <https://doi.org/10.1016/j.jmatprotec.2003.11.051>
20. Sames, W.J., List, F.A., Pannala, S., et al.: The metallurgy and processing science of metal additive manufacturing. *Int. Mater. Rev.* **61**(5), 315–360 (2016). <https://doi.org/10.1080/09506608.2015.1116649>
21. Basak, A., Das, S.: Epitaxy and microstructure evolution in metal additive manufacturing. *Annu. Rev. Mater. Res.* **46**(1), 125–149 (2016). <https://doi.org/10.1146/annurev-matsci-070115-031728>
22. Zhu, Y.Y., Tang, H.B., Li, Z., et al.: Solidification behavior and grain morphology of laser additive manufacturing titanium alloys. *J. Alloy. Compd.* **777**, 712–716 (2019). <https://doi.org/10.1016/j.jallcom.2018.11.055>
23. Vyshnepolskyi, Y., Pavlenko, D., Tkach, D., Dvirnyk, Y.: Parts diamond burnishing process regimes optimization made of INCONEL 718 Alloy via selective laser sintering method. In: 2020 IEEE 10th International Conference Nanomaterials: Applications and Properties, Sumy, p. 02SAMA01-1. IEEE (2020). <https://doi.org/10.1109/NAP51477.2020.9309661>
24. Pavlenko, D.V.: Effect of porosity parameters on the strength of gas turbine compressor blades made of titanium alloys. *Strength Mater.* **51**(6), 887–899 (2020). <https://doi.org/10.1007/s11223-020-00139-0>
25. Markov, O., Kukhar, V., Zlygoriev, V., et al.: Improvement of upsetting process of four-beam workpieces based on computerized and physical modeling. *FME Trans.* **48**(4), 946–953 (2020). <https://doi.org/10.5937/fme2004946M>
26. Tarasov, A., Altukhov, A., Gribkov, E., Abdulov, A.: Development and FEM modeling of a new severe plastic deformation process according to the reverse shear scheme. *Model. Simul. Eng.* **2019**, 8563830 (2019). <https://doi.org/10.1155/2019/8563830>
27. Seabra, M., Azevedo, J., Araújo, A., et al.: Selective laser melting (SLM) and topology optimization for lighter aerospace components. *Procedia Struct. Integr.* **1**, 289–296 (2016). <https://doi.org/10.1016/j.prostr.2016.02.039>
28. Motallebi, R., Savaedi, Z., Mirzadeh, H.: Additive manufacturing – a review of hot deformation behavior and constitutive modeling of flow stress. *Curr. Opin. Solid State Mater. Sci.* **26**(3), 100992 (2022). <https://doi.org/10.1016/j.cossms.2022.100992>
29. Plankovskyy, S., Popov, V., Shypul, O., et al.: Advanced thermal energy method for finishing precision parts. In: Gupta, K., Pramanik, A. (eds.) *Advanced Machining and Finishing*, pp. 527–575. Elsevier, Amsterdam (2021). <https://doi.org/10.1016/B978-0-12-817452-4.00014-2>
30. Tkachenko, D., Tsegelnyk, Y., Myntiuk, S., Myntiuk, V.: Spectral methods application in problems of the thin-walled structures deformation. *J. Appl. Comput. Mech.* **8**(2), 641–654 (2022). <https://doi.org/10.22055/jacm.2021.38346.3207>



3D Concrete Printing Technology: Implementing Tasks in Ukraine

Oleh Kulaienko^(✉)  and Oleksii Kabus 

Kharkiv National University of Civil Engineering and Architecture, 40 Sumska Street,
Kharkiv 61002, Ukraine
kulaienko.oleh@kstuca.kharkov.ua

Abstract. This paper describes the development tasks of localized for Ukraine 3D concrete printing technology, the ways of design, manufacture and testing in industrial conditions a technological equipment set as a part of Smart Manufacturing conception in construction. It is necessary to create design documentation, technological regulations, guidelines and special software for technology implementation. As the same the object of novelty should be the technology of manufacturing special concrete mixtures localized for raw materials available in Ukraine. According to the project objectives, it justified the use BIM technologies, which corresponds to the target program of the Ministry of Regional Development of Ukraine. The work results should be the solution for the mass construction of affordable durable middle-class housing for the housing stock in Ukraine restoration.

Keywords: Construction 3D printer · CNC machines · Multidisciplinary

1 Introduction

Construction technologies used by construction companies in Ukraine do not allow to effectively solve the problem of rapid low-rise housing construction in the middle price sector with the necessary characteristics of energy efficiency, ergonomics, engineering [1]. Suburban low-rise buildings are not economically attractive for large construction companies due to the high cost of individual design and organization of the construction process for each individual building, but the public demand for housing of this class is growing. In addition, due to the destruction of a large number of residential buildings during the hostilities in Ukraine, the issue of mass construction of affordable durable middle-class housing for the long-term restoration of Ukraine's housing stock is already on the agenda. There is a need to reduce the cycle of construction production from design to construction. At the same time, the individuality of each house remains is important.

The solution to the problem is the introduction of modern technologies of additive production or 3D-printing of concrete structures in the construction industry [2, 3]. The technology allows for mass construction of suburban settlements with the individuality of each of the buildings in the shortest possible time. The final cost of such houses is

much lower than analogues. The use of technology allows to significantly update the housing stock of Ukraine.

The essence of the technology is to layer-by-layer build-up of concrete mix with special characteristics for the formation of building structural elements [4]. The main equipment for the implementation of this process is a construction 3D printer. This is a machine with a CNC system, designed to supply the construction mixture according to a given contour program [5–7]. This program is formed in the process of designing a building or a separate structure using Building Information Model (BIM) technologies [8].

The main advantages of the technology are the high speed of construction of the main structures of the building and low cost compared to traditional technologies, such as construction of brick or monolithic reinforced concrete. In this case, the design of any structure and complexity with pre-set characteristics can actually be formed. Thus, a significant intensification of housing production with high performance can be achieved.

An additional advantage of the technology is the high flexibility in the objects design and construction with atypical architectural solutions, which significantly increases the aesthetic value of the building. The field of the technology application is the construction of low-rise buildings or the manufacture of complex shape concrete structures without the use of formwork.

This technology has been actively developing in the world for 15 years. The leaders in its implementation are the United States, China, the UAE, Denmark and the Netherlands. Ukraine is also developing materials and creating basic equipment for 3D printing, but there are currently no complete technological solutions to ensure the full cycle of building construction. The main problems in the introduction of this technology are:

- high cost of imported basic equipment, as well as the actual lack of ability to service this equipment by foreign manufacturers. This creates great risks for the developer during implementing this technology;
- lack of regulatory framework, practical and organizational recommendations for design and construction;
- lack of localized technology for the production of concrete mix for 3D printing;
- lack of domestic specialists in the implementation of 3D printing technology.

The solution of the given complex of problems will allow to introduce this technology in the construction industry of Ukraine and to provide construction of high-quality social housing or buildings with complex architectural forms. The use of construction 3D printing in future programs for the restoration of socio-economic infrastructure of the eastern regions of Ukraine is also promising.

2 Project Problem Formulation

The research team of Kharkiv National University of Civil Engineering and Architecture (KhNUCEA) proposes a project to implement the latest technologies of concrete 3D-printing for low-rise buildings, taking into account local characteristics of materials and construction management. Currently, the project has no analogues in Ukraine. Existing

solutions are not comprehensive and solve only the problems of operation of special equipment, not the introduction of technology as a whole.

According to the project objectives, it is planned to attract BIM technologies, which corresponds to the target program of the Ministry of Regional Development of Ukraine.

The object of novelty should be the technology of manufacturing special concrete mixtures localized for raw materials available in Ukraine according to the recommendations [9–11]. At present, the technology of production of works and materials for the mixtures manufacture are available only with the purchase of foreign basic equipment.

Fundamentally new in Ukraine is the design and manufacture of construction 3D-printer with a set of supply equipment for the full cycle of construction of the building directly on the construction site.

The project includes an experimental study of individual structures obtained by new technology using the developed equipment and materials. This will allow to develop the necessary additions to the State building codes.

3 Project Implementation Stages

Project Implementation Stages (SPI) and performance indicators are listed below.

– SPI 1. Development of the Technical Task for the Complex Manufacture

Objectives: Determination of technological and operational parameters of structures, materials and equipment for the implementation of 3D printing.

- Task 1. Analysis of raw materials for the manufacture of mixtures adapted for 3D printing.
- Task 2. Prototype analysis of machines, software and technological complexes that implement the technology of buildings and individual structures 3D printing.
- Task 3. Development of a technical task for the manufacture of mechanical equipment, software and technology of materials for 3D printing.

Performance Indicators: Terms of reference for the manufacture of equipment and software.

– SPI 2. Technology Design

Objectives: Development of technological bases and design documentation for the manufacture of equipment and technology for buildings 3D printing.

- Task 1. Development of technology for materials production for 3D-printing adapted in Ukraine.
- Task 2. Development of working design and engineering documentation for the manufacture of basic and auxiliary mechanical equipment.
- Task 3. Development of experimental building structures models, which are manufactured according to the proposed technology, using BIM.

- Task 4. Development of BIM integrated software.

Performance Indicators: Technological regulations for the manufacture of materials for 3D printing, design documentation for the main and auxiliary equipment, BIM-models of typical building structures, software module for the interpretation of structural models in the executive G-code for the CNC system.

– SPI 3. Equipment Set Production

Objectives: Creation of experimental research material base for testing 3D printing technology of buildings.

- Task 1. Placing an order for the manufacture of the complex according to the project.
- Task 2. Production of a coordinate machine.
- Task 3. Manufacture of auxiliary equipment.

Performance Indicators: Tender for the manufacture of equipment according to the project, producing of the coordinate machine experimental sample, producing of the auxiliary equipment set according to the project.

– SPI 4. Experimental Test of the Complex

Objectives: Experimental assessment of technological characteristics of the complex, identification and elimination of shortcomings at the design stage.

- Task 1. Assembly and commissioning of the complex on the experimental site.
- Task 2. Fabrication of individual building structures on the experimental site.
- Task 3. Testing of individual structures for compliance with building codes.

Performance Indicators: Commissioning of an experimental sample of a complex for 3D printing, production of 10 typical building structures using 3D printing technology, protocol of laboratory structural characteristics testing.

– SPI 5. “Project-Equipment-Building” Testing in Industrial Conditions

Objectives: Confirmation of the technology effectiveness in conditions of construction site.

- Task 1. Development of a design paper of the building using BIM technologies.
- Task 2. Coordination of the project with the developer.
- Task 3. Complex installation for 3D printing of the building on the construction site.
- Task 4. Construction works execution.

Performance Indicators: Working design of construction using the proposed technology, commissioning of the complex in terms of construction production, experimental sample of the building made by 3D printing technology.

– SPI 6. Work Results Generalization

Objectives: Results analysis and technology preparation for mass implementation.

- Task 1. Development of the design documentation package for the manufacture of a complex for 3D-printing, taking into account modifications.
- Task 2. Development of recommendations and additions to the relevant regulations for the implementation 3D printing technology in Ukraine.
- Task 3. Estimation of the actual economic effect of using 3D printing technology of buildings.
- Task 4. Publication of research results.

Performance Indicators: Design documentation for the 3D-printing complex, recommendations and additions to the building codes of Ukraine, report on economic indicators and marketing plan for technology implementation, sustainable project development plan.

4 Results

The following methods are used:

- analysis of prototypes;
- the principle of interchangeability and unification of components in the design of equipment [12, 13];
- the principle of availability of materials and components in the design of technology [14, 15].

The work has a scientific and applied nature and includes 4 main stages:

- design of basic equipment based on the analysis of prototypes [16–18];
- design of special construction mixtures, laboratory study of their properties and testing on the construction site [19, 20]
- design and experimental study of individual structures and materials for their manufacture [21];
- generalization of results in the form of recommendations to regulatory documents.

The design of the main equipment takes place according to the terms of reference agreed with the existing construction companies. It is planned to develop and manufacture a portal coordinate machine with the size of the effective working area ($L \times W \times H$) $12 \times 9 \times 6$ m. These dimensions are typical for most low-rise residential buildings. Type of machine control – industrial CNC system using high-precision dynamic servo for positioning the working tool. It is also planned to develop a special mobile complex of auxiliary equipment (mixer and concrete pump) for placement directly on the construction site. All components and components are purchased, installed and serviced in Ukraine.

Mixtures for 3D-printing with concrete are selected individually depending on the specified design characteristics, printer specifications and printing parameters. The key is to choose the right type of cement, maximum size of aggregates, types and concentrations of chemical, mineral additives and fiber, which provide special properties associated with 3D printing technology [10]. When designing the composition of mixtures, in addition to standard requirements, you need to consider the need for:

- obtaining mixtures with rheological properties that provide uninterrupted pumping and extrusion of the mixture, the density and geometry of the layer without its spreading, the formation of voids and rupture sites;
- ensuring the required duration of open time during which the material is used for pumping and extrusion;
- providing the time required for the erection of one layer without compromising adhesion to the next layer;
- acceleration of initial processes of hardening of cements to avoid deformation of material from own weight in process of addition of new layers;
- control and reduction of destructive processes from shrinkage of concrete, which can be much more important than when concreting in the formwork due to the large open surface;
- taking into account the difference in strength between normally laid and layered concrete.

The outlined issues require detailed experimental research and systematization. The result is the development of methods for designing and controlling the properties of mixtures and printed concrete. This will allow to adjust the printing process in order to build structures with specified geometric dimensions, physical and mechanical properties and reliability.

Scientific and practical tasks within the project determine its multidisciplinary. Specialists in construction design, construction materials science, mechanical engineering, industrial electronics, BIM technologies are involved in the project. The project is planned to involve architects, specialists in the organization of construction production, the economy of the enterprise.

The work includes the creation of a prototype complex for 3D printing, which requires the purchase of materials and components for its manufacture. Design work is performed on the basis of KhNUCEA.

The complex includes:

- CNC coordinate machine to provide the movement of the print head;
- printing head for concrete extrusion;
- concrete mix preparation system;
- concrete mix supply system;
- software package for 3D printing buildings design.

Upon completion of the project, the obtained equipment and materials will be used as an experimental laboratory complex of the KhNUCEA smart construction laboratory to provide training for 3D printing specialists for enterprises of the construction industry of

Ukraine for both university students and third parties. It is also planned to use commercial equipment for construction works by Ukrainian enterprises.

To conduct experimental studies of the composition of special concrete mixtures, it is necessary to purchase raw materials. In the process of experiments, samples of structures must be destroyed on laboratory presses to obtain strength characteristics. The research uses the testing laboratory of building materials, products and structures of KhNUCEA (certificate of compliance of the measurement system with the requirements of DSTU ISO 10012:2005 for № 01–0064/2018 of June 16, 2018), which is designed to determine the deformation-strength and other characteristics of materials and structures, development of projects to strengthen building elements and extend their life, research and implementation of new building materials, ways to increase the strength of load-bearing structures, soil characteristics and foundations [22].

The project team has created a set of physical and chemical methods for studying the hardening of binders and concrete. Thermokinetic analysis and temperature-time monitoring of cements and concretes hardening with additives were carried out. The results of research work were implemented in the development of DSTU and in the use of complex additives in concrete [23, 24].

The production base of the main equipment complex is PE “Axicon” [25], whose specialists have experience in the manufacture and implementation of large portal coordinate machines with CNC. A prototype of a multifunctional coordinate machine with a working area size of $8000 \times 3000 \times 1000$ mm (Fig. 1) was developed and manufactured for the installation of special technological equipment to ensure various technological processes, including concrete extrusion (Fig. 2). The drive part of the machine allows to move a portal weighing up to 3000 kg with a speed up to 2000 mm/min. The control system is based on Siemens Sinumeric 808D Advanced. This allows you to use the equipment in an open construction site.

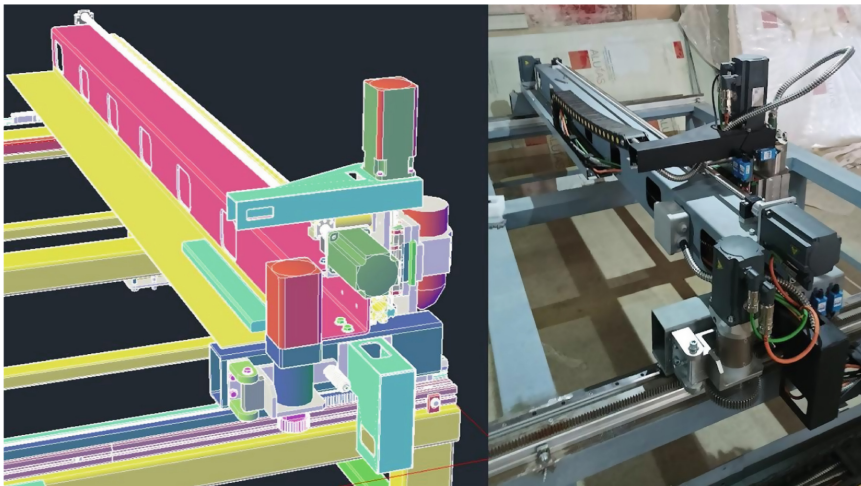


Fig. 1. Portal large dimensional machine. CAD-model and prototype.

5 Conclusion

The result of the work should be the development and implementation of a technological complex for 3D printing of buildings. It is planned to create design documentation, technological regulations, guidelines and special software for technology implementation. With the help of the complex it is possible to print individual low-rise buildings with an area of up to 100 m² and mass low-rise buildings. It is planned to launch the complex into serial production.

Advantages of the complex in comparison with foreign analogues:

- lower cost of equipment (30–50%);
- better performance due to the use of available components and the ability to service equipment components;
- technologies for the production of raw materials for construction from raw materials available in Ukraine;
- localization of technology for building codes of Ukraine.

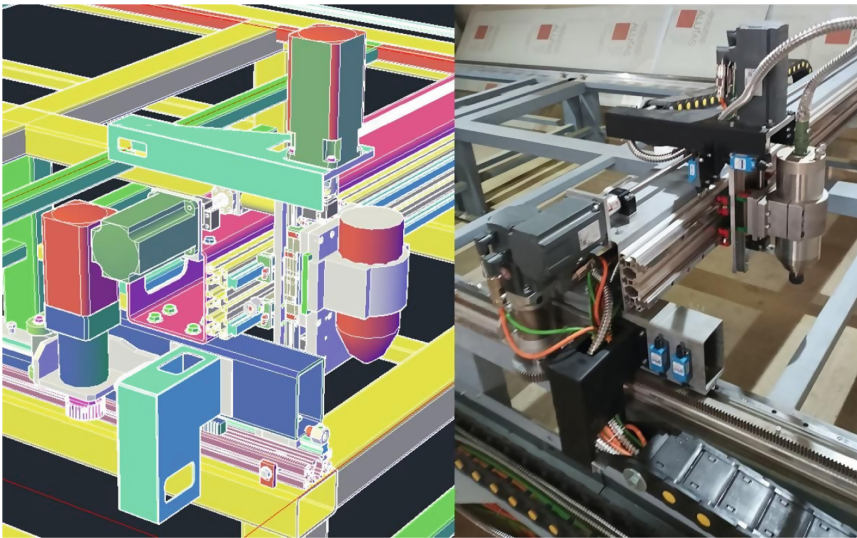


Fig. 2. Multifunctional machine support. CAD-model and prototype.

The project aims to introduce the latest technologies of concrete 3D-printing of low-rise buildings. The result of the work should be the solution of the problem of mass construction of affordable durable middle-class housing for the long-term restoration of the housing stock in Ukraine. An important aspect of the work is the change of the architectural environment on the basis of fundamentally new construction technologies. The proposed technology can be used for housing construction in the reconstruction of the eastern regions of Ukraine, for housing construction for servicemen, as well as for prefabricated military facilities.






References

1. Babaev, V., Sukhonos, M., Starostina, A., Beletsky, I.: Improving the processes of cost management in the construction and energy projects. *East. Eur. J. Enterpr. Technol.* **4**(3), 10–17 (2016). <https://doi.org/10.15587/1729-4061.2016.75515>
2. Jipa, A., Dillenburger, B.: 3D printed formwork for concrete: state-of-the-art, opportunities, challenges, and applications. *3D Print. Addit. Manuf.* **9**(2), 84–107 (2022). <https://doi.org/10.1089/3dp.2021.0024>
3. Sharma, S., Mitra, S., Adesina, A., Das, S.: Construction industry with 3D printer: a new era. In: Maiti, D.K., et al. (eds.) *Recent Advances in Computational and Experimental Mechanics*, vol II. LNME, pp. 311–324. Springer, Singapore (2022). https://doi.org/10.1007/978-981-16-6490-8_26
4. Schuldt, S.J., Jagoda, J.A., Hoisington, A.J., Delorit, J.D.: A systematic review and analysis of the viability of 3D-printed construction in remote environments. *Autom. Constr.* **125**, 103642 (2021). <https://doi.org/10.1016/j.autcon.2021.103642>
5. Cui, H., Li, Y., Cao, X., et al.: Experimental study of 3D concrete printing configurations based on the buildability evaluation. *Appl. Sci.* **12**(6), 2939 (2022). <https://doi.org/10.3390/app12062939>
6. Cao, X., Yu, S., Cui, H., Li, Z.: 3D Printing devices and reinforcing techniques for extruded cement-Based materials: a review. *Buildings* **12**(4), 453 (2022). <https://doi.org/10.3390/buildings12040453>
7. Guamán-Rivera, R., Martínez-Rocamora, A., García-Alvarado, R., et al.: Recent developments and challenges of 3D-printed construction: a review of research fronts. *Buildings* **12**(2), 229 (2022). <https://doi.org/10.3390/buildings12020229>
8. Gradeci, K., Labonnote, N.: On the potential of integrating building information modelling (BIM) for the additive manufacturing (AM) of concrete structures. *Constr. Innov.* **20**(3), 321–343 (2020). <https://doi.org/10.1108/CI-07-2019-0057>
9. Chen, Y., He, S., Gan, Y., et al.: A review of printing strategies, sustainable cementitious materials and characterization methods in the context of extrusion-based 3D concrete printing. *J. Build. Eng.* **45**, 103599 (2022). <https://doi.org/10.1016/j.jobe.2021.103599>
10. Roussel, N.: Rheological requirements for printable concretes. *Cem. Concr. Res.* **112**, 76–85 (2018). <https://doi.org/10.1016/j.cemconres.2018.04.005>
11. Muthukrishnan, S., Ramakrishnan, S., Sanjayan, J.: Technologies for improving buildability in 3D concrete printing. *Cem. Concr. Compos.* **122**, 104144 (2021). <https://doi.org/10.1016/j.cemconcomp.2021.104144>
12. Kombarov, V., Tsegelnyk, Y., Plankovskyy, S., et al.: Investigation of the required discreteness of interpolation movement parameters in cyber-physical systems. *Periodica Polytechnica Mech. Eng.* **66**(1), 1–9 (2022). <https://doi.org/10.3311/PPme.17884>
13. Aksonov, Y., Kombarov, V., Tsegelnyk, Y., et al.: Visualization and analysis of technological systems experimental operating results. In: 2021 IEEE 16th International Conference on Computer Sciences and Information Technologies (CSIT), Lviv, vol. 2, pp. 141–146. IEEE (2021). <https://doi.org/10.1109/CSIT52700.2021.9648592>
14. Kondratiev, A., Píšťek, V., Purhina, S., et al.: Self-heating mould for composite manufacturing. *Polymers* **13**(18), 3074 (2021). <https://doi.org/10.3390/polym13183074>
15. Shupikov, A.N., Smetankina, N.V.: Non-stationary vibration of multilayer plates of an uncanonical form. The elastic immersion method. *Int. J. Solids Struct.* **38**(14), 2271–2290 (2001). [https://doi.org/10.1016/S0020-7683\(00\)00166-9](https://doi.org/10.1016/S0020-7683(00)00166-9)
16. Kajzr, D., Brousek, J., Petr, T., et al.: New design of PLC-based robotic control system for concrete printing in building construction. *MM Sci. J.* **2021**, 5346–5352 (2021). https://doi.org/10.17973/MMSJ.2021_12_2021051

17. Wolfs, R.J.M., Bos, F.P., van Strien, E.C.F., Salet, T.A.M.: A real-time height measurement and feedback system for 3D concrete printing. In: Hordijk, D.A., Luković, M. (eds.) *High Tech Concrete: Where Technology and Engineering Meet*, pp. 2474–2483. Springer, Cham (2018). https://doi.org/10.1007/978-3-319-59471-2_282
18. Tsegelnyk, Y., Kombarov, V., Plankovskyy, S., et al.: Investigation of the portal-type machine tool gear-belt gearbox. *Int. J. Mechatron. Appl. Mech.* **1**(11), 1–8 (2022)
19. Borziak, O., Chepurna, S., Zidkova, T., et al.: Use of a highly dispersed chalk additive for the production of concrete for transport structures. *MATEC Web Conf.* **230**, 03003 (2018). <https://doi.org/10.1051/mateconf/201823003003>
20. Şahin, H.G., Mardani-Aghabaglou, A.: Assessment of materials, design parameters and some properties of 3D printing concrete mixtures; a state-of-the-art review. *Constr. Build. Mater.* **316**, 125865 (2022). <https://doi.org/10.1016/j.conbuildmat.2021.125865>
21. Asprone, D., et al.: Structural design and testing of digitally manufactured concrete structures. In: Roussel, N., Lowke, D. (eds.) *Digital Fabrication with Cement-Based Materials. RILEM State-of-the-Art Reports*, vol. 36, pp. 187–222. Springer, Cham (2022). https://doi.org/10.1007/978-3-030-90535-4_6
22. Usherov-Marshak, A.V., Kabus, A.V.: Calorimetric monitoring of early hardening of cement in the presence of admixtures. *Inorg. Mater.* **49**(4), 430–433 (2013). <https://doi.org/10.1134/S0020168513040183>
23. Kabus, O., Kulaienko, O., Ryabushko, A., et al.: Temperature-time monitoring of concrete hardening of a wind farm foundation. *IOP Conf. Ser. Mater Sci. Eng.* **907**, 012037 (2020). <https://doi.org/10.1088/1757-899X/907/1/012037>
24. Ubyivovk, A., Samorodov, A., Kupreichyk, A.: Laboratory experimental research of loading friction forces acting on the lateral surface of tapered piles in structurally unstable soils. *IOP Conf. Ser. Mater. Sci. Eng.* **708**, 012074 (2019). <https://doi.org/10.1088/1757-899X/708/1/012074>
25. AXICON PE: Homepage. <https://axicon.tech/>. Accessed 10 May 2022



Investigation of Control Algorithms for Machine Tool Coupled Axes

Oleksandr Aksonov , Yevgen Tsegelnyk  ^(✉), Volodymyr Kombarov ,
Sergiy Plankovskyy , and Yevhen Aksonov 

O. M. Beketov National University of Urban Economy in Kharkiv, 17 Marshala Bazhanova
Street, Kharkiv 61002, Ukraine
y.tsegelnyk@kname.edu.ua

Abstract. Modern trends in the development of mechanical engineering and the construction industry include the necessity to create large-sized machine tools, equipment for 3D printing of buildings, and other technological systems with a complex kinematic structures. As a rule, such equipment contains organs driven by several servo drives. The control of this equipment is carried out with applying various coupled-axes control algorithms. An application of CNC-based software and hardware complex for the experimental investigation of such algorithms is proposed. The principles of organizing various schemes to control coupled-axes are considered. The capabilities of the complex for recording a large number of experimental data in the process of controlling such equipment are shown. Examples of experimental investigations of coupled axes control algorithms are presented.

Keywords: Coupled axes · Servo drives · CNC · Software and hardware complex

1 Introduction

The main trend in the development of modern mechanical engineering is the automation of manufacturing processes for large-sized tooling and processing of complex spatial parts and assemblies [1–3]. Automation in the construction industry is developing not only in the field of production of building materials, components, and equipment but also in the construction of entire buildings using innovative 3D printing technologies [4–7]. The basis of technological systems that implement such processes is large-sized equipment with a complex kinematic structure [8]. As a rule, such equipment contains organs driven by several servo drives. This implies the necessity to apply the control algorithms for coupled axes.

There are various tasks that require the application of multi-motor systems. Each such task has its own peculiarities and is solved using specific schemes and algorithms of coupled control.

One of such tasks is backlash compensation. It can be solved by using special algorithms for single-motor [9] or multi-motor control schemes. For example, to improve

the positioning accuracy, the use of master-slave control for the double pinion and rack is considered, taking into account the torque of both motors [10]. A similar task of improving the accuracy of the rack and pinion of the rotary table of a vertical lathe using dual servo motor driving system is considered in [11]. The use of twin-motor tandem schemes for backlash compensation in rack and pinion gears of large-sized machine tools is discussed in [12].

Gantry-type machine tool is widely applied. For such a scheme, it is important not only to ensure accuracy but also to synchronize the motors (to minimize mutual error). Improving synchronization accuracy through the use of a cross-coupled controller is discussed in [13]. A similar synchronization task is solved for broaching machine with cross-coupling feedforward control in [12].

The use of linear drives in machines with dual-drive gantry systems is promising. Decoupling control of an industrial dual linear drive moving gantry stage based on a physical dynamic model of the machine is proposed in [14]. The task of providing dynamic characteristics and accuracy of a linear dual-drive gantry system with low structural rigidity is considered in [15]. Cross-coupling control can be organized using a special algorithm of the CNC software [10, 11, 15, 16], or a separate device [12, 13, 17].

With an increase in dimensions and an increase in the requirements of accuracy, it becomes necessary to combine different solutions using coupled schemes, which greatly increases the number of interacting elements. The development of such schemes cannot be carried out without mathematical modeling [10, 18–21] and experimental investigations [11, 14, 22, 23]. Such investigations, as a rule, are carried out with the use of specialized stands. However, an increase in the dimensions of the equipment creates certain difficulties in carrying out experimental research and debugging. In this regard, the control system for such equipment should have additional functionality that provides the possibility of investigating and debugging processes directly on the equipment [23, 24]. In turn, the complication of the structure and number of interacting elements of the equipment under investigation implies the necessity to register parameters, the number of which may exceed several hundred. However, this possibility is not provided by world leaders of CNC systems manufacturing.

The aim of the paper is the development of a hardware-software complex that allows to combine control schemes for complex technological systems and to register the required number of parameters for studying control processes. In order to achieve this aim, it is necessary to solve the following tasks:

- to provide the possibility of implementing various coupled schemes and their combinations;
- to ensure the registration and analysis of large number of control parameters of complex technological systems;
- to test the complex by investigating the functioning of various coupled schemes.

2 Coupled-Axes Control Algorithms

Coupled-axes control implies the interaction of at least two servo drives. In Fig. 1 shown various variants of the interaction schemes.

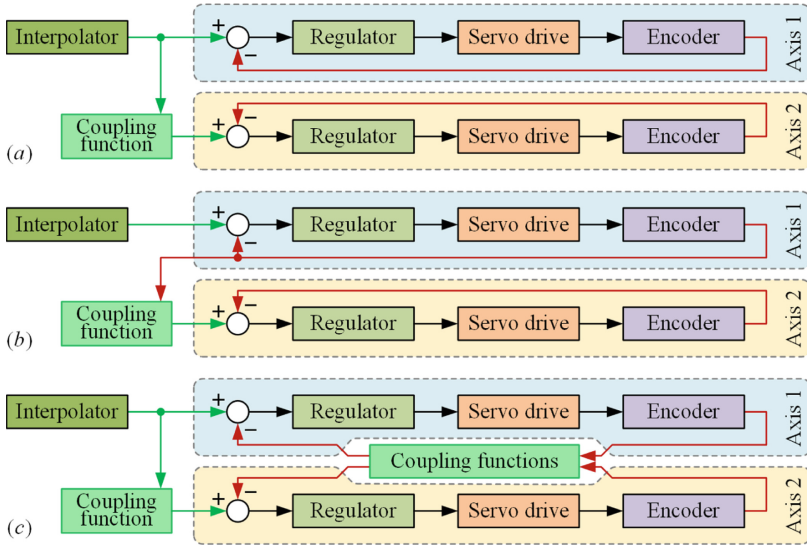


Fig. 1. Various coupled schemes: (a) “Tandem control”; (b) “Master-Slave control”; (c) scheme with a cross-coupled control.

The simplest scheme to implement is the “Tandem control” (Fig. 1a) with common reference motion command and independent feedback. As a rule, such a scheme is used for synchronous control of the gantry axis. Relevant for various equipment where high synchronization accuracy is not required [13]. For such a scheme, the synchronization error Δ_{Σ} is determined by the sum of the errors of the servo drives:

$$\Delta_{\Sigma} = \Delta_1 + \Delta_2.$$

In Fig. 1b the “Master-Slave control” scheme is shown. In this scheme the reference motion command for the slave servo drive is formed from the feedback of the master servo drive. As a rule, such a scheme is used to organize the interaction of drives with significantly different dynamics. An example of implementation of this scheme is the synchronization of the tool movement with the position of the rotating spindle. However, such an organization can lead to the formation of a clock delay in the synchronization of the movement of the slave drive. In this case, the synchronization error Δ_{Σ} is determined by the error of the driven axis and the magnitude of the delay. In Fig. 1c shown a scheme with a cross-coupled control function. This scheme provides feedback correction taking into account the mutual influence of servo drives errors. This solution reduces the synchronization error:

$$\Delta_{\Sigma} < \Delta_1 + \Delta_2.$$

In addition, control schemes may include the use of several different types of control signals, feedback, and various combinations of them. For example, in the axis control loop, accelerometer sensors [25] and dynamometers [26] can be used, which are integrated into the equipment design to take into account force factors and vibrations that

occur during processing. In the technological system, not only the process of mechanical displacements but also other processes can be controlled. For example, to provide the required composition of the gas mixture in impulse thermal deburring [27], an interdependent supply control of components with feedback on temperature and pressure is used. Thus, the CNC system must be able to define structural elements with different types of reference motion commands and feedback.

Coupled-axes control can be implemented using additional specialized devices [17] or a specialized multiaxis servo drives [28, 29]. In some cases, not only the interaction of two servo drives but also the organization of more complex schemes may be required. For example, to solve the problem of synchronizing an axis movement with the position of a rotating spindle using tandem drives that provide backlash sampling in gantry system, a combination of several variants of axes coupling schemes is required (Fig. 2). The example shows an axis interaction for a machine where the Z-axis is controlled by two motors with cross-coupled control, the Y-axis is controlled by four motors in parallel-serial connection and all six motors can be controlled in the mode of synchronizing with a spindle.

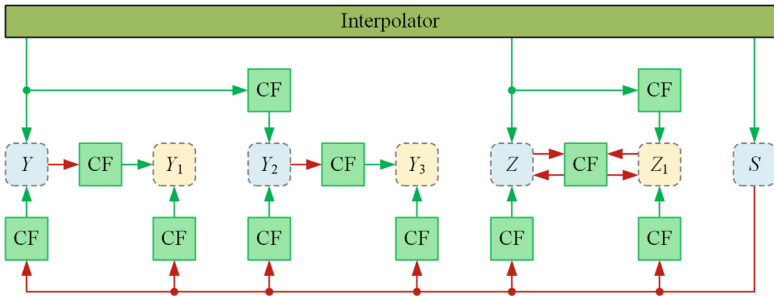


Fig. 2. An example of a complex coupled axes control: CF is the coupling function.

One of the ways to solve this problem is the software organization of coupled axes control in the CNC [30, 31] using general industrial servo drives. Such drives are generally available and cheaper compared to specialized ones. The CNC system for equipment with a combined coupled axes control must have the flexibility and variability in setting up links. In addition, in order to solve research problems, it is necessary to be able to register a lot number of parameters directly in the control process. In this paper, we consider one of the possible implementations of such a problem using the CNC-based software and hardware complex [23, 24].

3 An Application of CNC-Based Complex for the Experimental Investigations of Coupled Axes Control Algorithms

The software and hardware complex [23, 24] is a two-level PC-based CNC system. The operator panel unit of complex is implemented on a Windows PC and performs the tasks of preparing control programs and communicating with an operator. The real-time unit

is implemented on a PC with a real-time OS (Fig. 3a). It provides tasks of interpolation, motion control, automation control, communication with the operator panel and other devices. At the program level, these tasks are implemented using the appropriate modules. Axes are controlled through the “Logic devices”, which are included in the structure of the “Virtual controllers” modules. Several virtual controllers can be placed both on one computing device and distributed among several devices. In the first case, data exchange between virtual controllers is carried out through a virtual network, and in the second, through a real network. Presented in this paper experimental investigations was carry out with applying single computing device configuration of real-time unit.

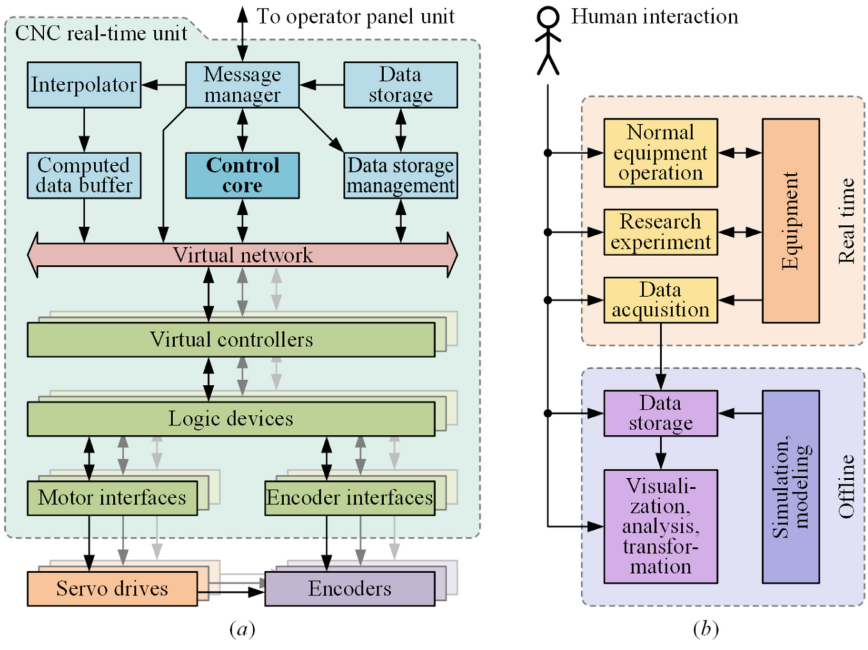


Fig. 3. CNC-based complex: (a) real-time unit structure; (b) application for investigation.

The “Data storage” module of the complex software provides registration of parameters during the investigation. It is possible to save several hundred parameters for each axis. The procedure for obtaining experimental data and their processing is shown in Fig. 3b. Data registration is performed in real-time in parallel with the process of equipment control. Visualization and results processing is carried out in offline mode.

To implement coupled-axes control in the considered CNC-based complex, the following scheme of axes interaction is proposed (Fig. 4). The axes whose data are to be used in the control of other axes are designated as the master axis, and the axes that use this data are designated as the coupled (slave) axis.

Each master axis transfers the necessary data to a special area of memory – “Master data buffer”. The “Regulator” module of coupled axis receives data from this buffer to “Coupled links information” registers. “Regulator” module processes received data

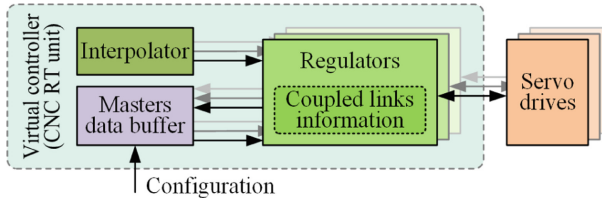


Fig. 4. Organization of axes interaction for coupled-axes control.

according to the given configuration. Data processing algorithms are represented by software-implemented coupling functions. Such an organization allows the implementation of various coupling schemes, including cross-coupled control (Fig. 1c), and their combinations (Fig. 2). The absence of direct data exchange between the controllers of interacting axes ensures the unification of the description of interactions and the possibility of placing controllers on separate computing devices.

Thus, the implementation of the proposed method of the axes interaction provides the possibility of organizing various coupling schemes and their combinations. The implementation of the proposed interaction method into the considered software and hardware complex makes it possible to ensure the registration and analysis of a large number of control parameters for complex technological systems.

4 Experimental Investigations of Cross-Coupled Control

An experimental investigation of the coupled control was carried out on the example of the control of a two-motor gantry scheme with cross-coupling control (Fig. 1c). The possibility of increasing the positioning and synchronization accuracy in the case of controlling servo drives with different accuracy parameters was investigated. The initial setting of the servo drives provided the movement with different positioning servo errors. At a feed rate of 5.8 m/min, the Z drive moved with an average error of 98.6 μm , and the Z₁ drive moved with error 3.2 μm . The control was carried out according to a proportional law with velocity feedforward.

The positioning accuracy was investigated using the multiplicative cross-coupling function (MC) with different K_{out} values (Fig. 5). When applying the cross-coupling factor $K_{out} = 0$ the scheme is equivalent to “Tandem control” scheme (Fig. 1a) with common reference motion command and independent feedback (Fig. 6). In this case, the errors of the Z and Z₁ axes correspond to the initial setting. The average synchronization error was $\Delta_{\Sigma} = 95.4 \mu\text{m}$.

As K_{out} increases from 0 to 2.5, the synchronization improves, and Δ_{Σ} decreases to 15.9 μm . The positioning accuracy of the Z-axis increases, and Δ_Z decreases to 57.5 μm . The positioning accuracy of the Z₁ axis decreases, and Δ_{Z_1} increases to 41.5 μm . The amplitude of oscillations changes insignificantly and amounts to 6 μm for the Z-axis and 11 μm for the Z₁ axis, and the synchronization error amplitude does not exceed 16 μm . With a further increase in the coefficient K_{out} , there is no improvement in synchronization, but the amplitude of the oscillations increases. At $K_{out} = 3$ undamped oscillations arise.

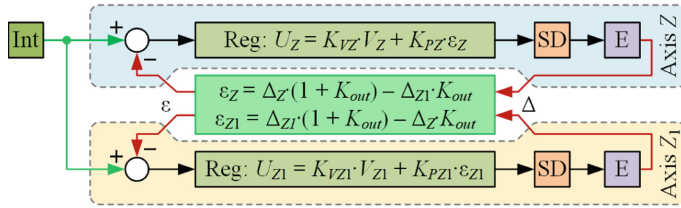


Fig. 5. Model with multiplicative cross-coupling function (MC).

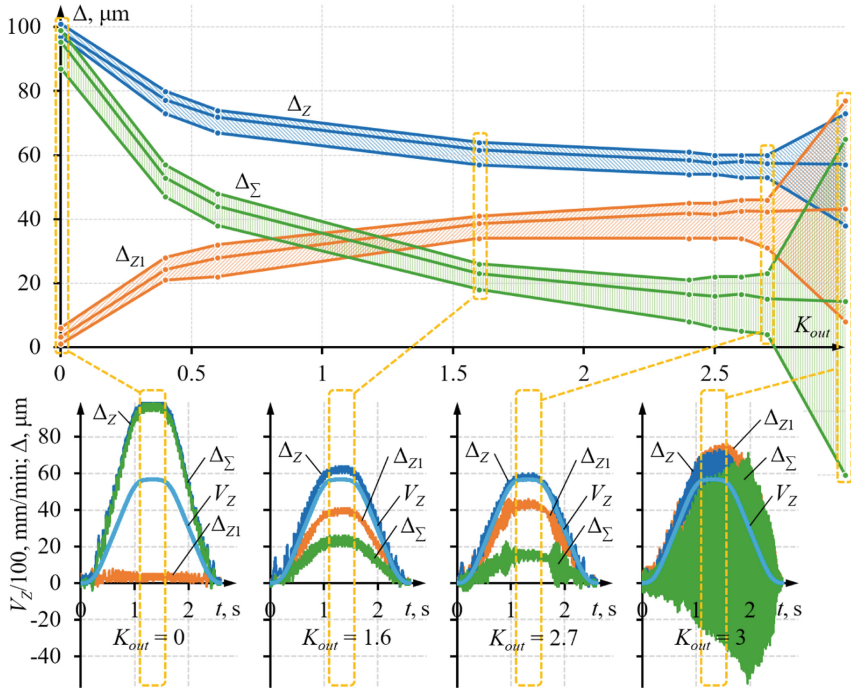


Fig. 6. Positioning accuracy of cross-coupling control with using the MC model.

The expression for calculating the corrected error in the investigated MC model is characterized by taking into account the influence of the coupling axis and correcting its own error by the factor $(1 + K_{out})$. This causes the total position error gain to increase significantly. As a result, for this model, it is impossible to unambiguously determine what is the reason for the variation in the error value: a variation in the total gain or the influence of cross-coupling.

To investigate the separate effect of the feedback gain and cross-coupling, a model with a simple cross-coupling (SC) function (Fig. 7) was applied.

The behavior of positioning errors was investigated for various values of the K_{out} coefficient in the range of the position error gain K_{PZ} of the main regulator of both axes from 10 to 60. As expected, with an increase in the K_{PZ} coefficient, the error decreases

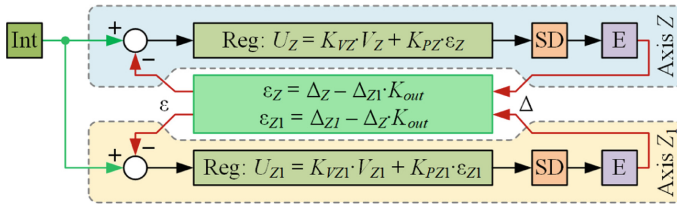


Fig. 7. Model with simple cross-coupling function (SC).

(Fig. 8a). As the cross-coupling coefficient K_{out} increases from 0 to 0.65, the synchronization of the axes improves and the accuracy of both axes decreases simultaneously (Fig. 8b). For $K_{out} = 0.5$ and $K_{PZ} = 28$, the change in error for the Z-axis is $14 \mu\text{m}$ (44%) and for the Z_1 axis is $23 \mu\text{m}$ (3700%). In this case, the synchronization error Δ_Σ is reduced by $11 \mu\text{m}$ (34%).

The investigations of two models of cross-coupling control showed the possibility to increase the synchronization accuracy of the two-motor gantry scheme with cross-coupling control with different accuracy of servo drives. However, positioning accuracy at a constant gain in the proportional controller deteriorates as the cross-coupling coefficient increases. The investigated functions can be applied to tasks where the synchronization accuracy is more important than the positioning accuracy.

Thus, the performed approbation of the complex with coupled-axes control showed its effectiveness in carrying out experimental investigations of the functioning of various coupled control schemes.

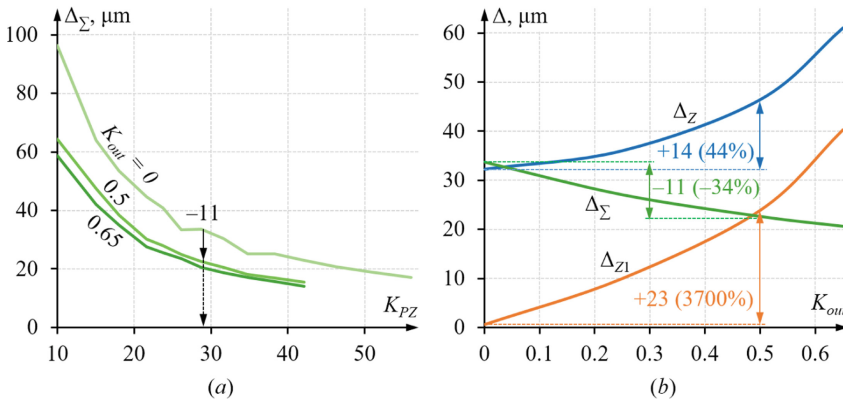


Fig. 8. Positioning accuracy of cross-coupling control with using the SC model: (a) depending on K_{PZ} coefficient, (b) depending on K_{out} coefficient.

5 Conclusion

Large-sized machine tools, equipment for 3D printing of buildings and other technological systems with a complex kinematic structure contains organs driven by several

servo drives. The control of this equipment is carried out with applying various coupled-axes control algorithms. The principles of organizing various schemes for axes coupled control are considered.

The possibility of combining control schemes for complex technological systems and registering the required number of parameters for studying control processes is considered. An application of CNC-based software and hardware complex for this task is proposed. A method for organizing the interaction of coupled-axes control in the considered complex, which provides the possibility of implementing various coupled control schemes and their combinations is proposed.

An experimental investigation of cross-coupling control of a gantry scheme driven by two servo drives with different accuracy was performed. Two options for cross-coupling functions are considered. Investigations have shown the possibility of increasing the synchronization accuracy in these schemes. With a constant proportional gain variation of cross-coupling gain leads to positioning accuracy deteriorating. The considered cross-coupling functions are effective for tasks, in which the synchronization accuracy is more important than the positioning accuracy.

Developed hardware-software complex allows to combine of control schemes for complex technological systems and recording a large number of data. The approbation of the complex showed its effectiveness in experimental investigations of the functioning of coupling control algorithms.

References

1. Pavlenko, D., Dvirnyk, Y., Przysowa, R.: Advanced materials and technologies for compressor blades of small turbofan engines. *Aerospace* **8**(1), 1–16 (2021). <https://doi.org/10.3390/aerospace8010001>
2. Kondratiev, A., Píšťek, V., Purhina, S., et al.: Self-heating mould for composite manufacturing. *Polymers* **13**(18), 3074 (2021). <https://doi.org/10.3390/polym13183074>
3. Shelyagin, V., Zaitsev, I., Bernatskyi, A., et al.: Contactless monitoring of welding processes with computer processing of acoustic emission signals. In: 2018 14th International Conference on Advanced Trends in Radioelectronics, Telecommunications and Computer Engineering (TCSET), Lviv-Slavske, pp. 706–710. IEEE (2018). <https://doi.org/10.1109/TCSET.2018.8336298>
4. Kombarov, V., Kryzhyvets, Y., Biletskyi, I., et al.: Numerical control of fiberglass pipe bends manufacturing. In: 2021 IEEE 2nd KhPI Week on Advanced Technology (KhPIWeek), Kharkiv, pp. 357–362. IEEE (2021). <https://doi.org/10.1109/KhPIWeek53812.2021.9570068>
5. Jipa, A., Dillenburger, B.: 3D printed formwork for concrete: state-of-the-art, opportunities, challenges, and applications. *3D Print. Addit. Manuf.* **9**(2), 84–107 (2022). <https://doi.org/10.1089/3dp.2021.0024>
6. Liu, J., Nguyen-Van, V., Panda, B., et al.: Additive manufacturing of sustainable construction materials and form-finding structures: a review on recent progresses. *3D Print. Addit. Manuf.* **9**(1), 12–34 (2022). <https://doi.org/10.1089/3dp.2020.0331>
7. Sharma, S., Mitra, S., Adesina, A., Das, S.: Construction industry with 3D printer: a new era. In: Maiti, D.K., et al. (eds.) *Recent Advances in Computational and Experimental Mechanics*, Vol. II. LNME, pp. 311–324. Springer, Singapore (2022). https://doi.org/10.1007/978-981-16-6490-8_26

8. Ji, W., Wang, Y., Liu, H., Wang, L.: Interface architecture design for minimum programming in human-robot collaboration. *Procedia CIRP* **72**, 129–134 (2018). <https://doi.org/10.1016/j.procir.2018.03.013>
9. Farouki, R.T., Swett, J.R.: Real-time compensation of backlash positional errors in CNC machines by localized feedrate modulation. *Int. J. Adv. Manuf. Technol.* **119**(9–10), 5763–5776 (2021). <https://doi.org/10.1007/s00170-021-08515-z>
10. Franco, O., Beudaert, X., Erkorkmaz, K.: Effect of rack and pinion feed drive control parameters on machine tool dynamics. *J. Manuf. Mater. Process.* **4**(2), 33 (2020). <https://doi.org/10.3390/jmmp4020033>
11. Jiang, H., Fu, H., Han, Z., Jin, H.: Elimination of gear clearance for the rotary table of ultra heavy duty vertical milling lathe based on dual servo motor driving system. *Appl. Sci.* **10**(11), 4050 (2020). <https://doi.org/10.3390/app10114050>
12. Lu, W., Ji, K., Dong, H., Zhang, J., Wang, Q., Guo, L.: Double position servo synchronous drive system based on cross-coupling integrated feedforward control for broacher. *Chin. J. Mech. Eng.* **30**(2), 272–285 (2017). <https://doi.org/10.1007/s10033-017-0077-5>
13. Ishizaki, K., Sencer, B., Shamoto, E.: Cross coupling controller for accurate motion synchronization of dual servo systems. *Int. J. Autom. Technol.* **7**(5), 514–522 (2013). <https://doi.org/10.20965/ijat.2013.p0514>
14. Gomand, J., Kestelyn, X., Bearee, R., Barre, P.J.: Dual-drive gantry stage decoupling control based on a coupling model. *ElectroMotion* **15**(2), 94–98 (2008)
15. Li, C., Yao, B., Zhu, X., Wang, Q.: Adaptive robust synchronous control with dynamic thrust allocation of dual drive gantry stage. In: 2014 IEEE/ASME International Conference on Advanced Intelligent Mechatronics, Besacon, pp. 316–321. IEEE (2014). <https://doi.org/10.1109/AIM.2014.6878098>
16. Kombarov, V., Tsegelnyk, Y., Plankovskyy, S., et al.: Investigation of the required discreteness of interpolation movement parameters in cyber-physical systems. *Periodica Polytechnica Mech. Eng.* **66**(1), 1–9 (2022). <https://doi.org/10.3311/PPme.17884>
17. Shih, Y.T., Chen, C.S., Lee, A.C.: A novel cross-coupling control design for bi-axis motion. *Int. J. Mach. Tools Manuf.* **42**(14), 1539–1548 (2002). [https://doi.org/10.1016/S0890-6955\(02\)00109-8](https://doi.org/10.1016/S0890-6955(02)00109-8)
18. Pliuhin, V., Sukhonos, M., Bileckiy, I.: Object oriented mathematical modeling of electrical machines. In: 2020 IEEE 4th International Conference on Intelligent Energy and Power Systems (IEPS), Istanbul, pp. 267–272. IEEE (2020). <https://doi.org/10.1109/IEPS51250.2020.9263158>
19. Dobrotvorskiy, S., Kononenko, S., Basova, Y., Dobrovolska, L., Edl, M.: Development of optimum thin-walled parts milling parameters calculation technique. In: Ivanov, V., Trojanowska, J., Pavlenko, I., Zajac, J., Peraković, D. (eds.) *DSMIE 2021. LNME*, pp. 343–352. Springer, Cham (2021). https://doi.org/10.1007/978-3-030-77719-7_34
20. Shupikov, A.N., Smetankina, N.V.: Non-stationary vibration of multilayer plates of an uncanonical form. The elastic immersion method. *Int. J. Solids Struct.* **38**(14), 2271–2290 (2001). [https://doi.org/10.1016/S0020-7683\(00\)00166-9](https://doi.org/10.1016/S0020-7683(00)00166-9)
21. Kolar, P., Sulitka, M., Fojtu, P., et al.: Cutting force modelling with a combined influence of tool wear and tool geometry. *Manuf. Technol.* **16**(3), 524–531 (2016). <https://doi.org/10.21062/ujep/x.2016/a/1213-2489/MT/16/3/524>
22. Tsegelnyk, Y., Kombarov, V., Plankovskyy, S., et al.: Investigation of the portal-type machine tool gear-belt gearbox. *Int. J. Mech. Appl. Mech.* **2022**(11), 295–302 (2022). <https://doi.org/10.17683/ijomam/issue11.41>
23. Aksonov, Y., Kombarov, V., Fojtů, O., et al.: Investigation of processes in high-speed equipment using CNC capabilities. *MM Sci. J.* **2019**(04), 3271–3276 (2019). https://doi.org/10.17973/MMSJ.2019_11_2019081

24. Aksonov, Y., Kombarov, V., Tsegelnyk, Y., et al.: Visualization and analysis of technological systems experimental operating results. In: 2021 IEEE 16th International Conference on Computer Sciences and Information Technologies (CSIT), Lviv, vol. 2, pp. 141–146. IEEE (2021). <https://doi.org/10.1109/CSIT52700.2021.9648592>
25. Javed, A.R., Sarwar, M.U., Khan, S., et al.: Analyzing the effectiveness and contribution of each axis of tri-axial accelerometer sensor for accurate activity recognition. *Sensors* **20**(8), 2216 (2020). <https://doi.org/10.3390/s20082216>
26. Alipanahi, A., Mahboubkhah, M., Barari, A.: Cross-sensitivity control in a novel four-component milling dynamometer for simultaneous measurement of tri-axial forces and torque. *Measurement* **191**, 110788 (2022). <https://doi.org/10.1016/j.measurement.2022.110788>
27. Plankovskyy, S., Popov, V., Shypul, O., et al.: Advanced thermal energy method for finishing precision parts. In: Gupta, K., Pramanik, A. (eds.) *Advanced Machining and Finishing*, pp. 527–575. Elsevier, Amsterdam (2021). <https://doi.org/10.1016/B978-0-12-817452-4.00014-2>
28. He, J., Jiang, X., Zhang, C., et al.: Multiaxis servo synergic control based on sliding mode controller. *J. Control Sci. Eng.* **2019**, 9249270 (2019). <https://doi.org/10.1155/2019/9249270>
29. Grigoriev, S.N., Martinov, G.M.: An ARM-based multi-channel CNC solution for multi-tasking turning and milling machines. *Procedia CIRP* **46**, 525–528 (2016). <https://doi.org/10.1016/j.procir.2016.04.036>
30. Beckhoff: TwinCAT CNC: Overview. <https://infosys.beckhoff.com/english.php?content=../content/1033/tccncprogramming/html/programmingofaxescouplings.htm&id=>. Accessed 10 May 2022
31. Siemens: Axes, coupled motion. <https://mall.industry.siemens.com/mall/en/WW/Catalog/Products/10352826?tree=CatalogTree>. Accessed 10 May 2022



Technological Equipment and Automation Control of the Three-Dimensional Structures Laser Welding Process in Different Spatial Positions

Artemii Bernatskyi^(✉) , Mykola Sokolovskiy , Volodymyr Lukashenko ,
Oleksandr Siora , and Nataliia Shamsutdinova 

E. O. Paton Electric Welding Institute of the National Academy of Science of Ukraine, 11
Kazymyra Malevycha Street, Kyiv 03150, Ukraine
bernatskyi@paton.kiev.ua

Abstract. The problem of automation of the welding process of steel and alloy complex profiles is present in many industries. In this study, the problem of automation of the laser welding process control when welding complex three-dimensional structures in different spatial position was studied. In the first part of the investigation, a centralized hardware-software complex was developed to ensure that the laser welding in different spatial positions is carried out properly. The developed hardware-software complex has the ability to be operated in both manual and automatic modes for the ease of practical preparation of the experiment. In the second part of the study, a set of technological equipment in the form of a laboratory stand was developed. The developed laboratory stand is designed for experimental research of technological features of laser welding of steels and alloys in different spatial positions. In testing, the hardware-software complex, coupled to the laboratory stand have procured control joints, adherent to current quality standards. As a result of this study, the testing of the hypothesis, according to which, the conditions of laser welding in different spatial positions are associated with a stable balance between the forces acting on the free surface of the liquid metal of the melt bath, became possible.

Keywords: Laser welding · Process automation · Spatial positions · Laser technological equipment

1 Introduction

The pace of development and progress in various sectors of the economy is directly related to the degree of their automation [1–3]. This applies to the various processes: management, transport, production, etc. [4–6]. Analysis of scientific papers shows that there are more and more publications, devoted to the study of the automation problem of various processes in recent years [7–9].

The problem of automation of the welding process of complex profiles of steels and alloys is present in many industries [10–12]. Various welding methods are successfully

used to solve it [13–15]. However, under a number of circumstances (such as large dimensions, complex profiles, large mass, etc.), there is a need for welding in spatial positions that differ from the standard low position, the proficient usage of which accentuates a need for the study of the latest welding technologies as well as creation of equipment, capable of an automated process. In such conditions it is not only necessary to take into account the physical effects that accompany laser welding, but to use them to our advantage [16–18]. For example, taking the forces of gravity and surface tension into account makes it possible to influence the degree of the penetration channel opening when moving the welding bath in different directions [19–21]. Taking the aforementioned features into account allows to obtain a set of technological process maps for welding of joints in different spatial positions, necessitating the development of required algorithms for these processes, as well as appropriate automated technological equipment. Algorithms for the implementation of automation of the three-dimensional laser welding processes of steel and alloy structures in different spatial positions are designed to work in various different options [22–24]. These actions are necessary and sufficient to perform the process of three-dimensional laser welding of steel and alloy structures in different spatial positions [25–27]. Authors describe “different spatial positions of welding” as the possibility of arbitrary location of the heat source (laser beam) velocity vector in space. To develop these automation algorithms, researchers use various ways, based on the results of theoretical or experimental studies, as well as their combinations [28–30].

The analysis of publications showed that the vast majority of scientific papers are devoted to the study of laser welding in the “low” spatial position. Some scientific papers, which study the influence of spatial position in laser welding on the structure, shape, mechanical characteristics and dimensions of welded joints, relate more directly to the technological aspects of the laser welding process, performed on existing equipment. These studies made it possible to conduct experiments at a specific inclination angle of the welding plane, without considering the possibility of its variation. Therefore, the results of previously conducted studies are disparate and cannot be systematized. This is the case due to a lack of attention to solving the problem of creating specialized automated technological equipment.

The main aim of this study is the development of automation algorithms for laser welding of steel and alloy three-dimensional structures in different spatial positions is aimed at describing the list of actions, as well as development of appropriate equipment required to perform the process of laser welding in different spatial positions while achieving the specified qualities of the welding seams – reliability, strength, needs, etc. The other aim of this study was to conduct experimental research on laser welding of steels and alloys in different spatial positions, where the authors have resorted to the creation of experimental equipment in the form of a laboratory stand for automated welding in spatial positions, different from the “lower” position.

2 Methods

The automation algorithm for the process of laser welding of steel and alloy three-dimensional structures describes the patterns of movement of focused laser radiation along a complex trajectory of the product (coordinates, linear velocity, acceleration in

some parts of the seam, etc.), and controls laser radiation relative to the surface of the sample, etc.). According to the developed algorithm for automation of laser welding of steel and alloy three-dimensional structures in different spatial positions, to simplify the problem of three-dimensional welding of structures, a complex spatial welding trajectory was proposed to divide it into so-called spatial primitives, i.e. individual welds (butt, T-shaped, overhanging and angular), welded in certain spatial positions. This made it possible to consider particular problems of laser welding in different spatial positions, that are related to the automation of welding processes.

The implementation of the operation control modes of the complex is carried out on the basis of the laser welding process technological maps obtained by welding control samples of welded joints of steels and alloys in different spatial positions. Verification of the effectiveness of the developed algorithm was performed upon creation of the hardware and software complex described below.

3 Results and Discussion

The developed hardware-software complex (hereinafter – “HSC” or “the complex”) is designed to automate the laser welding process control. The object of automation in this complex is the process of laser welding of large three-dimensional structures in different spatial positions. The HSC consists of a set of units, devices and software modules that are meant to ensure that the laser welding in different spatial positions is carried out properly. The complex must be able to move the focused laser beam in different spatial positions along a pre-set linear trajectory. It must be able to provide an interface to enable a manual selection of the position of both start- and end- points of the focused laser beam linear trajectory before the laser welding process. The HSC must also be able to set the speed of the focused laser beam linear movement during the laser welding process.

The HSC has a centralized structure, with the only governing body of it being the “Control Unit”. The structure of the complex is shown in Fig. 1.

The main elements of the HSC are: a linear movement module, a laser and a control unit. Operation of the complex is carried out using work algorithms in manual and automatic modes which are realized as a set of programs in C language. These algorithms are located in the independent memory of the microcontroller – the central element of the control unit. Additional elements of the HSC are: the power sources for the laser, the control unit and the linear module. During laser welding, the radiation is transported along the fiber optic cable to the focusing lens, which is located inside the laser welding head. The laser welding head is secured to the carriage of the linear module and moves together with it over the course of the work of the complex in a manual or automatic mode.

As shown in Fig. 1, the complex should consist of the following basic elements: the control unit, the laser, the movement module, the mounting unit, a part blank, a control system as well as the power supply unit(s). The HSC must be equipped with a system for transmitting and receiving control and diagnostic (information) signals.

To perform the task of laser welding in different spatial positions of the developed HSC, it was integrated with the laser radiation generator power supply unit, as well as the linear movement module. The laser radiation generator power supply comes

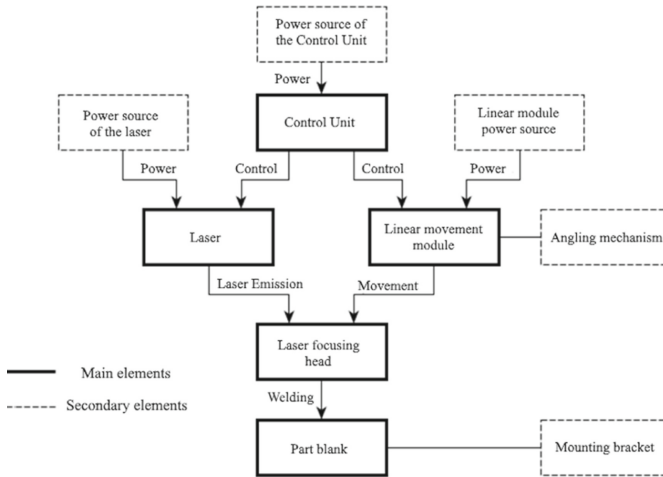


Fig. 1. Structure of the developed hardware-software complex (HSC).

equipped with a control interface that allows us to transmit and receive signals. The linear movement module was equipped with an interface, responsible for movement control. The developed HSC has the ability to be operated in both manual and automatic modes. The manual mode is designed for the movement of the carriage, belonging to the linear movement unit, in preparation for the laser welding process, carried out in different spatial positions. The automatic mode of operation is designed to perform the process of laser welding of steels and alloys in different spatial positions. The diagnostic information of the hardware-software complex is displayed on the LCD screen.

The developed HSC can be optionally equipped with a system, responsible for regulation of the laser radiation output power. In such case, the productivity and flexibility of the laser welding process can be increased via reduction of the time spent on reprogramming the parameters of the laser generator.

The first phase of the creation of the HSC is the independent development and manufacture of parts and assemblies, such as:

- the control unit;
- the mounting bracket;
- the tilting devices for the linear movement module.

The second phase of the creation of the hardware-software complex is the assembly of the manufactured parts and assemblies. The developed software package is designed to perform the following functions:

- registration of control (command) inputs by the operator of the installation;
- programming the position of the start- and end- point of the welding trajectory;
- display of information (diagnostic) messages;
- transmission of control pulses to the linear movement module;
- registration of the state of end sensors;

- execution of the laser welding working cycle.

The control unit (CU) is designed to store and execute the control algorithms of the hardware-software complex. The control algorithms are created using software, operating with C programming language, compiled into machine code and loaded into the independent memory of the ATmega 328 microcontroller, which provides a layer of autonomy to the work process of the system.

The control algorithm is executed in a cyclical manner, while waiting for the control inputs from the operator. Upon receipt of a specific input from the operator of the algorithm selects the subroutine, associated with the desired input.

The main subroutines include:

- “zeroing” – search of the absolute starting position of the carriage;
- control of the starting/ending point of the trajectory;
- electric brake control of the servo;
- adjustment of the working/idling speed;
- turning the emission of the laser radiation on/off.

The main subroutine is that of the “working” cycle, required to carry out the laser welding process. This work cycle is only performed if the operator has already set the position of the start and end points of the welding path and has performed the “zeroing” of the servo. Execution of the “working” cycle is compliant with the following sequence:

- movement of the carriage to the starting point of the trajectory;
- inclusion of laser radiation to the welding path;
- moving the carriage with the specified speed to the endpoint of the trajectory;
- exclusion of the laser radiation from the welding path.

Thus, the first task of this study was performed and a mock-up of the hardware-software complex, designed to ensure the process of laser welding of steel and alloy structures in different spatial positions, was developed.

The goal of the second part of the study was to create the technological equipment in the form of a laboratory stand, designed for experimental research of technological features of laser welding of steels and alloys in different spatial positions.

The laboratory stand was designed to create and test technologies for laser welding of different (butt, T-shaped, corner and lap) welded joints of steels and alloys with a thickness, varying from 0.3 mm to 20.0 mm. The stand is a single assembly, consisting of interconnected electromechanical and electronic components, as well as a technological laser. The welding head movement is carried out in the *X* and *Z* coordinates. The stand includes the following components: a two-coordinate manipulator; a mobile platform; a mounting bracket for clamps; control and automation units. Technical characteristics of the stand are shown in Table 1. Let’s take a better look at the structure of the laboratory stand and its components, the model of which is shown in Fig. 2.

The created laboratory stand uses two linear servo drives, based on synchronous AC motors. The voltage on the motor windings is controlled by servo amplifiers (frequency converters), in which the feedback on their positioning is provided by the incremental

Table 1. Technical characteristics of the laboratory stand for experimental studies of technological features of laser welding of steels and alloys in different spatial positions.

Characteristic		Value
Number of axles, pcs		2
Maximum load capacity, kg		20
ON duration at + 25 °C, not less than, %		50
Power consumption, up to, kW		35
Repeatability, not worse than, mm		± 0.08
Acceleration along the axes, m/sec ²		1
Overall dimensions of the manipulator, mm		700 × 1500 × 1600
Welding speed, cm/s		0–25
Weight of the manipulator, no more than, kg		500
- Length of a motion in Z coordinate, mm		1170
- Length of a motion in X coordinate, mm		540
Coordinate positioning accuracy, μm	X	± 70
	Z	± 50
Maximum speed of movement along the coordinate axles, cm/s	X	25
	Z	25

encoders. The shafts of the encoders are rigidly connected to the motor shafts. Nominal speed of rotation of engines is $50 \text{ rps} = 3000 \text{ rpm}$.

Both servo drives use ball screws to convert rotational motion into linear motions. The pitch of the screws in both systems is 10 mm/rev. Both servos are configured for external control of positioning using pulses, as well as the speed of movement by means of the “Step/Dir” digital interface. The “Dir” input of the control interface is designed to control the direction of carriage movement. The installation of both servo drives was done in such a way that when one pulse is applied to the “Step” input, the carriage moves 10 μm forward or backward depending on the signal on the “Dir” input. Structurally, the linear modules are mechanically connected to each other in a three-section system. The first section is a fixed frame, which is the basis of the whole system (position 9 in Fig. 2). The size of the fixed frame is 1620 × 650 mm, it is welded from steel channels №12. The second and third sections are linear modules (positions 1 and 2 in Fig. 2). The second section is connected to the first using a rotating hinge mechanism (position 10 in Fig. 2). This mechanism allowed us to angle the second section from the vertical position at a chosen angle between 0° to 90° (Fig. 3).

The inclination of the frame is possible at the 30°, 45°, 60° and 90° discrete angles. The fixation of the movable frame position at the different angles is carried out using side rails as well as M20 bolts. The side rails are mounted on the axles of the fixed frame housings. At the moment, the frame tilt mechanism is not equipped with a servo system, so the adjustment of angular deviation is carried out manually. The linear module,

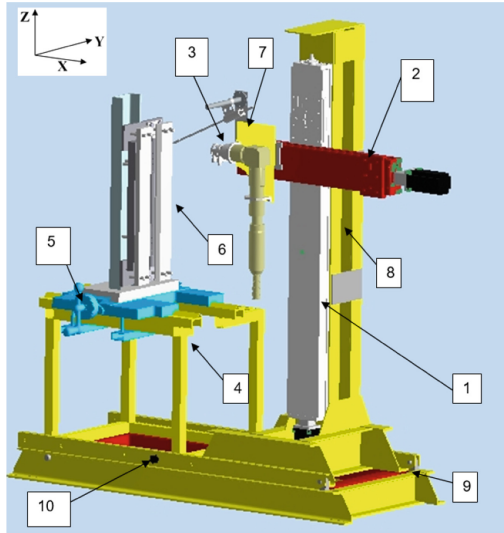


Fig. 2. Laboratory stand model, where 1 – is the module of linear movement along the Z-axis; 2 – modulus of linear displacement along the X-axis; 3 – welding head; 4 – clamp for fixing welding specimens; 5 – platform for moving the clamp in the XY plane; 6 – clamp with the test sample; 7 – bracket for mounting the welding head; 8 – column; 9 – fixed frame; 10 – base of the frame.

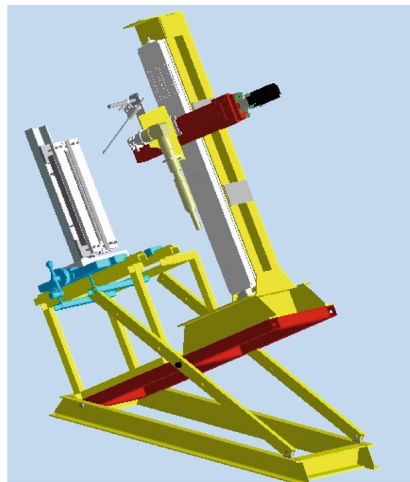


Fig. 3. Model of the stand in an inclined position.

mounted on this section, is mounted on a column with a height of 1650 mm (position 8 in Fig. 2), which is welded from steel channels № 16.

The third section (position 2 in Fig. 2) is rigidly attached to the carriage of the second section. The laser head (position 3 in Fig. 2) is fixed to the carriage of the third

section using brackets (position 7 in Fig. 2). In its initial position, the second section is located vertically (Fig. 2). With this connection, each of the linear movement modules is responsible for moving the laser head parallel to one of the Cartesian coordinate system directions, namely – the second section being responsible for the movement along the Z coordinate, and the third – for movement along the X coordinate. The range of movement for the X coordinate is 540 mm, and for the Z coordinate – 1170 mm. A personal computer running under the Linux operating system is used to organize and control the movement along the contour. A modified real-time operating system kernel is used to increase reliability. This allows us to ensure proper guaranteed runtime for I/O operations for specified time intervals. The software, designed to control the movement of the contour, allows us to configure the numerical control system to calculate the trajectory of contour movement, as well as to provide control for the electrical automation. The built-in interpolator allows us to program movement of linear, circular and cubic spline segments of the trajectory in 2-dimensional and 3-dimensional coordinate systems. Different external interfaces (such as the serial port, USB port, etc.) can be used for communication of the control unit with the external equipment.

A draft of the design documentation, with which the technological equipment in the form of the laboratory stand was created to carry out experimental researches of technological features of laser welding processes of steels and alloys in various spatial positions, was developed. In Fig. 4 shown a photograph of the created technological equipment in the form of a laboratory stand for experimental research of technological features of laser welding of steels and alloys in different spatial positions.



Fig. 4. Laboratory stand for laser welding of steels and alloys in different spatial positions.

Verification of the functional capabilities of the created technological equipment was performed during experimental research on laser welding of steels and alloys in different

spatial positions [19, 26]. The experiments were conducted using a Nd:YAG solid-state “DY044” laser with a wavelength of 1.06 μm , manufactured by “ROFIN-SINAR” (Germany).

The created stand and auxiliary technological equipment (brackets, clamps, fasteners, etc.) lets us obtain butt, T-shaped, corner and lap welded joints of steels and alloys in a wide range of technological parameters. Welding was conducted on plates of steels and alloys at different angles: 90°, 60°, 45°, 30°, 0°. In all variants (other than the “lower” position), welding was performed “uphill” and “downhill”.

The level of quality of welded joints was determined according to current standards. According to the requirements of these standards, three quality levels have been established, which correspond to a certain range of maximum permissible sizes of defects and relate to welded joints. The angle of inclination, at which the highest quality connection (with the fewest defects) was obtained, was determined. Laser welding of steel and alloy control joints in different spatial positions was performed.

The promising areas of further development for the technological equipment, created in this study, are: improvement of the design of the laboratory stand towards providing additional possible welding angle values as well as the possibility of changing the angle in the middle of a welding operation; usage of the system to create new technological applications not only for lasers, but also for laser-arc hybrid welding, as well as laser-assisted plasma arc welding; usage to create the latest technologies not only welding but also laser surfacing and heat treatment.

4 Conclusion

The hardware and software basis for experimental testing of the hypothesis, according to which, the conditions of laser welding in different spatial positions are associated with the constant maintenance of a stable balance between the forces acting on the free surface of the liquid metal of the melt bath, was created. A new laboratory stand for automated laser welding in different spatial positions, different from the “lower” position, was created. A system of automated technological equipment in the form of a laboratory stand that provides the ability to obtain butt, T-shaped, angular and seam welded joints of steels and alloys in different spatial positions with a wide range of technological parameters, was created.

References






1. Aksonov, Y., Kombarov, V., Tsegelnyk, Y., et al.: Visualization and analysis of technological systems experimental operating results. In: 2021 IEEE 16th International Conference on Computer Sciences and Information Technologies (CSIT), vol. 2, pp. 141–146. IEEE, Lviv (2021). <https://doi.org/10.1109/CSIT52700.2021.9648592>
2. Kyrychenko, H., Berdnychenko, Y., Strelko, O., Shcherbyna, R.: Application of the automated system at the change of technology of work of reference stations on the railway. In: Proceedings of the 25 International Conference Transport Means 2021, Pt. II, pp. 782–786. Kaunas University of Technology, Kaunas (2021)

3. Duriagina, Z., et al.: Optimized filling of a given cuboid with spherical powders for additive manufacturing. *J. Oper. Res. Soc. China* **9**(4), 853–868 (2020). <https://doi.org/10.1007/s40305-020-00314-9>
4. Přístěk, V., Kučera, P., Fomin, O., Lovska, A.: Effective mistuning identification method of integrated bladed discs of marine engine turbochargers. *J. Marine Sci. Eng.* **8**(5), 379 (2020). <https://doi.org/10.3390/jmse8050379>
5. Kombarov, V., Sorokin, V., Tsegelnyk, Y., et al.: Numerical control of machining parts from aluminum alloys with sticking minimization. *Int. J. Mech. Appl. Mech.* **1**(9), 209–216 (2021). <https://doi.org/10.17683/ijomam/issue9.30>
6. Strelko, O., Yurchenko, O., Vasilova, H., et al.: Theoretical prerequisites for the development of multimodal transport-logistic technologies in cooperation with Ten-T network. In: Nechyporuk, M., et al. (eds.) *ICTM 2021. LNNS*, vol. 367, pp. 1041–1050. Springer, Cham (2022). https://doi.org/10.1007/978-3-030-94259-5_80
7. Severino, A., Martseniuk, L., Curto, S., Neduzha, L.: Routes planning models for railway transport systems in relation to passengers' demand. *Sustainability* **13**(16), 8686 (2021). <https://doi.org/10.3390/su13168686>
8. Statyvka, Y., Kyrychenko, H., Strelko, O., Berdnychenko, Y.: Control of technological processes using a fuzzy controller of the system for management of cargo delivery by railway. *Acta Sci. Polonorum Adm. Locorum* **20**(3), 241–251 (2021). <https://doi.org/10.31648/aspal.6808>
9. Babyak, M., Keršys, R., Neduzha, L.: Improving the dependability evaluation technique of a transport vehicle. In: *Proceedings of the 24 International Conference Transport Means 2020, Pt. II*, pp. 646–651. Kaunas University of Technology, Kaunas (2020)
10. Zavdovtsev, A., Poznyakov, V., Baudin, T., et al.: Effect of heat treatment on the mechanical properties and microstructure of HSLA steels processed by various technologies. *Mater. Today Commun.* **28**, 102598 (2021). <https://doi.org/10.1016/j.mtcomm.2021.102598>
11. Fomin, O., Lovska, A., Skliarenko, I., Klochkov, Y.: Substantiating the optimization of the load-bearing structure of a hopper car for transporting pellets and hot agglomerate. *East.-Euro. J. Enterpr. Tech.* **1**(7), 103, 65–74 (2020). <https://dx.doi.org/https://doi.org/10.15587/1729-4061.2020.193408>
12. Lobanov, L.M., Pashchyn, M.O., Mikhodui, O.L., Goncharov, P.V., Sydorenko, Y.M., Ustymenko, P.R.: Influence of the accompanying heating on the efficiency of electrodynamic treatment of amg6 aluminum alloy welded joints. *Strength Mater.* **53**(2), 222–226 (2021). <https://doi.org/10.1007/s11223-021-00278-y>
13. Korzhyk, V., Khaskin, V., Grynyuk, A., et al.: Comparison of the features of the formation of joints of aluminum alloy 7075 (Al-Zn-Mg-Cu) by laser, microplasma, and laser-microplasma welding. *East.-Eur. J. Enterpr. Technol.* **1**(12), 38–47 (2022). <https://doi.org/10.15587/1729-4061.2022.253378>
14. Semenov, I., Krivtsun, I., Demchenko, V., et al.: Modelling of binary alloy (Al–Mg) anode evaporation in arc welding. *Modell. Simul. Mater. Sci. Eng.* **20**(5), 055009 (2012). <https://doi.org/10.1088/0965-0393/20/5/055009>
15. Sydorets, V., Korzhyk, V., Khaskin, V., et al.: On the thermal and electrical characteristics of the hybrid plasma-MIG welding process. *Mater. Sci. Forum* **906**, 63–71 (2017). <https://doi.org/10.4028/www.scientific.net/MSF.906.63>
16. Shelyagin, V., Krivtsun, I., Borisov, Y., et al.: Laser-arc and laser-plasma welding and coating technologies. *Avtom. Svarka* **8**, 49–54 (2005)
17. Bagherzadeh, S.A., Shamsipour, M., Kholoud, M.J., Dehkordi, M.H.R.: ANN modeling and multiobjective genetic algorithm optimization of pulsed laser welding of Ti6Al4V alloy sheets with various thicknesses. *J. Laser Appl.* **33**(1), 012056 (2021). <https://doi.org/10.2351/7.0003356>

18. Bernatskyi, A., Khaskin, V.: The history of the creation of lasers and analysis of the impact of their application in the material processing on the development of certain industries. *Hist. Sci. Technol.* **11**(1), 125–149 (2021). <https://doi.org/10.32703/2415-7422-2021-11-1-125-149>
19. Bernatskyi, A., Berdnikova, O., Sydorets, V., et al.: Laser welding of stainless steel 321 in different welding positions. *Solid State Phenom.* **313**, 106–117 (2021). <https://doi.org/10.4028/www.scientific.net/SSP.313.106>
20. Fang, C., Xin, J., Dai, W., et al.: Deep penetration laser welding of austenitic stainless steel thick-plates using a 20 kW fiber laser. *J. Laser Appl.* **32**(1), 012009 (2020). <https://doi.org/10.2351/1.5094176>
21. Chang, B., Yuan, Z., Cheng, H., et al.: A study on the influences of welding position on the keyhole and molten pool behavior in laser welding of a titanium alloy. *Metals* **9**(10), 1082 (2019). <https://doi.org/10.3390/met9101082>
22. Singh, A., Cooper, D.E., Blundell, N.J., et al.: Modelling of weld-bead geometry and hardness profile in laser welding of plain carbon steel using neural networks and genetic algorithms. *Int. J. Comput. Integr. Manuf.* **27**(7), 656–674 (2014). <https://doi.org/10.1080/0951192X.2013.834469>
23. Gao, Y., Zhong, P., Tang, X., et al.: Feature extraction of laser welding pool image and application in welding quality identification. *IEEE Access* **9**, 120193–120202 (2021). <https://doi.org/10.1109/ACCESS.2021.3108462>
24. Liu, B., Jin, W., Lu, A., et al.: Optimal design for dual laser beam butt welding process parameter using artificial neural networks and genetic algorithm for SUS316L austenitic stainless steel. *Opt. Laser Technol.* **125**, 106027 (2020). <https://doi.org/10.1016/j.optlastec.2019.106027>
25. Zhang, M., Tang, K., Zhang, J., Mao, C., Hu, Y., Chen, G.: Effects of processing parameters on underfill defects in deep penetration laser welding of thick plates. *Int. J. Adv. Manufact. Technol.* **96**(1–4), 491–501 (2018). <https://doi.org/10.1007/s00170-018-1613-x>
26. Bernatskyi, A., Sydorets, V., Berdnikova, O., et al.: Pore formation during laser welding in different spatial positions. *Solid State Phenom.* **303**, 47–58 (2020). <https://doi.org/10.4028/www.scientific.net/SSP.303.47>
27. Chang, B., Yuan, Z., Pu, H., et al.: A comparative study on the laser welding of Ti6Al4V alloy sheets in flat and horizontal positions. *Appl. Sci.* **7**(4), 376 (2017). <https://doi.org/10.3390/app7040376>
28. Kombarov, V., Sorokin, V., Tsegelnyk, Y., Plankovskyy, S., Aksonov, Y., Fojtů, O.: S-shape feedrate scheduling method with smoothly-limited jerk in cyber-physical systems. In: Ciobață, D.D. (ed.) *ICoRSE 2021*. LNNS, vol. 305, pp. 54–68. Springer, Cham (2022). https://doi.org/10.1007/978-3-030-83368-8_6
29. Bakhtiyari, A.N., Wang, Z., Wang, L., Zheng, H.: A review on applications of artificial intelligence in modeling and optimization of laser beam machining. *Opt. Laser Technol.* **135**, 106721 (2021). <https://doi.org/10.1016/j.optlastec.2020.106721>
30. Romanova, T., Stoyan, Y., Pankratov, A., et al.: Sparsest balanced packing of irregular 3D objects in a cylindrical container. *Eur. J. Oper. Res.* **291**(1), 84–100 (2021). <https://doi.org/10.1016/j.ejor.2020.09.021>



Automation of the Pneumatic Impulse Mandreling Technological Process

Vitalii Voronko¹ , Yuri Dyachenko² , Iryna Voronko² , Oleksandr Zastela² ,
and Vladyslav Voronko² 

¹ O. M. Beketov National University of Urban Economy in Kharkiv, 17 Marshala Bazhanova Street, Kharkiv 61002, Ukraine

² National Aerospace University “Kharkiv Aviation Institute”, 17 Chkalova Street, Kharkiv 61070, Ukraine
i.voronko@khai.edu

Abstract. At most enterprises, fundamental technologies remain undeveloped, without which the transition to digital/smart enterprises is impossible. Manufacturers are not able to rebuild their organizational structure and change long-standing traditions. The transition should be carried out by upgrading equipment, supplementing existing equipment or replacing it completely. That is why the purpose of this paper is to develop an addition to the existing multifunctional robotic complexes in the form of a power unit. The power unit itself is a variant of automation of an existing manual device that can work in a new generation enterprise. During the processing of holes in airplane structures by the proposed device, the junction (elastic clamp), which connects it with the robot, feels the load. This device can facilitate the work of the foreman in the shop and facilitate the transition to digital manufacturing. The article discusses three schematic diagrams that ensure the connection of the power unit with the robot and a description of its operation during the mandreling process.

Keywords: Robotic complex · Manipulator · Industrial robots · Pneumatic impulse device for mandreling · Power unit · Mandreling process · Pneumatic electromagnetic valves

1 Introduction

The robotic complex (RC) is a component of flexible automated manufacturing. This is a complex technological system in terms of its technological purpose, layout and degree of automation [1]. This system combines both the executive means of implementing and equipping a specific technological process, and the means of controlling and mathematical software [2–4]. Industrial robots, consisting of a mechanical arm and a reprogrammed control system, are important components of automated flexible manufacturing systems (FMS) [5].

High Accuracy Robots such as FANUC (Japan), KUKA (Germany), ABB (Sweden, Switzerland), Kawasaki (Japan), Motoman Yaskawa (Japan, USA) are designed to perform high precision tasks. The robots of the high-accuracy range are used for various work in the aviation and automotive industries:

- *drilling, riveting and bolting*. Simultaneous drilling, filling and riveting process. KUKA Robotics robots work in pairs on both sides. The robot on the outside of the fuselage drills a hole by inserting the fastener (filling the hole) and driving it in, while the robot on the inside acts as an anvil for the fastener, which is hammered in to properly deform the fastener edge and create a rivet. Robots protect airline workers from shock loads on their shoulders and arms (vibration sickness) and reduce rework costs [6];
- *cutting (automated robot performs the stacking process and cutting tape in the production of composite aircraft)*. Robotic laser cutting systems have the flexibility and versatility to improve quality at every stage of their application, resulting in improved end product quality. The execution speed depends on the laser power, the absorption efficiency and the material stiffness. The most common are CO₂ lasers (carbon dioxide lasers) and fiber lasers (solid-state lasers (SSL)), mounted on industrial robots. All robotic laser cutting systems are completely safe, and operators use safety goggles [7, 8].
- *sealing*. FANUC robots are used in the aerospace industry for drilling and riveting, coating and painting, aluminum structural welding and polishing. For sealing on structural elements such as spars, medium sized robots of the M-710iC series are well used, using machine vision to find flaws in welds and apply sealant [9];
- *painting*. Specialized explosion-proof robots enable faster paint application, improved finish quality and significant weight savings [9];
- *priming*. Automation of this operation is very effective when combined with painting. An example is the use of 7-axis robots' model KJ314 for simultaneous processing of structural elements by priming and painting in one stand [9];
- *welding*. The Fabricator robots create deep and narrow welds, join dissimilar materials, make workpieces of different dimensions, while creating minimal heat-affected zones in materials [10];
- *friction joining*. Technology of butt welding of friction joints in the assembly of aircraft fuselages without rivets (Kawasaki Robotics, USA). Kawasaki uses two very rigid robots to connect fuselage sections with rivets or Robots for Friction Spot Joining (RFSJ) – an innovative method of joining metal. Similar to friction-displacement welding, which uses frictional heat and pressure to join materials, RFSJ can replace rivets and fasteners, creating a joint without a head, hole, or recess [11];
- *gluing (applying glue to the surface simultaneously with quality control)*. Modern aircraft are made of both metal and composites. In this case, the skins are assembled by gluing. And now the process of applying glue to the surface with simultaneous quality control is carried out by robots [12];
- *location and setting in the assembly position*. The research group (Fraunhofer Institute of Technology) designed and implemented a system of flexible grippers on a CFRP (carbon-fiber-reinforced plastic) frame. The flexible grip features a simple and comfortable array of suction cups sitting on strong joints with spacers mounted on a CFRP frame that provides stability. The weight of the grip is much less than the metal one. Therefore, works equipped with a gripping system will be able to demonstrate higher accuracy when gripping a structural element, basing it and placing it in the required position. Transportation of massive structures with such clamps allows them to maintain their shape, avoiding slight bending [13];

- *bolted connections*. Automation of the bolt setting process is carried out by universal robots of the UR5 type. Lightweight flexible robot UR5 (Universal Robots) with an actual load of up to 5 kg automates repetitive assembly tasks that can be a dangerous task for a worker [9];
- *plasma treatment*. Plasma surface treatment technology provides good adhesion, removes moisture, cleans the surface of the element before further processing (gluing, painting, varnishing and coating). The application of this treatment is suitable for plastic, rubber, metal and composite parts;
- *control system (laser control system from Premium Aerotech during the manufacturing of the A350 aircraft)*. The mobile laser tracking system allows precise positioning of robot heads during aircraft construction. The robot places the structural element in the required position, then the measurement system automatically turns on. The robot informs the measuring system its location, and the system informs it to make corrections. The communication is then terminated. The structural element is installed in place, and the tracker can adjust the position of the next robot's head [14].

The analysis shows that in the field of aerospace production for operations with constant repeatability, where it is necessary to ensure high accuracy, the choice is given in favor of robots [15]. Automated drilling, fastening, riveting [6], painting [9], composite production [16–18] and other types of work – factories of the future.

Fully automating an aircraft or engineering plant is a complex process and huge costs, but the desire for competitiveness and product quality encourages the manufacturer to break new ground. Therefore, one of the objectives of the study is the modification of the pneumatic impulse device, which will be used in the robotic complex system.

An important aspect is the development of specific power unit control schemes, which will take into account the technical characteristics of the robotic complex (manipulator), the type of its drive (electric, electrohydro-pneumatic) [19], its control system (cyclic or positional), positioning accuracy [20, 21], features and specifics of the control program development, the number of freedom degrees, the possibility of active control, etc.

A way is proposed to solve the above problems by analyzing the design of the existing model of a manual pneumatic impulse device for mandrel (PIDM) PIDM-100. Taking into account the drive mechanism of the PIDM-100 device, it is possible to develop a scheme for starting the power unit, which will be compatible with a multifunctional robot.

2 Conditions for Optimal Integration of the Device (Power Unit) into the Robotic Complex Environment

The effectiveness of the power units use made according to the design of the pneumatic impulse device for mandreling PIDM-100 in the robotic processes of mandreling holes is determined by the conditions for their rational integration into the RC environment. A prerequisite for this is the pneumatic impulse device PIDM-100, which implements the possibility of one-sided access to the places of operations due to the reverse action for removing the tool from the hardened hole. The device PIDM-100 has sufficient energy capabilities, high performance, reliability, uses compressed air of 0.5 MPa as an energy

carrier, which is similar to the drives of most RC components, and has a sufficient degree of autonomy. Considering all of the above, it becomes obvious that:

- pneumatic impulse mandreling of holes is the most effective method of surface-plastic deformation, which provides an increase in the cyclic durability of the aircraft;
- there is a need to study the technological parameters of reverse pneumatic impulse mandreling of holes in structures made of aviation materials with the establishment of their features and optimal use under conditions of multifactorial impact;
- pneumatic impulse device PIDM-100 requires modernization and the creation on its basis of a power unit that implements reverse mandrel with the possibility of its operation using the control systems (CS) developed for this in the robotic complex environment;
- the organization of the interconnected and coordinated functioning of the power unit in the robotic complex system is the most important purpose of the CS. At the same time, the power unit control system should ensure its interaction with the control program (CP) of manipulators – industrial robots (IR), i.e. joint functioning of the constituent elements of a single technological system “Energy Unit – Robotic Complex – Object”;
- it is necessary to evaluate the mutual influence of the design and technological parameters of the process, the power unit characteristics, the IR manipulator with a gripping jig on the accuracy of location, positioning of the power unit and its dynamic adjustment to ensure adaptation in the robotic complex coordinate system;
- a methodology (algorithm) is required for developing a technology for pneumatic impulse reverse mandreling of holes in structures made of aviation materials, which will take into account the research results and technological recommendations for adapting the process in the robotic complex environment.

3 The Concept of Compatibility the System Interaction

The integration of pneumatic impulse reverse mandreling of holes technology in aircraft structures into the robotic complex coordinate system is implemented by the compatibility of the functioning and interaction of the power unit operation principle, its CS with the CP of the manipulator-robot as a single technological system “Power Unit – Robotic Complex – Object”.

As a power unit, a modified pneumatic impulse device for mandreling PIDM-100 is used, which corresponds to the process in terms of its functional purpose according for the principle of its operation [22–24]. Important in the modernization of the manual device PIDM-100 is the replacement of the handle with a trigger mechanism for an air distribution collector that connects the power unit with the actuating elements of its control system. In addition, in the design of the power unit, the pre-striker cavity is bled down directly into the atmosphere. This allows (in comparison with PIDM-100) to significantly simplify the design, improve the reliability, performance and stability of the power unit. And also, due to a decrease in back pressure in the pre-striker cavity, to increase the impact efficiency (energy) by increasing the speed of the striker during its acceleration. The reliability of damping excessive process energy has been increased with the help of an additionally designed air cushion for the mandrel holder.

Adapted for functioning as part of a robotic complex, a pneumatic impulse power unit for reverse hole mandreling has a number of qualitative advantages:

- sufficient specific energy supply (the ratio of energy to the acceptable mass of the power unit), high efficiency. The efficiency of the mandreling process is ensured by a regulated excess of energy for the guaranteed implementation of one-time direct and reverse impacts, which greatly simplifies the power unit control system and guarantees the stability of the qualitative technological parameters of the process;
- energy stability and its regulation possibility, ensuring the implementation of the process with optimal (recommended) technological modes;
- work reliability, which implies the reliability of the power unit design, the stability in response time and the tool (mandrel) operational life;
- overall dimensions and shape contribute to the embed ability into the robotic complex system and the accesses possibility to the amplification zone, spatial manipulation, as well as ensuring the location accuracy (coaxiality of the power unit installation bases with the mandrel tool axis) when using, if possible, standard IR manipulator gripping jigs, taking into account their characteristics, reliability of installation and fixing;
- constructive and functional compatibility with the robotic complex control device, the manipulator controller, the property of complementarity and redistribution of control functions and their flexibility, as well as the similarity (or uniformity) in the use of energy carriers (or energy units);
- minimum force and inertial loads of recoil impact on the IR executive bodies of the robotic complex and the gripping jigs of the IR manipulator in the process of performing operations. These force actions affect the accuracy of coordinate positioning. At the same time, the functions of the manipulator (IR) of the robotic complex, accompanied by significant power technological loads, are assigned to the power unit;
- versatility, allowing the use of the power unit for various assembly operations (riveting, calking, punching holes, setting bolts with tension, etc.) with minor structural modifications (or readjustments);
- high productivity that reduces the total cycle time while reducing the main time and time for auxiliary transitions. This increases the efficiency of the assembly process;
- ease of maintenance, interchangeability during debugging, readjustment and development of the control program;
- the possibility of simultaneous operation of the power unit with other executive elements connected by a single (or homogeneous) control system, including a single control program (combination of operations, for example, preparing holes, setting fasteners, punching, riveting, control, etc.);
- operation efficiency, energy carrier availability and minimal consumption;
- manufacturability of the power unit design (simplicity, lack of scarce materials, low manufacturing costs, the presence of unified structural elements, etc.);
- satisfactory sanitary-hygienic and environmental indicators;
- work safety;
- the implementing feedback possibility of the power unit control system with the robotic complex control program prevents the occurrence of unforeseen deviations of the technological process from the standard situation.

4 Power Unit Control for Adapting the Process of Pneumatic Impulse Mandreling Holes

Structurally, the power unit (Fig. 1) is a receiver 2 fixed in the corps 1, with a shaft 3 located in it coaxially with the possibility of its axial movement. A striker 4 is located in the shaft, distributing it into pre-striker and behind-striker (with a rear socket) cavities 5 and 6, respectively. In front of the shaft, a working tool-mandrel 7 is mounted, held by a mandrel holder 8. The pre-striker cavity 5 can be connected to the atmosphere using windows 9 in the shaft 3. Alternately, the supply of compressed air from the receiver 2 to the pre-striker and behind-striker cavity is provided by a stepped distribution sleeve 10 located coaxially on the outer surface of the shaft, mounted in the circular chamber 11. The power unit contains an air distribution collector 12, four channels of which are connected: 13 with the receiver 2; 14 with the circular chamber 11; 15 with behind-striker cavity 6; 16 with atmosphere (drainage, output).

The manipulator, with the help of the gripping jig, holds the power unit and the controller associated with it, and moves in a single coordinate system of the robotic complex in which the object is located.

In order to adapt the process of pneumatic impulse mandreling of holes in the robotic complex coordinate system, an electropneumatic, pneumo-electromagnetic, pneumatic mechanical power unit control system has been developed. Each of these schemes has its own characteristics and advantages. Figure 1, for example, shows a pneumatic impulse power unit for mandreling holes and a control system using pneumatic electromagnetic valves (EMV).

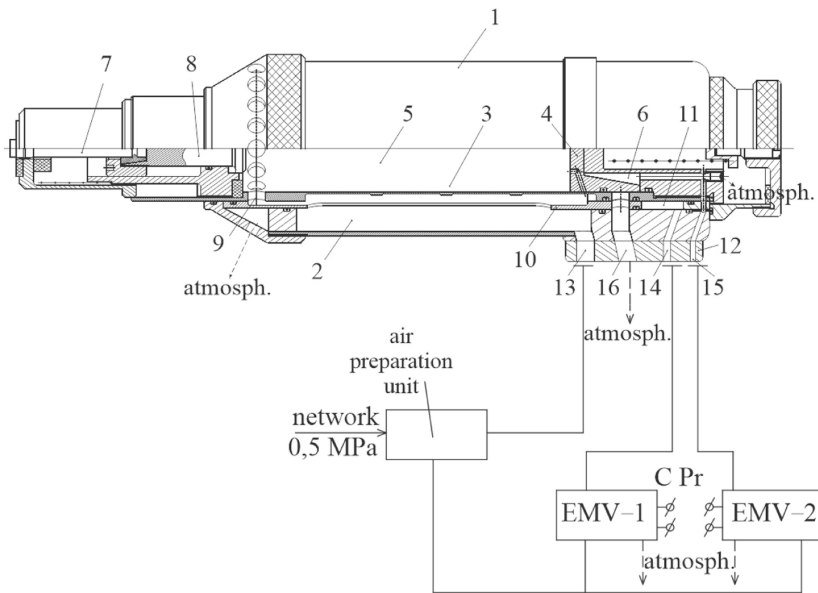


Fig. 1. Power unit of the pneumatic impulse device for reverse mandreling with a control system using pneumatic electromagnetic valves.

The control system of pneumatic impulse power units with the help of pneumatic EMV is based on the use of the control electrical network of the controller. According to the control program, pneumatic one-way EMV provide compressed air injection into the corresponding cavity of the power unit and ejection from it into the atmosphere. Some of the power unit control functions is assigned in the principal scheme of its operation. The energy carrier is supplied through an air preparation unit (APU), which cleans the air and regulates its pressure, and hence the energy.

The operation principle of the control system for pneumatic impulse power units using pneumatic electromagnet valves in the technological system “Power Unit – Robotic Complex – Object” is shown by a simplified (without taking into account the time factor) cyclogram (Table 1).

Table 1. Power unit control cyclogram.

Pos. No.	State of the system	Transition content	The manipulator controller control program of the robotic complex			Power unit
			Manipulator with power unit	EMV-1	EMV-2	Position of elements
1	Initial state	Processing of the manipulator movement trajectory with the power unit by the system Connection to the pneumatic network	Tool feed to the equidistant axis of a hole's group for mandreling Turning on Energy supply to the APU	No-voltage (off)		The initial position of the power unit elements (see Fig. 1)
2	Positioning	Fixing the power unit on the mandreling hole axis (pre-impact position)	Moving the power unit along the mandreling hole axis; self-centering, fixing it at a given point	Powered (on)	No-voltage (off)	Separating sleeve 10 in the rear position Mandrel holder 7 with mandrel 8 immersed by the value of the mandreling stroke
3	Direct impact	Direct hole mandreling	Holding in a fixed position (see point 2)	Powered (on)		Distribution sleeve 10 (see point 2) Acceleration of the striker 4, impact on the mandrel holder 8 with mandrel 7 The striker is in the forward position

(continued)

Table 1. (continued)

Pos. No.	State of the system	Transition content	The manipulator controller control program of the robotic complex			Power unit
			Manipulator with power unit	EMV-1	EMV-2	Position of elements
4	Reverse impact	Reverse hole mandreling	Holding in a fixed position (see point 3)	No-voltage (off)		Separating sleeve 10 in forward position The striker 4 accelerates in the opposite direction, the impact of the striker on the rear cap of the shaft, the striker moves to the rear position in socket 6
5	Return to initial state			No-voltage (off)		The initial position of the power unit elements (see Fig. 1)
6	Initial state	Trajectory movement for positioning the next hole	Fixing at a given point of the next hole axis (by step)			

The process of pneumatic impulse reverse mandreling of holes can be adapted to the robotic complex environment under the following conditions:

- the technological parameters stability of the object (tolerances for the diameters of hardened holes, the correctness of their shape, the relative position, range, hole pitch, etc.);
- stability and reliability, sufficient power equipment of the power unit;
- the correctness of the manipulator control program, which ensures the accuracy of positioning the power unit in the robotic complex coordinate system;
- reliable functional interconnection and interaction of the power unit elements with its control system.

These conditions are necessary, but they are not sufficient, since they do not fully provide the property of adaptability – a guarantee that the axis of the working tool-mandrel will coincide directly at its pre-impact moment with the axis of the hole to be hardened. Such accurate positioning before impact is not only an important requirement for automated production in the robotic complex environment, but also an indisputable condition for the quality of the impulsed hole mandreling process.

The process of pneumatic impulse mandreling of holes is carried out in a complex technological system “Robotic Complex – Object – IR Manipulator – Gripping Jig – Power Unit”. Even in the most perfect and well-coordinated system, functional (both system and random) errors can occur. Important for the positioning accuracy (coincidence of the mandrel axes and the hardened hole) is basing – a fixed spatial location of the object in the robotic complex coordinate system.

This determines the accuracy of coordinate movements and positioning of the robot-manipulator according to the control program and the clarity of binding of the power unit control subsystem.

Figure 2 shows the second of the power unit control “Pneumatic mechanical control scheme of the power unit”.

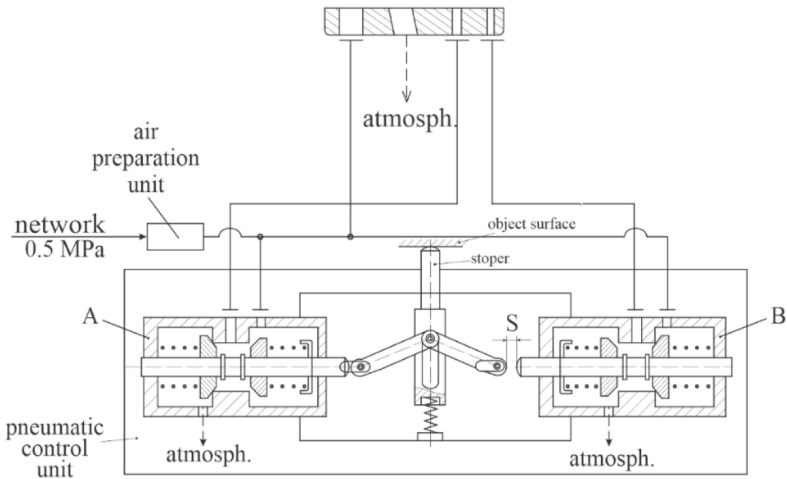


Fig. 2. Pneumatic-mechanical control scheme of the power unit.

The difference here is the replacement of the EMV with air distribution valves A and B. Valve A provides control of the air distribution sleeve 32 (similar to EMV-1). The valve B (similar to the EMV-2) provides compressed air supply to the socket 8 and the shift of the striker 5 with its subsequent acceleration for a direct blow.

The third proposed scheme “Electropneumatic control scheme of the power unit” is a control system with a partial feedback function (Fig. 3). A similar power unit is controlled by an air distribution collector.

But the basic elements contain built-in special sensors, and the connection of these sensors allows you to implement feedback (“Power Unit – Control Program”). In case of a failure, the sensors do not close the electrical circuit and block the process (stopping the accident).

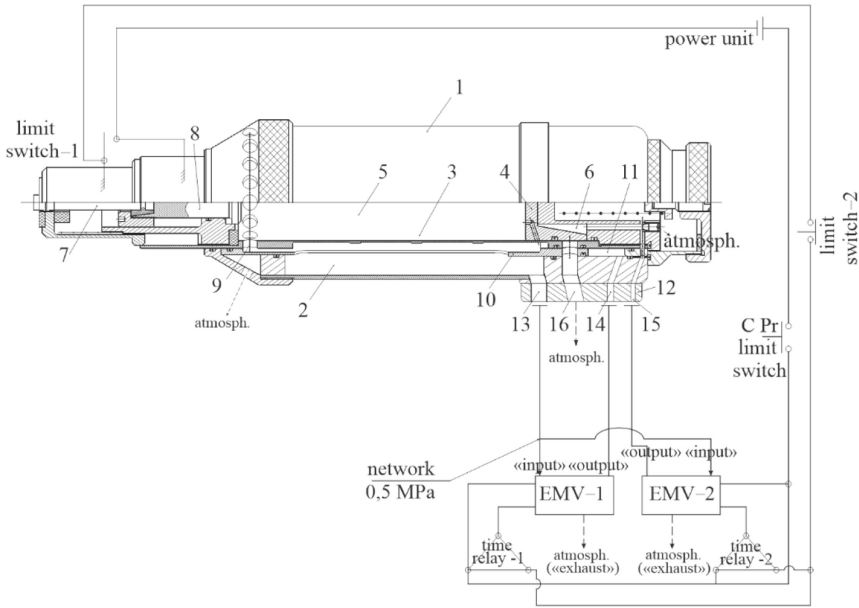


Fig. 3. Electropneumatic control scheme of the power unit.

5 Conclusion

On the basis of the manual pneumatic impulse device for mandreling holes in aircraft structures, new equipment and schemes for embedding it into multifunctional CNC machines were proposed.

The real possibilities of a particular device for burnishing (energy unit) are considered: energy data embedded in the design, specific designs of moving impact elements, etc.

This tool, operating in the robotic complex system, provides one-way access to the object. Direct-reverse mandreling with the help of a power unit finally processes the hardened hole. With a reverse impact, a smoothing mandreling is obtained: at this moment, the stress-strain state and roughness finally change. Such mandreling requires less energy and is realized at low strain rates.

Unlike other impulsed assembly and mounting processes (for example, riveting, coinage, countersink and other processes where the amount of energy determines the quality of the controlled parameters), mandreling does not require normalized energy values, but, on the contrary, its randomness is preferred, as well as for impulsed hole punching.

As an example of embedding equipment in modern production, three schematic diagrams of power unit control were shown. This will enable enterprises to use existing equipment and embed modernized devices (power unit) into already functioning robotic complex.

For this, a functional connection of the computer program of the robotic complex with the means of the power unit was provided. The work shows the principle of power unit

control system operation is shown, which gives an understanding of the full operation cycle of the device during the hole mandreling process.

A model of the process of pneumatic impulse mandreling of holes in a complex technological system “Robotic Complex – Object – IR Manipulator – Gripping Jig – Power Unit” has been developed, which describes the interaction between the components of this system.

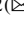
References

1. Krivtsov, V.S., Voronko, V.V., Zaytsev, V.Y.: Advanced prospects for the development of aircraft assembly technology. *Sci. Innov.* **11**(3), 11–18 (2015). <https://doi.org/10.15407/sci11.03.011>
2. Aksonov, Y., Kombarov, V., Tsegelnyk, Y., et al.: Visualization and analysis of technological systems experimental operating results. In: 2021 IEEE 16th International Conference on Computer Sciences and Information Technologies (CSIT), vol. 2, pp. 141–146. IEEE, Lviv (2021). <https://doi.org/10.1109/CSIT52700.2021.9648592>
3. Kritskiy, D., Pohudina, O., Kovalevskiy, M., et al.: Powder mixtures analysis for laser cladding using OpenCV library. In: Nechyporuk, M., et al. (eds.) *Integrated Computer Technologies in Mechanical Engineering – 2021. LNNS*, vol. 367, pp. 924–937. Springer, Cham (2022). https://doi.org/10.1007/978-3-030-94259-5_72
4. Zhengning, Y., Yongli, Z.: An evolution-Simulation-verification framework of aviation products in the future. In: 2020 IEEE 2nd International Conference on Civil Aviation Safety and Information Technology (ICCASIT), pp. 1004–1007. IEEE, Weihai (2020). <https://doi.org/10.1109/ICCASIT50869.2020.9368801>
5. Kalscheuer, F., Eschen, H., Schüppstuhl, T.: Towards semi automated pre-assembly for aircraft interior production. In: Schüppstuhl, T., et al. (eds.) *Annals of Scientific Society for Assembly, Handling and Industrial Robotics 2021*, pp. 203–213. Springer, Cham (2022). https://doi.org/10.1007/978-3-030-74032-0_17
6. Yu, T.B., Zhang, X., Xu, X.L., et al.: Researches on virtual machining simulation of flexible manufacturing cell based on KUKA robot. *Key Eng. Mater.* **621**, 499–504 (2014). <https://doi.org/10.4028/www.scientific.net/KEM.621.499>
7. Plankovskyy, S., Tsegelnyk, Y., Shypul, O., Pankratov, A., Romanova, T.: Cutting irregular objects from the rectangular metal sheet. In: Nechyporuk, M., Pavlikov, V., Kritskiy, D. (eds.) *Integrated Computer Technologies in Mechanical Engineering. AISC*, vol. 1113, pp. 150–157. Springer, Cham (2020). https://doi.org/10.1007/978-3-030-37618-5_14
8. Bogue, R.: Lasers in manufacturing: a review of technologies and applications. *Assem. Autom.* **35**(2), 161–165 (2015). <https://doi.org/10.1108/AA-07-2014-066>
9. Bogue, R.: The growing use of robots by the aerospace industry. *Ind. Robot.* **45**(6), 705–709 (2020). <https://doi.org/10.1108/IR-08-2018-0160>
10. Bernatskiy, A., Sydorets, V., Berdnikova, O.M., et al.: Pore formation during laser welding in different spatial positions. *Solid State Phenom.* **303**, 47–58 (2020). <https://doi.org/10.4028/www.scientific.net/SSP.303.47>
11. Goushegir, S.M., Amancio-Filho, S.T.: Friction spot joining (FSpJ). In: Amancio-Filho, S.T., Blaga, L.-A. (eds.) *Joining of Polymer-Metal Hybrid Structures: Principles and Applications*, pp. 61–99. John Wiley & Sons, New York (2018). <https://doi.org/10.1002/9781119429807.ch3>
12. Ebnesajjad, S., Landrock, A.H.: *Adhesives Technology Handbook*. William Andrew, London (2015). <https://doi.org/10.1016/C2013-0-18392-4>

13. Mei, B., Zhu, W.: Accurate positioning of a drilling and riveting cell for aircraft assembly. *Robot. Comput. Integr. Manuf.* **69**, 102112 (2021). <https://doi.org/10.1016/j.rcim.2020.102112>
14. Apmann, H., Busse, M., Du, J.-Y., Köhnke, P.: Automated manufacture of fibre metal laminates to achieve high rate of production. *Lightweight Des. Worldwide* **10**(4), 28–33 (2017). <https://doi.org/10.1007/s41777-017-0037-x>
15. Kihlman, H., Ossbahr, G., Engström, M., Anderson, J.: Low-cost automation for aircraft assembly. SAE Technical Paper, 2004–01–2830 (2004). <https://doi.org/10.4271/2004-01-2830>
16. Kondratiev, A., Píšťek, V., Purhina, S., et al.: Self-heating mold for the composite manufacturing. *Polymers* **13**(18), 3074 (2021). <https://doi.org/10.3390/polym13183074>
17. Smetankina, N., Kravchenko, I., Merculov, V., Ivchenko, D., Malykhina, A.: Modelling of bird strike on an aircraft glazing. In: Nechyporuk, M., Pavlikov, V., Kritskiy, D. (eds.) *Integrated Computer Technologies in Mechanical Engineering*. AISC, vol. 1113, pp. 289–297. Springer, Cham (2020). https://doi.org/10.1007/978-3-030-37618-5_25
18. Dveirin, O.Z., Andreev, O.V., Kondrat'ev, A.V., Haidachuk, V.Y.: Stressed state in the vicinity of a hole in mechanical joint of composite parts. *Int. Appl. Mech.* **57**(2), 234–247 (2021). <https://doi.org/10.1007/s10778-021-01076-4>
19. Zablodskiy, M., Gritsyuk, V., Pliuhin, V., Biletskyi, I.: The surface characteristics features of the electromagnetic field of the rotor of a polyfunctional electromechanical converter. In: *2021 International Conference on Electrical, Computer, Communications and Mechatronics Engineering (ICECCME)*, pp. 1–5. IEEE, Mauritius (2021). <https://doi.org/10.1109/ICECCME52200.2021.9590872>
20. Kombarov, V., Tsegelnyk, Y., Plankovskyy, S., et al.: Investigation of the required discreteness of interpolation movement parameters in cyber-physical systems. *Period. Polytech. Mech. Eng.* **66**(1), 1–9 (2022). <https://doi.org/10.3311/PPme.17884>
21. Kombarov, V., Sorokin, V., Tsegelnyk, Y., Plankovskyy, S., Aksonov, Y., Fojtů, O.: S-shape feedrate scheduling method with smoothly-limited jerk in cyber-physical systems. In: Ciobotă, D.D. (ed.) *ICoRSE 2021*. LNNS, vol. 305, pp. 54–68. Springer, Cham (2022). https://doi.org/10.1007/978-3-030-83368-8_6
22. Kryvtsov, V.S., Vorobiov, I.A., Chystiak, V.G., Voronko, V.V.: Pneumatic impulse device for hole mandreling. UA Patent **81550**, 10 (2008)
23. Krivtsov, V.S., Vorob'ev, Y.A., Voron'ko, V.V.: Advanced devices for mandreling bores. *Kuznechno-Shtampovochnoe Proizvodstvo (Obrabotka Metallov Davleniem)* **12**, 18–30 (2004)
24. Vorobiov, I., Maiorova, K., Voronko, I., et al.: Creation and improvement principles of the pneumatic manual impulse devices. In: Nechyporuk, M., et al. (eds.) *Integrated Computer Technologies in Mechanical Engineering – 2021*. LNNS, vol. 367, pp. 178–191. Springer, Cham (2022). https://doi.org/10.1007/978-3-030-94259-5_17



Ensuring Functional Stability of Technological Processes as Cyberphysical Systems Using Neural Networks

Valentyn Sobchuk¹ , Iryna Zamrii²  , and Serhii Laptiev¹ 

¹ Taras Shevchenko National University of Kyiv, 60 Volodymyrska Str., Kyiv 01033, Ukraine
sobchuk@knu.ua

² State University of Telecommunications, 7 Solomianska Str., Kyiv 03110, Ukraine
irinafraktal@gmail.com

Abstract. Complex technical systems form multilevel structures and are built to perform special tasks. By analogy with natural systems, the development of such systems leads to the complication of their functioning and the emergence of new properties, such as, in fact, functional stability. Widespread use of artificial intelligence in technological processes as cyber-physical systems allows for management based on fundamental approaches to the stability of complex systems. Depending on the complexity of the organization of enterprise information systems and the level of analysis, the property of functional stability can be manifested in the form of resistance to errors, reliability, survivability, fault tolerance, adaptability, noise immunity and more. The characteristics that ensure the functional stability of technological systems and control of dynamic processes of production processes of metalworking in machine-building enterprises on the basis of non-linear dynamics, fractal analysis and artificial intelligence are studied. Taking into account the peculiarities of metal cutting processes, the universal construction of neural network models of the machining process based on an artificial counter-neural neural network is proposed and substantiated. To ensure the functional stability of the production process at machine-building enterprises and enterprises of the mining and metallurgical complex, an intelligent system of analysis and forecasting of the dynamic stability of the technological process of cutting with the help of parallel calculations is proposed.

Keywords: Technological process · Functional stability · Dissipative systems · Neural network · Kohonen network

1 Introduction

The main achievements of the transformation of the global information infrastructure and large-scale automation of production are the actual merger of automated production technologies, data exchange, and production into a single self-regulatory system with minimal or no human intervention in the production process. Currently, there is a mass introduction of cyber-physical systems [1, 2] in the production and breakthroughs in the

fields of artificial intelligence, robotics, Internet of Things, autonomous transport, nanotechnology, autonomous machines, drones, virtual assistants, and translators, guides, quantum computers, etc. Taken together, this has a significant impact on the functioning of the state, business, science, and people, which leads to constant modification of existing concepts and theories and gives new meaning to a wide range of commonly used terms and concepts in many areas of human activity.

One of the consequences of the revolutionary trend in the development of modern industry, i.e. Industry 4.0, is a significant expansion of the object composition of technical systems, and the areas of their use. In particular, as a result of expanding the range of objects for the operation of complex technical systems, including information and variations of combinations of these objects, there is a requirement to expand the technical and object composition of the systems themselves. Such systems include machines, apparatus, devices, equipment, equipment, and their elements in the form of components, blocks, units, etc. It is a set of intelligent technical and cyber-physical systems and information networks, which by their nature are mostly complex or super-complex systems [3, 4]. Studies of the nature of cyber-physical systems themselves, as well as the methodological basis for building cyber-physical security systems of critical infrastructure based on modeling the behavior of antagonistic agents in security systems, are discussed in [5].

On the other hand, we are experiencing a real boom in the development of artificial intelligence technologies and their widespread introduction into the production processes of modern enterprises. Thus, in [6, 7] self-organizing neural networks, known as Kohonen maps, are used to diagnose the state of technical systems. A self-organizing neural network is used to diagnose equipment malfunctions. This uses the ability of the network to compress data, i.e. to represent a set of points by the weight vector of one neuron. Fundamental here is the assumption that each class of defects generates a certain change in the characteristics of the equipment. The neuron that wins the competition is characterized by either normal operation or a malfunction. Neural networks with self-organization activate one neuron, which allows locating the damaged element regardless of the state of the rest. In [7], the Kohonen neural network is used to diagnose the chemical process of melting metals.

Thus, to ensure the functional stability of technological processes of industrial enterprises, it is possible to widely use different classes of neural networks [8]. Training of neural networks taking into account the condition of functional stability of the technological process will ensure efficient operation of both production equipment and current product quality control.

The article [9] deals with issues related to the use of artificial neural networks in solving problems of identification and control of nonlinear dynamical systems. The characteristics of the network, which is the result of the use of fuzzy logic apparatus in the classical SMAS neural network, are studied. It is proved [10] that the use of artificial intelligence is a practical and perfect tool for solving large-scale problems of complex technical systems.

The paper [11] emphasizes the crucial role of network feedback in determining reliable management strategies, providing a dynamic benchmark for other management methods and opening promising research in the management of complex networks with

nonlinear dynamics. As shown in [12–14], nonlinear dynamics is a very effective tool for solving engineering problems.

The application of the theory of nonlinear dynamics and neural networks for optimization in enterprises with complex technical processes was studied in [15–17].

In [18] the stability of the technological system of processing at high-speed turning was investigated and the modeling of the dynamic stability of the system was performed. The models are based on vibroacoustic time series of signals generated as a result of machining. Adjustable and control parameters are determined and, depending on their set, changes in the dynamics of the system on the attractor on different models are investigated. A comparative analysis of mathematical models of nonlinear dynamics is used to study the behavior of the technological system and verify their adequacy [19–22].

It follows from the analysis that a sufficient number of scientific papers have been devoted to the issue of ensuring functional stability, but there is no clearly defined approach to ensuring the functional stability of technological processes of cyber-physical systems using neural networks. Therefore, research in this area is relevant.

2 Metal Cutting Processes Characteristics

Metal cutting processes are more competitive in terms of accuracy, quality, and efficiency compared to other molding methods. The basis of the cutting process is plastic deformation and destruction of the cutting layer. The process of plastic deformation of the cut layer causes deformation of the elastic elements of the general system of the machine. Dynamic instability of the cutting process causes a decrease in the roughness of the machined surface and tool wear, which necessitates a reduction in the modes of machining parts and productivity [8].

Cutting materials, such as stainless and refractory steel, their alloys, are subject to deformation hardening. They are characterized by intense vibration, characteristic sawdust, and increased tool wear. In carbon steels, the main impurity is carbon, which, located at the grain boundaries, can contribute to their fragility. As the temperature increases, the diffusion mobility of carbon increases, which promotes the sliding of the grain, increases, and changes the shape of the sawdust. Therefore, the degree of deformation of the cut layer and the cutting force is reduced.

The susceptibility of cutting materials to deformation before curing depends on their electronic and dislocation structure, energy defect in the packing of material crystals in the grain, the presence, strain rate, temperature, type of lattice, etc., and speed of softening processes. In [8], the peculiarities of the mechanisms of destruction of metals with increasing strain rates under tensile conditions with different crystal lattices were studied in detail. The analysis of fractures is given, which allows connecting this effect with the fragile destruction of sawdust elements., with increasing strain rate and increasing yield strength of materials with decreasing deformation localization area.

Along with these integral factors that characterize the processing of metals by cutting, it should be noted that this process is also characterized by modes of self-oscillation. In fact, experimental studies indicate [8] the presence of a self-oscillating regime of structural changes during the deformation of materials undercut conditions. The internal source causes the phase shift of the cutting force and the occurrence of self-oscillations

in the periodic localization of plastic deformation in the cutting system. The motion of localized deformation waves propagates from the free surface to the cutting blade. The deformation wave in the cut layer also moves to the blade, causing periodic loss of contact of the tool with the workpiece. In the first approximation, the energy of localized deformation waves can be determined as follows

$$\Delta U_D = E_0 \cdot \rho = \alpha \cdot G \cdot b^2 \cdot \rho,$$

where ΔU_D is the energy of elastic deformation, E_0 is the specific energy of deformation corresponding to the unit of dislocation length, ρ is the dislocation density, G is the shear modulus, α is the coefficient. The amplitude of the deformation wave h is estimated as follows:

$$\varepsilon = 2 \ln \left(\frac{h}{d_k} \right),$$

where ε is the degree of deformation, d_k is the cell size (fragment $\sim 1/\sqrt{\rho}$).

In [8] the conditions of deterministic chaos in dynamic machining processes are also studied. It is shown that three degrees of freedom of the elastic system of a metalworking machine are enough for the development of chaotic movements. On this basis, a dynamic model is proposed and various scenarios of chaos of the elastic system of the metalworking machine are studied, in particular the soliton scenario of chaos of the elastic system of the machine (see Fig. 1), as one of the most probable scenarios. Construction of attractors, estimation of d_F of fractal dimension [23] and λ Lyapunov exponents in the direction of force P_z and P_y showed that smaller values of d_F correspond to the attractor in the direction of force P_y and has zero value λ .

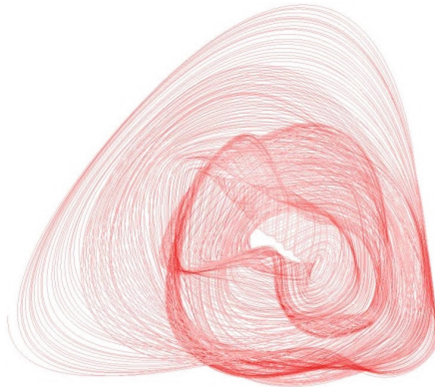


Fig. 1. View of the reconstructed attractor generated by the chaos of the elastic system of the metalworking machine.

Theoretical studies have shown that the transition from laminar motion of particles of material processed in cut layers to the vortex, i.e. dynamic chaos, may be associated with the formation of solitons here. The energy of localized deformation waves can be determined as follows.

3 Application of Neural Network Theory in Machining Processes Modeling

The ability to model nonlinear processes, work with noisy data, and adaptability makes it possible to use neural networks to solve a wide range of problems. Consider the management of machining processes in the fields of digital engineering based on neural networks. This is possible only on the basis of studying the phenomena that accompany the process of plastic deformation of metals and self-oscillations during metal cutting. A promising area of a comprehensive study of sawdust processes, cutting dynamics, and the mechanism of formation of the surface layer of the work piece is a systematic energy approach [8], according to which the machining process should be considered as a system of dissipative processes:

$$A_c = A_d + A_{fr(f)} + A_{fr(t)} + A_{gr}, \tag{1}$$

where A_c is the work of cutting, A_d is the work of deformation in the area of shear, $A_{fr(f)}$ and $A_{fr(t)}$ is the work of friction force of the front and rear face of the tool, respectively, A_{gr} is the work spent on destroying the growth. Each of the components of the system has its own properties and nature of behavior. If all possible manifestations of the system are reduced to the sum of the manifestations of its components, then such a system is simple. Methods of analysis are traditionally used to describe simple systems, the essence of which is the sequential decomposition of the system into components and the construction of models of increasingly simple elements. This is basically a method of mathematical modeling, in which models are described in the form of equations, and predicting the behavior of the system is based on their solutions.

An example of such an approach to the formalization of the cutting process are currently widely used mathematical models of machining (see Fig. 2), based on empirical power dependences of the initial characteristics of the cutting process on the parameters and geometry of the tool:

$$A(v, s, t, \varphi, \varphi_1, \dots) = C_A v^\alpha s^\beta t^\gamma \varphi^k \varphi_1^\eta \dots k_1 k_2 \dots k_n.$$

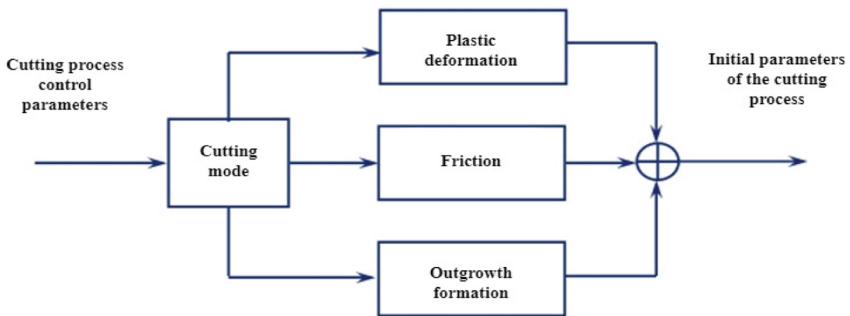


Fig. 2. Scheme of the cutting process in the form of a system of dissipative processes.

The universal method of constructing neural network models of the machining process on the basis of an artificial neural network of counter propagation can be described as follows:

- Step 1. Formation of a training sample that characterizes a wide range of conditions of the technological process and consists of vectors $\Psi(\tau_i)$ available for physical measurement of diagnostic information about the process and, corresponding to them, vectors of output parameters $\mathcal{P}(\tau_i)$.
- Step 2. Generalization and classification of input images $\Psi(\tau_i)$ diagnostic information in order to determine the set $\Theta(\Psi)$ of possible phase states of the technological process by self-learning Kohonen layer.
- Step 3. Comparison of each individual phase state Θ_k of the process with the most probable values of its initial parameters \mathcal{P}'_k by studying the Grossberg layer.

Estimation of instantaneous values of dependent cutting parameters is based on the structural-energy representation of the machining process in the form of a system of dissipative processes described by energy Eq. (1). The task of modeling each of the parameters (1) is to create a training sample of signals that characterizes the phase transitions of the cutting process (explicit or vague) due to changes in the controlled value, and the corresponding training of the neural network.

When using neural network models, the first question is the choice of a specific network architecture (the number of layers and the number of neurons in each of them). Then there is the process of learning the network, which is essentially a fit of the model implemented by the network, to the available training data that characterize the different options for the conditions of the technological process being modeled. The error for a particular network configuration is determined by running through the network all available observations of the input parameters \mathcal{U} of the process and comparing the output values \mathcal{W}_i model with the actual values of the output parameters \mathcal{W} process. All such differences are summed by the so-called error function, the value of which is the network error. Training is carried out until the network error reaches an acceptably small value (see Fig. 3).

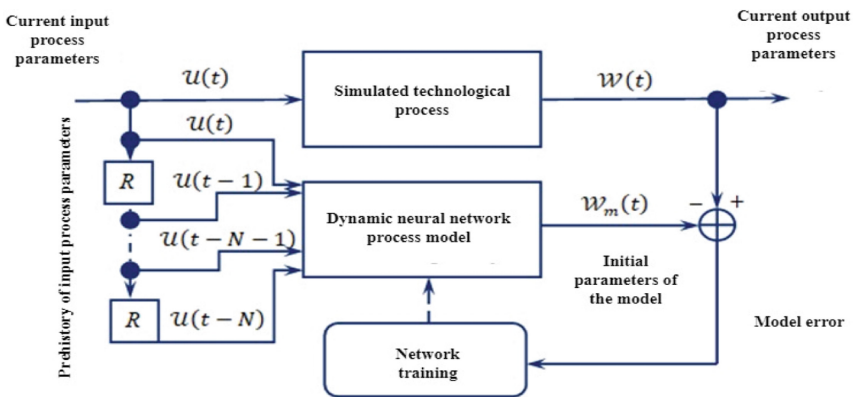


Fig. 3. Scheme of learning a dynamic neural network model of the technological process.

The network obtained as a result of training expresses the patterns present in the data. In this approach, it is the functional equivalent of the relationships between variables, similar to those built in traditional modeling. However, unlike traditional models, in the case of networks, these dependencies cannot be written explicitly. Often neural networks implement very high quality models; however, they are a typical example of a non-theoretical approach to research. In this approach, the main effort is focused solely on the practical result. In this case, the adequacy of the model, rather than the essence of the mechanisms underlying the phenomenon.

In practice, it is not always possible to fully model the entire process. In this case, it is useful to build a model of any of its components, the most important in terms of initial parameters of the process or the least convenient for direct measurements and, as a rule, therefore little studied. Such partial models can be useful for diagnosing the process as a whole. Naturally, the input data for these models will not be the vector $\mathcal{U}(t)$ control, and the vector $\Psi(t)$ of any intermediate parameters of the technological process, obtained as a result of physical measurements.

For example, the use of a dynamic neural network model of the oscillating system “tool-detail” of a metal-cutting machine allows for an effective way to diagnose vibrations that are self-excited in the cutting process. Information about the relative vibrations of the tool and the work piece can be obtained only as a result of indirect measurements. The main task of the analysis of such data is to determine the qualitative and quantitative characteristics of the recorded signals and to judge the true state of the dynamic processes occurring in the cutting zone. Therefore, we have a convenient tool for diagnosing the functional stability of the work center of the technological process, which allows you to detect malfunctions of the unit, which will localize the fault and eventually take action to continue operating until the completion of the technological operation.

Determining the parameters of the technological system that provide a stable mode of operation for its intended purpose (machining) is an urgent task. In real production, the determination of the optimal values of the modes of processing and adjustment of the machine is carried out using reference books and the experience of the technologist. However, the reference material often gives only approximate calculations of the parameters of the adjustment of the machine and does not take into account the dynamic characteristics of the machines, which can differ significantly from each other. The solution to this problem can be the development of an individual dynamic passport of the machine (work center), which allows an automated mode to determine the optimal modes of operation and their adjustment.

The real technological system is described by a large number of parameters that to some extent affect the initial parameters of the cutting system, such as vibration, temperature, force, and deformation, which, in turn, determine the productivity and quality of the treated surface. Accounting for all parameters in the process model is not possible. As a rule, in any complex hierarchical dissipative system, from the standpoint of a synergetic approach, there are parameters of order that determine the behavior of the system as a whole.

To identify patterns between the input parameters of the cutting process based on experimental data (cutting mode, machined material, method of fixing the work-piece, tool geometry, geometric parameters of the workpiece) and output (amplitude, frequency,

fractal dimension of the attractor [23]) in [8] used recurrent neural network adapted for regression analysis. After training, a regression neural network model of the cutting process was created, which allows to model any combination of input parameters of the cutting process and analyze the values of the output, thereby determining the margin and stability of the system in a wide range. The input layer of the neural network consists of 21 main neurons, which receive information about the vector S_t and additional neurons, which receive the values of the vector of the previous dynamic state S_{t-1} from the source neurons through the feedback channel. Thus, the neural network model takes into account the current processing conditions, as well as the previous dynamic state, which significantly increases the accuracy of modeling. The source layer consists of 4 main neurons that characterize the vector of the current dynamic state of the cutting process S_t , which contains information about the amplitude of self-oscillations, fractal dimension of the attractor, signal entropy, senior Lyapunov and 10,000 additional neurons, each responsible for a frequency in the spectrum. Neural network learning is implemented by the method of inverse error propagation.

Given the large amount of data in the digitized signal of acoustic emission (see Fig. 4), the problem of learning performance and neural network becomes relevant. A modern approach to increasing its productivity is the technology of parallel computing. Parallelization can be performed both on the CPU cores and with the use of GPU cores. In the problems of spectral analysis with further training of the neural network, it is advisable to divide the frequency spectrum of the signal into certain zones.

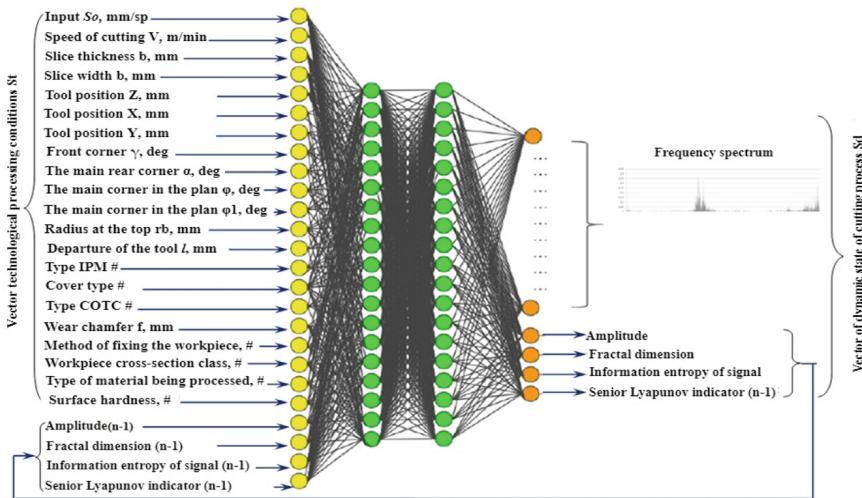


Fig. 4. Neural network model of technological process of cutting.

To increase the productivity of computing should be integrated into the control system of the production center of the technological process by increasing the productivity of neural networks and the speed of their learning, the use of GPU cores and nVidia CUDA technology.

4 Intelligent System of Dynamic Stability Analysis and Forecasting

Development of a dynamic passport of the work center of the technological process based on neural networks with a parallel learning algorithm allows to determine the areas of dynamic stability of the cutting process on specific equipment and assign optimal processing and adjustment of the work center. Approaches to nonlinear dynamics make it possible to build attractors of the cutting system and to assess their fractal dimension, as well as to detect chaotic self-oscillations during cutting and loss of stability of the cutting system. The use of parallel computing algorithms NVIDIA CUDA significantly accelerates the learning process of the neural network, which allows them to be used in systems of operational diagnostics of dynamic stability of technological systems in production.

Modern intelligent systems integrated into process control include a database of the dynamic state of the cutting process, a neural network for the stability of the cutting process, a neural network for classifying the cross-sections of the workpiece, and signal analysis software.

The database contains information about the vector of technological parameters St and the corresponding vector of the dynamic state Sd , obtained during experimental studies or equipment operation [8]. After accumulating a certain amount of information in the database, the neural network model of the stability of the cutting process is trained, which connects the values of the vector of technological parameters St with the corresponding values of the vector of the dynamic state of the cutting process Sd (see Fig. 5). The input layer of the neural network consists of 13 neurons, the input of which receives information about the vector of technological parameters of St . The source layer consists of 4 main neurons that characterize the dynamic state vector of the cutting process, which contains information about the amplitude of self-oscillations. The fractal dimension of the attractor, signal entropy, and 10,000 additional neurons, each responsible for a frequency in the spectrum. Neural network learning is a method of inverse error propagation. Due to a large amount of incoming data, parallel computing (GPU) approaches and NVidia CUDA technology are used, in particular a specialized cuDNN library, which allows increasing learning productivity by 5–7 times.

The influence of the shape of the workpiece on the vector of the dynamic state of the cutting process is taken into account using its 3D model. Based on the Boolean subtraction operation, a 3D model of the workpiece is subtracted from the 3D model of the working space of the work center bounded by a prismatic solid. Then through the interval dz cross-sections of the formed figure are constructed. The resulting cross sections are covered with a grid with cells of size dx . Cells in which there is no solid body, due to the Boolean subtraction operation, take the value “1”, and in cells in which there is a solid body, the value “0”. From the obtained values of the cells, a matrix is formed, which reflects the geometric features of the part in a particular section and the location of the working space of the work center. The resulting matrix is fed to the input of an artificial neural network, which on the basis of Kohonen’s self-learning algorithm forms classes of sections. The obtained classes of sections are recorded in the database and used in the process of learning the neural network model of stability (functional stability) of the cutting process.

After training, the neural network is able to simulate the dynamic state of the cutting process, forming on the source layer of neurons vector of the dynamic state of the cutting process Sd_m based on data about the vector of technological parameters St_m . By changing the value of the vector St_m , it is possible to model different dynamic states to further select the technological parameters that provide the most dynamically stable cutting modes, thereby increasing the efficiency of machining, and thus ensuring the functional stability of the process.

Developed intelligent system for diagnostics and management of dynamic stability of the cutting process, can be implemented on the basis of modeling processing at the production center for cutting metals with carbide metalworking tools (see Fig. 5). It is necessary that the input of the neural network model receives the vector of technological parameters St_m ($V = 1$ m/s, $t = 4$ mm, $S_o = 0.1$ mm/r). And at the output of the artificial neural network the corresponding vector of the dynamic state of the cutting process Sd_m is formed. As a variable component of the vector St_m , you can choose the value of Z is the position of the caliper of the machine on the Z axis of mm, which can vary in steps of 0.01 mm in the range, for example, from 0 to 350 mm. This technique allows you to form a vector Sd_m throughout the processing of the workpiece.

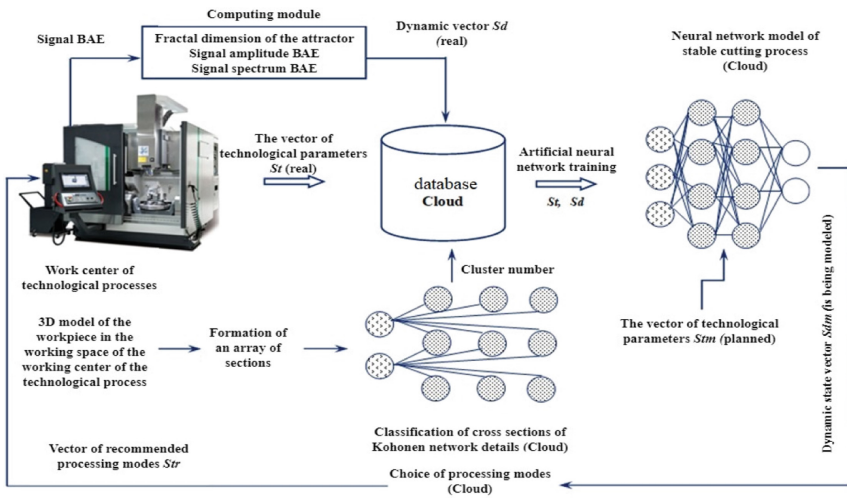


Fig. 5. Schematic diagram of an intelligent system for diagnosing and managing the dynamic stability of the technological process of cutting.

The proposed intelligent system for diagnosing and managing the dynamic stability of the technological process of cutting is a necessary condition for ensuring the functional stability of the production process.

Ensuring the practical observance of the model parameters within the real production process will guarantee its functional stability within the time interval as long as the parameters of the technology center will satisfy the calculated model parameters. The system will become functionally unstable when the parameters go beyond the set of design parameters, which will lead to a loss of dynamic stability of the work center and

will require stopping the process or its correction, tool replacement, operating modes, and more.

5 Conclusion

The universal method of construction of neural network models of machining process on the basis of the artificial neural network of counter propagation is given. Based on the research, an intelligent system of analysis and forecasting of dynamic stability of the technological process of cutting with the use of parallel calculations was chosen. The method of building neural network models of the machining process on the basis of an artificial neural network of counter-propagation guarantees the fulfillment of the necessary conditions to ensure the functional stability of the production process.

In the future, it is planned to continue the study of functionally stable technological processes using artificial intelligence methods. The focus will be on modeling such processes, taking into account the characteristics of the working environment, the materials used, and the impact of physical processes that accompany the relevant technological processes.

References

1. Edward, A., Sanjit, A.: Introduction to Embedded Systems. A Cyber-Physical Systems Approach. MIT Press, London (2017)
2. Shyr, W.J., Juan, H.C., Tsai, C.Y., Chang, Y.J.: Application of cyber-physical system technology on material color discrimination. *Electronics* **11**, 920 (2022). <https://doi.org/10.3390/electronics11060920>
3. Muammer, E., Lo'ai, T., Fadi, M.: The security concerns on cyber-physical systems and potential risks analysis using machine learning. *Procedia Comput. Sci.* **201**, 527–534 (2022). <https://doi.org/10.1016/j.procs.2022.03.068>
4. Latif, S., Wen, F., Band, S., et al.: AI-empowered, blockchain and SDN integrated security architecture for IoT network of cyber physical systems. *Comput. Commun.* **181**, 274–283 (2021). <https://doi.org/10.1016/j.comcom.2021.09.029>
5. Yevseiev, S., Ponomarenko, V., Laptiev, O., et al.: Synergy of Building Cybersecurity Systems. PC Technology Center, Kharkiv (2021). <https://doi.org/10.15587/978-617-7319-31-2>
6. Sujeet, S., Shankar, S., Subramaniaswamy, V.: A hypergraph based Kohonen map for detecting intrusions over cyber-physical systems traffic. *Futur. Gener. Comput. Syst.* **119**, 84–109 (2021). <https://doi.org/10.1016/j.future.2021.02.001>
7. Xu, Y., Ran, J., Chen, H.: Kohonen neural network classification for failure process of metallic organic coating in corrosion environment. *Metals* **7**(4), 147 (2017). <https://doi.org/10.3390/met7040147>
8. Kabaldin, Y.G., Shatagin, D.A.: Artificial intelligence and cyberphysical machining systems in digital production. *Russ. Eng. Res.* **40**(4), 292–296 (2020). <https://doi.org/10.3103/S1068798X20040115>
9. Rudenko, O., Bezsonov, O., Lebediev, O.: Adaptive control over nonlinear objects using the robust neural network FCMAC. *East.-Eur. J. Enterpr. Technol.* **2**(4), 4–14 (2018). <https://doi.org/10.15587/1729-4061.2018.128270>

10. Johnson, C., Laurell, C., Ots, M., Sandstrom, C.: Digital innovation and the effects of artificial intelligence on firms' research and development – Automation or augmentation, exploration or exploitation? *Technol. Forecast. Soc. Chang.* **179**, 121636 (2022). <https://doi.org/10.1016/j.techfore.2022.121636>
11. Jorge, G., Gang, Y., Réka, A.: Structure-based control of complex networks with nonlinear dynamics. *PNAS* **114**(28), 7234–7239 (2017). <https://doi.org/10.1073/pnas.1617387114>
12. Guo, J., Qiu, B., Hu, C., Zhang, Y.: Discrete-time nonlinear optimization via zeroing neural dynamics based on explicit linear multi-step methods for tracking control of robot manipulators. *Neurocomputing* **412**, 477–485 (2020). <https://doi.org/10.1016/j.neucom.2020.05.093>
13. Gospodinova, E., Gospodinov, M., Negreva, M.: Nonlinear dynamics methods for analysis of ECG signals. In: *Proceedings of the 21st International Conference on Computer Systems and Technologies 2020*, pp. 194–200. ACM (2020). <https://doi.org/10.1145/3407982.3408000>
14. Ohrimenko, O.I., Maltsev, I.M., Rokotyanskaya, V.V., Vilisova, M.L.: The theory of nonlinear systems as an instrument for solving engineering problems. *MATEC Web Conf.* **226**, 04040 (2018). <https://doi.org/10.1051/mateconf/201822604040>
15. Lipski, J., Zaleski, K.: Optimisation of milling parameters using neural network. In: *ITM Web of Conferences*, vol. 15, p. 01005 (2017). <https://doi.org/10.1051/itmconf/20171501005>
16. Khrustalev, M., Rumyantsev, D., Tsar'kov, K.: Optimization of quasilinear stochastic control-nonlinear diffusion systems. *Autom. Remote. Control.* **78**(6), 1028–1045 (2017). <https://doi.org/10.1134/S0005117917060054>
17. Zhu, Q., Wang, Y., Zhao, D., et al.: Review of rational (total) nonlinear dynamic system modelling, identification, and control. *Int. J. Syst. Sci.* **46**(12), 2122–2133. <https://doi.org/10.1080/00207721.2013.849774>
18. Ostapchuk, A.K., Kuznetsova, E.M., Dmitrieva, O.V.: Estimation of the stability of the machining technological system using nonlinear dynamics mathematical models. In: *2018 International Multi-Conference on Industrial Engineering and Modern Technologies*, pp. 1–4. IEEE, Vladivostok (2018). <https://doi.org/10.1109/FarEastCon.2018.8602523>
19. Sobchuk, V., Zamrii, I., Vlasyk, H., Tsvietkova, Y.: Strategies for control automated production centers to ensure the functional stability of enterprise information systems. In: *2021 IEEE 3rd International Conference on Advanced Trends in Information Theory*, pp. 61–66. IEEE, Kyiv (2021). <https://doi.org/10.1109/ATIT54053.2021.9678784>
20. Zheng, W., Zhang, Z., Sun, F., Wen, S.: Robust stability analysis and feedback control for networked control systems with additive uncertainties and signal communication delay via matrices transformation information method. *Inf. Sci.* **582**, 258–286 (2022). <https://doi.org/10.1016/j.ins.2021.09.005>
21. Trung, V., Thinh, N.: Approach to spacecraft functional stability in changes in moments of inertia. *Procedia Comput. Sci.* **103**, 549–555 (2017). <https://doi.org/10.1016/j.procs.2017.01.056>
22. Berezovska, Y.: Ensuring functional stability of the information system with limited output information about certain random values. *Telecommun. Inf. Technol.* **4**, 69–79 (2020)
23. Barabash, O., Koptiika, O., Zamrii, I., Sobchuk, V., Musienko, A.: Fraktal and differential properties of the inversor of digits of Q_s -representation of real number. In: Sadovnichiy, V.A., Zgurovsky, M.Z. (eds.) *Modern Mathematics and Mechanics*. UCS, pp. 79–95. Springer, Cham (2019). https://doi.org/10.1007/978-3-319-96755-4_5



S-Shape Feedrate Profile with Smoothly-Limited Jerk for Threading Movements Synchronization in CNC Machining

Volodymyr Kombarov¹ , Volodymyr Sorokin² , Yevgen Tsegelnyk¹  ,
Sergiy Plankovskyy¹ , and Yevhen Aksonov¹ 

¹ O. M. Beketov National University of Urban Economy in Kharkiv, 17 Marshala Bazhanova Street, Kharkiv 61002, Ukraine

y.tsegelnyk@kname.edu.ua

² National Aerospace University “Kharkiv Aviation Institute”, 17 Chkalova Street, Kharkiv 61070, Ukraine

Abstract. The threaded surface is an important element of various technical products, such as leadscrew, worm drive, high-pressure gas, oil tubing, etc. The accuracy of the manufacture of the threaded surface largely determines its reliability and durability. Threaded surface machining on CNC equipment requires accurate synchronization of the periodic movements of the tool with the continuous rotation of the spindle. One of the possible options for organizing such synchronization in a two-level CNC system is observed. Mathematical models of movement at the acceleration stage of the longitudinal movement axis synchronized with the spindle have been developed. Models based on uniformly accelerated motion and motion with a smooth change in differential characteristics such as speed, acceleration, and jerk are considered. An S-shaped feedrate profile using the \sin^2 function is applied. The movement of the longitudinal axis at thread machining is synchronized with the position of the rotating spindle. The problem of axis acceleration at synchronized movement on a section of a given length with the implementation of an S-shaped feed profile is solved. The proposed model is implemented in the two-level CNC. The results of its experimental studies are presented.

Keywords: Threading · CNC · S-shaped feedrate profile · Smooth jerk · Axis synchronization

1 Introduction

Threaded joints and parts with helical surfaces are widely used in various industries of mechanical engineering, mining and municipal economy [1–3]. At the current level of manufacturing equipment development, most of the parts with critical threaded and helical surfaces are manufactured on CNC equipment [4, 5]. The high-accuracy requirements are imposed upon threaded surfaces, which significantly affects both the characteristics of products and their durability and reliability, for example, high pressure gas and oil tubing, etc. [6, 7]. The leaders of modern machine tool manufacturing produce equipment

that provides these requirements. However, the requirements for the accuracy increase over time [8, 9]. Accordingly, the task of equipment accuracy improving for various purposes, and in particular for threading, does not lose its relevance.

The control bodies on high feeds cannot immediately respond to variations in the tool path in sections with bends, due to the influence of inertia forces [10]. One of the areas of investigations and innovation related to improving the accuracy of CNC equipment [11] and servo drives [12, 13] is the development of mathematical models [14], and methods for controlling the machine tools movement, taking into account differential characteristics, such as speed, acceleration and jerk. Modern CNC systems use intelligent feedrate scheduling methods implemented by Look-ahead algorithms [15, 16] in order to avoid inertial throws due variation the tool movement direction.

This trend is most pronounced in the development of feedrate scheduling systems for high-speed machining. A large number of the S-shape feedrate models are proposed. Have been proposed S-shape profiles based on the polynomials: with trapezoidal acceleration [17], with a discontinuous jerk [18], with jerk continuous [19] etc. Proposed S-shape feedrate profiles based on the trigonometric functions: profile with continuous acceleration and discontinuous jerk [20], with continuous jerk [21] and seven-interval model of S-shaped profile with smoothly-limited jerk [22]. It was experimentally shown in [22] that the use of S-shape feedrate profile with smoothly-limited jerk contributes to an increase in the accuracy of movement of machine organs compared to S-shape profile with trapezoidal acceleration and jerk limited.

For the threading process on CNC equipment, it is necessary to ensure that several motion tool axes are synchronized with the position of the rotating spindle. The longitudinal movement axis is most susceptible to the formation of dynamic errors. These errors can be reduced by applying an S-shaped feedrate profile with a smooth variation in the differential characteristics. The problem of acceleration of the longitudinal axis movement in synchronization with the position of a rotating spindle during movement in a section of a given length with the implementation of an S-shaped feedrate profile with using the \sin^2 function is considered in this paper.

2 Threading Control in a Two-Level CNC System

Despite the extremely wide variety of threaded and helical surfaces designs, in their manufacture using extractive technologies, the same type of processing cycles for multi-pass threading are used. In Fig. 1a shown the typical toolpath used in threading cycles. At the same time, for the shaping implementation, it is necessary to perform a synchronized movement of three axes at once: rotation of the spindle S , movement of the Z -axis along with the pitch of the helix thread, movement and positioning of the X -axis on the corresponding size of the diameter of the machined surface. Due to the equipment design features and differences in inertia, the dynamic characteristics of the spindle and tool movement axes differ significantly. For this reason, traditional approaches to coordinating the axes movements involved in shaping through interpolation [23, 24] will not provide the required accuracy. As a result, the tool movement during the formation of threaded surfaces is carried out in synchronization with the spindle. In this paper, synchronization of the longitudinal movement axis is considered as the most prone to the formation of a dynamic error.

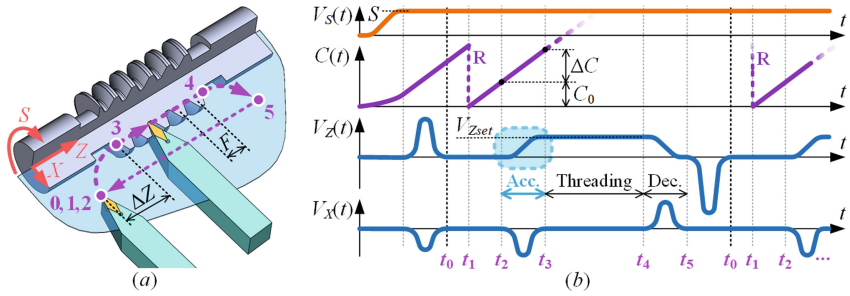


Fig. 1. Threading process: (a) the tool paths characteristic sections; (b) diagram of the axes interaction during threading; R is the reset spindle angle value at zero label position.

In Fig. 2 shown the threading control scheme, including the longitudinal axis and the spindle control. The initial information for processing a specific part is generated in CAD/CAM and transferred to CNC as a G-code, which contains a minimum set of data about the parameters of the helix thread forming. In the two-level CNC system used by the authors for experimental studies [25, 26], the tasks of code interpretation and motion interpolation are distributed between two PC. Code interpretation is performed without using real-time mode and involves data conversion and the formation of “Machine code” in a format convenient for use in equipment control.

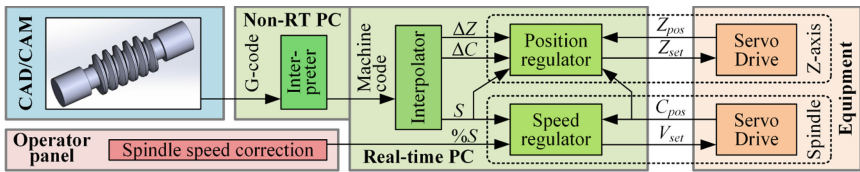


Fig. 2. Threading process control scheme.

The “Interpolator” and “Regulator” modules work on a PC in real-time, but clocked at a different pace to eliminate the “information deprivation” in the “Regulator” module. In the normal mode of movement, the “Interpolator” module transmits to the “Regulator” module data on variation in the position and speed for each control cycle. Data is transmitted via a virtual network, which ensures the unification of the communication of these modules, both within a single PC and when the “Regulator” modules are placed on separate PCs in a distributed system. Such an organization implies a significant limitation on the number and type of transmitted parameters.

Transferring data to the “Regulator” module in synchronization mode with the position of a rotating spindle has similar limitations. In this regard, the possibility of restoring the motion model using a limited set of parameters should be provided. In addition, in the process of converting data from a G-code to a set of input parameters in the “Regulator”, errors may accumulate. The algorithm for calculating the synchronized movement in the “Regulator” module must exclude the influence of such errors.

A typical trajectory and the diagram of the axes movement during threading is shown in Fig. 1. The process is carried out at a constant predetermined spindle speed S . Parameter $C(t)$ shows the actual position of the rotating spindle. Before the start of the cycle (t_0), the tool is positioned at the starting point. At zero label position (t_1), the $C(t)$ value is zeroed, the X, Z axes “Regulator” modules enter to the spindle tracking mode. After the spindle position C_0 is reached (t_2), the acceleration starts. During the acceleration, the speed of the Z -axis increases to V_{Zset} over a section ΔZ (t_3). The V_{Zset} is determined by the spindle speed S and the helix pitch F . By this time, the spindle should change position by ΔC . The threading stage is executed at the speed of the synchronized movement V_{Zset} until the end of the threading section (t_4). The synchronized motion mode is completed by retracting the tool from the workpiece surface along the X -axis and decelerating the Z -axis to zero speed (t_5). The repetition of the cycle is carried out after returning to the start point in the mode of traditional interpolation. For the proposed model, the parameters $S, C_0, \Delta C, \Delta Z$ are used as initial data.

Due to the peculiarities of the two-level CNC system architecture (Fig. 2), the formation of model parameters is carried out in the “Interpreter” module for the value S specified by the G-code. The actual spindle speed may differ due to drive setting errors. In addition, the spindle speed can be adjusted during processing. Thus, the motion model must provide the correct acceleration of the axis in the mode of the spindle’s actual position (C_{pos}) tracking, regardless of the actual speed being executed.

In this paper, mathematical models of the longitudinal axis acceleration synchronized with the spindle based on uniformly accelerated motion and motion with a smooth jerk are considered. An experimental comparison of the accuracy of the longitudinal axis movement in the application of these models is carried out.

3 Mathematical Model of Uniformly Accelerated Motion

The mathematical model of the longitudinal axis movement in the acceleration section during threading should provide a clear synchronization of the spindle speeds V_S and the longitudinal axis movement $V_Z(t)$. The spindle speed (deg/s) is determined as

$$V_S = 6S, \quad (1)$$

where S is the value of the spindle speed specified in the G-code (rpm). During acceleration of the Z -axis, the spindle performs uniform motion at a speed V_S . Then, the expression for the time t required to reach an arbitrary position ΔC_{pos} can be written as

$$t = \Delta C_{pos}/6S. \quad (2)$$

The expression for determining the time t_{acc} required to reach the position ΔC

$$t_{acc} = \Delta C/6S. \quad (3)$$

The speed of the Z -axis at the end of the acceleration section V_{Zset} depends on the thread pitch F and the spindle speed and is equal to the speed on the threading section

$$V_{Zset} = (F \cdot S)/60. \quad (4)$$

For the accepted boundary conditions $V_{Z0}(t_0) = 0$; $Z(t_0) = Z_0$ the equations for variation the speed and position of the longitudinal axis can be written as

$$V_Z(t) = a_{acc} \cdot t, \quad (5)$$

$$Z(t) = Z_0 + \Delta Z(t) = Z_0 + (a_{acc} \cdot t^2)/2. \quad (6)$$

The longitudinal axis acceleration is carried out for some time t_{acc} up to the speed V_{Zset} . From Eq. (5), taking into account (4), obtain the value of the acceleration time

$$t_{acc} = (F \cdot S)/(60 \cdot a_{acc}). \quad (7)$$

The expression for the variation in position during uniformly accelerated motion at the end of the acceleration section can be written from (6) taken into account (3)

$$\Delta Z = (a_{acc} \cdot \Delta C)/(72 \cdot S^2). \quad (8)$$

From here we get the expression for the acceleration required for the spindle and the longitudinal axis coordinated movement

$$a_{acc} = 72 \cdot S^2 \cdot \Delta Z / \Delta C^2. \quad (9)$$

From Eq. (5), taking into account (3), (4) and (9), we obtain a relation between the thread pitch and the displacements of the spindle and the Z-axis

$$F = 720 \cdot \Delta Z / \Delta C. \quad (10)$$

To control the Z-axis in the spindle tracking mode according to Fig. 2, the axes displacements must be represented as a function of the spindle position ΔC_{pos} . To do this, using simple Eq. (6), taking into account (2) and (9), we obtain

$$Z(\Delta C_{pos}) = Z_0 + \Delta C_{pos}^2 \cdot \Delta Z / \Delta C. \quad (11)$$

During the program execution, the spindle speed may differ from the one specified in the G-code. Equation (11) relates the position of the Z-axis to the spindle position and does not use such parameters as time t and spindle speed S . It is obvious that the synchronization of the Z-axis movement with the spindle using the Eq. (11) is not sensitive to errors in the actual speed of the spindle rotation and can be used in CNC. However, such a model of the longitudinal axis movement in the acceleration section during threading does not provide a smooth change in the differential movement characteristics, which is necessary to ensure high machining accuracy.

4 Mathematical Model of Motion with a Smooth Jerk

In the paper [27] proposed a simplified three-interval model S-shaped feedrate profile with smoothly-limited jerk using the \sin^2 function and shows its application in the CNC. In the feedrate scheduling system, the problem of ensuring the minimum time of

movement along the processing trajectory is solved while observing the limitations of the differential movement characteristics. The length of the trajectory section on which the movement speed is changed is used as one of the limitations, but it is allowed to accelerate to a given speed on a section of arbitrary length. In contrast to feedrate scheduling CNC systems [28, 29], during threading it is necessary to ensure the simultaneous achievement of the required speed of the longitudinal axis movement and the specified position of the spindle and the longitudinal axis. In this case, the possibility of a deviation in the spindle speed from the theoretically specified one is allowed. It is necessary to solve the problem of determining the motion parameters of the longitudinal axis, in which, at a given length, the speed of movement necessary for synchronization with the speed of spindle rotation will be achieved.

In Fig. 3. Shown a diagram of a variation of the Z-axis differential movement characteristics in the synchronization mode with the spindle position. To describe the Z-axis movement, the model with a smooth jerk proposed in [27] is used. However, for the purposes of describing the movement during threading, the motion model is considered not as a function of time, but as a function of the parameter p . The value of the parameter p is defined as the ratio of the spindle position ΔC_{pos} to the specified speed of its rotation or to the specified revolutions S , taking into account Eq. (1)

$$p = \Delta C_{pos}/V_S = \Delta C_{pos}/(6S). \tag{12}$$

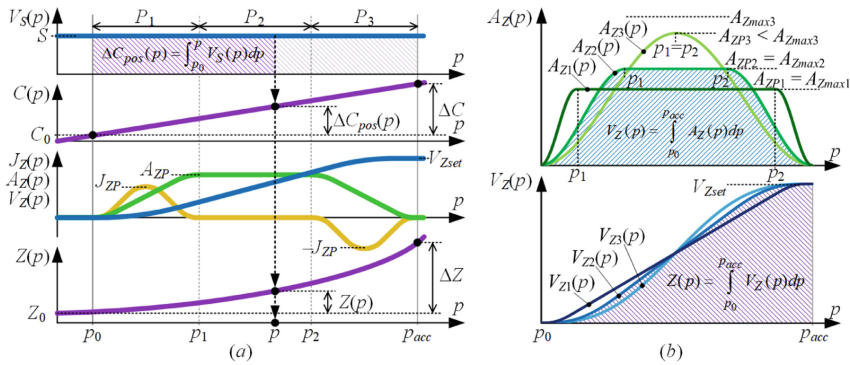


Fig. 3. Diagram of kinematic motion parameters: (a) variation the differential movement characteristics of the longitudinal axis Z with the spindle rotation S; (b) acceleration limitation.

The acceleration section of the longitudinal axis corresponds to its movement in the interval of parameter change from $p_0 = 0$ to p_{acc}

$$p_{acc} = \Delta C/V_S = \Delta C/(6S). \tag{13}$$

For the accepted conditions $V_{Z0}(p_0) = 0$; $Z(p_0) = Z_0$ the Z-axis speed is given by

$$V_Z(p_{acc}) = (F \cdot S)/60. \tag{14}$$

Additionally the following boundary conditions should be observed to achieve the smoothness of motion during acceleration: $A_Z(p_0) = A_Z(p_{acc}) = 0$; $J_Z(p_0) = J_Z(p_{acc}) = 0$. The traveled distance ΔZ for the acceleration section is given in the machine code, the position variation function is determined according to the S-shape feedrate profile (Fig. 3), which usually includes three intervals.

$$\Delta Z = \int V_Z dp, P_i = [p_{i-1}, p_i], i \in [1, 3], \tag{15}$$

Acceleration starts at the time corresponding to the value of the parameter p_0 and finishes at the time corresponding p_{acc} . The model covers the following intervals:

- P_1 is an acceleration from $A_Z(p_0) = 0$ to $A_Z(p_1) = A_{ZP}$, the duration is Δp_1 ;
- P_2 is a motion with constant acceleration $A_Z(p_1 \dots p_2) = const$, the duration is Δp_2 ;
- P_3 is an acceleration from $A_Z(p_2) = A_{ZP}$ to $A_Z(p_3) = 0$, the duration is $\Delta p_3 = \Delta p_1$.

In the particular case, intervals of constant acceleration P_2 may be not used. At each i interval parameter from it start is defined as.

$$\tau(p) = (p - p_{i-1}), p \in P_i. \tag{16}$$

Full parameter variation interval for the acceleration process

$$p_{acc} = \Delta p_{acc} = \Delta p_1 + \Delta p_2 + \Delta p_3 = 2 \cdot \Delta p_1 + \Delta p_2. \tag{17}$$

The jerk variation law is based on the \sin^2 function with period defined by angular frequency $\omega(s^{-1})$. Value of ω is calculated from the condition $\sin^2(\omega \cdot \Delta p_1) = 0$:

$$\omega = \pi / \Delta p_1.$$

In accordance with the proposed model, we write equation to determine the velocity

$$V_Z(p) = \begin{cases} J_{ZP} \cdot FV(p), & p \in P_1, \\ A(p_1) \cdot \tau(p) + V(p_1), & p \in P_2, \\ A(p_1) \cdot \tau(p) - J_{ZP} \cdot FV(p) + V(p_2), & p \in P_3, \end{cases} \tag{18}$$

where $FV(p) = 0.25 \cdot (\tau(p))^2 - (\sin(\omega \cdot \tau(p)) / (2 \cdot \omega))^2$.

The position of the longitudinal axis movement is defined as

$$Z(p) = Z_0 + \Delta Z(p). \tag{19}$$

Equation to determine the distance traveled during acceleration:

$$\Delta Z(p) = \begin{cases} J_{ZP} \cdot FS(p), & p \in P_1, \\ A(p_1) \cdot \tau(p)^2 / 2 + V_Z(p_1) \cdot \tau(p) + Z(p_1), & p \in P_2, \\ A(p_1) \cdot \tau(p)^2 / 2 - J_{ZP} \cdot FS(p) + V_Z(p_2) \cdot \tau(p) + Z(p_2), & p \in P_3, \end{cases} \tag{20}$$

where $FS(p) = \tau(p)^3 / 12 - \tau(p) / (8 \cdot \omega^2) + (\sin(2 \cdot \omega \cdot \tau(p))) / (16 \cdot \omega^3)$.

The acceleration, velocity and traveled distance, which will be achieved at the end of P_1 interval (at the p_1), in accordance with the proposed model are defined as:

$$A_{ZP}(p_1) = 0.5 \cdot J_Z \cdot \Delta p_1, \quad (21)$$

$$V_{ZP}(p_1) = 0.25 \cdot J_Z \cdot \Delta p_1^2, \quad \Delta Z(p_1) = J_Z \cdot \Delta p_1^3 \cdot \left(1/12 - 1/(8 \cdot \pi^2)\right), \quad (22)$$

The velocity and traveled distance, which will be achieved at the end of P_2 interval (at the p_2), in accordance with the proposed model [27] are defined as:

$$V_Z(p_2) = V_{Zset} - 0.25 \cdot J_Z \cdot \Delta p_1^2 \quad (23)$$

$$\Delta Z(p_2) = 0.5 \cdot V_{Zset} \cdot (\Delta p_2) + S(\Delta p_1). \quad (24)$$

From (18), (22) and (17), obtain the speed at the end of the acceleration section

$$V_{Zset} = V_Z(p_{acc}) = 0.5 \cdot J_{ZP} \cdot (\Delta p_1^2 - \Delta p_1 \cdot \Delta p_2) = 0.5 \cdot J_{ZP} \cdot (\Delta p_1 \cdot \Delta p_{acc} - \Delta p_1^2). \quad (25)$$

The distance traveled in the acceleration section is determined by the equation

$$\Delta Z(p_{acc}) = 0.5 \cdot V_{Zset} \cdot \Delta p_{acc} = 0.5 \cdot V_{Zset} \cdot (2 \cdot \Delta p_1 + \Delta p_2). \quad (26)$$

From Eq. (23), taking into account (4), obtain an equation to determine the range of the parameter variation in the acceleration section

$$\Delta p_{acc} = 120 \cdot \Delta Z / (S \cdot F). \quad (27)$$

From (24), (17) and (13), obtain the relation between the thread pitch and the displacements of the spindle and the longitudinal axis in the acceleration section

$$F = 720 \cdot \Delta Z / \Delta C. \quad (28)$$

Equation (25) for the proposed S-shaped profile with smoothly-limited jerk is similar to Eq. (10) for uniformly accelerated movement. The relation of the considered parameters in Eq. (28) does not explicitly depend on the spindle speed. The number of intervals in the implemented S-shaped feedrate profile in the acceleration section of the Z-axis depends on the ratio of the required acceleration and its limitation

$$A_{ZP} \leq A_{Zmax}. \quad (29)$$

In Fig. 3b shown that when condition (29) is satisfied, the interval P_2 is absent, and the value of the variation in the parameter in the interval P_1 for a two-interval acceleration profile is determined by the relation between the axis movement and the spindle position and, taking into account (13), is determined by the equation

$$\Delta p_{1_2i} = 0.5 \cdot \Delta p_{acc} = \Delta C / (12 \cdot S). \quad (30)$$

If condition (29) the acceleration is carried out using a three-interval profile. The acceleration at the end of the interval P_1 will correspond to the $A_{Z\max}$ limit. Considering this, the duration of the interval P_1 , obtain from expressions (25), (21):

$$\Delta p_{1_a\max} = \Delta p_{acc} - V_{Zset}/A_{Z\max}. \quad (31)$$

In the acceleration section, in order to form an S-shaped feedrate profile that satisfies the condition for ensuring a synchronized movement speed at a given travel length, it is necessary to choose the smallest value Δp_1 :

$$\Delta p_1 = \min(\Delta p_{1_a\max}, \Delta p_{1_2i}). \quad (32)$$

Using Eqs. (25), (26) we find the value of the jerk J_{ZP} required for movement in the acceleration section for both two-interval and three-interval profiles

$$J_{ZP} = 0.25 \cdot \Delta Z / (\Delta p_1 \cdot \Delta p_{acc}^2 - \Delta p_1^2 \cdot \Delta p_{acc}) \quad (33)$$

In accordance with the proposed model, the calculation of the Z-axis movement parameters during acceleration section is performed in the following order:

- determination of the intervals for variation of the parameter p , p_{acc} by Eq. (13), Δp_{1_amax} by Eq. (31), Δp_{1_2i} by expression (30);
- determination of the number of intervals (32) and the duration of the interval P_2 in accordance with (17);
- calculation of the required jerk J_{ZP} according to Eq. (33);
- in the threading process, depending on the position ΔC_{pos} , the parameter p is calculated according to the Eq. (12) and the parameters of movement and positioning according to the model (18), (20).

It is obvious that the calculation of the motion parameters of the longitudinal axis in accordance with the proposed mathematical model is quite simple for their implementation in the CNC. The complexity of the calculation algorithm is commensurate with the complexity of the algorithm of the model of uniformly accelerated movement. The model provides the ability to control motion in the acceleration section according to a limited set of initial data, including variation in the positions of the longitudinal axis ΔZ and spindle ΔC in the acceleration frame, as well as the specified spindle speed S . The parameters of the acceleration section must satisfy the condition (28), which ensures that the speed necessary for threading is reached in the section of a given length. The model is not sensitive to deviations in the value of the spindle speed and allows threading with a significant variation in the spindle speed.

5 Experimental Investigations

Experimental investigations were carried out on equipment with a two-level CNC system. Movement of the machine axis with AC servomotor Estun EMG-10APA22 was investigated. Registration and processing of experimental data was carried out using a CNC-based software and hardware complex [25, 26].

The tool movement corresponding to the manufacturing operation of the left-hand worm screw was studied (Fig. 1a). The experiment investigate the behavior of servo error $\delta(t)$ during the movement of the Z-axis in a fixed-length acceleration section. A comparison of servo error $\delta(t)$ obtained during acceleration using the uniformly accelerated motion model (Fig. 4a) and the model using the S-shaped profile with a smoothly-limited jerk (Fig. 4b) is performed. Table 1 summarizes the Z-axis movement parameters in the acceleration section and the resulting servo error values.

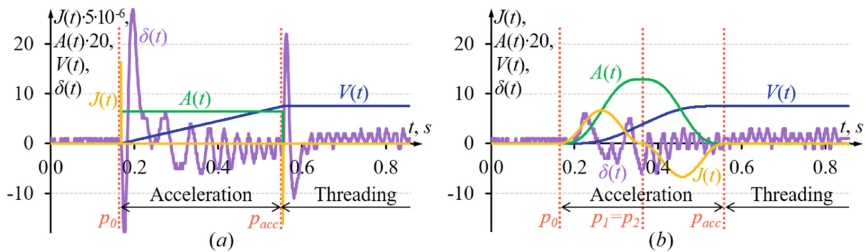


Fig. 4. Longitudinal axis servo error $\delta(t)$: (a) using the uniformly accelerated motion model; (b) using the model with smoothly-limited jerk S-shaped feedrate profile.

Table 1. The longitudinal axis movement parameters in the acceleration section

	Unit	Linear	S-shape
Acceleration stage duration	s	0.39	0.39
Threading federate	m/min	7.5	7.5
Maximum acceleration	m/s ²	0.325	0.65
Maximum jerk	m/s ³	325000	7
Maximum servo error at acceleration stage	μm	27	6
Maximum servo error at threading stage	μm	22	3

As expected, when applying a uniformly accelerated motion (Fig. 4a), servo error $\delta(t)$ occurs after a sharp variation in acceleration at the beginning of the acceleration section (p_0) and after it is completed (p_{acc}). At the beginning, the servo error reaches values of $-17 \dots +27 \mu\text{m}$, but this does not affect the machining accuracy, since there is no contact with the workpiece in this position. After the acceleration is completed, and threading is beginning, the servo error reaches values of $-11 \dots +22 \mu\text{m}$, which directly affects the machining accuracy. For this reason, most CNC system manufacturers recommend that the thread start point (Fig. 1a, pos. 3) be set outside the workpiece, which cannot always be done due to the nature of the workpiece design. In addition, this nature of the movement has a negative effect on the equipment, as it increases its wear and tear.

When the model with a smoothly-limited jerk S-shaped feedrate profile (Fig. 4b) servo error $\delta(t)$ is applied, the behavior of the error changes significantly. At the initial stage of acceleration outside the workpiece, servo error oscillations occur within $\pm 6 \mu\text{m}$.

By the end of acceleration before proceeding to threading, the value of servo error stabilizes at the level of $-1 \dots +3 \mu\text{m}$, which corresponds to its value in the steady-state. This allows to set the start point of the thread (Fig. 1a, pos. 3) directly on the part and facilitates the execution of technological operations for processing parts with a limited length of the acceleration section. In addition, the smooth motion reduces wear and tear, extending the life of the equipment.

Based on the results of the investigation, the proposed model S-shape feedrate profile with a smoothly-limited jerk for synchronization of threading movements was implemented into the production. In Fig. 5a shown the process adjustment the left-hand worm screw manufacturing, and in Fig. 5b – examples of manufactured parts.

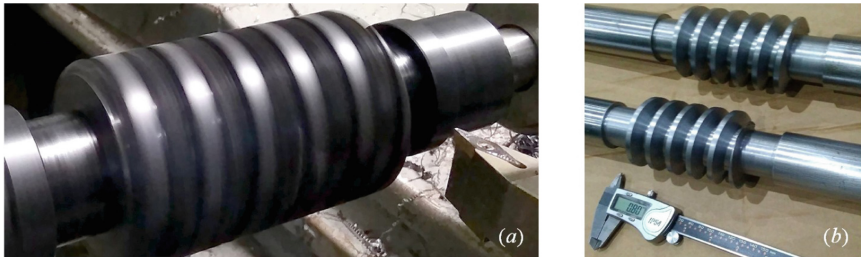


Fig. 5. Worm screw manufacturing: process adjustment (a) and manufactured parts (b).

6 Conclusion

The paper considers the urgent problem of increasing the accuracy of equipment when synchronizing the tool movement with the position of the spindle in CNC.

Mathematical models of movement at the acceleration stage of the longitudinal axis synchronized with the spindle have been developed. Models based on uniformly accelerated motion and motion with a smooth change in differential characteristics such as speed, acceleration and jerk are considered. A parameters necessary to set the movement in the acceleration section has been determined, taking into account the limitations of the amount of data transmitted to the controlled axle controller module.

The problem of axis acceleration at synchronized movement on a section of a given length with the implementation of an S-shaped profile are solved. S-shaped profile with using the \sin^2 function is applied. The proposed model provides acceleration to the required speed in a section of a given length, regardless of the actual spindle speed. The proposed model, in comparison with the uniformly accelerated motion model, provides a reduction in the positioning error at the threading stage from $22 \mu\text{m}$ to $3 \mu\text{m}$ and facilitates the execution of technological operations with a limited length of the acceleration section. The calculating complexity of the proposed algorithm is commensurate with the complexity of the algorithm for uniformly accelerated motion. The proposed model is implemented in the CNC and in the manufacturing process.

References

1. Dayong, T., Yu, Z., Wannian, L.: Simulation analysis and test of the thread joint of high strength directional drill pipe with large through hole. *J. Phys: Conf. Ser.* **1314**, 012115 (2019). <https://doi.org/10.1088/1742-6596/1314/1/012115>
2. Siora, O.V., Bernatskiy, A.V.: Development of basic processing methods of laser welding of joints of dissimilar metals. *Metallofiz. Noveishie Tekhnol.* **33**, 569–576 (2011)
3. Shupikov, A.N., Smetankina, N.V.: Non-stationary vibration of multilayer plates of an uncanonical form. the elastic immersion method. *Int. J. Solids Struct.* **38**(14), 2271–2290 (2001). [https://doi.org/10.1016/S0020-7683\(00\)00166-9](https://doi.org/10.1016/S0020-7683(00)00166-9)
4. Pavlenko, D., Dvirnyk, Y., Przysowa, R.: Advanced materials and technologies for compressor blades of small turbofan engines. *Aerospace* **8**(1), 1–16 (2021). <https://doi.org/10.3390/aerospace8010001>
5. Dodok, T., Čuboňová, N., Císar, M., et al.: Influence of CNC milling strategies on complex surface machining. In: *IOP Conference Series: Materials Science and Engineering*, vol. 776, no. 1, p. 012002 (2020). <https://doi.org/10.1088/1757-899X/776/1/012002>
6. Trykoz, L., Kamchatnaya, S., Pustovoitova, O., Atynian, A.: Reinforcement of composite pipelines for multipurpose transportation. *Trans. Probl.* **13**(1), 69–79 (2018). <https://doi.org/10.21307/tp.2018.13.1.7>
7. Kondratiev, A., Pštěk, V., Purihina, S., et al.: Self-heating mould for composite manufacturing. *Polymers* **13**(18), 3074 (2021). <https://doi.org/10.3390/polym13183074>
8. Djurdjanovic, D., Mears, L., Niaki, F.A., et al.: State of the art review on process, system, and operations control in modern manufacturing. *J. Manuf. Sci. Eng.* **140**(6), 061010 (2018). <https://doi.org/10.1115/1.4038074>
9. Dobrotvorskiy, S., Basova, Y., Dobrovolska, L., Sokol, Y., Kazantsev, N.: Big challenges of small manufacturing enterprises in industry 4.0. In: Ivanov, V., Trojanowska, J., Pavlenko, I., Zajac, J., Peraković, D. (eds.) *DSMIE 2020. LNME*, pp. 118–127. Springer, Cham (2020). https://doi.org/10.1007/978-3-030-50794-7_12
10. Kombarov, V., Kryzhyvets, Y., Biletskiy, I., et al.: Numerical control of fiberglass pipe bends manufacturing. In: *2021 IEEE 2nd KhPI Week on Advanced Technology*, pp. 357–362. IEEE, Kharkiv (2021). <https://doi.org/10.1109/KhPIWeek53812.2021.9570068>
11. Kombarov, V., Tsegelnyk, Y., Plankovskyy, S., et al.: Investigation of the required discreteness of interpolation movement parameters in cyber-physical systems. *Period. Polytech. Mech. Eng.* **66**(1), 1–9 (2022). <https://doi.org/10.3311/PPme.17884>
12. Pliuhin, V., Sukhonos, M., Bilecki, I.: Object oriented mathematical modeling of electrical machines. In: *2020 IEEE 4th International Conference on Intelligent Energy and Power Systems*, pp. 267–272. IEEE, Istanbul (2020). <https://doi.org/10.1109/IEPS51250.2020.9263158>
13. Zablodskiy, M., Gritsyuk, V., Pliuhin, V., Biletskiy, I.: The surface characteristics features of the electromagnetic field of the rotor of a polyfunctional electromechanical converter. In: *2021 International Conference on Electrical, Computer, Communications and Mechatronics Engineering (ICECCME)*, pp. 1–5. IEEE, Mauritius (2021). <https://doi.org/10.1109/ICECCME52200.2021.9590872>
14. Kurin, M.O., Surdu, M.V.: The concept of the mechanism and kinetics of influence of mechanochemical processes on edge cutting machining. *Metallofiz. Noveishie Tekhnol.*, **39**(3), 401–424 (2017). <https://doi.org/10.15407/mfint.39.03.0401>
15. Chen, Y., Ji, X., Tao, Y., Wei, H.: Look-ahead algorithm with whole S-curve acceleration and deceleration. *Adv. Mech. Eng.* **5**, 974152 (2013). <https://doi.org/10.1155/2013/974152>
16. Qin, Q., Huang, J., Yao, J.: A real-time adaptive look-ahead speed control algorithm for FDM-based additive manufacturing technology with Hbot kinematic system. *Rapid Prototyping J.* **25**(6), 1095–1107 (2019). <https://doi.org/10.1108/RPJ-11-2018-0291>

17. Erkorkmaz, K., Altintas, Y.: High speed CNC system design. Part I: jerk limited trajectory generation and quintic spline interpolation. *Int. J. Mach. Tools Manufact.* **41**(9), 1323–1345 (2001). [https://doi.org/10.1016/S0890-6955\(01\)00002-5](https://doi.org/10.1016/S0890-6955(01)00002-5)
18. Liu, Q., Liu, H., Yuan, S.: High accurate interpolation of NURBS tool path for CNC machine tools. *Chin. J. Mech. Eng.* **29**(5), 911–920 (2016). <https://doi.org/10.3901/CJME.2016.0407.047>
19. Fan, W., Gao, X.S., Yan, W., Yuan, C.M.: Interpolation of parametric CNC machining path under confined jounce. *Int. J. Adv. Manufact. Technol.* **62**(5), 719–739 (2012). <https://doi.org/10.1007/s00170-011-3842-0>
20. Lee, A.C., Lin, M.T., Pan, Y.R., Lin, W.Y.: The feedrate scheduling of NURBS interpolator for CNC machine tools. *Comput. Aided Des.* **43**(6), 612–628 (2011). <https://doi.org/10.1016/j.cad.2011.02.014>
21. Ni, H., Yuan, J., Ji, S., et al.: Feedrate scheduling of NURBS interpolation based on a novel jerk-continuous ACC/DEC algorithm. *IEEE Access* **6**, 66403–66417 (2018). <https://doi.org/10.1109/ACCESS.2018.2813334>
22. Kombarov, V., Sorokin, V., Fojtů, O., et al.: S-curve algorithm of acceleration/deceleration with smoothly-limited jerk in high-speed equipment control tasks. *MM Sci. J.* **2019**(04), 3264–3270 (2019). https://doi.org/10.17973/MMSJ.2019_11_2019080
23. Nittler, K.M., Farouki, R.T.: A real-time surface interpolator methodology for precision CNC machining of swept surfaces. *Int. J. Adv. Manufact. Technol.* **83**(1–4), 561–574 (2015). <https://doi.org/10.1007/s00170-015-7552-x>
24. Zhong, W., Luo, X., Chang, W., et al.: A real-time interpolator for parametric curves. *Int. J. Mach. Tools Manufact.* **125**, 133–145 (2018). <https://doi.org/10.1016/j.ijmachtools.2017.11.010>
25. Aksonov, Y., Kombarov, V., Fojtů, O., et al.: Investigation of processes in high-speed equipment using CNC capabilities. *MM Sci. J.* **2019**(04), 3271–3276 (2019). https://doi.org/10.17973/MMSJ.2019_11_2019081
26. Aksonov, Y., Kombarov, V., Tsegelnyk, Y., et al.: Visualization and analysis of technological systems experimental operating results. In: 2021 IEEE 16th International Conference on Computer Sciences and Information Technologies (CSIT), vol. 2, pp. 141–146. IEEE, Lviv (2021). <https://doi.org/10.1109/CSIT52700.2021.9648592>
27. Kombarov, V., Sorokin, V., Tsegelnyk, Y., Plankovskyy, S., Aksonov, Y., Fojtů, O.: S-shape feedrate scheduling method with smoothly-limited jerk in cyber-physical systems. In: Ciobotă, D.D. (ed.) *ICoRSE 2021*. LNNS, vol. 305, pp. 54–68. Springer, Cham (2022). https://doi.org/10.1007/978-3-030-83368-8_6
28. Huang, J., Lu, Y., Zhu, L.M.: Real-time feedrate scheduling for five-axis machining by simultaneously planning linear and angular trajectories. *Int. J. Mach. Tools Manuf.* **135**, 78–96 (2018). <https://doi.org/10.1016/j.ijmachtools.2018.08.006>
29. Sun, Y., Jia, J., Xu, J., et al.: Path, feedrate and trajectory planning for free-form surface machining: a state-of-the-art review. *Chin. J. Aeronaut.* **35**(8), 12–29 (2022). <https://doi.org/10.1016/j.cja.2021.06.011>

Smart City



World Experience of Smart City Development

Tetiana Pushkar^(✉) , Daria Serogina , Krystyna Mykhailova ,
Hanna Zhovtyak , and Hanna Sobolieva

O. M. Beketov National University of Urban Economy in Kharkiv,
17 Marshala Bazhanova Street, Kharkiv 61002, Ukraine
Tetyana.Pushkar@kname.edu.ua

Abstract. The concept of urban development is becoming a central idea of urban development in the active form of the information society. Accelerating digital transformation processes, the development of information and communication technologies will replace a significant number of processes of the urban environment, urban management, living conditions, and the use of urban services. The paper aims to analyze the world experience of smart city growth, approaches to assessing and ranking cities according to the degree of development of components that define the city as “smart”, as well as taking into account such experience in building the smart city development strategies in Ukraine. An analysis of world experience has indicated that the main factor in ensuring the success of US cities as “cities of the future” is considered by most researchers to be information and communication technologies. The study considers the first attempt to estimate and build a ranking list of smart cities. Based on which invention processes, best practices, and implementation measures will contribute to their further development. IMD and the Singapore University of Technology and Design (SUTD) have suggested the Global Smart City Index (SCI), which is designed to measure a balanced strategy to the economic and technological aspects of smart cities and more humanitarian dimensions of urban life. The study presents an overview of the central segments of SCI, the main aspects of the survey methodology in its formation, the division of cities into groups for the development of components of a Smart City.

Keywords: Smart city · Sustainable development · Urban development · The global index of smart cities · Development strategies · Digital environment

1 Introduction

The development of the concept of smart cities is an integral part of sustainable regional development. The modern city, along with the active development of digital infrastructure involves the creation of systems for the integration of urban development management with high-tech production and high-tech systems to ensure the livelihood of cities. To address pressing urban issues, local governments around the world have adopted smart metropolis programs. They promote digital technologies to optimize urban governance and interaction between government and non-government actors in the pursuit of

sustainable development [1]. Smart governance acts as a socio-technical approach that reconciles technological potential with new forms of cooperation between local authorities and citizens to solve urban problems based on the principles of sustainability [2, 3]. However, research on the concept of smart cities should move away from the contextual understanding of smart governance, as different spatial conditions have different urban priorities and circumstances that cause different dynamics of joint governance with the support of information and communication technologies [4].

Considering the wide range of research on smart cities, and substantiation of strategies for their development in Ukraine, it should be noted that to a large extent the study of Ukrainian authors reflects the basic approaches and principles of smart cities that define this concept in the world. The definition of a smart city is mainly based on its features, such as the integration of information and communication technologies with urban systems, the creation of innovative infrastructure, improving the quality of life based on them, and they promote sustainable development. McKinsey Global Institute, defines the concept of a smart city as a highly intelligent integrated city, characterized by a combination of technologies that stimulate the integration of social environment and entrepreneurship, emphasizing the integration of urban systems with modern trends in technological development [5]. Experts at Vienna University of Technology: European Smart Cities in developing smart city concepts focus on the fact that such a city combines competitive attractiveness and sustainable development, or “a city where new infrastructure links combine energy, transport and communication” [6]. Smart cities are testing grounds for the EU for measures that can stimulate employment growth because that is where digital technologies can be combined with innovative infrastructure and new services [7]. The possibilities of smart cities in the formation of new approaches to the creation of relevant and modern systems of integration of urban systems are especially emphasized at this stage of their development. Smart cities are fast-growing cities that capture the field for new experiments in several important areas, from urban planning, sustainable energy, and transport strategies to social inclusion and talent mobilization [8]. However, in the context of the formation of smart cities in Europe in the current digitalization of society and the dimensions of integration, the implementation of smart cities in the “old” cities is becoming increasingly important. The problem of managing the involvement of participants in the formation of a smart old town in the context of cultural heritage has a special sound in this aspect [9]. Undoubtedly, the issues of integration of the latest digital technologies and urban systems with the preservation of historical and cultural heritage are of great relevance for the cities of Ukraine. The combination of cultural, sociological, economic, and technological aspects is a prerequisite for the successful implementation of the concept of smart cities. A vital issue in the implementation of smart city development strategies is the perception of the latest changes by city residents. The comfortable digital environment of the city is, first of all, the attitude and the possibility to include and use all the advantages of a smart city by its inhabitants. This study is devoted to the implementation of strategies for the development of smart cities and attempts to assess the development of these processes through the prism of their perception by city residents.

2 World Experience in the Expansion of Smart Cities

The debate over the future of urban development in many Western countries is increasingly influencing the discussion of smart cities.

The European Economic and Social Committee in its research on the development of smart cities determines that the sustainability of cities will be the result of a smart combination of more mature and inventive technologies, integrated (European, national and local) platforms, modern infrastructure, energy efficiency, more efficient services tailored to needs. Population and users [6].

The tendencies of recent years in smart city initiatives in the world, identify the main opportunities and issues that have been accessed and data collection, the usefulness of such initiatives for consumers, and the economic viability of such solutions [10]. Another trend in determining the development of smart city strategies, which outlines the possibility of their implementation are role and expansion of systems for measuring the effectiveness of management technologies and government programs [11]. Along with the technical, technological, organizational, and managerial aspects of the functioning of smart cities, it is impossible to deny the importance of spatial expansion and regional features. The spatial and socio-economic context, which is seen as a major driver of organizational innovation, can be particularly vital for cities. Cities, as dense agglomerations with economic entities, concentrated skilled human capital, and developed infrastructure, are often associated with innovation [12]. The experience of the formation of smart Swiss cities shows that the availability of research institutions and the high density of cities are crucial for their development, whereas population, new housing, and participation in international networks seem less critical [13].

Recent studies of smart city development strategies demonstrate some division in queries that question whether smart city development should be based on: a technological or holistic strategy; model of cooperation; top-down or bottom-up approach; or one-dimensional or integrated logic of interference in processes. The example of European cities (Amsterdam, Helsinki, Barcelona and Vienna) provides an opportunity to identify several ideas about what strategic principles guide the development of smart cities in Europe [14]. The main focus is on the maturity of transparency of open data systems in smart cities, which are seen as a basis for supporting the emergence of sustainable, interest-oriented residents of smart cities [15]. Examples of the experience of smart cities in Europe are the cities of Spain, where the government promotes urban development in the direction of digital transformation, integration of the Internet of Things (IoT), and improving the social cohesion of residents. Areas of action for the implementation of strategies conducted in the European metropolis focus on a holistic approach and specialization (tourism or intelligent buildings), modern technology, software, and digital management [16].

The experience of its closest neighbor, Poland, is important for Ukraine. Poland's experience in implementing the smart cities strategy includes gradual adaptation processes and new forms of urban policy. Smart cities, in the case of the Polish practice act, are a form of urban policy that has emerged and reflects the tension between contemporary and more traditional forms of urban governance and economic, environmental, and social pursuits [17].

The current debate on smart cities is increasingly concentrated on the relationship between knowledge and communication technologies and sustainability, mainly in connection with the current configuration of cities in the so-called “smarting” process [18]. Based on existing concepts of cooperation and participation in the field of smart city, an example of how information and communication technologies can promote joint governance in the city and increase participation and involvement of its residents in urban development, we can identify three Brazilian cities that manage municipal operations centers to “become smarter”: Rio de Janeiro, Porto Alegre and Belo Horizonte [19].

Smart city modeling introduces an emphasis on the static e-government policy to pragmatic IoT (Internet of Things) solutions that are constantly dynamic in response to citizens and the environment [20]. More and more regions of the world are focusing on high-tech cities as drivers of economic growth. An illustration of understanding the importance of implementing the concept of smart cities as “growth points” is Cape Town (South Africa). As a smart city, Cape Town can contribute to the socio-economic growth of Africa by adopting the principles of the Smart Africa Manifesto for Socio-Economic Development [20].

Within the framework of the initiatives of the European Economic and Social Committee (EESC) on the development of smart city strategies, the Smart Islands Project is being executed, which has launched a study of trends in the evolution of smart specialization in Europe. In 2015 and 2016, a delegation of EESC members will carry out fact-finding missions to six EU islands. The project focuses on the island of Ile d’Ye in France, Mallorca in Spain, Favignana in Italy, Samsa in Denmark, Kifnos in Greece, and Saaremaa in Estonia.

The EESC noted the development of big data in tourism and the QR project in emergencies in Mallorca, the online community in Samsa, virtual service and services for the elderly in Saaremaa, and the smart Marina Ahoy solution for small ports in Estonia [21].

The EESC has overseen several initiatives, such as the offshore wind farm and the reduction of traffic on the island of Ile; solar energy, energy efficiency, and sustainable mobility in Favignana, use of straw from local farms for collective heating systems on Samsa, foreword of renewable energy sources in the energy complex on Kitnos, Samsa Energy Academy, public fountains with filtered water to prevent plastic waste and plastic waste the area of the Egadi Islands [21].

The Smart Islands initiative later became part of the EU’s Smart Cities projects. The Smart Cities project is a follow-up to the conclusion of the European Economic and Social Committee (EESC) on smart cities as a driving force for the new European industrial policy, adopted in July 2015. Smart cities can be a driving force for the development of new European industrial policies that can influence the development of specific manufacturing sectors, greatly expanding the benefits of the digital economy. To achieve this, the EESC notes the maximum approximation to the development model, which is more perfect and efficient than those used so far [7]. The initiative examined the implementation of the “Smart City” strategy in the sample of two cities – Lisbon (Portugal), and La Rochelle (France) [22].

The World Economic Forum, in collaboration with the President of the G20, will lead a new global effort to establish universal standards and guidelines for smart city

technology. One of the directions in the construction of the Global Smart Cities Alliance will focus its efforts on expanding the use of technology in public places and encouraging the basic principles of sustainable urban development, including transparency, confidentiality, and security [23].

The growth of smart cities as a global procedure, despite the common approaches to the main components, has its regional features.

In 2017, two institutions, IMD and Singapore University of Technology and Design (SUTD), decided to join forces to create a Smart City Index (SCI). At the moment, this is the first attempt to evaluate and build a ranking list of smart cities, based on which to identify those innovative processes, best practices, and implementation measures that will contribute to the further development of these processes. SCI is a global index designed to assess a balanced view of the economic and technological aspects of smart cities, on the one hand, and the more humanitarian measurements of urban life, such as quality of life and inclusiveness, on the other. Based on the rating and its associates, a rating of 118 cities around the world is formed (Table 1).

Table 1. Rating scale of smart cities according to the IMD methodology and Singapore University of Technology and Design (SUTD) (according to [24]).

No	Group	Quartile	Scale
1	Groups 1	The highest quartile	AAA-AA-A-BBB- BB
2	Groups 2	Second quartile	A-BBB- BB-B- CCC
3	Groups 3	The third quartile	BB-B- CCC-CC-C
4	Groups 4	The lowest quartile	CCC-CC-C-D

The methodology of evaluation and rating construction includes:

- each city belongs to one of the four groups, based on the values obtained;
- ratings for each city are calculated based on the correlation of the city relative to another city in the group;
- IMD-SUTD Smart City Index (IMI-SUTD) measures residents’ perceptions of issues related to the structures and technologies available to them in their city;
- assessment is based on the perception of certain factors 120 inhabitants of each city.
- two components are identified that require perception from residents: the first component – “Structure”, which relates to existing urban infrastructure, the second – “Technology”, which reveals the development of technologies and their implementation in the city, a description of technological support and services available for residents;
- each level is assessed in five key areas: health and safety, mobility, activities, opportunities, and governance;
- the final score for each city is calculated by the perception of residents of their city in all components and key areas [24].

Cities are divided into four groups based on the United Nations Human Development Index (HDI). In each HDI group, cities are allocated a “rating scale” (from AAA to D)

based on the assessment of the perception of the city resembled the assessments of all other cities in the same city.

In 2021, IMD-SUTD experts identified a smart city as “an urban environment that uses technology to increase the benefits and reduce the disadvantages of urbanization for its citizens.” According to the data, access to better air quality and medical services has become a priority in such smart cities around the world after the outbreak of the pandemic [24]. In 2021, the first three areas on the SCI IMD-SUTD were Singapore (first place), Zurich (second place), and Oslo (third place) (Table 2).

Table 2. Top ten cities according to the SCI IMD-SUTD index in 2021.

Place in the ranking	City	Smart City rating 2021	Structure	Technologies	Smart City rating 2021
1	Singapore	AAA	AAA	AAA	1
2	Zurich	AA	AAA	A	3
3	Oslo	AA	AAA	A	5
4	Taipei	A	A	A	8
5	Lausanne	A	AAA	A	new
6	Helsinki	A	AA	A	2
7	Copenhagen	A	AA	A	6
8	Geneva	A	AA	A	7
9	Auckland	A	A	A	4
10	Bilbao	BBB	A	BBB	24

Let’s consider how the main expansion trends are outlined and the level of SCI IMD-SUTD for leading cities is determined. In assessing the development of the processes of becoming a smart city, the answers to the questions asked to all respondents in Singapore were distributed as follows:

- are you ready to provide personal information to improve congestion? (67.3%);
- are you comfortable using face recognition technology to reduce crime? (73.0%);
- do you think that the availability of information on the Internet has supplemented your trust in the authorities? (75.3%);
- the share of your daily payment transactions that are non-cash (67.9%).
- In Zurich, respondents answered as follows:
 - are you ready to provide personal information to improve congestion? (69.4%);
 - are you comfortable using face recognition technology to reduce crime? (59.9%);
 - do you think that the availability of data on the Internet has increased your trust in the authorities? (68.1%);
 - the share of your daily payment transactions that are non-cash (73.4%).

Table 3. Assessment by Kyiv respondents of the factors of the “Structure” component in the assessment of SCI IMD-SUTD in 2021 [16] (summarized by the authors).

No	The evaluating factor	Percentage of positive feedback from respondents
Health and safety		%
1	Basic sanitation meets the needs of the poorest areas	68,1
2	Satisfaction with waste recycling services	73,2
3	Public safety is not an issue	57,8
4	Air pollution is not a problem	41,3
5	Providing medical ambassadors is satisfactory	82,6
6	Finding a home with a rent of 30% or less of your monthly salary is no problem	23,6
Mobility		
1	Congestion is not a problem	36,0
2	Public transport is satisfactory	59,9
Activity		
1	Greenery is satisfactory	70,7
2	Cultural events (shows, bars, museums) are satisfactory	66,4
Opportunity (work and study)		
1	Job search services are affordable and easy	58,5
2	Most children have access to good schools	69,4
3	Local educational institutions provide lifelong learning	53,8
4	Businesses are creating new jobs	55,4
5	Any minority feels comfortable and has equal conditions	56,7
Management		
1	Information on local government is available and open	57,4
2	The corruption of city officials is not a cause for concern	50,0
3	Residents contribute to local government decision-making	53,2

Among the 118 cities in the world, which were rated by the SCI IMD-SUTD rating, the rating comprised only one city in Ukraine - Kyiv, which took 82nd place in the ranking.

Thus, the modern world, given the growth of urbanization and the development of urban agglomerations, is evolving into a world of “smart cities”. Each city, taking into account general trends, has its exceptional features and certain priorities for development and digital modification, which can be a useful experience for the execution of processes for the “smart specialization” of cities in Ukraine.

3 Mechanisms for Implementing Smart City Development Strategies

As it was mentioned before, only one Ukrainian city, Kyiv, was included in the IMD-SUTD Smart City Index (SCI IMD-SUTD). The functions defined during the rating and the built profiles of cities are a certain tool for substantiating strategies for the formation of smart cities, determining organizational measures, as they outline problematic issues from the point of view of residents.

The rating was determined, as mentioned above, for the assessment of the two components “Structure” and “Technology”. The most complicated issues in the segment “Structure” residents identified as air pollution, the ability to find housing with rent equal to 30% or less of monthly salary; significant traffic jams on streets and roads; corruption of city officials (Table 3).

The main complex issues in the component “Technology” respondents from among the residents of Kyiv identified: the available websites or applications that allow you to effectively control air pollution; car-sharing applications reduce congestion; bicycle rental has reduced congestion; public access to public finance information has reduced corruption; public participation in online voting and surveys of city governments and authorities has increased.

In Kyiv, respondents answered as follows:

- are you ready to provide personal data to improve congestion? (72.9%);
- are you comfortable using face recognition technology to reduce crime? (76.9%);
- do you think that the availability of information on the Internet has increased your trust in the authorities? (56.4%);
- the share of your daily payment transactions that are non-cash (69.0%) [16].

Compared to other cities in the ranking, Kyiv has a fairly low level of reviews by residents on trust in local councils and local self-government, significant problems in resolving traffic. The question “Congestion is not a problem” received the least number of positive answers from respondents.

Therefore, accomplishing comparative analysis and use of the IMI-SUTD SCI rating, in particular the survey methodologies offered in this rating, can be an influential tool for developing smart cities (Table 4).

The formation of smart cities is an objective process of information society development and significant transformations in economic processes. The fact that the capital of Ukraine was included in one of the first rankings of smart cities already serves as a certain indicator of the development of smart cities in the country. The concept of “Smart City” has been proclaimed in many cities of Ukraine (for example, Odesa, Kharkiv), but

Table 4. Assessment by Kyiv respondents of the factors of the “Technology” component in the assessment of SCI IMD-SUTD in 2021 [16] (summarized by the authors).

No	The evaluating factor	Percentage of positive feedback from respondents
Health and safety		%
1	Online reporting on city maintenance issues provides a quick solution	55,0
2	Websites or applications allow residents to easily distribute or sell things they no longer need	50,7
3	Free public WI-FI has improved access to city services	58,0
4	Surveillance cameras allow residents to feel safe	53,0
5	Websites or applications are available to effectively control air pollution	46,1
6	The organization of medical receptions online has improved access	63,1
Mobility		
1	Car-sharing applications have reduced congestion	43,4
2	Add that allow you to identify and route to free parking spaces reduce travel time	59,8
3	Bicycle rental has reduced congestion	48,6
4	Online timing and ticket sales have made it easier to use public transportation	70,0
5	The city provides information about traffic jams through mobile phones and applications	62,1
Activity		
1	Buying tickets for performances and museums online has made it easier to visit	83
Opportunity (work and study)		
1	Internet access to job lists made it easier to find a job	82,7
2	IT skills are provided in schools at a sufficient level	54,6

(continued)

Table 4. (continued)

No	The evaluating factor	Percentage of positive feedback from respondents
3	The online services provided by the city have facilitated the opening of new businesses	52,7
4	The current speed and reliability of the Internet meet the needs of the connection	74,1
Management		
1	Internet public access to information on city finances has reduced corruption	34,4
2	Public participation in online voting and polls by city governments and authorities has increased	48,6
3	There is an online platform where city residents offer ideas that improve their lives	54,7
4	Processing identity documents online has reduced waiting times	72,9

the level of evolution of these processes is still in the process of differing and identifying indicators that need to be evaluated. That is why the world experience, which concerns not only the tools for the formation of smart cities but also the assessment of the level of this development, can become the basis for the construction of approaches to assessment in Ukraine.

Using a methodology that evaluates leaders among intelligent cities who are pioneers in using the latest digital technologies of urban development, provides an opportunity not only to resemble the best examples but also to determine the experience that evolves into a driver of growth and can be successfully applied to Ukrainian cities.

4 Conclusion

The quickness of building smart cities for Ukraine shortly will only increase, which will be actively promoted by national processes of creating a digital society, the development of digital governance, and the establishing of a nationwide system of digital services for citizens. However, the understanding is that proclaiming the Smart City strategy does not always reflect the reality of constructing a smart city system. The world experience of consistent implementation of comprehensive procedures to the construction of urban smart techniques, their integration into city life, and the gradual perception of these strategies by city residents is not only useful for Ukrainian cities but can be the basis for long-term programs for smart cities in Ukraine implementation.

The modern city cannot be “smart”, the question arises only in the evolution of technologies that allow it to be smarter and effectively facilitate sustainable urban development, which is reflected in improving the living standards of residents. Effective tools

can be developed “solid” and “service” information and communication infrastructures, as well as tools that have already proven themselves in world practice: blockchain technology, the creation of municipal operations centers, and the use of digital twin cities. Instructing comparative analyzes with the world’s leading cities on the expansion of these processes can contribute to the formation of effective strategies for the development of “smart” cities, which can be facilitated by accomplishing regular surveys and analogizing the results of the SCI IMD-SUTD index.

Profitable areas of research in terms of implementing smart city strategies in Ukraine are the issue of constructing a favorable digital environment for urban residents, which addresses a wide range of social and economic issues.

References

1. Cimander, R., Royo, S., Yetano, A.: Citizen panels on climate targets: ecological impact at collective level. In: Aichholzer, G., Kubicek, H., Torres, L. (eds.) *Evaluating e-Participation*. PAIT, vol. 19, pp. 243–264. Springer, Cham (2016). https://doi.org/10.1007/978-3-319-25403-6_12
2. Meijer, A., Bolívar, M.P.R.: Governing the smart city: a review of the literature on smart urban governance. *Revue Int. des Sci. Adm.* **82**(2), 417–435 (2016). <https://doi.org/10.3917/risa.822.0417>
3. Meijer, A., Thaens, M.: Urban technological innovation: developing and testing a sociotechnical framework for studying smart city projects. *Urban Aff. Rev.* **54**(2), 363–387 (2018). <https://doi.org/10.1177-2F1078087416670274>
4. Tomor, Z., Meijer, A., Michels, A.: Smart governance for sustainable cities: findings from a systematic literature review. *J. Urban Technol.* **26**, 3–27 (2019). <https://doi.org/10.1080/10630732.2019.1651178>
5. Woetzel, J., Remes, J., Boland, B., et al.: *Smart cities: Digital solutions for a more livable future*. McKinsey Global Institute (2018). <https://www.mckinsey.com/business-functions/operations/our-insights/smart-cities-digital-solutions-for-a-more-livable-future>. Accessed 10 May 2022
6. Vienna University of Technology: *European Smart Cities* (2015). <http://www.smart-cities.eu>. Accessed 10 May 2022
7. European Union: Opinion of the European Economic and Social Committee on ‘Smart cities as drivers for development of a new European industrial policy (own-initiative opinion)’. Official Journal of the European Union, (2015). <https://eur-lex.europa.eu/legal-content/EN/TXT/?uri=CELEX%3A52015IE0586>. Accessed 04 May 2022
8. Bris, A., Cabolis, C., Chan, H.C., Lanvin, B.: *Sixteen Shades of Smart: How Cities Can Shape Their Own Future*. Institute for Management Development, Lausanne (2019)
9. Snis, U.L., Olsson, A.K., Bernhard, I.: Becoming a smart old town – How to manage stakeholder collaboration and cultural heritage. *J. Cult. Herit. Manag. Sustain. Dev.* **11**(4), 627–641 (2021). <https://doi.org/10.1108/JCHMSD-10-2020-0148>
10. Hasija, S., Shen, Z.J., Teo, C.P.: Smart city operations: modeling challenges and opportunities. *M&SON – Manufact. Serv. Oper. Manag.* **22**(1), 203–213 (2020). <https://doi.org/10.1287/MSOM.2019.0823>
11. Argento, D., Grossi, G., Jaaskelainen, A., et al.: Governmentality and performance for the smart city. *Acc. Audit. Acc. J.* **33**(1), 204–232 (2020). <https://doi.org/10.1108/AAAJ-04-2017-2922>

12. Bibri, S.E.: On the sustainability of smart and smarter cities in the era of big data: an interdisciplinary and transdisciplinary literature review. *J. Big Data* **6**(1), 1–64 (2019). <https://doi.org/10.1186/s40537-019-0182-7>
13. Duygan, M., Fischer, M., Pärli, R., Ingold, K.: Where do smart cities grow? The spatial and socio-economic configurations of smart city development. *Sustain. Cities Soc.* **77** (2021). <https://doi.org/10.1016/j.scs.2021.103578>
14. Mora, L., Deakin, M., Reid, A.: Strategic principles for smart city development: a multiple case study analysis of European best practices. *Technol. Forecast. Soc. Chang.* **142**, 70–97 (2019). <https://doi.org/10.1016/j.techfore.2018.07.035>
15. Orejon-Sanchez, R.D., Crespo-Garcia, D., Andres-Diaz, J.R., et al.: Smart cities' development in Spain: a comparison of technical and social indicators with reference to European cities. *Sustain. Cities Soc.* **81** (2022). <https://doi.org/10.1016/j.scs.2022.103828>
16. Lnenicka, M., Nikiforova, A., Luterek, M., et al.: Transparency of open data ecosystems in smart cities: definition and assessment of the maturity of transparency in 22 smart cities. *Sustain. Cities Soc.* **82**, 103906 (2022). <https://doi.org/10.1016/j.scs.2022.103906>
17. Masik, G., Sagan, I., Scott, J.: Smart city strategies and new urban development policies in the polish context. *Cities* **108**, 102970 (2021). <https://doi.org/10.1016/j.cities.2020.102970>
18. Bifulco, F., Tregua, M., Amitrano, C., D'Auria, A.: ICT and sustainability in smart cities management. *Int. J. Public Sect. Manag.* **29**(2), 132–147 (2016). <https://doi.org/10.1018/IJPSM-07-2015-0132>
19. Pereira, G., Cunha, M., Lampoltshammer, T., et al.: Increasing collaboration and participation in smart city governance: a cross-case analysis of smart city initiatives. *Inf. Technol. Dev.* **23**(3), 526–553 (2017). <https://doi.org/10.1080/02681102.2017.1353946>
20. Arnardu, A.N., Francke, E.: Cape town: a smart city for African socio-economic development. *Suid-Afrikaanse Tydskrif vir Natuurwetenskap en Tegnologie* **40**(1), 140–148 (2022). <https://doi.org/10.36303/SATNT.2021.40.1.843>
21. European Economic and Social Committee: TEN Section Report on the Smart Islands: Project (2015). <https://www.eesc.europa.eu/our-work/publications-other-work/publications/ten-section-report-smart-islands-project#downloads>. Accessed 10 May 2022
22. European Economic and Social Committee. Smart Cities Project – Related Events (2015). <https://www.eesc.europa.eu/en/our-work/publications-other-work/project/smart-cities-project/events>. Accessed 10 May 2022
23. World Economic Forum: An unprecedented Global Alliance for Smart City Technology Launched to Counter Rising Tensions (2019). <https://www.weforum.org/press/2019/06/world-economic-forum-to-lead-g20-smart-cities-alliance-on-technology-governance>. Accessed 10 May 2022
24. IMD: Smart City Observatory. <https://www.imd.org/smart-city-observatory/home>. Accessed 10 May 2022



Perspectives on Socially and Environmentally Just Circular Cities: The Case of Naples (Italy)

Patrizia Ghisellini¹  , Renato Passaro¹ , and Sergio Ulgiati^{1,2} 

¹ University of Naples Parthenope, 80 Via Ammiraglio Ferdinando Acton,
80133 Naples, Italy

patrizia.ghisellini@uniparthenope.it

² Beijing Normal University, 19 Xinwai Avenue, Beijing 100875, China

Abstract. This study starts by evaluating the evolution and current state of the concept of circular city. The latter can be included within a wider window of urban brandings which share in common the visions and applications in cities of more sustainable patterns. We adopted a multiple case study approach to evaluate the adoption of the concept of circular city in Naples. Some organizations located in such area have been selected as they are performing diverse and innovative practices of CE that we framed within the interpretative model of circular development by Williams (2021). Naples has already defined its vision of smart city but lacks of a circular city vision. The results of this study could provide useful insights to the policy makers of the city as well as contribute to the existing research. The analyzed organizations with their CE practices improve the local environment and generate social development promoting much radical models and visions of CE applications in cities. The case studies instill of new opportunities the CE transition in cities suggesting to look at beyond its conventional mindset in waste management and recycling model and showing its potential in reducing the negative externalities of the linear and recycling models.

Keywords: Circular cities · Smart cities · Naples

1 Introduction

The concept of circular city has many theoretical and practical origins and can be traced back since to the principles of urban environmentalism emerged from the 1980s [1]. In this perspective, many developed urban brandings and experiences such as those about the eco-cities, eco-towns, sustainable cities, smart cities, resilient cities, low carbon cities, inclusive cities [2] reflect both the visions and variety of nuances and responses of cities towards the need for being more environmentally and socially sound [3]. Such models (in particular eco-cities and eco-towns) also underline the need for monitoring the input and output flows to better adapt cities to natural resource limits and prevent the generation of waste [1] and in so doing transitioning toward zero waste goals [4]. The concepts of smart cities and sustainable cities seem the most linked to the concept of circular economy [2, 3]. Both smart and circular urban systems share the need for cities

of being more sustainable [3] and suggest the optimization of resources use achieved by means of technological digital instruments [1]. Certainly, the concept of smart city is a precursor of the circular city concept as shown by the experience of Genova in Italy [5]. However, in the circular economy (CE) framework the digital instruments are only one of the factors characterizing such model. In parallel, the current debate on just CE transition and the contribution of CE to a sustainable human development and a more inclusive society [6] could be enablers for the smart cities concept to take into more account the effects of technologies on people and the social inequalities that could arise e.g. by the unequal access of people towards the digital technologies [7, 8]. The Just transition to CE stresses to look at the social changes embedded in the transition process and the associated technological changes giving attention to the issues of participation, democracy, decent and quality labor, gender, global justice and good quality of life.¹

A circular city seems oriented in matching the concept of sustainability in all its three dimensions as reflected in current indicatory frameworks that e.g. many European cities (e.g. Amsterdam, Rotterdam, Paris, London and so on) are adopting and developing [9–12]. The model of CE, in itself, requires a considerable change in how a society produces and consumes in order to transform existing unsustainable societal patterns [13] as well as how it values resources, goods, well-being of people and environment. Therefore, rethinking the concept of cities in a more circular way raises the concern of applying it thoroughly and radically in order for the CE to contribute to a just sustainable development [6, 14] and the environmental challenges ahead. The adoption of a model of CE mainly focused on recycling waste as a practice [15] probably could fail the opportunity of addressing the current global environmental goals and reduce the social inequalities of the current linear-recycling economy models [16]. CE practices such as reduction by design, reuse and repair are considered essential to reduce the extraction of raw materials [17] and the related social inequalities between exporting and importing countries [18, 19].

Large and small cities across the globe are implementing the CE in their visions and plans [11] and are showing that it is possible to expand the current focus on recycling waste towards other practices in the waste hierarchy, e.g., prevention, repair, reuse, refurbishing, energy efficiency and renewable energies, cleaner urban mobility, urban forestry and urban agricultural programs [20, 21]. The adoption of a circular approach for cities is also suggested as an opportunity of regeneration for cities against the unsustainable development and linear patterns of the past [22, 23]. The concept and the researches on urban mining, addressed to maximizes the economic value of the urban waste streams, are in line with the planning and designing of sustainable cities whereas they connect local material and energy loops [24].

The scientific community is trying to define a circular city, namely how could it be envisioned and approached by policy-makers [11], supporting them towards identifying tools and indicators appropriate to monitor the CE transition [9, 12]. In this regard, a circular city can be defined as a city that applies the CE principles (eliminate, circulate and regenerate in a participative way with all the city's stakeholders (e.g. public administrations, citizens, universities and research centers, private and non-profit organizations,

¹ JUST2CE, A Just Transition to Circular Economy, <https://just2ce.eu/>. Accessed 10 May 2022.

environmental and cultural associations) with the purpose of realizing a future city that strives for a better sustainability [1].

Concerns for the circular city are also emerging in the political-institutional realm. Highlighting that a growing number of cities and regions are actively testing and improving circularity in their urban activities, United Nations in 2016 started the United for Smart Sustainable Cities Initiative (U4SSC) which provide information exchange and partnership building towards circular cities. This initiative is in line with the UN 2030 Agenda for Sustainable Development with one of the 17 goals dedicated to sustainable cities (SDG1). In 2021 the European Union has launched the Circular Cities & Regions Initiative (CCRI), as part of the New Circular Economy Action Plan. Therefore, in this study our research aims are the following:

- evaluate an interpretative framework in the literature useful to study the development of CE in cities and apply it to a case study;
- explore the transition to the CE adoption in the city of Naples by means of some bottom-up initiatives (from civil society organizations) and mixed ones (participative public initiatives);
- evaluate qualitatively the potential environmental and social benefit of such initiatives to provide feedbacks to the policy-makers of the city;
- contributing to improve the current understanding of the circular development in Naples and the application of the concept of circular city [22, 25, 26];
- exploring the relationships between the concepts of smart city and circular city contributing with new insights to the current debate in the international literature [2].

2 Material and Methods

2.1 Circular Economy Transition in Italian Cities

Italy is currently highly committed in the scale-up of CE at different levels (macro, meso and micro). At macro level, some cities such as Milan, Prato and Bari² have been identified as pilot cities in the CE transition by the Ministry of Ecological Transition due to their dimension, particular experiences on the CE and geographical position. The city of Prato is partner of other European Cities within the EU Urban Agenda Partnership on Circular Economy. However, many other urban initiatives are flourishing and show how they are contributing positively to the well-being of the local communities creating a connection between place-based sustainability [27] and CE [28].

In this study, our aim is evaluating the transition to the model of circular city in Naples, that is the largest municipality in the Metropolitan area of Naples grouping a total number of 92 municipalities (Fig. 1). Naples is located in Campania Region in Southern Italy.

Naples has developed since the year of 2014 its vision of smart city in the areas of mobility, sustainable development, tourism identity, creative environment and innovation and strategic vision of the future. The city has not yet a specific plan for developing a

² Circular Economy City of Prato, <https://cittadiprato.it/EN/Sezioni/620/Circular-economy/>. Accessed 10 May 2022.

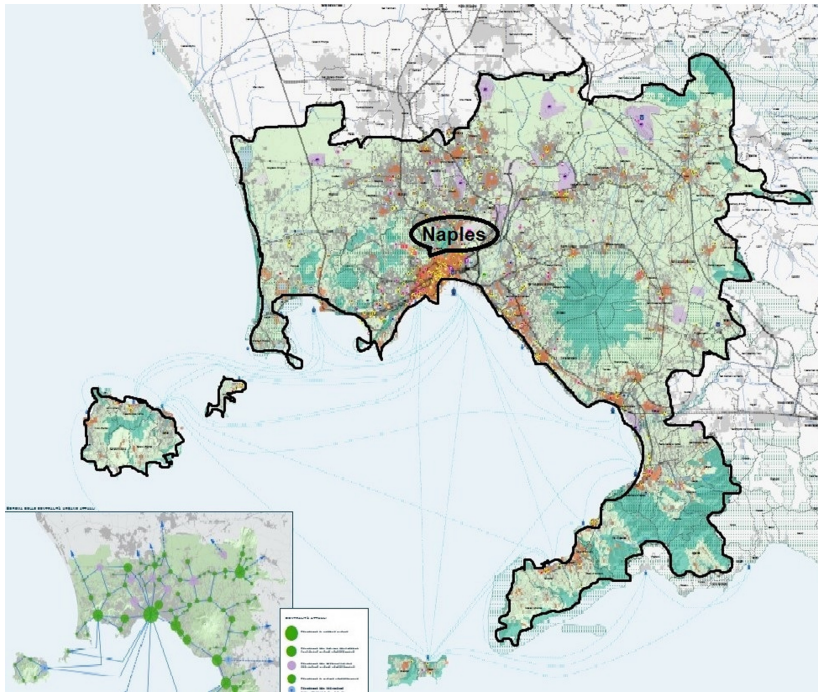


Fig. 1. Location of Naples and the metropolitan city of Naples.

circular city but it is currently participating to projects funded by the European Union about the development of CE in specific sectors. In particular, this year has started the project “Biocircular cities”³ which considers as pilot area the Metropolitan City of Naples (that also includes the city of Naples) and other two European cities: Barcelona (Spain) and Pazardzhik (Bulgaria). The three pilot cities aim to explore opportunities and challenges in closing the loops for municipal organic waste streams and local industrial agro-food and forestry sectors. The Metropolitan city of Naples has an important agro-food industry with many by products available for which to explore new circular and more sustainable businesses (such as those of the tomato, lemon, olive oil, wine processing industry). The project involves a consortium of organizations and administrations of the three areas. The ENEA (Italian National Agency for New Technologies, Energy and Sustainable Economic Development) research center of Naples is also part of the consortium. The final goal of this project is proposing new political instruments and roadmaps in the wider area of EU drawing insights from the experiences of the tree pilot areas.

In this study, we will show some further initiatives of CE in Naples performed by small organizations as the CE development also concerns grassroots initiatives contributing to add further insights to the existing research on the adoption of the circular city model in Naples [22, 25].

³ Biocircularcities, <https://www.bbi.europa.eu/projects/biocircularcities>. Accessed 10 May 2022.

The analyzed case studies comprise small entrepreneurs, environmental associations, and start-ups located in Naples. With such realities we have had the opportunity to collaborate in the last years in some research projects. The CE practices performed by them can be classified in different thematic areas drawing insight from the circular development model in cities proposed by [20] and described in the next section.

2.2 Research Method

As a first step in this study, we performed a literature review for searching in the recent literature an interpretative model useful to analyze the CE development of cities in a broader vision. We identified in the literature the model by [20]. Figure 2 shows that such model considers three types of actions (ecological regenerative, adaptive and looping). These can be performed in combination during the process of the circular development and their performances monitored in ecological, social and economic terms. Circular actions in the loop dimension are related to the repair, reuse, refurbishing, recycling and recover of waste resources whereas the ecologically regenerative actions entail e.g. the adoption of green infrastructures that contribute to regenerate the urban environment and its ecological functions. Finally, adaptive actions aim to render much adaptive the urban environment, its spaces and its communities to the changing needs of the city and the limits of the natural environment in order to be more resilient [20]. Then we adopted a multiple case study approach (by selecting four case studies involved in previous/current research projects of the authors) to collect data for evaluating the transition to a circular city in Naples. We combined both analysis of the documents provided by the founders/participants of the organizations and interviews to them. The last step has been the validation and discussion of the case studies results compared to the previous literature on circular economy, circular cities, smart cities.

3 Results and Discussion

The analysis of the development of the circular city model in Naples by means of the description of four case studies investigated evidences the following results in terms of adoption of CE practices and related social and environmental benefits.

3.1 Start-Up “Remade in Rione Sanità”: Local WEEE and Plastic Waste Recycling

Remade in Rione Sanità is a laboratory and a social enterprise that experiments innovative models for waste management at urban level combining innovation and technology, social development and environmental sustainability with the aim of creating both CE awareness and new forms of entrepreneurship linked to the CE.

Their activity consists in the collection and recycling of some type of plastic and waste electrical and electronic equipment (WEEE) components (e.g.: copper from cables and motherboard’s pin) in the urban area of Naples close to their laboratory. The goal of the latter is to propose a new and alternative local model of waste management and recycling compared to the existing one managed by the local public administrations.



Fig. 2. The classification of the circular economy implementation into three types of strategies: looping, ecologically regenerative and adaptive as suggested by the model of [20].

Such alternative model could be replicable and useful for creating a network of micro enterprises spread throughout the urban territory for a more decentralized and small-scale management of some type of waste. The recycling of plastic and e-waste in the local social enterprise overcome the transport of such type of waste over long distances due to the lack of recycling plants in the close proximities of Naples reducing the environmental impacts (energy consumption and CO₂ emissions) and the related social and economic costs (e.g., pollution, lost employment and development opportunities). Remade in Rione Sanità, with its economic activity, also contributes to the socio-economic development of a particular area of Naples suddenly renewed for criminal events in so avoiding its marginalization compared to the city centre.

3.2 “Fab Lab” in Naples

Fab Lab is the acronym of Fabrication Laboratory. The latter are composed of one room or more rooms or a building where the so-called makers manufacture or repair manufactured goods. In Naples and other Italian cities, the Fab Lab movement has launched their initiatives since the year 2010. Torino with “Stazione Futuro” in the year 2011 and Rome with “Makers!” in the year 2012 organized the first important events contributing to disseminate the knowledge about Fab Lab in the country [29]. The main idea at the centre of Fab Lab is contributing to the sharing of knowledge in the internet. They are strongly convinced that ideas have a public nature and do not have a private property as they grow and are improved by means of the contribution of the participants

to the Fab Lab who also can suggest the most adequate technologies or the use of open sources programs. The aim at the end is to realize the best final product within the cooperative efforts of the maker and the Fab Lab people [29].

The Fab Lab in Naples has been founded in 2013 and is a non-profit association of makers, professionals and companies performing the design, research and development of products and digital fabrication. The reference stakeholders are both public and private organization such as schools, universities, designers, architects, engineers, makers, programmers, artisans, university students, simply curious and DIY enthusiasts) who share their skills and the use of devices, machines and technologies available in the locals of the Fab Lab for the Digital Fabrication and the creation and shape of their ideas. The association gives a fundamental importance to the collaboration between the Fab Lab participants, the access to the technologies for the production, the sharing and the culture of doing as fundamental factors for the development of sustainable innovation.⁴

3.3 “Altra Napoli” Association: Regeneration of Buildings, Urban Lands and Life of Young People

Altra Napoli is a non-profit association founded in the year 2005 by a group of Neapolitan people who decided to commit themselves in relaunching and regenerating some most degraded areas of the city of Naples even if they no more live in that city. Since 2005 the association has received and invested 9 million euros developing more than 50 projects and involving about 1000 young people contributing to create work opportunities for many of them. The activities and goals of the association are centered on the regeneration of the endogenous resources of the territory of Naples, on the valorization of human capital and on the development of a social enterprise model. The activities of “Altra Napoli” consists in the following:

- developing urban regeneration projects in degraded areas of Naples with the goal of improving the well-being of residents and the cultural and social growth of youth people;
- create social entrepreneurial projects by means of the creation of cooperatives composed by youths;
- Valorize the talent of children by means of education, music and theater activities;

Among the 50 projects they developed so far, those related to the urban regeneration regard the creation of the Oranges Garden that is a green space located in the Rione Sanità area of the city open to children and their families. Such garden project is particularly important since the low availability of green spaces in such area of the city. Regeneration projects also involved the renovation of the seventeenth-century cloister and its current use as a meeting space for young people, the creation of a multifunctional space for children in the former sacristy of a church for after school activities and ludic-recreational laboratories, music and new technologies educational programs. Moreover, Altra Napoli also contributed to the recovery of San Gennaro catacombs and of the paleo-Christian Basilica of San Gennaro.

⁴ Fab Lab Napoli, <https://www.facebook.com/fablabnapoli>. Accessed 10 May 2022.

3.4 “Green Italia”: Green Mobility for 15 Minute-Naples

This association is involved in the cultural promotion of a renewal of the urban environment of the city of Naples. The future well-being of the city, is considered in fact by the Association very precarious without interventions aimed e.g. to reforest the city to prevent the further worsening of the so-called “island heat” effect. Without intervention the city risks of facing 55 days of extreme heat by 2049 which could almost double by 2081.

The association is also firmly convinced of the importance of reducing the vehicles traffic for improving the livability of Naples and shift toward the vision of Naples at 15 min as developed by Carlos Moreno. His approach is designing urban programs and policies having people rather than cars at the center who become the main actors in the urban transformation for better sustainability.⁵ At this regard, Green Italia evidence that past important events (e.g. G7 Summit and America’s Cup) provided the opportunity of adopting pedestrianization programs being very beneficial in reducing local pollution and smog as well as revitalizing Naples in the world aligning itself with the actions of other European Cities.

In this perspective, Green Italy is currently proposing more sustainable mobility alternatives in the plans of the local administration and supporting the pedestrianization project of the entire seafront to create a “green line” from the historic center to the sea part of the city.

3.5 “Urban Green Infrastructure” Project of Portici

The municipality of Portici, part of the Metropolitan City of Naples, has launched a new “Air Heritage” project that has been the winner of the European Call “Urban Innovative Actions”.

With “Air Heritage” Portici aims to improve the quality of the urban air environment by perceiving a reduction by 20% of particulate matter (PM₁₀ and PM_{2.5}), NO₂ (Nitrogen Dioxide), CO (Carbon Monoxide) and O₃ (Ozone) by means of different solutions such as soft mobility promoting the use of the so called “Pedibus” (Pedestrian Bus) in almost all the schools as well as encouraging at least the 20% of children to reach the schools by walking. The project also considers central the role of green infrastructures (such as urban forestry, parks and green gardens, urban kitchen garden, green facades and green roofs) in contributing to achieve the goals of pollution reduction. The innovation of the project is the involvement of the citizens in the planning of the urban green infrastructures of the city by means of the participatory maps tool. The latter supports the enhancement of the green infrastructures planning in quantitative (increasing the availability of green infrastructures) and qualitative terms paying attention to the methods of combination of trees and shrubs species, that will be also selected taking into account their capacity of pollutants removal and mitigation of the effects of climate change. Every citizen, by filling in a simple form online and selecting the reference place on the participatory map, can become a “guardian of the green”. The administrators of the city will evaluate all the proposals and suggestions from the citizens, their feasibility and the appropriate

⁵ The 15 min City, <https://www.15minutecity.com/>. Accessed 10 May 2022.

tools for implementing their suggestions. The project is realized with Legambiente, one of the main Italian environmental associations.

The environmental and social benefits of urban greening projects are well-known and studied by the international literature [30, 31]. For example, urban trees provide a wide range of ecosystems services as well as social, economic, health, visual and aesthetics benefits [31]. With regard to the ecosystem's services, they are related to a long list comprising carbon storing/sequestration, air quality improvement, storm water runoff reduction and improvement of water quality, energy use, habitat preservation and biodiversity, noise reduction, microclimate maintenance in buildings and in the urban environment. In this latter case, they play an important role in mitigating the so-called "heat island effect" in summer while they protect buildings from the cold wind in winter [30, 31].

Finally, with regard to the social benefits these projects contribute to enhance the liveability of people in cities creating a nicer and more inspiring urban environment where to live as well as work. They in fact contribute to increase the biodiversity in the urban context and create a sense of community for the urban dwellers. In that, urban trees and green areas also give to cities a high aesthetic, landscape and relational value since they represent key elements of spaces for socializing, relax, sports and recreation.

4 Conclusion

The goal of this study was showing and disseminating current experiences and alternative models of the CE development in cities unlocking its conventional mindset on waste management and recycling (performed in big plants located many kilometers outside the city), in that way improving the awareness of its potential to contribute to a place-based sustainable just development and giving better value on the quality of resources, materials and products rather than on their quantity.

We have chosen the city of Naples to improve our understanding of the circular development in cities by adopting a multi-case study approach of circular activities performed by some local organizations or within projects. Since 2014 Naples has been defined by the local municipality as a smart city with specific goals to achieve. Currently, Naples is also a pilot city with other two cities (Barcelona and Pazardzhik) in the European project "Biocircularcities" that aims to identify new development opportunities for unexploited streams of bio-circular processes and products as well as evaluate the main challenges in such development, their environmental and economic sustainability. The final goal is leverage lessons in developing new policy tools and roadmaps useful in the larger EU context.

The results of the multiple case study evidence that by developing looping activities at the local level of the city (e.g.: reuse/recycling WEEE to create new products) or refurbishing historical buildings, urban lands and spaces for youth development and employment, as well as strengthen the network of green mobility and infrastructures (by means of participative projects), the development of a broad vision of CE has the potential of rendering cities and their communities, infrastructures and spaces more adaptive to their changing needs and those of the natural environment, thus providing environmental, economic and social benefits for the city and its communities.

Acknowledgment. This research received funding from the European Commission's research programme Horizon 2020-SC5-2020-2 scheme, Grant Agreement 101003491 (JUST Transition to Circular Economy project).





References

1. Prendeville, S., Cherim, E., Bocken, N.: Circular cities: Mapping six cities in transition. *Environ. Innovation Soc. Transitions* **26**, 171–194 (2018). <https://doi.org/10.1016/j.eist.2017.03.002>
2. Crippa, J., Silva, M.G., Ribeiro, N.D., Ruschel, R.: Urban branding and circular economy: a bibliometric analysis. *Environ., Dev. Sustain.* 1–28 (2022). <https://doi.org/10.1007/s10668-022-02173-1>
3. Shukla, S., Hait, S.: Smart waste management practices in smart cities: current trends and future perspectives. In: Hussain, C., Hait, S. (eds.) *Advanced Organic Waste Management*, pp. 407–424. Elsevier, Amsterdam (2022). <https://doi.org/10.1016/B978-0-323-85792-5.00011-3>
4. Zaman, A.U., Lehmann, S.: The zero waste index: a performance measurement tool for waste management systems in a 'zero waste city.' *J. Clean. Prod.* **50**, 123–132 (2013). <https://doi.org/10.1016/j.jclepro.2012.11.041>
5. Del Borghi, A., et al.: Waste management in Smart Cities: the application of circular economy in Genoa (Italy). *Impresa Progetto Electron. J. Manage.* **4**, 1–13 (2014)
6. Schröder, P., Lemille, A., Desmond, P.: Making the circular economy work for human development. *Resour. Conserv. Recycl.* **156**, 104686 (2020). <https://doi.org/10.1016/j.resconrec.2020.104686>
7. Kolotouchkina, O., Barroso, C.L., Sánchez, J.L.M.: Smart cities, the digital divide, and people with disabilities. *Cities* **123**, 103613 (2022). <https://doi.org/10.1016/j.cities.2022.103613>
8. March, H.: The Smart City and other ICT-led techno-imaginaries: any room for dialogue with Degrowth? *J. Clean. Prod.* **197**, 1694–1703 (2018). <https://doi.org/10.1016/j.jclepro.2016.09.154>
9. Coleman, N., Fiorentino, G., Fotopoulou, S., et al.: A roadmap for the integration of assessment methods for the transition towards a Circular Economy. Deliverable D2.5 Retrace project, H2020 MSCA-ITN-2018 (2022)
10. Papageorgiou, A., Henrysson, M., Nuur, C., Sinha, R., Sundberg, C., Vanhuysse, F.: Mapping and assessing indicator-based frameworks for monitoring circular economy development at the city-level. *Sustain. Cities Soc.* **75**, 103378 (2021). <https://doi.org/10.1016/j.scs.2021.103378>
11. Paiho, S., et al.: Towards circular cities – Conceptualizing core aspects. *Sustain. Cities Soc.* **59**, 102143 (2020). <https://doi.org/10.1016/j.scs.2020.102143>
12. Fusco Girard, L., Nocca, F.: Moving towards the circular economy/city model: which tools for operationalizing this model? *Sustainability* **11**(22), 6253 (2019). <https://doi.org/10.3390/su11226253>
13. Bocken, N.M., Short, S.W.: Unsustainable business models – recognising and resolving institutionalised social and environmental harm. *J. Clean. Prod.* **312**, 127828 (2021). <https://doi.org/10.1016/j.jclepro.2021.127828>
14. Morgan, A.: Inclusive place-based education for 'Just Sustainability.' *Int. J. Incl. Educ.* **16**(5–6), 627–642 (2012). <https://doi.org/10.1080/13603116.2012.655499>
15. Ghisellini, P., Cialani, C., Ulgiati, S.: A review on circular economy: the expected transition to a balanced interplay of environmental and economic systems. *J. Clean. Prod.* **114**, 11–32 (2016). <https://doi.org/10.1016/j.jclepro.2015.09.007>

16. Mah, A.: Future-proofing capitalism: the paradox of the circular economy for plastics. *Glob. Environ. Polit.* **21**(2), 121–142 (2021). https://doi.org/10.1162/glep_a_00594
17. Haas, W., Krausmann, F., Wiedenhofer, D., Heinz, M.: How circular is the global economy? An assessment of material flows, waste production, and recycling in the European Union and the world in 2005. *J. Ind. Ecol.* **19**(5), 765–777 (2015). <https://doi.org/10.1111/jiec.12244>
18. Fubini, F.: *Il vulcano*. Longanesi, Milano (2020)
19. Brown, M.T., Ulgiati, S.: Understanding the global economic crisis: a biophysical perspective. *Ecol. Model.* **223**(1), 4–13 (2011). <https://doi.org/10.1016/j.ecolmodel.2011.05.019>
20. Williams, J.: Circular cities: what are the benefits of circular development? *Sustainability* **13**(10), 5725 (2021). <https://doi.org/10.3390/su13105725>
21. Ghisellini, P., Santagata, R., Zucaro, A., Ulgiati, S.: Circular patterns of waste prevention and recovery. *E3S Web Conf.* **119**, 00003 (2019). <https://doi.org/10.1051/e3sconf/201911900003>
22. Bosone, M., Nocca, F., Fusco Girard, L.: The circular city implementation: cultural heritage and digital technology. In: Rauterberg, M. (ed.) *HCII 2021*. LNCS, vol. 12794, pp. 40–62. Springer, Cham (2021). https://doi.org/10.1007/978-3-030-77411-0_4
23. Bosone, M.: Culture as a driver of circular urban regeneration. In: Viola, S., Ul Abedin, Z. (eds.) *Cultural and Creative Industries. Technological Innovation for the Built Environment*, pp. 140–142. La Scuola di Pitagora, Napoli (2020)
24. Arora, R., Paterok, K., Banerjee, A., Saluja, M.S.: Potential and relevance of urban mining in the context of sustainable cities. *IIMB Manag. Rev.* **29**(3), 210–224 (2017). <https://doi.org/10.1016/j.iimb.2017.06.001>
25. Girard, L.F.: Towards the implementation of the circular economic model in metropolitan cities: the case of naples. In: Suzuki, S., Patuelli, R. (eds.) *A Broad View of Regional Science*. NFRSAP, vol. 47, pp. 303–328. Springer, Singapore (2021). https://doi.org/10.1007/978-981-33-4098-5_16
26. Santagata, R., Zucaro, A., Viglia, S., Ripa, M., Tian, X., Ulgiati, S.: Assessing the sustainability of urban eco-systems through Emergy-based circular economy indicators. *Ecol. Indic.* **109**, 105859 (2020). <https://doi.org/10.1016/j.ecolind.2019.105859>
27. Balvanera, P., et al.: Interconnected place-based social–ecological research can inform global sustainability. *Curr. Opin. Environ. Sustain.* **29**, 1–7 (2017). <https://doi.org/10.1016/j.cosust.2017.09.005>
28. Ghisellini, P., Ulgiati, S.: Circular economy transition in Italy. Achievements, perspectives and constraints. *J. Cleaner Prod.* **243**, 118360 (2020). <https://doi.org/10.1016/j.jclepro.2019.118360>
29. Vittoria, M.P., Naapolitano, P.: The informal community for the contemporary city. *Fab Lab as an opportunity of learning and participative labor*. *L’Industria* **1**, 63–84 (2017). [in Italian]
30. Song, X.P., Tan, P.Y., Edwards, P., Richards, D.: The economic benefits and costs of trees in urban forest stewardship: a systematic review. *Urban For. Urban Greening* **29**, 162–170 (2018). <https://doi.org/10.1016/j.ufug.2017.11.017>
31. Roy, S., Byrne, J., Pickering, C.: A systematic quantitative review of urban tree benefits, costs, and assessment methods across cities in different climatic zones. *Urban For. Urban Greening* **11**(4), 351–363 (2012). <https://doi.org/10.1016/j.ufug.2012.06.006>



Regional Waste Management System Improvement Strategy Based on Sustainable Development Principles

Olga Khandogina¹(✉) , Natalia Mushchynska¹ , Olena Dymchenko¹ ,
and Nataliia Obukhova² 

¹ O. M. Beketov National University of Urban Economy at Kharkiv, 17 Marshala Bazhanova Street, Kharkiv 61002, Ukraine

olga.khandogina@kname.edu.ua

² Kharkiv National University of Civil Engineering and Architecture, 40 Sumska Street, Kharkiv 61002, Ukraine

Abstract. The paper reviews the main indicators for decision-making process in the field of waste management at the local level. Development of sustainable integrated waste management system requires comprehensive consideration and assessment of many factors. Nevertheless, a small number of indicators are usually used for assessing the development scenarios of the waste management system. The purpose of the study is to identify the most important aspects of the waste management system and to formulate general principles for ensuring the sustainability of solid waste management systems performance and development at the regional level. Analysis of previous studies shows the variety of approaches to classify indicators of sustainable development in the field of solid waste management. Large number of factors, a small number of observations and unknown dynamic relationships between variables are shown to be reasons for complex problems in solid waste management decision-making. An expert assessment was made to investigate the officials' and practitioners' vision on waste management systems performance and strategies development. The set of economic, social, environmental, and technical indicators was selected and assessed by the group of experts. The analysis shows that mainly economic indicators are considered by local authorities and other stakeholders involved in regional waste management strategies development and implementation while social and environmental aspects are out of sight. At the same time financing of waste management system is not systematic and consistent and the amount of funding is extremely insufficient. The main principles for sustainable performance and development of the waste management system were formulated in the paper as the following: principle of national development strategies integration, principle of application of an effective monitoring and forecasting system, principle of differentiation of the development strategies at the regional level, principle of considering the stakeholders' interests.

Keywords: Regional development strategy · Sustainable development indicators · Waste management

1 Introduction

Waste generation is tightly connected with all aspects and stages of human activity, closely related to energy and material conservation. It affects environment, ecosystems existence and reproduction, life and health of the population. The waste management sector is a powerful source of greenhouse gas emissions, which is unacceptable regarding the implementation of the new European green policy based on transition to a climate-neutral society. Therefore, the regional sustainable development is inextricably linked to the reliability, efficiency and safety of integrated waste management systems. The problem of waste management system is of high level of concern of the transformation period [1, 2]. The necessity to reform the waste management system and to improve legislative and regulatory documents contribute to developing projects, plans and programs aimed at improving the solid waste management system at the level of regions and individual municipalities or communities. The problem is that not all elements of these systems are given due attention, which makes the decision-making process inefficient. Thus, a small number of indicators are used for assessing the development scenarios of the waste management system to determine the further development strategy on regional level.

Development of integrated documents that will determine the state or regional policy in the field of waste management over the years and decades (such as numerous regional waste management programs, regional waste management plans, which are currently being developed to implement the National Waste Management Strategy), as well as decision-making by local authorities, require comprehensive consideration and assessment of many factors. An important condition for an integrated approach is the awareness of key groups of stakeholders about modern technologies, solutions. They need to have systematic approach to solving problems, understanding the risks and threats that may hinder the implementation of planned activities.

Therefore, understanding the mechanisms of selecting scenarios for the waste management systems development at the local level, and, if necessary, adjusting them by increasing the level of knowledge in this and related fields, their transfer to competent persons, is an important prerequisite for sustainable performance and development of solid waste management systems [3].

Modern society, as well as technologies of domestic production, are characterized by high material and energy consumption, which leads to loss of resources, environmental degradation, waste accumulation. The issue of Ukraine's backwardness in terms of solid waste management technologies is especially relevant in the context of European integration of Ukraine's economy. Therefore, the creation of effective, complex integrated regional waste management systems will solve a range of social, environmental, and economic problems.

2 Literature Review

Supporting the decision-making process in waste management in world practice is most often carried out through the use of life cycle assessment, cost-benefit analysis and multi-criteria decision-making [4–6]. The first two methods focus on environmental and economic aspects, respectively, while the latter considers a set of environmental,

economic and social criteria. The development, implementation and monitoring of local or regional waste management strategies should take into account compliance with regulations, the possibility of using the best-known technologies, public involvement, improving the quality of life, approximation to the principles of the circular economy, etc. [7]. The importance of considering environmental factors, particularly related to municipal waste, in the analysis of socio-economic development and planning of regional development strategies, has been considered by many scientists [8–10].

Therefore, the important prerequisite for the creation of sustainable and efficient solid waste management systems could be defined as following: understanding the mechanisms for selecting scenarios of solid waste management systems development at the local level; considering economic, environmental, social, technical and organizational aspects of their planning and implementation; ensuring compliance with basic European principles, and, if necessary, adjusting mechanisms of scenario selection by raising the level of knowledge in this and related fields, their transfer to competent persons etc. There are many approaches to classify indicators of sustainable development in the field of solid waste management at different levels of administrative and territorial organization [9, 11, 12]. Multidimensional analysis of the solid waste management system and the development of optimization economic and environmental management models and decision-making algorithms on this basis still remain relevant for scientific research.

Prominent economists tried to determine the optimal ratio of economic, industrial, market factors that would provide the economic system with a dynamic equilibrium and sustainable development. The complex problems arising in solid waste management decision-making are associated with a large number of factors, a small number of observations and unknown dynamic relationships between variables.

Provided literature review and own previous research allowed to formulate the hypothesis as follows:

- H1: Not all socio-environmental factors are identified as important while making decisions on the developing strategies of solid waste management systems improvement.
- H2: The economic tools used to build a solid waste management system in Ukraine are unbalanced and need significant revision.
- H3: The development of regional waste management strategies should be based on the principles of sustainable development, which will ensure a well balanced approach.

The aim of the study is to identify the most important aspects of the waste management system and to formulate general principles for ensuring the sustainability of solid waste management systems performance and development at the regional level. To achieve the purpose the following tasks were fulfilled: to define the indicators for assessment, to conduct expert survey, to process the received data, to determine generalized principles which should be considered to ensure the sustainability of waste management systems.

3 Research Methods and Methodology

Method of expert assessments is proposed in the paper to identify the most important aspects of the waste management system, considering the experience, knowledge and skills of professionals and decision makers. Expert evaluation is an important way to obtain and analyze qualitative data for solving problems of management, planning, forecasting etc. The main stages of expert evaluation are the preparatory stage (determination of the purpose and objectives of expert evaluation, formation of expert groups and formulation of evaluation procedures), choice of expert information obtaining method, the research, processing of expert evaluation results and analysis of information.

The expert assessment was carried out with the involvement of a group of experts consisting of representatives of local governments, waste management companies in the Dergachi district of Kharkiv region.

37 indicators were identified to assess the scenarios of waste management system development, including 11 main economic indicators, 10 – social and organizational, 11 – environmental, 5 technical (see Fig. 1) [13].

Experts received questionnaires where the importance of each indicator in choosing a scenario for the waste management system development could be estimated. The most important factor according to the expert received a score of “5”, and the least important – “1”.

The Kendall concordance coefficient was used to determine the degree of expert agreement. Its calculation is performed by expression (1):

$$W_k = \frac{12S}{m^2(n^3 - n)} \tag{1}$$

where m is the number of correlated factors, n is number of observations, S is the sum of the squared deviations of the sum of ranks by m factors from their arithmetic mean, calculated by expression (2):

$$S = \sum_{i=1}^n \left(\sum_{j=1}^m R_{gij} - \sum_{j=1}^m \overline{R_{gij}} \right)^2 \tag{2}$$

where R_g is the rank assigned to the i -th value of the j -th attribute.

In the provided estimation the associated ranks are present, so the Eq. (1) will be as follows eq. (3):

$$W_k = \frac{12S}{m^2(n^3 - n) - m \cdot \sum_{j=1}^m T_j} \tag{3}$$

where T_j is the index of associated ranks in j -ranking.

The analysis was performed using the STATISTICA package. According to the calculation results, with considering the associated ranks, the concordance coefficient is established as 0.4284. The concordance coefficient is measured in the range from 0 to 1, with 0 corresponding to inconsistency, 1 – complete consistency. The concordance coefficient from 0.3 to 0.7 can be considered as average.

Indicators for assessment of waste management scenarios	Economic	<ul style="list-style-type: none"> 1.1. Investment costs 1.2. Annual operational costs 1.3. Annual revenue from recovery of materials and energy 1.4. Total costs of WM system 1.5. Regional added value 1.6. Costs per waste management subsystem 1.7. Ratio of revenues from MSW fees and expenditures for WM 1.8. Costs of waste management in the GNP of the city 1.9. Costs of waste management per person as % of minimum wage 1.10. Costs of waste management per person as % of income per person 1.11. Subsidies or grants per person
	Social and governance	<ul style="list-style-type: none"> 2.1. Public acceptance 2.2. Job creation 2.3. User convenience and complexity 2.4. Urban space consumption 2.5. Odour caused by waste treatment transport and treatment 2.6. Noise 2.7. Visual impact 2.8. Traffic 2.9. Length of time required for the introduction of the scenario 2.10. Availability of space for new treatment plants
	Environmental	<ul style="list-style-type: none"> 3.1. Separated collection rate 3.2. Material recovery rate 3.3. Energy recovery rate 3.4. Waste landfilling rate (Landfill volume required) 3.5. Untreated waste landfilling rate 3.6. Biodegradable waste diversion rate 3.7. Greenhouse gas emissions 3.8. Reaching the objectives of the Strategies for Waste Management 3.9. Locally relevant air pollutants from waste treatment and disposal 3.10. Locally relevant emissions into water from waste treatment and disposal 3.11. Waste amounts per costs of disposal
	Technical	<ul style="list-style-type: none"> 4.1. Technical reliability 4.2. Requirement of qualified personnel and maintenance requirements 4.3. Sensitivity to quantity of input material 4.4. Sensitivity to quality of input material 4.5. Autarky in the waste treatment

Fig. 1. List of indicators for expert assessment.

Spearman’s rank correlation computed on ranks shows the result of 0.3876. According to the t-Test of Spearman’s rank correlation the calculated t-value is less than the table value at an alpha level of 0.05 which means the rank correlation coefficient is statistically significant and the rank correlation between the scores is significant.

4 Results and Discussion

The result of Friedman's rank analysis of variance and determination of Kendall concordance are given in Table 1, where data were sorted by the average rank.

Since in this assessment, the score of 5 was set as the most important (according to the experts) indicators, the greater the weight of the indicators corresponds to the greater the value of the average rank. The level of significance is less than 0.05, which indicates significant differences between indicators.

Table 1. Friedman's rank analysis of variance and Kendall concordance.

Indicator	Average rank	The sum of ranks	Average	Standard deviation
2.7	4.500	67.5	2.267	0.798809
2.8	6.800	102.0	2.667	0.487950
2.6	7.433	111.5	2.800	0.774597
1.5	8.867	133.0	2.933	0.703732
3.7	10.933	164.0	3.000	1.414214
1.7	11.133	167.0	3.267	0.457738
3.3	13.700	205.5	3.333	1.046536
3.9	14.133	212.0	3.400	0.828079
1.11	15.333	230.0	3.600	0.736788
3.6	15.567	233.5	3.533	0.990430
3.2	15.800	237.0	3.533	0.833809
3.5	16.000	240.0	3.600	0.828079
2.9	16.400	246.0	3.600	0.828079
3.10	17.367	260.5	3.667	0.899735
2.5	17.433	261.5	3.667	0.723747
4.2	18.100	271.5	3.600	1.352247
4.4	18.633	279.5	3.867	0.639940
3.4	19.167	287.5	3.867	0.639940
4.3	19.200	288.0	3.867	0.639940
4.5	19.667	295.0	3.933	0.593617
1.10	20.267	304.0	4.000	0.654654
2.3	20.267	304.0	3.933	0.593617
1.3	21.033	315.5	4.067	0.883715
1.6	21.833	327.5	4.133	0.833809
3.1	21.833	327.5	4.067	0.883715

(continued)

Table 1. (continued)

Indicator	Average rank	The sum of ranks	Average	Standard deviation
3.8	21.900	328.5	4.067	0.593617
3.11	22.400	336.0	4.067	0.961150
1.9	23.000	345.0	4.200	0.560612
2.2	23.733	356.0	4.200	0.560612
2.10	24.100	361.5	4.200	0.676123
1.2	25.600	384.0	4.400	0.632456
2.4	25.600	384.0	4.333	0.487950
4.1	27.500	412.5	4.467	0.639940
2.1	27.800	417.0	4.533	0.639940
1.8	28.100	421.5	4.600	0.507093
1.4	30.167	452.5	4.733	0.457738
1.1	31.700	475.5	4.867	0.351866

Table shows that the most significant indicators of the expert assessment are investment costs, the total cost of the waste management system and the share of waste management costs in GRP. All of them belong to the group of economic indicators.

The least important indicators (according to the experts) were visual impact, transport conditions and noise levels - factors that can lead to a deterioration in the quality of residents life, environmental pollution and social tensions. However, one should remember that the ranking does not consider the distance between the factors.

In order to determine the most important group of indicators according to the experts, ranking by the method of average scores was conducted. To do this, the average score given by each expert within a certain group of indicators was determined (Table 2).

Table 2. Ranking of groups of indicators by the method of average

Experts	Groups of indicators			
	Group1	Group 2	Group 3	Group 4
1	4.45	3.4	2.91	3.2
2	4	3	3.36	4.4
3	3.82	3.7	3.91	4.2
4	4	3.7	3.91	4.2
5	3.82	3.6	4.27	3.8
6	4.73	4.3	4.27	4.4

(continued)

Table 2. (continued)

Experts	Groups of indicators			
	Group1	Group 2	Group 3	Group 4
7	3.82	3.6	3.55	4
8	3.73	3.7	4	4.2
9	4.36	3.2	2.36	2.8
10	4.45	3.9	4.45	4.2
11	3.73	3.5	4.09	3.8
12	4.36	4.1	4.27	4.6
13	4.09	3.7	3.55	3.8
14	4	3.8	3.64	4
15	3.73	3.1	2.18	3.6
The sum of ranks	61.09	54.3	54.72	59.2
The arithmetic mean of the ranks	4.07	3.62	3.65	3.95
Rank	1	4	3	2

This situation can lead to imbalance of the waste management system, as it does not take into account all possible threats. For example, insufficient attention to indicator 3.7 “Greenhouse gas emissions” and the choice of waste management scenario, which is characterized by increased greenhouse gas emissions, leads not only to environmental pollution, but also to increased taxes on pollutant emissions into the air in the future, and as a result to the general rise in costs of the waste management system elements. However, such causation is often overlooked by decision makers due to the lack of a systematic approach.

The economic instruments used as a priority to ensure the performance and development of the waste management system are imperfect and do not perform their functions in full. This is manifested in the opacity of tariff policy, the presence of debts from consumers of services, the refusal to enter into agreements. Economic incentives to limit the amount of waste generated are almost non-existent, and containment tools are also ineffective, including through an imperfect control system. There is no system of interaction with producers of goods, which would provide the possibility of utilization of consumption waste or packaging, there is no system of extended producer responsibility. The level of investment in this area is insufficient. Financing of waste management is not systematic and consistent (Fig. 2).

The main source of waste management system funding in Ukraine is local budgets. In 2018 the annual costs spent for waste management system was in the range from UAH 1,201 thousand (Zakarpatska region) to UAH 185,438 thousand (Donetska region). Total financing in Ukraine amounted to UAH 1,004,674 thousand (including UAH 141,330 thousand from the state budget, UAH 696,017 thousand from local budgets, UAH 59,260 thousand from loans, and UAH 108,067 thousand UAH from other sources). In Fig. 3

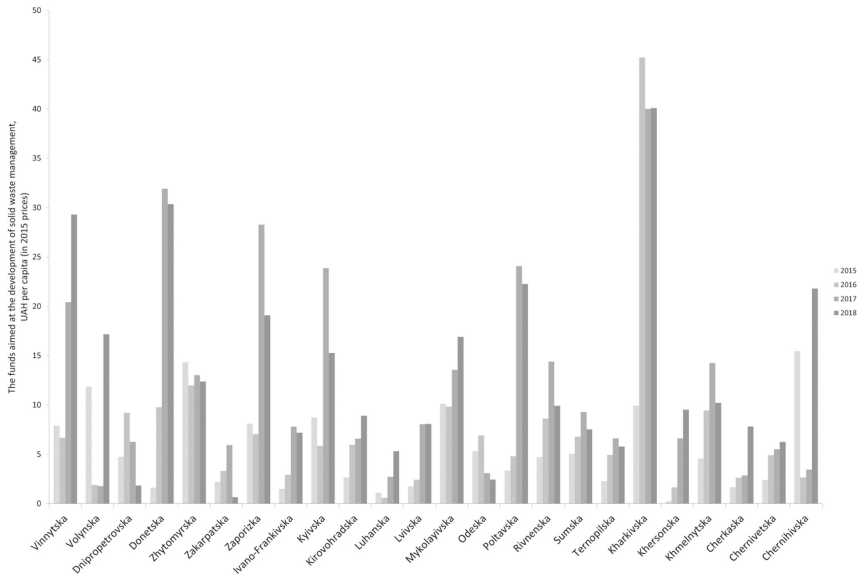


Fig. 2. Dynamics funds directed to the waste management development in the regions of Ukraine per capita in the prices in 2015, considering consumer price indices (Ministry of Development of Communities and Territories of Ukraine, n.d.)

shown the ratio in the financing of various aspects of the waste management system in the regions of Ukraine.

In 2018 the vast majority of regions spent less than 30% of the total amount of funds on the construction of new landfills and the reconstruction of existing ones. In 8 regions, however, these objects of expenditures were not funded at all. This may partly explain the catastrophic situation with the municipal waste disposal sites in our country. Most of the money is spent on upgrading of special vehicles and containers used for waste collection and transportation. However, the destructive processes observed in the market of waste management services cannot ensure the proper operation of technical means and lead to their rapid failure, which in turn leads to a constant need to finance this category of costs without significant quality improvement.

The World Bank estimates that the cost of regional waste management systems for low-income countries can average up to 20% of the total budget. In middle-income countries, waste management expenditures account for more than 10% of local budgets and about 4% for high-income countries [14].

In Ukraine, funds allocated for the financing of waste management range from only 0.01% (Zakarpatska region) to 0.7% (Donetska region) of the region’s budget expenditures, about 0.2% in the country. This amount of funding is extremely insufficient to ensure the functioning of all elements of the system, and, moreover, does not allow the implementation of measures for its complex reform.

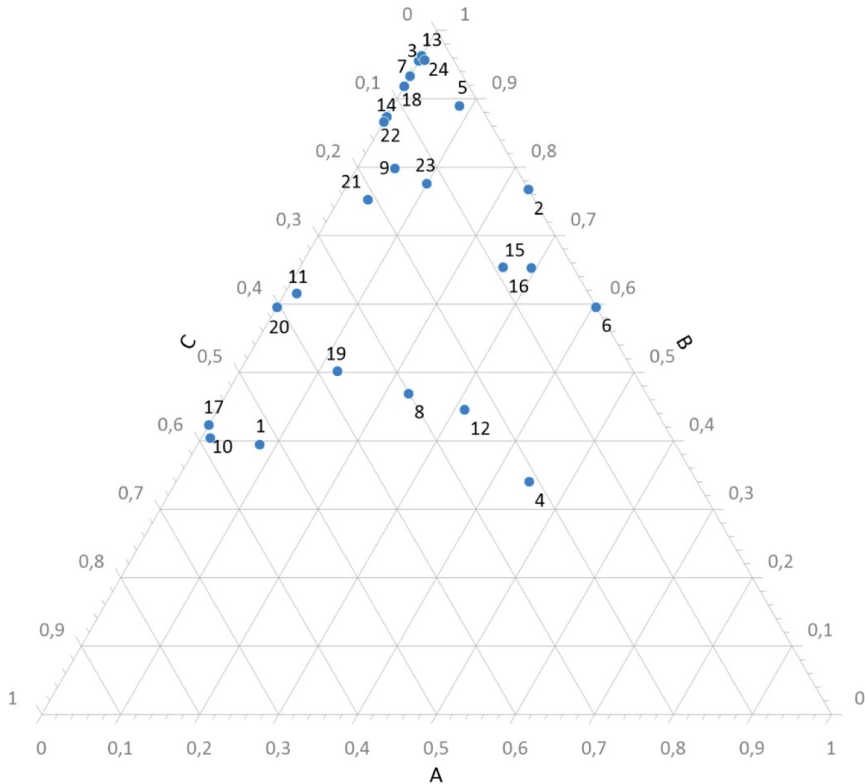


Fig. 3. The ratio of funds aimed at the development of various elements of the waste management system (Ministry of Development of Communities and Territories of Ukraine, n.d) A – funds for waste disposal sites, B – funds for technical means for solid waste collection, C – other costs (Regions: 1 – Vinnytska, 2 – Volynska, 3 – Dnipropetrovska, 4 – Donetsk, 5 – Zhytomyska, 6 – Zakarpatska, 7 – Zaporizka, 8 – Ivano-Frankivska, 9 – Kyivska, 10 – Kirovohradska, 11 – Luhanska, 12 – Lvivska, 13 – Mykolayivska, 14 – Odeska, 15 – Poltavska, 16 – Rivnenska, 17 – Sumska, 18 – Ternopilska, 19 – Kharkivska, 20 – Khersonska, 21 – Khmelnytska, 22 – Cherkaska, 23 – Chernivetska, 24 - Chernihivska).

5 Conclusion

The development and implementation of new management methods, modern innovative technologies and approaches, state support for innovative development of the solid waste management sector is of crucial necessity for solving problems of the mentioned sphere. Institutional support of waste management as a set of rules and institutions establishing coordination is a key issue in the process of forming and implementing national and regional policies in this area.

Attention to the following generalized principles should be paid to ensure the sustainability of the performance and development of waste management systems:

1. The principle of national development strategies integration. It is necessary to consider the national goals of sustainable development and ensure their achievement, particularly by achieving the goals for the waste management system [15].
2. The principle of application of an effective monitoring and forecasting system. A comprehensive system for data monitoring and possible waste management scenarios forecasting considering all groups of indicators should be implemented, rather than focusing the attention of decision-makers only on economic ones. This principle will also allow to effectively balance the allocation of budget funds to the development of various elements of waste management.
3. The principle of differentiation of the development strategies at the regional level. Clustering of regions according to the indicators of regional waste management systems development [16, 17], allows to develop differentiated strategies to increase the efficiency of waste management systems at the regional level. At the same time, there are still common problems that affect the state of waste management system and each of the regional systems separately.
4. The principle of considering the stakeholders' interests. The effective performance of the waste management system strongly depends on its organizational structure, effective distribution of management functions, powers and responsibilities between all elements and participants (Ministry of Community and Territorial Development, Ministry of Ecology and Environmental Protection, Department of Housing, Department of Ecology, State Environmental inspection, Local governments, Companies operating in the field of waste management, the media, NGOs, Population, Scientists, Investors). Providing mechanisms to increase the involvement of major groups of stakeholders should be implemented to create conditions for the functioning of effective integrated regional solid waste management systems.

References

1. Skryhan, H., Shilova, I., Khandogina, O., Abashyna, K., Chernikova, O.: Waste management in post-soviet countries: how far from the EU? *Detritus* **3**, 193–203 (2018). <https://doi.org/10.31025/2611-4135/2018.13657>
2. Papagiannis, F., Gazzola, P., Burak, O., Pokutsa, I.: A European household waste management approach: intelligently clean Ukraine. *J. Environ. Manage.* **294**, 113015 (2021). <https://doi.org/10.1016/j.jenvman.2021.113015>
3. Coban, A., Ertis, I.F., Cavdaroglu, N.A.: Municipal solid waste management via multi-criteria decision making methods: a case study in Istanbul, Turkey. *J. Cleaner Prod.* **180**, 159–167 (2018). <https://doi.org/10.1016/j.jclepro.2018.01.130>
4. Goulart Coelho, L.M., Lange, L.C.: Applying life cycle assessment to support environmentally sustainable waste management strategies in Brazil. *Resour. Conserv. Recycl.* **128**, 438–450 (2018). <https://doi.org/10.1016/j.resconrec.2016.09.026>
5. Goulart Coelho, L.M., Lange, L.C., Coelho, H.M.: Multi-criteria decision making to support waste management: a critical review of current practices and methods. *Waste Manage. Res.* **35**(1), 3–28 (2017). <https://doi.org/10.1177/0734242X16664024>
6. Karmperis, A.C., Aravossis, K.G., Tatsiopoulos, I.P., Sotirchos, A.: Decision support models for solid waste management: Review and game-theoretic approaches. *Waste Manage.* **33**, 1290–1301 (2013). <https://doi.org/10.1016/j.wasman.2013.01.017>

7. Zorpas, A.A.: Strategy development in the framework of waste management. *Sci. Total Environ.* **716**, 137088 (2020). <https://doi.org/10.1016/j.scitotenv.2020.137088>
8. Lakioti, E.N., Moustakas, K., Komilis, D.P., Domopoulou, A.E.: Sustainable solid waste management: socio-economic considerations. *Chem. Eng. Trans.* **56**, 661–666 (2017). <https://doi.org/10.3303/CET1756111>
9. Wilson, D.C., et al.: ‘Wasteaware’ benchmark indicators for integrated sustainable waste management in cities. *Waste Manage.* **35**, 329–342 (2015). <https://doi.org/10.1016/j.wasman.2014.10.006>
10. Zhang, J., Qin, Q., Li, G., Tseng, C.: Sustainable municipal waste management strategies through life cycle assessment method: a review. *J. Environ. Manage.* **287**, 112238 (2021). <https://doi.org/10.1016/j.jenvman.2021.112238>
11. Deus, R.M., Bezerra, B.S., Battistelle, R.A.G.: Solid waste indicators and their implications for management practice. *Int. J. Environ. Sci. Technol.* **16**(2), 1129–1144 (2018). <https://doi.org/10.1007/s13762-018-2163-3>
12. Cetrulo, N.M., Cetrulo, T.B., Dias, S., Ramos, T.B.: Solid waste indicators in local sustainability assessment: a literature review. *Ambient. Soc.* **23**, 1–31 (2020). <https://doi.org/10.1590/1809-4422asoc20190028r3vu2020L5AO>
13. Den Boer, E., Den Boer, J., Jager, J.: Waste management planning and optimisation - Handbook for municipal waste prognosis and sustainability assessment of waste management systems. Ibidem-Verlag, Stuttgart (2005)
14. Kaza, S., Yao, L.C., Bhada-Tata, P., Van Woerden, F.: What a Waste 2.0: a Global Snapshot of Solid Waste Management to 2050. World Bank, Washington, DC (2018). <https://doi.org/10.1596/978-1-4648-1329-0>
15. Rodić, L., Wilson, D.C.: Resolving governance issues to achieve priority sustainable development goals related to solid waste management in developing countries. *Sustainability* **9**(3), 404 (2017). <https://doi.org/10.3390/su9030404>
16. Güteryüz, D.: Evaluation of waste management using clustering algorithm in megacity Istanbul. *Environ. Res. Technol.* **3**(3), 102–112 (2020). <https://doi.org/10.35208/ert.764363>
17. Sharma, N., Litoriya, R., Sharma, A.: Application and analysis of K-means algorithms on a decision support framework for municipal solid waste management. In: Hassanien, A.E., Bhatnagar, R., Darwish, A. (eds.) *AMLTA 2020. AISC*, vol. 1141, pp. 267–276. Springer, Singapore (2021). https://doi.org/10.1007/978-981-15-3383-9_24



Application of an Innovative Monolithic Mechanical Seismometer for Urban Vibroscape Monitoring

Marco Casazza¹ (✉) , Rocco Romano² , and Fabrizio Barone¹ 

¹ University of Salerno, Department of Medicine, Surgery and Dentistry “Scuola Medica Salernitana”, 84081 Baronissi, Italy

mcasazza@unisa.it

² University of Salerno, Department of Pharmacy, 84084 Fisciano, Italy

Abstract. Urbanization process produces relevant negative impacts that need to be monitored. Within smart cities, extensive networks of standalone environmental sensors, potentially integrable within cloud computing capabilities, should serve as the basis of innovative near real-time monitoring systems, being able to characterize and to detect the variability of urban environmental parameters. While the interest is often concentrated on air quality and acoustic noise, other parameters might be of interest, including vibrations, since they can exert a relevant impact on human health and urban assets (buildings and infrastructures). This work focuses on the application of an innovative broadband monolithic mechanical seismometer, produced and commercialized by Advanced Scientific Sensors and Systems (Adv3S™), used as a stand-alone sensor to detect the features of the vibroscape (i.e.: the totality of vibrations of natural and anthropic origin). Results contain some examples of raw data, measured in the city of Napoli (Italy), proving the effectiveness of the sensor in detecting the urban vibroscape features. The sensor, having a low operational cost and high integrability into data networks, could be relevant in the context of smart cities, considering different applications, ranging from the structural health monitoring of urban assets to civil protection purposes.

Keywords: Sensor · Seismometer · Urban vibroscape

1 Introduction

The global urbanization process, characterized by growth of population in cities, higher concentrations of economic activities and increasing consumption of natural resources is producing relevant negative effects both on human health and on environmental conditions. In order to understand the causes and to develop effective strategies aimed at the reduction of these effects, it is necessary a reliable and deep understanding of the causes affecting the quality of life in cities and the environment, providing the needed support to urban managers and policy-makers in the development of effective transition strategies and actions aiming at the implementation of sustainable cities and communities, in agreement with the 11th Sustainable Development Goal, and toward good health and

well-being (3rd Sustainable Development Goal). It is, therefore, clear that the quality of this approach is strongly dependent on an accurate knowledge of the environmental conditions, measured with geographically distributed monitoring systems, often integrating a large number of different typologies of sensors. Within this context, it is also well known that extensive networks of standalone environmental sensors, potentially integrable within cloud computing capabilities, should serve as the basis of innovative near real-time monitoring systems, being able to characterize and to detect the variability of urban environmental parameters [1].

Furthermore, the design and implementation of a distributed monitoring system, synthesis of different classes and typologies of sensors, must be well integrated within ICT infrastructures, that play a crucial role within the smart cities context [2].

Previous works focused, in particular, on the development of different air quality and noise monitoring technologies and their applications in Smart Cities [3, 4]. However, these parameters are not the only environmental parameters of interest for public health reasons. This is the case of vibrations, that are a known cause of annoyance for urban residents [5] and potential adverse health effects, such as sleep disturbance, where a dose-effect relation was found for different levels of exposure to vibrations [6], as well as other symptoms, such as headaches, dizziness, nausea, fatigue, insomnia, and/or chronic anxiety [7].

In the case of acoustic noise, considering, in particular, the vibrations within the range of 20 Hz–20.000 Hz, the concept of soundscape was coined, in order to synthetize the totality of noise generated by natural and anthropogenic sources characterizing a given space [8, 9]. However, recent studies suggested that also infrasound vibrations are a relevant source of stimuli for different living species, being also the most common form of signaling through mechanical communication [10]. This is why the concept of vibroscape was coined, as synthesis of the totality of vibrations generated by biological, geophysical and anthropogenic sources, being detected and characterizing a given space [11]. Despite the huge applications of vibration studies for civil (e.g., structural health monitoring) and industrial (e.g., components and material fatigue) purposes, as well as the monitoring activities for geophysical (i.e., earthquakes or prospection) or other specific research purposes (e.g., research on gravitational waves), a little attention was paid in the past in relation to anthropogenic [12] and biological [13] sources of vibrations. Thus, the characterization of vibroscape in different contexts, such as urban areas, will likely become a relevant field of investigation, due to its implications for public health and for the structural health monitoring of urban assets (building and infrastructures).

On the other hand, the above studies, although often devised for specific purposes and with well-defined goals, if analyzed from a general and synthetic point of view, clearly show the need of implementation of globally geographically distributed monitoring systems integrating different classes of sensors aimed at monitoring different and independent environmental variables, such as the need of implementation of reliable standalone sensors and systems for local monitoring aimed at focusing on specific areas with increased accuracy and precision.

In any case, the critical point of every local and/or geographically distributed monitoring system is determined mainly by the sensors, whose typology and quality in term of precision, accuracy, band, sensitivity, stability and directionality determine the global quality of the monitoring network and, consequently, the quality of the knowledge that

it is possible to obtain from the measurements. Among the different typologies of sensors, it is known that seismic sensors, especially seismometers, have the advantage of producing a minor environmental impact on the quality of detected signals with respect to other sensors, still keeping very high levels of sensitivity and very large detection bands, especially in the low frequency region [14].

This work focuses on the application of an innovative broadband monolithic mechanical seismometer as a standalone sensor, tested, for the first time in the literature, as an instrument for urban vibroscape measurement. In particular, results will highlight the main findings derived from the field test of an implemented stand-alone version of the system, based on the above seismometer, being used to monitor the urban vibroscape.

2 Materials and Methods

2.1 The Monolithic Mechanical Seismometer

As pointed above, the standalone system version used for these first tests of the urban vibroscape measurement, produced by Advanced Scientific Sensors and System (Adv3S™), consists of a high-quality compact size, low power consumption, transportable DAQ system powered with external batteries and equipped with a highly directional horizontal high-sensitivity broadband mechanical seismometer. Actually the version we have used for the tests is the minimal version of an adaptive transportable urban vibroscape system, since it has been designed as a modular system remotely controllable and fully expandable, although still compact, to acquire up to 120 sensors of different typologies (seismic, acoustic, etc.) with very high signal-to-noise ratio and large band, especially in the low frequency region.

The mechanical monolithic seismometer (SE-10HL), used for this first application of (seismic) vibroscape monitoring, is a real horizontal seismometer (no force feedback control configuration), produced and commercialized by Advanced Scientific Sensors and Systems (Adv3S™). It consists of a mechanical monolithic oscillator (model GK19A – class EB-100), based on an innovative Watt's Linkage architecture developed by the Applied Physics Research group of the University of Salerno [15–19], equipped with a high-sensitive LVDT readout system, necessary to convert the output mechanical signal in an electronic signal for data acquisition. The technical characteristics of the seismometer SE-10HL are detailed in Table 1.

Finally, although the model used for these tests is already effective for a vibroscape application, it is important to stress that the characteristics of sensitivity, band, size and weight of the sensor can be defined at the vibroscape network global design level, being the mechanical oscillator fully scalable in terms of resonance frequency, size and weight, limited in its performances only by its thermal noise, so that the real and final performances of the sensor are actually determined only by the readout system choice [15, 20] that, in our case, is a commercial LVDT system. In fact, a different readout choice (e.g. optical, interferometric, capacitive, LVDT enhanced, etc.) can increase the sensitivity of the sensor of two-three orders of magnitude both in sensitivity and in band, in the low frequency region).

The DAQ system is based on the 24-bit National Instruments™ FieldDAQ, model FD-11603, whose characteristics are detailed in Table 2, based the Ethernet standard

for data acquisition and remote control of the units. The acquisition system, in turn, was connected to a portable computer running Windows 10 operating system in order to collect the data for further elaboration. Sampled data were originally saved in *.tdms file format, being the proprietary file format output of the used DAQ.

Table 1. Technical characteristics of the horizontal seismometer model SE-10HL from Advanced Scientific Sensors and Systems (Adv3S™).

Basic architecture	Model CHIPA – class EB-100 monolithic folded pendulum (Pat.)
Configuration	Seismometer (open loop)
Natural frequency	3.80 Hz ± 10%
Mass displacement	±0.8 mm ± 10%
Readout	LVDT (commercial)
LVDT sensor	MHR-010 (Measurement Specialities, Inc.)
Band	DC – 100 Hz
Sensitivity	72 V/mm ± 10%
Spectral sensitivity	$<10^{-8} \text{ m}/\sqrt{\text{Hz}}$ (3.50 Hz < f < 100 Hz)
Input voltage (dual)	±18 V (min)–±30 V (max)
Output signal (dual)	±10 V (range)
Dimensions	200 (l) × 80 (w) × 110 (h) (mm)
Weight	1750 g
Operating temperature	–40 °C–85 °C

Table 2. Technical characteristics of the National Instruments model FD-11603 Data Acquisition System (DAQ).

Number of channels	8 analogic input channel
Isolation	Galvanic isolation between channels and to chassis
Input voltage range	±10.5 V
ADC type	24 bits
ADC resolution	Delta-Sigma (with analogic prefiltering)
Sample mode	Simultaneous
Time bases	
<i>Frequency</i>	13.1072 MHz; 12.8 MHz; 12.288 MHz; 10.24 MHz
<i>Accuracy</i>	±30 ppm maximum
Sampled data rate range	

(continued)

Table 2. (continued)

<i>Minimum</i>	500 Samples/s	
<i>Maximum</i>	102.4 kSamples/s	
Accuracy		
<i>Temperature</i>	<i>Gain error</i>	<i>Offset error</i>
5 °C to 40 °C, typical	0.013%	0.001%, 0.105 mV
5 °C to 40 °C, maximum	0.037%	0.01%, 1.05 mV
−40 °C to 85 °C, maximum	0.062%	0.02%, 2.1 mV
Stability		
<i>Gain drift</i>	±4 ppm/°C	
<i>Offset drift</i>	±5 mV/°C	

The control system interface, developed by Adv3S™ to act a Supervisor for the management and control of the DAQ system is a software device running on the portable computer. In particular, this supervisor controls and synchronizes both the data acquisition and storage through a dedicated Ethernet network, managing the data storage in frames. This technical choice makes it possible to build open and large data archiving, leaving completely open the possibility of a full integration of data analysis software, open or commercial, in a completely independent way from the proprietary data acquisition technologies.

The Supervisor is managed, also remotely, through a graphical page, used for the configuration of the system at the beginning of each acquisition run (e.g. sampling frequency, number and position of sensors, temporal length of the frames, etc.). A second graphical page is equipped, instead, with a graphical window displaying in real-time selected channels during the data acquisition phase, operation necessary to check the correct signal acquisition procedure, but very useful also as a tool for the periodic maintenance of the whole system.

2.2 Raw Data Elaboration

Raw Data frame were elaborated using MATLAB™. In particular, the *.tdms frame files were converted into a structure in MATLAB™, applying an algorithm, made available through MathWorks File Exchange service [21]. The extracted data contains all the details about the measurement, as well as the measured time series, that were converted into displacement values (meters), using the signal conversion factor as reported in the SE-10HL characteristics (Table 1), that is ($1 \text{ m} \equiv 72,000 \text{ V}$).

Then, the characteristic instrumental response, being specific of each type of seismometer, was removed. In particular, a specific MATLAB script, derived from a published research work, was used [22]. This allowed to remove the instrumental response from the datasets used for this work.

Nevertheless, in order to provide the reader with the real raw data, to give a global view of the measurements, without any action determined by dedicated and specialized

data analysis methods and techniques, we prefer to present in the following only raw data, simply converted in displacement units, using the conversion factor as reported on the characteristics of the sensors (Table 1). This choice does not modify the data spectral structure, since, as largely reported in the literature, the instrument transfer function is a second order transfer function, so that, beyond the mechanical oscillator resonance frequency, in general clearly visible in the spectral data figures, the system response is unitary, while below the resonance frequency, the spectral response must be enhanced by 40 dB/decade (the sensor attenuates the signal in the low frequency band with an attenuation coefficient equal to 40 dB/decade).

2.3 Field Measures

Field measures were conducted from February to April 2022. The standalone system was located in the urban center of Napoli (Italy), close to a main road of the historical center, characterized by a high traffic load and by the passage of a subway under the same area. Figure 1 identifies the sampling point and the sampling area.



Fig. 1. Aerial view of the measure area in Napoli (Italy), with measure point evidenced as red dot. Scale and North orientation are reported within the view. On the top-right, the position of Napoli municipality in Italy.

3 Results and Discussion

3.1 Results

Displayed results consist in a graphic representation of a sub-set of converted raw data, serving as representative examples, proving the effectiveness of the system in detecting

the urban vibroscape and its characteristics. In particular, the presented data, acquired from the SE-10HL seismometer oriented in the North-East direction, span a temporal length of about 2 days starting from February 7, 2022 at 22:29:03 (UTC + 1), sampled at a frequency of 2083 Hz. Although the DAQ system can sustain a sampling frequency up to 100 kHz, we preferred to choose a lower sampling frequency, in order to minimize the amount of data storage for a long-term acquisition, since this test was mainly aimed at looking to seismic signals (vibrations), generally in a band up to a few tenth of Hz. Nevertheless, the chosen sampling frequency guarantees a full coverage of the band of interest, especially in the low frequency region, still keeping the level of the digital noise introduced by the 24-bit ADC lower than the electronic noise of the seismometer.

Although not instrument-corrected, the data (Fig. 2) show already very interesting preliminary features. It is important to stress that the system, although fully capable, has not been developed for strong motion measurements (earthquakes, etc.), but its main feature is that of measuring the seismic background and its forcing, a very relevant source of information for the study the vibration pollution introduced by environment conditions and anthropic activity. The signal is lower at night hours (Fig. 3b) than at daytime hours (Fig. 3a), showing a clear increase of the site seismic background noise at low frequencies (Fig. 4a), in this case mainly due to anthropic activities.

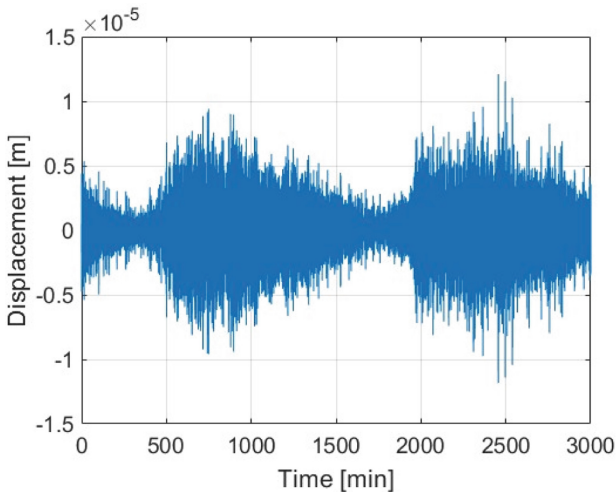


Fig. 2. Long-term temporal sequence (night and day) of extracted seismometric raw data, expressed in units of m.

Although a deeper analysis has to be done in order to understand the different possible causes that can generate these effects, polluting, in some sense, the environment, the pictures clearly show some already clear things. In fact, while the peak at about 4 Hz (Fig. 4a and Fig. 4b) is the resonance peak of the seismometer (that disappears one the data are instrumentally corrected), a very interesting bunch of peaks appears within the band 1–10 Hz, that can be attributed to the resonance frequencies (modes) of the building

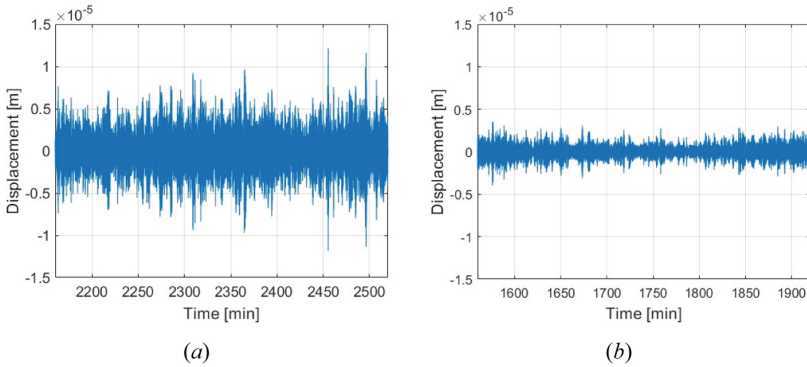


Fig. 3. Extracted sub-set of seismometer raw data, measured as displacement, expressed in units of m, derived from Fig. 2: (a) Day-time temporal sequence; (b) Night-time temporal sequence. The difference in amplitude of displacement oscillations between day and night data is clearly visible from the two figures. Both scales (abscissa and the ordinate axes) have been preserved in the two figures to be equal to Fig. 2.

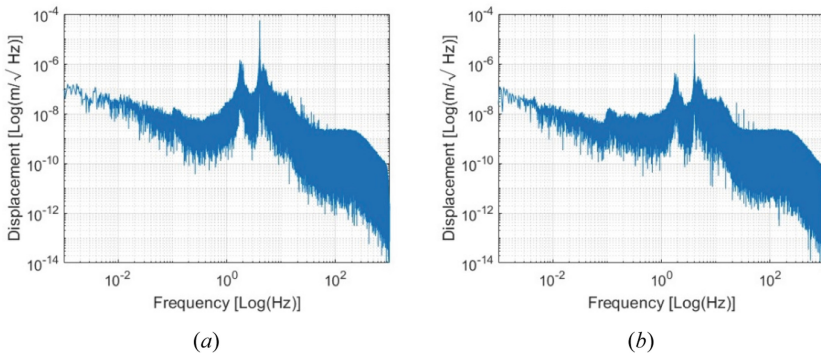


Fig. 4. Signal spectra, derived from the extracted sub-set of seismometer raw data represented in Fig. 3. (a) Day-time signal spectrum; (b) Night-time signal spectrum. Data, plotted in Log-Log scale, represent the signal displacement, in units of $(m/\sqrt{\text{Hz}})$, with respect to the frequency, in units of Hz.

where the systems has been installed, increasing during the daylight due to anthropic forcing (traffic, underground, etc.).

Interesting are also the peaks at low frequency, that is about 100 MHz, that can be attributed to seismic noise generated by the sea (Fig. 4a and Fig. 4b), since this location is very close to the seaside. In fact, these peaks do not decrease during the night, and in general change their amplitude and size, due to the changing sea conditions.

3.2 Discussion

The results of field tests performed in the city of Napoli confirm the effectiveness of the monolithic mechanical seismometer within a standalone system for monitoring the

urban vibroscape, with particular reference to the background noise and to its dynamical evolution according to the environment conditions and anthropic activity.

The advantage of using the selected seismometer is its high performance and low noise [22], higher sensitivity at lower frequencies with respect to other high-quality sensors, often unable to detect signals lower than 0.5 Hz [23], sometimes very expensive, being relevant for the identification of some phenomena of geophysical interests, such as regional earthquake sources (typical frequency band: 0.2 Hz–0.5 Hz) [24].

Besides the relevance of data for public health interest, as stated in the introduction, the raw data, derived from this standalone system, based on the above-described monolithic mechanical seismometer, could be used in several relevant urban applications, as already proved by the literature. These include, among the others, the evaluation of impacts on built heritage due to traffic-induced vibrations [25, 26], structural health of structures or buildings [27], knowing that fundamental natural frequencies of buildings lower than 10 storeys-high falls between 1 Hz and 10 Hz [28], the quantification of structural impacts on cultural heritage [29], where the same sensors were used for monitoring the Trajan Arch in the city of Benevento (Italy) [30, 31], but also the permanent distributed monitoring system of the Neptune Temple in the Archeological Park of Paestum (Italy) operational since 2021 [32], as well as emergency and civil protection applications [33].

4 Conclusion

This work proved the capability of an innovative monolithic mechanical sensor, produced and distributed by the firm Advanced Scientific Sensors and Systems (Adv3S™), to be integrated into a standalone solution for the characterization of urban vibroscape. The system, here used in a different configuration for being applied to different field test, can be deployed in integration with a data storage and transmission unit. Thus, the installation and operativity of such systems in different measuring points, having the characteristic of having a low operational cost and high integrability into data networks, could be relevant in the context of smart cities. In particular, collected raw data can find different relevant applications in the urban context, being already recognized by the literature.

Considering the sensors characteristics and their capability to detect different relevant phenomena of natural and anthropogenic origin, future research will be oriented toward the implementation of different tailored applications. Within this context, smart cities can represent a relevant area of application, being useful for managers and planners for protecting the existing urban assets, as well as the population, in the case of specific circumstances, such as those related to civil protection.

Acknowledgements. Authors wish to thank the firm Advanced Scientific Sensors and Systems (Adv3STM) for providing the instrumentation necessary to make the measurements presented in this work. Marco Casazza acknowledges the financing of his working position through the Italian Ministry of University PON fund, Azione IV.4 Asse IV “Istruzione e ricerca per il recupero – REACT-EU”.

References

1. Bibri, S.E., Krogstie, J.: Environmentally data-driven smart sustainable cities: applied innovative solutions for energy efficiency, pollution reduction, and urban metabolism. *Energy Inform.* **3**(1), 1–59 (2020). <https://doi.org/10.1186/s42162-020-00130-8>
2. Wong, M., Wang, T., Ho, H., Kwok, C., Keru, L., Abbas, S.: Towards a Smart City: development and application of an improved integrated environmental monitoring system. *Sustainability* **10**(3), 623 (2018). <https://doi.org/10.3390/su10030623>
3. Bacco, M., Delmastro, F., Ferro, E., Gotta, A.: Environmental monitoring for smart cities. *IEEE Sens. J.* **17**, 7767–7774 (2017). <https://doi.org/10.1109/JSEN.2017.2722819>
4. Anachkova, M., Domazetovska, S., Petreski, Z., Gavriloski, V.: Design of low-cost wireless noise monitoring sensor unit based on IoT concept. *J. Vibroeng.* **23**, 1056–1064 (2021). <https://doi.org/10.21595/jve.2021.21709>
5. Pedersen, E.: City dweller responses to multiple stressors intruding into their homes: noise, light, odour, and vibration. *Int. J. Environ. Res. Public. Health* **12**, 3246–3263 (2015). <https://doi.org/10.3390/ijerph120303246>
6. Persson Waye, K., et al.: Assessing the exposure-response relationship of sleep disturbance and vibration in field and laboratory settings. *Environ. Pollut.* **245**, 558–567 (2019). <https://doi.org/10.1016/j.envpol.2018.09.082>
7. Epstein, M.J.: Healing the urban soundscape: reflections and reverberations. *Cities Health* **5**, 74–81 (2021). <https://doi.org/10.1080/23748834.2019.1676628>
8. McAlexander, T.P., Gershon, R.R., Neitzel, R.L.: Street-level noise in an urban setting: assessment and contribution to personal exposure. *Environ. Health* **14**, 18 (2015). <https://doi.org/10.1186/s12940-015-0006-y>
9. Gill, S.A., Grabarczyk, E.E., Baker, K.M., Naghshineh, K., Vonhof, M.J.: Decomposing an urban soundscape to reveal patterns and drivers of variation in anthropogenic noise. *Sci. Total Environ.* **599–600**, 1191–1201 (2017). <https://doi.org/10.1016/j.scitotenv.2017.04.229>
10. Šturm, R., López Díez, J.J., Polajnar, J., Sueur, J., Virant-Doberlet, M.: Is it time for ecotremology? *Front. Ecol. Evol.* **10**, 828503 (2022). <https://doi.org/10.3389/fevo.2022.828503>
11. Šturm, R., et al.: Hay meadow vibroscape and interactions within insect vibrational community. *iScience* **24**(9), 103070 (2021). <https://doi.org/10.1016/j.isci.2021.103070>
12. Riahi, N., Gerstoft, P.: The seismic traffic footprint: Tracking trains, aircraft, and cars seismically. *Geophys. Res. Lett.* **42**, 2674–2681 (2015). <https://doi.org/10.1002/2015GL063558>
13. Farina, A., Eldridge, A., Li, P.: Ecoacoustics and multispecies semiosis: naming, semantics, semiotic characteristics, and competencies. *Biosemiotics* **14**(1), 141–165 (2021). <https://doi.org/10.1007/s12304-021-09402-6>
14. Wang, H., Quan, W., Wang, Y., Miller, G.: Dual roadside seismic sensor for moving road vehicle detection and characterization. *Sensors* **14**, 2892–2910 (2014). <https://doi.org/10.3390/s140202892>
15. Acernese, F., Giordano, G., Romano, R., De Rosa, R., Barone, F.: Tunable mechanical monolithic sensor with interferometric readout for low frequency seismic noise measurement. *Nucl. Instrum. Methods Phys. Res. Sect. Accel. Spectrometers Detect. Assoc. Equip.* **617**(1–3), 457–458 (2010). <https://doi.org/10.1016/j.nima.2009.10.112>
16. Barone, F., Giordano, G., Acernese, F., Romano, R.: Watts linkage based large band low frequency sensors for scientific applications. *Nucl. Instrum. Methods Phys. Res. Sect. Accel. Spectrometers Detect. Assoc. Equip.* **824**, 187–189 (2016). <https://doi.org/10.1016/j.nima.2015.11.015>

17. Barone, F., Giordano, G.: Mechanical accelerometers. In: Wiley Encyclopedia of Electrical and Electronics Engineering, pp. 1–28. John Wiley & Sons, Inc., Hoboken (2015)
18. Barone, F., Giordano, G.: The UNISA folded pendulum: a very versatile class of low frequency high sensitive sensors. *Measurement* **118**, 339–347 (2018). <https://doi.org/10.1016/j.measurement.2017.09.001>
19. Barone, F., Giordano, G.: A new typology of DC tiltmeter based on the Watt's linkage architecture. *Sens. Actuators Phys.* **281**, 264–277 (2018). <https://doi.org/10.1016/j.sna.2018.08.015>
20. Travasso, F.: Low temperature performances of a monolithic folded pendulum sensor for the third generation of interferometric detectors of gravitational waves. In: The international GRAvitational-wave Science & technology Symposium (GRASS 2018). Padova (Italy) (2018)
21. Humphreys, B.: ConvertTDMS (v10) (2022)
22. Haney, M.M., Power, J., West, M., Michaels, P.: Causal instrument corrections for short-period and broadband seismometers. *Seismol. Res. Lett.* **83**, 834–845 (2012). <https://doi.org/10.1785/0220120031>
23. Acernese, F., De Rosa, R., Giordano, G., Romano, R., Barone, F.: Tunable mechanical monolithic horizontal accelerometer for low frequency seismic noise measurement. Paper presented at the SPIE Europe Remote Sensing, Berlin, Germany, 17 Sept 2009
24. Guillier, B., et al.: The SESAME team: Influence of instruments on the H/V spectral ratios of ambient vibrations. *Bull. Earthq. Eng.* **6**, 3–31 (2008). <https://doi.org/10.1007/s10518-007-9039-0>
25. Tasič, I.: Interdependent quality control of collocated seismometer and accelerometer. *J. Seismolog.* **22**(6), 1595–1612 (2018). <https://doi.org/10.1007/s10950-018-9788-z>
26. D'Alessandro, A., et al.: Urban seismic networks, structural health and cultural heritage monitoring: the National Earthquakes Observatory (INGV, Italy) Experience. *Front. Built Environ.* **5**, 127 (2019). <https://doi.org/10.3389/fbuil.2019.00127>
27. Baraccani, S., Azzara, R.M., Palermo, M., Gasparini, G., Trombetti, T.: Long-term seismometric monitoring of the two towers of Bologna (Italy): modal frequencies identification and effects due to traffic induced vibrations. *Front. Built Environ.* **6**, 85 (2020). <https://doi.org/10.3389/fbuil.2020.00085>
28. Hsu, T.-Y., Yin, R.-C., Wu, Y.-M.: Evaluating post-earthquake building safety using economical MEMS seismometers. *Sensors* **18**, 1437 (2018). <https://doi.org/10.3390/s18051437>
29. Roselli, I.: Urban transport vibrations and cultural heritage sites in Rome: the cases of the temple of Minerva Medica and of the catacomb of Priscilla. Presented at the SUSTAINABLE CITY 2017, Seville, Spain, 18 Sept 2017
30. Barone, F., Giordano, G.: Mechanical monolithic inertial sensors for historical and archeological heritage real-time broadband monitoring. In: D'Amico, S., Venuti, V. (eds.) *Handbook of Cultural Heritage Analysis*, pp. 1137–1166. Springer, Cham (2022). https://doi.org/10.1007/978-3-030-60016-7_39
31. Petti, L., Barone, F., Mammone, A., Giordano, G.: Static and dynamic behaviour assessment of the Trajan Arch by means of new monitoring technologies. *The Int. Arch. of the Photogram., Remote Sens. Spatial Inf. Sci.* **XLII-2/W5**, 567–574 (2017). <https://doi.org/10.5194/isprs-archives-XLII-2-W5-567-2017>
32. Petti, L., Barone, F., Greco, D., Zuchtriegel, G.: Innovative structural monitoring as tool of preservation and valorization of monumental architectures: the case of Neptune Temple. Presented at the Sustainable Conservation of UNESCO and other Heritage Sites through Proactive Geosciences, Egypt, 10 Dec 2019

33. Hayashi, K., Saito, T., Horioka, T., Sato, E.: Implementation of real-time seismic diagnostic system on emergency management center buildings: system introduction and operational status on municipal government office buildings. *J. Civ. Struct. Heal. Monit.* **9**(4), 529–541 (2019). <https://doi.org/10.1007/s13349-019-00349-4>



The Sustainable and Smart Mobility Strategy: Country Comparative Overview

Olga Kunytska¹  , Luca Persia² , Norbert Gruenwald³, Diana Datsenko¹ ,
and Malgorzata Zakrzewska⁴ 

¹ National Transport University, 1 Mykhaila Omelianovycha-Pavlenka Street,
Kyiv 01001, Ukraine

olga.kunytska@ntu.edu.ua

² Sapienza University of Rome, 5 Aldo Moro Piazzale, 00185 Rome, Italy

³ University of Applied Science: Technology, Business and Design, 14 Philipp-Müller-Straße,
23966 Wismar, Germany

⁴ University of Szczecin, 22A Papieża Jana Pawła II Aleja, 70453 Szczecin, Poland

Abstract. Mobility is an integral part of everyday life and affects the well-being of European citizens. At the same time, the negative consequences of transport use – traffic accidents, noise and deteriorating air quality – can be observed in almost all cities. Mobility has a significant environmental impact, being responsible for over 27% of all greenhouse gas emissions. One of the goals of The Sustainable and Smart Mobility Strategy, which is part of the European Green Deal package, is to reduce greenhouse gas emissions in the transport sector. The Strategy contains 82 initiatives that should transform the countries transport system into a smart, competitive, safe, inclusive and affordable one. This European Union policy document is transforming the European transport system so that transport emissions are reduced by 90% by 2050 and cities become more resilient to future crises. The purpose of this article is to analyze the implementation and realization of the Strategy in the countries of Italy, Germany, Poland and Ukraine.

Keywords: Smart city · Sustainability · Smart mobility · Sustainable city

1 Introduction

The world's biggest cities have faced challenges throughout their history from growing populations and environmental degradation. And although mobility is part of citizens' daily lives and affects their well-being, the transport sector is responsible for almost a quarter of greenhouse gas emissions [1].

Recently, the difficulties of the transport sector have been compounded by the impact of the COVID-19 epidemic – the number of passenger transport journeys has fallen crucial and there is a need to redesign the urban environment towards greater social distance in public transport, on the streets and in other public spaces.

One of the responses to these challenges is the implementation of a Sustainable and Smart Mobility Strategy ('the Strategy'). The experience of developed countries in

responding to the COVID-19 pandemic in the first half of 2020 has shown that sustainable mobility measures and organizational solutions have proven to be some of the most needed in practice.

The Strategy released at the end of 2020 is part of the EU Green Deal [1]. The strategy lays the foundation for the digitalization of the European transport system as well as for its greening and resilience to future crises.

2 Literature Review

The concept of sustainable transport, like the more general sustainable city concept, is an interdisciplinary, practice-oriented approach that implements current theoretical positions in ecology, economics, urban planning, health, etc. When analyzing the research on the topic, two directions can be indicated:

1. Studies that directly examine sustainable transport as a distinct field.
2. Studies that examine related fields and consider sustainable mobility in the context of their research aspect. For example, in the context of sustainable or smart city issues, urban planning approaches urbanism and design, healthy life-styles, etc.

Sustainable mobility has been addressed in several seminal studies since the mid-1980s when motorization in developed countries reached its peak [2, 3]. The first works focused on academic critiques of private car-oriented transport planning as well as investigating so-called transport paradoxes and describing the effects of induced demand. It has been investigated that, as a result of the expansion of the street network, the authorities are provoking new demand for road infrastructure, disproportionately exceeding the value of the road resource added.

Car users, responding to increased road infrastructure and new opportunities for shorter travel times, etc., are increasing their use of cars, including shifting from public transport to private cars. Studies show that a 10% increase in road capacity increases the number of vehicles by 3–6% in the short term and by 6–10% in the long term [4] (the Lewis-Mogridge paradox [5], Braes' paradox [6], Dawn's paradox [7].) The key conclusion from the reviewed works is that to create an efficient transport system, it is not the expansion of infrastructure but the introduction of regulatory measures that create a system of incentives to use the most efficient types of mobility.

These conclusions are in line with the main objectives of The Sustainable and Smart Mobility Strategy [1]. And although its main purpose is to transform the European transport system so that transport emissions are reduced by 90% by 2050 compared to 2017, and make cities more resilient to future crises, as an interdisciplinary concept, the Strategy is in close contact with other related theories of urban development.

The paper considers examples of the implementation of the Strategy for four countries – Italy, Germany, Poland and Ukraine.

3 Italy Case Study

3.1 The Need for a Sustainable, Smart and Resilient Mobility Strategy in Italy

The transport sector (in its different modes) contributes significantly to greenhouse gas emissions in Italy, and the situation could worsen in the near future. In fact, measures to contain the COVID-19 pandemic have strongly affected population mobility showing an increase in 2020 in the proportion of people who habitually travel to work only by private modes of transport (75.0%) [8], rather than more sustainable modes of transportation such as public transportation.

In this scenario, current Italian planning policies are addressed to ensure sustainable mobility in road transport (especially in the changing of the car fleet from more polluting vehicles to the less-ones) with particular reference to the renewal of local public transport vehicles and interventions aimed at encouraging the use of zero impact transport modes such as cycling and electric micro-mobility, but also with reference to maritime transport.

3.2 Sustainable Mobility

In line with the greenhouse gas emission reduction targets (55% by 2030 and 90% by 2050) set out in the 2019 European “Green Deal” Communication, Italy approved the same year the National Strategic Plan for Sustainable Mobility [9].

The Plan is intended for the renewal of the bus fleet of local and regional public transport services and for the promotion and improvement of air quality with innovative technologies. The 2018 Budget Law has established the opportunity to use up to 100 million euros to finance experimental and innovative sustainable mobility projects, in line with the Sustainable Urban Mobility Plans (SUMP) for the implementation of alternative fueled vehicles or boats and related support infrastructure, presented by municipalities and metropolitan cities.

A second pillar contributing to sustainable mobility in urban areas is the SUMP. As of September 2021, 196 SUMP have been initiated, 53 of them approved and 45 adopted and 98 are in the process of being drafted [10].

With regard to cycling, the cornerstone of planning for the development of cycling and the implementation of the national network of cycling is represented by the National Plan for Cycling Mobility. The Plan is articulated with reference to two areas of intervention, relating, respectively, to the development of cycling in urban and metropolitan areas and the implementation of cycling on routes defined as regional, national and European levels.

3.3 Smart Mobility

Smarter Italy is a program promoted by the Ministry of Economic Development (MISE), the Ministry of University and Research (MUR) and the Minister for Technological Innovation and Digitization which aims to improve the life of communities and citizens through the experimentation in the territories of emerging technological solutions in different areas: mobility, environment, personal well-being and cultural heritage [11]. The financial endowment for the Smarter Italy program is over 90 million euros.

The first action of the Smarter Italy program involves the definition of one or more innovative tenders for the development of solutions that improve the mobility and logistics of Italian cities according to the “Smart city” paradigm. The action involves, as hosts: The Municipalities that have joined the experimentation of the 5G network and 12 “Villages of the Future”. The hosts expressed their needs for innovation in terms of traffic, pollution, livability of historic centers, usability of industrial districts. These needs can be scalable throughout the national territory. On the basis of the needs that emerged, a public consultation was launched with market operators: companies, start-ups, universities, research centers. The winning solutions will be tested on the territories of the proposing municipalities.

Another important element of the Italian smart mobility strategy is smart roads. The former Ministry of Infrastructure and Transport (MIT) issued 2018 the Smart Road Decree [12], indicating which are the new smart services concerning the roads, and where and when they will be carried out. The government expects to invest a total of 1 billion euros in the coming years for digitization projects, including the 3,000 km of smart road.

In the first phase, by 2025, action is taken on the Italian infrastructures belonging to the European TEN-T network, and on the entire motorway network. Progressively, the services will be extended to the entire road network of the integrated national transport system.

3.4 Resilient Mobility

Resilient mobility is mainly addressed by the National Recovery and Resilience Plan (NRP), which includes a package of investments and reforms divided into six missions, two of them relevant to mobility [13]. Mission 2 is contributing especially to sustainable mobility, by including actions relating to hydrogen testing for road and rail transport and investment in electric buses and the development of more sustainable local transport,

Mission 3: Infrastructures for Sustainable Mobility is more relevant to resilient mobility. It provides interventions to complete the main high-speed and high-capacity railway corridors, integrating them with the regional rail network and making the whole rail network safe. In close connection with the strategic framework of the Mission 3, on the basis of national resources, investments will also be made for Road Safety 4.0, in order to improve the safety and climate/seismic resilience of bridges and viaducts, using the solutions provided by technological innovation and with a view to adapting to climate change.

In Fig. 1 shown the change in the modal share for passenger and freight transport between 2019 and 2030 following the implementation of the actions in the NRP. Thanks to the reduction in average rail travel times throughout the country with a more marked increase in accessibility in the economically more vulnerable areas, there is a significant increase in the modal share of both freight and passenger transport by rail.

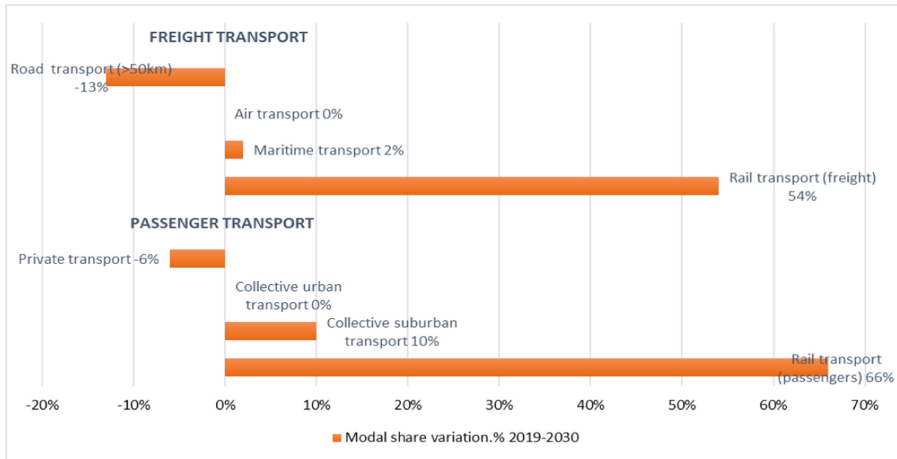


Fig. 1. Passenger transportation modal split 2019 and 2030 as a result of NRP implementation (% values) [14].

However, the NRP lacks an integrated approach to road safety. This is addressed in the recent National Road Safety Plan 2030 (NRSP). The NRSP adopts the Safe System approach suggested at the international level to achieve the goal of zero road deaths and serious injuries by 2050 through intermediate steps. It is a new model that tackles the issue of road safety by adopting an integrated vision that simultaneously takes into account the various aspects that affect risk factors.

4 Germany Case Study

4.1 The Need for a Sustainable, Smart and Resilient Mobility Strategy in Germany

In Germany, the mobility volume between 2010 and 2030, as formulated in the Federal Transport Infrastructure Plan (BVWP) 2030. According to it, freight traffic will grow by 38%.

An important approach to counteract this circumstance is the expansion and new construction of the modes of transport and their transport capacity with only limited possibilities to increase the traffic area.

In many cases, the expansion or new construction of traffic areas even leads to disproportionately high additional traffic. When choosing a mode of transport in the direction of supposedly more efficient mobility modes such as car-sharing or ride-hailing, this is made more difficult by the fact that it leads to the substitution of bicycle and pedestrian traffic by these emission-intensive modes, as could be demonstrated with the example of Uber [15].

4.2 Sustainable and Smart Mobility

On average, German drivers spent 457,000 h in traffic jams – that's what the ADAC reported at the end of last year. Current approaches to solutions using micro-mobility

solutions such as e-scooters or hailing/sharing offers usually only lead to an undesirable substitution of emission-free alternatives (pedestrian/bicycle traffic) and are therefore not suitable in their current form. Mobility will continue to change and develop as a result of ongoing digitalization [16].

Smart Mobility is not a solution, but the future. Many metropolises and regions in Germany already offer their passengers the option of using an app to switch between different means of transport. However, these offers always remain on the respective network connected mobility systems limited.

In the Aachen region, a seamless, digital mobility service is being made available with a so-called mobility broker “movA”. The offer can be accessed via PC, laptop or smartphone and links public transport with other mobility providers so that in addition to buses and trains, numerous sharing offers such as e-scooters, pedelecs or taxis are also available as on-demand solutions.

EUROPEANMOBILITYWEEK (EMW) is the European Commission’s flagship awareness-raising campaign on sustainable urban mobility. It promotes behavioral change in favour of active mobility, public transport, and other clean, intelligent transport solutions.

In 2022, the winners of the European Awards for Sustainable Mobility 2021 were crowned in Brussels, including the two EMW Awards. Kassel (Germany) walked away with the EMW Award 2021, it impressed the jury with its creative activities, which brought local and regional transport partners together to pro-mote behavioral changes in children and adults. The city also implemented a number of permanent measures, including road safety signs near schools and the redesign of two busy streets for bicycle use. That are a few examples and show that Germany is one of the world leaders in sustainable, innovative and efficient mobility solutions.

4.3 Mobility Network

Germany has a long history of successful changes and transformations in the transport sector. The German Partnership for Sustainable Mobility (GPSM) is an initiative by the Federal German Ministry for Economic Cooperation and Development (BMZ) and the Ministry for the Environment, Nature Conservation, Building and Nuclear Safety (BMUB). The German Partnership for Sustainable Mobility is serving as a guide for sustainable mobility and green logistics solutions in Germany. As a platform for exchanging knowledge, expertise and experiences, GPSM supports the transformation towards sustainability in developing and emerging countries. It serves as a network of information from academia, businesses, civil society and associations [17].

The German Partnership for Sustainable Mobility (GPSM) has become ‘TUMI Friends’ (Transformative Urban Mobility Initiative) and continues to serve as a guide for sustainable mobility and green logistics solutions in Germany. As a platform for exchanging knowledge, expertise and experiences, TUMI Friends supports the transformation towards sustainability in developing and emerging countries. It serves as a network of information from academia, businesses, civil society and associations.

5 Poland Case Study

5.1 Sustainable and Smart Mobility Strategies in Poland

Urban policy in Poland is based on three main documents: The Strategy for Responsible Development (SOR) (2017), the National Strategy for Regional Development (KSRR) of 2019 and the National Urban Policy (KPM) of 2015 [18]. These documents construct the main areas of activities and define the most crucial challenges facing cities and also present a vision of city development. The need for changes in individual and collective mobility (including through the promotion of collective transport) is also addressed in the Strategy for the Sustainable Development of Transport up to 2030, which was adopted in 2019. As [19] research indicates, in Poland:

- there is an emphasis on ‘hard’ development factors and physical infrastructure investments in the areas of transport, energy and ICT;
- hard infrastructure projects are planned regionally, reflecting inter-municipal cooperation requirements mandated by EU policy;
- in terms of prioritization within strategies, transportation is by far the central area of focus, followed by energy efficiency and ICT;
- efficiency gains in public service provision were inferred through their digitalization on official municipal websites.

5.2 Smart City Policies in Polish Cities

However, more and more cities in Poland are making an attempt to be considered the smartest, researches indicate four main metropolises as the smartest cities in Poland. Namely: Warsaw, Wroclaw, Cracow, and Gdansk. As indicated in Table 1, mentioned cities vary considering using Smart City policies, implementing both “hard” and “soft” types. Examples of each type of policies were indicated in Table 2 and Table 3.

Table 1. Projects related to Smart City policies in the smartest cities of Poland [20].

Cities and their metropolitan areas	Hard infrastructure/tangible resources				Soft skills/intangible capital			
	Energy	Transportation	Water and waste	ICT	Education	Health	Social care	Participation (e-governance)
Warsaw		X						
Warsaw Metro	X	X						X
Krakow				X				
Krakow Metro	X	X						
Łódź	X	X		X				

(continued)

Table 1. (continued)

Cities and their metropolitan areas	Hard infrastructure/tangible resources				Soft skills/intangible capital			
	Energy	Transportation	Water and waste	ICT	Education	Health	Social care	Participation (e-governance)
Łódź Metro	X	X						
Wrocław		X						
Wrocław Metro	X	X		X				
Poznań	X	X	X	X	X		X	X
Poznań Metro	X	X		X				
Gdańsk	x	X	x	X	X			X
Gdańsk Metro		x		X				

Table 2. Projects related to Smart City policies (area: e-government) in the smartest cities of Poland [20].

Categories	Warsaw	Krakow	Łódź	Wrocław	Poznań	Gdańsk
Management	<ul style="list-style-type: none"> • Open access to municipal services 24/7 • Management of schools • Open data 	<ul style="list-style-type: none"> • Land information system • Order and waste in city app • Car-sharing 		<ul style="list-style-type: none"> • Virtual citizens advisor <ul style="list-style-type: none"> • Real estate market • Mobile assistant – app • Individual license plates <ul style="list-style-type: none"> • City council software • Land information system • Public administration services for residents • Electronic document management in city hall <ul style="list-style-type: none"> • Queue system • Sign language interpreter • One phone number to city hall <ul style="list-style-type: none"> • Open data • Public telecommunication net 	<ul style="list-style-type: none"> • Public admin. Services for residents • Electronic document management in city hall • Open data • Electronic system of booking visits • Open data • Land information system • System of grants proceeding • Operational and strategic risk managing system • Web survey 	<ul style="list-style-type: none"> • Map of city order • City apps • ISO 37120 standard • Land information system • Integration of urban telecommunication subsystems for better managing • System for management in education • Public administration services for residents • Open data • System for planning of city’s budget • Queue system

Table 3. Projects related to Smart City policies (area: social actions) in the smartest cities of Poland [20].

Categories	Warsaw	Krakow	Łódź	Wroclaw	Poznań	Gdańsk
Education				<ul style="list-style-type: none"> • Explain Everything for schools • Scholarships for university students • School in the city (in public institutions) • Integrated system of education management • Telecommunications connections among schools 	<ul style="list-style-type: none"> • Recruitment to schools 	<ul style="list-style-type: none"> • Smart apps by students • Support in ICT solutions for public sector by universities
People	<ul style="list-style-type: none"> • Support for senior citizens • Civic budget • Web portal of volunteering 	<ul style="list-style-type: none"> • Civic budget • Guide for disabled - app 	<ul style="list-style-type: none"> • Civic budget • Electronic search of dead people in cemeteries • Web system for dialog • Tele-care 	<ul style="list-style-type: none"> • Support for NGO's • City guide • Support for senior citizens • City blogs • Public consultations web portal • Civic budge 	<ul style="list-style-type: none"> • Civic budget • Web system for dialog • Addresses in city • Electronic job exchange • Electronic search of dead people in cemeteries • Warnings system 	<ul style="list-style-type: none"> • Civic budget
Living (place)	<ul style="list-style-type: none"> • System of notification about events • Internet hot-spots 	<ul style="list-style-type: none"> • Green places and events in city – app • Internet hot-spots 	<ul style="list-style-type: none"> • Internet hot-spots • City guide 	<ul style="list-style-type: none"> • Regeneration of trade streets • Events and leisure time in city • Cultural events • Co-operatives and self-made buildings • Health events • Urban events card • Internet hot-spots 	<ul style="list-style-type: none"> • Green places – app • Churches in city • City guide • Airport guide • Smart zoo • Exchange of handbooks • E-books from city's libraries • Internet hot-spots 	<ul style="list-style-type: none"> • Adoption of animals • Cultural events • Conventions in the city – app • Internet hot-spots

Polish cities appear to be partially successful in the implementation of Smart Cities strategies. There is a slightly change to be observed especially in such areas as cooperation, increased digitalization of services and meeting needs [20]. The biggest obstacles that are addressed consider: lack of resources and experience and technical capacity [20]. Eventhugh, as researches indicate there is potential for gradual change and innovation, a balance between business interests and innovations, technological change, local government responsibilities and citizen needs is key to maintaining sustainable development and improving the quality of life in cities [19, 20].

6 Ukraine Case Study

6.1 Importance of Sustainable and Smart Mobility Strategy for Ukraine

Emissions of greenhouse gases from transport in Ukraine account for about 10–12% of all greenhouse gas emissions per year [21], and emissions of harmful pollutants into the air from transport 35–40% [22]. In large cities emissions from transport can account for up to 90% of all emissions. A shift to low or zero-emission transport is therefore important for Ukraine.

There are some differences in the objectives declared by the EU and Ukraine: The European Union aims to reduce emissions from transport by 90% and to create a climate-neutral continent by 2050, while Ukraine aims to become carbon neutral by 2060. However, despite these differences in the declared objectives of the EU and Ukraine, the key priorities of the Mobility Strategy fully correspond to the goals and objectives of Ukraine in cooperation with the EU.

6.2 Priority Areas for Ukraine's Development

Development of Cycling Infrastructure

20 Ukrainian cities and united territorial communities have developed and approved cycling infrastructure plans. However, there are not enough bicycle lanes in Ukrainian cities (Fig. 2) [23].

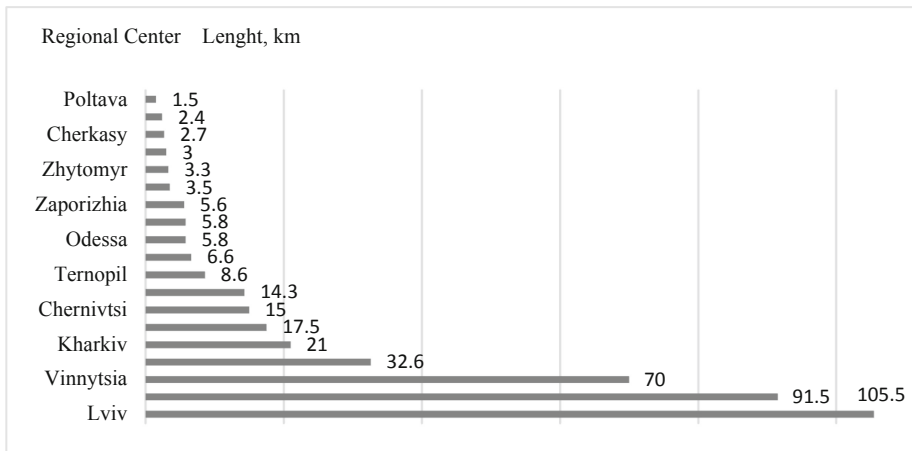


Fig. 2. Length of bicycle lanes in regional centers of Ukraine, km (April 2020) [25].

Development of Electric Mobility

Ukraine is already creating incentives for the development of electric vehicles thanks to easier taxation for the import of electric vehicles. As a result, the electric vehicle market

in Ukraine is growing: as of January 1, 2022, over 33 thousand electric vehicles were registered, and in 2021 Ukrainians purchased 8.8 thousand electric-powered cars [24]. Specialized chargers have not yet been introduced for trucks, so there are only light trucks in the country.

A priority for electric mobility is to expand the network of charging stations - there are 8,529 electric vehicle charging stations in Ukraine, September 2020 [25].

Development of Sustainable Urban Mobility Plans for Ukrainian Cities

The integration of Ukraine's transport network into the TEN-T requires the fulfilment of the network development requirements. In particular, the cities that are "nodes" of the network must develop Sustainable Urban Mobility Plans. As of the end of 2021, the 8 cities have Sustainable Urban Mobility Plans (SUMP) (Table 4).

Table 4. Development of a Sustainable Urban Mobility Plan for Ukrainian cities, 2021.

City	Zhytomyr	Ivano-Frankivsk	Lviv	Mykolayiv	Poltava	Kharkiv	Kherson	Ternopil
Deadline	2019	2015	2020	2018	2018	2021	2021	2022
Funded by	Grant GIZ	Grant GIZ	Grant GIZ	Budget funds	Grant GIZ	Grant GIZ	Grant EBRD	Budget funds
Developer	Dornier	PTV & Dreberis	Lviv-avtodor	A + C	Dornier	Dornier	Egis	Dornier

Micro Mobility as a "LAST-MILE" Solution

Micro-mobility in Ukraine is evolving. The number of bicycle couriers has increased by 35–48% since autumn 2019 compared to the same period in 2020, this is due to the growth of e-commerce and a corresponding change in customer behavior [26].

Around 5% of the cyclists observed in the survey used a bicycle rental service. The increased popularity of micro-mobility was a consequence of quarantine restrictions and interruption of public transport. This boom in micro-mobility has opened up many problems in urban infrastructure and traffic law.

6.3 Changes as a Result of the Strategy Implementation

When analyzing the impact created on the transport sector in Ukraine by the adoption of the Sustainable and Smart Mobility Strategy, several trends can be identified:

- the Strategy may have a negative impact on the Ukrainian road business transporting cargo to Europe, as more rail freight becomes a priority. This trend is evident in the decreasing number of transport permits Ukraine receives;
- the Strategy encourages the development of multimodal complexes at Ukraine's western border crossings with the EU. This will contribute to a change in the investment policy of European banks for infrastructure projects in Ukraine.

It should be noted that the actions initiated to implement the Strategy have been suspended or even set back due to the impact of military operations in Ukraine since

February 2022. Thus, as of late April 2022, according to the State Agency of Ukrainian Highways “Ukravtodor” the number of public roads destroyed due to military operations is 23,000 km of roads. In addition, 273 structures, including bridges and overpasses, were destroyed. The total amount of damage reaches – EU 26 billion for roads, and 1.2 billion for bridges [27]. According to preliminary expert estimates, about 500 thousand cars have been irretrievably lost due to hostilities in Ukraine. Another 300 thousand vehicles have left the territory of Ukraine. In total, about one million cars have been withdrawn from the active part of the car fleet.

7 Conclusion

This paper reviews the main initiatives of The Sustainable and Smart Mobility Strategy published by the EU in December 2020. One of the goals of the Strategy, which is part of the European Green Deal package, is to reduce greenhouse gas emissions in the Transport sector.

The paper examines the implementation of The Strategy in Italy, Germany, Poland and Ukraine. Identification of the main drivers of each country for Strategy points performance. The priority areas for realization are presented and the difficulties faced by the countries in implementing the Strategy initiatives are highlighted.





References

1. EU Commission: Annex to the Communication from the Commission to the European Parliament, the European Council, the Council, the European Economic and Social Committee and the Committee of the Regions. The European Green Deal, Brussels (2019)
2. Williams, K. (ed.): Spatial Planning, Urban Form and Sustainable Transport. Routledge (2017). <https://doi.org/10.4324/9781315242668>
3. Schiller, P., Kenworthy, J.: An Introduction to Sustainable Transportation. Routledge, London (2017). <https://doi.org/10.4324/9781315644486>
4. Litman, T.: Smart Congestion Relief-Comprehensive Evaluation of Traffic Congestion Costs and Congestion Reduction Strategies. Victoria Transport Policy Institute (2021)
5. Burnewicz, J.: Economic paradoxes in transport. *Transp. Econ. Logistics* **67**, 11–21 (2017). <https://doi.org/10.5604/01.3001.0010.5774>
6. Ma, J., Li, D., Cheng, L., Lou, X., Sun, C., Tang, W.: Link restriction: Methods of testing and avoiding braess paradox in networks considering traffic demands. *J. Transp. Eng., Part A: Syst.* **144**(2), 04017076 (2018). <https://doi.org/10.1061/JTEPBS.0000111>
7. Albers, G.W.: Late window paradox. *Stroke* **49**(3), 768–771 (2018). <https://doi.org/10.1161/STROKEAHA.117.020200>
8. ISTAT: Annual Report 2020: The Situation of the Country. Rome, Italy (2020)
9. Camera dei Deputati: La Mobilita Sostenibile. Rome, Italy (2022) [in Italian]
10. Osservatorio PUMS: L'Osservatorio – I PUMS in Italia: stato dell'arte. <https://www.osservatoriopums.it/osservatorio/pums>. Accessed 10 May 2022
11. Ministry of Economic Development of Italy: Decree of 31 January 2019. Allocation of resources from the Fund for Sustainable Growth for the implementation of calls for intelligent public demand. Rome, Italy (2019)
12. The Ministry of Infrastructure and Transport of Italy: Decree 28 February 2018. Implementation methods and operational tools of road testing of Smart Road solutions and connected and automatic driving. Rome, Italy (2018)

13. Italiano, Governo: Piano Nazionale di Ripresa e Resilienza (PNRR). Rome, Italy (2021)
14. Ministero delle Infrastrutture e della mobilità sostenibili: Cambiamenti climatici, infrastrutture e mobilità. Rome, Italy (2022)
15. Graehler, M., Richard, A., Gregory D.: Understanding the recent transit ridership decline in major US cities: Service cuts or emerging modes. Paper presented at 98th Annual Meeting of the Transportation Research Board. Washington, DC (2019)
16. Kazmaier, M., Taefi, T.T., Hettesheimer, T.: Techno-economical and ecological potential of electric scooters: a life cycle analysis. *European J. Transp. Infrastruct. Res.* **20**(4), 233–251 (2020). <https://doi.org/10.18757/ejtir.2020.20.4.4912>
17. TUMI Friends. <http://www.german-sustainable-mobility.de>. Accessed 10 May 2022
18. Polish Ministry of Infrastructure and Development: National Urban Policy 2023. Warsaw, Poland (2015)
19. Masik, G., Sagan, I., Scott, J.W.: Smart City strategies and new urban development policies in the Polish context. *Cities* **108**, 102970 (2021). <https://doi.org/10.1016/j.cities.2020.102970>
20. Bielińska-Dusza, E., Hamerska, M., Żak, A.: Sustainable mobility and the Smart City: a vision of the city of the future: the case study of Cracow (Poland). *Energies* **14**(23), 7936 (2021). <https://doi.org/10.3390/en14237936>
21. UNFCCC: National Greenhouse Gases Inventory Report, Ukraine 2020. Kyiv, Ukraine (2021)
22. Air emissions from mobile transport means by regions. http://www.ukrstat.gov.ua/operativ/operativ2020/ns/vzrpgz_reg_2019.html. Accessed 10 May 2022
23. Micromobility has approached Ukraine. <https://blog.liga.net/user/vsamoilenko/article/36936>. Accessed 10 May 2022
24. Ministry of Infrastructure of Ukraine: Ukravtodor Approved the Action Plan to Support Electric Mobility. Kyiv, Ukraine (2022)
25. Developing the infrastructure for electric cars. Green expedition. <https://ukrainer.net/infrastructure-for-electric-cars/>. Accessed 10 May 2022
26. Kunytska, O., Comi, A., Danchuk, V., Vakulenko, K., Yanishevskiy, S.: Optimizing last mile delivering through the analysis of shoppers' behaviour. In: Sierpiński, G., Macioszek, E. (eds.) *Decision Support Methods in Modern Transportation Systems and Networks*. LNNS, vol. 208, pp. 129–147. Springer, Cham (2021). https://doi.org/10.1007/978-3-030-71771-1_9
27. Ukravtodor counted how many roads were destroyed during the war. <https://www.avtomir.ua/news/ukraine/ukravtodor-pidrahuvav-skilky-dorig-zrujnovano-pid-chas-vijny/>. Accessed 10 May 2022



Definition of the e-Scooter Sharing Stations Number and Location Under a Lack of Data: A Case Study of the City District in Dnipro

Olha Svichynska^{1,2} , Kateryna Serhienko^{1,2} , Stanislav Svichynskyi^{1,2} ,
and Vitalii Chyzhyk^{1,2} 

¹ Kharkiv National Automobile and Highway University, 25 Yaroslava Mudrogo Street,
Kharkiv 61002, Ukraine

tsl@khadi.kharkov.ua

² Modern Solutions Group, Ltd., Dnipro 49040, Ukraine

Abstract. In Ukrainian cities, the number of users of bicycles, usual and electric scooters, and e-unicycles increased in recent years. All these vehicles are a direct alternative to walking trips or short-distance transport trips. During the COVID-19 pandemic, the micromobility has become a safe option to travel in the open air which ensured the possibility to keep social distance and reduce the number of contacts in comparison with public transport. This paper presents the approach to defining the rational number and location of e-scooter sharing stations under limited data. To estimate the number of the sharing stations, the station capacity, potential daily demand for e-scooter trips and the locations of available e-scooters were used. The locations of sharing stations were defined concerning walking accessibility, demand coverage and remoteness from the shortest path of the vehicle commissioned to collect the scooters for recharging or replace the scooter batteries on-site. The research was conducted by the example of Sobornyi district in Dnipro, Ukraine. Apart from the number and location of sharing stations, the potential flows of e-scooter riders were modeled. These findings are relevant because they can provide local authorities and sharing operators with the information for well-grounded decisions on public space and street design, micromobility infrastructure extension as well as planning of the sharing system performance indicators.

Keywords: e-Scooter · Micromobility · Sharing station · Micro-vehicle infrastructure · Shared mobility

1 Introduction

At the beginning of the COVID-19 pandemic, the society had experienced chaos in the field of passenger transportation, and most of the population had to stay home while some people found themselves searching for an alternative to their usual mode of travelling. In Ukraine, the users of bicycles, usual and electric scooters (e-scooters), e-unicycles and hoverboards become more frequent, and the use of these micromobility vehicles (also

called micro-vehicles) become an alternative to walking or short-distance transport trips. An example is also the USA where nearly 60% of all trips by micro-vehicles are made for a distance up to 5 miles [1].

This mode of transport is safe and truly mobile as it allows planning the personal trips in the open air, keeping a social distance and reducing the number of contacts in comparison with ‘usual transport’ trips.

In our country, micromobility trips are purely studied, and the research of these trips is actual because the information about the demand for this type of travel will allow better planning of walking and micromobility trips and defining rational locations of the sharing stations at the city streets.

According to foreign information agencies, the majority of the users use micro-vehicles to make home-based work trips or get to the public transport stop if the distance allows it. Therefore, the lanes for bikes and e-scooters have been built in many cities to avoid conflict situations with pedestrians on the pavements and drivers on the carriageways.

This trend is also relevant to our country, where the use of bicycles and e-scooters becomes popular causing an increase in the number of sharing stations and charging points, but with the slow development or even absence of dedicated lanes or paths. At the same time, there happen the situations in big cities when these stations have low demand or, on the contrary, a low capacity.

In the modern world, there exist opportunities to use data from mobile apps to monitor a wide list of indicators which are of interest to the operators, researchers and core departments in the city councils. Among these indicators are micromobility vehicle locations, travel speed, distance travelled by each user, battery condition, etc. [2]. The study of these indicators supports the development of the micromobility system.

There is no secret that usually, the research projects in Europe are large-scale and deep, and the micromobility studies are not the exception. But what a researcher should do if he or she faces a lack of data or resources? Unfortunately, such a situation is common in Ukrainian reality, and to address this issue this paper presents the approach to calculating the rational number of e-scooter sharing stations, their locations and the influence on the potential demand under the conditions of a lack of data and resources.

2 Literature Review

2.1 Rising Demand for e-Scooter Trips and the Ways to Organize Them

E-scooter sharing services have appeared on the global market in 2018 owing to Lime, Inc. And Bird, Inc., USA. Just in a couple of years, e-scooters have rapidly spread across the US and European cities. In two years after the launch of the e-scooters production in California, one of the start-ups in e-scooter sharing appeared to be able to enter the market in more than 100 cities on almost all continents and service millions of riders.

Generally, electric transport development advanced the occurrence of ‘shared mobility’. At present, this term covers different types of sharing services: car-sharing, bike-sharing and micromobility vehicle sharing. These lines of business are carried on by the famous company Uber which is also one of the major investors in the start-ups in the production of e-scooters and development of the mobile apps for sharing systems [3].

E-scooters along with other road vehicles should operate according to law. Development of the corresponding regulations is under the jurisdiction of a government and local authorities. Different cities reacted to the trend of shared mobility and associated problems in different ways. These problems still exist, and they are as follows.

Because of the fact that e-scooters are used in public spaces, it is difficult to ensure the safety of their use. Uncontrolled scooter parking can negatively influence the mobility of vulnerable people like blind or visually impaired persons, elderly people and children. Also, among the problems caused by uncontrolled scooter parking is the blocking of the pavements, passageways, entrances to the buildings, pedestrian crossings and public transport stops.

The governments in many countries addressed these problems through the development of the laws which introduce the rules on the use of e-scooters on public roads. These rules regulate the fines for a ride on pavements and footpaths, the minimum number of sharing stations, the license fee for one micro-vehicle, the areas restricted for parking, minimal rider age, permitted maximal speed, the presence of obligatory equipment (license plates, indicators, rear lights, brakes), etc. The rules of this type are developed and introduced in the United Kingdom Malta, France, Germany, Italy, Bulgaria and other countries [4–7].

A usual operating model for sharing operators consists in placing e-scooters in the city downtown near the sights, transport hubs (stops, stations) and other places with high pedestrian flows. Dockless system of e-scooter operation allows riders to start and finish their trip almost wherever they want and accordingly plan ‘door-to-door’ trips but it increases the number of vandalism and theft incidents and makes the logistics more complicated for the operator. During the day, the e-scooter battery level decreases, and the operator commissions a carrier to collect scooters with low batteries and deliver them to a charging point where they should be charged at night. The charging point is usually a big parking lot with corresponding chargers. After the charging, e-scooters should be delivered to the predefined places, and the cycle starts again. Some operators practice the change of dead batteries to charged ones on-site. It excludes the need to transport scooters. To deliver charged batteries, cargo bikes can be used.

The high popularity of e-scooters caused problems in Stockholm, Sweden, where 7 sharing operators have over 20 000 vehicles. As a result, the streets were crowded with these units, and to solve the problem, 100 sharing stations of 10 units capacity were established. It put the micromobility in order and freed some space.

According to Swedish Transport Agency, improved bicycle infrastructure is one of the most important prerequisites to avoiding accidents with e-scooters. At that, the improvements should include sharing the space of bike stations with micromobility vehicles. These points are also supported by the research of the Norwegian Institute of Transport Economics which showed that the dedicated sharing stations can significantly improve the situation with safety in cities [3]. In addition, in 2021 International Transport Forum published the report “Reversing Car Dependency” where they recommend redistributing road and parking spaces between public transport, bicycles, e-scooters, and other micro-vehicles and cars to make micromobility a much more attractive alternative for travelling [8, 9]. If we go over to the specific cases of stimulating the use of e-scooters and improving safety, the following examples can be presented.

Voi Technology AB warns riders against parking at the car parks and stimulates users to leave the scooters at the stations by providing them with discounts. Joint research of Voi and S-Bahn in Stuttgart in autumn 2020 showed that the presence of e-scooter sharing stations increases the number of public transport trips. Passenger volume on the rail increased 35% when Voi set up the stations at the railway station and joined services with S-Bahn in commercial and digital format through the integration of S-Bahn services into the ‘mobility as a service’ Mobimeo platform.

All of these show that establishing the e-scooter sharing stations instead of dockless operation is an effective measure to:

- improve the safety of the riders and other road users;
- increase the quality of micromobility service;
- increase the number of trips combined with public transport (owing to the use of e-scooters as a feeder transport mode);
- reduce the number of cars in cities.

It makes the research of the methods to define a rational number of e-scooter sharing stations actual, especially in Ukrainian conditions.

2.2 Approaches to Optimize Scooter Sharing System Operation

E-scooter sharing systems are usually introduced by municipalities, public-private partnerships or private companies. One of the main issues in sharing system establishment is to define rational locations of sharing stations and charging points. Existing models to solve this task are aimed at determining the optimal location of the stations, fleet size, station capacity, and the number of available scooters at each station taking into account initial investments which should be less than the given budget [10, 11].

The necessary location of the station can be chosen using the models based on the information about scooters’ location, station capacity, area coverage and rider movements. These models allow optimizing total costs, transportation costs and demand coverage [12].

In 2013, US researchers presented the inventory model to manage docking stations by introducing the function of unsatisfied user demand to assess service quality. This optimization model determines the rational network of the stations with the highest demand coverage in each of the assigned zones under the restriction of scooter rent cost and level of service. In this case, the demand is measured as the number of trips in the zones that should be assigned in a way which ensures acceptable walking distance to the station within a zone. The input parameters for the model are user demand, maximal and minimal station capacity, the cost of station setup, the cost of e-scooters, the cost of transportation related to scooter charging, total investments and total cost of sharing system operation, discounting and cash flows during the project implementation. The outputs of the model are the location of the stations in each zone and their capacity, the expected number of trips, the size of the scooter fleet and the number of e-scooters which should be available at each station to maximize demand and annual income [13]. At that, there should be a few free spaces at each station to allow parking for arriving riders. It was recommended to take the number of free spaces as 25% of station capacity.

Apart from the model above, there exists a methodology to define e-scooter station locations with the use of integer linear programming. It takes into account user demand, required investments, operational costs and different pricing schemes aimed to maximize net profit. In this methodology, demand for trips is taken as optimization criteria under the restriction of the available budget. Defined station locations should result in maximum area coverage and maximum satisfaction of the covered demand. The advantage of the methodology is that the mathematical model in it allows the minimization of both user costs and operator (investor) costs [14].

The analysis above revealed that the success in micromobility development substantially depends on the rational solutions in three essential issues of strategic planning and day-to-day e-scooter sharing system operation which are as follows:

- the number and location of sharing stations in the coverage area;
- the capacity of sharing stations;
- the demand for e-scooter trips.

To find the solution to these issues under a lack of data, a case study of the city district in Dnipro, Ukraine, was conducted.

3 Methodology to Define the Number and Location of e-Scooter Sharing Stations Under a Lack of Data

3.1 Data Availability, Restrictions and General Assumptions

Currently, Dnipro has a dockless scooter sharing system which is operated by ‘Kiwi’ [15]. During the system operation, there arose an issue of chaotic scooter parking all around the city, which is the common problem of dockless systems. This parking caused not only the inconveniences for pedestrians but the risk of vandalism, theft and extra fuel consumption for delivering the e-scooters to the charging point.

So, the problem of scooter parking organization became a reason to do this research. In the beginning, there was an attempt to collect data and statistics for thorough mathematical modelling, and it was expected to get GPS tracks for e-scooter trips (including scooter pick-up and drop-off points), trip time and distance, travel speed and rental time. But unfortunately, during the communication with the operator, the request for these data was refused, that is the common situation for the data requests from initiative researchers and even research institutions in Ukraine.

In view of limited resources and without access to desired data it was decided to study the situation in one of the city districts. Because of the high popularity of micro-vehicles owing to the recreational zones (square and promenade) and available bike lane, the Sobornyi district was chosen. Another decision was to collect data about the locations of available e-scooters during the day on the authors’ own from open sources.

This information is available in real-time in the smartphone app, and it became the ground to develop the methodology to define the rational location of e-scooter sharing stations. During the methodology development, it was decided that (1) the station capacity, (2) area coverage based on walking access distances and (3) the closeness to the shortest path of the vehicle collecting e-scooters for charging should be considered.

Given that at present there are no sharing stations, no data about factual demand for scooters and no details on scooter trips, existing methods and criteria reviewed in Sect. 2 and aimed to evaluate the rationality of station locations cannot be applied in full or without modification for this case. It caused the need to search for other criteria which would be applicable in the study. As a result, the average Euclidean distance between sharing station and the line of the shortest path of the vehicle that collects e-scooters for charging was chosen. This distance is always the straight link between two points in Euclidean space that can be calculated using the following formula:

$$d_{pq} = \sqrt{\sum_{i=1}^n (p_i - q_i)^2}, \quad (1)$$

where n is the number of coordinates (in two-dimensional space, this is x- and y-coordinates or longitude and latitude which are used in present-day mapping websites); p, q are the values of the coordinates.

This distance is important for both the user and the operator:

- the user will always know the exact location of the station, and accordingly where he or she can rent the scooter;
- the reduction of the mentioned distance will allow an operator to reduce the time for manoeuvring and fuel consumption for the vehicle that collects the abandoned and discharged scooters.

Apart from the abovementioned distance, the location of the sharing stations should be defined with regard to:

- the budget for station setup;
- the distance between adjacent stations which should preferably be within the range between 200 m and 800 m. This is the acceptable distance which the user is ready to walk to rent the scooter [10];
- city areas (street and public spaces) permitted for scooter parking according to local legislation;
- restriction on the distance between sharing station and carriageway. It should be equal to or more than 3 m [10].

3.2 The Steps to Define the Rational Location of the Stations: A Case Study of Sobornyi District in Dnipro

Given that the criterion of sharing stations' location, the factors and restrictions influencing these locations are determined, the steps to define rational locations of sharing stations were developed. These steps are as follows:

- the first step is marking the locations of available e-scooters on the map;
- the second step is the identification of the shortest path of the vehicle that should collect e-scooters for charging;

- the third step is measuring the distance between each marked location and the line of the shortest path of the vehicle;
- the fourth step is grouping the e-scooters into assumed zones according to the considered capacities of the sharing stations;
- the fifth step is the assignment of the sharing station location in each zone according to the restrictions defined above.

During the first step, e-scooter locations had been identified by processing the screenshots from the smartphone app. The number of scooters and their location were monitored during the period from 7:00 to 9:00 and from 17:00 to 19:00. The observations in the Sobornyi district showed that these are periods of high demand for e-scooter trips, and they coincide with rush hours. It can be explained by the population's need to get to work in the morning and come back in the evening. Also, evening trips appeared to be more frequent due to the use of e-scooters for recreation.

The screenshots were made several times in each of the chosen periods depending on the changes in scooter availability – each screenshot was aimed to reflect relatively significant changes in the location of available scooters in the Sobornyi district. This work was performed for 17 days between 26 October and 14 November 2021. As a result, 364 scooter locations were identified. This number is more than enough for a pilot survey and can be considered sufficient for the solution of tasks in this study where no demand stratification is required [16].

After the identification of e-scooter locations, these data were mapped in Google MyMaps. Each scooter location in MyMaps was complemented with the information about the date and the number of e-scooters at the location if there were several available scooters in one place (point).

During the second step, the shortest path of the vehicle that should collect e-scooters for charging was identified and mapped.

During the third step, each e-scooter location was connected to the line that shows the shortest path of the vehicle using the link right-angled to the shortest path line. The length of these links is the Euclidean distance between the scooter location and the vehicle's shortest path. These distances were recorded in the common table.

There were a lot of e-scooters chaotically located along the shortest path line. Meanwhile, according to the European standards [10], the distance between sharing station and the carriageway should be equal to or more than 3 m. Therefore, the fourth step implied the grouping of the e-scooters into assumed zones.

According to the reviewed literature, most e-scooter sharing stations in Europe have a capacity of between 7 and 20 scooters. Thus, the zones had been assigned to 'cover' the number of closely located scooters that correspond to the mentioned capacity.

During the fifth step, the potential location of sharing station in each assigned zone was defined. To do this, the simple median method [17] was used. Each location was reviewed according to restrictions listed at the end of Sect. 3.1. It should be noted that the choice of the method is up to the tasks of the study, researcher preferences and available data. The example of the results which were obtained after abovelisted steps is presented in Fig. 1.

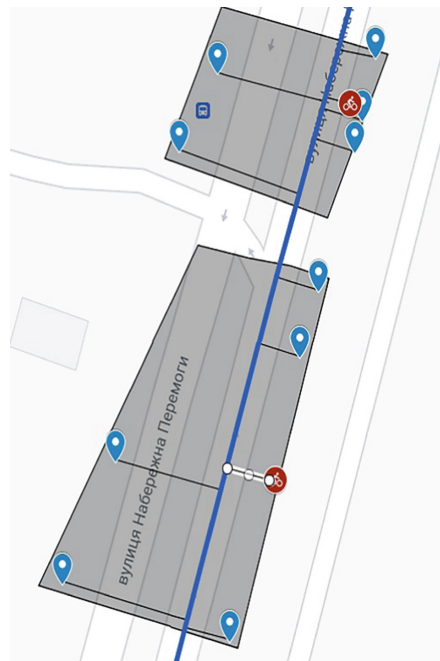


Fig. 1. The screenshot from MyMaps with the assumed zones and the potential locations of sharing stations: blue markers show available e-scooters location; grey areas are the areas of assumed zones; the thick blue line shows the shortest path of the vehicle that should collect e-scooters for charging; thin straight black lines show Euclidean distances between scooter locations and the vehicle's shortest path line; red markers show potential locations of sharing stations.

After the last step, it was important to analyze the number of potential sharing stations as well as Euclidean distances between scooter and station locations and the vehicle's shortest path line.

Euclidean distance between each scooter location and the vehicle's shortest path line is the lower estimate of the distance that should be covered to collect the scooter for charging or replace the battery on-site. It allows estimating the average Euclidean distance for the current (dockless) sharing system and the station-based sharing system with the stations located according to the developed methodology. As a result, the average Euclidean distance for the station-based sharing system appeared to be 28.6% less than the distance for the current sharing system – these distances are 15 m and 21 m correspondingly. This result supports the expediency of the establishment of the sharing stations and the change of the sharing system operation model.

The number of potential sharing stations appeared to be equal to 78. It seems to be high and can cause unreasonable costs and problems because this number of stations in the Sobornyi district can 'crowd' it. To address this issue, the possibility to merge certain stations complemented with demand modelling was considered.

3.3 Review of the Sharing Stations Mapping

The final step of the methodology is to check whether the number of sharing stations can be reduced or not. Since the determined number of sharing stations seems to be too high for the Sobornyi district, it was decided to search for a way to reduce this number. In the beginning, the daily number of scooter rents was estimated as the ratio of the total number of marked locations in the zone to the number of days to which these locations refer. This ratio can be used as an estimate of the daily user demand in the zone. For modeling purposes, the ratio is reasonable to round up to the nearest integer.

After that, the average station capacity with respect to the daily demand in 78 potential sharing stations was calculated and turned to be equal to 14 units. Then, the scooter locations were regrouped into new zones according to this average capacity. New potential locations of the sharing stations in these zones were defined using the simple median method and with regard to the restriction on the distance between adjacent stations (200 m to 800 m). As a result, the number of sharing stations was reduced to 17. Their location is presented in Fig. 2.

To answer the question about the rationality of new station locations, Euclidean distances between these locations and the vehicle’s shortest path line were calculated. The average Euclidean distance for 17 new sharing station locations appeared to be equal to 9 m. It is 40% less than the distance for the previous case with 78 sharing stations. It allows a further decrease in the time and costs required to recharge scooters (or replace batteries).

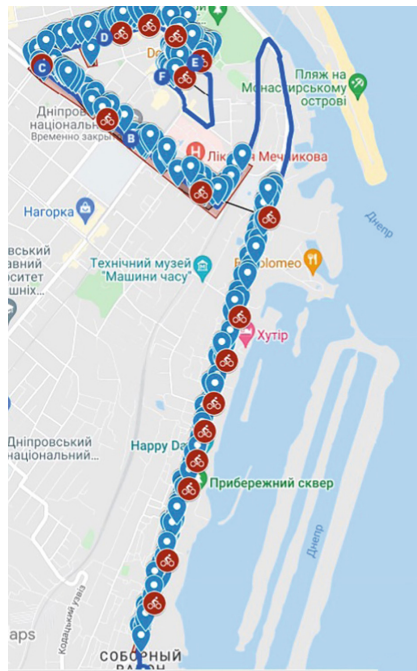


Fig. 2. Revised sharing station mapping.

Additional assessment of revised sharing station locations was performed in PTV Visum software [18, 19]. The demand model was built on the base of daily user demand in each zone and the ‘deterrence’ function estimated by the results of interviewing [the interview results which contain trip length distribution fitted to 109 recorded trip lengths are presented in Svichynska O., Sergienko K. Determination of the regularities in the random parameters of the trips made using the micromobility vehicles. Municipal economy of cities 161(1), 206–2011 (2021)]. The plot of the function appeared to be similar to well-known plots of trip length frequency distribution [20]. It supports the correctness of the data obtained during the interviews and the relevancy of their use in modeling. The modeling in Visum resulted in the potential daily flows of scooter riders, Fig. 3.

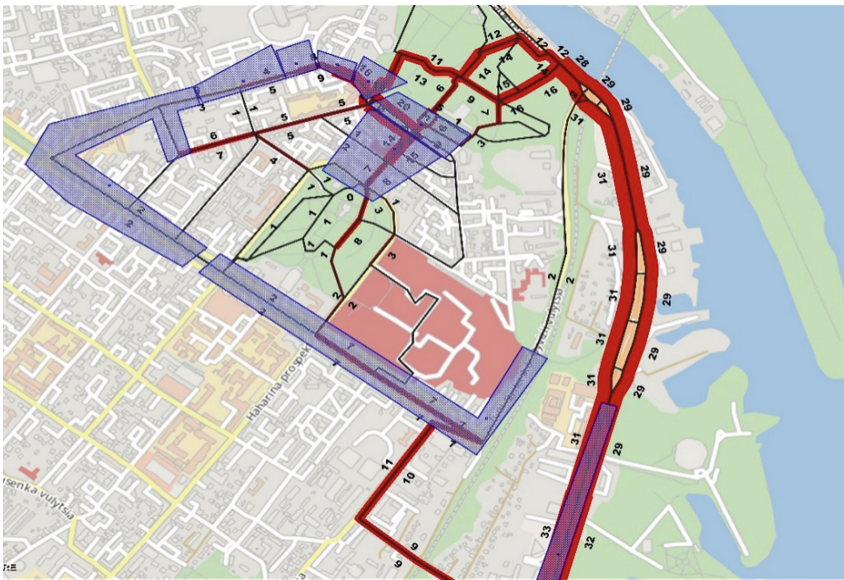


Fig. 3. Potential daily flows of scooter riders in Sobornyi district in Dnipro, Ukraine.

The figure shows the flows on the network where the bike lane is available (most of the thick red bars) and where there is no bike lane but the riders use the streets, pavements and footways as alternatives to the ‘main’ lane to get to the destinations (blue areas on the map). It is good information for the development of the measures to extend the micromobility infrastructure in the Sobornyi district and attract new users.

Summarizing the above, it should be noted that the defined sharing station mapping can be considered a good but an initial result that was received under a lack of data – it is based on the analysis of the location of e-scooters that were available for rent (364 locations were considered) and supported by the data from short user survey (109 trip lengths were recorded during the interviews). Thus, the received sharing station mapping and rider flows modeling results are satisfactory as an initial evaluation of user demand

and the data for preliminary estimation of the resources needed to cover it by station-based servicing.

To improve the obtained results and substantiate them by modeling, it is reasonable to increase the number of scooter locations for analysis, widen the period of their recording, extend the sample size of the user survey, study the trip purposes (demand strata), analyze tracks and organize scooter counts. It will allow collecting sufficient data and creating a better background for final decisions.

4 Conclusion

The developed methodology allows defining the number and location of e-scooter sharing stations under a lack of data – to use it, it is necessary to know only the location of available e-scooters during the day. The methodology is applicable for the case when the local authority or sharing operator intends to change the dockless operation model to a station-based one. As an output of the application, defined sharing station locations will allow an operator to reduce the costs of the collection of discharged scooters or the replacement of the batteries.

To obtain the best results, it is reasonable to increase the sample of scooter locations, conduct a full-scale user survey, collect and analyze scooter tracks as well as organize scooter counts to gather data for modeling purposes.

The combination of the methodology outputs with the modelling of the potential flows of e-scooter riders opens the opportunities for well-grounded decisions on public space and street design that will ensure the safety of pedestrians and road users. Also, modelling results will allow an operator to estimate demand for e-scooters and plan income as well as budget for fleet renewal.

References


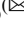


1. National Household Travel Survey (NHTS): Federal Highway Administration – Department of Transportation, Washington (2021). <http://nhts.ornl.gov>
2. Huber, S., Lißner, S., Francke, A.: Utility of GPS data for urban bicycle traffic planning in Germany: potentiality, limitations and prospects. *Int. J. Transp. Dev. Integr.* **3**(1), 1–14 (2019). <https://doi.org/10.2495/TDI-V3-N1-1-14>
3. Li, A., Zhao, P., Liu, X., Mansourian, A., Axhausen, K.W., Xiaobo, Q.: Comprehensive comparison of e-scooter sharing mobility: evidence from 30 European cities. *Transport. Res. Part D: Transp. Env.* **105**, 103229 (2022). <https://doi.org/10.1016/j.trd.2022.103229>
4. Bozzi, A.D., Aguilera, A.: Shared e-scooters: a review of uses, health and environmental impacts, and policy implications of a new micro-mobility service. *Sustainability* **13**(16), 8676 (2021). <https://doi.org/10.3390/su13168676>
5. Lipovsky, C.: Free-floating electric scooters: representation in French mainstream media. *Int. J. Sustain. Transp.* **15**(10), 778–787 (2021). <https://doi.org/10.1080/15568318.2020.1809752>
6. Laa, B., Leth, U.: Survey of e-scooter users in Vienna: who they are and how they ride. *J. Transp. Geogr.* **89**, 102874 (2020). <https://doi.org/10.1016/j.jtrangeo.2020.102874>
7. Gu, T., Kim, I., Currie, G.: To be or not to be dockless: empirical analysis of dockless bikeshare development in China. *Transport. Res. Part A: Policy Pract.* **119**, 122–147 (2019). <https://doi.org/10.1016/j.tra.2018.11.007>

8. Leydesdorff, L.: Summary and conclusions. In: *The Evolutionary Dynamics of Discursive Knowledge*. QQASSC, pp. 209–215. Springer, Cham (2021). https://doi.org/10.1007/978-3-030-59951-5_11
9. Edel, F., Wassmer, S., Kern, M.: Potential analysis of e-scooters for commuting paths. *World Electr. Veh. J.* **12**(2), 56 (2021). <https://doi.org/10.3390/wevj12020056>
10. Fazio, M., Giuffrida, N., Le Pira, M., Inturri, G., Ignaccolo, M.: Bike oriented development: selecting locations for cycle stations through a spatial approach. *Res. Transport. Bus. Manage.* **40**, 100576 (2021). <https://doi.org/10.1016/j.rtbm.2020.100576>
11. Nikiforiadis, A., Aifadopoulou, G., Grau, J., Boufidis, N.: Determining the optimal locations for bike-sharing stations: methodological approach and application in the city of Thessaloniki, Greece. *Transp. Res. Procedia* **52**, 557–564 (2021). <https://doi.org/10.1016/j.trpro.2021.01.066>
12. Reck, D.J., Haitao, H., Guidon, S., Axhausen, K.W.: Explaining shared micromobility usage, competition and mode choice by modelling empirical data from Zurich, Switzerland. *Transport. Res. Part C: Emerg. Technol.* **124**, 102947 (2021). <https://doi.org/10.1016/j.trc.2020.102947>
13. Frade, I., Ribeiro, A.: Bike-sharing stations: a maximal covering location approach. *Transport. Res. Part A: Policy Pract.* **82**, 216–227 (2015). <https://doi.org/10.1016/j.tra.2015.09.014>
14. Choron, R.L., Sakran, J.V.: The integration of electric scooters: useful technology or public health problem? *Am. J. Public Health* **109**(4), 555–556 (2019). <https://doi.org/10.2105/AJPH.2019.304955>
15. Kiwi Homepag: <https://ride.kiwi/>. Accessed 10 May 2022
16. Horbachov, P., Makarichev, O., Svichynskiy, S., Ivanov, I.: Framework for designing sample travel surveys for transport demand modelling in cities. *Transportation* **49**(1), 115–136 (2021). <https://doi.org/10.1007/s11116-021-10168-6>
17. Mu, W., Tong, D.: On solving large p-median problems. *Environ. Planning B: Urban Analytics City Sci.* **47**(6), 981–996 (2020). <https://doi.org/10.1177/2399808319892598>
18. Karami, Z., Kashef, R.: Smart transportation planning: data, models, and algorithms. *Transp. Eng.* **2**, 100013 (2020). <https://doi.org/10.1016/j.treng.2020.100013>
19. Lovelace, R.: Open source tools for geographic analysis in transport planning. *J. Geogr. Syst.* **23**(4), 547–578 (2021). <https://doi.org/10.1007/s10109-020-00342-2>
20. Horbachov, P., Svichynskiy, S.: Theoretical substantiation of trip length distribution for home-based work trips in urban transit systems. *The J. Transport Land Use* **11**(1), 593–632 (2018). <https://doi.org/10.5198/jtlu.2018.916>

Transport Technologies and Logistics



Changing Drivers' Cognitive Characteristics at Twilight in Freight Transportation

Oleksii Prasolenko , Dmytro Burko  , and Vitalii Chumachenko 

O. M. Beketov National University of Urban Economy in Kharkiv, 17 Marshala Bazhanova Street, Kharkiv 61002, Ukraine
dmytro.burko@kname.edu.ua

Abstract. The paper is devoted to the issues of the freight transportation in the cities at twilight. A group of drivers aged from 20 to 40 years with a total driving experience of 3 to 16 years were studied. Drivers drove along well-known routes in twilight and with further darkness. The drivers' attention indicators using the Pupil Labs headset, as well as changes in the functional state using indicators of heart rate, respiratory rate, galvanic skin response were measured. Drivers were divided into two groups with a driving experience of up to 10 years or more. The research results indicate a significant difference in the shifts of the functional state during movement along the routes for both groups. Drivers with less driving experience were less alert and more emotionally stressed. At the same time, drivers of both groups experienced significant difficulties in reducing lighting in the event of conflict situations while driving. At the same time, energy costs significantly exceeded the boundary indicators, and attention indicators deteriorated. This fact was observed when the level of illumination of the environment is less than 50 lx.

Keywords: Driver's functional state · Freight vehicle · Twilight · Human factor · Electrocardiogram · Traffic safety

1 Introduction

The safety of road freight transport in cities [1] is one of the important aspect of ensuring the normal life process of residents of modern megalopolises. To reduce the load on the transport network and speed up the delivery of goods in many cities around the world, product delivery is organized at night. The key role in ensuring the reliability and timeliness of the transport process, in such cases, is assigned to the driver. Studies conducted in Sweden at different times of the day showed that the most dangerous time for a driver, in terms of safety, is at three in the morning in winter and at four in the morning in summer; in addition, driving safety is largely dependent on the state of drowsiness caused by early morning driving [2]. Studies conducted in Alabama (USA) indicate the presence of various factors affecting the severity of the accident, which in most cases relate to the driver, his condition (fatigue), and age. The results of this study indicate a close relationship between driver's behavior and the occurrence of severe injuries associated with vehicle accidents [3]. According to the statistics of traffic

accidents per 100 thousand transport vehicles: 26 in the morning twilight hours; 2 in the day light hours; 65 in the evening twilight hours; 4 at night. The accidents for the most severe consequences happen at night. The severity of road accidents increases by 30–40% in the darkness, that shown by several studies. The problem of the human factor in ensuring road safety at twilight is to determine the mechanisms of perception and processing of information by the driver in accordance with the traffic situation. The speed of information processing by the driver is influenced by the following factors: functional and emotional state, illumination, road conditions, presence of obstacles on a certain section of the road, presence and condition of road marking, road signs, road equipment, traffic lights, etc. [4, 5].

Thus, the safety of the freight transportation in urban conditions depends entirely on the condition of the driver, his psychophysiological characteristics and traffic conditions. A clear understanding of the processes that change the functional state of the driver in freight transportation in the city will allow to ensure the safety of road users at twilight.

2 Research Significance

About 90% of the driver receives the information through vision. In the darkness, the road illumination has a great importance for vision. In order for the eyes to recognize the subject, a certain level of illumination is required [6]. The objects can be recognized by the silhouette – when the brightness of the object is below the brightness of the surrounding background, or when the brightness of the obstacle is greater than the surrounding background. The greatest difficulties for the driver occur with the sudden changes in the illumination of the road, when driving in low light conditions. The rapid change in light levels causes irritation of the retina, and there is temporary blinding. Blinding time varies widely and can last from a few seconds to a few minutes [5]. Changing of the lighting also affects the reaction time of the driver. Untimely or inaccurate reactions often lead to road accidents. The driver may not always be able to see the trajectories of other cars or to see a pedestrian suddenly appeared on the roadway. The reaction time in this case can vary widely from 0.4 to 2.5 s depending on the professional experience and individual psychophysiological characteristics of the driver [7]. It has also been founded that the functional state of the driver and the mobility of his nervous processes changes with age; these factors influence the reaction time of the driver [8], and accident rates. At the same time, on driving safety is influencing the driving experience. In the study [9], approximately 16,000 drivers were investigated, and a comparison of unexperienced and experienced drivers was made, indicating that the time to get into the first accident was shorter for drivers with less experience. In addition, the study found that night driving and exceeding speed limits in urban conditions create the same conditions for getting into an accident for both unexperienced and experienced drivers. The study of the effect of gender differences in drivers on the accident probability also observed when driving at night. Night driving reduces the time before the first crash among women, but not among men. In this case, the risk of an accident increases with excessive speed, but the effect of speed is much higher for men than for women among more experienced drivers. Particular attention is paid to the relationship between drivers' age and the probability of their involving into an accident [10, 11]. It has been established that the age and experience of the driver have independent effects on the risk of involving into an accident,

ceteris paribus, mileage. Studies have shown that young drivers had significantly higher accident rates than older drivers, especially drivers over 25 years old. Other studies [12] explain the effect of night lighting on driving speeds and the perception of visual information of the driving environment by drivers. In the result of modeling the speeds of movement, it was found out that their value is significantly influenced by the lighting parameters in various traffic conditions (sunny, cloudy, dark etc.). Driving at night worsens the statistics of traffic accidents [13] and creates the preconditions for increased interest to the problems of night driving through the understanding of the processes in the behavior of the driver in low light conditions. Comparison of the choice of speeds by drivers in the daytime and at night is carried out, and, significant factors that affect the choice of speeds under various lighting conditions are identified. Modern trends in the cities transport infrastructure development are reflected in the characteristics of mathematical models that describe the technical and economic parameters of the functioning of freight transport systems [14, 15]. The influence of the driving environment on the occurrence of driving risks is considered in sufficient detail in the study [16, 17]. It was considered 17 risk factors; the greatest influence on the driver is affected by the weather, traffic flow, travel time and average speed on the route. According to the authors [1], the driver's work in different road conditions is characterized by certain levels of tension. Different intensity of work causes the driver different rates of energy consumption at different rates and driving conditions. The study of freight traffic safety indicators shows more generalized factors for reducing traffic safety indicators such as: characteristics of vehicles, roads, and drivers [18].

It should be noted that existing approaches to assessing traffic safety in cities do not fully consider the influence of the functional state of the driver on the effectiveness of the transport process. Moreover, the problem of assessing the driver's condition while driving on city routes at twilight has not been sufficiently studied.

3 Objective and Hypotheses

The purpose of the study is to determine the effect of traffic parameters on city streets on the performance of the driver's work at twilight. The method of determining the impact of conflict situations while driving at twilight on the drivers' attention indicators and functional state is developed. Scientific interest is the dynamics changes of drivers' functional state and attention depending on light changing in the evening twilight.

4 Methodology

While driving through the city streets, the driver consumes a certain amount of energy. External respiration parameters are used to determine the amount of energy consumed by the driver. Energy consumption means the amount of kcal/min spent. The author of [4] indicates that the number of inhalation and exhalations of the driver depends on the heart rate. Accordingly, the amount of energy consumed by the driver can be determined by the formula:

$$\Delta E = 0,075(C - C_o)S, \quad (1)$$

where ΔE is the shift of energy cost while driving, kcal/min; C , C_0 are the frequencies of the external respiration of the driver when driving on the road and in the background, cycle/min; S is the driver's body area, m^2 ; 0.075 – proportionality coefficient.

The driver's body area according to [4] is determined by the nomogram (Fig. 1).

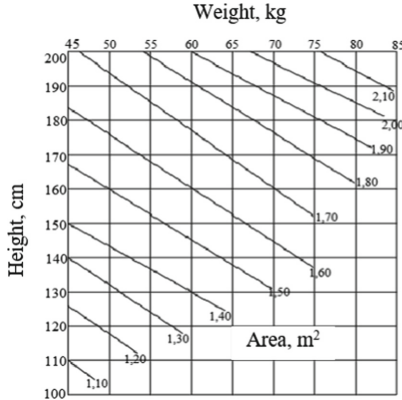


Fig. 1. Nomogram for determining the driver's body area.

Investigations of the external respiration rate of the driver while driving on the road and in the background, were performed using a pneumogram (Fig. 1). The Neulog sensor was used to record the parameters of respiration (Fig. 2).

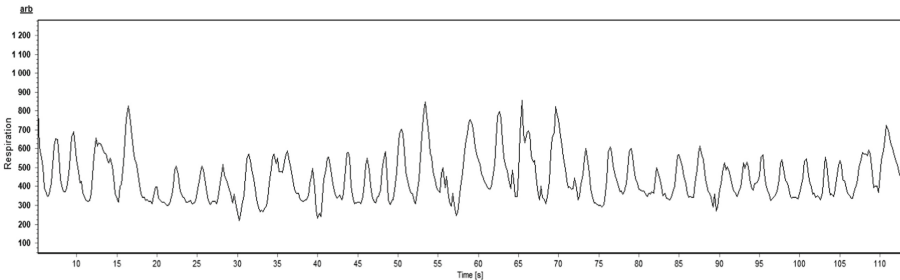


Fig. 2. An example of a driver's external respiration rate recording.

To determine the influence of traffic factors during the driver's interaction in the traffic flow, the dangerous braking parameters of the driver while driving in conflict situations, were considered. For recording the deceleration parameters was used a racelogic device [1]. The conflict's situation indicator is a speed or trajectory changing of the car. The degree of danger of such situation is characterized by the negative longitudinal and lateral accelerations that occur during the car maneuvering. The danger degree of conflicts is divided into three types: light, medium and critical (Table 1) [4].

Table 1. Conflict situations by the danger degree.

Criteria of conflict situations	Acceleration, m/s ² , for a conflict situation		
	Light, K1	Medium, K2	Critical, K3
Longitudinal acceleration	2.9 ± 0.8	3.0 ± 0.7	>3.8
Lateral acceleration	1.4 ± 0.2	1.4 ± 0.2	>1.7

In case of danger, the driver has lateral and longitudinal accelerations (g-forces), which are vectors of speeds, that have magnitudes and directions. The following approach is suggested for these parameters' registration. For determining the strength of a conflict situation, it's not enough just to add two speeds together or accelerations. If the two forces are directed at right angles from each other, the Pythagorean theorem can be used to get the total value of the two forces (for adding the two velocities and accelerations' vectors) (Fig. 3).

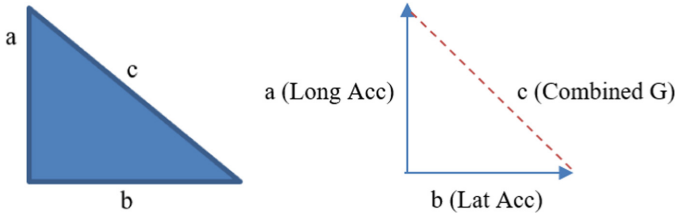


Fig. 3. Scheme and principle of determining the strength of the “combined G”.

Then the magnitude of the two forces can be determined by the formula:

$$a^2 + b^2 = c^2, \tag{2}$$

where *a* is the longitudinal acceleration, Long Acc (g); *b* is the lateral acceleration, Lat Acc (g); *c* is the combined, “combined G” (Fig. 3).

In addition, each conflict causes a changing in the area under the curve of deceleration of the car (Fig. 5). The area under the “combined G” curve (mathsChannel) is an important indicator that shows the vehicle's motion vector and the longitudinal (lateral) accelerations over time. The analysis of each conflict situation is based on the characteristic' definition of “combined G” in accordance with Fig. 3–4. The using of “VBOX Test Suite” software (Fig. 5) defines the limits of changing the “combined G”- parameters. This indicator depends not only on the forces of longitudinal and lateral acceleration, but also on the duration of action of a certain factor.

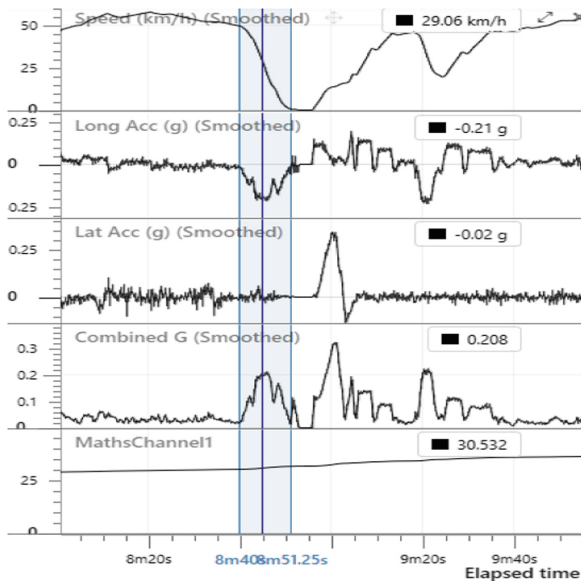


Fig. 4. Driving parameters in the experiment.

Measure						
VBOX0024						
Channel	At Start	At End	Difference	Max	Min	Avg
Speed (km/h)	49.49	0.71	-48.78	49.49	0.71	25.26
Long Acc (g)	-0.02	-0.05	-0.04	-0.01	-0.21	-0.12
Lat Acc (g)	-0.01	0.00	0.01	0.06	-0.03	0.00
Combined G	0.019	0.015	-0.004	0.211	0.015	0.123
MathsChannel1	29.977	31.362	1.385	31.362	29.977	30.652
Elapsed time (s)	520.00	531.20	11.20	--	--	--
Distance (m)	4528.43	4607.03	78.59	--	--	--

Fig. 5. Calculation of parameters in traffic conflicts.

Studies show that in emergency situations, when a person does not have time to make a conscious decision, emotions act as a command signal to start a chain of actions aimed at self-preservation. Emotions influence the activity in conscious decisions. An emotional state that exceeds the optimum disorganizes the driver’s activity. Attention depends on the emotional state of the driver. The main properties of attention are: concentration, stability, switching, volume and distribution. The driver spends a certain amount of time fixing his gaze to evaluate the trajectory or position of the objects in the traffic environment. Significant emotional stress increases the time of fixing the gaze, the driver’s field of vision narrows. The driver does not have time to receive and process the received information. It causes driver errors. [1, 19].

To determine the impact of conflicts on driver characteristics, were used indicators of attention changing at twilight. The driver's attention indicator was determined by the formula:

$$A_{driver} = \frac{\sum_{i=1}^k T_{d_i}}{T_{mov}} \cdot 100, \tag{3}$$

where T_{d_i} is the time of fixing the gaze of the driver on a certain i -th object of driving environment; k is the number of fixations of the driver's gaze; T_{mov} is the total travel time.

The number of fixations of the driver's gaze was determined by the formula:

$$N_F = \frac{\sum_{i=1}^k d_i}{T_{mov}}, \tag{4}$$

where d_i is the fixing the driver's gaze on a certain i -th object of the driving environment, un.

The functional state of the driver can be determined by the results of electrophysiological shifts:

- heart rate shift:

$$\Delta F = \frac{F - F_0}{F_0} \cdot 100 \tag{5}$$

- skin's conductivity shift:

$$\Delta GSR = \frac{GSR - GSR_0}{GSR_0} \cdot 100 \tag{6}$$

- respiratory shift, cycles/min.:

$$\Delta C = \frac{C - C_0}{C_0} \cdot 100, \tag{7}$$

where F is the heart rate indicator; GSR is galvanic skin response; C is the driver's breathing parameters while driving; F_0, GSR_0, C_0 are relevant indicators when the driver was in a calm state (measured separately for each driver in the morning).

5 Experimental Research

Experimental studies of changes in drivers' attention and functional state in the evening twilight were performed on different categories of city streets. The study involved drivers from 20 to 40 years old with driving experience from 3 to 16 years. "Pupil Labs" eye tracking glasses were used to investigate drivers' attention. Studies of lightness changes at twilight were performed using a "Neulog light" device. The "VBOX racelogic" was used for recording the car's driving parameters. The functional state of the driver was determined by the results of electrophysiological shifts in heart rate using the Holter

device, the electrical conductivity of the skin using the Neulog GSR device, and the external respiration rate of the driver using Neulog Respiration Monitor Belt.

Before and after the tests, background electrophysiological indicators of the characteristics of the drivers' functional state were recorded. Registration of indicators of the drivers' functional state was performed in the sitting position in a relaxed state with closed eyes. Comparison of these indicators of functional state with indicators during surveys are presented in Table 2 for drivers with 3–5 years of experience, and in Table 3 for drivers with experience of 10–16 years.

Studies were performed on different categories of city streets in the evening twilight (after sunset). The driver in the car after sunset performed the movement. The experiments' time matched with the evening rush hour. In accordance with this, the obtained indicators show the results with the maximum load on the driver. While registering the drivers' gaze, the level of illumination was simultaneously recorded in the evening twilight. In Fig. 6 shows the fixation of the driver's gaze while illumination changing on a specific object of the driving environment.

The experiment was carried out according to the following scheme. The driver arrived at the place where the experiment began before the twilight. Thus, the driver's warming-up time was considered at the beginning of the experiment. Then the drivers made trips along the known routes after sunset for 30 min. Figure 7 presents the patterns of the driver's attention changing, which was defined as the ratio of the total time of gaze fixation to the total travel time (3), the patterns of change the number of fixations of the driver's gaze, which were defined as the ratio of the number of fixations to the total travel time (4) and change of functional driver's state (5)–(7).

Table 2. Electrophysiological indicators of the characteristics of the functional state of drivers with 3–5 years of experience.

Electrophysiological indicators	Averages before the survey	Averages after the surveys	Averages during surveys
Galvanic skin response (GSR), μs	1.37	3.81	5.68
Respiration rate, cycle/min	21.8	24.4	30.4
Heart rate, beats/min	72.1	83.4	92.7
Glance fixation time, sec	–	–	0.292

Table 3. Electrophysiological indicators of the characteristics of the functional state of drivers with experience of 10–16 years.

Electrophysiological indicators	Averages before the survey	Averages after the surveys	Averages during surveys
Galvanic skin response (GSR), μs	1.28	2.55	3.59
Respiration rate, cycle/min	20.2	22.4	27
Heart rate, beats/min	69.5	75.7	86.1
Glance fixation time, Sec	–	–	0.246

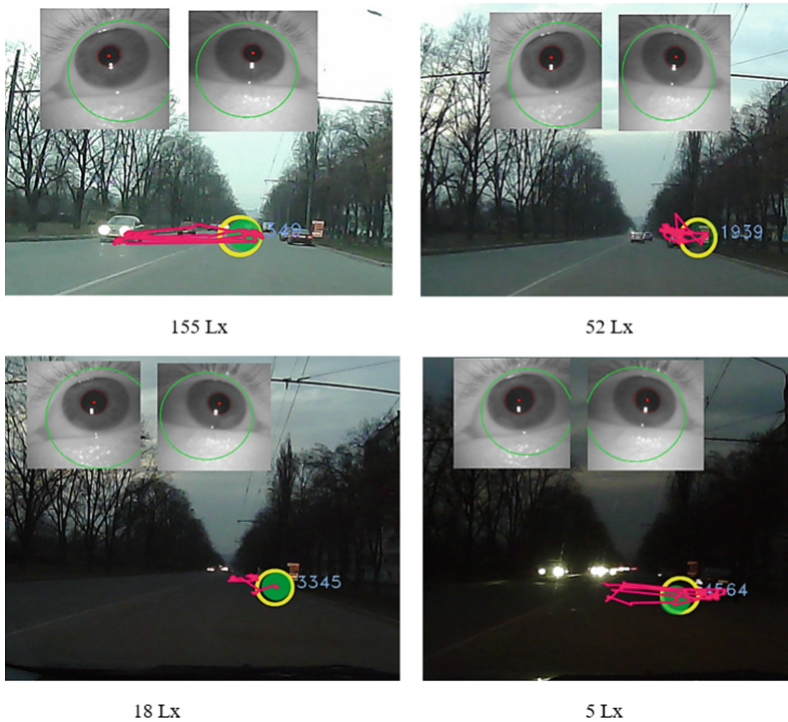


Fig. 6. An example of fixation of the driver's gaze and its parameters at evening twilight.

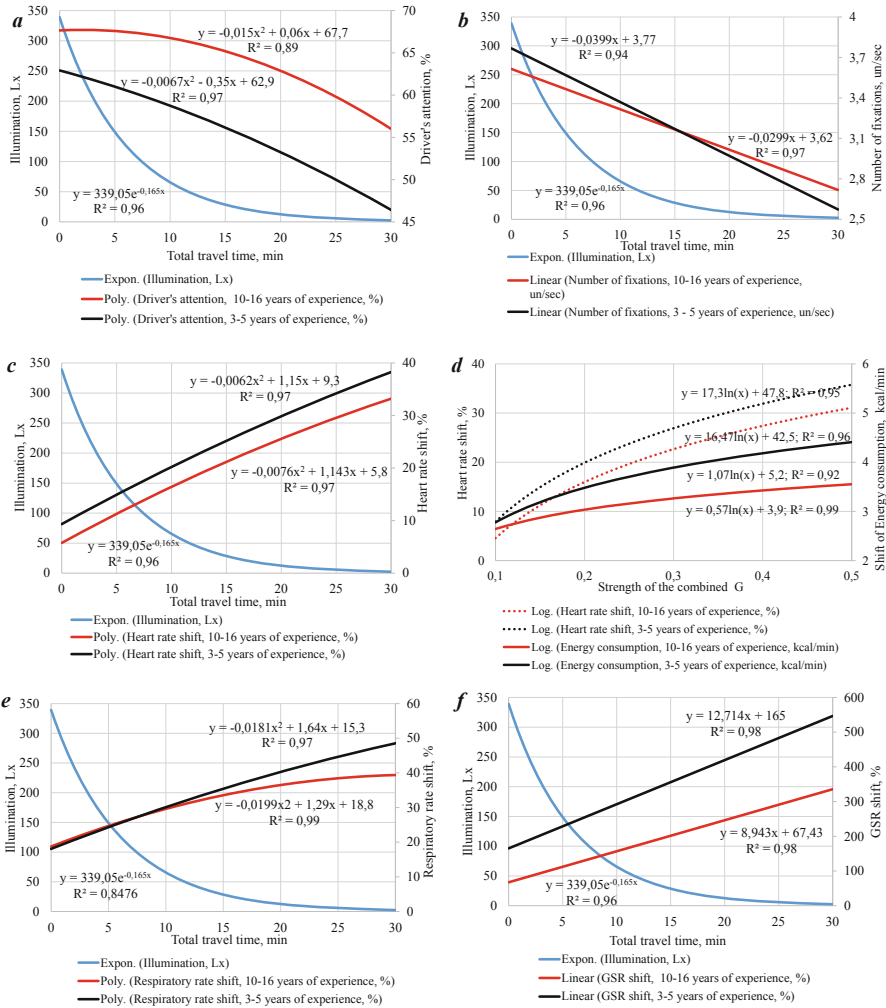


Fig. 7. (a) driver's attention changing; (b) change in the number of fixations of the driver's gaze; (c) effect of illumination on heart rate shift; (d) driver's energy consumption according to conflict situations; (e) effect of illumination on the respiratory rate shift; (f) effect of illumination on the GSR shift.

6 Conclusion

Experimentally obtained dependence in the indicator driver's attention changing and the number of the gaze fixations at evening twilight can be used for multifactorial models' formation, considering the parameters of traffic on different categories of streets. The driver's attention is highly reduced in the evening twilight. The driver, when the illumination changes from 50 lx or less, experiences visual fatigue from the constant search for objects on the road. At the same time, the number of fixations is significantly reduced, as the driver spends more time identifying and searching for the necessary elements of

the traffic environment, pedestrians, etc. Danger for the driver causes a stressful state, which is expressed in an increase in the driver's respiratory rate and a change in the functional state. The main factor influencing on the amount of energy consumed in such conditions is the interaction of the driver with the factors of the traffic situation. These factors require the driver to take some driving actions: acceleration, deceleration and certain reactions when driving. It has been established that when the illumination changes at twilight, the energy consumption increases by an average of 30%. In this case, the maximum rate of energy consumption for the driver is 12.6 kJ/min, i.e., 2.9 kcal/min. In heavy urban traffic, the driver performs 40–50 operations per 1 km of road.

These operations include stopping the car, engaging/disengaging the clutch, switching the control levers, braking the car (including without disengaging the clutch, turning the turn signal on and off, significantly speeding up, significant maneuvering with steering, traffic lights and road signs monitoring). That is, the number of driver's operations is influenced by many factors, both from the driver's side and from the side of the road situation. All the driver's actions listed above are associated with a certain amount of energy according to each specific traffic situation that can be classified as "conflict" and needs further investigation. The presented studies are covering a wide range of issues regarding to the changes drivers' functional state depending on the factors of the road environment at twilight.

The obtained dependences of the drivers' functional state, changing under different illumination, showed that at low illumination levels in the evening twilight rapidly increase shifts of the drivers' functional state. Thus, the driver's energy consumption while driving depends on the types of conflict situations and the level of illumination. In addition, it was found that for drivers with less than 10 years of experience, functional state's shifts were more important than for other drivers. Such drivers also had less attention indicators than experienced drivers with more than 10 years of driving experience. Therefore, for improving traffic safety in freight transport at night, and especially at twilight, it is advisable to involve experienced drivers.

The direction of further investigation could be the identifying significant differences in the drivers' reaction time and changes in their cognitive characteristics for the two studied groups with different driving experience.



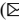


References

1. Prasolenko, O., Burko, D., Tolmachov, I., Gyulyev, N., Galkin, A., Lobashov, O.: Creating safer routing for urban freight transportation. *Transp. Res. Procedia* **39**, 417–427 (2019). <https://doi.org/10.1016/j.trpro.2019.06.044>
2. Åkerstedt, T., Kecklund, G., Hörte, L.G.: Night driving, season, and the risk of highway accidents. *Sleep* **24**(4), 401–406 (2001). <https://doi.org/10.1093/sleep/24.4.401>
3. Adanu, E.K., Hainen, A., Jones, S.: Latent class analysis of factors that influence weekday and weekend single-vehicle crash severities. *Accid. Anal. Prev.* **113**, 187–192 (2018). <https://doi.org/10.1016/j.aap.2018.01.035>
4. Gavrilov, E.V.: *Systematology Transport*, vol. 5. Knowledge of Ukraine, Kharkiv (2008)
5. Grüner, M., Ansoerge, U.: Mobile eye tracking during real-world night driving: a selective review of findings and recommendations for future research. *J. Eye Mov. Res.* **10**(2), 1 (2017). <https://doi.org/10.16910/jemr.10.2.1>

6. González-Hernández, B., et al.: The driver's visual perception research to analyze pedestrian safety at twilight. *Transport. Res. Procedia* **45**, 827–834 (2020). <https://doi.org/10.1016/j.trpro.2020.02.087>
7. Healey, J.A., Picard, R.W.: Detecting stress during real-world driving tasks using physiological sensors. *IEEE Trans. Intell. Transp. Syst.* **6**(2), 156–166 (2005). <https://doi.org/10.1109/TITS.2005.848368>
8. Makishita, H., Matsunaga, K.: Differences of drivers' reaction times according to age and mental workload. *Accid. Anal. Prev.* **40**(2), 567–575 (2008). <https://doi.org/10.1016/j.aap.2007.08.012>
9. Ayuso, M., Guillén, M., Pérez-Marín, A.M.: Time and distance to first accident and driving patterns of young drivers with pay-as-you-drive insurance. *Accid. Anal. Prev.* **73**, 125–131 (2014). <https://doi.org/10.1016/j.aap.2014.08.017>
10. Lam, L.T.: Distractions and the risk of car crash injury: the effect of drivers' age. *J. Safety Res.* **33**(3), 411–419 (2002). [https://doi.org/10.1016/S0022-4375\(02\)00034-8](https://doi.org/10.1016/S0022-4375(02)00034-8)
11. McCart, A.T., Mayhew, D.R., Braitman, K.A., Ferguson, S.A., Simpson, H.M.: Effects of age and experience on young driver crashes: review of recent literature. *Traffic Inj. Prev.* **10**(3), 209–219 (2009). <https://doi.org/10.1080/15389580802677807>
12. Bassani, M., Catani, L., Cirillo, C., Mutani, G.: Night-time and daytime operating speed distribution in urban arterials. *Transport. Res. F: Traffic Psychol. Behav.* **42**, 56–69 (2016). <https://doi.org/10.1016/j.trf.2016.06.020>
13. Bella, F., Calvi, A., D'Amico, F.: Analysis of driver speeds under night driving conditions using a driving simulator. *J. Safety Res.* **49**, 45-e1 (2014). <https://doi.org/10.1016/j.jsr.2014.02.007>
14. Shpachuk, V., Chuprynin, A., Garbuz, A., Suprun, T.: A multifactor analysis of the rail transport car that passes over a joint unevenness with respect to the phases of its motion. *Eastern-Eur. J. Enterp. Technol.* **7**(91), 55–61 (2018). <https://doi.org/10.15587/1729-4061.2018.121584>
15. Burko, D., Lobashov, O., Prasolenko, O., Gyulyev, N., Kumar, C.: Establishing patterns of the urban transport flows functioning on urban network parameters. *Transport. Res. Procedia* **48**, 793–800 (2020). <https://doi.org/10.1016/j.trpro.2020.08.082>
16. Niu, S., Ukkusuri, S.V.: Risk assessment of commercial dangerous-goods truck drivers using geo-location data: a case study in China. *Accid. Anal. Prev.* **137**, 105427 (2020). <https://doi.org/10.1016/j.aap.2019.105427>
17. Benlagha, N., Charfeddine, L.: Risk factors of road accident severity and the development of a new system for prevention: new insights from China. *Accid. Anal. Prev.* **136**, 105411 (2020). <https://doi.org/10.1016/j.aap.2019.105411>
18. Rahimi, E., Shamshiripour, A., Samimi, A., Mohammadian, A.K.: Investigating the injury severity of single-vehicle truck crashes in a developing country. *Accid. Anal. Prev.* **137**, 105444 (2020). <https://doi.org/10.1016/j.aap.2020.105444>
19. Wang, J., Wu, J., Li, Y.: The driving safety field based on driver–vehicle–road interactions. *IEEE Trans. Intell. Transp. Syst.* **16**(4), 2203–2214 (2015). <https://doi.org/10.1109/TITS.2015.2401837>



Informational Characteristics of Objects to the Driver's Perception Field in Urban and Suburban Conditions

Iryna Lynnyk , Svitlana Chepurna , Kateryna Vakulenko  ,
and Nadiia Kulbashna 

O. M. Beketov National University of Urban Economy in Kharkiv, 17 Marshala Bazhanova street, Kharkiv 61002, Ukraine

Kateryna.Vakulenko@kname.edu.ua

Abstract. Analyzed the mathematical models of car movement according to urban space and the human factor. Presented the mathematical model, which is considered the most productive due using the moment that depend on the motivational forces of a person, but due to the lack of information on characteristics of road factors for movement by urban conditions, its practical use is difficult. According to the results of experimental research, the signal values objects of movement in urban conditions were established and the signal values of objects of the movement for suburban conditions were formalized. These signal values are used to calculating the information characteristics of the driver's perception in the model for calculating vehicle speeds and traffic flow. The research of the signal values of the objects of perception by drivers allows calculating the absolute organization and the current entropy of objects of perception by drivers who determines the behavior of movement by car subsequently. Information characteristics are used in models for estimate and prognostication of the ecological state in the city streets and highways, prognostication of the evolution in the ergonomic system "driver – vehicle – transport network – environment".

Keywords: Probability · Informational characteristics · Human factor · Urban traffic conditions · Suburban traffic conditions · Driver

1 Introduction

Nowadays there is no doubt that the movement of the car is the result of subjective purposeful human activity [1, 2]. The decision to use the human factor when modeling traffic flows solving problems of organizing traffic were provided by scientists since 1954, it was provided that the behavior of a person on the roadway, his attitude to traffic flow is limited by some rules which are connected by need to provide safety movement of vehicle [3]. The results of this research were found their continuation in the researchers of many scientists [4, 5], in which were set up indicators, criteria that are allowed to include person to standards and methods of design road and are formulated recommendations and requirements of a person to highways [6, 7].

At the same time most mathematical models of the car movement are based on Newtonian dynamic, when structure doesn't show the influence of purposeful human activity (for example the Filippov's model, that used to solve system of simply differential equations). The mathematical and computer model for the vehicle system, use to study the lateral stability of the car and the mathematical models, which allow to carry out research of stability or response [8, 9], comfort, and optimization the design characteristics for the various parameters of the vehicle system were developed by scientist without considering the human factor and the moment that depend on the motivational forces of a person [10, 11].

The following mathematical model [3] is considered the most productive due to additive program forces and using the moment that depend on the motivational forces of a person (1):

$$\left. \begin{aligned} m\ddot{x}_2 &= F_{e2} + F_{p2}, \\ m\ddot{x}_3 &= F_{e3} + F_{p3}, \\ J\ddot{\Psi} &= M_{E1} + M_{p1} \end{aligned} \right\}, \tag{1}$$

where m and J is the mass and moment of inertia of a vehicle about the axis y_1 perpendicular to the plane $y_2 y_3$; F_{e2}, F_{e3}, M_{E1} are the natural force and moment; F_{p2}, F_{p3}, M_{p1} are the program force and moment.

The solution to a system (1) was allowed to receive formulas that describing the dependence upon the speed of movement from the design and maintenance characteristics of the vehicle, all set of road factors, and the psychological condition of the driver under the mode acceleration of the vehicle, in the braking mode with the engine none disconnected, in the braking mode with the engine disconnected, in coasting mode [3].

The choice mode of the movement carried out by the driver based on the selection formula:

$$\rho = \text{sign} \cdot (M_i V_i^0 - M_{i+1}), \tag{2}$$

where M is the motivation force; V_i^0 us the speed of satisfying the need.

Motivation forces calculated according to the dependences:

$$M = n(V - V_H), \tag{3}$$

where:

$$V_H = a + bk_c + cK_c^2, \tag{4}$$

$$K_c = \frac{H}{Q}, \tag{5}$$

$$H = -n \sum_{i=1}^n P_i \log_2 P_i - n \sum_{i=1}^n (1 - P_1) \log_2 (1 - P_i), \tag{6}$$

$$Q = n^2 + n \sum_{i=1}^n P_i \log_2 P_i - n \sum_{i=1}^n (1 - P_1) \log_2 (1 - P_i), \tag{7}$$

$$V_{n2} = \frac{V_{n3}}{2} + \frac{V_{n3}}{2} \cdot \left(1 - \frac{H_{m0} - 36}{r}\right), \quad (8)$$

$$H_m = n^2, \quad (9)$$

$$r = H_{mk} - H_{m0}, \quad (10)$$

where n is the number of objects in the driver's field of perception; P_i is the signal indicator of the i -th object; H_{mk} is the maximum entropy in the driver's field of perception at coefficient load of road $K_3 = 1$; H_{m0} is the maximum entropy in the driver's field of perception at coefficient load of road $K_3 = 0$; a, b, c are the coefficients depend on H_{mk} .

Practical use the mathematical model (1) is difficult due to the lack of information characteristics of road factors for urban traffic conditions and its classification. Information characteristics by suburban traffic conditions were determined [3] for some characteristics of the object, but these characteristics were not classification.

Therefore, the aim of our study is to establish information characteristics of road factors for urban and suburban movement conditions that is basis of experimental studies, and in the future, it can help to increase the safety of road users.

2 Materials and Methods

The study of the regularities in the formation of the driver's information loading during road traffic was carried out according to the results of research arrivals of moving laboratories by disordered mode of movement, that is, with the speed acceptable for the driver. The experiments were conducted in the summer on the streets in Kharkiv, Ukraine. Cars based on Ford Transit were used as moving laboratory that were equipped information and computing systems IVK HADI-2. The following Table 1 gives the plot characteristics, where were spent experiments.

During the research arrivals, the actual speed and trajectory of the moving laboratories, as well as the electrophysiological characteristics of the driver's body condition (electrocardiogram (ECG), galvanic and skin reaction (GSR) according to the Fere's method) were continuously registered.

At the same time, the moments of connection between different objects on the environment were recorded. The background characteristics in the functional condition to the driver's organism were recorded by the beginning of the experiments and after their completion. Registration of these characteristics was checked in the "sitting" position and in relaxed condition. These characteristics are shown in Table 2.

Comparison of these data is allowed to set up the availability of a pre-start the driver's body reaction.

Table 1. The plot characteristics where were spent experiments.

Characteristics	Units	Used values
The width of the carriageway on the streets	m	From 12 to 24
Longitudinal slope	‰	From 3 to 50
Radius of curves on the plan	m	From 0 to 190
Number of bands movement	–	4–6
Condition to covering of road	–	Dry, clean
The separator width between the bands of movement are either not, or equal	m	2,5
Width of the street in the red lines	m	From 29 to 150
Visibility	m	From 50 to 500
Distance from the carriageway to the sidewalk	m	0 to 36
The distance to the building	m	From 5 to 60
Tramway bed	–	The existence of a tramway bed or lack of one, or it is located separated from the carriageway, or in the middle of the street
Traffic intensity	Thousand vehicles/day	from 9,0 to 28,1

Table 2. The background characteristics in the functional condition to the driver's organism.

Electrophysiological indicators	Units	The average value of the indicators before the beginning of the experiments	The average value of the indicators after finishing of the experiments
Resistance between electrodes	kOhm	27.5	26.0
A person's respiratory rate	cycle/min	17.0	15.36
Galvanic and skin reaction	area, cm ²	0.1023	0.0656
Galvanic and skin reaction	amplitude, kOhm	0.06875	0.05833
Galvanic and skin reaction (number of waves per minute)	number of waves per minute	0.195	0.2
Heart rate	beats/min	83.31	81.46
P/T electrocardiogram (ECG)	%	10.163	9.697

3 Results

When processing the experimental data, the limiting indicator of the condition to the circulatory system was determined by the formula:

$$R_l = \frac{\sum_{i=1}^n R_i}{n_1} - \sigma_R, \tag{11}$$

where R_i is the width of the i -th RR-ECG interval, mm; σ_R is the average deviation of the RR-interval; n_1 is the number of elements in the sample of ECG RR-intervals and included at least 400 RR-intervals.

The signal indicator of the object environment was estimated according to the probability that the actual indicator of the RR-interval R_f during the meeting with this object would be less than the limiting R_l :

$$P_j = \frac{n_2}{N}, \tag{12}$$

where n_2 – the number of events, when $R_f < R_l$; N – the total amount of the meeting with the object of the environment.

The use of Eq. (12) to estimate the signal indicator of the object environment has appeared accepted only for discrete objects. Discrete objects include such which the difference in angular speed of the formation points of their contour is less than the driver’s differential perception boundary. During a meeting with non-discrete objects, it is determined to be more difficult to establish their signal indicator. In the same way, their assessment was performed by a calculation method based on the establishment of a regression connection between the signal indicator of the object with a coefficient of the accident that is presented in Fig. 1.

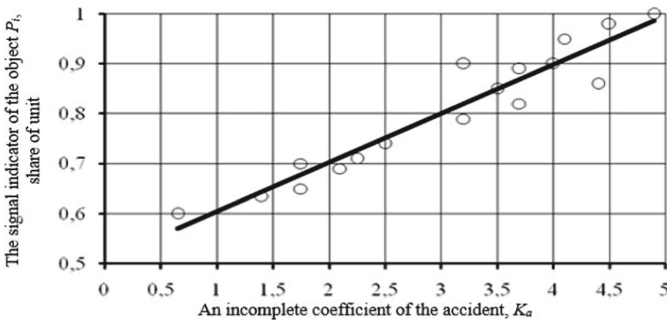


Fig. 1. Regression of the signal indicator of the object according to the coefficient of accident.

The coefficient of double correlation between the probability P_i and the coefficient of the accident K_a has been equal to $+0.96684 \pm 0.06019$. The calculated t -criterion for the reliability of the calculated coefficient of correlation has been $t_p = 16.06225$. Comparing this indicator with the boundary indicator $t_m = 2.093$ by importance $P = 0.05$ and the number of degrees’ freedom $f = 19$, it has appeared that $t_p \gg t_g$.

Correspondingly, the coefficient of correlation is calculated and is quite reliable that is evidenced by a strong connection between the probability P_i and the incomplete coefficient of the accident K_a [3]. The alignment to the connections P_i between the geometric and physical characteristics of the elements in the driver's field of perception using the least-squares method is allowed to receive empirical formulas for assessing the indicator of P_i and their tabulated values that are presented in Table 3, 4, 5 and 6.

Table 3. Dependences on the probabilities of finding objects in the driver's field of perception in a condition are dangerous for movement on the characteristics of these objects (for urban traffic conditions).

Object characteristic	Designation	Units	Connection of the probability P_i with the object characteristic
The width of the carriageway on the streets	B_{car}	m	$P_1 = 0,198 \cdot e^{-0,087B_{car}} + 0,5$
Longitudinal slope	i	%	$P_2 = 1,5 - (1 - 0,079) \cdot e^{-0,0036 \cdot i }$
Radius of curves in the plan	R	m	$P_3 = 0,0624 \cdot e^{-0,00736 \cdot R} + 0,5$
Difference in the width of the carriageway on the roads and bridges	d	m	$P_4 = 0,8325 - 0,209 \cdot d + 0,038 \cdot d^2$
The distance between building and road	Z	m	$P_5 = \frac{3,124}{Z} + 0,595$
Distance from road visibility:			
- in the plan	L_v	m	$P_6 = 0,58 + 0,92 \cdot e^{-0,0096 \cdot L_v}$
- in the profile	L_v	m	$P_6 = 0,58 + 0,92 \cdot e^{-0,0074 \cdot L_v}$
Types of intersection by the traffic intensity - at different levels	N	Thousand vehicles/ Day	$P_7 = 0,56$
- annular intersection	N	Thousand vehicles/ day	$P_8 = 0,60$
- unequipped intersection	N	Thousand vehicles/ day	$P_9 = 0,143 \cdot e^{0,022 \cdot N} + 0,5$
- intersection with traffic light regulation	N	Thousand vehicles/ day	$P_9 = 0,098 \cdot e^{0,024 \cdot N} + 0,5$
- connecting roads with traffic lights	N	Thousand vehicles/ day	$P_7 = 0,079 \cdot e^{0,029 \cdot N} + 0,5$
Pedestrian crossing outside the intersection by the pedestrian traffic intensity	N_2	Thousand people/ day	$P_8 = 0,571 + 0,015 \cdot N_2$
The distance from the carriageway to the sidewalks	L_{walk}	m	$P_9 = 0,5 + 0,21 \cdot e^{-0,06 \cdot L_{walk}}$
- for streets where a lot of pedestrians	L_{walk}	m	$P_9 = 0,5 + 0,28 \cdot e^{-0,07 \cdot L_{walk}}$

Table 4. The probabilities of finding objects in the driver's field of perception in a condition are dangerous for movement (for urban traffic conditions).

The name of the object in the field of perception	Numerical characteristics of the object
	Numerical values of probabilities
The condition carriageway on the street	Slippery (dirty, icy)
	$P_{10} = 0,68$
	Slippery (wet)
	$P_{10} = 0,64$
	Dry, clean
	$P_{10} = 0,6$
	Rough
	$P_{10} = 0,58$
Prohibiting traffic sign	$P_{11} = 0,785$
Warning traffic sign	$P_{12} = 0,743$
Directional traffic sign	$P_{13} = 0,74$
Order traffic sign	$P_{14} = 0,98$
Marking of the carriageway on the street:	Axial solid
	$P_{15} = 0,55$
	Axial dotted
	$P_{15} = 0,505$
	solid edge
	$P_{15} = 0,6$
The tram tracks	Be located outside of the road
	$P_{16} = 0,65$
	Be located at the axis of the street
	$P_{17} = 0,85$
	Be located near of the road
	$P_{17} = 0,75$

The correlation coefficients for the presented mathematical models range from 0.917 to 0.999. The coefficients of determination for the presented mathematical models range from 0.944 to 0.998.

Table 5. The probabilities of finding objects in the driver’s field of perception in a condition are dangerous for movement taking into account the number of street lanes and the intensity of the vehicle’s movement (for urban traffic conditions).

The name of the object in the field of perception	Numerical characteristics of the object							
	Numerical values of probabilities							
Number of lanes	1	2	3	4	2	3	4	6
Movement of vehicle	One-way streets				Two-way street			
With an intensity up to 15 thousand vehicles/day	$P_{18} = 0,65$	$P_{18} = 0,62$	$P_{18} = 0,56$	–	$P_{18} = 0,65$	$P_{18} = 0,61$	$P_{18} = 0,58$	$P_{18} = 0,56$
With an intensity more than 15 thousand vehicles/day	$P_{18} = 0,69$	$P_{18} = 0,65$	$P_{18} = 0,6$	$P_{18} = 0,55$	$P_{18} = 0,69$	$P_{18} = 0,65$	$P_{18} = 0,6$	$P_{18} = 0,58$

Table 6. The probabilities of finding objects in the driver’s field of perception in a condition are dangerous for movement considering the location of objects along the road and the possibility of oncoming and overtaking (for urban traffic conditions).

The name of the object in the field of perception	Numerical characteristics of the object				
	Numerical values of probabilities				
Public transport station	Number of lanes				
	1	2	3	4	5
With two-way street	–	$P_{19} = 0,66$	$P_{19} = 0,61$	$P_{19} = 0,6$	$P_{19} = 0,56$
With one-way street	$P_{19} = 0,67$	$P_{19} = 0,66$	$P_{19} = 0,63$	–	–
Tree by the roadside		For trucks $P_{20} = 0,71$ For vehicles $P_{20} = 0,796$			
Children by the roadside		$P_{21} = 0,885$			
Person by the roadside		$P_{22} = 0,87$			
Overtaking a motorcycle/bicycle		$P_{23} = 0,825$			
Oncoming a motorcycle/ bicycle		$P_{24} = 0,8$			
Oncoming a truck		$P_{25} = 0,714$			
Oncoming a vehicle		$P_{26} = 0,672$			
Overtaking a vehicle		$P_{27} = 0,78$			

Using this regression connection and information on the incomplete coefficient of the accident is allowed to determine the signal indicators of non-discrete objects at the traffic environment for suburban traffic conditions in according to data [3] that are presented in Table 7. The correlation coefficients for the presented mathematical models range from 0,813 to 0,999.

Table 7. Dependences on the probabilities of finding objects in the driver's field of perception in a condition are dangerous for movement on the characteristics of these objects (for suburban traffic conditions).

Object characteristic	Designation	Units	Connection of the probability P_i with the object characteristic
The width of the carriageway on the streets:			
- with fortified roadside	b_{car}	m	$P_1 = 0,010 \cdot b_{car}^2 - 0,164 \cdot b_{car} + 0,751$
- with unfortified roadside	b^l_{car}	m	$P_1 = 3,94 \cdot b^{1-1,56}_{car}$
Width of roadside	b_2	m	$P_2 = -0,061 \cdot n \cdot (b_2) + 0,170$
Longitudinal slope:			
- without separation of movement transport	$i1$	%	$P_3 = -0,155 \cdot l \cdot n(i_1) - 0,376$
- with separation of movement transport	$i2$	%	$P_3 = 0,084 \cdot e^{0,007 \cdot i_2}$
Radius of curves in the plan	$R1$	m	$P_4 = 8,8709R_1^{-0,062}$
Difference in the width of the carriageway on the roads and bridges	d_1	m	$P_5 = 0,037 \cdot d_1^2 - 0,172 \cdot d_1 + 0,292$
Length of straight sections on the road	L_{st}	km	$P_6 = 0,004 \cdot L_{st} + 0,088$
Types of intersection:			
- at different levels	-	-	$P_7 = 0,035$
- the intersection into one level	X	-	$P_7 = 0,361 \cdot l \cdot n(x) - 0,680$
Visibility on the intersection by an adjacent road	L_{b1}	m	$P_8 = 38,30 \cdot L_{b1}^{-1,53}$
Distance from building to the road	$Z1$	m	$P_9 = 0,003Z_1^2 - 0,113Z_1 + 1,289$
Distance from road visibility:			
- in the plan	L_{b2}	m	$P_{10} = -0,101 \cdot n(L_{b2}) + 0,774$
- in the profile	L_{b3}	m	$P_{10} = -0,161 \cdot n(L_{b3}) + 1,124$
The intersection at the one level by the traffic intensity on the main road	N	Thousand vehicles/day	$P_{11} = 0,121 \cdot e^{0,000N}$

The driver's reaction time plays an important role in creating traffic safety and the probability by the emergence of road accidents largely depends on it [12, 13]. Changes in the driver's condition have affected the parameters of the transport process and the

reliability of the system “man – equipment – environment”, especially in traffic jams [14]. In this case, a change in the driver’s reaction has been occurring when the traffic situation changes, at that jumpily. The changing reactions of the driver a periodic during a change in the information load of the environment are presented in the form of a system with rectangular impulses. One of the most effective ways of mutual adaptation of the driver and driving conditions is speed regulation using different types of the characteristic at object and information interaction of the driver by the environment. These characteristics are made a distinction for urban traffic conditions as for suburban traffic conditions. These indicators are presented in Table 8 and Table 9.

Table 8. The probabilities of finding objects in the driver’s field of perception in a condition are dangerous for movement (for suburban traffic conditions).

The name of the object in the field of perception	Numerical characteristics of the object
	Numerical values of probabilities
The condition carriageway on the street	Slippery (dirty, icy)
	$P_{12} = 0,25$
	Slippery (wet)
	$P_{12} = 0,20$
	Dry, clean
	$P_{12} = 0,13$
	Rough
	$P_{12} = 0,10$
	Very rough
	$P_{12} = 0,075$
Prohibiting traffic sign	$P_{13} = 0,285$
Warning traffic sign	$P_{14} = 0,243$
Directional traffic sign	$P_{15} = 0,24$
Order traffic sign	$P_{16} = 0,48$

Table 9. The probabilities of finding objects in the driver’s field of perception in a condition are dangerous for movement considering the location of objects along the road and the possibility of oncoming and overtaking (for suburban traffic conditions).

The name of the object in the field of perception	Numerical characteristics of the object			
	Numerical values of probabilities			
	Number of lanes			
	2–3	Without dividing lanes	With dividing lanes	With intersections in different levels

(continued)

Table 9. (continued)

The name of the object in the field of perception	Numerical characteristics of the object			
	Numerical values of probabilities			
	$P_{17} = 0,10$	$P_{17} = 0,15$	$P_{17} = 0,065$	$P_{17} = 0,035$
Children by the roadside		$P_{18} = 0,385$		
Person by the roadside		$P_{19} = 0,285$		
Overtaking a motorcycle or bicycle		$P_{20} = 0,325$		
Oncoming a motorcycle or bicycle		$P_{21} = 0,300$		
Oncoming a truck and bus		$P_{22} = 0,214$		
Oncoming a vehicle		$P_{23} = 0,1715$		
Overtaking a vehicle		$P_{24} = 0,28$		
A vehicle which is overtaken moving laboratory		$P_{25} = 0,4$		

4 Conclusion

According to the results of experimental studies, the signal indicator objects of the traffic environment in urban conditions were established and the firstly, the signal indicator objects of the traffic environment for suburban conditions were formalized. There signal indicators have used to calculate the informational characteristics in the driver's field of perception in the model for calculating vehicle speeds and traffic flow. Use data of tables are allowed to calculate absolute organization and current entropy of object in the driver's field of perception that, in the future, the schedule of vehicles movement is determined.

The proposed informational characteristics were implemented in the method of estimating air pollution, which has been applied at Jubilee Avenue in Kharkiv city, as a result main measures to improve the state of atmospheric air had been proposed [15]. Based of it the informational characteristics could found their further development in the model for assessing and predicting the ecological condition of city streets and highways, predicting the evolution of the ergonomic system "driver – vehicle – transport network –environment".






References

1. Ahangari, S., Jeihani, M., Anam Ardeshiri, M., Rahman, M., Dehzangi, A.: Enhancing the performance of a model to predict driving distraction with the random forest classifier.

- J. Transport. Res. Board **2675**(11), 612–622 (2021). <https://doi.org/10.1177/03611981211018695>
2. Evtiukov, S., Karelina, M., Terentyev, A.: A method for multi-criteria evaluation of the complex safety characteristic of a road vehicle. *Transport. Res. Procedia* **36**, 149–156 (2018). <https://doi.org/10.1016/j.trpro.2018.12.057>
 3. Gavrilov, E.: *Systematology Transport*, vol. 5: Ergonomics. Knowledge of Ukraine, Kharkiv (2008)
 4. Kang, X., Namgung, M., Fujiwara, A., Kim, W., Wang, W.: Analysis of vehicle maneuverability and driving characteristics on a curved road condition. *KSCE J. Civ. Eng.* **23**(1), 420–432 (2019). <https://doi.org/10.1007/s12205-018-1803-y>
 5. Shaju, A., Kumar Pandey, A.: Modelling transient response using PAC 2002-based tyre model. *Veh. Syst. Dyn.* **60**(1), 20–46 (2022). <https://doi.org/10.1080/00423114.2020.1802048>
 6. Gruppelaar, V., van Paassen, M.M., Mulder, M., Abbink, D.A.: A perceptually inspired driver model for speed control in curves. In: 2018 IEEE International Conference on Systems, Man, and Cybernetics (SMC), pp. 1257–1262. IEEE, Miyazaki (2018). <https://doi.org/10.1109/SMC.2018.00220>
 7. Mahmoud, N., Abdel-Aty, M., Cai, Q.: Factors contributing to operating speeds on arterial roads by context classifications. *J. Transp. Eng., Part A: Syst.* **147**(8), 04021040 (2021). <https://doi.org/10.1061/JTEPBS.0000548>
 8. Chakraborty, M., Gates, T.: Assessing safety performance on urban and suburban roadways of lower functional classification: a comparison of minor arterial and collector roadway segments. *engrXiv Preprint* (2021). <https://doi.org/10.31224/osf.io/wgpn7>
 9. Yao, Z., Wang, Y., Liu, B., Zhao, B., Jiang, Y.: Fuel consumption and transportation emissions evaluation of mixed traffic flow with connected automated vehicles and human-driven vehicles on expressway. *Energy* **230**, 120766 (2021). <https://doi.org/10.1016/j.energy.2021.120766>
 10. Biondi, F., Alvarez, I., Jeong, K.A.: Human–vehicle cooperation in automated driving: a multidisciplinary review and appraisal. *Int. J. Hum.-Comput. Inter.* **35**(11), 932–946 (2019). <https://doi.org/10.1080/10447318.2018.1561792>
 11. Afanasieva, I., Galkin, A.: Assessing the information flows and established their effects on the results of driver’s activity. *Arch. Transp.* **45**(1), 7–23 (2018). <https://doi.org/10.5604/01.3001.0012.0938>
 12. Galkin, A., Davidich, N., Melenchuk, T., Kush, Y., Davidich, Y., Lobashov, O.: Modelling truck’s transportation speed on the route considering driver’s state. *Transport. Res. Procedia* **30**, 207–215 (2018). <https://doi.org/10.1016/j.trpro.2018.09.023>
 13. Prasolenko, O., Burko, D., Tolmachov, I., Gyulyev, N., Galkin, A., Lobashov, O.: Creating safer routing for urban freight transportation. *Transport. Res. Procedia* **39**, 417–427 (2019). <https://doi.org/10.1016/j.trpro.2019.06.044>
 14. González-Hernández, B., et al.: The driver’s visual perception research to analyze pedestrian safety at twilight. *Transport. Res. Procedia* **45**, 827–834 (2020). <https://doi.org/10.1016/j.trpro.2020.02.087>
 15. Lynnyk, I., Vakulenko, K., Lezhneva, E.: Analysis of the air quality in considering the impact of the atmospheric emission from the urban road traffic. In: Macioszek, E., Sierpiński, G. (eds.) *Research Methods in Modern Urban Transportation Systems and Networks*. LNNS, vol. 207, pp. 13–27. Springer, Cham (2021). https://doi.org/10.1007/978-3-030-71708-7_2



Real Time Driver Alertness System Based on Eye Aspect Ratio and Head Pose Estimation

Ronak Mundra¹ , Avireni Srinivasulu^{1,2} , Cristian Ravariu³ ,
Appasani Bhargav⁴ , and Sarada Musala⁵ 

¹ JECRC University, Jaipur 303905, India
avireni@jecrcu.edu.in

² K. R. Mangalam University, Gurugram 122103, India

³ Politehnica University of Bucharest, 313 Splaiul Independentei, Bucharest, Romania

⁴ Kalinga Institute of Industrial Technology, Bhubaneswar 751024, India

⁵ Vignan's Foundation for Science Technology and Research, Guntur 522213, India

Abstract. Drowsy driving is one of the main causes of traffic accidents that leads to the loss of men and material. There are two methods to detect the alertness of the driver: first method focuses on the driver's performance and second method focuses on the driver's state. Furthermore, methods focusing on driver's state are of two types groups: methods using brain signals and methods using image processing. This paper presents a real-time image processing system to detect the alertness of a driver based on the estimation of eye-aspect ratio (EAR) and the head-pose (HP) estimation. A camera is used to obtain the data of the driver and computer vision based methods are used to detect driver's state. The video segments captured by the camera are analyzed using image processing techniques. The EAR and the HP are continuously estimated to detect the alertness of a vehicle driver. The proposed scheme will have benefits in minimizing the accidents by alerting the driving about his current state.

Keywords: Driver monitoring · Driver drowsiness detection · Head pose · Eye aspect ratio (EAR)

1 Introduction

With the increase in the number of vehicles worldwide, auto collisions are one of the main causes of human loss. As per the report of the World Health Organization (WHO), car crashes are one of the main ten reasons for human death. As per a 2012 survey directed by the National Sleep Foundation, one among every five pilots concede that they have made a genuine mistake, and one out of six trained administrators and transporters say that they have had a “close to miss” because of drowsiness [1]. In 2008, the National Highway Traffic Safety Administration estimates that 100000 police reports' on vehicle crashes were the direct results of driver drowsiness resulting in 1550 deaths, 71000 injuries, and \$12.5 billion in monetary losses [2].

Three primary methodologies are used to identify driver absentmindedness, namely, physiological, driving-conduct based, and visual-include based methodologies. Physiological methodologies include examination of imperative signals, for example, cerebrum action, pulse, and heartbeat rate. For instance, Khushaba *et al.* [3] fostered a fluffy shared data based wavelet parcel change model to gauge the tiredness level from a bunch of electroencephalogram, electrooculogram, and electrocardiogram signals. Notwithstanding, the physiological methodologies frequently require anodes that are connected to the driver's body, which are meddlesome in nature and, thus ly, may make disturbance to the driver. Driving-behaviour-information-based approaches evaluate the driver's performance over time.

Based on the variations in the lateral position, speed, steering wheel angle, acceleration, and breaking, the system determines, if the driver is alert or not. Liang *et al.* [4] developed a real-time approach for detecting distraction using the driver's eye movements and driving performance data collected in a simulator environment called the in-vehicle information system. Drowsy people often produce unique visual features on the face such as eye blinking, yawning, and eye and head movements. Hammoud *et al.* [5] had proposed a driver laziness discovery framework that gauges the situation with the eyes in the close infrared range. Moriyama *et al.* [6] have assessed the eye state by making itemized layouts of the shape and surface of the eyelid. As a broadly acknowledged visual measure for sluggishness identification, the level of eyelid conclusion (PC) tallies the quantity of eye flickers of the driver [7]. These methods are based mainly on the eye movements and the driving performance of the driver [8–15].

This paper presents the continuous monitoring of the driver's alertness by estimating the eye aspect ratio (EAR) and the head pose (HP). The information needed for the estimation is captured using a single camera and the parameters are obtained using the OpenCV library implemented in Python. The proposed scheme estimates the EAR and HP angles from a face object in a live video stream captured by the camera [16–19].

The organization of the paper is as follows: the next section describes the detection of EAR based on facial features. The third section presents the estimation of the HP. The proposed algorithm for detecting the state of the driver is proposed in section four. In section five the experimental results are presented and finally in section six, the conclusion is discussed.

2 Facial Landmark and Ear Detection Review

There are a variety of facial landmark detectors, but all methods are essentially to try to localize and label the various facial regions, such as, mouth, right eyebrow, left eyebrow, right eye, left eye, nose and jaw.

The pre-trained facial landmark detector is available inside the dlib library and is used to estimate the location of 68 (x, y) -coordinates that map the facial structures on the face. As discussed in the above section, the condition of eyes demonstrates the state of the driver. In [3] a method of ellipse fitting was proposed to describe the shape of pupil. As shown in Fig. 1, the method first segments the pupil using the traditional image processing techniques. Then, an ellipse is fitted with the white pixels, which represent the shape of the eyes. Lastly, the ratio of major and minor axes of the ellipse was used

to evaluate the state of eyes. However, the performance depends on other factors as well as discussed below:

1. The pixel values are sensitive. Image segmentation depends on the surrounding environment.
2. In practical application, the pixel values between the pupils and glasses are very close, which lead to wrong ellipse fitting, when the driver is wearing glasses.

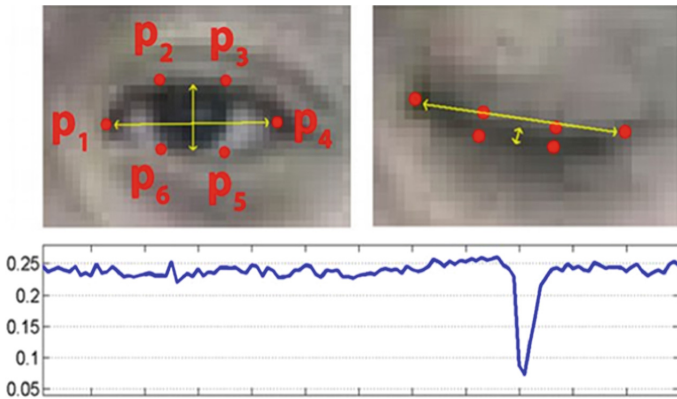


Fig. 1. Eyes landmarks. Upper: Eye landmark coordinate. Bottom: reading of EAR [7].

In this paper, we design a new more stable parameter based on Dlib toolkit to evaluate the state of driver’s eyes. It is more stable and precise than ellipse fitting method thanks to avoiding the traditional image process.

As shown in Fig. 1, for particular eye, we have six centres passed on around to discover the circumstance of eye. The development of eyes accomplishments has basic separations among two state either open or close. In [4], EAR was use to save the squint rehash. EAR can be handled by the circumstance of eyes achievements by [7]:

$$EAR = \frac{\|P_2 - P_6\| + \|P_3 - P_5\|}{2\|P_1 - P_4\|} \tag{1}$$

where $P_x, x = 1, 2, 3, 4, 5, 6$ is the coordinate of eyes landmarks. As shown in Fig. 1, when EAR is 0.2 or above means eyes consider as open otherwise close.

3 The Head Pose Estimation

In computer vision the posture of an object alludes to its overall direction and position regarding a camera. You can change the posture by either moving the item regarding the camera, or the camera concerning the item.

The posture assessment issue depicted in this instructional exercise is frequently alluded to as Perspective-n-Point issue or PNP in computer vision language. As we shall

find in the accompanying segments in more detail, in this issue the objective is to discover the posture of an item when we have an adjusted camera, and we know the areas of n 3D focuses on the article and the relating 2D projections in the Fig. 2.

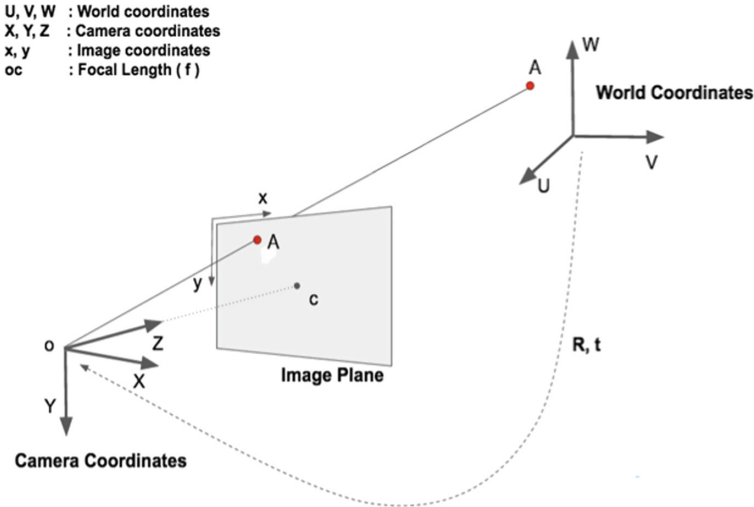


Fig. 2. 3D coordinates projected on image frame [6].

Let’s assume that we know the location of a point in the 3D co-ordinate system. If we know the rotation (a 3×3 matrix) and translation (a 3×1 vector) of the coordinate with respect to the camera coordinates, the location of the point in the camera coordinate system can be calculated using the following equation.

$$\begin{bmatrix} X \\ Y \\ Z \end{bmatrix} = \begin{bmatrix} r_{00} & r_{01} & r_{02} & t_x \\ r_{10} & r_{11} & r_{12} & t_y \\ r_{20} & r_{21} & r_{22} & t_z \end{bmatrix} \begin{bmatrix} U \\ V \\ W \\ 1 \end{bmatrix}. \tag{2}$$

A 3D rigid object has only two kinds of motions with respect to a camera. One is translation and second is rotation. There are three organized frameworks in play here. The 3D directions of the different facial highlights as appeared above are in world directions. In the event that if we knew the rotation and translation (for example present), we could change the 3D focuses in world directions to 3D focuses in camera organizes. The 3D focuses in camera facilitates that can be projected onto the picture plane (for example picture organize framework) utilizing the natural boundaries of the camera (central length, optical focus and so on)

$$s \begin{bmatrix} X \\ Y \\ Z \\ 1 \end{bmatrix} = \begin{bmatrix} r_{00} & r_{01} & r_{02} & t_x \\ r_{10} & r_{11} & r_{12} & t_y \\ r_{20} & r_{21} & r_{22} & t_z \end{bmatrix} \begin{bmatrix} U \\ V \\ W \end{bmatrix}, \tag{3}$$

where s is the scale factor, it exists in equation because we don't know the depth of the image, (X, Y, Z) is 3D coordinate of point A in camera coordinate system and (U, V, W) is 3D coordinate of point A in world coordinate system. The joint rotation–translation matrix $[R|t]$ contains extrinsic parameters r_{ij} and t_i . The POSIT algorithm is used to estimate the position in three dimensions of a known object.

This equation can be solved using a method called the direct linear transform (DLT). After solving the same we get the equation shown as under

$$s \begin{bmatrix} X \\ Y \\ 1 \end{bmatrix} = \begin{bmatrix} f_x & 0 & c_x \\ 0 & f_y & c_y \\ 0 & 0 & 1 \end{bmatrix} \begin{bmatrix} r_{11} & r_{12} & r_{13} & t_1 \\ r_{21} & r_{22} & r_{23} & t_2 \\ r_{31} & r_{32} & r_{33} & t_3 \end{bmatrix} \begin{bmatrix} U \\ V \\ W \end{bmatrix}, \quad (4)$$

where f_x and f_y are the focal lengths in the x and y directions, and is the optical center.

In OpenCv the function **solvePnP** can be used to estimate pose. We can use this function on several algorithms for pose estimation using the parameter flag. By default, this function use `SOLVE_ITERATIVE` which is required for DLT solution.

In OpenCV there are two new methods **SOLVEPNP_DLS** and **SOLVEPNP_UPNP**. The important thing in `SOLVEPNP_UPNP` is that it tries to estimate camera internal parameters also.

`SOLVEPNP_UPNP` Method is based on the paper [11]. In this case the function also estimates the parameters f_x and f_y assuming that both have the same value. Then the camera Matrix is updated with the estimated focal length.

4 Proposed Algorithm Flow Diagram

A normal camera is being utilized for portraying the face and its highlights. There is a need of speakers too for disturbing the driver to keep the driver away from feeling snoozing. In this proposed project there are four different parts:

- Face detection,
- Eye detection,
- Eye blinking detection,
- Head Pose Estimation.

By using OpenCv Dlib library we get face part. It distinguishes the face and introduces the interaction of languor discovery continuously, and also, for identifying area of facial highlights like eye, eye flickering developments, mouth and so on. Once, eyes are being identified, their developments are determined per outline.

In this case, after determining the eyes we can perform some mathematical operations on this as stated above and calculated eye aspect ratio (EAR). Along with this we can locate the head and track that in real time. Thus, we can track 5 points like nose tip, corner of both eyes, and corner of chicks and chin point. By using all these points we make an angle by which we can determine the particular degree of head from the centre.

If this angle is more than the threshold limit, for example, 45° for some consecutive frame then we can say that driver is not seeing in front for whatsoever reason and then we play an alarm to alert the driver. We can better understand this with the help of flow diagram as seen in Fig. 3.

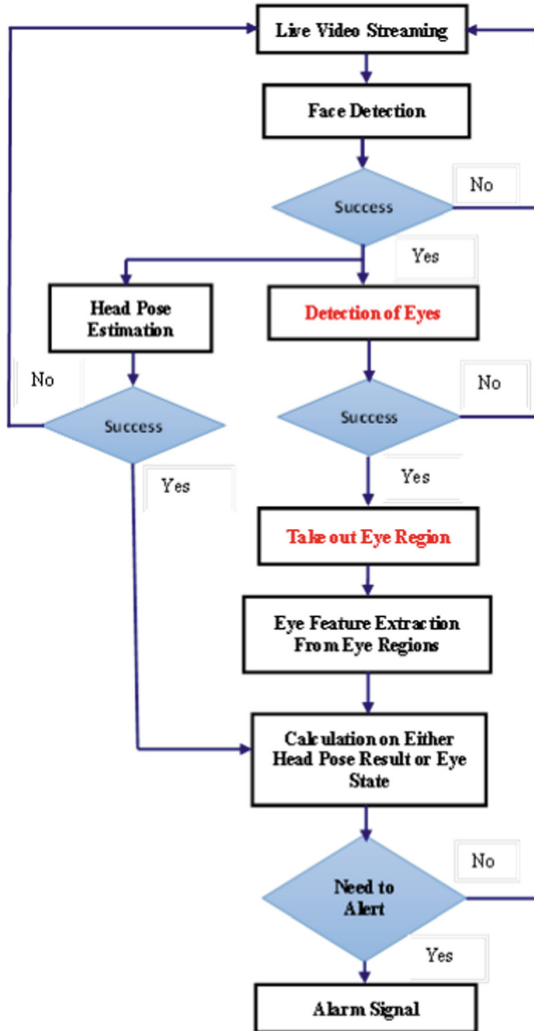


Fig. 3. System flow.

5 Experimental Results

The proposed detection framework was tested on different individuals. It only recognizes the right individual (the driver) and ignores the other individuals. Additionally, the

method can recognize each individual by the face and it also labels them. The OpenCv library was to recognize face. Next, the EAR is estimated in real-time. When the EAR is below the threshold a warning is issued. The EAR is estimated continuously in the real time. These results are shown in Fig. 4, 5 and 6.



Fig. 4. Normal open eye.



Fig. 5. Closed eye.

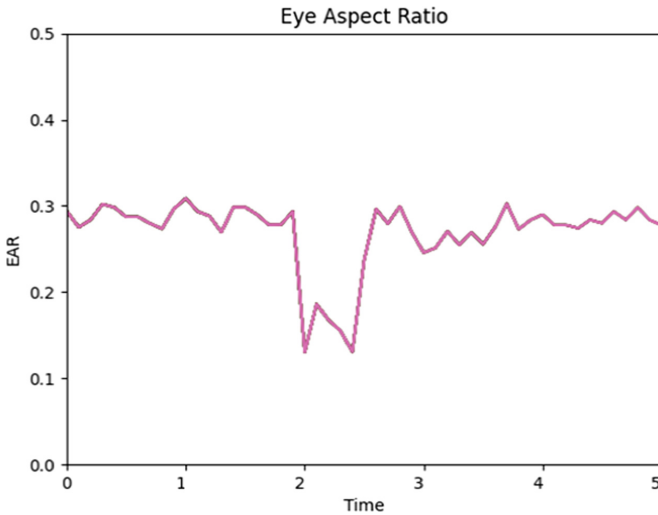


Fig. 6. Eye aspect ratio graph.

Next result is for head pose estimation that you can see in the below figures from Fig. 7, 8 and Fig. 9.



Fig. 7. Right side watching.



Fig. 8. Left side watching.

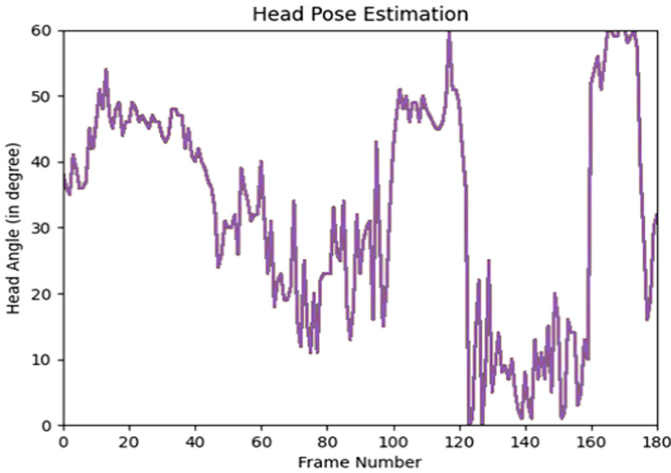


Fig. 9. Head pose estimation graph.

6 Conclusion

Examination on languid driving identification calculation is perhaps the main techniques to lessen car crashes. As we probably are aware that, there are critical individual contrasts, particularly the size of eyes, between various individuals. It is quick enough to contemplate the individual contrasts when we concentrate on the calculation dependent on computer vision.

In this paper, we propose another driving languor discovery calculation. We present a strategy for computation for eye angle proportion and head present assessment for sharpness of the driver. The test shows that framework works reliably.

In future, we can improve this technique in such a manner that it can also maintain the speed of vehicle and emergency break if needed along with alert signal. With help of this we can control the final damage up to a certain level.

References

1. Ren, Z., Yuan, J., Meng, J., Zhang, Z.: Robust part-based hand gesture recognition using kinect sensor. *IEEE Trans. Multimedia* **15**(5), 1110–1120 (2013). <https://doi.org/10.1109/TMM.2013.2246148>
2. Mengyuan, L., Liu, H., Chen, C.: Robust 3d action recognition through sampling local appearances and global distributions. *IEEE Trans. Multimedia* **20**(8), 1932–1947 (2018). <https://doi.org/10.1109/TMM.2017.2786868>
3. Tolba, A.: Content accessibility preference approach for improving service optimality in internet of vehicles. *Comput. Netw.* **152**, 78–86 (2019). <https://doi.org/10.1016/j.comnet.2019.01.038>
4. Kong, X., Xia, F., Li, J., Hou, M., Li, M., Xiang, Y.: A Shared bus profiling scheme for smart cities based on heterogeneous mobile crowdsourced data. *IEEE Trans. Ind. Inf.* **16**(2), 1436–1444 (2020). <https://doi.org/10.1109/TII.2019.2947063>
5. Mbouna, R.O., Kong, S.G., Chun, M.-G.: Visual analysis of eye state and head pose for driver alertness monitoring. *IEEE Trans. Intell. Transp. Syst.* **14**(3), 1462–1469 (2013). <https://doi.org/10.1109/TITS.2013.2262098>
6. ProgrammerSought: Head posture detection. <https://www.programmersought.com/article/52424662140/>. Accessed 10 May 2022
7. Jung, T., Kim, S., Kim, K.: Deep vision: Deepfakes detection using human eye blinking pattern. *IEEE Access* **8**, 83144–83154 (2020). <https://doi.org/10.1109/ACCESS.2020.2988660>
8. Khushaba, R.N., Kodagoda, S., Lal, S., Dissanayake, G.: Driver drowsiness classification using fuzzy wavelet-packet-based feature-extraction algorithm. *IEEE Trans. Biomed. Eng.* **58**(1), 121–131 (2010). <https://doi.org/10.1109/TBME.2010.2077291>
9. You, F., Li, X., Gong, Y., Wang, H., Li, H.: A real-time driving drowsiness detection algorithm with individual differences consideration. *IEEE Access* **7**, 179396–179408 (2019). <https://doi.org/10.1109/ACCESS.2019.2958667>
10. Luo, C., Zhang, J., Jun, Y., Chen, C.W., Wang, S.: Real-time head pose estimation and face modeling from a depth image. *IEEE Trans. Multimedia* **21**(10), 2473–2481 (2019). <https://doi.org/10.1109/TMM.2019.2903724>
11. Brandt, T., Stemmer, R., Rakotonirainy, A.: Affordable visual driver monitoring system for fatigue and monotony. In: 2004 IEEE International Conference on Systems, Man and Cybernetics (IEEE Cat. No. 04CH37583), vol. 7, pp. 6451–6456. IEEE, Hague (2004). <https://doi.org/10.1109/ICSMC.2004.1401415>
12. Ullah, A., Ahmed, S., Siddiqui, L., Faisal, N.: Real time driver's drowsiness detection system based on eye conditions. *Int. J. Sci. Eng. Res.* **6**, 3 (2015)
13. Omidyeganeh, M., Javadtalab, A., Shirmohammadi, S.: Intelligent driver drowsiness detection through fusion of yawning and eye closure. In: 2011 IEEE International Conference on Virtual Environments, Human-Computer Interfaces and Measurement Systems Proceedings, pp. 1–6. IEEE, Ottawa (2011). <https://doi.org/10.1109/VECIMS.2011.6053857>
14. Penate-Sanchez, A., Andrade-Cetto, J., Moreno-Noguer, F.: Exhaustive linearization for robust camera pose and focal length estimation. *IEEE Trans. Pattern Anal. Mach. Intell.* **35**(10), 2387–2400 (2013). <https://doi.org/10.1109/TPAMI.2013.36>
15. Tirupathireddy, A., Sarada, M., Srinivasulu, A.: Energy-efficient approximate adders for DSP applications. *Analog Integr. Circ. Sig. Process* **107**(3), 649–657 (2021). <https://doi.org/10.1007/s10470-020-01768-w>
16. Gupta, D.K., et al.: Hybrid gravitational-firefly algorithm based load frequency control for hydrothermal two-area system. *Mathematics* **9**(7), 712 (2021). <https://doi.org/10.3390/mat9070712>

17. Saini, J.K., Srinivasulu, A., Kumawat, R.: High-performance low-power 5:2 compressor with 30 CNTFETs using 32 nm technology. *Int. J. Sens. Wireless Commun. Control* **9**(4), 462–467 (2019). <https://doi.org/10.2174/2210327909666190206144601>
18. Saini, J.K., Srinivasulu, A., Kumawat, R.: Low power-high speed magnitude comparator circuit using 12 CNFETs. In: 2018 International SoC Design Conference (ISOCC), pp. 145–146. IEEE, Daegu (2018). <https://doi.org/10.1109/ISOCC.2018.8649969>
19. Banerjee, S., et al.: A triple band highly sensitive refractive index sensor using terahertz metamaterial perfect absorber. *Prog. Electromagnet. Res. M* **107**, 13–24 (2022). <https://doi.org/10.2528/PIERM21100701>



Modeling the Impact of Technology and Arranging Commuter Passenger Transportation by Competing Modes of Transport

Tetiana Hrushevska , Oleh Strelko  ^(✉), Anatoliy Horban , Liubov Soloviova ,
and Oleksandra Soloviova 

State University of Infrastructure and Technologies, 9 Kyrylivska Street, Kyiv 04071, Ukraine
olehstrelko@duit.edu.ua

Abstract. The aim of the paper is to improve and to optimize the system for arranging commuter passenger transportation and improving the quality of transport services by modeling the impact of technology and arranging commuter passenger transportation on their volumes in a competitive environment in the transport market. The processes of development of any system associated with the modernization or the introduction of new technology and equipment have common properties. Accordingly, commuter transport should be considered in relation to the external environment. It is advisable to solve problems of this class specifically with the help of a systematic approach. The commuter passenger transportation system is difficult to study, because it contains a large number of components that are in various relationships. The components of this system are passengers of different social groups, vehicles, infrastructure facilities, financial flows, information flows, etc. With reference to the above-mentioned subject, the study of the system for arranging commuter passenger transportation should be approached from the standpoint of system analysis, when a system is understood as a set of elements that are in relationships and connections with each other and form a certain integrity and unity. In order to mathematically describe the system for arranging commuter passenger transportation, it is necessary to describe the properties of the input stream of homogeneous events – the structure of the system, the characteristics of the service, the flow of orders. The theory of waiting lines is applied in this. The methods of the theory of waiting lines are well studied and widely used to solve various problems in transport. This also applies to the commuter passenger transportation industry. The probability of preference for choosing a rail transport by a potential passenger, taking into account the totality of technological, organizational, and economic parameters that affect the traffic flow and reflect the conditions for the transportation of passengers by various modes of transport.

Keywords: Railway transport · Mathematical modeling · Suburban railway · Passenger transportation

1 Introduction

The processes of development of any system associated with the modernization or the introduction of new technology and equipment have common properties [1–3]. Accordingly, commuter transport should be considered in relation to the external environment [4]. It is advisable to solve problems of this class specifically with the help of a systematic approach. The commuter passenger transportation system is difficult to study, because it contains a large number of components that are in various relationships [5–7]. The components of this system are passengers of different social groups, vehicles, infrastructure facilities, financial flows, information flows, etc. [8–10]. With reference to the above-mentioned subject, the study of the system for arranging commuter passenger transportation should be approached from the standpoint of system analysis [11–13], when a system is understood as a set of elements that are in relationships and connections with each other and form a certain integrity and unity.

Mathematical modeling is one of the most important tools in solving various transport problems [14–16] and it is one of the most common methods in the study of transport processes and phenomena [17–19].

The aim of the paper is to improve and to optimize the system for arranging commuter passenger transportation and improving the quality of transport services by modeling the impact of technology and arranging commuter passenger transportation on their volumes in a competitive environment in the transport market.

2 Literature Review

The methodological basis for the development of mathematical models of arranging commuter passenger transportation is a systematic approach, the implementation of which should be based on the fundamental provisions of the theory of transport systems and relevant applied methods. The methodological foundations and practical aspects of the functioning of passenger transport are reflected in the works that consider the problems optimizing vehicle design to minimize damaging track forces [20], highlighting recent trends to identify the foremost research areas whose advancement will reduce the environmental impact of this sector [21], new conceptual framework and pragmatic strategies for transit priority implementation in car-centric cities [22], technical and regulatory problems and barriers which are considered to prevent or impede the use of drones for parcel and passengers transportation [23], theoretical frameworks, sampling and estimation methods and indicators relevant to designing empirical built environment and transit use research [24], the transformation of the transport market, being the effect of changes on the market of goods and services and economic growth, the reasons for using railway transport in servicing urban and agglomeration traffic [25] and other studies [26–28].

The most common and important criteria in the analysis of the commuter passenger transportation system are quality, reliability, number of passengers carried, competitiveness, efficiency of arranging, and the like. The basic tool for conducting a comprehensive analysis of the activity of commuter passenger transportation is factor analysis. The theoretical and practical foundations of the factor analysis methodology are shown in the

works [29–31]. Factor analysis is applied as a form of quantities and constants, the value of which is determined on the basis of statistical data and probabilistic ideas about transport processes.

3 Research Methodology

In order to mathematically describe the system for arranging commuter passenger transportation, it is necessary to describe the properties of the input stream of homogeneous events – the structure of the system, the characteristics of the service, the flow of orders. The theory of waiting lines is applied in this. The methods of the theory of waiting lines are well studied and widely used to solve various problems in transport [32–34]. This also applies to the commuter passenger transportation industry.

It is necessary to note the theory of games and decisions among the methods based on the probability theory, which studies mathematical models, where the participants in the transportation process – the players (railway and vehicular transport) have different interests and have to achieve goals using certain strategies.

Methods of the probability theory, the theory of waiting lines and mathematical statistics should be used in the calculation and analysis of passenger flows in commuter traffic routes. Using these methods, it is possible to identify certain patterns in the formation of passenger flows within the transport hub.

The authors of [35] conventionally divided the methods used in the study of transport processes into descriptive and mathematical ones. Thus, descriptive methods do not provide a quantitative measurement for assessing the processes under study. Therefore, mathematical methods of two directions are mainly discussed: deterministic and probabilistic ones. In the first case, transport is considered to be as a certain mechanism, and its components – stations, hubs, sections, traffic routes – as links interconnected by rigid analytical dependencies. In the second case, it is assumed that the operational processes are probable, correlational, and not uniquely determined.

If we talk about mathematical methods, then varieties of the linear programming method are widely used in transport. In linear programming problems, the conditions that are imposed on the range of permissible variable values are determined by a system of linear inequalities, while the desired value is a linear function of the same variables. It is expedient to use linear programming methods in this study in order to determine the size of train traffic on commuter routes.

4 Results and Discussion

In order to study the impact of technology and arranging commuter passenger transportation on their volumes in the conditions of competition in the transport market, we can apply both the experience of building similar mathematical models [12, 17] and the analogy with Markovian processes [19], in which the system passes from state S_i to state S_j (and it is in them with probabilities p_i and p_j) under the influence of certain flows of events, which (flows) have intensity λ_{ij} . Under the conditions of setting the problem of the spatial distribution of passengers in the network, a complete description of the state

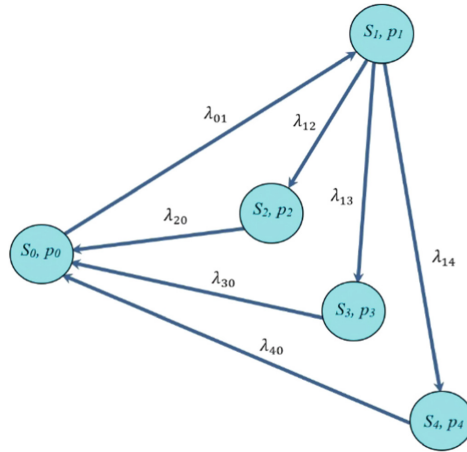


Fig. 1. An approximate graph of system states (S_i, p_i – i -th state of the system and the probability of finding the system in the i -th state), where S_0, p_0 – no passengers; S_1, p_1 – presence of passengers, choice of transport; S_2, p_2 – transportation by railway; S_3, p_3 – transportation by road; S_4, p_4 – transportation by private mode of transport (a private vehicle).

of the transportation system is to determine the behavior of the passenger in choosing a traffic route. An approximate graph of system states is shown in Fig. 1.

Let us consider the system of the competitive transport market “passenger – alternative carriers”, where the number of passengers in a certain period of time can be transported by rail or road, and the decision is made by the passenger, taking into account the economic, organizational-and-technological, and other advantages or disadvantages of these modes of transport. The hypothesis is that the intensity of the flow of events depends on the economic, organizational, and technological parameters of the transport service, different messages of which make the flow intensities more or less intense and different states of the system – more or less probable.

As S_2 state, we will consider the transportation of passengers by the rail transport chosen for this, S_3 – state – transportation by road, and S_4 – state – transportation by a private mode of transport (a vehicle). Thus, these three modes of transport are considered to be as competitive, alternative ones. We assign the described states to their probabilities and write down the system of flow balance equations for the final probabilities of the states. This system, compiled according to known rules [35], has the form:

$$\begin{cases} \lambda_{01} \cdot p_0 = \lambda_{20} \cdot p_2 + \lambda_{30} \cdot p_3 + \lambda_{40} \cdot p_4, \\ (\lambda_{12} + \lambda_{13} + \lambda_{14}) \cdot p_1 = \lambda_{01} \cdot p_0, \\ \lambda_{20} \cdot p_2 = \lambda_{12} \cdot p_1, \\ \lambda_{30} \cdot p_3 = \lambda_{13} \cdot p_1, \\ \lambda_{40} \cdot p_4 = \lambda_{14} \cdot p_1, \\ p_0 + p_1 + p_2 + p_3 + p_4 = 1. \end{cases} \quad (1)$$

From this system of equations, we first will find p_1 , and then all other state probabilities:

$$p_1 = \frac{1}{1 + \frac{\lambda_{12} + \lambda_{13} + \lambda_{14}}{\lambda_{01}} + \frac{\lambda_{12}}{\lambda_{20}} + \frac{\lambda_{13}}{\lambda_{30}} + \frac{\lambda_{14}}{\lambda_{40}}}, \tag{2}$$

$$p_2 = p_1 \cdot \frac{\lambda_{12}}{\lambda_{20}}, \tag{3}$$

$$p_3 = p_1 \cdot \frac{\lambda_{13}}{\lambda_{30}}, \tag{4}$$

$$p_4 = p_1 \cdot \frac{\lambda_{14}}{\lambda_{40}}, \tag{5}$$

$$p_0 = p_1 \cdot \frac{\lambda_{12} + \lambda_{13} + \lambda_{14}}{\lambda_{01}}. \tag{6}$$

If we assume that each state of the transportation system is carried out with equal probability, then the most probable distribution of flows is found.

Now, we will determine the intensity of passenger flow based on the above hypothesis, using both natural and economic parameters of transport services. Therefore, the intensities of passenger flows are as follows:

$$\lambda_{01} = \frac{B}{T}, \tag{7}$$

where B is the economic benefit of a passenger from traffic by public transport compared to private transport, UAH; T is the period of time (hours, days, etc.), hours.

$$B = C_v - \frac{(C_a + C_r + C_{pr})}{3}, \tag{8}$$

where C_v is the fare while traveling by private vehicle, UAH; C_a is the fare when traveling by public vehicular transport, UAH; C_r is the railway ticket price, UAH; C_{pr} is the fare when traveling by a private vehicle, UAH

$$C_{pr} = \frac{C_v}{K}, \tag{9}$$

where K is the number of passengers in a private vehicle.

The economic benefit calculated by formula 8 contains the average cost of traffic by public transport (including private vehicles) $-\frac{(C_a + C_r + C_{pr})}{3}$, which is due to: firstly, the proximity of the rates of rail and vehicular transport in nearby commuter areas in a competitive environment; secondly, the initial equiprobability of the passenger's choice of one or another mode of transport

$$C_v = \frac{C_a^v}{t_s \cdot 365} + \frac{gf \cdot C_f \cdot l_{ad}}{100}, \tag{10}$$

where C_a^v is the original cost of a vehicle, UAH; t_s is the service life, years; l_{ad} is the average dally vehicle run, km; g_f is the fuel cost (calculation is made on the example of gasoline); C_f is the fuel consumption rate per 100 km; C_a is the ticket price in public vehicular transport, UAH.

It is probably difficult to argue that the transition from the state “no passengers” to the state “presence of passengers” is the more likely, the greater the benefit that the transportation of passengers can provide. For example, the greater the difference in the cost of transportation by private vehicles compared to public transport, the more intense the passenger flow λ_{01} will be. Thus, the determination of the flow intensity λ_{01} is based on quite logical economic premises.

The intensities of flows λ_{12} , λ_{13} and λ_{14} , which predetermine the passenger’s choice of one of the three modes of transport (railway, vehicular, or private vehicle) are determined using the following considerations. The value λ_{1j} should be calculated as follows:

$$\lambda_{1j} = \frac{C_v - Q_j}{z_j}, \tag{11}$$

where Q_j is the cost of a passenger’s ticket required for its implementation by the j -th mode of transport ($j = 2$ – rail transport, $j = 3$ – vehicular transport, $j = 4$ – private vehicle), UAH; z_j is the total time of passenger transport service containing the following components, hours

$$z_j = \tau_j + \frac{T \cdot q_j}{A_m} + \frac{L_j}{V_j}, \tag{12}$$

where A_m is the volume of passenger transportation that should be carried out during a period of time T (hours, days, etc.), passengers; τ_j is the time before the start of the trip (for example, the time of approaching the railway station, approaching commuter ticket offices, parking, time to buy a ticket), hours; $\frac{T \cdot q_j}{A_m}$ is the average departure interval of vehicles (departure waiting time), determined using already known values, hours; $\frac{L_j}{V_j}$ is the duration of the passenger’s stay in the process of transportation, depending on its distance L_j and speed V_j , hours.

The rates of λ_{20} , λ_{30} and λ_{40} flows (generally λ_{j0}) that return the system to the «no passengers» state after the completion of the transportation of passengers for a period of time are as follows:

$$\lambda_{j0} = \frac{Q_j}{T}. \tag{13}$$

Obviously, the greater the specific economic benefits from the transportation of passengers per unit of time, the faster the transportation of passengers (the system returns to the “no passengers” state) is, but only in order to start a new cycle of receiving benefits (returns to the state “presence of passengers”).

After the above formulas, let us write out the formula (3) in expanded form

$$p_2 = p_1 \cdot \frac{\lambda_{12}}{\lambda_{20}},$$

$$p_2 = \frac{\frac{C_v}{Q_2} - 1}{z_2 \cdot \left[\frac{1}{T} + \frac{C_v - 1}{z_2} + \frac{C_v - 1}{z_3} + \frac{K - 1}{z_4} + \frac{1}{B} \cdot \left(Q_2 \cdot \frac{C_B - 1}{z_2} + Q_3 \cdot \frac{C_v - 1}{z_3} + \frac{C_v}{z_4} \cdot \left(1 - \frac{1}{K} \right) \right) \right]} \tag{14}$$

Equation (14), which in expanded form reflects the dependence of the probability of preference (chances) for choosing a rail transport by a potential passenger, shows that these chances depend on a set of technological, organizational, and economic parameters that reflect the conditions for the transportation of passengers by different modes of transport that compete with each other. It was clear that this dependence has a non-linear complex character and the z_2 , z_3 , and z_4 variables, in turn, depend on other parameters.

With the given output, the probability of choosing rail transport P_{rt} , if the passenger has no other choice than between rail, vehicular transport, and a private vehicle, will be: $P_{rt} = \frac{p_2}{p_2 + p_3 + p_4}$ (this calculation method is correct, since the probabilities of choosing one or another mode of transport are the probabilities of events that form a complete group, the sum of probabilities of which is always equal to one).

The formula for the probability of choosing a rail transport by a potential passenger takes the form:

$$P_{rt} = \frac{\frac{C_v}{Q_2} - 1}{\left(\frac{C_v}{Q_2} - 1 \right) + \frac{z_2}{z_3} \cdot \left(\frac{C_v}{Q_2} - 1 \right) + \frac{z_2}{z_4} \cdot (K - 1)} \tag{15}$$

The formula for the probability of choosing a vehicular transport by a potential passenger takes the form:

$$P_{at} = \frac{\frac{1}{z_3} \cdot \left(\frac{C_v}{Q_3} - 1 \right)}{\frac{1}{z_2} \cdot \left(\frac{C_v}{Q_2} - 1 \right) + \frac{1}{z_3} \cdot \left(\frac{C_v}{Q_3} - 1 \right) + \frac{K - 1}{z_4}} \tag{16}$$

The formula for the probability of choosing a private vehicle by a potential passenger takes the form:

$$P_{pr} = \frac{\frac{K - 1}{z_4}}{\frac{1}{z_2} \cdot \left(\frac{C_v}{Q_2} - 1 \right) + \frac{1}{z_3} \cdot \left(\frac{C_v}{Q_3} - 1 \right) + \frac{K - 1}{z_4}} \tag{17}$$

The study of the P_{rt} dependence on the totality of these parameters and conditions has been carried out using calculations, the results of which are shown in Figs. 2–4.

As can be seen from Fig. 2, the probability of preference for rail transport falls on the morning and evening peak periods and during the morning and evening recession, on the contrary, the probability of preference decreases in favor of the transport system with a higher speed of passenger delivery, with a shorter service time that satisfies the passenger’s requirements for transport services.

Figure 3 shows how, depending on the number of passengers in a private vehicle, the probability of a preference for rail transport changes. It can range from 23 to 66%, taking into account a period of a day and the number of passengers in a private vehicle.

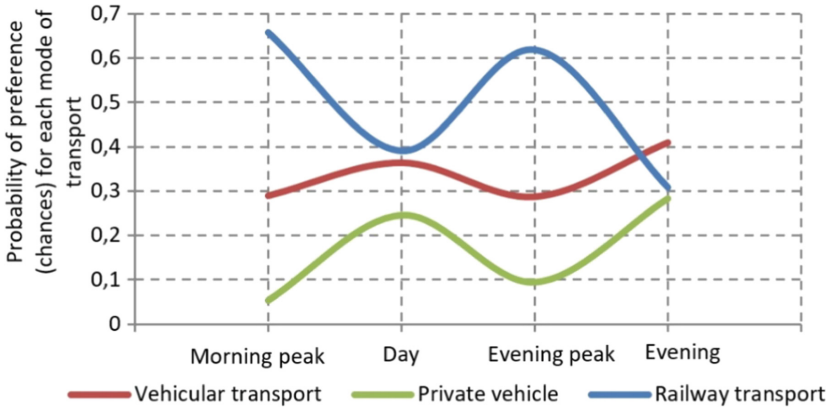


Fig. 2. Dependence of the probability of a passenger giving preference to each of the modes of transport (the chances of a mode of transport) on the period of the day.

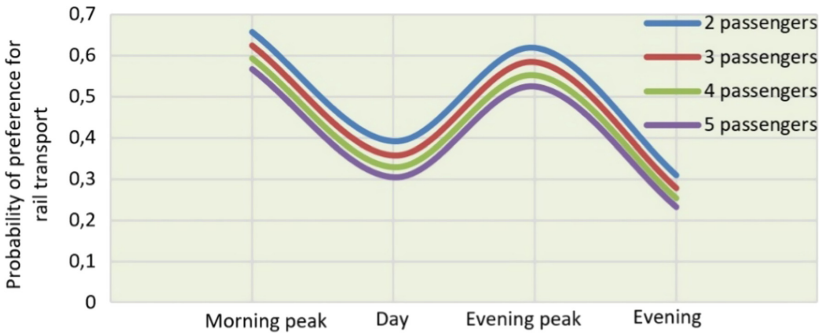


Fig. 3. Dependence of the probability of choosing a rail transport by a passenger on the number of passengers in a private vehicle.

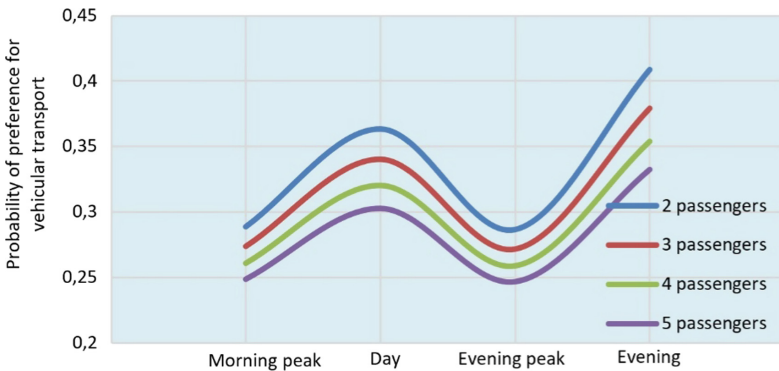


Fig. 4. Dependence of the probability that a passenger gives preference to public road transport on the number of passengers in a private vehicle.

After analyzing Fig. 4, it can be seen that the probability of the preference for vehicular transport during the morning and evening recession increases and it can range from 25% to 41%, depending on the number of passengers in a private vehicle and a period of a day.

It should be noted that each mode of transport is characterized by its own cost indicators: a ticket price for trip in public transport (vehicular or rail one) or the cost per passenger for a trip in a private vehicle; as well as depending on the arranging of its work, the total duration of the passenger's trip z_j . In order for the calculation results to be comparable for different modes of transport, we will take the maximum trip distance for all possible ways of its implementation as $L = 70$ km. Moreover, it should be taken into account that with different methods of making a trip, different vehicles, differing in passenger capacity (number of passengers), as well as their different average speeds at different times of a day, are used. For example: rail transport does not know such a phenomenon as traffic jams, however, both in vehicular transport (both public and private one), their negative impact on speed in the morning and evening peak hours is very noticeable, which should be taken into account when modeling. As can be seen from Fig. 5. Dependence of the probability of a passenger giving preference to rail transport during peak hours on the ticket price. Under the same conditions, the higher the cost of transportation is, the less likely the advantage of rail transport will be (if there is another transport system with a lower cost of transportation). Similarly, the amount of passenger flow can be affected by the transport time of a passenger service, the deviation of the actual time of transportation from the calculated one, and other factors.

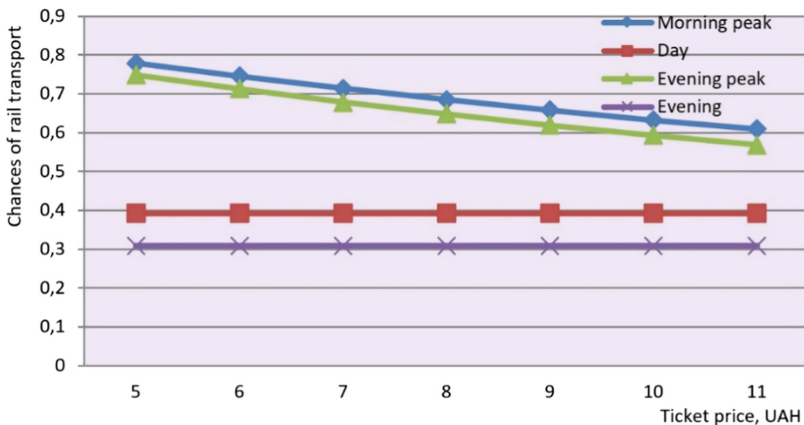


Fig. 5. Dependence of the probability of a passenger giving preference to rail transport during peak hours on the ticket price.

Authors of other studies have come to similar conclusions [17, 19]. Modeling the impact of technology and arranging commuter passenger transportation on their volumes in a competitive environment in the transport market is an effective means of improving and optimizing the system for arranging commuter passenger transportation [5] and improving the quality of transport services [8, 25].

In a competitive environment in the market of transport services, the vehicle-to-population ratio is increasing, which leads to increased requirements for public transport [22, 24, 26]. Therefore, in order to remain a competitive mode of transport, it is necessary to fully meet the needs of passengers during transportation, as well as to improve the quality of service.

5 Conclusion

The application of the developed model makes it possible to determine the probability of preference for choosing a rail transport by a potential passenger, taking into account the totality of technological, organizational, and economic parameters that affect the traffic flow and reflect the conditions for the transportation of passengers by various modes of transport. It can be argued that the most influential factors that attract passengers or repel them from one or another type of transportation are the following: the duration of the passenger's stay on the road; time of departure and arrival both at the main and intermediate stations; comfort level in trains; fare; traffic safety; independence from climatic conditions; initial and final time costs related to arranging a trip.

References

1. Soloviova, L., et al.: Container transport system as a means of saving resources. IOP Conference Series: Earth and Environmental Science **459**(5), 052070 (2020). <https://doi.org/10.1088/1755-1315/459/5/052070>
2. Kombarov, V., et al.: Investigation of the required discreteness of interpolation movement parameters in cyber-physical systems. Periodica Polytechnica Mechanical Engineering **66**(1), 1–9 (2022). <https://doi.org/10.3311/PPme.17884>
3. Kyrychenko, H., Strelko, O., Berdnychenko, Y.A.: Influence of existing operational conditions on compliance with car handling standards. IOP Conference Series: Earth and Environmental Science **666**(4), 167754 (2021). <https://doi.org/10.1088/1755-1315/666/4/042054>
4. Severino, A., Martseniuk, L., Curto, S., Neduzha, L.: Routes planning models for railway transport systems in relation to passengers' demand. Sustainability **13**(16), 8686 (2021). <https://doi.org/10.3390/su13168686>
5. Mohammadi, A., Amador-Jimenez, L., Nasiri, F.: Reliable, effective, and sustainable urban railways: a model for optimal planning and asset management. J. Constr. Eng. Manag. **146**(6), 04020057 (2020). [https://doi.org/10.1061/\(ASCE\)CO.1943-7862.0001839](https://doi.org/10.1061/(ASCE)CO.1943-7862.0001839)
6. Ghalehkhondabi, I., Ardjmand, E., Young, W.A., Weckman, G.R.: A review of demand forecasting models and methodological developments within tourism and passenger transportation industry. Journal of Tourism Futures **5**(1), 75–93 (2019). <https://doi.org/10.1108/JTF-10-2018-006>
7. Ammirato, S., et al.: A systematic literature review of revenue management in passenger transportation. Meas. Bus. Excell. **24**(2), 223–242 (2020). <https://doi.org/10.1108/MBE-09-2019-0096>
8. Pshinko, O., Charkina, T., Martseniuk, L., Orlovska, O.: Hubs as a key tool for improving the quality of the service and development of multimodal passenger traffic. Transport Problems **17**(1), 201–214 (2022). <https://doi.org/10.20858/tp.2022.17.1.17>

9. Strelko, O., et al.: Historical milestones of creation of computers technology automated system for passenger transportations management “Express” on the railway transport in the USSR. In: 2019 IEEE 2nd Ukraine Conference on Electrical and Computer Engineering (UKRCON), pp. 1214–1219. IEEE, Lviv (2019). <https://doi.org/10.1109/UKRCON.2019.8879892>
10. Matuška, J.: Railway system accessibility evaluation for wheelchair users: Case study in the Czech Republic. *Transport* **32**(1), 32–43 (2017). <https://doi.org/10.3846/16484142.2014.941396>
11. Hryhorak, M., Lyakh, O., Sokolova, O., et al.: Multimodal freight transportation as a direction of ensuring sustainable development of the transport system of Ukraine. *IOP Conference Series: Earth and Environmental Science* **915**(1), 012024 (2021). <https://doi.org/10.1088/1755-1315/915/1/012024>
12. Christoforou, Z., Corbillé, E., Farhi, N., Leurent, F.: Managing planned disruptions of mass transit systems. *Transportation Research Record* **2541**(1), 46–55 (2016). <https://doi.org/10.3141/2541-06>
13. Yin, J., et al.: Research and development of automatic train operation for railway transportation systems: a survey. *Transportation Research Part C: Emerging Technologies* **85**, 548–572 (2017). <https://doi.org/10.1016/j.trc.2017.09.009>
14. Bibik, S., et al.: Formulation of the mathematical model for the planning system in the carriage of dangerous goods by rail. *IOP Conference Series: Materials Science and Engineering* **985**(1), 012024 (2020). <https://doi.org/10.1088/1757-899X/985/1/012024>
15. Tiutkin, O., Keršys, R., Neduzha, L.: Comparative analysis of options for strengthening the railway subgrade with vertical elements. In: *Proceedings of the 25th International Conference Transport Means 2021, Pt. II*, pp. 604–608. Kaunas University of Technology, Kaunas (2021)
16. Lovska, A., Fomin, O., Přítěk, V., Kučera, P.: Dynamic load modelling within combined transport trains during transportation on a railway ferry. *Appl. Sci.* **10**(16), 5710 (2020). <https://doi.org/10.3390/app10165710>
17. Cacchiani, V., et al.: An overview of recovery models and algorithms for real-time railway rescheduling. *Transportation Research Part B: Methodological* **63**, 15–37 (2014). <https://doi.org/10.1016/j.trb.2014.01.009>
18. Statyvka, Y., Kyrychenko, H., Strelko, O., Berdnychenko, Y.: Control of technological processes using a fuzzy controller of the system for management of cargo delivery by railway. *Acta Scientiarum Polonorum Administratio Locorum* **20**(3), 241–251 (2021). <https://doi.org/10.31648/aspal.6808>
19. Fu, Q., Liu, R., Hess, S.: A review on transit assignment modelling approaches to congested networks: a new perspective. *Procedia Soc. Behav. Sci.* **54**, 1145–1155 (2012). <https://doi.org/10.1016/j.sbspro.2012.09.829>
20. Jaiswal, J.: Railways must adopt a system approach. *Int. Railw. J.* **45**(3), 21–23 (2005)
21. Epicoco, N., Falagario, M.: Decision support tools for developing sustainable transportation systems in the EU: A review of research needs, barriers, and trends. *Research in Transportation Business & Management*, 100819 (2022). <https://doi.org/10.1016/j.rtbm.2022.100819>
22. Reynolds, J., Currie, G.: New approaches and insights to managing on-road public transport priority. In: *Handbook of Public Transport Research*, pp. 172–201. Edward Elgar Publishing, Cheltenham (2021). <https://doi.org/10.4337/9781788978668.00017>
23. Kellermann, R., Biehle, T., Fischer, L.: Drones for parcel and passenger transportation: A literature review. *Transportation Research Interdisciplinary Perspectives* **4**, 100088 (2020). <https://doi.org/10.1016/j.trip.2019.100088>
24. Aston, L., Currie, G., Kamruzzaman, M., Delbosc, A.: Methodologies for empirical research on the link between the built environment and transit use. In: *Handbook of Public Transport Research*, pp. 30–55. Edward Elgar Publishing, Cheltenham (2021). <https://doi.org/10.4337/9781788978668.00008>

25. Pietrzak, O., Pietrzak, K.: The role of railway in handling transport services of cities and agglomerations. *Transportation Research Procedia* **39**, 405–416 (2019). <https://doi.org/10.1016/j.trpro.2019.06.043>
26. Hansson, J., Pettersson, F., Svensson, H., Wretstrand, A.: Preferences in regional public transport: a literature review. *Eur. Transp. Res. Rev.* **11**(1), 1–16 (2019). <https://doi.org/10.1186/s12544-019-0374-4>
27. Grzelec, K., Jagiełło, A.: The effects of the selective enlargement of fare-free public transport. *Sustainability* **12**(16), 6390 (2020). <https://doi.org/10.3390/su12166390>
28. Zhang, L., Long, R., Chen, H., Geng, J.: A review of China's road traffic carbon emissions. *J. Clean. Prod.* **207**, 569–581 (2019). <https://doi.org/10.1016/j.jclepro.2018.10.003>
29. Little, R.J., Rubin, D.B.: *Statistical Analysis with Missing Data*. John Wiley & Sons, Hoboken (2019). <https://doi.org/10.1002/9781119013563>
30. Jabłoński, A., Jabłoński, M.: Digital safety in railway transport – Aspects of management and technology. Springer, Cham (2022). <https://doi.org/10.1007/978-3-030-96133-6>
31. Kaldaras, L., Akazez, H., Krajcik, J.: A methodology for determining and validating latent factor dimensionality of complex multi-factor science constructs measuring knowledge-in-use. *Educ. Assess.* **26**(4), 241–263 (2021). <https://doi.org/10.1080/10627197.2021.1971966>
32. Grippa, P., Schilcher, U., Bettstetter, C.: On access control in cabin-based transport systems. *IEEE Trans. Intell. Transp. Syst.* **20**(6), 2149–2156 (2018). <https://doi.org/10.1109/TITS.2018.2864551>
33. Cevallos-Torres, L., Botto-Tobar, M.: Case study: Logistical behavior in the use of urban transport using the monte carlo simulation method. In: *Problem-Based Learning: A Didactic Strategy in the Teaching of System Simulation*, pp. 97–110. Springer, Cham (2019). https://doi.org/10.1007/978-3-030-13393-1_6
34. Aniyeri, R., Nadar, R.: Passengers queue analysis in international airports terminals in Kerala using multiphase queuing system. *Int. J. Math. Operat. Res.* **12**(1), 1–30 (2018). <https://doi.org/10.1504/IJMOR.2018.088566>
35. Cox, D.R., Miller, H.D.: *The Theory of Stochastic Processes*. CRC Press, Boca Raton (1977)



Effective Functioning of Intelligent Transport Systems as One of the Main Factors for Supporting Sustainable Urban Development

Viktor Danchuk¹ (✉) , Antonio Comi² , and Olga Kunytska¹ 

¹ National Transport University, 1 Mykhaila Omelianovycha-Pavlenka Street, Kyiv 01001, Ukraine

v.danchuk@ntu.edu.ua

² University of Rome Tor Vergata, 50 Via Cracovia, 00133 Rome, Italy

Abstract. The non-linear dynamic (bifurcation) nature of modern socio-economic processes has led to the emergence of the concept of sustainable development of society. The concept implies the use of innovative environmental, energy- and material-saving technologies, the preservation of the integrity and stability of socio-economic, biological and physical natural systems under conditions of limited resources. One of the main drivers of sustainable development is the high efficiency of designing, implementing and developing Intelligent Transport Systems (ITS). This paper considers the theoretical concepts of sustainable functioning and development of the transport system as an open non-linear dynamic system, within the framework of the generalized Lorenz model. The interaction between three dynamic variables is considered: the level of application of modern innovative technologies in ITS, the level of efficiency of various institutions that ensure the implementation and functioning of ITS, and the control factor, which determines the influence of the external environment on the current state of functioning of the transport system, including the urban street and road network (SRN). Based on the results of simulation studies, the conditions for the sustainable functioning of the ITS have been identified, which are associated with proactive activities to improve and timely implementation of information and communication technologies in the ITS; continuous controlling of the state of functioning of the transport system; implementation of a high degree of coordination and synchronized interaction between the processes of development, implementation, and use of the ITS.

Keywords: Sustainable development · Synergetic · Lorenz system · Transport system management · Intelligent Transport Systems

1 Introduction

Current trends in the acceleration of scientific and technological progress and, as a result, the active introduction of fast-changing science-intensive innovative technologies with short life cycles, globalization, the complication and mutual influence of the processes of

socio-economic development of civilization determine the non-linear dynamic (bifurcation) nature of the flow of socio-economic processes. This, under certain conditions, can lead to the unpredictability of capital markets, uncertainty and volatility of the business environment, uneven economic development in different countries, severe financial and economic crises, and irreversible processes of global environmental destruction.

These factors led to the emergence of the concept of sustainable development of society based on the combination of three areas: economic, social and environmental. This implies the adoption of measures aimed at the optimal use of limited resources and the use of environmentally friendly nature, energy, and material-saving technologies, maintaining the integrity and stability of socio-economic, biological and physical natural systems.

In line with this, the UN adopted the Sustainable Development Goals (SDGs), which are a kind of call to action coming from all countries, aimed at improving the well-being and protecting our planet [1].

One of the main goals adopted for the sustainable development of society is SDG 11 – Make cities and human settlements inclusive, safe, resilient and sustainable. And here, in authors' opinion, one of the main factors that can ensure the sustainable development of cities in the development, deployment and effective operation of intelligent transport systems (ITS). Indeed, accelerated motorization under conditions of underdeveloped urban road networks (URN), is accompanied by several negative economic, social and environmental consequences. Among the main consequences are a sharp decline in the efficiency of transport systems, a loss of control over logistics operations in the delivery of goods, a deterioration in the mobility and comfort of road users, and an increase in environmental pollution.

As the experience of the last decades shows, one of the main, often the only ways to solve these problems is the development and implementation of ITS using modern information and communication technologies. Effective use of ITS leads to:

- increase the mobility and comfort of the population in transport by eliminating congestion, prioritizing public transport, as well as timely road maintenance;
- improve the safety and efficiency of the functioning and management of transport systems;
- reduce the negative impact on the environment, improving the ecological situation in cities.

Meanwhile, the analysis shows [2–12] that improving the efficiency of ITS functioning as one of the main factors in enhancing the sustainability and livability of a city is not always determined only by the level of use of modern ICT. Often, the sustainable development of a city, along with the use of modern ICT, is also determined by the degree of coordination, cooperation, synchronized action between business units, scientific institutions engaged in the development and implementation of appropriate ITS modules, and public institutions, transport and logistics enterprises, which must ensure the effective implementation and operation of these ITSs [13–15].

In addition, if in the leading countries the problems of intellectualization of transport systems have been dealt with since the 90s, the creation of ITS took place in a

complex, systematic way, with the development of strategies and tactics for the creation, implementation and development of ITSs. Unfortunately, in Ukraine, this is done locally, sporadically in the absence of a national strategy for the development of ITS in the country. Generally speaking, today there is no general theoretical justification for the need for such coordination to ensure the sustainable functioning and development of ITS as one of the main factors in ensuring the sustainable development of cities.

This paper considers the concept of sustainable functioning and development (evolution) of transport systems, which is based on the synergetic Lorentz model. This model considers the interaction between three dynamic variables: the level of application of modern innovative technologies in ITS (I), the level of efficiency of various institutions that are responsible for the implementation or take part in the functioning of the ITS (F), and the controlling factor of the external environment is an indicator that characterizes the current state of the functioning of the transport system (p), for example, the urban road network (URN). Needs to note the URN in a certain way depends on various factors of the nonlinear dynamics of the external environment – a sharp increase congestion of URN sections, a sharp decrease in throughput due to the inefficient use of transport infrastructure, a significant deterioration in the environmental situation, etc.

2 Synergetic Theory of Transport Systems Sustainable Development

Recent studies show [2–4] that in modern conditions the socio-economic development of society, as a complex open non-equilibrium system, is a nonlinear dynamic transformation associated with the transition from one stable state to another through a series of intermediate nonequilibrium, unstable (often chaotic) structurally heterogeneous states. Here, when the fluctuations of the external socio-economic environment exceed certain critical values, there comes a moment (bifurcation point). At this point, the changes in parameters lead to an abrupt transition of the system to a qualitatively different state, to a new development trajectory (bifurcation stage of system development). At the same time, a bifurcation point is a branching point of various alternative development options that can lead to the implementation of fundamentally different both stable (attractors) and unstable scenarios for the development of the system.

At the present stage of the development of scientific research to describe the behavior of nonlinear dynamic systems, the nature and mechanisms of the manifestation of the corresponding effects, the ideas and methods of synergetic based on the theory of dynamic systems and no equilibrium thermodynamics are most widely used [5, 6]. Synergetic is a scientific direction that studies the processes of self-organization in open non-linear non-equilibrium dissipative systems of different nature (physical, technical, socio-economic, psychophysical, cognitive, etc. [7–9]).

At the same time, the creator of the concept and basic principles of ITS design, implementation and development, Joseph M. Sussman, in his seminal work [12], argued that the main drivers of sustainable development of society as an open socio-economic system are technology, organizational and institutional relations, and the external environment. Here, the external environment is the controlling parameter for the degree of the synchronized, coherent interaction between the processes of developing and using

innovative technologies in society and the institutions responsible for their effective use, taking into account environmental externalities (importance of clean air and water policies, global warming, energy, social justice, etc.) [10, 11].

At the same time, since transport in modern conditions is one of the determining factors in the formation of society, innovative technologies are also the main drivers of modern transport systems development (Fig. 1) [12]. Here, the efficiency of transport systems functioning as a control parameter is determined by the degree of synchronized, coordinated interaction between the processes of development, implementation, use of modern ICT in transport and institutional relations between entities that ensure their effective functioning, taking into account the goals of sustainable development of systems of the appropriate dimension [12, 16].

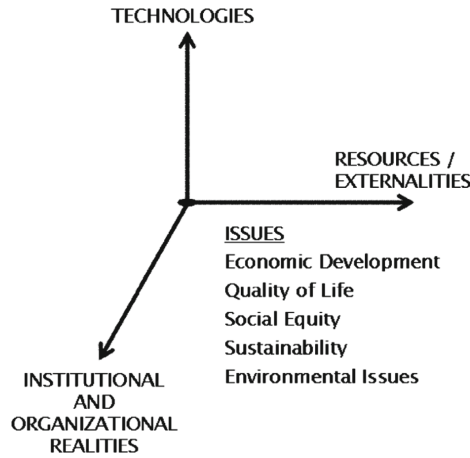


Fig. 1. Drivers of transport system development [12].

More over, [12] provides a theoretical justification for the need to use the fractal approach (self-similarity) to ensure the effective functioning of transport systems of any dimension, which is one of the main approaches in synergetic to describe the collective self-consistent behavior of open nonlinear systems based on the principles of self-organization [17]. According to [12], the presented concept of sustainable development of transport systems should be reflected at all levels of functioning of transport systems of the appropriate dimension (Fig. 2): on all timeframes, from real-time to strategic planning; at all geographic scales, from urban to global; at all organizational levels, from modal to the integrated supply chain.

Here, a variety of approaches, including advanced models in operations research, simulation modelling, econometrics, etc., need to be used to ensure effective real-time management of transport systems of any dimension through modern ICT [12]. At the same time, an appropriate qualitative analysis framework needs to be used to deal with new and more complex institutional realities in transport.

Following the above, within the framework of the fractal approach, we will consider the transport system at the city level as an open non-linear dynamic dissipative system.

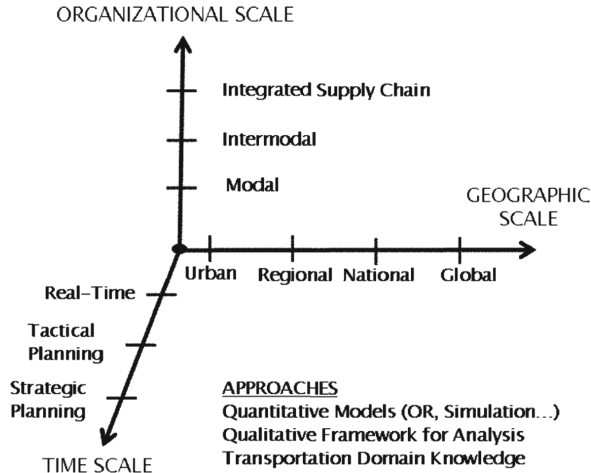


Fig. 2. Transport system dimensions according to [12].

The sustainable functioning and development of which largely determines the sustainable development of the city. Then, it is reasonable to describe the evolution of functioning of such a system in the framework of synergetic representations, which generalize the thermodynamic picture of phase transformations [18].

At the same time, we are based on the Lorenz system [18] with three dynamic variables (order parameter, associated field and control parameter), which corresponds to the simplest synergetic system that is self-organizing. By analogy with [12], in our case, these variables are the level of application of modern innovative technologies in ITS (I), the level of performance of various institutions responsible for the implementation and participating in the functioning of ITS (F), and the indicator characterizing the current state of operation of the transport system (p), for example, the urban road network (URN), which depends in a certain way on various factors of non-linear dynamics of the environment (a sharp increase in the congestion of URN sections, a sharp decrease in throughput due to the inefficient use of transport infrastructure, a significant deterioration in the environmental situation etc.). In this formulation, the problem is reduced to finding solutions to the system of self-consistent equations of evolution of these three dynamic variables.

Then, in the framework of the synergetic Lorenz model, the evolution of the transport system functioning as a result of the influence of internal and external nonlinear environment factors is described by a system of self-consistent nonlinear differential equations, which in relative units has the following form [18]:

$$\begin{cases} \dot{I} = -I + F, \\ \delta \cdot \dot{F} = -F + I \cdot p, \\ h \cdot \dot{p} = (p_e - p) - I \cdot F. \end{cases} \quad (1)$$

Here $\dot{I}, \dot{F}, \dot{p}$ are the time derivatives of I, F, p ; $\delta = \tau_F/\tau_I, h = \tau_p/\tau_I, p_e$ are the system parameters, τ_I, τ_F, τ_p are the corresponding relaxation times, on which the rates of

change (reaction) I, F, p depend under the influence of various negative factors of the nonlinear environment. p_e is an effective parameter that just determines the effect of various factors of the nonlinear environment on the evolution of the dynamic variables I, F, p of the system.

To solve the system of differential Eqs. (1) describing the prediction of the evolution of transport system operation perturbed by the nonlinear external environment, it is necessary to construct according to a standard scheme [19, 20] a bifurcation diagram, namely, to find special (stationary) points of system phase portrait (stationary system states) and to study these points (states) for stability.

The analysis carried out according to [19, 20] of the system (1) indicates the presence of three stationary points: p. O with coordinates $(I_c, F_c, p_c) = (0, 0, p_e)$, and p. P_1 and P_2 with coordinates $P_1(\sqrt{p_e - 1}, \sqrt{p_e - 1}, p_e)$, $P_2(-\sqrt{p_e - 1}, -\sqrt{p_e - 1}, p_e)$ respectively. It turns out that stationary points P_1 and P_2 arise and exist when $p_e \geq 1$.

When changing p_e from 0 to 1, there is one steady state at point O with coordinates $(Q, F, p) = (0, 0, p_e)$. At $p_e = 1$ there is a bifurcation: the equilibrium position at p. O becomes unstable and two stable stationary states appear at points P_1 and P_2 with coordinates $P_1(\sqrt{p_e - 1}, \sqrt{p_e - 1}, 1)$ and $P_2(-\sqrt{p_e - 1}, -\sqrt{p_e - 1}, 1)$.

Thus, even in the case of the simplest synergetic model in the form of a deterministic Lorentz system, there are two attractors (points P_1 and P_2) – stable stationary modes, into one of which, depending on the initial conditions, the system follows, passing through a series of intermediate transition states. At the same time, the influence of fluctuations of the external environment p_e can lead to the realization of essentially different trajectories (scenarios) of such transition, and, hence, to the possibility of realization with a certain probability of qualitatively different final steady states of such system. The mutual consistency of dynamic variables I, F, p in our case is determined by the ratio $\delta = \tau_F/\tau_I$, $h = \tau_p/\tau_I$ of response rates I, F, p to abrupt changes in the external environment p_e , affecting the state of the transport system, including URN.

3 Results and Discussion

In contrast to [18], where the synergistic effects of the macroeconomic system were studied in adiabatic approximation, the solutions of the Lorentz system (1) will be sought in general numerically, using the standard scheme [19]). The analysis of system (1) will be performed by changing the parameter in the range $\{0; p_e\}$ for fixed values of δ, h , and some initial values of I, F, p . Numerical simulation was performed using the computer mathematical calculations system MathCad.

Let at a certain point of time t_0 the state of the transport system be described by some values of dynamic variables I_0, F_0, p_0 and parameters δ, h, p_e . If p_e does not change significantly (in our case from 0 to 1), then the transport system is in a dynamically stable state and all current external negative fluctuations in this system (e.g. increased congestion on sections of urban road networks, deterioration of environmental characteristics due to improper vehicle operation, etc.) are neutralized by the application of appropriate organizational and technical measures.

With a sharp increase in p_e ($p_e \gg 1$), associated, for example, with a dramatic increase in motorization, significant environmental degradation, etc., as shown by the

results of the simulation study (Fig. 2), an unstable state (bifurcation) of the transport system emerges at p . O , whose evolution from the bifurcation point (p . O) can lead over time to one of two alternative steady states (p . P_1 and p . P_2).

This means that, given the above system characteristics (1), if the development (evolution) of the transport system results from the effective implementation and operation of innovative technologies in the ITS in synchronized, coordinated interaction with the relevant institutions, then the transport system will move to a highly efficient and sustainable state of operation (Fig. 3: p . P_1 , $\delta = 5$, $h = 2$, $p_e = 10$, $I_0 = 0.01$, $F_0 = 0.01$, $p_0 = 0.01$). In the opposite case, the transport system, having passed through a series of intermediate non-equilibrium, unstable states, enters a low-efficient state of operation (Fig. 3: p . P_2 , $\delta = 5$, $h = 2$, $p_e = 10$, $I_0 = -0.01$, $F_0 = -0.01$, $p_0 = 0.01$).

The analysis also shows that the functioning of the transport system, as an open non-linear dynamic system, becomes unstable at the bifurcation point (p . O) and sensitive to arbitrarily small differences in the initial values of the indicators that characterize its current state. This means that almost all trajectories of transport system evolution, however close at the beginning, are exponentially divergent, which may eventually lead to the realization of fundamentally different (alternative) system trajectories (Fig. 2). This result demonstrates the need for continuous, proactive improvement of the ITS in the effective operation of the various institutions involved in the implementation and operation of the ITS. To ensure the sustainable development of the urban transport system, as one of the main factors of sustainable urban development, it is necessary to timely improve and implement modern ICT in the ITS based on the results of continuous monitoring of the transport system, as well as conducting, within adequate models, procedures for forecasting its possible states under various influences of the external environment.

To confirm this conclusion, simulation studies of the evolution of the transport system under different magnitudes of the environmental influences described by the indicator p_e (Fig. 4) were carried out. Here, the transport system is characterized by the following values at a given point in time t_0 : $\delta = 5$, $h = 2$, $I_0 = 0.08$, $F_0 = 0.01$, $p_0 = 0.01$. Note that, in this case, the level of efficiency of modern innovative technologies in ITS $I_0 = 0.08$ is significantly higher than in the previous case ($I_0 = 0.01$, Fig. 3). At the value of the effective influence parameter of the external environment $p_e = 10$ we have a stable (focus) high-efficiency state of the transport system (Fig. 4a), as in the previous case (Fig. 3, p . P_1). When the negative influence of the non-linear external environment is increased to $p_e = 12$, the high-efficiency state becomes less stable with a certain probability of transition to the low-efficient state (Fig. 4b).

However, when the negative influence of the nonlinear environment reaches a threshold value (for $\delta = 5$, $h = 2$, the calculations according to [1–20] give $(p_e)_{\text{thr}} = 35$), the functioning of the transport system corresponds to a state of deterministic chaos (strange attractor [20], see Fig. 4c). Here, its functioning takes place under crisis conditions and becomes unpredictable under any system parameters (1). This means that in such a situation, even with the maximum mobilization of all resources and capabilities, achieving a highly effective steady-state in the development of the transport system is at least problematic. The optimal solution here seems to be a radical structural and functional

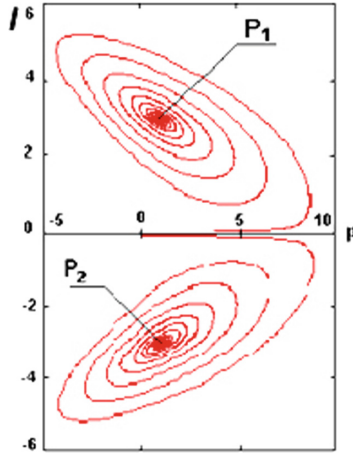


Fig. 3. The phase portrait of the transition of the transport system into a high-efficiency profitable steady-state (p, P_1 , initial conditions: $I_0 = 0.01, F_0 = 0.01, p_0 = 0.01$) and a low-efficient steady-state (p, P_2 , initial conditions: $I_0 = -0.01, F_0 = -0.01, p_0 = 0.01$) for $\delta = 5, h = 2, p_e = 10$. The projection of the phase portrait onto the plane $\{I, p\}$ is shown for clarity.

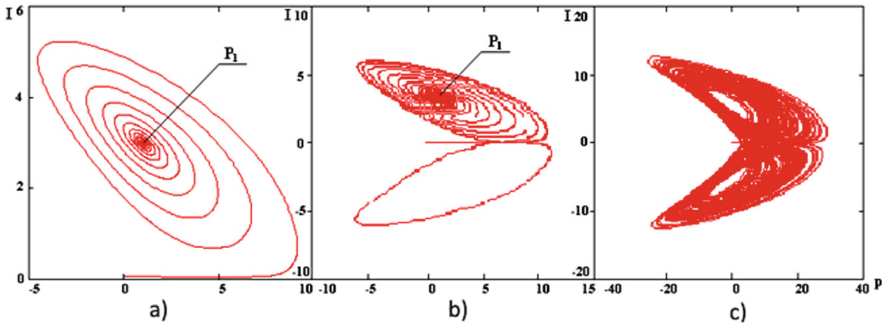


Fig. 4. Projection of the phase portrait of the evolution of the transport system onto the plane $\{I, p\}$ within model (1) for $\delta = 5, h = 2, I_0 = 0.08, F_0 = 0.01, p_0 = 0.01$ and different values of the effective parameter p_e : (a) $p_e = 10$; (b) $p_e = 12$; (c) $(p_e)_{thr} = 35$.

reorganization of the functioning of the transport system, which is associated with a high level of technical and economic costs.

Thus, based on the non-linear-dynamic (synergetic) nature of transport system functioning, its sustainable development should be carried out through continuous purposeful (management) and spontaneous (self-organization) structural and functional transformation, which adequately corresponded to the current state of external environment influence. In addition, a high degree of coordination, synchronized and coordinated interaction between the processes of development, implementation, and use of ITS on the one hand, and the processes of organizational and productive involvement of the relevant institutions and economic entities involved in the provision and use of transport services, on the other hand, is essential for the effective, sustainable development of

the transport system. Let us consider this with the help of an example. $\delta = 5, h = 2, p_e = 10, I_0 = 0.01, F_0 = 0.01, p_0 = 0.01$.

Let at a certain point of time t_0 the state of the transport system be described by the following values of the dynamic variables: $I_0 = 0.08; F_0 = 0.01, p_0 = 0.01$ which coincide with those considered in the previous case (Fig. 4). However, the dynamic parameters acquire the following values $h = 5, \delta = 2, p_e = 12$ (Fig. 5a).

Analysis (1) shows that the responsiveness of the institutions responsible for ensuring the effective implementation and use of ITS to negative changes in the external environment $\delta = \tau_F/\tau_I = 2$ is lower than in the previous case, where $\delta = \tau_F/\tau_I = 5$. This leads to the evolution of the transport system to a low-efficient steady state under the influence of the non-linear external environment (Fig. 5a) in contrast to the previous case (Fig. 4b).

The situation does not change even with a significant increase δ : the operation of the transport system is still characterized by low efficiency after a phase transition under the influence of the external environment (Fig. 5b for $\delta = 5$). Only for $\delta = 10$, with other values of dynamic variables and parameters being equal, the transport system enters a highly efficient steady state of functioning (Fig. 5c) in a non-linearly changing external environment. The sustainable highly effective functioning of ITS in URN, as one of the main factors of sustainable development of the city, is realized, can be ensured if certain ratios between the rates of response to external negative factors of the processes characterizing the level of introduction and application of modern innovative technologies in ITS (I), and the processes characterizing the level of activity of various institutions and organizations to ensure effective introduction and functioning of these ITS (F) are observed.

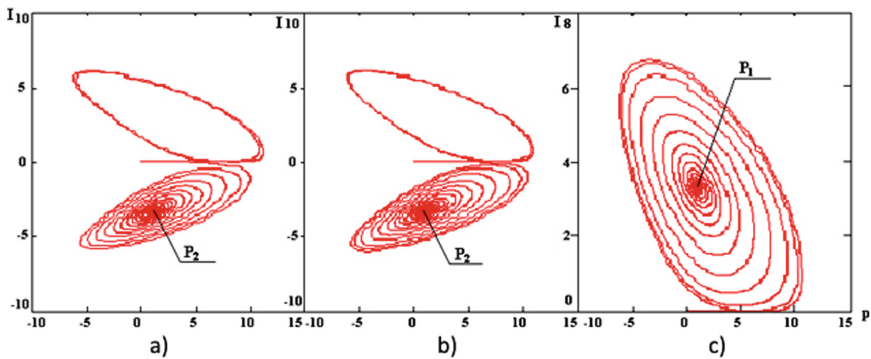


Fig. 5. Projection of the phase portrait of the evolution of the transport system on the plane $\{I, p\}$ within the model (1) for $p_e = 12, h = 5, I_0 = 0.08, F_0 = 0.01, p_0 = 0.01$ and different values of the parameter δ : (a) $\delta = 2$; (b) $\delta = 5$; (c) $\delta = 10$.

4 Conclusions

This paper develops theoretical concepts of sustainable functioning and development of the transport system within the framework of the Lorenz synergistic model, which

considers the interaction between three dynamic variables: the level of application of modern innovative technologies in ITS, the level of efficiency of various institutions ensuring the implementation and operation of ITS, and the controlling factor, which determines the influence of the environment on the current state of functioning of the transport system. The results obtained are general and, given the fractal nature (self-similarity) of synergistic systems, should apply to transport systems of any dimension: at all timeframes – from real-time to strategic planning; geographical scales – from urban to global; at all organizational levels – from modal to integrated supply chain. Based on the results of simulation studies, the conditions and mechanisms for the sustainable functioning and development of the ITS have been determined.

On the one hand, they include those associated with proactive activities for the improvement and timely implementation of information and communication technologies in ITS; continuous monitoring of the state of operation of the transport system; implementation of a high degree of coordination, synchronized and coordinated interaction between the processes of development, implementation and use of ITS. It also takes into account those processes of organizational and production activities of the relevant institutions that ensure high efficiency of ITS functioning, taking into account the objectives of sustainable development of systems of the corresponding dimension. At the same time, the legislative, financial and public-private cooperation activities of state institutions are aimed at achieving the environmental, social and economic goals of sustainable development of the city, region, state and transnational community as a whole.






References

1. Johnson, J., Nowak, A., Ormerod, P., Rosewell, B., Zhang, Y.-C. (eds.): *Non-Equilibrium Social Science and Policy*. UCS, Springer, Cham (2017). <https://doi.org/10.1007/978-3-319-42424-8>
2. Saviotti, P., Stanley, J.: *Evolutionary Theories of Economic and Technological Change. Present Status and Future Prospects*. Routledge, London (2018)
3. Kolomiets, S.: Categories of synergetics in economic research: nonlinearity of socio-economic systems. *Scientific Notes of Vernadsky TNU. Ser.: Economy and Management* **31**(3), 191–197 (2020). <https://doi.org/10.32838/2523-4803/70-3-66> [in Ukrainian]
4. Gardini, L., Gori, L., Guerrini, L., Sodini, M.: Introduction to the focus issue “nonlinear economic dynamics”. *Chaos: An Interdisciplinary Journal of Nonlinear Science* **28**(5), 055801 (2018). <https://doi.org/10.1063/1.5039304>
5. Turkmen, O.: *Synergetic Theory of Life*. Matador, Leicester (2014)
6. Prigogine, I., Stengers, I.: *Order Out of Chaos*. Verso Books (2018)
7. Puchkovska, G.O., et al.: Resonance dynamical intermolecular interaction in the crystals of pure and binary mixture n-paraffins. *J. Mol. Struct.* **708**(1–3), 39–45 (2004). <https://doi.org/10.1016/j.molstruc.2004.02.010>
8. Danchuk, V., Bakulich, O., Svatko, V.: Building optimal routes for cargo delivery in megacities. *Transport and Telecommunication* **20**(2), 142–152 (2019). <https://doi.org/10.2478/tjtj-2019-0013>
9. Schiepek, G., et al.: Synergetics in psychology: patterns and pattern transitions in human change processes. In: Wunner, G., Pelster, A. (eds.) *Selforganization in Complex Systems: The Past, Present, and Future of Synergetics*. UCS, pp. 181–208. Springer, Cham (2016). https://doi.org/10.1007/978-3-319-27635-9_12

10. Schrotten, C., et al.: Research for Tran Committee. EPRS (2020)
11. European Commission: Communication from the commission Europe 2020: A strategy for smart, sustainable and inclusive growth. Brussels (2010)
12. Haghghat, A.K., Ravichandra-Mouli, V., Chakraborty, P., Esfandiari, Y., Arabi, S., Sharma, A.: Applications of Deep Learning in Intelligent Transportation Systems. *Journal of Big Data Analytics in Transportation* **2**(2), 115–145 (2020). <https://doi.org/10.1007/s42421-020-00020-1>
13. Comi, A., Sassano, M., Valentini, A.: Monitoring and controlling real-time bus services: a reinforcement learning procedure for eliminating bus bunching. *Transportation Research Procedia* **62**, 302–309 (2022). <https://doi.org/10.1016/j.trpro.2022.02.038>
14. Russo, F., Comi, A.: Providing dynamic route advice for urban goods vehicles: the learning process enhanced by the emerging technologies. *Transportation Research Procedia* **62**, 632–639 (2022). <https://doi.org/10.1016/j.trpro.2022.02.078>
15. Russo, F., Comi, A.: Sustainable urban delivery: the learning process of path costs enhanced by information and communication technologies. *Sustainability* **13**(23), 13103 (2021). <https://doi.org/10.3390/su132313103>
16. Sornette, D.: *Critical Phenomena in Natural Sciences*. SSSYN. Springer, Berlin, Heidelberg (2016). <https://doi.org/10.1007/3-540-33182-4>
17. Olemskoi, A., Katsnelson, A.: *Synergetics of Condensed Medium*. URSS, Moscow (2010). [in Russian]
18. Thomson, W.: *Theory of Vibration with Applications*. CRC Press, London (2017)
19. Chen, Z., Li, Y., Liu, X.: Noise induced escape from a nonhyperbolic chaotic attractor of a periodically driven nonlinear oscillator. *Chaos: An Interdisciplinary Journal of Nonlinear Science* **26**(6), 063112 (2016). <https://doi.org/10.1063/1.4954028>
20. Feldman, D.: *Chaos and Dynamical Systems*. Princeton University Press, Princeton (2019)



Influence of the City Transport Route Network Discrete Model Geometrical Parameters on a Quality of a Passenger Traffic System Operation

Serhii Pustiulha , Volodymyr Samchuk^(✉) , Viktor Samostian ,
Valentyn Prydiuk , and Valerij Dembitskij 

Lutsk National Technical University, 75 Lvivska Street, Lutsk 43018, Ukraine
volodsam@gmail.com

Abstract. The research is dedicated to an investigation of an influence of geometrical parameters of a discrete model of the city transport route network on a quality of a passenger traffic system operation and to a discovery of the priority criteria of the developed characteristics while searching for the ways of improvement of its structural components. Quality characteristics of the city passenger routes network substantially depend on a complexity of their geometrical configuration and topological structure. Afterwards, a development of a city routes network goes, as a rule, by the way of complication of a travel routes topological structure and of interrelation between geometrical characteristics of their separate elements. Such a trend allows to make a conclusion about the necessity of elaboration of the effective mathematical methods of modeling of the new ones and of optimization of the existing networks, on the base of which there would be situated the algorithms of the quantity evaluation of a quality of the city transport system operation on the base of an all-round analysis of geometrical parameters of the route schemes discrete models. In the present research work there were examined and analyzed the discrete models of geometrical images, their main characteristics, there were offered the methods of determining of separate parameters of the geometrical structures concerning the determining of optimal ways of improvement of the technical and technological characteristics of a city transport network. All the examined images can be set as principles of analysis of its accessibility and determining of the possibilities and ways of improvement of the already existing routes network.

Keywords: Transport route network · Field of fractal type · Discrete cell model · Transport accessibility

1 Introduction

While solving the practical problems concerning an analysis and identification of some objects on the pictures, the actual task is to determine certain fields that correspond to the

informative characteristics of given structures (schemes, maps, photos of the surfaces, photos of the materials and some their combinations).

For summarizing of the necessary information about the objects on the pictures and its application for solving some specific tasks, it is necessary to have a methodology and the algorithms of calculating of the main characteristics of the objects on the pictures: the parameters of their form, a geometrical structure, an objects composition, other characteristics. Basing on the analysis of the determined characteristics, there are generalized some conclusions about the objects types, the examined picture quality concerning the determining of the ways of improvement of its technical and technological characteristics [1]. Along with that it is clear that the base of analysis is composed by exactly the geometrical characteristics either of its entire picture, or of its separate fragments.

Second aspect of the problem is that a majority of pictures is, on practice, the totalities of the complex, “chaotic-cut” objects and they are identified as fractal or quasifractal images. It’s exactly a fractal dimension (together with other geometrical characteristics) that can become a base for evaluation and effective improvement of characteristics initially of a model, but then of real objects respectively [2].

2 Literature Review

There exist a lot of researches dedicated to an analysis and treatment of the pictures [3–5]. Among them there can be separated the researches in a field of alarm systems, quality control systems of different goods, the searches of identification of the objects and text documents, the scientific studies concerning medical diagnostics and other.

In the before-mentioned studies there are solved, as a rule, three classic problems concerning graphical pictures: a problem of picture synthesis, that is to get it by a description, a problem of analysis, that is to get a description by a picture, a problem of picture treatment, that is to get a new picture basing on the existing one. Computer technique and information technologies are actively used while solving all these problems. But the problems of developing of the algorithms of effective presentation and analysis of the pictures that contain the objects of evidently fractal type, are still actual. In the researches [6, 7] an effectiveness of the methods of fractal geometry to determine the main technological characteristics and to predict the ways of optimisation of the objects that have fractal structure, is shown. The methods of discrete presentation of fractal objects, the manners of identification, the algorithms of their dimension calculating, the use of complex geometrical characteristics to work out the ways of improvement of examined images are the actual problems both in theoretical and practical aspects.

3 Research Methodology

The geometrical characteristics of the objects form the basis of solving the majority of practical problems. If these characteristics are calculated and analyzed on the base of pictures of objects and sets, it is necessary to determine their list, the methods of calculating and priority in the measurement order. Mostly, the picture fragment measured parameters can be the next: an identification of an object type, its topological dimension,

the linear dimensions, a perimeter, an area, the form parameters (convexity, concentricity, compactness, roundness), the static moments of closed areas and other characteristics.

Because of the discreteness of a picture of, for example, an examined city transport network (see Fig. 1a), two variants of calculating its geometrical characteristics are possible: contour and “skeletal”. At contour method every point of a picture is treated as a discrete element (can be a pixel) and has a dimension equal to its area correspondingly. Linear distances between nearby points are equal to a unit of a scale of discrete presentation. While using “skeletal” method of calculating the geometrical characteristics, it is considered that a point is situated in the centre of sampling element. Thus, a calculating of vertical and horizontal distances between separate points is made by the linear dimensions of sampling element, the diagonal ones are determined as a hypotenuse of a right triangle.

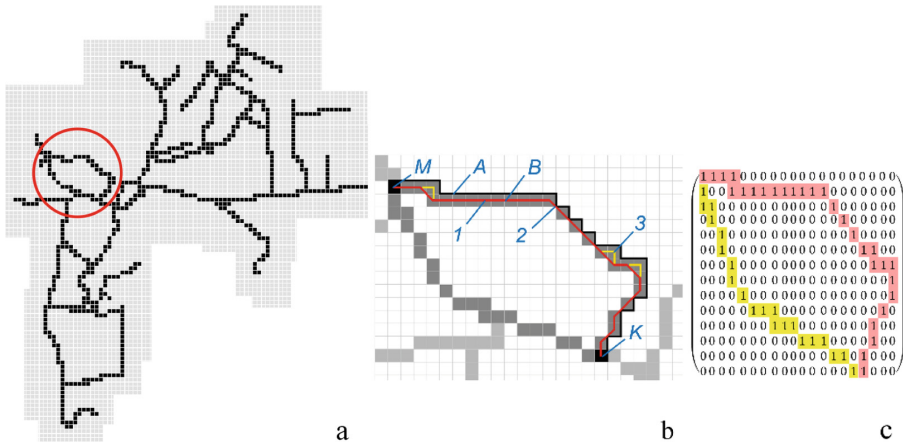


Fig. 1. Discrete pixel model of a city routes network, the scheme of “skeletalization” of the fragment and its matrix implementation. *A* – segment length on the base of contour method. *B* – segment length on the base of skeletal method. *M, K* – end points of curvilinear discrete fragment of a curve.

Both methods are right and on the short steps of sampling give the results that have slight, that is admissible, error. That is why, while solving practical problems, one can choose more algorithmically convenient way. But except calculating the geometrical characteristics, a created discrete model of a picture should predict a maximum informational content and a possibility of reverse passage to its continuous presentation. That is exactly a “skeletal” method of calculating of linear dimensions that mostly corresponds to the requirements of our formulated practical problem. On Fig. 1b there are given the discrete pixel models of geometrical elements of network and there are offered the schemes of their “skeletalization”.

One can notice that the offered discrete cell models of the unidimensional images have an ambiguous “skeletalization” (1 – right, 2 – diagonal, 3 – mixed). Within a solving of our practical problem, while choosing a form of “skeleton” on an area of discretely presented image, a diagonal connexion type of nearby points would have a priority.

Let's show an effectiveness of such choice while modelling and identifying some geometrical images. For discrete model of a curve segment the important characteristics are: a topological (fractal) dimension of an object, a degree of rectilinearity and its length. A topological dimension is determined by the extreme (end) points of a discrete model and by calculating a fractal dimension. The model limits are the zero-dimensional images. A fractal dimension of a segment in a process of scaling approaches to 1, that is – an object is unidimensional, and an area of an object model is equal to zero.

A degree of rectilinearity of separate segments is determined by a relation of calculated parameter of length of a discrete model of segment by a “skeletal” method to a distance between the end points of an object. A length of a discrete model of a transport network segment is determined by a matrix of “skeleton” (see Fig. 1c), built with taking into consideration the types of coherence of separate discrete elements.

According to a model, N_L is the cells with direct neighbours (neighbourhood – line), N_P is the cells with indirect neighbours (neighbourhood – point). While having for one cell both vertical and horizontal neighbours with a limit – line, two connections are replaced by the diagonal one (see Fig. 1b).

A model length while using a “skeletal” method is calculated according to a formula:

$$L_M = unit(n \cdot Ng_L + k \cdot N_T), \tag{1}$$

where Ng_L is a horizontal distance between the centres of nearby cells of a model; Nv_L is a vertical distance between the centres of nearby cells of a model; N_T is a diagonal distance between the centers of nearby cells of a model; $unit$ is the scale parameters of an elementary discrete cell; n and k is a number of horizontal and vertical elements of skeleton correspondingly.

A length between the end points of an object is calculated:

$$L_{go} = \sqrt{(unit(Ng - 1))^2 + (unit(Nv - 1))^2}, \tag{2}$$

where Ng is a number of the model cells of a segment in horizontal direction; Nv is a number of the model cells of a segment in vertical direction.

For rectilinear segments, situated horizontally, vertically and at an angle 45° – a degree of rectilinearity of a discrete model W_{lin} would be always equal to 1. In all other cases $W_{lin} \approx 1.01 \div 1.05$.

For curvilinear discrete model (see Fig. 1b) the basic geometrical characteristics would be: a topological (fractal) dimension of an object, a degree of curvilinearity, a model perimeter, the parameters of a form of closed curves and other characteristics.

A topological dimension is determined by the end points (for open curves) of a discrete model and by a calculating of fractal dimension of an element. The limits of a discrete model fragment are the zero-dimensional images (points M and K). A fractal dimension of an object, in a process of scaling, approaches to 1, that is – an object is unidimensional.

A matrix model of a transport network segment is shown at Fig. 1c. A length of a curvilinear section $M-K$ is determined according to an Eq. (1).

A degree of curvilinearity of a section $M-K$ is determined by a relation of a calculated parameter of a model section length L_{M-K} to a distance between the end points of an object M and K .

If $L_{go} = 0$ – curve line is closed. Then, instead of a length of curve section according to a “skeletal” method, there is calculated a perimeter of a closed curve model, for example P_{M-M} . In general view a perimeter is presented as a function $P_{M-M} = f(N_{gL}, N_{vL}, N_T)$. As $L_{go} = 0$ – there is no sense to calculate a degree of curvilinearity for closed curve.

The parameters of a closed curve model form (convexity, concentricity, compactness and roundness) would have more geometrical informational content in such a case. To determine the listed geometrical characteristics of a binary picture of a closed curve model, it is necessary, first of all, to build on its end points a limitary rectangular shell (see Fig. 2), and secondary to determine a cell that would present a weight centre (i_{cg}, j_{cg}) of a closed field of a curve discrete model.

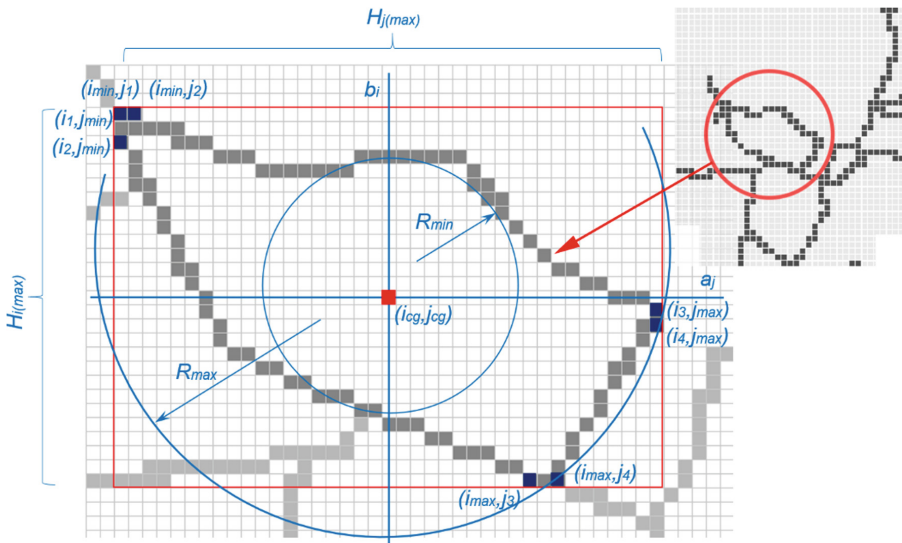


Fig. 2. Scheme of calculating the geometrical parameters of a city transport network fragment in binary reference.

The discrete coordinates of a field weight centre are calculated by the formulas:

$$i_{cg} = \frac{\sum_{(i,j) \in (R-Q)} i}{\sum_{(i,j) \in R} unit \cdot n - \sum_{(i,j) \in Q} unit \cdot k}, j_{cg} = \frac{\sum_{(i,j) \in (R-Q)} j}{\sum_{(i,j) \in R} unit \cdot n - \sum_{(i,j) \in Q} unit \cdot k}, \quad (3)$$

where a dominator of the expressions (3) is an area of inner field of a given model. If a value of desired discrete quantities i_{cg} , or j_{cg} is non-integral, one should use the rules of mathematic rounding to integral values.

An area is determined as an amount of all elementary cells of a model of closed field R , except for the limiting cells – set Q . If a scaled cell coefficient is taken for unit, one would have a formula:

$$S_{in} = \sum_{(i,j) \in R} unit \cdot n - \sum_{(i,j) \in Q} unit \cdot k. \quad (4)$$

Afterwards, a degree of convexity C_1 of a discrete pixel model of a closed curve would be determined by a proximity of its full area R to an area of limiting rectangular shell – $Hi(max) \times Hj(max)$

$$C_1 = \frac{\sum_{(i,j) \in R} unit \cdot n}{(i(max) \times j(max))unit}. \tag{5}$$

The closer the given index is to 1, the bigger is a degree of convexity of a discrete model. As a second form parameter would be considered a degree of concentricity C_2 of a discrete model of closed curve. It is determined by a relation of the radiuses, inscribed R_{min} and circumscribed R_{max} from a weight centre, of the circles (see Fig. 2).

$$C_2 = \frac{R_{min}}{R_{max}} = \frac{\min \sqrt{(i_k - i_{cg})^2 + (j_k - j_{cg})^2}}{\max \sqrt{(i_k - i_{cg})^2 + (j_k - j_{cg})^2}}. \tag{6}$$

An important geometrical parameter is a degree of compactness C_3 . A circle has the biggest compactness. That is why a proximity of the areas of a closed curve discrete model and a circle with the same perimeter would be determined by C_3 . Respectively, a perimeter and an area of a figure are equal $P_f = f(N_{gL}, N_{vL}, N_T)$, $S_f = \sum_{(i,j) \in R} unit \cdot n$.

An area of a circle with a perimeter P_f is calculated:

$$S_k = \frac{P_f^2}{4\pi}. \tag{7}$$

A degree of a model compactness, taking into consideration (7), looks like:

$$C_3 = \frac{4\pi \sum_{(i,j) \in R} unit \cdot n}{P_f^2}. \tag{8}$$

A degree of roundness of a closed curve discrete model is a very interesting index from a geometrical point of view. It can be calculated by two ways that gives almost equal results in a majority of cases. A parameter is rather sensible to a cut, oscillating behavior of a limit of discrete curve model and can immediately, without using the fractal algorithms, classify the objects of fractal or non-fractal type.

The first way is based on a calculating of relation of a perimeter square of given field to its area:

$$C_4 = \frac{P_f^2}{S_f}. \tag{9}$$

The second way consists in determination of relation of a middle deviation of the discrete image limiting cells from a field weight centre to a middle square deviation of the same cells from a weight centre:

$$C_5 = \frac{\frac{1}{K} \sum_0^{K-1} |(i_k, j_k) - (i_{cg}, j_{cg})|}{\sqrt{\frac{1}{K} \sum_0^{K-1} ((i_k, j_k) - (i_{cg}, j_{cg}))^2}}. \tag{10}$$

The bigger value have the parameters of roundness C_4 or C_5 of a curve discrete model, the bigger is the possibility to predict a fractal behavior of an examined field.

A limiting rectangular (see Fig. 2), that restrains the maximum and minimum values i and j of the black cells of a discrete model, determines, together with a weight centre, the basic axes of a closed geometrical image that also influence the form characteristics and play an important role while determining a model orientation in space.

The next elements of the images models identification are the closed fields of non-fractal and fractal types. If a discrete cell model of a picture or of picture fragment has at least one black cell that has 8 black neighbors by 8-coherence, one can consider that a given model presents a two-dimensional non-fractal image, or a field with a dimension from 1 to 2 of fractal type.

The limits of such object are a unidimensional set of cells of fractal or non-fractal type with at minimum two black neighbors by 8-coherence. These limiting cells are in the base of developing a “skeleton” of a field limit.

For a discrete model of two-dimensional image the basic geometrical characteristics are: a topological (fractal) dimension of an object, a perimeter value, an area of object model, a convexity, a concentricity, a compactness, a roundness, the static moments, Euler characteristic etc.

A topological dimension is determined inductively by a dimension of the limits of a discrete model and by a calculating of its fractal dimension. As it was before-mentioned, a limit of a discrete model (for non-fractal images) is a unidimensional set of cells with a determined “skeleton”, respectively, a topological dimension of an object is equal to 2. A fractal dimension of a discrete model, while scaling, for a cell calculating method, also approaches to 2.

A perimeter of a closed field discrete model. This value is considered as a contour characteristic of two-dimensional images, that is why a “skeletal” calculating method is applied to it. A perimeter is determined taking into account all the cell types of an image limit N_{vL}, N_{gL}, N_T .

A distance between the vertical and horizontal neighbors is equal to unit, a distance between the diagonal ones – to $unit \cdot \sqrt{2}$. While having for one cell of a “skeleton” simultaneously both vertical and horizontal neighbors with a number of pairs – s , two connections N_{vL} and N_{gL} are replaced by one diagonal N_T .

Afterwards, a perimeter of a limiting line of a cell model of two-dimensional image is calculated by a length of a “skeleton”:

$$P_M = ((n - s) \cdot N_{gL} + (m - s) \cdot N_{vL} + (k + s) \cdot N_T) \cdot unit, \tag{11}$$

where n is a total number of horizontal linear connections N_{gL} between the cells of a model limit; m is a total number of vertical linear connections N_{vL} between the cells of

a model limit; k is a total number of diagonal point connections N_T between the cells of a model limit.

The static moments have a wide application at a process of analysis and geometrical identification of the pictures of closed fields. While having a matrix picture model, it is easy to determine the main of them.

Thus, a zero moment $\mu_{00} = S_f$ is calculated as an amount of elementary cells of inner field of an object model and completely corresponds to its area. The moments of first order that are normalized to this area, $\mu_{01} = i_{cg}$, $\mu_{10} = j_{cg}$ as it is before-mentioned, are equal to the coordinates of a field weight centre.

The central moments of first order that are normalized to a field area, can give an information about a form roundness of a field limiting contour, and central moments of second order show how symmetrical the field is correspondingly to the horizontal and vertical axes:

$$\mu_{11} = \frac{\sum_{(i,j) \in R-Q} (i - i_{cg})(j - j_{cg})}{S_f}, \mu_{02} = \frac{\sum_{(i,j) \in R-Q} (i - i_{cg})^2}{S_f}, \mu_{20} = \frac{\sum_{(i,j) \in R-Q} (j - j_{cg})^2}{S_f}. \quad (12)$$

Two-dimensional fields and their discrete cell structures can have even more complicated structure by its topology (combined sets, enclosure, “nicks” etc.). A complexity of such structures can be evaluated by Euler number that characterises an inclusion of the fields in each other, a number of openings or “nicks” inside a given combined object.

4 Results

The before examined and analyzed discrete models of geometrical images, their main characteristics, the offered methods of determination of separate parameters of geometrical structures are closely linked with a concrete practical problem – a determination of optimal ways of improvement of technical and technological characteristics of a city transport network [8–10].

According to a discrete model of a city transport network (see Fig. 1a), there are separated the next geometrical elements that compose a picture base: the models of right and unclosed curve lines, the models of closed curves, the discrete models of the fields of non-fractal and fractal types, the binary models of combined structures. All the examined images are important for identification of the network elements and can be set as principals of analysis of its accessibility and for determination of the possibilities and ways of improvement of the existing routes net. Thus, for example, the diametral, radial and tangential routes of passenger transport are described by the discrete models of the unclosed curve lines, the shortest distances between the transport junctions are the straight line models, the circle routes are presented as the closed images of fractal and non-fractal types. The pictures of separate transport city districts are modeled as the closed curvilinear fields, and a superposition of route schemes in separate transport junctions are described by the discrete models of combined structures [11, 12].

An offered identification method of the picture elements can become a base for an analysis of an existing state of the city route network, but the only identification is not enough to elaborate the offers concerning the routes improvement. That is why for every

element of route network there are determined the basic geometrical characteristics, there are given the criteria of priority of their influence on a routes network quality, there are elaborated the algorithms of calculation of the basic parameters for a discrete model of the routes schemes. Inside a set of geometrical characteristics as both a whole network and its separate components, there are distinguished: a topological (fractal) dimension, the linear dimensions, a perimeter, an area, the parameters of a discrete image form (a convexity, a concentricity, a compactness, a roundness), the static moments of the closed fields and other that indirectly influence the technical and technological characteristics of a route network. For example: the linear dimensions, an image perimeter are a measure of routes extension, of distances between the stop points, of distances between the basic transport junctions; an area of closed fields is a basic value to determine and to correct the form parameters, that, in their way, are the determinant for a maximum transport accessibility of separate points and territories on a city map; the static moments together with an index of fractal dimension, characterize a compactness of a route schemes network on a determined territory; the Euler numbers give an information about a “critical layout”, that is an inaccessibility of some city zones for transport service [13–15].

As a result of conducted researches, there was offered a hypothesis that a city is considered optimal by a transport accessibility if an amount of the chains lengths that connect all the cells of a discrete cell model of a city, is minimal (see Fig. 3). Such an optimal network model has a fractal structure, and its separate components are considered transport accessible, if: for each of them there exist a possibility to get in any other cell of a discrete city map model; the total extension of the routes, and correspondingly a time of their passage, are minimal; a number of changes to reach a desirable purpose is minimal; a maximum number of routes goes through a determined point.



Fig. 3. Hypothesis of a transport accessibility model.

Let's show an effectiveness of an offered methodology at an example of determination of the indices of transport accessibility in Lutsk city as a whole and the possible ways of its improvement. For this purpose let's impose on a city map an existing transport network of the buses and trolleybuses routes and let's make its binarization. Let's make a sampling of a received map taking into account the conditions of distance of any point not more than 500 m to a route network, and let's determine a number of cells that cover it (in this case there are 354 of them, Fig. 4a).

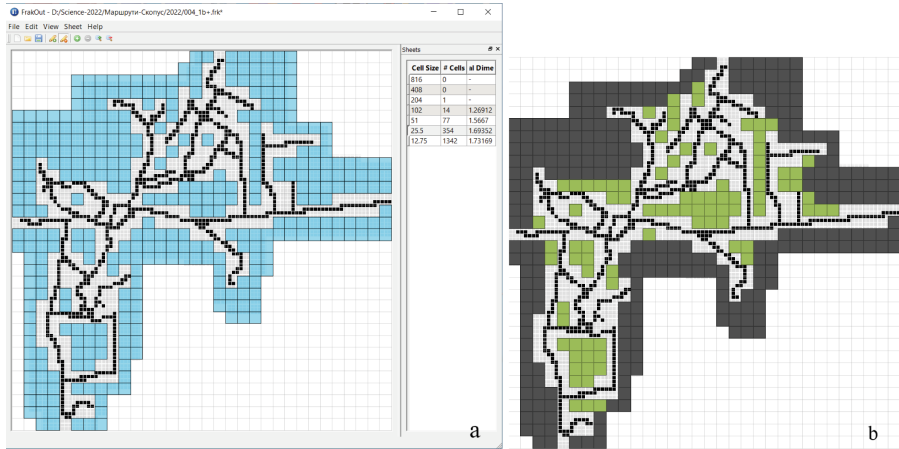


Fig. 4. Graphical presentation of an optimization methodology of the city routes network according to its accessibility: (a) algorithm of determination of fractal dimension of a city routes network; (b) correction of the city routes schemes basing on the analysis of fractal dimension.

Next, let's determine the zones on a discrete map model that are completely inaccessible for transport service while satisfying the standardized requirements. Such "dead" zones are coloured grey (see Fig. 4b), a total number of the cells that describe them, is equal to 267. With the help of special algorithms one can calculate a fractal dimension of a city map discrete model provided that an indice of transport accessibility is equal to 0. A fractal dimension of such a model is equal to 1.84.

Let's calculate a fractal dimension in a condition of an existing route network of Lutsk city. It is equal to 1.69.

A conducted fractal analysis clearly shows a tendency to improvement of a transport accessibility in a city – it's a decrease of a fractal dimension of presented model. A practical application of given idea and calculations comes to a correction of the city route schemes to liquidate the green zones of an offered model, with a purpose to greatly decrease its fractal dimension, that is – an improvement of the indices of a city transport network accessibility in general (see Fig. 4b). A model with a dimension close to 1 would be characterized by an ideal transport accessibility.

Besides, according to the before-mentioned algorithms, it is possible to determine the quality indices of transport sufficiency for given model: a total extension of a route into the necessary point, an approximate time of travel by a route, a possible number of

changes to reach a purpose, a number of possible variants of the vehicles choice on a route to get to a point of destination and other.

Though, while critically evaluating the results of made researches, it is necessary to mention that the offered fractal methodology of searching the ways of improvement of a city transport accessibility is only one of the possible approaches of determination of the optimal ways of improvement of technical and technological characteristics of a transport network, but not a final solution of a problem of optimization of transport accessibility.

5 Conclusion

In the present research work there was examined an influence of geometrical parameters of a discrete model of the city transport route network on a quality of a passenger traffic system operation and there were circumscribed the criteria of priority of taking into consideration the geometrical characteristics while searching the ways of improvement of the transport network structure components. There were elaborated the methods of pictures identification and there were distinguished separate geometrical elements of a discrete model of the city transport network that significantly influence a quality of a passenger traffic.

There were elaborated the algorithms and the methods of calculating the geometrical characteristics of picture identification for determination and further effective correction of technical and technological characteristics of the city transport structure.

References

1. Ablamejko, S.V., Nedz'ved', A.M.: Processing of Optical Images of Cellular Structures in Medicine. OIPI NAN Belarusi (2005)
2. Feder, J.: Fractals. Springer, Boston (1988). https://doi.org/10.1007/978-1-4899-2124-6_4
3. Mohan, V.M., Kanaka Durga, R., Devathi, S., Srujan Raju, K.: Image Processing Representation Using Binary Image; Grayscale, Color Image, and Histogram. In: Satapathy, S.C., Raju, K.S., Mandal, J.K., Bhateja, V. (eds.) Proceedings of the Second International Conference on Computer and Communication Technologies. AISC, vol. 381, pp. 353–361. Springer, New Delhi (2016). https://doi.org/10.1007/978-81-322-2526-3_37
4. Serino, L.: Skeletonization of Gray-Tone Images Based on Region Analysis. In: Sanfeliu, A., Martínez Trinidad, J.F., Carrasco Ochoa, J.A. (eds.) CIARP 2004. LNCS, vol. 3287, pp. 495–502. Springer, Heidelberg (2004). https://doi.org/10.1007/978-3-540-30463-0_62
5. Marszałek, M., Schmid, C.: Accurate object Recognition with Shape Masks. *Int. J. Comput. Vision* **97**, 191–209 (2012). <https://doi.org/10.1007/s11263-011-0479-2>
6. Pustiulha, S., et al.: Fractal diagnostics of the degree of fuel atomization by diesel engine injectors. *Eastern-European Journal of Enterprise Technologies* **6**(8), 40–46 (2017). <https://doi.org/10.15587/1729-4061.2017.116104>
7. Pustiulha, S., Holovachuk, I., Samchuk, V., Samostian, V., Prydiuk, V.: Improvement of the Technology of Tribostate Application of Powder Paints Using Fractal Analysis of Spray Quality. In: Ivanov, V., et al. (eds.) DSMIE 2019. LNME, pp. 280–289. Springer, Cham (2020). https://doi.org/10.1007/978-3-030-22365-6_28
8. Dubovik, V.O.: Methods for assessing the transport accessibility of the territory. *Reg. Stud.* **4**(42), 11–18 (2013)

9. Bonenberg, W., Bonenberg, A., Dong, L., Zhou, M.: Transport Accessibility as a Factor of Spatial Development on the Example of the Poznan Metropolitan Area, Poland. In: Charytonowicz, J., Maciejko, A., Falcão, C.S. (eds.) AHFE 2021. LNNS, vol. 272, pp. 294–301. Springer, Cham (2021). https://doi.org/10.1007/978-3-030-80710-8_36
10. Ribeiro, J., Fontes, T., Soares, C., Borges, J.L.: Accessibility as an indicator to estimate social exclusion in public transport. *Transportation Research Procedia* **52**, 740–747 (2021). <https://doi.org/10.1016/j.trpro.2021.01.019>
11. Renzi, A., Ferranti, P.: Efficient and nice – urban accessibility and public transport. In: *Quality of Life in Urban Landscapes*. UBS. Springer, Cham (2018). https://doi.org/10.1007/978-3-319-65581-9_12
12. Horák, J., Ivan, I., Voženílek, V., Tesla, J.: Multidimensional Evaluation of Public Transport Accessibility. In: Ivan, I., Horák, J., Inspektor, T. (eds.) GIS OSTRAVA 2017. LNGC, pp. 149–164. Springer, Cham (2018). https://doi.org/10.1007/978-3-319-61297-3_11
13. Fuglsang, M., Hansen, H.S., Münier, B.: Accessibility Analysis and Modelling in Public Transport Networks – A Raster Based Approach. In: Murgante, B., Gervasi, O., Iglesias, A., Taniar, D., Apduhan, B.O. (eds.) ICCSA 2011. LNCS, vol. 6782, pp. 207–224. Springer, Heidelberg (2011). https://doi.org/10.1007/978-3-642-21928-3_15
14. Cavallaro, F., Dianin, A.: An innovative model to estimate the accessibility of a destination by public transport. *Transp. Res. Part D: Transp. Environ.* **80**, 102256 (2020). <https://doi.org/10.1016/j.trd.2020.102256>
15. Benenson, I., Ben-Elia, E., Rofe, Y., Rosental, A.: Estimation of Urban Transport Accessibility at the Spatial Resolution of an Individual Traveler. In: Thakuriah, P., Tilahun, N., Zellner, M. (eds.) *Seeing Cities Through Big Data*. SG, pp. 383–404. Springer, Cham (2017). https://doi.org/10.1007/978-3-319-40902-3_21



Improvement of the System of Arranging Commuter Passenger Transportation Based on the Kyiv Transport Hub

Oleh Strelko^(✉) , Tetiana Hrushevska , Vasyl Gaba , Yuliia Berdnychenko ,
and Hanna Kyrychenko 

State University of Infrastructure and Technologies, 9 Kyrylivska Street, Kyiv 04071, Ukraine
olehstrelko@duit.edu.ua

Abstract. Methods for improving the arrangement of commuter railway transportation are based on a systematic analysis of the structure of passenger flows and the uneven distribution of them in time and space, which is the basis for establishing the patterns of formation of passenger flows and the necessary resources for their transport service. The arrangement of commuter passenger transportation can be improved by regulating the intervals of trains and the passenger capacity of their train sets, which together will ensure their optimal population, minimal unproductive costs for commuter train traction, and more comfortable conditions for passengers. In order to rationally use passenger rolling stock and to improve the convenience and comfort of passengers, it is necessary to constantly conduct research on the capacity of train carriages in commuter trains, depending on seasonality, the level of service, the quality of services provided, as well as the departure interval and the distance of passenger transportation. At the same time, “natural” methods of such studies (which are rather laborious and expensive ones) should be supplemented by their theoretical generalization. The nature of the uneven distribution of passenger flows by periods of the day, directions of transportation has been analyzed and the patterns of fluctuations in passenger flows have been clarified. On this basis, a mathematical model for the formation of commuter train passenger flows has been developed. With its use, the necessary technological parameters for the arrangement of transportation and rolling stock have been established, which was used as a systemic factor in improving the system for organizing commuter passenger transportation based on the Kyiv transport hub.

Keywords: Passenger traffic · Population of suburban trains · Train intervals · Railway transport · Integrated curves · Commuter railway transportation · Transport Hub

1 Introduction

The extensive network of Ukrainian railways and its high carrying capacity [1–3], regularity and versatility of transportation [4–6], regardless of the time of year and climatic

conditions in the face of fierce competition, determine the important role of rail passenger commuter transportation in the transport service of the capital of Ukraine, the city of Kyiv, and other large cities [7]. Performing an important social function, often at the expense of its own resources and without proper state support, Ukrainian rail transport meets the needs of the train capacity in passenger transportation. However, the efficiency and safety of the functioning of the system for arranging commuter railway passenger transportation is determined by the resources available in it, the sufficiency and compliance of which with the functions performed by the systems should be considered in the interaction of various aspects [8–10]. Rapid wear of the rolling stock and very slow rates of its renewal are observed [11–13].

Modern conditions for the implementation of commuter passenger transportation in the system of operational and commercial activities of railways have led to an increase in their cost and unprofitability. It so happened historically that in the post-Soviet space, passenger transportation has always been unprofitable on almost all routes, including commuter ones [14, 15]. According to statistics, the damage to Ukrzaliznytsia (hereinafter referred to as the “UZ”) from passenger transportation in commuter traffic exceeds UAH 5 billion per year on average [4]. At the same time, own coverage of losses at the expense of income from commuter transportation is currently no more than 20%. The remainder of the losses – 80% – is covered by Ukrzaliznytsia through cross-financing from the profits of freight transportation, which leads to a slowdown in the development of the industry due to the loss of funds and resources.

The arrangement of commuter passenger transportation by rail should, on the one hand, most fully meet the needs of passengers and, on the other hand, ensure the best use of transportation facilities. The safety of train traffic and the safety of passengers in railway transport in Ukraine [4, 13, 16], as in Italy [17], India [18], China [19], Ghana [20], Poland [21], Germany [22], and other countries, remains the highest priority [23].

The aim of the paper is to improve the system for arranging commuter passenger transportation on the example of the Kyiv transport hub by mathematical modeling of the formation of passenger flows of commuter trains.

2 Literature Review

In foreign countries, as well as in Ukraine, there is fierce competition between different modes of passenger transport [24–26]. In modern conditions in all countries of the world, a characteristic feature of the commuter rail transport operation is its active participation in interurban transportation [27–29]. Therefore, in recent years, the existing urban railways in many large cities of the world have been intensively developed, modernized, and supplied with new comfortable rolling stock [30]. In large metropolitan areas, separate routes have been allocated for commuter traffic, which allow increasing the capacity of passenger traffic [31]. Most of the world’s railways are experiencing an increase in the passenger transportation volume in commuter traffic, although the share of passenger transport in the development of these transportations is not the same for different countries [32].

The main goal in the arrangement systems of passenger transportation in most countries of Europe is the desire to implement flexible adaptive technologies aimed at maximizing the satisfaction of the population’s needs for transportation at minimal costs for

organizing the transportation process [18, 21, 27]. Their traffic management technologies are based on the principle of adaptation to fluctuations in the level of demand for transportation, which is reflected in flexible measures of operational regulation of the transportation process, aimed mainly at regulating passenger train compositions. One of the latest achievements is the passenger traffic implementation on a modular basis, which provides for the constructive and technological possibility of quickly changing train sets at the corresponding stations, if necessary, in order to adapt. This principle of arranging passenger traffic has become widespread in such countries as Germany, France, the Netherlands, etc.

The experience of other countries is useful in that it confirms the need to pay attention to both core activities and additional services on the railway network. In the field of arranging transportation, the efforts of foreign countries are aimed at solving the issues of improving the train schedule, applying the clock schedule, providing technical equipment for commuter sections, and determining the parameters of a promising rolling stock.

As a whole, the quality of transport services in the system of railway passenger transportation can be assessed by such indicators as an annual volume of traffic, a passenger turnover, an average travel distance, and a number of trips per person.

3 Research Methodology

The nature of the uneven distribution of passenger flows by periods of the day, directions of transportation has been analyzed and the patterns of fluctuations in passenger flows have been clarified. On this basis, a mathematical model for the formation of commuter train passenger flows has been developed. With its use, the necessary technological parameters for the arrangement of transportation and rolling stock have been established, which was used as a systemic factor in improving the system for organizing commuter passenger transportation based on the Kyiv transport hub.

4 Results and Discussion

In order to rationally use passenger rolling stock and to improve the convenience and comfort of passengers, it is necessary to constantly conduct research on the capacity of train carriages in commuter trains, depending on seasonality, the level of service, the quality of services provided, as well as the departure interval and the distance of passenger transportation. At the same time, “natural” methods of such studies (which are rather laborious and expensive ones) should be supplemented by their theoretical generalization.

Since passenger flow is a determining factor in the choice of rolling stock, train intervals, and other parameters, it is necessary to analyze the capacity of commuter trains and to develop theoretical provisions for determining the number of train carriages in commuter trains. Therefore, the development of theoretical provisions for determining the required number of cars in suburban trains, taking into account the mentioned unevenness is an urgent need.

The uneven departure of passengers in the morning, afternoon, and evening hours is determined by the requirements for the frequency of commuter trains, the required fleet

of rolling stock, the number of train carriages in the train, and the general arrangement of commuter traffic in large railway junctions. Having reliable statistical data on each commuter train capacity during the day, it is possible to accurately and reasonably determine the set of commuter trains, in accordance with the actual passenger flow. To do this, on the basis of statistical data on each commuter train capacity for the days of the week of each season of the year, it is possible to determine (to select) the theoretical distribution law in the following order.

First, assume that the commuter train capacity is a variable random variable. As a confirmation of this, Table 1 shows the capacity values of one of the commuter trains on the Fastiv – Kyiv route, which runs daily.

Table 1. Calculation of the average commuter train capacity and dispersion of the investigated value.

The value of the intervals in the category (passengers in the train)	The average value of the interval in the category, X_i	Number of values in interval, m_i	$h_i = \frac{m_i}{\sum m}$	$X_i \cdot h_i$	$X_i - X_m$	$(X_i - X_m)^2$	$(X_i - X_m)^2 \cdot h_i$
302–394	348	4	0.007	2.53	–602.14	362576.96	2636.92
395–503	449	6	0.011	4.90	–501.14	251144.94	2739.76
504–596	550	14	0.025	14.01	–400.14	160114.93	4075.65
597–705	651	35	0.064	41.46	–299.14	89486.92	5694.62
706–798	752	52	0.095	71.14	–198.14	39260.90	3711.94
799–907	853	92	0.167	142.76	–97.14	9436.89	1578.53
908–1000	954	145	0.264	251.63	3.86	14.87	3.92
1001–1109	1055	95	0.173	182.31	104.86	10994.86	1899.11
1110–1202	1156	60	0.109	126.16	205.86	42376.84	4622.93
1203–1311	1257	29	0.053	66.30	306.86	94160.83	4964.84
1312–1404	1358	11	0.020	27.17	407.86	166346.81	3326.94
1405–1513	1459	2	0.004	5.31	508.86	258934.80	941.58
1514–1606	1560	2	0.004	5.67	609.86	371924.78	1352.45
1607–1715	1661	2	0.004	6.04	710.86	505316.77	1837.52
1716–1808	1762	1	0.002	3.20	811.86	659110.76	1198.38
Total	–	$\sum m = 550$	1.000	$X_m = 950.59$	–	–	$D[X] = 40585.11$

These data have been determined by field observations by traveling in an electric train and data from the reports of inspectors-auditors for the spring and summer periods of 2021 have been also used.

The sum of the third column gives the total number of observations $\sum m = 550$; the sum of the fourth column, which shows the frequency of values of a train capacity in certain intervals, is always equal to one, $\sum h_i = 1$; the sum of the fifth column determines the average value of train capacity $X_m = 950.59$; the sum of the eighth one is the studied value dispersion $D[X] = 40585.11$. The K parameter, characterizing the train capacity fluctuations shall be determined by the formula [33]:

$$K = \frac{X_m^2}{D[X]}, \tag{1}$$

where X_m is the average value of commuter train capacity; $D[X]$ is the studied value dispersion.

In order to give the proper form to the distribution, it is necessary to construct a polygon, plotting the average value of the interval in the discharge along the abscissa axis, and the number of values in the interval, shown in Fig. 1, – along the ordinate axis. The distribution law shall be determined from the shape of the polygon and the K parameter value [33].

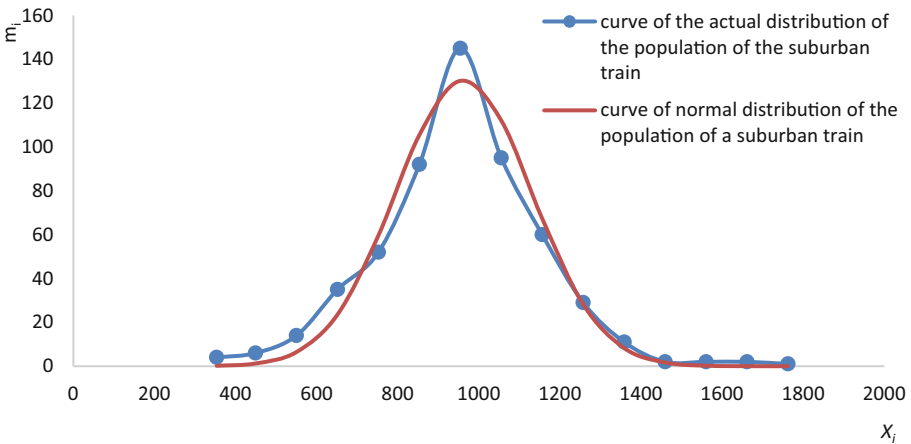


Fig. 1. Comparison of actual and normal distribution of commuter train capacity.

If the value of the parameter is $K \geq 10$, then we can assume that the commuter train capacity is distributed, according to the normal law, if $K \approx 6$, the distribution is close to normal, and if $2 \leq K < 6$, we have the Erlang distribution. Depending on the K parameter, we can assume that the commuter train capacity will have either a normal distribution, or a truncated normal distribution, or an Erlang distribution [33]. Given that the K parameter is greater than 10, we can conclude that the commuter train capacity in the Fastiv direction has a truncated normal distribution.

In many commuter trains, the capacity will have the same distribution laws. Therefore, the processing of statistical data and forecasting can be carried out both for each commuter train and for groups of trains.

After processing the statistical data, identifying the distribution law of commuter train capacity, it is necessary to calculate the value of the distribution functions and to plot a family of integral curves of train capacity for groups of trains with the same laws, but with different average values of train capacity.

For the truncated normal distribution of commuter train capacity, the distribution function shall be determined by the formula [33]:

$$F(X_i) = \frac{F(u) - F(\xi)}{1 - F(\xi)}, \tag{2}$$

For a normal distribution, the distribution function shall be determined by the formula:

$$F(X_i) = F(u), \tag{3}$$

where X_i is the stochastic random variable, passengers; $F(u)$ is distribution function corresponding to the normal law; $F(\xi)$ is function of the normalized truncation point;

$$u = \frac{X_i - X_m}{\sigma}, \xi = -\frac{X_m}{\sigma};$$

σ is the standard deviation of the number of passengers on the train.

The σ value shall be determined by the formula [27]:

$$\sigma = \sqrt{D[X]}, \tag{4}$$

In this case, $\sigma = \sqrt{40585.11} = 201.46$ passengers per train.

The values of the ordinary and truncated ordinary distribution functions shall be determined from mathematical and statistical tables [33].

The variation coefficient, showing how much greater the dispersion of random variables compared to the average value, shall be determined by the formula:

$$V = \frac{\sigma}{X_m}. \tag{5}$$

Commuter passenger trains can run short, medium, and long distances. In order to improve the capacity of electric commuter trains, it is necessary to provide for their possible limit train capacity with different options for laying lines on the train schedule and the characteristics of these trains.

The maximum allowable capacity of commuter trains with a different number of train carriages in the commuter train and taking into account the standing passengers can be determined as follows:

$$N_a = O_a \cdot \sum M \tag{6}$$

where O_a is the allowable commuter train overcapacity coefficient (1.1–1.3); $\sum M$ is the total number of seats on the train.

The maximum allowable capacity of commuter trains with a different number of train carriages in the set of commuter trains, taking into account the standing passengers,

determines the comfort of the trip of commuter passengers. It is believed that in the commuter transportation, standees can be used when traveling to the nearest stops. However, passengers traveling for a distance of 20–30km or more should be provided with seats. This value has been obtained on the basis that in the rolling stock, it is allowed to stand (meaning in the aisles of a train carriage and vestibules) two or three people per 1 m² of free space.

In Fig. 2 shown a family of train capacity integral curves for groups of trains with the same distribution laws (truncated normal one), but different average values of train capacity X_m . The abscissa shows the number of passengers in the commuter train and the ordinate shows the value of the differential probability density distribution function of the commuter train capacity.

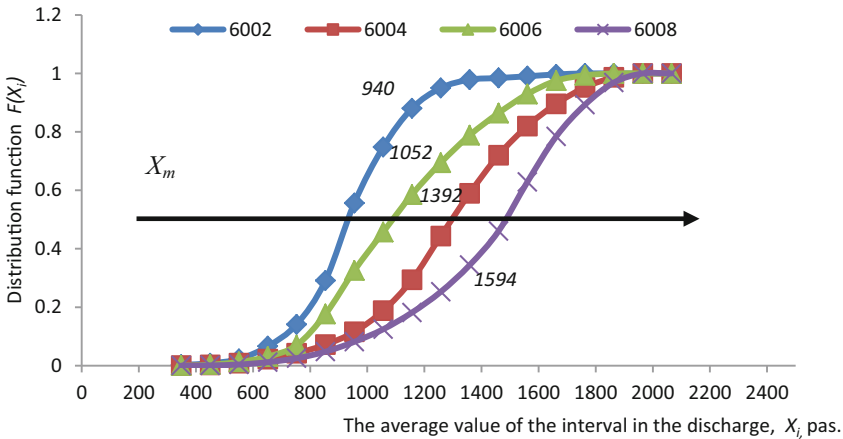


Fig. 2. Family of integral curves of truncated normal distribution of commuter train capacity.

From the analysis of the data obtained from the integral function of the accumulation of passengers on the platform for different trains, a generalized approximation formula has been obtained:

$$F(F_i) = \frac{1}{1 + e^{-\left(\frac{X_i - X_m}{140}\right)}} \tag{7}$$

Based on Eq. (7), a family of approximating integral curves has been built (see Fig. 3). As follows from the formula (7), the average number of passengers in a train corresponds to the value of 0.5 of the integral function ($F(X_m) = 0.5$). On Fig. 3 this corresponds to the points of intersection of the horizontal line at the level of 0.5 with the integral curves.

How to use theoretical results in practice? In order to make decisions about the number of train carriages in electric train sets, it is possible to quickly take data on the average capacity of each train within one to two weeks. The allowable commuter train overcapacity coefficient can be taken from 1.1 to 1.3. Having determined the maximum allowable train capacity for a certain number of train carriages, according to the schedule

(see Fig. 3), it is necessary to check whether this number of train carriages will be enough to transport such a number of passengers, that is, the probability $P(X_i \leq N_d)$ that the number of passengers in the train will not exceed the maximum allowable commuter train capacity $P(X_i \leq N_d) = F(X_i)$. The number of train carriages will be sufficient while $F(X_i) \approx 0.9$ (if this level of probability shall be considered sufficient for practical purposes).

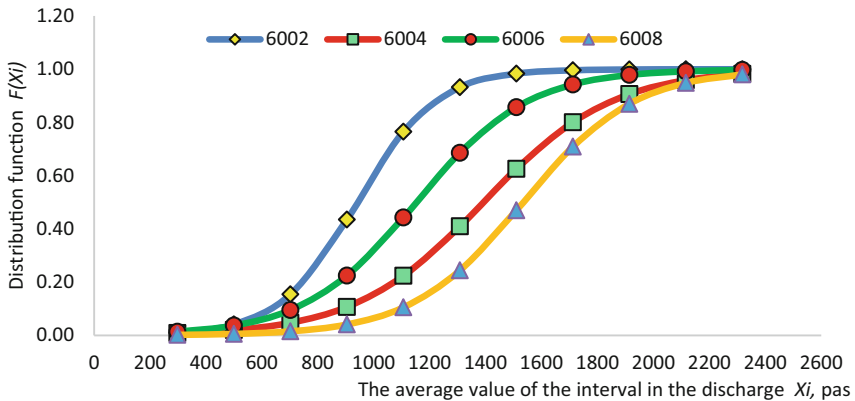


Fig. 3. A family of approximated integral curves of the truncated normal distribution of the commuter train capacity.

From Eq. (7), we can obtain the inverse dependence of the number of passengers, taking into account the value of the integral function:

$$X_i = X_m - 140 \ln\left(\frac{1}{F(X_i)} - 1\right). \tag{8}$$

For $F(X_i) = 0.9$ we get:

$$X_{max} = X_m + 307 \tag{9}$$

Figure 4 shows the dependence of X_m on the time of departure of trains. With the help of the theoretical data obtained, a method for determining the number of train carriages in the train set, depending on the time of departure, has been developed. Let us give an example of the calculation by this method.

Let us take the train starting at 6:08. According to the approximation formula, we shall obtain the average number of passengers in the train $X_m = 1,410$ passengers. According to Eq. (9), the maximum number of passengers is 1,717 people.

In order to transport such a number of passengers, it is necessary to have 12 train carriages in the train set, which is technically impossible. Conclusion: since the maximum composition of the train is 10 train carriages, it is necessary to change the timetable in order to avoid overcrowding of the train.

The probability that a commuter train will have more passengers than the maximum allowable train capacity is:

$$P(X_i > N_d) = 1 - F(X_i) \tag{10}$$

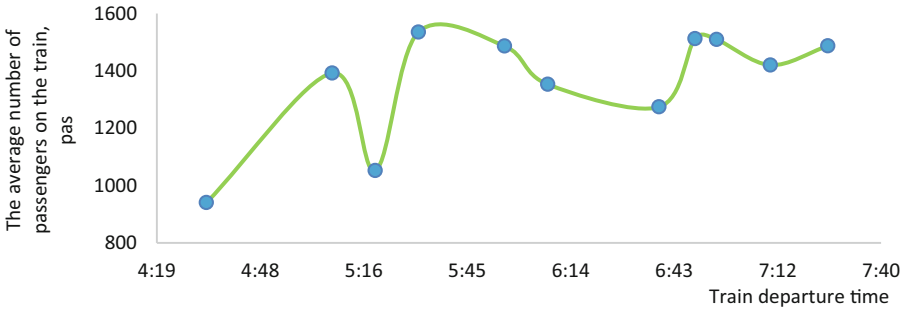


Fig. 4. Dependence of the average number of passengers from the time of train departure.

Since the main part of the sets of commuter trains in the Kyiv railway hub are the trains of the ER-9M series, the average number of seats in one train carriage is 100. Accordingly, if the number of train carriages in a train is 10, the maximum allowable train capacity should not exceed 1,500 passengers, with eight train carriages – 1200, with six train carriages – 900, with four – 600 passengers.

The results obtained are in good agreement with the data of similar studies. As the analysis shows, the systems for arranging commuter and regional passenger transportation by railroads in different countries have features both different from Ukraine and common with it and with each other [1, 4, 23]. Recently, the use of integrated transport systems, the application of new technological and organizational methods for arranging commuter transportation has become more widespread [19, 22, 30]. Methods of improving the arrangement of commuter rail transportation are based on a systematic analysis of the structure of passenger flows and the unevenness of their distribution in time and space, which is the basis for establishing patterns of formation of passenger flows and the necessary resources for their transport services [27, 30, 32]. The experience of arranging passenger traffic in Slovenia [27], Italy [31], China [23], indicates the prospects for using the commuter transportation technology on the railways of Ukraine of the modular principle of organizing traffic, which can also be one of the rational ways for the further development of the industry.

5 Conclusion

The arrangement of commuter passenger transportation can be improved by regulating the intervals of trains and the passenger capacity of their train sets, which together will ensure their optimal train capacity, minimal unproductive costs for commuter train traction, and more comfortable conditions for passengers.

The data from scheduled surveys of commuter train capacity should be used as the initial statistical information based on which mathematical models of commuter train capacity are built as a function of their train capacity, inter-train interval, and passenger capacity of trains, which allows improving the commuter train capacity arrangement.

The nature of the uneven distribution of passenger flows by periods of the day, directions of transportation has been analyzed and the patterns of fluctuations in passenger

flows have been clarified, and on this basis, the necessary technological parameters for arranging transportation and rolling stock have been identified, which was used as a systemic factor in improving the system of commuter passenger transportation using the example of the Kyiv transport hub. Since the main part of the sets of commuter trains in the Kyiv railway hub are the trains of the ER-9M series, the average number of seats in one train carriage is 100. Accordingly, if the number of train carriages in a train is 10, the maximum allowable train capacity should not exceed 1,500 passengers, with eight train carriages – 1200, with six train carriages – 900, with four – 600 passengers.

References






1. Pshinko, O., Charkina, T., Martseniuk, L., Orlovska, O.: Hubs as a key tool for improving the quality of the service and development of multimodal passenger traffic. *Transport Problems* **17**(1), 201–214 (2022). <https://doi.org/10.20858/tp.2022.17.1.17>
2. Fesovets, O., et al.: Container transportation by rail transport within the context of Ukraine's European integration. In: *Proceedings of the 23rd International Scientific Conference Transport Means*, pp. 381–386. Kaunas University of Technology, Kaunas (2019)
3. Gutnyk, M., Radohuz, S.: The impact of decisions of Mining Industrialists Congresses on the Industrial Revolution increasing in Ukraine in the late XIX century. *History of Science and Technology* **10**(1), 50–61 (2020). [https://doi.org/10.32703/2415-7422-2020-10-1\(16\)-50-61](https://doi.org/10.32703/2415-7422-2020-10-1(16)-50-61)
4. Mandych, O., et al.: The organizational and economic policy of the state administration of development of railway transport of Ukraine. *SHS Web of Conferences* **67**, 02007 (2019). <https://doi.org/10.1051/shsconf/20196702007>
5. Strelko, O., et al.: Historical milestones of creation of computers technology automated system for passenger transportations management “Express” on the railway transport in the USSR. In: *2019 IEEE 2nd Ukraine Conference on Electrical and Computer Engineering (UKRCON)*, pp. 1214–1219. IEEE, Lviv (2019). <https://doi.org/10.1109/UKRCON.2019.8879892>
6. Fomin, O., Lovska, A., Horban, A.: Historical aspects of construction and operation of train ferry routes. *History of Science and Technology* **11**(2), 351–382 (2021). <https://doi.org/10.32703/2415-7422-2021-11-2-351-382>
7. Kulbovskiy, I.I., Aharkov, O.V., Kharuta, V.S., Halushko, M.M.: Main criteria of complex evaluation of subway train power facility technological productive potential. *IOP Conference Series: Materials Science and Engineering* **1021**(1), 012007 (2021). <https://doi.org/10.1088/1757-899X/1021/1/012007>
8. Kyrychenko, H., Strelko, O., Berdnychenko, Y.A.: Influence of existing operational conditions on compliance with car handling standards. *IOP Conference Series: Earth and Environmental Science* **666**(4), 042054 (2021). <https://doi.org/10.1088/1755-1315/666/4/042054>
9. Zelenko, Y., Bezovska, M., Skvireckas, R., Neduzha, L.: The impact of motor oils quality on improving the reliability in operation of traction rolling stock. In: *Proceedings of the 24 International Conference Transport Means 2020*, Pt. II., pp. 568–572. Kaunas University of Technology, Kaunas (2020)
10. Bibik, S., et al.: Formulation of the mathematical model for the planning system in the carriage of dangerous goods by rail. *IOP Conference Series: Materials Science and Engineering* **985**(1), 012024 (2020). <https://doi.org/10.1088/1757-899X/985/1/012024>
11. Okorokov, A., et al.: Research that have exhausted their standard resource into a possibility to prolong the time of operation of universal open top wagon bodies. *Eastern-European Journal of Enterprise Technologies* **3**(7), 20–26 (2018). <https://doi.org/10.15587/1729-4061.2018.131309>

12. Babyak, M., Keršys, R., Neduzha, L.: Improving the dependability evaluation technique of a transport vehicle. In: Proceedings of the 24 International Conference Transport Means 2020, Pt. II., pp. 646–651. Kaunas University of Technology, Kaunas (2020)
13. Romanova, T., et al.: Sparsest balanced packing of irregular 3D objects in a cylindrical container. *Eur. J. Oper. Res.* **291**(1), 84–100 (2021). <https://doi.org/10.1016/j.ejor.2020.09.021>
14. Ugnenko, Y., et al.: Innovative geoinformation systems for the design of communication paths. In Environmental Engineering. In: Proceedings of the International Conference on Environmental Engineering (ICEE), vol. 11, pp. 1–9. Vilnius Gediminas Technical University, Vilnius (2020). <https://doi.org/10.3846/enviro.2020.693>
15. Kurhan, D., Kurhan, M., Hmelevska, N.: Development of the high-speed running of trains in Ukraine for integration with the international railway network. *Acta Polytechnica Hungarica* **19**(3), 207–218 (2022). <https://doi.org/10.12700/APH.19.3.2022.3.16>
16. Fomin, O., Lovska, A., Píšťek, V., Kučera, P.: Dynamic load effect on the transportation safety of tank containers as part of combined trains on railway ferries. *Vibroengineering Procedia* **29**, 124–129 (2019). <https://doi.org/10.21595/vp.2019.21138>
17. Coppola, P., De Fabiis, F.: Impacts of interpersonal distancing on-board trains during the COVID-19 emergency. *Eur. Transp. Res. Rev.* **13**(1), 1–12 (2021). <https://doi.org/10.1186/s12544-021-00474-6>
18. Nunes, L., Rangwala, L., Pai, M.: Mainstreaming photo-and video-based documentation as method for establishing a level of service framework for the Mumbai suburban railway System. *Transportation Research Record* **2675**(12), 175–185 (2021). <https://doi.org/10.1177/03611981211028606>
19. Tang, L., et al.: Scheduling local and express trains in suburban rail transit lines: Mixed–integer nonlinear programming and adaptive genetic algorithm. *Comput. Oper. Res.* **135**, 105436 (2021). <https://doi.org/10.1016/j.cor.2021.105436>
20. Alimo, P.K., et al.: Factors causing low demand for a suburban passenger train in Sekondi-Takoradi. *J. Transp. Geogr.* **98**, 103268 (2022). <https://doi.org/10.1016/j.jtrangeo.2021.103268>
21. Pietrzak, O., Pietrzak, K.: The role of railway in handling transport services of cities and agglomerations. *Transportation Research Procedia* **39**, 405–416 (2019). <https://doi.org/10.1016/j.trpro.2019.06.043>
22. Sarker, R.I., Mailer, M., Sikder, S.K.: Walking to a public transport station: Empirical evidence on willingness and acceptance in Munich, Germany. *Smart and Sustainable Built Environment* **9**(1), 38–53 (2019). <https://doi.org/10.1108/SASBE-07-2017-0031>
23. Zhang, M., Dong, W., Sun, X., Ji, Y.: A method for enhancing global safety of regional rail transit based on coordinative optimization of passenger flow assignment and train scheduling. *J. Phys: Conf. Ser.* **1624**(4), 042036 (2020). <https://doi.org/10.1088/1742-6596/1624/4/042036>
24. Dykan, V., et al.: Public management of railway transport development based on the principles of a systematic approach. *Journal: Scientific Horizons* **24**(8), 98–107 (2021). [https://doi.org/10.48077/scihor.24\(8\).2021.98-107](https://doi.org/10.48077/scihor.24(8).2021.98-107)
25. Hörl, B., Dörr, H., Wanjek, M., Romstorfer, A.: METRO. FREIGHT. 2020—strategies for strengthening rail infrastructure for freight transport in urban regions. *Transportation Research Procedia* **14**, 2776–2784 (2016). <https://doi.org/10.1016/j.trpro.2016.05.478>
26. Lutzemberger, G., Musolino, A., Rizzo, R.: Automated people mover: a comparison between conventional and permanent magnets MAGLEV systems. *IET Electrical Systems in Transportation* **7**(4), 295–302 (2017). <https://doi.org/10.1049/iet-est.2017.0004>
27. Ambrož, M., Korinšek, J., Blaž, J., Prebil, I.: Integral management of public transport. *Transportation Research Procedia* **14**, 382–391 (2016). <https://doi.org/10.1016/j.trpro.2016.05.090>

28. Shevchenko, A., et al.: Ways of introduction of the high-speed movement of passenger trains in Ukraine. *MATEC Web of Conferences* **230**, 01014 (2018). <https://doi.org/10.1051/mateconf/201823001014>
29. Mohammadi Pirouz, H., Hajizadeh, A.: A highly reliable propulsion system with onboard uninterruptible power supply for train application: topology and control. *Sustainability* **12**(10), 3943 (2020). <https://doi.org/10.3390/su12103943>
30. Codina, E., Rosell, F., Cadarso, L., Marín, Á.: Setting services in public transit lines in short time periods under time-varying demand. *Transportation Research Procedia* **22**, 615–624 (2017). <https://doi.org/10.1016/j.trpro.2017.03.054>
31. Torti, A., et al.: A general bi-clustering algorithm for object data with an application to the analysis of a Lombardy railway line. *Int. J. Approximate Reasoning* **142**, 161–177 (2022). <https://doi.org/10.1016/j.ijar.2021.12.003>
32. Zhou, L., Liu, Y.J., Yu, L., Liu, Y.: Research on the spatial-system-based rail transit systems of the world cities. *Procedia Engineering* **137**, 699–708 (2016). <https://doi.org/10.1016/j.proeng.2016.01.307>
33. Cox, D.R., Miller, H.D.: *The Theory of Stochastic Processes*. CRC Press, Boca Raton (1977)



Public Transit Crowding Estimation Indicators: Comparative Analysis, Conditions of Application, Interaction

Denys Ponkratov , Yuriy Davidich , Denys Kopytkov^(✉) , Ganna Samchuk ,
and Yevhen Kush 

O. M. Beketov National University of Urban Economy in Kharkiv, 17 Marshala Bazhanova
Street, Kharkiv 61002, Ukraine
denys.kopytkov@kname.edu.ua

Abstract. The article deals with the issues of the public transit crowding estimation. Attention is paid to the fact to estimate the vehicle crowding level, the indicators of various nature and conditions of application can be used. A comparative analysis revealed that passenger density and area assumed for one standing passenger indicators were the objective characteristics of the vehicle occupancy level. Their values do not depend on passenger capacity and interior planning of the vehicle, but they do not reflect the occupancy of seats. The application of the load factors makes it possible to estimate the entire range of vehicle occupancy. However, from the standpoint of the crowding discomfort in public transport, they must be adjusted based on the passenger density indicator. It was found that under the same passenger density conditions the load factor value for different bus sizes may significantly differ due to various ratio of the number of seats to the total capacity of the vehicles. To describe the interaction between occupancy indicators, the analytical formulas were proposed to take into account as variables fraction of the number of seats in the total capacity of the vehicle and normalized number of passengers standing per square meter accepted for total capacity calculation. The obtained research results can be used to solving the tasks of public transit operation and revealing the in-vehicle comfort estimation.

Keywords: Load factor · Passenger density · Passenger capacity · Occupancy level · Vehicle area assumed for one standing passenger

1 Introduction

Public transit should provide a high level of service. Despite the comprehensive nature of the service indicator, one of its most important factors is crowding level. Overcrowded conditions are one of the leading causes of trip discomfort feeling. As a result, the transit vehicles' occupancy rate should be restricted to some values. In-vehicle crowding estimation has been done via a series of indicators of various features and conditions of application. At the same time, it complicates the assessment and analysis of the passenger trip conditions originating from different occupancy indicators to solve both research

and practical public transit problems. In view of the above, conducting a comparative analysis of occupancy indicators, identifying their application conditions, and revealing dependencies between them are the relevant tasks for mass transportation operation.

2 Literature Review

Presently there is no researchers' common opinion regarding the unified crowding indicator. Papers [1–3] emphasize that an increase in a passenger vehicle crowding level affects the passenger trip parameters to be manifested in the following aspects: the discomfort growth – making a trip with an increase in a vehicle crowding becomes less comfortable for passengers; the fail-to-board probability – provides the conditions when several passengers are unable to board the first vehicle arrived at the stop and are forced to wait for the arrival of the next one; the service reliability – with an increase in the vehicle crowding, the waiting and trip time increases due to a decrease in the operating regularity, a longer vehicle dwell time at intermediate stops and headway. In turn, the mass transit occupancy level affects the passengers' transport behavior, for example, a path choice [4, 5].

The most comfortable travel conditions are those when the passenger can travel in a sitting position. Acceptable conditions can be considered when the vehicle is not overcrowded, and the trip is not too long. Uncomfortable conditions arise when the vehicle is overcrowded. With an increase in the vehicle crowding level, the passengers' trip conditions worsen. It also should be taken to those commuters who travel in a sitting position [6].

When establishing the nature of the discomfort caused by vehicle crowding, researchers conduct a survey and analyze subjective scores [7–9]. This approach made it possible to determine the respondents' attitude to a vehicle crowding rate when traveling and to rank the factors according to their significance.

A survey of public transport passengers [10] found that the most significant causes of overcrowding discomfort are over-closeness, physical load while standing, and noise and smell in a vehicle. It was also revealed that women and high-income passengers are more sensitive to the trip conditions. The authors [11] made a similar conclusion.

The results [12] indicated that the vehicle crowding level leads to a significant discomfort increase which can be measured through the utility function change. The study of Santiago (Chile) showed that the utility function of the travel path increases by 29% if the passenger density increases from 1–2 pass./m² to 3–4 pass./m², and by 73% with an increase in density from 3–4 pass./m² to 5–6 pass./m². Paper [13] demonstrated that vehicle overcrowding may have a greater importance than waiting from the passengers' viewpoint.

When choosing the vehicles' service frequency, the vehicle peak-load factor should be considered in the busiest route section. The peak-load factor choice allows managing the required number of route-operated vehicles [14, 15].

To assess the passenger vehicle occupancy level, the following indicators are used: the number of passengers standing per 1 square meter (passenger density) (α); area assumed for one standing passenger (F_{sp}); load factor calculated as the “on-board passengers number-to-vehicle total capacity” ratio (γ); load factor determined as the “on-board

passengers number-to-vehicle seating capacity” ratio (LF). Table 1 shows the various authors’ approaches to the determination of crowding indicators.

Table 1. Review of crowding indicators application.

Authors	Problem to be solved	α , pass./m ²	γ	LF	F_{sp} , m ² /pass
Cats & Hartl [1]	Modeling public transport on-board congestion	–	–	+	–
Qu <i>et al.</i> [2]	Estimating wait time and passenger load in a saturated metro network	–	+	–	+
Yap <i>et al.</i> [4]	Crowding valuation in urban tram and bus transportation	+	–	+	–
Márquez <i>et al.</i> [5]	Explanation of in-vehicle crowding in a choice context between bus rapid transit and metro	+	–	–	–
Yan <i>et al.</i> [6]	Determination of the optimal solution to the seating capacity for a 12 m city bus	+	–	–	–
Börjesson & Rubensson [8]	Finding of the relationship between performance level and satisfaction for crowding and reliability	–	–	+	–
Wang & Zacharias [9]	Measure of the physical and human factors impacting travel comfort on mass urban rail transport	+	–	–	–
Haywood <i>et al.</i> [10]	Survey conducting to investigate the crowding effect on public transport	+	–	–	–
Basu & Hunt [11]	Valuing of attributes influencing the attractiveness of suburban train service	+	–	–	–
Batarce <i>et al.</i> [12]	Valuation of comfort in public transportation	+	–	–	–
Batarce <i>et al.</i> [13]	Valuing crowding in public transport	–	–	+	–
Lin & Tang [14]	Optimization of urban public transport lines	–	+	–	–
Börjesson & Fung [15]	Finding of the optimal prices and frequencies for buses	–	+	–	–
Shao <i>et al.</i> [16]	Influence of in-vehicle crowding on passenger travel time value evaluation	+	–	–	–

At the same time, the passenger density is a more objective indicator to embrace the trip conditions [16]. According to [7], the critical crowding level is of a different value for various regions. Thus, in countries of the European Union and Australia, the normalized value is 4 pass./m²; USA – 5 pass./m²; China (bus transportation) – 8 pass./m².

3 Comparative Analysis of Occupancy Indicators

The passenger vehicle total capacity can be represented as follows:

$$q_{total} = q_{seat} + q_{stand} = q_{seat} + F_{floor} \cdot \alpha_n, \quad (1)$$

where q_{seat} is the number of seats in a vehicle (seating capacity), pass.; q_{stand} is the number of standing places in a vehicle, pass.; F_{floor} is the standing passengers' floor space, m^2 ; α_n is the normalized number of passengers standing per 1 square meter accepted for total capacity calculation, pass./ m^2 .

The value of these indicators in a particular route section can be determined by the following relationships. The number of passengers standing per 1 square meter (passenger density):

$$\alpha = \begin{cases} 0, & \text{if } N_{pass} \leq q_{seat} \\ \frac{N_{pass} - q_{seat}}{F_{floor}}, & \text{if } N_{pass} > q_{seat} \end{cases} \quad (2)$$

where N_{pass} is the number of the on-board passengers, pass.

The area assumed for one standing passenger (m^2 /standing passenger):

$$F_{sp} = \frac{F_{floor}}{N_{pass} - q_{seat}} = \frac{1}{\alpha}, N_{pass} > q_{seat}, \text{ pass./}m^2. \quad (3)$$

Load factor calculated as the "on-board passengers number-to-vehicle total capacity" ratio:

$$\gamma = \frac{N_{pass}}{q_{total}}. \quad (4)$$

Load factor determined as the "on-board passengers number-to-vehicle seating capacity" ratio:

$$LF = \frac{N_{pass}}{q_{seat}}. \quad (5)$$

Since F_{floor} is usually not presented in the vehicles' specification, the Eq. (2) considering (1) can be represented in a more convenient form:

$$\alpha = \begin{cases} 0, & \text{if } N_{pass} \leq q_{seat} \\ \frac{(N_{pass} - q_{seat}) \cdot \alpha_n}{q_{total} - q_{seat}}, & \text{if } N_{pass} > q_{seat} \end{cases} \quad (6)$$

Occupancy level change for Mercedes Conecto G bus ($q_{seat} = 40$, $q_{total} = 150$) is shown in Fig. 1. Calculations were performed at $\alpha_n = 8$ pass./ m^2 .

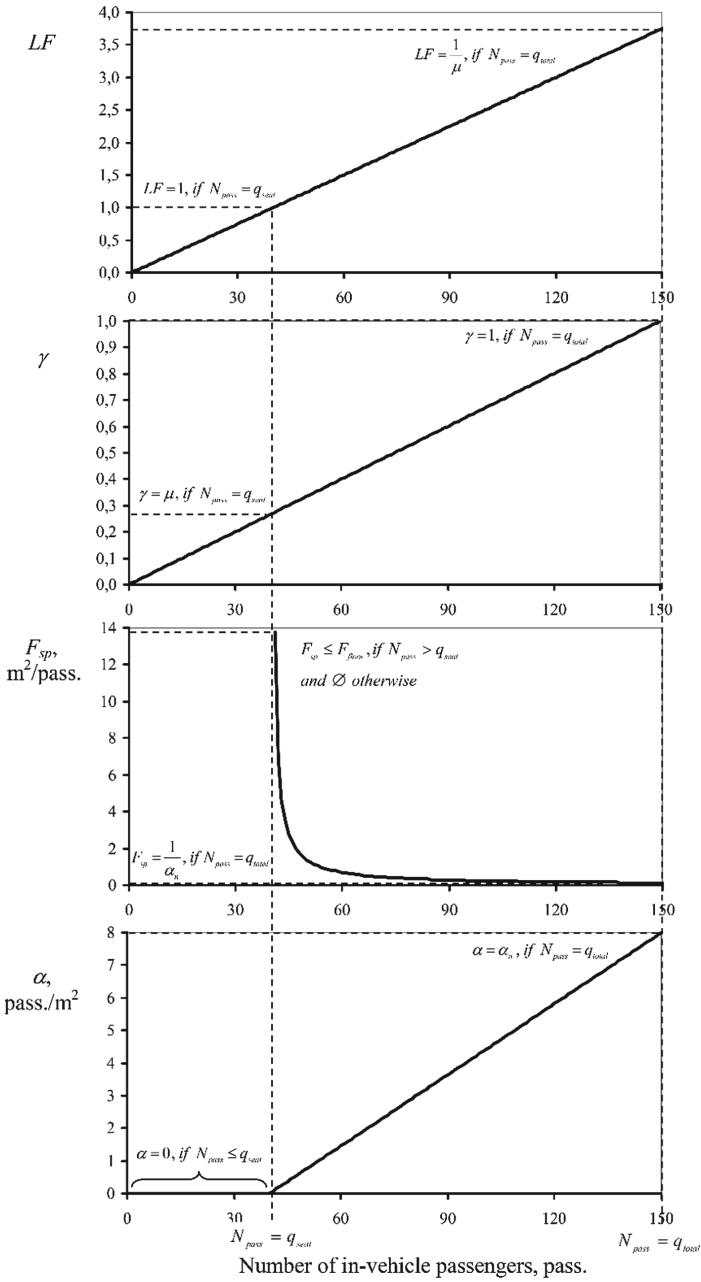


Fig. 1. Graph of the occupancy level change for Mercedes Conecto G bus.

As can be seen in Fig. 1, with the increase in the number of on-board passengers, which does not exceed the bus seating capacity, the passenger density is 0 pass./m². Further growth in the number on-board passengers leads to an α linear increase. In this case, when the number of on-board passengers reaches the vehicle total capacity, the passenger density is equal α_n . The area assumed for one standing passenger is the inverse of the passenger density. From the graph, it can be observed that the function is uncertain, if $N_{pass} \in [0; q_{seat}]$. However, this statement is justified by the assumption that if there are free seats, all passengers will use them and travel standing only if all seats are occupied. However, as noted in [7], some passengers are prone to travel standing despite the availability of seats.

The F_{sp} maximum value is observed, if one on-board passenger travels standing, and is equal F_{floor} . Further increase in the number of on-board passengers affects on its decrease in hyperbolic function. Providing that $N_{pass} = q_{total}$, the area assumed for one standing passenger is equal $1/\alpha_n$.

The disadvantage of the passenger density and the area assumed for 1 standing passenger indicators is that they do not characterize the occupancy of seats. However, these indicators are objective and convenient for crowding valuation.

The γ and LF vehicle occupancy indicators are linear and increasing with in-vehicle passenger's volume. The limit value of the γ indicator to encompass the full occupancy of seats is equal μ (the share of the number of seats in the vehicle total capacity). The LF indicator characterizes the occupancy rate of seats. Accordingly, full occupancy of seats for travel is achieved by $LF = 1$. This condition is met regardless of the vehicle capacity.

In the case when the number of in-vehicle passengers is equal to the vehicle total capacity, the γ value is 1.0, and the LF value can be determined as follows:

$$LF = 1/\mu, \text{ if } N_{pass} = q_{total}, \quad (7)$$

where $\mu = q_{seat}/q_{total}$ is the share of the number of seats in the vehicle total capacity.

According to the considered conditions, the values exceeding $\gamma = 1$ and $LF = 1$ correspond to the passenger density of more than 8 pass./m². Originating from the comparative analysis of vehicle occupancy indicators, Table 2 was formed. In Table 2, it can be observed that vehicle occupancy indicators depend on the α_n and μ parameters.

Analysis of urban bus specifications (Table 3) showed that with increasing the bus size, there is a tendency to reduce the share of the number of seats in the vehicle total capacity. In Table 3, for the Bogdan A201.10 bus ($q_{total} = 48$) ratio of the number of seating and standing places in the bus total capacity is equal to 50%. At the same time, for the Mercedes Conecto G ($q_{total} = 150$, articulated bus) percent of the number of seating and standing places in the bus total capacity is 26.7 and 73.3%, respectively.

Table 2. Application features of vehicle occupancy indicators.

Vehicle occupancy indicator	Characteristic of seat occupancy level	Conditions of full occupancy of seats	Indicator function change	Conditions of full vehicle occupancy
α , pass./m ²	No	$\alpha > 0$ pass./m ²	piecewise-linear	$\alpha \geq \alpha_n$
F_{sp} , m ² /pass	No	$F_{sp} \leq F_{flow}$	hyperbolic	$F_{sp} \geq 1/\alpha_n$
γ	Yes	$\gamma \geq \mu$	linear	$\gamma \geq 1$
LF	Yes	$LF \geq 1$	linear	$LF \geq 1/\mu$

Table 3. Characteristics of urban bus passenger capacity.

Bus model	Bus length, mm	Seating places	Standing places	Total passenger capacity (passenger density of 8 pass./m ²)	Percentage of seating and standing places in bus total capacity, %	
					seating	standing
Mercedes-Benz Sprinter 318cdi	6945	19	–	19	100.0	–
Bogdan 201.10	7880	24	24	48	50.0	50.0
Karsan Atak	8315	21	39	60	35.0	65.0
Mercedes Conecto	12134	26	75	101	25.7	74.3
Mercedes Conecto G	18124	40	110	150	26.7	73.3

4 Conditions of Application

From the comparative analysis of vehicle occupancy indicators, it is possible to conclude the following: passenger density and area assumed for one standing passenger indicators are objective characteristics of the vehicle occupancy level, which do not depend on passenger capacity and vehicle interior planning, but they do not reflect the occupancy of seats; application of the load factors makes it possible to estimate the entire range of vehicle occupancy, however, from the standpoint of the crowding discomfort in public transport, they must be adjusted based on the passenger density indicator; under the same, the passenger density and the load factor value for different bus sizes may significantly differ due to various share of the number of seats in the total vehicle's capacity; with the increase in vehicle passenger capacity there is a tendency to reduce the share of the number of seats in the vehicles' total capacity.

5 Crowding Indicators Interrelation

Given the above, it is an important task to formalize the relationship between the stated public transit vehicles occupancy indicators. Passenger density is the indicator that is inverse to area assumed for one standing passenger:

$$\alpha = \frac{1}{F_{sp}}, F_{sp} > 0. \quad (8)$$

At the same time, the opposite dependence is as follows:

$$F_{sp} = \frac{1}{\alpha}, \alpha > 0. \quad (9)$$

The load factor determined as the “the on-board passengers number-to-vehicle total capacity” ratio (γ) based on the passenger density (α) can be found as:

$$\gamma = \mu(\alpha_n) + (1 - \mu(\alpha_n)) \frac{\alpha}{\alpha_n}, \alpha \geq 0. \quad (10)$$

From the Eq. (10), the α and γ relation can be represented by:

$$\alpha = \begin{cases} 0, & \text{at } \gamma \leq \mu(\alpha_n); \\ \frac{\alpha_n \cdot (\gamma - \mu(\alpha_n))}{1 - \mu(\alpha_n)}, & \text{at } \gamma > \mu(\alpha_n). \end{cases} \quad (11)$$

Substituting (8) in (10), the formula should be obtained to determine γ from the F_{sp} value:

$$\gamma = \mu(\alpha_n) + \frac{1 - \mu(\alpha_n)}{\alpha_n \cdot F_{sp}}, F_{sp} > 0. \quad (12)$$

In this way, the reverse formula can be represented like this:

$$F_{sp} = \frac{1 - \mu(\alpha_n)}{\alpha_n \cdot (\gamma - \mu(\alpha_n))}, \gamma > \mu(\alpha_n). \quad (13)$$

Considering Eq. (4) the number of in-vehicle passengers can be determined as:

$$N_{pass} = q_{seat} \cdot LF. \quad (14)$$

Substituting Eq. (11) in (4) results in:

$$\gamma = \frac{q_{seat}}{q_{total}} \cdot LF = \mu(\alpha_n) \cdot LF. \quad (15)$$

The inverse formula is:

$$LF = \frac{\gamma}{\mu(\alpha_n)}. \quad (16)$$

After substituting (10) in (16), it can be found:

$$LF = 1 + \frac{1 - \mu(\alpha_n)}{\mu(\alpha_n)} \times \frac{\alpha}{\alpha_n}. \quad (17)$$

After converting inverse formula should be obtained:

$$\alpha = \begin{cases} 0, & \text{if } LF \leq 1; \\ \frac{\alpha_n \cdot \mu(\alpha_n)}{1 - \mu(\alpha_n)} (LF - 1), & \text{if } LF > 1. \end{cases} \quad (18)$$

Substituting (8) into (17) gives the result:

$$LF = 1 + \frac{1 - \mu(\alpha_n)}{\mu(\alpha_n) \cdot \alpha_n \cdot F_{sp}}, \quad F_{sp} > 0. \quad (19)$$

And after transforming the inverse formula is:

$$F_{sp} = \frac{1 - \mu(\alpha_n)}{\mu(\alpha_n) \cdot \alpha_n \cdot (LF - 1)}, \quad LF > 1 \quad (20)$$

The occupancy indicators interrelation diagram was developed (Fig. 2). This scheme allows determining the required occupancy indicators from the initial indicator. The graphic interrelation of occupancy indicators change is presented in Fig. 3.

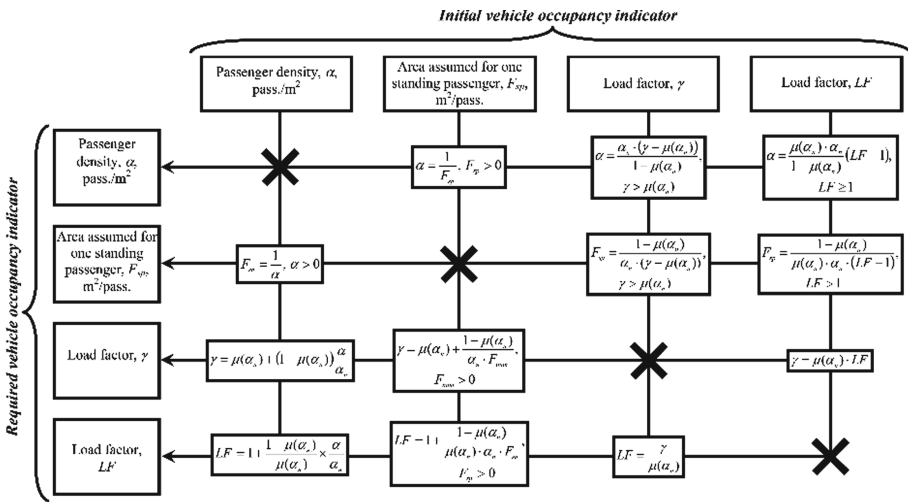


Fig. 2. Occupancy indicators interrelation diagram.

For example, for initial data $\alpha_n = 8\text{pass./m}^2$, $\mu(\alpha_n) = 0.2$ and $= 8\text{pass./m}^2$ occupancy indicators are as follows: $= 0.5\text{m}^2/\text{pass.}$; $\gamma = 0.4$; $LF = 2.0$.

Thus, there is a clear dependence between the passenger density indicator (α) and the area assumed for one standing passenger (F_{sp}). The interrelation between stated indicators does not depend on the planning characteristics of the vehicle interior and its passenger capacity. At the same time, in determining γ and LF indicators an important role is given to the share of the number of seats in the total capacity of the vehicle ($\mu(\alpha_n)$) and the normalized number of passengers standing per 1 square meter accepted for total capacity (α_n).

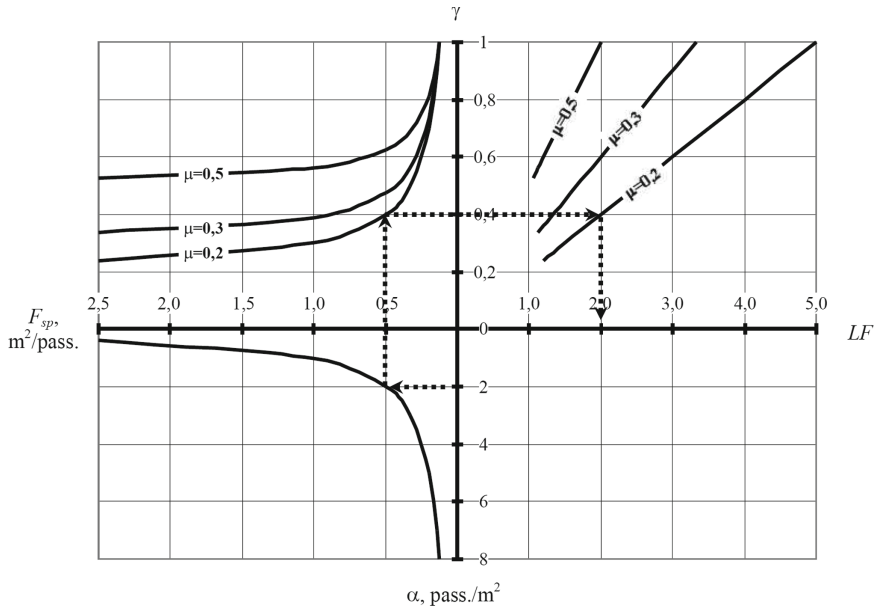


Fig. 3. Graph of occupancy indicators change ($\alpha_n = 8 \text{ pass./m}^2$).

6 Conclusion

From the comparative analysis of vehicle crowding indicators, it is possible to draw the following conclusions: passenger density and area assumed for one standing passenger indicator are the objective characteristics of the level of vehicle occupancy, which do not depend on passenger capacity and interior planning of the vehicle, but they do not reflect the occupancy of seats; application of the load factors makes it possible to estimate the entire vehicle occupancy range, however, if considered from the standpoint of the crowding discomfort in public transport, these indicators must be adjusted from the passenger density value; under the same, the passenger density conditions, the load factor indicator for different bus sizes may significantly differ due to various share of the number of seats in the total vehicle capacity; with the vehicle passenger capacity increase there is a tendency to reduce the share of the number of seats in the total capacity of the vehicles.

Analytical formulas were given to describe the relationship between occupancy rates, which consider as variables the share of seats in the total capacity of the vehicle and the normalized number of passengers per square meter taken to calculate the total capacity.

However, it should be noted that the approach proposed can be applied if the vehicle's total capacity is determined with the same standardized space for one standing passenger. In some cases, it may differ, and gross vehicle weight restrictions may also have an effect.

From a practical viewpoint, the results obtained can be used in determining the optimal frequency and vehicle capacity in public transit lines and choosing the measures for urban transportation crowding reduction. The research direction of the approach may


be the following: crowding cost estimation, modeling of public transportation on-board congestion, modeling of capacity constraints in transit assignment models.

References

1. Cats, O., Hartl, M.: Modelling public transport on-board congestion: comparing schedule-based and agent-based assignment approaches and their implications. *J. Adv. Transp.* **50**(6), 1209–1244 (2016). <https://doi.org/10.1002/atr.1398>
2. Qu, H., Xu, X., Chien, S.: Estimating wait time and passenger load in a saturated metro network: a data-driven approach. *J. Adv. Transp.* **2020**, 4271871 (2020). <https://doi.org/10.1155/2020/4271871>
3. Noursalehi, P., Koutsopoulos, H.N., Zhao, J.: Predictive decision support platform and its application in crowding prediction and passenger information generation. *Transp. Res. Part C: Emerg. Technol.* **129**, 103139 (2021)
4. Yap, M., Cats, O., van Arem, B.: Crowding valuation in urban tram and bus transportation based on smart card data. *Transportmetrica A: Transport Sci.* **16**(1), 23–42 (2020). <https://doi.org/10.1080/23249935.2018.1537319>
5. Márquez, L., Alfonso, J.V., Poveda, J.C.: In-vehicle crowding: Integrating tangible attributes, attitudes, and perceptions in a choice context between BRT and metro. *Transp. Res. Part A: Policy Pract.* **130**, 452–465 (2019). <https://doi.org/10.1016/j.tra.2019.09.061>
6. Yan, S., Cao, J., Zhao, Z.: Seating Provision and Configuration of a 12m City Bus Considering Passenger Crowding. *Int. J. Automot. Technol.* **21**(5), 1223–1231 (2020). <https://doi.org/10.1007/s12239-020-0116-6>
7. Li, Z., Hensher, D.A.: Crowding in public transport: a review of objective and subjective measures. *J. Public Transp.* **16**(2), 107–134 (2013). <https://doi.org/10.5038/2375-0901.16.2.6>
8. Börjesson, M., Rubensson, I.: Satisfaction with crowding and other attributes in public transport. *Transp. Policy* **79**, 213–222 (2019). <https://doi.org/10.1016/j.tranpol.2019.05.010>
9. Wang, B., Zacharias, J.: Noise, odor and passenger density in perceived crowding in public transport. *Transp. Res. Part A: Policy Pract.* **135**, 215–223 (2020). <https://doi.org/10.1016/j.tra.2020.03.013>
10. Haywood, L., Koning, M., Monchambert, G.: Crowding in public transport: Who cares and why? *Transp. Res. Part A: Policy Pract.* **100**, 215–227 (2017). <https://doi.org/10.1016/j.tra.2017.04.022>
11. Basu, D., Hunt, J.D.: Valuing of attributes influencing the attractiveness of suburban train service in Mumbai city: A stated preference approach. *Transp. Res. Part A: Policy Pract.* **46**(9), 1465–1476 (2012). <https://doi.org/10.1016/j.tra.2012.05.010>
12. Batarce, M., Muñoz, J.C., de Dios Ortúzar, J., et al.: Use of mixed stated and revealed preference data for crowding valuation on public transport in Santiago, Chile. *Transp. Res. Record* **2535**(1), 73–78 (2015). <https://doi.org/10.3141/2F2535-08>
13. Batarce, M., Muñoz, J.C., de Dios Ortúzar, J.: Valuing crowding in public transport: Implications for cost-benefit analysis. *Transp. Res. Part A: Policy Pract.* **91**, 358–378 (2016). <https://doi.org/10.1016/j.tra.2016.06.025>
14. Lin, H., Tang, C.: Analysis and optimization of urban public transport lines based on multiobjective adaptive particle swarm optimization. *IEEE Transactions on Intelligent Transportation Systems*, 1–13 (2021). <https://doi.org/10.1109/TITS.2021.3086808>
15. Börjesson, M., Fung, C.M., Proost, S.: Optimal prices and frequencies for buses in Stockholm. *Econ. Transp.* **9**, 20–36 (2017). <https://doi.org/10.1016/j.ecotra.2016.12.001>
16. Shao, M., Xie, C., Li, T., Sun, L.: Influence of in-vehicle crowding on passenger travel time value: Insights from bus transit in Shanghai, China. *Int. J. Transp. Sci. Technol.* 1–13 (2021). <https://doi.org/10.1016/j.ijst.2021.09.001>



A Formal Method of Trust Computation in VANET: A Spatial, Temporal and Behavioral Approach

Abdullah Alharthi^{1,2}(✉) , Qiang Ni¹ , Richard Jiang¹ ,
and Mohammad Ayoub Khan² 

¹ Lancaster University, Lancaster LA1 4WY, UK
a.m.alharthi@lancaster.ac.uk

² University of Bisha, Bisha 67714, Saudi Arabia
amallharthy@ub.edu.sa

Abstracts. VANETs (vehicular Ad-hoc Networks) are a subclass of Mobile Ad-hoc Networks (MANETs) that are currently playing a key role in Intelligent Transportation Systems (ITS). A VANET is a vehicle-assisted network that develops a dynamic topology over time. VANETs are developed to assist two sorts of applications: safety and non-safety. Non-safety applications ensure that vehicle occupants travel in safety and have access to essential entertainment, whereas safety applications are designed to protect people and public property. The existing VANET requirements are concerned with privacy and security issues, but they don't address how to assess the behavior of certified vehicles. A valid vehicle, for instance, could broadcast inaccurate data to a central monitoring system, causing the system to make an erroneous decision. Improved traffic safety and efficiency can be achieved via the use of VANET. However, in an untrusted environment, vehicles have difficulty determining the legitimacy of incoming messages. Trust, data accuracy, and dependability of data being broadcasted via the communication channel are the primary challenges in VANET. Depending on a variety of characteristics, vehicles can determine how trustworthy a given vehicle is based on how well it processes the received message. Therefore, a formal method of trust computation of vehicles is needed. The proposed framework is based on the spatial, temporal and behavioral parameters such as reputation, message correctness, participation degree, message similarity, message freshness, and vehicle age to compute the trust.

Keywords: Formal method · Trust · Reputation · VANET

1 Introduction

The origin of VANET (Vehicular Ad Hoc Networks) is the “Internet of Things (IoT).” The IoT is the major technology of driving autonomously. The Internet of vehicle (IoV) system integrates inter-vehicular communication and improved communication technology site [1]. The three main communication components of the VANET system are vehicular mobile internet, intra-vehicular communication, and inter-vehicular communication [2].

A major trend in the environment of IoV is the addressing of communication mishaps amongst different devices in various domains like safety, traffic control, and infotainment. Communication applications are limited in their interoperability due to the issues concerning availability, privacy, and accessibility. This is why the applications operate independently. So many attempts have been made to increase interoperability and reduce application complexity [3–5]. The various attempts pay attention to developing multiple interaction platform frameworks that enable various devices and vehicles to communicate on the IoV environments. The major types of vehicular communication include vehicle-to-vehicle (V2V), vehicle-to-infrastructure (V2I), and vehicle-to-cloud (V2C).

This had to do with exchanging information wirelessly about the position and speed of surrounding vehicles to avoid crashes, ease congestion and improve the environment. Every node will send, retransmit signals, and a mesh network, meaning every node (car, smart traffic signal, etc.) could send, capture, and retransmit signals [6]. It is essential for developing countries [7].

In the field of Intelligent Transportation Systems (ITS), VANETs are a subclass of IoT, which are now playing an important role in the development of new technologies. The VANET generates a dynamic topology over time with the use of vehicles (Fig. 1). VANETs are being developed to assist with two types of applications: those requiring safety and those requiring non-safety. In contrast to non-safety applications, which are intended to keep vehicle safe while also providing them with vital entertainment, safety applications are intended to keep people and public resources safe. OBUs (Onboard Units) and RSUs (Road-side Units) are the two primary types of VANET units, with the former being the more common (RSUs). RSUs are stationed at the side of the road, whereas OBUs are mounted within the cars themselves. In addition to privacy and security concerns, the present VANET regulations do not address how to evaluate the performance of approved cars. When a genuine car broadcasts malicious data to a central monitoring system, the system may make an incorrect decision, resulting in the vehicle being towed. These attacks not only have the potential to damage transportation efficiency, but they may also result in accidents that put people's lives in danger. A trust system must be established in order for VANETs to function properly. In order to compute each car's associated trust value, a system would need to be able to identify each vehicle, and developing a pseudonyms method that would operate well inside a reputation system is a challenging challenge to solve successfully.

Many trust computing approaches have been proposed in the existing literature; however, they don't provide a general paradigm for trust calculation in the VANET environment. Due to the VANET platform, it is essential that all components of trust be specified, including knowledge gathering, processing and the generation of quantifiable value in the process.

We have proposed trust metrics for spatial knowledge, temporal experience, and behavior pattern based on a large number of trust attributes to represent the characteristics and experiences of the vehicle during the interaction in the network. To evaluate the proposed method, we have generated the dataset which describe most of the scenario of the vehicle in the network. Thereafter, the proposed method is applied to obtain the reputation of the vehicle.

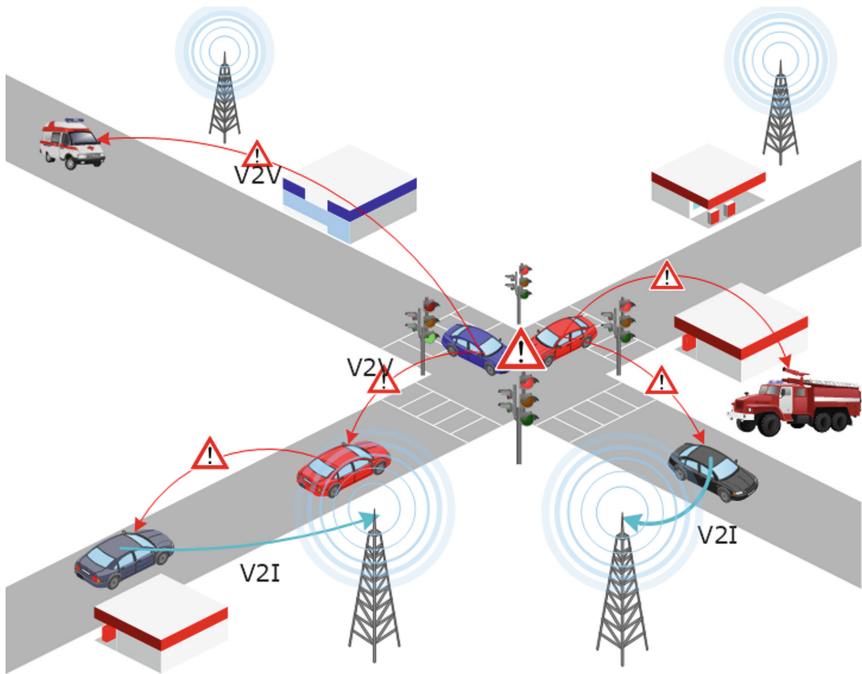


Fig. 1. Communication model in VANET

The rest of this paper is organized as follow: Sect. 2, presents the background and related work in the trust computation. Section 3 presents the proposed formal method to compute the trust. Section 4 presents the dataset generation and reputation obtained from the dataset. Finally, Sect. 5 presents conclusion.

2 Background and Related Work

Trust management has the potential to be a cost-effective solution for addressing VANET security and privacy issues. Through the formal methods of a trust management system that is based on reputation and identity evaluation, it may be able to reward trustworthy cars while flagging untrustworthy vehicles in VANETs, therefore assuring trustworthy message broadcasting. The centralised and distributed forms of trust management may be classified into two categories: centralized trust management and distributed trust management [8]. Within the centralised architecture [9–11], trust management is managed by one or more centralised servers. When it comes to administering centralised servers, however, a large number of resources are required, and the server itself is open to attacks by malicious individuals who may cause major issues as a result of single points of failure. Instead of a centralized approach, researchers [12–14] have attempted to solve these difficulties through the use of a distributed architecture in which trust is measured by RSU rather than a centralized one. In order to overcome the problem of single points of failure, the distributed model has implemented a system in which the communication ranges of each RSU are largely responsible for trust management.

By identifying dishonest vehicles and removing compromised messages from the network, VANET's trust and reputation models are designed to provide secure and reliable data distribution. Yang et al. [15] proposed a VANET architecture based on similarity-based trust and reputation, which necessitated the verification of messages after they arrived. To determine the degree of similarity between unrelated non-linear datasets, the authors have employed a similarity mining approach. Agents' suggestions and outcomes were merged in a reputation evaluation model. Instantly, the trust and reputation values of a communication are affected when the message content is reviewed. BARS (blockchain-based anonymous reputation system) introduced in [16], is another method for trust management. It uses two forms of blockchain authentication: presence-based and absence-based. Pseudonyms are assigned to the public keys in order to protect the privacy of the vehicles. The broadcast messages stored on a single blockchain define a vehicle's reputation. Researchers found that BARS can increase broadcast message reliability while safeguarding driver privacy at the same time. The Lightweight Self-Organized Trust (LSOT) structure is recommended by the authors of [17]. In this paradigm, trust certificates and suggestions are collected by self-organizing nodes. ART (Attack-Resistant Trust) was proposed by Li and Song [18] to measure the trustworthiness of data and vehicles in VANETs. In VANETs, node trust is used to assess the trustworthiness of nodes, whereas data trust is used to validate data. The ART model was put to the test to see if it could ward off harmful attacks, and the results show that it can. Based on reputation, experience, and knowledge, [19] provides three trust indicators. To date, the vehicle's reputation reflects its ability to exchange data with all relevant systems. The experience component takes into account how well the trustee and the trustor have been able to communicate thus far. Direct trust is established by the trustee's knowledge. An augmentation of the natural deduction calculus unsecured by Primiero et al. [20] was offered as a proof-theoretic model for trust and reputation in VANETs. Consistency checks were done at each vehicle-algorithm contact to ensure that the algorithm worked as intended. A temporal metric was used to rate the service qualities based on parameterized feedback messages, as a consequence of this reputation system. Data interchange on VANETs, as well as the maintenance of trust, was the subject of work by Javaid et al. [21]. Using a cryptographic fingerprint, the DrivMan system verifies the authenticity of each vehicle's data. In order to secure the privacy of vehicles, infrastructure units provide certificates. Data integrity and uniqueness may be provided by DrivMan in VANETs to ensure the secure and reliable operation of intelligent cars.

3 Formal Method

Trust is built on many dimensions throughout the time. After each new communication with vehicle, trust scores are automatically updated. In the trust computation a new interaction is evaluated, computed, and experienced. Therefore, the formal models are necessary because they specify the trust qualities or characteristics that are universally recognized (Khan et al., 2018). In order to value the trust score, only the data generated by vehicle may be directly used. As a result, it appears to be critical to specify the scope, duration, and context of the trust. The trustworthiness of a vehicle device may be defined as follows.

Definition: The trust T_{ij} of a vehicle V_i is defined as $T \in [0, 1]$ which is evaluated by the vehicle i based on the existing knowledge, interactions and behavior in a specific context and time. Depending on the interaction between the vehicles in the network, the trust score may be different. If two vehicles have different experience after interaction, their trust in the vehicle and its interactions might be different. A trust score is therefore a mix of the vehicle specific attributes and the interaction factors. The quality of the interaction and the trust score are both affected by the score T , which expresses the distinctive characteristic score value of the vehicle.

A weight w can be used to indicate the importance of a given characteristics. Hence, each individual vehicle trust may be represented using the (1).

$$Trust (V_i^j) = \prod_{j=1}^n (T_{ij})^{w_n}, j = 1, 2, 3, \dots, n. \tag{1}$$

The trust T_{ij} of vehicle i computed by vehicle j is based on existing reputation $R_{i,j}^{(n-1)}$ of vehicle defined in (2) and (3).

$$T_{ij} = f_T(R_{i,j}^{(n)}), \quad 0 < R_{i,j}^{(n)} \leq 1, \tag{2}$$

$$T_{ij} = \begin{cases} 0, & R_{i,j}^{(n)} < t_h \\ 1, & R_{i,j}^{(n)} > t_h \end{cases} \quad T_{ij} [0, 1]. \tag{3}$$

Average Trust: Average trust of vehicle i can be computed by summing all the trust values given by n vehicles as shown in (4):

$$T_{ij} = \frac{\sum_{j=1}^n T_{ij}}{n}. \tag{4}$$

Reputation: The proposed reputation model offers a unique approach based on spatial, temporal and behavioral aspects such as participation degree, vehicle age, and computation of vehicle reputation. The reputation $R_{i,j}^{(n)}$ sss of the vehicle i computed by vehicle j for the n^{th} message at time t is the correctness of the message C_t^i , age α , participation degree θ , the smoothing coefficient β , and existing reputation $R_{i,j}^{(n-1)}$ which can be computed by (5)

$$R_{i,j}^{(n)} = \begin{cases} \alpha + \theta + (\beta R_{i,j}^{(n-1)} + (1 - \beta) C_t^i), & n > 1, \\ \alpha + \theta + C_t^i, & n = 1, \end{cases} \tag{5}$$

where

$$\left\{ \begin{array}{l} \alpha = (t - t_{Reg}) + (t - t_0), \\ \theta = \frac{N^+}{N}, \\ N = N^+ + N^-, \\ N^+ = \sum_{k=1}^n M_k, N^- = \sum_{l=1}^n M_l, N > 0, \\ C_t^i = f_c(M), C_t^i \in [0, 1], \end{array} \right.$$

$$f_c(M) = S(M_i, M_j)w_1 + f_f(M_i)w_2 + f_d(M_i, M_j)w_3. \tag{6}$$

The trust of all the vehicles can be stored into $n \times n$ matrix as follows:

	V_1	V_2	V_3	V_n
V_1	T_{11}	T_{12}	T_{13}	T_{1n}
V_2	T_{21}	T_{22}	T_{23}	T_{2n}
V_3	T_{31}	T_{32}	T_{33}	T_{3n}
...
V_n	T_{n1}	T_{n2}	T_{n3}	T_{nn}

The trust of a vehicle i computed by vehicle j at time t is represented by the T_{ij}^t . After extracting the trust feature vector X_j , every pair of the vehicle can be represented as shown in (7) to produce the m samples.

$$[X]_{p \times q} = \left[[\mathbb{S}]^T, [\mathbb{T}]^T, [\mathbb{B}]^T \right] \tag{7}$$

The $\mathbb{S}, \mathbb{T}, \mathbb{B}$ refers to the spatial, temporal and behavioral parameters respectively. The participation degree θ is an important parameter to compute the trust of a vehicle. The participation degree indicates the amount of participation in the network. More participation will indicate that vehicle is active which can be ascertained using the number of messages classified as correct which were sent with respect to the total number of messages sent. The N^+ represents the total number of messages which were classified as correct or positive. The N represents the total number of messages which includes correct and incorrect message. The vehicle age α represents the real of the vehicle and age in the network. The real age refers to the date when vehicle was registered with motor vehicle department (MVD while the network age refers to time elapse between the first participation time t_0 and current participation time t . Vehicle age parameter is providing the real age of the vehicle since started participating in the network. The function of correctness f_c is defined over many parameters such message similarity, freshness of the message, closeness of senders, and authenticity of the message as shown in (6).

4 Results

We have produced data for simulation of proposed formal method which has 24 characteristics, a typical trust computation dataset, as the experimental dataset to demonstrate

the feasibility of our method. Table 1 provides a full description of the dataset. In all, there were a total of 100,000. According to the available statistics, the non-trustworthy vehicle is 2.08661%. A common method for data normalization known as min–max normalization is employed to ensure that all characteristics are consistent. A decimal between zero and one is used to represent each characteristic’s lowest value, while the maximum value is converted to a 1. An Intel Pentium CPU running Python 3.6 was used to execute the simulation (Windows 10 operating system, 2.6 GHz Intel Core i7 processor, 16.0 GB RAM). It has taken into account most of the typical network parameters such as packet length, TTL, total forwarded packets, total backward packets, failure type, option type, road condition, speed, weather, time scenario, lane type, traffic scenario, packet type, and location etc. as shown in Table 1. All the 24 features describe the scenario of a vehicle that constitutes spatial \mathbb{S} , temporal \mathbb{T} and behavior \mathbb{B} parameters. The dataset defines the important numerical attributes which participate in reputation computation are number of packets forwarded, the average size of packet, the time when message has originated, message communication type and status, title to live in the network and the port number.

Table 1. Dataset description

Feature	Details
source	IP address of the source vehicle
destination	IP address of the destination vehicle
detection_target	IP address of the detection node
destination_port	Destination port address
Total_Fwd_Packets	Total number of forwarded packets
Total_Bkwd_Packets	Total number of backward packets
Total_Length_of_Fwd_Packets	Size of the forwarded packets
Total_length_of_Bkwd_Packets	Size of backward packets
Flow_Packet_Per_Second	Flow per second of packet
Average_packet_Size	Average size of the packet
Time_Stamp	Time when packet originated
TTL	Title to live
Reputation	Reputation of the sender
OT	0: default, 1 request, 2 reply, 3 transmission result
Failure	0: no malicious behavior, 1: malicious behavior), 2: Failure caused by non-malicious behaviours. 3: transmission result
Road_Condition	‘Dry’, ‘wet’, ‘Icy’

(continued)

Table 1. (continued)

Feature	Details
Speed Scenario	'Accelerating', 'constant', 'Deaccelerating'
Time_Scenario	'Dawan', 'Day', 'Dusk', 'Night'
Weather Scenario	'Clear', 'Foggy', 'Raining', 'Snowing', 'Windy'
Lane_Type	'Winding', 'UpHill', 'Straight', 'Intersection', 'Curve', 'DownHill'
Traffic_Scenario	'Car on 1 side', 'Car on 2 sides', 'Car on 3 sides', 'Car on 4 sides', 'No cars'
Packet_Type	'General', 'Safety', 'Traffic'
Latitude, Longitude	Position of vehicle

Table 2. Sample output of the reputation computation

IP address	Port	Time stamp	TTL	Reputation
20.100.168.125	4244	Thu Jan 27 02:32:40 2022	147	0.947461244
20.100.168.34	2624	Thu Jan 27 02:32:40 2022	86	0.61587248
20.100.168.177	1064	Thu Jan 27 02:32:40 2022	116	0.656448565
20.100.168.187	1892	Thu Jan 27 02:32:40 2022	221	0.593758417
20.100.168.210	3417	Thu Jan 27 02:32:40 2022	213	0.995342545
20.100.168.95	1260	Thu Jan 27 02:32:40 2022	218	0.615054778
20.100.168.228	2221	Thu Jan 27 02:32:40 2022	162	0.834318201
20.100.168.171	4892	Thu Jan 27 02:32:40 2022	171	0.443103195
20.100.168.4	1329	Thu Jan 27 02:32:40 2022	242	0.921932154
20.100.168.11	3739	Thu Jan 27 02:32:40 2022	202	0.897358896
20.100.168.105	3951	Thu Jan 27 02:32:40 2022	255	0.703708723
20.100.168.236	2959	Thu Jan 27 02:32:40 2022	138	0.221071998
20.100.168.90	1316	Thu Jan 27 02:32:40 2022	161	0.913946538
20.100.168.53	4766	Thu Jan 27 02:32:40 2022	111	0.724440567
20.100.168.225	4510	Thu Jan 27 02:32:40 2022	112	0.324995418
20.100.168.230	2240	Thu Jan 27 02:32:40 2022	171	0.444987762
20.100.168.192	2768	Thu Jan 27 02:32:40 2022	104	0.679105299
20.100.168.52	1064	Thu Jan 27 02:32:40 2022	218	0.361281827
20.100.168.167	3071	Thu Jan 27 02:32:40 2022	173	0.297529623
20.100.168.114	3443	Thu Jan 27 02:32:40 2022	220	0.438722483
20.100.168.115	2145	Thu Jan 27 02:32:40 2022	70	0.780719787

(continued)

Table 2. (continued)

IP address	Port	Time stamp	TTL	Reputation
20.100.168.223	2311	Thu Jan 27 02:32:40 2022	184	0.519106395
20.100.168.33	3110	Thu Jan 27 02:32:40 2022	243	0.597114853
20.100.168.121	4671	Thu Jan 27 02:32:40 2022	114	0.655051857
20.100.168.106	4468	Thu Jan 27 02:32:40 2022	156	0.813050019
20.100.168.76	2328	Thu Jan 27 02:32:40 2022	140	0.31932139
20.100.168.110	3498	Thu Jan 27 02:32:40 2022	168	0.265870971

5 Conclusion

The primary challenge in the upcoming VANET infrastructure is about the trust of vehicle. Depending on a variety of characteristics, vehicles can determine how trustworthy a given vehicle is based on how well it processes the received message. These characteristics can be categorized into spatial, temporal and behavioral parameters such as reputation, message correctness, participation degree, message similarity, message freshness, and vehicle age to compute the trust. Therefore, it becomes critical to compute trust and reputation in a vehicular network. This is why trust computation and categorization are so critical to the security of the vehicular network. The dynamic nature of trust and reputation data, as opposed to static data, creates new issues for existing systems. Thus, in this work a formal method of trust computation of vehicles has been proposed. To verify the correctness of method the dataset is generated and thereafter reputation has been computed.

References

1. Gandhi, M., Khan, M.A.: Performance analysis of metrics of broadcasting protocols in VANET. In: 2014 Innovative Applications of Computational Intelligence on Power, Energy and Controls with their impact on Humanity (CIPECH), pp. 315–321. IEEE, Ghaziabad (2014). <https://doi.org/10.1109/CIPECH.2014.7019048>
2. Xu, L., Zhou, X., Khan, M.A., et al.: Communication quality prediction for Internet of vehicle (IoV) networks: an elman approach. *IEEE Trans. Intell. Transport. Syst.* **23**, 19644–19654 (2021). <https://doi.org/10.1109/TITS.2021.3088862>
3. Khan, W.U., Li, X., Ihsan, A., et al.: NOMA-enabled optimization framework for next-generation small-cell IoV networks under imperfect SIC decoding. *IEEE Transactions on Intell. Transport. Syst.* 1–10 (2021). <https://doi.org/10.1109/TITS.2021.3091402>
4. Nanjie, L.: Internet of Vehicles your next connection. *WinWin Magazine* 11, (2011)
5. Wan, J., Zhang, D., Zhao, S., et al.: Context-aware vehicular cyber-physical systems with cloud support: architecture, challenges, and solutions. *IEEE Commun. Mag.* **52**(8), 106–113 (2014). <https://doi.org/10.1109/MCOM.2014.6871677>
6. Howard, B.: V2V: What are vehicle-to-vehicle communications and how do they work? *Extreme Tech.* <https://www.extremetech.com/extreme/176093-v2v-what-are-vehicle-to-vehicle-communications-and-how-does-it-work>. Accessed 25 May 2022

7. Zorkany, E.M.: Vehicle To Vehicle “V2V” Communication: Scope, Importance, Challenges. Research Directions and Future. Benthanopen. <https://benthamopen.com/FULLTEXT/TOTJ-14-86>. Accessed 25 May 2022
8. Lu, Z., Qu, G., Liu, Z.: A survey on recent advances in vehicular network security, trust, and privacy. *IEEE Trans. Intell. Transp. Syst.* **20**(2), 760–776 (2018). <https://doi.org/10.1109/TITS.2018.2818888>
9. Li, X., Liu, J., Li, X., Sun, W.: RGTE: A reputation-based global trust establishment in VANETs. In: 2013 5th International Conference on Intelligent Networking and Collaborative Systems, pp. 210–214. IEEE, Xi’an (2013). <https://doi.org/10.1109/INCoS.2013.91>
10. Li, Q., Malip, A., Martin, K.M., et al.: A reputation-based announcement scheme for VANETs. *IEEE Trans. Veh. Technol.* **61**(9), 4095–4108 (2012). <https://doi.org/10.1109/TVT.2012.2209903>
11. Bißmeyer, N., Njeukam, J., Petit, J., Bayarou, K.M.: Central misbehavior evaluation for vanets based on mobility data plausibility. In: Proceedings of the Ninth ACM International Workshop on Vehicular Inter-Networking, Systems, and Applications, pp. 73–82. ACM (2012). <https://doi.org/10.1145/2307888.2307902>
12. Raya, M., Papadimitratos, P., Gligor, V.D., Hubaux, J.P.: On data-centric trust establishment in ephemeral ad hoc networks. In: IEEE INFOCOM 2008-The 27th Conference on Computer Communications, pp. 1238–1246. IEEE, Phoenix (2008). <https://doi.org/10.1109/INFCOM.2008.180>
13. Monir, M., Abdel-Hamid, A., El Aziz, M.A.: A categorized trust-based message reporting scheme for VANETs. In: Awad, A.I., Hassanien, A.E., Baba, K. (eds.) *Advances in Security of Information and Communication Networks. SecNet 2013*. CCIS, vol. 381, pp. 65–83. Springer, Berlin, Heidelberg (2013). https://doi.org/10.1007/978-3-642-40597-6_6
14. Huang, X., Yu, R., Kang, J., Zhang, Y.: Distributed reputation management for secure and efficient vehicular edge computing and networks. *IEEE Access* **5**, 25408–25420 (2017). <https://doi.org/10.1109/ACCESS.2017.2769878>
15. Yang, N.: A similarity based trust and reputation management framework for VANETs. *Int. J. Future Generation Commun. Network.* **6**(2), 25–34 (2013)
16. Lu, Z., Wang, Q., Qu, G., Liu, Z.: BARS: A blockchain-based anonymous reputation system for trust management in VANETs. In: 2018 17th IEEE International Conference On Trust, Security And Privacy In Computing And Communications/12th IEEE International Conference On Big Data Science And Engineering (TrustCom/BigDataSE), pp. 98–103. IEEE, New York (2018). <https://doi.org/10.1109/TrustCom/BigDataSE.2018.00025>
17. Liu, Z., Ma, J., Jiang, Z., et al.: LSOT: a lightweight self-organized trust model in VANETs. *Mob. Inf. Syst.* **2016**, 7628231 (2016). <https://doi.org/10.1155/2016/7628231>
18. Li, W., Song, H.: ART: an attack-resistant trust management scheme for securing vehicular ad hoc networks. *IEEE Trans. Intell. Transp. Syst.* **17**(4), 960–969 (2015). <https://doi.org/10.1109/TITS.2015.2494017>
19. Truong, N.B., Lee, G.M.: Trust evaluation for data exchange in vehicular networks. In: 2017 IEEE/ACM Second International Conference on Internet-of-Things Design and Implementation (IoTDI), pp. 325–326. IEEE, Pittsburgh (2017)
20. Primiero, G., Raimondi, F., Chen, T., Nagarajan, R.: A proof-theoretic trust and reputation model for VANET. In: 2017 IEEE European Symposium on Security and Privacy Workshops (EuroS&PW), pp. 146–152. IEEE, Paris (2017). <https://doi.org/10.1109/EuroSPW.2017.64>
21. Javaid, U., Aman, M.N., Sikdar, B.: DrivMan: Driving trust management and data sharing in VANETS with blockchain and smart contracts. In: 2019 IEEE 89th Vehicular Technology Conference (VTC2019-Spring), pp. 1–5. IEEE, Kuala Lumpur (2019). <https://doi.org/10.1109/VTCSpring.2019.8746499>



Research of the Freight Trains Movement Stability with a Network Effect

Andrii Prokhorchenko , Mikhail Kravchenko , Olena Malakhova ,
Grygorii Sikonenko , and Halyna Prokhorchenko  

Ukrainian State University of Railway Transport, 7 Feyerbakh Square, Kharkiv 61050, Ukraine
prokhorchenko@kart.edu.ua

Abstract. In the article for railway systems of mixed traffic without observing the movement of freight trains, the stability of the movement of freight trains was researched, with a network effect. Models of the influence of research parameters, the intensity of traffic and the average mass of trains for the total duration of trains were found. Based on correlation analysis and hierarchical clustering, the influence of these parameters on the total duration of trains along the main lines at the railway region is numerically proved. Based on the results of the analysis of Dendrograms, clusters of the interdependence of lines with various routes on the network were identified. From the analysis of the hierarchical structure of clusters, a clear division into two groups can be observed, depending on the existence of a positive and negative correlation. The lines and routes that most affect the stability of train movement are determined. The results of hierarchical clustering prove that as the mass of trains increases, the duration on the route is reduced. The proposed methodology and the results will allow you to form more complex management strategies at tactical and strategic levels for railway systems without observing the traffic schedule.

Keywords: Railway system · Stability · Clusterogram

1 Introduction

For effective transport systems, including railway [1–4], it is important to have the ability to function without changing operational indicators, to be equilibrium and maintain constant time. Nevertheless, railway systems with a predominant cargo traffic in peak periods of loads fall to a high level of disorganization of traffic schedule – congestion on the overloaded network lines are created, cargo delivery time is increased, which violates the stability of traffic flow, and, as a result, leads to losses. Such railway systems include the railways of North America, China, India, Kazakhstan, Ukraine and similar to them in many other countries of the world. A separate difficulty in ensuring the stability of traffic arises in railway systems without observing the movement of freight trains, where trains are sent after performing normative technological operations, do not comply with a clearly established movement schedule. This is the so-called principle of departure by “readiness” [5, 6]. Such systems differ from railway systems with a graph

of freight trains of countries such as Germany, France, Great Britain, Poland and the like. Compliance with the normative schedule of train movement allows you to study accurately the influence of various factors on the stability of the movement of traffic flows. Considering that the lack of a traffic schedule for trains leads to a significant uncertainty of the transportation process, which is difficult to foresee, the study of the stability of the movement of freight trains is more complex and little researched. Therefore, studies aimed at determining the causes that lead to overloading the railway network and, as a result, to violation of the stability of the movement of freight trains, are relevant.

The problem of researching the stability of the movement of traffic flows is considered in scientific work in several main areas. In the first direction of the study, they are aimed at studying the influence of the mass and speed of trains on the stability of the movement of traffic flows. In these studies, the main attention is paid to the physical parameters that affect the movement of the train, the technical properties of traction and economic criteria. Thus, the paper [7] proposes a methodology for determining the optimization of the mass of the train, depending on the profile of the track and parameters of the locomotive to ensure stable parameters of the trips on the line. The papers [8, 9] examine the change in the speed of the train that moves on the line as a stochastic process based on dynamic modeling of movement. The formation of train delays depending on the speed of movement is researched in papers [10, 11]. The research of [12] is interesting, which is devoted to the study of the interdependence of the density and intensity of the train on the basis of the principles of the Fundamental Diagram of Traffic Flow [13]. The construction of the relationship is made for two interval traffic control systems: Discrete Control Blocks and Moving Blocks. The authors note that the results of the research can be used to analyze the stability of trains in the route in different trains management systems and in operating conditions quickly. Nevertheless, research data is devoted to the study of the influence of various factors on the stability of the movement of train flow only in a separate area. This is a disadvantage and does not allow comprehensively evaluate the mutual influence of movement parameters on an extensive network, taking into account the network effect [14].

The second direction corresponds to the task of ensuring the stability of movement based on the optimization of train parameters for the effective use of the capacity and carry ability of the railway infrastructure. The paper [15] examine the effect of trains characteristics with heterogeneous movement on the throughput of sites. In paper [16], it proposes to use the metaheuristic model of annealing to rationalize trains of various categories to increase absolute throughput. In paper [17], the methodological approaches to the determination of capacity are sore and each influencing factor is separately analyzed in the details, which ensures the stability of the train.

We can share a direction dedicated to increasing the stability of transportation by searching for rational routes and a train schedule. These methods are used in conditions of restrictions on the development of railway infrastructure. In paper [18], a train method is proposed to select the route of each train on the railway region, taking into account the stability of the train. In paper [19] for choosing a route offers a model of integer programming to simultaneous determination of the route of the movement and schedule based on spatial-temporal modeling. This approach allows you to take into account the change in network loading during different periods of transportation. The paper of [20]

is devoted directly to evaluation of the stability of the movement schedule on the line, depending on the complexity of operations. It is proposed to investigate the stability of the schedule, taking into account the number of conflicts. The paper [21] uses the theory of stability for analyzing schedules for sensitivity and resistance to delays train based on a linear systematic description of the railway schedules using the mathematical apparatus of Max-Plus System theory. The advantage of this method is the ability to take into account the network effect, but its use is limited only by the study of processes in railway systems in compliance with the schedule.

From the above analysis, we can conclude that researches based on an integrated approach to the recovery of the interdependence of the parameters of traffic flows on their overall stability on the main routes are practically absent. The purpose of this research is to determine the causes of a violation of the stability of movement, taking into account the network effect and theoretical substantiation of the effects of the parameters of traffic flows, such as the intensity and mass of trains, on the stability of the movement of freight flows on the key routes of the railway training region.

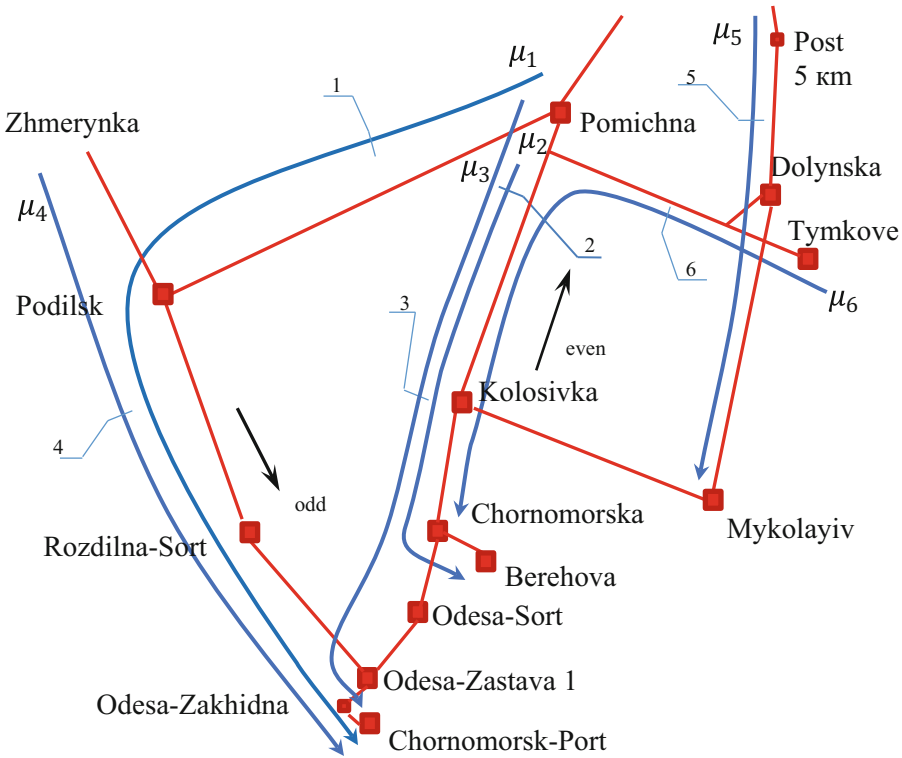
The remainder of this article is organized as follows. In Sect. 2, we explain in detail the proposed methodology. The results of the calculations of clusterograms of the interconnection of the intensity of traffic and the average mass of trains in the researched lines for the total duration of trains along the main routes are presented in Sect. 3. Finally, we will discuss the results in the last section.

2 Proposed Methodology

This goal was achieved by studying the mutual influence of traffic flows on a freight railway region based on the macro - core approach. In this research, under the stability of the movement of freight trains, the ability of the railway system is functioning, without changing on the main routes of the standards for the duration of cargo, even in the conditions of the system violation - overload of the system during the peak loading season. Ensuring this duration of traffic flows on the main routes in different periods of transportation during the freight year can be considered as finding the railway system in equilibrium and the availability of the opportunity to maintain stability over time.

Based on the previous analysis of operating conditions, it was found that usually on the extensive infrastructure of the railway network, the routes of the main routes are intersected and duplicated, and therefore one can evaluate their relationship and take into account the so-called “network effect” [14].

Considering that the railway system of Ukraine refers to vertically integrated railway roads of mixed traffic without observing the movement of freight trains, it is proposed to take a separate iron training ground for research. One of the “narrow places” of the joints of the railway systems of Ukraine with the largest sea ports of the country is the training ground of the Odessa Railway of Ukrzaliznytsia JSC. The graph of the railway network is shown on Fig. 1.



- 1 - Pidhorodna - Obkhidna;
- 2 - Pomichna-Kolosivka;
- 3 - Kolosivka-Chornomorska;
- 4 - Podilsk-Myhayeve;
- 5 - Post 5 km-Dolynska;
- 6 - Post 124 km-Kropyvnytska

Fig. 1. Graph of the landfill railway network of regional branch of Odesa Railway JSC Ukrzaliznytsia and traffic routes train flow.

The routes of the movement of the train flow μ_i , where $i = \overline{1, 6}$ shown in Fig. 1 with blue arrows, indicate the main directions of the carriage of wagon flowing into seaports. μ_1 – Pomichna – Podilsk – Chornomorsk-Port route; μ_2 – Pomichna – Berehova; μ_3 - Pomichna - Chornomorsk-Port; μ_4 - Podilsk – Chornomorsk-Port, μ_5 - Tymkovo – Chornomorska, μ_6 - Post 5 km – Mykolayiv. It is proposed on each of the μ_i - routes, highlight the line j , where $j = \overline{1, 6}$ which, in its operational conditions, affects the total duration of trains along the route.

Based on previous studies [13] interdependence of the speed of the intensity of trains on the line in the work is proposed to investigate the effect of intensity and a related parameter with a given indicator – the average mass of freight trains for the duration of the traffic freight flow on the route. To take into account the fluctuations of the indicators, data for the period I-III quarters and IV quarter in 2019 and 2020 were used. The fourth quarter characterizes the period of peak load and allows you to identify factors that affect the stability of train flow in the conditions of network overload, which arose in the fourth quarter of 2019. In terms of volume 2019, it was a record for transporting goods

in Ukraine. For analysis, data of the form “CO-4AR” was used. Report on the work and indicators of the use of rolling stock. Section 3. Indicators of the use of rolling stock for train - areas and directions”.

To check the hypotheses about the presence of connections between the variables, the correlation analysis method has been used. Checking existing connections is proposed to be performed on the basis of calculating the Pearson’s correlation coefficient [22]. The advantage of the parametric method of Pearson’s correlation is its simplicity and the speed of establishing the tightness of linear connections, which is sufficient at the first stage of research data. For a more detailed identification of routes with related levels of interdependence, the method of hierarchical clustering is proposed for constructing clusterograms [23] – which is a combined thermal card – dendrogram that allows you to detect the internal interdependence of the studied lines and routes.

Checking the significance of the distinction between the correlation coefficients from zero is performed using the hypothesis of the criterion of the Student – the zero hypothesis is discarded [24]. The established correlations are reliable at $p < 0.05$. The construction of clusterograms is made in the Matlab environment using “Average” connection method [25].

3 Results

Based on the above research methodology in the work, calculations of the clusterogram of the interconnection of the intensity of movement and the average mass of the train in the studied areas for the total duration of traffic flow on the main routes were carried out. In the Fig. 2 shown the dendroting clusterogram of the hierarchical relationship of the number of freight trains that proceeded on the line per day to the total duration of traffic on routes. From the analysis of the hierarchical structure of clusters, a clear division into two groups can be observed, depending on the existence of a positive and negative correlation. The cluster with a negative correlation includes lines 6, 2, 3rd increase in the intensity of traffic flow in these lines, leads to a decrease in the duration of the train on almost all the routes of the test training ground. Lines 1, 5, 4 belong to the cluster with a positive correlation – they can be called critical for the region with negative consequences, since an increase in the intensity of trains on these lenis leads to a slowdown of the movement of the train on almost all routes.

Line 4 – Podilsk-Myhayeve has correlation relations, which can be described as “very significant” with routes μ_3 ($r = 0.87$), μ_1 ($r = 0.88$), μ_4 ($r = 0.92$), μ_5 ($r = 0.98$) Negative correlation ($r = -0.9$), characterized as “very significant” [26], has a line 6 – Post 124 km- Kropyvnytska, which lies on the route Tymkove-Chornomorska, with the route- Pomichna – Podilsk – Chornomorsk-Port (μ_1). This can be explained by the only source of cargo flow, consisting of the cargo of the mining and metallurgical complex and partially during the peak period of loads from grain cargo, which follow from the stations of regional branches of the South, Donetsk and Dnieper Railways (through Pyatykhatky), that is, an increase in the daily number of trains by The line 6 – Post 124 km-Kropyvnytska will affect the intensity and reduce the load of the line on the μ_1 route, and, as a result, the movement of the tribute on this route will accelerate.

Additionally, mutual influence can be explained by the high values of the correlation relations of the μ_1 route with other lines that are indirectly interdependent at different

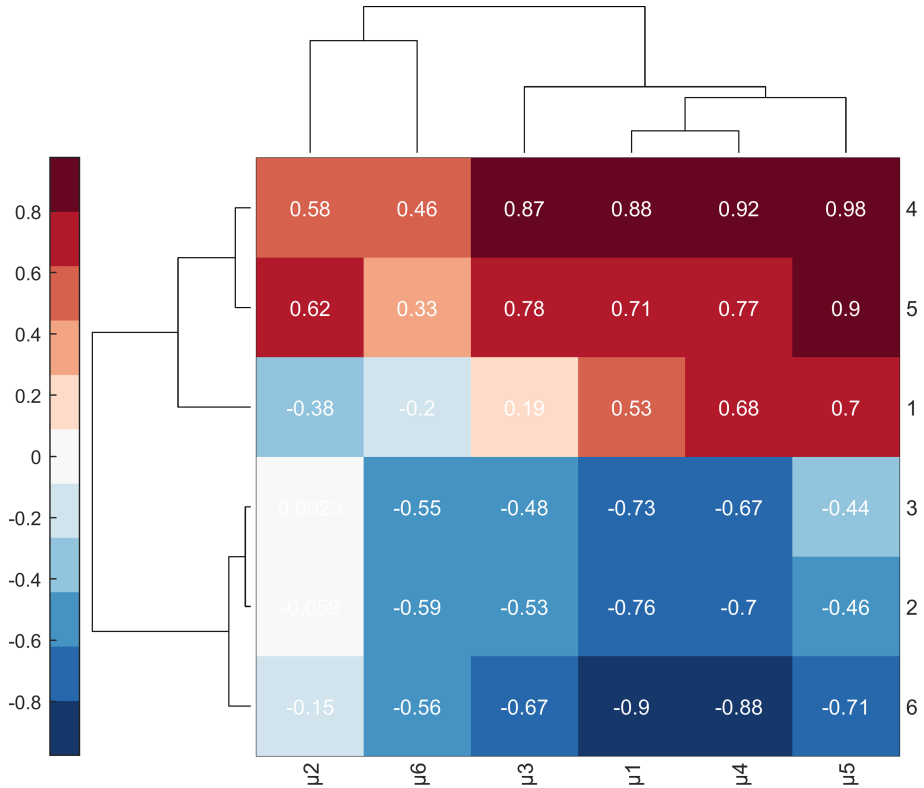


Fig. 2. Clustrogram of the interconnection of the intensity of traffic flow on the routes studied, to the total duration of traffic flow on routes during the I-III and IV quarters of 2019 and 2020.

levels of dendrograms with line 6. Line 4 - Podilsk-Myhayeve has correlation relations, which can be described as “very significant” with routes μ_3 ($r = 0.87$), μ_1 ($r = 0.88$), μ_4 ($r = 0.92$), μ_5 ($r = 0.98$) Negative correlation ($r = -0.9$), characterized as “very significant” [26], has a line 6 - Post 124 km- Kropyvnytska, which lies on the route Tymkove-Chornomorska, with the route - Pomichna – Podilsk – Chornomorsk-Port (μ_1). This can be explained by the only source of cargo flow, consisting of the cargo of the mining and metallurgical complex and partially during the peak period of loads from grain cargo, which follow from the stations of regional branches of the South, Donetsk and Dnieper Railways (through Pyatykhatky), that is, an increase in the daily number of trains by The line 6 – Post 124 km- Kropyvnytska will affect the intensity and reduce the load of the line on the μ_1 route, and, as a result, the movement of the tribute on this route will accelerate. Additionally, mutual influence can be explained by the high values of the correlation relations of the μ_1 route with other lines that are indirectly interdependent at different levels of dendrograms with line 6.

Considering that the average mass of freight trains affects the speed of movement and determines the everyday amount on the line [27] in work, it is proposed to deepen the research. The average mass of freight trains [3500 ÷ 4750 tons] is a controlled

parameter, which interconnects the throughput and defense capacity of the line and the railway region as a whole. The clusterogram of the relationship between the average mass of trains on the lines to the total duration of traffic flows on the routes in which these lines are included in Fig. 3.

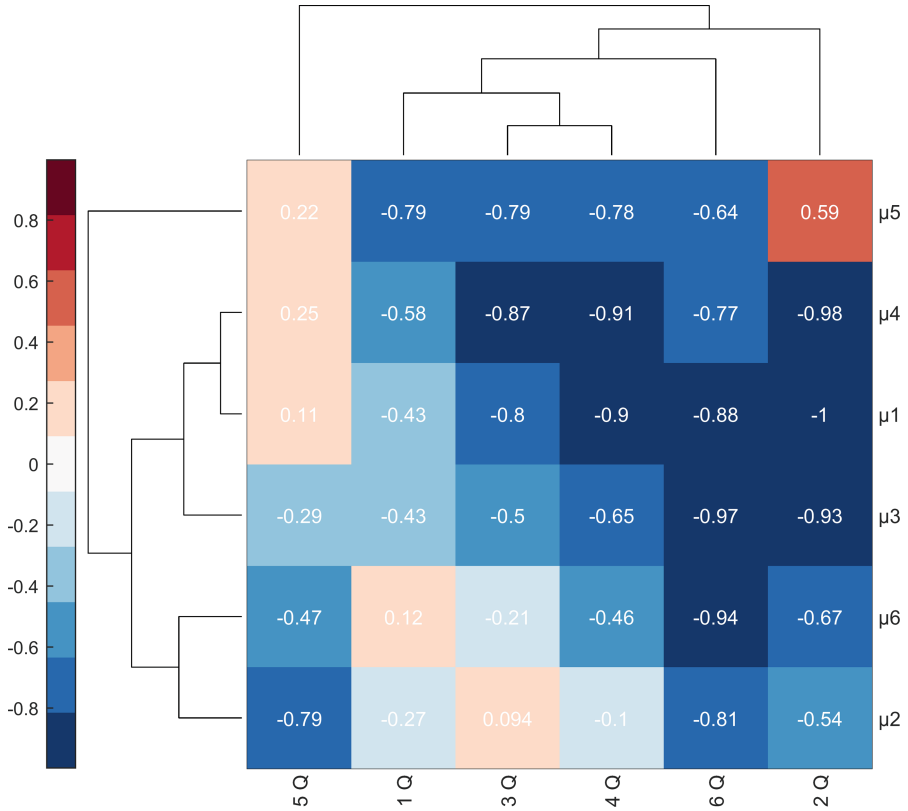


Fig. 3. The clusterogram of the interconnection of the average mass of trains on routes, which are explored for the total duration of trains on the routes of the I-III and IV quarters of 2019 and 2020.

Analysis of the cluster dendrogram of the interconnection of the average mass of trains on routes, which are explored for the total duration of traffic flow on the routes (Fig. 3) showed that at the first level, the μ_3 - Pomichna – Chornomorsk-Port and μ_4 - Podilsk – Chornomorsk-Port are combined along the columns of the correlation matrix. – Podolsk – Chernomorsk-Port. First of all, this is due to the similarity in the technical characteristics of these lines and the similarity of the structure of the freight flow following these routes. At the second level, is added to these clusters the route is poured- μ_1 - Pomichna – Podilsk – Chornomorsk-Port. The proximity of the data of this cluster is explained by the unification of the mass of the trains following the route together – the line 4 Podilsk-Myhayeve.

At the first level of horizontal analysis, the Dendrogram of the Odbvsterates the routes μ_1 Pomichna – Podilsk – Chornomorsk-Port and μ_4 - Podilsk – Chornomorsk-Port, which indicates similar trains conditions, types of traffic schedule and line speed, especially the general part of the route without the priority of the priority vagon flow. The previous clusters with μ_3 - Pomichna – Chornomorsk-Port has a slightly smaller connection (the second level of the association), and a similar degree of distances between the elements has a route μ_2 - Pomichna – Berehova with μ_6 - Post 5 km – Mykolayiv. Clusters μ_2 , μ_3 and μ_2 , μ_3 have a common part of the rout: the line 2 - Pomichna-Kolosivka and the line 3 – Kolosivka – Chornomorska and, accordingly, interdependent conditions of the trains. The rest of the associations should not be taken into account, since the degree of interconnected elements is low, that is, we can talk about the “elbow” of the cluster dendrogram [28].

Analyzing the correlations between the length of stay on the route and the mass of the trains, we can conclude that the data of almost all clusters, except μ_5 , are able to be controlled by controlled parameters. The correlation coefficient on these routes of specified operational indicators varies within $r = [-0.87 \div -1]$, which indicates a significant negative connection. The negative value of the correlation coefficient shows that with an increase in the mass of the train, the total time on the line decreases. Thus, with an increase in the mass of the train on the line 6 - Post 124 km – Kropyvnytska with a high degree of correlation, the travel time on the routes μ_2 ($r = -0,81$), μ_6 ($r = -0,94$), μ_3 ($r = -0,97$) and μ_1 ($r = -0,88$). This is due to the interdependence of the movement of train flow. Since part of the μ_3 route trains follow the routes μ_2 and μ_6 and the degree of correlation is significant (-0.93 and 0.97 accordingly), then an increase in the mass of trains of the cluster μ_3 can positively be displayed on the total time of the train on the line by reducing the number of trains of the third cluster and reducing flow density. This statement is especially important for lines with intensive traffic, which can be attributed the line 2 – Pomichna – Kolosivka and the line 3 – Kolosivka – Chornomorska.

Although the correlation coefficient on the horizontal cluster μ_5 varies in the range from the low ($r = 0,21$) to the negative high ($r = -0,79$), it will not be possible to significantly affect the total time being on the route when the mass of the train increases. This is due to the relatively low intensity of movement - the number of trains varies within $[8.51 \div 14.59]$ trains per day, that is, the departure of trains occurs in a sparse environment.

4 Conclusion

The results of the calculations of clusterograms for the first time numerically allowed us to assess the impact of the intensity of movement and the average mass of trains on the line to the total duration of traffic flow along the main routes at the railway network region, taking into account the network effect. Based on the results of the analysis of dendograms, clusters of the interdependence of lines with various routes on the network were identified. A cluster with a negative correlation is determined, which includes the line 6 - Post 124 km – Kropyvnytska, the line 2 – Pomichna – Kolosivka, the line 3 – Kolosivka – Chornomorska where, increasing the intensity of the train in these areas, leads to a decrease in the duration of the train on almost all routes of region. The results

of hierarchical clustering prove that, with an increase in the mass of the train on the line 6 - Post 124 km – Kropyvnytska with a high degree of correlation, the travel time on the routes μ_2 , μ_6 , μ_3 and μ_1 will be reduced with a high degree of correlation. These results will allow you to form more complex management strategies at the tactical and strategic levels. The proposed method of macroanalysis using the construction of clusterograms of the interconnection of operational indicators of individual lines for the duration of trains on routes allows you to identify the most influencing causes of the stability of the movement of freight trains, taking into account the network effect.

References

1. Boyer, S., Blandin, S., Wynter, L.: Stability of transportation networks under adaptive routing policies. *Transp. Res. Procedia* **7**, 578–597 (2015). <https://doi.org/10.1016/j.trpro.2015.06.030>
2. Iryo, T., Smith, M.J., Watling, D.: Stabilisation strategy for unstable transport systems under general evolutionary dynamics. *Transp. Res. Procedia* **38**, 421–440 (2019). <https://doi.org/10.1016/j.trpro.2019.05.023>
3. Irina, T., Moroz, M., Zahorianskyi, V., et al.: Management of the logistics component of the grain harvesting process with consideration of the choice of automobile transport technology based on the energetic criterion. In: 2021 IEEE International Conference on Modern Electrical and Energy Systems (MEES), Kremenchuk, pp. 1–5. IEEE (2021). <https://doi.org/10.1109/MEES52427.2021.9598768>
4. Masiuk, V., Galan, O., Prokhorchenko, A., Tverdomed, V.: An agent-based simulation for optimizing the parameters of a railway transport system. *CEUR Workshop Proc.* **3013**, 121–128 (2021)
5. Butko, T., Prokhorchenko, A., Golovko, T., Prokhorchenko, G.: Development of the method for modeling the propagation of delays in noncyclic train scheduling on the railroads with mixed traffic. *East. Eur. J. Enterp. Technol.* **1**(3), 30–39 (2018). <https://doi.org/10.15587/1729-4061.2018.123141>
6. Butko, T., Kostienikov, O., Parkhomenko, L., et al.: Forming an automated technology to manage freight transportation along a direction. *East. Eur. J. Enterp. Technol.* **1**(3), 6–13 (2019). <https://doi.org/10.15587/1729-4061.2019.156098>
7. Al-Shumari, A.: Weight and speed optimization for goods trains on cargo-intensive railway sections. In: Manakov, A., Edigarian, A. (eds.) *TransSiberia 2021*. LNNS, vol. 402, pp. 211–220. Springer, Cham (2022). https://doi.org/10.1007/978-3-030-96380-4_24
8. Corman, F., Trivella, A., Keyvan-Ekbatani, M.: Stochastic process in railway traffic flow: models, methods and implications. *Transp. Res. Part C Emerg. Technol.* **128**, 103167 (2021). <https://doi.org/10.1016/j.trc.2021.103167>
9. Huisman, T., Boucherie, R.J.: Running times on railway sections with heterogeneous train traffic. *Transp. Res. Part B Methodol.* **35**(3), 271–292 (2001). [https://doi.org/10.1016/S0191-2615\(99\)00051-X](https://doi.org/10.1016/S0191-2615(99)00051-X)
10. Carey, M., Kwieceński, A.: Stochastic approximation to the effects of headways on knock-on delays of trains. *Transp. Res. Part B Methodol.* **28**(4), 251–267 (1994). [https://doi.org/10.1016/0191-2615\(94\)90001-9](https://doi.org/10.1016/0191-2615(94)90001-9)
11. Xu, X., Li, K., Yang, L., Ye, J.: Balanced train timetabling on a single-line railway with optimized velocity. *Appl. Math. Model.* **38**(3), 894–909 (2014). <https://doi.org/10.1016/j.apm.2013.07.023>

12. de Rivera, A.D., Dick, C.T.: Illustrating the implications of moving blocks on railway traffic flow behavior with fundamental diagrams. *Transp. Res. Part C Emerg. Technol.* **123**, 102982 (2021). <https://doi.org/10.1016/j.trc.2021.102982>
13. Garber, N.J., Hoel, L.A., Rao, K.R.: *Traffic and Highway Engineering*. Cengage Learning, Patparganj (2015)
14. Landex, A., Nielsen, O.A.: Network effects in railway systems. In: 2007 European Transport Conference, Leiden, p. 16 (2007)
15. Dingler, M.H., Lai, Y.C., Barkan, C.P.: Impact of train type heterogeneity on single-track railway capacity. *Transp. Res. Rec.* **2117**(1), 41–49 (2009). <https://doi.org/10.3141/2117-06>
16. Yaghini, M., Nikoo, N., Ahadi, H.R.: An integer programming model for analysing impacts of different train types on railway line capacity. *Transport* **29**(1), 28–35 (2014). <https://doi.org/10.3846/16484142.2014.894938>
17. Černá, L., Ľupták, V., Šulko, P., Blaho, P.: Capacity of main railway lines – Analysis of methodologies for its calculation. *Naše More* **65**(4), 213–217 (2018). <https://doi.org/10.17818/NM/2018/4SI.9>
18. Sama, M., Pellegrini, P., D’Ariano, A., et al.: A routing filter for the real-time railway traffic management problem based on ant colony optimization. *Transp. Res. Procedia* **10**, 534–543 (2015). <https://doi.org/10.1016/j.trpro.2015.09.007>
19. Meng, L., Zhou, X.: Simultaneous train rerouting and rescheduling on an N-track network: a model reformulation with network-based cumulative flow variables. *Transp. Res. Part B Methodol.* **67**, 208–234 (2014). <https://doi.org/10.1016/j.trb.2014.05.005>
20. Delorme, X., Gandibleux, X., Rodriguez, J.: Stability evaluation of a railway timetable at station level. *Eur. J. Oper. Res.* **195**(3), 780–790 (2009). <https://doi.org/10.1016/j.ejor.2007.06.062>
21. Goverde, R.M.: Railway timetable stability analysis using max-plus system theory. *Transp. Res. Part B Methodol.* **41**(2), 179–201 (2007). <https://doi.org/10.1016/j.trb.2006.02.003>
22. Gallagher, R.H.: *A Correlation Study of Methods of Matrix Structural Analysis*. Elsevier Science, Kent (2014)
23. Eisen, M.B., Spellman, P.T., Brown, P.O., Botstein, D.: Cluster analysis and display of genome-wide expression patterns. *Proc. Natl. Acad. Sci.* **95**(25), 14863–14868 (1998). <https://doi.org/10.1073/pnas.95.25.14863>
24. Johnson, R., Bhattacharyya, G.: *Statistics: Principles and Methods*. Wiley, Hoboken (2019)
25. Gdeisat, M., Lilley, F.: *MATLAB® by Example: Programming Basics*. Elsevier, Amsterdam (2013). <https://doi.org/10.1016/C2012-0-03351-0>
26. Chaddock, R.E.: *Principles and Methods of Statistics*. Houghton Mifflin, Boston (1952)
27. Prokhorchenko, A., Malakhova, O., Gurin, D., et al.: Development of a methodology for determining an energy efficient technology for the freight transportation on a singletrack railway line. *IOP Conf. Ser. Mater. Sci. Eng.* **1021**, 012009 (2021). <https://doi.org/10.1088/1757-899X/1021/1/012009>
28. Antunes, N.M., Ramos, C.M., Sousa, C.M.: Who are the tourists sharing content on social media? Behaviour and characteristics. *J. Spat. Organ. Dyn.* **6**(3), 237–257 (2018)



Efficiency Assessments of the Parking and Time Restrictions Implementation in Kharkiv by Applying the Logistics Sustainability Index Methodology

Mariia Olkhova¹  , Dmytro Roslavl'tsev¹ , Antonio Comi² ,
and Olga Plyhun¹ 

¹ O. M. Beketov National University of Urban Economy in Kharkiv,
17 Marshala Bazhanova Street, Kharkiv 61002, Ukraine
m.olhova@kname.edu.ua

² University of Rome Tor Vergata, 50 Via Cracovia, 00133 Rome, Italy

Abstract. Large cities have experienced problems associated with high traffic congestion especially during peak periods, followed by several serious problems of an environmental, time and economic character. At the same time, a large contribution to this is due to freight transport. The paper aims to assess the primary possible implementation of a parking ban and time window for trucks due to reduce the negative effects of freight transport in Kharkiv including decreasing traffic congestion, environmental improvement, and economic impact. To achieve this goal, two initiatives are introduced, considering their impact on traffic participants and stakeholders, namely reducing congestion and, therefore, traffic delays, emissions, noise, improving road safety for both pedestrians and drivers on a selected section of the road network of the city of Kharkiv. The assessment of the measures considered is based on the Logistics Sustainability Index methodology using a Multi-Actor Multi-Criteria Analysis.

Keywords: Parking restriction · City logistics · Sustainability · Time window

1 Introduction

According to the world ranking of road congestion in cities (Traffic Index 2021, Tom-Tom), the Ukrainian cities of Kyiv, Odesa, Kharkiv, and Dnipro are occupied the first places in terms of traffic taking 3rd, 6th, 12th and 25th place, respectively. Compared to the EU countries, the level of motorization in Ukraine is growing more rapidly, which only worsens the conditions of moving in the city [1]. Traffic jams lead to longer travel times, more delays, more fuel consumption, emissions, noise, and vibrations. One of the reasons for this is the long-term implementation of sustainable policy in EU cities through the economic, regulation, and infrastructural measures in contrast to Ukrainian cities where this process is at the beginning stage. Simultaneously, a large contribution to unsustainable city functioning is due to freight transport moving within the cities.

Urban freight transport and logistics are inherently interdisciplinary and are influenced by several factors related to the behavior of different stakeholders. Residents of urban areas, transport and logistics companies, manufacturing companies, information and communication technology providers and municipal authorities, in particular, function in the complex urban conditions that they create and at the same time affect the conditions of the city. Planning freight in the city is a complex process and public authorities usually do not have enough information on specific issues, while private companies involved in the organization and implementation of urban freight are aware of the technical aspects. Insufficient coordination of city logistics entities and the availability of information, however, contribute to poor urban planning and integration of urban freight transport. There is almost no collection of data on freight within the city, even if they exist, the data are not representative. This leads to the fact that the city authorities have no idea about the current situation in the field of freight transport, which means that it is impossible to develop the necessary measures and strategies [2].

2 Literature Review

The measures that will be proposed to be implemented in Kharkiv have already been applied in the different cities. From the literature review, the study relates to the congestion management strategy well-known in the developed countries and their policy in contrast with Ukrainian cities and their authorities where implementation of the parking policy has not based on a holistic approach. The parking regulation in Ukraine concerns private cars in the city centers and slightly freight vehicles. There are regulations resolutions and road signs that ban the movement of HGV in the cities, and no one is concerned regulation of truck parking and loading/unloading. But the issue should be started to study and assessed the possibility of implementation and impact in the Ukrainian megalopolis. Bearing in mind that the local administrations are faced with the presence of greater constraints in terms of the use of space and time [3]. Meanwhile, freight traffic causes a disproportionate number of externalities and the current bay configuration leads to greater mobility impacts than some of the proposed systems [4]. The behavior of truck deliveries is distinctly different from commuter parking: trucks do not cruise for parking spaces, and demand for goods delivery is driven by customers and is practically inelastic to the delivery costs [5]. Nevertheless, the introduction of traffic and parking restrictions is one of the most sensitive and controversial aspects of the implementation of transport policy in the cities [6].

The flagman of the regulation of traffic and climate change actions is in London. There are a lot of cases of mobility regulation. Since 2008, London has operated one of Europe's largest Low Emission Zones (LEZ). Covering the entire city, the LEZ specifies emission requirements for heavy vehicles driven in the city all year round. As a result of the Congestion Charge, LEZ, Ultra-LEZ, and London Lorry Control Scheme are part of a comprehensive package of measures to reduce congestion and improve air quality, as well as provide incentives, resources and opportunities for city residents and industry stakeholders to transition to cleaner and more efficient vehicles [7, 8]. A truck zone, where the vehicles must not stop or park during the hours shown on the sign unless dropping off or picking up goods in a truck over 4.5 tons gross vehicle mass, is applied in Sydney,

Australia [9]. An “environmental fee” for all trucks of 3.5 tons or more is established in Paris. Simultaneously, in Australia, as well as in Europe and the USA, it is common to have special licenses for trucks – permission to enter an area where there are no parking and/or drive-through signs [10]. As a result, the most effective solution to the problem of illegal parking is high fines and infrastructure that provides recreation for truck drivers in special legal places: quality-guarded gas stations, and motels. Also, it should be noted that an effective solution is time restrictions which improve the ecology of large cities and increase road safety. An attractive counterproposal from the authorities is to obtain special permits for transport companies (their drivers) – licenses to enter restricted areas for trucks, each of which is issued individually according to the cargo transported and the type of transport.

It is widespread in EU, when local authorities are motivated by a special projects such as CIVITAS, EiT urban Mobility, Interreg etc. for the development of parking regulation as a part of a holistic approach to sustainable development and climate change policy. Thus, a lot of events are provided by the project teams for all stakeholders with the crucial aim to share their results and demonstrate the relevance and impact to the cities (for instance upcoming Park4SUMP, European Parking Association Congress 2022) [11, 12]. Except for the project initiatives there is scientific research devoted to the evaluation of the parking regulation of freight vehicles. A complex analysis of the current state of parking areas out and inside the cities of the Slovak Republic has been conducted. The lack the parking lots based on surveys conducted has been determined, namely the proposal for the development of a number of public parking areas for road freight transport in urban areas [13]. The analysis of the current parking lots and facilities were evaluated in the Czech Republic, city of Jindrichuv Hradec, using the TOPSIS method for making-decision on two proposals. It was highlighted that static traffic or parking lots are one of the most problematic areas of transport in urban areas [14].

Freight operations are out of legal schedules, and parking spaces are insufficient and inadequate to meet the demand in Cali’s city center of Colombia a Multi-Actor Multi-Criteria Analysis was applied for the evaluation of strategies aimed at improving logistics operations including several objectives such as noise reduction, social impacts, and even political priorities. In a conclusion, the authors declaimed that the real needs of freight operations in city centers should be dealt with from an urban space planning perspective and not exclusively from a traffic perspective. City planners misunderstand the land use demand for loading and unloading operations, but also the different alternatives to mitigate its externalities [15].

The deep research is provided in the city of Lisbon, Portugal by using micro modeling by creation of parking demand models based on the data from an establishment-based freight survey and a parking observation exercise. Bay systems’ ability in reducing double-parking impacts was assessed via a set of indicators. Loading/unloading bays are generally viewed as an effective way to avoid freight vehicles double-parking, but are often misused by non-freight vehicles [4]. An on-street parking model for downtowns in urban centers that incorporates the often-neglected delivery demand of delivery trucks has been developed for downtown Toronto. It was investigated the study of the relationship between passenger vehicles’ parking and truck delivery behaviors and provided

tools for policy makers to optimize the trade-offs in parking space allocation, pricing, and aggregate network congestion [5].

The paper aims to assess firstly the possible implementation of city logistics measures such as a parking ban and time window for trucks for achieving reducing of the negative effects of freight in Kharkiv. The assessment of the measures considered is based on the Logistics Sustainability Index methodology, the Iterreg project [16].

3 Kharkiv Case Study

3.1 Study Area

The study area is located near a ring road, in a residential area with developed business activities and infrastructure in Kharkiv, Oleksiyivka district, Fig. 1. This section of road was recently repaired, so it has a good road surface. However, accidents happen in some of its sections.

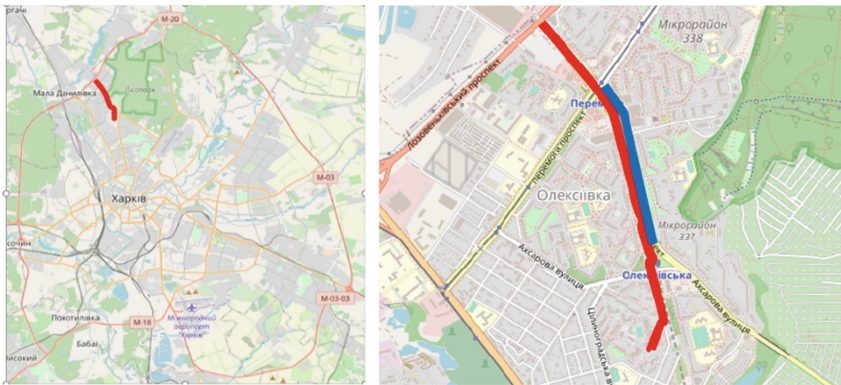


Fig. 1. Study area: Ludwig Svobody Avenue: █ – Ludwig Svobody Avenue in Kharkiv; █ – studied part of Ludwig Svobody Avenue.

Oleksiyivka is a “young” district in relation to the city of Kharkiv and has a rapid pace of development. The study area has many both grocery and domestic stores, cafes and restaurants, as well as the market. Economic activity is developing rapidly, every year new points of sale and recreation are opened here which, in turn, is a reason for increasing freight moving. The total length of the avenue is 2.23 km, the studied section – 0.94 km. Detailed characteristics of traffic proportion and noise level by peak periods are presented in Fig. 2.

It should be noted that despite the predominant number of private cars in the morning and evening periods, the main source of noise is cargo flows. The studied area is a part of the avenue where problems related to trucks occur more often, namely inappropriate parking of large vehicles near intersections. Firstly, it reduces the safety of pedestrians (especially at night) when crossing a wide roadway. Secondly, this parking increases traffic delays for public transport (especially for trolleybuses which must use their own

lane). Trucks are parked away from crosswalks by 1–2 m and almost every intersection on this road part has public stopping points. Another problem that should be noted is the performance of loading and unloading operations during the buyer’s rush hour. The following subsection describes in detail the proposed measures to solve the above problems.

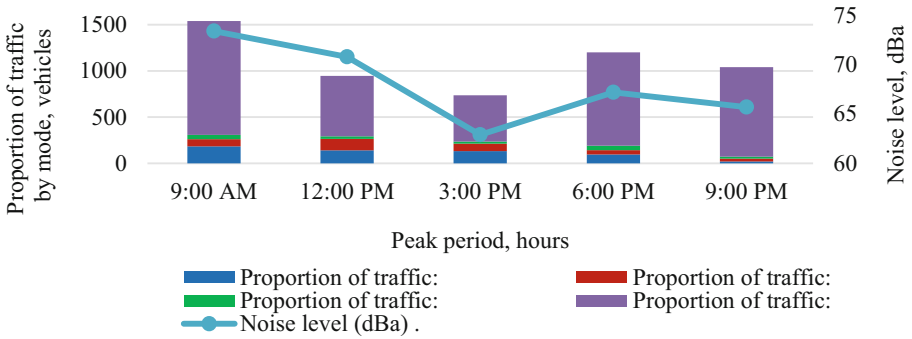


Fig. 2. Characteristic of traffic proportion and noise level by peak periods.

3.2 Description of the Measures

Several problems and the measures proposed to solve them are presented in detail in Table 1.

Table 1. Description of measure

Problem	Measure	Expected result
Parking of HGV on roads for recreational purposes, making it difficult to get through during rush hours;	Parking ban for trucks	Increasing road capacity and reduce traffic delays, since HGV take up a lot of space on the road;
Parking of HGV near intersections which worsens visibility, especially at night		Increasing visibility of pedestrians and other vehicles on the road, reducing delays in traffic, increasing traffic safety
High proportion of freight vehicles during the morning rush hour for the purpose of loading and unloading operations which increases traffic delays	Time restrictions	Loading and unloading operations by HGV from 9PM to 9AM and by LGV – from 10AM to 5PM will reduce traffic congestion and significantly reduce the proportion of freight vehicles during rush hours

Similarly, it should be noted that the reduction in the number of trucks on the street sections, which will result from the implementation of restrictions, will optimize the movement of public transport vehicles, positively affect the punctuality and regularity of service, contributing to the competitiveness of this transport mode.

Technical analysis of the measure “Parking ban for trucks” is presented in Fig. 3. Installation of road signs and, as a result, the change of the traffic scheme by the local authority must be coordinated with the relevant departments of the National Police [16]. Technical analysis of the Time Restrictions measure is presented in Fig. 4.

Parking ban for trucks	requires the installation of appropriate road signs at the beginning and end of the street in both directions (4 units);	
	the cost of project implementation takes into account the purchase and installation of road signs (about 66 euro for signs);	
	requires the approval of the local authorities;	encouraging local authorities to use online resources that have accessible information about permitted downtime;
		alerting drivers to possible resting places.

Fig. 3. Technical analysis of measure “Parking ban for trucks”.

Time restrictions	requires the installation of appropriate road signs at the beginning and end of the street in both directions (4 units);	
	the cost of project implementation takes into account the purchase and installation of road signs (about 87 euro for signs);	
	according to natural observations, the majority of logistics operations occur during the peak of customer activity – from 5 pm (regarding LGV), so performing these operations at off-peak times would be the best option;	
	requires the approval of the local authorities;	coordination with local store owners of time restrictions;
	requires the approval of the supply chain participants;	the question of the availability of staff ready to accept goods in limited time, as well as payment for labor (if required) is raised.

Fig. 4. Technical analysis of measure “Time restrictions”.

To install road signs, an initiator must apply to the City Council and receive permission for installing road signs [17]. According to DSTU 4100:2014 of Ukraine [18], the installation of road signs without an agreement with the Ministry of Internal Affairs of Ukraine according to the Law of Ukraine “About Road Traffic” is prohibited.

The expected environmental and social impact of the measures are offered in Table 2.

Table 2. Environmental and social impact of the measures

Measure	Environmental change	Social change
Parking ban for trucks	Increasing capacity due to the free lane (or part of it) will reduce traffic delays and increase the flow rate, thereby reducing the number of emissions	Ensures the safety of pedestrians and drivers, especially at night
Time restrictions	Significant reduction of noise in the residential area in peak periods and the level of vibration that destroys the road surface	Reducing the noise level of nearby areas, but negative for the owner of the stores can be

The next step is to determine the impact of these possible measures to be implemented on the stakeholders. Detailed information is obtainable in Table 3.

Table 3. Impact analysis by stakeholder

Group of stakeholders	Positive impact	Negative impact
Local authorities	<ol style="list-style-type: none"> 1. Accidents risk reduction 2. Minimum inconvenience caused by UFT 3. Improve livability 4. Additional finance for budget as a result of violations 	<ol style="list-style-type: none"> 1. Additional costs for realization project (but not so high) 2. Lawsuits for violation/restriction of entrepreneurial activities
Receivers	<ol style="list-style-type: none"> 1. Increase of load & unload availability because of no peak period of customer activity 2. On time delivery of products, with a shot lead-time 3. Reducing the time and costs spent on cargo inspection 	Not for all of them because of changing in the goods acceptance schedule – lawsuits for violation/restriction of activities
Logistics service providers/carriers	<ol style="list-style-type: none"> 1. Increase of vehicle productivity 2. Accidents risk reduction 3. More availability of curbside space and time and reduction of conflict between cargo vehicles and other road users 	Change in the delivery schedule (but temporary) – lawsuits for violation/restriction of activities

(continued)

Table 3. (continued)

Group of stakeholders	Positive impact	Negative impact
Suppliers/shippers	1. Are benefited with better service level due to the reduction of the lead time in the last mile	Change in the delivery schedule (but temporary)
Residents/local population	1. Traffic congestion and local air and noise pollution emission reduction 2. Accidents risk reduction 3. Dwell-time operations do not disturb the shopping process	Noise and vibration increasing at night, but will not exceed the normative values

3.3 Scenario Before and After

In the “before” context, in the studied area were moving 327 HGV and 575 LGV during peak periods with a speed of flow 35–40 km/h. In the “after” scenario it is assumed reduction of HGV and LGV proportion during the peak period and change in noise level (increasing at night, but reduced equilibrium distribution during the day) and increasing of speed. A summary of the two scenarios is reported in Table 4.

Table 4. Summary of the two scenarios supposed

Features	Before	After
Number of HGV during peak period, cars	327	295
Number of LGV during peak period, cars	575	450
Noise level at day, dB	62.9–73.4	63–70
Noise level at night (after 9 PM), dB	50–55	55–57
Speed of flow, km/h	35–40	45–50

Although most HGV pass through in transit, some part of the vehicles has dwell-time operations at the selected site. It is assumed that after the implementation of the measures, this portion will operate at night which will help to reduce the proportion of trucks in the flow and, accordingly, increase the speed of movement and reduce delays. The situation is similar for LGV, however, the measures suggest that this mode of transport will be unloaded during off-peak periods, thus increasing the share of LGV from 10 am to 5 pm, and at other times LGV are only eligible for transit passage. Since the LGV flow will prevail in the daytime, the noise will be higher (or stay at the same level) and distributed equally during the day but will not exceed the normative values. If we talk about HGV, we should not expect high noise levels at night because the flow of individual vehicles will be reduced to 100 units per hour which in total will not exceed the normative values of noise levels at night, namely – 45 dB.

However, it should be noted that meanings in Table 4 obtained near the road, but there are greenery plantings along the road – forest plantations – which represent a sanitary protection zone and prevent the spread of noise to the adjacent areas (in this case – residential buildings). The width of this zone is about 85–90 m, therefore the noise level near residential buildings meets the standard values.

3.4 Impact Assessment

Logistics Sustainable Index methodology, that developed according to the project SULPiTER, Interreg Central Europe, is applied to provide the impact assessment of proposed initiatives. Logistics Sustainability Index (LSI), a Multi-stakeholders Multi Criteria Decision Analysis tool used to aggregate normalized values of indicators into a unique index. This index is able to assess the city logistics measure's impacts over a given impact area, and eventually aggregate different indexes to assess the overall convenience of a measure [19]. The calculation process of the LSI is composed of six steps: selection of the impact area, criteria, indicator, weighing process, value normalization and LSI calculation. The choice of the impact area depends on the primary and secondary objectives of the cities or the stakeholders. Three major impact areas were highlighted for assessing the impact – economy, environment, transport, and mobility, Table 5.

These indicators were taken into consideration due to the possibility to evaluate during the observation. The monetization of economy and energy data including investment costs, management, and personnel were determined on the basis of the average salary of the workers in the region concerned [20]. The monetization of road signs and their installation depends on size, material and composition. The monetization of the noise level has been made following the guidelines of SULPiTER [16]. Firstly, it was necessary to determine the population exposed to noise pollution by observation which is done by multiplying the population density and the pertinence surface. Then, the percentage of a-few/not-annoyed people, the percentage of annoyed people and the percentage of very annoyed people for road transport.

The indicators of the Environment impact area (CO, NO₂, SO₂, NMVOC, PM₁₀, NH₃, CO₂ concentrations) have been calculated using the methodology for calculating emissions of pollutants and greenhouse gases into the air from vehicles [21] based on the average number of vehicles, fuel consumption rates by vehicle type, and specific emissions in kilograms per kilogram of fuel. The cost of each gram of a certain emission per 1 kg of diesel fuel was taken according to the SULPiTER Handbook [16], and monetization was done based on the calculations made. Then, the same methodology has been applied for the “after” scenario. The number of accidents has been computed in the “before” scenario through the statistical data. Not a single fatality with or without a pedestrian on the selected road segment has occurred in the past year.

The use of indicators of different contexts, nature and values in a common assessment methodology, requires establishing a commensurate scale, thus making indicator values dimensionless. This had been achieved by means of the normalization of values of each criteria and indicator into the set of dimensionless real numbers [16].

Table 5. Indicators of the two scenarios supposed

Impact area (weight)	Criterion	Indicator	Unit	Before	After
Economy and energy (0,32)	Development	Local/regional development	Likert scale	4	5
	Benefits	Strength and diversification of local economy	Likert scale	1	3
		Costs	Investment costs	€	0
		Management	€	0	500
		Personnel	€	0	600
		Equipment/materials/infrastructure	€	0	153
	Economics and financial risks	Reduction of the foreseen capacity of freight transport system in a city	Likert scale	3	4
		Delayed receipt of funds	Likert scale	3	4
UFT activity economic aging		Likert scale	3	4	
Environment (0,33)	Air quality	CO emission	g/year	5,13	4,25
		NMVOE emission	g/year	1,05	0,87
		N _{ox} emission	g/year	0,02	0,02
		PM emission	g/year	0,59	0,49
		NH ₃ emission	g/year	0,15	0,13
		SO ₂	g/year	4,4	3,7
	GHG emissions	CO ₂ emission	g/year	480,5	398
	Noise	Noise level	dB (A)	48	46,5
Transport and mobility (0,35)	Level of service	Punctuality	%	60	90
		Market response	%	60	80
		Customer satisfaction	Likert scale	3	5
		Supply chain visibility	Likert scale	3	5
	Safety and security	Accidents	Number/veh-km	4	1
	Transport system	Violations	%	30	5
	UFT vehicles	Load factor	%	60	90
		Vehicle utilization factor	%	50	90
	IT, infrastructure and technology	Underdeveloped transport infrastructure	Likert scale	2	4

(continued)

Table 5. (continued)

Impact area (weight)	Criterion	Indicator	Unit	Before	After
		Low quality of transport infrastructure	Likert scale	1	3
		Limitations at developing and changing the existing infrastructure	Likert scale	3	4
		Infrastructure usage	Likert scale	1	4

3.5 Logistics Sustainability Index (LSI)

Calculation of Logistics Sustainability Index (LSI) is based on the weighted sum model is represented in Fig. 5.

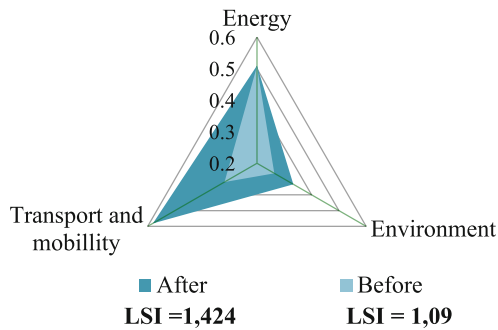


Fig. 5. Impact areas' performances in the “before” and “after” scenario.

Based on the calculations, the greatest improvement is observed in the transport and mobility area. Economy and energy remained almost at the same level, there is a slight improvement because the implementation of these measures requires costs. The environment has also improved.

4 Conclusion

In this paper, it was proposed to introduce firstly in Kharkiv city logistics measures such as Parking ban for trucks and Time Restrictions to reduce the negative effect of trucks on the road of Oleksiyivka district of the city. The effectiveness of the measures had been assessed by applying Logistics Sustainable Index methodology. Based on the calculations, the greatest improvement is observed in Transport and mobility – from 0,319 to 0,581. I consider this impact area to be the most important among those chosen because its improvement will lead to improvements in other areas. Economy and energy remained almost at the same level, there is a slight improvement because the implementation of these measures requires costs – from 0,508 to 0,51. The environment has also improved from 0,264 to 0,333. The total LSI increased from 1,09 to 1,424.

It's the first attempt to apply city logistics measures in a Ukrainian city. It's expected that the experience of evaluating and implementing different initiatives for achieving a sustainable city transport system in Ukrainian cities will be shared and adopted from the best practices of cities. It's obvious, that such an approach has its pros and cons, but it allows complex to consider the implementation of city logistics initiatives and make a decision about the necessity of its implementation, or reconsider the impact areas, criteria if required. However, it's a respectable instrument, that allows introducing for policymakers and stakeholders impact of all areas in the city of the initiatives. The flexibility of such methodology allows adapting this instrument to different cities with diverse characteristics and requirements and assessing its impact.






References

1. Galkin, A., Lobashov, O., Capayova, S., et al.: Perspective of decreasing of road traffic pollution in the cities. In: International Multidisciplinary Scientific GeoConference Surveying Geology and Mining Ecology Management, vol. 18, pp. 547–554. SGEM (2018). <https://doi.org/10.5593/sgem2018/4.2/S19.071>
2. Olkhova, M., Roslavtsev, D., Galkin, A.: The comparative method of assessing city logistics measure. In: Sierpiński, G., Macioszek, E. (eds.) Decision Support Methods in Modern Transportation Systems and Networks. LNNS, vol. 208, pp. 163–174. Springer, Cham (2021). https://doi.org/10.1007/978-3-030-71771-1_11
3. Russo, F., Comi, A.: Sustainable urban delivery: the learning process of path costs enhanced by information and communication technologies. *Sustainability* **13**(23), 13103 (2021). <https://doi.org/10.3390/su132313103>
4. Alho, A.R., e Silva, J.A., de Sousa, J.P., Blanco, E.: Improving mobility by optimizing the number, location and usage of loading/unloading bays for urban freight vehicles. *Transp. Res. Part D Transp. Environ.* **61**, 3–18 (2018). <https://doi.org/10.1016/j.trd.2017.05.014>
5. Amer, A., Chow, J.Y.: A downtown on-street parking model with urban truck delivery behavior. *Transp. Res. Part A Policy Pract.* **102**, 51–67 (2017). <https://doi.org/10.1016/j.tra.2016.08.013>
6. Gärling, T.: Effectiveness, public acceptance, and political feasibility of coercive measures for reducing car traffic. In: Gärling, T., Steg, L. (eds.) Threats from Car Traffic to the Quality of Urban Life, pp. 313–324. Emerald Group Publishing Limited, Bingley (2007). <https://doi.org/10.1108/9780080481449-017>
7. C40 Cities: C40 Good Practice Guides: London - Charging Zones to Promote ULEVs. <https://www.c40.org/case-studies/c40-good-practice-guides-london-charging-zones-to-promote-ulevs>. Accessed 10 May 2022
8. London Councils: About the London Lorry Control Scheme. <https://www.londoncouncils.gov.uk/services/london-lorry-control/about-llcs>. Accessed 10 May 2022
9. NSW Government: Parking rules. <https://www.nsw.gov.au/driving-boating-and-transport/roads-safety-and-rules/parking/parking-rules>. Accessed 10 May 2022
10. Australian Taxation Online: Continuing movement permission. <https://www.ato.gov.au/Forms/Continuing-movement-permission/>. Accessed 10 May 2022
11. Park4SUMP high level meeting: new parking standards & preparing buildings and cities for zero-emission mobility. <https://www.eltis.org/participate/events/park4sump-high-level-meeting-new-parking-standards-preparing-buildings-and-cities>. Accessed 10 May 2022
12. European Parking Association (EPA) Congress 2022. <https://www.eltis.org/participate/events/european-parking-association-epa-congress-2022>. Accessed 10 May 2022

13. Gnap, J., Kubíková, S.S.: Possible effects of lacking parking areas for road freight transport on logistics and transport safety. *Transp. Res. Procedia* **44**, 53–60 (2020). <https://doi.org/10.1016/j.trpro.2020.02.009>
14. Lizbetin, J., Bartuska, L.: The issue of addressing the lack of parking spaces for road freight transport in cities – a case study. *Open Eng.* **10**(1), 209–215 (2020). <https://doi.org/10.1515/eng-2020-0025>
15. Cruz-Daraviña, P.A., Suescún, J.P.: Freight operations in city centers: a land use conflict in urban planning. *Land Use Policy* **108**, 105575 (2021). <https://doi.org/10.1016/j.landusepol.2021.105575>
16. SULPiTER: The Logistics Sustainability Index Handbook. Final Version. Interred Central EU (2017)
17. sud.ua: Whether local governments should coordinate the installation of road signs with National Police units. <https://sud.ua/ru/news/publication/181311-vs-rozyasniv-chi-povinni-organi-mistsevogo-samovyaduvannya-pogodzhuvati-vstanovlennya-dorozhnikh-znakiv-z-pidrozdilami-natsionalnoyi-politsiyi>. Accessed 10 May 2022
18. DSTU 4100:2014. Traffic Safety. Road signs. General specifications. Rules of application. <https://service-znak.com.ua/>. Accessed 10 May 2022
19. Comi, A., Persia, L., Polimeni, A., et al.: A methodology to design and assess scenarios within SULPS: the case of Bologna. *Transp. Res. Procedia* **46**, 269–276 (2020). <https://doi.org/10.1016/j.trpro.2020.03.190>
20. The average salary of a road worker in Ukraine. Statistics of salaries of Road Worker in Ukraine. <https://ua.trud.com/ua/salary/2/78669.html>. Accessed 10 May 2022
21. Methodology for calculating emissions of pollutants and greenhouse gases in the air from vehicles. https://ukrstat.org/uk/metod_polog/metod_doc/2008/452/metod.htm. Accessed 10 May 2022



Directions for Improving the Efficiency of Intermodal Transport

Ludmiła Filina-Dawidowicz¹  , Alla Selivanova² , Daria Możdrzeń¹ ,
and Sara Stankiewicz¹ 

¹ West Pomeranian University of Technology in Szczecin, 41 Piastów Avenue, 71065 Szczecin, Poland

ludmila.filina@zut.edu.pl

² Odesa National University of Technology, 112 Kanatna Street, Odesa 65039, Ukraine

Abstract. Intermodal transport deals with carriages of freights in intermodal loading units using different transport modes, without goods reloading while modes changing. This kind of transport is intensively developing worldwide, and its efficiency is regularly increased. The article aims to investigate the directions for improving the efficiency of intermodal transport of goods. The case study of Polish market was analyzed, and opinions of practitioners involved in intermodal transport operation were investigated. The activities that may improve intermodal transport efficiency were determined. The questionnaire survey was developed and filled in by the group of intermodal transport companies' representatives. Research results analysis revealed that automation of handling processes and infrastructure quality improving are the main activities perceived by respondents' group as the most essential for improving the efficiency of intermodal transport. The results of the research may be useful for transport and logistics companies, as well as decision-makers who are involved in intermodal transport development.

Keywords: Intermodal transport · Transport efficiency · Development directions

1 Introduction

Intermodal freight transport is dynamically developing worldwide, including individual European Union (EU) countries [1]. This kind of transport deals with transport of loads in intermodal loading units (e.g. containers, swap bodies, semitrailers, etc.) using infrastructure and transport means of different modes of transport (e.g. maritime, rail, road, etc.) [2]. The whole transport process is planned and organized by forwarder or multimodal transport operator. This process includes cargo carriage, as well as handling operations performed at intermodal terminals located in seaports (ferry and container terminals) and in the hinterland (rail-road terminals) [3].

Intermodal transport is considered to be the most environmentally friendly alternative to road transport that generates relatively high emissions [4], and its development is supported by the number of legal acts [5]. Intermodal transport implementation allows to efficiently reduce the handling duration and relieve congestion at every transshipment point [6]. It is believed that intermodal transport plays significant role in reducing

logistics costs and constitutes efficient way of organizing transportation activities [7]. The attention is paid to the fact that intermodal transport is developing much faster as compared to transport of loads using other technologies [8]. This deals with the need to carry out specific actions aimed at continuously increasing its efficiency. Conducted available literature analysis revealed that individual countries undertake the number of activities aimed at improving intermodal transport operation. However, the activities that may improve intermodal transport efficiency, considering opinions of different groups of practitioners involved in intermodal transport operation, were analysed to the small extent. Research question was formulated as follows: “How the efficiency of intermodal transport may be improved, considering practitioners’ viewpoint?”

The paper aims to explore the directions for improving the efficiency of intermodal freight transport. The activities that are considered by practitioners as the most important for enhancing intermodal transport efficiency were determined and analyzed in detail. The paper includes literature review part and description of methodology used to conduct the research. The Results section presents the outcomes of conducted investigations and shows the directions of improving efficiency of intermodal transport. In order to sum up the conclusions have been drawn.

2 Literature Review

Efficiency of transport process is dependent on effectiveness of work organization of all transport participants [9]. It deals with the result of the actions undertaken and is described by the ratio of achieved results (e.g. profits from the activity, etc.) and the incurred inputs (e.g. financial resources, etc.). It is often analyzed using in time- and costs related aspects [10].

Intermodal transport efficiency improvement needs innovations implementation. For that purpose, significant funds are required. Therefore, detailed needs analysis allows to set the list of solutions and activities to be implemented effectively [11].

Transport infrastructure is one of the basic elements of intermodal transport systems that condition its efficient and effective development [12]. The density and high quality of linear (e.g. roads) and punctate (e.g. transshipment terminals) infrastructure elements of individual transport modes determine its availability. The development and improvement of infrastructure extends the scope of transport operations, allows for the acquisition of new markets for transport services and influences economy of urbanized areas [13]. Several favorable conditions for the development of intermodal transport were identified by Smolnik [14]. Among these conditions favorable geographic position, expanding terminals’ infrastructure, rail transport development potential was mentioned. Moreover, optimal localization of intermodal terminals within transport network conditions future cargo carriages [15].

The means of transport used to transport intermodal loading units should be adapted to potential of the existing transport infrastructure. Additionally, the structure of the rolling stock of the individual modes of transport has to be adjusted to handle any type of intermodal loading unit [16]. Its differentiation enables the selection of the appropriate type of transport mean for cargo carriage within the individual links of the transport chain. The age and technical condition of the rolling stock affects, among others the level of

transport safety and costs of the transport process (e.g. fuel consumption). Rolling stock constitutes an area susceptible to the implementation of innovative solutions, due to the need to increase the level of transport safety and reduce the negative impact of transport on the natural environment.

The difficulties to perform cargo handling operations may influence intermodal transport efficiency [17]. The improvement of technological solutions applied in this area affects, among others, the possibility of uninterrupted handling and control of transported cargo conditions. Intermodal terminals are the key transshipment points for servicing intermodal loading units and transport means [18]. Within these facilities the efforts are made to improve handling processes of cargo and transport means, which may result in shortening their duration, simplifying the documentation flow (e.g. in electronic form with the use of modern systems), reducing the level of costs and energy consumption, etc.

It was emphasized that road freight transport dominates the terrestrial transport market, and increasing of the share of other transport modes, especially rail transport is needed [19]. The attention was also put to the need to optimize intermodal networks improving sustainable transport efficiencies [20]. Furthermore, intermodal terminals' layout may allow to reduce the total cost and time of containers transport from the port to their destination [6].

The implementation of innovative technical and technological solutions is currently carried out on a large scale in many areas of intermodal transport. It makes it possible to relieve employees and automate processes, influencing duration of preformed activities and increasing their efficiency [18].

Information flow and sharing is necessary for processes management in intermodal transport. Multi-source information may cause information conflicts and reduce efficiency of transport activities [21]. Therefore, optimization of information sharing processes and information flow improvements are carried out.

In the available literature the attention is also paid to the need to promote intermodal transport [22]. Agamez-Arias and Moyano-Fuentes [23] put attention to frames elements and variables that impact intermodal transport systems' logistics efficiency. They mention i.e. the quality of service, information and communication systems, and freight planning and linkages among system operators to provide an adequate service. Consequently, reliable cooperation between enterprises is very important to assure the processes efficiency. It was highlighted that cooperation and joint planning of activities will allow more efficient use of available resources and thereby optimize transportation costs [10]. Innovative organizational solutions within intermodal transport chains, implementing a variety of digital applications, support the provision of services and the implementation of individual transport processes.

Educated management staff is crucial for the effective functioning of transport companies. It makes strategic, tactical, and operational decisions, which require a wide range of staff' knowledge and experience. It is also responsible for implementing innovations in the enterprise. The effectiveness of the application of new solution will be influenced, among others, by the level of experience and competence of the company's employees [3, 24].

Intermodal transport is supported by state authorities and international intermodal transport associations in individual countries [8, 25]. The measures needed to improve development of intermodal transport in Poland were identified by Mindur and Paweńska [26]. The attention was put to the need of preparation of a legal act on granting financial aid for intermodal transport, creating dedicated Intermodal Transport Fund for supporting the development of this transport system, creating a legal basis for using environmental protection fund and other activities.

Furthermore, series of planning programs to improve intermodal transport efficiency have been proposed in different countries [27]. For example, in Poland “The Strategy for Sustainable Development of Transport until 2030” [5] has defined strategic viewpoint on national transport development. It is assumed that the development of intermodal transport should be approached systematically, various investments and non-investment activities should be applied in relation to intermodal transport elements, including linear and punctate infrastructure, rolling stock, loading units, legal regulations, etc. [28]. Moreover, in Poland general directions of intermodal transport development are specified in the document “Directions for the Development of Intermodal Transport until 2030 with a perspective until 2040” [28]. This document defines the main goal for the development of intermodal transport, which deals with creating optimal conditions for intermodal integration in the Polish transport system and increasing the use of rail transport in intermodal transport. The objectives and measures for the development of intermodal transport include the emergence of comprehensive projects for the use of intermodal transport in supply chains, improving the competitiveness of intermodal transport, digitization of intermodal transport.

Based on available literature analysis it may be stated that there is a need to investigate activities that are currently perceived by practitioners as the most and least important to improve intermodal transport efficiency.

3 Methodology

The literature review was carried out to collect information necessary to conduct investigations. Based on the results of this review, the questionnaire survey was developed. The questionnaire was prepared in electronic form in Polish and was divided into two parts. First part allowed to set respondent’s profile, the second one contained thematic questions. The practitioners were asked to answer the following question: “What would you suggest in order to increase the level of efficiency in intermodal transport?”.

Based on conducted literature review the activities that may be essential to increase the efficiency of intermodal transport were identified. These activities included:

- More financial resources allocated to innovations implementation (A1),
- Conducting detailed needs analyzes (A2),
- Improving the quality of transport infrastructure (A3),
- Implementation of innovative transport means (A4),
- Improving handling techniques and technologies in terminals (A5),
- Increasing the share of rail transport in intermodal transport (A6),
- Extension the network of intermodal terminals (A7),

- Automation of transshipment processes (A8),
- Improving information flow (A9),
- Greater promotion of intermodal transport (A10),
- Improving cooperation between enterprises (A11),
- Increasing the level of staff qualifications (A12),
- Financial incentives and other types of governmental support for entrepreneurs (A13).

The case study of Polish intermodal transport market was considered. In 2020 in Poland 34 intermodal terminals were involved in loading units' service (Fig. 1) [29]:

- 4 handled sea-rail and sea-road shipments (terminals located in seaports),
- 30 handled rail-road shipments (rail-road terminals).



Fig. 1. Location of intermodal terminals in Poland [29].

According to Central Statistical Office [29] in 2020 the total annual throughput capacity of intermodal transport terminals in Poland was 8.2 million TEU, including 5.2 million TEU serviced in terminals located at seaports, and 3.0 million TEU – in rail-road terminals. In 2020 a 5% increase in transshipment was observed compared to 2019. A total of 77.9 million tons of containerized cargo were handled at intermodal terminals, including:

- 29.2 million tons – carried by maritime transport means (which accounted for 37.4% of the total cargo transhipped in intermodal terminals),

- 25.5 million tons – transported by roads (32.7%),
- 23.3 million tons – carried by railway transport means (29.9%).

The survey was carried out in Poland in September and October 2021. The developed questionnaire was sent to 53 intermodal transport companies in electronic form by email. Among these companies there were: container and ferry terminals located in seaports, rail-road intermodal terminals and freight forwarding companies that plan, organize, and monitor carriages of goods using intermodal transport.

The questionnaire was filled in by 21 representatives of intermodal transport companies. Then, the obtained results were analyzed in detail, and conclusions have been drawn.

4 Results

The respondents who filled in the survey were managers employed in intermodal transport terminals located in seaports (7 persons) and rail-road terminals (7 persons), as well as there were 7 forwarders working in transport and forwarding companies.

The distribution of answers put in the first part of questionnaire survey, while investigating respondents' profile, is presented in Fig. 2. Among the respondents were men (86%) and women (14%) with different work experience (up to 25 years).

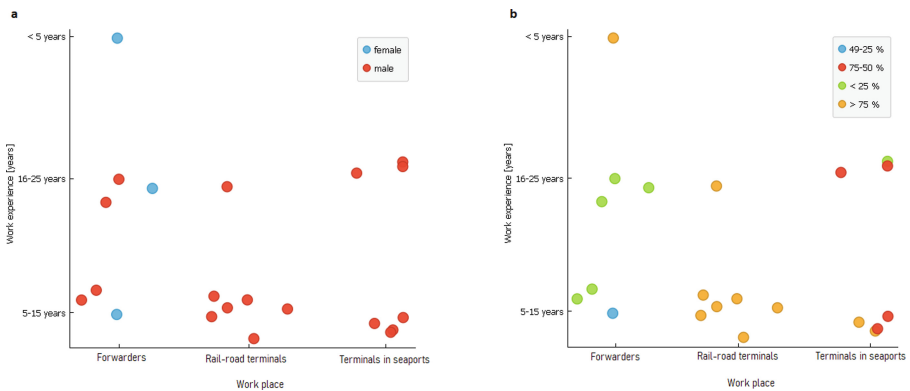


Fig. 2. The answers to questions related to practitioner's profile: (a) respondent's gender; (b) the number of orders that are related to intermodal transport in companies represented by the practitioners.

The companies represented by practitioners were involved in servicing orders related to intermodal transport: 48% of respondents worked in companies that serviced more than 75% of analyzed orders within company's activity, 28% of respondents indicated that the number of mentioned orders serviced in represented companies was below 25%, 19% of respondents were employed in companies servicing 75–50% of orders dealing with intermodal transport, and 5% (1 person) mentioned that the share of considered orders is about 49–25%

In second part of the survey, the respondents were enquired to suggest the activities to increase the level of efficiency in intermodal transport. The practitioners were asked to rate individual activities in Likert scale [30] from 1 to 5, where 1 – the least important activity, 5 – the most important activity. Achieved answers analysis allowed to create the ranking of selected activities and determine the most and the least important actions that may increase the efficiency of intermodal transport (Fig. 3).

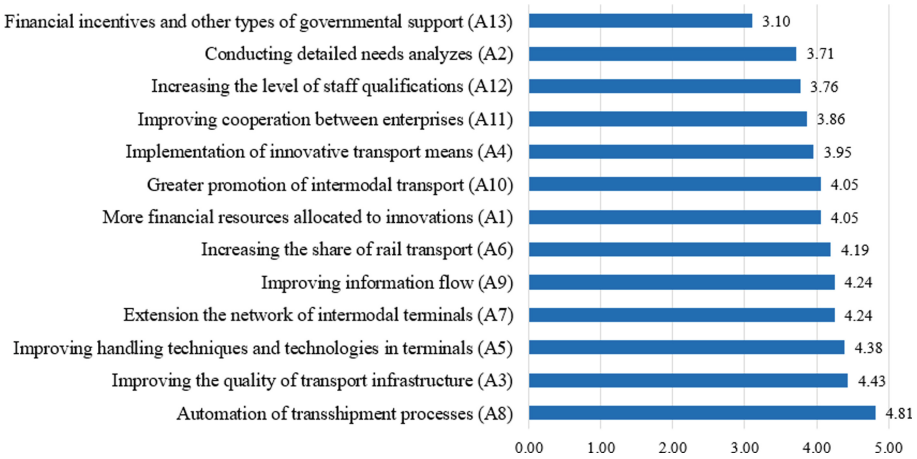


Fig. 3. Responds to the question: “What would you suggest in order to increase the level of efficiency in intermodal transport?” (mean values).

Results analysis allowed to conclude that according to respondents’ opinion, it is necessary to invest in transshipment processes automation (activity A8) to increase the level of intermodal transport efficiency. This activity received the highest rates given by 18 practitioners. The needed actions should also concern the upgrading of infrastructure quality of individual transport modes (A3), as well as improving of handling techniques and technologies within intermodal terminals (A5).

The lowest scores were given to activities such as: financial incentives and other types of governmental support for entrepreneurs (A13) and conducting detailed needs analyzes (A2), increasing the level of staff qualifications (A12), which lead to the conclusion that the problems with the efficiency of intermodal transport are mainly of a technical and technological and/or organizational nature. It was also possible to set the activities ranking within analyzed groups of respondents (Fig. 4 and Table 1).

Results analysis showed that all respondents’ groups had the same viewpoint on the most important activity to improve intermodal transport efficiency (Table 1) indicating automation of transshipment processes (A8). However, it should be noted that there were differences in viewpoints on other selected activities, taking into account their impact on intermodal transport efficiency.

Representatives of intermodal terminals located in seaports gave high ratings to improving handling techniques and technologies in intermodal terminal (A5) and increasing the share of rail transport in intermodal transport (A6). In their opinion the

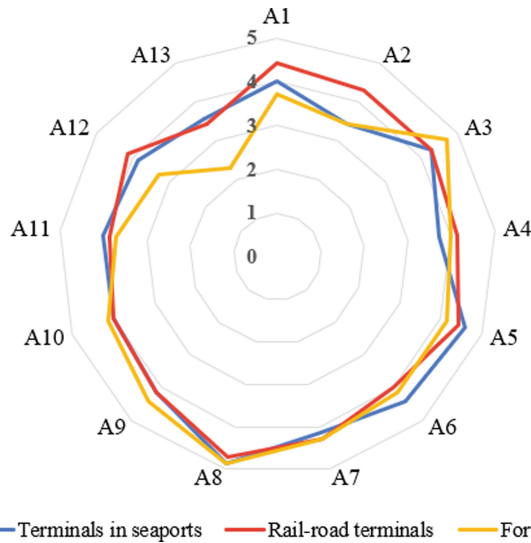


Fig. 4. Answers to the question: “What would you suggest in order to increase the level of efficiency in intermodal transport?”, considering individual respondents’ groups (mean values).

Table 1. Ranking of activities influencing intermodal transport efficiency, considering respondents’ groups.

Terminals in seaports		Rail-road terminals		Forwarders	
Activity	Mean value	Activity	Mean value	Activity	Mean value
A8	4.86	A8	4.71	A8	4.86
A5	4.57	A1	4.43	A3	4.71
A6	4.43	A5	4.43	A9	4.43
A3	4.29	A2	4.29	A7	4.29
A7	4.14	A3	4.29	A5	4.14
A9	4.14	A7	4.29	A6	4.14
A1	4.00	A4	4.14	A10	4.14
A10	4.00	A9	4.14	A4	4.00
A11	4.00	A12	4.14	A1	3.71
A12	3.86	A6	4.00	A11	3.71
A4	3.71	A10	4.00	A2	3.43
A13	3.57	A11	3.86	A12	3.29
A2	3.43	A13	3.43	A13	2.29

least important activity that influence intermodal transport efficiency was conducting detailed needs analyzes (A2), financial incentives and other types of governmental support for entrepreneurs (A13) and implementation of innovative transport means (A4). It could be concluded that terminals' needs analyzes were already done, the needs and ways to receive financial incentives have been identified.

In turn, representatives of rail-road terminals besides improving handling techniques and technologies (A5) gave the same points to the need to allocate more financial resources to the development and implementation of innovations within terminals (A1). The least important activities in their opinion are: financial incentives and other types of governmental support for entrepreneurs (A13), improving cooperation between enterprises (A11) and greater promotion of intermodal transport (A10). It may be stated that terminals had already created cooperation schemes with their clients, however, innovative solution in rail-road terminals are still needed.

Forwarders' representatives mentioned the important impact of improving the quality of transport infrastructure (A3) and improving information flow (A9), that is directly related to the nature of the work performed. According to their viewpoint the least important actions are financial incentives and other types of governmental support for entrepreneurs (activity A13 received the lowest grades among other groups of respondents), increasing the level of staff qualifications (A12) and detailed needs analyzes (A2). Based on conducted literature analysis and the results of survey it was possible to determine the main directions of intermodal transport efficiency improvement, considering the practitioners' viewpoint (Table 2).

Table 2. Main directions of intermodal transport efficiency improvement, considering the practitioners' viewpoint.

Direction	Activity indicator
Improving handling operations	A5, A8
Infrastructure quality improvement	A3, A6, A7
Improvement of processes organization	A9, A11, A12
Transport means improvement	A4
Improvement of financial and governmental support	A1, A13
Promotion and detailed needs analysis	A2, A10

It should be noted that identified directions (Table 2) are in line with intermodal transport development strategies in Poland, however, reflect the practitioners' needs and priorities that may be taken into account by decision-makers who directly select and implement particular actions.

5 Conclusion

The article aimed at determining the activities needed to increase intermodal transport efficiency, considering practitioner's viewpoint. Thirteen activities that may allow to

improve this efficiency were identified and analyzed in detail. Based on collected data analysis it was possible to develop a ranking of activities to increase the efficiency level of intermodal transport. Automation of transshipment processes got the highest rates among the considered actions. The importance of improving the quality of infrastructure in individual transport modes, as well as the need to modernize handling techniques and technologies used in intermodal terminals were also indicated.

It should be emphasized that opinions of considered respondents' groups varied. All groups ranked the need to increase the level of automation of transshipment processes as the most important to improve efficiency of intermodal transport. Such activity implementation requires significant investments, however, allows to reduce operational cost and handling processes duration. Research results also revealed the current needs and directions to improve intermodal transport efficiency seen by practitioners. These needs deal mainly with operational activity improvement.

It should be noted that research results are limited to Polish market conditions that may influence the achieved results. However, the investigation outcomes show the directions that may be chosen by decision-makers to improve the efficiency of intermodal transport. The results of the research may be useful for transport enterprises, logistics and forwarding companies, as well as decision-makers who are involved in intermodal transport operation and strategies development.

The directions of our future research will cover investigation of possibilities and needs for implementation of innovations in intermodal transport.

References


1. Rokicki, T., Ochnio, L., Bórawski, P., et al.: Development of intermodal transport in the EU countries. *Eur. Res. Stud. J.* **24**(4B), 300–308 (2021)
2. Wiśnicki, B., Dyrda, A.: Analysis of the intermodal transport efficiency in the Central and Eastern Europe. *Naše More* **63**(2), 43–47 (2016). <https://doi.org/10.17818/NM/2016/2.1>
3. Filina-Dawidowicz, L., Kostrzewski, M.: The complexity of logistics services at transshipment terminals. *Energies* **15**(4), 1435 (2022). <https://doi.org/10.3390/en15041435>
4. Jacyna, M., Wasiak, M., Lewczuk, K., et al.: Decision problems in developing proecological transport system. *Rocznik Ochrona Srodowiska* **20**, 1007–1025 (2018)
5. gov.pl: Strategia Zrównoważonego Rozwoju Transportu do 2030 roku. <https://gov.pl/attachment/8ca82ea2-ddf5-4cff-8bfc-b7d7bfb1237b>. Accessed 10 May 2022
6. Abu Aisha, T., Ouhimmou, M., Paquet, M., Montecinos, J.: Developing the seaport container terminal layout to enhance efficiency of the intermodal transportation system and port operations—case of the Port of Montreal. *Marit. Policy Manag.* **49**(2), 181–198 (2022). <https://doi.org/10.1080/03088839.2021.1875140>
7. Ge, J., Shi, W., Wang, X.: Policy agenda for sustainable intermodal transport in China: an application of the multiple streams framework. *Sustainability* **12**, 3915 (2020). <https://doi.org/10.3390/su12093915>
8. Mindur, L., Mindur, M.: Intermodal Transport on Selected Continents. In: Sładkowski, A. (ed.) *Modern Trends and Research in Intermodal Transportation*. SSDC, vol. 400, pp. 125–195. Springer, Cham (2022). https://doi.org/10.1007/978-3-030-87120-8_3
9. Galkin, A.: Mechanisms for increasing of transportation efficiency using joint service of logistics systems. *Arch. Transp.* **49**(1), 7–24 (2019). <https://doi.org/10.5604/01.3001.0013.2770>

10. Karišik, A., Škerlič, S., Muha, R.: Time efficiency model for identification of development potentials in urban logistics. *Promet Traffic Transp.* **33**(3), 437–450 (2021). <https://doi.org/10.7307/ptt.v33i3.3662>
11. Kush, Y., Tonkoshkur, M., et al.: The efficiency of food supply chain engineering (case study in Ukraine). *Arch. Transp.* **55**(3), 51–71 (2020). <https://doi.org/10.5604/01.3001.0014.4222>
12. Czapiewska, G.: The importance of intermodal transport in Poland in the context of sustainable development. *Prace Komisji Geografii Komunikacji PTG* **23**(3), 69–83 (2020)
13. Snquz-Daz, C.: Transport infrastructure quality and logistics performance in exports. *Economics* **9**(1), 107–124 (2021). <https://doi.org/10.2478/eoik-2021-0008>
14. Smolnik, P.: The prospects for growth of the intermodal transport in Poland. In: Conference Quality Production Improvement – CQPI, vol. 3, no. 1, pp. 53–62. Sciendo (2021). <https://doi.org/10.2478/cqpi-2021-0006>
15. Gnap, J., Senko, Œ, Drliciac, M., Kostrzewski, M.: Modeling of time availability of intermodal terminals. *Transp. Res. Procedia* **55**, 442–449 (2021). <https://doi.org/10.1016/j.trpro.2021.07.007>
16. Jacyna, M., Jachimowski, R., Szczepaski, E., Izdebski, M.: Road vehicle sequencing problem in a railroad intermodal terminal-simulation research. *Bull. Pol. Acad. Sci. Techn. Sci.* **68**(4), 1135–1148 (2020). <https://doi.org/10.24425/bpasts.2020.134643>
17. Szczepaski, E., Jacyna, M., Jachimowski, R., et al.: Decision support for the intermodal terminal layout designing. *Arch. Civ. Eng.* **67**(2), 611–630 (2021). <https://doi.org/10.24425/ace.2021.137188>
18. Kostrzewski, M., Kostrzewski, A.: Analysis of operations upon entry into intermodal freight terminals. *Appl. Sci.* **9**(12), 558 (2019). <https://doi.org/10.3390/app9122558>
19. Daduna, J.R.: Intermodal competition in freight transport - political impacts and technical developments. In: Mes, M., Lalla-Ruiz, E., Vo, S. (eds.) ICCL 2021. LNCS, vol. 13004, pp. 642–660. Springer, Cham (2021). https://doi.org/10.1007/978-3-030-87672-2_42
20. Han, B., Shi, S., Gao, H., Hu, Y.: A sustainable intermodal location-routing optimization approach: a case study of the Bohai Rim region. *Sustainability* **14**(7), 3987 (2022). <https://doi.org/10.3390/su14073987>
21. Xiaoping, Q., Juan, L., Fatimah, R., Chen, J.: Activity efficiency model in business process under conflict information and its application. *Int. J. Comput. Intell. Syst.* **14**(1), 528–536 (2021). <https://doi.org/10.2991/ijcis.d.201215.004>
22. Milewski, D., Winicki, B.: Modelling intermodal transport systems – directions for scientific research. *Res. J. Univ. Gdask Transp. Econ. Logist.* **17**, 35–43 (2017)
23. Agamez-Arias, A., Moyano-Fuentes, J.: Intermodal transport in freight distribution: a literature review. *Transp. Rev.* **37**(6), 782–807 (2017). <https://doi.org/10.1080/01441647.2017.1297868>
24. Filina-Dawidowicz, L., Gajewska, T.: Examination of importance and range of comprehensive service for refrigerated containers in seaports. *Int. J. Appl. Manag. Sci.* **10**(1), 26–43 (2018)
25. Tamannaei, M., Zarei, H., Rasti-Barzoki, M.: A game theoretic approach to sustainable freight transportation: competition between road and intermodal road–rail systems with government intervention. *Transp. Res. Part B Methodol.* **153**, 272–295 (2021). <https://doi.org/10.1016/j.trb.2021.09.002>
26. Mndur, L., Pawska, M.: Methods of promoting intermodal transport development in the Federal Republic of Germany, France and Italy in years 1990–2016 – conclusions for Poland. *Transp. Probl.* **14**(2), 135–143 (2019). <https://doi.org/10.20858/tp.2019.14.2.12>
27. Yan, H., Guo, L.: A Study on the development status and planning of Guangzhou’s rail-water intermodal transport: a case study of Huangpu port. In: CICTP 2020, pp. 3343–3354. ASCE (2020). <https://doi.org/10.1061/9780784482933.288>
28. gov.pl: Kierunki rozwoju transportu intermodalnego do 2030 r. z perspektyw do 2040 r. <https://gov.pl/attachment/63382ca4-c027-4d00-9b03-99bbad9dbf1e>. Accessed 10 May 2022

29. stat.gov.pl: Transport intermodalny w Polsce w 2020 roku. <https://stat.gov.pl/obszary-tematyczne/transport-i-lacznosc/transport/transport-intermodalny-w-polsce-w-2020-roku,14,5.html>. Accessed 10 May 2022
30. Joshi, A., Kale, S., Chandel, S., Pal, D.: Likert scale: explored and explained. *Br. J. Appl. Sci. Technol.* 7(4), 396–403 (2015). <https://doi.org/10.9734/BJAST/2015/14975>



Analysis of Urban Freight Distribution Management Methods on the Principles of “Green Logistics”

Olesia Hriekova^(✉) 

O. M. Beketov National University of Urban Economy in Kharkiv, 17 Marshala Bazhanova Street, Kharkiv 61002, Ukraine

olesia.hriekova@kname.edu.ua

Abstract. Transport network of the city is an important component and serves for distribution of different goods. The effective and sustainable solution of the distribution of goods in urban areas follows the concepts of City logistics. It is aimed at fast and reliable transportation of goods in terms of effective and ecological standards of distributions. Therefore, the researchers are looking for different approaches that allow for fast and reliable logistics operations carried out by vehicles and waste disposal services. The wide application of environmentally friendly vehicles in urban logistics can help to mitigate such problems as environmental pollution, global warming, etc. To shed light on the introduction of environmentally friendly vehicles in urban logistics, the article conducted a systematic review of the empty list literature on this topic.

Keywords: Green logistics · Vehicle Routing Problem · Ecologistics · Environment

1 Introduction

Among researchers in different fields and industries, environmental impact has recently increasingly been considered. Therefore, decisions are made considering the ecological factor and do not leave logistics aside, because it is one of the main sources of different pollution [1].

Recently, you can see a greater interest in the concepts of sustainable development. And from the point of view of logistics, and to sustainable transport. The distribution of goods, characterized by movement between distribution centers, warehouses and retail activities, is an integral part of urban activity. Automobiliation and traffic growth have a significant impact on sustainable development. Because of the resulting congestion, urban traffic is responsible for 40% of CO₂ emissions and 70% of other pollutants. As for noise emissions and air pollution, the movement of freight vehicles is 40%. All European cities are concerned with this issue [2].

Due to the spread of e-commerce and the latest management principles (“just in time” and others), the demand for cargo distribution in the city grows year by year. The

pandemic COVID-19 was also an important aspect of the growing demand for distribution of huge daily volumes [3]. At present, problems have emerged due to the increase in traffic in the cities, namely: congestion, air pollution, lack of public space, noise emissions, etc. All factors reduce the quality of life of the inhabitants. The paper [4] found that City logistics has a significant impact on the following aspects of sustainability: economic (cost of supplies, etc.), environmental (CO₂ emissions, noise pollution) and social (congestion in the city on others). To solve these problems, the authorities pay attention to initiatives on sustainable development (for example, the use of more environmentally friendly vehicles, the policy is aimed at rules of freight distribution, such as the load capacity of the vehicle, introduction of time windows, etc. [5]). In the White paper of 2011, highlights transport goals pursued by the European Union and government policy in this sector. The document refers to reducing greenhouse gas emissions by 60% in 2050 in the transport sector. It should be mentioned that in White paper of 2011 on transport also considered ways of achieving energy and ecological goals (technological innovations, which can increase energy efficiency of vehicles, introduction of new technologies and engines for environmentally friendly transport).

2 Literature Review

2.1 Definitions and Basic Principles of “Green Logistics”

Also, among European countries there is a belief that for several reasons it is necessary to use more ecological vehicles («green» vehicles – with an intensity of emissions up to 120 g of CO₂ emissions per km). Because of this, the European Committee pays much attention to environmental issues, all sectors and organizations are under pressure to implement relevant policies. Therefore, the interest in the development of “green logistics” (GL) by companies, government and society is growing especially because traditional logistics cannot meet the requirements of the present and has a direct impact on the environment. Transport is the source of environmental pollution and the user of natural resources, so the environmental issue cannot remain outside the scope.

In [6] the term GL is defined as the practice of chain management of logistics systems and strategies, with emphasis on reducing ecological and energy traces of distribution of goods which is focused on materials processing, waste management, packaging and transportation.

Many researchers pay attention to the definition of GL and its description. Such work of authors [7] noted the components of GL, namely: all kinds of activity connected with eco-efficient management of return flows of products and information between production and consumption. Researchers define GL: how to manage the green supply network; the activities of organizations considering environmental components and integrating it into supply chain management to change environmental performance [8]. The main green logistics activities include different distribution strategies that assess the environmental impact, reduce energy use in logistics operations, reduce waste and manage it. This term is also considered from the point of view of sustainable development, where it is defined as «production and distribution of goods in a sustainable order, considering ecological and social factors» [9]. The definition of WCED (1987) sustainable development and corporate responsibility corresponds to the interpretation of GL.

Therefore, the principles of «green logistics» are becoming more and more attention due to the deterioration of the environment all over the world [10].

Three pillars of sustainable development can be applied to GL. As noted in the definitions of this term earlier, in the past, companies coordinated their logistics activities (distribution of goods, freight transportation, warehousing, packaging, material processing and data collection and management to meet the demand of customers on the minimum costs, which are related to monetary conditions). Now stakeholders pay more attention to the environment, so the negative impact on it is seen as one of the factors of cost. Many companies consider the external costs of logistics operations related to the environment (climate change, environmental pollution, noise). GL is an attempt to identify ways to reduce these external effects and achieve a more sustainable balance between environmental, economic, and social goals [11].

Over the past 40 years, GL has been several ways, for example:

- reduction of transport costs [12],
- City logistics [13],
- corporate environmental strategies in the field of logistics [14],
- reverse logistics [15],
- management of the «green» supply chain [11].

GL also presents three perspectives: public (for private sectors), operational (for strategic planning) and local (for global). The first prospect of GL refers to those who have begun to push the government to implement a policy of mitigating the devastating effects of the movement of goods. The private sector has also begun to formulate environmental strategies at the corporate level. Efficiency is aimed at increasing corporate commitment to GL. The local and global perspective is focused on the relevant impact on the environment of air pollution, vibration, noise, accidents, etc. [13].

Nowadays the term GL is often used as “the result of logistics activity, which is primarily motivated by environmental considerations”. The term GL is also defined as the use of cost-saving, convenient options for transportation, but the priority is the company image [14]. GL is often known as “environmental logistics”, defined as “understanding and minimizing the environmental consequences of logistics” [15]. These measures are intended to assess the environmental impact on transport, which reduces fuel consumption and the use of different types of resources.

And in the paper [16] there are four factors that influence GL, namely: company, consumers, governments, and society. Consumers have their own requirements for «green» products and services. Customers, especially with high environmental awareness, may require products delivered by clean vehicles or products that have a minimum emission, forcing suppliers to move to “green solutions”. In general, external and internal factors that influence the adoption of environmental policy by companies can be divided. Pressure of stakeholders, environmental regulations, industrial sector, company size, geographical location of retailers, internationalization, strategic attitude, position in the value chain, management relations and motivation, manager characteristics and human resources are the appropriate environmental and organizational changes that often appear in the work of different researchers considering such topics.

The principles of GL were being studied not so long ago. One of the important articles written on this subject is the paper [14]. The authors considered various ways of solving the existing problems, among them: reduction of the intensity of freight vehicles, distribution of goods on less coal-fired vehicles, increase of the efficiency of transport vehicles, increase of energy efficiency of freight operations, decrease of CO₂ emissions while using freight vehicles, decarbonization of warehouse operations and other things. The most important in spreading the problems of GL is that stakeholders take responsibility for the negative impact on the environment from their activities. Therefore, companies are considering the possibility of including environmental thinking in their business strategies, for example in Polish companies [14].

As noted in the paper [17], achievement of the goals of GL is based on two strategies: to promote the introduction of environmentally friendly vehicles; to develop and implement political measures to reduce the negative impact of urban distribution. In their work, the researchers found that the number of works published in this field and similar directions has grown rapidly in recent years.

2.2 Vehicle Routing Problem

In 1959, the Vehicle Routing Problem (VRP), which deals with the distribution of goods between stakeholders with known needs, was highlighted. This problem is described on the matrix (network of urban roads). In turn, it consists of road areas, the location of retailers, warehouses and transport links. Sections of the road – arcs (directional or non-directional, depending on the possibility to move in one or both directions). The location of stakeholders is represented by nodes. The basic variant of VRP is the Capacity Vehicle Routing Problem (GVRP), in which each vehicle has a limited load capacity, each retailer is associated with a fixed demand that cannot be divided. Route optimization results in significant savings from previous researchers estimates from 5 to 30% or from 5 to 20%.

There are the following variants of VRP: limited distance, limited time windows for distribution of goods, the problem of reverse transport (VRPB), self-delivery and delivery (VRPPD).

Various goods are transported by vehicles, which account for 25% of the city's street traffic. With the allocation of problems with transport, growth of population of cities and pressure of the public, the number of research of urban logistics has increased. Despite growing interest in this topic, City VRP is not considered enough. Urban logistics is the process of full optimization of the logistics and transport activities of private companies in urban areas, considering the transport environment, congestion and energy consumption within the market economy. Also, the goal of urban logistics is global optimization of logistics systems in the urban area, considering the costs and benefits of the schemes for the public and private sectors. In the paper [18] the author has allocated four types of stakeholders: guides of goods, carriers, residents and administrators. The goals of goods on the goal are sales of products with the maximum level of service. Carriers provide services for distribution of goods from freight forwarders to retailers, minimizing transport costs. Residents want to have a living environment (free of pollution, congestion and accidents). On the other hand, city authorities are more interested in improving the economic and ecological state of the city.

Researchers have highlighted that VRP is a mathematical programming model. In 1964 the authors proposed a principal heuristic method [19]. Over the past decades, research of VRP models and their solutions have been conducted and published. Real-time traffic information was a key driving force in City VRP [20], to build smart routes. Thus, a method of data collection such as Floating Car Data has appeared. Also, some cities have introduced a policy to reduce the difference in air pollution and noise by entering time windows for moving vehicles. At present, one of the fundamentals of “green policy” is fuel and environmental issues.

2.3 The Position of Stakeholders Regarding the Solution of VRP

Optimization of routes by vehicles in cities is caused by two goals, namely: reduction of congestion, increase of mobility of transport services of goods in urban areas at minimal costs and positive contribution to environment and sustainable development by reduction of pollution and noise or improvement of life of inhabitants of the city. But depending on the involved stakeholders, their goals differ. The position of the state authorities can contradict individual results and goals of private stakeholders, whose aim is to increase their economic benefits. The control of traffic flows is carried out by carriers, but local authorities can influence them by means of the introduction of appropriate rules. The combination of different goals and influence makes the vehicle routing models very different. Designed for local authorities to assess the impact of the new policy are theoretical. On the part of private companies, the aim is to satisfy the daily demand of consumers at minimal costs.

Local government policy can be implemented as a restriction of access to certain special zones during certain periods. The initial problem is known as a Vehicle Routing Problem with Access time Windows (VRPATW). The access time windows (TW) differ from TW in VRP: they restrict access to the total corresponding zone (limited zone). They do not relate to the time of delivery, but to the time of day when vehicles can enter. In paper, the authors [21] show that this type of regulation imposes additional costs on carriers and makes them attract more vehicles. Limited access policy principles can be combined with the introduction of a distribution center (CDC) in a system where goods are shipped to cleaner vehicles for last-mile delivery. Under this regulation, prohibited areas are valid for some types of vehicles and distribution is not limited in time. The authors [22] show how this will reduce the number of freight vehicles in the city center. And model this configuration as a two-stage VRP (2E-VRP) and assess how CDC can reduce overall costs compared to VRP costs. In work [23] the decisions concerning time windows and the task of synchronization of different categories of vehicles are considered in more detail. The authors [24] also research the impact of TW restrictions and vehicle movement on distribution of goods in cities. They calculate routes with the classic VRPTW solution, changing the data to simulate the different scenarios they want to compare. Also, develop an app to help authorities assess different scenarios of the delivery system based on a single CDC located near a medium-sized city. The problem that arises is the Multi-Trip VRP of TW, which considers both self-driving and delivery, as well as a different fleet of vehicles.

The planners need to consider several important aspects. The first of them is a strong connection in urban areas between time of day and time on the road. Several authors

follow this line and include time dependence to their VRP models [25]. According to the results, it is evident how this helps to reduce CO2 emissions by 7%, and decisions calculated without considering time-dependent on the road, lead to up to 60% of missed time windows when estimated according to traffic time.

Also, an important characteristic of cities, which cannot be ignored, is their dynamics. There are the following technical solutions to combat unforeseen events: fleet monitoring during operation and response to them by means of a reasonable regulation of the route of vehicles. This information can be used to optimize a route [26].

Also, an important aspect to consider is the structure of the road network, especially in old cities: narrow streets, availability of parking places, often one-way traffic directions [21]. Due to structural features and restrictions, there is a problem with entering the city center for large freight vehicles. And the capacity of smaller vehicles causes an excessive quantity of trips during the day. Therefore, the optimization of the route differs from the traditional VRP, where one trip is allowed for each vehicle. Many authors who researched this situation (in the context of urban logistics) [27]. The first who considered the distribution of various goods in Berlin, fresh food in Duisburg or drinks in Dortmund, demonstrated how it helps to better use time windows and vehicle capacity. Cooperation and collaboration among companies are also topics of great interest [27]. Authors show how sharing systems can improve service quality, cost of routing, and reduce CO2 emissions.

At present, considerable attention is paid to the development of transport infrastructure, modern mechanical and mathematical models are offered. In particular, this applies to electric transport, considering both economic parameters [28] and technical issues of operation [29].

3 Research Results Analysis

The paper considers several topical issues that have been researched by various Ukrainian authors. Highlighting the criteria that interested us, a significant number of articles related to other issues were removed. Table 1 presents only those elements that remained in the selection, which is 126 works.

The data obtained were structured over the years into lists and the key topics they reveal were analyzed. All published works considered the country in which the articles were published. Selected works have been published in Ukraine.

Table 1. Search by database according to category filters.

Search by Google Scholar	Records
“Green Logistics”	99
Vehicle Routing Problem	27

In Fig. 1a,b shown 99 and 27 scientific articles broken down by year, as defined in the databases. In addition, based on this, we can note the growing trend of research in

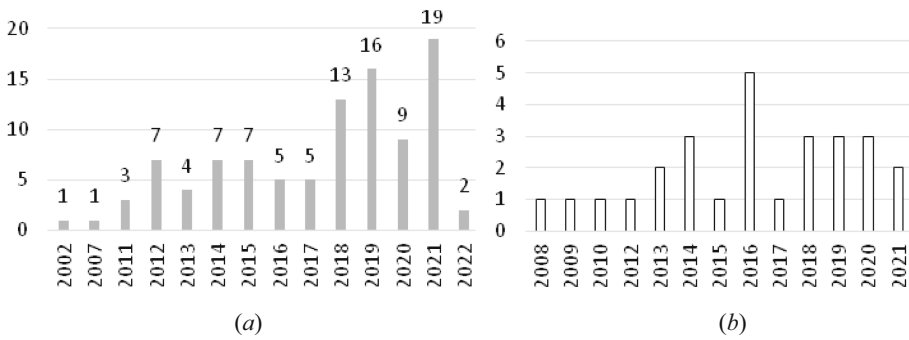


Fig. 1. Annual scientific publications on: (a) GL; (b) VRP

these areas. Regarding Fig. 1a, it can be concluded that in 2002 the topic of GL research began. Subsequently, it was studied steadily, but since 2018 the number of studies has increased almost 3 times. With the growing importance of «green logistics» in the world, draw attention to this research topic, which has been growing ever since. In 2021, the largest rate of published articles. Thus, Fig. 1b shows that the consideration of Vehicle Routing Problems began in 2008, and in 2016 most articles on this topic were published. After 2016, we can say that research in this area continues.

Table 2. Main keywords risen by research.

Keywords	Records
Green Logistics, approaches, principles	99
Enterprise/manufacture based on GL	54
Reduce resource use/use of alternative energy	53
Government level/norms and standards in GL	64
Logistics management considering the principles of GL	47
Waste management/reverse concept	64
Green Logistics in sustainable development	37
Cost minimization due to implementation GL/VRP solution	44
Modern technologies/real-time monitoring when VRP is solved	40
Stakeholders in GL/when solving VRP	38
Term “Ecologistics”	21
The impact of globalization on GL	16
Environmental safety	13
Management/marketing in GL	11
Ecological vehicles in GL	7
Vehicle Routing Problem	21
Time window (TW)/Restrictions	13

Therefore, we will consider the main keywords and topics that are found in the work under consideration. Table 2 presents a list of keywords in the researchers and the quantity of publications, respectively.

Therefore, in the first group of search queries, the most mention of GL, application at enterprises, use of resources and maintenance of “green” policy at the government level is mentioned. Note that waste management and disposal were also frequent issues in the review of the paper investigated.

When considering the Vehicle Routing Problem, it has been highlighted that the studies often consider stakeholders (especially consumers and producers). Also, when researching this topic often use a restriction policy such as the introduction of time windows in service.

Table 3. Crossing Matrix (search area vs keywords) based in the records.

Research area																		
#Records		99	54	53	64	47	64	37	44	40	38	21	16	13	11	7	21	13
		Green Logistics, approaches, principles	Enterprise / manufacture based on GL	Reduce resource use / use of alternative energy	Government level / norms and standards in GL	Logistics management considering the principles of GL	Waste management/reverse concept	Green Logistics in sustainable development	Cost minimization due to implementation GL/VRP solution	Modern technologies/real-time monitoring when VRP is solved	Stakeholders in GL / when solving VRP	Term “Ecologistics”	The impact of globalization on GL	Environmental safety	Management / marketing in GL	Ecological vehicles in GL	Vehicle Routing Problem	Time window (TW) / Restrictions
45	Logistics	45	21	18	25	19	21	9	17	10	11	7	4	5	3	4	6	4
6	Management	6	4	4	4	4	3	3	-	3	2	-	-	-	2	-	-	-
13	Ecology	13	8	7	5	3	12	6	3	4	3	7	4	2	3	1	-	-
33	Economy	23	16	11	19	11	15	9	10	5	10	4	4	4	-	1	3	2
10	Sustainable development	10	3	9	10	5	9	9	4	4	3	2	3	2	1	-	-	-
2	Marketing	2	2	1	1	2	1	1	1	1	1	1	1	-	2	-	-	-
5	Modeling	-	-	1	-	-	-	-	2	1	3	-	-	-	-	-	2	1
7	Computer mathematics	-	-	-	-	-	-	-	2	3	5	-	-	-	-	-	3	3
5	Transport engineering	-	-	3	-	3	3	-	5	9	-	-	-	-	-	1	7	3

More detailed use of keywords is described in Table 3. The published papers are broken down by topics and the number of mentions in each of them has been allocated. So, we see that the most works are written in the sphere of logistics and economy.

The largest number of mentions of the term GL, also many “enterprises and manufacturers”. Because the papers emphasize that responsibility falls on these stakeholders. The mention of the state and government levels is conditioned by the necessity to implement the relevant environmental policy. It is the state objects that should be directed to save the environment.

Note that a new concept is introduced – “Ecologistics”, which is mentioned in works 21 times in different spheres of research.

As for the consideration of publications on the search for “Vehicle Routing Problem”, different spheres of research consider this issue. Such as logistics, economics, modeling, computer mathematics. The introduction of restrictions (time windows) in algorithms of route construction and introduction of modern technologies (real-time data collection) is considered.

4 Conclusion

The paper examined 126 articles published by Ukrainian scientists and researchers related to topics of GL and VRP. From the search in the web-resource Scholar and several various works, only those publications that met the request are allocated. For the first time such a deep analysis of literature in the field of GL and VRP was carried out.

At the first stage of the analysis of publications the tendency of increasing interest to the first and second themes was formed. We have concluded that in 2002 the topic of research of GL was started. It has been researched steadily since then, but since 2018 the number of papers has increased almost 3 times. With the increasing importance of GL in the world, the research topic, which has since grown in 2021, is the largest indicator of published articles. Although 2022 has just begun, 2 works on this topic have already been published. And publications on the topic of the Vehicle Routing Problem began in 2008, and in 2016 the most articles on this topic were published. After 2016, research in this area continues.

At the second stage the keywords were analyzed. Therefore, it is possible to highlight related research topics. For example, publications of GL have a rich number of mentions of manufacturers and enterprises. The papers emphasize that these stakeholders should bear responsibility for environmental pollution from processes. And the technologies and approaches that will help solve this issue are presented. The publications also emphasize the importance of the government policy aimed at environmental protection. Note that in different spheres the given aspect is considered, namely: logistics, management, ecology, economy, sustainable development, marketing.

As for publications on the topic VRP, different spheres of research consider this issue. Such as logistics, economics, modelling, computer mathematics. The introduction of restrictions (time windows) in algorithms of route construction and introduction of modern technologies (real-time data collection) is considered.

Based on such research, it is planned to develop models and methods of organization of the process of urban cargo transportation, proceeding from principles of GL.


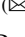




References

1. Perboli, G., Rosano, M.: Parcel delivery in urban areas: opportunities and threats for the mix of traditional and green business models. *Transp. Res. Part C Emerg. Technol.* **99**, 19–36 (2019). <https://doi.org/10.1016/j.trc.2019.01.006>
2. Janjevic, M., Knoppen, D., Winkenbach, M.: Integrated decision-making framework for urban freight logistics policy-making. *Transp. Res. Part D: Transp. Environ.* **72**, 333–357 (2019). <https://doi.org/10.1016/j.trd.2019.05.006>
3. Schwerdfeger, S., Boysen, N.: Optimizing the changing locations of mobile parcel lockers in last-mile distribution. *Eur. J. Oper. Res.* **285**(3), 1077–1094 (2020). <https://doi.org/10.1016/j.ejor.2020.02.033>
4. Gatta, V., Marcucci, E., Nigro, M., et al.: Public transport-based crowdshipping for sustainable city logistics: assessing economic and environmental impacts. *Sustainability* **11**(1), 145 (2018). <https://doi.org/10.3390/su11010145>
5. Awasthi, A., Adetiloye, T., Crainic, T.G.: Collaboration partner selection for city logistics planning under municipal freight regulations. *Appl. Math. Model.* **40**(1), 510–525 (2016). <https://doi.org/10.1016/j.apm.2015.04.058>
6. Rodrigue, J.-P., Slack, B. Comtois, C.: Green logistics. In: Brewer, A.M., et al. (eds.) *Handbook of Logistics and Supply-Chain Management*, vol. 2, pp. 339–350. Emerald Group Publishing Limited, Bingley (2017). <https://doi.org/10.1108/9780080435930-021>
7. Patella, S.M., Grazieschi, G., Gatta, V., et al.: The adoption of green vehicles in last mile logistics: a systematic review. *Sustainability* **13**(1), 6 (2020). <https://doi.org/10.3390/su13010006>
8. Holguín-Veras, J., Amaya-Leal, J., Wojtowicz, J., et al.: *Improving Freight System Performance in Metropolitan Areas: a Planning Guide*. The National Academies Press, Washington (2015). <https://doi.org/10.17226/22159>
9. Doolun, I.S., Ponnambalam, S.G., Subramanian, N., Kanagaraj, G.: Data driven hybrid evolutionary analytical approach for multi objective location allocation decisions: automotive green supply chain empirical evidence. *Comput. Oper. Res.* **98**, 265–283 (2018). <https://doi.org/10.1016/j.cor.2018.01.008>
10. Zhang, S., Lee, C.K., Chan, H.K., et al.: Swarm intelligence applied in green logistics: a literature review. *Eng. Appl. Artif. Intell.* **37**, 154–169 (2015). <https://doi.org/10.1016/j.engappai.2014.09.007>
11. Lyon, T.P., Maxwell, J.W.: Corporate social responsibility and the environment: a theoretical perspective. *Rev. Environ. Econ. Policy* **2**(2), 240–260 (2008). <https://doi.org/10.1093/reep/ren004>
12. Muñoz-Villamizar, A., Montoya-Torres, J.R., Faulin, J.: Impact of the use of electric vehicles in collaborative urban transport networks: a case study. *Transp. Res. Part D Transp. Environ.* **50**, 40–54 (2017). <https://doi.org/10.1016/j.trd.2016.10.018>
13. McKinnon, A., Browne, M., Whiteing, A., Piecyk, M. (eds.): *Green Logistics: Improving the Environmental Sustainability of Logistics*. Kogan Page Publishers, London (2017)
14. Arza Santas, J.: *Análisis de la distribución urbana sostenible de mercancías en el Casco Antiguo de Pamplona*. Dissertation, Public University of Navarre (2019)
15. Trushkina, N.V.: Green economy as a key vector for the transformation of Italy's logistics system. In: IX International Scientific and Practical Conference “Advancing in research, practice and education”, pp. 35–40. International Science Group, Florence (2022). <https://doi.org/10.46299/ISG.2022.I.X>. (in Ukrainian)
16. Lohre, D., Gotthardt, R.: Carbon footprinting in einer nachhaltig ausgerichteten Logistik. In: Deckert, C. (ed.) *CSR und Logistik. MCSR*, pp. 65–86. Springer, Heidelberg (2021). https://doi.org/10.1007/978-3-662-63570-4_3

17. Ren, R., Hu, W., Dong, J., et al.: A systematic literature review of green and sustainable logistics: bibliometric analysis, research trend and knowledge taxonomy. *Int. J. Environ. Res. Public Health* **17**(1), 261 (2020). <https://doi.org/10.3390/ijerph17010261>
18. Letnik, T., Marksel, M., Luppino, G., et al.: Review of policies and measures for sustainable and energy efficient urban transport. *Energy* **163**, 245–257 (2018). <https://doi.org/10.1016/j.energy.2018.08.096>
19. Clarke, G., Wright, J.W.: Scheduling of vehicles from a central depot to a number of delivery points. *Oper. Res.* **12**(4), 568–581 (1964). <https://doi.org/10.1287/opre.12.4.568>
20. Gmira, M., Gendreau, M., Lodi, A., Potvin, J.Y.: Managing in real-time a vehicle routing plan with time-dependent travel times on a road network. *Transp. Res. Part C Emerg. Technol.* **132**, 103379 (2021). <https://doi.org/10.1016/j.trc.2021.103379>
21. Masson, R., Trentini, A., Lehuédé, F., Malhéné, N., Péton, O., Tlahig, H.: Optimization of a city logistics transportation system with mixed passengers and goods. *EURO J. Transp. Logist.* **6**(1), 81–109 (2015). <https://doi.org/10.1007/s13676-015-0085-5>
22. Perboli, G., Tadeim, R., Fadda, E.: New valid inequalities for the two-echelon capacitated vehicle routing problem. *Electron. Notes Discrete Math.* **64**, 75–84 (2018). <https://doi.org/10.1016/j.endm.2018.01.009>
23. Grangier, P., Gendreau, M., Lehuédé, F., Rousseau, L.M.: An adaptive large neighborhood search for the two-echelon multiple-trip vehicle routing problem with satellite synchronization. *Eur. J. Oper. Res.* **254**(1), 80–91 (2016). <https://doi.org/10.1016/j.ejor.2016.03.040>
24. Boschetti, M., Maniezzo, V.: A set covering based matheuristic for a real-world city logistics problem. *Int. Trans. Oper. Res.* **22**(1), 169–195 (2015). <https://doi.org/10.1111/itor.12110>
25. Rabbani, M., Bosjin, S., Yazdanparast, R., Saravi, N.: A stochastic time-dependent green capacitated vehicle routing and scheduling problem with time window, resiliency and reliability: a case study. *Decis. Sci. Lett.* **7**(4), 381–394 (2018). <https://doi.org/10.5267/j.dsl.2018.2.002>
26. Marujo, L.G., Blanco, E.E., Mota, D.O., Leite, J.M.L.G.: The use of public railway transportation network for urban intermodal logistics in congested city centres. In: Marinov, M., Piip, J. (eds.) *Sustainable Rail Transport*. LNM, pp. 187–207. Springer, Cham (2020). https://doi.org/10.1007/978-3-030-19519-9_6
27. Leonardi, J.: Sustainable solutions in urban freight & logistics management: European experiences. Paper presented at FFIJ-Michelin Foundation Workshop City Logistics for Sustainable and Liveable Cities, EHESS, Paris, 25 January 2021
28. Shpachuk, V., Chuprynin, A., Garbuz, A., Suprun, T.: A multifactor analysis of the rail transport car that passes over a joint unevenness with respect to the phases of its motion. *East. Eur. J. Enterp. Technol.* **1**, 55–61 (2018). <https://doi.org/10.15587/1729-4061.2018.121584>
29. Shpachuk, V., Chuprynin, A., Daleka, V., Suprun, T.: Simulation of impact interaction of rail transport carriage in a butt roughness zone. *Sci. J. Silesian Univ. Technol. Ser. Transp.* **106**, 141–152 (2020). <https://doi.org/10.20858/sjsutst.2020.106.12>



Efficiency of “Green” Logistics Technologies in Multimodal Transportation of Dangerous Goods

Denis Lomotko¹  , Oleksandr Ohar¹ , Dmytro Kozodoi¹ ,
Vitalii Barbashyn² , and Mykola Lomotko¹ 

¹ Ukrainian State University of Railway Transport, 7 Feuerbach Square, Kharkiv 61050, Ukraine
den@kart.edu.ua

² O. M. Beketov National University of Urban Economy in Kharkiv, 17 Marshala Bazhanova Street, Kharkiv 61002, Ukraine

Abstract. The improvement of the technology for performing international and domestic transportation of dangerous goods through the use of container and piggyback trains is considered. It has been established, that these technologies have significant advantages in terms of reducing the negative impact on the environment in comparison with the delivery of dangerous goods only by certain modes of transport. A brief feature of the main environmental characteristics of the routes of multimodal trains is given and assessed the negative impact of each type of transport separately and as part of a multimodal system on the environment. It has been established, that reducing the share of unimodal road transport, replacing them with multimodal ones with the participation of rail, sea and river modes of transport, makes it possible to increase environmental friendliness when transporting big numbers of dangerous goods - this reduces the number of flights during transportation and reduces the harmful impact on the environment. The ways of further development of “green” logistics as a safety factor in the transportation of dangerous goods in containers and piggyback are proposed.

Keywords: Container · Green logistic · Multimodal transportation · Railway · Environmental impact · Dangerous goods · Glory of Ukraine

1 Introduction

The emergence of “green” logistics, as a concept for ecologically rationally designing and operation of logistics systems, refers to the methodology of sustainable economic development. According to experts, transport accounts for about 8% of all carbon pollution of atmospheric air on the planet, therefore, the introduction of “green” technologies in logistics activities will make it possible to take certain steps to preserve the climate on the planet. In this regard, research and development of technologies for multimodal transportation of dangerous goods are relevant [1, 2].

Automobile transport, except affecting the atmospheric air, carries out contaminates soil, water resources, acoustic pollution of the environment and has a high probability

of significant negative consequences as a result of road accidents during the transport of dangerous goods. Therefore, a strategic direction for the development of “green” logistics in the transport of dangerous goods is the refusal or reduction of the share of transport in favor of more environmentally rail transport.

2 Relevance

According to experts, transport accounts for 8% of all carbon dioxide emissions on the planet, storage facilities – another 3% [1]. In this regard, the widespread introduction of “green” technologies in logistics activities will make a significant contribution to the preservation of the climate on the planet, suitable for safe human life. Synonymous with the term “green” logistics experts call ecological logistics.

The development of combined and multimodal transport provides for the creation of a unified system for the functioning of the transport system, in particular rail and road, which makes it possible to carry out transport services on a scheme “door-to-door” and “just-in-time”. As a result, on the railways of many countries run piggyback, container trains and route container groups, as well as trains of combined transport [3].

The purpose of the paper is a brief analysis of the state of container and piggyback transportation of dangerous goods, consideration of the advantages and disadvantages of operating various types of transport and their impact on environmental safety. The task “green” logistics to reduce the negative impact of transport on the environment is the integration of various modes of transport, the implementation of their interaction with minimal involvement of automobile transportation. Thus, it will be the task of organizing multimodal or intermodal transportation and the formation of promising multimodal transport chains.

3 Research Methodology

If the main function of traditional logistics is the optimal management and coordination of all types of logistics flows in order to meet the needs of customers with minimal costs, then “green” logistics pays great attention to external costs associated with climate change, air, water and soil pollution, noise influence in order to achieve a sustainable balance between economic performance, the environment and the requirements of society regarding safety standards. Container and piggyback transportation in comparison with traditional delivery methods is currently the most widespread technology, contributing to the development of “green” logistics.

Analyzing the above advantages of modes of transport, it can be noted, that none of them is universal. Each mode of transport is cost-effective and environmentally friendly only with certain characteristics of the dispatch. For rail and water transport are cost-effective bulk shipments over long distances. Automobile transportation is beneficial to use for the transportation of small consignments of cargo over relatively short distances, but its environmental performance raises certain questions.

Effective measures that will allow the development and strengthening of container and piggyback transportation of goods include:

- improvement of legislative acts on multimodal transport and combined transport, will become a prerequisite for the creation of a modern regulatory framework for the transport of dangerous goods, harmonized with the EU regulatory framework;
- further development of the network of logistics centers in terms of replenishment and renewal of specialized rolling stock for dangerous goods;
- differentiation of freight and passenger traffic in order to reduce transport risks;
- introduction of special environmental tariffs and financial and economic support from the state.

In the work systematizes the main regulatory instruments in the field of decarbonization of transport and logistics [4]. They are aimed at reducing greenhouse gas emissions into the atmosphere, increasing the practical significance of the concept of “green” logistics and allowing to form an organizational mechanism for implementing the principles of sustainable development in logistics activities. The role of railway, air and water transport in air pollution is insignificant. According to the State Statistics Service of Ukraine, emissions of pollutants into the air from road transport in 2018 amounted to 1,358.4 thousand tons, railway transport – 27.6 thousand tons, that is, the relative excess of emissions from automobile transport is 49 times [3, 5, 6]. Taking into account the level of cargo turnover in the research year (road transport – 42569.5 mln tkm, railway transport – 186344.1 mln tkm), without a large error, we can consider the specific average level of emissions of pollutants in the country into the atmosphere from road transport – 31.910 g/tkm, from railway transport – 0.148 g/tkm. Long-term studies of leading scientists in the world, the results of which were published by the Intergovernmental Commission on Climate Change in its report in 2018 (see [1, 5, 7]), showed that in the period from 1970 to 2010, emissions of such modes of transport as road transport, international aviation, domestic aviation, international and coastal shipping are showing a steady upward trend [4, 5] and is shown in Fig. 1.

Operators of multimodal transportation and operators of container and piggyback terminals are faced with the task of meeting the requirements for ensuring transport safety and environmental protection in terms of the implementation of an environmental management system in accordance with the international standard ISO 14001 (DSTU ISO 14001) “Environmental management systems. Requirements and guidance for use” [7, 8]. This standard contains information and a system of measures for a specific plurality environmental aspect.

Railway transport enterprises are objects that have a negative impact on people in the form of physically dangerous and harmful factors. In addition, the activity of transport under the influence of hazardous and harmful chemical factors of dangerous goods leads to environmental pollution and increase cost on its restoration. Taking into account requirements, an environmental criterion for assessing transport risk is proposed in general form, calculated as the value of financial damage from the negative impact of the vehicle and its cargo on the environment [7]

$$B = P \cdot (B_a + B_w + B_l + B_{sa} + B_{fn} + B_{fl}), \quad (1)$$

where, P is the probability of an adverse event occurring during the transportation of dangerous goods; B_a is the damage from air pollution, million UAH; B_w is the damage

from water pollution, million UAH; B_l is the damage from pollution and land degradation, million UAH; B_{sa} is the damage from the spread of harmful substances in the surrounding area, million UAH; B_{fn} is the damage to fauna, million UAH; B_{fl} is the damage to flora, million UAH.

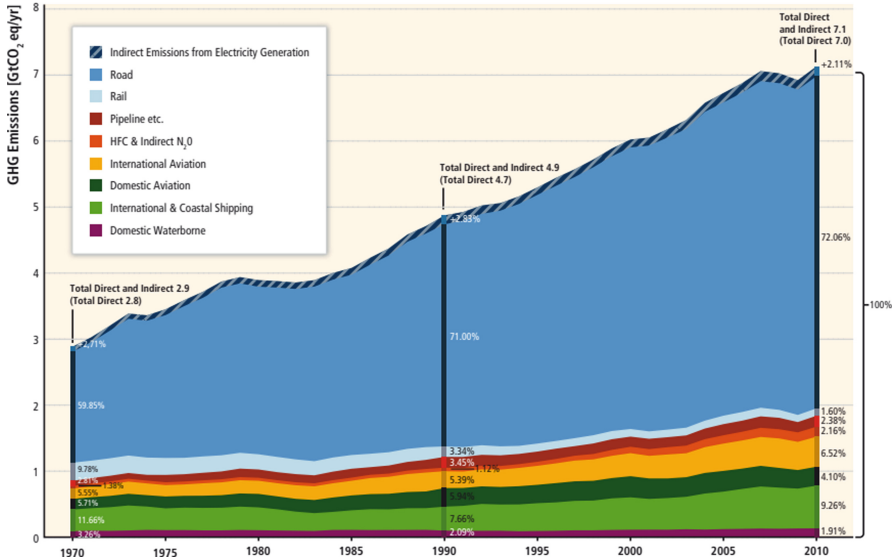


Fig. 1. Trends in the increase of harmful emissions by mode of transport [4].

One of the ways to develop and improve the technology for performing international transportation of dangerous goods is the use of piggyback trains. Piggyback transportation is a type of combined transport in which road trains (tractors with semi-trailers, cars with trailers), semi-trailers, swap bodies are used as cargo units.

A diagram of the organization of conventional (unimodal) and multimodal transportation of goods is shown in Fig. 2. In case of unimodal transportation, it is considered that the entire route distance L_{pr} is realized by one mode of transport. In case of multimodal transportation, the route distance consists of the initial sections with the participation of road transport L_{a1} , the main transportation $L_{3(M)}$ by rail transport (water transport) and the final sections of delivery by road transport L_{a2} . At the terminals, the interaction of modes of transport is implemented, a cargo unit (container) is reloaded and shunting work is performed with a duration of T_{term} (further it is assumed that it will be 1 h at each terminal on the train route).

The flexibility and adaptability of the dangerous goods delivery system is realized due to the rapid movement of reliable information using electronic data interchange (EDI). The main principles of EDI are the exclusion of multiple data entry, acceleration and increase in the accuracy of logistic information by automating data entry, the use of modern intelligent systems and cognitive technologies processing information flows. Practical solutions in the field of improving the quality of logistics services are manifested in ensuring the acceleration of order execution and shortening delivery times, the use of

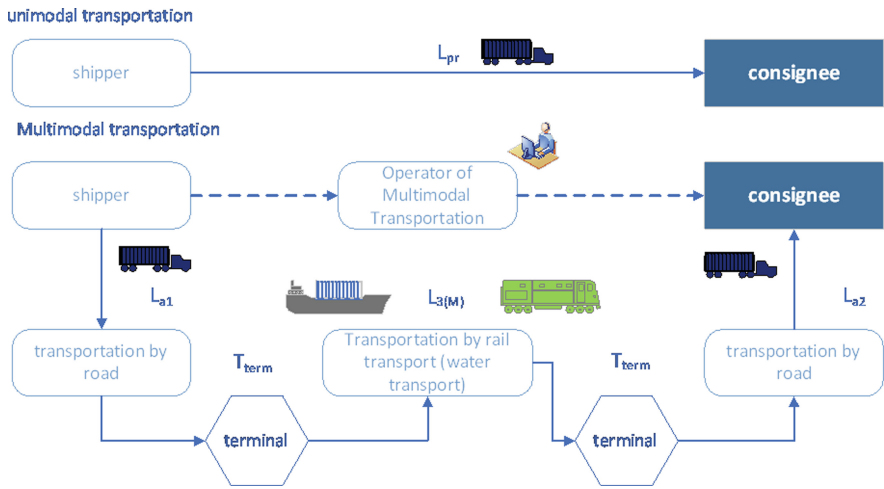


Fig. 2. General scheme of organization of unimodal and multimodal transportation of dangerous goods.

cross-docking concepts, a just-in-time system, a quick response system (QR), the use of bar codes and RFID tags, strategies for determining the exact location based on GPS [2, 6, 9].

4 Research Results

In the framework of multimodal “green” logistics, analysis of existing and prospective logistics channels for the movement of dangerous goods was carried out in order to identify their influence on the environment. In part of improving the level of preservation of dangerous goods due to innovative packaging, the following areas of activity should be envisaged: the use of environmentally acceptable packaging materials, the creation of a system for the return of packaging materials, disposal of packaging and goods, unsuitable for their intended use [10–12].

If we consider the activities of each type of transport separately, then each of them has a negative impact on the environment. Exception is railway transport, due to a significant share of electric traction, constantly reducing harmful emissions.

Share of road transport is 72% of all emissions. Therefore, it is obvious that with a combination of various types of transport in a piggyback scheme of cargo delivery, the harm from the effects of pollutants contained in the exhaust gases and substances of a technically sound tractor truck will be minimize. In particular, emission indicators CO_2 for rail transport are low compared to road and water transport: according to the estimates, transporting 1000 tons of dangerous goods by rail requires three times less energy than transporting them by road transport. The approximate level of specific emissions of exhaust gases are given in Table 1 [5, 6, 13–15].

Taking into account the data in the Table 1, an assessment of energy costs and harmful emissions into the environment was made during the transportation of containers by various modes of transport:

Table 1. Specific emissions of exhaust gases [5].

Type of transport	Specific emissions of exhaust gases, kg/h						
	Carbon monoxide (CO)	Nitric oxide (NO _x)	Hydrocarbon (CH)	Soot (C)	Sulfur oxide (SO _x)	Plumbum (Pb)	Benzo(a)pyrene
Internal combustion engine truck	1.104	0.0120	0.1776	–	0.00168	0.00045	0.26 · 10 ⁻⁶
Diesel truck	0.171	0.0486	0.0180	0.0042	0.0045	–	0.38 · 10 ⁻⁶
Shunting locomotive	6.410	12.400	3.540	0.380	1.870	–	0.80 · 10 ⁻⁶
Ocean vessel	4.812	15.390	3.849	0.962	0.962	–	0.80 · 10 ⁻⁶

- average specific electricity consumption by an electric locomotive 0.6040...0.6552 kW·h/TEU·km;
- average unit consumption of electricity for railway electric traction, taking into account losses in the power supply system 0.6647...0.7208 kW·h/TEU·km;
- average specific emissions of harmful substances on railway electric traction CO = 0.0033...0.0038 g/TEU·km, NO_x = 0.8170...0.8174 g/TEU·km, SO_x = 0.8696...0.8763 g/TEU·km (with mixed mode of power generation by power plants fuel oil/coal);
- average specific emissions of harmful substances when performing shunting work CO = 320.50 g/TEU·h, NO_x = 620.1 g/TEU·h, SO_x = 93.50 g/TEU·h (diesel locomotive ChME-3 in mode engine Ne = 75% of the full power, the composition of the shunting train is accepted for 10 cars);
- average specific emissions of harmful substances during the transportation of containers by sea (for example, a container ship of the type Emma Maersk with a 14-cylinder diesel engine with a capacity of 80800 kW) CO = 8.1955...13.3927 g/TEU·km, NO_x = 2.5625...4.1875 g/TEU·km, SO_x = 1.8750...3.0562 g/TEU·km (specific fuel consumption is expertly accepted as 205 g/kW·h.);
- average specific emissions of harmful substances from a truck CO = 13.194 g/TEU·km, NO_x = 3.750 g/TEU·km, SO_x = 3.200 g/TEU·km (6-cylinder diesel engine, average speed 60 km/h, full container load).

Thus, it has been proven that railway transport is the most environmentally friendly in terms of CO, NO_x, SO_x emissions into the atmosphere. In Fig. 3 shown a comparison of the specific polluting effect on the environment when transporting a 20-foot container (TEU) with dangerous goods by various modes of transport.

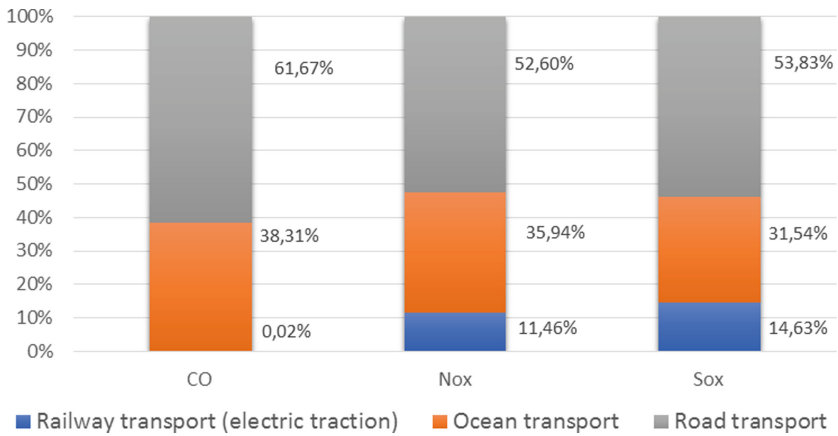


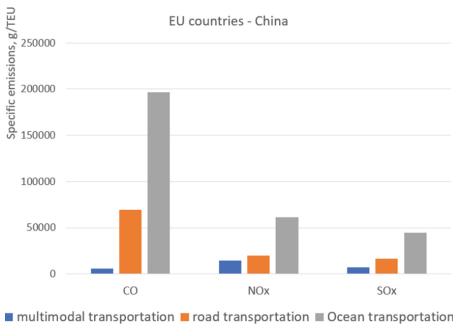
Fig. 3. Comparison of the specific polluting effect on the environment when transporting a 20-foot container (TEU) with dangerous goods by various modes of transport

In order to compare the quantitative assessment of harmful emissions into the environment during the transportation of containers with dangerous goods by various methods and modes of transport along the routes of delivery by some container trains and similar unimodal routes, based on the scheme (see [6, 7, 16]), a Table 2 has been constructed. The table takes into account that the distance to follow the route by different modes of transport depends on the topology of the corresponding communication routes.

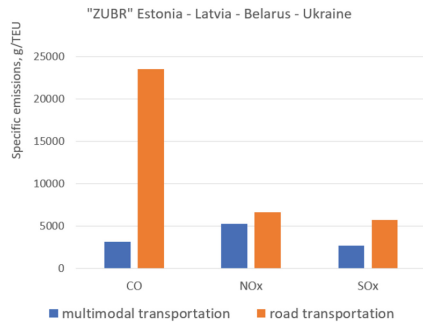
In Fig. 4 shown a comparison of the assessment of harmful emissions into the environment during the transportation of containers with dangerous goods along the considered routes. The analysis showed that the most environmentally friendly is the multimodal container transportation technology, but in terms of NO_x emissions during transportation over relatively short distances (up to 500 km), transportation by road can be conventionally considered more environmentally friendly (under normal weather conditions). If we take into account the impact of the deterioration of natural conditions (snowfall, ice, low temperatures, heavy rains), then even at such short distances, vehicles are inferior to railway ones in terms of environmental indicators [17, 18]. Except to these factors of air pollution, it is also necessary to take into account the harmful effects of the operation of trucks on the state of the roads, the level of noise pollution of the environment, the criteria for the safety of people when using various technologies for the transport of dangerous goods. Taking into account the expected minimization of the movement of road transport when performing piggyback transportation, the likelihood of injury to a person by the remnants of dangerous goods during a road accident, also decreases.

Table 2. Estimation of the amount of harmful emissions into the environment during the transportation of containers with dangerous goods by various methods and modes of transport, g/TEU.

Multimodal route, distance and estimated duration of the route	Emissions on a multimodal route: by train (Additional emissions for initial/final and shunting operations)	Total emissions of the multimodal route	Unimodal emissions from transport (road, water)
“Viking”, combined transport train, Lithuania - Belarus - Ukraine - Bulgaria - Moldova/Romania/Georgia - Azerbaijan, $L_3 = 1766$ km, $t_{pr} = 59$ h	CO 5.83 NO _x 1 442.82 SO _x 1 535.71 (CO 2 865.28 NO _x 2 930.40 SO _x 758.00)	CO 2 871.11 NO _x 4 373.22 SO _x 2 293.71	$L_{pr} = 1486$ km CO 19 606.28 NO _x 5 572.5 SO _x 4 755.2
“ZUBR”, container transportation, Estonia - Latvia - Belarus – Ukraine $L_3 = 2162$ km, $t_{pr} = 84$ h	CO 7.13 NO _x 1 766.35 SO _x 1 880.08 (CO 3 185.78 NO _x 3 550.50 SO _x 851.50)	CO 3 192.91 NO _x 5 316.85 SO _x 2 731.58	$L_{pr} = 1782$ km CO 23 511.71 NO _x 6 682.50 SO _x 5 702.40
EU countries - China, container transportation, Altinkol – Mostiska $L_3 = 6333$ km, $t_{pr} = 360$ h (15 days)	CO 20.8989 NO _x 5 174.061 SO _x 5 507.1768 (CO 6 070.28 NO _x 9 131.40 SO _x 1 693.00)	CO 6 091.18 NO _x 14 305.46 SO _x 7 200.17	$L_{pr} = 5244$ km CO 69 189.34 NO _x 19 665.00 SO _x 16 780.80 (Ocean transport CO 196 692.00 NO _x 61 500.00 SO _x 45 000)



(a)



(b)

Fig. 4. Comparison of the specific environmental impact of the transport of a 20-foot container (TEU) with dangerous goods.

5 Application Prospects

The above factors of the possibility of using piggyback transportation of dangerous goods is a multi-criteria task, therefore, in the future, it must be formalized in order to scientifically substantiate the rational time for preparing a piggyback train for a trip and the probability of failure-free reception or passage of trains by the transport system, protection from physical hazards and harmful factors, increasing safety level, technical capability and processing capacity places of locations piggyback terminals.

6 Conclusion

The introduction of “green” logistics technologies in general when using container and piggyback transportation of dangerous goods makes it possible to highlight the following promising areas of activity:

- investing in the development and construction of new logistics and multimodal centers, which improve the efficiency of logistics operations and indicators of transportation of dangerous goods;
- introduction of specialized technologies in warehouses for the purpose of rational organization of warehouse logistics. As a result, there will be a reduction in storage areas and energy consumption, an increase in safety indicators when performing cargo operations with dangerous goods;
- development of the transport system, incl. transport interchanges, construction of new roads, optimization of routes for transporting dangerous goods in order to reduce emissions of harmful gases;
- reducing the share of unimodal road transport, replacing them with multimodal ones with the participation of rail, sea and river modes of transport, makes it possible to increase environmental friendliness when transporting big numbers of dangerous goods – this reduces the number of flights during transportation and reduces the harmful impact on the environment;
- informing consumers about the environmental direction of the carrier’s and multimodal operator’s activities by labeling the packaging with special signs, increasing the importance of the environmental impact on the quality of life of consumers and the market stability of the carrier during the implementation of activities;
- development and stimulation of waste processing, reduction of tariffs for the disposal residues of container and packaging, development of container transport, providing for the minimization of packaging.

The prospect of “green” logistics today should be linked to the requirements of ISO 14001 (DSTU ISO 14001) “Environmental management systems. Requirements and guidance for use” [8]. It is recognized worldwide as a tool for creating an effective environmental management system. With the correct implementation of the provisions standard ISO 14001 for the entire structure of the organization of multimodal transportation, it is possible to achieve two goals at once: creating conditions for reducing the harmful impact on the environment, subject to the maximum preservation of financial resources.



References

1. Lomotko, D., Krasnoshtan, O.: Innovative approach to increase of operational speed and productivity. *Her. Natl. Transp. Univ.* **1**(48), 188–202 (2021). <https://doi.org/10.33744/2308-6645-2021-1-48-188-202>. (in Ukrainian).
2. Carbone, V., Moatti, V., Schoenherr, T., Gavirneni, S.: From green to good supply chains: halo effect between environmental and social responsibility. *Int. J. Phys. Distrib. Logist. Manag.* **49**(8), 839–860 (2019). <https://doi.org/10.1108/IJPDLM-12-2017-0382>
3. Ghadge, A., Wurtmann, H., Seuring, S.: Managing climate change risks in global supply chains: a review and research agenda. *Int. J. Prod. Res.* **58**(1), 44–64 (2020). <https://doi.org/10.1080/00207543.2019.1629670>
4. Palanivelu, P., Dhawan, M.: Green logistics. White Paper, TATA Consultancy Services Limited (2010)
5. Lomotko, D.V., Prymachenko, H.O., Kovalova, O.V., et al.: Use of modern logistics technologies in terms of saving resources. *IOP Conf. Ser. Mater. Sci. Eng.* **1021**, 012041 (2021). <https://doi.org/10.1088/1757-899X/1021/1/012041>
6. State Statistics Service of Ukraine: Emissions of pollutants and carbon dioxide into the atmosphere 1990–2019 (2019). http://www.ukrstat.gov.ua/operativ/menu/menu_u/ns.htm Accessed 10 May 2022. (in Ukrainian)
7. Galkin, A., Olkhova, M., Iwan, S., et al.: Planning the rational freight vehicle fleet utilization considering the season temperature factor. *Sustainability* **13**(7), 3782 (2021). <https://doi.org/10.3390/su13073782>
8. DSTU ISO 14001:2015: Environmental management systems – requirements and guidelines for use. Ukrainian Research and Training Center of Standardization, Certification and Quality, Kyiv (2016). (in Ukrainian)
9. Mutanov, G., Ziyadin, S., Serikbekuly, A.: Application of system-dynamic modeling to improve distribution logistics processes in the supply chain. *Commun. Sci. Lett. Univ. Zilina* **22**(3), 29–39 (2020). <https://doi.org/10.26552/com.C.2020.3.29-39>
10. Intergovernmental Panel on Climate Change: Transport. In: *Climate Change 2014: Mitigation of Climate Change: Working Group III Contribution to the IPCC Fifth Assessment Report*, pp. 599–670. Cambridge University Press, Cambridge (2015). <https://doi.org/10.1017/CBO9781107415416.014>
11. Olabi, A.G., Maizak, D., Wilberforce, T.: Review of the regulations and techniques to eliminate toxic emissions from diesel engine cars. *Sci. Total Environ.* **748**, 141249 (2020). <https://doi.org/10.1016/j.scitotenv.2020.141249>
12. Lomotko, D., Kovalov, A., Kovalova, O.: Formation of fuzzy support system for decision-making on merchantability of rolling stock in its allocation. *East. Eur. J. Enterp. Technol.* **6**(3), 11–17 (2015). <https://doi.org/10.15587/1729-4061.2015.54496>. (in Ukrainian)
13. Blanckenberg, N.: Extensive List of Fulfillment Companies and Services for eCommerce. *StoreYaBlog* (2019). <https://blog.storeya.com/2018/11/list-of-fulfillment-companies>. Accessed 10 May 2022
14. Lankauskienė, R., Vidickienė, D., Gedminaitė-Raudonė, Ž.: Evolution of short food supply chain theory and practice: two-sided networks and platforms. *Energies* **15**(3), 1137 (2022). <https://doi.org/10.3390/en15031137>
15. Tucki, K., Orynych, O., Wasiak, A., et al.: A computer tool using OpenModelica for modelling CO₂ emissions in driving tests. *Energies* **15**(3), 995 (2022). <https://doi.org/10.3390/en15030995>
16. Carter, C.R., Washispack, S.: Mapping the path forward for sustainable supply chain management: a review of reviews. *J. Bus. Logist.* **39**(4), 242–247 (2018). <https://doi.org/10.1111/jbl.12196>

17. Farooque, M., Zhang, A., Thürer, M., et al.: Circular supply chain management: a definition and structured literature review. *J. Clean. Prod.* **228**, 882–900 (2019). <https://doi.org/10.1016/j.jclepro.2019.04.303>
18. Mogno, C., Fontaras, G., Arcidiacono, V., et al.: The application of the CO₂MPAS model for vehicle CO₂ emissions estimation over real traffic conditions. *Transp. Policy* **124**, 152–159 (2020). <https://doi.org/10.1016/j.tranpol.2020.01.005>



The Strategic Positioning in the International Maritime Logistics

Iuliia Samoilyk¹ (✉)  and Viktoriia Nykonchuk² 

¹ Poltava State Agrarian University, 1/3 Skovorody Street, Poltava 36003, Ukraine

iuliia.samoilyk@gmail.com

² National University of Water and Environmental Engineering, 11 Soborna Street,

Rivne 33028, Ukraine

v.m.nykonchuk@nuwm.edu.ua

Abstract. The strategic vectors of the maritime logistics system development by countries have been substantiated. Trends in logistics development under the globalization condition have been identified. It has been proven that maritime logistics plays an important role in the world trade and economies development. It has been justified those countries that have access to the sea or ocean occupy leading positions in the ranking of countries with a high value of the Logistics Performance Index. The components of the maritime logistics system's effective development have been identified and the maritime logistics leaders have been defined. An analysis of the destructive factors impacts on the trade and the economy, as a whole, development, in particular the pandemic in the world and military action in Ukraine impact, has been carried out. Quantitative and qualitative indicators of the world's leading ports development have been analyzed, in particular the different types vessels number, including depending on the flag, their carrying capacity, time spent in the port. The maritime trade development in the context of the main sea routes using: Non-mainline East West, North-South, South-South, Intra-regional, has been analyzed. With the help of cluster analysis, the main groups of countries that play a leading role in the international maritime logistics system formation have been identified and their development strategic directions have been substantiated.

Keywords: Logistics · Logistics system · International logistics · Maritime logistics · Sea freight · Development strategy

1 Introduction

The market relations development in modern situations is characterized primarily by the closeness and effectiveness of partnerships that arise in the production and commercial activities of economic entities process. Under conditions of intensifying competition and accelerating the pace of socio-economic activity, logistics problems have been becoming increasingly important. Under the deepening globalization impact, the goods around the world delivery have more accessible to most consumers, both at the state level and to individuals. Logistics service is getting less tangible for the average consumer that

characterizes the high level of these services' quality. At the same time, given the growing demand for goods around the world, the deepening of the international labor division, and globalization processes in international logistics, new problems appeared, the solution of which requires effective strategic solutions. The goods transportation plays the leading role in the system of logistics management.

In the international logistics, maritime transport is very important. This carriage type has a lot of advantages over other cargo transportation types, including low cost, large volumes of transportation, clear and unambiguous rules, legal rules of sea transportation, certain sea routes, etc. However, under the conditions of geopolitical changes, increasing globalization, increasing the level of international competitiveness, and entering the market of new stakeholders, there are new challenges in the international maritime logistics field.

2 Literature Review

The scientific literature has contained much research on transport logistics. For example, Topolšek *et al.* [1] noted that there are also a number of different curricula and disciplines, such as: transport economics, transport logistics, logistics management and more. All of these names are often associated with the content of the plan, planning, organization, management and control of human, material, information and financial flows. However, in practice they are often correlated and misused [2]. Problems of transport logistics in various industries, including maritime logistics, are considered by Komelina *et al.* [3], Zos-Kior *et al.* [4], Gani [5], Soner *et al.* [6], Song *et al.* [7], Talley [8]. These works are multi-vector and allow us to assess the state, level of development and strategic management of logistics in the world and individual regions. Blyde and Molina [9] study the logistics infrastructure and the international location of fragmented production, but the features of maritime logistics in this study are not considered. Maritime transport is a very important component of the world economy. More than 80% of the world's trade in goods is through the maritime logistics system. Yan *et al.* [10] proposed new approaches to maritime transport research. Scientists summarize the research topics of maritime transport and classical approaches developed to address them. Talley [8] divided sea transport into "sea part" and "port part". This idea is objective because it characterizes two different directions of maritime transport. Shi and Li's research [11] in the field of maritime logistics is very complex. They concluded that the most popular areas of research in this area are shipping market analysis, ship management, green shipping, safety and security of shipping and management of a shipping company. The most popular topics in the port area are port management, performance and competitiveness assessment, and terminal management. The authors identified seven methods of maritime logistics research, namely: literature review, economic modeling, SIQO (interviews, surveys, observations and questionnaires), case studies, MES (mathematical, econometric and statistical analysis), CCCQ (conceptual analysis), substantive, comparative and qualitative analysis), and modeling [11].

The regional aspect of maritime logistics is being studied by Amin *et al.* [12]. They focused on maritime logistics in the economic development of the archipelago in eastern Indonesia. Alamá-Sabater *et al.* [13] note that the connection of the transport network in

logistics systems can increase the flow of industrial goods between countries. Interesting opinion of Bensassi *et al.* [14], who said that the quality of maritime transport infrastructure is urgent to maintain the efficiency of maritime logistics systems to increase economic added value and competitiveness in international trade.

Thus, the issue of logistics is of interest to many scientists, some areas of research in this area are studied quite comprehensively. However, strategic issues in the development of maritime logistics need further research, especially in view of new trends in globalization in this area.

3 Purpose of the Research, Data and Methodology

The purpose of the study is the substantiation the strategic vectors of maritime logistics system development by countries, identify trends in logistics under the globalization condition, components of maritime logistics system's effective development, identify leaders in maritime logistics, and analyze the impact of destructive factors on trade and the economy as a whole, quantitative and qualitative indicators of the world's leading ports development evaluation. Data from the World Bank, UNCTAD, the world's leading ports, and personal calculations were used for the study.

For the research, methods of analysis, monographic, comparison, graphic, economic-statistical methods, and method of cluster analysis were used.

4 Strategic Direction of the Maritime Logistics Development

4.1 The Level of Logistics System Development and Maritime Trade

The logistics system development requires effective mechanisms and strategic decisions. The modern system of trade and commodity chains formation needs new logistical approaches, which are based on the awareness of the country's strategic position on a globalization scale. The relationship between the countries is deepening, so if the logistics strategy of the one country changes, there will be changes in the entire logistics system. An example is the hostilities in Ukraine's impact.

Due to blocked ports in the spring of 2022, the ships movement is impossible. The war in Ukraine affected about 25% of world grain trade and led to rising world prices, food inflation and reduced access to food in Ukraine's and Russia's importing countries, in particular, wheat and sunflower oil. Wheat supply from Ukraine is more than 10% of annual wheat consumption for 15 countries. For example, this is 28% of Indonesia's needs, 21% – Bangladesh, and Egypt imports almost 80% of its wheat from Russia and Ukraine. In 2021, Ukraine exported agricultural products to more than 180 countries and most to the EU, it is almost 30% [15]. Due to hostilities in the south of Ukraine, seaports have been blocked, logistics and economic chains have been severed, and as a result, Ukrainian producers need of an uninterrupted raw materials supply, including fuel, seeds, plant protection products, fertilizers, spare parts and other goods, and also, suffer from a lack of strategic products.

To assess the level of logistics development and formulate appropriate strategies for the management of logistics systems in the international context, it is advisable to analyze the Logistics Performance Index (LPI) (Table 1).

Table 1. TOP-10 countries by the LPI, 2007–2018, summarized by authors on the basis of [1]

Heading level	2007		2010		2012		2014		2016		2018	
	Rank	Score	Rank	Score	Rank	Score	Rank	Score	Rank	Score	Rank	Score
Germany	3	4.10	1	4.11	4	4.03	1	4.12	1	4.23	1	4.20
Sweden	4	4.08	3	4.08	13	3.85	6	3.96	3	4.20	2	4.05
Belgium	12	3.89	9	3.94	7	3.98	3	4.04	6	4.11	3	4.04
Austria	5	4.06	19	3.76	11	3.89	22	3.65	7	4.10	4	4.03
Japan	6	4.02	7	3.97	8	3.93	10	3.91	12	3.97	5	4.03
Netherlands	2	4.18	4	4.07	5	4.02	2	4.05	4	4.19	6	4.02
Singapore	1	4.19	2	4.09	1	4.13	5	4.00	5	4.14	7	4.00
Denmark	13	3.86	16	3.85	6	4.02	17	3.78	17	3.82	8	3.99
United Kingdom	9	3.99	8	3.95	10	3.90	4	4.01	8	4.07	9	3.99
Finland	15	3.82	12	3.89	3	4.05	24	3.62	15	3.92	10	3.97

The LPI report presents the latest worldwide view on trade logistics performance across more than 160 countries as seen by logistics professionals. This biennial information on logistics infrastructure, service provision, crossborder trade facilitation, and other aspects is invaluable for policy makers, traders, and a wide audience of other stakeholders, including researchers and teachers. The LPI survey data provide numerical evidence on how easy or difficult it is in these countries to transport general merchandise – typically manufactured products in unitized form. The six main indicators of the international part of the LPI summarize on a five-point scale the assessments of logistics professionals worldwide trading with the country. The domestic part of the LPI indicates the quality and availability of key logistics services within a country, but due to the small number of responses, these data are more informative in comparisons by region or income group [1].

The highest LPI values during all years of LPI calculating were in Germany, except in 2007, when Singapore took first place and Germany – third place. In 2018, the German LPI was 4.2 of 5. High performance for this country is due primarily to the developed infrastructure, advantageous geographical location, effective management and strategic logistics management. Germany uses all modes of transport, including powerful ports, which allows for efficient shipping and trade. It should be noted that all TOP-10 countries in the logistics efficiency index have strong ports and developed maritime trade. Thus, the sea plays an important role in ensuring the efficiency of logistics and the economy as a whole. Ukraine ranks 69th in the ranking with a score of 2.83.

Reliability of the supply chain plays an important role in the efficiency of logistics in the context of globalization. Consignees want to have high confidence in when and how deliveries will take place. Supply chain security is a problem not only in cost and time, but also in the quality of shipment. In recent years, trade volumes have increased significantly, particularly in maritime trade. The exception is 2020, as trade and consumption have declined significantly under the influence of coronavirus, so this year is not indicative for analysis (Table 2).

Table 2. International maritime trade, 1970–2020 (millions of tons loaded) [16].

Year	Tanker trader	Marin bulk	Other dry cargo	Total (all cargoes)
1980	1871	608	1225	3704
1990	1755	988	1265	4008
2000	2163	1186	2635	5984
2005	2422	1579	3108	7109
2006	2698	1676	3328	7702
2007	2747	1811	3478	8036
2008	2742	1911	3578	8231
2009	2641	1998	3218	7857
2010	2752	2232	3423	8408
2011	2785	2364	3626	8775
2012	2840	2564	3791	9195
2013	2828	2734	3951	9513
2014	2825	2964	4054	9842
2015	2932	2930	4161	10023
2016	3058	3009	4228	10295
2017	3146	3151	4419	10716
2018	3201	3215	4603	11019
2019	3163	3218	3690	11071
2020	2918	3181	4549	10648

The most popular types of shipping in the world are tanker trade and marin bulk. The total volume of maritime trade in the world was 10648 millions of tons loaded in 2020, it is on 423 million tons loaded (3,8%) les as in 2019. In 2021–2022, trade resumed, albeit with some restrictions. In 2020, the pandemic impacted to the world economy, cutting production activity and consumption, so supply, demand and logistics decreased. By UNCTAD information, all major trading economies saw imports and exports rise above pre-pandemic levels in the fourth quarter of 2021, with trade in goods increasing more strongly in the developing world than in developed countries. The world trade in goods remained strong and trade in services finally returned to its pre-COVID-19 levels. The value of global trade reached a record level of 28.5 trillion USA dollar in 2021.

That's an increase of 25% on 2020 and 13% higher compared to 2019, before the COVID-19 pandemic struck. While most global trade growth took hold during the first half of 2021, progress continued in the year's second half. After a relatively slow third quarter, trade growth picked up again in the fourth quarter, when trade in goods increased by almost 200 billion USA dollar, achieving a new record of 5.8 trillion USA dollar. Trade in services rose by 50 billion USA dollar to reach 1.6 trillion USA dollar, just above pre-pandemic levels. Positive growth rates are expected for both trade in goods

and services, albeit only marginally, keeping trade values at levels similar to the last three months of 2021 [17].

The positive for international trade in 2021 is primarily the result of rising commodity prices, lifting pandemic restrictions and restoring demand through economic stimulus. In the future, global demand for organic products is expected to grow.

4.2 Features of the Maritime Transport in the International Context

In view of the structure of shipping, it is worth considering the types of ships that are most popular in the world. In the world bulk carriers are most used – 879725 thousand dead-weight tons (42.47%) in 2020 and 913032 thousand dead-weight tons (42.77%) in 2021. All numbers of this types of carriers increased in 3.79% (Fig. 1). A bulker carrier is a type of dry cargo vessel specialized for the transportation of goods in bulk, grain, coal, ore, cement, etc.

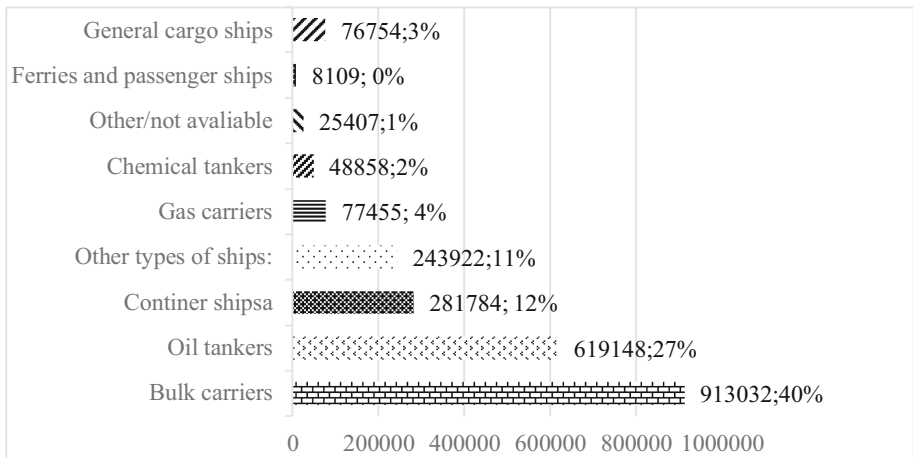


Fig. 1. A World fleet by principal vessel type, 2021 (thousand dead-weight tons and percentage), summarized by the authors on the basis of [16].

Dimensions and weight, connecting devices for transportation by different modes of transport, as well as for equipment that unloads and loads them, doorway, etc. brought to the relevant standards. Thanks to various types of containers, today container transportation of any dimension’s freights, and also the goods which need low temperature at transportation is possible. Thus, the largest share of transportation in the world is carried out with the help of bulk vessels. They are divided into large and small vessels (Fig. 2).

Most are transported by large vessels, in particular 3181 million tons in 2020, which is 1.1% less than in 2019. The largest amount of iron was transported – 1503 million tons or 47.2%. In second place is coal – 1165 million tons, or 36.6% in 2020, but compared to 2019 by 9.3% less. Such reductions are primarily related to the coronavirus pandemic. In addition, global demand for coal is gradually declining as a result of a global strategy to reduce extractive industries due to their significant impact on the environment and,

consequently, the development of alternative energy. Also popular is grain transportation, which accounts for 16.1% of all large-scale transportation. Despite the pandemic, in 2020 the volume of transportation of these products increased from 478 million tons to 512 million tons, or 7.1%. This is due to the growing demand for food, despite the destructive factors. As for small-sized transportation, their total volume is 38.4%, in particular, this type of maritime transport is mostly used for the delivery of steel and timber products.

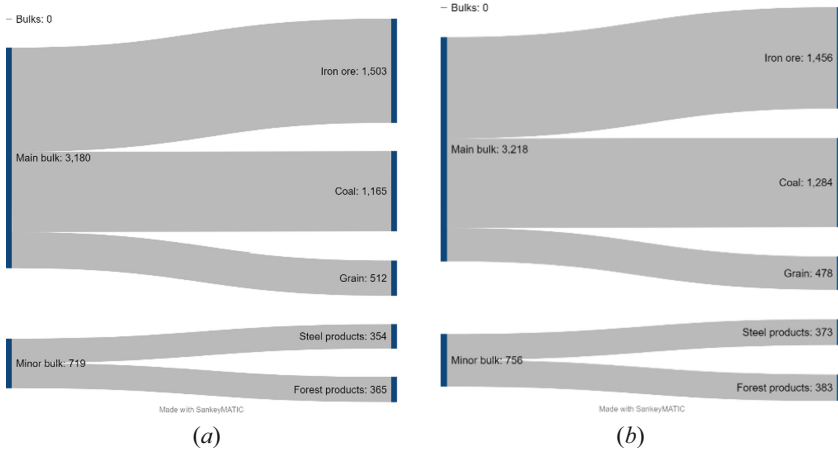


Fig. 2. Dry bulk trade 2019 (a) and 2020 (b) (million tons and percentage change), created by the authors in Sankey MATIC on the basis of [16].

The main trade route is the Main East-West, which carries 39.7% of container traffic. In 2020, the volume of container trade on the main routes East-West amounted to 59168.7 billion TEU, which is 8.6% more than in 2016 and 2% less than in 2018, a decrease in 2020 due to the effects of the coronavirus pandemic. It is worth noting the growing role of other maritime trade routes. The turnover on other routes in 2020 amounted to 90 trillion TEU, which is 11.3% more than in 2016. The intra-regional route is popular. In this way, the turnover in 2020 amounted to 40 trillion TEU, which is 11.6% more than in 2016. The volume of South-South trade increased significantly – 18.6% and amounted to 18.4 trillion TEU. The turnover on the East-West Non-Trunk Route in 2020 amounted to 19.3 trillion TEU, which is 7.2% more than in 2016. The smallest share in turnover is occupied by the North-South route – 11.9 trillion dollars. In general, we can note the growth of trade on all trade routes. In 2020, the total volume of world maritime trade amounted to 149.2 trillion dollars, which is 10.2% more than in 2016. The world’s largest ports are concentrated in China. International transportation is a major component of China’s foreign trade. The world’s ten largest ports are located in China. Shanghai is China’s main seaport. It occupies an advantageous geographical position (located between the northern and southern parts of China, direct access to the sea). Main export-import specialization: oil products, metal, ore, lumber, various equipment, knitwear, agricultural products (especially grain), coal, fertilizers. The port of Shanghai

is capable of receiving and handling up to 25 million containers per year, while the port’s capacity is constantly increasing [18].

In 2021, the port of Singapore increased container turnover by 1.6% compared to the previous year to 37.47 million TEU, which is a record in its history. The total volume of cargo handling in the port of Singapore in 2021 increased by 1.4% to 599 million tons. The largest shipowners of various types are Japan, Greece and China.

The cost of Bulk Carriers in Japan is 39564 million USA dollars, Greece – 39853 million of USA dollars, China – 34735 million of USA dollars. (Fig. 3). In terms of container value, Germany ranks first with 24,166 million USA dollars (Germany’s largest port is Hamburg). According to other types of ships, China ranks first. Japan is the leader in all types of ships, and the leaders include Greece, China, the United States, Singapore, Norway, Germany, Great Britain, Hong Kong, and South Korea.

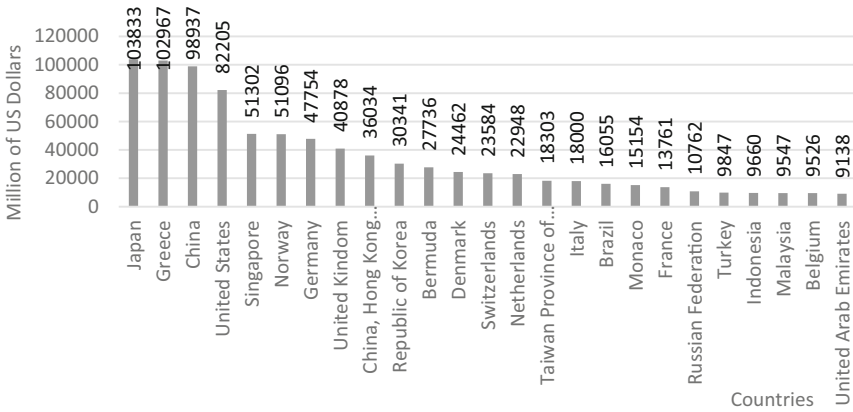


Fig. 3. Top 1 – ship-owning economies, as of 1 January 2021 (millions USA dollars), created by the authors on the basis of [16]

4.3 Strategic Positioning and Maritime Logistics Development Vectors in the International Dimension

To assess the strategic position of the state in the global logistics system, it is necessary to analyze a number of indicators. In particular, the departures from the ports of the country’s frequency indicators are important, as well as the capacity of ships served in the respective ports (Fig. 4).

Using a set of indicators such as Logistics Performance Index, number of vessels (national flag and foreign flag), deadweight tonnage (national flag and foreign flag), number of arrivals, median time in port (days), average container carrying capacity (TEU) per vessel, maximum container carrying capacity (TEU) of vessels, we will carry out the cluster analysis.

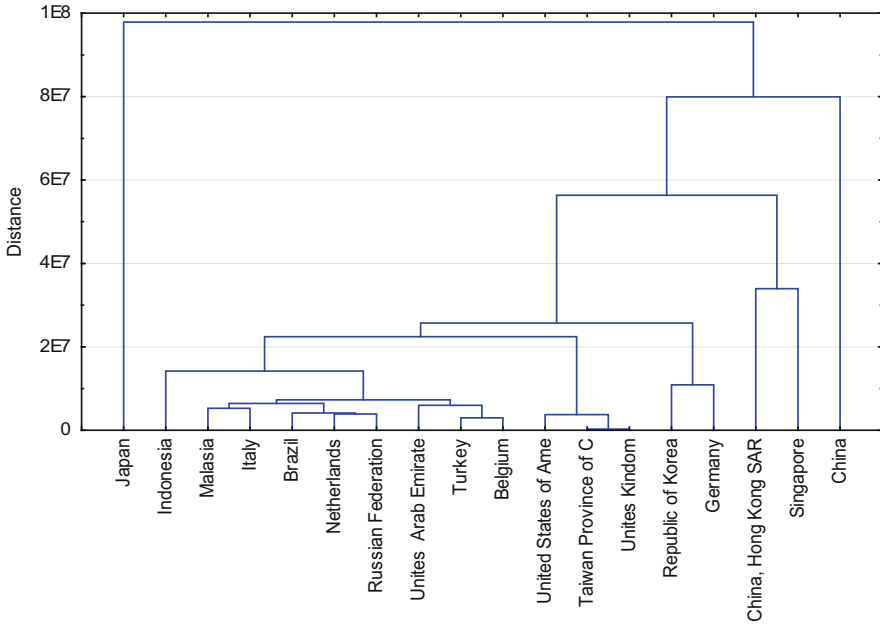


Fig. 4. Vertical hierarchical dendrogram of leading maritime countries clustering according to the set of maritime logistics development indicators.

As a result of the cluster analysis 6 clusters of the countries on signs similarity are formed. It is advisable for China and Japan into a separate cluster to be divided. These countries have unique characteristics for the development of maritime logistics. For each cluster formed, it is advisable to propose an appropriate strategic vector for the development of the maritime logistics system (Table 3).

Table 3. Strategic vectors of maritime logistics development based on the results of cluster analysis.

Routes	Characteristics	Strategic development vectors
China	The level of logistics development is slightly above average, the world's largest number of vessels and their carrying capacity, the average length of stay in port	Strategy for the development of the logistics management system, speeding up the process of loading, loading and unloading, increasing the number of average load capacity days
Japan	High level of logistics development, the world's largest number of vessels under foreign flag, the second largest in the world in terms of total cargo capacity, the shortest length of stay in port and the smallest average cargo capacity of a container vessel	Increasing the number of ships under its own flag (improving legislation), increasing the fleet of ships with higher carrying capacity
Singapore, China, Hong Kong, Republic of Korea	High level of logistics development, significant number of vessels owned, their maximum carrying capacity, average time spent in port	Increasing the number of vessels, reducing the time of their service in the port
Unites Kingdom, Germany, USA, Taiwan	High level of logistics development, average number of vessels owned, their maximum carrying capacity, average time spent in port	Increasing the number of ships, fleet renewal
Turkey, Belgium, UAE, Russian Federation, Netherlands	The level of logistics development is below average, the average number of vessels owned, their maximum carrying capacity, significant time spent in port	Strategy of logistics development, increase in the number of vessels, renewal of the fleet, reduction of their service time in the port
Italy, Brazil, Malasia	The level of logistics development is below average, relatively fewer vessels are owned; average capacity is the average time spent in port	Development of logistics, strengthening in its niche

5 Conclusion

Maritime logistics plays an important role in the development of world trade and economies. Those countries that have access to the sea or ocean occupy the leading positions in the ranking of countries with a high value of the Logistics Efficiency Index. The first place in this indicator is occupied by Germany with a value of 4.2. Also, among the leaders Sweden, Belgium, Austria, Japan, Netherlands, Singapore.

Maritime trade is carried out in the following main ways: Non-mainline East West is it the trade involving Western Asia and the Indian Sub-continent, Europe, North America, and East Asia; North-South is it the trade involving Oceania, Sub-Saharan Africa, Latin America, Europe, and North America; South-South route involve Oceania, Western Asia, East Asia, Sub-Saharan Africa and Latin America; Intra-regional is the trade within Europe, Africa, Asia, North America, Latin America and Oceania.

The cluster analysis identifies six main groups of countries that play a leading role in shaping the international maritime logistics system. The main indicators that determine the vector of strategic development of maritime logistics are: the number of ships of different types, including depending on the flag, their carrying capacity, time spent in port.

Areas of further research are to substantiate the impact of the maritime logistics system development on the “blue economy”.





References

1. Topolšek, D., Čižiūnienė, K., Ojsteršek, T.C.: Defining transport logistics: a literature review and practitioner opinion based approach. *Transport* **33**(5), 1196–1203 (2018). <https://doi.org/10.3846/transport.2018.6965>
2. Tongzon, J., Heng, W.: Port privatization, efficiency and competitiveness: Some empirical evidence from container ports (terminals). *Transport. Res. Part A: Policy Pract.* **39**(5), 405–424 (2005). <https://doi.org/10.1016/j.tra.2005.02.001>
3. Komelina, O.V., Samoilyk, I.V., Boldyrieva, L.M., Krapkina, V.V.: The management of organizational processes of the transport use in construction. In: Onyshchenko, V., Mammadova, G., Sivitska, S., Gasimov, A. (eds.) *ICBI 2019. LNCE*, vol. 73, pp. 601–608. Springer, Cham (2020). https://doi.org/10.1007/978-3-030-42939-3_59
4. Zos-Kior, M., Kuksa, I., Samoilyk, I., Storoška, M.: Methodology for assessing globalisation development of countries. *Economic Annals—XXI* **168**(11–12), 4–8 (2017). <https://doi.org/10.21003/ea.V168-01>
5. Gani, A.: The logistics performance effect in international trade. *Asian J. Shipping Logist.* **33**(4), 279–288 (2017). <https://doi.org/10.1016/j.ajsl.2017.12.012>
6. Soner, O., Akyuz, E., Celik, M.: Statistical modelling of ship operational performance monitoring problem. *J. Mar. Sci. Technol.* **24**(2), 543–552 (2018). <https://doi.org/10.1007/s00773-018-0574-y>
7. Song, L., van Geenhuizen, M.: Port infrastructure investment and regional economic growth in China: Panel evidence in port regions and provinces. *Transp. Policy* **36**, 173–183 (2014). <https://doi.org/10.1016/j.tranpol.2014.08.003>
8. Talley, W.K.: Maritime transportation research: topics and methodologies. *Marit. Policy Manag.* **40**(7), 709–725 (2013). <https://doi.org/10.1080/03088839.2013.851463>
9. Blyde, J., Molina, D.: Logistic infrastructure and the international location of fragmented production. *J. Int. Econ.* **95**(2), 319–332 (2015). <https://doi.org/10.1016/j.jinteco.2014.11.010>

10. Yan, R., Wang, S., Zhen, L., Laporte, G.: Emerging approaches applied to maritime transport research: Past and future. *Communications in Transportation Research* **1**, 100011 (2021). <https://doi.org/10.1016/j.commtr.2021.100011>
11. Shi, W., Li, K.X.: Themes and tools of maritime transport research during 2000–2014. *Marit. Policy Manag.* **44**(2), 151–169 (2017). <https://doi.org/10.1080/03088839.2016.1274833>
12. Amin, C., Mulyati, H., Anggraini, E., Kusumastanto, T.: Impact of maritime logistics on archipelagic economic development in eastern Indonesia. *Asian J. Shipping Logist.* **37**(2), 157–164 (2021). <https://doi.org/10.1016/j.ajsl.2021.01.004>
13. Alamá-Sabater, L., Márquez-Ramos, L., Suárez-Burguet, C.: Trade and transport connectivity: a spatial approach. *Appl. Econ.* **45**(18), 2563–2566 (2013). <https://doi.org/10.1080/00036846.2012.669466>
14. Bensassi, S., Márquez-Ramos, L., Martínez-Zarzoso, I., Suárez-Burguet, C.: Relationship between logistics infrastructure and trade: Evidence from Spanish regional exports. *Transport. Res. Part A: Policy Pract.* **72**, 47–61 (2015). <https://doi.org/10.1016/j.tra.2014.11.007>
15. Port of Hamburg: Top 20 Container Ports. <https://www.hafen-hamburg.de/en/statistics/top-20-container-ports/>. (Accessed 03 May 2022)
16. UNCTAD: Review of Maritime Transport 2021. United Nations, Geneva (2021)
17. UNCTAD: Global trade hits record high of \$28.5 trillion in 2021, but likely to be subdued in (2022). <https://unctad.org/news/global-trade-hits-record-high-285-trillion-2021-likely-be-subdued-2022>. (Accessed 03 May 2022)
18. Sazonets, O., Nykonchuk, V., Kozakevych, A.: The influence of intellectual capital and innovations on the economic development of the world and national economy. *Economic Annals—XXI* 190(5–6), 23–32 (2021). <https://doi.org/10.21003/ea.V190-03>



Urban Street and Road Network Reconstruction Problems

Lina Hasenko¹ , Tetyana Lytvynenko¹ , Viktoriia Ivaskenko² ,
and Mohamed Elgandour¹ 

¹ National University “Yuri Kondratyuk Poltava Polytechnic”, 24 Pershotravnevyj Avenue,
Poltava 36011, Ukraine

ab.Hasenko_LV@nupp.edu.ua

² O. M. Beketov National University of Urban Economy in Kharkiv, 17 Marshala Bazhanova
Street, Kharkiv 61002, Ukraine

Abstract. The paper analyses the current large cities street and road network condition. As a result it is determined that in recent decades in developed cities around the world is taking place a large-scale streets reconstruction, as well as the development of norms, standards, new principles and techniques according to which there will be a place not only for cars but also for pedestrians (including low-mobile population groups), cyclists, cafes, verandas, street shops, etc. in the city. The problems of the street-road network are investigated and the main tasks of the reconstruction of street-road networks are formulated. Three main groups of measures for the reconstruction of the street and road network have been identified: planning measures (introducing changes to the planning structure of the city, redistribution of street and road space, construction of artificial structures, parking lots, arrangement of roundabouts, introduction of means to ensure the inclusiveness of the street and road space and ensure drainage from streets and roads), organizational measures (orientation of the central streets in settlements on pedestrian traffic, encouragement of movement by public and light personal transport and the maximum possible reduction of transit traffic through settlements), operational measures (information support, “green waves” introduction, off-street car parks creation and installation of noise barriers).

Keywords: Changing priorities · Inclusive space · Traffic organization

1 Introduction

Since the 1970s, many cities around the world have begun to review the road environment quality. The function of transit space has become insufficient [1]. There was a need for streets to be also places for meetings, knowledge sharing, cultural leisure, and city life [2]. This process continues to this day. Many cities around the world are actively involved in this process. Streets large-scale reconstruction (see Figs. 1, 2) are the proof of that, as well as the development of norms, standards, new principles and techniques according to which the city will have a place not only for cars but also for pedestrians (including low-mobile population groups), cyclists, cafes, verandas, street shops, etc. [3].



Fig. 1. Changing the urban space distribution in Dusseldorf, Germany. Source: <https://imgur.com/gallery/KjMC2bQ>.



Fig. 2. Changing the distribution of urban space in St. Paul, Minnesota, USA. Source: <https://www.stateofplace.co/our-blog/2018/2/loveable-streets>.

2 Literature Review

For example, in Paris there is a Strategic Plan for Relocation (Plan de déplacements urbain, PDU) for 10 years, which sets specific goals to change the citizens' behavior [4]. It formulates the main objectives, such as reducing of air pollution, increasing of population mobility, quality zoning of public space, stimulating of economic development and others. The strategic plan determines the general outline of relocations in the city, and landscaping projects remain under the auspices of the city hall and are created in working order. On the one hand, it allows constantly design approaches updating, on the other – unique environment creating, even on the smallest street or square.

By the end of the 1970s, London streets design and improvement was based on two documents: “Design and Layout of Roads in Built-Up Areas” and “Roads in Urban Areas” [5]. These norms have been criticized for stimulating the growth of motor vehicles. The result of the struggle to move away from the idea of building new roads was issued in 1977 “Residential Roads and Footpaths Layout Considerations”. Since the early 2000s, there has been a demand in society to shift the main focus of street design from motorists to pedestrians and locals. In 2007, the National Department of Transport published a guide “Manual for Streets” [6]. This document set new standards for design process, landscaping activities and environmental design elements. The second edition of the 2010 Manual, which covers all roads and streets in England and Wales, is currently available.

In Toronto, the principles and approaches to the city development in general, as well as street and public spaces in particular, are set out in many documents and regulations [7]. They are based on “Toronto Official Plan”, adopted in 2010. The plan is constantly changing – with the passage of time, changing current urban needs, as well as public requirements. “Urban Design Guidelines” takes the general recommendations contained in the “Toronto Official Plan” to the next level and details the objectives of the Plan, translating them into the desired results – the design of specific spaces and buildings. “Urban Design Streetscape Manual” is more of an online reference resource than a standalone document. The online system is open to all external users. The potential developer can carry out the project according to recommendations contained in system, requirements, and also arrangement options for a specific street.

3 Research Prerequisites

The current trends in the development of street and road network in cities include:

- growth of cities and building density [8];
- growth of urban population;
- growth in the number of cars per 1,000 inhabitants;
- growth in the number of accidents, environmental, social and other problems related to traffic.

The problem of road accidents in Ukraine is recognized as extremely acute, especially in the last decade, due to the mismatch of road transport infrastructure to the society and the state urgent needs in safety when traveling on highways and road users discipline low level [9, 10].

The press service of Internal Affairs Ministry recently announced sad statistics (see Fig. 3): in Ukraine, on average, one accident occurs every three minutes, one person is injured every fifteen minutes, and one person dies every three hours.

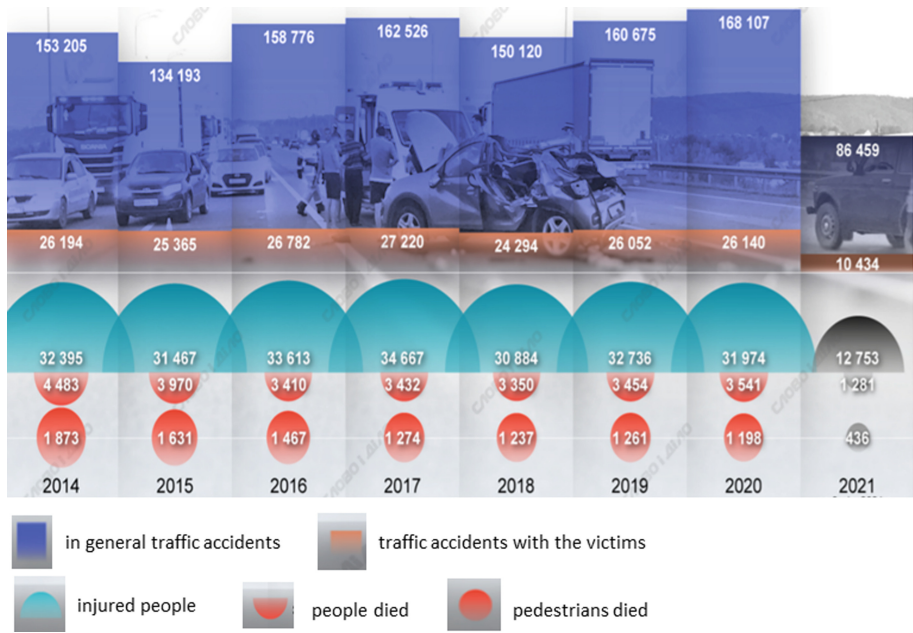


Fig. 3. Accident statistics in Ukraine. Source: <https://www.slovovidilo.ua/2021/07/21/infografika/suspilstvo/dtp-ukrayini-skilky-lyudej-travmuyetsya-hyne-dorohax>.

The motor vehicles number is growing every year, and the new roads and streets construction and expansion does not prevent congestion. Therefore, it is necessary to develop modern principles and techniques for existing street and road networks improving, including technical, safety and environmental requirements.

Starting the urban transport and road network reconstruction, designers should solve problems that would achieve the following goals:

- more even traffic flows distribution throughout the road network;
- minimization of transport mileage when traveling between any two points in the city (the actual route should not be much longer than the distance between points on the overhead line) [11];
- road network differentiation by type of predominant transport modes and traffic organization (freight transport, cars and passengers, high-speed traffic, etc.);
- convenience of connections with the suburban area and transport hubs of systems providing long-distance and interstate connections;
- reduction of traffic flows harmful effects on residential neighbourhoods, recreation areas, areas of historic buildings that have architectural and artistic value, as well as on the residents health [12].

Traffic safety analysis shows that in the road network structure there are traditionally dangerous areas, which should be considered in the first place when developing reconstruction measures.

Developing methods and measures for large cities road network reconstruction should be guided by domestic regulations and positive foreign experience.

4 Results

Based on research of three main measures groups for urban street and road network reconstruction have been identified:

– planning measures;

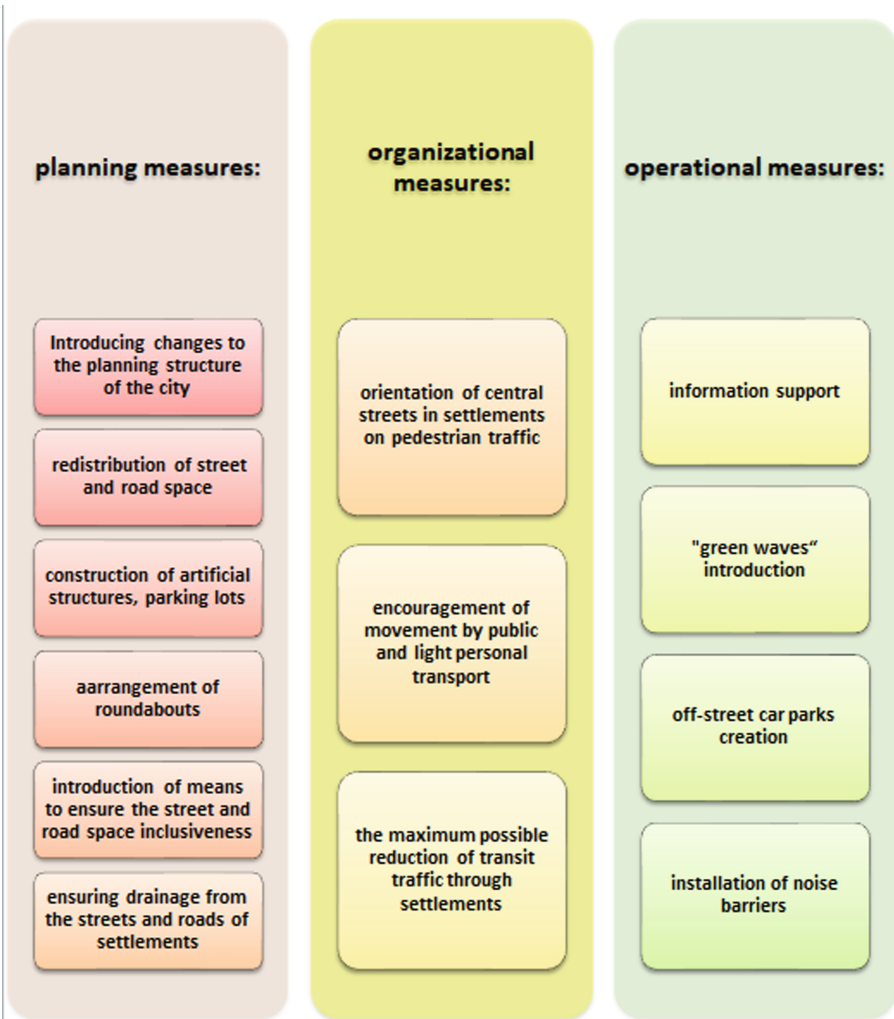


Fig. 4. Measures for urban street and road network reconstruction.

- organizational;
- operational.

The defined measures in turn are divided into receptions and means (see Fig. 4).

4.1 Planning Measures

The most large-scale and complex for the road network settlement reconstruction in order to improve it, are planning measures, which in turn consist of: introducing changes to the planning structure of the city, redistribution of street and road space, construction of artificial structures, parking lots, arrangement of roundabouts, introduction of means to ensure the inclusiveness of the street and road space and ensure drainage from streets and roads in settlements.

Introducing changes to the planning structure of the city first of all can be connected with consolidation of centre building, removal from it a part of enterprises and establishments, especially those which are ecologically dangerous or for the functioning demand considerable freight or passenger transportations. To reduce transit through the centre, for example, the transformation of radial planning structure of the main road network may be envisaged: supplementing it with ring roads, tangential connections along the boundaries of city central and peripheral zones; reconstruction of the existing and new main network construction.

Measures for the **redistribution of street and road space** include:

- *pilot measures* (temporary marking, fencing and change of traffic organization);
- *intermediate steps of reconstruction* (application of new markings, installation of stationary and sliding columns, mobile flower beds, containers with young trees or bushes, large natural stones, lanterns, benches, etc.);
- *comprehensive streets and spaces reconstruction* (widening of sidewalks, relocation of curbs, allocation or bicycle paths separation, elements installation to slow down car traffic, etc.).

Construction of artificial structures, parking lots in settlements can often include the new bridges construction, overpasses and transport interchanges at various levels, the arrangement of above-ground and underground parking.

Arrangement of roundabouts is becoming increasingly common in developed countries. The main advantages of such intersections introduction:

- bandwidth is virtually unaffected, and sometimes exceeds traditional intersections;
- safety increases, the number of accidents decreases, as well as their severity;
- traffic calms down;
- it is possible to organize heavy traffic without traffic lights;
- provides a simple organization of a large number of paths merging;
- movement comfort is promoted by a psychological component – there is no “main” in movement.

The introduction of means to ensure the inclusiveness of the street and road space includes the provision of spatial orientation (by tactile tiles, voice notifications, traffic indicators, including Braille); installation of ramps to overcome height differences; elevated pedestrian crossings and public transport stops (see Fig. 5), etc.

Ensuring drainage from streets and roads in settlements can be achieved by means of vertical planning in combination with open and closed drainage structures.

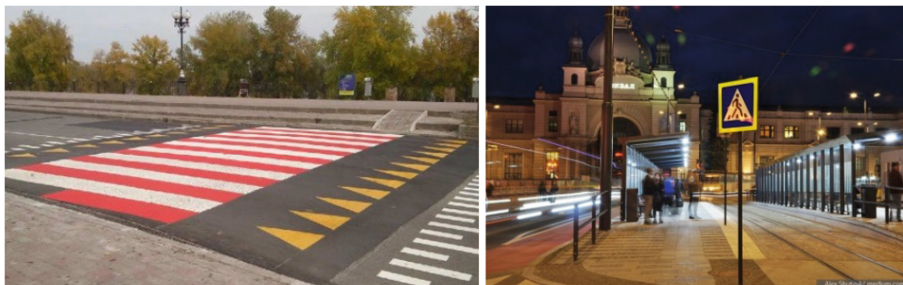


Fig. 5. Elevated pedestrian crossing and public transport stop. Sources: <https://cmr.pb.org.ua/projects/archive/52/show/20>; <https://hmarochos.kiev.ua/2020/06/03/yakymy-mayut-buty-yak-isni-zupynty-gromadskogo-transportu-arhitektor-poyasnyuye-na-prykkladah/>.

4.2 Organizational Measures

World experience proves that even investing significant funds in the road network development, it is impossible to solve the problem of movement in large cities by providing only comfortable movement for cars.

That is why organizational measures for urban street and road network reconstruction should include orientation of central streets in settlements on pedestrian traffic, encouragement of movement by public and light personal transport and the maximum possible reduction of transit traffic through settlements.

Orientation of central streets in settlements on pedestrian traffic appropriate, and in some cities necessary, taking into account the following factors:

- most urban centres have historically not been designed for large amounts of transport;
- the historic centres of cities are attractive for contemplation. Once there, citizens have the opportunity to feel the so-called “spirit of the old city”, see the facades of houses and their details. All this requires a “human scale” and an atmosphere that is almost impossible to achieve with heavy car traffic [13];
- such measures encourage residents to move more on foot and think about the feasibility of using private transport without much need.

While implementing such measures, it is necessary to provide places for storing cars outside pedestrian streets, as well as to create places for pedestrian recreation.

Measures for **encouragement of movement by public and light personal transport**, which can be performed as part of streets reconstruction, are:

- identification of specialized lanes for public and light personal transport (bicycles, scooters, segways, etc.);
- construction of comfortable, safe and accessible public transport stops;
- arrangement of infrastructure for light personal transport (parking [14], repair, maintenance, and power supply of such transport modes [15]).

Outside of street reconstruction, measures to encourage public and light personal transport are appropriate, such as:

- social advertising of such types of relocation [16];
- increasing the public transport attractiveness [17] (rolling stock renewal, proper maintenance, timely cleaning and repair, traffic optimization [18, 19]);
- introduction of social support for public transport, which will make transportation free or affordable (competitive compared to the private cars use).

Maximum possible reduction of transit traffic through settlements can be implemented by bypass roads building and appropriate road signs installing. In world practice, there is also experience in the use of underground space [20] to pass transit traffic (see Fig. 6).

4.3 Operational Measures

Operational measures to improve the road traffic safety and comfort include: information support, “green waves” introduction, off-street car parks creation and installation of noise barriers.

Information support of road traffic should reduce the over-mileage by road users, increase the comfort and traffic safety on the streets. Means of information support (road signs, signposts, information boards, plates with street names and addresses, etc.) should be aimed at both pedestrians and drivers.

“Green waves” introduction is to establish a traffic light connection that ensures the inclusion of green signals to the moments of vehicles compact groups approach. The average vehicles speed in the city should be 40–50 km/h, this speed when introducing the “green wave” should guarantee the driver non-stop travel along the entire highway from intersection to intersection due to coordinated switching of traffic light signals.

This will increase the capacity of regulated intersections, reduce travel time and decrease emissions by reducing braking and acceleration while vehicles are moving [21].

Off-street car parks creation – one of the necessary measure to increase the capacity of urban streets and roads, as the lack of such parking forces drivers to use extreme lanes as parking [22]. Given the lack of space in most cities, especially their historic centres, it is advisable to consider the possibility of multi-level parking lots (overground and underground) using automated parking.

Installation of noise barriers usually appropriate along high-speed highways passing by residential and public areas. The barriers installation can significantly reduce noise pollution, and is also a physical barrier between the roadway and surrounding areas, which prevents the sudden appearance of people and animals on the road.

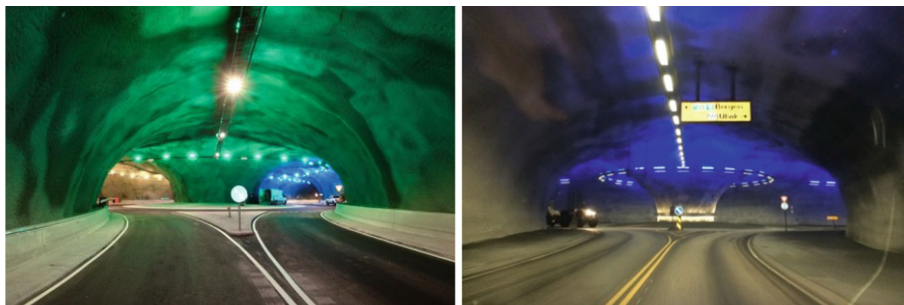


Fig. 6. Underground roads: in the Faroe Islands in Denmark (left); in Norway (right). Source: <https://edition.cnn.com/travel/article/eysturoy-tunnel-roundabout-faroe-islands/index.html>, https://www.reddit.com/r/europe/comments/der2fu/yet_another_roundabout_in_norway_but_this_one_is/

5 Conclusion

The problem of road accidents in Ukraine is recognized as extremely acute, especially in the last decade, due to the mismatch of road transport infrastructure to the society and the state urgent needs in safety when traveling on highways and road users discipline low level.

Analysing the current state of street and road network in large cities, we can conclude that the process of transition from the attitude to the streets as a transit space to their consideration as public space – for meetings, knowledge sharing, cultural leisure and city life is underway in many cities.

Many cities around the world are actively involved in this process. Streets large-scale reconstruction are the proof of that, as well as the development of norms, standards, new principles and techniques according to which the city will have a place not only for cars but also for pedestrians (including low-mobile population groups), cyclists, cafes, verandas, street shops, etc.

Based on research of three main measures groups for urban street and road network reconstruction have been identified:

- planning measures: introducing changes to the city planning structure, redistribution of street and road space, construction of artificial structures, parking lots, arrangement of roundabouts, introduction of means to ensure the inclusiveness of the street and road space and ensure drainage from streets and roads;
- organizational measures: orientation of the central streets in settlements on pedestrian traffic, encouragement of movement by public and light personal transport and the maximum possible reduction of transit traffic through settlements;
- operational measures: information support, “green waves” introduction, off-street car parks creation and noise barriers installation.

Traffic safety analysis shows that in the road network structure there are traditionally dangerous areas, which should be considered in the first place when developing reconstruction measures.

Developing methods and measures for large cities road network reconstruction should be guided by domestic regulations and positive foreign experience.

References

1. McClymont, K., Bedinger, M., Beevers, L., et al.: Understanding urban resilience with the urban systems abstraction hierarchy (USAH). *Sustain. Cities Soc.* **80**, 103729 (2022). <https://doi.org/10.1016/j.scs.2022.103729>
2. Lytvynenko, T., Gasenko, L.: Peculiarities of infrastructure designing for the movement of individual environmental friendly vehicles. *Period. Polytech. Transp. Eng.* **43**(2), 81–86 (2015). <https://doi.org/10.3311/PPtr.7593>
3. Galkin, A.: Urban environment influence on distribution part of logistics systems. *Arch. Trans.* **42**(2), 7–23 (2017). <https://doi.org/10.5604/01.3001.0010.0522>
4. Rossman, V.: *Capital Cities: Varieties and Patterns of Development and Relocation*. Routledge, London (2018). <https://doi.org/10.4324/9781315735061>
5. Davies, H.W.E.: Continuity and change: the evolution of the British planning system, 1947–97. *Town Planning Rev.* **69**(2), 135–152 (1998)
6. Jones, P., Marshall, S., Boujenko, N.: Creating more people-friendly urban streets through ‘link and place’ street planning and design. *IATSS Res.* **32**(1), 14–25 (2008). [https://doi.org/10.1016/S0386-1112\(14\)60196-5](https://doi.org/10.1016/S0386-1112(14)60196-5)
7. Bista, S., Hollander, J.B., Situ, M.: A content analysis of transportation planning documents in Toronto and Montreal. *Case Stud. Trans. Policy* **9**(1), 1–11 (2021). <https://doi.org/10.1016/j.cstp.2020.06.007>
8. Rosati, U., Conti, S.: What is a smart city project? An urban model or a corporate business plan?. *Proc. – Soc. Behav. Sci.* **223**, 968–973 (2016). <https://doi.org/10.1016/j.sbspro.2016.05.332>
9. Lytvynenko, T., Tkachenko, I., Gasenko, L.: Principles of the road beautification elements placing. *Period. Polytech. Transp. Eng.* **45**(2), 94–100 (2017). <https://doi.org/10.3311/PPtr.8592>
10. Afanasieva, I., Galkin, A.: Assessing the information flows and established their effects on the results of driver’s activity. *Arch. Trans.* **45**(1), 7–23 (2018). <https://doi.org/10.5604/01.3001.0012.0938>
11. Wong, Y.Z., Hensher, D.A., Mulley, C.: Mobility as a service (MaaS): Charting a future context. *Trans. Res. Part A: Policy Practice* **131**, 5–19 (2020). <https://doi.org/10.1016/j.tra.2019.09.030>
12. Avila-Palencia, I., Panis, L.I., Dons, E., et al.: The effects of transport mode use on self-perceived health, mental health, and social contact measures: a cross-sectional and longitudinal study. *Environ. Int.* **120**, 199–206 (2018). <https://doi.org/10.1016/j.envint.2018.08.002>
13. Azizibabani, M., Bemanian, M., Yeganeh, M.: Investigation of the effects of applying social sustainability components on residential satisfaction. *J. Sustain. Architect. Civil Eng.* **29**(2), 49–61 (2021). <https://doi.org/10.5755/j01.sace.29.2.29217>
14. Wu, Y.H., Kang, L., Hsu, Y.T., Wang, P.C.: Exploring trip characteristics of bike-sharing system uses: Effects of land-use patterns and pricing scheme change. *Int. J. Trans. Sci. Technol.* **8**(3), 318–331 (2019). <https://doi.org/10.1016/j.ijst.2019.05.003>
15. Deb, S., Tammi, K., Kalita, K., Mahanta, P.: Review of recent trends in charging infrastructure planning for electric vehicles. *Wiley Interdis. Rev. Energy Environ.* **7**(6), e306 (2018). <https://doi.org/10.1002/wene.306>

16. Sulikova, S., Brand, C.: Investigating what makes people walk or cycle using a socio-ecological approach in seven European cities. *Transport. Res. F: Traffic Psychol. Behav.* **83**, 351–381 (2021). <https://doi.org/10.1016/j.trf.2021.10.008>
17. Porru, S., Misso, F.E., Pani, F.E., Repetto, C.: Smart mobility and public transport: Opportunities and challenges in rural and urban areas. *J. Traffic Trans. Eng. (English Ed.)* **7**(1), 88–97 (2020). <https://doi.org/10.1016/j.jtte.2019.10.002>
18. Olaverri-Monreal, C.: Autonomous vehicles and smart mobility related technologies. *Informations J.* **8**(2), 17–24 (2016)
19. Petersen, N.C., Rodrigues, F., Pereira, F.C.: Multi-output deep learning for bus arrival time predictions. *Trans. Res. Proc.* **41**, 138–145 (2019). <https://doi.org/10.1016/j.trpro.2019.09.025>
20. Admiraal, H., Cornaro, A.: Future cities, resilient cities – The role of underground space in achieving urban resilience. *Underground Space* **5**(3), 223–228 (2020). <https://doi.org/10.1016/j.undsp.2019.02.001>
21. Chai, H., Zhang, H.M., Ghosal, D., Chuah, C.N.: Dynamic traffic routing in a network with adaptive signal control. *Trans. Res. Part C: Emerg. Technol.* **85**, 64–85 (2017). <https://doi.org/10.1016/j.trc.2017.08.017>
22. Parmar, J., Das, P., Dave, S.M.: Study on demand and characteristics of parking system in urban areas: A review. *Journal of Traffic and Transportation Engineering (English Edition)* **7**(1), 111–124 (2020). <https://doi.org/10.1016/j.jtte.2019.09.003>

Author Index

A

Airapetian, Tamara, 360
Aksonov, Oleksandr, 547
Aksonov, Yevhen, 547, 593
Alharthi, Abdullah, 775
Ali, Osamah Ihsan, 420
Appasani, Bhargav, 248
Arsenyeva, Olga, 315
Avramov, Konstantin, 477

B

Babaiev, Volodymyr, 115, 302
Bacherikov, Dmytro, 237
Bajdor, Paula, 277
Barbashyn, Vitalii, 831
Barone, Fabrizio, 644
Bazilevych, Kseniia, 107
Bazilo, Constantine, 202, 225
Berdnikova, Olena, 381, 513
Berdnychenko, Yuliia, 752
Bernatskyi, Artemii, 513, 558
Bhargav, Appasani, 707
Biletskyi, Ihor, 75, 412
Bondarenko, Maksym, 225
Bulaienko, Maryna, 3
Burko, Dmytro, 683
Butkevych, Mykola, 107

C

Casazza, Marco, 644
Chepurna, Svitlana, 695
Chuhai, Andrii, 25
Chumachenko, Tetyana, 86
Chumachenko, Vitalii, 683

Chyzhyk, Vitalii, 669
Comi, Antonio, 729, 795

D

Danchuk, Viktor, 729
Datsenko, Diana, 656
Davidich, Yuriy, 764
Dembitskij, Valerij, 740
Derevianko, Ihor, 477
Dril, Nataliia, 290
Dulfan, Hanna, 412
Dushkin, Stanislav, 349
Dvirnyk, Yaroslav, 525
Dyachenko, Yuri, 569
Dymchenko, Olena, 290, 612

E

Elgandour, Mohamed, 854
Epoyan, Stepan, 360

F

Faure, Emil, 225
Fedorovich, Oleg, 163
Filimonov, Sergey, 237
Filimonova, Nadiia, 237
Filina-Dawidowicz, Ludmiła, 808
Fomin, Oleksandr, 258

G

Gaba, Vasyl, 752
Galkina, Olena, 349
Ghadekar, Premanand, 128
Ghisellini, Patrizia, 621
Ghonge, Mangesh, 96

Gil, Mykola, 35
 Gordienko, Sergii, 368
 Greshta, Viktor, 403
 Gruenwald, Norbert, 656
 Gupta, Kapil, 489
 Gurina, Galina, 393
 Gyurika, István Gábor, 420

H

Haiduchok, Oleksandr, 360
 Halchenko, Volodymyr, 202, 237
 Hasenko, Lina, 854
 Horban, Anatoliy, 717
 Hriekova, Olesia, 820
 Hrushevska, Tetiana, 717, 752
 Hryhorenko, Svitlana, 381
 Hussain, Talib, 128

I

Illiasenko, Yevhenii, 432
 Infante, Luis, 14
 Ivasenko, Viktoriia, 854

J

Jakab, Miklós, 420
 Janda, Mario, 177
 Jiang, Richard, 775

K

Kabus, Oleksii, 537
 Kachare, Tejas, 96, 128
 Kakade, Siddharth, 96
 Kalmykov, Oleg, 115
 Kaptsov, Ivan, 325
 Kaptsova, Nataliya, 325
 Kapustenko, Petro, 315
 Khabarova, Hanna, 337
 Khademi, Anahita, 151
 Khademian, Sepehr, 151
 Khan, Mohammad Ayoub, 775
 Khandogina, Olga, 632
 Khaskin, Vladislav, 432
 Khokhlov, Maksym, 513
 Khomiak, Olha, 14
 Khudiakov, Illia, 302
 Klemeš, Jiří Jaromír, 315
 Kombarov, Volodymyr, 547, 593
 Kondratiev, Andrii, 444, 466
 Kopytkov, Denys, 764
 Korytchenko, Kostyantyn, 177
 Korzyk, Volodymyr, 432
 Kostenko, Oleksandr, 3
 Kostin, Valeriy, 381
 Kozodoi, Dmytro, 831
 Kozub, Pavlo, 393

Kozub, Svetlana, 393
 Kravchenko, Mikhail, 785
 Kravchuk, Oleksandr, 360
 Krivosheev, Serhiy, 177
 Krivtsov, Serhii, 86
 Krykun, Valentyn, 258
 Kulaienko, Oleh, 537
 Kulbashevska, Tetiana, 57, 75
 Kulbashna, Nadiia, 695
 Kunytska, Olga, 656, 729
 Kush, Yevhen, 764
 Kushnarova, Olga, 381, 513
 Kuzenkov, Oleksandr, 213
 Kuznetsov, Valeriy, 140
 Kuznetsov, Vitaliy, 213
 Kyrychenko, Hanna, 752
 Kyrychenko, Volodymyr, 57, 75
 Kyzym, Mykola, 290

L

Laptiev, Serhii, 581
 Litvinchev, Igor, 25
 Liutova, Olga, 403
 Lomakina, Olga, 337
 Lomotko, Denis, 831
 Lomotko, Mykola, 831
 Lubov, Denis, 412
 Lukashenko, Volodymyr, 558
 Lynnyk, Iryna, 695
 Lys, Daria, 258
 Lytvynenko, Tetyana, 854

M

Maladhari, Pradunya, 128
 Malakhova, Olena, 785
 Martynov, Serghii, 349
 Meniailov, Ievgen, 86
 Merkulov, Dmytro, 456
 Merkulova, Alyona, 456
 Mishra, Sunil Kumar, 248
 Misura, Serhii, 456
 Moroz, Natalia, 368
 Możdrzeń, Daria, 808
 Mundra, Ronak, 707
 Musala, Sarada, 266, 707
 Mushchynska, Natalia, 632
 Mykhailova, Krystyna, 609

N

Nabokina, Tetyana, 444, 466
 Ni, Qiang, 775
 Nigade, Siddharth, 96
 Nikolenko, Anatoliy, 213
 Nykonchuk, Viktoriia, 842

O

Obukhova, Nataliia, 632
 Ohar, Oleksandr, 831
 Olkhova, Mariia, 795
 Orlov, Andrii, 258

P

Padalko, Halyna, 107
 Pakhomov, Yuriy, 163
 Palahin, Volodymyr, 65
 Palahina, Elena, 65
 Paleyeva, Katerina, 325
 Passaro, Renato, 621
 Pati, Avadh, 248
 Patsuk, Volodymyr, 35
 Pavlenko, Dmytro, 502, 525
 Pedash, Oleksii, 525
 Peleshenko, Sviatoslav, 432
 Persia, Luca, 656
 Phokane, Thobadingoe Craven, 489
 Piddubna, Lidiia, 57, 189
 Plankovskyy, Sergiy, 547, 593
 Pliuhin, Vladyslav, 189, 302
 Plyhun, Olga, 795
 Polishchuk, Oleg, 477
 Polozhaenko, Sergii, 258
 Ponkratov, Denys, 764
 Prasolenko, Oleksii, 683
 Prokhorchenko, Andrii, 785
 Prokhorchenko, Halyna, 785
 Prokhorov, Oleksandr, 163
 Prokhorov, Valeriy, 163
 Prydiuk, Valentyn, 740
 Pushkar, Tetiana, 609
 Pustiulha, Serhii, 740

R

Ravariu, Cristian, 266, 707
 Reshetchenko, Alona, 337
 Romano, Rocco, 644
 Romanova, Tatiana, 25
 Roslavitsev, Dmytro, 795
 Rudachenko, Olha, 290

S

Saienko, Natalia, 393
 Salenko, Oleksandr, 477
 Samchuk, Ganna, 764
 Samchuk, Volodymyr, 740
 Samoilyk, Iuliia, 842
 Samostian, Viktor, 740
 Selivanova, Alla, 808
 Semenets, Oleksandr, 456
 Semenov, Oleksandr, 412

Sergieiev, Viktor, 57, 75
 Serhiienko, Kateryna, 669
 Serhiienko, Serhii, 140
 Serogina, Daria, 609
 Shalomoev, Vadim, 403
 Shamsutdinova, Nataliia, 558
 Shatalov, Oleksii, 163
 Shcheretskyi, Volodymyr, 432
 Shekhovtsov, Sergiy, 25
 Shevchenko, Tamara, 349
 Shevtsova, Maryna, 444, 466
 Shintre, Snehal, 96
 Shmukler, Valeriy, 115
 Shypul, Olga, 177
 Sikchi, Sagar, 128
 Sikonenko, Grygorii, 785
 Sinkevych, Oleksiy, 140
 Siora, Oleksandr, 513, 558
 Skripinets, Anna, 393
 Smachylo, Valentyna, 290
 Smetankina, Natalia, 456
 Smirnov, Daniil, 65
 Sobchuk, Valentyn, 581
 Sobolieva, Hanna, 609
 Sokolovskyy, Mykola, 558
 Soloviova, Liubov, 717
 Soloviova, Oleksandra, 717
 Sorokin, Volodymyr, 593
 Sravani, Kesanasetty Leela, 266
 Srinivasulu, Avireni, 266, 707
 Stankiewicz, Sara, 808
 Starostka-Patyk, Marta, 277
 Stetsyuk, Petro, 14, 25
 Stopkin, Vasyl, 213
 Strelko, Oleh, 717, 752
 Sukhonos, Maria, 189, 302
 Sukhorukov, Gennadiy, 360
 Svichynska, Olha, 669
 Svichynskyy, Stanislav, 669

T

Tarasov, Oleksandr, 502, 525
 Teliura, Natalia, 337, 412
 Teterov, Vitaliy, 302
 Titkov, Evgeniy, 381
 Tkach, Daria, 502, 525
 Torba, Yuriy, 502
 Trembovetska, Ruslana, 202
 Tryputen, Mykola, 213
 Tsapko, Nataliia, 337
 Tsaritsynskyy, Anton, 444, 466
 Tsegelnyk, Yevgen, 189, 547, 593
 Tuz, Viacheslav, 225

U

Uhodnikova, Olena, [368](#)
Ulgiati, Sergio, [621](#)
Uspensky, Borys, [477](#)
Usyk, Liudmyla, [225](#)

V

Vakulenko, Kateryna, [695](#)
Vambol, Oleksii, [444](#), [466](#)
Varbanov, Petar Sabev, [315](#)
Vedavyas, Arepalli, [248](#)
Vergunov, Sergey, [45](#)
Vergunova, Nataliia, [45](#)
Viatkin, Kostiantyn, [368](#)
Viatkin, Roman, [368](#)
Volianska, Nina, [140](#)
Voliansky, Roman, [140](#)

Voronko, Iryna, [569](#)

Voronko, Vitalii, [569](#)

Voronko, Vladyslav, [569](#)

Y

Yaskov, Georgiy, [25](#)

Yeresko, Oleksandr, [177](#)

Z

Zablodskiy, Mykola, [189](#)

Zakrzewska, Malgorzata, [656](#)

Zamrii, Iryna, [581](#)

Zarytskyi, Oleksandr, [3](#)

Zastela, Oleksandr, [569](#)

Zhovtyak, Hanna, [609](#)

Zhydkov, Volodymyr, [14](#)